

THE BIOLOGICAL BULLETIN

PUBLISHED BY
THE MARINE BIOLOGICAL LABORATORY

SEP 09 1998

Associate Editors

JAMES A. BLAKE, ENSR Marine & Coastal Center, Woods Hole
LOUIS E. BURNETT, Grice Marine Biological Laboratory, College of Charleston
WILLIAM D. COHEN, Hunter College, City University of New York
CHARLES D. DERBY, Georgia State University
SHINYA INOUÉ, Marine Biological Laboratory
RUDOLF A. RAFF, Indiana University

Editorial Board

PETER B. ARMSTRONG, University of California, Davis	MARK W. MILLER, Institute of Neurobiology, University of Puerto Rico
ANDREW R. CAMERON, California Institute of Technology	TATSUO MOTOKAWA, Tokyo Institute of Technology
THOMAS H. DIETZ, Louisiana State University	YOSHITAKA NAGAHAMA, National Institute for Basic Biology, Japan
RICHARD B. EMLET, Oregon Institute of Marine Biology, University of Oregon	SHERRY D. PAINTER, Marine Biomedical Institute, University of Texas Medical Branch
DAVID EPEL, Hopkins Marine Station, Stanford University	K. RANGA RAO, University of West Florida
DAPHNE GAIL FAUTIN, University of Kansas	BARUCH RINKEVICH, Israel Oceanographic & Limnological Research Ltd.
WILLIAM F. GILLY, Hopkins Marine Station, Stanford University	RICHARD STRATHMANN, Friday Harbor Laboratories, University of Washington
ROGER T. HANLON, Marine Biological Laboratory	STEVEN VOGEL, Duke University
GREGORY HINKLE, University of Massachusetts, Dartmouth	J. HERBERT WAITE, University of Delaware
MAKOTO KOBAYASHI, Hiroshima University of Economics	SARAH ANN WOODIN, University of South Carolina
MICHAEL LABARBERA, University of Chicago	RICHARD K. ZIMMER-FAUST, University of California, Los Angeles
DONAL T. MANAHAN, University of Southern California	
MARGARET MCFALL-NGAI, Kewalo Marine Laboratory, University of Hawaii	

Editor: MICHAEL J. GREENBERG, The Whitney Laboratory, University of Florida

Managing Editor: PAMELA L. CLAPP, Marine Biological Laboratory

AUGUST, 1998

Printed and Issued by
LANCASTER PRESS, Inc.

3575 HEMPLAND ROAD
LANCASTER, PA

Cover

Expression of endostyle-specific genes in a 1-month-old adult of an ascidian (*Ciona intestinalis*), revealed by *in situ* hybridization in a whole mount. Ascidians, or tunicates, are ubiquitous marine animals; they are also primitive chordates and therefore share the characteristic features of the phylum Chordata with the cephalochordates and vertebrates. But the endostyle, a pharyngeal secretory structure associated with food collection, is also found in ascidians, amphioxus, and larval lampreys; moreover, the endostyle is transformed into the thyroid gland in the course of vertebrate evolution. Therefore, the endostyle-specific genes are key markers that should help to elucidate, not only the development of the organ itself, but also the evolution of the chordates. Michio Ogasawara and Noriyuki Satoh of Kyoto University are pursuing these matters; details of their work are reported in this issue.

CONTENTS

IMAGING AND MICROSCOPY

- Piston, David W.**
Concepts in Imaging and Microscopy. Choosing objective lenses: the importance of numerical aperture and magnification in digital optical microscopy 1

RESEARCH NOTES

- Hárosi, Ferenc I., Ione Hunt von Herbing, and Jeffrey R. Van Keuren**
 Sickling of anoxic red blood cells in fish 5
- Stuart, J. A., E. L. Ooi, J. McLeod, A. E. Bourns, and J. S. Ballantyne**
 D- and L- β -hydroxybutyrate dehydrogenases and the evolution of ketone body metabolism in gastropod molluscs 12
- Rodhouse, Paul G.**
 Physiological progenesis in cephalopod molluscs . . . 17

DEVELOPMENT AND REPRODUCTION

- Holm, Eric R., Brian T. Nedved, Eugenio Carpizo-Ituarte, and Michael G. Hadfield**
 Metamorphic-signal transduction in *Hydroides elegans* (Polychaeta: Serpulidae) is not mediated by a G protein 21

PHYSIOLOGY

- Leys, Sally P., and Henry M. Reiswig**
 Transport pathways in the neotropical sponge *Aplysina* 30
- Nair, P. Satish, and William E. Robinson**
 Calcium speciation and exchange between blood and extrapallial fluid of the quahog *Mercenaria mercenaria* (L.) 43
- Nakatani, Isamu, Yoshinori Okada, and Takuji Kitahara**
 Induction of extra claws on the chelipeds of a crayfish, *Procambarus clarkii* 52

ECOLOGY AND EVOLUTION

- Ogasawara, Michio, and Noriyuki Satoh**
 Isolation and characterization of endostyle-specific genes in the ascidian *Ciona intestinalis* 60
- Maruyama, Tadashi, Masaharu Ishikura, Satoru Yamazaki, and Satoru Kanai**
 Molecular phylogeny of zooxanthellate bivalves . . . 70

NEUROBIOLOGY AND BEHAVIOR

- Cobb, Christopher S., and Roddy Williamson**
 Electrophysiology and innervation of the photosensitive epistellar body in the lesser octopus *Eledone cirrhosa* 78

* * *

- Annual Report of the Marine Biological Laboratory . . . R1**

THE BIOLOGICAL BULLETIN

THE BIOLOGICAL BULLETIN is published six times a year by the Marine Biological Laboratory, 7 MBL Street, Woods Hole, Massachusetts 02543.

Subscriptions and similar matter should be addressed to Subscription Manager, THE BIOLOGICAL BULLETIN, Marine Biological Laboratory, 7 MBL Street, Woods Hole, Massachusetts 02543. Subscription per year (six issues, two volumes): \$195 for libraries; \$95 for individuals. Subscription per volume (three issues): \$97.50 for libraries; \$50 for individuals. Back and single issues (subject to availability): \$40 for libraries; \$20 for individuals.

Communications relative to manuscripts should be sent to Michael J. Greenberg, Editor-in-Chief, or Pamela L. Clapp, Managing Editor, at the Marine Biological Laboratory, 7 MBL Street, Woods Hole, Massachusetts 02543. Telephone: (508) 289-7428. FAX: 508-457-1924. E-mail: pclapp@mbl.edu.

<http://www.mbl.edu/BiologicalBulletin/>

The home page for the electronic companion to THE BIOLOGICAL BULLETIN—the *Marine Models Electronic Record*—and other BIOLOGICAL BULLETIN publications is available on the World Wide Web at the address shown above.

THE BIOLOGICAL BULLETIN is indexed in bibliographic services including *Index Medicus* and MEDLINE, *Chemical Abstracts*, *Current Contents*, *Elsevier BIOBASE/Current Awareness in Biological Sciences*, and *Geo Abstracts*.

Printed on acid free paper,
effective with Volume 180, Issue 1, 1991.

POSTMASTER: Send address changes to THE BIOLOGICAL BULLETIN, Marine Biological Laboratory,
7 MBL Street, Woods Hole, MA 02543.

Copyright © 1998, by the Marine Biological Laboratory
Periodicals postage paid at Woods Hole, MA, and additional mailing offices.
ISSN 0006-3185

INSTRUCTIONS TO AUTHORS

The Biological Bulletin accepts outstanding original research reports of general interest to biologists throughout the world. Papers are usually of intermediate length (10–40 manuscript pages). A limited number of solicited review papers may be accepted after formal review. A paper will usually appear within four months after its acceptance.

Very short, especially topical papers (less than 9 manuscript pages including tables, figures, and bibliography) will be published in a separate section entitled "Research Notes." A Research Note in *The Biological Bulletin* follows the format of similar notes in *Nature*. It should open with a summary paragraph of 150 to 200 words comprising the introduction and the conclusions. The rest of the text should continue on without subheadings, and there should be no more than 30 references. References should be referred to in the text by number, and listed in the Literature Cited section in the order that they appear in the text. Unlike references in *Nature*, references in the Research Notes section should conform in punctuation and arrangement to the style of recent issues of *The Biological Bulletin*. Materials and Methods should be incorporated into appropriate figure legends. See the article by Lohmann *et al.* (October 1990, Vol. 179: 214–218) for sample style. A Research Note will usually appear within two months after its acceptance.

The Editorial Board requests that regular manuscripts conform to the requirements set below; those manuscripts that

do not conform will be returned to authors for correction before review.

1. **Manuscripts.** Manuscripts, including figures, should be submitted in triplicate. (Xerox copies of photographs are not acceptable for review purposes.) The submission letter accompanying the manuscript should include a telephone number, a FAX number, and (if possible) an E-mail address for the corresponding author. The original manuscript must be typed in no smaller than 12 pitch or 10 point, using double spacing (including figure legends, footnotes, bibliography, etc.) on one side of 16- or 20-lb. bond paper, 8 by 11 inches. Please, no right justification. Manuscripts should be proofread carefully and errors corrected legibly in black ink. Pages should be numbered consecutively. Margins on all sides should be at least 1 inch (2.5 cm). Manuscripts should conform to the *Council of Biology Editors Style Manual*, 5th Edition (Council of Biology Editors, 1983) and to American spelling. Unusual abbreviations should be kept to a minimum and should be spelled out on first reference as well as defined in a footnote on the title page. Manuscripts should be divided into the following components: Title page, Abstract (of no more than 200 words), Introduction, Materials and Methods, Results, Discussion, Acknowledgments, Literature Cited, Tables, and Figure Legends. In addition, authors should supply a list of words and phrases under which the article should be indexed.

2. **Title page.** The title page consists of a condensed title or running head of no more than 35 letters and spaces, the manuscript title, authors' names and appropriate addresses, and footnotes listing present addresses, acknowledgments or contribution numbers, and explanation of unusual abbreviations.

3. **Figures.** The dimensions of the printed page, 7 by 9 inches, should be kept in mind in preparing figures for publication. We recommend that figures be about 1 times the linear dimensions of the final printing desired, and that the ratio of the largest to the smallest letter or number and of the thickest to the thinnest line not exceed 1:1.5. Explanatory matter generally should be included in legends, although axes should always be identified on the illustration itself. Figures should be prepared for reproduction as either line cuts or halftones. Figures to be reproduced as line cuts should be unmounted glossy photographic reproductions or drawn in black ink on white paper, good-quality tracing cloth or plastic, or blue-lined coordinate paper. Those to be reproduced as halftones should be mounted on board, with both designating numbers or letters and scale bars affixed directly to the figures. All figures should be numbered in consecutive order, with no distinction between text and plate figures and cited, in order, in the text. The author's name and an arrow indicating orientation should appear on the reverse side of all figures.

Color: *The Biological Bulletin* will publish color figures and plates, but must bill authors for the actual additional cost of printing in color. The process is expensive, so authors with more than one color image should—consistent with editorial concerns, especially citation of figures in order—combine them into a single plate to reduce the expense. On request, when supplied with a copy of a color illustration, the editorial staff will provide a pre-publication estimate of the printing cost.

4. **Tables, footnotes, figure legends, etc.** Authors should follow the style in a recent issue of *The Biological Bulletin* in preparing table headings, figure legends, and the like. Because of the high cost of setting tabular material in type, authors are asked to limit such material as much as possible. Tables, with their headings and footnotes, should be typed on separate sheets, numbered with consecutive Roman numerals, and placed after the Literature Cited. Figure legends should contain enough information to make the figure intelligible separate from the text. Legends should be typed double spaced, with consecutive Arabic numbers, on a separate sheet at the end of the paper. Footnotes should be limited to authors' current addresses, acknowledgments or contribution numbers, and explanation of unusual abbreviations. All such footnotes should appear on the title page. Footnotes are not normally permitted in the body of the text.

5. **Literature cited.** In the text, literature should be cited by the Harvard system, with papers by more than two authors cited as Jones *et al.*, 1980. Personal communications and material in preparation or in press should be cited in the text only, with author's initials and institutions, unless the material has been formally accepted and a volume number can be supplied. The list of references following the text should be headed Literature Cited, and must be typed double spaced on separate

pages, conforming in punctuation and arrangement to the style of recent issues of *The Biological Bulletin*. Citations should include complete titles and inclusive pagination. Journal abbreviations should normally follow those of the U. S. A. Standards Institute (USASI), as adopted by BIOLOGICAL ABSTRACTS and CHEMICAL ABSTRACTS, with the minor differences set out below. The most generally useful list of biological journal titles is that published each year by BIOLOGICAL ABSTRACTS (BIOSIS List of Serials; the most recent issue). Foreign authors, and others who are accustomed to using THE WORLD LIST OF SCIENTIFIC PERIODICALS, may find a booklet published by the Biological Council of the U.K. (obtainable from the Institute of Biology, 41 Queen's Gate, London, S.W.7, England, U.K.) useful, since it sets out the WORLD LIST abbreviations for most biological journals with notes of the USASI abbreviations where these differ. CHEMICAL ABSTRACTS publishes quarterly supplements of additional abbreviations. The following points of reference style for THE BIOLOGICAL BULLETIN differ from USASI (or modified WORLD LIST) usage:

A. Journal abbreviations, and book titles, all underlined (for *italics*)

B. All components of abbreviations with initial capitals (not as European usage in WORLD LIST *e.g.*, *J. Cell. Comp. Physiol.* NOT *J. cell. comp. Physiol.*)

C. All abbreviated components must be followed by a period, whole word components *must not* (*e.g.*, *J. Cancer Res.*)

D. Space between all components (*e.g.*, *J. Cell. Comp. Physiol.*, not *J.Cell.Comp.Physiol.*)

E. Unusual words in journal titles should be spelled out in full, rather than employing new abbreviations invented by the author. For example, use *Rit Vísindafélag Islandinga* without abbreviation.

F. All single word journal titles in full (*e.g.*, *Veliger, Ecology, Brain*).

G. The order of abbreviated components should be the same as the word order of the complete title (*i.e.*, *Proc.* and *Trans.* placed where they appear, not transposed as in some BIOLOGICAL ABSTRACTS listings).

H. A few well-known international journals in their preferred forms rather than WORLD LIST or USASI usage (*e.g.*, *Nature, Science, Evolution* NOT *Nature, Lond., Science, N.Y.; Evolution, Lancaster, Pa.*)

6. **Reprints, page proofs, and charges.** Authors of articles in black and white (no color figures) receive their first 50 reprints (without covers) free of charge. Color reprints and additional black-and-white reprints may be purchased; authors will receive order forms. Reprints normally will be delivered about 2 to 3 months after the issue date. Authors (or delegates for foreign authors) will receive page proofs of articles shortly before publication. They will be charged the current cost of printers' time for corrections to these (other than corrections of printers' or editors' errors). Other than these charges for authors' alterations, *The Biological Bulletin* does not have page charges.

Concepts in Imaging and Microscopy

**Choosing Objective Lenses:
The Importance of Numerical Aperture
and Magnification
in Digital Optical Microscopy**

DAVID W. PISTON

*Department of Molecular Physiology and Biophysics, Vanderbilt University,
Nashville, Tennessee 37232-0615*

Abstract. Microscopic images are characterized by a number of microscope-specific parameters—numerical aperture (NA), magnification (M), and resolution (R)—and by parameters that also depend on the specimen—for example, contrast, signal-to-noise ratio, dynamic range, and integration time. In this article, issues associated with the microscope-specific parameters NA, M, and R are discussed with respect to both widefield and laser scanning confocal microscopies. Although most of the discussion points apply to optical microscopy in general, the main application considered is fluorescence microscopy.

Introduction

The objective lens is arguably the most important component of any light microscope (Keller, 1995). Advances in digital imaging have completely changed the way that optical microscopy is performed, and have also changed the relevant specifications for objective lenses. Although lens design, construction, and quality have improved to keep up with the requirements of modern light microscopy, the markings on the lenses remain as they have been for decades. On the objective lens shown in Figure

1, the word ‘FLUAR’ describes the type of lens design; although all manufacturers use similar types of designs, the nomenclature varies from company to company. The next most notable feature on the objective lens is the magnification (M), which in the illustration is 100 \times . It is written in the largest font of all the specifications, yet as is discussed here, it is not the most important parameter. This distinction belongs to the numerical aperture (NA), which is written next to the magnification, but in a smaller font, and in this case is 1.30. The immersion medium for this objective is also given. Below the magnification and numerical aperture, the tube length (∞) and the coverslip thickness (0.17 mm) are given. Currently all manufacturers are offering infinity-corrected optics (denoted by the ∞ symbol), and most lenses are optimally corrected for a number 1.5 coverslip, nominally 170- μ m thick. Both of these parameters are important, but the objective lens will still function adequately for many applications with other tube lengths and coverslip thicknesses. However, because the manufacturers perform chromatic corrections in different ways, multi-color experiments—for instance, co-localization of two different colored immunofluorescent probes—should be performed using only sets of optics that were designed to work together. This applies not only to mixing lenses of different manufacturers, but also to mixing older and newer lines of optics. The working distance of the objective (the depth into the sample to which the lens can focus before it runs into the sample) is also a very important parameter, especially for confocal microscopy in thick biological samples. Despite the critical nature of this spec-

Received 13 February 1998; accepted 28 May 1998.

E-mail: dave.piston@mcmail.vanderbilt.edu

This is the second in a series of articles entitled ‘‘Concepts in Imaging and Microscopy.’’ This series is supported by the Opto-Precision Instruments Association (OPIA) and was introduced with an editorial in the April 1998 issue of this journal (*Biol. Bull.* **194**: 99). The first article in the series was written by Dr. Kenneth R. Castleman and appeared in the same issue (*Biol. Bull.* **194**: 100–107).



Figure 1. An objective lens with typical markings. Although this is a Zeiss lens, most manufacturers use similar markings.

ification, the working distance is not marked on most lenses. Nikon has now started writing the working distance on their CFI60 optics, and it is hoped that this trend will be followed by the other manufacturers.

This short article describes the relative importance of magnification and numerical aperture for digital optical microscopy. Traditionally, observations made with optical microscopes were detected by eye, and in this case, the size of the detector pixels—given by physiological factors in the human eye—is not optimal, so the magnification was increased so the sample could be “seen” better. In digital imaging, however, the magnification can be determined by the combination of resolution and detector pixel size. To understand the relative importance of NA and magnification, we must consider the basics of image formation and the effect of lens parameters on the resolution and information content in optical microscopy. Because the resolving power of an optical microscope is dependent only on the numerical aperture, magnification should be thought of as a secondary parameter whose optimal value can be determined by the NA, detector pixel size, and other instrument-independent imaging parameters. Thus, NA is a more important parameter than magnification in digital imaging. The practical implications of this conclusion are described for two commonly used modes of fluorescence imaging: widefield epi-fluorescence microscopy with a CCD camera as the detector, and laser scanning confocal microscopy with photomultiplier tube detectors.

Basics of Image Formation

As might be guessed by looking at the markings on any objective lens, the magnification and numerical aper-

ture are important for the image-formation properties of an optical microscope. Magnification for an optical instrument is defined as the relative enlargement of the image over the object. Although at first glance it would seem best to use the highest magnification possible, the maximal useful magnification is limited by the resolution of the imaging instrument (as described in the next paragraph). The definition of numerical aperture is more complicated. NA is defined by the half-angle of the objective’s collection cone (α) and the index of refraction of the immersion medium (n), and is expressed by $NA = n \cdot \sin(\alpha)$ (Inoué and Spring, 1997, p. 32). The larger the cone of collected light, the higher the NA, and the more light that will be collected. Thus in practice, NA can be thought of as the amount of light that is collected by the objective lens: a high-NA lens collects more light than a low-NA lens. An analogy is with telescopes: a larger telescope collects more light just as a lens with a larger NA collects more light. Most optical microscopes also offer the option of secondary magnification between the objective lens and the detector. Use of such extra magnification may sometimes be required (see Table 1), but should be avoided if possible since extra light loss is introduced.

As suggested above, resolution (as determined by the basic diffraction principles of light) limits the useful magnification in an optical microscope. Resolution (R) is defined as the smallest distance that two objects can be apart and still be discerned as two separate objects. There are many mathematical definitions for resolution, but a simple and reasonable approximation is $R = \lambda / (2 \cdot NA)$, where λ is the wavelength of the light (Inoué and Spring, 1997, p. 31). This relationship indicates that when using a high-NA lens and 500-nm (blue-green) light, the smallest resolvable distance is ~ 200 nm, or $0.2 \mu\text{m}$, which agrees well with experimental values. One frequent point of confusion for microscope users is the difference between spatial resolution (the ability to distinguish multiple objects) and spatial precision (the ability to localize a single object). Many image-processing enhancements can be used to increase the precision of localization. For example, the path of a single microtubule can be determined to ~ 10 nm precision by pixel-fitting (*e.g.*, Ghosh and Webb, 1994) or deconvolution methods (*e.g.*, Agard *et al.*, 1989; Carrington *et al.*, 1990; Holmes *et al.*, 1995). However, this is *not* 10-nm resolution; 10-nm resolution means that two microtubules that are 10-nm apart can be recognized as two separate tubules. If multiple objects are small and close together (that is, close enough that they cannot be resolved), then no amount of image processing can differentiate between several individual objects and a single object.

Since there is a minimum resolvable distance for every microscope, continuing to increase the magnification past a certain point will no longer increase the information

content of the image. Further magnification beyond this point is sometimes referred to as "empty" or meaningless magnification. This is analogous to any digital image on a computer, where pixelation is observed when an image is magnified on the screen (this can be seen, for example, by repeatedly using the "zoom in" command in Adobe Photoshop). So the question obviously arises, how should the correct magnification be chosen? A good rule is to use the Nyquist criterion, which basically says that one should collect two points per resolution size (Inoué and Spring, 1997, p. 513). Collecting images in this manner maximizes the information content.

The use of $\lambda/(2 \cdot NA)$ for the resolution criterion, and of $R/2$ for the sampling rate are both arbitrary. Many microscopists select other resolution criteria, but all of these choices are only mathematical approximations of the same physical properties. Use of any other resolution criteria would not affect the arguments presented here, although the numbers (*e.g.*, those shown in Table I) would change slightly.

Some attention should also be given to special considerations for fluorescence microscopy (Rost, 1992). Since fluorescence is subject to fluorophore saturation and photobleaching effects that do not affect other optical methods, the highest possible light collection efficiency is desirable. This consideration dictates that the highest possible NA should be used. However, the highest NA lenses (NA = 1.40) are usually of a "plan-Apochromat" design; this type of lens consists of up to 14 elements and has a lower transmittance than a "Fluor" design. Also, if aqueous samples are used, the actual NA is limited to ~ 1.2 because of total internal reflection for higher collection angles at the interface between water and coverslip (Inoué and Spring, 1997, pp. 53–55). For these reasons, fluorescence from an aqueous sample appears brighter through a 100 \times /1.30 NA FLUAR (as shown in Fig. 1) than through a 100 \times /1.40 plan-Apochromat objective lens.

Finally, it should be noted that improvements in almost every aspect of lens design and construction (*e.g.*, computer design of complex lens combination, automated grinding of arbitrary lens shapes, new optical materials for both lenses and coatings, and computer-controlled thin film deposition for precise optical coatings) make modern objective lenses superior to and more reliable than older lenses. Although many older lenses are superb, variables during their construction made finding a good one somewhat challenging, and many researchers just took what came. Today's lenses are consistently of high quality, and also offer higher transmission efficiency and lower autofluorescence than did older lenses.

Numerical aperture, magnification, and resolution in widefield microscopy

In a digital widefield (conventional fluorescence) microscope, the image is projected onto an imaging detector

(usually a CCD camera) that takes the place of the eye. Thus, to optimize the information content of the resulting digital image, the pixels on the detector must be matched to the desired image resolution. As described above, the radius of a diffraction-limited spot, $R_{\text{diff}} \approx \lambda/(2 NA)$, is a good quantity to use for the definition of resolution. In the image plane, this spot will still give the smallest resolvable object, but the width of the spot will now be $M \cdot R$. Based on the Nyquist criterion, the desired sampling rate should be twice the resolution, so we want a pixel size in the object of $R_{\text{samp}} \approx R_{\text{diff}}/2$. In practice, the pixel size in widefield microscopy is fixed by the imaging camera used, so the magnification is the only variable that can be adjusted. For the purposes of these calculations, we can assume $\lambda = 0.5 \mu\text{m}$ (a good approximation for fluorescein (FITC) imaging). We can determine the optimal M to be used for a given pixel size by matching the sampling resolution in the image plane to the pixel size (P) by $P = M \cdot R_{\text{samp}}$. Table I shows the results of this calculation for two typical pixel sizes: $24 \mu\text{m}$ (an older SITe 512D CCD chip) and $6.8 \mu\text{m}$ (the more modern Kodak KAF1400 CCD chip). As can be seen from the table, the older chips (with their larger pixel sizes) require higher magnification. For these larger pixels, an extra intermediate magnification of 2.5 would be required to maximize the information content of an image collected with a 100 \times /1.3 NA objective lens, and in fact cameras that use the older SITe chip usually have some extra magnification built into them. As micro-fabrication technology continues to advance, however, the need for high magnification lenses will decrease. Obviously, it is not possible to purchase a 72 \times /1.30 NA lens (although given the popularity of the KAF1400 CCD chip, perhaps it should be), so these optimal magnifications can only serve as a guide for selection of the best objective lens. Further calculations, such as those presented in the table, reveal that a camera with a pixel size of $5.4 \mu\text{m}$ would be ideal for use with many existing lenses, such as 60 \times /1.4 NA, 40 \times /0.90 NA, and 25 \times /0.60 NA. It should be noted, however, that as pixel sizes get smaller, the dynamic range of the detector may be reduced. For instance, the $5.4\text{-}\mu\text{m}$ pixels would likely be filled by fewer than 20,000 counts, which would limit the detector to 14-bit dynamic range. This is in contrast to larger pixel sizes (*i.e.*, the $24 \mu\text{m}$ in the SITe 512D CCD chip), which can easily deliver > 16 -bit dynamic range. For applications that require high precision, such as deconvolution methods, smaller pixels may be unworkable.

Numerical aperture, magnification, and resolution in laser scanning microscopy

Much has been made of the improvement in resolution provided by confocal microscopy. But this improvement is at best minimal, and is only attained for extremely

Table I

Optimal magnification for detectors with different pixel sizes calculated for five numerical apertures

	Numerical aperture (NA)				
	1.40	1.30	0.90	0.60	0.30
Calculated resolutions (μm)					
R_{diff}	0.18	0.19	0.28	0.42	0.83
R_{samp}	0.090	0.095	0.140	0.210	0.415
Magnification (\times)					
24- μm pixels*	267	253	171	114	58
6.8- μm pixels†	76	72	49	32	16

* Represents the SITe512D CCD chip.

† Represents the Kodak KAF1400 CCD chip.

small pinholes. In practical fluorescence microscopy, the pinhole must be opened somewhat to increase the efficiency of fluorescence collection. In fact, the pinhole is almost always opened enough to negate any resolution enhancement (Sandison *et al.*, 1995). In this practical case, there is an improvement in rejection of out-of-focus background, but the resolution is still given by $R_{\text{diff}} \approx \lambda / (2 \text{ NA})$, so the ideal sampling resolution remains as shown in Table I.

A key point in laser scanning microscopy is that there is no longer a fixed pixel size. Because the field over which the laser is scanned can be varied (this variation is usually called "zoom," or more appropriately "electronic zoom," and is analogous to using an optical zoom lens), the sampling resolution can be easily changed. For this reason, users often have a lot of trouble choosing lenses when they switch to laser scanning confocal microscopy. For instance, a $40\times$ lens with a zoom factor of 2.5 is basically equivalent to a $100\times$ lens with no extra zoom. Thus, a $40\times/1.3$ NA lens should be chosen over an equivalent $100\times/1.3$ NA lens, because it offers a potentially larger field of view with no fall-off in light collection or resolution.

In laser scanning confocal microscopy, two other parameters must be considered. First is the size of the detector pinhole, which depends on the magnification. Most confocal microscopes have an adjustable pinhole that is easily set to match the magnification (*e.g.*, for equivalence, a $60\times$ lens needs a pinhole 1.5-fold larger than a $40\times$ lens). Secondly, the lens design for confocal microscopy may, in some cases, be more important than either M or NA. This is especially true for co-localization experiments, in which the chromatic corrections of a plan-Apochromat make it preferable despite its lower light-collection efficiency (the same trade-off must be considered for any three-dimensional microscopies based on

widefield and deconvolution methods, as well). Regardless of the lens design, however, a lower magnification lens (of equivalent NA) is almost always preferable, because it offers a larger field-of-view, and delivers equivalent resolution.

Acknowledgments

This work was supported by an Arnold and Mabel Beckman Foundation Young Investigator Award, NIH grant DK53434, and the Vanderbilt Cell Imaging Resource (underwritten by CA68485 and DK20593).

Literature Cited

- Agard, D. A., Y. Hiraoka, P. Shaw, and J. W. Sedat. 1989. Fluorescence microscopy in three dimensions. *Methods Cell Biol.* **30**: 353–377.
- Carrington, W. A., K. E. Fogarty, and F. S. Fay. 1990. 3D fluorescence imaging of single cells using image restoration. Pp. 53–72 in *Non-invasive Techniques in Cell Biology*. J. K. Foskett and S. Grinstein, eds. Wiley-Liss, New York.
- Ghosh, R. N., and W. W. Webb. 1994. Automated detection and tracking of individual and clustered cell surface low density lipoprotein receptor molecules. *Biophys. J.* **66**: 1301–1318.
- Holmes, T. J., S. Bhattacharyya, J. A. Cooper, D. Hanzel, V. Krishnamurthi, W. Lin, B. Roysam, D. H. Szarowski, and J. N. Turner. 1995. Light microscopic images reconstructed by maximum likelihood deconvolution. Pp. 389–402 in *The Handbook of Biological Confocal Microscopy*, 2nd Edition. J. Pawley, ed. Plenum, New York.
- Inoué, S., and K. R. Spring. 1997. *Video Microscopy: the Fundamentals*, 2nd Edition. Plenum, New York.
- Keller, H. E. 1995. Objective lenses for confocal microscopy. Pp. 111–126 in *The Handbook of Biological Confocal Microscopy*, 2nd Edition. J. Pawley, ed. Plenum, New York.
- Rost, F. W. D. 1992. *Fluorescence Microscopy*. Cambridge University Press, Cambridge, UK.
- Sandison, D. R., D. W. Piston, R. M. Williams, and W. W. Webb. 1995. Resolution, background rejection, and signal-to-noise in widefield and confocal microscopy. *App. Optics* **34**: 3576–3588.

Sickling of Anoxic Red Blood Cells in Fish

FERENC I. HÁROSI^{1,*}, IONE HUNT VON HERBING², AND JEFFREY R. VAN KEUREN³

¹Laboratory of Sensory Physiology, Marine Biological Laboratory, Woods Hole, Massachusetts 02543, and Department of Physiology, Boston University School of Medicine, Boston, Massachusetts 02118; ²School of Marine Sciences, University of Maine, Orono, Maine 04469; and ³Biology Department, Woods Hole Oceanographic Institution, Woods Hole, Massachusetts 02543

The occurrence of the mutant hemoglobin Hb S in human red blood cells results in sickle cell anemia. This disease, including its genetic and molecular bases, has been extensively investigated and is well understood (1,2). The presence of deoxy-induced sickling of animal erythrocytes is largely unknown, however. We examined red blood cells (RBCs) from several fish species in vitro under aerated and anoxic conditions. Our polarized light microscopic techniques were aimed at establishing correlations between erythrocyte morphology, state of oxygenation, spectral absorbance, linear dichroism, and linear birefringence. We found no fish with intracellular HbO₂ polymerization; but there were intraerythrocytic aggregations of deoxy Hb with a high degree of either molecular order or disorder. The ordered aggregates in the RBCs of Atlantic cod, haddock, and toadfish were remarkably similar in dichroic ratio magnitudes and birefringence to those in human RBCs that contain HbS. Therefore, fish hemoglobins appear to be good models of sickling disorders and polymerization-related phenomena. The consequences of sickling on animal health and fish aquaculture remain to be studied.

Aggregates of hemoglobin in fish erythrocytes have been reported since 1865 (cited in ref. 3). Nevertheless, former studies have failed to establish causal relationships between Hb aggregation, the state of oxygenation, and the attendant optical properties of erythrocytes (4–6). As a chance microspectrophotometric observation, we discovered linearly dichroic absorption of light by Hb in larval fish erythrocytes. This linear dichroism—*i.e.*, the dependence of the absorp-

tion coefficient on polarization direction—was associated with abnormal RBC shape, or “sickling,” the common term for this condition. The cells with the distorted morphology contained intracellular “bodies” with high concentrations of deoxyhemoglobin; for the sake of simplicity we call these bodies “erythroosomes.”

Erythroosomes are therefore intraerythrocytic, anisotropic aggregates of polymerized deoxy Hb that become visible in the light microscope because the refractive index of Hb is higher than that of the surrounding medium. Erythroosomes exhibit linear dichroism as well as linear birefringence and occur in varied forms. In the RBCs of larval haddock and cod, for example, they may appear as V, U, or “banana”-shaped structures; but at other stages, or in different species, they may be shaped like needles or rods. The sickled fish erythrocytes encountered to date have always been associated with deoxy Hb, and not the oxygenated form. Indeed, the sickling that appeared was readily reversible by aeration; that is, the erythroosomes disappear and the affected cells resume their normal shape upon oxygenation. Moreover, repeated cycles of anoxia and normoxia cause concomitant cycles of intracellular hemoglobin aggregation and dispersion. In these characteristics, sickling in fish mimics sickling in man.

Our initial observations of sickling were made on 8- and 60-day-old larval haddock (*Melanogrammus aeglefinus*, family Gadidae) as well as on 118- and 125-day-old Atlantic cod (*Gadus morhua*, family Gadidae), all of which derived from stocks originating in the Bay of Fundy, Canada. Because we did not know whether sickling in fish is restricted to the developmental stages of particular species or is a more widespread phenomenon, we extended our investigation to wild-caught and cultured specimens of several species from four other geographical locations.

Received 25 February 1998; accepted 5 June 1998.

* To whom correspondence should be addressed. E-mail: fharosi@mbl.edu

Typical spectral behavior of larval Atlantic cod RBC is illustrated in Figure 1. Erythrocytes with undistorted shape yielded the expected absorption spectrum for HbO_2 as shown in panel a: the Soret (or γ) band peaks at 414 nm and is not dichroic (dichroic ratio of 1). This is consistent with the presence of a random ensemble of HbO_2 molecules (α - and β -band peaks are at 574 and 540 nm, respectively). In marked contrast, the Soret-band in panel b peaks at 430 nm and shows significant linear dichroism with a peak ratio of about 2. The latter is indicative of an orderly arrangement of the chromophores *in situ* (no α -band and shifted β peak to 554 nm); thus the cod Hb behaves like the human Hb S. RBCs of juvenile Atlantic cod (age, 227 and 272 days) obtained from the Narragansett Laboratory of the National Marine Fisheries Service (Rhode Island), also sickled extensively (92%–95% of all cells) under anoxic conditions. Therefore, RBC sickling in cod and haddock is limited neither to an isolated stock nor to a specific age group, but is present in both larval and juvenile stages.

Of the 12 fish species tested, however, only 4 species exhibited sickling under our experimental conditions. These were the two gadids (Atlantic cod and haddock), the toadfish (*Opsanus tau*, family Batrachoididae), and the tautog (*Tautoga onitis*, family Labridae). Because all vertebrate hemoglobins are intracellular heterotetramers of the type $\alpha_2\beta_2$ (except for those of the cyclostomes) (1), and because sickling is controlled by the molecular makeup of the Hb molecules (1, 2), variations in sickling among the species appear to be due to variations in the globins. Such variability is in keeping with known amino acid variations in the α and β chains for which a great variety of mutations have been uncovered (1). In addition to interspecies variations, intraspecies variations were observed between different life history stages in tautog, but not haddock. In haddock, sickling occurred in all stages; but in tautog, sickling was common in the larva, rare in the juvenile stage, and absent in the adult.

Sickling in wild-caught adult toadfish was distinctive for the large erythrocytes produced. Under normoxic conditions, adult toadfish RBCs appeared as flattened ovoids containing isotropic HbO_2 (Fig. 2a); but in a sealed enclosure under anoxic conditions, virtually every RBC with an undamaged cell membrane sickled. Examples are shown in Figure 2b–d. The empirical Soret-band dichroic ratios determined for 100 erythrocytes yielded values between 1.3 and 2.5, with the distribution peaking at 2. Similar results were obtained with cod and haddock, so the erythrocytes in these three species resemble human sickle cells, which have yielded similar dichroic (polarization) ratio distributions peaking at 2.1 (7, 8).

RBC sickling in 37-day-old larval tautog was quite different from that in the former three species. Here, the most common path of aggregation followed the rims of

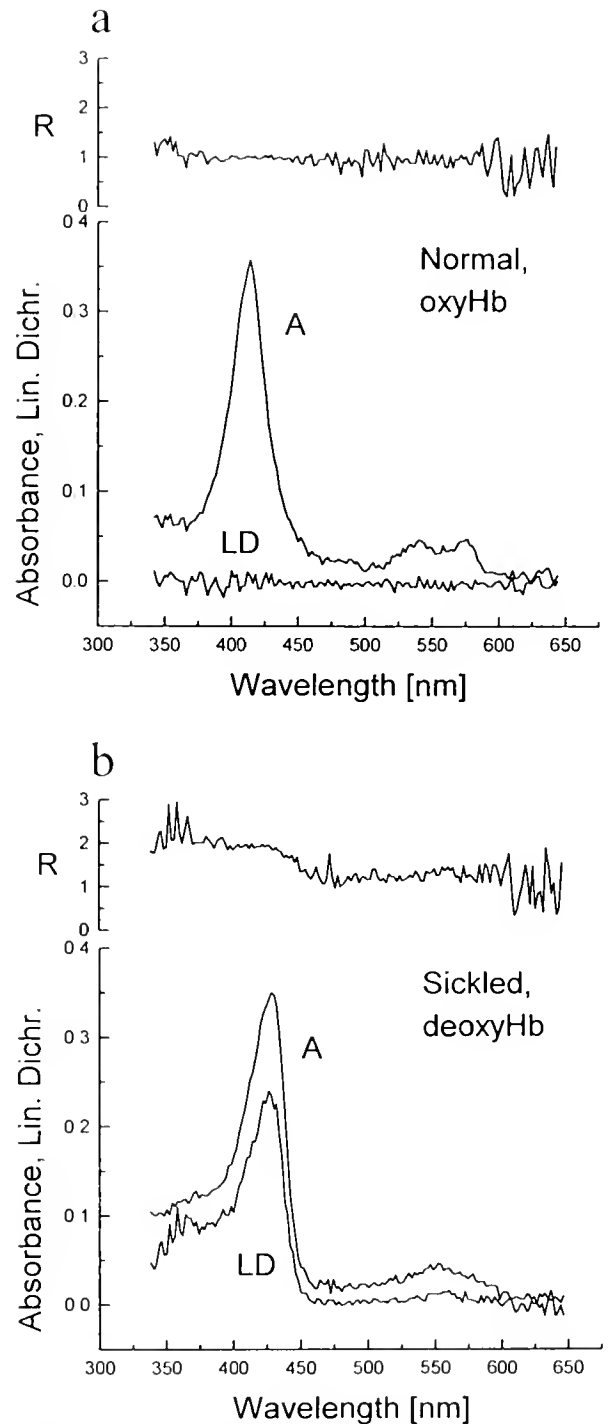


Figure 1. Larval Atlantic cod erythrocyte spectra under oxygenated (a) and deoxygenated (b) conditions: absorbance, A; linear dichroism, LD; and dichroic ratio, R. Absorbance was defined as $A = \log(I_t/I_r)$, where I_t and I_r are transmitted fluxes through sample and reference volumes of the preparation. Linear dichroism was proportional to transmission modulation by sample anisotropy, which was calibrated with an external polarizer to yield 1.0 full-scale value. Polarized absorbance components were determined (26, 27) parallel with erythrocyte length for A_{\parallel} , and perpendicular to it for A_{\perp} . The dichroic ratio was computed as $R = A_{\parallel}/A_{\perp}$.

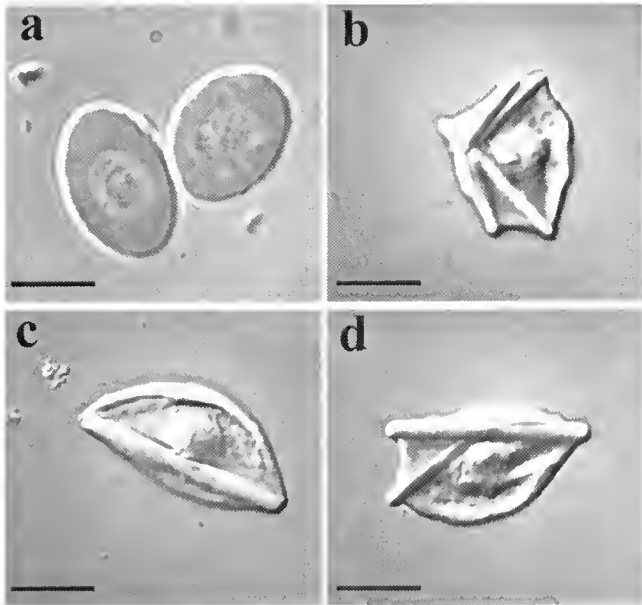


Figure 2. Photomicrographs of adult toadfish erythrocytes (nucleated, as all non-mammalian erythrocytes [9]) obtained with a Zeiss Axiophot 2 microscope in differential interference contrast mode (objective: Plan Apochromat, 63/1.4, oil immersion). (a) Normal cells containing HbO₂ with spectra like those of Fig. 1a. (b–d). Sickled cells under anoxic condition, each with spectra similar to those depicted in Fig. 1b. Scale bars, 10 μ m.

the erythrocytes, usually forming elliptical and closed structures. The transverse-to-tangential dichroic ratio around the cells were nearly uniform, with $R \sim 1.5$. These results imply a flexible fibrous aggregation of Hb in which a degree of parallelism prevails. Unlike the toadfish case, tautog Hb polymerization seems to be too feeble to distort cells into "sickles"; rather it occurs along existing cellular features, such as hooplike microtubules (9).

Hemoglobin gelation in the summer flounder (*Paralichthys dentatus*, family Bothidae) is markedly different from that in either the toadfish or the tautog. Anoxic erythrocytes in the flounder may contain intraerythrocytic clumps without sickling. Aggregates of deoxy Hb in flounder remained isotropic and did not gel into regular structures. They exhibited no linear dichroism ($R \sim 1$). To distinguish isotropic from anisotropic aggregation, we regarded a cell to be sickled only when the Soret-band's linear dichroism was at least 10% above isotropic (i.e., $R \geq 1.1$; see Table I).

Because a linearly dichroic sample should also have anisotropic polarizability, sickle cells would be expected to exhibit linear birefringence as well. Indeed, this has been observed (10) and measured (3) for human sickle cells. We found fish erythrocytes to be also birefringent. Figure 3a illustrates how toadfish erythrocytes may "light up" between crossed polarizers in various color-

ations depending on their orientation with respect to the polarizer's passing direction; they are the darkest at 0° and 90°, and brightest near 45° and 135°.

Retardance and absorbance spectra obtained from a typical toadfish erythrocyte are depicted in Figure 3b. The retardance spectrum shows two peaks, one at 445–450 nm and the other at 585–590 nm; these peaks correspond to the longwave half-maxima of the γ and β -bands (with peaks at 430 and 556 nm, respectively). Although the latter behavior is consistent with *anomalous dispersion* (11,12), we currently lack a quantitative interpretation. The theory of anomalous dispersion describes variations in the relationship between refractive index and wavelength through regions of strong absorption: the index first declines with increasing wavelength, and then sharply rises before declining again to a higher plateau on the longwave side of an absorption band. The presence of the erythrocyte's linear dichroism complicates matters. Here, the stronger absorption coincides with the slow direction of retardance, and the weaker absorption with the fast direction. Therefore, the two principal refractive indices undergo unequal dispersion and thus yield an "anomalous retardance." Whereas we expected erythrocytes to have *two intrinsic birefringent components*, one due to the heme groups and the other to the globin chains, their further delineation does not appear possible at present. Based on multiple determinations of retardance shown in Figure 3b (and assuming that the width of the erythrocyte equals its thickness), the average *specific* retardance ($n = 16$) was in the range of 8.4 ± 1.4 nm/ μ m (450 nm) to 2.7 ± 0.6 nm/ μ m (540 nm). Thus, the average difference in the principal refractive indices, $|n_e - n_o|$, was variable in the visible spectrum between $2.7 - 8.4 \times 10^{-3}$. This range of values is to be compared with that of crystalline quartz, where the difference between the principal refractive indices is 9×10^{-3} . The explanation for erythrocyte hues also follows from Figure 3b. Since light transmission of an erythrocyte between crossed polarizers is proportional to retardance at each wavelength, and because peak retardance occurs around 450 nm, the transmitted flux should cause blue visual sensation at white illumination. If, on the other hand, retardance is also elevated for longer wavelengths (expected for thicker erythrocytes), increased transmission would result throughout the spectrum, yielding desaturated shades of blue.

The principal axes of birefringence were directly observable in polarized light by sample rotation. For toadfish erythrocytes, these correspond to their short and long dimensions, as can be seen in Figure 3a. However, a compensator is also needed if the slow direction is to be distinguished from the fast. To accomplish this, we used the Pol-Scope (13, 14), which is equipped with an automatic compensator. Figure 3c depicts brightness-encoded retardance images of several anoxic toadfish erythrocytes,

Table I

Fish erythrocyte properties: absorbance maxima and sickling

Species	Stage	OxyHb λ_{\max} [nm]				DeoxyHb λ_{\max} [nm]			
		γ	β	α	Sickling	γ	β	α	Sickling (%)*
Atlantic cod (<i>Gadus morhua</i>)	Larval	414	540	574	—	430	554	—	+ (~100)
	Juven.	414	540	574	—	430	554	—	+ (~95)
Haddock (<i>Melanogrammus aeglefinus</i>)	Larval	†	†	†	†	430	556	—	+ (~100)
	Juven.	414	540	575	—	430	556	—	+ (95)
	Adult	414	542	575	—	430	556	—	+ (91)
Toadfish (<i>Opsanus tau</i>)	Adult	414	540	576	—	430	556	—	+ (99)
Tautog (<i>Tautoga onitis</i>)	Larval	414	540	575	—	430	556	—	+ (~90)
	Juven.	414	542	576	—	430	556	—	+ (~1)
	Adult	414	542	576	—	430	556	—	—
Summer flounder (<i>Paralichthys dentatus</i>)	Juven.	414	542	576	—	430	560	—	—
Killifish (<i>Fundulus heteroclitus</i>)	Juven.	414	544	575	—	430	556	—	—
Sheepshead minnow (<i>Cyprinodon variegatus</i>)	Juven.	415	540	578	—	428	560	—	—
Blueback herring (<i>Alosa aestivalis</i>)	Juven.	414	539	575	—	430	555	—	—
Atlantic silverside (<i>Menidia menidia</i>)	Juven.	415	540	576	—	430	560	—	—
Smooth dogfish (<i>Mustelus canis</i>)	Adult	414	544	575	—	430	556	—	—
Little skate (<i>Raja erinacea</i>)	Adult	413	538	576	—	429	555	—	—
Common white sucker (<i>Catostomus commersoni</i>)	Adult	414	540	576	—	430	555	—	—

* In this column, + indicates the occurrence of optically anisotropic intraerythrocytic aggregates; ~ percentage was obtained by visual inspection of cell morphology; other fractions were based on measurable Soret-band linear dichroism ($R \geq 1.1$). The numeric values we regard only as approximate indicators of sickling, because polymerization is reversibly dependent on subtle variations in environmental conditions. Factors promoting sickling were anoxic conditions, low pH (6.9) and elevated temperature (29°C), analogous to those reported previously for Hb S.

† Unavailable data.

revealing bundles of linear molecular aggregation. Another cell from the same preparation is shown in Figure 3d, where an erythrocyte retardance image with superimposed black lines indicates local slow axis direction; this direction is approximately transverse to the long dimension of the erythrocyte. The line scans of erythrocyte retardance are consistent with a model of fibrous molecular order which, taken together with the slow direction of retardation and coincident strong absorption, is in harmony with the presence of bundles of polymerized hemoglobin molecules with their planar porphyrin groups oriented nearly perpendicular to the length of the aggregation. These features have also been found in normal human reduced-hemoglobin crystals and in sickle cells from anemia patients (3).

Our polarized light microscopic observations are complementary to the structural information provided by electron microscopy. Thomas (15) used the latter technique on red cells of cod (*Gadus callarias*) and reported a paracrystalline organization for hemoglobin in erythrocytes. For atomic-scale comparison of fish hemoglobins with Hb S, it will be necessary to combine data from several techniques, as has been done for the various forms of human hemoglobin, including refined methods in electron

microscopy (16), X-ray crystallography (17), and analyses of globin mutations based on amino acid sequence information (18).

The current investigation notwithstanding, we can only speculate how widespread sickling is among the nearly 20,000 extant fish species. But given the richly varied environments that fishes inhabit, a great variability in fish hemoglobins is probable. Also probable is that the evolution of fish hemoglobins has responded to various environmental stresses in many species. Thus, we anticipate fish hemoglobins to emerge as a rich resource for genetic, evolutionary, molecular, and pathophysiological studies. The variety of sickling hemoglobins may lead to new model systems, not only for a human disease, but also for studies of fundamental importance such as polymerization, force generation (19), and the identification of molecular contacts that make paracrystal formation possible.

The phenomenon of sickling may also have practical relevance to marine fish aquaculture. Fish in culture are often under heightened stress (e.g., insufficient oxygenation, high bacterial load, and low pH), and they are consequently prone to infections and high mortality rates. Because a propensity for sickling could increase mortality

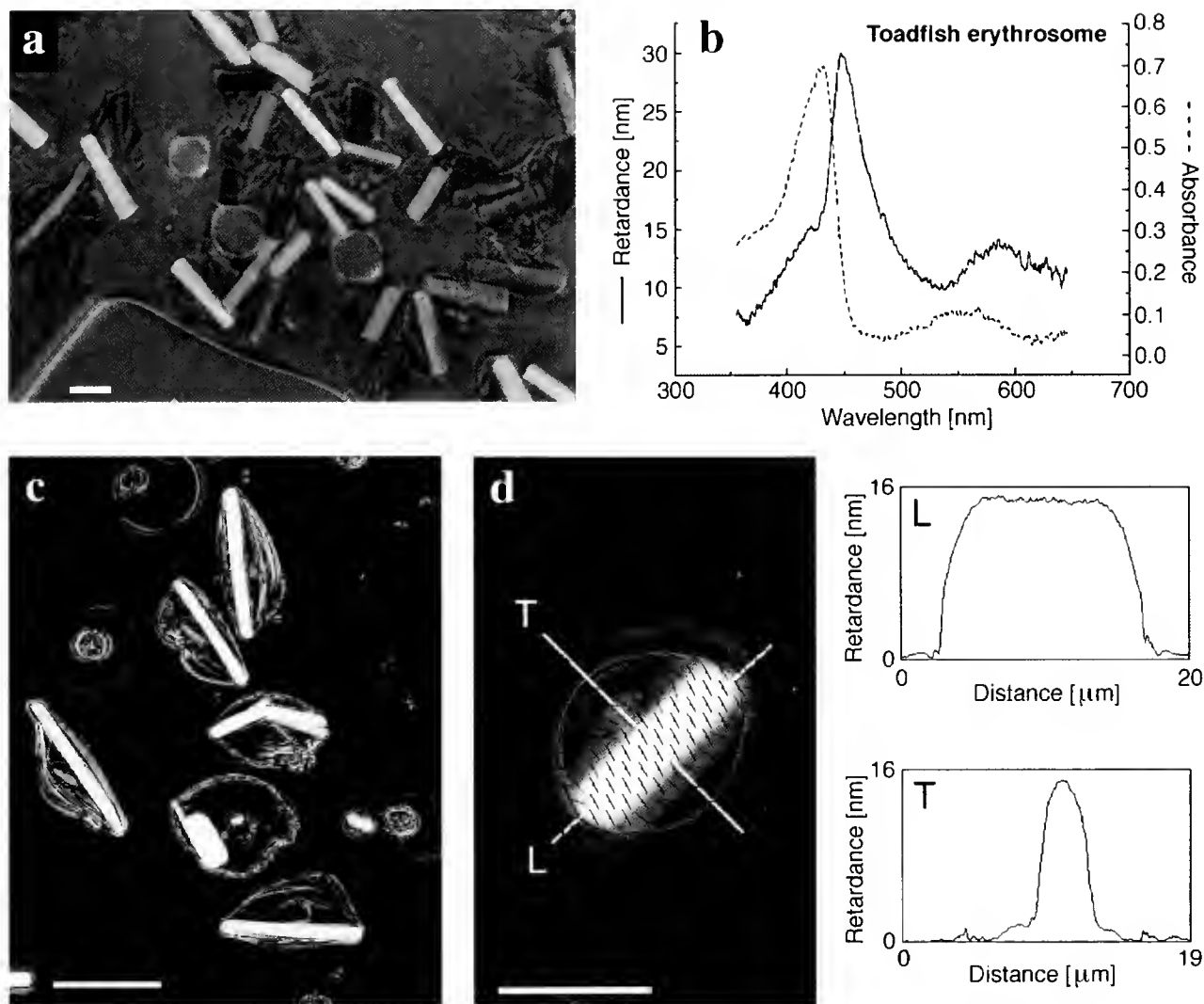


Figure 3. Toadfish erythrocytes. (a) Unstained, anoxic preparation between crossed polarizers at white light illumination (photographed in a Zeiss Axiophot 2 microscope on Kodak Ektachrome 160T film). (b) Retardance (solid) and absorbance (dashed) spectra of an isolated erythrocyte ($3.6 \times 9 \mu\text{m}$). (c) Retardance images from sickled and ghost cells measured at 546 nm with the Pol-Scope (13,14). The retardance for each picture element (pixel) was encoded in gray between 0 (black) and 16 nm (white). (d) Another Pol-Scope image of retardance with two line scans (inserts): longitudinal (L) and transverse (T) to the erythrocyte. Scale bars, $10 \mu\text{m}$.

ties, the molecular characterization of sickling hemoglobins in fishes and their attendant physiological manifestations are of paramount importance. The phenomenon is also relevant to restocking programs aimed at reestablishing dwindling groundfish populations.

Summary

Sickling in fish red blood cells is described, and the phenomenon is shown to occur in several species. By correlating the morphology of RBC with spectral absorption of Hb *in situ*, sickling is associated with the presence

of deoxyhemoglobin. The polymerization of deoxy Hb is inferred from optical anisotropies measured in single cells. The magnitude of linear dichroism and the nature of linear birefringence detected in fish "erythrocytes" show close kinship to the corresponding properties determined previously from human sickle cells and hemoglobin crystals. The range of oxygen tension for sickling has not been determined and, therefore, we do not know whether it is within physiological limits. Also unknown is whether sickling in fish is pathological or, perhaps, reflective of a physiological condition with as yet obscure significance. In either case, however, further investiga-

tions promise to provide new insights into the requisite conditions that produce intracellular hemoglobin polymerization.

Methods

Sample preparation. Experiments were conducted at room temperature (20°–23°C). Our primary buffer (marine teleost Ringer's solution) contained (in mM): NaCl 140, KCl 2.5, CaCl₂ 1.5, MgSO₄ 1, NaH₂PO₄ 0.5, NaHCO₃ 0.5, and HEPES 10, adjusted to pH 7.3 with NaOH. This was used (air-saturated) in about 10-fold excess to dilute whole blood for oxygenated preparations. Samples for microscopy were prepared in between two No. 1½ cover glasses sealed around the edge with a molten mixture of paraffin and Vaseline. The usual procedure was to place 3 µl of blood on a thoroughly cleaned (20, 21) microscope cover glass, either with or without a poly-L-lysine (P-1274, Sigma) coating (22, 23), add and mix 15–30 µl of desired buffer, cover, blot, and seal. Anoxic preparations were obtained in one of four ways: (1) By letting metabolically active blood cells deplete O₂. The effectiveness of this method is variable; for extensive sickling to occur, it may take from a few hours to 2–3 days. (2) By mounting erythrocytes and metabolically active retinal cells together in a sealed preparation, where complete deoxygenation may take only 30–120 min. This was the condition under which we first observed sickling. (3) By using N₂-purged dithionite solution (from 100 mM Na₂S₂O₄ stock) (24) and N₂-purged buffer (1:1) in preparing blood samples. (4) By the use of a calcium-free buffer (marine teleost Ringer without added calcium, containing 1 mM EGTA, at pH 6.9, and purged with N₂ for 1 h) and blood stored under light mineral oil (Paraffin, Fisher Scientific). The purpose of the oil is to keep the blood airtight, as previously reported (10). Additionally, we found that the oil prevents clotting for long periods (tested up to 8 weeks for toadfish blood); the latter method was found most effective in producing large, well-aligned erythrocytes.

Determination of absorbance and linear dichroism. We used the dichroic microspectrophotometer (25–27) with a measuring beam cross section of about 0.6 × 2 µm on cells in optical isolation. This instrument is a single-beam, phase-modulated, polarized light microscope equipped with automatic, wavelength-scanning and recording photometry. Glycerin immersion-type microscope objectives were used for both condenser (32×/0.4 Ultrafluar, Zeiss) and objective (100×/1.3 UV-F100, Nikon). Visualization was implemented with infrared light and a video camera system with tape recording.

Linear birefringence determination. The laboratory instrument was built around a modified Axiovert 10 (Zeiss) microscope utilizing quartz components and fiberoptic

links between a 150-W xenon light source (Oriel Corp.) and a spectrograph-detector combination. Its adjustable cross section microbeam (about 1.5 × 4 µm) was passed through a rotatable polarizer (Glan-Thompson type); the condenser (32×/0.4 Ultrafluar, Zeiss); the preparation affixed to a rotatable, sliding stage; the objective (100×/1.2 Ultrafluar, Zeiss); and a slidable analyzer (HN38S, Meadowlark Optics). The transmitted light was collected and focused on the entrance slit of a spectrograph (MonoSpec 18, Jarrell Ash), which in turn dispersed it over an intensified diode array detector (Model 1455B, EG&G PARC). Electronic scanning of the latter provided records of spectral responses in the range of 350–650 nm. This instrument was also capable of determining absorbance and linear dichroism from static transmission measurements taken at appropriate sample orientations and polarizer settings. For the determination of linear birefringence, the preparation was positioned between crossed polarizers with the sample's principal ("slow" and "fast") axes oriented at ±45° to the direction of polarization. The basis for signal processing was provided by the formula $I(\lambda) = I_p(\lambda)\{\sin^2[\Gamma(\lambda)/2] + 1/EF\}$, where $I(\lambda)$ is the transmitted flux at sample retardance of $\Gamma(\lambda)$ radians, $I_p(\lambda)$ the flux through the system for polarizer and analyzer axes set parallel [with $\Gamma(\lambda) = 0$], and EF is the extinction factor defined as $EF = I_p(\lambda)/I_c(\lambda)$ with $I_c(\lambda)$ being the transmitted flux for crossed polarizers (28). It followed from the foregoing that $\sin^2[\Gamma(\lambda)/2] = [I(\lambda) - I_c(\lambda)]/I_p(\lambda)$, wherefrom the retardance (in nm) at wavelength λ (nm) could be obtained as $\Gamma(\lambda) \approx \{[I(\lambda) - I_c(\lambda)]/I_p(\lambda)\}^{1/2} \lambda/\pi$ (assuming equality between the sine of small angles and their values in radians). The latter relationship was implemented on data sets from spectral scans of $I(\lambda)$, $I_c(\lambda)$ and $I_p(\lambda)$ by software operations using ORIGIN (Microcal Software). Birefringence is linked to retardance by the optical path difference in the sample between the fast and slow waves propagating through thickness d , $\Gamma(\lambda) = |n_e - n_o|d$, where n_e and n_o are the refractive indices along the two principal directions. The instrument's retardance determinations were tested on mica flakes as microscopic targets; the retardance and azimuth of the targets were previously measured (at 546 nm) in the PolScope (13, 14). Good agreement was found between results of the two instruments for the retardance range used in this work.

Acknowledgments

The authors are grateful to D. Martin-Robichaud (St. Andrew's Biological Station, Department of Fisheries and Oceans, St. Andrew, N.B., Canada) for adult haddock blood; to L. Kling (Aquaculture Research Center, University of Maine) for providing cod and haddock larval and juvenile specimens; to L. J. Buckley and J. Allen (NOAA/

NMFS/NEFSC—Narragansett Laboratory, Rhode Island) for juvenile cod specimens; to G. Klein MacPhee (Graduate School of Oceanography, University of Rhode Island) for tautog and flounder specimens; to D. Perry, J. Hughes, and S. Burgh (NOAA/NMFS—Milford, Connecticut) for adult tautog blood; and to several colleagues at the Marine Biological Laboratory for supplying blood samples from various other organisms. We also thank R. Oldenbourg and K. Katoh for discussions and assistance with the Pol-Scope measurements, R. L. Nagel for advice, and I. Novales Flamarique for help with some experiments. Supported by grants from the US Public Health Service (EY04876 to F.I.H.), from Sea Grant development funds (to I.H.v.H.) and from the National Science Foundation (OCE 931-3680 to J.R.V.K.).

Literature Cited

1. Bunn, H. F., and B. G. Forget. 1986. *Hemoglobin: Molecular, Genetic and Clinical Aspects*. Saunders, Philadelphia.
2. Eaton, W. A., and J. Hofrichter. 1987. Hemoglobin S gelation and sickle cell disease. *Blood* **70**: 1245–1266.
3. Perutz, M. F., and J. M. Mitchinson. 1950. State of haemoglobin in sickle-cell anaemia. *Nature* **166**: 677–679.
4. Yoffey, J. M. 1929. A contribution to the comparative histology and physiology of the spleen, with reference chiefly to its cellular constituents. I. In fishes. *J. Anat.* **63**: 314–344.
5. Dawson, A. B. 1932. Intracellular crystallization of hemoglobin in the erythrocytes of the northern pipefish, *Syngnathus fuscus*. *Biol. Bull.* **63**: 492–495.
6. Hansen, V. K., and K. G. Wingstrand. 1960. Further studies on the non-nucleated erythrocytes of *Maurollicus Mülleri*, and comparisons with the blood cells of related fishes. Pp. 1–15 in *Dana-Report No. 54*, A. F. Host, Copenhagen.
7. Hofrichter, J., D. G. Hendricker, and W. A. Eaton. 1973. Structure of hemoglobin S fibers: optical determination of the molecular orientation in sickled erythrocytes. *Proc. Natl. Acad. Sci. USA* **70**: 3604–3608.
8. Eaton, W. A., and J. Hofrichter. 1981. Polarized absorption and linear dichroism spectroscopy of hemoglobin. Pp. 175–261 in *Methods in Enzymology*, Vol. 76, *Hemoglobins*. E. Antonini, L. Rossi-Bernardi, and E. Chiancone, eds. Academic Press, New York.
9. Cohen, W. D. 1991. The cytoskeletal system of nucleated erythrocytes. *Int. Rev. Cytol.* **130**: 37–84.
10. Sherman, I. J. 1940. The sickling phenomenon, with special reference to the differentiation of sickle cell anemia from sickle cell trait. *Bull. Johns Hopkins Hosp.* **67**: 309–324.
11. Jenkins, F. A., and H. E. White. 1957. *Fundamentals of Optics*. McGraw-Hill, New York.
12. Born, M., and E. Wolf. 1975. *Principles of Optics*. Pergamon Press, Oxford.
13. Oldenbourg, R., and G. Mei. 1995. New polarized light microscope with precision universal compensator. *J. Microsc.* **180**: 140–147.
14. Oldenbourg, R. 1996. A new view on polarization microscopy. *Nature* **381**: 811–812.
15. Thomas, N. W. 1971. The form of haemoglobin in the erythrocytes of the cod, *Gadus callarias*. *J. Cell Sci.* **8**: 407–412.
16. Crepeau, R. H., and S. J. Edelstein. 1984. Polarity of the 14-strand fibers of sickle cell hemoglobin determined by cross-correlation methods. *Ultramicroscopy* **13**: 11–18.
17. Padlan, E. A., and W. E. Love. 1985. Refined crystal structure of deoxyhemoglobin S. I. Restrained least-squares refinement at 3.0-Å resolution. *J. Biol. Chem.* **260**: 8272–8279.
18. Nagel, R. L., et al. 1980. β -Chain contact sites in the haemoglobin S polymer. *Nature* **283**: 832–834.
19. Inoué, S. 1997. The role of microtubule assembly dynamics in mitotic force generation and functional organization of living cells. *J. Struct. Biol.* **118**: 87–93.
20. Inoué, S. 1986. *Video Microscopy*. Plenum Press, New York.
21. Fuseler, J. W. 1975. Mitosis in *Tilia americana* endosperm. *J. Cell Biol.* **64**: 159–171.
22. Mazia, D., G. Schatten, and W. Sale. 1975. Adhesion of cells to surfaces coated with polylysine. *J. Cell Biol.* **66**: 198–200.
23. Burr, A. H., and F. I. Hárosi. 1985. Naturally crystalline hemoglobin of the nematode *Mermis nigrescens*. An *in situ* microspectrophotometric study of chemical properties and dichroism. *Biophys. J.* **47**: 527–536.
24. Nagel, R. L., and H. Chang. 1981. Methods for the study of sickling and hemoglobin S gelation. Pp. 760–792 in *Methods in Enzymology*, Vol. 76, *Hemoglobins*. E. Antonini, L. Rossi-Bernardi, and E. Chiancone, eds. Academic Press, New York.
25. Hárosi, F. I., and E. F. MacNichol, Jr. 1974. Dichroic Microspectrophotometer: a computer assisted, rapid, wavelength-scanning photometer for measuring linear dichroism in single cells. *J. Opt. Soc. Am.* **64**: 903–918.
26. Hárosi, F. I. 1982. Recent results from single-cell microspectrophotometry: cone pigments in frog, fish and monkey. *Color Res. Applic.* **7** (No. 2, Part 2): 135–141.
27. Hárosi, F. I. 1987. Cynomolgus and rhesus monkey visual pigments: application of Fourier transform smoothing and statistical techniques to the determination of spectral parameters. *J. Gen. Physiol.* **89**: 717–743.
28. Inoué, S., and R. Oldenbourg. 1995. Microscopes. Pp. 17.1–17.52 in *Handbook of Optics*, Vol. II, 2nd ed. M. Bass, ed. McGraw-Hill, New York.

D- and L- β -Hydroxybutyrate Dehydrogenases and the Evolution of Ketone Body Metabolism in Gastropod Molluscs

J. A. STUART, E. L. OOI, J. McLEOD, A. E. BOURNS, AND J. S. BALLANTYNE

Department of Zoology, University of Guelph, Guelph, Ontario, Canada, N1G 2W1

*In vertebrate animals, ketone bodies, synthesized primarily from stored lipid, are important metabolic substrates (1). During starvation, ketone bodies, acetoacetate (Acac) and β -hydroxybutyrate (BHB), are oxidized by some extrahepatic tissues at high rates, and thus perform the important function of sparing limited glycogen stores (1, 2). The enzyme β -hydroxybutyrate dehydrogenase (BHBDH), which catalyzes the interconversion of the ketone bodies, is found in all mammals and most vertebrates, but is absent in most invertebrates (1, 3), including marine molluscs (4). The highest measured BHBDH activities in the animal kingdom, however, are found in the hearts of terrestrial gastropod molluscs (5, 6). We have recently demonstrated that, in tissues of the terrestrial gastropod *Cepaea nemoralis*, two unique and previously unknown isoforms of BHBDH occur (5). The isoforms differ from the well-characterized mitochondrial membrane-bound D-BHBDH found in all other animals (7) in that they are cytosolic, and one isoform is specific for the L-enantiomer of BHB. Here we identify patterns in the evolution of these enzyme isoforms in the Gastropoda. BHBDH activities, stereospecificity and subcellular compartmentalization were measured in gastropod species representing four major groups with freshwater and terrestrial representation: Neritimorpha (primitive gilled gastropods), Architaenioglossa (more advanced gilled gastropods), Basommatophora (freshwater pulmonates), and Stylommatophora (terrestrial pulmonates). Mapping*

of these data onto a phylogeny of the Gastropoda (8) indicates that cytosolic D- and L-BHBDH have arisen a single time, in an ancestral stylommatophoran. All gastropods of the order Stylommatophora possess this unique organization of ketone body metabolism, which has not been found elsewhere in the animal kingdom.

Activities and subcellular distributions of D- and L-BHBDH were measured in hepatopancreas and, in some cases, heart and kidney of gastropods by fractionating tissues into mitochondrial and cytosolic fractions, and assaying enzyme activities in each fraction (Table I). Recovery of mitochondria in the "mitochondrial fraction" was 79% or greater for hepatopancreas from all species, based on the distribution of activity of cytochrome C oxidase (CCO), an exclusively mitochondrial, membrane-bound enzyme (Table I). A large proportion of these mitochondria maintained structural integrity, as indicated by the low leakage (less than 23% in all cases) of the matrix enzyme citrate synthase (CS). The subcellular distributions of D-BHBDH approximated those of CCO and CS in the hepatopancreas of all Neritopsina, Architaenioglossa, and Basommatophora, with less than 28% of total activity occurring in the cytosolic fraction. In these species, L-BHBDH activity was either not detected or was less than 6% of D-BHBDH activity. The low L-BHBDH activities detected in *Helisoma* and *Physa* were likely the result of contaminating D-BHB, present as an impurity, in the commercial L-BHB preparation (the L-BHB preparation contained up to 0.4% D-BHB). Alternatively, it is possible that these low activities were due to trace levels of L-BHBDH, indicating a transitional state in which both mitochondrial and cytosolic isoforms are present.

The contamination of the mitochondrial fraction of the stylommatophoran *Bradybaena* hepatopancreas with cytosolic lactate dehydrogenase (LDH) was low (7%). The

Received 7 May 1997; accepted 6 April 1998.

To whom correspondence should be addressed. E-mail: jballant@uoguelph.ca

Abbreviations: Acac, acetoacetate; BHB, β -hydroxybutyrate, BHBDH, β -hydroxybutyrate dehydrogenase; CCO, cytochrome C oxidase; CS, citrate synthase; LDH, lactate dehydrogenase.

Table 1

Activities of β -hydroxybutyrate dehydrogenase (BHBBDH) and marker enzymes in mitochondrial and cytosolic compartments of gastropod hepatopancreas*

Genus	Fraction [†]	Enzyme activity ($\mu\text{mol}/\text{min}/\text{g}$ wet tissue weight) [‡]					
		CCO	CS	DL-BHBBDH	D-BHBBDH	L-BHBBDH	LDH
Stylommatophora							
<i>Archachatina</i>							
hepatopancreas	tissue	n.m.	n.m.	n.m.	0.13 \pm 0.06	0.77 \pm 0.09	n.m.
heart	tissue	n.m.	n.m.	n.m.	35.74 \pm 8.60	n.d.	n.m.
kidney	tissue	n.m.	n.m.	n.m.	0.54 \pm 0.10	0.58 \pm 0.08	n.m.
<i>Bradybaena</i>							
	mito	1.25 \pm 0.10	0.83 \pm 0.11	0.14 \pm 0.08	0.21 \pm 0.12	0.14 \pm 0.08	0.33 \pm 0.1
	cytosol	0.16 \pm 0.06	0.22 \pm 0.06	0.85 \pm 0.06	0.23 \pm 0.08	0.98 \pm 0.14	4.35 \pm 0.8
<i>Arion</i>							
	mito	1.10 \pm 0.11	1.90 \pm 0.10	n.d.	n.d.	n.d.	n.m.
	cytosol	0.03 \pm 0.01	0.21 \pm 0.04	2.44 \pm 0.09	0.07 \pm 0.04	2.60 \pm 0.11	n.m.
Basommatophora							
<i>Physa</i>							
	mito	0.87 \pm 0.08	4.71 \pm 0.50	1.02 \pm 0.28	3.07 \pm 0.73	n.d.	n.m.
	cytosol	0.17 \pm 0.08	1.37 \pm 0.34	0.53 \pm 0.18	0.99 \pm 0.19	0.22 \pm 0.04	n.m.
<i>Helisoma</i>							
	mito	4.85 \pm 0.65	3.58 \pm 0.29	0.52 \pm 0.15	1.94 \pm 0.44	n.d.	n.m.
	cytosol	0.04 \pm 0.04	0.39 \pm 0.08	0.12 \pm 0.05	0.13 \pm 0.04	0.09 \pm 0.01	n.m.
<i>Stagnicola</i>							
hepatopancreas							
	mito	2.81 \pm 0.21	1.40 \pm 0.20	2.97 \pm 0.14	7.00 \pm 0.67	n.d.	0.38 \pm 0.2
	cytosol	0.76 \pm 0.08	0.18 \pm 0.06	0.67 \pm 0.10	1.01 \pm 0.19	n.d.	1.25 \pm 0.2
heart							
	mito	9.48 \pm 0.85	5.72 \pm 3.66	n.m.	13.20 \pm 1.96	n.d.	6.00 \pm 3.3
	cytosol	5.01 \pm 2.96	1.95 \pm 0.55	n.m.	11.61 \pm 1.85	n.d.	34.57 \pm 1.7
Neritopsina							
<i>Helicina</i>							
	mito	6.54 \pm 1.24	1.49 \pm 0.11	0.45 \pm 0.09	0.53 \pm 0.32	n.d.	0.17 \pm 0.1
	cytosol	0.31 \pm 0.11	0.37 \pm 0.25	0.25 \pm 0.18	0.21 \pm 0.10	n.d.	1.72 \pm 0.8
Architaenioglossa							
<i>Campeloma</i>							
	mito	2.12 \pm 0.12	1.82 \pm 0.11	0.46 \pm 0.27	0.65 \pm 0.04	n.d.	n.d.
	cytosol	0.01 \pm 0.01	0.06 \pm 0.02	0.07 \pm 0.02	0.15 \pm 0.06	n.d.	n.d.
<i>Pomacea</i>							
hepatopancreas							
	mito	1.82 \pm 0.62	0.89 \pm 0.45	1.68 \pm 0.63	1.53 \pm 0.70	n.d.	0.44 \pm 0.2
	cytosol	0.03 \pm 0.01	0.25 \pm 0.06	0.19 \pm 0.11	0.33 \pm 0.13	n.d.	0.48 \pm 0.01
heart							
	mito	3.25 \pm 1.35	17.05 \pm 1.87	n.m.	0.55 \pm 0.18	n.d.	0.32 \pm 0.1
	cytosol	0.81 \pm 0.37	14.18 \pm 2.73	n.m.	0.09 \pm 0.05	n.d.	7.73 \pm 2.3
kidney							
	mito	2.97 \pm 1.83	4.09 \pm 0.56	n.m.	0.47 \pm 0.09	n.d.	0.44 \pm 0.3
	cytosol	0.15 \pm 0.10	0.31 \pm 0.05	n.m.	0.14 \pm 0.10	n.d.	0.92 \pm 0.4

* Most gastropods were collected from fields and ponds near the University of Guelph, in Guelph, Ontario, Canada, or purchased (*Pomacea*, *Campeloma*) from local aquarium stores. The terrestrial prosobranchs, *Helicina orbiculata*, were collected near Jacksonville, Florida. The giant African snails, *Archachatina ventricosa*, were from our laboratory population established with animals provided by the Toronto Metro Zoo. All snails and slugs were kept in terraria or aquaria at room temperature ($22^\circ \pm 2^\circ\text{C}$) and fed lettuce. We observed no effect of duration of time spent under these conditions on BHBBDH compartmentation or enantiomeric specificity. Taxonomic classification of gastropods was as in Ponder and Lindberg (10) (Table II).

A. ventricosa tissues were not fractionated. They were prepared as in Stuart and Ballantyne. (4) For enzyme measurements in all other gastropods, excised tissues were placed in approximately 20 volumes of sucrose buffer (100 mM sucrose, 20 mM N-[2-hydroxyethyl]piperazine-N'-[2-ethanesulfonic acid] (HEPES), pH 7.5). Cells were disrupted by five passes of a Potter-Elvehjem homogenizer operated at low speed (<100 rpm). This homogenate was centrifuged at $10,000\times g$ for 10 min to separate it into mitochondrial (pellet) and cytosolic (supernatant) fractions. The mitochondrial pellet was resuspended in a volume of buffer equal to the original buffer addition, thus maintaining equal the dilution of both fractions. Both fractions were sonicated with three 5-s bursts of a Vibra-Cell sonicator (Sonics & Materials Inc., Danbury, CT) set to 80% output, 50 watts. These preparations were used directly in the measurement of enzymes.

We used CCO to mark the mitochondrial membrane, CS to mark the leakage of matrix enzymes from mitochondria damaged in the fractionation process, and LDH to evaluate the contamination of the mitochondrial fraction with cytosolic enzymes. CCO, CS, and LDH were measured as in Stuart and Ballantyne. (4) The assays for D-, L- and DL-BHBBDH contained 2 mM NAD and either 200 mM D- or L-BHB or 400 mM DL-BHB, respectively (BHB omitted for control) in 50 mM imidazole, pH 8.0. All chemicals were purchased from Sigma Chemical Co. (St. Louis, MO).

[†] "tissue" = whole tissue homogenate; "mito" = mitochondrial fraction; "cytosol" = cytosolic fraction.

[‡] CCO = cytochrome C oxidase; CS = citrate synthase; LDH = lactate dehydrogenase. DL-, D- and L-BHBBDH = activity measured with racemic mixture of DL- β -hydroxybutyrate, high-purity D- β -hydroxybutyrate, and high-purity L- β -hydroxybutyrate, respectively. n.d. = not detected; n.m. = not measured. Values are means \pm standard error; $n = 5$.

low L-BHBDH activity observed in the mitochondrial fraction thus can be attributed to cytosolic contamination. Low D-BHBDH activities in *Bradybaena*, *Arion*, and *Archachatina* hepatopancreas were likely due to contaminating L-BHB in the commercial D-BHB preparation (L-BHB contamination was up to 2%). As we used a [D-BHB] of 20 mM in the assays, as much as 0.4 mM L-BHB could have been present.

Heart and kidney were fractionated in the same way as the hepatopancreas. Fractionation of heart tissue resulted in a lower recovery of mitochondria and greater leakage into the cytosol of mitochondrial matrix enzymes (Table I), perhaps because of the small size of these tissues (*Stagnicola* hearts averaged 0.8 mg; *Pomacea* hearts averaged 10 mg). Nonetheless, the distribution of BHBDH activity approximated those of CCO and CS in these tissues, indicating that BHBDH activity is localized to the mitochondria in basommatophoran heart and architaenioglossan heart and kidney. In all of these tissues, BHBDH was specific for D-BHB, with no oxidation of L-BHB observed.

The pattern of D- and L-BHBDH distribution in *Archachatina* (Table I) parallels that seen in *Cepaea*. In *C. nemoralis* tissues, no mitochondrial form of BHBDH was found (5). Instead, a cytosolic L-BHBDH was present in hepatopancreas and kidney, and a cytosolic D-BHBDH was found in heart and kidney. Similarly, D-BHB was oxidized by *Archachatina* heart and kidney homogenates and L-BHB was oxidized by kidney and hepatopancreas. This configuration of BHBDH organization appears to be characteristic of the Stylommatophora.

We investigated the evolution of cytosolic BHBDH isoforms by mapping the occurrence of the mitochondrial D-BHBDH and cytosolic L-BHBDH of gastropod hepatopancreas onto a gastropod phylogeny (8) using the MacClade (9) software program (Fig. 1). Mollusc phylogenies based upon morphological (10) and molecular (8, 11–13) data support the monophyly of Gastropoda, within which pulmonates are monophyletic. Within Pulmonata, the Stylommatophora and Basommatophora are each also monophyletic.

For this analysis, we have considered the presence of mitochondrial D-BHBDH to be the ancestral condition. Though BHBDH activity is undetectable in marine gastropods, it is found in all freshwater and terrestrial gastropods that we have studied. Thus, the enzyme appears to have first arisen in a gastropod ancestral to these groups. Our phylogenetic analysis suggests that the cytosolic L-BHBDH isoform evolved a single time in an ancestral stylommatophoran. Gastropods of this order are almost exclusively terrestrial and compose the vast majority of terrestrial snails and slugs (14). To test whether the presence of L-BHBDH correlates with terrestriality, we included the distantly related terrestrial gilled gastropod

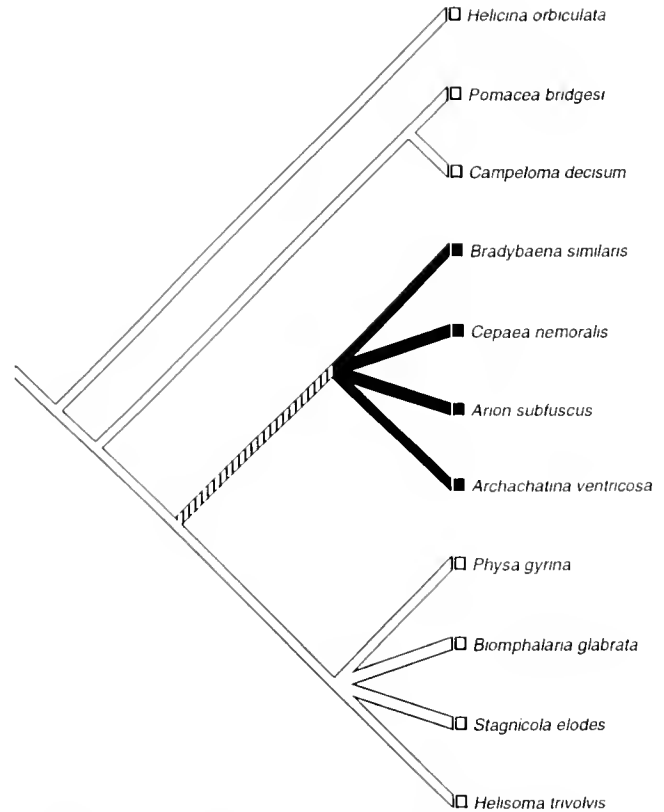


Figure 1. Phylogenetic relationships among freshwater and terrestrial gastropod taxa used in this study. Unfilled lines represent the presence of mitochondrial D- β -hydroxybutyrate dehydrogenase (and absence of L- β -hydroxybutyrate dehydrogenase). Filled lines denote the presence of cytosolic L- β -hydroxybutyrate dehydrogenase (and absence of D- β -hydroxybutyrate dehydrogenase). Hatched line = equivocal occurrence of L- β -hydroxybutyrate dehydrogenase, denoting that the enzyme arose at an undetermined point along this lineage. *Cepaea nemoralis* data are from Stuart and Ballantyne (5). *Biomphalaria glabrata* data are from Meyer et al. (15).

Helicina (Neritimorpha) in our analysis. The absence of L-BHBDH in *Helicina*, however, suggests that the occurrence of this isoform correlates exclusively with phylogenetic position.

A general upregulation of BHBDH activities appears to have occurred in tissues of pulmonate gastropods. In pulmonate hearts, exceptionally high activities of D-BHBDH (approximately two orders of magnitude greater than in *Pomacea* heart) (Table I) suggest that D-BHB is particularly important as a metabolic substrate in these tissues. High activities of all enzymes of ketone body metabolism in *Stagnicola elodes*, *C. nemoralis*, and *A. ventricosa* indicate a substantial flux through this pathway in all pulmonates. D-BHB levels in hemolymph are as high as those of glucose in the basommatophoran pulmonate *Biomphalaria glabrata* (15). These snails, and tissues isolated from them, actively oxidize ketone bodies. BHB

Table II

Higher classification (10) of gastropod species used for measurements of BHBBDH activity

Gastropoda
Orthogastropoda
Neritimorpha
Helicinoidea
<i>Helicina orbiculata</i> (terrestrial)
Apogastropoda
Architaenioglossa
Viviparoidea
<i>Campeloma decisum</i> (freshwater)
<i>Pomacea bridgesi</i> (freshwater)
Heterobranchia
Euthyneura
Pulmonata
Basommatophora
<i>Physa gyrina</i> (freshwater)
<i>Helisoma trivolvis</i> (freshwater)
<i>Stagnicola elodes</i> (freshwater)
Stylommatophora
<i>Archachatina ventricosa</i> (terrestrial)
<i>Bradybaena similaris</i> (terrestrial)
<i>Arion subfuscus</i> (terrestrial)

appears, therefore, to be an important metabolic substrate in pulmonate snails. Unlike mammals, these snails show a decrease in D-BHB levels in the hemolymph during starvation, suggesting that pulmonates may routinely use ketone bodies as energy substrates, whereas mammals confine their use to times of starvation. This difference may be related to a decreased emphasis on amino acid metabolism and a low capacity for extrahepatic oxidation of fatty acids in pulmonates. The metabolic organization of tissues in these organisms suggests that they use ketone bodies which, unlike fatty acids, are freely soluble, as a means of transporting lipid carbon from central stores to peripheral tissues for oxidation.

In stylommatophoran pulmonates, upregulation of BHBBDH activity has been followed by the elaboration of new isoforms of the enzyme. This may have occurred through an initial loss of the transmembrane amino acid sequence from the membrane-bound mitochondrial BHBBDH, to allow the enzyme to function in the cytosol. In stylommatophoran hepatopancreas and kidney, this enzyme may have been further modified to act upon L-BHB rather than D-BHB. However, this scenario for the occurrence of cytosolic BHBBDH isoforms assumes divergence from the ancestral mitochondrial D-BHBBDH. Alternatively, the cytosolic enzymes could derive from other proteins, unrelated to the mitochondrial D-BHBBDH, and have achieved functional similarity through evolutionary convergence. This convergence appears to have occurred in the evolution of D- and L-LDHs in bacteria (16). On the other hand, divergence of cytosolic L-BHBBDH from

cytosolic D-BHBBDH is suggested by the difficulty of separating these isoforms when they are electrophoresed together on a gel that separates proteins on the bases of size and charge (5). Analyses of primary structures are necessary to determine the relatedness of the three BHBBDH isoforms.

The use of both enantiomers of a single metabolic substrate in routine energy metabolism is unusual in the animal kingdom, though other examples of this phenomenon exist among molluscs. Both D- and L-alanine are found in tissues of some marine bivalves. The occurrence of D-alanine appears to be related to a role in osmoregulation (17). Both D- and L-specific isoforms of LDH also occur within individual cephalopods (18), although the physiological significance of these has not been established. The advantages of the stylommatophoran cytosolic BHBBDH isoforms are also not immediately obvious. The existence of both D- and L-BHBBDH may allow the metabolic partitioning of BHB between specific tissues. Enzyme activities indicate that ketone bodies could be synthesized in the kidney from fatty acids under normal conditions. Both D- and L-BHBBDH are present in stylommatophoran kidneys, which are thus able to produce both forms of BHB. Each of these enantiomers of BHB may be specifically targeted to a tissue, with D-BHB being oxidized by heart and L-BHB by hepatopancreas. This adaptation could be related to the apparently greater role for ketone bodies in the intermediary metabolism of pulmonate gastropods—*i.e.*, a refining of a much-used pathway.

The phylogenetic pattern of hepatopancreas BHBBDH stereospecificity and subcellular distribution in gastropods suggests that L-BHBBDH, and perhaps also D-BHBBDH, could be valuable characters for assessing phylogenetic relationships within the Gastropoda. Both enzymes can be rapidly and inexpensively assayed. The presence of hepatopancreas L-BHBBDH may be a useful defining characteristic of the Stylommatophora. As such, it will be especially interesting to identify which isoforms of BHBBDH are present in tissues of the Archiopulmonata, a group of much-debated phylogenetic position. Certainly, the presence of L-BHBBDH in stylommatophoran gastropods should be noted by population geneticists, as staining of electrophoretic gels of gastropod tissues with racemic DL-BHB mixtures will give results that are a function, in part, of the phylogenetic position and tissue of the snail examined.

Acknowledgments

We thank John Colbourne for help with phylogenetic analyses. Also, thanks to Drs. Fred G. Thompson and Harry G. Lee, and Tom Mason, Invertebrate Curator at the Toronto Metro Zoo, for their assistance with finding and identifying gastropod species.

Literature Cited

1. Newsholme, E. A., and A. R. Leech. 1983. *Biochemistry for the Medical Sciences*. John Wiley, New York.
2. Robinson, A. M., and D. H. Williamson. 1980. Physiological roles of ketone bodies as substrates and signals in mammalian tissues. *Physiol. Rev.* **60**: 143–187.
3. Beis, A., V. A. Zammit, and E. A. Newsholme. 1980. Activities of 3-hydroxybutyrate dehydrogenase, 3-oxoacid CoA-transferase and acetoacetyl-CoA thiolase in relation to ketone-body utilisation in muscles from vertebrates and invertebrates. *Eur. J. Biochem.* **104**: 209–215.
4. Stuart, J. A., and J. S. Ballantyne. 1996. Correlation of environment and phylogeny with the expression of β -hydroxybutyrate dehydrogenase in the mollusca. *Comp. Biochem. Physiol.* **114B**: 153–160.
5. Stuart, J. A., and J. S. Ballantyne. 1997. Tissue specific forms of β -hydroxybutyrate dehydrogenase oxidize the D- or L-antiomers of β -hydroxybutyrate in the terrestrial gastropod *Cepaea nemoralis*. *J. Exp. Zool.* **278**: 115–118.
6. Stuart, J. A., and J. S. Ballantyne. 1997. Importance of ketone bodies in the intermediary metabolism of the terrestrial snail *Archachatina ventricosa*: evidence from enzyme activities. *Comp. Biochem. Physiol.* **117B**: 197–201.
7. Lehninger, A. L., H. C. Sudduth, and J. B. Wise. 1960. D-beta-hydroxybutyric dehydrogenase of mitochondria. *J. Biol. Chem.* **235**: 2450–2455.
8. Harasewych, M. G., S. L. Adamkewicz, J. A. Blake, D. Saudek, T. Spriggs, and C. J. Bult. 1997. Phylogeny and relationships of pleurotomariid gastropods (Mollusca: Gastropoda): an assessment based on partial 18S rDNA and cytochrome *c* oxidase I sequences. *Mol. Mar. Biol. Biotech.* **6**: 1–20.
9. Maddison, W. P., and D. R. Maddison. 1992. *MacClade: Analysis of Phylogeny and Character Evolution Version 3.0*. Sinauer, Sunderland, MA.
10. Ponder, W. F., and D. R. Lindberg. 1997. Towards a phylogeny of gastropod molluscs—an analysis using morphological characters. *Zool. J. Linn. Soc.* **6**: 83–265.
11. Winnepeninckx, B., T. Backeljau, and R. De Wachter. 1994. Small ribosomal subunit RNA and the phylogeny of Mollusca. *The Nautilus Supplement 2*: 98–110.
12. Tillier, S., M. Masselot, J. Guerdoux, and A. Tillier. 1994. Monophyly of major gastropod taxa tested from partial 28S rRNA sequences, with emphasis on euthyneura and hot-vent limpets Peltospiroidea. *The Nautilus Supplement 2*: 122–140.
13. Rosenberg, G., G. S. Kuncio, G. M. Davis, and M. G. Harasewych. 1994. Preliminary ribosomal RNA phylogeny of gastropod and unionoidean bivalve mollusks. *The Nautilus Supplement 2*: 111–121.
14. Solem, A. 1985. Origin and diversification of pulmonate land snails. Pp. 269–293 in *The Mollusca, Vol. 10—Evolution*, E. R. Trueman and M. R. Clarke, eds. Academic Press, Toronto.
15. Meyer, R., W. Becker, and M. Klimkewitz. 1986. Investigations on the ketone body metabolism in *Biomphalaria glabrata*: influence of starvation and of infection with *Schistosoma mansoni*. *J. Comp. Physiol. B.* **156**: 563–571.
16. Kaplan, N. O., and M. M. Ciotti. 1961. Evolution and differentiation of dehydrogenases. *Ann. N.Y. Acad. Sci.* **94**: 701–722.
17. Matsushima, O., and Y. S. Hayashi. 1992. Metabolism of D- and L-alanine and regulation of intracellular free amino acid levels during salinity stress in a brackish-water bivalve *Corbicula japonica*. *Comp. Biochem. Physiol.* **102A**: 465–471.
18. Mulcahy, P., A. Cullina, and P. O'Carra. 1997. Both D- and L-specific lactate dehydrogenases co-exist in individual cephalopods. *Comp. Biochem. Physiol.* **116A**: 143–148.

Physiological Progenesis in Cephalopod Molluscs

PAUL G. RODHOUSE

British Antarctic Survey, Natural Environment Research Council, High Cross, Madingley Road, Cambridge CB5 9BG, UK

The coleoid cephalopods (cuttlefish, squid and octopus) arose from their shelled ancestors during the late Devonian; they diversified in the Jurassic but did not radiate substantially until the Tertiary. Since then they have coevolved with the fish (1). Squid are less efficient energetically than fish (2) but have survived alongside them by evolving highly opportunistic reproductive and feeding strategies (3, 4) as well as rapid jetting and inking for escape and defense. Little is known about the life history strategies of the fossil forms, but the only surviving shelled cephalopods, the nautilus, have relatively long life spans and are iteroparous; that is, in common with most members of other molluscan classes, they breed more than once during their lives. In contrast, all other living cephalopods are generally short lived (usually 1 year) and have monocyclic reproduction and a semelparous life history. The short-lived semelparous coleoids are typified by the mid-latitude ommastrephid squid which provide the basic model considered here. This family is relatively primitive and biologically well known. Its members are essentially monocyclic, but some species may spawn their eggs in batches (5, 6), although there is no evidence of this in laboratory spawnings (7). Most loliginid squid, at least in temperate seas, have a life cycle similar to that of the ommastrephids, despite having different spawning habits. A comparison of the lifetime energetics and growth pattern of benthic, iteroparous molluscs with those of the pelagic, semelparous ommastrephids shows that, although some squid may attain a length of 1 m or more, the allocation of their energy resource among growth components is essentially characteristic of the early life, especially the first year, of iteroparous forms. The lifetime energy budget of these squid thus seems to have evolved by physiological progenesis, a process in which

maturation is accelerated while other aspects of the physiology are more typical of the juvenile.

The life cycle of most benthic marine molluscs (bivalves and gastropods) is characterized by a relatively short egg and larval stage, a long adult life span (usually several years), and iteroparity (8). Feeding rates of herbivorous and carnivorous species decline relative to body mass over the lifetime, and the mass exponent for feeding rate is invariably less than for metabolic rate (9). These allometric relationships between consumption rate, metabolic rate, and body mass mean that, as body size increases, the amount of energy produced by food consumption decreases relative to the amount of energy lost as heat. The relative scope for growth therefore decreases with size, and this is the physiological basis for the steadily decreasing gross and net growth efficiency with age (10). Annual production of somatic tissue reaches a maximum during the first half of the life span and declines thereafter, whereas gamete production increases asymptotically. Somatic production exceeds gamete production during early life, but is later exceeded by gamete production, which eventually dominates tissue growth. Lifetime energy budgets have been estimated for some bivalves and gastropods (11, 12), and the general pattern of energy allocation is illustrated in Figure 1a. Lifetime energetics is dominated by respiratory losses in the form of heat. A substantial proportion of total production is allocated to shell organics, and this, together with the energy cost of mineralization (13), reduces the energy available for tissue growth in these benthic forms.

The physiological energetics of *Nautilus*, which probably resembles that of the ancestors of the living coleoids in many respects, differs substantially from that of the coleoids with respect to reproduction (14). *Nautilus* has a life span of more than 4 years, and its reproduction is iteroparous, so in many respects its lifetime energy budget resembles that of the iteroparous benthic molluscs.

Relative to most iteroparous molluscs, including *Nautilus*, the life cycle of the semelparous cephalopods is char-

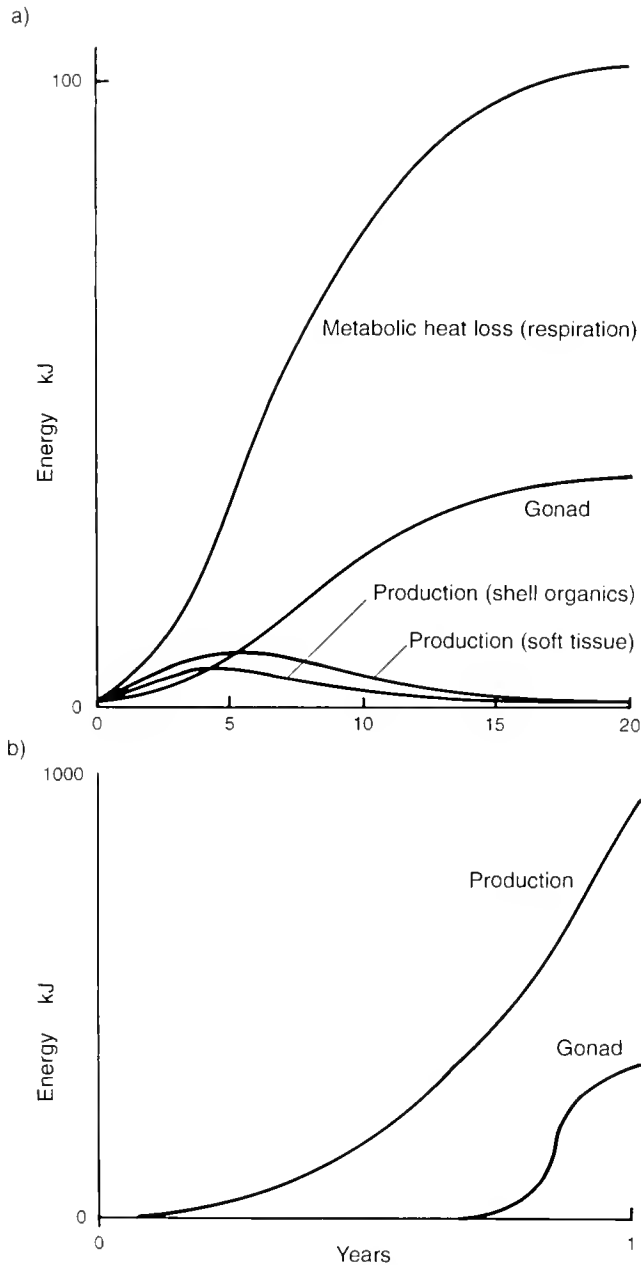


Figure 1. Energy, in kilojoules (kJ), allocated to the different components of growth and metabolism: (a) over the 20-year lifetime of a long-lived, iteroparous benthic bivalve (*Ostrea edulis*); (b) over the one-year lifetime of a short-lived semelparous cephalopod (*Illex argentinus*).

acterized by long egg, paralarval, and juvenile phases, and by a short adult life. Feeding and metabolic rates are higher than in other molluscs (15), and empirically determined mass exponents for feeding and metabolic rate are higher than in benthic molluscs—0.79 [feeding] and 0.96 [metabolism] for the squid *Illex illecebrosus* (16) compared with mean values of 0.58 ± 0.12 [feeding] and 0.70 ± 0.13 [metabolism] for 36 and 50 benthic species,

respectively (9). The mass exponent for metabolic rate has long been thought to be close to 1.0 in small organisms (< 50 mg) and approaching 0.75 in larger ones (17). This exponent has been suggested to derive from the weighted sum of body surface area and volume (18). Squid appear to fall between the predicted values for large and small organisms. The exponent for feeding rate is lower than for metabolic rate, but the difference between these exponents in the *I. illecebrosus* example is less than in the longer-lived iteroparous molluscs (9), implying relatively higher scope for growth at larger body size in the squid. This is reflected in relatively high growth efficiencies (15). Somatic tissues grow for most of the squid life span, but gonad growth is rapid once sexual maturation is initiated. *Illex argentinus*, with a life span of about a year, starts to mature in about 7 or 8 months and reaches full maturity by 12 months (19). Lifetime production of soma and gonad in *I. argentinus* has been estimated from data on growth and allometry combined with biochemical composition (19, 20). The pattern of energy allocation among soma and gonad in the squid differs fundamentally from the pattern in the long-lived iteroparous molluscs (Fig. 1b). Production of somatic tissue continues until full sexual maturity; and even in the latter part of the life span, when the squid is reaching maturity, somatic growth remains in excess of gonad production. This pattern of energy allocation among soma and gonad closely resembles that of the first year of the longer-lived iteroparous molluscs. Suitable data on lifetime metabolic heat losses in cephalopods are not available for comparison with the benthic forms.

The declining relative scope for growth and increasing allocation of energy to reproduction is the mechanism underlying the form of the asymptotic growth curve followed by these longer-lived iteroparous molluscs. The von Bertalanffy growth function is commonly used in ecology and fisheries science to model asymptotic growth of animals (21) and has provided an adequate fit to most data for annual growth increments in iteroparous molluscs. The equation is generally given as:

$$l_t = L_\infty [1 - e^{-K(t - t_0)}]$$

in which l_t is length at time t , L_∞ is length at infinite age, K is the rate constant at which L_∞ is approached, and t_0 is effectively a scaling factor that displaces the curve along the age axis to fit the data. Seasonality of growth has also been modeled by substituting day-degrees for time in the von Bertalanffy model (22, 23):

$$l_D = L_\infty [1 - e^{-K_D(D - D_0)}]$$

in which l_D is length at D day-degrees, K_D is the rate constant determined as K/D_y (D_y is the annual sum of day-degrees) and $D_0 = t_0 \cdot D_y$. This models the effects of

seasonal temperature variation only and not, for example, changes in food available to suspension feeders grazing on seasonal phytoplankton blooms. The von Bertalanffy model rarely, if ever, fits growth during the juvenile phase (usually the first year of life), hence the necessity for the mathematical convenience of the term t_0 , as the fitted model rarely passes through the origin. The poor fit of the von Bertalanffy function to growth of the juvenile phase is probably due to the combined effects of seasonality of growth in the first year and different patterns of energy allocation during the pre-reproductive phase of early development.

The high growth efficiency of squid, together with their relatively low investment in gonadal growth, results in high growth rates throughout the life span (24). This efficiency is accentuated by their semelparity, because the reduction in growth rate, due in iteroparous forms to the energetic costs of repeat spawning, is not experienced. The age of ommastrephids taken from the field has been estimated from daily growth increments in the statolith. These data show that growth in mantle length of adults up to sexual maturity can generally be fitted by a simple linear model (19, 25). But there are no data covering the whole life span of ommastrephids, including the brief post-spawning phase, so the form of the growth curve towards the end of life is not known. The allometric coefficient in ommastrephids is generally close to 3.0 (24), so the linear phase of growth in mantle length is accompanied by a power curve reflecting growth in mass. Where detailed measurements have been made on squid, growth in mass is best fitted by an exponential growth function for early life and a power function for the latter phase (24, 26). Modeling studies also suggest that lifetime growth is influenced by temperature, especially in the post-hatching period (27, 28). This is reflected in field data, which indicate different growth patterns in squid hatched in different seasons and, by inference, at different temperatures (19, 29, 30), as well as in laboratory studies (27) in which squid were exposed to different water temperatures after hatching.

Squid appear to exhibit physiological progenesis in the sense that they reach full maturity over a short life span during which their lifetime energy budget resembles that typical of the early life of iteroparous molluscs, a time when growth rate and growth efficiency are relatively high, when production is dominated by somatic growth, and when reproductive investment (proportion of body mass released as gametes) is relatively low. In squid, low reproductive investment is compensated for by traits that minimize juvenile mortality: relatively large hatchlings, direct development, protective egg coatings, and the rapid, jet-propelled escape response possessed even by hatchling squid (3). Although the evolutionary processes of progenesis and neoteny have usually been attributed

to morphological phenomena (paedomorphosis) (31), applying the concept of progenesis to physiological energetics provides a useful insight into the evolution of patterns of cephalopod growth and reproduction.

For much of their life span, squid occupy the juvenile phase of the generalized molluscan life cycle that is not readily fitted by the von Bertalanffy growth function. Because this function rarely fits the growth data for squid or other cephalopods (32), they have been compared with larvae of other taxa that do not grow asymptotically (33). If, as has been argued, the von Bertalanffy function is fundamentally applicable to squid (34), they probably die before, or very soon after, approaching the asymptotic phase. The principal factors that underlie the complicated and highly variable growth trajectories of these molluscs are changes in the allocation of energy resources between soma and gonad; seasonality of growth rate, modulated by food availability and temperature; and the confounding effects of hatching season on lifetime growth rate. The underlying lifetime pattern of energy allocation and the consequent growth characteristics of the cephalopods suggest that these traits have evolved through physiological progenesis, in which sexual maturation has been accelerated, while the energy budget retains features found in the juvenile phase of other classes of molluscs.

Acknowledgments

I thank Daniel Pauly for encouraging me to get these ideas down on paper and the anonymous reviewers who made numerous helpful criticisms.

Literature Cited

1. Packard, A. 1972. Cephalopods and fish: the limits of convergence. *Biol. Rev.* **47**: 241–307.
2. O'Dor, R. K., and D. M. Webber. 1986. The constraints on cephalopods: why squid aren't fish. *Can. J. Zool.* **64**: 1591–1627.
3. Calow, P. 1987. Fact and theory—an overview. Pp. 351–365 in *Cephalopod Life Cycles*, Vol. 2. *Comparative Reviews*. P. R. Boyle, ed. Academic Press, London.
4. Rodhouse, P. G., and Ch. M. Nigmatullin. 1996. Role as consumers. In *The Role of Cephalopods in the World's Oceans*. M. R. Clarke, ed. *Phil. Trans. R. Soc. Lond.* **351**: 1003–1022.
5. Harman, R. F., R. E. Young, S. B. Reid, K. M. Mangold, T. Suzuki, and R. F. Hixon. 1989. Evidence for multiple spawning in the tropical oceanic squid *Sthenoteuthis oualaniensis* (Teuthoidea: Ommastrephidae). *Mar. Biol.* **101**: 513–519.
6. Laptikhovskiy, V., and Ch. M. Nigmatullin. 1992. Egg size, fecundity and spawning in females of the genus *Illex* (Cephalopoda: Ommastrephidae). *ICES J. Mar. Sci.* **50**: 393–403.
7. O'Dor, R. K., N. Balch, and T. Amaratunga. 1982. Laboratory observations of midwater spawning by *Illex illecebrosus*. *NAFO SCR Doc. No. 82/VI/5*. 8 pp.
8. Yonge, C. M., and T. E. Thompson. 1976. *Living Marine Molluscs*. Collins, London. 288 pp.
9. Bayne, B. L., and R. C. Newell. 1983. Pp. 407–515 in *The Mollusca* Vol. 4. *Physiology* Part 1. A. S. M. Saleuddin and K. M. Wilbur, eds. Academic Press, New York.

10. Bayne, B. L., J. Widdows, and R. J. Thompson. 1976. Physiological integrations. Pp. 261–191 in *Marine Mussels*, B. L. Bayne, ed. Cambridge University Press, Cambridge.
11. Rodhouse, P. G. 1978. Energy transformations by the oyster *Ostrea edulis* L. in a temperate estuary. *J. Exp. Mar. Biol. Ecol.* **34**: 1–22.
12. Branch, G. M. 1982. The biology of limpets: physical factors, energy flow and ecological interactions. *Oceanogr. Mar. Biol. Annu. Rev.* **19**: 235–380.
13. Palmer, A. R. 1981. Do carbonate skeletons limit the rate of body growth. *Nature* **292**: 150–152.
14. Ward, P. D. 1987. *The Natural History of Nautilus*. Allen and Unwin, London. 267 pp.
15. Wells, M. J., and A. Clarke. 1996. Energetics: the cost of living and reproducing for an individual cephalopod. *Phil. Trans. R. Soc. Lond. B* **351**: 1083–1104.
16. O'Dor, R. K., and M. J. Wells. 1987. Energy and nutrient flow. Pp. 109–133 in *Cephalopod Life Cycles*, Vol. 2. *Comparative Reviews*. P. R. Boyle, ed. Academic Press, London.
17. Zenthen, E. 1953. Oxygen uptake as related to body size in organisms. *Quart. Rev. Biol.* **28**: 1–12.
18. Kooijman, S. A. L. M. 1993. *Dynamic energy budgets in biological systems*. Cambridge University Press, Cambridge. 350 pp.
19. Rodhouse, P. G., and E. M. C. Hatfield. 1990. Dynamics of growth and maturation in the cephalopod *Illex argentinus* (Teuthoidea: Ommastrephidae). *Phil. Trans. R. Soc. Lond. B* **329**: 299–241.
20. Clarke, A., P. G. Rodhouse, and D. J. Gore. 1994. Biochemical composition in relation to the energetics of growth and maturation in the ommastrephid squid *Illex argentinus*. *Phil. Trans. R. Soc. Lond. B* **344**: 201–212.
21. Pitcher, T. J., and P. J. B. Hart. 1982. *Fisheries Ecology*. Croom Helm, New York. 414 pp.
22. Ursin, E. 1963. On the incorporation of temperature in the von Bertalanffy growth equation. *Medd. Danm. Fisk.-og. Havunders* **4**: 1–16.
23. Bayne, B. L., and C. M. Worrall. 1980. Growth and production of mussels *Mytilus edulis* from two populations. *Mar. Ecol. Prog. Ser.* **3**: 317–328.
24. Forsythe, J. W., and W. F. Van Heukelem. 1987. Growth. Pp. 135–156 in *Cephalopod Life Cycles*, Vol. 2. *Comparative Reviews*. P. R. Boyle, ed. Academic Press, London.
25. Rosenberg, A. A., K. F. Wihorg, and I. M. Beck. 1980. Growth of *Todarodes sagittatus* (Lamarck) (Cephalopoda: Ommastrephidae) from the Northeast Atlantic, based on counts of statolith growth rings. *Sarsia* **66**: 53–57.
26. Forsythe, J. W., and R. T. Hanlon. 1989. Growth of the Eastern Atlantic squid, *Loligo forbesi* Steenstrup (Mollusca: Cephalopoda). *Aquacult. Fish. Manage.* **20**: 1–14.
27. Forsythe, J. W. 1993. A working hypothesis on how seasonal temperature change may impact the growth of young cephalopods. Pp. 133–143 in *Recent Advances in Cephalopod Fisheries Biology*, T. Okutani, R. K. O'Dor, and T. Kubodera, eds. Tokai University Press, Tokyo.
28. Grist, E. P. M., and S. des Clers. 1998. How seasonal temperature variations may influence the structure of annual squid populations. *IMA J. Math. Appl. Med. Biol.* **15**: 1–23.
29. Arkhipkin, A., and A. Mikheev. 1992. Age and growth of the squid *Sthenoteuthis pteropus* (Oegopsida: Ommastrephidae) from the Central East Atlantic. *J. Exp. Mar. Biol. Ecol.* **163**: 261–276.
30. Arkhipkin, A., and V. Laptikhovskiy. 1994. Seasonal and interannual variability in growth and maturation of winter-spawning *Illex argentinus* (Cephalopoda, Ommastrephidae) in the Southwest Atlantic. *Aquat. Living Resour.* **7**: 221–232.
31. Gould, S. J. 1977. *Ontogeny and Phylogeny*. Harvard University Press, Cambridge. 501 pp.
32. Jackson, G. D., and J. H. Choat. 1992. Growth in tropical cephalopods: an analysis based on statolith microstructure. *Can. J. Fish. Aquat. Sci.* **49**: 218–228.
33. Alford, R. A., and G. D. Jackson. 1993. Do cephalopods and larvae of other taxa grow asymptotically? *Am. Nat.* **141**: 717–728.
34. Pauly, D. In press. Why squids—though not fish—may be better understood by pretending they are. *S. Afr. J. Mar. Sci.*

Metamorphic-Signal Transduction in *Hydroides elegans* (Polychaeta: Serpulidae) Is Not Mediated by a G Protein

ERIC R. HOLM, BRIAN T. NEDVED, EUGENIO CARPIZO-ITUARTE,
AND MICHAEL G. HADFIELD*

Kewalo Marine Laboratory, University of Hawaii, 41 Ahui St., Honolulu, Hawaii 96813

Abstract. Evidence from larvae of hydrozoans, gastropods, and barnacles suggests that G protein-coupled receptors mediate induction of settlement and metamorphosis in response to environmental cues. We examined responses of larvae of the serpulid polychaete *Hydroides elegans* to neuropharmacological agents to determine if G protein-coupled receptors or their associated signal-transduction pathways regulated induction of metamorphosis by bacterial cues. Larvae of *Hydroides elegans* metamorphose rapidly and in high proportions when exposed to bacterial biofilms. Neither the G-protein activator Gpp[NH]p nor the inhibitor GDP- β -S affected metamorphosis. Although the nonspecific phosphodiesterase inhibitors IBMX, theophylline, and papaverine induced larvae to metamorphose, RO-20-1724 (an inhibitor selective for cAMP-specific phosphodiesterase IV) and the cyclic nucleotide analogs db-cAMP and db-cGMP had no effect on metamorphosis. The adenylyl cyclase activator forskolin inhibited responses of larvae to inductive bacterial biofilms. These apparently conflicting results may be due to side effects of IBMX, theophylline, papaverine, and forskolin on ion transport. The phorbol ester TPA, an activator of protein kinase C, also had no effect on larval metamorphosis. These experiments indicate that G protein-coupled receptors and signal transduction by the

adenylyl cyclase/cyclic AMP or phosphatidylinositol/diacylglycerol/protein kinase C pathways are not components of the morphogenetic pathway that is directly responsible for processing metamorphic cues in *H. elegans*.

Introduction

Several decades of research have demonstrated the importance of biochemical and physical cues in determining, on small spatial scales, where larvae of marine invertebrates settle and metamorphose (see Scheltema, 1974; Crisp, 1984; Svane and Young, 1989, for reviews). Identification of the exact nature and ecological role of exogenous cues remains an active field of study. Over the last 20 years, however, increased attention has focused on the physiological mechanisms underlying detection of these cues and the initiation of metamorphosis. The approach generally taken in this work consists of exposing larvae to solutions of potentially neuroactive compounds, in the presence or absence of a cue, and noting the responses. Although such experiments may be difficult to interpret (Pawlik, 1990; Leitz, 1997), a common theme is developing from the results.

In the marine invertebrate larvae that have been most extensively studied, it appears that G protein-coupled receptors and their associated signal-transduction pathways play an important role in regulating metamorphosis. In the hydrozoans *Hydractinia echinata* (Müller, 1985; Leitz and Müller, 1987; Leitz and Klingmann, 1990; Schneider and Leitz, 1994) and *Mitrocomella polydiademata* (Freeman and Ridgway, 1990), the phosphatidylinositol/diacylglycerol/protein kinase C (PI/DAG/PKC) pathway transduces the metamorphic signal provided by bacterial cues. In addition, Leitz and Wirth (1991) found that *H. echinata*

Received 23 December 1997; accepted 27 May 1998.

* To whom correspondence should be addressed. E-mail: hadfield@hawaii.edu

Abbreviations: AC/cAMP, adenylyl cyclase/cyclic AMP; db-cAMP, dibutyryl-cyclic AMP; db-cGMP, dibutyryl-cyclic GMP; DMSO, dimethyl sulfoxide; FSW, filtered seawater; GDP- β -S, guanosine 5'-O-(2-thiodiphosphate); Gpp[NH]p, 5'-guanylylimidodiphosphate; IBMX, 3-isobutyl-1-methylxanthine; PI/DAG/PKC, phosphatidylinositol/diacylglycerol/protein kinase C; TPA, phorbol-12-myristate-13-acetate.

metamorphosed in response to the G-protein activators ortho- and metavanadate, suggesting that G protein-coupled receptors are involved in the process. Schneider and Leitz (1994) proposed that the bacterial inducer of metamorphosis acted by first binding to a G protein-coupled receptor. In the barnacle *Balanus amphitrite*, two signal-transduction systems, the adenylate cyclase/cyclic AMP (AC/cAMP) pathway (Rittschof *et al.*, 1986; Clare *et al.*, 1995) and the PI/DAG/PKC pathway (Yamamoto *et al.*, 1995; Holm *et al.*, unpubl. data), appear to regulate metamorphosis. Clare (1996) proposed a model linking the two pathways; in this model the exogenous metamorphic cue was bound to a G protein-coupled receptor. Finally, in the abalone *Haliotis rufescens*, the AC/cAMP pathway transduces the metamorphic signal provided by compounds found on the surface of crustose coralline algae, while the PI/DAG/PKC pathway facilitates the response to these compounds (Morse *et al.*, 1980; Trapido-Rosenthal and Morse, 1985, 1986; Baxter and Morse, 1987; Morse, 1990, 1991). The receptor of the metamorphic cue did not appear to be associated with a G protein, but evidence suggested that the separate, facilitating pathway was activated by binding of amino acids to a G protein-coupled receptor (Baxter and Morse, 1987, 1992; Wodicka and Morse, 1991).

G protein-coupled receptors and their associated signal-transduction pathways present a compelling general model for detection of a variety of stimuli in an exceptionally broad range of organisms (Carr, 1992). It is not clear, however, whether the regulation of metamorphosis by G proteins is a general feature of marine invertebrate larvae (Hadfield, 1998). For larvae of *Haliotis rufescens*, at least, a G protein-coupled receptor does not bind the metamorphic signal (Baxter and Morse, 1987). There are several other classes of receptors (Féger *et al.*, 1994) that could conceivably function in marine larvae to detect exogenous cues for settlement and metamorphosis. These include lectins, which have been implicated in the metamorphosis of larvae of the spirorbid polychaete *Janna brasiliensis* (Kirchman *et al.*, 1982; Maki and Mitchell, 1985), and ligand-gated ion channels.

To test the hypothesis that G protein-coupled receptors or the AC/cAMP and PI/DAG/PKC signal-transduction pathways regulate metamorphosis in the serpulid polychaete *Hydroïdes elegans*, we examined the response of larvae of this species to various neuropharmacological agents. *Hydroïdes elegans* (Haswell, 1883) is a common member of the shallow subtidal fouling community throughout tropical and warm temperate seas (Hadfield *et al.*, 1994). In the laboratory, competent larvae settle and metamorphose after as little as 15 min of exposure to bacterial biofilms (Hadfield *et al.*, 1994; Carpizo-Iltuarte and Hadfield, 1998). Experiments with larvae of other polychaetes, including *Capitella capitata* Sp. 1 (Biggers

and Laufer, 1992), *Phragmatopoma lapidosa californica* (Jensen and Morse, 1990; Pawlik, 1990), and *Hydroïdes elegans* from Hong Kong (Bryan *et al.*, 1997), indicate that the AC/cAMP pathway may be involved in metamorphosis. Our results, however, suggest that G protein-coupled receptors and their associated signal-transduction pathways *do not* play a direct role in regulating metamorphosis in *Hydroïdes elegans*.

Materials and Methods

Obtaining and culturing larvae

We collected sexually mature *Hydroïdes elegans* from the surface of plastic screens previously placed in the water in Pearl Harbor, Hawaii, to serve as a substratum for settlement of larvae and subsequent growth of recruits. Clumps of worms were removed from the screens and placed into dishes of seawater filtered through a 0.22- μm filter (hereafter, FSW). When we broke open their tubes, ripe male and female worms released gametes, and fertilization took place within minutes (see also Wisely, 1958; Hadfield *et al.*, 1994).

After several hours we separated developing larvae from adult worms and debris by sieving, and transferred the larvae to beakers of FSW so as to realize a density in culture of 5–10 larvae ml^{-1} . Larvae were reared at room temperature ($25^\circ \pm 2^\circ \text{C}$) and fed daily with *Isochrysis galbana* (Tahitian strain) at a density of about 6×10^4 cells ml^{-1} . Every 2 days, larvae were transferred to fresh FSW. Under these conditions we obtained metamorphically competent larvae 4–6 days after fertilization.

Assays for metamorphosis

We tested for metamorphosis of larvae in response to potentially neuroactive compounds by conducting assays in still water. In these assays larvae were introduced to polystyrene petri dishes (Falcon 1006, 50×9 mm; Fisher, 60×15 mm) containing 4–5 ml of a solution of the agent of interest. Larvae were added in a volume of FSW between 15 and 25 μl , yielding from 2 to 113 larvae per dish. Four or five replicate assays for each experimental treatment were conducted at room temperature and, when compounds were light labile, in darkness.

For each experiment, appropriate control treatments were also tested. Controls for metamorphic competence ('Biofilm') consisted of petri dishes containing FSW and a biofilmed surface, either a 1.6- cm^2 chip of polystyrene or a piece of plastic screen. We obtained biofilms by soaking these substrata in flowing seawater for at least 5 d. Petri dishes containing only FSW served as negative controls. For experiments in which we examined inhibitory effects, larvae were added to dishes containing both the test solution and a biofilmed surface. Test solutions

were made by diluting stock solutions of the compound of interest in FSW. Stock solutions were prepared by dissolving the compound in either FSW or dimethyl sulfoxide (DMSO). When the stock solution included DMSO, we ran controls for the potential effects of DMSO on metamorphosis.

We scored metamorphosis of larvae after 24 h of continuous exposure to the test compounds. Larvae were considered to have metamorphosed if they had permanently attached to the surface of the petri dish (or the biofilmed substratum); constructed either a primary (proteinaceous) tube or both a primary and a calcareous, secondary tube; and exhibited differentiation of the head region into the branchial crown. Some compounds evoked abnormal metamorphosis in a small proportion of larvae. Such larvae did not construct primary or secondary tubes but did show evidence of metamorphosis, including loss of the prototroch and development of the branchial crown. Except for assays with the phosphodiesterase inhibitor IBMX (see Results section below), we counted these larvae as metamorphosed.

Neuropharmacological agents

We tested 10 compounds for their effects on metamorphosis. We chose these compounds to differentiate the roles that G proteins, the AC/cAMP signal-transduction pathway, or the PI/DAG/PKC signal-transduction pathway might play in metamorphosis (Table 1). Neuropharmacological agents tested included 5'-guanylylimidodiphosphate (Gpp[NH]p), guanosine 5'-O-(2-thiodiphosphate) (GDP- β -S), 3-isobutyl-1-methylxanthine (IBMX), theophylline, papaverine, RO-20-1724, dibutyryl-cAMP (db-cAMP), dibutyryl-cGMP (db-cGMP), forskolin, and phorbol-12-myristate-13-acetate (TPA). Gpp[NH]p is a nonhydrolyzable GTP analog that activates G proteins. Provocation of a response by Gpp[NH]p or other GTP analogs has been proposed as a criterion for involvement of G proteins in a given process (Gilman, 1987). GDP- β -S is a nonhydrolyzable GDP analog that inhibits activation of G proteins. IBMX, theophylline, and papaverine inhibit phosphodiesterases that hydrolyze cAMP and cGMP. Whereas these compounds inhibit phosphodiesterases in general, RO-20-1724 is a selective inhibitor of the mammalian cAMP-specific phosphodiesterase IV (Thompson, 1993). Dibutyryl-cAMP and -cGMP are analogs of cAMP and cGMP, respectively, that may penetrate cell membranes more freely than cAMP and cGMP (Posternak and Weimann, 1974) and may also be resistant to hydrolysis by phosphodiesterases (Cheung and Lin, 1974; Posternak and Weimann, 1974). Forskolin activates adenylyl cyclase (Seamon *et al.*, 1981), the enzyme that catalyzes generation of cAMP. TPA activates protein kinase C. Müller (1985) and Freeman and Ridgway (1990)

found TPA, among the phorbol esters, to be the most effective inducer of metamorphosis in the hydrozoans *Hydractinia echinata* and *Mitrocomella polydiademata*, respectively. Table 1 provides a brief description of the activity of each of the compounds tested and their predicted effect on metamorphosis of larvae of *Hydroides elegans*.

Except for Gpp[NH]p and RO-20-1724, the concentration ranges we tested for these compounds spanned effective concentrations previously determined to induce metamorphosis in larvae of other marine invertebrates. We could find no comparable data for Gpp[NH]p and RO-20-1724. RO-20-1724 was obtained from Calbiochem, San Diego, California; all other compounds were purchased from Sigma, St. Louis, Missouri.

Statistical analysis

The results of the experiments were analyzed using either two-sample *t*-tests or Wilcoxon rank-sum tests. The percentage of larvae metamorphosing in each replicate petri dish was subjected to the angular transformation, and the means and variances for each treatment were calculated. Variances for the two treatments to be compared were then tested for homogeneity using the *F*-max test (Sokal and Rohlf, 1981). If variances were homogeneous, the transformed data were compared by two-sample *t*-test. Otherwise the untransformed data were analyzed by the nonparametric Wilcoxon rank-sum test. All *t*-tests were calculated by hand; the nonparametric tests were conducted using the NPARIWAY procedure in SAS (SAS Institute Inc., 1989). Significant results were identified using the sequentially rejective Bonferroni procedure (Holm, 1979; Rice, 1989) to correct for multiple tests.

Results

Compounds affecting the activity of G proteins

Neither the G-protein activator Gpp[NH]p nor the inhibitor GDP- β -S affected metamorphosis of the larvae of *Hydroides elegans* (Fig. 1A, B). In the absence of a stimulatory bacterial biofilm, Gpp[NH]p did not induce metamorphosis (Fig. 1A), and GDP- β -S failed to inhibit metamorphosis in response to a biofilmed surface (Fig. 1B).

Compounds affecting the AC/cAMP transduction pathway

In two separate trials, the phosphodiesterase inhibitors IBMX, theophylline, and papaverine all induced metamorphosis in the absence of a biofilm (Fig. 2A, B). Concentrations at which we observed maximal responses were the same in both trials; 10^{-4} M for IBMX (*t*-test, $P < 0.001$, both trials), 10^{-3} M for theophylline (*t*-test, $P <$

Table 1

Compounds tested for effects on metamorphosis of larvae of *Hydroides elegans*

	Activity	Predicted effect on metamorphosis
Compounds affecting G proteins		
Gpp [NH] p	Activates G proteins	Induction
GDP- β -S	Inhibits activation of G proteins	Inhibition
Compounds affecting the AC/cAMP signal-transduction pathway		
IBMX	Inhibits phosphodiesterases*	Induction
Theophylline	Inhibits phosphodiesterases*	Induction
Papaverine	Inhibits phosphodiesterases*	Induction
RO-20-1724	Inhibits cAMP-specific phosphodiesterase IV*	Induction
db-cAMP	Increases intracellular cAMP	Induction
db-cGMP	Increases intracellular cGMP	Induction
Forskolin	Activates adenylate cyclase*	Induction
Compounds affecting the PI/DAG/PKC signal-transduction pathway		
TPA	Activates protein kinase C	Induction

A brief description of the activity of each compound is provided (Activity). Predicted Effect describes the result one would expect if G proteins, or the affected signal-transduction pathway, mediated responses of larvae to metamorphic cues. See text for details.

* Activity increases intracellular cAMP or cGMP.

0.001, both trials), and 10^{-5} M for papaverine (*t*-test, $P < 0.001$, trial 1; *t*-test, $P < 0.005$, trial 2). IBMX at 10^{-3} M caused a large number of larvae to metamorphose without constructing a primary or secondary tube. Figure 2 shows only the percentage of larvae that had undergone normal metamorphosis (characterized by permanent attachment to the substratum and construction of either a primary or secondary tube, see Materials and Methods) when exposed to IBMX at 10^{-3} M. Papaverine was a much less effective inducer of metamorphosis than either IBMX or theophylline, with a maximum mean percentage of metamorphosis $< 20\%$, as compared to $> 80\%$ for both IBMX and theophylline (Fig. 2A, B). Exposure of larvae to theophylline at 10^{-2} M was fatal. In the second trial (Fig. 2B) both IBMX (rank-sum test, $P < 0.05$) and papaverine (rank-sum test, $P < 0.05$) inhibited normal metamorphosis at their highest concentrations, although the effects were not strong. These compounds may have been toxic at the highest concentrations we tested. The selective phosphodiesterase inhibitor RO-20-1724 exhibited no inductive effects (Fig. 3).

Neither the adenylate cyclase activator forskolin, the cAMP analog db-cAMP, nor the cGMP analog db-cGMP induced metamorphosis in the absence of biofilm (Fig. 4). In the presence of a stimulatory biofilm, however, 10^{-4} M forskolin strongly inhibited metamorphosis (Fig. 5A, *t*-test, forskolin vs. DMSO control, $P < 0.001$). Inhibition did not appear to be the result of toxicity, as larvae exposed to 10^{-4} M forskolin in this experiment and in the absence of biofilm swam and behaved normally. We

observed no mortality in these trials. Neither db-cAMP nor db-cGMP inhibited responses of larvae to biofilms (Fig. 5B).

Compounds affecting the PI/DAG/PKC transduction pathway

Exposure of larvae to the phorbol ester TPA caused no significant induction of metamorphosis as compared to the appropriate DMSO controls (Fig. 6).

Table II lists the compounds tested, their predicted effect on metamorphosis of larvae of *Hydroides elegans* if G protein-coupled receptors or the AC/cAMP or PI/DAG/PKC signal-transduction pathways mediated responses of larvae to metamorphic cues, and the effect we observed in our experiments.

Discussion

A growing body of research on the effects of neuropharmacological agents on marine invertebrate larvae suggests that G protein-coupled receptors and their associated signal-transduction pathways are important regulators of larval settlement and metamorphosis, either directly through sensation and processing of exogenous metamorphic cues, or indirectly by modifying responses to these cues. It is not clear, however, whether this role for G proteins in metamorphosis is a characteristic of all marine invertebrate larvae (Hadfield, 1998). Our experiments indicate that G protein-coupled receptors or signal transduction by the AC/cAMP or PI/DAG/PKC pathways

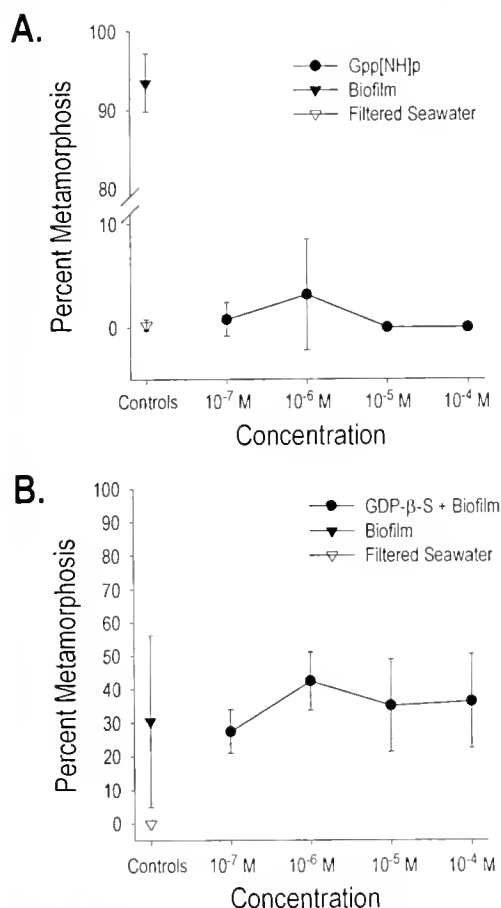


Figure 1. Metamorphosis of larvae of *Hydroides elegans* exposed to activators and inhibitors of G proteins. (A) Response to the G-protein activator Gpp [NH]p. (B) Effect of the G-protein inhibitor GDP-β-S on metamorphosis in response to bacterial biofilms. Points represent means of 4 replicates; error bars are standard deviations.

do not mediate responses of larvae of the serpulid polychaete *Hydroides elegans* to metamorphic cues.

If cues for settlement and metamorphosis of larvae of *H. elegans* were bound by a G protein-coupled receptor, we would have expected competent larvae to (1) metamorphose when exposed to the GTP analog Gpp[NH]p, and (2) fail to respond to inductive bacterial biofilms when those biofilms were presented in combination with GDP-β-S, a competitive inhibitor of G protein activation by GTP. We observed no increase in metamorphosis over FSW control treatments in the presence of Gpp[NH]p (Fig. 1A), and no inhibition of response of larvae to biofilmed surfaces when exposed to GDP-β-S (Fig. 1B). These results imply that the receptors responsible for detecting the metamorphic cue in *H. elegans* are not associated with G proteins.

The absence of evidence for the involvement of G protein-coupled receptors does not exclude the possibility that the metamorphic signal is transduced by either the

AC/cAMP or PI/DAG/PKC pathways. Baxter and Morse (1987) found that Gpp[NH]p and GDP-β-S did not directly affect metamorphosis of larvae of *Haliotis rufescens*, but larvae were induced to metamorphose by application of forskolin, IBMX, and theophylline, suggesting that the metamorphic signal was likely to be transduced by the AC/cAMP pathway, although not by a G protein-coupled receptor (Baxter and Morse, 1987; Morse, 1990).

If signal transduction by the AC/cAMP pathway were a necessary event in the metamorphic sequence in *Hydroides elegans*, then competent larvae should have metamorphosed when exposed to the phosphodiesterase inhibitors, db-cAMP, and the adenylate cyclase activator forskolin. The nonspecific phosphodiesterase inhibitors IBMX, theophylline, and papaverine induced significant levels of metamorphosis (Fig. 2); however, we observed no effect of the selective inhibitor RO-20-1724 (Fig. 3). Additionally, neither forskolin nor db-cAMP caused larvae to metamorphose (Fig. 4). Forskolin had the opposite

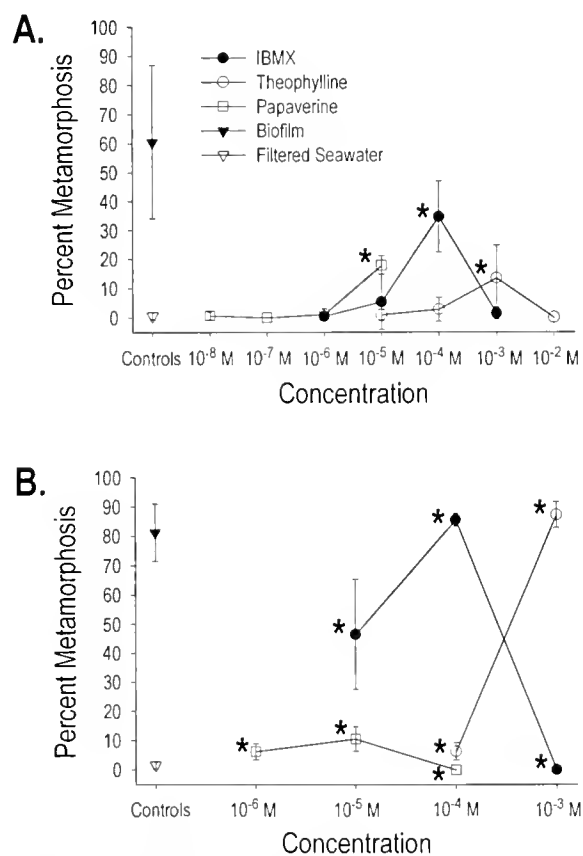


Figure 2. Metamorphosis of larvae of *Hydroides elegans* exposed to the phosphodiesterase inhibitors IBMX, theophylline, and papaverine. (A) and (B) present results from two separate trials. Note that the concentration ranges (x axes) differ between trials. Points represent means of 5 replicates in (A), 4 replicates in (B); error bars are standard deviations. * - significantly different from the FSW control treatment at $P \leq 0.05$.

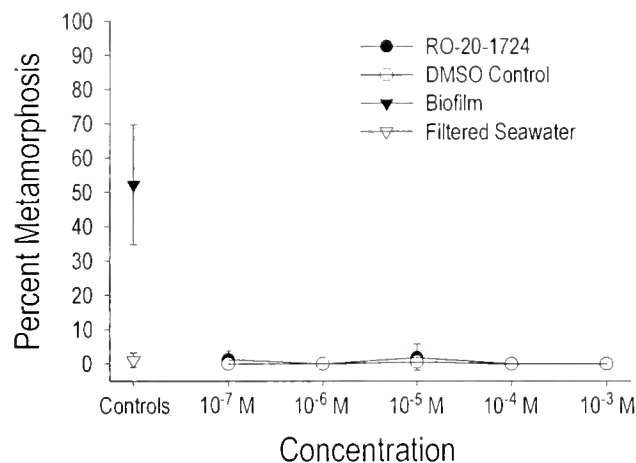


Figure 3. Metamorphosis of larvae of *Hydroides elegans* exposed to RO-20-1724, a selective inhibitor of the mammalian cAMP-specific phosphodiesterase IV. Exposure of larvae to DMSO served as the control for the RO-20-1724 treatment. Points represent means of 4 replicates; error bars are standard deviations.

effect, inhibiting metamorphosis of *H. elegans* in response to bacterial biofilms (Fig. 5).

Alternatively, the metamorphic signal may be transduced by cGMP. IBMX, theophylline, and papaverine are not selective for any of the cyclic nucleotide phosphodiesterase isozymes (Thompson, 1993); they inhibit phosphodiesterases that hydrolyze cGMP as well as those that hydrolyze cAMP. Exposure of larvae to db-cGMP, however, neither induced (Fig. 4) nor inhibited (Fig. 5B) metamorphosis.

Although the results presented here appear to be contra-

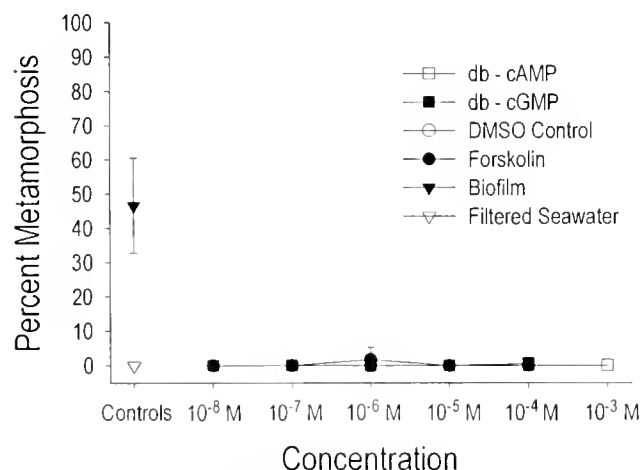


Figure 4. Metamorphosis of larvae of *Hydroides elegans* exposed to the cyclic nucleotide analogs db-cAMP and db-cGMP, and the adenylate cyclase activator forskolin. Exposure of larvae to DMSO served as the control for the forskolin treatment. Points represent means of 4 replicates; error bars are standard deviations.

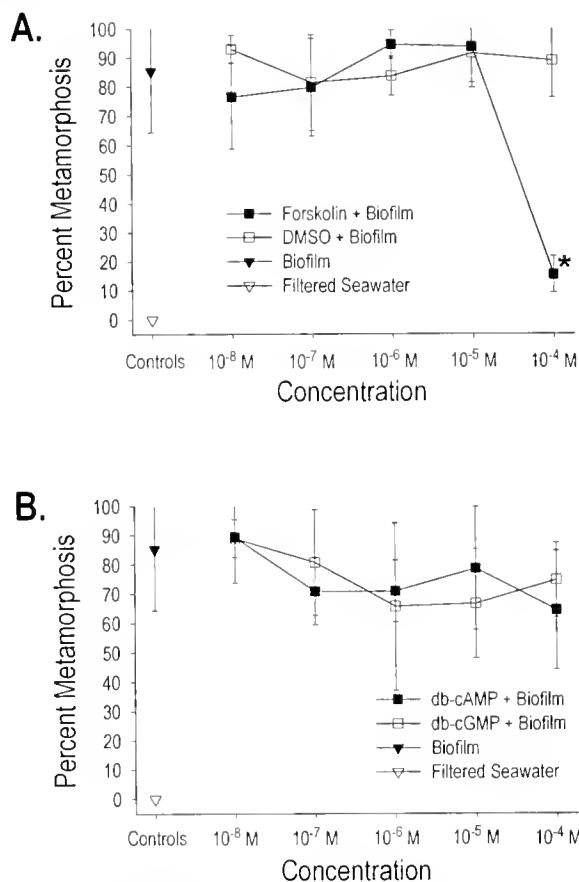


Figure 5. Metamorphosis of larvae of *Hydroides elegans* exposed to bacterial biofilms in combination with forskolin, db-cAMP, and db-cGMP. (A) Response to biofilmed surfaces in the presence of forskolin. The DMSO + Biofilm treatment served as the control for larvae exposed to forskolin. (B) Response to biofilmed surfaces in the presence of db-cAMP and db-cGMP. Points represent means of 4 replicates; error bars are standard deviations. * - significantly different from the control treatment at $P \leq 0.05$.

dictory, they may be explained by the effects on ion transport of some of the compounds used. IBMX (Kopf *et al.*, 1983; Simasko and Yan, 1993; Usachev and Verkhatsky, 1995), theophylline (Kopf *et al.*, 1983), and papaverine (Fujioka, 1984; Iguchi *et al.*, 1992) all have effects on calcium transport that can be either independent of or stronger than their effects on intracellular cAMP levels. Forskolin can block both potassium (Watanabe and Gola, 1987; Coombs and Thompson, 1987; Hoshi *et al.*, 1988; Garber *et al.*, 1990) and calcium (Park and Kim, 1996) channels, and desensitize acetylcholine receptors (Wagner and Pallotta, 1988; White, 1988), independently of its effects on cAMP. Calcium ions are important second messengers in the metamorphic pathway of some hydrozoan larvae (Freeman and Ridgway, 1987, 1990), and may serve the same function in larvae of polychaetes (Han *et al.*, 1993) and barnacles (Rittschof *et al.*, 1986; Clare,

1996). Metamorphosis of larvae of several phyla of marine invertebrates can be induced or inhibited by elevated concentrations of potassium (reviewed in Woollacott and Hadfield, 1996) or by application of potassium-channel blockers (reviewed in Pawlik, 1990). The exact mechanism by which potassium affects metamorphosis has yet to be determined.

Ongoing research in our laboratory indicates that calcium and potassium play important roles in the metamorphic morphogenesis of *H. elegans*. Addition of calcium ions to FSW enhances metamorphosis in the presence of biofilms, and pulse application of potassium induces metamorphosis in the absence of other cues (unpubl. data; Carpizo-Ituarte and Hadfield, 1996, 1998). Calcium and potassium channel blockers inhibit metamorphosis in response to cesium pulses and bacterial films, respectively (unpubl. data; Carpizo-Ituarte and Hadfield, 1998). It seems likely that the results we observed after application of the nonspecific phosphodiesterase inhibitors and forskolin are due to their effects on ion transport, rather than on cAMP or cGMP levels. This conclusion is supported by the lack of inhibitory or stimulatory effects from db-cAMP, db-cGMP, or the selective phosphodiesterase inhibitor RO-20-1724. On the basis of this evidence, we conclude that the AC/cAMP pathway does not transduce the metamorphic signal in larvae of *H. elegans*.

Our data also indicate that metamorphosis does not require signal transduction by the PI/DAG/PKC pathway. We attempted to induce metamorphosis with the protein kinase C activator TPA, the phorbol ester found to be the most effective stimulator of metamorphosis in two species of hydrozoans (Müller, 1985; Freeman and Ridgway, 1990). No effect was observed, implying that the PI/DAG/PKC pathway does not directly participate in the meta-

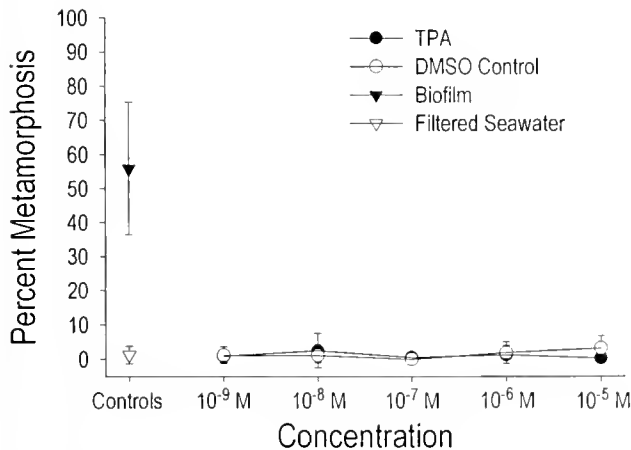


Figure 6. Metamorphosis of larvae of *Hydroides elegans* exposed to the protein kinase C activator TPA. Exposure of larvae to DMSO served as the control for the TPA treatment. Points represent means of 4 replicates; error bars are standard deviations.

Table II

Predicted and observed effects of compounds tested on larvae of Hydroides elegans

	Effect on metamorphosis	
	Predicted	Observed
Compounds affecting G proteins		
Gpp [NH] p	Induction	None
GDP- β -S	Inhibition	None
Compounds affecting the AC/cAMP signal-transduction pathway		
tBMX	Induction	Induction
Theophylline	Induction	Induction
Papaverine	Induction	Induction
RO-20-1724	Induction	None
db-cAMP	Induction	None
db-cGMP	Induction	None
Forskolin	Induction	Inhibition
Compounds affecting the PI/DAG/PKC signal-transduction pathway		
TPA	Induction	None

See Table I and the text for descriptions of the activity of each compound. Predicted Effect describes the result one would expect if G proteins, or the affected signal-transduction pathway, mediated responses of larvae to metamorphic cues.

morphic process. The possibility that G proteins and the PI/DAG/PKC pathway transduce signals that modify responses of larvae to the metamorphic cue, as in *Haliotis rufescens* (Trapido-Rosenthal and Morse, 1985; Baxter and Morse, 1987), cannot be eliminated, however.

Our results indicate that neither G protein-coupled receptors nor signal transduction by the AC/cAMP or PI/DAG/PKC pathways are components of the morphogenetic pathway (in the sense of Baxter and Morse, 1987) directly responsible for sensation and processing of bacterial settlement cues in larvae of *Hydroides elegans*. We are investigating the possibility that the receptors that detect these cues are either ligand-gated ion channels similar to amino acid taste receptors in channel catfish (Teeter *et al.*, 1990; Brand *et al.*, 1991), or lectins such as those suggested to mediate responses to bacterial biofilms in larvae of the spirorbid polychaete *Janua brasiliensis* (Kirchman *et al.*, 1982; Maki and Mitchell, 1985).

Acknowledgments

This research was funded by grants from the Office of Naval Research to C. M. Smith and MGH (No. N00014-95-1-0196), and MGH (N00014-95-1-1015). EC-1 was supported in part by a scholarship for graduate studies from CONACYT/UABC, Mexico. We thank D. Rittschof and two anonymous reviewers for valuable comments on preliminary drafts of the manuscript.

Literature Cited

- Baxter, G., and D. E. Morse. 1987. G protein and diacylglycerol regulate metamorphosis of planktonic molluscan larvae. *Proc. Natl. Acad. Sci. USA* **84**: 1867–1870.
- Baxter, G. T., and D. E. Morse. 1992. Cilia from abalone larvae contain a receptor-dependent G protein transduction system similar to that in mammals. *Biol. Bull.* **183**: 147–154.
- Biggers, W. J., and H. Laufer. 1992. Chemical induction of settlement and metamorphosis of *Capitella capitata* Sp. 1 (Polychaeta) larvae by juvenile hormone-active compounds. *Invertebr. Reprod. Dev.* **22**: 39–46.
- Brand, J. G., J. H. Teeter, T. Kumazawa, T. Huque, and D. L. Bayley. 1991. Transduction mechanisms for the taste of amino acids. *Physiol. Behav.* **49**: 899–904.
- Bryan, P. J., P.-Y. Qian, J. L. Kreider, and F.-S. Chia. 1997. Induction of larval settlement and metamorphosis by pharmacological and conspecific associated compounds in the serpulid polychaete *Hydroides elegans*. *Mar. Ecol. Prog. Ser.* **146**: 81–90.
- Carpizo-Ituarte, E., and M. G. Hadfield. 1996. Biofilm and ionic stimulation of metamorphosis in the polychaete *Hydroides elegans*. *Am. Zool.* **36**: 10A.
- Carpizo-Ituarte, E., and M. G. Hadfield. 1998. Stimulation of metamorphosis in the polychaete *Hydroides elegans* Haswell (Serpulidae). *Biol. Bull.* **194**: 14–24.
- Carr, W. E. S. 1992. Recurring themes and variations: an overview and introduction. *Biol. Bull.* **183**: 143–146.
- Cheung, W. Y., and Y. M. Lin. 1974. Purification and characterization of cyclic 3', 5'-nucleotide phosphodiesterase from bovine brain. *Methods Enzymol.* **38**: 223–239.
- Clare, A. S. 1996. Signal transduction in barnacle settlement: calcium re-visited. *Biofouling* **10**: 141–159.
- Clare, A. S., R. F. Thomas, and D. Rittschof. 1995. Evidence for the involvement of cyclic AMP in the pheromonal modulation of barnacle settlement. *J. Exp. Biol.* **198**: 655–664.
- Coombs, J., and S. Thompson. 1987. Forskolin's effect on transient K current in nudibranch neurons is not reproduced by cAMP. *J. Neurosci.* **7**: 443–452.
- Crisp, D. J. 1984. Overview of research on marine invertebrate larvae, 1940–1980. Pp. 103–126 in *Marine Biodeterioration: an Interdisciplinary Study*, J. D. Costlow and R. C. Tipper, eds. Naval Institute Press, Annapolis, Maryland.
- Féger, J., S. Gil-Faloon, and C. Lamaze. 1994. Cell receptors: definition, mechanisms and regulation of receptor-mediated endocytosis. *Cell Mol. Biol.* **40**: 1039–1061.
- Freeman, G., and E. B. Ridgway. 1987. Endogenous photoproteins, calcium channels and calcium transients during metamorphosis in hydrozoans. *Roux's Arch. Dev. Biol.* **196**: 30–50.
- Freeman, G., and E. B. Ridgway. 1990. Cellular and intracellular pathways mediating the metamorphic stimulus in hydrozoan planulae. *Roux's Arch. Dev. Biol.* **199**: 63–79.
- Fujioka, M. 1984. Lack of a causal relationship between the vasodilator effect of papaverine and cyclic AMP production in the dog basilar artery. *Br. J. Pharmacol.* **83**: 113–124.
- Garber, S. S., T. Hoshi, and R. W. Aldrich. 1990. Interaction of forskolin with voltage-gated K⁺ channels in PC12 cells. *J. Neurosci.* **10**: 3361–3368.
- Gilman, A. G. 1987. G proteins: transducers of receptor-generated signals. *Annu. Rev. Biochem.* **56**: 615–649.
- Hadfield, M. G. 1998. Research on settlement and metamorphosis of marine invertebrate larvae: past, present and future. *Biofouling* **12**: 9–29.
- Hadfield, M. G., C. C. Unabia, C. M. Smith, and T. M. Michael. 1994. Settlement preferences of the ubiquitous fouler *Hydroides elegans*. Pp. 65–74 in *Recent Developments in Biofouling Control*, M. F. Thompson, R. Nagabhushanam, R. Sarojini, and M. Fingergerman, eds. Oxford and IBH Pub. Co., New Delhi.
- Holm, S. 1979. A simple sequentially rejective multiple test procedure. *Scand. J. Statist.* **6**: 65–70.
- Hoshi, T., S. S. Garber, and R. W. Aldrich. 1988. Effect of forskolin on voltage-gated K⁺ channels is independent of adenylate cyclase activation. *Science* **240**: 1652–1655.
- Iguchi, M., T. Nakajima, T. Hisada, T. Sugimoto, and Y. Kurachi. 1992. On the mechanism of papaverine inhibition of the voltage-dependent Ca⁺⁺ current in isolated smooth muscle cells from the guinea pig trachea. *J. Pharmacol. Exp. Ther.* **263**: 194–200.
- Ilan, M., R. A. Jensen, and D. E. Morse. 1993. Calcium control of metamorphosis in polychaete larvae. *J. Exp. Zool.* **267**: 423–430.
- Jensen, R. A., and D. E. Morse. 1990. Chemically induced metamorphosis of polychaete larvae in both the laboratory and ocean environment. *J. Chem. Ecol.* **16**: 911–930.
- Kirchman, D., S. Graham, D. Reish, and R. Mitchell. 1982. Lectins may mediate in the settlement and metamorphosis of *Janua* (*Dexiospira*) *brasilensis* Grube (Polychaeta: Spirorbidae). *Mar. Biol. Lett.* **3**: 131–142.
- Kopf, G. S., C. A. Lewis, and V. D. Vacquier. 1983. Methylxanthines stimulate calcium transport and inhibit cyclic nucleotide phosphodiesterases in abalone sperm. *Dev. Biol.* **99**: 115–120.
- Leitz, T. 1997. Induction of settlement and metamorphosis of cnidarian larvae: signals and signal transduction. *Invertebr. Reprod. Dev.* **31**: 109–122.
- Leitz, T., and G. Klingmann. 1990. Metamorphosis in *Hydractinia*: studies with activators and inhibitors aiming at protein kinase C and potassium channels. *Roux's Arch. Dev. Biol.* **199**: 107–113.
- Leitz, T., and W. A. Müller. 1987. Evidence for the involvement of PI-signaling and diacylglycerol second messengers in the initiation of metamorphosis in the hydroid *Hydractinia echinata* Fleming. *Dev. Biol.* **121**: 82–89.
- Leitz, T., and A. Wirth. 1991. Vanadate, known to interfere with signal transduction, induces metamorphosis in *Hydractinia* (Coelenterata; Hydrozoa) and causes profound alterations of the larval and postmetamorphic body pattern. *Differentiation* **47**: 119–127.
- Maki, J. S., and R. Mitchell. 1985. Involvement of lectins in the settlement and metamorphosis of marine invertebrate larvae. *Bull. Mar. Sci.* **37**: 675–683.
- Morse, A. N. C. 1991. How do planktonic larvae know where to settle? *Am. Sci.* **79**: 154–167.
- Morse, D. E. 1990. Recent progress in larval settlement and metamorphosis: closing the gaps between molecular biology and ecology. *Bull. Mar. Sci.* **46**: 465–483.
- Morse, D. E., H. Duncan, N. Hooker, A. Baloun, and G. Young. 1980. GABA induces behavioral and developmental metamorphosis in planktonic molluscan larvae. *Fed. Proc.* **39**: 3237–3241.
- Müller, W. A. 1985. Tumor-promoting phorbol esters induce metamorphosis and multiple head formation in the hydroid *Hydractinia*. *Differentiation* **29**: 216–222.
- Park, T.-J., and K.-T. Kim. 1996. Cyclic AMP-independent inhibition of voltage-sensitive calcium channels by forskolin in PC12 cells. *J. Neurochem.* **66**: 83–88.
- Pawlik, J. R. 1990. Natural and artificial induction of metamorphosis of *Phragmatopoma lapidosa californica* (Polychaeta: Sabellariidae), with a critical look at the effects of bioactive compounds on marine invertebrate larvae. *Bull. Mar. Sci.* **46**: 512–536.
- Posternak, T., and G. Weimann. 1974. The preparation of acylated derivatives of cyclic nucleotides. *Methods Enzymol.* **38**: 399–409.
- Rice, W. R. 1989. Analyzing tables of statistical tests. *Evolution* **43**: 223–225.
- Rittschof, D., J. Maki, R. Mitchell, and J. D. Costlow. 1986. Ion and

- neuropharmacological studies of barnacle settlement. *Netherlands J. Sea Res.* **20**: 269–275.
- SAS Institute Inc. 1989.** *SAS/STAT User's Guide, Version 6, 4th ed.* SAS Institute Inc., Cary, North Carolina. 846 pp.
- Scheltema, R. S. 1974.** Biological interactions determining larval settlement of marine invertebrates. *Thalassia Jugosl.* **10**: 263–296.
- Schneider, T., and T. Leitz. 1994.** Protein kinase C in hydrozoans: involvement in metamorphosis of *Hydractinia* and in pattern formation of *Hydra*. *Roux's Arch. Dev. Biol.* **203**: 422–428.
- Seamon, K. B., W. Padgett, and J. W. Daly. 1981.** Forskolin: unique diterpene activator of adenylate cyclase in membranes and intact cells. *Proc. Natl. Acad. Sci. USA* **78**: 3363–3367.
- Simasko, S. M., and S. Yan. 1993.** 3-Isobutyl-1-methylxanthine inhibits sustained calcium current independently of cyclic AMP in neuronal and endocrine cells. *Mol. Pharmacol.* **44**: 622–627.
- Sokal, R. R., and F. J. Rohlf. 1981.** *Biometry*. W. H. Freeman, San Francisco. 859 pp.
- Svane, I., and C. M. Young. 1989.** The ecology and behaviour of ascidian larvae. *Oceanogr. Mar. Biol. Annu. Rev.* **27**: 45–90.
- Teeter, J. H., J. G. Brand, and T. Kumazawa. 1990.** A stimulus-activated conductance in isolated taste epithelial membranes. *Biophys. J.* **58**: 253–259.
- Thompson, W. J. 1993.** Cyclic nucleotide phosphodiesterases: pharmacology, biochemistry and function. Pp. 287–313 in *Intracellular Messengers*. C. W. Taylor, ed. Pergamon Press, Oxford.
- Trapido-Rosenthal, H. G., and D. E. Morse. 1985.** L- α , ω -diamino acids facilitate GABA induction of larval metamorphosis in a gastropod mollusc (*Haliotis rufescens*). *J. Comp. Physiol. B.* **155**: 403–414.
- Trapido-Rosenthal, H. G., and D. E. Morse. 1986.** Availability of chemosensory receptors is down-regulated by habituation of larvae to a morphogenetic signal. *Proc. Natl. Acad. Sci. USA* **83**: 7658–7662.
- Usachev, Y., and A. Verkhratsky. 1995.** IBMX induces calcium release from intracellular stores in rat sensory neurones. *Cell Calcium* **17**: 197–206.
- Wagoner, P. K., and B. S. Pallotta. 1988.** Modulation of acetylcholine receptor desensitization by forskolin is independent of cAMP. *Science* **240**: 1655–1657.
- Watanabe, K., and M. Gola. 1987.** Forskolin interaction with voltage-dependent K channels in *Helix* is not mediated by cyclic nucleotides. *Neurosci. Lett.* **78**: 211–216.
- White, M. M. 1988.** Forskolin alters acetylcholine receptor gating by a mechanism independent of adenylate cyclase activation. *Mol. Pharmacol.* **34**: 427–430.
- Wisely, B. 1958.** The development and settling of a serpulid worm, *Hydroides norvegica* Gunnerus (Polychaeta). *Aust. J. Mar. Freshwater Res.* **9**: 351–361.
- Wodicka, L. M., and D. E. Morse. 1991.** cDNA sequences reveal mRNAs for two G α signal transducing proteins from larval cilia. *Biol. Bull.* **180**: 318–327.
- Woollacott, R. M., and M. G. Hadfield. 1996.** Induction of metamorphosis in larvae of a sponge. *Invertebr. Biol.* **115**: 257–262.
- Yamamoto, H., A. Tachibana, K. Matsumura, and N. Fusetani. 1995.** Protein kinase C (PKC) signal transduction system involved in larval metamorphosis of the barnacle, *Balanus amphitrite*. *Zool. Sci.* **12**: 391–396.

Transport Pathways in the Neotropical Sponge *Aplysina*

SALLY P. LEYS^{1,3} AND HENRY M. REISWIG²

¹Department of Biology, University of Victoria, Victoria, British Columbia, Canada, V8W 3N5;

²Redpath Museum and Biology Department, McGill University, 859 Sherbrooke St., Montreal, Quebec, Canada; and ³Bellairs Research Institute of McGill University, St. James, Barbados

Abstract. Strands of cells distinct from the rest of the tissue were found running lengthwise through the endosome of four species of the sponge *Aplysina*. Although the strands were more highly pigmented than the adjacent tissue and could be removed intact with forceps, ultrastructural studies revealed no obvious barrier separating the cells in the strands from the rest of the tissue. The strands consist of stretches of elongate cells tightly aligned along densely bundled collagen fibrils, and areas of other elongate cells that possess numerous filopodia. When sponges were fed fluorescent latex beads *in situ*, beads were taken up and transported specifically into the strands; eventually they were found at the tip of the sponge and further down the stalk, away from the site of feeding. Beads injected into endosomal strands were also transported upwards in the strands to the tip of the sponge. Video microscopy of cells in strands that had been exposed along a portion of their length showed no bulk movement of cells; but individual cells were seen moving in both directions along the strands at $0.025\text{--}0.04\ \mu\text{m}\cdot\text{s}^{-1}$. The endosomal cell strands are suggestive of a primitive nutrient transport pathway in sponges.

Introduction

Sponges were the first multicellular animals to arise from unicellular protists during early metazoan evolution, at least 600 million years ago (Steiner *et al.*, 1993; Reitner and Mehl, 1995), and their tissue organization, accordingly, is quite simple. Sponges are diploblastic metazoans that possess no organ systems; their tissues consist of a limited number of cell types that surround and penetrate a mesohyl of collagen. The entire animal is organized

around canals and chambers through which water is channeled for feeding and respiration.

Within the Porifera, however, some groups differ markedly from this fundamental plan. The Hexactinellida, for example, are mostly syncytial (Reiswig, 1979; Mackie and Singla, 1983), a condition that allows symplastic transport of food (Perez, 1996; Wyeth *et al.*, 1996) and rapid conduction of action potentials that control the feeding current (Leys and Mackie, 1997). The Cladorhizidae, on the other hand, are deep-sea demosponges that are effectively carnivorous and lack flagellated chambers, which are otherwise a key poriferan character (Vacelet and Boury-Esnault, 1995). In a group as old as the Porifera, other exceptions to the basic sponge plan probably exist.

One intriguing possibility lies within demosponges of the genus *Aplysina*. These sponges, which are known as bacteriosponges for the vast number of bacteria living within their mesohyl, belong to the Verongida, an order that contains numerous pharmaceutically interesting chemicals (Bergquist *et al.*, 1991; Ciminiello *et al.*, 1994, 1997). An unusual feature of some sponges in this genus is the presence of longitudinal strands of elongate cells in the endosome. The strands, up to $100\ \mu\text{m}$ in diameter and particularly densely populated by bacteria, constitute a quasi-tissue that runs vertically through sponges of tube, chimney, and rope-form alike.

Despite their prominence in these sponges and their marked absence in other members of the phylum studied to date, the strands have received only passing mention in the literature. Tsurumi and Reiswig (1997) suggested that the "endosomal" tissue strands in *Aplysina cauliformis* (a rope-form sponge) serve as migration routes for rapid transport of cells for tip growth. Similar elongate cells, in the endosome and around the water canals in *Verongia* (synonymous with *Aplysina*), were suggested

to be contractile cells that act together to control water flow through the canal system (Vacelet, 1966). To have tested either of these hypotheses would have required cell labeling studies and, if possible, video-enhanced-contrast microscopy of live tissue, techniques that were not readily available until recently. We have now undertaken both approaches and present here a detailed description of the endosomal tissue strands and their role in transport of materials.

Materials and Methods

Description of the sponges and collection site

Aplysina cauliformis (probably synonymous to *A. fulva*), a neotropical rope-form sponge, grows at the tip (Wulff, 1990), reaching about 1 cm in diameter, but up to several meters in length. It is pink or purple on the outside and yellow inside. At depths of 7–10 m, *A. cauliformis* is typically branched and grows only 20–30 cm in height. *Aplysina lacunosa* is a mustard-yellow tube-form sponge. The tubes are 10–50 cm in length and can occur singly, but more often several of them bud from the same base. The tubes are 5–10 cm in diameter with an atrial diameter of 2–5 cm. *Aplysina rigida*, a branching stick-form sponge, is pink outside and yellow on the inside, but is both thicker (up to 5 cm in diameter) and taller (up to 1 m in height in 7-m-deep waters) than *A. cauliformis*. *Aplysina fistularis* is a robust, branching, stick-form sponge in Barbados, but it may be tube-form in other habitats in the Caribbean. *A. fistularis* is yellow outside and has an irregular outer surface, but it lacks the lacunae characterizing *A. lacunosa*; it is 3–5 cm in diameter and reaches 20–30 cm in height at depths of 7–10 m.

Species of *Aplysina* were manipulated *in situ* and collected by scuba from coral rubble at a depth of 7–10 m off the Bellairs Research Institute, St. James, Barbados (13°10'N, 59°40'W).

Field experiments

Latex bead feeding. Plastic bags (4 × 7 cm) open at both ends were slipped over the branches of *A. cauliformis* *in situ* and, about 5–10 cm from the top, were gently secured at both ends with plastic twist ties (Figs. 1 and 2a). A plastic syringe and needle were used to inject the bag with 5 ml of 1- μ m fluorescent latex beads (Molecular Probes, Eugene, OR) diluted 1:5 with seawater. The beads were not treated with serum to prevent clumping, because trial experiments showed that clumping did not interfere with bead uptake. The bead-filled bags were left on the sponges for 4 h and then removed; the beads had been cleared from the bags during this period. Two branches were collected for fixation at 4 and 24 h, and 2, 3, 7, 11, and 13 days after feeding. The sponges were cut off at a

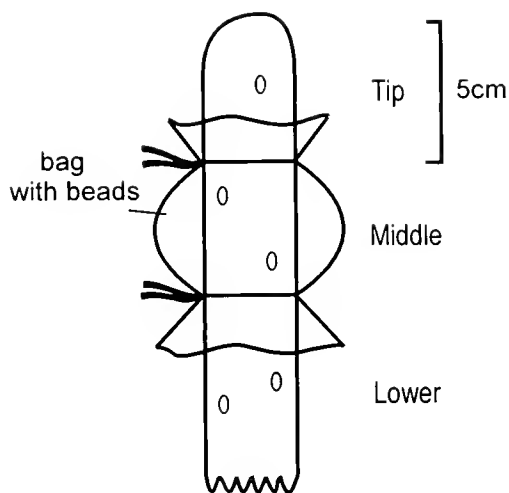


Figure 1. Diagram of a branch of *Aplysina cauliformis* showing the attachment of a plastic bag that is used to feed latex beads to the sponge. Also shown are the three segments (Tip, Middle, and Lower) that the branch was cut into; the segments were used in determining the fate of the beads.

point 15 cm from the top, placed in a plastic bag, and taken to the laboratory, where each piece was cut into three segments: the top 5 cm (Tip), the middle 5 cm where the bag had been secured (Middle), and the bottom 5 cm (Lower) (Fig. 1). The segments were fixed in 2% paraformaldehyde in seawater and placed in the refrigerator at about 4°C. After 4 hours the fixative was poured off and replaced with fresh, cold 2% paraformaldehyde.

Insertion of latex beads. Whole branches of *A. cauliformis* attached to loosely buried coral rubble were collected in plastic bags (with the coral) and brought into the laboratory; the sponges were never removed from seawater. The sponge branches were cut 7 cm from the tip, but not quite in two; thus a hinge of tissue still connected the tip segment to the main stem. The sponge was placed in a large bucket of seawater and, with the aid of a dissecting microscope poised over the bucket, 1- μ m latex beads were injected with a plastic syringe and needle onto a severed cell strand and its immediate area. The wound was sewn together with dental floss and the sponges were returned to the field no more than 4 h after collection and reattached with plastic cable ties to other pieces of coral rubble. Preliminary experiments showed that, despite wave action, the wound healed and new tissue grew over the dental floss within 1–2 days. Sponges treated in this way were recollected 1, 2, 3, 7, 11, and 13 days after wounding, cut into three segments as described above, and fixed in 2% paraformaldehyde in seawater.

Laboratory analysis of field experiments

Sponge pieces were transported while still in fixative to the University of Victoria, British Columbia, Canada, where

they were rinsed in phosphate-buffered saline (PBS) for 4 h, infiltrated overnight in 1:1 PBS and Tissue Tek (O.C.T. Compound 4583, Sakura Finetechnical, Tokyo), and embedded in 100% Tissue Tek by freezing in liquid nitrogen. Blocks of embedded tissue were stored at -20°C . Longitudinal sections ($30\ \mu\text{m}$) from each segment (Tip, Middle, and Lower) of one of the two branches from each collection period were cut on a cryomicrotome. Sections were mounted on slides coated with poly-L-lysine and stored at -20°C . Sections were viewed with a Leitz Aristoplan epifluorescence microscope equipped with the FITC filter (450–490-nm excitation) through which the tissue appeared green and orange and the latex beads bright yellow. Latex beads were counted in 10 sections chosen at random from each segment of the sponge for every time interval of collection. The location of the beads was scored as follows: i) in the tissue (*i.e.*, in or near the flagellated chambers) of the sponge; ii) at the edges of water canals; and iii) in cell strands. Where beads were too numerous to count (for example in the pieces collected within the first 24 h after treatment), 100 beads were first counted, and estimates of every hundred beads visible thereafter were made. Selected sections were later stained in hematoxylin and eosin but not cleared in xylene, and then mounted in PBS-glycerol. This procedure allowed us to see the location of beads within the strands.

Video microscopy

Pieces of *A. cauliformis* were transferred to flow-through seawater tanks at the Bellairs Research Institute without removal from seawater. A 4-cm piece of a sponge branch was cut in two lengthwise with a sharp disposable scalpel. Where a strand was exposed without damage along a portion of its length, the piece of branch was tied with dental floss to a glass microscope slide with the cut surface against the slide. With the exposed strand facing upwards, the slide was rested on supports at either end in a flow-through perfusion chamber so that the sponge did not touch the bottom of the dish. The perfusion cham-

ber was set on the stage of a Zeiss compound microscope and the strands were filmed with a $10\times$ objective lens for up to 5 h using a Panasonic CCD color video camera; the image was digitally enhanced with an Omnex real-time digital image processor (Imagen Corp.) and recorded on Fuji video tapes in real time with a Panasonic VCR. Photographs were taken from the monitor of a Technitron television with a Nikon FG camera on TMAX 400 ASA film.

Bright field microscopy

Pieces of *A. cauliformis* were cut in half lengthwise to expose the tissue strands and placed strand-side up, in a 5-cm diameter dish of seawater, on the stage of a Leitz Orthoplan microscope. The exposed surface was illuminated with two adjustable microscope lamps, and photographs were taken on 100 ASA Fujicolor print film.

Electron microscopy

Tissue strands were dissected, with a scalpel and fine forceps, out of freshly collected sponge branches. Strands and whole pieces of sponge with exposed strands were fixed in a cocktail of cold 1% osmium tetroxide and 2% glutaraldehyde in 0.45 M sodium acetate buffer, pH 6.4, and 10% sucrose in the final volume. Pieces were kept in the refrigerator at 4°C for 4 h, and the fixative was then changed. After 16 to 20 h, the fixative was poured off, and the tissue was rinsed in 0.45- μm Millipore-filtered seawater and stored in 70% ethanol for transport to the University of Victoria, British Columbia. Tissue strands and pieces of sponge were then further dehydrated to 100% ethanol, stained *en bloc* in 0.5% uranyl acetate overnight at the 80% ethanol stage, rinsed three times in propylene oxide, infiltrated overnight in 1:1 Epon (Taab 812) and propylene oxide, and embedded in 100% Epon at 60°C . Silver sections were cut on a Reichert ultramicrotome with a diamond knife, stained with lead citrate, and viewed in a Hitachi 8000 transmission electron microscope.

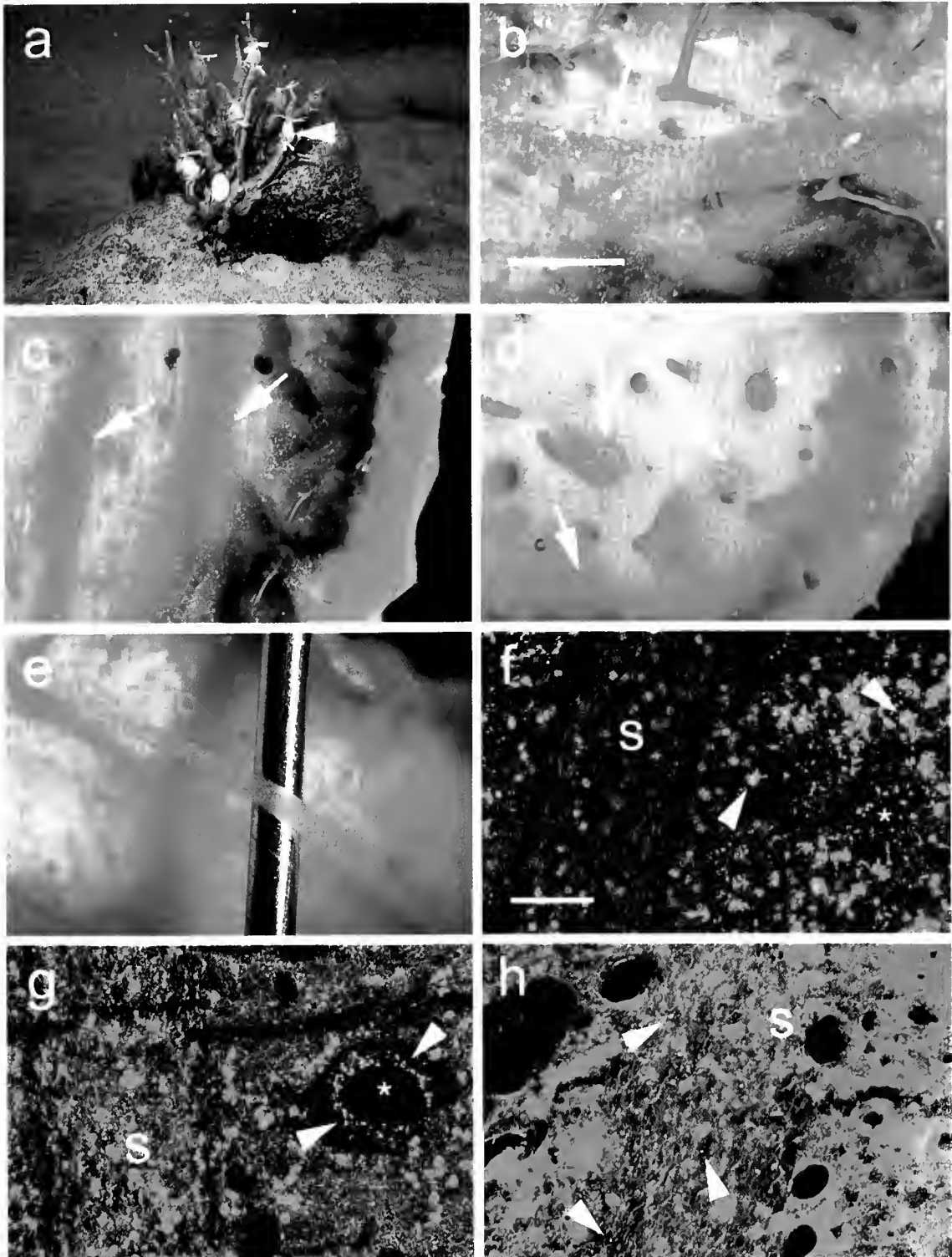
Figure 2. (a) *Aplysina cauliformis* attached to coral rubble, with plastic bags (arrowhead) filled with latex beads attached to each branch. Latex beads were "fed" to the sponge branches in the plastic bags, and the fate of ingested materials was determined. (b–e) Live tissue strands of *A. cauliformis*. Bar: 1 mm. (f–h) Latex beads in longitudinal sections of preserved sponge branches. Bar: $50\ \mu\text{m}$. (b) A strand in a longitudinal section of a sponge. The strand (arrow) is darker than the adjacent tissue and divides to go around the spongin skeleton. The arrowhead indicates a piece of the broken spongin skeleton. (c) Two exposed strands (arrows) in a longitudinal section are similar in color to the tissue at the outer layer of the sponge. (d) A cross section of a sponge branch showing three strands (arrows), which are easily identified by their pink color and by their slight separation from the neighboring tissue. Polychaete worms (*) are an abundant macrosymbiont in these sponges and either use water canals or fashion their own pathways through the sponge. (e) A tissue strand can be lifted up with a dissecting needle, indicating the integrity and slight elasticity of the strands. (f) Four hours after feeding, latex beads (arrowheads) were well distributed throughout the tissue but were not in the strands (s). (g) Two days after feeding, the beads (arrowheads) were predominantly in the tissues around the water canals (*); strands (s). (h) Eleven days after feeding, the beads (arrowheads) were only found in the tissue strands (s) of the tip segment of the branches. Very few were found in other tissues of the sponge at this time.

Results

Description of the strands

The tissue of *A. cauliformis* contained longitudinal strands running from the base to the tip of the sponge (Fig. 2b). The strands were darker than the adjacent tissue (Fig. 2b). The strands were darker than the adjacent tissue.

and were flecked here and there by white cells that appeared to be highly refractile. The strands were most similar in color to the tissue at the cortex (Fig. 2e) and the tissue at the tip of the sponge. Up to 12 strands could be identified in any one cross section of a sponge branch (Fig. 2d). Strands ranged in diameter from 20 to 100 μm .



but the diameter of any one strand was rather uniform for its entire length. Strands could be traced for at least 3 cm and often for more than 6 cm along a sponge branch. The strands tended to be straight, with only slight bends and turns where they coursed around the spongin skeleton (e.g., Fig. 2b), and there were no cross-connections between strands. Typically, strands branched or forked at the tip of the sponge, and if a strand was located along the cortex or edge of the sponge, a branch was often directed towards the cortex.

The strands were sufficiently separate from the rest of the tissue in the sponge that they could be lifted by one end with forceps and gently pulled free from the sponge. The strands were slightly elastic, as can be seen by the ability of a dissecting needle to pull a portion of a strand away from the sponge tissue (Fig. 2c). However, more than a moderate pulling resulted in the breakage and slow curling of the excised ends. Occasionally, when they were pulled out of the sponge, the strands frayed at the edges and pieces at the edges were left behind. Other parts of the sponge lacked this integrity and could not be removed intact from the sponge.

Examination of the live tissues of *A. lacunosa*, *A. fistularis*, and *A. rigida* revealed tissue strands in all three species. Strands were always distinctly more pink than the surrounding tissue, up to 100 μm in diameter, and traceable for at least 3 cm, and often for the full length of the sponge. Sections 1-cm thick cut with a scalpel from top to bottom of these sponges revealed fewer strands at the base than at the middle or tip of the sponge, and none of the strands were especially close to the cortex. In one section of *A. lacunosa*, 24 different strands were identified. Most of the strands could be followed for 4 cm or more along the length of the sponge.

Electron microscopy

Ultrastructural examination revealed no clear barrier separating the tissue strands from the rest of the sponge tissue. Only in one instance was a string of connected cells 60- μm long found at the edge of the strand. More commonly the edges of strands were lined simply by collagen. Strands were identifiable in sections of the sponge tissue by the presence of an increased number of aligned elongate cells, vast numbers of bacteria, and a much denser collagenous mesohyl in which the collagen fibrils were often aligned in a single direction (Fig. 3A, B). Elongate cells (40–50- μm long and 2.5–4- μm wide) with numerous filopodia were separated laterally by about 10 μm (Fig. 3A). These cells typically lacked conspicuous nucleoli and contained many small vesicles. Other cells in the strands (possibly spherulous cells) were stretched around large vesicles containing an electron-dense material (Fig. 3A). Along particularly dense bands of aligned collagen there were highly elongate cells with a well-

developed cytoskeleton (Figs. 3B, 4A). Cells in the strand were often found in the process of phagocytosing bacteria (e.g., Fig. 4B).

The tissue outside of the strands consisted mostly of a comparatively loose collagenous mesohyl containing numerous bacteria, although fewer than in the strands; scattered amoeboid-like cells; and flagellated chambers. The sponge cortex consisted of many spherulous cells containing large inclusions, and some elongate cells embedded in collagen that was not aligned in any particular direction (Fig. 4C).

Strands from other species of *Aplysina* were identical in ultrastructure to those in *A. cauliformis*. Cells in strands that were preserved after they had been forced to recoil at the edges by cutting and tweezing appeared no different than those in strands that had been fixed while still within the sponge. In both cases, cells were elongate when lying beside aligned collagen fibrils and irregularly ovoid when not.

Feeding and insertion of latex beads

In the feeding experiment, the beads were first seen in the flagellated chambers and pinacoderm (Fig. 5a) and later in cells in the mesohyl (Figs. 5B and 2f). Four hours after feeding, beads were found in all the sponge tissues of the middle segment except the cell strands (Fig. 2f). By 2 to 3 days after feeding the beads were concentrated in the tissues around the water canals (Fig. 2g). At this time only a few beads were found in the cell strands. However, 7 to 11 days after feeding, many beads were found in the tip segment, where they were specifically lodged in the cell strands (Fig. 2h); very few were found in adjacent tissues. Closer examination of selected stained sections showed that the beads were within the cells in these strands. At this level of resolution it appeared that the beads were in the elongate cells rather than in the spherulous cells, but the strands with beads were not examined by electron microscopy to confirm this observation.

The relative proportion of beads in the tissue, at the edges of canals, and in the tissue strands over the course of 13 days after latex bead feeding and insertion is shown in Figures 6 and 7. In the feeding experiment (Figs. 6A and 7A) most latex beads in the middle segment were first found in the sponge tissues (triangles) and later at the edges of water canals (squares) during the first week after feeding. The number of beads in the middle segment declined during the second week after feeding. Although many beads were counted in the strands in the middle segment at day 2 (see Table I), these were far outnumbered by those beads that were counted around the edges of the canals and in the tissue at this time. In the second week, 22% of the beads counted in all segments were in the strands in the tip segment 11 days after feeding (Fig.

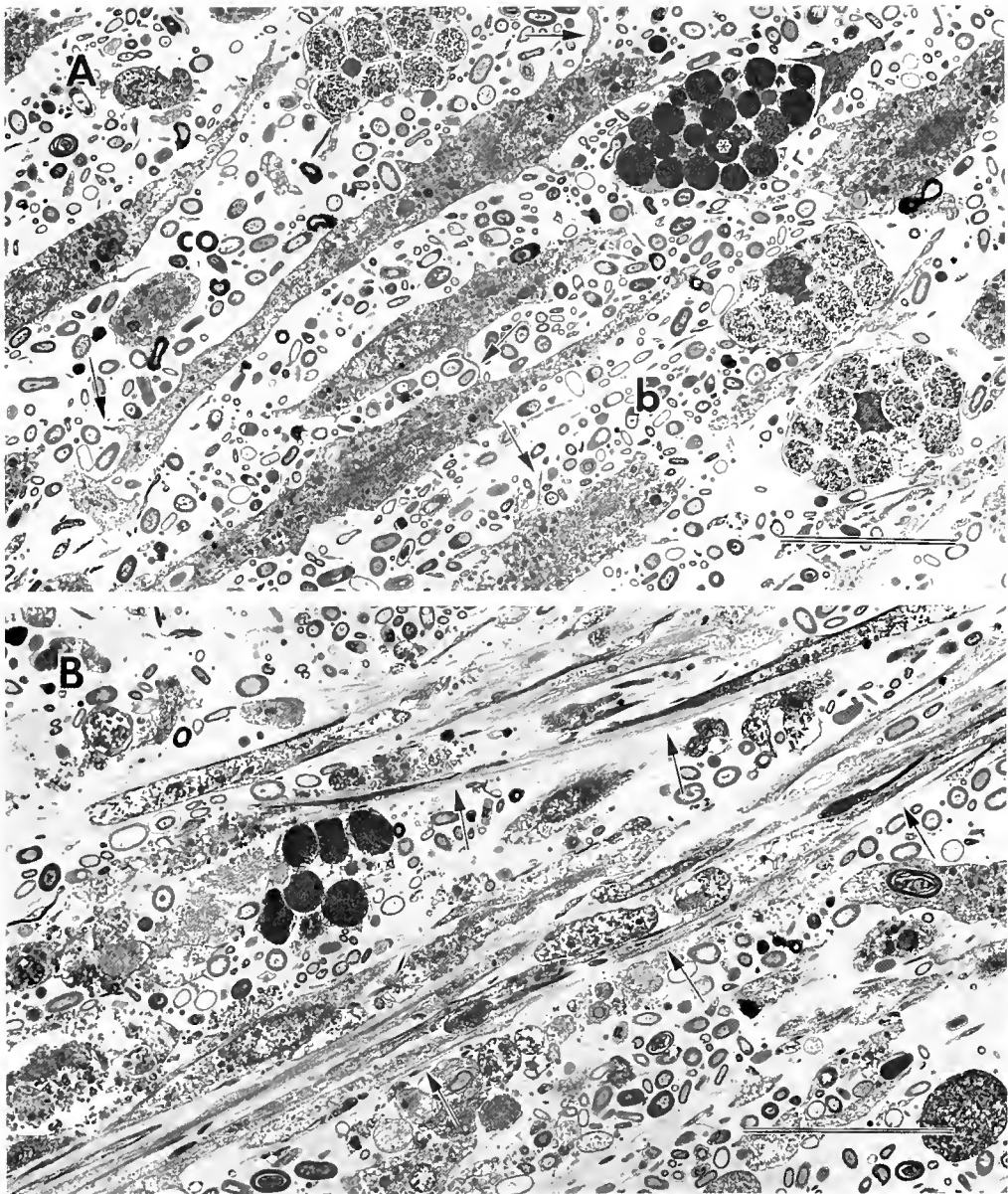


Figure 3. Longitudinal sections of tissue strands from *Aplysina cauliformis* (transmission electron microscopy). (A) A section showing several elongate cells with numerous filopodia (arrows). These cells lie lengthwise throughout the strand within a bacteria-filled (b) collagenous mesohyl (co). Other cells in the strands contain large inclusions of electron-dense material (*). Bar: 10 μ m. (B) Some cells in the tissue strands were highly elongate and were tightly aligned within dense bundles of collagen fibrils (arrows). Bar: 10 μ m.

6A: tip segment). However, 7 to 11 days after feeding, 95% of all the beads counted in the tip segment alone were in the strands (Fig. 7A). Many beads were found around the water canals in the lower segment in the feeding experiment. A week after feeding, 63% of the beads counted in the lower segment were found in the strands (Fig. 6A: lower segment).

Latex beads that were inserted into the sponge branches about 7 cm from the tip were transported predominantly

upward to the tip 2 weeks after insertion (Fig. 6B: tip segment); very few beads reached the segment of the sponge below the insertion point. One day after their insertion, the beads were abundant in the general tissue of the sponge in the middle segment, much as was found in the feeding experiment. After 3 days a large proportion of the beads were found at the edges of the water canals, and a few (5%) were in the tissue strands in the middle segment. Whereas the number of beads counted in the

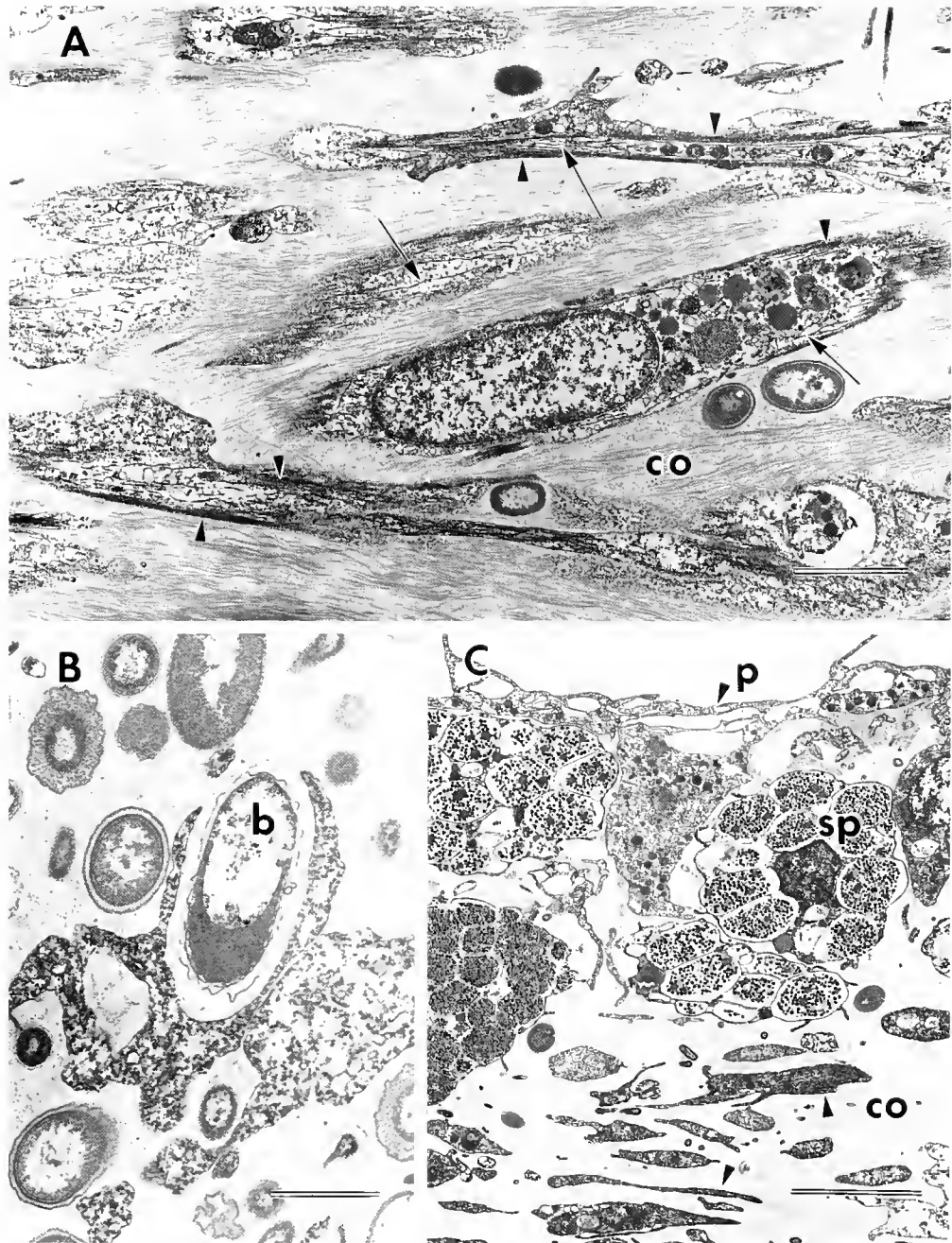


Figure 4. Aspects of the cell strands and the cortex of *Aplysina cauliformis* (transmission electron microscopy). (A) A higher magnification of cells among densely bundled collagen fibrils (co) in strands, showing bundles of electron-dense fibrils, which may be microfilaments (arrowheads), and of microtubules (arrows), in the cells. The microtubules were identified as such from their diameter in high magnification electron micrographs. Bar: 2 μm . (B) An example of a cell within a strand in the process of engulfing a bacterium (b) Bar: 1 μm . (C) The cortex of the sponge. Just inside the dermal layer or pinacoderm (p) are numerous spherulous cells (sp) with large inclusions, and individual elongate cells (arrowheads) lying in a collagenous mesohyl (co). These elongate cells are far shorter than those in the strands and are not in large tracts of aligned collagen fibrils. Bar: 5 μm .

middle segments declined toward the end of the second week, their number in the tip segment increased at this time. After 7 days, 42% of the beads counted in the tip

segment were in the strands; 13 days after feeding, however, most beads in the tip segment were in the tissue (Fig. 7B).

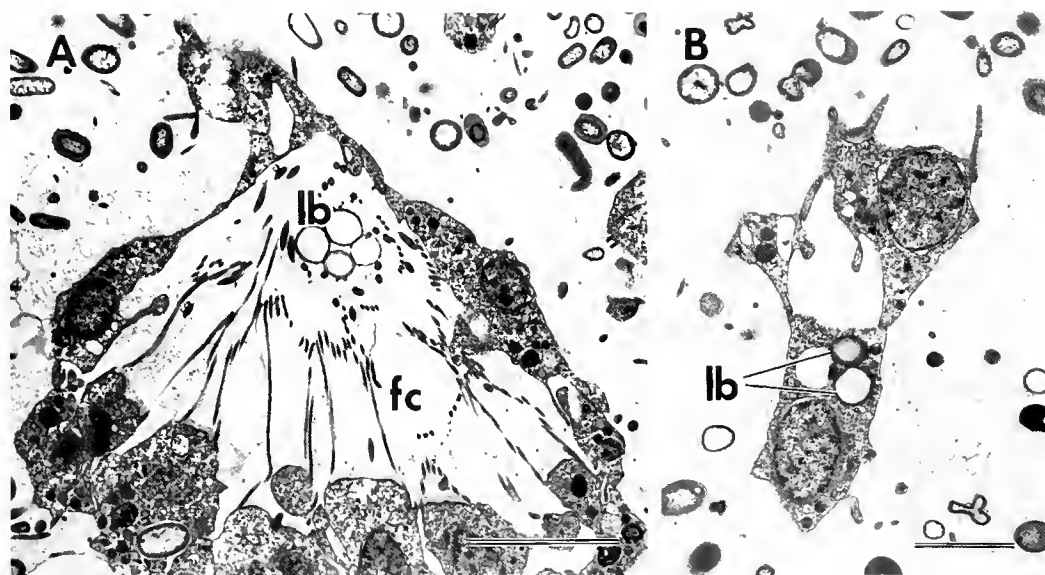


Figure 5. Latex bead uptake by *Aplysina cauliformis* (transmission electron microscopy). (A) Four hours after feeding, latex beads (lb) were found in flagellated chambers (fc) and (B) in ameboid cells in the mesohyl. Bar (A): 5 μm ; (B): 2 μm .

Video microscopy

Attempts to record movement of cells in the tissue strands of *Aplysina* were hampered by the opacity of the tissue strands; indeed, only cells at the edges of strands could be monitored by transmitted light microscopy. Consequently, strands that were exposed by cutting the sponge branch longitudinally were illuminated from above, and viewed at a low magnification with a 10 \times objective lens. The image was magnified by both the video camera and the digital image processor. With this system, highly refractile cells, which may correspond to the spherulous cells shown in Figure 3A, were the most conspicuous element in the strands; the movements of the smaller cells could not be monitored. The refractile cells showed no obvious movement as a group in either direction along the strand. Nevertheless, more than 2 h after filming began on the sponge, several individual cells definitely moved along the strand in both directions at rates of 0.025 $\mu\text{m} \cdot \text{s}^{-1}$ to 0.04 $\mu\text{m} \cdot \text{s}^{-1}$ ($n = 8$) (Fig. 8). Thus, the movement was probably not caused by contraction of the strand after wounding.

Discussion

Endosomal tissue strands have not been described in sponges other than the genus *Aplysina*, nor is there any record that a specialized structure is involved in the distribution of particulates in sponges. We have shown here, however, that when latex beads are fed to *A. cauliformis*, they are taken up and transported into the tissue strands; eventually they end up at the tip of the sponge or further down the stalk.

Sponges are well-known to have highly motile cells, whose rate of movement (2 to 21 $\text{mm} \cdot \text{day}^{-1}$; Bond, 1992)—although slower than that of crawling by *Amoeba*—is comparable to, and even faster than crawling by fibroblasts and neutrophils (Bray, 1992). Furthermore, at the growing edge of sponges, these cells (particularly those of a similar type) often become aligned in tracts (Bond and Harris, 1988). Similar tracts of cells, sometimes referred to as cell "cords," have been described in various demosponges where their suggested role has been in growth (Brien, 1976), regeneration (Lévi, 1960), and remodeling (Diaz, 1979). In each of these cases, the primary role of the cell cords was thought to be in skeletogenesis (Simpson, 1984), as demonstrated by Teragawa (1986) for the keratose sponge *Dysidea etheria*. However, none of these tracts or cords of cells is so permanent a structure within the sponge, nor so widespread and morphologically uniform within a genus, as the endosomal tissue strands in *Aplysina*. Nor can any of those tracts be so readily extracted from the rest of the tissue as can *Aplysina*'s tissue strands.

The bead uptake experiments here show that the strands are involved in transport of materials taken in during feeding. Most of the beads that were fed or inserted into the sponges were excreted within a week; relatively few ended up in the strands, which suggests that most of the food taken in by flagellated chambers and the adjacent pinacoderm is probably distributed to cells locally, and wastes are probably expelled from the same area. However, a role for the strands as transport pathways is supported by the observation that a substantial proportion of beads were in the strands in the tip segment 2 weeks after

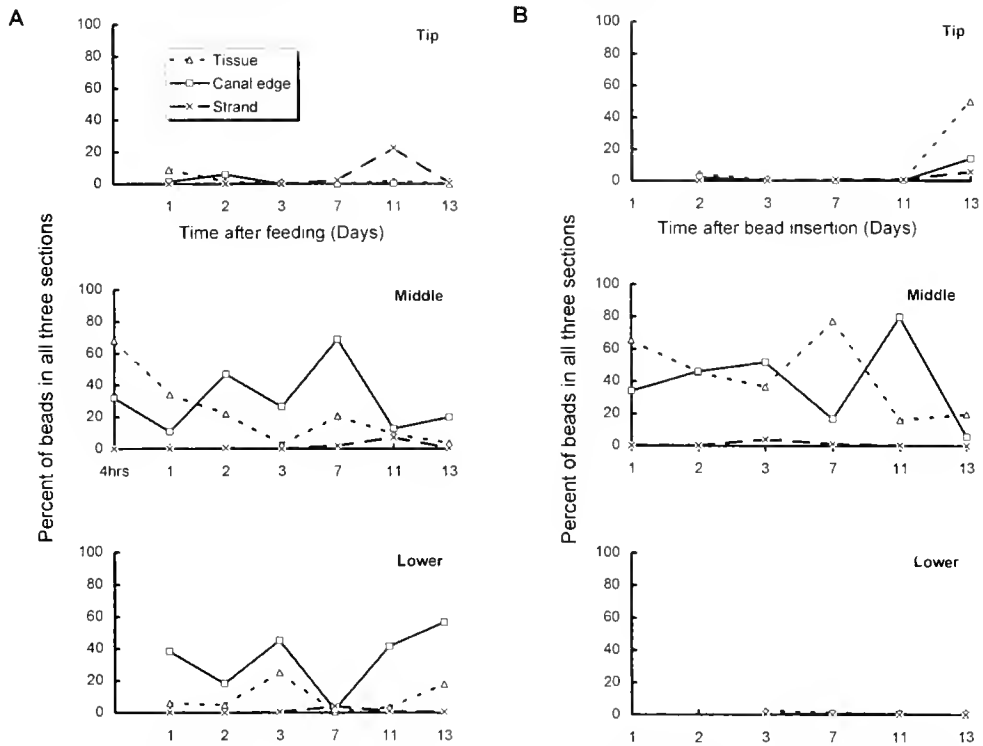


Figure 6. Latex bead experiments. Percent of the total number of beads counted in all sections of all three segments (Tip, Middle, and Lower) at each time interval, in the tissue (triangles), at the canal edges (squares), and in the strands (crosses): (A) feeding; (B) insertion. See text for explanation.

the middle portion of the sponge was fed. The beads found in the strands 2 days after the sponges were fed were far outnumbered by the beads counted around the

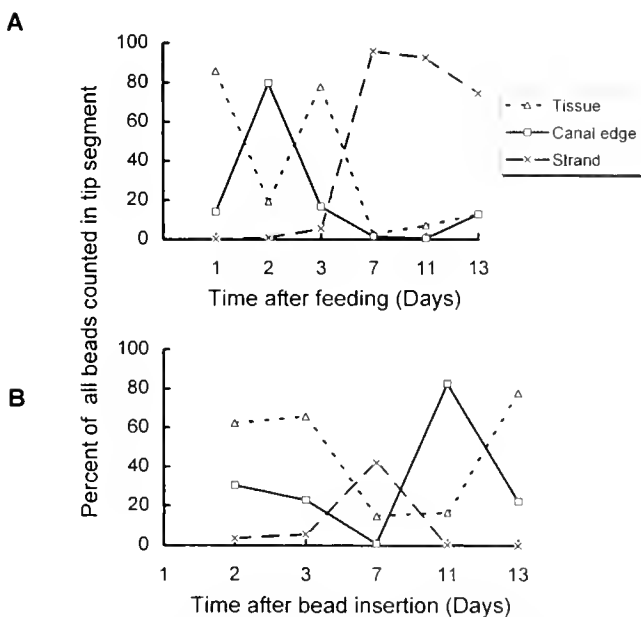


Figure 7. Latex bead experiments. Percent of all the beads counted in the tip segments only: (A) feeding; (B) insertion. See text for explanation.

canal edges or in the tissue (see Table 1). The delayed appearance of the beads in the tip segment 7 days after feeding is best explained by the time required for the cells transporting the beads to crawl first to the strands and then along the strands to the tip, where they accumulated. That downward transport also occurs is suggested by the number of beads found in strands in the lower segments a week after feeding, and later around the water canals. The beads found around the canal edges in the lower segment may have been transported down and then moved to the canals for excretion, or they may have been re-ingested after excretion from the middle section.

Aplysina fulva has been shown to grow rapidly, at an average rate of $2 \text{ cm} \cdot \text{month}^{-1}$ (minimum $0.2 \text{ cm} \cdot \text{month}^{-1}$, maximum $15 \text{ cm} \cdot \text{month}^{-1}$; calculated from Wulff, 1990). For this rate of growth, rapid translocation of materials to the tip would be necessary despite the ability of flagellated chambers at the tip to take in and distribute nutrients locally. Downward transport might supply regions of the sponge that possibly feed less and function primarily as a stalk. Video microscopy showed that individual cells moved within strands for distances of $30 \mu\text{m}$ or more at a rate of 2.2 to $3.5 \text{ mm} \cdot \text{day}^{-1}$. At this rate of movement, material could be transported 5 cm in 2 weeks, if transported more or less in a straight line. The large numbers of bacteria in the strand might support the energy require-

Table 1

The number of latex beads counted in the tissues, around the water canals, and in the strands of each segment of fed branches of *Aplysina cauliformis*

Collection period	Segment ^a	Number of beads			Total per segment	Total per day (all segments)	Percent of beads in each segment/day
		In each segment region ^b					
		Tissue	Canal edge	Strand			
day 1, 4 h	Middle	20,000	9,400	7	29,407	29,407	
day 1, 24 h	Lower	572	3,765	20	4,357	9,792	44.5
	Middle	3,348	1,060	6	4,414		45.1
	Tip	876	144	1	1,021		10.4
day 2	Lower	5,116	19,400	65	24,581	106,472	23.1
	Middle	23,400	49,950	548	73,898		69.4
	Tip	1,554	6,366	73	7,993		7.5
day 3	Lower	2,890	5,219	48	8,157	11,536	70.7
	Middle	319	3,042	0	3,361		29.1
	Tip	14	3	1	18		0.2
day 7	Lower	78	355	766	1,199	18,554	6.5
	Middle	3,806	12,753	346	16,905		91.1
	Tip	12	7	431	450		2.4
day 11	Lower	1,090	12,779	290	14,159	30,698	46.1
	Middle	2,843	3,914	2,212	8,969		29.2
	Tip	535	37	6,998	7,570		24.7
day 13	Lower	1,148	3,617	39	4,804	6,394	75.1
	Middle	247	1,274	30	1,551		24.3
	Tip	5	5	29	39		0.6

^a Lower, Middle, and Tip segments of each sponge branch fed latex beads.

^b Beads were counted in 10 sections from each segment of sponge (Lower, Middle, Tip) each day, and were noted as being in three regions of the segment: Tissue (flagellated chambers and associated tissues); Canal edge (cells specifically around the edges of water canals); and Strand (only within cell strands).

ments of so many moving cells, and this notion is substantiated by the ample phagocytosis of bacteria seen in cells in the tissue strands.

The presence of tissue strands in tube- and stick-forms of *Aplysina* suggests that the mechanism of transport is efficient for growth regardless of sponge form, and indeed has been maintained by at least four species in this genus. Whether more distantly related verongioid sponges also possess tissue strands or similar structures for nutrient transport or other functions is not known.

Feeding in sponges has been well-documented, and with the exception of the two examples cited in the introduction, the Cladorhizidae and the Hexactinellida, particle uptake in sponges occurs at the choanocytes in the flagellated chambers or at the pinacoderm-lined incurrent canals. Food is transferred *via* food vacuoles from the choanocytes to amebocytes, which deliver the nutrients locally to other cells, and wastes are excreted *via* the excurrent canals (Kilian, 1952; Weissenfels, 1976; Willenz, 1980; Imsieke, 1994). Directional translocation of cells and nutrients occurs in gemmule formation (Rasmont and de

Vos, 1974) and during oogenesis (Fell, 1983), but this transport occurs over very short distances. Hexactinellid sponges possess perhaps the longest transport pathway known in the Porifera, but translocation is intrasyncytial and occurs through a highly dynamic three-dimensional network of reticulated tissue, rather than along fixed pathways (Wyeth *et al.*, 1996; Leys, 1998).

Although sponges have not previously been shown to possess specific transport pathways for nutrients, all invertebrates have developed means of distributing nutrients. Many higher invertebrates such as ascidians, most echinoderms, and crustaceans have a well-developed fluid circulatory system with numerous types of hemocytes which, in addition to their many other functions, transport nutrients. Others invertebrates, however, move food around in a much slower manner: branching corals translocate nutrients to the tip of branches for tip growth (Buchsbbaum Pearse and Muscatine, 1971); gorgonians have cells that travel through the stem canals and solenia, a collagenous filled mesohyl, to deliver nutrients to the other tissues of the animal (Murdoch, 1978); fixed pan-

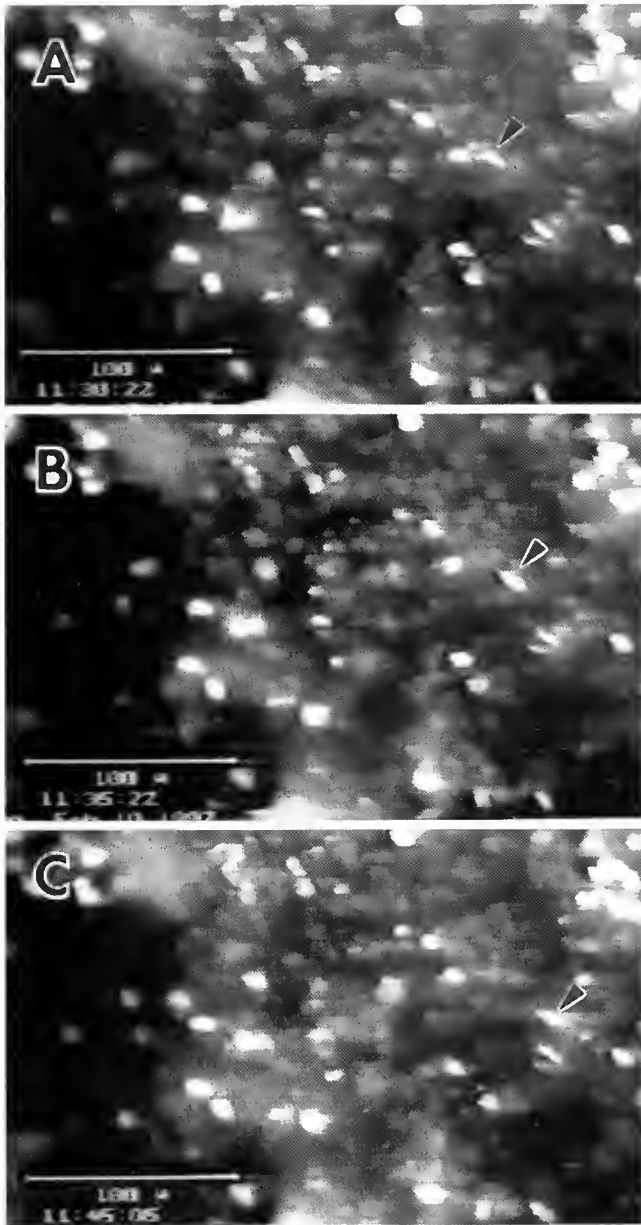


Figure 8. Cell movement in tissue strands (video microscopy). A highly refractile cell (arrowheads) was traced as it moved for $30\ \mu\text{m}$ along a tissue strand at $0.033\ \mu\text{m}\cdot\text{s}^{-1}$. Time of frames: (A) 0 min; (B) 5 min; (C) 15 min. Bar: $100\ \mu\text{m}$.

chymal cells in turbellarians are thought to act as a sort of stationary intracellular circulatory system (Pedersen, 1961); and acid phosphatase staining has shown that amoebocytes in the hemal lacuna of erinoids (again, a collagen-filled pathway) are involved in digestion and transport of nutrients (Heinzeller and Welsch, 1997).

We cannot rule out a role for the tissue strands in contracting the ostia and water canals to control water flow as suggested for the elongate cells in *Verongia* (Vacelet, 1966); nonetheless, there is little evidence to sup-

port this hypothesis. Although some cells in the strands have what appears to be a highly developed actin cytoskeleton, and the strands recoiled gently after being cut, none of the strands were wrapped around the water canals or ostia sufficiently to be able to reduce water flow if contracted. Furthermore, localized patches of elongate cells were present in valve- or sphincter-like structures around the water canal system, and these quite possibly function in controlling water flow through the sponge as suggested by Vacelet (1966), and by Reiswig (1971) for those sponges in which flow is not controlled by flagellar activity. The facts that video microscopy did not reveal all cells in the strands to be moving, and that not all cells in the strands are elongate, could also be taken as evidence against the transport hypothesis. But the thickness ($100\ \mu\text{m}$) of the strands allowed only a few cells at the edges of strands to be observed at high magnification by video microscopy. Despite the low magnification and use of epi-illumination, a few of the highly refractile cells could be clearly seen to travel for significant distances along the length of the strand.

It could also be true, however, that not all the cells in the strand transport material. Thin sections of the strands showed that only some cells in the strands had a highly developed actin cytoskeleton and were aligned along densely bundled collagen fibrils. Other cells were clearly elongate with filopodia at either end, but were not associated with the densely bundled collagen fibrils. Fibroblasts in culture orient themselves along grooves in culture dishes (Carter, 1967; Clark *et al.*, 1980), and on collagen substrates they take on a bipolar spindle morphology with filopodia at either end (Elsdale and Bard, 1972). Furthermore, Harris (1987) has demonstrated that the forces exerted by fibroblasts in culture are far greater than is necessary for cell crawling, and that the prime function of these cells is to bundle and align collagen to prepare the path for migratory cells (Stopak and Harris, 1982).

An analogous situation could exist in *Aplysina* strands. We suggest that the role of the highly elongate cells with a well-developed actin cytoskeleton is primarily to bundle and align the collagen fibrils, creating a pathway that cells transporting nutrients can recognize and follow, thereby allowing the rapid transport of materials either to the tip or to the base of the sponge (Fig. 9). In this fashion, apoplastic nutrient transport by amoeboid cells has become specialized in the genus *Aplysina* to the extent that these sponges have a differentiated structure that parallels fluid transport systems in other animals, but is a typically novel poriferan solution.

Acknowledgments

We thank the director and staff at the Bellairs Research Institute (BRI) of McGill University, in Barbados, for the use of facilities while we were conducting the field work

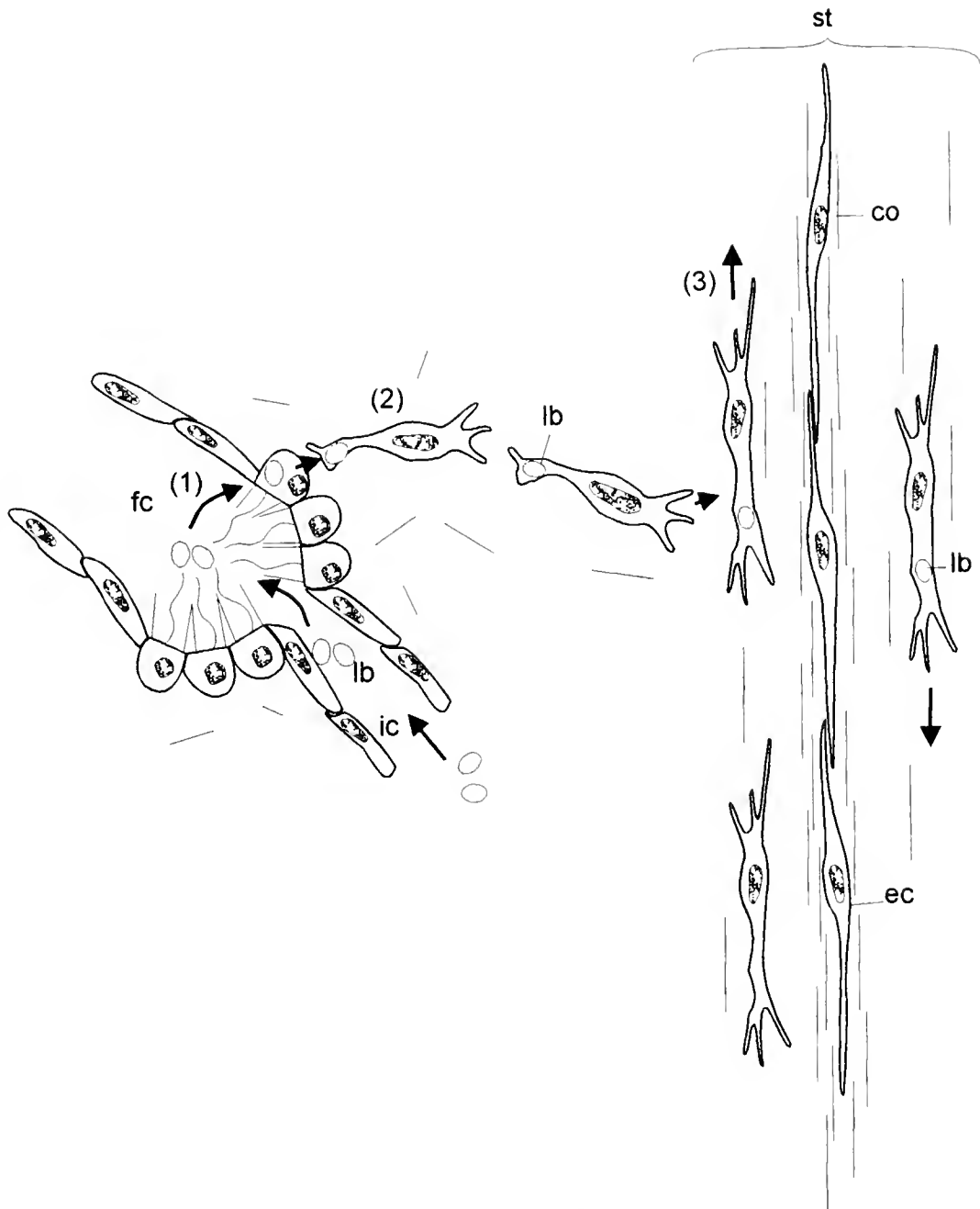


Figure 9. Diagram of the proposed route taken by latex beads (lb) that were fed to *Aplysina cauliformis*. Beads are taken in via the incurrent canals (ic) to the flagellated chambers (fc), where they are ingested (1) by choanocytes. The beads are then transferred to wandering amoebocytic cells (2), which encounter strands of elongate cells (ec) and highly bundled collagen fibrils (co). The amoebocytic cells follow the direction of the collagen, thereby transporting the latex beads up and down the strand (3) as shown by the arrows.

for this study. We also thank L. Verhegge, M. Tsurumi, and G. O. Mackie for comments on the manuscript. This research was supported by a Commander C. Bellairs Post-doctoral Fellowship from BRI and McGill University to SPL, and by a research grant from the Natural Science and Research Council of Canada (OGPOO 1427) to G.O.M.

Literature Cited

- Bergquist, P. R., P. Karuso, R. C. Cambie, and D. J. Smith. 1991. Sterol composition and classification of the Porifera. *Biochem. Syst. Ecol.* 19: 17–24.
- Bond, C. 1992. Continuous cell movements rearrange anatomical structures in intact sponges. *J. Exp. Zool.* 263: 284–302.

- Bond, C., and A. K. Harris. 1988. Locomotion of sponges and its physical mechanism. *J. Exp. Zool.* **246**: 271–284.
- Bray, D. 1992. *Cell Movements*. Garland, New York.
- Brien, P. 1976. La croissance des spongillidae. Formation des choanocytes et des spicules. *Bull. Biol. Fr. Belg.* **110**: 211–252.
- Buchsbaum Pearse, V., and L. Muscatine. 1971. Role of symbiotic algae (zooxanthellae) in coral calcification. *Biol. Bull.* **141**: 350–363.
- Carter, S. B. 1967. Haptotaxis and the mechanism of cell motility. *Nature* **213**: 256–260.
- Ciminiello, P., V. Costantino, E. Fattorusso, S. Magno, A. Mangoni, and M. Pansini. 1994. Chemistry of verongida sponges, II: Constituents of the Caribbean sponge *Aplysina fistularis* forma *Fulva*. *J. Nat. Prod.* **57**: 705–712.
- Ciminiello, P., E. Fattorusso, M. Forino, S. Magno, and M. Pansini. 1997. Chemistry of Verongida sponges VIII. Bromocompounds from the Mediterranean sponges *Aplysina aerophoba* and *Aplysina cavernicola*. *Tetrahedron* **53**: 6565–6572.
- Clark, P., P. Connolly, A. S. G. Curtis, and C. D. W. Wilkinson. 1980. Topographical control of cell behavior II. Multiple grooved substrata. *Development* **108**: 635–644.
- Diaz, J.-P. 1979. Variations, différenciations et fonctions des catégories cellulaires de la demosponge d'eaux saumâtres, *Suberite massa*, Nardo, au cours du cycle biologique annuel et dans des conditions expérimentales. Doctoral Thesis, Université des Sciences et Techniques du Languedoc, France. Pp. 167–169.
- Elsdale, T., and J. Bard. 1972. Collagen substrata for studies on cell behavior. *J. Cell Biol.* **54**: 626–637.
- Fell, P. E. 1983. Porifera. Pp. 1–29 in *Reproductive Biology of Invertebrates. Oogenesis, Oviposition, and Oosorption*, K. G. Adiyodi and R. G. Adiyodi, eds. John Wiley, Chichester.
- Harris, A. K. 1987. Cell motility and the problem of anatomical homeostasis. *J. Cell Sci. Suppl.* **8**: 121–140.
- Heinzeller, T., and U. Welsch. 1997. Crinoidea. Pp. 9–148 in *Microscopical Anatomy of Invertebrates*. F. W. Harrison and F.-S. Chia, eds. Wiley-Liss, New York.
- Imsieke, G. 1994. Ingestion and digestion of *Chlamydomonas reinhardtii* (Volvocales) by the freshwater sponge *Spongilla lacustris* (Spongillidae). Pp. 371–376 in *Sponges in Time and Space*. R. W. M. van Soest, T. M. G. van Kempen, and J.-C. Braekman, eds. A. A. Balkema, Rotterdam.
- Kilian, E. F. 1952. Wasserströmung und Nahrungsaufnahme beim Süßwasserschwamm *Ephydatia fluviatilis*. *Anschr. Vergleich. Physiol.* **34**: 407–447.
- Lévi, C. 1960. Reconstitution de l'éponge *Ophlitaspongia seriata* (Grant) à partir de suspensions cellulaires. *Cah. Biol. Mar.* **1**: 353–358.
- Lays, S. P. 1998. Fusion and cytoplasmic streaming are characteristics of at least two hexactinellids: examination of cultured tissue from *Aphrocallistes vastus*. Pp. 215–226 in *Sponge Sciences—Multidisciplinary Perspectives*. Y. Watanabe and N. Fusetani, eds. Springer-Verlag, Tokyo.
- Lays, S. P., and G. O. Mackie. 1997. Electrical recording from a glass sponge. *Nature* **387**: 29–31.
- Mackie, G. O., and C. L. Singla. 1983. Studies on hexactinellid sponges. I Histology of *Rhabdocalyptus dawsoni* (Lambe, 1873). *Philos. Trans. R. Soc. Lond. B* **301**: 365–400.
- Murdoch, G. R. 1978. Circulation and digestion of food in the gastrovascular cavity of gorgonian corals. *Bull. Mar. Sci.* **28**: 363–370.
- Pedersen, K. J. 1961. Studies on the nature of planarian connective tissue. *Z. Zellforsch. Mikrosk. Anat.* **53**: 569–608.
- Perez, T. 1996. La rétention de particules par une éponge hexactinellide, *Oopsacas minuta* (Leucopsacasidae): le rôle du réticulum. *C. R. Acad. Sci. Ser. III Sci. Vie* **319**: 385–391.
- Rasmont, R., and L. De Vos. 1974. Etude cinématographique de la gemmulation d'une éponge d'eau douce *Ephydatia fluviatilis*. *Arch. Biol.* **85**: 329–341.
- Reiswig, H. M. 1971. *In situ* pumping activities of tropical demospongiae. *Mar. Biol.* **9**: 38–50.
- Reiswig, H. M. 1979. Histology of hexactinellida (Porifera). *Colloq. Int. Cent. Natl. Rech. Sci.* **291**: 173–180.
- Reitner, J., and D. Mehl. 1995. Early paleozoic diversification of sponges: new data and evidences. *Geol. Palaont. Mitt. Innsbruck* **20**: 335–347.
- Simpson, T. L. 1984. *The Cell Biology of Sponges*. Springer Verlag, New York.
- Steiner, M., D. Mehl, J. Reitner, and B. D. Erdtmann. 1993. Oldest entirely preserved sponges and other fossils from the Lowermost Cambrian and new facies reconstruction of the Yangtze platform (China). *Beliner Geoviss. Abh.* **9**: 293–329.
- Stopak, D., and A. K. Harris. 1982. Connective tissue morphogenesis by fibroblast traction. *Dev. Biol.* **90**: 383–398.
- Teragawa, C. K. 1986. Sponge dermal membrane morphology: histology of cell-mediated particle transport during skeletal growth. *J. Morph.* **190**: 335–347.
- Tsurumi, M., and H. M. Reiswig. 1997. Sexual versus asexual reproduction in an oviparous rope-form sponge *Aplysina cauliformis* (Porifera; Verongida). *Invertebr. Repr. Dev.* **32**: 1–9.
- Vacelet, J. 1966. Les cellules contractiles de l'éponge cornée *Verongia cavernicola* Vacelet. *C. R. Acad. Sci. Paris* **263**: 1330–1332.
- Vacelet, J., and N. Boury-Esnault. 1995. Carnivorous sponges. *Nature* **373**: 333–335.
- Weissenfels, N. 1976. Bau und Funktion des Süßwasserschwamms *Ephydatia fluviatilis* L. (Porifera). III. Nahrungsaufnahme, Verdauung und Defäkation. *Zoomorphologie* **85**: 73–88.
- Willenz, P. 1980. Kinetic and morphological aspects of the particle ingestion by the freshwater sponge *Ephydatia fluviatilis*. Pp. 163–178 in *Nutrition in the Lower Metazoa*. D. C. Smith and Y. Tiffon, eds. Pergamon Press, Oxford.
- Wulff, J. L. 1990. Patterns and processes of size change in Caribbean demosponges of branching morphology. Pp. 425–435 in *New Perspectives in Sponge Biology*, K. Ruetzler, ed. Smithsonian Institution Press, Washington, DC.
- Wyeth, R. C., S. P. Lays, and G. O. Mackie. 1996. Use of sandwich cultures for the study of feeding in the hexactinellid sponge *Rhabdocalyptus dawsoni* (Lambe, 1892). *Acta Zool.* **77**: 227–232.

Calcium Speciation and Exchange Between Blood and Extrapallial Fluid of the Quahog *Mercenaria mercenaria* (L.)

P. SATISH NAIR AND WILLIAM E. ROBINSON*

*University of Massachusetts Boston, Environmental, Coastal and Ocean Sciences Department,
100 Morrissey Blvd., Boston, Massachusetts 02125-3393*

Abstract. Calcium and small organic molecules (*e.g.*, tyrosine, MW 181 Da) introduced into the extrapallial fluid (EPF) of the quahog *Mercenaria mercenaria* exhibit rapid fluxes across the outer mantle epithelium and are distributed throughout the circulatory system within 3 h. Larger molecules (*e.g.*, bovine serum albumin, MW 66,000 Da) are less readily exchanged between EPF and blood. The protein compositions of blood plasma and EPF are different, with at least seven protein bands expressed more prominently in the EPF. Equilibrium dialysis experiments reveal that Ca^{2+} constitutes only 2% of the total Ca in plasma; most of the Ca (85%) is bound to macromolecules, and the remaining 13% is present as dialyzable low molecular weight moieties. This distribution cannot be explained by speciation of inorganic Ca alone, since the MINTEQA2 equilibrium speciation model predicts that 79%–86% of the Ca should be present as Ca^{2+} , with the remainder as CaSO_4 (20%–13%). However, inclusion of a weakly Ca-binding organic molecule ($\log_{10} K_a \approx 2 M^{-1}$) into MINTEQA2 could fully reconcile modeling with experimental measurements. Results suggest that calcium transport in blood plasma and EPF is mediated by a suite of proteins and small organic ligands with a low affinity for Ca.

Introduction

A variety of invertebrates secrete CaCO_3 exoskeletons. Unraveling the mechanisms involved in these secretory processes requires an understanding of the microenviron-

ment within the compartment immediately adjacent to the site of CaCO_3 incorporation. The molluscan shell-formation system, for example, consists of a series of compartments, the most important of which are the inner shell surface, the extrapallial space, and the outer mantle epithelium (Crenshaw, 1980). Extrapallial fluid (EPF), a blood-like fluid contained in the extrapallial space, is considered to be the microenvironment for the deposition of shell (Wilbur, 1972; Marsh and Sass, 1983; Saha *et al.*, 1988) by an organic matrix-mediated process (Weiner, 1984; Wheeler *et al.*, 1988; Keith *et al.*, 1993). In bivalve molluscs, the muscular attachment of the mantle to the shell along the pallial line further divides the shell-forming compartment into two distinct zones. The marginal zone, outside the pallial line, is associated with the highest rate of shell deposition and contributes to increases in the height and length of the shell. The central zone, within the pallial line, is associated with both deposition (thickening) and redissolution of shell (Wheeler *et al.*, 1975; Hudson, 1992).

The EPFs associated with the marginal and central zones may have different chemical composition, in keeping with the functional differences between the two zones (Wilbur and Saleuddin, 1983). Studies on the composition of EPF have concentrated almost exclusively on the fluid from the central zone because the quantities of EPF available from the marginal zone are minuscule, making it difficult to obtain samples (Crenshaw, 1980). The central zone EPF contains a complex mixture of inorganic ions (Crenshaw, 1972a; Wada and Fujinuki, 1976) and organic components including amino acids, proteins, acid mucopolysaccharides, carbohydrates, and probably lipids (Misogianes and Chasteen, 1979; Marsh and Sass, 1983; Wilbur and Bernhardt, 1984). One or more of these com-

Received 20 August 1997; accepted 4 May 1998.

* Author to whom correspondence should be addressed. E-mail: robinsonw@umbksy.cc.umb.edu

ponents constitute the organic matrix, which in turn is considered to regulate CaCO_3 crystal nucleation, morphology, orientation, density, and growth (Wheeler and Sikes, 1984; Wheeler *et al.*, 1988; Kawaguchi and Watabe, 1993; Falini *et al.*, 1996).

Extrapallial fluid and blood are thought to be separate compartments, a conclusion based on differences in their inorganic composition (Crenshaw, 1972a). Nevertheless, inorganic ions in the EPF are probably derived from blood, while the origin of its organic constituents is still a matter of debate. The outer mantle epithelium is known to synthesize and secrete proteins, enzymes, and some organic matrix precursors into the EPF (Wilbur, 1972; Wheeler and Harrison, 1982; Saleuddin and Kunigelis, 1984; Bielefeld *et al.*, 1993; Miyamoto *et al.*, 1996). It is possible that some constituents are also synthesized elsewhere and transported into the EPF by the blood (Wilbur, 1972; Wilbur and Saleuddin, 1983). Little work has been done on the exchange of organic compounds between the blood and EPF of bivalves.

Ions involved in shell formation (Ca^{2+} , HCO_3^- , and CO_3^{2-}) are apparently freely exchanged between the EPF, the blood, and the external medium (Greenaway, 1971; Wilbur and Saleuddin, 1983). Fluxes of these ions between the EPF and blood are probably bidirectional, and occur through the outer mantle epithelium. Studies on calcium movement across the epithelia of various species indicate the existence of two major pathways, namely paracellular (Neff, 1972; Karbach, 1992; Bielefeld *et al.*, 1993; Newman and Robinson, unpubl. data) and transcellular routes. The latter uptake route involves Ca entry by simple diffusion (Sorenson *et al.*, 1980; Coimbra *et al.*, 1988), or through channels (Beirão *et al.*, 1989; Lucu, 1994), and subsequent intracellular transport by Ca-binding proteins (Bawden, 1989; Feher *et al.*, 1992), Ca vesicles (Jones and Davis, 1982; Akins and Tuan, 1993), or as calcareous concretions (Graf and Meyran, 1983; Ziegler, 1996). Transfer of Ca between the external medium and EPF has been examined *in vivo* (Crenshaw and Neff, 1969; Akberali, 1980; Dillaman and Ford, 1982), although *in vivo* demonstrations of exchanges between EPF and blood are lacking.

The present study was designed to investigate *in vivo* the exchange of Ca^{2+} and organic compounds between the central zone EPF and the blood of the bivalve *Mercenaria mercenaria* (L.). The speciation of Ca and the protein composition of blood plasma and EPF were examined in relation to this Ca exchange.

Materials and Methods

Mercenaria mercenaria (quahogs; length 65–75 mm) were purchased locally and maintained in glass aquaria filled with aerated Instant Ocean (30 PSU), at 10°C. They

were fed with mixed cultures of *Isochrysis galbana* and *Dunaliella tertiolecta* thrice weekly.

Circulation experiments

Exchange of radiolabeled compounds of different sizes between EPF and blood of the quahog were studied by a series of injection experiments. The compounds studied were the inorganic cation $^{45}\text{Ca}^{2+}$ (MW = 40 Da) as CaCl_2 , the free amino acid ^3H -tyrosine (MW = 181 Da), and the macromolecule ^{14}C -bovine serum albumin (BSA; MW = 66,000 Da). Each compound was introduced into the central zone extrapallial space of the right shell. Its redistribution was monitored by periodic sampling of the EPF from the left and right sides, and blood drawn from the anterior and posterior adductor muscles.

Access to the EPF was obtained by drilling through the central zone of the shell using a Dremel high-speed cutter with a circular burr. Powdered shell generated during the drilling was removed with a suction tube connected to a vacuum pump. Drilling was stopped just before the edge of the burr penetrated the inner shell surface, and the extrapallial space was exposed by gently teasing away the innermost nacreous layer with a needle.

Injections and EPF sample withdrawals were performed using a micro-syringe with a bent needle, taking care not to damage the underlying mantle tissue. The holes in the shell were sealed with hot glue immediately after injection or sampling. Blood samples from the anterior and posterior adductor muscles were withdrawn by inserting a micro-syringe needle between the shells. Just enough shell adjacent to the adductor muscles was removed to facilitate needle insertion. Typically, each experiment consisted of injecting 10 μl of radiolabel (Ca^{2+} = 1.9, tyrosine = 0.67, and BSA = 0.025 mCi/ml) and withdrawing 50 μl of sample at intervals over a period of 4–4.5 h. The injected volume was $\leq 0.05\%$ of the total blood volume, as determined from the relationship of shell length to blood volume for *M. mercenaria* (Robinson and Ryan, 1988).

Quahogs were held out of water during the duration of the experiment, then dissected and inspected for damage to mantle tissue. Samples from animals with damaged mantles were rejected. Blood and EPF samples thus collected were placed in borosilicate scintillation vials, mixed with 10 ml of scintillation fluid (Packard Hionic Fluor), and left overnight in the dark to reduce chemiluminescence. Radioactivity was counted using a Packard 1500 Tri-Carb liquid scintillation counter, corrected for background counts. In an additional experiment, cold BSA instead of ^{14}C -BSA was injected into quahogs (10 μl , 100 mg/ml), and EPF and blood samples were withdrawn at 3 h and 6 h. Those samples were analyzed by electrophoresis, as described below.

Calcium measurements

Shells of *M. mercenaria* ($n = 10$) were cracked and pried open to drain mantle cavity seawater (Robinson and Ryan, 1988). Whole blood was then collected by dissecting tissues from the shells and draining the tissues into an acid-cleaned Falcon tube over a 30-min period. Blood thus collected could be contaminated by very small amounts of EPF that had leaked through the damaged mantle. Cell-free plasma was obtained by centrifugation at $1750 \times g$ for 10 min. 'Total Ca' in the plasma was determined by the *o*-cresolphthalein complexone method (Kessler and Wolfman, 1964; Sigma Diagnostics procedure no. 587), with absorbance measured at 575 nm using a Kontron Uvikon spectrophotometer. Optical densities were converted to mM using a CaCO_3 standard curve, which was linear between 1 mM and 7 mM (detection limit = 0.3 mM).

'Free Ca' (Ca^{2+}) was measured using an Orion EA 910 specific ion meter fitted with an Orion 93-20 Ca ion-specific electrode (ISE) and 90-01 single junction reference electrode. A 5-ml sample was combined with 0.1 ml of ionic strength adjustor (4 M KCl), continuously stirred, and maintained at 4°C. Millivolt readings were converted to mM Ca^{2+} using a standard curve (mv vs. \log_{10} mM Ca^{2+}) prepared from CaCO_3 , which followed the Nernst equation and had a detection limit of 0.07 mM. 'Bound Ca' was defined as inorganic Ca compounds and Ca bound to organic ligands (calculated as the difference between total Ca and Ca^{2+}).

Dialysis experiments

Individual blood plasma samples (3 ml; $n = 10$) were dialyzed against 30 ml of oyster maintenance solution (Tripp *et al.*, 1966; prepared without Ca) in Spectra/Por-7 dialysis bags (MWCO 1000 Da). Dialysis was conducted at 10°C for 48 h on a rotary shaker (100 rpm). 'Dialyzable Ca' was defined as free Ca plus Ca bound to ligands <1000 Da, which would include low molecular weight organic compounds and inorganic Ca species. 'Nondialyzable Ca' was defined as Ca bound to ligands (primarily organic) >1000 Da. At the end of dialysis, concentrations of total Ca and free Ca were measured on samples withdrawn from inside the dialysis bags (dialyzable + nondialyzable Ca) and from the external solution (dialyzable Ca). Nondialyzable Ca concentration was calculated by subtraction.

Calcium speciation modeling

Results from dialysis experiments were compared to theoretical estimates of Ca speciation by using the equilibrium speciation model MINTQA2/PRODEFA2 (Allison *et al.*, 1991). Values for the molar concentration of the

major inorganic ions (Na^+ , K^+ , Ca^{2+} , Mg^{2+} , Cl^- , SO_4^{2-} , and total CO_2) in blood and EPF of *M. mercenaria* were obtained from Crenshaw (1972a). Since blood SO_4^{2-} and CO_2 concentrations were not available, the corresponding EPF values (Crenshaw, 1972a) were substituted as an approximation. The total CO_2 molarity provided by Crenshaw (1972a) was entered in the model as CO_3^{2-} . MINTQA2 was run using various permutations of the given concentrations to understand more clearly changes in Ca speciation with changing blood and EPF composition. This included adding a hypothetical Ca-binding protein to examine organic Ca speciation. The MINTQA2 model provided percentage distributions of free, inorganic, and organic Ca species formed under the given conditions.

Electrophoresis

Plasma and EPF were subjected to discontinuous SDS-polyacrylamide gel electrophoresis (SDS-PAGE) using the method of Laemmli (1970), with a 3% stacking and 7.5% resolving gel. Protein concentrations in the samples [plasma = 1.34 ± 0.15 mg/ml, $n = 5$; EPF = 0.97 ± 0.17 mg/ml, $n = 5$; determined by Bradford's (1976) dye binding method] were adjusted by dilution such that the amount of protein applied per lane was 40–60 μg . Stacking (100 V d.c.; 2 h) and resolving (200 V d.c.; 4 h) were carried out at 15°C. Gels were stained either with 0.1% Coomassie brilliant blue R-250 (Hames and Rickwood, 1981) or with a periodic acid-silver stain for glycoproteins, as described by Dubray and Bezard (1982). Protein molecular weights were determined by comparison with a standard mixture containing myosin (205 kDa), β -galactosidase (116 kDa), phosphorylase B (97.4 kDa), BSA (66 kDa), ovalbumin (45 kDa), and carbonic anhydrase (29 kDa).

Results

Quahogs injected with $^{45}\text{Ca}^{2+}$ and ^3H -tyrosine showed a progressive decrease in radioactive counts in the right shell EPF, the site of injection (Fig. 1a, b). Concentrations of both materials decreased 3 orders of magnitude over a period of 4 to 4.5 h. Samples of blood from the anterior and posterior adductor muscles and of EPF from the left shell exhibited a corresponding increase in $^{45}\text{Ca}^{2+}$ and ^3H -tyrosine counts. Counts from the four sampling points converged at approximately 3 h, indicating complete mixing of the introduced radiolabel with the blood. The high molecular weight BSA, on the other hand, showed less tendency to redistribute into the circulatory system (Fig. 1c). Although a decline in BSA concentration was observed in the right EPF, a difference of 3 orders of magnitude remained between counts at the point of injection and at the three other sampling sites at 4 h post-injection.

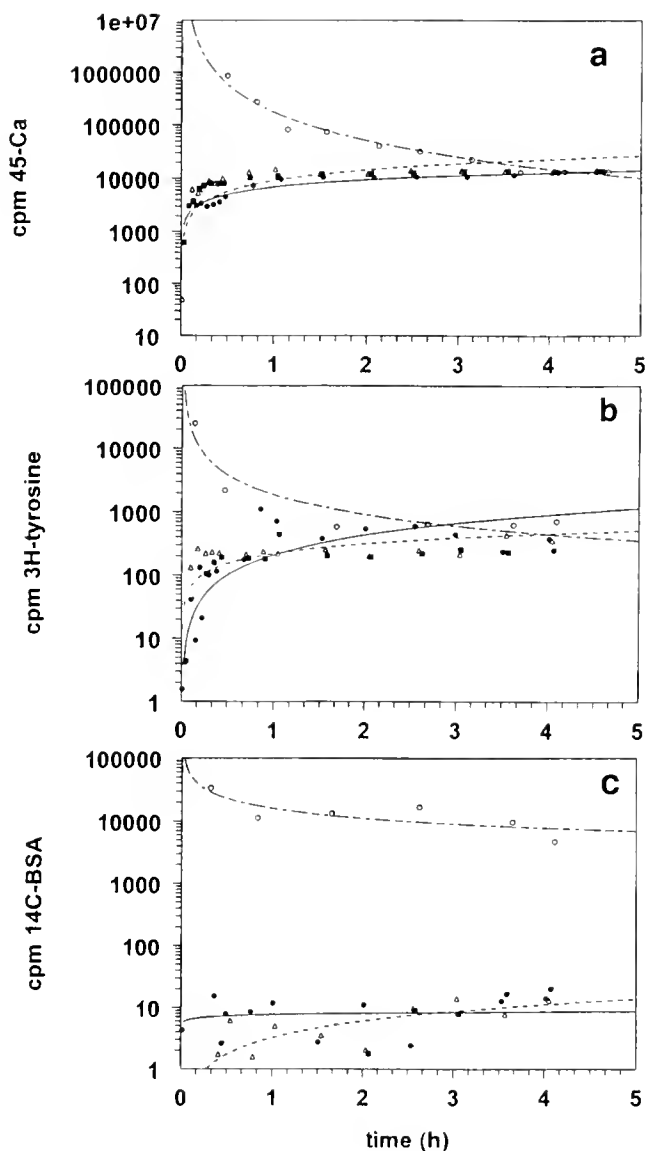


Figure 1. Radioactivity (cpm) in *Mercenaria mercenaria* extrapallial fluid (EPF) and blood following injection of (a) ^{45}Ca (MW = 40), (b) ^3H -tyrosine (MW = 181), and (c) ^{14}C -BSA (MW = 66 kDa) into the right shell EPF. Extrapallial fluid samples were drawn from the central zone of the right (—○—) and left (—●—) shells; blood samples were drawn from the anterior (—△—) and posterior (—■—) adductor muscles. Lines were drawn by a logarithmic-fit function using SlideWrite Plus[®] V4.0.

Furthermore, ^{14}C -BSA concentration in the left shell EPF appeared to remain constant over the 4-h period. The time required for the introduced BSA to become homogeneous with the blood was estimated to be at least 22 h.

A confirmatory experiment using nonlabeled BSA was performed to determine whether the BSA remained solubilized in EPF or became adsorbed to the mantle tissue during the course of the experiment. SDS-polyacrylamide gels of EPF and blood plasma showed that the 66-kDa

band of BSA was present only in the right shell EPF (the point of introduction) in samples taken 3 h and 6 h post-injection (results not shown). Staining intensities of the bands at 3 and 6 h were similar, indicating that the BSA was not bound to tissues. If BSA was present in the left shell EPF and in the plasma samples at 3 and 6 h, it was below the detection limits of SDS-PAGE.

The shapes of the semilog plots in Figure 1 indicate a rapid decrease in injected counts during the first 30 min, followed by a longer phase of gradual decline and attainment of an apparent steady state over the next 4–4.5 h. This suggests that the release of radiolabel from the EPF may be biphasic. Apparent depuration constants (k_{d2}) were calculated from the slopes of tangents to the initial and final portions of the plots. Depuration constants for the rapid phase (k_{d1}) were estimated as 9.7, 12.0, and 2.4 h^{-1} for ^{45}Ca , ^3H -tyrosine, and ^{14}C -BSA, respectively, whereas constants for the slow phase (k_{d2}) were 0.1, 0.08, and 0.04 h^{-1} . Biological half-lives calculated from the k_{d2} values were 6.9 h for ^{45}Ca , 8.7 h for ^3H -tyrosine, and 17.3 h for ^{14}C -BSA.

The mean concentration of total Ca measured in the blood plasma of 10 quahogs was $10.9 \pm 1.3 \text{ mM}$, of which $0.4 \pm 0.1 \text{ mM}$ was free Ca^{2+} . Bound Ca was estimated as $10.5 \pm 1.2 \text{ mM}$. Equilibrium dialysis of the plasma samples revealed that the majority of bound Ca (7.2 mM; Table I) was nondialyzable (*i.e.*, bound to ligands >1000 Da), but 1.1 mM was dialyzable, and 0.2 mM was free Ca. These concentrations reflect a 78% recovery of total Ca following dialysis; the remainder was presumably bound to the walls of the dialysis bags. Expressed as percentage of total Ca recovered, bound Ca (nondialyzable and dialyzable) and free Ca^{2+} amounted to 84.7, 12.9, and 2.4%, respectively (Table I).

Inorganic Ca speciation obtained by MINTQA2 predicted that a high proportion of plasma Ca should be present as free Ca^{2+} (78.9%; Table II, permutation 1), and the remainder as bound Ca (primarily CaSO_4 , 20.2%). However, this prediction is inconsistent with the values of 2.4% free Ca^{2+} and 12.9% bound-dialyzable Ca obtained by the dialysis experiments (Table I). If the SO_4^{2-} concentration used in model permutation 1 (46.1 mM, Crenshaw, 1972a) was replaced by the seawater SO_4^{2-} concentration (28.2 mM, Mantoura *et al.*, 1978), the distribution of CaSO_4 was reduced to 13.1% and 12.5% for plasma and EPF, respectively (Table II, permutation 2). The theoretical prediction of free Ca^{2+} (85.9% in plasma) was even further out of line with the measured Ca^{2+} concentrations.

Inclusion of Ca-binding organic ligands (*e.g.*, proteins) in the milieu is a way to reconcile this discrepancy with free Ca^{2+} . Serum albumin in vertebrate blood, for instance, binds free Ca with an affinity constant ($\log_{10} K_a$) of 2 M^{-1} and a binding capacity of 16 Ca ions per molecule

Table I

Distribution of calcium in *Mercenaria mercenaria* blood plasma

Ca	Concentrations in mM		Percentage of total Ca recovered	
	Nondialyzable	Dialyzable	Nondialyzable	Dialyzable
Bound*	7.2 ± 0.9	1.1 ± 0.2	84.7 ± 10.6	12.9 ± 2.4
Free (Ca ²⁺)†	nd	0.2	nd	2.4

Note: Values expressed as mean ± SD, $n = 10$. Results were obtained by equilibrium dialysis.

* Represents the difference between total Ca and free Ca²⁺.

† nd = not detected.

(Putnam, 1975). A hypothetical Ca-binding protein with 15 independent Ca-binding sites per molecule was included in the model, and the resulting Ca speciation was tested under a range of concentrations (0.1 to 100 mM protein) and affinity constants ($\log_{10} K_a = 2-6 M^{-1}$). Free Ca distributions of less than 2.5% were obtained in the 10–100 mM range at affinity constants 2 and 3 M^{-1} , and in the 0.1–10 mM range at K_a s 4–6 M^{-1} (Fig. 2). For instance, 60 mM protein with a $\log K_a$ of 2.1 M^{-1} resulted in 2.3% free Ca²⁺ and 96.7% Ca-protein complex in the plasma (Table II, permutation 3). If a 1:5 protein:Ca ratio were modeled, three times as much protein would be required to bind the same amount of Ca.

SDS-PAGE was carried out to compare the protein profiles of plasma and EPF. Seventeen distinct bands ranging in size from 30 to greater than 230 kDa could be detected in EPF by Coomassie brilliant blue staining (Fig. 3). Blood plasma, on the other hand, revealed 15 bands, 5 of which (MW = 157, 125, 42, 35, and 34 kDa) stained faintly but were detected by scanning densitometry (results not shown). Two prominent protein bands (MW = 74 and 51 kDa) were observed only in the EPF. These band patterns were consistent in samples from four quahogs, although the intensity of staining varied between animals. Four bands in the EPF (MW = 212, 157, 142,

and 74 kDa) and two in plasma (MW = 212 and 142 kDa) stained positive for glycoproteins by the highly sensitive periodic acid-silver staining technique.

Discussion

Results of the tyrosine circulation experiment indicate that small organic compounds, in the range of a few hundred daltons, are probably freely exchanged between the EPF and the blood. These compounds behave like Ca with respect to their rate of transport across the outer mantle epithelium. A size increase of about 2 orders of magnitude may, however, drastically limit the passage of a molecule across this epithelium. Bovine serum albumin (MW = 66 kDa), for example, was not rapidly redistributed with the blood. From the cold BSA injection experiment, it was apparent that BSA was retained in the EPF in solution, and not taken up by or bound to the outside of the underlying tissue. Similarly, the SDS-PAGE results identified two protein bands in the EPF (MW > 50 kDa) that were not detected in the plasma, indicating that the outer mantle epithelium contains an effective barrier to at least some high molecular weight proteins. These observations are consistent with those of Bielefeld *et al.* (1993), who found the outer mantle epithelium of the

Table II

Theoretical speciation of calcium in *Mercenaria mercenaria* blood plasma and extrapallial fluid

Model permutation*	Sample	Ca ²⁺	CaSO ₄	CaHCO ₃ ⁺	CaOH ⁺	Ca-Protein
1	Plasma	78.9	20.2	<0.9	trace	0
	EPF	85.9	19.3	<0.9	trace	0
2	Plasma	85.9	13.1	<0.9	trace	0
	EPF	86.5	12.5	<0.9	trace	0
3	Plasma	2.3	1.0	0	0	96.7
	EPF	2.2	0.9	0	0	96.9

Note: Values expressed as percentage of total calcium. Results were obtained using the equilibrium speciation model MINTEQA2 (Allison *et al.*, 1991).

* Permutations: (1) concentrations of inorganic ions taken from Crenshaw (1972a); (2) sulfate concentration decreased from 46.1 to 28.2 mM; (3) 60 mM of hypothetical Ca-binding protein (15:1 Ca:protein) with $\log_{10} K_a$ of 2.1 M^{-1} added.

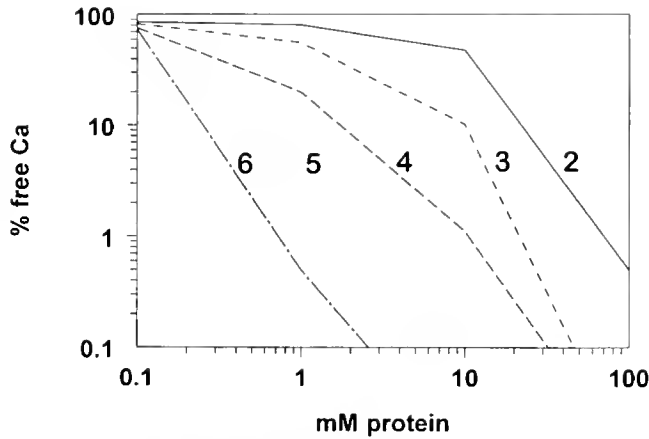


Figure 2. Percentage distribution of free Ca (ionic Ca^{2+}) in the blood plasma of *Mercenaria mercenaria* in the presence of a hypothetical Ca-binding protein with 15 Ca-binding sites. The lines represent a range of binding affinity constants tested ($\log_{10} K_a = 2-6 M^{-1}$). Data were generated using the equilibrium speciation model MINTEQA2 (Allison *et al.*, 1991).

snail *Biomphalaria glabrata* impermeable to injected horseradish peroxidase (MW = 40 kDa).

An important factor governing the direction of Ca flux across the outer mantle epithelium is anaerobiosis. Anaerobiosis induced upon shell closure is accompanied by redissolution of CaCO_3 from the shell to maintain a more uniform plasma pH through the bicarbonate buffering system (Crenshaw and Neff, 1969; Hudson, 1992; Littlewood and Young, 1994). This leads to a net Ca flux away from the central zone EPF. On the other hand, injury to the shell causes remobilization of Ca into the EPF. Calcium for shell repair is derived predominantly from the calcium cells of the mantle and foot (see Watabe, 1983), by dissolution of CaCO_3 and $\text{Ca}_3(\text{PO}_4)_2$ spherules. Because the quahogs in our experiments had damaged shells and were kept out of water for as long as 4.5 h, the 3-h timeframe for Ca exchange in this study probably reflected opposing Ca fluxes resulting from anaerobiosis and attempts at shell repair.

Other studies have found similar timeframes for Ca exchange in bivalves. ^{45}Ca introduced in the seawater took 2 h to reach a steady state with the mantle in *Argopecten irradians* (Wheeler *et al.*, 1975), and Crenshaw and Neff (1969) detected radioactivity in the EPF of *M. mercenaria* 2.75 h after ^{45}Ca was added to the seawater. *Scrobicularia plana* showed rapid shell dissolution about 2 h after the onset of salinity stress (Akberali, 1980). These results indicate that the timeframes involved in both inward Ca flux (for shell deposition and repair) and outward flux (for shell redissolution due to salinity and anaerobic stress) may be similar. The total Ca concentration for blood plasma found in this study (10.9 mM) is similar to

reported values for *M. mercenaria* (10.5 mM; Crenshaw, 1972a) and *Mytilus edulis* (12.6 mM; Bayne, 1976). Knowledge of total Ca concentrations, however, is of little value in understanding the processes involved in shell formation. These processes can only be inferred in light of Ca speciation (*i.e.*, the distribution of ionic Ca^{2+} , inorganic Ca species, and organically bound Ca chelates). Shell deposition in molluscs occurs only when Ca^{2+} and CO_3^{2-} are present in concentrations exceeding their solubility products (Wilbur and Saeluddin, 1983). Whereas CO_3^{2-} is derived from both the external medium and metabolic CO_2 (Dillaman and Ford, 1982), Ca must be obtained externally, and transported via the blood to the EPF. Different Ca species may be involved in each step of this process.

The MINTEQA2 model predicts the distribution of free and bound Ca in blood plasma as 78.9% and 21.1%, respectively. However, this prediction is inconsistent with the 2.4% free Ca and the 12.9% bound-dialyzable Ca obtained by the dialysis experiments. The model-derived figure of 20.2% CaSO_4 is probably an overestimate of inorganic Ca, because the SO_4^{2-} concentration (46.1 mM)

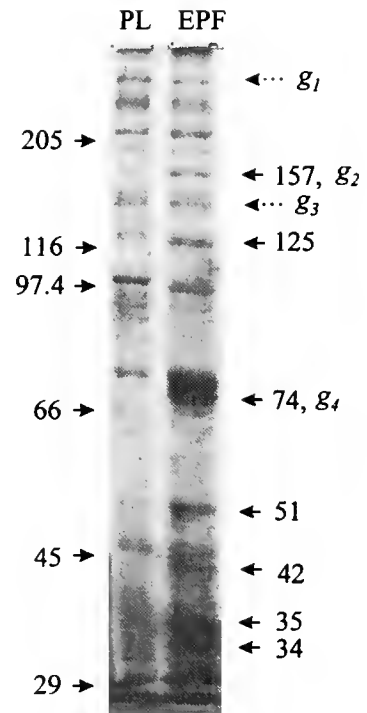


Figure 3. Comparison of *Mercenaria mercenaria* blood plasma (left lane) and extrapallial fluid (EPF; right lane) proteins ($\sim 50 \mu\text{g}/\text{lane}$) by 7.5% SDS-PAGE stained with Coomassie brilliant blue. The positions of molecular weight markers (kDa) are indicated on the left; 7 protein bands predominant in the EPF are marked on the right. Bands that stained positive as glycoproteins by periodic acid-silver staining are indicated as g_1-g_7 . Bands g_1 (212 kDa) and g_3 (142 kDa) were detected in both plasma and EPF.

reported by Crenshaw (1972a) was obtained by hydrolysis of ester sulfates, and therefore is at least partly organic in nature. Replacing Crenshaw's SO_4^{2-} concentration with that of seawater SO_4^{2-} reduces CaSO_4 to 13.1%, a figure almost identical (coincidentally) to the bound-dialyzable fraction. However, the high percentage of Ca^{2+} predicted by MINTEQA2 is still not explained.

It is apparent that inorganic speciation alone does not explain the very low percentage of free Ca^{2+} obtained experimentally. Calcium-binding organic ligands are the only species that can plausibly account for this difference. If analogous to vertebrate blood (Putnam, 1975; Scott and Bradwell, 1983), Ca-binding proteins in quahog plasma and EPF probably exhibit nonspecific, low-affinity binding with high binding capacities. Although the molar concentrations and affinity constants (K_a) of quahog Ca-binding proteins are not known, inclusion of a single protein (1:15 Ca binding, with a $\log K_a$ of $2.1 M^{-1}$) in the MINTEQA2 model resulted in free Ca distributions similar to those obtained by dialysis. Although the assumption of a single protein is simplistic, these binding characteristics compare well with Ca binding by serum albumin. Organic matrices of bivalve shells possess both somewhat high-affinity ($\log K_a = 4-5 M^{-1}$) and low-affinity ($\log K_a = 3-4 M^{-1}$) Ca-binding components (Wheeler and Sikes, 1984).

Interestingly, the contribution of SO_4^{2-} to Ca speciation became negligible whenever proteins were added and free Ca was reduced below 5%. This suggests that CaSO_4 is not a major Ca species in plasma and EPF, and that the 12.9% bound-dialyzable fraction obtained by dialysis consists primarily of low molecular weight organic Ca-binding ligands. Such ligands, including amino acid anions, carboxylate, salicylate, and ascorbate, are found in blood plasma, and are known to bind a variety of cations (May *et al.*, 1977). Taken together, these results indicate that *M. mercenaria* has a multi-component Ca transport system consisting of low molecular weight ligands as well as one or more proteins. This is consistent with a previous finding by Misogianes and Chasteen (1979) for *Mytilus edulis* EPF.

Because of the predominance of organically bound Ca in quahog plasma, one must wonder about the sequence of events following our injection of CaCl_2 into the EPF of the quahog. In all likelihood, the injected Ca was rapidly reportioned among a variety of inorganic and organic ligands, with most of the Ca binding to EPF proteins. Because similar proteins are also present in the plasma, any free Ca initially entering the plasma would also be bound to proteins, and subsequently equilibrated with tissue Ca. Calcium binding in EPF could actually be slightly greater or stronger than Ca binding to plasma proteins, because five proteins present in the EPF are not prominent in the plasma, and two are absent. The results of our gel

electrophoresis indicate that any EPF Ca-protein complexes with a molecular weight greater than about 30 kDa would translocate to the plasma slowly. Yet we observed a rapid flux of ^{45}Ca between the EPF and the plasma (with an apparent steady state established within 3 h). Therefore, the binding of Ca with these EPF proteins must be relatively weak, in agreement with MINTEQA2 modeling. Weak binding would allow a rapid exchange of Ca among all of the possible inorganic and organic species present in blood and EPF, and would explain how Ca can be translocated rapidly while the larger molecular weight proteins are exchanged much more slowly.

The prominent 157-kDa glycoprotein band seen in the EPF is similar in size to a 160-kDa protein isolated from the soluble shell matrix of *M. mercenaria* by Crenshaw (1972b). This matrix protein also stained positively with the glycoprotein-specific stains ponceau S and alcian blue, and is believed to bind Ca and help in CaCO_3 crystal nucleation. Similar calcium-binding proteins have been isolated from the EPF and shell matrices of other bivalves (Samata, 1990; Donachy *et al.*, 1992). Shell injury triggers the outer mantle epithelium to secrete glycoproteins, mucoproteins, and mucopolysaccharides into the EPF (Timmermans, 1973; Meenakshi *et al.*, 1975; Watabe, 1983). The 74- and 51-kDa protein bands we found exclusively in the EPF could represent components of these secretions.

In summary, the experiments conducted in this study demonstrate *in vivo* that Ca and small organic molecules are readily exchanged between the EPF and blood of *M. mercenaria*. The passage of macromolecules across the outer mantle epithelium is restricted, and extrapallial fluid and plasma differ in their protein compositions. Inorganic speciation modeling predicts that concentrations of free Ca^{2+} in plasma and EPF are vastly higher than those obtained experimentally. This discrepancy can be overcome by including organic ligands in Ca speciation models for both biological fluids. Most of the Ca in blood plasma and EPF is bound to macromolecules, and the remainder to small organic ligands. Calcium is transported by a system of one or more relatively weakly binding proteins and smaller organic molecules.

Acknowledgments

Research was funded by the National Institutes of Health grant RO3 RR08693-01. We thank two anonymous reviewers for their comments and helpful suggestions on the manuscript.

Literature Cited

- Akberali, H. B. 1980. ^{45}Ca uptake and dissolution in the shell of *Scrobicularia plana* (da Costa). *J. Exp. Mar. Biol. Ecol.* **43**: 1-9.

- Akins, E. A., and R. S. Tuan. 1993. Transepithelial calcium transport in the chick chorioallantoic membrane II. Compartmentalization of calcium during uptake. *J. Cell Sci.* **105**: 381–388.
- Allison, J. D., D. S. Brown, and K. J. Novo-Gradac. 1991. *MINTEQA2/PRODEFA2, a Geochemical Assessment Model for Environmental Systems*. U.S. EPA/600/3-91/021. Athens, Georgia.
- Bawden, J. W. 1989. Calcium transport during mineralization. *Anat. Rec.* **224**: 226–233.
- Bayne, B. L., ed. 1976. *Marine Mussels—Their Ecology and Physiology*. Cambridge University Press, Cambridge. 506 pp.
- Beirão, P. S., and J. H. M. Nascimento. 1989. Sodium- and calcium-dependent mechanisms on the action potential of the secretory epithelium of a clam mantle. *J. Exp. Biol.* **145**: 395–402.
- Bielefeld, U., K. H., Körtje, H. Rahmann, and W. Becker. 1993. The shell-forming mantle epithelium of *Biomphalaria glabrata* (Pulmonata): ultrastructure, permeability and cytochemistry. *J. Moll. Stud.* **59**: 323–338.
- Bradford, M. M. 1976. A rapid and sensitive method for the quantitation of microgram quantities of protein utilizing the principle of protein-dye binding. *Anal. Biochem.* **72**: 248–254.
- Coimbra, J., J. Machado, P. L. Fernandes, H. G. Ferreira, and K. G. Ferreira. 1988. Electrophysiology of the mantle of *Anodonta cygnea*. *J. Exp. Biol.* **140**: 65–88.
- Crenshaw, M. A. 1972a. The inorganic composition of molluscan extrapallial fluid. *Biol. Bull.* **143**: 506–512.
- Crenshaw, M. A. 1972b. The soluble matrix from *Mercenaria mercenaria* shell. *Biomimetalisation* **6**: 6–11.
- Crenshaw, M. A. 1980. Mechanisms of shell formation and dissolution. Pp. 115–132 in *Skeletal Growth of Aquatic Organisms*, D. C. Rhoads and R. A. Lutz, eds. Plenum Press, New York.
- Crenshaw, M. A., and J. M. Neff. 1969. Decalcification at the mantle-shell interface in molluscs. *Am. Zool.* **9**: 881–885.
- Dillaman, R. M., and S. E. Ford. 1982. Measurement of calcium carbonate deposition in molluscs by controlled etching of radioactively labeled shells. *Mar. Biol.* **66**: 133–143.
- Donachy, J. E., B. Drake, and C. S. Sikes. 1992. Sequence and atomic-force microscopy analysis of a matrix protein from the shell of the oyster *Crassostrea virginica*. *Mar. Biol.* **114**: 423–428.
- Dubray, G., and G. Bezar. 1982. A highly sensitive periodic acid-silver stain for 1,2-diol groups of glycoproteins and polysaccharides in polyacrylamide gels. *Anal. Biochem.* **199**: 325–329.
- Falini, G., S. Albeck, S. Weiner, and L. Addadi. 1996. Control of aragonite or calcite polymorphism by mollusc shell macromolecules. *Science* **271**: 67–69.
- Feber, J. J., C. S. Fullmer, and R. H. Wasserman. 1992. Role of facilitated diffusion of calcium by calbindin in intestinal calcium absorption. *Am. J. Physiol.* **262**: C517–C526.
- Graf, E., and J. C. Meyran. 1983. Premolt calcium secretion in mid-gut posterior caeca of the crustacean *Orchestia*: ultrastructure of the epithelium. *J. Morphol.* **177**: 1–23.
- Greenaway, P. 1971. Calcium regulation in the freshwater mollusc *Limnaea stagnalis* (L.) (Gastropoda: Pulmonata). II. Calcium movements between internal calcium compartments. *J. Exp. Biol.* **54**: 609–620.
- Hames, B. D., and D. Rickwood. 1981. *Gel Electrophoresis of Proteins: A Practical Approach*. IRL Press, Oxford. 290 pp.
- Hudson, R. L. 1992. Ion transport by the isolated mantle epithelium of the freshwater clam, *Unio complanatus*. *Am. J. Physiol.* **263**: R76–R83.
- Jones, R. G., and W. L. Davis. 1982. Calcium-containing lysosomes in the outer mantle epithelial cells of *Anblema*, a fresh-water mollusc. *Anat. Rec.* **203**: 337–343.
- Karbach, U. 1992. Paracellular calcium transport across the small intestine. *J. Nutr.* **122**: 672–677.
- Kawaguchi, T., and N. Watabe. 1993. The organic matrices of the shell of the American oyster *Crassostrea virginica* Gmelin. *J. Exp. Mar. Biol. Ecol.* **170**: 11–28.
- Keith, J., S. Stockwell, D. Ball, K. Renillard, D. Kaplan, T. Thannhauser, and R. Sherwood. 1993. Comparative analysis of macromolecules in mollusc shells. *Comp. Biochem. Physiol.* **105B**: 487–496.
- Kessler, G., and M. Wolfman. 1964. An automated procedure for the simultaneous determination of calcium and phosphorous. *Clin. Chem.* **10**: 686–687.
- Laemmli, U. K. 1970. Cleavage of structural proteins during the assembly of the head of bacteriophage T4. *Nature* **227**: 680–685.
- Littlewood, D. T. J., and R. E. Young. 1994. The effect of air-gaping behaviour on extrapallial fluid pH in the tropical oyster *Crassostrea rhizophorae*. *Comp. Biochem. Physiol.* **107A**: 1–6.
- Luca, C. 1994. Calcium transport across isolated gill epithelium of *Carcinus*. *J. Exp. Zool.* **268**: 339–346.
- Mantoura, R. F. C., A. Dickson, and J. P. Riley. 1978. The complexation of metals with humic materials in natural waters. *Estuarine Coastal Mar. Sci.* **6**: 387–408.
- Marsh, M. E., and R. L. Sass. 1983. Calcium-binding phosphoprotein particles in the extrapallial fluid and innermost lamella of clams. *J. Exp. Zool.* **226**: 193–203.
- May, P. M., P. W. Linder, and D. R. Williams. 1977. Computer simulation of metal-ion equilibria in biofluids: models for the low-molecular-weight complex distribution of calcium (II), magnesium (II), manganese (II), iron (II), copper (II), zinc (II), and lead (II) ions in human blood plasma. *J. Chem. Soc. Dalton Trans.* **6**: 588–595.
- Meenakshi, V. R., P. L. Blackwelder, P. E. Hare, K. M. Wilbur, and N. Watabe. 1975. Studies on shell regeneration—I. Matrix and mineral composition of the normal and regenerated shell of *Pomacea paludosa*. *Comp. Biochem. Physiol.* **50A**: 347–351.
- Misogianes, M. J., and N. D. Chasteen. 1979. Extrapallial fluid: a chemical and spectral characterization of the extrapallial fluid of *Mytilus edulis*. *Anal. Biochem.* **100**: 324–334.
- Miyamoto, H., T. Miyashita, M. Okushima, S. Nakano, T. Morita, and A. Matsushiro. 1996. A carbonic anhydrase from the nacreous layer in oyster pearls. *Proc. Natl. Acad. Sci. USA* **93**: 9657–9660.
- Neff, J. M. 1972. Ultrastructure of the outer epithelium of the mantle in the clam *Mercenaria mercenaria* in relation to calcification of the shell. *Tissue Cell* **4**: 591–600.
- Putnam, F. W. 1975. *The Plasma Proteins: Structure, Function, and Genetic Control*. Vol. 2. Academic Press, New York. 423 pp.
- Robinson, W. E., and D. K. Ryan. 1988. Transport of cadmium and other metals in the blood of the bivalve mollusc *Mercenaria mercenaria*. *Mar. Biol.* **97**: 101–109.
- Saha, A., T. K. Jana, and A. Choudhury. 1988. The extrapallial fluid of *Macoma birninnica*: an environment for calcium carbonate deposition. *Philipp. J. Sci.* **117**: 395–399.
- Saleuddin, A. S. M., and S. C. Kuniyelis. 1984. Neuroendocrine control mechanisms in shell formation. *Am. Zool.* **24**: 911–916.
- Samata, T. 1990. Ca-binding glycoproteins in molluscan shells with different types of ultrastructure. *Veliger* **33**: 190–201.
- Scott, B. J., and A. R. Bradwell. 1983. Identification of the serum binding proteins for iron, zinc, cadmium, nickel and calcium. *Clin. Chem.* **29**: 629–633.
- Sorenson, A. K., D. S. Wood, and L. B. Kirschner. 1980. Electrophysiological properties of resting secretory membranes of lamelli-branch mantles. *J. Gen. Physiol.* **75**: 21–37.
- Timmermans, L. P. 1973. Mantle activity following shell injury to the pond snail, *Limnaea stagnalis* L. *Malacologia* **14**: 53–61.

- Tripp, M. R., L. A. Bisignani, and M. T. Kenny. 1966.** Oyster amoebocytes *in vitro*. *J. Invert. Path.* **8**: 137-140.
- Wada, K., and T. Fujinuki. 1976.** Biomineralization in bivalve molluscs with emphasis on the chemical composition of the extrapallial fluid. Pp. 175-190 in *The Mechanisms of Mineralization in the Invertebrates and Plants*, N. Watabe and K. M. Wilbur, eds. University of South Carolina Press, Columbia.
- Watabe, N. 1983.** Shell repair. Pp. 289-316 in *The Mollusca*, vol. 4, A. S. M. Saleuddin and K. M. Wilbur, eds. Academic Press, New York.
- Weiner, S. 1984.** Organization of organic matrix components in mineralized tissues. *Am. Zool.* **24**: 945-951.
- Wheeler, A. P., and E. W. Harrison. 1982.** Subcellular localization and characterization of HCO_3^- -ATPase from the mantle of the freshwater clam, *Anodonta cataracta*. *Comp. Biochem. Physiol.* **71B**: 629-636.
- Wheeler, A. P., and C. S. Sikes. 1984.** Regulation of carbonate calcification by organic matrix. *Am. Zool.* **24**: 933-944.
- Wheeler, A. P., P. L. Blackwelder, and K. M. Wilbur. 1975.** Shell growth in the scallop *Argopecten irradians*. I: Isotope incorporation with reference to diurnal growth. *Biol. Bull.* **148**: 472-482.
- Wheeler, A. P., K. W. Rusenko, D. M. Swift, and C. S. Sikes. 1988.** Regulation of *in vitro* and *in vivo* CaCO_3 crystallization by fractions of oyster shell organic matrix. *Mar. Biol.* **98**: 71-80.
- Wilbur, K. M. 1972.** Shell formation in molluscs. Pp. 103-145 in *Chemical Zoology*, vol. VII, M. Florkin and B. T. Scheer, eds. Academic Press, New York.
- Wilbur, K. M., and A. M. Bernhardt. 1984.** Effects of amino acids, magnesium, and molluscan extrapallial fluid on crystallization of calcium carbonate: *in vitro* experiments. *Biol. Bull.* **166**: 251-259.
- Wilbur, K. M., and A. S. M. Saleuddin. 1983.** Shell formation. Pp. 235-287 in *The Mollusca*, vol. 4, A. S. M. Saleuddin and K. M. Wilbur, eds. Academic Press, New York.
- Ziegler, A. 1996.** Ultrastructural evidence for transepithelial calcium transport in the anterior sternal epithelium of the terrestrial isopod *Porcellio scaber* (Crustacea) during the formation and resorption of CaCO_3 deposits. *Cell Tissue Res.* **284**: 459-466.

Induction of Extra Claws on the Chelipeds of a Crayfish, *Procambarus clarkii*

ISAMU NAKATANI^{1*}, YOSHINORI OKADA², AND TAKUJI KITAHARA¹

¹Department of Biology, Faculty of Science, Yamagata University, Yamagata 990-8560, Japan;

²Department of Biology, Faculty of Science, Okayama University, Okayama 700-8530, Japan

Abstract. In a crayfish, *Procambarus clarkii*, growth of an extra claw was induced by making a V-shaped wound in the proximal end of the propodus of the second and third chelipeds. Two nerve bundles were damaged by the wounding. Some type of extra growth developed on the propodi of 13 of the damaged chelipeds: a pair of extra claws (2 chelipeds), a pair of extra dactyls (1 cheliped), a single extra dactyl (2 chelipeds), and a single slight projection (8 chelipeds). The extra claws and dactyls developed from the peripheral side of the propodus away from the wound site. One of a pair of extra dactyls and the single extra dactyls could be moved only slightly, either manually or by the crayfish. The other extra dactyls could be moved by the crayfish. Muscles were associated with each of the extra and primary claws. The muscles attached to the double extra claw or dactyl were innervated by nerve bundles that were branches from the primary thick nerve bundles. One possible explanation for these findings is that the severed nerve fibers in the thick nerve bundles regenerate, elongate into aberrant roots, and form extra claws or dactyls.

Introduction

The occurrence of double claws has been observed in the past. They have been reported to occur naturally on the cheliped of the American lobster, *Homarus americanus*, from the primary propodus near the dactyl (Faxon, 1881) and from the base of the primary propodus (Cole, 1910). In the crayfish, *Procambarus clarkii*, extra claws have been reported to occur naturally on the first and third chelipeds (Nakatani *et al.*, 1997). Both of these extra

claws developed from the base of the primary propodus. These crayfish were not able to move the dactyls of the extra claws, although they could be moved manually. Nerve bundles were observed to branch from the primary thick nerve bundles into the extra claw on the third cheliped (Nakatani *et al.*, 1997).

Lateral outgrowths on the first cheliped of crayfish can be induced by wounding. In one study (Murayama *et al.*, 1994), outgrowths developed in about 10% of wounded chelipeds. This percentage was increased to 61.9% by increasing the width and depth of the wound and removing the tissue in the wounded area (Nakatani, 1996). Many of these outgrowths have serrations and hooks. However, there is no articulation between the primary propodus and the new structure. These structures, hereafter called "lateral outgrowths," may be distinguished from an extra claw or extra dactyl by the absence of an articulation.

The objectives of the present study were to induce the growth of extra claws and to investigate the degree of movement and innervation of the extra growth.

Materials and Methods

The experimental crayfish

Crayfish (*Procambarus clarkii*) of both sexes were collected, without regard to molting stage, from ponds in the suburbs of Yamagata City, Yamagata, Japan. The length of the carapace varied from 15.2 to 36.6 mm. We used both intact and eyestalk-ectomized specimens because eyestalk removal promotes growth and decreases molt interval (Fingerman and Fingerman, 1974; Nakatani and Otsu, 1979; 1981; Suzuki, 1980).

Wounds

The dorsal side of the base of the propodus of the second and third chelipeds was wounded using small scis-

Received 1 August 1997; accepted 7 May 1998.

* To whom correspondence should be addressed. E-mail: nakatani@sci.kj.yamagata-u.ac.jp

sors. The V-shaped incision was made to a depth of about half the width of the base of the propodus (Fig. 1). The ventro-median tissues were destroyed by inserting a needle (1 mm in diameter) into the wound. In 34 crayfish, a total of 134 chelipeds were wounded. Both eyestalks of five of the crayfish were removed from the base 10 to 20 days post-operation.

Rearing wounded crayfish

From September 1996 to March 1997, the wounded crayfish were reared until they had molted two or three times. The animals were kept separately in individual containers (300 × 240 × 105 mm) under a natural photoperiod at room temperature (18°–26°C). Prawn pellets (Super B; Nihon Nosan Industry, Japan) and dry persimmon leaves were placed in the rearing containers so that the crayfish could feed on them *ad libitum*.

Sensory neuron responses

A cheliped with extra dactyls was cut off at the base of the merus and held on a glass slide by rubber bands. The exoskeleton at the base of the merus was removed and the nerve bundles were exposed. To detect responses from the sensory neurons, the point of a needle was used to push the extra dactyls in a closing direction. Action potentials from the exposed nerve bundles were recorded extracellularly, using suction electrodes.

Mechanical force exerted by closure of dactyls

Measurements were taken on the force exerted by closing the dactyls. The cheliped with double extra dactyls was cut off at the base of the merus and prepared as described above. Nerve bundles were stimulated using a pair of tungsten hook electrodes. Repetitive pulses (single pulse, 10 ms in duration; 20 Hz) were applied for 0.5–2 s to hook electrodes connected to an electronic stimulator (SEN1101; Nihon Kohden, Japan). The mechanical force exerted by closure of each of the two dactyls was recorded

simultaneously with a thermal array recorder (TRA1100; Nihon Kohden) via a high-gain force-displacement transducer (SB-1T-H; Nihon Kohden) coupled mechanically to the tip of the dactyl by a silk thread filament.

The sensory nerve responses and mechanical force were recorded at room temperature (23°–28°C).

Observations on nerve bundles and muscles

Observations were made on the nerve bundles and muscles of the propodus. The exoskeletons of the propodus and carpus of the above-mentioned chelipeds were removed, and nerve bundles and muscles were exposed and placed in physiological solution for crustaceans (van Harreveld, 1936). The nerve bundles were stained with a 0.005% solution of methylene blue dissolved in physiological solution and were observed under a dissecting microscope. The stained chelipeds were then fixed overnight at 0°C in a 20% formalin solution acidified to pH 3.8 with an acetate buffer. The muscles were observed with a dissecting microscope and a polarizing light microscope (BHSP, Olympus, Japan).

Results

Development of extra structures

Data on extra structure development are shown in Table I. Most of the chelipeds healed normally, but 13 (9.7%) formed extra structures. A pair of claws, a pair of dactyls, and single dactyls developed from the side away from the wound, and single, slight projections developed at the wound. These projections ranged in size from 0.3 to 1.8 mm at the second or third post-operation molt. Because extra structures developed at such a low frequency, we cannot draw any conclusions about the effect of eyestalk removal on their development.

Morphology of extra claws

A pair of extra claws that developed on one of the damaged chelipeds is shown in Figure 2. Here, the dactyl and pollex were torn off at the first post-operation molt. However, a pair of projections 0.6-mm long developed on the remaining untorn part (arrowheads in Fig. 2A). Two extra claws appeared on the propodus near the primary dactyl, and the primary dactyl and pollex regenerated at the second molt. The lengths of the three dactyls (Fig. 2B, a, b, c) and the single contralateral dactyl were 0.5, 1.9, 1.7, and 3.3 mm, respectively.

The three claws elongated at the third molt, and the shape of each claw was normal. There was no boundary among the propodi of these claws. The lengths of these three dactyls (Fig. 2C, a, b, c) and the single contralateral dactyl were 2.9, 3.7, 3.7, and 4.4 mm, respectively.

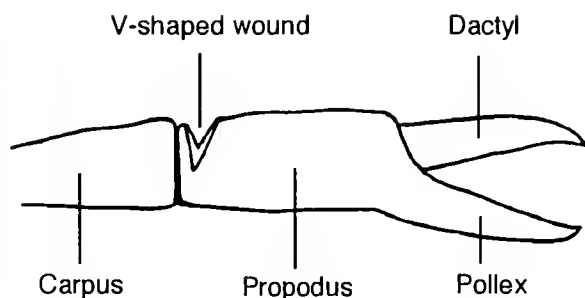


Figure 1. Diagram of the second cheliped of the crayfish showing V-shaped wound at the base of the propodus.

Table 1

Summary of wounding experiment in the crayfish *Procambarus clarkii* (values represent number of chelipeds)

	Wounded ¹	Autotomized ²	Developed extra structures ³				Healed normally ⁴
			Double		Single		
			Claws	Dactyls	Dactyl	Projection	
Eyestalks							
With	114	10	1	1	1	8	93
Without	20	1	1	0	1	0	17

¹ A total of 134 chelipeds from 34 crayfish received a V-shaped incision. After 10 to 20 days, both eyestalks were removed from 5 of the animals (20 chelipeds).

² Some animals autotomized chelipeds post-operatively.

³ Extra structures developed in 13 chelipeds.

⁴ Most of the chelipeds healed normally, with no outgrowths.

Morphology of a pair of extra dactyls

Two dactyls appeared on one of the chelipeds of a crayfish with eyestalks. The V-shaped wound seemed to have healed normally at the first molt. However, extra dactyls appeared on the right second cheliped at the second molt (Fig. 3, a, b). The extra dactyls developed on the primary propodus near the primary dactyl, although the wound was made at the base of the propodus. The primary claw was angled about 45° to the left of the propodus near the primary dactyl. The angle of the extra dactyls and the primary claw was about 90°. The extra dactyls a and b of Figure 3 are hereafter called "extra dactyl a" and "extra dactyl b," respectively. The lengths of the carapace, extra dactyls a and b, and primary and contralateral dactyls were 39.5, 2.9, 3.1, 5.1, and 3.1 mm, respectively.

Morphology of single extra dactyl

A single extra dactyl that developed on the propodus of the second right cheliped at the second molt is shown in Figure 4. The extra dactyl was located between the base of the primary propodus and the base of the primary dactyl. The extra and primary dactyls were 2.0- and 3.7-mm long, respectively.

Movement of the extra and primary dactyls

In the example shown in Figure 2, the crayfish could move the primary dactyl but not the two extra dactyls at the second molt. Extra claw b was usually in an open position, but opened readily when it was closed manually. After the third molt, the crayfish could move the extra and primary dactyls. It always moved these three dactyls asynchronously and often spontaneously moved the primary dactyl synchronously with extra dactyl b. These

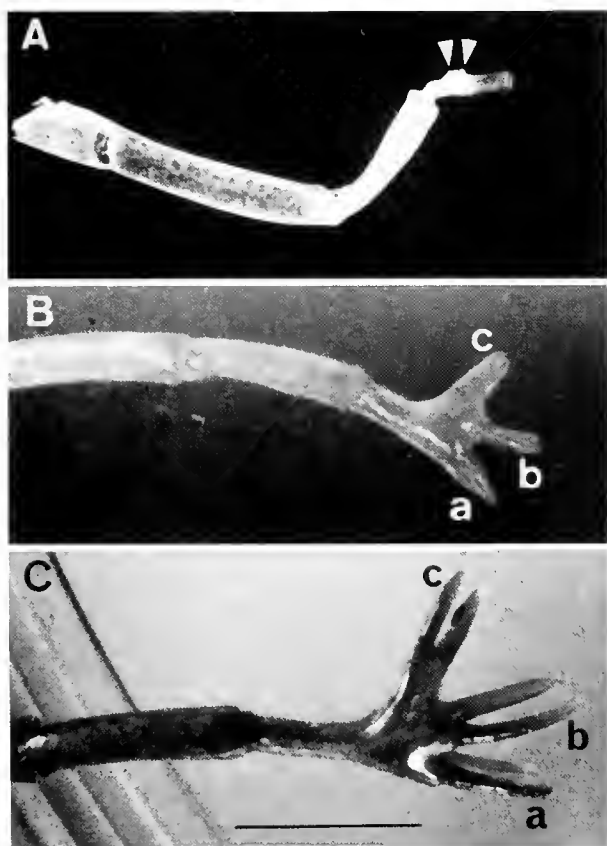


Figure 2. Development of extra claws on the third cheliped of the crayfish after a wound was made in the propodus. Both eyestalks were removed at the base on day 11 after wounding. (A) Two projections 0.6-mm long (arrowheads) developed on the propodus, but the dactyl and pollex were torn off at the first post-operation molt. (B) The projections developed into two poor claws at the second molt, and the untorn remaining part regenerated the dactyl and pollex. (C) The claws developed fully at the third molt. A and B, the castoff exuvia after the second and third molts, respectively. a, primary claw; b and c, extra claws. Bar = 5.0 mm.

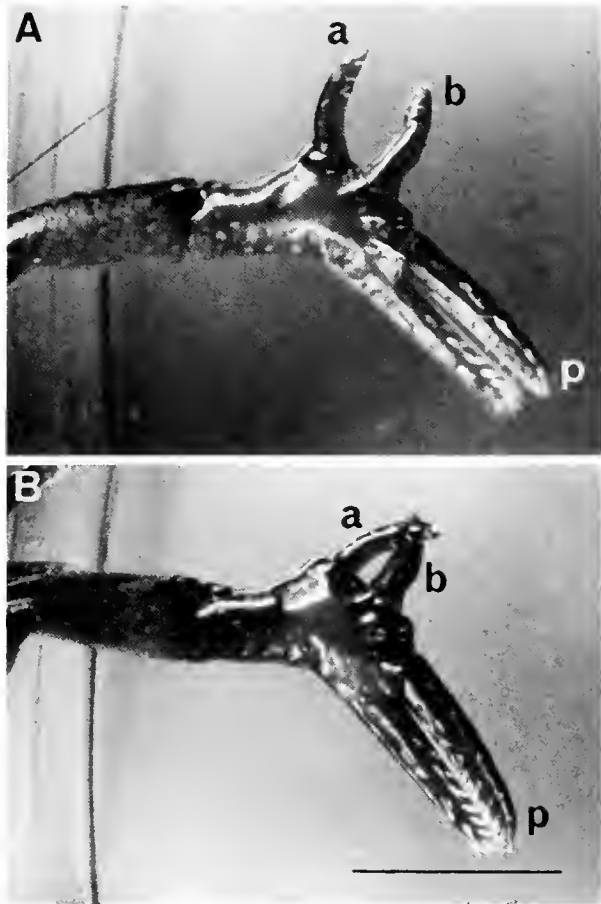


Figure 3. Two extra dactyls on the right second cheliped produced after the propodus was wounded. (A) Extra dactyls in the open state. (B) Extra dactyls in the closed state. a and b, extra dactyls; p, primary dactyl. Bar = 5.0 mm.

three dactyls would move synchronously when one of them was touched.

In the diagram shown in Figure 3, the crayfish could move the extra dactyls and the primary dactyl. When it was picked up, it moved the extra dactyl a more frequently than the primary dactyl. However, it moved these dactyls simultaneously if one of them was touched. The single extra dactyl in Figure 4 and extra dactyl b in Figure 3 could be moved only slightly, either manually or by the crayfish.

Muscles and innervation

Muscles were observed to correspond to each claw in the propodus. In view of their locations, these muscles could control the opening and closing of the three claws. The closer muscles are shown in Figure 5A.

Four muscles in the propodus with two extra dactyls (Fig. 3) were dissected out as shown in Figure 6B. In this figure, muscles m1, m2, m3, and m4 are the closer muscle

of the primary dactyl, the closer muscles of extra dactyls b and a, and the opener muscle of extra dactyl a, respectively. The mean (\pm standard error of the mean) lengths of 10 sarcomeres of each of these muscles after being fixed with formalin solution were 6.4 ± 0.3 , 6.2 ± 0.3 , 7.7 ± 0.4 , and $5.8 \pm 0.5 \mu\text{m}$.

There were two thick nerve bundles in the intact propodus of the second cheliped (Fig. 6A); one ran toward its dactyl along the boundary between the opener and closer muscles; the other ran to its pollex along the closer muscle. The extra dactyls shown in Figure 3 were innervated with nerve bundles from the primary nerve trunks. A thick nerve bundle ran toward the primary dactyl between the two closer muscles (Fig. 6B, m2 and m3) of the extra dactyls. At the proximal part of the propodus, the nerve bundle ran between the closer muscle of the primary dactyl (m1) and the opener muscle of the extra dactyl a (m4) (Fig. 6B, C).

In a propodus with two extra claws, the nerve bundles branched to each claw from the primary nerve trunk (Fig. 5B).

Extracellular recording

An extracellular recording was made from the nerve bundle at the merus of the cheliped with two extra dactyls. The neuron in the nerve bundle responded to the push toward closing of extra dactyl b (Fig. 7). However, the neuron did not generate action potentials when the dactyl moved in the opposite direction. Therefore this response might be the action potential from proprioceptors.

Mechanical force generated by dactyl movement

The mechanical force generated by the movement of the primary and extra dactyls in response to electrical



Figure 4. A single extra dactyl that developed on the right second cheliped. Both eyestalks were removed on day 12 after the cheliped was damaged. The arrowhead shows an articulation. Bar = 5.0 mm.

stimulation of the nerve bundle in the merus was measured. The force generated by the primary dactyl was about 8- and 3-fold greater than that generated by extra dactyls a and b, respectively (Fig. 8). The primary dactyl moved spontaneously and asynchronously with the extra dactyls just before the electrical stimuli were applied to the nerve bundles (Fig. 8A, A').

Discussion

There have been previous reports of double extra claws developing from the carpus (Bateson, 1894) and coxa (Przibram, 1921) of the crayfish (*Astacus fluviatilis*) and from the propodus of the cheliped of lobster (*Homarus americanus*) (Cole, 1910). Recently, two extra claws that

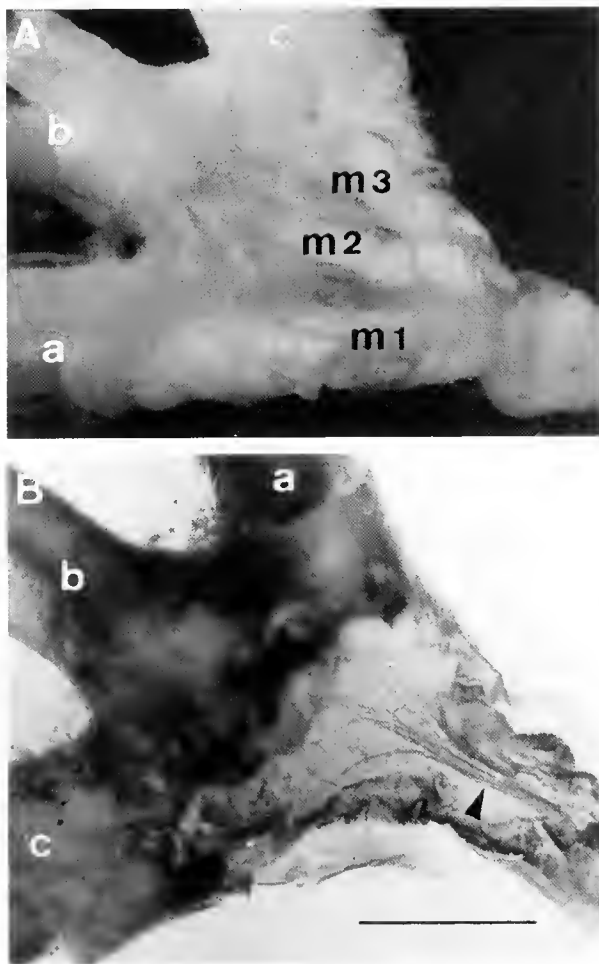


Figure 5. Innervation and muscles in the propodus of a cheliped with two induced extra claws. The cheliped is the same as that shown in Figure 2C. (A) Muscles corresponding to each claw (dorsal view). (B) The nerve trunks in the primary propodus branch, and each branched nerve bundle innervates a claw (ventral view). a, primary claw; b and c, extra claws; m1, m2, and m3, closer muscles associated with the primary claw (a) and extra claws (b, c), respectively. Arrowhead shows the nerve trunks. Bar = 1.0 mm.

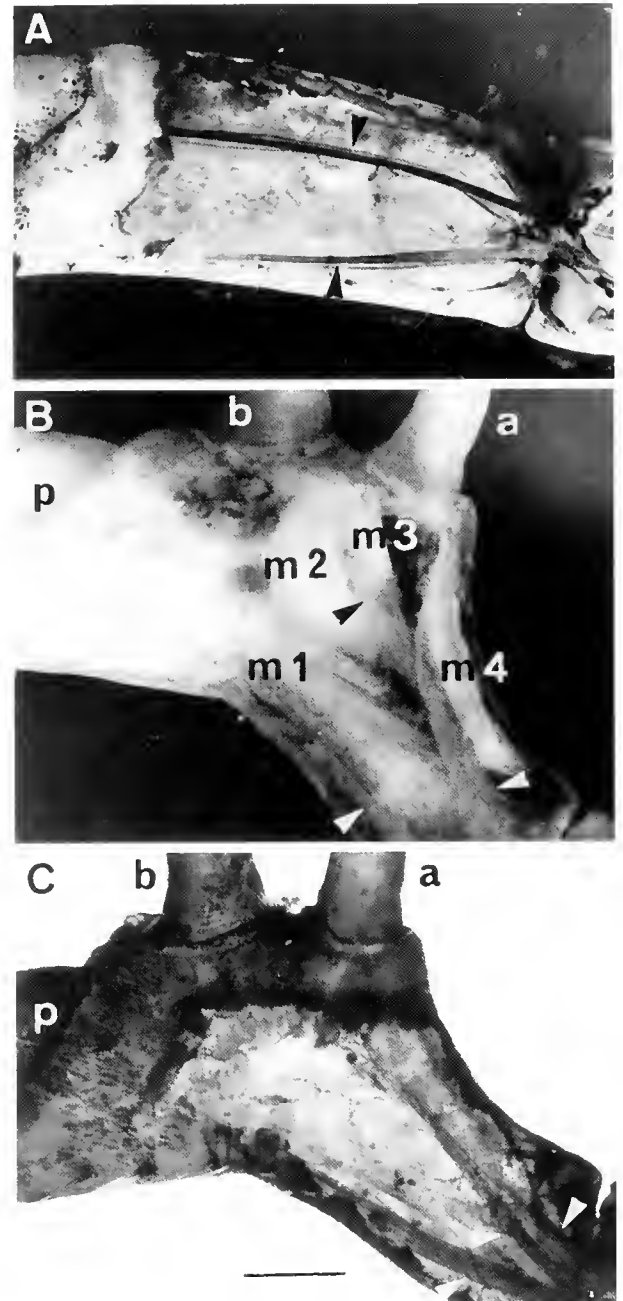


Figure 6. Innervation and muscles in a propodus with double extra dactyl and in a normal cheliped. The cheliped with extra dactyls is the same as that shown in Figure 3. (A) Two nerve bundles (arrowheads) in the propodus of the second cheliped. (B and C) Branched nerve bundles from the primary nerve trunks (arrowheads) innervate the extra dactyls. m1, closer muscle of the primary claw; m2 and m3, closer muscles of the extra dactyls b and a, respectively; m4, opener muscle of the extra dactyl a. a, b, and p are extra dactyl a, extra dactyl b, and primary dactyl, respectively. Bar = 1.0 mm.

developed naturally in *P. clarkii* were described (Nakatani *et al.*, 1997). These single claws were borne on the first and third chelipeds—one on each propodus. The extra



Figure 7. Extracellular recording from nerve trunks in the merus of a cheliped with extra dactyls. Thick bar signifies manual closing of the extra dactyl shown in Figure 3.

claws induced in the present study are essentially similar to those naturally occurring ones. The naturally occurring extra claws reported by Cole (1910) and Nakatani *et al.* (1997) developed from the base of the primary propodus. Lateral outgrowths from experimental incisions developed from the wounded site on the outer surface of the propodus (Murayama *et al.*, 1994; Nakatani, 1996). Thus, in the present study, the wound was made at the base of the propodus. However, all of the extra claws or extra dactyls developed on the distal side of the wound. This suggests that the extra claws reported by Cole (1910) and

Nakatani *et al.* (1997) were caused by damage at a site more proximal to the extra claw—for example, at the carpus.

Although there were no extra propodi, the shape and location of the a pair of extra dactyls observed in this study were similar to those of the naturally occurring one reported by Faxon (1881) on the cheliped of *H. americanus*. As in the present study, these extra claws developed away from the base of the propodus. The propodi of the extra claws described by Faxon were about one-sixth as long as the extra dactyls, and each was separated from its primary propodus by an articulation.

Lateral outgrowths on chelipeds have been assumed to result from the abnormal healing of a natural wound (Suzuki and Odawara, 1971; Shelton *et al.*, 1981; Okamoto, 1991; Nakatani *et al.*, 1992). Many of those outgrowths consisted of a pair of projections without any articulation. The proximal and distal surfaces of the wound each developed one projection, and they faced each other as mirror images (Nakatani, 1996). However, in the present study, the extra dactyls developed away from the damaged site. Different mechanisms may be involved in the development of a lateral outgrowth and of an extra claw or dactyl. In the propodus it was observed that one nerve trunk runs in the direction of the pollex and another to the dactyl.

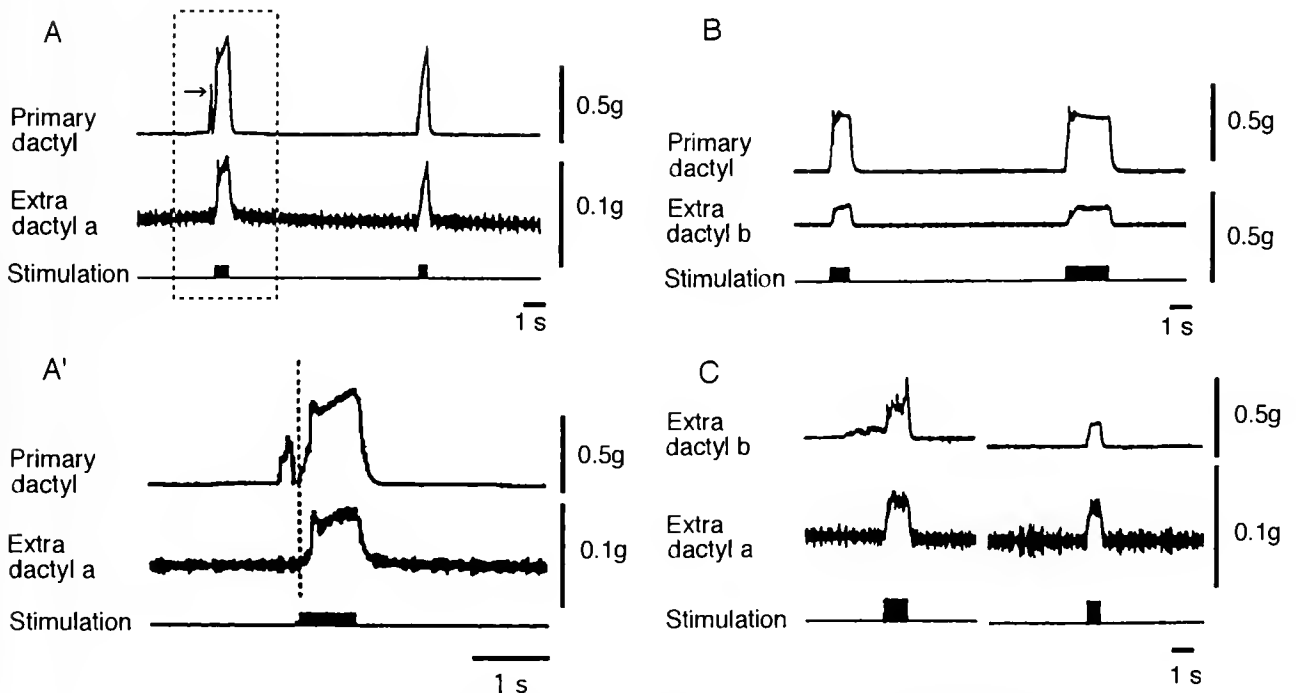


Figure 8. Movements of the primary and extra dactyls. The movements generated by each of two of three dactyls were recorded simultaneously when repetitive pulses (single pulse, 10 ms in duration; 20 Hz) were applied to the nerve trunks in the merus, which was monitored in each bottom trace. The same cheliped shown in Figure 3 was used. A', the time-scale for enclosed part with broken line in A was magnified 4-fold.

Lateral outgrowths were induced by wound damage of the nerve trunk that runs toward the pollex (Nakatani, 1996). Meanwhile, in the present study, both nerve trunks may have been damaged by wounding, because of the depth of the wound and the location of the nerve trunks.

The crayfish reported by Nakatani *et al.* (1997) could not move the dactyl of its natural extra claws, despite the presence of muscles and nerve bundles. In contrast, all of the extra dactyls in the present study could be moved by the crayfish. Further studies are needed to explain this difference, but some speculation is possible. Closer and opener muscles, and innervation of these muscles, are necessary for a crayfish to move its dactyls. The crayfish claw is moved by two muscles controlled by five efferent axons: one inhibitor and one excitor to the opener muscle, and one inhibitor and two exciters—a “fast” and a “slow”—to the closer muscle (van Harreveld and Wiersma, 1937; Wiens, 1976). Both the primary and extra claws can be functional if the axons are adequately branching and innervate the muscles of each claw. The primary and extra dactyls may move synchronously if the above-mentioned axons branch to each muscle. However, the crayfish observed in this study could move all three dactyls synchronously or asynchronously. Atwood (1973) reported that a wide variety of synaptic mechanisms and muscle fiber properties permit delicate control within a simple framework in the crayfish claw. The articulation of the dactyl also affects its mobility. An extra dactyl could be moved only slightly by hand, even though it had well-developed closer and opener muscles, and innervation (Fig. 6B, C).

For an extra claw or dactyl to develop, some of the severed nerve fibers must separate from the primary nerve trunks. The present results suggest that severed nerve fibers regenerate; some of them elongate to form aberrant roots and extra claws or extra dactyls. Aberrant roots have been observed in the abdominal nerve cord of the crayfish *P. simulans* by Bittner *et al.* (1974). They reported that neurons projected aberrant roots toward the periphery after the third abdominal ganglion was removed. Also, Goransson *et al.* (1988) showed that in crayfish *P. clarkii*, the regenerating neurons would orient themselves in the proper direction to make connections toward the preferred target area. Further, the neurons do not respond to positional cues during the first week of regeneration.

Other studies have shown that transplanted tissues can induce growth of new structures. Kao and Chang (1996) proved that dactyl, pollex, and ischium tissues of the crab claw all had claw-transforming activity if they were autotransplanted into the autotomized stump of the fourth walking leg. Furthermore, by autotransplantation of a pollex into the eye sockets, a claw with complete proximal segments (ischium, merus, carpus and manus) developed (Kao and Chang, 1997). In the cockroach *Blattella ger-*

manica, graft/host junctions of the leg regenerated segmented structures consisting of two copies of all structures distal to the point of the junction (French, 1976). French (1976) speculated that the graft and host do not heal together and interact, but rather regenerate autonomously in mirror-image symmetry of the original graft and host levels. Further studies are needed to explore related issues in crayfish.

Acknowledgments

We are grateful to Dr. Toshiyuki Nishida, Professor Emeritus, University of Hawaii, for his valuable comments and for improving the manuscript.

Literature Cited

- Atwood, H. L. 1973. An attempt to account for the diversity of crustacean muscles. *Am. Zool.* **13**: 357–378.
- Bateson, W. 1894. *Materials for the Study of Variation, Treated With Especial Regard to Discontinuity in the Origin of Species*: xvi. Macmillan, London, New York. 598 pp.
- Bittner, G. D., M. L. Ballinger, and J. L. Larimer. 1974. Crayfish CNS: minimal degenerative-regenerative changes after lesioning. *J. Exp. Zool.* **189**: 13–36.
- Cole, L. J. 1910. Description of an abnormal lobster cheliped. *Biol. Bull.* **18**: 252–268.
- Faxon, W. 1881. On some crustacean deformities. *Bull. Mus. Comp. Zool.* **8**: 257–274.
- Fingerman, M., and S. W. Fingerman. 1974. The effects of limb removal on the rates of ecdysis of eyed and eyestalkless fiddler crabs, *Uca pugnator*. *Zool. Jb. Physiol. Bd.* **78**: 301–309.
- French, V. 1976. Leg regeneration in the cockroach. *Blattella germanica* II. Regeneration from a non-congruent tibial graft/host junction. *J. Embryol. Exp. Morphol.* **35**: 267–301.
- Goransson, L. G., W. P. Hunt, and S. J. Velez. 1988. Regeneration studies on a crayfish neuromuscular system. II. Effect of changing the nerve entry point into the muscle field on the gradient of innervation. *J. Neurobiol.* **19**: 141–152.
- Kao, H. W., and E. S. Chang. 1996. Homeotic transformation of crab walking leg into claw by autotransplantation of claw tissue. *Biol. Bull.* **190**: 313–321.
- Kao, H. W., and E. S. Chang. 1997. Limb regeneration in the eye sockets of crabs. *Biol. Bull.* **193**: 393–400.
- Murayama, O., I. Nakatani, and M. Nishita. 1994. Induction of lateral outgrowths on the chelae of the crayfish, *Procambarus clarkii* (Girard). *Crust. Res.* **23**: 69–73.
- Nakatani, I. 1996. Morphology of lateral outgrowths induced on chelipeds of the crayfish, *Procambarus clarkii* (Girard). *Crust. Res.* **25**: 142–150.
- Nakatani, I., and T. Otsu. 1979. The effects of eyestalk, leg, and uropod removal on the molting and growth of young crayfish, *Procambarus clarkii*. *Biol. Bull.* **157**: 182–188.
- Nakatani, I., and T. Otsu. 1981. Relation between the growth and the molt interval in the eyestalkless crayfish, *Procambarus clarkii*. *Comp. Biochem. Physiol.* **68A**: 549–553.
- Nakatani, I., K. Yamauchi, and O. Murayama. 1992. Abnormalities found in the chela of the crayfish, *Procambarus clarkii* (Girard). *Res. Crust.* **21**: 207–209.
- Nakatani, I., Y. Okada, and T. Yamaguchi. 1997. An extra claw on the first and on the third cheliped of the crayfish, *Procambarus clarkii* (Decapoda, Cambaridae). *Crustaceana* **70**: 788–798.

- Okamoto, K. 1991.** Abnormality found in the cheliped of *Geryon affinis granulatus* Sakai. *Res. Crust.* **20**: 63–65.
- Przibram, H. 1921.** Die Bruchdreifachbildung im Tierreich. *Wilhelm Roux Arch. Entw-Mech. Org.* **48**: 205–444.
- Shelton, P. M. J., P. R. Truby, and R. G. J. Shelton. 1981.** Naturally occurring abnormalities (Bruchdreifachbildungen) in the chelae of three species of Crustacea (Decapoda) and a possible explanation. *J. Embryol. Exp. Morphol.* **63**: 285–304.
- Suzuki, H., and T. Odawara. 1971.** Malformation found in the chelipeds of two edible crabs. *Res. Crust.* **4–5**: 191–195.
- Suzuki, S. 1980.** The effects of leg-removal to the molting of the crab, *Sesarma (Holometopus) haematocheir*. *Res. Crust.* **10**: 61–68.
- van Harreveld, A. 1936.** A physiological solution for freshwater crustaceans. *Proc. Soc. Exp. Biol.* **34**: 428–432.
- van Harreveld, A., and C. A. G. Wiersma. 1937.** The triple innervation of crayfish muscle and its function in contraction and inhibition. *J. Exp. Biol.* **14**: 448–461.
- Wiens, T. J. 1976.** Electrical and structural properties of crayfish claw motoneurons in an isolated claw-ganglion preparation. *J. Comp. Physiol.* **112**: 213–233.

Isolation and Characterization of Endostyle-Specific Genes in the Ascidian *Ciona intestinalis*

MICHIO OGASAWARA* AND NORIYUKI SATOH

Department of Zoology, Graduate School of Science, Kyoto University, Sakyo-ku, Kyoto 606-01, Japan

Abstract. The endostyle is a special organ in the pharynx of Urochordata, Cephalochordata, and Cyclostomata. It may have arisen in the common ancestor of these taxa, along with a shift to internal feeding for extracting suspended food from the water. In addition, the endostyle has a functional homology to the vertebrate thyroid gland. The endostyle is therefore one of the structures key to the understanding of the origin and evolution of chordates. In the present study, we isolated and characterized cDNA clones for four endostyle-specific genes, *CiEnds1*, *CiEnds2*, *CiEnds3*, and *CiEnds4*, of the ascidian *Ciona intestinalis*. Although the predicted amino acid sequences of the gene products CiENDS1, CiENDS2, and CiENDS3 showed no similarity to known proteins, their mean hydropathy profiles suggest that they are secretory proteins. In addition, CiENDS3 contained a unique repeat of 10 amino acids [R(QPCI)-(RRPC)I]. *CiEnds1* and *CiEnds2* were expressed in zone 6, a protein-secreting glandular element of the endostyle, and *CiEnds3* was expressed in zone 2, another secretory zone. *CiEnds4*, a cytoplasmic actin gene, was predominantly expressed in zones 3 and 5, which are supporting elements of the endostyle. The amino acid sequences of CiENDS1 and CiENDS2 resembled each other. In addition, they resembled a zone-6-specific gene product (HrENDS2) of another ascidian, *Halocynthia roretzi*. The results suggest that these genes are conserved among ascidian species, and therefore they (as well as *CiEnds3* for the protein with a unique motif) may be useful probes for further analyses of molecular mechanisms involved in endostyle development.

Introduction

The endostyle is a specialized organ in the pharynx of tunicates, cephalochordates, cyclostomates, and certain

prosobranchiates (Orton, 1912). The ascidian endostyle forms a trough-shaped structure in the ventral wall of the pharynx which extends from the fore-part of the pharynx to the esophagus (see Figs. 1A and 2D). In 1834, Lister first investigated how food particles in the feeding current are trapped in the pharynx of appendicularians. Fol (1876) found that the food is trapped by a mucous substance produced from the endostyle of tunicates. Thereafter, the ascidian endostyle has been intensively investigated by histological and ultrastructural observations (Olsson, 1963, 1965; Aros and Viragh, 1969; Fujita and Nanba, 1971); by the examination of ¹²⁵I incorporation (Thorpe *et al.*, 1972; Dunn, 1974); by histochemical detection of thyroperoxidase (Fujita and Sawano, 1979); and by partial purification of thyroperoxidase and its enzyme activity (Dunn, 1980).

It is commonly considered that the endostyle of lower chordates may be a homolog and primitive antecedent of the vertebrate thyroid gland, mainly because the organ incorporates iodine (Barrington, 1957, 1958; Salvatore, 1969). However, the endostyle is a mucus-secreting and food-collecting organ, and the ability to concentrate iodine is restricted to a small region of the organ (Olsson, 1963). The general organization of the ascidian endostyle is depicted in Fig. 1B. The cells of this organ are differentiated into eight or nine strips, or zones, that run parallel to one another in longitudinal orientation. The cells of each zone are highly specialized in morphology and function. The cells of zones 7, 8, and 9, like the thyroid cells of higher vertebrates, have an iodine-concentrating activity. The cells of zones 2, 4, and 6 have numerous secretory granules. These cells are believed to secrete the proteins or mucoprotein related to the digestion of food. The cells of zones 1, 3, and 5 are considered supporting elements and also as elements that might play a role in catching and transporting food.

We are interested in molecular developmental mecha-

Received 23 February 1998; accepted 20 May 1998.

* To whom correspondence should be addressed. E-mail: ogasawara@ascidian.zool.kyoto-u.ac.jp

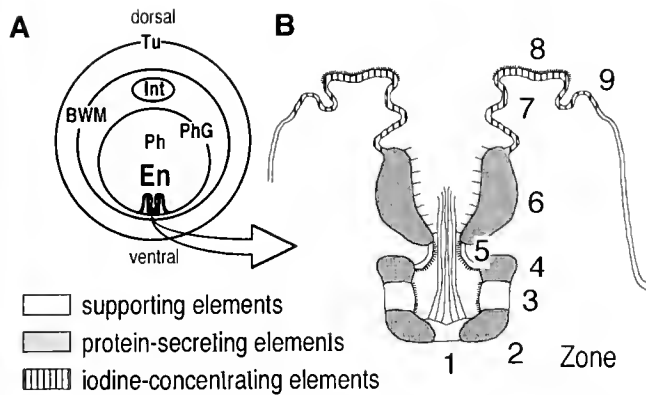


Figure 1. Diagram of the ascidian endostyle. (A) Transverse section of the adult body showing the position of the endostyle (En) in the ventral wall of the pharynx (Ph). BWM, body wall muscle; Int, intestine; PhG, pharyngeal gill; Tu, tunic. (B) Enlargement of the endostyle showing compositional elements or zones of the endostyle. Zones 1, 3, and 5 are supporting elements; zones 2, 4, and 6 are protein-secreting glandular elements; and zones 7, 8, and 9 are iodine-concentrating elements, equivalent to the thyroid gland of vertebrates. [Based on descriptions of Barrington (1957), Thorpe *et al.* (1972), Fujita and Nanba (1971), and Dunn (1974)].

nisms that permitted or accelerated the advent of chordates. The phylum Chordata consists of the subphyla Urochordata (tunicates), Cephalochordata (amphioxus), and Vertebrata. Chordates are categorized as deuterostomes, along with two other invertebrate groups, echinoderms and hemichordates, as was supported by molecular phylogenetic studies (Wada and Satoh, 1994; Turbeville *et al.*, 1994). Chordates share several characteristic features including a notochord, a dorsal hollow nerve cord, and pharyngeal gill slits. In addition, lower chordates (including tunicates, amphioxus, and lampreys) share an endostyle. We have emphasized that these hallmarks of the chordate body plan apparently evolved with the emergence of creatures resembling tadpole larvae (Satoh, 1995; Satoh and Jeffery, 1995). Therefore, investigations of the organization of these structures are of salient importance in attempts to understand the origin of chordates.

Coincidentally with this change in the mode of larval locomotion, most of the primitive chordates or chordate ancestors may have shifted their feeding system to the use of pharyngeal gill slits for extracting suspended food from the water and of an endostyle for secreting mucus to catch the food particles (*e.g.*, Brusca and Brusca, 1990). This possibility suggests that, in addition to the notochord and nerve cord, the pharyngeal gill and endostyle are key organs that can be used to explore molecular mechanisms involved in the emergence of chordates. In other words, we believe that the origin and evolution of chordates may be approached by isolating genes specific to the pharyngeal gill or endostyle and by analyzing how these genes

are organized during evolution in various deuterostomes. In previous studies, we isolated cDNA clones for pharyngeal gill-specific genes (*HrPhG1* and *HrPhG2*; Tanaka *et al.*, 1996) and for endostyle-specific genes (*HrEnds1* and *HrEnds2*; Ogasawara *et al.*, 1996) from the ascidian *Halocynthia roretzi*, which belongs to the order Pleurogona. Both endostyle-specific genes are expressed in zone 6 and encode secreted proteins. In the present study, we attempted the isolation of cDNA clones for endostyle-specific genes from *Ciona intestinalis*, which belongs to the order Enterogona. If both ascidian species conserve endostyle-specific structural genes, they may serve as models for the investigation of the molecular mechanisms involved in the organization of other chordate groups.

Materials and Methods

Biological materials

Adults of *Ciona intestinalis*, *C. savignyi*, and *Styela clava* were collected near the Marine BioSource Education Center of Tohoku University, Onagawa, Miyagi and Otsuchi Marine Research Center, Ocean Research Institute, University of Tokyo, Iwate, Japan. After the dissection of adult specimens, tissues and organs were quickly frozen in liquid nitrogen, and kept at -80°C until use.

Isolation of RNAs and construction of cDNA libraries

Total RNA was extracted from the endostyle and pharyngeal gill of *C. intestinalis* by the AGPC method (Chomczynski and Sacchi, 1987). Poly(A)⁺ RNA was purified with oligotex dT30 beads (Roche Japan, Tokyo). Complementary DNA was synthesized and cDNA libraries were constructed as described in a previous report (Ogasawara *et al.*, 1996). An endostyle cDNA library was constructed using a uni-ZAP-II vector (Stratagene, La Jolla, CA).

Isolation and sequencing of cDNA clones for endostyle-specific genes

The endostyle cDNA libraries were screened differentially. Duplicate filters of the library were made; one was hybridized with a [³²P]-labeled total cDNA probe prepared from 5 μg of poly(A)⁺ RNA of endostyle under high-stringency conditions, and the other was hybridized with a [³²P]-labeled total cDNA probe of pharyngeal gill under the same conditions. Plaques that showed positive hybridization with the endostyle probe but were negative for the pharyngeal-gill probe were selected and isolated by two rounds of screening. The specificity of the clones positive for the endostyle was confirmed by a Northern blot analysis. The clones were prepared for sequencing by controlled nested deletion from either the T3 or T7

side and sequenced using the ABI PRISM 377 DNA Sequencer (Perkin Elmer, Norwalk, CT).

Northern blot analysis

The Northern blot hybridization was carried out by the standard procedure (Sambrook *et al.*, 1989), and the filters were washed under high-stringency conditions. DNA probes for blot hybridizations were labeled with [³²P]-dCTP using a random primed labeling kit (Boehringer Mannheim, Heidelberg, Germany).

In situ hybridization

Juveniles of *C. intestinalis*, *C. savignyi*, and *Styela clava* were fixed in 4% paraformaldehyde in 0.5 M NaCl, 0.1 M MOPS buffer at 4°C for 12 h. Probes were synthesized by following the instructions from the supplier of the kit (DIG RNA Labeling kit; Boehringer Mannheim). The *in situ* hybridization of whole-mount specimens was carried out basically as described previously (Ogasawara *et al.*, 1996). For the *in situ* hybridization of sectioned specimens, samples were dehydrated with a graded series of alcohol, embedded in polyester wax (BDH), and sectioned at 6 µm.

Results

As in the case of the isolation of cDNA clones for the endostyle-specific genes of *H. roretzi* (Ogasawara *et al.*, 1996), differential screenings of a *C. intestinalis* endostyle cDNA library with total cDNA probes for the endostyle and pharyngeal gill yielded several cDNA clones specific to or enriched in the endostyle library. The preliminary *in situ* hybridization analysis of sectioned specimens demonstrated that transcripts of four cDNA clones were specific to the endostyle. We named the corresponding genes *CiEnds1* (*Ciona intestinalis* endostyle gene 1), *CiEnds2*, *CiEnds3*, and *CiEnds4*. During the screening procedures, we noticed that the *CiEnds1* transcript was abundant in the library, representing nearly 10% of the library clones. When 1 µg of poly(A)⁺ RNA of the endostyle was electrophoresed, we detected the transcript as a band stained with 0.5 µg/ml ethidium bromide (data not shown).

Characterization of cDNA clone for CiEnds1

As shown in Figure 2C, the Northern blot analysis of the *CiEnds1* transcript in various tissues and organs of a *C. intestinalis* adult detected the transcript of about 2.3 kb only in the endostyle. Hybridization signals were not detected in the pharyngeal gill, body-wall muscle, intestine, or gonad.

The nucleotide sequence of the cDNA clone for *CiEnds1* will appear under the accession number of AB010895 in the DDBJ, EMBL, and GenBank nucleotide

sequence databases. The insert of the cDNA clone consisted of 2265 nucleotides, including 17 adenylyl residues at the 3' end. The clone contained a single open reading frame (ORF) of 1950 nucleotides, which predicted a polypeptide of 650 amino acids (Fig. 2A). The calculated molecular mass (Mr) of the *CiEnds1*-encoded protein (CiENDS1) was 75.5 k.

CiENDS1 did not show any sequence motifs shared by transcriptional factors, a transmembrane domain, nuclear localization signals, or motifs found in growth factor proteins. However, as shown in Figure 2B, the mean hydropathy profiles of CiENDS1 showed that the N-terminus was highly hydrophobic. This region had a typical signal peptide sequence that consisted of a positively charged residue (amino acid position 2; K, Lys), a hydrophobic (3–13) region of 10–15 residues, a charged residue (position 15; S, Ser), and a residue containing the short side chain (position 16; A, Ala). A predicted cleavage site of the signal peptide was evident behind the Ala (position 16). This sequence motif strongly suggests that CiENDS1 is a secretory protein, with a probability of 82% determined by using the PSORT Program (Online, PSORT World Wide Web Server; Available: <http://psort.nibb.ac.jp>). In addition, CiENDS1 contained four putative N-linked glycosylation sites (Fig. 2A).

The *in situ* hybridization of whole-mount specimens demonstrated that the signals were restricted to the endostyle (Fig. 2D). In addition, the *in situ* hybridization of sectioned specimens demonstrated that the signals were not distributed over the entire regions of the endostyle but rather were restricted to zone 6 (Fig. 2E). No signals above background level were found in the control specimen hybridized with the sense probe (data not shown).

Characterization of cDNA clone for CiEnds2

The nucleotide sequence of cDNA clone for *CiEnds2* will appear under the accession number of AB010896 in the DDBJ, EMBL, and GenBank nucleotide sequence databases. The insert of the cDNA clone consisted of 2107 nucleotides, including 25 adenylyl residues at the 3' end. The occurrence of a 2.3-kb-long *CiEnds2* transcript only in the endostyle (Fig. 3C) suggested that the cDNA was close to full-length. The clone contained a single ORF of 1950 nucleotides, which also predicted a polypeptide of 650 amino acids (Fig. 3A). The calculated Mr of the *CiEnds2*-encoded protein (CiENDS2) was 77.3 k.

CiENDS2 may also be a secretory protein. As shown in Figure 3B, the mean hydropathy profiles of CiENDS2 showed that the N-terminus was highly hydrophobic. This region had a typical signal peptide sequence that consisted of a positively charged residue (amino acid position 2; K, Lys), a hydrophobic (3–13) region of 10–15 residues, a charged residue (position 15; N, Asp), and a residue

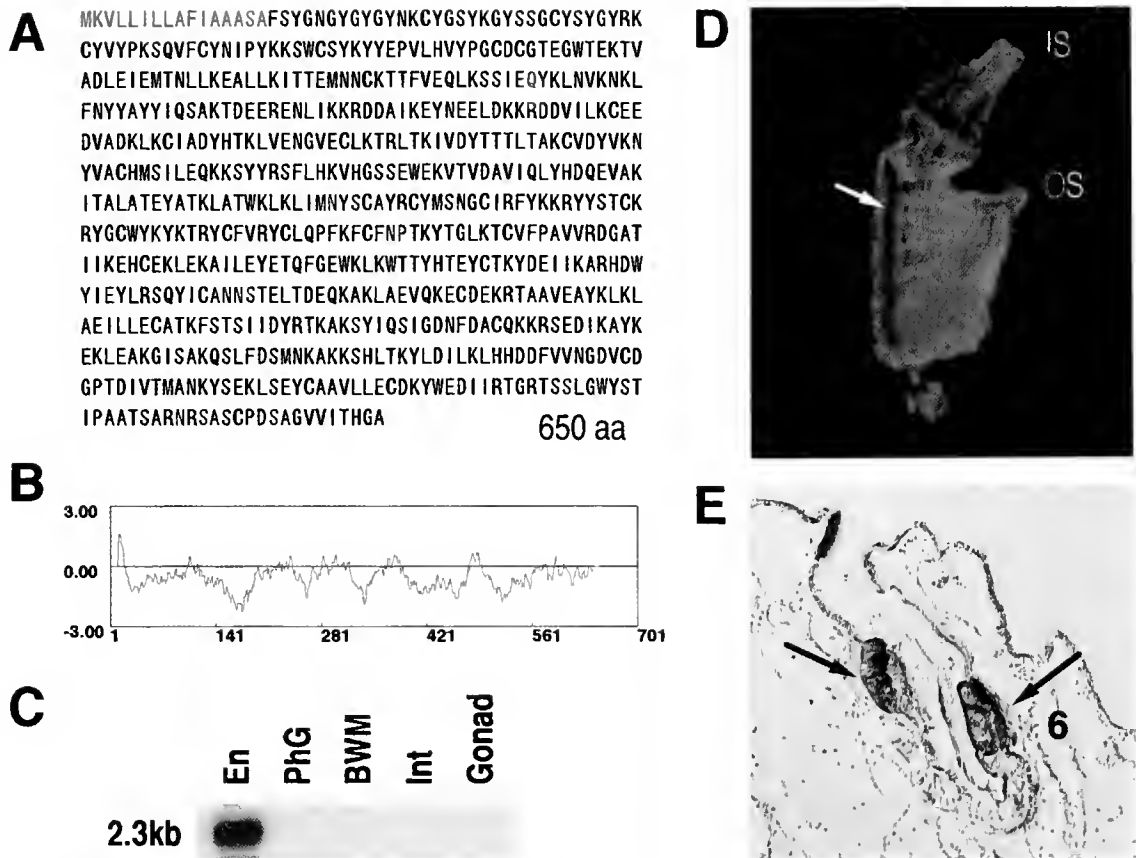


Figure 2. Characterization of the *CiEnds1* gene. (A) The predicted sequence of 650 amino acids of CiENDS1. The predicted signal peptide sequence is shown by red capitals, and putative N-linked glycosylation sites by green capitals. The nucleotide sequence for *CiEnds1* will appear under the accession number of AB010895 in the DDBJ, EMBL, and GenBank nucleotide sequence databases. (B) Mean hydropathy index of the CiENDS1 calculated across a window of 19 residues according to the method of Kyte and Doolittle (1982). The N-terminus of the protein is characterized by a 16-amino-acid-long hydrophobic region that contains the predicted signal peptide sequence (see text for details). This suggests that CiENDS1 is a secretory protein. (C) Distribution of *CiEnds1* transcript in tissues and organs of the adult. Northern blots of poly(A)⁺ RNA prepared from the endostyle (En), pharyngeal gill (PhG), body-wall muscle (BWM), intestine (Int), and gonad (Gonad) were hybridized with the random-primed [³²P]-labeled DNA probes, and the membrane was washed under high-stringency conditions. The *CiEnds1* transcript of about 2.3 kb in length was detected only in the endostyle. Each lane was loaded with 8 μ g of poly(A)⁺ RNA. (D, E) Localization of *CiEnds1* transcript, as revealed by *in situ* hybridization. IS, incurrent siphon; OS, outcurrent siphon. (D) A whole-mount specimen of a 1-month-old young adult and (E) a cross-section of an adult showing that the signal is restricted to the endostyle (D, arrow) and to zone 6 of the endostyle (E, arrows).

containing the short side chain (position 16; A, Ala). A predicted cleavage site of the signal peptide was evident behind the Ala (position 16). However, the results of the PSORT Program calculation showed that CiENDS2 seems to have an uncleaved N-terminal signal sequence. In addition, CiENDS2 contained a putative N-linked glycosylation site (Fig. 3A). CiENDS2 showed 48.3% identity at the amino acid level with CiENDS1, a finding that will be discussed later.

The *in situ* hybridization of whole-mount specimens demonstrated that the signals were restricted to the endo-

style (Fig. 3D), whereas that for sectioned specimens demonstrated that the signal was restricted to zone 6 (Fig. 3E). No signals above the background level were found in the other zones.

Characterization of cDNA clone for CiEnds3

The nucleotide sequence of cDNA clone for *CiEnds3* will appear under the accession number of AB010897 in the DDBJ, EMBL, and GenBank nucleotide sequence databases. The insert of the *CiEnds3* cDNA was

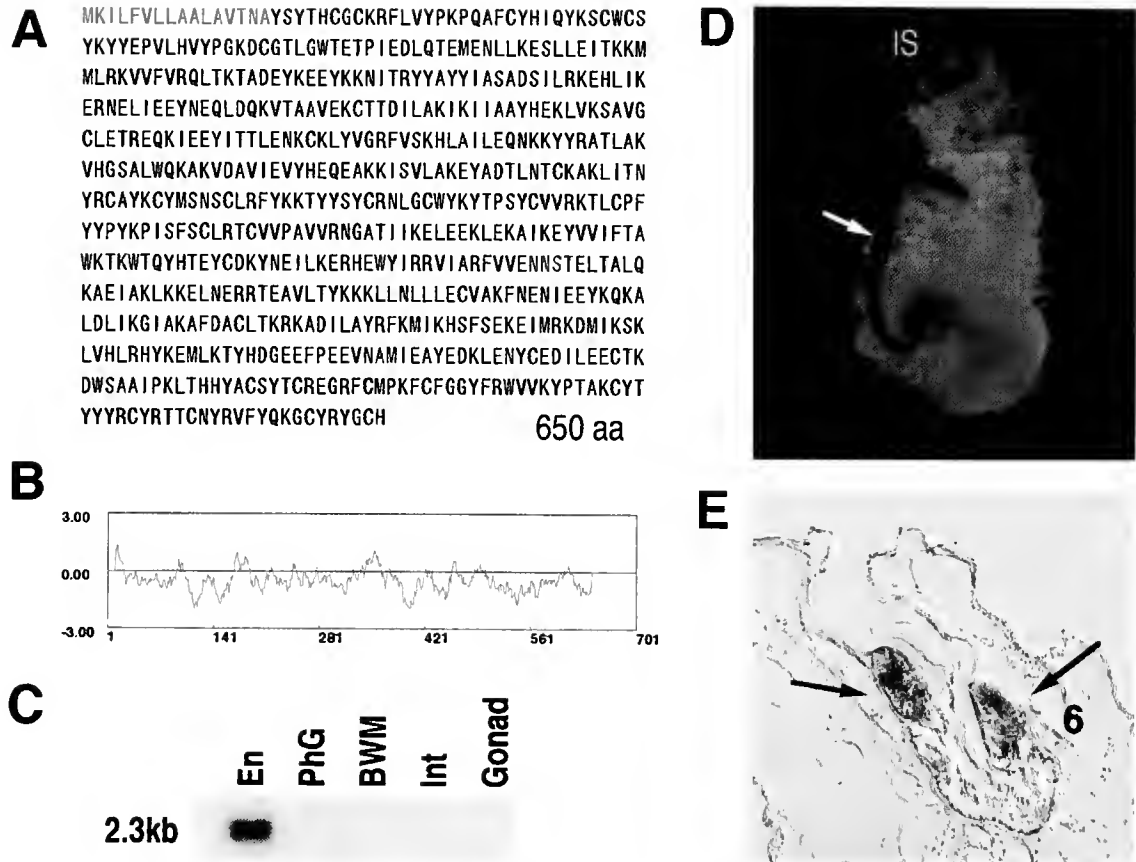


Figure 3. Characterization of the *CiEnds2* gene. (A) The predicted sequence of 650 amino acids of *CIENDS2*. The predicted signal peptide sequence is shown by red capitals, and a putative N-linked glycosylation site by green capitals. The nucleotide sequence for *CiEnds2* will appear under the accession number of AB010896 in the DDBJ, EMBL, and GenBank nucleotide sequence databases. (B) Mean hydropathy index of the *CIENDS2*, calculated as in the case of *CIENDS1*. (C) Distribution of *CiEnds2* transcript in tissues and organs of the adult. The *CiEnds2* transcript of about 2.3 kb in length was detected only in the endostyle. Each lane was loaded with 8 μ g of poly(A)⁺ RNA. (D, E) Localization of *CiEnds2* transcript, as revealed by *in situ* hybridization. IS, incurrent siphon. (D) A whole-mount specimen of a 1-month-old young adult and (E) a cross-section of an adult showing that the signal is restricted to the endostyle (D, arrow) and to zone 6 of the endostyle (E, arrows).

1319 nucleotides, including 17 adenyI residues at the 3' end. The Northern blot analysis demonstrated the occurrence of a 1.4-kb long *CiEnds3* transcript, which was detected only in the endostyle (Fig. 4C). This suggested that the cDNA was close to full-length. The clone contained a single ORF of 945 nucleotides, which predicted a polypeptide of 315 amino acids (Fig. 4A). The calculated Mr of the *CiEnds3*-encoded protein (*CIENDS3*) was 35.3 k.

CIENDS3 may also be a secretory protein. As shown in Figure 4B, the mean hydropathy profiles of *CIENDS3* showed that the N-terminus was highly hydrophobic. This region had a typical signal peptide sequence that consisted of a positively charged residue (amino acid position 2; R), a hydrophobic (3–13) region of 10–15 residues, a charged residue (position 15; T), and a residue containing

the short side chain (position 16; C). A predicted cleavage site of the signal peptide was evident behind the Cys (position 16). This sequence motif strongly suggests that *CIENDS3* is a secretory protein, with a probability of 58% determined by the PSORT Program.

In addition, *CIENDS3* contained a unique repeat of 10 amino acids (Fig. 4A). The repeat consisted of R(QPC1)(RRPC)I. This type of repeat has not been reported to date in the PDB, SWISSPROT, and PIR databases surveyed.

The *in situ* hybridization of whole-mount specimens demonstrated that the signals were restricted to the endostyle (Fig. 4D). In addition, the *in situ* hybridization of sectioned specimens demonstrated that the signal was restricted to zone 2 (Fig. 4E). No signals above the background level were found in the other zones.

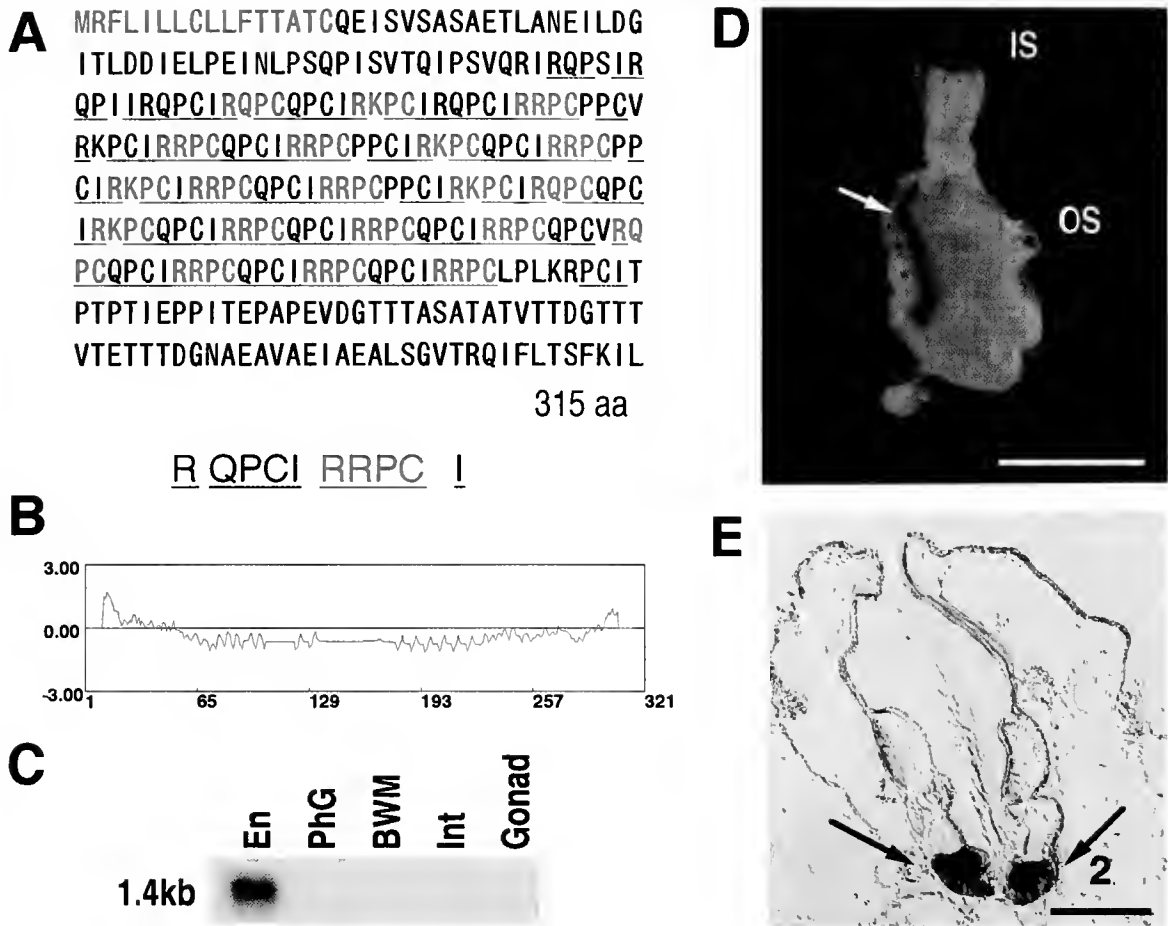


Figure 4. Characterization of the *CiEnds3* gene. (A) The predicted sequence of 315 amino acids of CiENDS3. The predicted signal peptide sequence is shown by red capitals. The sequence contained a characteristic repeat [R(QPC)I]RRPC[I]. The underlined amino acids are identical to those of the consensus sequences. The nucleotide sequence for *CiEnds3* will appear under the accession number of AB010897 in the DDBJ, EMBL, and GenBank nucleotide sequence databases. (B) Mean hydropathy index of the CiENDS3 calculated as in the case of CiENDS1. (C) Distribution of *CiEnds3* transcript in tissues and organs of the adult. Northern blots of poly(A)⁺ RNA prepared from the endostyle (En), pharyngeal gill (PhG), body-wall muscle (BWM), intestine (Int), and gonad (Gonad) were hybridized with the random-primed [³²P]-labeled DNA probes, and the membrane was washed under high-stringency conditions. The *CiEnds3* transcript of about 1.4 kb in length was detected only in the endostyle. Each lane was loaded with 8 μ g of poly(A)⁺ RNA. (D, E) Localization of *CiEnds3* transcripts, as revealed by *in situ* hybridization. IS, incurrent siphon; OS, outcurrent siphon. (D) A whole-mount specimen of a 1-month-old young adult (scale bar is 1 mm) and (E) a cross-section of an adult (scale bar is 100 μ m) showing that the signal is restricted to the endostyle (D, arrow) and to zone 2 of the endostyle (E, arrows).

Characterization of cDNA clone for CiEnds4

The *in situ* hybridization to isolate endostyle-specific cDNA clones demonstrated that the transcript of another clone (*CiEnds4*) was restricted to the zones 3, 5, and 7 (Fig. 5A). Strong signals were evident in zones 3 and 5, supporting elements of the endostyle; weak signals were also evident in zone 7, a putative iodine-concentrating element (Fig. 5A).

The insert of the *CiEnds4* cDNA was 1541 nucleotides, including 19 adenylyl residues in the 3' end. The clone

contained a single ORF of 1125 nucleotides, which predicted a polypeptide of 375 amino acids (data not shown). A cDNA clone for *C. intestinalis* cytoplasmic actin has been isolated and characterized in the laboratory of Dr. Takahito Nishikata of Konan University, Kobe, Japan (pers. comm.). The determination of the partial nucleotide sequence of *CiEnds4* cDNA clone revealed that *CiEnds4* encodes a cytoplasmic actin.

The above-mentioned results suggested that the gene or genes for one or more cytoplasmic actin are actively

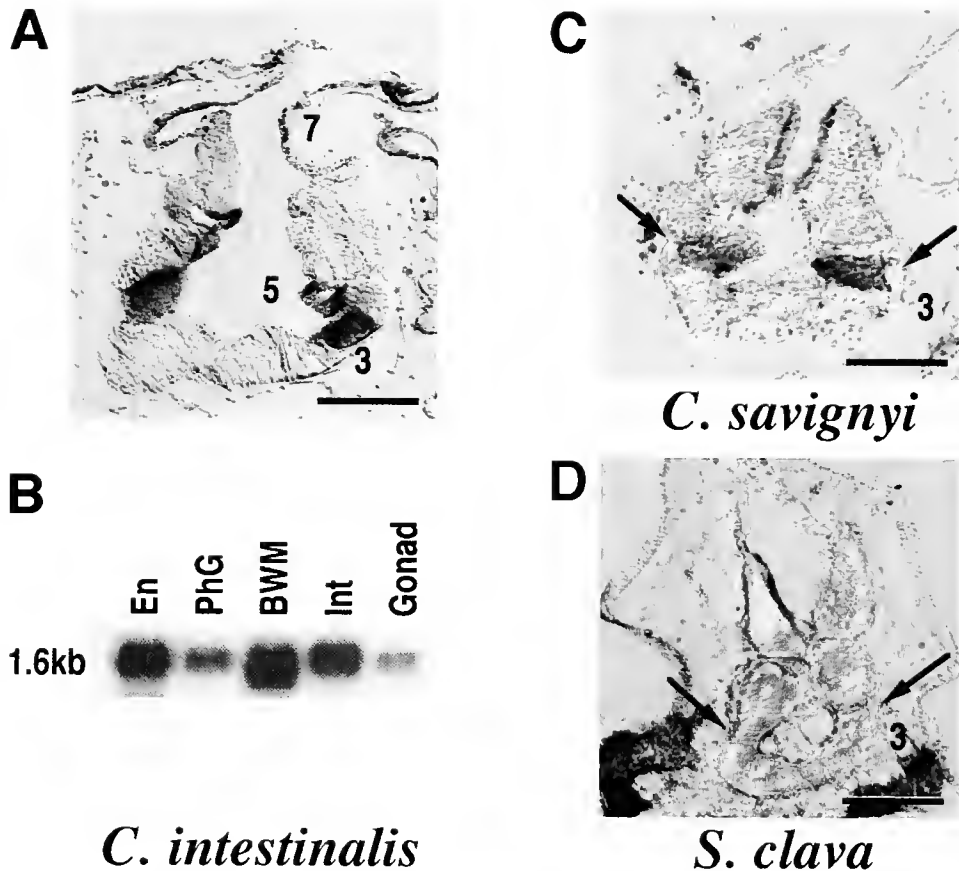


Figure 5. Characterization of the *CiEnds4* gene. The predicted amino acid sequence of CiENDS4 suggested that CiENDS4 is a cytoplasmic actin. (A) Localization of *CiEnds4* transcripts, as revealed by *in situ* hybridization. A cross-section of a young adult showing signals in zones 3, 5, and 7 of the endostyle. (B) Distribution of *CiEnds4* transcript in tissues and organs of the adult. Northern blots of poly(A)⁺ RNA prepared from the endostyle (En), pharyngeal gill (PhG), body-wall muscle (BWM), intestine (Int), and gonad (Gonad) were hybridized with the random-primed [³²P]-labeled DNA probes, and the membrane was washed under high-stringency conditions. The *CiEnds4* transcript of about 1.6 kb in length, or closely related molecules, was detected in the organs examined. Each lane was loaded with 8 μ g of poly(A)⁺ RNA. (C, D) Cross-reactivity of *CiEnds4* probe with zone 3 (arrows) of the endostyle of (C) *C. savignyi* and (D) *Styela clava*, as revealed by *in situ* hybridization (scale bars in A, C, and D are 100 μ m).

expressed in the supporting elements of the endostyle. We therefore examined, using the *CiEnds4* probe, whether the cytoplasmic actin gene is expressed in the supporting elements of the endostyle of two other ascidian species, *C. savignyi* and *Styela clava*. As shown in Figure 5C and D, the *CiEnds4* probe detected cytoplasmic actin transcripts in zone 3 of both species.

In addition, the Northern blot analysis demonstrated the occurrence of a 1.6-kb-long *CiEnds4* transcript not only in the endostyle but also in other organs including the pharyngeal gill, body-wall muscle, intestine, and gonad (Fig. 5B).

Discussion

In the present study, we isolated cDNA clones for four genes (*CiEnds1*, *CiEnds2*, *CiEnds3*, and *CiEnds4*), which

are expressed in different zones of the ascidian endostyle. *CiEnds1* and *CiEnds2* are expressed in zone 6 and encode peptides with similar amino acid sequences. *CiEnds3* is expressed in zone 2 and encodes a polypeptide with a novel repeat of 10 amino acids, tentatively called "ends-repeat." *CiEnds4* encodes a cytoplasmic actin that is expressed mainly in zones 3 and 5.

In a previous study, we characterized cDNA clones for two endostyle-specific genes, *HrEnds1* and *HrEnds2*, from the ascidian *H. roretzi* (Ogasawara *et al.*, 1996). Both genes are expressed in zone 6 and encode secreted proteins. Transcripts of both genes are abundant in the endostyle library; each represents about 10% of the cDNA clones of the library. As revealed by the present study, *CiEnds1* is also expressed in zone 6 and encodes a secreted protein. This transcript also represents the most

abundant species in the library. These results strongly suggest that zone 6 plays a major role in the secretion of mucus by the endostyle and has functions different from those of zones 2 and 4. This notion is consistent with a previous ultrastructural observation that the size and structure of the secretory granules in zone 6 differ from those of the other glandular zones 2 and 4 (Aros and Viragh, 1969). Zone 6 occupies the largest area in the endostyle and is characterized as the most developed glandular zone, containing abundant endoplasmic reticulum (Fujita and Nanba, 1971). Aros and Viragh (1969) and Fujita and Nanba (1971) reported that zone 6 contains at least two types of secretory granule—a large electron-dense granule and a smaller granule. Directly facing the pharynx in zone 6 is a wide exit for secretion; in contrast, zones 2 and 4 have only a very limited exit for secretion (Thorpe *et al.*, 1972).

When the amino acid sequences are compared for CiENDS1 and CiENDS2 (Fig. 6) and for CiENDS1, HrENDS2, and CiENDS2 (Fig. 7), these three polypeptides closely resemble each other: the sequence identity was 48.3% between CiEnds1 and CiEnds2, 22.2% between CiENDS1 and HrENDS2 (similarity 43.7%), and 22.8% between CiENDS2 and HrENDS2 (similarity 42.6%). Our previous genomic Southern blotting analysis of *HrEnds2* suggested that there are some other genes in the *H. roretzi* genome that contain a sequence similar to that of *HrEnds2*. In the present study, we isolated two cDNA clones from *C. intestinalis* that contained a sequence similar to that of *HrEnds2*. It is therefore likely that CiENDS1, CiENDS2, and HrENDS2 are members

of the same protein family, and it is possible that these genes were derived from a common ancestral gene.

The first aim of our studies is to isolate genes that are expressed in certain zones of secretory function, these genes being common in different species that belong to different orders of ascidians. In the present study, we first attempted the screening of *C. intestinalis* homologs of *HrEnds1* and *HrEnds2* with low-stringency hybridization conditions, using these genes as probes. Unfortunately, we could not isolate any homologs with the conditions we adopted. Therefore, we next tried the differential screening we used in a previous study (Ogasawara *et al.*, 1996), because we thought that if the nature of the endostyle is the same between *C. intestinalis* and *H. roretzi*, we might isolate homologous genes easily using this method. In the present screening, we were able to isolate an endostyle-specific cDNA clone for *CiEnds1*; this clone was highly expressed in zone 6 and contained a sequence similar to that of *HrEnds2*. In the further screening, we isolated *CiEnds2*, which was also expressed in zone 6 and contained sequences similar to that of *HrEnds2*. *CiEnds1*, *CiEnds2*, and *HrEnds2* may be related to each other and play an important role in the ascidian endostyle, and therefore they are good candidates for future studies.

Interestingly, the *CiEnds3* encodes a polypeptide with a novel repeat of 10 amino acids [the core repeat is 8 amino acids (QPC1)(RRPC)]. We tentatively call this the "ends-repeat." Because of its uniqueness and conserva-

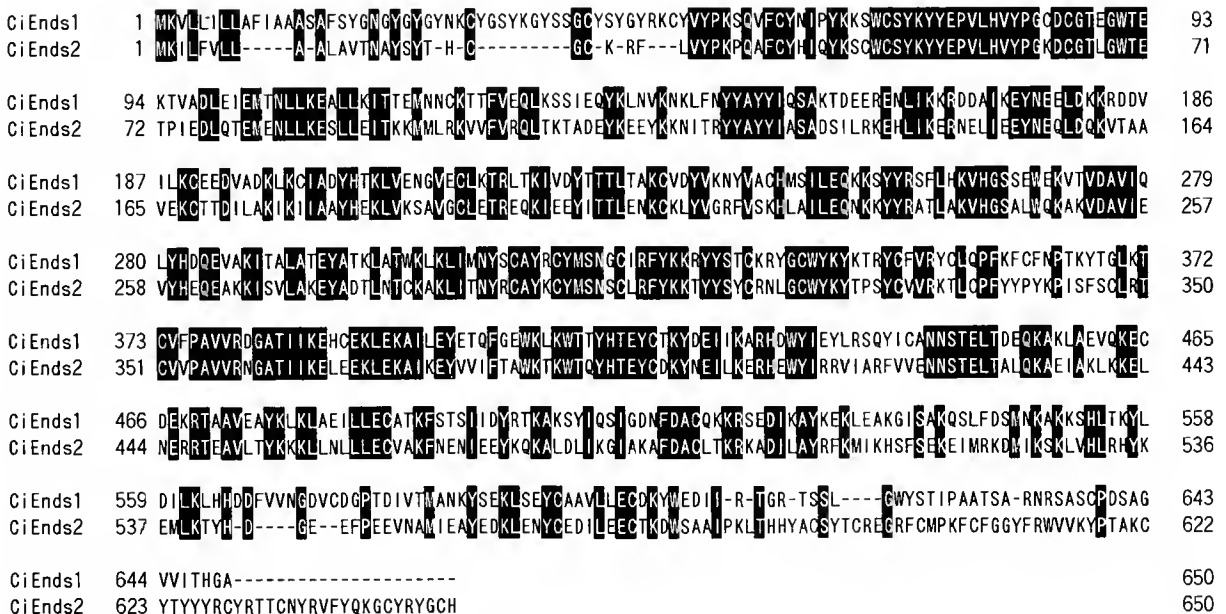


Figure 6. Alignment of the amino acid sequences of CiENDS1 and CiENDS2. Identical amino acids are enclosed by boxes. Gaps were induced to obtain the maximal similarity.

CiEnds1 aa	1	MKVLILLAFIAAASAFSYGN-----GYYGYNKKCYGSYKGYSSGCSYCYT-RKCYVYKSKVFCY	60
HrEnds2 aa	1	MKILIVLLSCLAVASAFGYGCSYRSYRYGRYINKYPSYGGYSKYSSYGSYKY-PSYG-6YNK-QYSY-6YKSHNGGYYHSSCYL-PPSECFY	88
CiEnds2 aa	1	MKILFVLLAALAVTHAYSYTHCGC-KRFLVY-----PKQAECY	38
CiEnds1 aa	61	NIPYKKSNGSYKYEPVHVYPGCGTEGWTEKTVADLEIEMTNLLKEALLKTTTEMNCKTTFVEQKSSIEQYKLNKVNKLFYYAYYI-	152
HrEnds2 aa	89	KGLFKNEWCTTAFYSVDLSYPPDDAKNIP-KANATDQVV-----ALLNKRTNVDKAEIAHQNRSDLLIVNRFKSEHTCTNRYASRIS	177
CiEnds2 aa	39	HIQYKSCNGSYKYEPVHVYPGCGCTLQWTEPTIEDLQTEMENLLKESLLEITKMMMLRKVVFRQLTKTADVEYKLYKKNLTRYAYYIA	131
CiEnds1 aa	153	-QSAKTD-EERENLIKRRDDAIKEYNEELDKKRDVILKCEEDVADKLCIADYHTKLVENGVECLKTRLTIVDYTTTAKCVDIVKNYVA	243
HrEnds2 aa	178	LAISKNDTTEQTRLETERDLAISNYDRSIEIQYNATKATSDAEAAARIKQKVIHFHDSIKIKFEQCYDTREAKITTFEEQLNTTAVKVKDYKT	270
CiEnds2 aa	132	---SADSILRKEHLIKERNELIEEYNEQLDQKVTAAVEKCTTDILAKIKIIAAYHEKLVKSAVGDLETREQLIEEYITLLENKCKLVGRFVS	221
CiEnds1 aa	244	CHMSILEQKKSYYRSFLHKVHGSSWEKVTVDAVIQLYHDQEVAKITALATEYATKLATWKLKIMNYSAYRCYMSNGCIRYKRYYSTCK	336
HrEnds2 aa	271	ALETDRDSSTAFAKAVLEKIGGTIAIPPSLVTEFENTFKVDE--KVT---KYDTDIDEKANDKTCYRALKCYQSSGLTFRNTYYQLP	357
CiEnds2 aa	222	KHLAILEQNKYYRATLAKVHGSAWQAKAVDAVIEVYHEQEAKKISVLAKYADTLNTCKAKIINRYCAYKCYMSNSCLREYKRYYSYCR	314
CiEnds1 aa	337	RYGCWYKYKTRYCFV-RYCL--QPFFKCFNPTKYGLKTVFPVAVVRDCAIIEKECEKLEKAILEYETQFGEWKLNNTYHTEYCTKYDEIT	426
HrEnds2 aa	358	FSG-KL-VALHYSEIQRTVLPYLKYYTWHKLEYNSLSTCONSTVNADKDVLEADWILNSNAVKAARIEMNFIDKHEGHSNYVDKLSL	448
CiEnds2 aa	315	NLGCWYKYTPSYCVV-RKTL--CPFYYPKPSFSLRTGVPAVVRNGATIIKELEKLEKAIKEYVVFIAWKTATQYHTEYCTKYNEIL	404
CiEnds1 aa	427	KARHDWYIEYLRSQVICANNSTELDEQAKLALEVQKCEDEKRTAAVEAYKLKLAELILECATKfstSTIDYRTKAKSYIQSTGDNFDACQKK	519
HrEnds2 aa	449	NSKNTAEVQKTKYKSLRDTGILTASDNAAISALQSSLEASKNATMIAEAKLKADRDSAEITGTASDAWEANINATVTNLQKYQDHLIT	541
CiEnds2 aa	405	KERHEWYIRRVIRFVVENNSTELALQKAEIAKLKKEINERTEAVLTYKKNLNLLECVAKFNENIEEYKQKALDILKIAKAFDACLIK	497
CiEnds1 aa	520	RSEDIKAYKEKLEAKGISAKQSLFDSMNKAKKSHLTKYLDILKLHDDVFNVDVCTGPTDIVTMANKYSEKSEYCAVLLCEDKYVEDII-	611
HrEnds2 aa	542	RTANINIIYINKVATLRNRKCELTNLKAVTEKNVDAAKAVI---NAWETGSANITDSAPATAWIKSYKQKLEVNDVYNSFEAHNVALE	630
CiEnds2 aa	498	RKADILAYRFKMIKHSFSEKIMRDKMIKSKLVHLRHYKEMLKYHD---GEEPEEVE--NAMI-EAEDKLENYCEDILEECTKDSAAIE	583
CiEnds1 aa	612	R-TGR-TSSL---GWSTIPAA TSA-RNRSASCP--DSAGVVI THGA-----	650
HrEnds2 aa	631	KLILDYECKYKIVGEYRVSPWRKPSFSNKTCYPTTGYLSHSCGYSSYTKPTSYHHHYYPKTTSTYYYPKTSGHYHTRTSGHY	717
CiEnds2 aa	584	KLTHHYAGSYTQREBRFCMPKFCFGYERWVVKYPTAK--CYTYYRCL-RTI-CNYRVFYQK-GCIRYGCH-----	650

Figure 7. Alignment of the amino acid sequences of CiENDS1, HrENDS2, and CiENDS2. Identical amino acids are enclosed by red boxes, and similar amino acids are enclosed by pink boxes. Gaps were induced to obtain the maximal similarity.

tion among the repeats, this gene is also a good candidate as a probe to explore common mechanisms involved in development and evolution of the endostyle.

There are some differences in the functions of endostyles among ascidian species. The zones that have iodine-concentrating activities (Kobayashi *et al.*, 1983) and thyroperoxidase activities (Dunn, 1974) are different between *H. roretzi*, *C. intestinalis*, and some other ascidians. However, we think that the functions and gene expressions of the endostyle are basically the same. Indeed, the present study isolated related genes, the nature of which (spatiotemporal expression and amount of the transcript) is the same in *C. intestinalis* and *H. roretzi*. Furthermore, *CiEnds4*, which encoded a cytoplasmic actin, was strongly expressed in zone 3 of *C. intestinalis*, *C. savignyi*, and *S. clava* (Fig. 5A, C, and D). In future studies, we should use these probes to isolate endostyle-specific genes from cephalochordates, cyclostomes, and hemichordates.

In addition to zones 2, 4, and 6 that secrete mucus, zones 8 and 9 are of special interest because other research has indicated that the vertebrate thyroid gland may be homologous with the endostyle of tunicates (Dunn, 1974; Fujita and Sawano, 1979; Kobayashi *et al.*, 1983), cepha-

lochordates (Tsuneki *et al.*, 1983; Fredriksson *et al.*, 1985; Ericson *et al.*, 1985), and larval lampreys (Egeberg, 1965; Fujita and Honma, 1969). In this and previous studies, we were not able to isolate cDNA clones for genes expressed in zones 8 and 9. The isolation of cDNA clones for genes specific to the thyroid-equivalent elements is very important for elucidating the evolutionary relationship of these elements among ascidians. In addition, the isolation and characterization of genes that are involved in the structure and function of vertebrate thyroid glands are of particular interest for future studies.

Acknowledgments

We thank all of the staff members of the Marine Bio-Source Education Center of Tohoku University, Onagawa, Miyagi and the Otsuchi Marine Research Center, Ocean Research Institute, University of Tokyo for their hospitality. We also thank Kazuko Hirayama for her technical assistance. M.O. is a predoctoral fellow of JSPS with a Monbusho research grant (No. 3535). This research was also supported by a Grant-in-Aid for Specially Promoted Research (No. 07102012) from the Monbusho, Japan, to N.S.

Literature Cited

- Aros, B., and S. Viragh. 1969. Fine structure of the pharynx and endostyle of an ascidian (*Ciona intestinalis*). *Acta Biol. Acad. Sci. Hung.* **20**: 281-297.
- Barrington, E. J. W. 1957. The distribution and significance of organically bound iodine in the ascidian *Ciona intestinalis* Linnaeus. *J. Mar. Biol. Ass. U.K.* **36**: 1-16.
- Barrington, E. J. W. 1958. The localization of organically bound iodine in the endostyle of Amphioxus. *J. Mar. Biol. Ass. U.K.* **37**: 117-126.
- Brusca, R. C., and G. J. Brusca. 1990. *Invertebrates*. Sinauer Associates, Sunderland, MA.
- Chomczynski, P., and N. Sacchi. 1987. Single-step method of RNA isolation by acid guanidinium thiocyanate-phenol-chloroform extraction. *Anal. Biochem.* **162**: 156-159.
- Dunn, A. D. 1974. Ultrastructural autoradiography and cytochemistry of the iodine-binding cells in the ascidian endostyle. *J. Exp. Zool.* **188**: 103-123.
- Dunn, A. D. 1980. Properties of an iodinating enzyme in the ascidian endostyle. *Gen. Comp. Endocrinol.* **40**: 484-493.
- Egeberg, J. 1965. Iodine-concentrating cells in the endostyle of Ammocoetes. *Z. Zellforsch. Mikrosk. Anat.* **68**: 102-115.
- Ericson L. E., G. Fredriksson, and T. Ofverholm. 1985. Ultrastructural localization of the iodination center in the endostyle of the adult amphioxus (*Branchiostoma lanceolatum*). *Cell Tissue Res.* **241**: 267-273.
- Fol, H. 1876. Über die Schleimdrüse oder den Endostyl der Tunicaten. *Morph. Jahrb.* **1**: 222-230.
- Fredriksson, G., L. E. Ericson, and T. Ofverholm. 1985. Electron-microscopic studies of iodine-binding and peroxidase activity in the endostyle of the larval amphioxus (*Branchiostoma lanceolatum*). *Cell Tissue Res.* **241**: 257-266.
- Fujita, H., and Y. Honma. 1969. Iodine metabolism of the endostyle of larval lampreys, Ammocoetes of *Lampetra japonica*. Electron microscopic autoradiography of 125-I. *Z. Zellforsch. Mikrosk. Anat.* **98**: 525-537.
- Fujita, H., and H. Nanha. 1971. Fine structure and its functional properties of the endostyle of ascidians, *Ciona intestinalis*. A part of phylogenetic studies of the thyroid gland. *Z. Zellforsch. Mikrosk. Anat.* **121**: 455-469.
- Fujita, H., and F. Sawano. 1979. Fine structural localization of endogenous peroxidase in the endostyle of ascidians, *Ciona intestinalis*. A part of phylogenetic studies of the thyroid gland. *Archi. Histol. Jpn.* **42**: 319-326.
- Kobayashi, H., K. Tsuneki, H. Akiyoshi, Y. Kobayashi, M. Nozaki, and M. Onji. 1983. Histochemical distribution of peroxidase in ascidians with special reference to the endostyle and the branchial sac. *Gen. Comp. Endocrinol.* **50**: 172-187.
- Kyte, J., and R. F. Doolittle. 1982. A simple method for displaying the hydrophobic character of a protein. *J. Mol. Biol.* **157**: 105-132.
- Lister, 1834. Cited in Fol, 1876, *op cit*.
- Ogasawara, M., K. J. Tanaka, K. W. Makabe, and N. Satoh. 1996. Expression of endostyle-specific genes in the ascidian *Halocynthia roretzi*. *Dev. Genes Evol.* **206**: 227-235.
- Olsson, R. 1963. Endostyles and endostylar secretions: a comparative histochemical study. *Acta Zool.* **44**: 299-329.
- Olsson, R. 1965. The cytology of the endostyle of *Oikopleura dioica*. *Ann. N. Y. Acad. Sci.* **118**: 1038-1051.
- Orton, J. H. 1912. The mode of feeding of *Crepidula* with an account of the current-producing mechanism in the mantle cavity, and some remarks on the mode of feeding in gastropods and lamellibranchs. *J. Mar. Biol. Ass. U. K.* **9**: 444-478.
- Salvatore, G. 1969. Thyroid hormone biosynthesis in Agnatha and Protochordata. *Gen. Comp. Endocrinol. Suppl.* **2**: 535-550.
- Sambrook, J., E. F. Fritsh, and T. Maniatis. 1989. *Molecular Cloning: A Laboratory Manual*, 2nd ed. Cold Spring Harbor Laboratory, Cold Spring Harbor, New York.
- Satoh, N. 1995. Towards a molecular understanding of developmental mechanisms underlying the origin and evolution of chordates. Pp. 267-290 in *Biodiversity and Evolution*, R. Arai, M. Kato, and Y. Doi, eds. The National Science Museum Foundation, Tokyo.
- Satoh, N., and W. R. Jeffery. 1995. Chasing tails in ascidians: developmental insights into the origin and evolution of chordates. *Trends Genet.* **11**: 354-359.
- Tanaka, K. J., M. Ogasawara, K. W. Makabe, and N. Satoh. 1996. Expression of pharyngeal gill-specific genes in the ascidian *Halocynthia roretzi*. *Dev. Genes Evol.* **206**: 218-226.
- Thorpe, A., M. C. Thorndyke, and E. J. Barrington. 1972. Ultrastructural and histochemical features of the endostyle of the ascidian *Ciona intestinalis* with special reference to the distribution of bound iodine. *Gen. Comp. Endocrinol.* **19**: 559-571.
- Tsuneki, K., H. Kobayashi, and M. Onji. 1983. Histochemical distribution of peroxidase in amphioxus and cyclostomes with special reference to the endostyle. *Gen. Comp. Endocrinol.* **50**: 188-200.
- Turbeville, J. M., J. R. Schulz, and R. A. Raff. 1994. Deuterostome phylogeny and the sister group of the chordates: evidence from molecules and morphology. *Mol. Biol. Evol.* **11**: 648-655.
- Wada, H., and N. Satoh. 1994. Details of the evolutionary history from invertebrates to vertebrates, as deduced from the sequences of 18S rDNA. *Proc. Natl. Acad. Sci. USA* **91**: 1801-1804.

Molecular Phylogeny of Zooxanthellate Bivalves

TADASHI MARUYAMA^{1,*}, MASAHARU ISHIKURA¹, SATORU YAMAZAKI²,
AND SATORU KANAI³

¹Marine Biotechnology Institute, Kamaishi Laboratories, Heita 3-75-1, Kamaishi-shi, Iwate 026-0001, Japan; ²Department of Marine Science, Tokai University, Shimizu-shi, Shizuoka 424-0902, Japan; and ³Bimolecular Engineering Research Institute, 6-2-3, Furuedai, Suita, Osaka 565-0874, Japan

Abstract. The aim of this research was to analyze the phylogenetic relationships of zooxanthellate bivalves belonging to the genera *Tridacna*, *Hippopus*, *Fragum*, and *Corculum* as well as to the closely related azooxanthellate bivalves belonging to *Vasticardium* and *Fulvia*. The small-subunit ribosomal RNA genes (18S rDNAs) from these bivalves were amplified by polymerase chain reaction with universal eukaryotic primers and were then sequenced. The sequence data from each species were analyzed by the neighbor-joining, maximum parsimony, and maximum likelihood methods, and phylogenetic trees were constructed. The results were essentially consistent with the morphological taxonomy of these bivalves. Thus, the zooxanthellate clams branch into two lineages, one composed of the genera *Fragum* and *Corculum* in the family Cardiidae, and the other composed of the genera *Tridacna* and *Hippopus* in the family Tridacnidae. However, present results indicate that the azooxanthellate clams analyzed (*Vasticardium flavum* and *Fulvia mitica*) are more likely to form a clade with the species of *Tridacna* and *Hippopus* than with those of *Fragum* and *Corculum*. This topology suggests that either the symbiosis with zooxanthellae occurred independently in each of two lineages, *Tridacna-Hippopus* and *Corculum-Fragum*, or the symbiosis was established in clams ancestral to the lineages of both the zooxanthellate clams and the azooxanthellate clams *Vasticardium* and *Fulvia*, and the latter lost the symbiotic relationship after the symbiotic clam lineages had diverged.

Introduction

Symbioses between marine invertebrates and microalgae have been known for years (Smith and Douglas, 1987; Trench, 1993). Although various microalgae—from cyanobacteria to diverse eukaryotic species—are known as symbionts, zooxanthellae (a common name for symbiotic dinoflagellates) dominate marine invertebrate symbioses, including those in corals, molluscs, flatworms, and protozoa. In bivalves, symbioses with microalgae are found in two distinct groups: freshwater clams in the genus *Anodonta* (Unionidae) that harbor a symbiotic green alga (zoochlorella) (Goetsch and Scheuring, 1926; Pardy, 1980); and the giant clams and related clams that harbor zooxanthellae. The giant clams belong to the genera *Tridacna* and *Hippopus* (Rosewater, 1965, 1982; Yonge, 1980) in the family Tridacnidae. Less well known clams harboring zooxanthellae belong to the genera *Corculum* (Kawaguti, 1950) and *Fragum* (Kawaguti, 1983a; Ohno *et al.*, 1995) in the family Cardiidae. No bivalve in any other family has been reported to have a symbiotic relationship with zooxanthellae.

Zooxanthellae are thought essential to the clams that contain them. Photosynthetic products secreted from the zooxanthellae are taken up by the giant clam and contribute nutrition (Fisher *et al.*, 1985; Griffiths and Streamer 1988; Klumpp *et al.*, 1992). No adult giant clam devoid of zooxanthellae has ever been found, though a partially albino *T. gigas* has been reported (Yellowlees *et al.*, 1993; Norton *et al.*, 1995). The zooxanthellae also benefit from the association: they lack UV-absorbing substances and are sensitive to UV light, but are protected by the mantle tissue of the host clam (Ishikura *et al.*, 1997).

The evolution of the symbiosis between the zooxanthel-

Received 17 January 1997; accepted 27 April 1998.

* To whom correspondence should be addressed. E-mail: tmaruyama@kamaishi.mbio.co.jp

lae and the clams has been enigmatic. Recently, however, the methods of molecular phylogeny have been applied to the relationship between zooxanthellae and various marine invertebrate hosts (Rowan and Powers, 1991, 1992; MacNally *et al.*, 1994). These reports have shown that symbiotic dinoflagellates from various hosts are diverse and that phylogenetic similarity among the dinoflagellates is not correlated with the phylogenetic affiliations of their hosts. These data support the concept that the symbioses between dinoflagellates and marine invertebrates are polyphyletic (Trench, 1992), but the phylogeny of the giant clams has not yet been subjected to molecular analysis.

Symbiosis with zooxanthellae occurs only in two closely related families of bivalves, Tridacnidae and Cardiidae (Ohno *et al.*, 1995). Although all of the eight living Tridacnidae clams contain zooxanthellae (Norton and Jones, 1992), this relationship occurs in only a few species in two genera of Cardiidae (Ohno *et al.*, 1995). To clarify the phylogenetic relationship of these zooxanthellate and azooxanthellate bivalves, we analyzed the 18S rDNA sequences from seven zooxanthellate tridacnid clams (five species of *Tridacna* and two of *Hippopus*), three zooxanthellate cardiid clams (one species of *Corculum* and two of *Fragum*), and two azooxanthellate cardiid clams (one species each of *Fulvia* and *Vasticardium*).

Materials and Methods

Collection of clam specimens

Tridacnid clams (*Tridacna maxima*, *T. squamosa*, and *Hippopus hippopus*), zooxanthellate cardiid clams (*Fragum fragum*, *F. uedo*), and an azooxanthellate cardiid clam (*Vasticardium flavum*) were collected in the Republic of Palau, Western Caroline Islands, during the cruises of the R/V *Sohgen-maru* in 1993–1994. *T. gigas*, *T. derasa*, and *H. porcellanus* were purchased from the PMDC (Palau Mariculture Demonstration Center). Live specimens of a zooxanthellate cardiid, *Corculum cardissa*, which had been collected from mariculture tanks for tridacnid clams, were gifts from PMDC. A live specimen of *Fragum fragum* collected in Okinawa, Japan, was a gift from Mr. Osumi of Ryukyus University. An azooxanthellate cardiid clam, *Fulvia mutica*, was purchased from a local fishery market in Shimizu, Japan. The shells were saved (except for those of *T. gigas*, which were lost during transportation) and were kindly identified by Prof. Okutani of Nihon University.

Extraction of DNA from the clams

Live clams were dissected, and the organs were separated and frozen at -20°C until used. The white part of

the gill or foot tissue (0.1–0.2 g), which was devoid of zooxanthellae, was homogenized in a glass homogenizer in 2–3 ml TE buffer (10 mM Tris-HCl, 100 mM EDTA, pH 8.0) containing 0.5% sodium dodecyl sulfate, and digested with proteinase K (100 $\mu\text{g}/\text{ml}$) at 50°C for 3 h (Wada *et al.*, 1992). The DNA was then extracted with TE buffer-saturated phenol and washed twice with a mixture of chloroform and isoamyl alcohol (24:1). An equal volume of 5 M ammonium acetate was then added, and the DNA was precipitated with cold ethanol, washed once with cold 70% ethanol, and dried.

Amplification of 18S rDNA and DNA sequence determination

A polymerase chain reaction (PCR) kit (Takara Shuzo, Kyoto, Japan) was used to amplify the 18S rDNA from 1 μg of genomic DNA. The manufacturer's instructions were followed; *i.e.*, 30 cycles comprising 93°C for 1.5 min, 58°C for 1.5 min, and 72°C for 2 min. The extension reaction at 72°C in the final cycle was prolonged to 10 min, and the PCR products were then frozen at -20°C until used. The universal eukaryotic primers used in the amplification of the 18S-rDNA were 5'-GGTTGATCCTGCCAGTAGTCATATGCTTG-3' (ss5) and 5'-GATCCTTCCGCAGGTTTCACCTACGGAAACC-3' (ss3). These sequences were reported to be located four nucleotides from the 5' and 3' ends, respectively, of the 18S-rRNA of *Prorocentrum micans*, a dinoflagellate (Herzog and Maroteaux, 1986; Rowan and Powers, 1992). Amplified DNAs were cloned in pT7 plasmids (Novagen, USA) with *E. coli* JM 109 as the host. At least three cloned DNAs amplified from the genomic DNA of an individual clam were sequenced for each clam species, using custom-made 20-b DNA primers (Japan BioService, Saitama), a Takara PCR sequence kit with an ABI-type 373A DNA sequencer.

Analysis of the sequence data

The 18S rDNA sequences were aligned using Clustal W (Thompson *et al.*, 1994) and gap and insertion regions removed with the software program RMINSDEL in MOLPHY-2.2 (Adachi and Hasegawa, 1994). The aligned sequences were then analyzed by the neighbor-joining (NJ) method (Saitou and Nei, 1987) using the DNADIST and NEIGHBOR programs (using the Kimura 2-parameter model; Kimura, 1980) in PHYLIP 3.57c (Felsenstein, 1995). The statistical significance of each cluster in the tree was evaluated with 1000 iterations of bootstrap resamplings and tree reconstructions (Felsenstein, 1985) using DNADIST, NEIGHBOR, SEQBOOT, and CONSENSE in PHYLIP 3.57c. The same sequences were analyzed by the maximum parsimony

(MP) method using the DNAPARS program in PHYLIP 3.57c. Decay analysis (Bremer, 1988, 1994; Winnepenninckx *et al.*, 1996) was also undertaken by using PHYLIP 3.57c. The sequence data of nine selected clams were further analyzed by the maximum likelihood (ML) method using the NUCML program adopting the Alpha/Beta ratio 2.0 model (Hasegawa *et al.*, 1985) in MOLPHY 2.2 (Adachi and Hasegawa, 1994). The tree with minimal AIC (Akaike Information Criterion), which is defined as $-2(\log\text{-likelihood}) + 2(\text{number of free parameters})$ (Akaike, 1974), was considered the most appropriate tree. The statistical significance of each cluster in the ML tree was evaluated by the bootstrap analysis with 1000 iterations. Phylogenetic trees were drawn with TreeView (Page, 1996) on a Macintosh computer.

Results

The PCR products

Lengths of the amplified 18S rDNAs (between the primers ss5 and ss3) from the zooxanthellate and azoo-

xanthellate cardiid clams were 1780–1875 bp—longer than the corresponding lengths in the other clams examined (1745–1772 bp) (Table 1). Those sequences were deposited in the DDBJ (DNA data base of Japan) under the accession numbers shown in Table 1. The clam shells (except *T. gigas*) were deposited in The National Science Museum in Tokyo with the specimen numbers listed in Table 1.

Phylogenetic trees

The alignment of 18S rDNA sequences of the clams is available on the web site of this journal at the following address:

<http://www.mbl.edu/html/BB/home.BB.html>

After removing the gaps and insertions, we analyzed 1698 sites within the sequences by the NJ and MP methods. Figure 1 shows a phylogenetic tree constructed by the NJ method. The 18S rDNA sequence of *Limicolaria kambel* (Gastropoda, Pulmonata, Achatinidae) was chosen as the outgroup. We also analyzed the data with the 18S rDNA

Table 1

Length of amplified 18S-rDNAs

Species	Place of collection	Length of the PCR products ¹	Accession number ²	Specimen number ³
Zooxanthellate bivalves (present work)				
<i>Tridacna gigas</i>	Palau	1780 bp	D84189	n.d.
<i>Tridacna derasa</i>	Palau	1803	D84658	NSMT-Mo70918
<i>Tridacna crocea</i>	Okinawa (Japan)	1803	D88908	NSMT-Mo70917
<i>Tridacna maxima</i>	Palau	1805	D84659	NSMT-Mo70919
<i>Tridacna squamosa</i>	Palau	1804	D84190	NSMT-Mo70916
<i>Hippopus hippopus</i>	Palau	1813	D84660	NSMT-Mo70914
<i>Hippopus porcellanus</i>	Palau	1813	D84661	NSMT-Mo70915
<i>Fragum fragum</i>	Palau	1865	D84662	NSMT-Mo70921
<i>Fragum fragum</i>	Okinawa (Japan)	1865	D84663	NSMT-Mo70920
<i>Fragum unedo</i>	Palau	1865	D84664	NSMT-Mo70922
<i>Corculum cardissa</i>	Palau	1875	D88909	NSMT-Mo70923
Azooxanthellate Cardiidae bivalves (present work)				
<i>Vasticardium flavum</i>	Palau	1852	D88910	NSMT-Mo70913
<i>Fulvia nutica</i>	Mikawa-bay (Japan)	1840	D88911	NSMT-Mo70912
Other bivalves (from database)				
<i>Spisula solidissima</i>		1772	L11270	
<i>Tresus nuttali</i>		1772	L11269	
<i>Placopecten magellanicus</i>		1745	X53899	
<i>Chlamys islandica</i>		1746	L11232	
<i>Mytilus edulis</i>		1757	L24489	
Gastropod (from database)				
<i>Limicolaria kambel</i>		1770	X66374	

¹ Length of the amplified DNA between but excluding primers ss5 and ss3.

² Accession number of the DNA sequence data in DNA Data Base of Japan.

³ Deposit number of the shell specimen in National Science Museum, Tokyo; n.d., not deposited.

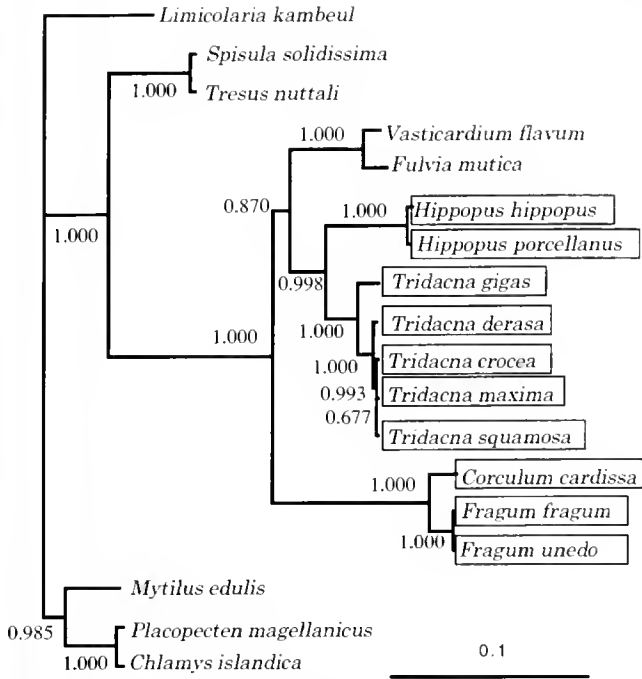


Figure 1. A phylogenetic tree of zooxanthellate and azooxanthellate clams, calculated by the neighbor-joining method adopting the Kimura 2-parameter model. Numbers at the nodes are the bootstrap values for the clades in 1000 replications. Box, zooxanthellate clam. Bar, 0.10 substitutions per site.

sequence of *Symbiodinium corculorum*, the symbiotic alga of *Corculum cardissa* (accession number L13717) as the outgroup; the results were the same as those with *L. kambeul* (data not shown). Clams belonging to the Pteriomorpha (*Mytilus edulis* in Mytilidae, and *Placopecten magellanicus* and *Chlamys islandica* in Pectinidae) made a clade that was clearly separated from those of the Heterodonta. In the heterodont branch, a clade including the families Tridacnidae and Cardiidae—and comprising all of the zooxanthellate clams examined, as well as two azooxanthellate clams, *V. flavum* and *F. mutica*—was clearly separated from another clade containing two species in the family Macridae (*Spisula solidissima* and *Tresus nuttali*). This clade was further resolved into three lineages: *Corculum-Fragum*, *Vasticardium-Fulvia*, and *Tridacna-Hippopus*. The NJ tree indicates that the zooxanthellate cardiids and azooxanthellate cardiids diverged before the zooxanthellate tridacnids. The bootstrap value at the node uniting the *Vasticardium-Fulvia* and *Tridacna-Hippopus* clades was 0.870, and that at the node uniting the *Vasticardium-Fulvia-Tridacna-Hippopus* and *Corculum-Fragum* clade was 1.000. This indicates that tridacnid clams are more likely to form a clade with clams of *Vasticardium-Fulvia* than with those of *Fragum-Corculum*. Three tridacnid clams, *T. maxima*, *T. squamosa*,

and *T. crocea*, are evidently very closely related, whereas *T. gigas* and *T. derasa* are relatively distant from them. *Fragum fragum* and *F. unedo* are very closely related, the identity between their 18S rDNA sequences being 99.8% (1861 out of 1865 bp).

The maximum parsimony (MP) method gave three equally most parsimonious trees of similar, but distinct, topologies (Fig. 2, A–C). The lengths of the trees were

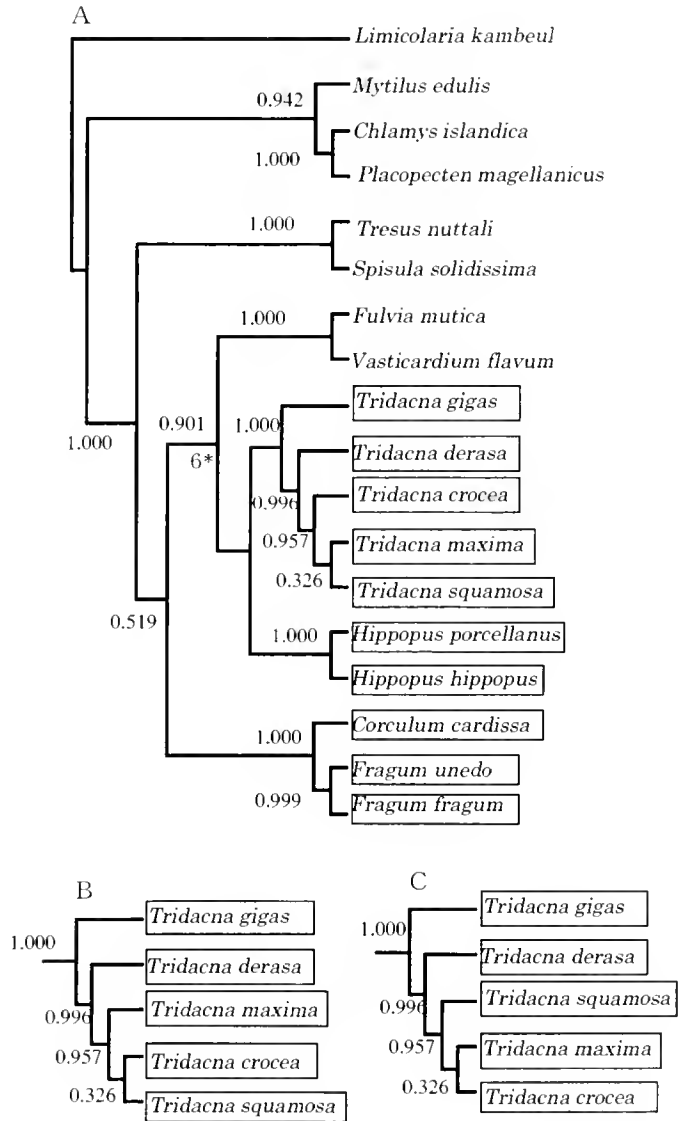


Figure 2. Phylogenetic trees of zooxanthellate and azooxanthellate clams, calculated by the maximum parsimony method. Three topologies were selected as the best tree; the differences were found in *Tridacna squamosa*, *T. crocea*, and *T. maxima*. (A) One of the best trees. (B and C) Parts of the two other trees showing the dissimilarities to A. Numbers at the nodes are the bootstrap values for the clades in 1000 replications. *, decay index. Box, zooxanthellate clam. Consistency index, 0.76; retention index, 0.88.

1019 steps. Consistency and retention indices of the three trees were 0.76 and 0.88, respectively. These trees had essentially the same topology as that obtained by the NJ method, except for the positions of the three closely related clams in the genus *Tridacna* (*T. squamosa*, *T. crocea*, and *T. maxima*). These differences suggest that the three species are closely related. In this tree, bootstrap value for the clade containing the tridacnid clams and *Vasticardium-Fulvia* was high (0.901). The decay index, which is the number of extra steps required before this clade collapsed, was calculated to be 6. These data suggest that the azooxanthellate cardiid lineage is more likely to form a clade with the zooxanthellate tridacnid clam lineage than with the zooxanthellate cardiid clam lineage. Lineages *Tridacna-Hippopus-Vasticardium-Fulvia* and *Corculum-Fragum* formed a clade, but the bootstrap value was relatively low (0.519).

Due to the computational limitations, we selected nine clam species for a maximum likelihood analysis; one from subclass Pteriomorpha (*Mytilus edulis*) as an outgroup, two from zooxanthellate Cardiidae (*Corculum cardissa* and *Fragum fragum*), two from azooxanthellate Cardiidae (*Vasticardium flavum* and *Fulvia mutica*), two from the genus *Tridacna* (*Tridacna gigas* and *T. derasa*), and two from *Hippopus* (*H. hippopus* and *H. porcellanus*). A total of 1713 sites were used for the ML analysis. The tree topology (Fig. 3), was essentially the same as that obtained by the NJ method. The bootstrap value at the node of *Tridacna-Hippopus* and *Vasticardium-Fulvia* was 0.76, and that of *Tridacna-Hippopus-Vasticardium-Fulvia* and *Corculum-Fragum* was 1.00. The differences between the minimal AIC (Akaike Information Criterion, as defined in the Materials and Methods) and the AICs of the other possible trees were greater than 15.5 ($\gg 1.0$), which suggests that the tree topology shown in Figure 3 is statistically significant.

To examine the genetic difference between individuals from two distant locations, 18S rDNA sequences of *F. fragum* collected from Okinawa and Palau were compared. The identity between them, 99.9% (1864 out of 1865 bp), indicated no significant difference between them.

Insertions and gaps

Table II shows the major gaps and insertions found in 18S rDNAs of cardiids and tridacnids when aligned with those of other clams, especially *Limicolaria kambeul*, listed in Table I. Designations of the regions of the 18S rRNA are shown according to Winnepennickx *et al.* (1992). The table includes any insertions and gaps longer than 10 b in any of the cardiids and tridacnids. Corresponding smaller gaps and insertions in other zooxanthel-

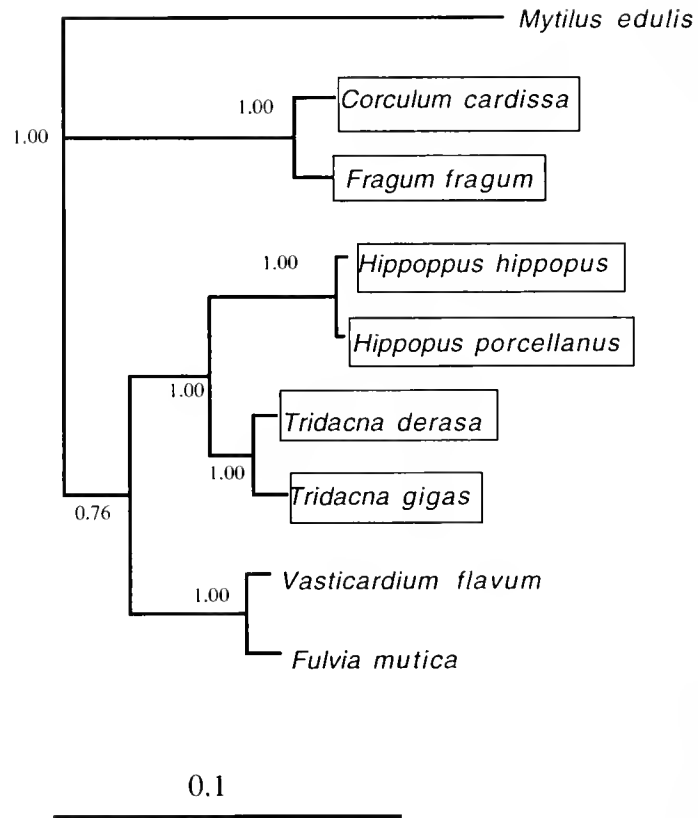


Figure 3. A phylogenetic tree of nine selected bivalves, including zooxanthellate and azooxanthellate clams, calculated by the maximum likelihood method. Bar indicates 0.1 base substitutions per site. Numbers at the nodes are the bootstrap values for the clades in 1000 replications. Box, zooxanthellate clam.

late clams are also shown. Insertions in the E10-1 region are restricted to the azooxanthellate cardiid clams, *V. flavum* and *F. mutica*. On the other hand, zooxanthellate clams have gaps in this region. Some of those insertions were aligned and are shown in Figure 4. The identity between E10-1 insertions of *V. flavum* and *F. mutica* is low (70%). While the inserts in *Corculum* and *Fragum* are similar to each other, those in *Hippopus* are different from those of *Corculum* and *Fragum*. Inserts in region 47 are restricted to *Tridacna*, but *T. gigas* lacks this insertion. Those of *T. squamosa* and *T. maxima* are the same: one base different from that of *T. crocea*, and two bases different from that of *T. derasa*.

Discussion

The tree topologies based on 18S rDNA sequences (Figs. 1–2) are consistent with the morphological taxonomy of Mytilidae, Pectinidae, and Mactridae (Morton, 1996). The family Tridacnidae comprises two genera, *Tridacna* and *Hippopus* (Rosewater, 1965, 1982). The genus

Table 11

Major insertions and gaps in 18S rDNAs in tridacnid and cardiid clams in comparison with those of *Limicolaria kamebeul*

	Regions*	Positions in the alignment†	Size (b)	Species‡
Insertions	E10-1	247-269	23	Vf
			22	Fm
	E21-2	768-782	15	Cc
			12	Ff, Fu
			11	Hh, Hp
			4	Vf, Fm
			3	Tg
			30	Ff, Fu
	41	1484-1513	27	Cc
			4	Vf, Fm, Hh, Hp, Tg, Td, Tc, Ts, Tm
	47	1879-1910	32	Ts, Tc, Tm
			31	Td
			8	Cc
			6	Fm
5			Fu, Ff, Vf, Tg	
Gaps	E10-1	232-281	25§	Hh, Hp, Tg, Td, Tc, Ts, Tm
		232-246	14	Cc, Fu, Ff

Gaps and insertions were detected in the aligned 18S rDNAs listed in Table 1.

* Regions in 18S rRNA of *Limicolaria kamebeul* designated in Winnepennickx *et al.* (1992).

† The alignment is available at the following URL:

<http://www.mbl.edu/html/BB/home.BB.html>

‡ Cc, *Corculum cardissa*; Fu, *Fragum unedo*; Ff, *Fragum fragum*; Vf, *Vasticardium flavum*; Fm, *Fulvia mutica*; Hh, *Hippopus hippopus*; Hp, *Hippopus porcellanus*; Tg, *Tridacna gigas*; Td, *Tridacna derasa*; Tc, *Tridacna crocea*; Ts, *Tridacna squamosa*; Tm, *Tridacna maxima*.

§ Very close gaps or insertions were combined.

Tridacna is further divided into three subgenera, *Tridacna*, *Persikima*, and *Chametrachea*. *Tridacna gigas* belongs to subgenus *Tridacna*; *T. derasa* to *Persikima*; and three species, *T. squamosa*, *T. maxima*, and *T. crocea*, belong to *Chametrachea*. This classical taxonomy also agrees well with the present tree topologies (Figs. 1–3). However, the present data are also in marked disagreement with the classical taxonomy: *i.e.*, the tridacnid clams, genera *Tridacna* and *Hippopus*, are more closely related to the cardiids *Vasticardium flavum* and *Fulvia mutica* than these clams of *Fragum* and *Corculum*, suggesting either that the family Cardiidae is paraphyletic or that tridacnids belong to the family Cardiidae. The correct interpretation—either the traditional taxonomy of Tridacnidae and Cardiidae or the present molecular view of these groups—is obscure. Molecular phylogenetic analyses using some other genes are underway and may answer this question.

The present results indicate that the divergence between the *Corculum-Fragum* lineage and that of *Vasticardium-Fulvia* is deeper than that between *Corculum-Fragum* and *Tridacna-Hippopus*. Because there is no evidence of symbiosis in clams of *Vasticardium* and *Fulvia*, clams in the

tridacnid and *Corculum-Fragum* lineages might have acquired symbiotic relationships with zooxanthellae independently after their divergence from the lineage of *Vasticardium-Fulvia*. An alternative explanation is that the clam ancestral to the three lineages acquired the symbiotic relationship with zooxanthellae, and only the lineage of azooxanthellate Cardiidae lost this characteristic. If the latter explanation is correct, there may be some traces of symbiosis, not yet reported, in some of the azooxanthellate Cardiidae. Further studies are necessary to distinguish between these two hypotheses.

Masuda *et al.* (1994) reported that extracts of mantle homogenates from tridacnid clams (*Tridacna derasa*, *T. maxima*, *T. crocea*, and *H. hippopus*) are much more stimulatory to the excretion of photosynthate by *T. derasa* zooxanthellae than are tissue extracts of zooxanthellate *Fragum* clams, other azooxanthellate bivalves, or gastropods. These may reflect the relative phylogenetic distance between tridacnids and zooxanthellate cardiids, although the active substance in the mantle homogenate is still not known.

Tridacna crocea larvae develop through several morphological stages: straight-hinge and prodissoconch,

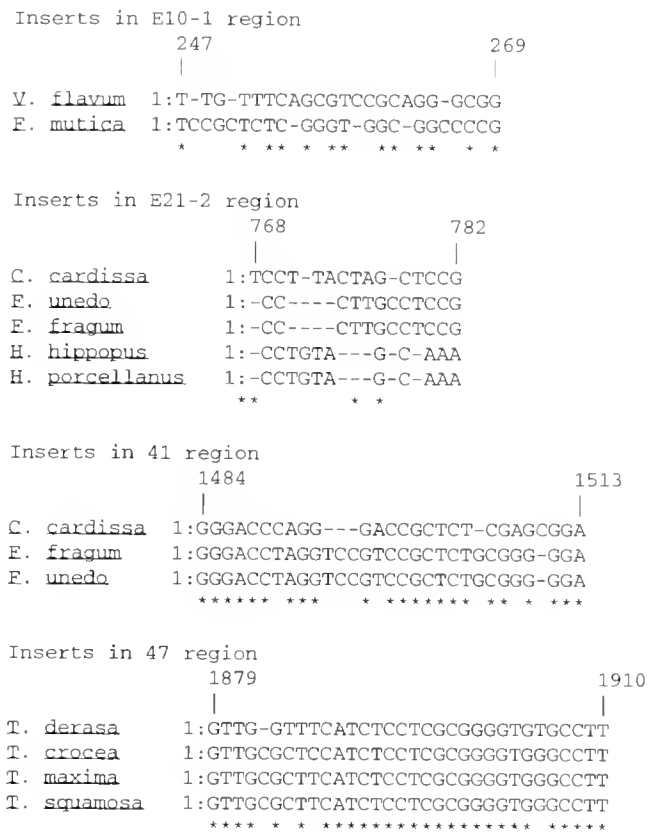


Figure 4. Inserts in 18S rDNAs of zooxanthellate tridacnids and cardiids, as well as in azooxanthellate cardiids, when aligned with 18S rDNA sequences of *Limicolaria kameul*, *Mytilus edulis*, *Placopecten magellanicus*, *Chlamys islandica*, *Spisula solidissima*, and *Tresus nutali*. *, identical base sequence. Numbers at both ends of the sequence indicate the position of the base in the aligned sequences, which are available at the following URL:

<http://www.mbl.edu/html/BB/home.BB.html>

cardiid, proto-tridacnid, and pre-hippopus, before reaching the final tridacnid stage (Kawaguti, 1983b). This suggests that the tridacnid clams evolved from the ancestral cardiid clam. The present phylogenetic topologies (Figs. 1–3) are consistent with this idea.

Insertions in E10-1 in azooxanthellate cardiids are found in the variable region. The identities between these insertion sequences are relatively low, but they might appear after divergence from both of the zooxanthellate cardiids and tridacnids. In region 47, the insertions are restricted to tridacnid clams, except *T. gigas*. This insertion might appear after divergence between *T. gigas* and other *Tridacna* species.

Fossil records of Tridacnidae species are known from the Eocene (Stasek, 1961) and those of *Fragum* only from the Miocene (Keen, 1980). No *Corculum* fossils have been found before the Recent (Keen, 1980). More detailed molecular phylogenetic study, in combination with physi-

ological and paleontological studies on the zooxanthellate and azooxanthellate bivalves, may give us insight into the evolution of symbiosis with zooxanthellae in bivalves.

Acknowledgments

Captain Imura and the crew of the R/V *Sohgen-maru* are acknowledged for the maintenance of the clams. We also thank the staff of the Coral Reef Research Foundation for collecting *Vasticardium flavum*, the staff of the Palau Mariculture Demonstration Center for providing *Corculum cardissa*, and Mr. Ohsumi for a specimen of *Fragum fragum*. We further thank Dr. Okutani of Nihon University for identifying the clams, Mrs. N. Yano for technical assistance, Dr. Ohno and Mr. Odo for discussions on the origins of symbiosis in clams, and Drs. R. A. Lewin and L. Cheng for critical reading of the manuscript. Dr. G. Hinkle is acknowledged for decay analysis. This work was performed as a part of the Industrial Science and Technology Frontier Program supported by the New Energy and Industrial Technology Development Organization. We deeply appreciate critical comments on the manuscript from the editors and reviewers.

Literature Cited

- Adachi, J., and M. Hasegawa. 1994. MOLPHY (program for molecular phylogenetics) 2.2. Institute of Statistical Mathematics, Tokyo.
- Akaike, H. 1974. A new look at the statistical model identification. *IEEE Trans. Autom. Contr.* **19**: 716–723.
- Bremer, K. 1988. The limits of amino acid sequence data in angiosperm phylogenetic reconstruction. *Evolution* **42**: 795–803.
- Bremer, K. 1994. Branch support and tree stability. *Cladistics* **10**: 295–304.
- Felsenstein, J. 1985. Confidence limits on phylogenies: an approach using the bootstrap. *Evolution* **39**: 783–791.
- Felsenstein, J. 1995. PHYLIP (Phylogeny Inference Package) 3.57c. University of Washington, Seattle, WA.
- Fisher, C. R., W. T. Fitt, and R. K. Trench. 1985. Photosynthesis and respiration in *Tridacna gigas* as a function of irradiance and size. *Biol. Bull.* **169**: 230–245.
- Goetsch, W., and L. Scheuring. 1926. Parasitismus und Symbiosis der Algengattung Chlorella. *Z. Morphol. Oekol. Tiere.* **7**: 221–253.
- Griffiths, D. J., and M. Streamer. 1988. Contribution of zooxanthellae to their giant clam host. Pp. 151–154 in *Giant Clams in Asia and the Pacific*, J. W. Copland and J. S. Lucas, eds. Australian Centre for International Agricultural Research, Canberra.
- Hasegawa, M., H. Kishino, and T. Yano. 1985. Dating of the human—age splitting by a molecular clock of mitochondrial DNA. *J. Mol. Evol.* **22**: 160–174.
- Herzog, M., and L. Maroteaux. 1986. Dinoflagellate 17S rRNA sequence inferred from the gene sequence: evolutionary implications. *Proc. Natl. Acad. Sci. USA* **83**: 8644–8648.
- Ishikura, M., C. Kato, and T. Maruyama. 1997. UV-absorbing substances in zooxanthellate and azooxanthellate clams. *Mar. Biol.* **128**: 649–655.
- Kawaguti, S. 1950. Observations on the heart shell, *Corculum cardissa* (L.), and its associated zooxanthellae. *Pac. Sci.* **4**: 43–49.

- Kawaguti, S. 1983a.** The third record of association between bivalve mollusks and zooxanthellae. *Proc. Jpn. Acad. Ser. B.* **59**: 17–20.
- Kawaguti, S. 1983b.** Metamorphosis of the boring clam, *Tridacna crocca*. *Proc. Jpn. Acad. Ser. B.* **59**: 67–70.
- Keen, A. M. 1980.** The pelecypod family Cardiidae: a taxonomic summary. *Tulane Stud. Geol. Paleontol.* **16**: 1–40.
- Kimura, M. 1980.** A simple model for estimating evolutionary rates of base substitutions through comparative studies of nucleotide sequences. *J. Mol. Evol.* **16**: 111–120.
- Klumpp, D. W., B. L. Bayne, and A. J. S. Hawkins. 1992.** Nutrition of the giant clam *Tridacna gigas* (L.). I. contribution of filter feeding and photosynthates to respiration and growth. *J. Exp. Mar. Biol. Ecol.* **155**: 105–122.
- Masuda, K., S. Miyachi, and T. Maruyama. 1994.** Sensitivity of zooxanthellae and non-symbiotic microalgae to stimulation of photosynthate excretion by giant clam tissue homogenate. *Mar. Biol.* **118**: 687–693.
- McNally, K. L., N. S. Govind, P. E. Thomé, and R. K. Trench. 1994.** Small-subunit ribosomal DNA sequence analyses and a reconstruction of the inferred phylogeny among symbiotic dinoflagellates (Pyrrophyta). *J. Phycol.* **30**: 316–329.
- Morton, B. 1996.** The evolutionary history of the bivalvia. Pp. 337–359 in *Origin and Evolutionary Radiation of the Mollusca*, J. Taylor, ed. Oxford University Press, New York.
- Norton, J. H., and G. W. Jones. 1992.** *The Giant Clam: An Anatomical and Histological Atlas*. Australian Centre for International Agricultural Research, Canberra. 142 pp.
- Norton, J. H., H. C. Prior, B. Baillie, and D. Yellowlees. 1995.** Atrophy of the zooxanthellal tubular system in bleached giant clams, *Tridacna gigas*. *J. Invertebr. Pathol.* **66**: 307–310.
- Ohno, T., T. Katoh, and T. Yamasu. 1995.** The origin of algal-bivalve photo-symbiosis. *Palaentology* **38**: 1–21.
- Page, R. D. M. 1996.** TreeView: An application to display phylogenetic trees on personal computers. *Comp. Appl. Biosci.* **12**: 357–358.
- Pardy, R. L. 1980.** Symbiotic algae and ¹⁴C incorporation in the freshwater clam, *Anodonta*. *Biol. Bull.* **158**: 349–355.
- Rosewater, J. 1965.** The family Tridacnidae in the Indo-Pacific. *Indo-Pac. Mollusca* **1**: 347–396.
- Rosewater, J. 1982.** A new species of *Hippopus* (Bivalvia: Tridacnidae). *Nautilus* **96**: 3–6.
- Rowan, R., and D. A. Powers. 1991.** A molecular genetic classification of zooxanthellae and the evolution of animal-algal symbioses. *Science* **251**: 1348–1351.
- Rowan, R., and D. A. Powers. 1992.** Ribosomal RNA sequences and the diversity of symbiotic dinoflagellates (zooxanthellae). *Proc. Natl. Acad. Sci. USA* **89**: 3639–3643.
- Saitou, N., and M. Nei. 1987.** The neighbor-joining method: a new method for reconstructing phylogenetic trees. *Mol. Biol. Evol.* **4**: 406–425.
- Smith, D. C., and A. E. Douglas. 1987.** *The Biology of Symbiosis*. Edward Arnold, London. 302 pp.
- Stasek, C. R. 1961.** The form, growth and evolution of the Tridacnidae (giant clams). *Arch. Zool. Exp. Gen.* **101**: 1–40.
- Thompson, J. D., D. G. Higgins, and T. J. Gibson. 1994.** CLUSTAL W: improving the sensitivity of progressive multiple sequence alignment through sequence weighting, position-specific gap penalties and weight matrix choice. *Nucleic Acids Res.* **22**: 4673–4680.
- Trench, R. K. 1992.** Microalgal-invertebrate symbiosis, current trends. Pp. 129–142 in *Encyclopedia of Microbiology* Vol.3. J. Leaderberg, ed. Academic Press, New York.
- Trench, R. K. 1993.** Microalgal-invertebrate symbioses: a review. *Endocytobiosis Cell Res.* **9**: 135–175.
- Wada, H., K. Makabe, M. Nakanishi, and N. Satoh. 1992.** Phylogenetic relationships between solitary and colonial ascidians, as inferred from the sequence of the central region of their respective 18S rDNAs. *Biol. Bull.* **183**: 448–455.
- Winnepennickx, B., T. Backeljau, Y. van de Peer, and R. D. Wachter. 1992.** Structure of the small ribosomal subunit RNA of the pulmonate snail, *Limicolaria kambeul*, and phylogenetic analysis of the Metazoa. *FEBS Lett.* **309**: 123–126.
- Winnepennickx, B., T. Backeljau, and R. De Wachter. 1996.** Investigation of molluscan phylogeny on the basis of 18S rRNA sequences. *Mol. Biol. Evol.* **13**: 1306–1317.
- Yellowlees, D., M. L. Dionisia-Sese, K. Masuda, T. Maruyama, T. Abe, B. Baillie, M. Tsuzuki, and S. Miyachi. 1993.** Role of carbonic anhydrase in the supply of inorganic carbon to the giant clam-zooxanthellate symbiosis. *Mar. Biol.* **115**: 605–611.
- Yonge, C. M. 1980.** Functional morphology and evolution in the Tridacnidae (Mollusca: Bivalvia: Cardiacea). *Rec. Aust. Mus.* **33**: 735–777.

Electrophysiology and Innervation of the Photosensitive Epistellar Body in the Lesser Octopus *Eledone cirrhosa*

CHRISTOPHER S. COBB^{1,*} AND RODDY WILLIAMSON^{1,2}

¹ *The Marine Biological Association of the UK, The Laboratory, Citadel Hill, Plymouth, PL1 2PB, UK; and* ² *Department of Biological Sciences, University of Plymouth, Drake Circus, Plymouth, PL4 8AA, UK*

Abstract. The innervation and responses to light of the cephalopod epistellar body were investigated in preparations isolated from the stellate ganglia of the lesser or northern octopus, *Eledone cirrhosa*. Extracellular generator potentials in response to flashes of light were recorded from these photosensitive vesicles, with the amplitude of the response being found to be dependent upon the intensity of the flash and the level of ambient illumination. Intracellular recordings from photoreceptor cells of the epistellar body showed that they had resting potentials of about -49 ± 7 mV (mean \pm SD, $n = 43$) and were depolarized by flashes of white, but not red (>650 nm) light. The evoked depolarization consisted of a transient component, followed by a steady plateau in which the amplitude of the depolarization was well correlated with the log of the stimulus intensity. The evoked depolarizations induced action potentials in the photoreceptor cells, with the frequency of firing being well correlated with the stimulus intensity. The morphologies of individual photoreceptor cells were visualized by intracellular injections of the fluorescent dye Lucifer yellow, and the path of the epistellar nerve across the stellate ganglion, into the pallial nerve, toward the brain was traced using the lipophilic dye Di-I. This pathway was confirmed physiologically by recording light-evoked responses from the cut end of the pallial nerve.

Introduction

Most cephalopods have, in addition to their retinal photoreceptor system, extraocular photoreceptors or photo-

sensitive vesicles (PSVs). The PSVs of octopods such as *Eledone moschata* are located inside the mantle sac and appear as a small pigmented vesicle on the ventral posterior margin of the stellate ganglion (Bauer, 1909; Young, 1936, 1971; reviewed in Mauro, 1977; Fig. 1). These PSVs have also been termed the 'epistellar bodies' (Young, 1929, 1936). The ultrastructure of the epistellar body of *E. moschata* shows packed arrays of photoreceptor cells with microvilli, reminiscent of rhabdomeres, but without dioptric apparatus (Nishioka *et al.*, 1962), together with an epistellar nerve running into the stellate ganglion (Young, 1936; Perrelet and Mauro, 1972). The epistellar photoreceptor system in *E. moschata* has been shown to contain the visual pigment rhodopsin, with a maximum absorption wavelength of 475 nm; this is very close to 470 nm, which is the maximum absorption wavelength of retinal rhodopsin in this octopod species (Nishioka *et al.*, 1966; Mauro, 1977). This wavelength is also close to electrophysiological estimates of spectral sensitivity in *E. moschata* (Nishioka *et al.*, 1966; Mauro, 1977). The accessory pigment retinochrome is also present in cephalopod PSVs (Hara and Hara, 1980; Ozaki *et al.*, 1983). Although preliminary evidence has indicated that the photoreceptor cells within the epistellar body of octopus give depolarizing responses to light (Mauro and Baumann, 1968; reviewed in Mauro, 1977), there has been no detailed study of these responses.

Previously we have shown that extracellular, light-induced generator potentials in the epistellar bodies of *Eledone cirrhosa* can be produced by light flashes of different intensity and duration, transmitted through the mantle sac wall of the octopus (Cobb *et al.*, 1995a,b). In addition, the normal circadian behavioral rhythm entrained by a

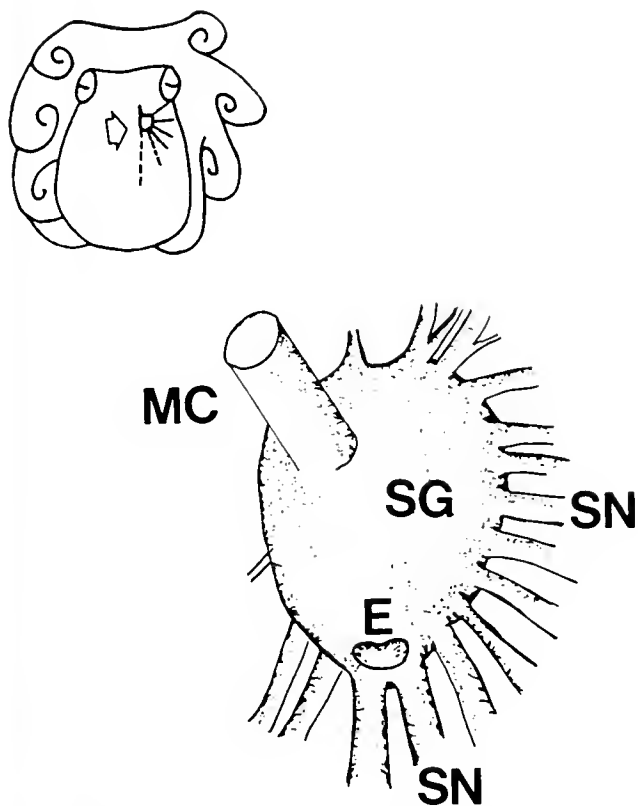


Figure 1. Diagrams showing the position of the photosensitive vesicle or epistellar body in an octopus (not to scale). Top left: dorsal right view of octopus showing position of stellate ganglion (arrow) attached to the inner surface of the dorsal mantle sac wall. Bottom right: ventral view of left stellate ganglion in the same orientation as top left, with epistellar body (E), stellate ganglion (SG), stellar nerve (SN), and mantle connective or pallial nerve (MC) indicated.

light-dark cycle is maintained after removal of the epistellar body in sighted octopus (Cobb *et al.*, 1995a,b). In the present study, we examine the capacity of the octopod extraocular photoreceptor system for light detection by characterizing the extracellular and intracellular responses to light flashes of increasing intensity and duration in the octopus *Eledone cirrhosa*. Lucifer yellow was used to stain iontophoretically and identify the photoreceptor cells in the octopus epistellar body; there was no evidence for dye coupling between these extraocular photoreceptor cells. It is also established that the epistellar body sends afferent nerves that pass across the stellate ganglion and connect with the central nervous system, *via* the mantle connective (pallial) nerve.

Materials and Methods

Collection and maintenance of experimental animals

The lesser or northern octopus, *Eledone cirrhosa* (dorsal mantle length 5–14 cm) used in this study were caught

offshore near the coast of Plymouth, UK, at a depth of 10–15 m and transported to laboratory holding tanks with flow-through, aerated seawater at 12°–18°C. To prevent the octopus from escaping, the side walls of the tank were lined with 1-cm-thick sheets of plastic foam (Boyle, 1981). Octopus were supplied with live crab (*Carcinus maenas*) food *ad libitum* and were maintained in the tank system for up to 9 months until required.

Electrophysiology

For electrophysiological recordings, an octopus was anesthetized with 3% ethanol in seawater and decapitated. The paired stellate ganglia and attached epistellar bodies were then removed from the dorsal mantle wall. The epistellar body and attached stellate ganglion were washed in fresh seawater and pinned out, ventral side up, in a Sylgard-lined recording dish filled with filtered artificial seawater (ASW: NaCl 470 mM, KCl 10 mM, MgCl₂ 50 mM, CaCl₂ 10 mM, MOPS (3-[N-Morpholine]propane-sulfonic acid) 10 mM, pH adjusted to 7.8, osmolarity 1010 mmol/kg). All subsequent electrophysiological recordings were made at room temperature (between 18° and 23°C).

Illumination stimuli were provided by a Schott KL1500 cold light source, with a quartz halogen bulb (Thorn EMI 15 V, 150 W). The light was passed through a standard heat filter into a glass fiber light guide and then, *via* an electronically controlled shutter and a second fiber light guide, to the ventral side of the stellate ganglion and epistellar body. The duration of the light flash was set by the electronic shutter (Uniblitz T132, Optilas Ltd, UK) to between 10 ms and 10 s. The light intensity was varied by inserting neutral density filters into the light path and was measured at the preparation level using a portable calibrated radiometer (Ealing Electro-optics, UK: model 27-5479). An additional, uncalibrated photocell was used to record the precise timing and duration of the stimulus light flashes. In some experiments, a red filter (Kodak 1A, UK, wavelength >650 nm) was introduced into the light path. Suction electrodes were used to take extracellular recordings from the mantle connective (pallial) nerve of the stellate ganglion in response to flashes of white or red light that were applied to the epistellar body of the preparation from two octopus.

The extracellular receptor potentials were recorded by inserting a low-resistance microelectrode (2 MΩ resistance when filled with ASW) into the epistellar body wall. Intracellular recordings from photoreceptor cells in isolated intact epistellar bodies were made using high-resistance microelectrodes of borosilicate glass capillaries with inner filaments (Clark Electrochemical, UK, GC-150F, 1.5 mm OD × 0.86 ID), filled with 3 M KCl and having tip resistances of 30–150 MΩ. A conventional

microelectrode amplifier (AxoClamp 2B amplifier, Axon Instruments, Inc. USA) was used for recording resting, generator, and receptor potentials and for injecting current pulses through the intracellular microelectrode. In some experiments, octopus photoreceptor cells were injected iontophoretically with the fluorescent naphthalimide dye Lucifer yellow CH (Stewart, 1978; Sigma, UK). For this the microelectrodes were back-filled with 3% Lucifer yellow in 1 M LiCl and had resistances of 150–200 M Ω . Injections of hyperpolarizing current (1.0 nA at 1 Hz) resulted in rapid movement of Lucifer yellow into the cells, and dye filling was considered complete after 30 min. Resting potential was recorded during cell impalement and generator potentials were recorded in response to light flashes, before switching to current injection in these experiments. Immediately after dye injection, the preparation was photographed in whole mount under an epifluorescent microscope, using color film (400 ASA).

For normal recordings, the signal from the microelectrodes was amplified and, together with the signal from the photocell monitor, was passed to a computer-controlled signal averager (CED 1401 computer interface running Sigavg software, Cambridge Electronic Design, UK). Typically, 5–10 responses were averaged to improve signal-to-noise ratios, and repeated light flash stimuli were separated by at least 20 s. The octopus preparations remained viable for at least 6 h. Illumination of the experimental 'darkroom' was provided by red safelight (>650 nm). Illumination of 0.1 $\mu\text{W}/\text{cm}^2$ with this red light was found not to cause a decrement in photoreceptor response.

Epistellar body innervation

Innervation of the epistellar body was studied by orthodromic filling from the epistellar body using the lipophilic dye Di-I (Honig and Hume, 1989) in 10 animals. With the aid of a dissecting microscope, the ASW was removed from the dish and a crystal of the fluorescent carbocyanine lipophilic dye Di-I (1,1'-dioctadecyl-3,3,3',3' tetramethylindocarbocyanine perchlorate, D-282 (Di-I C18(3)), Molecular Probes, Inc. USA) was placed inside the epistellar body of each stellate ganglion through an incision made with a fine steel pin or razor blade. The tissues were then fixed in 2.5% paraformaldehyde in 0.1 M phosphate buffer. A microscope with epifluorescence and a rhodamine filter (Nikon DM580) was used to map the progress of the orange Di-I fluorescence from the epistellar body, across the stellate ganglion, through axons and into the pallial nerve over several days. Tissues were cleared in 60% (w/v) meglumine iohalamate with 0.01% (w/v) sodium calciumedetate and 0.01% (w/v) sodium acid phosphate (product: Conray 280, May & Baker Ltd (Rhône-Poulenc Group), UK; Zill *et al.*, 1993), before the Di-I

stained axons were photographed (400 ASA Kodak black-and-white film), under the epifluorescence microscope with rhodamine filter set. Additional white light illumination was sometimes used to observe and photograph the relative positions of fluorescent Di-I-filled axons and the stellate ganglion tissue.

Results

Anatomy and innervation of the octopus epistellar body

Figure 2 shows the size, shape, and position of the epistellar body that contains the extraocular photoreceptors on the stellate ganglion of *Eledone cirrhosa*. The epistellar body is located at the ventral posterior margin of the ganglion and is commonly spherical (Fig 2A), although it sometimes appears divided into two or more compartments (Fig 2B). It is confined within the common capsule of connective tissue surrounding the ganglion, but is separated from the ganglionic neuronal cell bodies by one or more sheath layers. The epistellar body is usually orange in freshly dissected preparations, but the color may fade with time after dissection or be absent in some animals, particularly larger, older specimens.

In the course of the intracellular recordings described below, some photoreceptor cells ($n = 4$) were injected

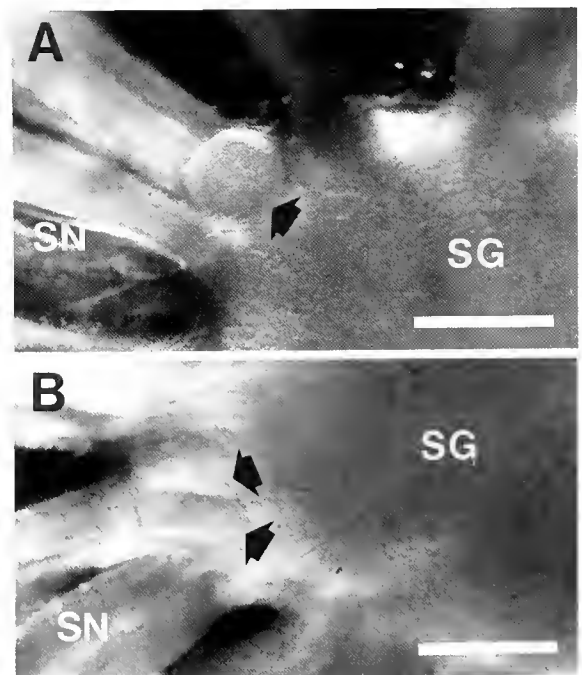


Figure 2. Epistellar body (arrows), stellate ganglion (SG), and stellate nerves (SN) of the octopus *Eledone cirrhosa*. The epistellar body is commonly spherical (A), but sometimes appears to be divided into two compartments (B). Scale bars are 1 mm.

with Lucifer yellow, a fluorescent dye (Fig. 3). The dye fills showed that the photoreceptors have a cell soma ($50\ \mu\text{m}$) that is located in the wall of the epistellar body and gives rise to a single axon, extending towards the periphery of the epistellar body. The axons from separate photoreceptor cells converge outside the epistellar body to form the 'epistellar' nerve. In addition, a process that may be as long as $100\ \mu\text{m}$ projects towards the center of the epistellar body, sometimes dividing or branching toward its distal end. No dye coupling between photoreceptors was observed in any of the cells that were well filled with dye.

Figure 4A shows an epistellar body, the attached stellate ganglion, and the connection of the mantle connective (pallial) nerve to the ganglion. For all cases ($n = 8$) in which the epistellar body and attached stellate ganglion preparations were filled with fluorescent Di-I (Fig. 4B, C, D), orthodromic fills indicated that the epistellar body gave off an 'epistellar' nerve (Fig. 4B, C, D) that passed across the stellate ganglion, into the mantle connective (pallial) nerve (Fig. 4B, C), and then, presumably, to the brain. The nerve bundle was more shallow in its path across the stellate ganglion in some preparations ($n = 2$) than in others. In these preparations, the epistellar nerve remained intact and branched, sometimes into three separate fiber bundles (Fig. 4B), only before entry to the mantle connective (pallial) nerve. In addition, these preparations showed a single nerve branch, which occurred close

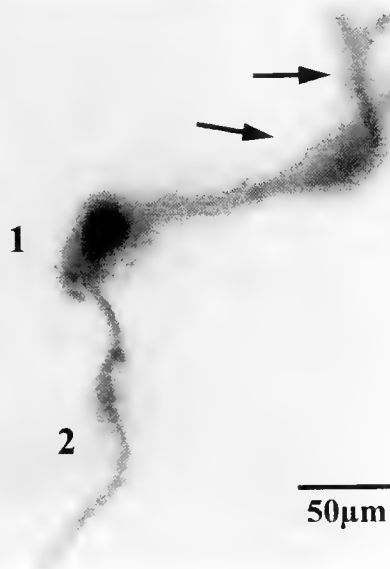


Figure 3. Iontophoretic microinjection of Lucifer yellow into an epistellar body photoreceptor cell. Detail of photoreceptor cell filled with Lucifer yellow showing cell soma (1) and axon process (2). Note long, branched process (arrows) that extends toward the center of the epistellar body.

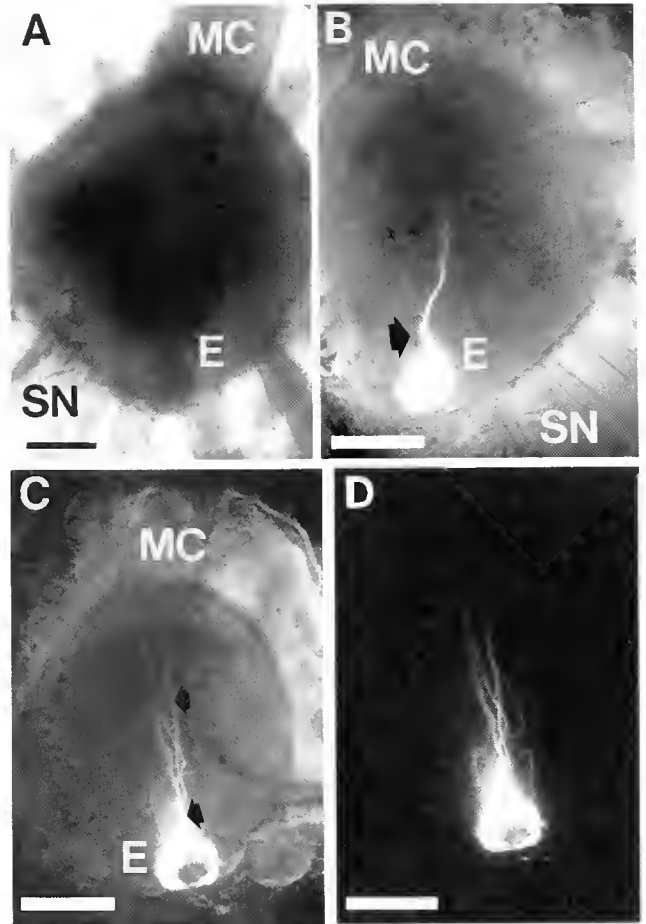


Figure 4. Innervation of the epistellar body. (A) Epistellar body and stellate ganglion of the octopus *Eledone cirrhosa*. The ovoid epistellar body (E) lies at the posterior end of the stellate ganglion near the origin of several stellar nerves (SN), opposite the mantle connective (pallial) nerve (MC). Scale bar is 1 mm. (B) Whole mount of epistellar body and stellate ganglion with orthodromic fluorescent Di-I-filled 'epistellar' nerve (arrow), epistellar body (E), stellate nerves (SN), and mantle connective (pallial) nerve (MC). Scale bar is 1 mm. (C) Whole mount of stellate ganglion with orthodromic fluorescent Di-I-filled epistellar body photoreceptor cell axons (arrows) connecting the epistellar body (E) and the mantle connective (pallial) nerve (MC). Scale bar is 1 mm. (D) Whole mount as in (C) under rhodamine-filtered light only, showing detail of Di-I-filled axons. Scale bar is 1 mm.

to the epistellar body. This branch separated from the epistellar nerve and passed deep into the stellate ganglion, to an unidentified destination (Fig. 4B). However, in most preparations examined ($n = 8$), the Di-I-filled epistellar nerve branched close to the epistellar body, forming numerous nerve bundles that passed into the mantle connective nerve and then toward the central nervous system (Fig. 4C, D). In addition to the epistellar nerve, these preparations showed two Di-I-filled nerves running from the side of the epistellar body in parallel to and on each side of the epistellar nerve (Fig. 4C, D). These parallel

nerve bundles then appeared to focus on the central path of the epistellar nerve bundles and pass into the center of the stellate ganglion (Fig. 4C, D), perhaps to the neuropil. The destination remains conjecture, however, because none of the preparations examined showed conclusive evidence of interaction between a Di-I-filled nerve fiber and the neuropil of the stellate ganglion.

Recordings from the mantle connective (pallial) nerve

To test whether light-evoked activity from the epistellar body could be observed in the mantle connective (pallial) nerve, suction electrode recordings were made from the cut end of the nerve as controlled light flashes were applied to the epistellar body. When white light was flashed, a compound action potential was observed, mainly comprising a large downward trough (Fig. 5). To test for artifacts and to determine the spectral sensitivity of the suction electrode response, a flash stimulus of red light was produced by using a >650 nm filter. Whereas a flash of white light evoked an extracellular voltage response in the mantle connective (pallial) nerve, a flash of red light, of the same duration, evoked no response (Fig. 5). The relatively long delay between stimulus and response does not permit any conclusions to be drawn about whether this is a direct or post-synaptic response; clearly the former would be expected.

Electrophysiology of the epistellar body photoreceptors

Generator potential responses induced by light flashes of constant duration but increasing intensity were recorded extracellularly from the epistellar body photoreceptors of the octopus, *Eledone cirrhosa* (Fig. 6A). The generator potential appeared as a short-latency downward deflection of the voltage trace, and the amplitude of the evoked response increased with increasing flash intensity. A graph of response against stimulus intensity (Fig. 6B) shows that the amplitude of the evoked response was well correlated to the log of light intensity across the entire range examined (Fig. 6B). The latency between the start

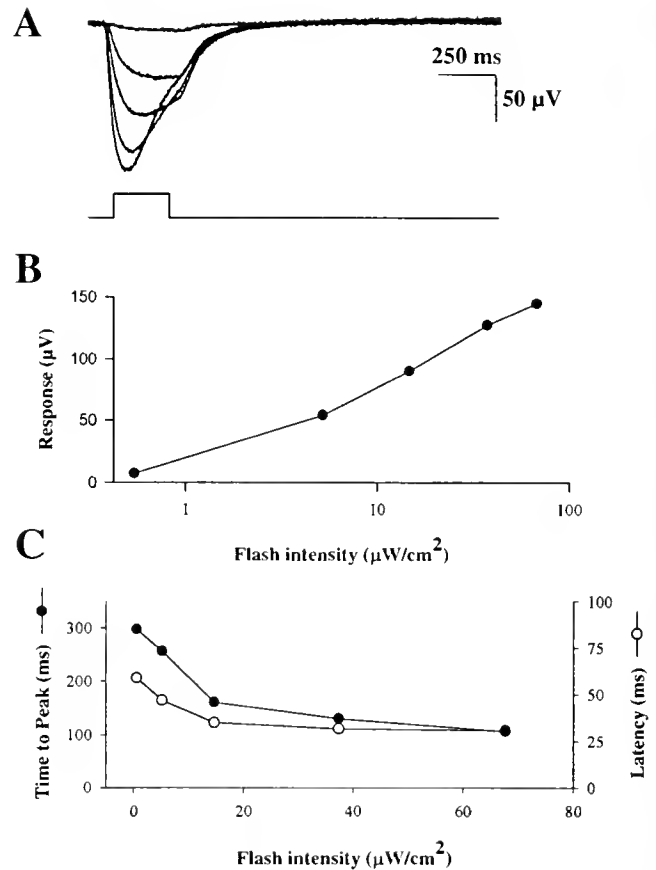


Figure 6. Epistellar body responses to change in intensity of the light stimulus. (A) Upper traces show generator potentials recorded extracellularly from photoreceptor cells in the epistellar body in response to a series of 250-ms-duration light flashes, as indicated in the lower trace, of increasing intensity. (B) Graph of log light-flash intensity against extracellular response amplitude. (C) Latency and rise time of the extracellular response with increasing stimulus intensity.

of the stimulus and the start of the photoreceptor response was between 40 and 25 ms, and this latency decreased with increased stimulus intensity (Fig. 6C). Increasing stimulus intensity was also linked with a decrease in the time from the start of the stimulus to the peak of the response or rise time (Fig. 6C). The epistellar photoreceptor cells needed some time to recover from each light flash: the extracellular response generated by a second flash given 2.5 s after the first was reduced by almost 80% (Fig. 7A). This decrease in response was evident up to 30 s after the first light flash. A plot of the response amplitude to the second flash (Fig. 7B) showed that the recovery had an exponential time curve with a time constant of almost 6 s. Similarly, the size of the extracellular response to a single light flash was affected by the intensity level of ambient illumination (Fig. 8). Figure 8A shows the extracellular responses to constant light flashes given after at least a 1-min exposure to three different

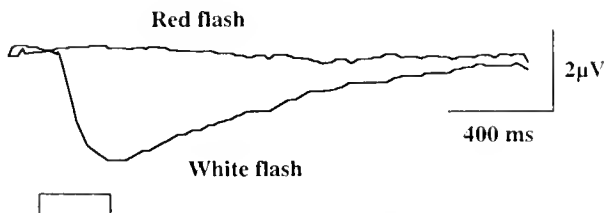


Figure 5. Light-evoked extracellular responses in the mantle connective (pallial) nerve of the stellate ganglion preparation recorded by suction electrode in response to flashes of white and red light. Duration of the light flash applied to the epistellar body is indicated in the bottom trace.

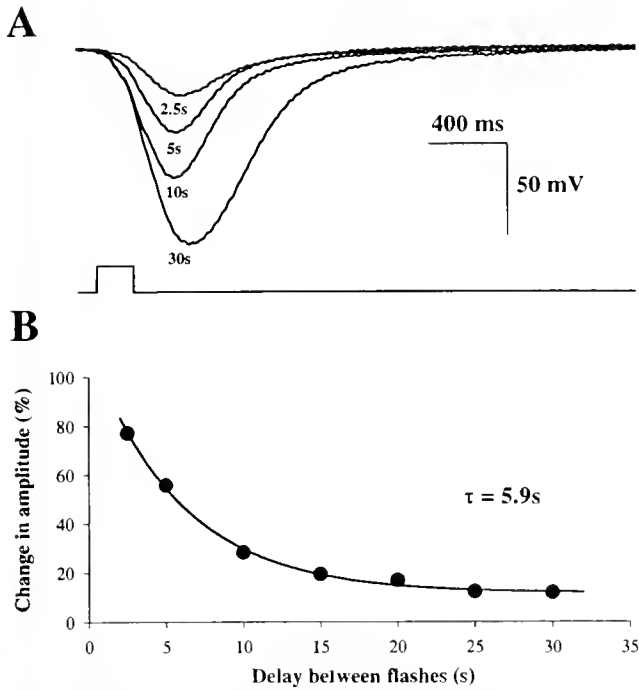


Figure 7. Adaptation or recovery responses between light flashes to the epistellar body. (A) Upper traces show examples of photoreceptor cell generator potentials recorded extracellularly from the octopus epistellar body in response to a series of 200-ms-duration light flashes with increased delay between flashes, but constant intensity (34 $\mu\text{W}/\text{cm}^2$), as indicated in the lower trace. (B) Amplitude of the extracellular response with increasing delay between flashes.

intensity levels of 'background' illumination. It can be seen that the greater the level of background illumination, then the smaller the extracellular response to the light flash; Figure 8B shows that the relationship is more-or-less exponential.

Intracellular recordings from individual photoreceptor cells demonstrated that, in the dark, these had membrane resting potentials of about $-49 \pm 7\text{ mV}$ (mean \pm SD, $n = 43$); such recordings could be maintained for up to 45 min. Epistellar body photoreceptors responded to a short flash of white light with a depolarization that often resulted in the firing of a burst of action potentials (Fig. 9). Although not studied in detail, this response was dependent on the wavelength of the light stimulus, for stimuli at wavelengths greater than 650 nm evoked no response (Fig. 9). This also provided confirmation that the response was not artifactual or related to other stimuli, such as the noise of the mechanical shutter. The amplitude of the intracellular receptor potential response varied with the intensity of the light flash (Fig. 10A). A graph of these responses (Fig. 10B), demonstrated that the amplitude of the depolarization was well correlated to the log of the light-flash intensity across the intensity range examined. Similarly, Figure 10B illustrates that the peak firing fre-

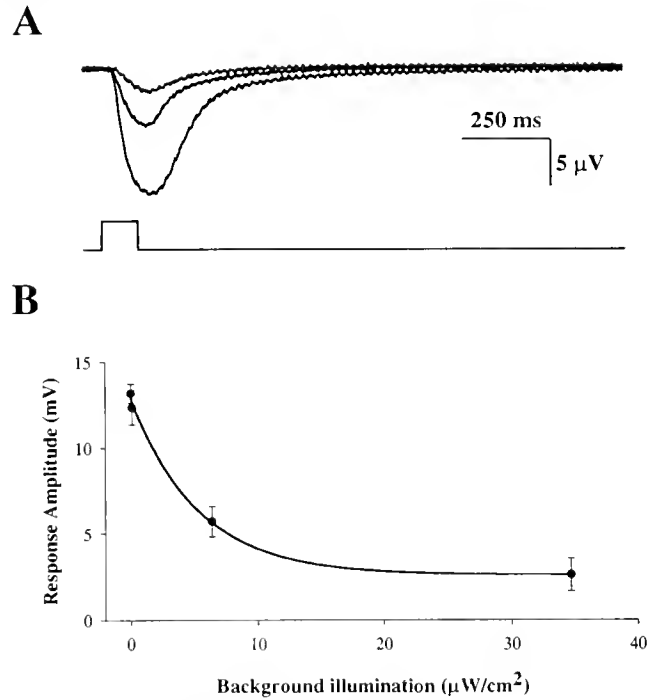


Figure 8. Effect of background illumination on the response of the epistellar body to light-flash stimuli. (A) Upper traces show examples of photoreceptor cell generator potentials recorded extracellularly from the octopus epistellar body in response to a 200-ms-duration light flash (intensity 167 $\mu\text{W}/\text{cm}^2$), as indicated in the lower trace, while subjecting the epistellar body to increased background illumination. (B) Amplitude of the extracellular response with increasing background illumination. In all cases each point represents the mean \pm SEM, $n = 10$ separate receptor responses.

quency of the resulting action potentials was well correlated to the log of the stimulus intensity and the conversion factor from receptor potential to action potentials or 'spikes' is about 2 spikes/mV depolarization; that value is within the range of other invertebrate spike encoding photoreceptor cells—for example 1 spike/mV in eccen-

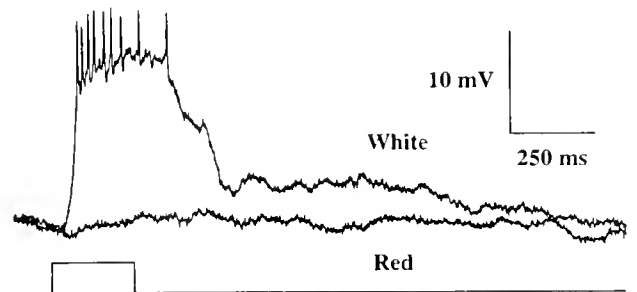


Figure 9. Intracellular receptor potential's response to white and red light (>650 nm) stimuli recorded from the same photoreceptor cell in an epistellar body. The lower trace indicates the time and duration of 250-ms light flashes. Light-flash intensity was 167 $\mu\text{W}/\text{cm}^2$ and resting potential was -53 mV in both cases.

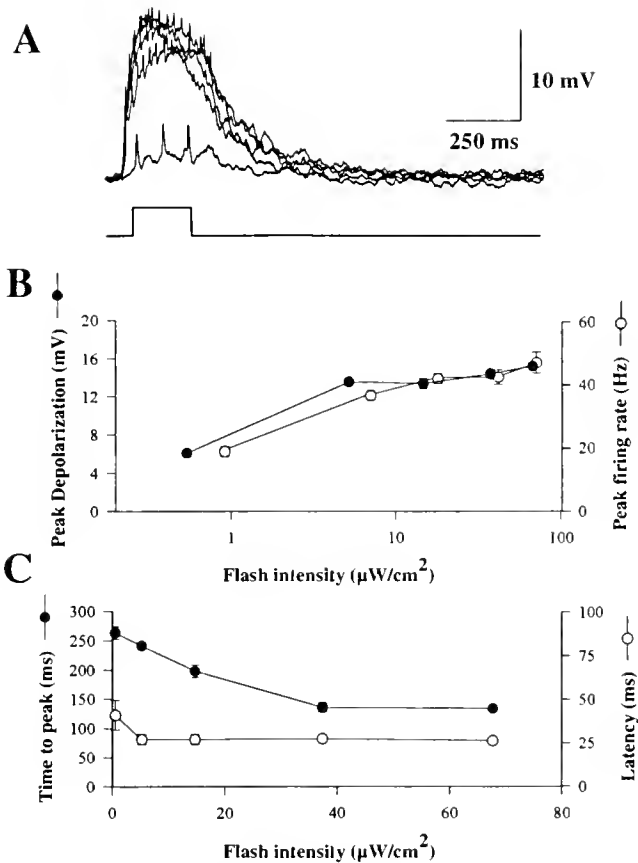


Figure 10. Typical intracellular receptor potentials recorded in a photoreceptor cell from an epistellar body, in response to change in light-flash stimulus intensity. Resting potential was -42 mV to -47 mV. (A) The upper traces show the photoreceptor potentials in response to the series of 250-ms-duration light flashes, as indicated in the lower trace in response to increased intensity. (B) Graph of light-flash intensity against response receptor potential amplitude and peak firing frequency. (C) Rise time and latency of receptor potentials against increased light stimulus intensity. In all cases each point represents the mean \pm SEM. $n = 10$ separate receptor potential responses to light-flash stimuli from a single photoreceptor cell. In some cases the SEM is too small to be visible.

tric cells from *Limulus polyphemus* (Behrens and Wulff, 1965). As already seen for the extracellular compound generator potentials, the time-to-peak depolarization for individual photoreceptor cells decreased with increasing stimulus intensity (Fig. 10C). However, stimulus-to-response latency for individual photoreceptor cells was fairly constant at around 25 ms for flashes of intensity greater than $5 \mu\text{W}/\text{cm}^2$, but longer for very weak flashes (Fig. 10C). The effect of long-duration (5 s and 10 s) but constant-intensity stimuli on the intracellular photoreponse was examined. There was an increase in the duration of the receptor potential as the light stimulus was lengthened from 5 s to 10 s, with the long-lasting plateau maintained for the duration of the stimulus and then

slowly decaying back to the normal resting potential for the photoreceptor cell (Fig. 11); this probably indicates that the action potentials do not actively invade the cell soma and are thus attenuated or absent in some soma recordings.

Discussion

A number of morphological and biochemical studies have shown that octopod and decapod cephalopods have extraocular photoreceptors (reviewed in Messenger, 1991). Young (1936) first described epistellar structures in several octopod genera; from histological considerations, he hypothesized that these might have a neurosecretory function. The epistellar body of *Octopus vulgaris* was later re-investigated in detail using electron microscopy and found to contain cells that have microvilli very like those found in the rhabdomeres of the extraocular photoreceptors seen in other molluscs and arthropods (Nishioka *et al.*, 1962). This work was later extended to include the epistellar bodies of *Eledone moschata* (Nishioka *et al.*, 1966); in it, electron microscopy gave further evidence for a rhabdomeric ultrastructure, and biochemical evidence indicated the presence of the photopigment rhodopsin. These studies thus implied that the neuronlike cells of the epistellar body were not neurosecretory, but photoreceptor cells. This agreed with comparative studies showing the presence of extraocular photosensitive cells in the central nervous systems of many other invertebrates—for example, in the caudal ganglion of the crayfish (Kennedy, 1963) and the molluscs *Aplysia californica* (Arvanitaki and Chalazonitis, 1961) and *Onchidium veruculatum* (Hisano *et al.*, 1972). Preliminary electrophysiological evidence demonstrating a light-evoked response from cephalopod epistellar body photoreceptor cells was first obtained by Mauro and Baumann (1968) in an octopus, *Eledone moschata*. Decapod cephalopods such as the

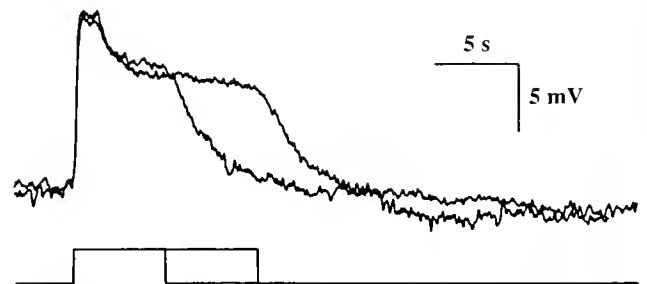


Figure 11. Intracellular receptor potentials recorded in a single photoreceptor cell from an epistellar body in response to constant intensity ($77 \mu\text{W}/\text{cm}^2$) and increased long-duration light stimuli. The receptor potentials recorded from a 5-s and 10-s light flash are shown as indicated by the stimulus marker in the bottom trace. Resting potential was -50 mV.

squid *Loligo vulgaris* and the cuttlefish *Sepia officinalis* also have PSVs, or 'parolfactory vesicles'; these are not located on the stellate ganglia, but lie underneath the cranial cartilage casing on and below the optic tract (Young, 1936; Perrelet and Mauro, 1972). These PSVs also have neuronlike cells with a rhabdomeric ultrastructure containing rhodopsin (Nishioka *et al.*, 1966; Baumann *et al.*, 1970) and their responses to light stimuli have been briefly reported for *Todarodes sagittatus* (Mauro and Sten-Knudsen, 1972; Mauro, 1977), *Loligo pealei* and *Loligo forbesi* (Sperling *et al.*, 1973; Cobb and Williamson, 1998).

Electrophysiology of extraocular photoreceptor cells

Using extracellular and intracellular recordings from extraocular photoreceptors in *Eledone cirrhosa*, the present study extends our understanding of the electrophysiology of epistellar body photoreceptors in cephalopods. The results show that the photoreceptors have cell resting potentials of about -49 ± 7 mV and respond to a flash of light with a depolarization consisting of a transient component, often accompanied by a burst of action potentials, followed by a steady-state or plateau depolarization. The amplitude of the evoked depolarization and the peak firing frequency of the cell were directly correlated with the intensity of the light flash. No 'quantum bumps' were observed in these recordings, although these have been reported in recordings from the extraocular photoreceptors of *Eledone moschata* (Mauro and Baumann, 1968), as well as from other invertebrates (Lisman and Brown, 1975).

The extracellular generator potentials recorded from the epistellar body of *Eledone cirrhosa* showed adaptational changes when the level of ambient illumination was increased in this study. This agrees well with the adaptational changes seen in retinal photoreceptors for cephalopods (Weeks and Duncan, 1974) and other invertebrates (Laughlin, 1989). It should be noted that there are no reports of screening pigments in cephalopod extra-retinal photoreceptors, so the mechanism of screening pigment migration cannot be invoked here. The observed decrease in the stimulus-to-response latency of the evoked intracellular depolarization (from about 40 ms to 25 ms) with increasing intensity is similar to that seen in photoreceptor latency measurements from the epistellar bodies of both *Eledone moschata* and *Eledone cirrhosa* (Mauro, 1977; Cobb *et al.*, 1995b) and also from the retina of *Sepioida atlantica*, a sepiolid cephalopod (Duncan and Weeks, 1973). The small differences between the latency values reported in this study (40 ms) and in the others (30 and 23 ms, respectively) are probably due to the different stimulus intensities used, for as shown above, the onset delay decreases with stimulus intensity.

When two extraocular photoreceptor cells from the same cluster in a parolfactory vesicle from a squid (*Loligo pealei*) were impaled simultaneously, partial electrical coupling was recorded in 1 out of 4 pairs of cells (Sperling *et al.*, 1973). In the present study, which used extraocular photoreceptor cells from the epistellar body of an octopus (*Eledone cirrhosa*), no evidence of Lucifer yellow dye coupling was observed. The lack of dye coupling may perhaps indicate a lack of electrical coupling, for the two are often well correlated, as, for example, in the horizontal cells of the turtle retina (Stewart, 1978) and in the pineal gland photoreceptors of teleost fish, where numerous gap junctions are present (Omura, 1984), and Lucifer yellow dye coupling has been observed (Nakamura *et al.*, 1986). However, electrical coupling is not always associated with dye coupling, particularly in molluscan preparations (Williamson, 1989; Ewadinger *et al.*, 1994).

Light-flash stimuli transmitted through the red filter (Kodak 1A, wavelength >650 nm) neither stimulated the PSVs from *Eledone cirrhosa* nor evoked an afferent response in the mantle connective nerve; therefore, this wavelength of red light (>650 nm), at the intensities used in this study, did not stimulate the photoreceptors. This outcome was perhaps to be expected, for the photoreceptors in both the retinal and extra-retinal systems of *Eledone moschata* have a rhodopsin absorption maximum around 470 nm (Nishioka *et al.*, 1966; Hamdorf *et al.*, 1968), and the red light stimuli are therefore likely to be outside the detection range of the photoreceptors, at the stimulus intensities employed here.

Innervation of the epistellar body

Orthodromic fills of the photoreceptor axons with fluorescent Di-I from the epistellar body of *Eledone cirrhosa* have shown nerve bundles passing from the epistellar body into the mantle connective (pallial) nerve. Microanatomical studies, silver-staining techniques, and electron microscopy were used in studies of the octopuses *Eledone moschata* and *Octopus vulgaris* to trace the 'epistellar nerve' from the photoreceptor cells of the epistellar body, through the stellate ganglion, to the mantle connective (pallial) nerve (Young, 1936; Cazal and Bogoraze, 1944; Nishioka *et al.*, 1966; Perrelet and Mauro, 1972). In addition, degeneration of nerve fibers running to the epistellar body was shown in *E. moschata* after the mantle connective nerve was cut (Young, 1936). The mantle connective (pallial) nerve is known to contain about 16,000 nerve fibers (Young, 1965), with two groups of efferent, and possibly two groups of afferent fibers (Young, 1971). In *E. moschata*, the epistellar nerve contains about 1500 afferent nerves (Perrelet and Mauro, 1972). Therefore, the selective nerve tracing in this study (using Di-I and electrophysiological recordings from the mantle connec-

tive (pallial) nerve) presents new evidence supporting the view that the epistellar nerve contains the afferent axons of extraocular photoreceptor cells, and that these axons conduct photoreceptive information to the central nervous system in the octopus. Whether such sensory information passes to the palliovisceral lobe of the octopus brain from nerves carried in the mantle connective (pallial) nerve remains to be determined.

In summary, this study provides further evidence for the presence of an active extraocular photoreceptor system in adult cephalopod molluscs. However, the functional role of the epistellar body and parolfactory vesicles in octopus and squid still remains enigmatic. The lack of a structurally organized retina or optical apparatus such as a lens, and the relatively deep location of all these PSVs argues against any function in visual image formation. Rather, it is generally assumed that in both octopods and decapods the extraocular photoreceptors play a role in monitoring ambient light levels over lengthy periods; that is, they function as a photometer (Mauro, 1977; Houck, 1977a,b), perhaps connected with seasonal reproductive activity (Baumann *et al.*, 1970), control of circadian activity rhythms in octopods (Houck, 1977ab, 1981, 1982), diel vertical migration in squid (Palmer and O'Dor, 1978), or even the feedback control of ventral photophores in midwater squid such as *Abralia trigonura* (Young, 1972, 1973; Young *et al.*, 1979).

Observations increasingly suggest that the influences of environmental light on the physiology and behavior of cephalopods may be detected not only by the eye, but also by an array of other photoreceptor organs, including the PSVs. Some of these photoreceptors still remain to be studied in detail—those located on the head of hatchling cuttlefish and squid (Sundermann, 1990), for example. Whether it is such extraocular receptors or the ocular sensory pathways that control such behavior as 'search' or 'avoidance' reactions to light (*e.g.*, in juvenile cephalopods) has not yet been examined.

Acknowledgments

The authors are grateful to Roger Swinfen and to the master and crew of the R.V. *Squilla* for supplies of octopus on which this work was based. This work was supported by the BBSRC (C.S.C). R.W. is a Wellcome Trust Senior Research Fellow.

Literature Cited

- Arvanitaki, A., and N. Chalazonitis. 1961. Excitatory and inhibitory processes initiated by light and infra-red radiations in single identifiable nerve cells (giant ganglion cells of *Aplysia*). Pp. 194–231 in *Nervous Inhibition*. E. Florey, ed. Pergamon Press, London.
- Bauer, V. 1909. Einführung in die Physiologie der Cephalopoden. Mit besonderer Berücksichtigung der im Mittelmeer häufigen Formen. *Mitt. Zool. Stat. Neapel*. **19**: 149–268.
- Baumann, F., A. Mauro, R. Millecchia, S. Nightingale, and J. Z. Young. 1970. The extra-ocular light receptors of the squid *Todarodes* and *Illex*. *Brain Res.* **21**: 275–279.
- Behrens, M. E., and V. J. Wulff. 1965. Light-initiated responses of retinula and eccentric cells in the *Limulus* lateral eye. *J. Gen. Physiol.* **48**: 1081–1093.
- Boyle, P. R. 1981. Methods for the aquarium maintenance of the common octopus of British waters, *Eledone cirrhosa*. *Lab. Anim.* **15**: 327–331.
- Cazal, P., and D. Bogoraze. 1944. La glande épistellaire du Poulpe (*Octopus vulgaris* Lam.) organe neurocrine. *Arch. Zool. Exp. et Gen.* **84**: 9–22.
- Cobb, C. S., and R. Williamson. 1998. Electrophysiology of extraocular photoreceptors in the squid *Loligo forbesi* (Cephalopoda: Loliginidae). *J. Molluscan Stud.* **64**: 111–117.
- Cobb, C. S., S. K. Pope, and R. Williamson. 1995a. Circadian rhythms to light-dark cycles in the lesser octopus, *Eledone cirrhosa*. *Mar. Freshw. Behav. Physiol.* **26**: 47–57.
- Cobb, C. S., R. Williamson, and S. K. Pope. 1995b. The responses of the epistellar photoreceptors to light and their effect on circadian rhythms in the lesser octopus, *Eledone cirrhosa*. *Mar. Freshw. Behav. Physiol.* **26**: 59–69.
- Duncan, G., and F. I. Weeks. 1973. Photoreception by a cephalopod retina *in vitro*. *Exp. Eye. Res.* **17**: 183–192.
- Ewaudinger, N. W., N. I. Syed, K. Lukowiak, and A. G. M. Bulloch. 1994. Differential tracer coupling between pairs of identified neurons of the mollusc *Lymnaea stagnalis*. *J. Exp. Biol.* **192**: 291–297.
- Hamdorf, K., J. Schwemer, and U. Taüber. 1968. Der Sehfärbstoff, die Absorption der Rezeptoren und die spektrale Empfindlichkeit der Retina von *Eledone moschata*. *Z. Vergh. Physiol.* **60**: 375–415.
- Hara, T., and R. Hara. 1980. Retinochrome and rhodopsin in the extraocular photoreceptor of the squid, *Todarodes*. *J. Gen. Physiol.* **75**: 1–19.
- Hisano, N., H. Tateda, and M. Kuwabara. 1972. Photosensitive neurons in the marine pulmonate mollusc, *Onchidium verruculatum*. *J. Exp. Biol.* **57**: 651–660.
- Honig, M. G., and R. L. Hume. 1989. DiI and DiO: versatile fluorescent dyes of neuronal labelling and pathway tracing. *Trends Neurosci.* **12**: 333–341.
- Houck, B. A. 1977a. A morphological and behavioral study of an extra-ocular photoreceptor in octopods. Ph.D. Thesis, University of Honolulu, Hawaii.
- Houck, B. A. 1977b. Photoreception in octopods: The role of ocular and extra-ocular photoreception in maintenance of locomotor activity rhythms [Abstract]. *Am. Zool.* **17**: 969.
- Houck, B. A. 1981. Locomotor activity and home selection in three species of Hawaiian octopods [Abstract]. *Am. Zool.* **21**: 967.
- Houck, B. A. 1982. Temporal spacing in the activity patterns of three Hawaiian shallow-water octopods. *Nautilus* **96**: 152–156.
- Kennedy, D. 1963. Physiology of photoreceptor neurons in the abdominal nerve cord of the crayfish. *J. Gen. Physiol.* **46**: 551–572.
- Laughlin, S. B. 1989. The roles of sensory adaptation in the retina. *J. Exp. Biol.* **146**: 39–62.
- Lisman, J. E., and J. B. Brown. 1975. Light-induced changes of sensitivity in *Limulus* ventral photoreceptors. *J. Gen. Physiol.* **66**: 473–488.
- Mauro, A. 1977. Extra-ocular photoreceptors in cephalopods. *Symp. Zool. Soc. Lond.* **38**: 287–308.
- Mauro, A., and F. Baumann. 1968. Electrophysiological evidence of photoreceptors in the epistellar body of *Eledone moschata*. *Nature* **220**: 1332–1334.
- Mauro, A., and O. Sten-Knudsen. 1972. Light-evoked impulses

- from extra-ocular photoreceptors in the squid *Todarodes*. *Nature* **237**: 342–343.
- Messenger, J. B. 1991.** Photoreception and vision in molluscs. Pp. 364–397 in *Evolution of the Eye and Visual System*. J. R. Cronly-Dillon and R. L. Gregory, eds. Macmillan, London.
- Nakamura, T., G. Thiele, and H. Meissl, H. 1986.** Intracellular responses from the photosensitive pineal organ of the teleost, *Phoxinus phoxinus*. *J. Comp. Physiol. A*. **159**: 325–330.
- Nishioka, R. S., I. Yasumasu, and H. A. Bern. 1962.** Ultrastructure of the epistellar body of the octopus. *Z. Zellforsch. Mikrosk. Anat.* **57**: 406–421.
- Nishioka, R. S., I. Yasumasu, A. Packard, H. A. Bern, and J. Z. Young. 1966.** Nature of vesicles associated with nervous system of cephalopods. *Z. Zellforsch. Mikrosk. Anat.* **75**: 301–316.
- Omura, Y. 1984.** Pattern of synaptic connections in the pineal organ of the ayu, *Plecoglossus altivelis* (Teleostei). *Cell Tissue Res.* **236**: 611–617.
- Ozaki, K., R. Hara, and T. Hara. 1983.** Histochemical localization of retinochrome and rhodopsin studied by fluorescence microscopy. *Cell Tissue Res.* **233**: 335–345.
- Palmer, B. W., and R. K. O'Dor. 1978.** Changes in vertical migration patterns of captive *Illex illecebrosus* in varying light regimes and salinity gradients. *Tech. Rep. Fish. Mar. Sci. Canada* **833**: 23.1–23.12.
- Perrelet, A., and A. Mauro. 1972.** Ultrastructure of nerves associated with the epistellar body of the octopod *Eledone moschata* and the parolfactory vesicles of the squid *Todarodes sagittatus*. *Brain Res.* **37**: 161–171.
- Sperling, L., J. E. Lisman, and A. Godfrey. 1973.** Light-evoked responses from the ventral parolfactory vesicles of *Loligo pealei* [Abstract]. *Biol. Bull.* **145**: 456.
- Stewart, W. W. 1978.** Functional connections between cells as revealed by dye-coupling with highly fluorescent naphthalimide tracer. *Cell* **14**: 741–759.
- Sundermann, G. 1990.** Development and hatching state of ectodermal vesicle organs in the head of *Sepia officinalis*, *Loligo vulgaris* and *Loligo forbesi* (Cephalopoda, Decabrachia). *Zoomorphology* **109**: 343–352.
- Weeks, F. I., and G. Duncan. 1974.** Photoreception by a cephalopod retina: response dynamics. *Exp. Eye Res.* **19**: 493–509.
- Williamson, R. 1989.** Electrical coupling between secondary hair cells in the statocyst of the squid *Alloteuthis subulata*. *Brain Res.* **486**: 67–72.
- Young, J. Z. 1929.** Sopra un nuovo organo dei cefalopodi. *Boll. Soc. Ital. Biol. Sper.* **4**: 1022–1024.
- Young, J. Z. 1936.** The giant nerve fibres and epistellar body of cephalopods. *Q. Jl. Microsc. Sci.* **78**: 367–386.
- Young, J. Z. 1965.** The diameters of fibres of the peripheral nerves of *Octopus*. *Proc. R. Soc. Lond. B.* **162**: 47–79.
- Young, J. Z. 1971.** *The Anatomy of the Nervous system of Octopus vulgaris*. Clarendon Press, Cambridge.
- Young, R. E. 1972.** Function of extra-ocular photoreceptors in bathypelagic cephalopods. *Deep-Sea Res.* **19**: 651–660.
- Young, R. E. 1973.** Information feedback from photoreceptors and ventral countershading in mid-water squid. *Pac. Sci.* **27**: 1–7.
- Young, R. E., C. F. E. Roper, and J. F. Walters. 1979.** Eyes and extraocular photoreceptors in midwater cephalopods and fishes: Their roles in detecting downwelling light for counterillumination. *Mar. Biol.* **51**: 371–380.
- Zill, S. N., S. F. Frazer, D. L. Macfarland, and S. E. Fish. 1993.** Characterization of insect sense organs and optical clearing of whole-mount preparations using Dil in fixed tissues. *J. Exp. Biol.* **175**: 299–303.

**Marine
Biological
Laboratory
Woods Hole
Massachusetts**

One Hundreth Report
for the Year 1997
One-Hundred and Ninth Year

Officers of the Corporation

Sheldon J. Segal, *Chairman of the Board of Trustees*

Frederick Bay, *Co-Vice Chair*

Mary J. Greer, *Co-Vice Chair*

James D. Ebert, *President of the Corporation*

John E. Burris, *Director and Chief Executive Officer*

Mary B. Conrad, *Treasurer*

Neil Jacobs, *Clerk of the Corporation*

Contents

Report of the Director and CEO	R1
Report of the Treasurer	R7
Financial Statements	R8
Report of the Library Director	R19
Educational Programs	
Summer Courses	R22
Short Courses	R26
Other Programs	R31
Summer Research Programs	
Principal Investigators	R33
Other Research Personnel	R34
Library Readers	R36
Institutions Represented	R37
Year-Round Research Programs	R42
Honors	R53
Board of Trustees and Committees	R59
Administrative Support Staff	R62
Members of the Corporation	
Life Members	R65
Members	R66
Associate Members	R76
Certificate of Organization	R79
Articles of Amendment	R79
Bylaws	R79

Photo credits:

W. Amos—R19
Beth Armstrong—R2 (top), R34, R37, R43
Ken Foreman—R5 (bottom), R31
Linda Golder—R59, R65
Roger Hanlon—R3 (top), R62
Richard Howard—R4 (top), R5 (top), R22, R26,
R30, R78
Tom Kleindinst—R45
Alan Kuzirian—R53
Beth Liles, R49
George Lower—R4 (bottom), R7
Chris Neill, R42
Bruce Peterson—R47
Janice Reed—R1



Report of the Director and Chief Executive Officer

The Marine Biological Laboratory had another exciting and successful year in 1997. We set our sights high and achieved a number of major goals for the Laboratory. We launched the first Semester in Environmental Sciences program for undergraduates from liberal arts colleges; recruited new investigators for our resident research programs; planned for and established new advanced summer courses; and found new and expanded ways to capitalize on the flexibility and sophistication of the Marine Resources Center.

These endeavors were supported by the tangible and intangible resources and energies generated by the laboratory's new fundraising campaign, *Discovery: The Campaign for Science at the Marine Biological Laboratory*, which was launched with a public celebration and street fair on August 8, 1997. In my report last year, I discussed the concerted planning process that set the stage for this campaign. By focusing our research and educational directions and priorities, we were able to announce last August a campaign goal of \$25 million to be raised by December 31, 2000.

I am pleased to say that, as of the spring of 1998, we have already raised \$14.5 million towards that goal. I have every reason to believe that we will meet, if not exceed our goal within the timeframe of the campaign.

Research at the MBL

We made great strides in the MBL's resident research centers and programs during 1997. The avenues for independent research broadened and diversified in each of MBL's programmatic areas, while our investigators found new ways to work together in various interdisciplinary pursuits.

The Josephine Bay Paul Center

Dr. Mitchell Sogin and his colleagues in the Josephine Bay Paul Center for Comparative Molecular

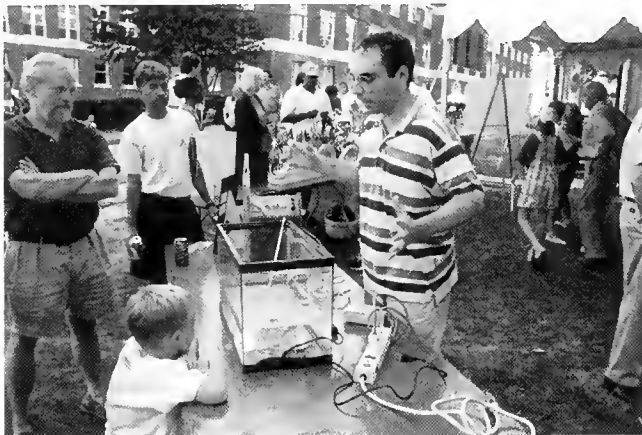
Biology and Evolution continued their important studies on the evolution of eukaryotes, most recently focusing on those found in extreme environments. An exciting development is a major grant from the National Institutes of Health to sequence the genome of *Giardia lamblia*, a water-borne human pathogen. Giardiasis is a major contributor to the enormous burden of human diarrheal diseases, which are second only to respiratory infections as causes of mortality and morbidity worldwide. While *Giardia* can be a deadly organism, it is manageable in terms of genome analysis because it has a relatively modest genome size of 12 million base pairs distributed onto five chromosomes.

Dr. Michael Cummings was recruited to the Bay Paul Center in 1997. He comes to the Center to study Mycobacteria as a means of understanding more clearly the evolution of pathogenicity and how various strains of tuberculosis develop drug resistance. Another member of the Bay Paul Center, Dr. Monica Riley, continues to travel world-wide sharing her expertise on the *E. coli* genome. She was a co-author in September on a paper published in the journal *Science* which reports the successful sequencing of the genome of the K-12 strain of the bacterium.

In 1997, Center scientist Dr. Neal Cornell and his co-workers conducted a molecular phylogenetic analysis for 5-aminolevulinic synthase, the first enzyme of heme biosynthesis. The analysis supports the suggestion that alpha-purple bacteria are the closest contemporary eubacterial relatives of eukaryotic mitochondria. The study also indicates that the massive gene duplication required for the evolution of true vertebrates had occurred when non-vertebrate jawless fish appeared, 400 to 500 million years ago.

The Ecosystems Center

The MBL's Ecosystems Center, co-directed by Drs. John Hobbie and Jerry Melillo, continues its leadership in environmental research on local and global scales.



For more than a decade, MBL scientists have led a Long-Term Ecological Research (LTER) project on the arctic tundra around Toolik Lake in Alaska. In 1997, scientists at the Center secured another LTER project grant of nearly \$3.4 million over six years from the National Science Foundation to study the Plum Island Sound system in northeastern Massachusetts. An LTER grant is important scientifically and institutionally because it allows long-term data collection and analysis in the same location and provides a solid base of funding with which to recruit scientists and research technicians for the project. We are proud of the Ecosystems Center team because they were the only group that was funded out of 21 proposal submissions nationwide.

In the southern hemisphere, our scientists have also been compiling data for more than a decade on the effects of deforestation on soil fertility and trace gas emissions in the rainforests in Brazil. Their work continues as they evaluate what effects changing and more aggressive agricultural practices are having on the Amazon Basin and the world.

In 1997, the MBL received a challenge grant of \$1 million from The Clowes Fund, Inc., of Indiana, to provide support for new and expanded facilities for The Ecosystems Center. Thanks to this grant, the MBL is now in the early stages of planning renovations and expansion that will nearly double the Center's existing laboratory, field staging, and office space. The plans also call for the creation of a new computer teaching laboratory in the Center.

The Marine Resources Center

Dr. Roger Hanlon has advanced his research agenda in the Marine Resources Center (MRC) with the introduction of the Program in Sensory Biology and Neuroethology and the Program in Scientific

Aquaculture. An MRC Advisory Committee has been constituted to review research directions and scientist recruitment strategies. Members of the Committee include Drs. Gerald Fischbach, Harvard Medical School; Irwin Levitan, Brandeis University; and Vilayanur Ramachandran, University of California, San Diego.

In the program on neuroethology, Dr. Hanlon and his colleagues study vision, balance, chemical sensing, and signaling to gain a better understanding of the output of neural activity, *i.e.*, the resultant behavior of an organism that has evolved through natural selection. Towards that end, Dr. Hanlon has recently been awarded research grants that will enable molecular and cellular studies on squid and cuttlefish. These marine organisms possess very large neurons and have evolved dramatic and rapidly changing skin patterning displays as evidence of aggressive and reproductive behaviors. Last summer, Hanlon and his colleagues performed a series of experiments in the MRC in which they discovered that squids are able to detect transparent prey at greater distances thanks to a specialized way of seeing known as polarization vision. The result is enhanced predation and feeding by the squid. Hanlon's findings appeared in the journal *Nature* in May 1998.

The second MRC initiative, the Program in Scientific Aquaculture, seeks to select organisms with defined genetic lines or at precise developmental stages for use as biomedical models, to attract industry and





commercial ventures to develop and test products in the MRC, and to study molecular and cellular mechanisms of disease processes and prevention.

Architectural Dynamics in Living Cells Program

MBL scientists continue as leaders in the design and use of advanced imaging systems to study the molecular definition and physical forces that affect the structure and function in living cells. Dr. Shinya Inoué, MBL Distinguished Scientist, received additional honors in 1997 for his contributions to light microscopy and was awarded the Ernst Abbe Award for Microscopy by the New York Microscopical Society. Inoué and his colleagues announced at the 1997 meeting of the American Society of Cell Biology the development of the Centrifuge Polarizing Microscope. This new microscope allows researchers to view architectural changes in cells at the subcellular level when exposed to high gravitational forces. This technical feat was the fruit of collaboration between scientists at the MBL, Olympus Optical Co., and Hamamatsu Photonics Corp.

Dr. Rudolf Oldenbourg and his associate Kaoru Kato, together with Dr. Peter Smith and Katherine Hammar of the BioCurrents Research Center, reported in 1997 on their observations of the dynamic behavior of actin molecules at the tip of growing nerve cells. These observations were made possible by the exceptionally high sensitivity and sharp image quality of Oldenbourg's Pol-Scope, which was developed in collaboration with Cambridge Research and Instrumentation, Inc.

Laboratory for Reproductive Medicine

Dr. David Keefe, of the Laboratory for Reproductive Medicine of Brown University and the Women and

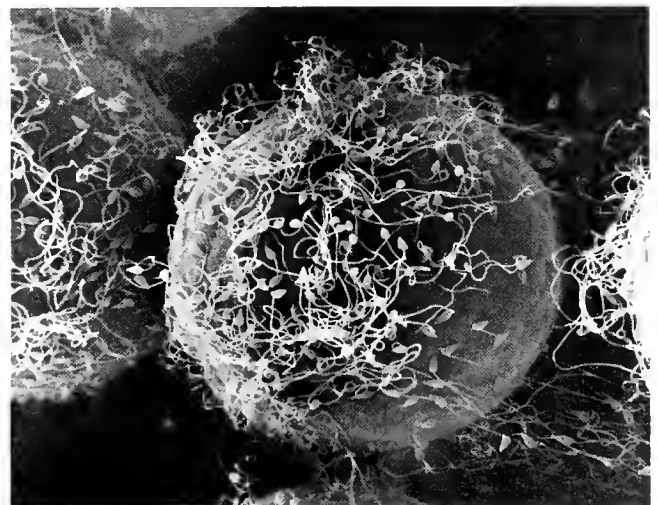
Infants Hospital in Providence, R.I., established a resident laboratory at the MBL in 1997. Here he investigates the mechanisms underlying age-related female infertility. Keefe uses technologies developed at the MBL to seek out clues that indicate whether an egg has been damaged with age and is therefore not viable. With the ion selective probe, developed in Peter Smith's BioCurrents Research Center, Keefe can detect the flow of certain ions in and out of the cell. This flow may reflect an egg's potential to develop successfully. He is also using Oldenbourg's Pol-Scope to study the egg's spindle; flaws in the spindle may be responsible for the faulty transfer of genetic material during cell division.

Laboratory of Aquatic Animal Health and Pathology

In 1997, scientists from the University of Pennsylvania's Laboratory of Aquatic Animal Health and Pathology, which is based at the MBL, continued their efforts to identify and treat diseases affecting marine organisms. They identified in toadfish an abscess of the abdominal organs caused by *Pseudomonas* sp. bacteria and a bacterial pericarditis disease caused by *Edwardsiella* sp. Dr. Roxanna Smolowitz continued her effort to culture QPX and describe the pathogenesis of the disease in susceptible strains of clams, while Dr. Robert Bullis and colleagues worked on ways to detect illegal chemical scrubbing of eggs in female lobsters.

Boston University Marine Program (BUMP)

BUMP Postdoctoral Fellow Frank Grasso organized and co-hosted an international workshop on "Plume Tracing" last year. Twenty-five scientists presented and debated the state-of-the-art in our knowledge of animals





following odor plumes to their source of release. Lobsters are animals that locate odor sources (for example, baited traps) under water without visual or auditory signals. Scientists in Dr. Jelle Atema's laboratory have developed a tool known as Robo-Lobster to perform the plume tracing task and to learn about the sensory input and signal processing used by lobsters.

Summer Research

The MBL's laboratories were again filled with scientists from all over the world during the summer of 1997. We welcomed back investigators with whom we have worked for a number of seasons and were able to share in the enthusiasm of scientists working here for the first time, either as fellows or as new principal investigators.

More than 400 scientists came to the MBL last summer to do their research, including 23 research fellows who received more than \$171,000 in fellowship awards. The summer research season is framed by the Poster Session in June and is capped off by the General Scientific Meetings in August. These events attest to the breadth and diversity of the multidisciplinary work at the MBL where presentations range from papers in ecology and population biology to cellular and molecular biology to vision and biophysics.

One of the highlights of the summer research season was Dr. Stephen Highstein's (Washington University) continuing work on the vestibular system of toadfish. The toadfish is an excellent marine model for studying how changes in pressure affect balance and equilibrium, because its vestibular system is similar to humans. Such studies teach us about motion sickness and dizziness, which are often signs of vestibular organ dysfunction. Highstein and his colleagues are focusing on the problems of nausea and dizziness experienced by astronauts when they get out beyond the earth's

gravity, a malady known as "space adaptation syndrome." As I write, four toadfish are passengers aboard the space shuttle Columbia, participants in an experiment designed to help scientists understand what happens in the vestibular system during an extended period in space.

Another area of research that is becoming increasingly important at the MBL is evolution and development or "evo-devo." Researchers from all over the world come to the MBL to learn more about how the dividing cells in an embryo decide which physiological role they will assume as the organism grows. For example, Drs. Mark Q. Martindale (University of Chicago), Jonathan Q. Henry (University of Illinois), and Barbara Boyer (Union College) take advantage of the wide variety of marine organisms available at the MBL to compare the developmental patterns of different kinds of embryos. They are studying relatively primitive animals like ctenophores whose development is simple enough that scientists can trace how a change in one cell or set of cells affects the whole organism as it grows. Ultimately, they hope to understand more clearly when and how organisms have diverged from their evolutionary ancestors.

The MBL's General Scientific Meetings are held annually in mid-August. This three-day meeting is an opportunity for summer and resident scientists to report on their most recent research results.

One highlight from the 1997 meeting is the finding from the laboratory of Robert Barlow (SUNY Health Science Center) that the lateral eyes of two species of horseshoe crabs—the Woods Hole species *Limulus polyphemus* and its Japanese counterpart *Tachypleus tridentatus*—are similar, but not alike. Both show the same nighttime circadian rhythms, but Barlow and co-workers found that the mechanism responsible for those rhythms differs between the two. The eye of *Limulus* is larger and contains more ommatidia than that of *Tachypleus*. As a result, the *Limulus* lateral eye





becomes more sensitive at night by capturing more photons. The smaller lateral eye of *Tachypleus* is nearly as sensitive, but due to its size is not able to catch as many photons as its Woods Hole relative. Instead, its photoreceptors make up for this deficiency by increasing gain, or the amount of information absorbed by the photoreceptors.

Education at the MBL

Summer Courses

The MBL's educational program in biology and biomedicine continues to be preeminent, with almost 400 students and 400 faculty coming to the MBL each summer for a superb hands-on scientific experience. The MBL now offers 20 courses each summer, three of which were developed in 1997. One of these, *Molecular Mycology: Current Approaches to Fungal Pathogenesis*, was taught for the first time during the summer of 1997. The others, *Frontiers in Reproduction: Molecular and Cellular Concepts and Applications*, and *Neural Development and Genetics of Zebrafish*, will be offered for the first time during the summer of 1998.

Competition for admission to these and all MBL courses is intense. The 368 students enrolled during the summer of 1997 were selected from 833 applications that were culled from 1521 inquiries. Students continue to come to MBL courses from throughout the world, with about 35% to 40% of them from foreign countries.

The popularity of the courses is one indication of their excellence. Another is the peer review process that surrounds the awarding of many of the funds that support the courses. For the first time in my and many of my colleagues' recollections, one of our summer courses, *Neural Systems and Behavior*, received a perfect score of

100 in its NIH review; *Neurobiology* also received near perfect marks from the NIH. This attests to the vision of the course directors and faculty and the quality of the curriculum that is offered at the MBL.

The generous support of a number of foundations, as well as the Federal government and a large cadre of individual donors is crucial to our ability to offer the best courses to the best students. Admission to many of the courses continues to be on a need-blind basis because of the scholarships we provide from these gifts and grants and from our endowment income.

Five course directors retired in 1997, including David Kleinfeld, University of California, San Diego, and David Tank, Lucent Technologies (Methods in Computational Neuroscience); Steve Hajduk, University of Alabama, Birmingham (Biology of Parasitism); Mark Mooseker, Yale University (Physiology); and Pierre Drapeau, Montreal General Hospital (Neurobiology and Development of the Leech). They will be replaced by William Bialek and Rob de Ruyter, NEC Research Institute (Methods in Computational Neuroscience); Ed Pearce, Cornell University (Biology of Parasitism); Kerry Bloom, UNC, Chapel Hill (Physiology); and Christie Sahley, Purdue University (Neurobiology and Development of the Leech). I thank all retiring course directors for their efforts on behalf of the MBL, and welcome our newest faculty members to the Laboratory.

Semester in Environmental Sciences

As I mentioned above, we are buoyed by the success of our first semester-long program in environmental science for undergraduates from liberal arts colleges. We welcomed 16 students for the inaugural semester which was held in the fall of 1997. Twenty-four liberal arts colleges and universities now participate in the consortium of institutions from which these students are drawn. The Ecosystems Center scientists who served as



faculty were impressed by the dedication and intellect of the group. I attended the student presentations before a large audience at semester-end and was impressed by the range and creativity of the research projects that they undertook. The semester proved a satisfying experience for all participants in this innovative new educational program, and it attests to the flexibility and commitment of the MBL in designing new and creative ways to further education in the life sciences.

MBL/WHOI Library

The Library is constantly responding to the challenges of straddling the traditional and the electronic modes of information transfer. This requires both technical achievement and renewal as well as the ongoing commitment to provide access to the best information essential to scientific research and teaching in the diverse Woods Hole scientific community. This charge translates into maintaining the unique, internationally acclaimed archival collection while, at the same time, being responsive to the fast-paced, complex, and demanding forces shaping electronic information delivery. So adept is the MBL/WHOI Library at this synthesis, that its director, Catherine Norton, is serving as President of the Boston Library Consortium, a group of academic, research, and hospital libraries.

Facilities

Our physical plant received significant attention during 1997. Major grants from the National Science Foundation and Colonial Gas Company provided nearly \$600,000 to renovate classrooms and laboratories in the Loeb building. Additional monies were spent to reconfigure and modernize research laboratories to accommodate newly appointed MBL scientists and expanded research needs.

MBL Trustees

At their November 1997 meeting, the Board of Trustees of the Marine Biological Laboratory elected Dr. John E. Dowling to serve as President of the MBL Corporation. Dowling succeeds Dr. James D. Ebert, who retired after serving as President for seven years. In recognition of his "outstanding service to the development of American science in general and his long-standing dedication to the Marine Biological Laboratory," the Board has designated Ebert an Honorary Member of the Board of Trustees.

Dr. Dowling is the Maria Moors Cabot Professor of

Natural Science at Harvard University, a long-time MBL summer investigator, and former MBL Trustee. His tenure as President of the MBL Corporation began with the March 1998 meeting of the Board.

Two New Trustees Join Board

At that same meeting, Mr. Sydney M. Cone, III, was elected a member of the Class of 2002. He is a partner with the law firm of Cleary, Gottlieb, Steen & Hamilton in New York City. He is also Starr Professor of Law of International Trade and Finance and the Director of the Center for International Law at New York Law School. He has served as a member of the MBL's Council of Visitors since 1996. Mrs. Robert W. (Jean) Pierce was elected as a member of the Class of 1999. She is a resident of Wellesley, Woods Hole, and Boca Grande, Florida. She is an incorporator of the Heritage Plantation in Sandwich, and serves on the boards of the Women's Club of Boca Grande and the Penzance Point Road Trust. Her late husband, Robert, served as a member of the MBL's Board of Trustees from 1990 to 1993.

Five Board Members Reappointed

Mr. John R. Lakian, Chairman of the Board of the Fort Hill Group, Inc.; Dr. Joan Ruderman, Marion V. Nelson Professor of Cell Biology at Harvard Medical School; Dr. Sheldon J. Segal, Distinguished Scientist at the Population Council; Dr. William T. Speck, President and CEO of Columbia-Presbyterian Medical Center; and Mr. Alfred Zeien, Chairman and CEO of Gillette, were also elected in 1997 as members of the Class of 2002.

Council of Scientific Advisors

I owe a debt of thanks to my colleagues here in Woods Hole and to the international network of scientific, philanthropic, and business colleagues who share their time, interest, leadership, and support to keep the Marine Biological Laboratory at the forefront of biology. During 1997, I was especially fortunate to receive input and advice from the Council of Scientific Advisors, a newly constituted group of eminent scientists. They include: Drs. Bruce Alberts, Thomas Eisner, Walter Gilbert, Eville Gorham, Marc Kirschner, and Carla Shatz. With their counsel and that from our Board of Trustees, the MBL Science Council, and all of you, I look forward to a bright and dynamic future for the Marine Biological Laboratory.

—John E. Burris



Report of the Treasurer

The year 1997 was a successful one for the Marine Biological Laboratory. The net assets of the Laboratory increased by \$6.2 M in 1997, from \$54.5 M to \$60.7 M. This increase was due to operations, the efforts of the capital campaign, and the success of our investment management activities. In accordance with generally accepted accounting principles, the Laboratory reported the results of operations after depreciation of \$1.5 M, resulting in unrestricted net assets decreasing by \$.8 M. This practice has masked a comparatively strong and healthy result of operations for the year. The capital campaign was responsible for a \$3.1 M increase in net assets and permanently restricted net assets through increased gifts; and our long-term investments increased \$4.9 M, resulting in a total return of 18.2% on our portfolio.

The 1997 balance sheet revealed an increase in liquidity as cash and short-term investments increased by \$.6 M to \$5.0 M and account for 50% of current net assets. Long-term investments increased by \$5.8 M. This increase was the result of \$2.1 M of new gifts,

market value increase of \$4.9 M, and a withdrawal of \$1.2 M to pay for scholarships and fellowships in accordance with the donors' instructions.

Land, buildings, and equipment, net of accumulated depreciation, decreased by \$.7 M as a result of the depreciation expense exceeding capital expenditures. This resulted in our inability to recover depreciation expense on federally funded capital projects.

The Laboratory continues to demonstrate the ability to attract funds from the federal government, from foundations, and from individuals. We are in the process of significantly upgrading the physical plant, making the Laboratory an even more attractive facility at which to do science. Our housing budget continues to generate surplus cash. With long-term investment growth and the strength of our capital campaign, the Marine Biological Laboratory will continue to provide a productive scientific experience for its community.

—Mary B. Conrad

Financial Statements

Coopers
& Lybrand

Coopers & Lybrand L.L.P.

a professional services firm

REPORT OF INDEPENDENT ACCOUNTANTS

To the Board of Trustees of
Marine Biological Laboratory
Woods Hole, Massachusetts

We have audited the accompanying balance sheet of Marine Biological Laboratory (the "Laboratory") as of December 31, 1997 and the related statements of activities and cash flows for the year then ended. These financial statements are the responsibility of the Laboratory's management. Our responsibility is to express an opinion on these financial statements based on our audit.

We conducted our audit in accordance with generally accepted auditing standards. Those standards require that we plan and perform the audit to obtain reasonable assurance about whether the financial statements are free of material misstatement. An audit includes examining, on a test basis, evidence supporting the amounts and disclosures in the financial statements. An audit also includes assessing the accounting principles used and significant estimates made by management, as well as evaluating the overall financial statement presentation. We believe that our audit provides a reasonable basis for our opinion.

In our opinion, the financial statements referred to above present fairly, in all material respects, the financial position of Marine Biological Laboratory as of December 31, 1997, and the changes in its net assets and its cash flows for the year then ended in conformity with generally accepted accounting principles.

Our audit was conducted for the purpose of forming an opinion on the basic financial statements taken as a whole. The supplemental schedule of functional expenses as of December 31, 1997 is presented for the purpose of additional analysis and is not a required part of the basic financial statements. Such information has been subjected to the auditing procedures applied in the audit of the basic financial statements and, in our opinion, is fairly stated, in all material respects, in relation to the basic financial statements taken as a whole.

Boston, Massachusetts
March 27, 1998

Coopers & Lybrand L.L.P.

Coopers & Lybrand L.L.P. is a member of Coopers & Lybrand International, a limited liability association incorporated in Switzerland.

MARINE BIOLOGICAL LABORATORY

BALANCE SHEETS

December 31, 1997

(with comparative totals as of December 31, 1996)

ASSETS	<u>1997</u>	<u>1996</u>
Cash and cash equivalents	\$ 560,801	\$ 391,528
Short-term investments, at market (Note C)	4,408,046	3,918,194
Accounts receivable, net of allowance for doubtful accounts of \$36,782 in 1997 and \$15,000 in 1996	1,221,781	762,860
Current portion of pledges receivable (Note H)	2,219,056	1,826,494
Receivables due for costs incurred on grants and contracts	1,157,165	1,114,082
Other assets	<u>560,269</u>	<u>482,992</u>
 Total current assets	 <u>10,127,118</u>	 <u>8,496,150</u>
Long-term investments, at market (Notes C and D)	35,614,151	29,763,495
Pledges receivable, net of current portion (Note H)	2,238,826	2,406,350
Plant assets, net (Notes E and F)	<u>20,026,580</u>	<u>20,695,624</u>
 Total long-term assets	 <u>57,879,557</u>	 <u>52,865,469</u>
 Total assets	 <u>\$68,006,675</u>	 <u>\$61,361,619</u>
 LIABILITIES AND NET ASSETS		
Current portion of long-term debt and capital leases (Note E)	229,657	204,108
Accounts payable and accrued expenses	1,494,948	1,536,015
Deferred income and advances on contracts	<u>384,258</u>	<u>321,998</u>
 Total current liabilities	 <u>2,108,863</u>	 <u>2,062,121</u>
Annuities and unitrusts payable	1,213,583	959,513
Long-term debt and capital leases, net of current portion (Note E)	2,567,370	2,591,973
Advances on contracts	<u>1,433,208</u>	<u>1,210,950</u>
 Total long-term liabilities	 <u>5,214,161</u>	 <u>4,762,436</u>
 Total liabilities	 <u>7,323,024</u>	 <u>6,824,557</u>
Commitments and contingencies (Notes F and H)		
Net assets:		
Unrestricted	18,729,311	19,371,978
Temporarily restricted	25,596,656	21,484,748
Permanently restricted	<u>16,357,684</u>	<u>13,680,336</u>
 Total net assets (Note B)	 <u>60,683,651</u>	 <u>54,537,062</u>
 Total liabilities and net assets	 <u>\$68,006,675</u>	 <u>\$61,361,619</u>

The accompanying notes are an integral part of the financial statements.

MARINE BIOLOGICAL LABORATORY

STATEMENT OF ACTIVITIES

for the year ended December 31, 1997

	<u>Unrestricted</u>	<u>Temporarily Restricted</u>	<u>Permanently Restricted</u>	<u>1997 Total</u>
Operating support and revenues:				
Government grants	\$ 9,986,800	—	—	\$ 9,986,800
Private contracts	1,178,192	—	—	1,178,192
Laboratory rental income	1,478,757	—	—	1,478,757
Tuition	399,703	—	—	399,703
Fees for conferences and services	3,085,616	—	—	3,085,616
Contributions	615,882	\$4,434,938	\$1,390,609	6,441,429
Investment income	471,832	1,238,151	—	1,709,983
Miscellaneous revenue	322,667	—	—	322,667
Present value adjustment to annuities	—	(165,504)	1,057	(164,447)
Net assets released from restrictions	<u>3,811,922</u>	<u>(3,871,922)</u>	<u>60,000</u>	<u>—</u>
Total operating support and revenues	<u>21,351,371</u>	<u>1,635,663</u>	<u>1,451,666</u>	<u>24,438,700</u>
Expenses:				
Research	11,031,914	—	—	11,031,914
Instruction	4,144,508	—	—	4,144,508
Conferences and services	1,487,705	—	—	1,487,705
Other programs (Note B)	<u>5,440,808</u>	<u>—</u>	<u>—</u>	<u>5,440,808</u>
Total expenses	<u>22,104,935</u>	<u>—</u>	<u>—</u>	<u>22,104,935</u>
Change in net assets before nonoperating activity	(753,564)	1,635,663	1,451,666	2,333,765
Nonoperating revenue:				
Total investment income and earnings	152,543	3,490,810	1,225,682	4,869,035
Less: investment earnings used for operations	<u>(41,646)</u>	<u>(1,014,565)</u>	<u>—</u>	<u>(1,056,211)</u>
Reinvested investment earnings	<u>110,897</u>	<u>2,476,245</u>	<u>1,225,682</u>	<u>3,812,824</u>
Total change in net assets	(642,667)	4,111,908	2,677,348	6,146,589
Net assets, beginning of year	<u>19,371,978</u>	<u>21,484,748</u>	<u>13,680,336</u>	<u>54,537,062</u>
Net assets, end of year	<u>\$18,729,311</u>	<u>\$25,596,656</u>	<u>\$16,357,684</u>	<u>\$60,683,651</u>

The accompanying notes are an integral part of the financial statements.

MARINE BIOLOGICAL LABORATORY

STATEMENTS OF CASH FLOWS

for the year ended December 31, 1997

(with comparative totals for the year ended December 31, 1996)

	<u>1997</u>	<u>1996</u>
Cash flows from operating activities:		
Change in net assets	\$ 6,146,589	\$ 6,375,604
Adjustments to reconcile change in net assets to net cash (provided by) from operating activities:		
Depreciation	1,483,203	1,473,878
Unrealized (gain) loss on investments	(1,740,501)	(1,765,532)
Realized (gain) loss on investments	(1,728,792)	(932,530)
Present value adjustment to annuities payable	164,447	(118,076)
Contributions restricted for long-term investment and annuities	(1,390,609)	(1,042,945)
Provision for bad debt	21,781	5,000
Provision for uncollectible pledges	89,620	—
Change in certain balance sheet accounts:		
Accounts receivable	(480,702)	(25,489)
Pledges receivable	(314,658)	(1,726,570)
Grants and contracts receivable	(43,083)	502,596
Other assets	(77,277)	(15,940)
Accounts payable and accrued expenses	(71,564)	(409,962)
Deferred income and advances on contracts	62,260	(59,539)
Annuities and unitrusts payable	120,052	—
Advances on contracts	222,258	757,875
	<u>2,463,024</u>	<u>3,018,370</u>
Net cash provided by operating activities		
Cash flows from investing activities:		
Purchase of property and equipment	(814,159)	(730,966)
Proceeds from sale of investments	23,450,218	7,293,473
Purchase of investments	(26,321,432)	(11,347,575)
	<u>(3,685,373)</u>	<u>(4,785,068)</u>
Net cash used in investing activities		
Cash flows from financing activities:		
Payments on annuities and unitrusts payable	(30,430)	(23,369)
Receipt of permanently restricted gifts	1,321,302	954,739
Annuity and unitrusts donations received	69,307	88,206
Loan proceeds	250,000	500,000
Payments on long-term debt and capital leases	(218,557)	(205,878)
	<u>1,391,622</u>	<u>1,313,698</u>
Net cash provided by financing activities		
Net increase (decrease) in cash and cash equivalents	169,273	(453,000)
Cash and cash equivalents at beginning of year	<u>391,528</u>	<u>844,528</u>
Cash and cash equivalents at end of year	<u>\$ 560,801</u>	<u>\$ 391,528</u>

The accompanying notes are an integral part of the financial statements.

Marine Biological Laboratory

Notes to Financial Statements

A. Background:

The Marine Biological Laboratory (the "Laboratory") is a private, independent not-for-profit research and educational institution dedicated to establishing and maintaining a laboratory or station for scientific study and investigation, and a school for instruction in biology and natural history. The Laboratory was founded in 1888 and is located in Woods Hole, Massachusetts.

B. Significant Accounting Policies:

Basis of Presentation

The accompanying financial statements have been prepared on the accrual basis of accounting and in accordance with the principles outlined in the American Institute of Certified Public Accountants' Audit Guide, "Not-For-Profit Organizations." The financial statements include certain prior-year summarized comparative information in total but not by net asset class. Such information does not include sufficient detail to constitute a presentation in conformity with generally accepted accounting principles. Accordingly, such information should be read in conjunction with the Laboratory's financial statements for the year ended December 31, 1996, from which the summarized information was derived.

The Laboratory classifies net assets, revenues, and realized and unrealized gains and losses based on the existence or absence of donor-imposed restrictions and legal restrictions imposed under Massachusetts State law. Accordingly, net assets and changes therein are classified as follows:

Unrestricted

Unrestricted net assets are not subject to donor-imposed restrictions of a more specific nature than the furtherance of the Laboratory's mission. Revenues from sources other than contributions are generally reported as increases in unrestricted net assets. Expenses are reported as decreases in unrestricted net assets. Gains and losses on investments and other assets or liabilities are reported as increases or decreases in unrestricted net assets unless their use is restricted by explicit donor stipulations or law. Expirations of temporary restrictions on net assets, that is, the donor-imposed stipulated purpose has been accomplished and/or the stipulated time period has elapsed, are reported as reclassifications between the applicable classes of net assets.

Temporarily Restricted

Temporarily restricted net assets are subject to legal or donor-imposed stipulations that will be satisfied either by the actions of the Laboratory, the passage of time, or both. These assets include gifts plus monies for which the specific, donor-imposed restrictions have not been met and pledges, annuities, and unitrusts for which the ultimate purpose of the proceeds is not permanently restricted. As the restrictions are met, the assets are released to unrestricted net assets. Also, realized/unrealized gains/losses associated with permanently restricted gifts which are not required to be added to principal by the donor are classified as temporarily restricted but maintain the donor requirements for expenditure.

Permanently Restricted

Permanently restricted net assets are subject to donor-imposed stipulations that they be invested to provide a permanent source of income to the Laboratory. These assets include gifts, pledges and trusts which require that the corpus be invested in perpetuity and only the income be made available for program operations in accordance with donor restrictions.

Nonoperating revenues include realized and unrealized gains on investments during the year as well as investment income on the master pooled investments. Investment income from short-term investments and investments held in trust by others is included in operating support and revenues. To the extent that nonoperating investment income and gains are used for operations as determined by the Laboratory's total return utilization policy (see below), they are reclassified from nonoperating to operating on the statement of activities as "Investment earnings used for operations." All other activity is classified as operating revenue. The Laboratory recorded net realized gains of \$1,728,792, net unrealized gains of \$1,740,501 and dividend and interest income of \$2,053,514 in 1997.

Cash and Cash Equivalents

Cash equivalents consist of resources invested in overnight repurchase agreements and other highly liquid investments with original maturities of three months or less.

Financial instruments which potentially subject the Laboratory to concentrations of risk consist primarily of cash and investments. The Laboratory maintains cash accounts with one banking institution. Investments are maintained primarily with two institutions.

Investments

Investments purchased by the Laboratory are carried at market value. Donated investments are recorded at fair market value at the date of the gift. For determination of gain or loss upon disposal of investments, cost is determined based on the first-in, first-out method. Investments with an original maturity of three months to one year are classified as short-term. All other investments are considered long-term.

In 1924, the Laboratory became the beneficiary of certain investments, included in permanently restricted net assets, which are held in trust by others. The Laboratory has the continuing rights to the income produced by these funds in perpetuity, subject to the contractual restrictions on the use of such funds. Accordingly, the trust has established a process to conduct a review every ten years by an independent committee to ensure the Laboratory continues to perform valuable services in biological research in accordance with the restrictions placed on the funds by the agreement. The committee met in 1994 and determined that the Laboratory has continued to meet the contractual requirements. The market

values of such investments are \$7,440,158 and \$6,214,477 at December 31, 1997 and 1996, respectively. The dividend and interest income on these investments totaled \$254,898 and \$224,324 in 1997 and 1996, respectively.

Investment Income and Distribution

For the master pooled investments, the Laboratory employs a total return utilization policy that establishes the amount of the investment return made available for spending each year. The Finance and Investment Committee has approved a standing policy that the withdrawal will be based on a percentage of the latest three-year average ending market values of funds. The market value includes the principal plus reinvested income, realized and unrealized gains and losses. Spending rates in excess of 5%, but not exceeding 7%, can be utilized if approved in advance by the Finance and Investment Committee of the Board of Trustees. For fiscal 1997, the Laboratory obtained approval to expend 6% of the latest three-year average ending market values of the investments. The 6% includes a 1½% administration fee for endowments. This fee was approved by the Laboratory's Board of Trustees for the years 1996–2000.

The net appreciation on permanently and temporarily restricted net assets is reported together with temporarily restricted net assets until such time as all or a portion of the appreciation is distributed for spending in accordance with the total return utilization policy and applicable state law.

Investment income on the pooled investment account is allocated to the participating funds using the market value unit method (Note D).

Plant Assets

Buildings and equipment are recorded at cost. Donated facility assets are recorded at fair market value at the date of the gift. Depreciation is computed using the straight-line method, beginning the month after the asset is placed in service, over the asset's estimated useful life. Estimated useful lives are generally three to ten years for equipment and 20 to 40 years for buildings and improvements. Depreciation expense for the year ended December 31, 1997 amounted to \$1,483,203 and has been recorded in the statement of activities in the appropriate functionalized categories. When assets are sold or retired, the cost and accumulated depreciation are removed from the accounts and any resulting gain or loss is included in unrestricted income for the period.

Annuities and Unitrusts Payable

Amounts due to donors in connection with gift annuities and unitrusts are determined based on remainder value calculations, as of December 31, 1997, with varied assumptions of rates of return and payout terms.

Deferred Income and Advances on Contracts

Deferred income includes prepayments received on Laboratory publications and advances on contracts to be utilized within the next year. Advances on contracts includes funding received for grants and contracts before it is earned. In certain circumstances, long-term advances are invested in the master pooled account until they are expended.

Revenue Recognition

Revenue is recognized at the time it is earned. The sources of revenue include grant payments from governmental agencies, contracts from private organizations, and income from the rental of laboratories and classrooms for research and educational programs. The tuition income is net of student financial aid of \$536,097 and \$479,000 in 1997 and 1996, respectively. Fees for conferences and other services include the following activities: housing, dining, library, scientific journals, aquatic resources and research services.

Contributions

Contribution revenue includes gifts and pledges. Gifts are recognized as revenue upon receipt. Pledges are recognized as temporarily or permanently restricted revenue in the year received and are recorded at the present value of expected future cash flows, net of allowance for unfulfilled pledges. Gifts and pledges, other than cash, are recorded at fair market value at the date of contribution.

Expenses

Expenses are recognized when incurred and charged to the functions to which they are directly related. Expenses that relate to more than one function are allocated among functions using various methodologies.

Other programs expense consists primarily of fundraising, year-round labs, and library room rentals, costs associated with aquatic resource sales and scientific journals. Total fundraising expense for 1997 is \$1,226,360.

Use of Estimates

The preparation of financial statements in conformity with generally accepted accounting principles requires management to make estimates and assumptions that affect the reported amounts of assets and liabilities and disclosure of contingent assets and liabilities at the date of financial statements and the reported amounts of revenues and expenses during the reporting period. Actual results could differ from those estimates.

Reclassification

Certain prior year amounts have been reclassified to conform with current year presentation. The reclassifications had no effect on net assets.

Tax-Exempt Status

The Laboratory is exempt from federal income tax under Section 501(c)(3) of the Internal Revenue Code.

R14 Annual Report

C. Investments:

The following is a summary of the cost and market value of investments at December 31, 1997 and 1996:

	<u>Market</u>		<u>Cost</u>	
	<u>1997</u>	<u>1996</u>	<u>1997</u>	<u>1996</u>
Certificates of deposit	\$ 40,000	\$ 55,350	\$ 40,000	\$ 55,350
Money market securities	2,168,958	3,469,588	2,168,958	3,469,589
U.S. Government securities	1,292,600	1,233,690	1,098,526	998,829
Corporate fixed income	2,587,861	3,431,333	2,472,653	3,278,396
Common stocks	5,279,266	3,793,156	4,271,853	2,742,841
Mutual funds	23,223,812	17,371,972	19,317,499	14,555,958
Limited partnerships	5,429,700	4,326,600	3,309,994	3,108,464
Total investments	<u>\$40,022,197</u>	<u>\$33,681,689</u>	<u>\$32,679,483</u>	<u>\$28,209,427</u>

Investment portfolios for the years ended December 31, 1997 and 1996 are as follows:

	<u>Market</u>		<u>Cost</u>	
	<u>1997</u>	<u>1996</u>	<u>1997</u>	<u>1996</u>
<u>Short-Term Investments</u>				
Certificates of deposit	\$ 40,000	\$ 55,350	\$ 40,000	\$ 55,350
Money market 1784 Fund	1,759,589	2,755,593	1,759,589	2,755,593
Common stocks	551,780	50,608	530,936	50,608
Mutual funds	<u>2,056,677</u>	<u>1,056,643</u>	<u>2,056,679</u>	<u>1,063,089</u>
Total	<u>4,408,046</u>	<u>3,918,194</u>	<u>4,387,204</u>	<u>3,924,640</u>
 <u>Long-Term Investments</u>				
Pooled investments:				
Master pooled investments	\$26,163,702	\$21,858,658	\$20,201,962	\$17,889,881
Separately invested:				
General Chase trust	5,846,916	4,898,630	4,986,443	3,926,959
Library Chase trust	1,593,242	1,315,847	1,358,149	1,065,008
Annuity and unitrust investments	<u>2,010,291</u>	<u>1,690,360</u>	<u>1,745,725</u>	<u>1,402,939</u>
Total	<u>35,614,151</u>	<u>29,763,495</u>	<u>28,292,279</u>	<u>24,284,787</u>
Total investments	<u>\$40,022,197</u>	<u>\$33,681,689</u>	<u>\$32,679,483</u>	<u>\$28,209,427</u>

D. Accounting for Pooled Investments:

Certain net assets are pooled for investment purposes. Investment income from the pooled investment account is allocated on the market value unit basis, and each fund subscribes to or disposes of units on the basis of the market value per unit at the beginning of the calendar quarter within which the transaction takes place. The unit participation of the funds at December 31, 1997 and 1996 is as follows:

	<u>1997</u>	<u>1996</u>
Unrestricted	4,192	4,415
Temporarily restricted	42,693	41,426
Permanently restricted	65,411	66,442
Advances on contracts	<u>6,506</u>	<u>6,493</u>
	<u>118,802</u>	<u>118,776</u>

Pooled investment activity on a per-unit basis was as follows:

	<u>1997</u>	<u>1996</u>
Unit value at beginning of year	\$ 186.35	\$ 159.37
Unit value at end of year	<u>220.30</u>	<u>186.35</u>
Total return on pooled investments	<u>\$ 33.95</u>	<u>\$ 26.98</u>

E. *Long-Term Debt:*

Long-term debt consisted of the following at December 31:

	<u>1997</u>	<u>1996</u>
Variable rate (5.50% at December 31, 1997) Massachusetts Industrial Finance Authority Series 1992A Bonds payable in annual installments through 2012	\$ 960,000	\$ 990,000
6.63% Massachusetts Industrial Finance Authority Series 1992B Bonds, payable in annual installments through 2012	1,280,000	1,330,000
5.8% The University Financing Foundation, Inc., payable in monthly installments through 2000	325,210	418,821
5.8% The University Financing Foundation, Inc., payable in monthly installments through 2002	231,817	—
Capital leases with various rates and due dates	<u>—</u>	<u>57,260</u>
	<u>\$2,797,027</u>	<u>\$2,796,081</u>

The aggregate amount of principal due on long-term debt for each of the next five fiscal years and thereafter is as follows:

1998	\$ 229,657
1999	243,274
2000	267,404
2001	173,664
2002	148,028
Thereafter	<u>1,735,000</u>
	2,797,027
Less current portion of long-term debt	<u>(229,657)</u>
	<u>\$2,567,370</u>

In 1992, the Laboratory issued \$1,100,000 Massachusetts Industrial Finance Authority (MIFA) Series 1992A Bonds and \$1,500,000 MIFA Series 1992B. These bonds pay varying annual interest rates ranging from 3.48% to 6.63%. Interest expense on this debt totaled \$141,899 for the year ended December 31, 1997. The Series 1992 A and B Bonds mature on December 1, 2012 and are collateralized by a first mortgage on certain Laboratory property.

The agreements related to these Bonds subject the Laboratory to certain covenants and restrictions. Under the most restrictive covenant of this debt, the Laboratory's operating surplus (before transfers), interest, expense and transfers from the quasi-endowment for debt service must equal or exceed all debt service payments, as defined by the agreement. The Laboratory was in compliance with these covenants and restrictions at December 31, 1997.

In 1996, the Laboratory borrowed \$500,000 with an interest rate of 5.8% from the University Financing Foundation, Inc. The interest expense for the year ended December 31, 1997 was \$21,829. The loan matures in 2000 and is collateralized by 69,440 shares of a fixed income mutual fund with a fair value of \$933,690 at December 31, 1997.

In 1997, the MBL borrowed \$250,000 with an interest rate of 5.8% per annum from the University Financing Foundation, Inc. The interest expense for the year ended December 31, 1997 was \$5,866. This loan matures 2002 and is collateralized by 69,440 shares of a fixed income mutual fund with a fair value of \$933,690 at December 31, 1997.

The Laboratory has a line of credit agreement with BankBoston from which it may draw up to \$1,000,000. No amounts were outstanding under this agreement as of December 31, 1997 and 1996.

R16 Annual Report

E. *Plant Assets:*

Plant assets consist of the following at December 31:

	<u>1997</u>	<u>1996</u>
Land	\$ 702,908	\$ 702,908
Buildings	32,419,072	31,730,830
Equipment	<u>4,300,932</u>	<u>4,270,278</u>
Total	37,422,912	36,704,016
Less: Accumulated depreciation	<u>(17,396,332)</u>	<u>(16,008,392)</u>
Plant assets, net	<u>\$20,026,580</u>	<u>\$20,695,624</u>

G. *Retirement Plan:*

The Laboratory participates in the defined contribution pension plan of TIAA-CREF (the "Plan"). The Plan is available to permanent employees who have completed two years of service. Under the Plan, the Laboratory contributes 10% of total compensation for each participant. Contributions amounted to \$715,858 and \$661,089 for the years ended December 31, 1997 and 1996, respectively.

H. *Pledges:*

Unconditional promises to give are included in the financial statements as pledges receivable and the related revenue is recorded in the appropriate net asset category. Unconditional promises to give are expected to be realized in the following periods:

	<u>1997</u>	<u>1996</u>
In one year or less	\$2,219,056	\$1,836,874
Between one year and five years	2,485,851	2,780,000
After five years	<u>80,000</u>	<u>—</u>
Total	4,784,907	4,616,874
Less: discount of \$227,025 in 1997 and \$373,650 in 1996 and allowance of \$100,000 in 1997 and \$10,380 in 1996	<u>(327,025)</u>	<u>(384,030)</u>
	<u>\$4,457,882</u>	<u>\$4,232,844</u>

Pledges receivable at December 31 have the following restrictions:

Research and education	\$3,787,882	\$4,232,844
Permanently restricted net assets	<u>670,000</u>	<u>—</u>
	<u>\$4,457,882</u>	<u>\$4,232,844</u>

I. *Postretirement Benefits:*

The Laboratory accounts for its postretirement benefits under Statement No. 106, "Employers' Accounting for Postretirement Benefits Other than Pensions," which requires employers to accrue, during the years that the employee renders the necessary service, the expected cost of benefits to be provided during retirement. As permitted, the Laboratory has elected to amortize the transition obligation over 20 years commencing on January 1, 1994.

The Laboratory's policy is that all current retirees and certain eligible employees who retired prior to June 1, 1994 will continue to receive postretirement health benefits. The remaining current employees will receive benefits; however, those benefits will be limited as defined by the Plan. Employees hired on or after January 1, 1995 will not be eligible to participate in the postretirement medical benefit plan.

Net postretirement benefits for 1997 and 1996 include:

	<u>1997</u>	<u>1996</u>
Service cost (benefits earned during period)	\$ 29,095	\$ 61,712
Interest cost (on projected benefit obligation)	135,892	149,149
Actual return on plan assets	(31,976)	(20,700)
Net amortization and deferral	<u>59,071</u>	<u>92,176</u>
Net postretirement benefits cost	<u>\$ 192,082</u>	<u>\$ 282,337</u>

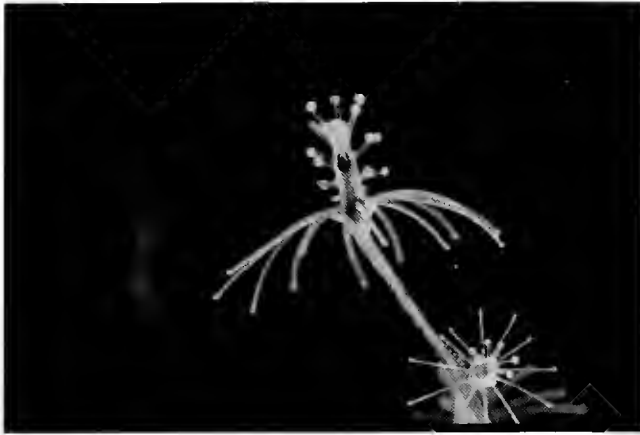
Below is a reconciliation of the funded status of the Plan at December 31, 1997 and 1996:

Accumulated postretirement benefit obligation:		
Retirees and dependents	\$1,439,899	\$1,369,787
Fully eligible active participants	163,188	230,290
Other active participants	<u>316,778</u>	<u>608,796</u>
Total	1,919,865	2,208,873
Market value of plan assets	<u>701,140</u>	<u>588,337</u>
Unfunded obligations	<u>1,218,725</u>	<u>1,620,536</u>
Unrecognized prior service cost (credit)	—	—
Unrecognized net (gain) loss	(191,078)	136,158
Unrecognized transition obligation	<u>1,389,159</u>	<u>1,475,981</u>
Accrued postretirement benefit cost	<u>\$ 20,644</u>	<u>\$ (8,397)</u>

The health care cost trend rate assumptions used in determining the projected benefit obligation begin at 9.5% in 1997 and gradually decrease to 5.0% in the year 2006 and thereafter. The effect of raising the assumed health care cost trend rate by one percentage point in each year would be to increase the accumulated postretirement benefit obligation as of December 31, 1997 by \$173,001 and to increase the aggregate of the service and interest cost components of net periodic postretirement benefit cost for the year then ended by \$14,528. The discount rate used in determining the accumulated postretirement benefit obligation is 7.5%, and the expected return on plan assets was 8.0%. During 1997, the Laboratory contributed \$192,082 to fund the Trust for these postretirement benefits.

MARINE BIOLOGICAL LABORATORY
SUPPLEMENTAL SCHEDULE OF FUNCTIONAL EXPENSES
for the year ended December 31, 1997

	<u>Research</u>	<u>Instruction</u>	<u>Conferences</u>	<u>Other</u>	<u>Facilities Maintenance</u>	<u>Administration</u>	<u>Library Services</u>	<u>Research Services</u>	<u>Aquatic Research Services</u>	<u>Total</u>
Salaries	\$ 3,188,396	\$ 368,776	\$ 346,380	\$ 636,238	\$ 1,045,652	\$ 1,722,940	\$ 346,574	\$ 344,199	\$ 239,100	\$ 8,238,255
Fringe benefits	852,100	99,599	93,522	171,739	282,421	468,136	93,575	92,934	64,557	2,218,583
Professional services	63,077	252,301	—	29,915	73,695	196,044	3,903	25	—	618,960
Subcontracts	981,132	—	957,949	3,127	—	—	—	—	—	1,942,208
Equipment	522,592	334,164	2,470	1,466	135,947	26,875	—	4,050	2,598	1,030,162
Supplies	537,402	391,223	40,850	110,557	217,796	138,744	15,073	353,334	42,422	1,847,401
Travel	501,316	193,823	(2,834)	31,135	8,334	39,363	10,707	915	95	782,854
Serials	627	1,466	—	15,846	628	1,305	476,119	346	—	496,337
Utilities	292	439	185,488	1,901	730,360	99,609	367	304	1,599	1,020,359
Depreciation	—	—	—	—	1,483,203	—	—	—	—	1,483,203
Other	223,503	300,789	216,477	331,173	493,236	472,017	111,450	195,312	82,656	2,426,613
Internal direct changes	359,010	801,051	(665,077)	98,639	(147,503)	28,593	49,906	(498,532)	(26,087)	—
Total	7,229,447	2,743,631	1,175,225	1,431,736	4,323,769	3,193,626	1,107,674	492,887	406,940	22,104,935
Indirect expense allocations	3,802,467	1,400,877	312,480	4,009,072	(4,323,769)	(3,193,626)	(1,107,674)	(492,887)	(406,940)	—
Total expenses	\$ 11,031,914	\$ 4,144,508	\$ 1,487,705	\$ 5,440,808	—	—	—	—	—	\$ 22,104,935



Report of the Library Director

One of the goals of the MBL's recently announced *Discovery Campaign* is to raise \$1 million in support of the MBL/WHOI Library. This is excellent news indeed for the library. Funding at this level will be a good start towards protecting for future generations of scientists one of the world's most comprehensive—and valuable—collections of books and journals in the biological, oceanographic, and ecological sciences. This support will also help in the development of information technology, which promises to play a vital role in the future of the library.

The way the library will serve scientists in the next decade will be very different from the way it serves them today. More and more the library is becoming a conduit rather than a repository of information, providing on-line access to the burgeoning electronic literature. But even as electronic delivery alters the library and the way it is used, the MBL's irreplaceable book and journal collection continues to be a national treasure that must be conserved.

The Library Committee has spent considerable time over the past year evaluating our collection as a whole, the library's physical plant, and the future of both the paper and electronic library. The committee found that even with the advent of more electronic resources in the library, still more room will soon be needed to house all the early monographic series now available in the stacks and the hardware required to serve the growing electronic resources.

With fellow members of the Boston Library Consortium, we are looking into the feasibility of having an off-site storage facility. If this plan is realized, we can look forward to a cooperatively run depository that will offer electronic retrieval and courier service as well as warehousing for some of our lesser used volumes, making room for other, ever expanding information resources.

Special collections

A new Special Collections area has been created in the third floor book section of the library through a

generous gift made in memory of Ivor Cornman. In this area, the expeditions, bound collected reprints, and books from the open shelves published before 1900 are being protected. Earlier works, currently on the open shelves in the stacks, are being cataloged and placed in the Rare Books Room.

Digital library

As we preserve the older collection, we are expanding the electronic collection. The library currently supports more than 300 full-text electronic journals on its web site (www.mbl.edu). We provide access to more than 35 commercial databases and provide public access to databases created here at the MBL on marine animals, *E. coli*, women-in-science, the Leuckart charts, and other educational material of interest to both scientists and students. From the Community of Science we have purchased funding and patent databases including the Expertise Database, which contains information on individual scientists and their projects. Woods Hole scientists who enter information about their work in the data bank are rewarded with timely information on available funding sources in their field.

The library continues to update to the latest versions of Internet Grateful Med and PubMed and InfoBank Search. The latter service includes newspaper, magazine, academic, and general reference searching targeted to our student and visitor populations. Bibliographies of relevant resources for the many summer courses held at the MBL have been created and can be accessed via the web. The Don Flescher photo collection of fish is a new database available from the library home page. It is comprised of 1500 pictures searchable by species, common name, catch area, or taxonomy.

Journal issues

One of the newest issues facing libraries, along with the continued rise in subscription prices, is the new

phenomena of publishers collecting electronic information at the "article level" when library users log into their sites. Vendors and publishers can now gather specific user data right down to the exact article, phrase, and words that someone pulls up or orders. What happens to this information? If this user information should be sold to the right company, it could become important for determining who else in the world is interested in, or perhaps working on, the same research problem. Will investigators hesitate to look at publishers' electronic sites for fear of competitors getting a hint of what they are working on? What protections can the library provide? A cloak of anonymity, possibly; but right now information on article use is transmitted almost exclusively to the publishers and not provided to the library.

Like other libraries, the MBL/WHOI Library is now managing licenses covering information content as opposed to purchasing the contents. At the same time, we are trying to negotiate protections for our users. Our newly appointed Technical Services Coordinator carries the responsibility of "watchdog" for these licenses. From the arena of fair use, we now are venturing into the arena of ethical use of information.

Ensuring access to today's electronic resources tomorrow is another major concern. Since 1991 the library has canceled more than 500 journal subscriptions. In 1991 we borrowed 1858 articles for our patrons. In 1997 we borrowed 3259, representing a 42% increase over six years. This practice will continue to increase as it becomes necessary to cancel titles in order to meet publishers' price increases for "must have" journals. As a result, electronic document delivery, whether providing documents for other libraries or retrieving materials for our own scientists, is becoming an ever-increasing component of the library's services.

Instruction

The new Science Reference Librarian has quickly expanded and improved the library's instructional programs on all four campuses (MBL, WHOI, Fisheries, and USGS). Training and course instruction is now provided for researchers and students, and new on-line bibliographies and reserve lists have been created for MBL summer courses. There continues to be high demand for new courses in how to search scientific databases. JAVA, Web page design, Windows 95, Powerpoint, etc.

Branch libraries

Jacqueline Riley, the Science Reference Librarian at the Fisheries, has implemented many new services

including launching a NEFSC library web page. The contract that provides library services for the National Marine Fisheries, while bringing a collegial interchange at the local level, presents some technological problems at the national level that resulted in different automated library systems. The marriage of two different library systems seemed to be impossible until a method was devised by Laurel Duda (MBL) and Maggie Rioux (WHOI) that allows both libraries to share bibliographic records without redundant effort (Duda, L.E. and M.A. Rioux, One Library, One Bib Record—Two OPACs, Two Systems, *Information Outlook* Vol. 2, No 3: 31–36).

A new library was incorporated into the design of the new WHOI Research Vessel *Atlantis*. Space was designed for a computer workstation with Internet access for the researchers and staff to fulfill their information needs while at sea. A reference collection, popular works, and a wonderful collection of World War II monographs donated by Ken Parada are also available aboard ship.

The Data Library, using the Library's integrated computer systems, has installed a new image server, providing photographic images of the WHOI scientific instrument collection. The new ALVIN archive catalog provides retrieval of individual ALVIN dive records through our local on-line catalog, MARINER, including all related media the data archive holds and hot links to images from the dives. More than 700 of the photographs in the MBL archives, including the late 1800 and early 1900 collection of MBL's Baldwin Coolidge photos, have also been cataloged and are available through MARINER and the Web.

A growing debate focusing on numerical data in the Earth and Environmental sciences and the issues relevant to the management of all non-text information was the focus of the Scientific Data Advisory Committee which met this past year at WHOI. The major problem identified was access to the data and how the library must make it easier for users of data sets to find, select, and retrieve that data. In order to do this the Data Library needs to encourage submission of data sets in a useable standard metadata format, with appropriate documentation. Because getting scientists to do the latter is referred to as "herding cats," the community needs to provide assistance and incentives.

The future

The National Library of Medicine awarded the library \$1,033,278 in support of the project titled, "Professional Services in Support of NLM's Outreach Efforts to Encourage the Use of Computers and Information Science in Medicine." With this support,

the library is able to plan for "change" over the next five years and to offer services that will fit evolving needs. However, all of the members of the scientific community must promote the value of academic access to information for research and teaching. They will also need to use innovative technology to improve scholarly communications without operating in an economic model tied to increasing costs from large commercial publishers. Libraries and administrators have realized that spiraling costs cannot be solved by strategies that merely include canceling titles and collective purchasing. Change must be effected through partnerships in new technologies, and the development of new models of publication and distribution.

While the new electronic environments offer opportunities to provide new services, we also need to think about the sustainability of the information ecosystem: managing the life cycle of information for preservation and access. This year the Florence Gould

Foundation awarded \$30,000 to the library for the preservation and conservation of the French scientific rare books in our collection. The library will make these books available electronically and will use some of the high-end translation dictionaries now available on our Web page that allows French to English translation.

As noted, one of the goals of the *Discovery Campaign* is to help preserve the library facility and the book and journal collections for future scholars. Managing this traditional collection will be much easier than managing the new electronic collection, which presents a number of new issues, not the least being the lack of planning for digital archival storage and migration to new technologies by the publishers. As we approach the 21st Century, "change" will be the MBL/WHOI Library's primary challenge.

—Catherine Norton



Educational Programs

Summer Courses

Biology of Parasitism: Modern Approaches (June 12–August 15)

Directors

Steven Hajduk, University of Alabama, Birmingham
Edward Pearce, Cornell University

Faculty

Robert Bullis, Marine Biological Laboratory
Harry Dickerson, University of Georgia
Steve Ealick, Cornell University
Christopher Hunter, University of Pennsylvania School of
Veterinary Medicine
Susan Little, University of Georgia
Phil LoVerde, State University of New York, Buffalo
David Russell, Washington University School of Medicine
Phillip Scott, University of Pennsylvania
David Sibley, Washington University School of Medicine
Christian Tschudi, Yale University School of Medicine
Buddy Ullman, Oregon Health Sciences University
Elisabetta Ullu, Yale University School of Medicine

Teaching Assistants

Laura Rosa Brunet, Cornell University
Nino Campobasso, Cornell University
Darrick Carter, Oregon Health Sciences University
Jaime Dant, Washington University Medical School
Jerome Drain, University of Alabama, Birmingham
Merle Elloso, University of Pennsylvania
Wendy Freebern, State University of New York, Buffalo
Maren Lingnau, Washington University School of Medicine
Carol Lopez-Estrano, Yale University

Joao Pedras-Vasconcelo, Cornell University Veterinary School
Elizabeth Sabin, Cornell University

Lecturers

Norma Andrews, Yale University School of Medicine
James Bangs, University of Wisconsin, Madison
Stephen Beverley, Harvard University School of Medicine
John Boothroyd, Stanford University
Karen Day, Oxford University, United Kingdom
John Donelson, University of Iowa College of Medicine
Paul Englund, Johns Hopkins University School of Medicine
Danel Goldberg, Washington University
Richard K. Grenis, University of Manchester, United Kingdom
Kasturi Haldar, Stanford University School of Medicine
John Heuser, Washington University School of Medicine
Stephen Hoffman, Naval Medical Research Institute
Peter Hotez, Yale University School of Medicine
William Jeffery, Pennsylvania State University
Patricia Johnson, University of California, Los Angeles
Richard Komuniecki, University of Toledo
Manfred Kopf, Basel Institute for Immunology, Switzerland
Jean Langhorne, Imperial College of Science and Technology,
United Kingdom
Timothy Nilsen, Case Western Reserve University
Marilyn Parsons, Seattle Biomedical Research Institute
William Petri, University of Virginia Health Sciences Center
Meg Phillips, University of Texas Southwest
Steven Reed, Infectious Disease Research Institute
Steve Reiner, University of Chicago
David Sacks, National Institutes of Health
Alan Sher, National Institutes of Health
Mitchell Sogin, Marine Biological Laboratory
Kenneth Stuart, Seattle Biomedical Research Institute
Sam Turco, University of Kentucky College of Medicine
C. C. Wang, University of California, San Francisco
Gary Ward, University of Vermont
Tom Wellem, National Institutes of Health

Dyann Wirth, Harvard University School of Public Health
 Maria Yazdanbakhsh, Leiden University, The Netherlands

Course Coordinator

Robert Sabatini, University of Alabama, Birmingham

Course Assistant

Brian Hondowicz, University of Pennsylvania

Laboratory Assistant

Joseph Paton, Tufts University

Students

Kimberly Brouwer, Johns Hopkins School of Public Health
 Maristela Camargo, Federal University of Minas Gerais, Brazil
 Soren Gantt, New York University School of Medicine
 Michelle Gleeson, University of Technology, Australia
 Meike Hensmann, Yale University
 David Jiang, Johns Hopkins University School of Medicine
 Andreas Lingnau, Washington University Medical School
 Gunnar Mair, Queen's University of Belfast, United Kingdom
 Antoinette Marsh, University of California, Davis
 Lillian Ouko, University of Pennsylvania
 Lisl Shoda, Washington State University
 Kevin Tan, National University, Singapore
 Carl Johan Treutiger, Karolinska Institute, Sweden
 Elisabeth Triplett, Cornell University
 Eric Villegas, University of Pennsylvania
 Ulrike Wille, University of Tübingen, Germany

Embryology: Concepts and Techniques in Modern Developmental Biology (June 15–July 26)

Directors

Marianne Bronner-Fraser, California Institute of Technology
 Scott Fraser, California Institute of Technology

Faculty

Andre Adoutte, Université Paris-Sud, France
 Rosa Beddington, National Institute for Medical Research, United Kingdom
 R. Andrew Cameron, California Institute of Technology
 Andrea Collazo, California Institute of Technology
 Eric H. Davidson, California Institute of Technology
 Richard Harland, University of California, Berkeley
 Lee Niswander, Memorial Sloan-Kettering Cancer Center
 James Posakony, University of California, San Diego
 Nadia Rosenthal, Massachusetts General Hospital
 Joel Rothman, University of California, Santa Barbara
 Joshua Sanes, Washington University School of Medicine
 John Saunders, Jr., Marine Biological Laboratory
 Martin Shankland, University of Texas
 Judith Venuti, Columbia University

Teaching Assistants

Maria Ina Arnone, California Institute of Technology
 Guillaume Balavoine, Wellcome/CRC Institute, United Kingdom
 Rebecca Beach, Hollins College
 Steve Gendreau, University of California, Santa Barbara

Gabrielle Kardon, Duke University
 Carmen Kirchhamer, Harvard University
 Anne Knecht, University of California, Berkeley
 Catherine Krull, California Institute of Technology
 Julie Kuhlman, Memorial-Sloan Kettering Cancer Center
 Eric Lai, University of California, San Diego
 Nicholas Lartillot, Université Paris-Sud, France
 David Nellesen, University of California, San Diego
 Craig Neville, Massachusetts General Hospital
 Robert Zeller, University of California, San Diego

Lecturers

Sean Carroll, University of Wisconsin
 Nancy Hopkins, Massachusetts Institute of Technology
 Michael Levine, University of California, Berkeley
 Tom Maniatis, Harvard University
 David McClay, Duke University

Course Coordinator

Linda Huffer, Marine Biological Laboratory

Course Assistants

Allison Freeman, Wheaton College
 Jason Rickles, Boston University School of Education

Students

Pia Aanstad, University of Newcastle, United Kingdom
 Dominique Bergmann, University of Colorado, Boulder
 Brian Cooper, National Institute for Medical Research, United Kingdom
 Wim Damen, München University, Germany
 Gregory Davis, University of Chicago
 Eric Finkelstein, State University of New York Health Science Center
 Paola Giuliano, Zoological Station, Italy
 Tiffany Heanue, Harvard University
 Sharon Hesterlee, University of Arizona
 Christoph Kaufmann, Massachusetts General Hospital
 Peter Ladurner, University of Innsbruck, Austria
 Walter Lerchner, National Institute for Medical Research, United Kingdom
 Per Lindahl, University of Göteborg, Sweden
 Matthew Marlowe, University of California, Berkeley
 Sean Megason, Harvard University
 Raffaella Melfi, Università Degli Studi di Palermo, Italy
 Axel Meyer, State University of New York
 Bennett Novitch, Harvard Medical School
 Catherine Olsen, University of California, Davis
 Eva Reissmann, Max-Planck-Institut, Germany
 Elaine Seaver, University of Texas, Austin
 James Spotts, California Institute of Technology
 Xin Sun, University of California, San Francisco
 Christina Takke, University of Köln, Germany
 Emily Walsh, University of California, San Francisco

Microbial Diversity (June 15–July 31)

Directors

Edward Leadbetter, University of Connecticut
 Abigail Salyers, University of Illinois

Faculty

Kurt Hanselmann, University of Zurich, Switzerland
Bruce Paster, Forsyth Dental Center
Rolf Schauder, University of Frankfurt, Germany

Teaching Assistants

Elena Barbieri, University of Urbino, Italy
Daniel Gisi, Swiss Federal Institute of Technology, Switzerland
David Graham, University of Illinois
Irena Levin, Forsyth Dental Center
Caroline Plugge, Wageningen Agricultural University, The Netherlands

Lecturers

Bianca Brahmshba, University of California, San Diego
Colleen Cavanaugh, Harvard University
Yehuda Cohen, Hebrew University of Jerusalem, Israel
Sharon Danielson, Rensselaer Polytechnic Institute
Daniel Distel, University of Maine
Stephen Farrand, University of Illinois, Urbana-Champaign
James Fleming, University of Tennessee
Tillman Gerngross, Metabolix, Inc., Cambridge
Robert Haselkorn, University of Chicago
Holger Jannasch, Woods Hole Oceanographic Institution
Jared Leadbetter, Michigan State University
Mark McBride, University of Wisconsin, Milwaukee
Terry Miller, New York State Department of Health
Duane Moser, Center for Great Lakes Studies, Milwaukee
Sandra Nierzwicki-Bauer, Rensselaer Polytechnic Institute
Thomas Pitta, Rowland Institute for Science
James Russell, Cornell University
Daad Saffarini, University of Massachusetts
Anglica Seitz, Harvard University
Nadja Shoemaker, University of Illinois
Alfred Spormann, Stanford University
David Stahl, Northwestern University
Anne Summers, University of Georgia
Andreas Teske, Woods Hole Oceanographic Institution
Pieter Visscher, University of Connecticut, Avery Point
John Waterbury, Woods Hole Oceanographic Institution
Lily Young, Rutgers University

Course Coordinator

Madeline Vargas, College of the Holy Cross

Course Assistant

Noah Horst, Tufts University

Students

Ehud Banin, Tel Aviv University, Israel
Fikry Barghuthy, Hebrew University, Israel
Brendan Bohannan, Michigan State University
Alfred Boyle, Rutgers University
Scott Dawson, University of California, Berkeley
Jeffrey Dugas, University of Connecticut
Kelly Evans, Queen's University, Canada
Deborah Hughes, Scripps Institution of Oceanography
Elke Jaspers, Universität Oldenburg, Germany
Hope Johnson, Stanford University
Sabine Krause, Max-Planck-Institut, Germany
Thomas Lie, University of Connecticut

David Long, Montana State University
Junko Munakata Marr, Colorado School of Mines
William Sobczak, Cornell University
Alexandra Stone, Ohio State University
Acharawan Thongmee, University of North Texas
Crisogono Vasconcelos, Universidade Federal Fluminense, Brazil
S. Wenuganen, Bogor Agricultural University, Indonesia
Ludek Zurek, University of Alberta, Canada

Neural Systems & Behavior (June 15–August 8)

Directors

Janis Weeks, University of Oregon
Harold Zakon, University of Texas, Austin

Faculty

Ronald L. Calabrese, Emory University
Catherine Carr, University of Maryland
Kathleen French, University of California, San Diego
David Glanzman, University of California, Los Angeles
Scott Hooper, Ohio University
Richard Hyson, Florida State University
Masashi Kawasaki, University of Virginia
William Kristan, University of California, San Diego
Richard Levine, University of Arizona
Pierre Meyrand, Université de Bordeaux, France
Michael Nusbaum, University of Pennsylvania School of Medicine
Glen Prusky, University of Lethbridge, Canada
William Roberts, University of Oregon
Gary Rose, University of Utah
Angela Wenning, Universität Konstanz, Germany

Teaching Assistants

Cecilia Armstrong, University of Oregon
Dawn Marie Blitz, University of Pennsylvania School of Medicine
Shanping Chen, University of California, Los Angeles
Richard Dyck, University of Lethbridge, Canada
Michael Ferrari, University of California, San Diego
Evelyn Field, University of Lethbridge, Canada
Matthew Friedman, Cornell University
Jorge Golowasch, Brandeis University
Andrew Hill, Emory University
Maria Kubke, University of Maryland
David Lenzi, University of Oregon
Lynne McAnelly, University of Texas
Tasha McMahon, University of California, Los Angeles
Geoffrey Murphy, University of California, Los Angeles
David Sandstrom, University of Arizona
Daphne Soares, University of Maryland
Laura Wolszon, Columbia University

Lecturers

George Augustine, Duke University Medical Center
Rita Balice-Gordon, University of Pennsylvania School of Medicine
David Clayton, University of Illinois
Roger Hanlon, Marine Biological Laboratory
Ron Hoy, Cornell University
Edward Kravitz, Harvard Medical School

Eduardo Macagno, Columbia University
Gina Turrigiano, Brandeis University

Scholars-in-Residence

Sascha du Luc, Salk Institute
Alan Gelperin, Bell Labs
Rebecca Johnston, Colby College
Simon Laughlin, University of Cambridge, United Kingdom

Course Assistants

Sarah Doernberg, Emory University
Sarah Gaines, Princeton University

Students

Emre Aksay, Bell Labs
Eric Bauer, University of Texas, Austin
Ben Bonham, University of California, San Francisco
Holly Campbell, University of Arizona
Randy Chitwood, University of Texas, San Antonio
Virginia de Sa, University of California, San Francisco
Teresa Esch, University of Virginia
Joe Fass, Michigan Tech University
Paul Gasser, Arizona State University
Timothy Holy, Princeton University
William Kargo, Allegheny University
Christopher Kilroy, University of North Carolina, Wilmington
Susan Laessig, University of Maryland, Baltimore
Lynne Merchant, University of California, San Diego
Leslie Osborne, University of California, Berkeley
Dorit Polnaï, Northeastern University
Rex Robison, Stanford University
Sen Song, Brandeis University
Ayako Yamaguchi, Columbia University
Shih-Rung Yeh, Georgia State University

Neurobiology (June 15–August 16)

Directors

Gary Banker, University of Virginia Medical School
Daniel Madison, Stanford University Medical Center

Section Directors

Michael Greenberg, Childrens' Hospital
Stephen Smith, Stanford University Medical Center

Faculty

Susan Birren, Brandeis University
Mark Bowlby, Wyeth-Ayerst Research
Gabriel Corfas, Childrens' Hospital
Kerry Delaney, Simon Fraser University, Canada
Donald Faber, Allegheny University of the Health Sciences
Steven Finkbeiner, Childrens' Hospital
Philip Haydon, Iowa State University
Stephen Jones, Case Western Reserve University
Maurice Kernan, State University of New York, Stony Brook
Stephen Lin, Wyeth-Ayerst Research
Ed McCleskey, Oregon Health Sciences University
Adam Rory McQuiston, Stanford University School of Medicine
Thomas Reese, National Institutes of Health
Morgan Sheng, Howard Hughes Medical Institute

Carolyn Smith, National Institutes of Health
Stuart Thompson, Stanford University
Li-Huei Tsai, Harvard Medical School
Susan Wray, National Institutes of Health
Joshua Zimmerberg, National Institutes of Health

Teaching Assistants

F. Woodward Hopf, Stanford University Medical Center
Alane Murdock, Stanford University Medical Center
Paul Pavlidis, Stanford University Medical Center
Alberto Pereda, Allegheny University
Martine Usdin, Stanford University Medical Center

Lecturers

Yadin Dudai, Weizmann Institute of Science, Israel
Justin Fallon, Brown University
Julie Ann Kauer, Duke University Medical Center
Maurine Linder, Washington University Medical School
Diane Lipscombe, Brown University
Luis Parada, University of Texas
Robert Rosenberg, University of North Carolina, Chapel Hill
Gary Ruvkun, Massachusetts General Hospital
Thomas Sudhof, University of Texas
Karel Svoboda, Cold Spring Harbor Laboratory
Roger Tsien, University of California, San Diego

Course Assistants

Tara Bennett, Dartmouth College
Eleanore Edson, Stanford University

Students

Alberto Bacci, University of Milano, Italy
Elizabeth Brown, Medical College of Virginia
Benjamin Cravatt, Scripps Research Institute
Samuel Hess, Cornell University
Warren Kim, Yale University School of Medicine
Stuart Licht, Massachusetts Institute of Technology
Johanna Montgomery, Otago University, New Zealand
Craig Nelson, Harvard University
Eric Norman, University of Pittsburgh
Rita Sattler, University of Toronto, Canada
Marilee Shelton, University of North Carolina, Chapel Hill
Stephan Sigrist, Max-Planck-Institut, Germany

Physiology: Cellular and Molecular Biology (June 16–July 27)

Directors

Kerry Bloom, University of North Carolina, Chapel Hill
Mark Mooseker, Yale University

Faculty

William Bement, University of Wisconsin
Richard Cheney, University of North Carolina, Chapel Hill
Jonathan Chernoff, Fox Chase Cancer Center
Ruth Empson, University of Oxford, United Kingdom
Antony Galione, University of Oxford, United Kingdom
Tom Hays, University of Minnesota, St. Paul
Daniel Kiehart, Duke University Medical Center
Daniel Lew, Duke University Medical Center



Mary Ann Sells, Fox Chase Cancer Center
 Edwin Taylor, University of Chicago
 Joseph S. Wolenski, Yale University
 Elaine Yeh, University of North Carolina, Chapel Hill

Teaching Assistants

Elaine Bardes, Duke University Medical Center
 Lisa Evans, Yale University
 Tama Hasson, Yale University
 Amanda Hayward-Lester, Yale University
 Gary Michael Idelchik, University of Wisconsin
 Min-gang Li, University of Minnesota, St. Paul
 Feng Liu, Fox Chase Cancer Center
 Craig Mandato, University of Waterloo, Canada
 Ruth Montague, Duke University Medical College
 Samara Reek-Peterson, Yale University
 Melissa Reeder, Fox Chase Cancer Center
 Rey Antonio Sia, Duke University Medical Center
 Jenny Sider, University of Wisconsin
 Andre Silvanovich, University of Minnesota, St. Paul

Lecturers

Sid Altman, Yale University
 Angelika Amon, Massachusetts Institute of Technology
 Van Bennett, Duke University
 John Chant, Harvard University
 Paul Forscher, Yale University
 Martin Hemler, Dana Farber Cancer Institute
 Laurinda Jaffe, University of Connecticut Health Center
 Jennifer Lippincott-Schwartz, National Institutes of Health
 Bruce Mayer, Harvard University
 Ben Neel, Beth Israel Hospital
 Terry Orr-Weaver, Massachusetts Institute of Technology
 Michael Snyder, Yale University
 Karl Swann, University of Connecticut Health Center
 Mark Terasaki, University of Connecticut Health Center
 Lew Tilney, University of Pennsylvania
 Pat Wadsworth, University of Massachusetts, Amherst
 Sandra Wolen, Yale University
 Tian Xu, Yale University Medical School
 Bruce Zetter, Harvard University

Course Coordinator

Dawn Grant, Louisiana State University Medical Center

Course Assistant

Rebekah Harrison, Stanford University

Students

Richard Bayliss, University of Cambridge, United Kingdom
 Dale Beach, University of North Carolina, Chapel Hill
 George Bell, University of Arizona
 Jill Broome, University of North Carolina, Chapel Hill
 Julie Canman, University of North Carolina, Chapel Hill
 Anthony DePass, University of Massachusetts, Amherst
 John Diggins, Providence College
 Jean-Emmanuel Faure, Centre National de la Recherche Scientifique, France
 Rip Finst, Emory University
 Gundula Gries, University of Pennsylvania
 Edward Guo, Columbia University
 William Heinz, Johns Hopkins University
 Maria Holzmann, University of Geneva, Switzerland
 G. Karthikeyan, Tata Institute of Fundamental Research, India
 Kaoru Katoh, Marine Biological Laboratory
 Reed Kelso, Yale University
 Tijs Ketelaar, Wageningen Agricultural University, The Netherlands
 Rosy Lee, Stanford University
 Laura Linz, Louisiana State University Medical Center
 Jonathan Lyon, Scripps Institute of Oceanography
 Paul Maddox, University of North Carolina, Chapel Hill
 Gregory McGillem, University of Alabama, Birmingham
 Spontaneous McKnight, University of Arizona
 Brian Nibbelink, University of Vermont
 Helen Nilsson, University of Göteborg, Sweden
 Nesrin Ozoren, University of Pennsylvania
 Omar Quintero, Duke University Medical Center
 Rachael Ream, Hopkins Marine Station
 Eric Reese, University of California, Riverside
 Yasushi Satoh, University of Tokyo, Japan
 Matthew Simmons, University of Florida
 Justin Skoble, University of California, Berkeley
 Aline Valster, University of Massachusetts, Amherst
 Gang Wang, University of Iowa
 Yihong Wang, Ohio University
 Kathryn White, Scripps Institute of Oceanography

Short Courses

Analytical & Quantitative Light Microscopy (May 8–May 16)

Directors

Greenfield Sluder, University of Massachusetts Medical Center, Worcester Foundation Campus
 David Wolf, University of Massachusetts Medical Center, Worcester Foundation Campus

Faculty

William B. Amos, Medical Research Council, United Kingdom
 Richard Cardullo, University of California, Riverside
 Walter Carrington, University of Massachusetts Medical School
 Jeff Gelles, Brandeis University
 Shinya Inoué, Marine Biological Laboratory
 Rudolf Oldenbourg, Marine Biological Laboratory
 Randi Salmon, University of North Carolina, Chapel Hill
 Rami Silver, Cornell University Medical College
 Kenneth Spring, National Institutes of Health

Yu-li Wang, University of Massachusetts Medical Center,
Worcester Foundation Campus
Warren Zipsel, Cornell University

Teaching Assistants

Christine Thompson, University of Massachusetts Medical Center,
Worcester Foundation Campus
Elizabeth Thompson, University of Massachusetts Medical Center,
Worcester Foundation Campus
Clare Waterman-Storer, University of North Carolina, Chapel Hill

Course Coordinator

Frederick Miller, University of Massachusetts Medical Center,
Worcester Foundation Campus

Students

Julia Avery, Yale University
Margaret Clarke, Oklahoma Medical Research Foundation
Carol Cogswell, University of Sydney, Australia
David Collings, North Carolina State University
Rossella Conti, Brandeis University
Carol Gregorio, University of Arizona, Tucson
Alexey Khodjakov, Wadsworth Center for Labs and Research
Helmut Knapp, Swiss Federal Institute of Technology, Switzerland
Stephen Lambert, University of Massachusetts Medical Center,
Worcester Foundation Campus
Jeannie Lee, Whitehead Institute
Edwin Levitan, University of Pittsburgh
Ilona Linnoila, National Cancer Institute
Frank Macaluso, Albert Einstein College of Medicine
Richard MacDonald, Massachusetts General Hospital
Ivana Novak, August Krogh Institute, Denmark
Joan Packenham, National Institute of Environmental Health
Sciences
Brigitta Peteri-Brunbäck, Astra Hässle AB, Sweden
Jonathan Pines, The Wellcome Trust/Cancer Research Campaign,
United Kingdom
Guillermo Romero, University of Pittsburgh
Ichiro Sase, Laboratory of Molecular Biophotonics, Japan
Shuji Toyonaga, Laboratory of Molecular Biophotonics, Japan
Shlomo Trachtenberg, National Institutes of Health
Steven Treisman, University of Massachusetts Medical Center
Stefan Wilhelm, Carl Zeiss, Inc., Germany
Ginger Withers, University of Virginia
Steven Wooding, Medical Research Council, United Kingdom
Ji-Hong Zang, Stanford University
Julianne Zimmerman, Payload Systems, Inc.

Medical Informatics (June 1–June 8)

Director

Daniel Masys, University of California, San Diego

Faculty

Paul Clayton, Columbia University
James Grigsby, University of Colorado Health Sciences Center
George Hripcsak, Columbia-Presbyterian Medical Center
Stephen Johnson, Columbia-Presbyterian Medical Center
Lawrence Kingsland, National Library of Medicine
David Landsman, National Library of Medicine
Donald D.A.B. Lindberg, National Library of Medicine

Richard Rodgers, National Library of Medicine
Jay Sanders, Global Telemedicine Group

Students

Michael Ashburn, University of Utah
Lynda Baker, Wayne State University
Janet Bangma, East Carolina University Health Sciences Library
Stephen Bartold, Texas Tech University Health Science Center
David Boilard, Medical College of Ohio
Sekum Boni-Awotwi, Howard University
Neil Busis, University of Pittsburgh
Laura Cailoux, Northwest Portland Area Indian Health Board
Thomas Clay, East Carolina University School of Medicine
May Dobal, Wayne State University
Janice Dreyer, Community Hospitals of Central California
Kathel Dunn, New York Academy of Medicine
David George, Reading Hospital & Medical Center
Gale Hannigan, Texas A&M University Health Science Center
Conor Heneghan, New York Eye & Ear Infirmary
Ruth Holst, Columbia Hospital
Arthur Huntley, University of California, Davis
Charles Jaffe, American College of Allergy
Juan Larach, Mission Neighborhood Health Center
Clare Leibfarth, Doctors Hospital of Stark County
Ethel Madden, Ochsner Medical Institutions
Faith Meakin, University of Florida
Peter Pevonka, University of Florida Health Science Center
Ted Rosenkrantz, University of Connecticut Health Center
Floyd Russell, West Virginia University
Gerald Segal, New York State Psychiatric Institute
Marcus Simpson, George Washington University
Elaine Trzebiatowski, Allina Health System
Amy Warner, University of Michigan
Ken Wolf, Charles R. Drew University of Medicine & Science

Methods in Computational Neuroscience (August 3–August 30)

Directors

David Kleinfeld, University of California, San Diego
David Tank, Bell Laboratories/Lucent Technologies

Faculty

Lawrence Abbott, Brandeis University
Moshe Abeles, Hebrew University of Jerusalem, Israel
Richard Andersen, California Institute of Technology
Robert Barlow, State University of New York Health Science
Center
William Bialek, NEC Research Institute
Thomas Collett, University of Sussex, United Kingdom
Rob de Ruyter van Steveninck, NEC Research Institute
Kerry Delaney, Simon Fraser University, Canada
Bard Ermentrout, University of Pittsburgh
David Hansel, Ecole Polytechnique, France
John Hopfield, Princeton University
Daniel Johnston, Baylor College of Medicine
Nancy Kopell, Boston University
Kevan Martin, Swiss Federal Institute of Technology, Switzerland
Kevin Martin, University of North Carolina, Chapel Hill
David McCormick, Yale University School of Medicine
Wolfram Schultz, Université de Fribourg, Switzerland
Terrance Sejnowski, Salk Institute

H. Sebastian Seung, Bell Laboratories
Arthur Sherman, National Institutes of Health
Karen Sigvardt, University of California, Davis
Frederick Sigworth, Yale University School of Medicine
Haim Sompolinsky, Hebrew University of Jerusalem, Israel
Mircea Steriade, Université Laval, Canada
David Terman, Ohio State University
Naftali Tishby, Hebrew University of Jerusalem, Israel
Misha Tsodyks, The Weizmann Institute, Israel
Steven Zucker, Yale University

Lab Instructors

Roderick Jensen, Wesleyan University
Terrance Kovacs, Bell Laboratories
John White, Boston University

Course Assistant

Joseph Paton, Tufts University

Students

Thomas Adelman, Cornell University
Yoram Ben Shaul, Hebrew University Hadassah School of
Medicine, Israel
Karl Deisseroth, Stanford University
Reiko Maki Fitzsimonds, University of California, San Diego
Galit Fuhrmann, Hebrew University of Jerusalem, Israel
Mark Goldman, Harvard University
Audrey Guzik, Allegheny University
Richard Hahnloser, Swiss Federal Institute of Technology,
Switzerland
Robert Harris, University of Cambridge, United Kingdom
Katrina MacLeod, California Institute of Technology
William Miller, Brandeis University
Jonathan Murnick, Harvard University Medical School
Louis Neltner, Ecole Polytechnique, France
Duane Nykamp, New York University
Anitha Pasupathy, Johns Hopkins University
Sharon Peled, Massachusetts Institute of Technology
Daniel Reich, Rockefeller University
Mark Schnitzer, Princeton University
Oren Shriki, Hebrew University of Jerusalem, Israel
Jonathan Simon, University of Maryland
William Vinje, University of California, Berkeley
Martin Wainwright, Harvard University
James Zackheim, Rutgers University

Microinjection Techniques in Cell Biology ***(May 20–May 27)***

Director

Robert B. Silver, Marine Biological Laboratory

Faculty

Suzanne Klaesstg, Cornell University
Douglas Kline, Kent State University
Gernot Presting, Institute of Plant Breeding, Germany
Eric Shelden, University of Michigan

Course Assistant

Lisa Mehlmann, University of Connecticut Health Center

Students

Annie Borgne, CNRS, France
Tao Cheng, Massachusetts General Hospital
Goffredo Cognetti, University of Palermo, Italy
Maxim Dorovkov, University of Medicine and Dentistry of New
Jersey/Robert Wood Johnson Medical School
William Faught, Medical University of South Carolina
Jennifer Hartt, University of Pennsylvania
Lorayne Jenkins, Wyeth Ayerst Research
Kathleen Jensen, U.S. Environmental Protection Agency
Shuxian Jiang, Harvard Institutes of Medicine
David Lagunoff, St. Louis University
Yoshiaki Omura, Heart Disease Research Foundation
Stelios Papaioannou, United Medical and Dental School of Guy's
and St. Thomas' Hospitals, United Kingdom
May Peñarroyo, De La Salle University, Philippines
Gloria Perez, Massachusetts General Hospital
Margherita Randazzo, University of Palermo, Italy
Vasantha Reddi, University of Virginia
Carol Reinisch, Tufts University School of Veterinary Medicine
Nancy Searby, NASA Ames Research Center/Stanford University
Jennifer Stephens, University of Oklahoma
Nirmala SundarRaj, University of Pittsburgh

Molecular Mycology: Current Approaches to Fungal Pathogenesis (August 10–August 30)

Directors

John Edwards, Jr., Harbor-UCLA Medical Center
Paul T. Magee, University of Minnesota
Aaron P. Mitchell, Columbia University

Lecturers

Arturo Casadevall, Albert Einstein College of Medicine
Gary T. Cole, Medical College of Ohio
Brendan Cormack, Stanford University School of Medicine
Jim Cutler, Montana State University
Judith Domer, Tulane Medical School
Scott Filler, Harbor-UCLA Medical Center
Gerald Fink, Whitehead Institute of Biomedical Research
Carol A. Kumamoto, Tufts University School of Medicine
Myra Kurtz, Merck Research Laboratories
June Kwon-Chung, National Institutes of Health
John McCusker, Duke University Medical Center
John Perfect, Duke University School of Medicine
Michael A. Pfaller, University of Iowa College of Medicine
Judith Rhodes, University of Cincinnati
Stewart Scherer, University of Minnesota School of Medicine
Brian Wong, Veterans Administration Connecticut Healthcare
System

Teaching Assistants

Janna Beckerman, University of Minnesota
Maria Soushko, Columbia University
Yang Xiao, Columbia University

Course Assistant

Joseph Paton, Tufts University

Students

James Alspaugh, Duke University
 Kent Buchanan, University of Oklahoma Health Sciences Center
 Enda Clarke, Royal Postgraduate Medical School, United Kingdom
 Marianne De Backer, Janssen Research Foundation, Belgium
 Maurizio Del Poeta, Duke University Medical Center
 Tamara Doering, Cornell University Medical School
 Roy Hopfer, University of North Carolina, Chapel Hill
 Margaret Hostetter, University of Minnesota
 Linda Janusek, Loyola University of Chicago
 Herbert Mathews, Loyola University of Chicago
 Frank-Michael Müller, National Cancer Institute
 Norbert Schnell, Zeneca Pharmaceuticals, United Kingdom
 Craig Thompson, Scriptgen Pharmaceuticals
 Jo-Anne van Burik, Fred Hutchinson Cancer Research Center
 Paul Verweij, University Hospital Nymegen, The Netherlands
 Mason Zhang, University of Nevada School of Medicine

Neurobiology & Development of the Leech
(August 9–August 30)*Directors*

Pierre Drapeau, McGill University, Canada
 Martin Shankland, University of Texas, Austin

Faculty

Andreas Baader, University of Zurich, Switzerland
 Irmgard Dietzel-Meyer, Ruhr-Universität Bochum, Germany
 Francisco Fernandez de Miguel, Universidad Nacional Autonoma, Mexico
 John Jellies, Western Michigan University
 Jorgen Johansen, Iowa State University
 Anna Kleinhaus, New York Medical College
 Eduardo Macagno, Columbia University
 Mark Martindale, University of Chicago
 Barbara Modney, Cleveland State University
 Kenneth Muller, University of Miami School of Medicine
 John Nicholls, University of Basel, Switzerland
 Christine Sahley, Purdue University
 Catherine Wedeen, New York Medical College
 David Weisblat, University of California

Course Assistant

Gabrielle Tomasky, Marine Biological Laboratory

Students

Istvan Albert, University of Notre Dame
 Dianne Allen, Louisiana State University Medical Center
 Maria Casanueva, Catholic University, Chile
 James Einum, Marquette University
 Chunfa Jie, Iowa State University
 Lynette Nguyen, Smith-Kettlewell Eye Research Institute
 Elizabeth Perruccio, New York Medical College
 Aloysius Phillips, Columbia University
 Giulietta Pinato, International School for Advanced Studies, Italy
 Subhabrata Sanyal, Tata Institute of Fundamental Research, India
 Daniel Shain, University of California, Berkeley
 Patrick Wigge, Medical Research Council, United Kingdom

Optical Microscopy and Imaging in the Biomedical Sciences (October 8–October 16)*Director*

Colin Izzard, State University of New York, Albany

Faculty

Joseph DePasquale, New York State Department of Health
 Robert Hard, State University of New York, Buffalo
 Brian Herman, University of North Carolina, Chapel Hill
 Shahid Khan, Albert Einstein College of Medicine
 Frederick Maxfield, Cornell University Medical College
 John Murray, University of Pennsylvania
 David M. Piston, Vanderbilt University
 Kenneth Spring, National Institutes of Health
 Jason Swedlow, Harvard University Medical School

Teaching Assistants

Ken Dunn, Indiana University Medical Center
 Lynda Pierini, Cornell University Medical College
 Wade Sigurdson, State University of New York, Buffalo
 Elizabeth Welnhofner, State University of New York, Buffalo

Lecturers

Jan Hinsch, Leica, Inc.
 Shinya Inoué, Marine Biological Laboratory
 H. Ernst Keller, Carl Zeiss, Inc.
 Rudolf Oldenbourg, Marine Biological Laboratory
 Martin Scott, Consultant in Scientific Imaging

Course Assistant

Kari Lavalli, Marine Biological Laboratory

Students

Diana Bartelt, St. John's University
 Michelle Burack, University of Virginia
 Dorthe Christensen, BioImage, Denmark
 Conan Cooper, University of Calgary, Canada
 John Crocker, University of Pennsylvania
 Leanne Delbridge, University of Melbourne, Australia
 Mark Drew, Johns Hopkins University
 Tracey du Laney, University of North Carolina, Chapel Hill
 Lars Hansen, Hagedorn Research Institute, Denmark
 Brian Helmke, University of Pennsylvania
 Robert Hughes, University of Washington
 Eleanor Kable, Sydney University, Australia
 Peter Kaplan, University of Pennsylvania
 Timothy King, University of Texas
 Thomas Kinraide, United States Department of Agriculture
 David Marcey, Kenyon College
 Susanne Pedersen, University of Copenhagen, Denmark
 Marli Robertson, University of Calgary, Canada
 Pascal Stein, Harvard Medical School
 David Swift, University of Pennsylvania
 James Thomson, University of Wisconsin
 Sebastian Tille, Carl Zeiss Jena, Germany
 Mariko Tokito, University of Pennsylvania
 Frances Wang, National Institute of Standards & Technology
 Karen Zito, University of California, Berkeley

Pathogenesis of Neuroimmunologic Diseases
(August 17–August 29)

Directors

Celia F. Brosnan, Albert Einstein College of Medicine
Jack Rosenbluth, New York University School of Medicine

Faculty

Barbara Barres, Stanford University School of Medicine
Etty Benveniste, University of Alabama, Birmingham
Joan Berman, Albert Einstein College of Medicine
Peter Charles, Albert Einstein College of Medicine
Patricia Coyle, State University of New York, Stony Brook
Robert Darnell, Rockefeller University
Judah Denburg, McMaster University, Canada
David Felten, University of Rochester
Robert M. Gould, New York State Institute of Basic Research
Diane Griffin, Johns Hopkins University
John Griffin, Johns Hopkins School of Medicine
William Hickey, Dartmouth-Hitchcock Medical Center
Gilla Kaplan, Rockefeller University
Paul Knopf, Brown University
Vijay Kuchroo, Brigham and Women's Hospital

Jon Lindstrom, University of Pennsylvania School of Medicine
James Martiney, Picower Institute for Medical Research
Steven Pfeiffer, University of Connecticut Health Center
Richard Ransohoff, Cleveland Clinic Foundation
Bruce Ransom, University of Washington School of Medicine
Anthony Reder, University of Chicago
J. M. Ritchie, Yale University School of Medicine
James Salzer, New York University Medical Center
Clifford Saper, Beth Israel Hospital
Moon Shin, University of Maryland, Baltimore
Michele Solimena, Yale University
Esther Sternberg, National Institutes of Health
J. Wayne Streilein, Scheppens Eye Research Institute
Byron Waksman, Foundation for Microbiology

Students

Amit Bar-Or, Massachusetts General Hospital
Rita Baron-Faust, WCBS NewsRadio 88
Alexei Boiko, Russian State Medical University, Russia
Emanuela Bonfoco, La Jolla Institute of Immunology
Laurent Coscoy, Pasteur Institute, France
Benedicte Dubois, Rega Institute, Belgium
Urszula Fiszler, Institute of Psychiatry & Neurology, Poland
Glen Greenough, Dartmouth-Hitchcock Medical Center
Carolyn Hohan, Cambridge Neuroscience Inc.
Liwei Hua, Albert Einstein College of Medicine
Kee-Ching Jeng, Taichung Veterans General Hospital, Taiwan
Pitagoras Justino, Universidade Federal de Uberlandia, Brasil
Bernd Kieseier, University of Würzburg, Germany
Pia Kivisakk, Karolinska Institute, Sweden
Dmitriy Labunsky, Institute of Neurology, Russia
Igor Leykin, Weizmann Institute of Science, Israel
Carrie McManus, Albert Einstein College of Medicine
Mary McMenamin, Oxford University, United Kingdom
Neelufar Mozaffarian, Albert Einstein College of Medicine
Marcin Mycko, Medical Academy of Lodz, Poland
Jitendra Patel, Zeneca Pharmaceuticals
Barry Singer, New York Hospital-Cornell Medical Center
Nevil Singh, Tata Institute of Fundamental Research, India
Sulpicio Soriano, Children's Hospital/Harvard Medical School

Workshop on Molecular Evolution
(August 3–August 15)

Directors

Daniel B. Davison, Bristol-Myers Squibb PR1
Mitchell Sogin, Marine Biological Laboratory

Faculty

W. Ford Doolittle, Dalhousie University, Canada
Douglas Eernisse, California State University
Joseph Felsenstein, University of Washington
Michael Gray, Dalhousie University, Canada
Robert Haselkorn, University of Chicago
David Hillis, University of Texas
Mike Holder, University of Houston
Richard Hudson, University of California, Irvine
Thomas Kaufman, Indiana University
David Maddison, University of Arizona, Tucson
Geoffrey McFadden, University of Melbourne, Australia
Lynn Miller, Genetics Computer Group, Inc.
Michael Miyamoto, University of Florida



Rasmus Nielsen, University of California, Berkeley
 Gary Olsen, University of Illinois
 William Pearson, University of Virginia
 Kevin Peterson, California Institute of Technology
 David Roos, University of Pennsylvania
 Pamela Soltus, Washington State University
 David Swofford, Smithsonian Institution
 John Wakeley, Nelson Biological Labs
 Bruce Walsh, University of Arizona, Tucson
 Sam Ward, University of Arizona, Tucson
 Carl Woese, University of Illinois, Urbana-Champaign

Teaching Assistant

Steven Thompson, Washington State University

Course Assistant

Udeni Amit, Marine Biological Laboratory

Students

Michael Alfaro, University of Chicago Field Museum of National History
 John Archibald, Dalhousie University, Canada
 Pamela Arnofsky, Woods Hole Oceanographic Institution
 Vijay Aswani, Smithsonian Tropical Research Institute
 Andrew Baker, University of Miami
 Anne Bansemir, Rutgers University
 Elizabeth Barratt, Zoological Society of London, United Kingdom
 Mary Bateson, Montana State University
 Christiane Biermann, State University of New York, Stony Brook
 Carine Blank, University of California, Berkeley
 Lisa Borghesi, Oklahoma Medical Research Foundation
 Adriana Briscoe, Harvard University
 Daniel Brumbaugh, University of Texas, Austin
 Nina Brunner, University of Essen, Germany
 Carmen Cadilla, University of Puerto Rico
 Susan Chien, University of Florida
 Manuela Coelho, University of Lisbon, Portugal
 Chris Conroy, University of Alaska Museum
 Colomban de Vargas, University of Geneva, Switzerland
 Joël Doré, Institut National de la Recherche Agronomique, France
 Mark Dorssi, University of Edinburgh, Scotland
 Amy Driskell, University of Chicago Field Museum of National History
 Lindsey Dubb, University of Washington
 Mary Eubanks, Duke University
 Jeffrey Fasick, University of Maryland Baltimore County
 Oisín Feeley, Dalhousie University, Canada
 Victor Fet, Marshall University
 Eric Gaidos, California Institute of Technology Jet Propulsion Laboratory/Woods Hole Oceanographic Institution
 Regine Großkopf, Max-Planck-Institut, Germany
 Gabriel Gutierrez, University of Seville, Spain
 Malin Heldtander, National Veterinary Institute, Sweden
 Hiromi Imamichi, SAIC Frederic
 Alex Jeffries, National Research Council, Canada
 Dana Jones, Centers for Disease Control and Prevention
 Marie-Josée LaForest, University of Montreal, Canada
 Kirsten Lindstrom, University of California, Berkeley
 Jaw-Ching Liu, University of Texas, Houston
 Lei Liu, University of Connecticut
 Frieder Mayer, University of Erlangen, Germany
 Damhnait McHugh, Harvard University
 Kirsten Nicholson, University of Miami

Link Olson, University of Chicago Field Museum of National History
 Bertil Pettersson, Royal Institute of Technology, Sweden
 Mary Poss, University of Washington
 Linda Prince, University of North Carolina, Chapel Hill
 Anne Marie Quinn, Yale University
 Patrick Reynolds, Hamilton College
 Frank Rosenzweig, University of Idaho
 Marco Salemi, Rega Institute, Belgium
 Andrew Salywon, Arizona State University
 Nikolaos Schizas, University of South Carolina
 Alastair Simpson, University of Sydney, Australia
 James Robert Stevens, University of Bristol, United Kingdom
 Suzanne Sukhdeo, Rutgers University
 Jin Gou Tong, Chinese University, Hong Kong
 Catherine Walton, University of Leeds, United Kingdom
 Hui Wang, University of Houston
 Jacqueline Weicker, University of Alaska, Fairbanks
 Connie Westhoff, University of Nebraska
 Adrian Whatmore, University of Warwick, United Kingdom
 Kenneth Wurdack, University of North Carolina, Chapel Hill

Other Programs

Semester in Environmental Science (September 8–December 19)

Directors

Jerry M. Melillo, Director
 Kenneth H. Foreman, Associate Director

Faculty

Charles Hopkinson, Aquatic Course Director
 Knute Nadelhoffer, Terrestrial Course Director
 John Hobbie, Microbial Ecology
 Edward Rastetter, Mathematical Modeling
 Anne Giblin
 Linda Deegan
 Bruce Peterson
 Christopher Neill
 Joe Vallino
 Mathew Williams



R32 Annual Report

Paul Steudler
Peter Siver, Faculty Fellow, Connecticut College

Research Assistants

Jeffrey Hughes
James Laundre
Jane Tucker
Lori Soucy
Kristin Tholke
Kathleen Regan
Beth Hooker
John Helfrich
Martha Downs
Amy Nolin
Kathleen Newkirk
Neil Bettez

Teaching Assistants

Martha Peterson
Michele Bahr
Patricia Micks
Bonnie Kwiatkowski
Robert Garritt
Nat Weston

Students

Toby Ahrens, Connecticut College
Hyacinth Armstrong, Mt. Holyoke College
Noah Bleich, Brandeis University
Abbey DeRocker, Bates College
Lynn Diener, Bard College
Janice Glass, Lafayette College
Sarah Jackson, Connecticut College
Samuel Kelsey, Dickinson College
Christy Meredith, Allegheny College
Sophie Parker, Wellesley College
Stephanie Parker, Middlebury College
Rachel Poretsky, Brandeis University
Shana Rapoport, Brandeis University
Amy Townsend-Small, Skidmore College
Marlene Tsie, Brandeis University
Rebecca Weidman, Carleton College

Teachers' Workshop: Living in the Microbial World (August 17–August 23)

Course Director

Lorraine Olendzenski, University of Connecticut

Course Assistant

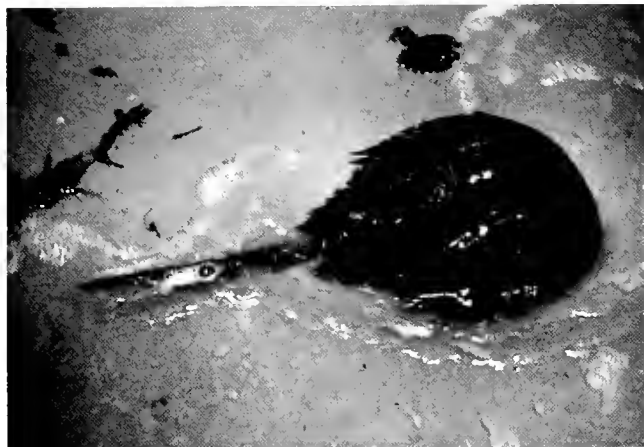
Andy Heaford, University of Connecticut

Presenters

Lynn Margulis, University of Massachusetts
Ricardo Guerrero, University of Barcelona, Spain
Steve Goodwin, University of Massachusetts, Amherst
Robert Bullis, Marine Biological Laboratory
Holger Jannasch, Woods Hole Oceanographic Institute
Greg Hinkle, University of Massachusetts, Dartmouth
Art Girard, Pfizer Central Research, Groton, CT
Norman Wainwright, Marine Biological Laboratory
Adrian Smith, Marine Biological Laboratory

Participants

Charles Anastasia, Mashpee High School
Diane E. Arnold, Bennie Dover Jackson Middle School
Catherine Baker, East Junior High School
Marcia A. Benvenuti, Bennie Dover Jackson Middle School
Florence Berdan, Parsippany Hills High School
Wesley Blauss, Indian Head Middle School
William Cerino, Lyme-Old Lyme High School
Paul J. Chamberlin, Nauset Regional High School
Elizabeth Check, Attleboro High School
Howard C. Estes, East Junior High School
Maryrose L. Flynn, Indian Head Middle School
Marsha R. Folger, Lyme-Old Lyme High School
Mary Johnson, Parsippany Hills High School, Brooklawn Middle School
Lucy Lupinacci, Griswold Intermediate School
Joreen Mattras, Griswold Intermediate School
Sheila E. McTigue, Lyme-Old Lyme High School
M. Susan O'Donnell, Indian Head Middle School
Jane Shute, Indian Head Middle School
Judith J. Trotta, Nauset Regional High School
James Watson, East Junior High School



Summer Research Programs

Principal Investigators

Armstrong, Clay, University of Pennsylvania
Armstrong, Peter B., University of California, Davis
Augustine, George J., Duke University Medical Center

Barbieri, Elena, Marine Biological Laboratory
Barlow, Jr., Robert B., State University of New York Health Science Center

Beaugé, Luis, Instituto M. y M. Ferreyra, Argentina
Bennett, Michael V. L., Albert Einstein College of Medicine
Berlin, Joshua, Bockus Research Institute
Bloom, George, University of Texas Southwestern Medical Center
Bodznick, David, Wesleyan University
Boron, Walter F., Yale University Medical School
Borst, David, Illinois State University
Boyer, Barbara, Union College
Brady, Scott T., The University of Texas Southwestern Medical Center, Dallas
Brown, Joel E., Albert Einstein College of Medicine
Browne, Carole, Wake Forest University
Burger, Max M., Friedrich Miescher Institute, Switzerland
Burgos, Mario, Universidad Nacional de Cuyo-Conicet, Argentina

Cardell, Robert R., University of Cincinnati
Casagrand, Janet, University of Colorado
Chappell, Richard L., Hunter College, City University of New York
Cohen, Lawrence B., Yale University School of Medicine
Cohen, William D., Hunter College, City University of New York
Corwin, Jeffrey, University of Virginia

De Weer, Paul, University of Pennsylvania School of Medicine
DeMont, Edwin, St. Francis Xavier University, Canada
Devlin, Leah, Penn State University
DiPolo, Reinaldo, IVIC, Venezuela

Eckberg, William, Howard University
Edwards, Donald, Georgia State University
Ehrlich, Barbara, University of Connecticut Health Center

Fay, Richard, Loyola University of Chicago
Fishman, Harvey M., The University of Texas Medical Branch, Galveston

Gadsby, David, The Rockefeller University
Garcia-Blanco, Mariano, Duke University Medical Center
Garrick, Rita Anne, Fordham University College, Lincoln Center

Giuditta, Antonio, University of Naples, Italy
Goldman, Robert D., Northwestern University Medical School
Gould, Robert, New York State Institute for Basic Research in Developmental Disabilities
Gray, John, Queen's University, Canada
Groden, Joanna, University of Cincinnati
Gundersen, Gregg, Columbia University

Haimo, Leah, University of California, Riverside
Halstead, Matthew, University of Auckland, New Zealand
Henry, Jonathan J., University of Illinois
Hershko, Avram, Technion, Israel
Highstein, Steven M., Washington University School of Medicine
Hines, Michael, Yale University School of Medicine
Holz, George, Massachusetts General Hospital
Hoskin, Francis, US Army Natick RD&E Center
Howze, Gwendolyn, Texas Southern University

Ip, Wallace, University of Cincinnati

Johnston, Daniel, Baylor College of Medicine
Joye, Samantha, Texas A&M University

Kaczmarek, Leonard, Yale University School of Medicine
Kaplan, Ilene M., Union College
Khan, Shahid, Albert Einstein College of Medicine
Khodakhah, Kamran, University of Pennsylvania
Klerkx, J.H.E.M., Utrecht University, The Netherlands
Kravitz, Edward, Harvard Medical School
Kuhns, William, The Hospital for Sick Children, Canada

Lafer, Eileen M., University of Texas Health Science Center
Landowne, David, University of Miami School of Medicine
Langford, George, Dartmouth College
Laskin, Jeffrey, University of Medicine and Dentistry of New Jersey
Layne, John, Duke University Marine Laboratory
Levandoski, Mark, Brown University
Lipicky, Raymond J., Food and Drug Administration
Llinás, Rodolfo R., New York University Medical Center
Lovett, Donald, The College of New Jersey

Martindale, Mark, University of Chicago
McNeil, Paul, Medical College of Georgia
Mensinger, Allen, Washington University School of Medicine
Metzals, Janis, University of Ottawa Faculty of Medicine, Canada
Minkoff, Charles, Duke University Medical Center
Miyakawa, Hiroyoshi, Tokyo University of Pharmacy and Life Science, Japan

R34 Annual Report

Moore, John, Duke University Medical Center

Nasi, Enrico, Boston University School of Medicine
Nguyen, Quoc Thang, University of California, Irvine

Palazzo, Robert, University of Kansas
Palma, Eleanora, Regina Elina Center Research Institute, Italy
Pant, Harish, National Institutes of Health
Parysek, Linda, University of Cincinnati
Pixley, Sarah, University of Cincinnati
Puga, Alvaro, University of Cincinnati

Quigley, James P., State University of New York, Stony Brook

Rakowski, Robert F., Finch University of Health Sciences/The
Chicago Medical School

Rasmussen, Howard, Medical College of Georgia
Ratner, Nancy, University of Cincinnati
Reese, Thomas S., National Institutes of Health
Rieder, Conly, Wadsworth Center
Ripps, Harris, University of Illinois College of Medicine
Rome, Larry, University of Pennsylvania
Rosenbluth, Jack, New York University Medical Center
Ross, William, New York Medical College
Ruderman, Joan V., Harvard Medical School
Russell, John M., Medical College of Pennsylvania

Saito, Takehito, University of Tsukuba, Japan
Schweizer, Felix, Duke University Medical Center
Shashar, Nadav, Marine Biological Laboratory
Sheetz, Michael, Duke University Medical Center
Simpson, Alastair, University of Sydney, Australia
Siver, Peter, Connecticut College
Sloboda, Roger D., Dartmouth College
Spann, Timothy, Northwestern University Medical School
Spiegel, Evelyn, Dartmouth College
Spiegel, Melvin, Dartmouth College
Standart, Nancy, University of Cambridge, United Kingdom
Steffen, Walter, Institute of Biochemistry and Molecular Cell
Biology, Austria
Stuart, Ann E., University of North Carolina, Chapel Hill
Sugimori, Mutuysuki, New York University Medical Center
Suszkiw, Janusz, University of Cincinnati

Takahashi, Megumi, Kanagawa Psychiatric Center, Japan
Telzer, Bruce, Pomona College
Tokumaru, Hiroshi, Duke University Medical Center
Tran, Phong, University of North Carolina, Chapel Hill
Troll, Walter, New York University Medical Center
Tytell, Michael, Bowman Gray School of Medicine, Wake Forest
University

Wachowiak, Matt, University of California, Berkeley
Weil, E. Jennifer, Marine Biological Laboratory
Whittaker, J. Richard, University of New Brunswick, Canada
Wicklein, Martina, University of Arizona

Zigman, Seymour, University of Rochester Medical School
Zottoli, Steven, Williams College
Zukin, R. Suzanne, Albert Einstein College of Medicine

Other Research Personnel

Abe, Terno, Niigata University, Japan
Altamirano, Anibal, University of Buenos Aires, Argentina



Anderson, Erik, St. Francis Xavier University, Canada
Antic, Srdjan, Yale University School of Medicine
Araneda, Ricardo, Albert Einstein College of Medicine
Armstrong, Clara, University of Pennsylvania

Baikie, Iain, Robert Gordon University, United Kingdom
Barrera, Jose, New York University Medical Center
Bearer, Elaine, Brown University
Becker, Julie, Temple University
Bezanilla, Francisco, University of California, Los Angeles
Bobb, David, Huston-Tillotson College
Boyle, Kim-Laura, Colby-Sawyer College
Brackenbury, Robert, University of Cincinnati
Breitwieser, Gerda E., Johns Hopkins School of Medicine
Brown, Euan, Marine Biological Association, United Kingdom
Burris, Jennifer, Carleton College

Carnall, Nicola, University of Cambridge, United Kingdom
Carvan, Michael, University of Cincinnati
Christman, Emily, Goucher College
Cimini, Ashley, Yale University
Claessens, Luc, Marine Biological Laboratory
Clay, John, National Institutes of Health
Clifford, Patrick, College of New Jersey
Connaughton, Martin, University of Pennsylvania
Cooper, Gordon, Yale University School of Medicine
Couch, Ernest, Texas Christian University
Cserjesi, Peter, Columbia University

Dadacay, Alma-Villa, Hunter College
Davis, Bruce A., Yale University
DePina, Ana, Dartmouth College
Dodge, Frederick, State University of New York Health Science
Center

Eddleman, Chris, University of Texas Medical Branch, Austin
Eds-Walton, Peggy, University of California, Riverside
Eyman, Maria, University of Naples, Italy

Fang, Jing, Yale University School of Medicine
Feinstein, Douglas, Cornell University
Fernandez-Busquets, Xavier, Friedrich Miescher Institut, Switzerland
Flamarique, Inigo, University of Victoria, Canada
Fukuda, Mitsunori, Tsukuba Life Science Center, Japan
Fukui, Yoshio, Northwestern Medical School

Gainer, Harold, National Institutes of Health
 Galbraith, James A., Duke University
 Gallant, Paul E., National Institutes of Health
 Gebhardt, Kelley, University of North Carolina, Chapel Hill
 Gerosa, Daniela, Friedrich Miescher Institute, Switzerland
 Goldman, Anne E., Northwestern University Medical School
 Gomez, Maria del Pilar, Boston University School of Medicine
 Goss, Thomas, Bancroft School
 Grant, Philip, National Institutes of Health
 Grassi, Daniel, Food and Drug Administration
 Gray, Richard, Baylor College of Medicine
 Grob, Marianne, Friedrich Miescher Institute, Switzerland
 Gross, Jeffrey, Duke University Medical College

Hagar, Robert, University of Connecticut Health Center
 Hambe, Bjorn, Lund University, Sweden
 Hirata, Kazunari, New York University Medical Center
 Hogan, Emilia M., Yale University Medical School
 Holmgren, Miguel, Massachusetts General Hospital
 Horner, Michael, University of Göttingen, Germany

Jarchow, Janina, Friedrich Miescher Institute, Switzerland
 Johannes, Eva, North Carolina State University
 Jonas, Elizabeth, Yale University School of Medicine

Kaftan, Edward, University of Connecticut Health Center
 Kamino, Kohtaro, Tokyo Medical and Dental University, Japan
 Katz, Benjamin, Williams College
 Keyoung, Jinsoo, Albert Einstein College of Medicine
 Khater, Kevin, Chicago Medical School
 Khuon, Satya, Northwestern University Medical School
 Klimov, Andrei, University of Pennsylvania
 Koroleva, Zoya, Hunter College
 Koulen, Peter, Max-Planck-Institute for Brain Research, Germany
 Krasne, Frank, University of California, Los Angeles
 Krasne, Sally, University of California, Los Angeles
 Kummer, Rebecca, Williams College

Lam, Ying-Wan, Yale University
 Lasser-Ross, Nechama, New York Medical College
 Lema-Foley, Christine, Hunter College
 Lew, Roger, York University, Canada
 Li, Lihong, Hunter College
 Linquist, Randall, Williams College
 Loboda, Andrey, University of Pennsylvania
 Ludin, Beat, Friedrich Miescher Institute, Switzerland
 Lyser, Katherine, Hunter College

MacGillivray, Patrick, St. Francis Xavier University, Canada
 Major, Guy, University Laboratory of Physiology, United Kingdom
 Malchow, Robert, University of Illinois, Chicago
 Marks, Andrew, Mount Sinai School of Medicine
 Martys, Jayme, Columbia University
 McCleskey, Ed, Vollum Institute
 McSweeney, Maireade, Bowdoin College
 Meigs, Bridget, Millbrook School
 Melishchuk, Alexey, University of Pennsylvania
 Meyers, Jason, University of Virginia
 Mikhailov, Alexei, Columbia University
 Molyneaux, Bradley, Dartmouth College
 Morgan, Jennifer, Duke University
 Mulligan, Megan, Columbia University
 Musani, Farrah, Williams College

Nakagawa, Masaya, New York University Medical Center
 Noailles, Pierre, Hunter College

O'Connor, Vincent, Max-Planck-Institute for Brain Research, Germany
 Ogan, Jeffrey, Illinois State University
 Onigman, Timna, Brown University

Parris, Tchaiko, Hunter College
 Pasman, Zvi, Duke University Medical Center
 Passaglia, Chris, State University of New York Health Science Center
 Patel, Leena, University of Illinois, Chicago
 Petersen, Jennifer, National Institutes of Health
 Petz, Anne, Wellesley College
 Piscopo, Stefania, University of Napoli, Italy
 Pivovarova, Natalia, National Institutes of Health
 Powers, Maureen, Vanderbilt University
 Pozzo-Miller, Lucas, National Institutes of Health
 Prasad, Kondury, University of Texas Health Science Center

Quinn, Kerry, University of Connecticut Health Center

Ramsey, John, Princeton University
 Ravula, Sharath, Texas A & M University
 Rebhun, Lionel, University of Virginia
 Rosenthal, Joshua, University of California, Los Angeles
 Ruta, Vanessa, Hunter College

Schlemmer, Etha, Hunter College
 Schlieff, Michelle, Hampshire College
 Searby, Nancy, NASA Ames Research Center
 Seyfarth, Ernst-August, J. W. Goethe-Universität, Germany
 Shaub, Amy, Illinois Wesleyan University
 Sheikh, Sarah, University of Edinburgh, United Kingdom
 Silva, Celso, Women's & Infants Hospital
 Simpson, Tracy, University of Hartford
 Singh, Satish, Yale University School of Medicine
 Smith, Benjamin, Southwestern University
 Smith, Cynthia R., Tufts University
 Smyers, Mark, University of Texas
 Sporhase-Eich, Ulrike, University of Göttingen, Germany
 Stenflo, Johan, Lund University, Sweden
 Stewart, Karen, Syracuse University
 Stockbridge, Norman, Food and Drug Administration
 Stokes, Darrell, Emory University
 Sudhot, Tom, University of Texas Southwestern Medical Center
 Suwa, Hiroshi, New York University Medical Center
 Swan, Justin, Wake Forest University
 Sweeney, Christina, Illinois Wesleyan University

Terasaki, Mark, University of Connecticut Health Center
 Thomas, Abraham, Jester Center
 Tokumaru, Hiroshi, Duke University Medical Center
 Tokumaru, Keiko, Duke University Medical Center
 Twersky, Laura, St. Peters College

Vasandani, Veena, University of Virginia

Wagg, Jonathan, The Rockefeller University
 White, Benjamin, Yale University
 Williams, Tracey, Howard University
 Wollert, Torsten, University of Rostock, Germany
 Womack, Mary, Duke University Medical School
 Wu, Peter, Columbia University

Zakevicius, Jane M., University of Illinois, Chicago
Zavilowitz, Joseph, Albert Einstein College of Medicine
Zecevic, Dejan, Yale University School of Medicine
Zeki, Semir, University College London, United Kingdom
Zhao, Jinhua, Yale University
Zigman, Bunnie R., University of Rochester Medical Center

Library Readers

Abbott, Jayne, Marine Research Inc.
Adelberg, Edward A., Yale University
Ahmadjian, Vernon, Clark University
Alkon, Daniel, National Institutes of Health
Allen, Garland E., Washington University
Alliegro, Mark, Louisiana State University Medical Center
Anderson, Everett, Harvard Medical School

Baccetti, Baccio, University of Siena, Italy
Barry, Susan R., Mount Holyoke College
Benjamin, Thomas L., Harvard Medical School
Bentham, Dolores A., SPC Associates, New York
Berne, Rosalyn W., University of Virginia
Bernhard, Jeffrey D., University of Massachusetts Medical Center
Bernheimer, Alan W., New York University
Borgese, Thomas A., Lehman College
Boyer, John, Union College
Burgess, David, Pittsburgh, PA

Campbell, Robert K., Ares Advanced Technology
Candelas, Graciela C., University of Puerto Rico
Cariello, Lucio, Stazione-Zoologica, Italy
Chaet, A. B., University of West Florida
Child, Frank M., Trinity College
Clark, Arnold M., University of Delaware
Clark, Denise, University of New Brunswick
Clark, Eloise E., Bowling Green State University
Clarkson, Kenneth L., Bell Labs, Lucent Technologies
Cogswell, Carol, University of Sydney, Australia
Cohen, Seymour S., American Cancer Society
Cohen, Leonard A., American Health Foundation
Cohen, Yehuda, Hebrew University of Jerusalem, Israel
Collier, Marjorie M., St. Peters College
Comoglio, Paolo, Institute for Cancer Research, Turino, Italy
Cooperstein, Sherwin J., University of Connecticut Health Center
Copeland, Eugene C., Woods Hole, MA
Cowling, Vincent F., SUNY, Albany

D'Allesio, Giuseppe, University of Naples
deToledo-Morrell, Leyla, Rush Medical College
Duncan, Thomas K., Nichols College

Epstein, Herman T., Brandeis University

Feldman, Susan C., New Jersey Medical School
Finch, Caleb E., University of Southern California
Frenkel, Krystyna, NYU Medical Center

Gehrke, Lee, Massachusetts Institute of Technology
German, James L., New York Blood Center
Goldman, Robert, Northwestern University Medical School
Goldstein, Moise H., Johns Hopkins University
Grodin, Joanna, University of Cincinnati
Gross, Paul, University of Virginia



Grossman, Albert, NYU Medical School
Gruner, John, Cephalon, Inc.

Haimo, Leah, University of California
Halvorson, Harlyn, University of Massachusetts, Dartmouth
Herskovits, Theodore T., Fordham University
Hunter, Robert, Gartnaval Royal Hospital

Ilan, Judith, Case Western Reserve University
Inoue, Sadayuki, McGill University, Canada
Issodorides, Marrietta, University of Athens, Greece

Jacobson, Allan S., University of Massachusetts Medical Center
Josephson, Beth, Ocean Arks International

Kaltenbach, Jane C., Mount Holyoke College
Kaminer, Benjamin, Boston University School of Medicine
Kamino, Kohtaro, Tokyo Medical & Dental University, Japan
Kaplan, Arnold, University of Illinois at Chicago
Karlin, Arthur, Columbia University
Kelly, Robert E., University of Illinois
Keynan, Alex, Israel Academy of Sciences and Humanities
King, Kenneth, Falmouth, MA
Klein, Donald, Colorado State University
Kramer, Fred R., Public Health Research Institute

1997 Library Room Readers

Daniel Alkon
National Institutes of Health

Lucio Cariello
Stazione-Zoolociga A. Dohrn

A. Chaet
University of Connecticut

Paolo Comoglio
Institute of Cancer Research, Turino, Italy

Giuseppe D'Alessio
University of Naples

Robert Goldman
Northwestern Univ. Medical School

Harlyn Halvorson
Marine Biological Laboratory

Alex Keynan
Israel Academy of Science

Hans Laufer
University of Connecticut

Joe L. Martinez
University of Texas, San Antonio

Michael Rabinowitz
Marine Biological Laboratory

George Reynolds
Princeton University

Gerald Weissman
NYU School of Medicine

Laderman, Aimlee D., Yale School of Forestry & Environmental Studies
 Laster, Leonard, University of Massachusetts Medical Center
 Laufer, Hans, University of Connecticut
 Lee, John J., City College of CUNY
 Leighton, Joseph, Aeron Biotechnology, Inc.
 Levy, Arthur L., St. Vincents Hospital of New York
 Lisman, John, Brandeis University
 Long, Carol, Allegheny University
 Lorand, Laszlo, Northwestern University Medical School
 Luckenbill-Edds, Louise, Ohio University

MacNichol, Edward F., Boston University School of Medicine
 Major, Guy, Oxford University
 Masland, Richard, Massachusetts General Hospital
 Martinez, Joe L., University of Texas, San Antonio
 Mauzerall, David, Rockefeller University
 Michaelson, James, MGH Cancer Center
 Miller, Daniel, Rockefeller University
 Mills, Eric L., Dalhousie University, Canada
 Mnkoff, Charles G., Duke University Medical Center
 Mitchell, Ralph, Harvard University
 Mizell, Merle, Tulane University

Nagel, Ronald L., Albert Einstein Institute
 Narahashi, Toshio, Northwestern University Medical School
 Nathans, Jeremy, Johns Hopkins University
 Naugle, John, NASA
 Nicaise, Mari-Luz, Université de Nice, France
 Nicaise, Ghislain, Université de Nice, France
 Nickerson, Peter A., SUNY, Buffalo

Pappas, George D., University of Illinois
 Pollen, Daniel A., University Massachusetts Medical Center
 Porter, Mary E., University of Minnesota
 Prusch, Robert D., Gonzaga University
 Przybyszewski, Andrew W., University of Massachusetts Medical Center

Rabinowitz, Michael, Marine Biological Laboratory
 Rafferty, Nancy S., Northwestern University
 Rafferty, Keen, Northwestern University
 Reynolds, George, Princeton University
 Rosenbluth, Raja, Simon Fraser University
 Rosenkranz, Herbert S., University of Pittsburgh
 Ryan, Terence E., Regeneron Pharmaceuticals

Sanger, Joseph W., University of Pennsylvania Medical School
 Sanger, Jean M., University of Pennsylvania Medical School
 Schauder, Rolf, University of Frankfurt, Germany
 Segal, Rosalind, Harvard Institute of Medicine
 Shepro, David, Boston University Microvascular Research
 Siwicki, Kathleen K., Swarthmore College
 Spector, Abraham, Columbia University
 Spotte, Stephen, University of Connecticut
 Sundquist, Eric, US Geological Survey
 Sweet, Frederick, Washington University School of Medicine

Tilney, Lewis, University of Pennsylvania
 Trager, William, The Rockefeller University
 Tweedell, Kenyon S., University of Notre Dame
 Tykocinski, Mark L., Case Western Reserve University

Van Holde, Kensal E., Oregon State University



Walton, Alan J., Cavendish Lab, Cambridge University, UK
 Warren, Leonard, Wistar Institute
 Weidner, Earl, Louisiana State University
 Weissman, Gerald, NYU Medical Center
 Whittaker, Victor P., Max-Planck-Institute for Biophysical Chemistry
 Yevick, George, Stevens Institute of Technology

Domestic Institutions Represented

AgBiotech Center
 Alabama, University of, Birmingham
 Alaska Museum, University of
 Alaska, University of
 Albert Einstein College of Medicine
 Allegheny University
 Allegheny University of the Health Sciences
 Allina Information Services
 American College of Allergy
 Arizona State University
 Arizona, University of

Bancroft School
 Baylor College of Medicine
 Bell Labs
 Beth Israel Medical Center
 Bockus Research Institute
 Boston University
 Boston University School of Education
 Boston University School of Medicine
 Bowdoin College
 Brandeis University
 Brigham and Women's Hospital

R38 Annual Report

Bristol-Myers Squibb PRI
Brown University

California Institute of Technology
California State University
California, University of, Berkeley
California, University of, Davis
California, University of, Irvine
California, University of, Los Angeles
California, University of, Riverside
California, University of, San Diego
California, University of, San Francisco
California, University of, Santa Barbara
Cambridge NeuroScience, Inc.
Carl Zeiss, Inc.
Carleton College
Case Western Reserve University
Center for Great Lakes Studies
Chicago Field Museum, University of
Chicago Medical School
Chicago, University of
Children's Hospital, Boston
Cincinnati Medical Center, University of
Cincinnati, University of
Cleveland Clinic Foundation
Cleveland State University
Colby College
Colby-Sawyer College
Cold Spring Harbor Laboratories
College of the Holy Cross
Colorado Health Science Center,
University of
Colorado School of Mines
Colorado, University of
Columbia Hospital Library
Columbia University
Columbia-Presbyterian Medical Center
Community Health Systems
Connecticut College
Connecticut Health Center, University of
Connecticut, University of
Cornell University
Cornell University Medical College
Cornell University Veterinary School

Dana Farber Center Institute
Dartmouth College
Dartmouth-Hitchcock Medical Center
Doctors' Hospital of Stark County
Drew University of Medicine & Science
Duke University
Duke University Marine Laboratory
Duke University Medical Center

East Carolina University
East Carolina University School of Medicine
Emory University
Eye Foundation Hospital

Finch University of Health Sciences
Florida State University
Florida, University of
Food and Drug Administration
Fordham University College, Lincoln Center

Forsyth Dental Center
Foundation of Microbiology
Fox Chase Cancer Center
Fred Hutchinson Cancer Research Center

Genetics Computer Group, Inc.
George Washington University
Georgia State University
Georgia, University of
Global Telemedicine Group
Goucher College

Hamilton College
Hampshire College
Harbor-UCLA Medical Center
Hartford, University of
Harvard Institutes of Medicine
Harvard Medical School
Harvard University
Harvard University School of Public Health
Heart Disease Research Foundation
Hollins College
Hopkins Marine Station
Houston, University of
Howard Hughes Medical Institute
Howard University
Hunter College
Huston-Tillotson College

Idaho, University of
Illinois State University
Illinois Wesleyan University
Illinois, University of
Indiana University
Indiana University School of Medicine
Infectious Disease Research Institute
Institute for Basic Research in
Developmental Disabilities
Iowa College of Medicine, University of
Iowa State University
Iowa, University of

Jester Center
Jet Propulsion Laboratory
Johns Hopkins University
Johns Hopkins University School of
Medicine
Johns Hopkins University School of Public
Health

Kansas, University of
Kent State University
Kentucky College of Medicine, University of

Laboratory of Kidney & Electrolyte
Metabolism
Leica, Inc.
Louisiana State University Medical Center
Loyola University of Chicago

Maine, University of
Marine Biological Laboratory
Marquette University
Marshall University

Maryland, University of
 Massachusetts General AIDS Research
 Center
 Massachusetts General Hospital
 Massachusetts Institute of Technology
 Massachusetts Medical School, University of
 Massachusetts, University of
 Medical College of Georgia
 Medical College of Ohio
 Medical College of Pennsylvania
 Medical University of South Carolina
 Meharry Medical College
 Memorial Sloan-Kettering Cancer Center
 Merck Research Laboratories
 Metabolix, Inc., Cambridge
 Miami, University of
 Michigan State University
 Michigan Technological University
 Michigan, University of
 Millbrook School
 Minnesota Medical School, University of
 Minnesota, University of
 Mission Neighborhood Health Center
 Montana State University
 Museum of Comparative Zoology Labs

 NASA Ames Research Center
 National Cancer Institute
 National Institute of Environmental Health
 Science
 National Institute of Standards & Technology
 National Institutes of Health
 National Library of Medicine
 Naval Medical Research Institute
 Nebraska, University of
 NEC Research Institute
 Nelson Biological Labs
 Nevada, University of
 New Jersey, College of
 New Jersey, University of Medicine and
 Dentistry
 New York Academy of Medicine
 New York Eye & Ear Infirmary
 New York Medical College
 New York State Department of Health
 New York State Institute for Basic Research
 New York State Psychiatric Institute
 New York University Medical Center
 New York University School of Medicine
 North Carolina State University
 North Carolina, University of
 North Carolina, University of, Chapel Hill
 North Texas, University of
 Northeastern University
 Northwestern University
 Northwestern University Medical School
 Notre Dame, University of
 NW Portland Area Indian Health Board

 Ochsner Medical Library
 Ohio State University
 Ohio University
 Oklahoma Health Sciences, University of
 Oklahoma Medical Research Foundation

Oregon Health Science University
 Oregon, University of

 Payload Systems, Inc.
 Pennsylvania School of Medicine,
 University of
 Pennsylvania School of Veterinary Medicine,
 University of
 Pennsylvania State University
 Pennsylvania, University of
 Picower Institute for Medical Research
 Pittsburgh School of Medicine, University of
 Pittsburgh, University of
 Pomona College
 Princeton University
 Providence College
 Puerto Rico, University of
 Purdue University

 Reading Hospital & Medical Center
 Rensselaer Polytechnic Institute
 Rochester Medical School, University of
 Rochester, University of
 Rockefeller University
 Rowland Institute for Science
 Rutgers University

 Salk Institute
 San Francisco State University
 Scheppens Eye Research Institute
 Scripps Institution of Oceanography
 Scripps Research Institute
 Scriptgen Pharmaceuticals
 Seattle Biomedical Research Institute
 Sloan Center for Theoretical Neurobiology
 Smith-Kettlewell Eye Research Institute
 Smithsonian Institution
 Smithsonian Tropical Research Institute
 South Carolina, University of
 Southwestern University Medical Center
 St. John's University
 St. Louis University School of Medicine
 St. Peters College
 Stanford University
 Stanford University Medical Center
 State University of New York Health
 Science Center
 State University of New York, Albany
 State University of New York, Buffalo
 State University of New York, Stony Brook

 Temple University
 Tennessee, University of
 Texas A&M University
 Texas A&M University College of Medicine
 Texas Christian University
 Texas Health Science Center, University of
 Texas M. D. Anderson Cancer Center,
 University of
 Texas Medical Branch, University of
 Texas Southern University
 Texas Southwestern Medical Center,
 University of
 Texas Tech University

R40 Annual Report

Texas, University of
Toledo, University of
Tufts University
Tufts University School of Medicine
Tufts University School of Veterinary
Medicine
Tulane University Medical School

U. S. Army Natick RD&E Center
U. S. Department of Agriculture
U. S. Environmental Protection Agency
Union College
Utah, University of

Vanderbilt University
Vermont, University of
Veterans Administration Connecticut
Healthcare System
Virginia Commonwealth University
Virginia Health Sciences Center,
University of
Virginia School of Medicine, University of
Virginia, University of
Vollum Institute

Wadsworth Center for Labs and Research
Wake Forest University
Wake Forest University, Bowman Gray
School of Medicine
Washington School of Medicine,
University of
Washington State University
Washington, University of
Wayne State University
Wellesley College
Wesleyan University
West Virginia University
Western Michigan University
Wheaton College
Whitehead Institute for Biomedical Research
Williams College
Wisconsin Regional Primate Research
Wisconsin, University of
Women & Infants Hospital
Woods Hole Oceanographic Institution
Worcester Foundation for Biomedical
Research
Wyeth-Ayerst Research

Yale University
Yale University School of Medicine

Zanvyl Krieger Mind Brain Institute
Zeneca Pharmaceuticals

Foreign Institutions Represented

Alberta, University of, Canada
Astra Hässle, Sweden
Auckland, University of, Australia
August Krogh Institute, Denmark

Basel, University of, Switzerland
Bogor Agricultural University, Indonesia
Bordeaux, University of, France
Brazil, University of, Brazil
Bristol, University of, United Kingdom
Buenos Aires, University of, Argentina

Calgary, University of, Canada
Cambridge, University of, United Kingdom
Carl Zeiss, Inc., Germany
Catholic University of Chile, Chile
CENA-USP, Brazil
Centre National de la Recherche Scientifique,
France
Chinese University of Hong Kong, Hong
Kong

Dalhousie University, Canada
De La Salle University, Philippines

Ecole Polytechnique, France
Edinburgh, University of, Scotland
Erlangen, University of, Germany

Federal University of Minas Gerais, Brazil
Frankfurt, University of, Germany
Fribourg, University of, Switzerland
Friedrich Meischer Institute, Switzerland

Geneva, University of, Switzerland
Göteborg, University of, Sweden
Göttingen, University of, Germany

Hagedorn Research Institute, Denmark
Hebrew University of Jerusalem, Israel
Hospital for Sick Children, Canada
Huddinge University Hospital, Sweden

I.V.I.C., Venezuela
Imperial College of Science, Technology and
Medicine, United Kingdom
Innsbruck, University of, Austria
International School of Advanced Studies,
Italy
Institut Nationale de la Recherche
Agronomique, France
Institut Pasteur de Lille, France
Institute for Marine Biosciences, Canada
Institute of Biochemistry and Molecular Cell
Biology, Austria
Institute of Neurology of Moscow, Russia
Institute of Plant Breeding, Germany
Instituto M. y M. Ferreyra, Argentina

J. W. Goethe-Universität, Germany
Janssen Research Foundation, Belgium
Julius-Maximilians-University, Germany

Kangawa Psychiatric Center, Japan
Karolinska Institute, Sweden

Laboratory of Molecular Biophotonics, Japan
Laval University School of Medicine,
Canada

- Leeds, University of, United Kingdom
Leiden, University of, The Netherlands
Lethbridge, University of, Canada
Lisbon, University of, Portugal
Lund University, Sweden
- Manchester, University of, United Kingdom
Marine Biological Association, United Kingdom
Max-Planck-Institut, Germany
McGill University, Canada
McMaster University, Canada
Medical Academy of Lodz, Poland
Medical Research Council, United Kingdom
Melbourne, University of, Australia
Milano, University of, Italy
Montreal, University of, Canada
Munich, University of, Germany
- Naples, University of, Italy
National Institute for Medical Research, United Kingdom
National University of Singapore, Singapore
National Veterinary Institute, Sweden
New Brunswick, University of, Canada
Niigata University, Japan
- Oldenburg, University of, Germany
Otago, University of, New Zealand
Ottawa, University of, Canada
Oxford, University of, United Kingdom
- Palermo, University of, Italy
Poland Institute of Psychiatry & Neurology, Poland
- Queen's University, Canada
Queen's University of Belfast, United Kingdom
- Rega Institute, Belgium
Regina Elena Center Research Institute, Italy
Robert Gordon University, United Kingdom
Rostock, University of, Germany
Royal Institute of Technology, Sweden
Royal Postgraduate Medical School, United Kingdom
Ruhr-Universität Bochum, Germany
Russian State Medical University, Russia
- School of Biological Sciences, United Kingdom
Seville, University of, Spain
Simon Fraser University, Canada
St. Francis Xavier University, Canada
Stazione Zoologica A. Dohrn, Italy
Sussex, University of, United Kingdom
Swiss Federal Institute of Technology, Switzerland
Sydney, University of, Australia
- Taichung Veterans General Hospital, Taiwan
Technion, Faculty of Medicine, Israel
Tel Aviv University, Israel
Tokyo Medical & Dental University, Japan
Tokyo, University of, Japan
Toronto, University of, Canada
Tsukuba Life Science Center, Japan
Tübingen, University of, Germany
- Universidad Nacional Autonoma, Mexico
Universidad Nacional de Cuyo-Conicet, Argentina
Universidade Federal Fluminense, Brazil
Universität GH Essen, Germany
Universität zu Köln, Germany
Université Paris-Sud, France
University College London, United Kingdom
University Hospital Nijmegen, The Netherlands
University Laboratory of Physiology, United Kingdom
University Newcastle upon Tyne, United Kingdom
University of Technology, Australia
Urbino, University of, Italy
Utrecht University, The Netherlands
- Victoria, University of, Canada
- Wageningen Agricultural University, The Netherlands
Waterloo, University of, Canada
Weizmann Institute of Science, Israel
Wellcome/CRC Institute, United Kingdom
- York University, Canada
- Zeneca Pharmaceuticals, United Kingdom
Zoological Society of London, United Kingdom
Zurich, University of, Switzerland

Year-Round Research Programs



Architectural Dynamics in Living Cells Program

Established in 1992, this program focuses on architectural dynamics in living cells—the timely and coordinated assembly and disassembly of macromolecular structures essential for the proper functioning, division, motility, and differentiation of cells; the spatial and temporal organization of these structures; and their physiological and genetic control. The program is also devoted to the development and application of powerful new imaging and manipulation devices that permit such studies directly in living cells and functional cell-free extracts. The Architectural Dynamics in Living Cells Program promotes interdisciplinary research and consists of resident core investigators and a cadre of adjunct members.

Resident Core Investigators

Danuser, Gaudenz, Postdoctoral Fellow
Inoué, Shinya, Distinguished Scientist
Kato, Kaoru, Postdoctoral Research Associate
Oldenbourg, Rudolf, Associate Scientist

Staff

Geer, Thomas, Research Assistant
Knudson, Robert, Instrumental Development Engineer
Maccaro, Jackie, Laboratory Assistant
MacNeil, Jane, Executive Assistant

Visiting Investigators

Burgos, Mario H., Universidad Nacional de Cuyo, Conicet, Mendoza, Argentina
Fukui, Yoshio, Northwestern University Medical School
Inoué, Theodore D., Universal Imaging Corporation, West Chester, PA
Okada, Naobumi, Olympus Corporation, Hachioji, Japan
Suzuki, Keisuke, Olympus Corporation, Hachioji, Japan
Takahashi, Hajime, Olympus Corporation, Hachioji, Japan
Tran, Phong, University of North Carolina, Chapel Hill

The Josephine Bay Paul Center for Comparative Molecular Biology and Evolution

Major emphasis in The Josephine Bay Paul Center for Comparative Molecular Biology and Evolution is placed upon comparative/phylogenetic studies of genes and genomes, molecular microbial

ecology/biodiversity, evolution of pathogenesis and evolution of host defense mechanisms in marine invertebrates. The center encourages studies of genotypic diversity across all phyla and promotes the use of modern molecular genetics and phylogeny to gain insights into the evolution of genes and genomes. The Marine Biology Laboratory has considerable strength in Comparative Molecular Biology and Evolution including Mitchell Sogin's studies of genome evolution and diversity of Eukaryotes, Monica Riley's Metabolic Database and evolutionary studies of protein sequences, Neal Cornell's comparative molecular studies of genes critical to heme biosynthesis, Norman Wainwright's studies of the molecular basis of host defense mechanisms in marine invertebrates, and Michael Cumming's work on evolution of pathogenesis in prokaryotes. Other collaborative projects include studies of P450 evolution between M. Sogin and John Stegeman's laboratory at Woods Hole Oceanographic Institution (WHOI), a molecular ecology component of the Long-Term Ecological Research project between M. Sogin's laboratory and J. Hobbie of the Ecosystems Center, and collaborative studies of molecular diversity among marine protists and bacteria with several eukaryotic microbiologists at WHOI.

Excellent resources for studies of molecular evolution exist in the form of automated DNA sequencing, well-equipped research laboratories, and powerful computational facilities. The Josephine Bay Paul Center for Comparative Molecular Biology and Evolution plays an active role in educational activities at the MBL. In addition to participating in the Parasitology and Microbial Diversity courses, it sponsors the Workshop in Molecular Evolution at the MBL which has gained an international reputation for excellence. This Workshop serves 60 students by offering a series of lectures and mini-symposia, which are complemented by a state-of-the-art computational facility. The Josephine Bay Paul Center for Comparative Molecular Biology and Evolution includes the laboratories of Neal Cornell, Michael Cummings, Monica Riley, Mitchell Sogin, and Norman Wainwright.

Resident Core Investigators

Sogin, Mitchell, Director and Senior Scientist
Cornell, Neal, Senior Scientist
Riley, Monica, Senior Scientist
Wainwright, Norman, Senior Scientist

Laboratory of Neal Cornell

Research in this laboratory is concerned with the comparative molecular biology of genes that encode the enzymes for heme biosynthesis, with particular emphasis on 5-aminolevulinate synthase, the first enzyme in the pathway. Because the ability to produce heme from common metabolic materials is a near universal requirement for living organisms, these genes provide useful indicators of molecular

aspects of evolution. For example, 5-aminolevulinic synthase in vertebrate animals and simple eukaryotes such as yeast and *Plasmodium falciparum* have high sequence similarity to the enzyme from the alpha-purple subgroup of eubacteria. This supports the suggestion that alpha-purple bacteria are the closest contemporary relatives of the ancestor of eukaryotic mitochondria. The analysis also raises the possibility that plant and animal mitochondria had different origins. Aminolevulinic synthase genes in mitochondria-containing protists are currently being analyzed to obtain additional insight into endosymbiotic events. Also, genes of primitive chordates are being sequenced to gain information about the large scale gene duplication that played a very important role in the evolution of higher vertebrates. Other studies in the laboratory have been concerned with the effects of environmental pollutants on heme biosynthesis in marine fish, and it has been shown that polychlorinated biphenyls (PCBs) enhance the expression of the gene for aminolevulinic synthase.

Staff

Cornell, Neal W., Senior Scientist
 Dunlap, Rachel, Research Associate
 Faggart, Maura A., Research Assistant
 Kreiling, Jill, Research Assistant
 Macarro, Jackie, Laboratory Assistant
 O'Neil, Brendan, Laboratory Assistant

Visiting Scientist

Fox, T. O., Harvard Medical School

Laboratory of Norman Wainwright

The mission of the laboratory is to understand the molecular defense mechanisms exhibited by marine invertebrates in response to invasion by bacteria, fungi, and viruses. The primitive immune systems demonstrate unique and powerful strategies for survival in diverse marine environments. The key model has been the horseshoe crab *Limulus polyphemus*. *Limulus* hemocytes exhibit a very sensitive LPS-triggered protease cascade which results in blood coagulation. Several proteins found in the hemocyte and hemolymph display microbial binding proteins that contribute to antimicrobial defense. Commensal or symbiotic microorganisms may also augment the antimicrobial mechanisms of macroscopic marine species. Secondary metabolites are being isolated from diverse marine microbial strains in an attempt to understand their role. Microbial participation in oxidation of the toxic gas hydrogen sulfide is also being studied.

Staff

Wainwright, Norman, Senior Scientist
 Child, Alice, Research Assistant

Visiting Investigator

Anderson, Porter, University of Rochester

Molecular Evolution of Genomes

The genome of the bacterium *Escherichia coli* contains all of the information required for a free-living chemoautotrophic organism to live, adapt, and multiply. The information content of the genome can be dissected from the point of view of understanding the role of each gene and gene product in achieving these ends. The many functions of *E. coli* have been organized in a hierarchical system representing



the complex physiology and structure of the cell. In collaboration with Dr. Peter Karp of SRI International, an electronic encyclopedia of information is being constructed on the genes, enzymes, metabolism, transport processes, regulation, and cell structure of *E. coli*. The interactive EcoCyc program is now publicly available and has graphical hypertext displays, including literature citations, on nearly all of *E. coli* metabolism, all genes and their locations, a hierarchical system of cell functions and some regulation processes. This work is continuing.

In addition, the *E. coli* genome contains valuable information on molecular evolution. We are analyzing the sequences of proteins of *E. coli* in terms of their evolutionary origins. By grouping like sequences and tracing back to their common ancestors, one learns not only about the paths of evolution for all contemporary *E. coli* proteins, but one extends even further back before *E. coli*, traversing millennia to the earliest evolutionary times when a relatively few ancestral proteins served as ancestors to all contemporary proteins of all living organisms. The complete genome sequence of *E. coli* and sophisticated sequence analysis programs permit us to identify evolutionary related protein families, determining ultimately what kinds of unique ancestral sequences generated all of present-day proteins. The data developed in the work has proved to be valuable to the community of scientists sequencing microbial genomes. *E. coli* data serve as needed reference points.

Staff

Riley, Monica, Senior Scientist
 Pelligrini-Toole, Alida, Research Assistant II
 Kerr, Alastair, Postdoctoral Research Associate

Program in Comparative Molecular Biology and Evolution: Laboratory of Mitchell L. Sogin

The Program in Molecular Evolution employs comparative phylogenetic studies of genes and genomes to define patterns of evolution that gave rise to contemporary biodiversity on the planet Earth. We are especially interested in discerning how the eukaryotic cell was invented as well as the identity of microbial groups that were ancestral to animals, plants, and fungi. We take advantage of the extraordinary conservation of ribosomal RNAs to define phylogenetic relationships that span the largest of evolutionary distances. These studies have overhauled traditional eukaryotic microbial classifications systems. We have discovered new evolutionary assemblages that are as genetically diverse and complex

as plants, fungi, and animals. The nearly simultaneous separation of these eukaryotic groups (described as the eukaryotic "Crown") occurred approximately one billion years ago and was preceded by a succession of earlier diverging protist lineages, some as ancient as the separation of the prokaryotic domains. At the same time this database provides a powerful tool for the newly emerging discipline of molecular ecology. Using the ribosomal RNA data-base and nucleic acid based probe technology, it is possible to detect and monitor microorganisms including those that cannot be cultivated in the laboratory. This strategy has revealed new habitats and major revelations about geographical distribution of microorganisms.

This past year we initiated a new project designed to unlock the secrets of genome evolution in the parasite *Giardia lamblia*. We selected *G. lamblia* as a model organism for genome analysis because of its well-recognized impact on human health, its relatively modest-sized genome containing 12 million base pairs distributed onto five chromosomes, and the insights it will provide about the origins of nuclear genome organization. Comparisons of several different gene families demonstrate *Giardia's* basal position in molecular phylogenies, which is consistent with the absence of several prominent organelles like mitochondria, peroxisomes, and mitotic spindles that characterize most eukaryotic cells. This genome project will complement an ongoing survey of genomic diversity from eukaryotic microorganisms that do not have mitochondria. We previously demonstrated that these taxa represent some of the earliest diverging lineages in the evolutionary history of eukaryotes. The objective is to develop a set of additional molecular markers for studying molecular evolution. These will be invaluable in unraveling sudden evolutionary radiations that cannot be resolved by rRNA comparisons and will provide insights into the presence or absence of important biochemical properties in the earliest ancestors common to all eukaryotic species.

Staff

Sogin, Mitchell L., Director and Senior Scientist
Amaral, Linda, Post Doctoral Research Associate
Edgcomb, Virginia, Post Doctoral Research Associate
Hinkle, Greg, Post Doctoral Research Associate
Morrison, Hilary G., Research Associate
Roger, Andrew, Post Doctoral Research Associate
Silberman, Jeff, Post Doctoral Research Associate

Visiting Investigators

Bahr, Michele, Ecosystems Center
Podar, Mircea, WHOI
Weil, Jennifer, Joslin Diabetes Center

BioCurrents Research Center

The Biocurrents Research Center (BRC), one of the NIH National Centers for Research Resources, has for many years been pioneering methods in the study of transmembrane currents and has hosted a variety of research pursuits. The Center provides visiting investigators access to a variety of unique technologies as well as new approaches to experimentation in the biomedical sciences.

Since the early 1980s, when this Biomedical Research Technology Program (BRTP) was established at the MBL, a number of probes have been introduced. Four systems are available or being developed at the BRC. All these probe technologies are based on the principles of a self-referencing electrode, maximizing sensitivity by noise and drift reduction. All the probes are non-invasive and generally placed in close proximity to the membrane of cells or tissues, in some cases at sub-micron distances. The two older techniques are designed to

measure the movement of ions across the membranes of living tissues or cells with the minimum of disturbance. The current probe, developed in 1974, is still available for the study of external current densities resulting from the general net balance of ion transport. Most use is made of the ion-selective probes (Seris), which measure and follow the transmembrane transport of specific ions such as calcium, potassium and protons. This system also can detect non-electrogenic transporters. Two newer techniques, which are finding their first successful applications on biological material, are the BioKelvin Probe and the non-invasive Oxygen Probe (Serp). The BioKelvin Probe measures voltages around living tissues in air. Recently, successful measurements were made of fields derived from growing corn seedlings responding to gravity and light. Experiments will apply this new instrument to the study of skin physiology. A radically different approach is being taken to the measurements of biocurrents using the Oxygen Probe. Presently applied to molecular oxygen, such a technique offers opportunity for the study of molecular transport using redox potentials. The prototype has made measurements of the oxygen consumption of a single neuron in culture with a spatial resolution of several μm^2 . We are currently developing further improvements to all our systems by incorporating super-resolution algorithms based on machine vision.

A state-of-the-art system offers non-invasive ion probes coupled with current and voltage clamp (both single, two electrode, and patch) along with ratio imaging via a recently purchased Zeiss Attofluor system, all of which are finding uses in the hosted biomedical studies, as well as BRC research and development.

Research by O. Shirihai, an MD/PhD student from Israel, who was at MBL as a Grass Fellow, is an example that brings together many aspects of a BRTP Center, resulting in discoveries that otherwise would not take place. While at the MBL he joined us to use the imaging capability of BRC. During that study he also applied the specialized Seris-electrodes to growing mammalian microglia, demonstrating, for the first time, a new member of the potassium/proton ATPase family in the central nervous system. The physiological demonstration was supported by immuno-histochemical work with antibodies made available to us through another Center visiting investigator, Dr. D. Brown of Harvard and Massachusetts General Hospital. The antibodies were raised by Adam Smolka in the Carolinas. As the microglia form a principal brain reactive cell, and are implicated in neurodegenerative diseases of the CNS, we believe these discoveries will be of fundamental biomedical importance.

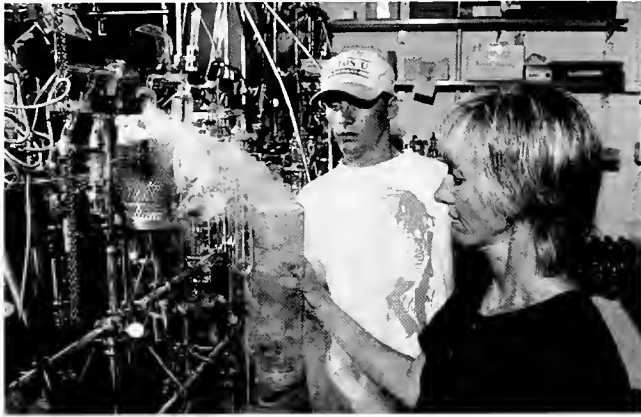
MBL year-round laboratories with which BRC is in active collaboration are the Laboratory of Rudolf Oldenbourg and the Laboratory of Reproductive Medicine, headed by David Keefe. Dr. Keefe and Dr. Peter Smith, BRC Director, are Co-Investigators on a grant to support the development of new technology to assess the developmental potential of preimplantation embryos and to study the pathophysiology of oocyte dysfunction.

Staff

Smith, Peter J. S., Director and Associate Scientist
Baikie, Iain D., Associate Scientist
Danuser, Gaudenz M., Visiting Scientist
Hammar, Katherine, Research Assistant
Jaffe, Lionel F., Senior Scientist
McLaughlin, Jane A., Research Assistant
Porterfield, D. Marshall, Research Associate
Sanger, Richard H., Senior Electronics Technician
Tamise, Catherine T., Graduate Student, University of Rhode Island

Visiting Scientist and Publications

This past year the Research Center hosted 25 visitors, 19 from the United States with the remaining from Canada, Israel, United



Kingdom and New Zealand. Scientific publications during the year numbered 21.

Boston University Marine Program

Faculty

Atema, Jelle, Professor of Biology, Director
 Dionne, Vincent, Professor of Biology, Acting Director
 Humes, Arthur, Professor of Biology Emeritus
 Kaufman, Les, Associate Professor of Biology
 Lobel, Phil, Associate Professor of Biology
 Valiela, Ivan, Professor of Biology
 Voigt, Rainer, Research Associate Professor
 Ward, Nathalie, Lecturer

Staff

Burns, Jennifer, Course Coordinator
 DiNunno, Paul, Research Assistant, Dionne Laboratory
 Hahn, Dorothy, Sr. Administrative Secretary
 Hall, Sheri, Program Manager
 Magee, Jennifer, Administrative Secretary
 Olson, Nancy, Program Assistant/Director's Secretary
 Proft, Heinz, Research Assistant, Lobel Laboratory
 Roberts, Brian, Research Technician, Valiela Laboratory
 Soucy, Lori, Research Assistant, Valiela Laboratory
 Tomasky, Gabby, Research Assistant, Valiela Laboratory
 Wheatley, MaryJo, Information and Development Officer
 Zackrisson, Rebecca, Course Coordinator

Postdoctoral Investigators

Basil, Jenny, Atema Laboratory
 Cebrian, Just, Valiela Laboratory
 Cohen, Anne, Lobel Laboratory
 Delay, Rona, Dionne Laboratory
 Eisthen, Heather, Dionne Laboratory
 Grasso, Frank, Atema Laboratory
 Lavalli, Kari, Atema Laboratory
 Trott, Thomas, Atema Laboratory

Visiting Faculty and Investigators

Epstein, Slava, Northeastern University
 Hanlon, Roger, Marine Biological Laboratory

Hecker, Barbara, Rutgers University
 Hinkle, Gregory, Marine Biological Laboratory
 Margulis, Lynn, University of Massachusetts, Amherst
 Moore, Michael, Woods Hole Oceanographic Institution
 Silver, Robert, Marine Biological Laboratory
 Simmons, Bill, Sandia National Laboratory
 Wainwright, Norman, Marine Biological Laboratory

Other

Dolan, Mike, Visiting Teaching Assistant
 Drucker, Sam, Visiting Teaching Assistant
 Witting, Jan, Visiting Teaching Assistant

Graduate Students

PhD Students

Existing

Batjakas, Ioannis
 Behr, Peter
 Dale, Jonathon
 Economakis, Alistair
 Farley, Lynda
 Hauxwell, Jennifer
 Herrold, Ruth
 Lindholm, James
 Ma, Diana
 McClelland, James
 Oliver, Steven
 Tamse, Armando
 Zhou, Qiao

New

Cole, Marci
 Kroeger, Kevin
 Piccillo, Bianca
 Sloan, Kevin
 Stieve, Erica
 Thoren, Erika
 Zhao, Jing

Masters Students

Existing

Ashcraft, Susan
 Barry, Kevin
 Bell, Kimberly
 Demary, Kristian
 Ewell, Cara
 Filson, Jean
 Heiskell, Marybeth
 Jefferson, Shawn
 Keith, Lucy
 Kerr, Lisa
 Paganessi, Laura
 Ryan, Pamela
 Searcy, Brian
 Thompson, Sarah
 Timmer, Edward
 Valentini, Stefanie
 Watson, Elise
 Wittenberg, Kim

New

Atkinson, Abby
 Baizer, Traci

Barlas, Margaret
Bowen, Jennifer
Cavanaugh, Joseph
DeCou, Dominique
Ferland, Amy
Griffin, Martin
Homkow, Laura
Lawrence, David
Smith, Spence
Tober, Joanna
Wright, Dana

Undergraduate Students

Spring 97

Balsys, Roman
Bentis, Christopher
Drucker, Sam
Schlimmer, Lisa
Singer, Emily
Strongin, Daniel
Wilkman, Jason

Fall 97

Adams, Elizabeth
Banik, Amy
Bell, Richard
Benjamin, Natasha
Berasi, Brenda
Brines, Zachary
Brown, Nicole
Camp, Sara
Dohogne, Michelle
Efros, Michelle
Frenz, Christopher
Furlong, Chris
Harris, Jennifer
Houghton, April
Hubert, Jessica
Jacobs, Jennafer
Joyce, Kelly
Kam, Adrienne
Krawczyk, Jaime
Levy, Ilan
Lolli, Amanda
Miller, Lauren
Paradise, Kristen
Rodriguez, Jennifer
Weaver, Matthew

Summer 1997 Interns

Duffy, Elisabeth
Elkins, Kim
Heberlig, Laura
Hoepfner, Susanne
Javonillo, Robert
Kinlan, Brian
Lee, Rosalynn
Markley, Jessamyn
Morlock, Summer
Taylor, David
Voss, Daniel
Whitman, Allison

Laboratory of Jelle Atema

Many organisms and cellular processes use chemical signals as their main channel of information about the environment. All environments are noisy and require some form of filtering to detect important signals. Chemical signals are transported by turbulent currents, viscous flow, and molecular diffusion. Receptor cells extract chemical signals from the environment through various filtering processes. In our laboratory, fish, marine snails, and crustacea have been investigated for their ability to use chemical signals under water. Currently, we use the lobster and its exquisite senses of smell and taste as our major model to study the signal-filtering capabilities of the whole animal and its narrowly tuned chemoreceptor cells.

Research in our laboratory focuses on amino acids, which represent important food signals for the lobster, and on the function and chemistry of pheromones used in lobster courtship. We examine animal behavior in the sea and in the lab. This includes social interactions and chemotaxis. To understand the role of chemical signals in the sea we use real lobsters and small untethered robots. Besides measurement and computer modeling of odor plumes and of the water currents lobsters generate to send and receive chemical signals, our research includes neurophysiology of receptor cells and anatomical studies of receptor organs and pheromone glands.

Laboratory of Vincent Dionne

Odors are powerful stimuli. They can focus the attention, elicit behaviors (or misbehaviors), and even resurrect forgotten memories. These actions are directed by the central nervous system, but they depend upon the initial transduction of chemical signals by olfactory receptor neurons in the nasal passages. More than just a single process appears to underlie odor transduction, and the intracellular pathways that are used are far more diverse than once thought. Hundreds of putative odor receptor molecules have been identified that work through several different second messengers to modulate the activity of various types of membrane ion channels. Our studies are being conducted with aquatic salamanders using amino acids and other soluble chemical stimuli which these animals perceive as odors. Using electrophysiological and molecular approaches, the research examines how these cellular components produce odor detection, and how odors are identified and discriminated.

Laboratory of Arthur G. Humes

Research interests include systematics, development, host specificity, and geographical distribution of copepods associated with marine invertebrates. Current research is on taxonomic studies of copepods from invertebrates in the tropical Indo-Pacific area, and poecilostomatoid and siphonostomatoid copepods from deep-sea hydrothermal vents and cold seeps.

The Laboratory of Les Kaufman

Current research projects in the laboratory deal with speciation and extinction dynamics of haplochromine fishes in Lake Victoria. We are studying the systematics, evolution, and conservation genetics of a species flock encompassing approximately 700 very recently evolved taxa, in the dynamic and heavily impacted landscape of northern East Africa. In the lab, we are studying evolutionary morphology, behavior, and systematics of these small, brightly colored cichlid fishes. Another area of study is developmental and skeletal plasticity in fishes; we are studying the diversity of bone tissue types in fishes, differential response to mineral and mechanical challenge, and matrotrophic *versus* environmental effects in the development of coral reef fishes. We also study the biological basis for marine reserves in

the New England fisheries. We are involved in collaborative research with NURC, NMFS, and others on the relative impact on groundfish stocks of juvenile habitat destruction *versus* fishing pressure.

Laboratory of Phillip Lobel

Fishes are the most diverse vertebrate group and provide opportunities to study many aspects of behavior, ecology, and evolution. We primarily study how fish are adapted to different habitats and the behavioral ecology of species interactions. Current research focuses on fish acoustic communication. We are also conducting a long-term study of the marine biology of Johnston Atoll, Central Pacific Ocean. Johnston Atoll has been occupied continuously by the military since the 1930s and proved a unique opportunity for assessing the biological impacts of island industrialization and effects on reefs. Johnston Atoll is the site of the US Army's chemical weapons demilitarization facility, JACADS.

Laboratory of Ivan Valiela

A focus of our work is the link between land use on watersheds and consequences in the receiving estuarine ecosystems. The work examines how landscape use and urbanization increase nutrient loading to groundwater and streams. Nutrients in groundwater are transported to the sea, and, after biogeochemical transformation, enter coastal waters. There, increased nutrients bring about a series of changes on the ecological components. To understand the coupling of land use and consequences to receiving waters, we study the processes involved, assess ecological consequences, and define opportunities for coastal management.

A second long-term research topic is the structure and function of salt marsh ecosystems, including the processes of predation, herbivory, decomposition, and nutrient cycles.

Calcium Imaging Laboratory

This laboratory investigates the roles of calcium patterns in development. Our main tool uses the aequorins, a family of luminescent proteins ultimately obtained from a jellyfish and long studied by Dr. Osamu Shimomura at the MBL. Aequorins can either be microinjected into cells or transgenically expressed without disturbing function or development. The patterns of luminescence that are emitted by aequorinated cells reveals changing patterns and levels of free calcium with the cell or its progeny. Much of what we know about the role of calcium in development has been obtained with the aequorins.

The four systems under present or planned investigation are the *Drosophila* egg (in collaboration with Carl Hashimoto at Yale), the zebrafish egg, the fucoid egg (in collaboration with Dr. Ken Robinson at Purdue), and the cellular slime mold, *Dictyostelium*.

Staff

Jaffe, Lionel, Senior Scientist
Créton, Robert, Research Associate

Center for Advanced Studies in the Space Life Sciences at the MBL

(supported by the National Aeronautics
and Space Administration)

The Marine Biological Laboratory and the National Aeronautics and Space Administration have established a cooperative arrangement with the formation of the Center for Advanced Studies in the Space



Life Sciences at the MBL. This Center serves as an interface between NASA and the basic science community, addressing issues of mutual interest. A series of symposia, workshops, and seminars are held at the MBL to advise NASA on a wide variety of topics in the life sciences, including cellular, molecular, developmental, plant, neuro-, and evolutionary biology. Special attention is directed at examining how gravity and its control impact on biological processes, and how variations in gravity can be used as a probe to better understand such processes. This center provides a forum for scientists to think and discuss, often for the first time, the role that gravity and other aspects of space flight may play in fundamental cellular and physiological processes. These interactions also serve to inform the community of research opportunities in the life sciences that are of interest to NASA. In addition, a newsletter will be published to disseminate this information to a wider audience.

During the past year the Center sponsored two workshops at the MBL: "Genetic Regulatory Networks in Embryogenesis and Evolution" held on June 11-14, 1997, chaired by Eric Davidson and David McClay; and "Evolution: A Molecular Point of View" held on October 24-26, 1997, chaired by Mitchell Sogin.

Staff

Dawidowicz, Lenny, Administrator
Amit, Udeni, Administrative Assistant
Nixon, Jennifer, Administrative Assistant

The Ecosystems Center

The Center carries out research and education in ecosystems ecology. Terrestrial and aquatic scientists work in a wide variety of ecosystems ranging from the streams, lakes and tundra of the Alaskan Arctic (limits on plant primary production) to sediments of Massachusetts Bay (controls of nitrogen cycling), to forests in New England (effects of soil warming on carbon and nitrogen cycling), and South America (effects on greenhouse gas fluxes of conversion of rain forest to pasture) and to large estuaries in the Gulf of Maine (effects of plankton and benthos of nutrients and organic matter in stream runoff). Many projects, such as those dealing with carbon and nitrogen cycling in forests, streams, and estuaries, use the stable isotopes ^{13}C and ^{15}N to investigate natural processes. A mass spectrometer facility is available. Data from field and laboratory research are used to construct mathematical models of whole-system responses to change. Some of these models are combined with geographically referenced data to produce estimates of how environmental changes affect key ecosystem indexes such as net primary productivity and carbon storage throughout the world's terrestrial biosphere.

R48 Annual Report

The results of the Center's research are applied, wherever possible, to the questions of the successful management of the natural resources of the earth. In addition, the ecological expertise of the staff is made available to public affairs groups and governmental agencies who deal with problems such as acid rain, coastal eutrophication, and possible carbon dioxide-caused climate change. The Semester in Environmental Science, a fall offering, was held for the first time in 1997. Sixteen students from 11 colleges participated in the program. There are opportunities for postdoctoral fellows.

Administrative Staff

Hobbie, John E., Co-Director
Melillo, Jerry M., Co-Director
Berthel, Dorothy J., Administrative Assistant
Chandler, Marsha, Administrative Assistant, Semester in Environmental Science
Donovan, Suzanne J., Executive Assistant
Foreman, Kenneth H., Associate Director of Environmental Studies Program
Nuñez, Guillermo, Research Administrator
Seifert, Mary Ann, Administrative Assistant
Scanlon, Deborah G., Executive Assistant, LMER Coordination Office

Scientific Staff

Hobbie, John E., Senior Scientist
Melillo, Jerry M., Senior Scientist
Peterson, Bruce J., Senior Scientist
Shaver, Gaius R., Senior Scientist
Giblin, Anne E., Associate Scientist
Hopkinson, Charles S., Senior Scientist
Nadelhoffer, Knute J., Associate Scientist
Deegan, Linda A., Associate Scientist
Rastetter, Edward B., Associate Scientist
Stuedler, Paul A., Senior Research Specialist
Neill, Christopher, Assistant Scientist
Pan, Yude, Research Associate
Vallino, Joseph J., Assistant Scientist
Williams, Mathew, Assistant Scientist
Xiao, Xiangming, Research Associate

Educational Staff Appointments

Currie, William, Visiting Postdoctoral Scholar, U.S. Department of Agriculture
Garcia, Diana, Postdoctoral Research Associate
Gough, Laura, Postdoctoral Research Associate
Hartley, Anne, Postdoctoral Research Associate
Herbert, Darrell A., Postdoctoral Research Associate
Holmes, Robert M., Postdoctoral Research Associate
Hughes, Jeffrey E., Postdoctoral Research Associate
Jablonski, Leanne, Postdoctoral Research Associate
Stieglitz, Marc, NOAA Global Climate Change Postdoctoral Fellow
Tian, Hanqin, Postdoctoral Research Associate

Technical Staff

Bahr, Michele P., Research Assistant
Bettez, Neil D., Research Assistant
Bryant, David M., Research Assistant
Canary, Jana D., Research Assistant
Caticala, Christina E., Research Assistant
Clark, Tamara, Research Assistant
Claessens, Luc, Research Assistant

Dornblaser, Mark M., Research Assistant
Downs, Martha R., Research Assistant
Garritt, Robert H., Senior Research Assistant
Helfrich, John V. K., III, Senior Research Assistant
Holland, Keri, Research Assistant
Hooker, Bethanie, Research Assistant
Kicklighter, David W., Senior Research Assistant
Kwiatkowski, Bonnie L., Research Assistant
Laundre, James A., Senior Research Assistant
Micks, Patricia, Research Assistant
Newkirk, Kathleen M., Research Assistant
Nolin, Amy L., Research Assistant
Pratt, Sara, Research Assistant
Regan, Kathleen M., Research Assistant
Ricca, Andrea, Research Assistant
Schwamb, Carol, Laboratory Assistant
Slavik, Karie A., Research Assistant
Soucy, Lori, Research Assistant
Thieler, Kama, Research Assistant
Thomas, Suzanne, Research Assistant
Tholke, Kristin S., Research Assistant
Tucker, Jane, Senior Research Assistant
Weston, Nat, Research Assistant
Wollheim, Wilfred M., Research Assistant

Consultants

Bowles, Frances P., Research Systems Consultant Principal, Research Designs
Bowles, Margaret C., Administrative Consultant
Golden, Heidi E., Research Consultant

Visiting Scientists and Scholars

Kling, George, Visiting Scientist, University of Michigan, Ann Arbor
Loya, Wendy, Visiting Scholar, Kansas State University
Seifert, Gabriel, CIEE Intern, Technical University of Wismar, Germany
Siver, Peter, Semester in Environmental Science Faculty Fellow, Connecticut College

Laboratory of Aquatic Animal Medicine and Pathology

The laboratory provides diagnostic, consultative research, and educational services to the institutions and scientists of the Woods Hole community concerned with marine animal health. Diseases of wild, captive, and cultured animals are investigated.

Staff

Abt, Donald A., Director and The Robert R. Marshak Term Professor of Aquatic Animal Medicine and Pathology, School of Veterinary Medicine, University of Pennsylvania
Bullis, Robert A., Research Associate in Microbiology, University of Pennsylvania
Leibovitz, Louis, Director Emeritus
McCafferty, Michelle, Histology Technician, University of Pennsylvania
Moniz, Priscilla C., Administrative Assistant
Smolowitz, Roxanna M., Research Associate in Pathology, University of Pennsylvania
Wadman, Elizabeth A., Microbiology Technician, University of Pennsylvania

Laboratory of Aquatic Biomedicine

Work in this laboratory centers on comparative immunopathology and molecular biology using marine invertebrates as experimental models. Examples of current research include determining the prevalence of leukemia in *Mya arenaria* (the soft shell clam) in Massachusetts. Monoclonal antibodies developed by this laboratory are being used to diagnose clam leukemia, identify and characterize a tumor-specific protein, and differentiate other leukemias in bivalve molluscs. Developmental and chemically-induced changes in gene expression and neuronal growth are also being studied in the surf clam, *Spisula solidissima*. Work in molecular biology is creating a clearer understanding of the comparative etiology and pathogenesis of tumors, particularly in environmentally impacted aquatic animals.

Staff

Reinisch, Carol L., Associate Scientist, MBL, and Chairperson,
Department of Environmental and Population Health, Tufts
University School of Veterinary Medicine
Jessen-Eller, Kathryn, Postdoctoral Fellow
Steele, Marjorie, Research Assistant
Barker, Colin, Laboratory Technician

Visiting Scientist

Barker, Lewellys, Senior Associate Department of International
Health, Johns Hopkins University School of Public Health

Student

Smith, Cynthia, Tufts University School of Veterinary Medicine

Laboratory of Cell Communication

Established in 1994, this laboratory is devoted to the study of intercellular communication. The research focuses on the cell-to-cell channel, a membrane channel built into the junctions between cells. This channel provides one of the most basic forms of intercellular communication in organs and tissues. The work is aimed at the molecular physiology of this channel, in particular, at the mechanisms that regulate the communication. Electrophysiological-, fluorescent-tracer-, and molecular biological techniques are used to this end. As was recently discovered in this laboratory, the channel is the conduit of growth-regulating signals. It is instrumental in a basic feedback loop whereby cells in organs and tissues control their number; in a variety of cancer forms it is crippled. Work is aimed now at the mechanisms of growth control and at correcting cancer growth by transferring the gene for the cell-to-cell channel protein from normal cells into the cancer cells. Molecular genetic techniques are used in this endeavor.

Staff

Loewenstein, Werner, Senior Scientist
Rose, Birgit, Senior Scientist
Jillson, Tracy, Research Assistant

Laboratory of Barbara and Bruce Furie

γ -Carboxyglutamic acid is a calcium-binding amino acid that is found in the conopeptides of the predatory marine cone snail, *Conus*. This laboratory has been investigating the biosynthesis of this amino acid in *Conus* and the structural role of γ -carboxyglutamic acid in the conopeptides. This satellite laboratory relates closely to the main



laboratory on the Harvard Medical School campus in Boston; the main focus of the primary laboratory is the synthesis and function of γ -carboxyglutamic acid in blood clotting proteins and the role of vitamin K.

Large numbers of cone snails from Fiji have been obtained and are being maintained in the Marine Resources Center. The marine cone snail is the sole invertebrate known to synthesize γ -carboxyglutamic acid (Gla). The venomous cone snail produces neurotoxic conopeptides, some rich in Gla, which it injects into its prey. To examine the biosynthetic pathway for Gla, we have studied the *Conus* carboxylase which converts glutamic acid to γ -carboxyglutamic acid. Of the *Conus* species tested, *C. bandanus*, *C. marmoreus*, *C. textile*, and *C. leopardus* had high specific γ -carboxylase activity. This activity has an absolute requirement for vitamin K. The *Conus* carboxylase has been extensively purified and its gene is being cloned. The *Conus* carboxylase substrates appear to contain a carboxylation recognition site on the conotoxin precursor. The *Conus* vitamin K-dependent carboxylase should be an excellent model for determining the mechanism of action of vitamin K in the synthesis of γ -carboxyglutamic acid.

Fifteen novel γ -carboxyglutamic acid-containing conopeptides have been isolated from the venom of *Conus textile*. The amino acid sequence, amino acid composition and molecular weights of these peptides have been determined. For several peptides, the cDNA encoding the precursor conotoxin has been cloned.

The three-dimensional structure of some of these Gla-containing conopeptides as well as conantokin G have been determined by 2D NMR spectroscopy. Complete resonance assignments were made from 2D ^1H NMR spectra via identification of intrasidue spin systems using ^1H - ^1H through-bond connectivities. NOESY spectra provided $d_{\alpha\text{N}}$, d_{NN} and $d_{\beta\text{N}}$ NOE connectivities and vicinal spin-spin coupling constants $^3J_{\text{HNH}}$ were used to calculate ϕ torsion angles. Structure generation based on interproton distance restraints and torsion angle measurements yield convergent structures generated using distance geometry and simulated annealing methods. The goal of this project is to determine the structural role of γ -carboxyglutamic acid in the Gla-containing conotoxins.

Staff

Barbara C. Furie, Scientist
Bruce Furie, Scientist
Johan Stenflo, Visiting Scientist
Eva Czerwiec, Postdoctoral Fellow
Gail Begley, Postdoctoral Fellow
Alan Rigby, Postdoctoral Fellow

Laboratory of Roger Hanlon

This laboratory investigates the behavior and neurobiology of cephalopods. Studies of various learning capabilities are currently being conducted, as are studies on reproductive strategies that include agonistic behavior, female mate choice, and sperm competition. The latter studies involve DNA fingerprinting to determine paternity and help assess alternative mating tactics. Currently we are studying sensory mechanisms and function of polarization vision in cephalopods. Complimentary field studies are conducted locally and on coral reefs. The functional morphology and neurobiology of the chromatophore system of cephalopods are also studied on a variety of cephalopod species, and image analysis techniques are being developed to study crypsis and the mechanisms that enable cryptic body patterns to be neurally regulated by visual input.

Staff

Hanlon, Roger, Senior Scientist
Boal, Jean, Postdoctoral Fellow
Shashar, Nadav, Postdoctoral Fellow

Visiting Investigators

Gabr, Howaida, Graduate Student, Suez Canal University, Panama
Wittenberg, Kim, Graduate Student, Boston University Marine Program

Laboratory of Shinya Inoué

Scientists in this laboratory study the molecular mechanism and control of mitosis, cell division, cell motility, and cell morphogenesis, with emphasis on biophysical studies made directly on single living cells, especially developing eggs in marine invertebrates. Development of biophysical instrumentation and methodology, such as polarization optical and video microscopy and digital image processing techniques, and exploration of their underlying theory are an integral part of the laboratory's effort.

Staff

Inoué, Shinya, Distinguished Scientist
Knudson, Robert, Instrument Development Engineer
Maccaro, Jackie, Laboratory Assistant
MacNeil, Jane, Executive Assistant

Laboratory of Alan M. Kuzirian

Research in the laboratory explores the functional morphology and ultrastructure of various organ systems in molluscs. The program includes mariculture of the nudibranch, *Hermisenda crassicornis*, with emphasis on developing reliable culture methods for rearing and maintaining the animal as a research resource. The process of metamorphic induction by natural and artificial inducers is being explored in an effort to understand the processes involved and as a means to increase the yield of cultured animals. Morphologic studies stress the ontogeny of neural and sensory structures associated with the photic and vestibular systems which have been used in learning and memory studies as well as the spatial and temporal occurrence of regulatory and transmitter neurochemicals. Concurrent with these morphologic studies is the development of new histologic techniques designed to facilitate the acquisition of morphologic and structural information supporting proposed physiologic processes.

Collaborative research includes histochemical investigations on strontium's role in initiating calcification in molluscan embryos (shell

and statoliths), as well as immunocytochemical labelling of cell-surface antigens, neurosecretory products, second messenger proteins involved with learning and memory, and intracellular transport organelles using mono- and polyclonal antibodies on squid (*Loligo pealei*) giant axons and *Hermisenda* sensory and neurosecretory neurons, both *in situ* and in cell culture. Toxicity studies detailing the effects of lead on *Hermisenda* learning and memory, feeding, and the physiology of cultured neurons are also being conducted.

Additional collaborative research includes DNA fingerprinting using RAPD-PCR techniques in preparation for isogenic strain development of laboratory-reared *Hermisenda* and hatchery produced bay scallops (*Argopectin irradians*) with distinct phenotypic markers for the rapid field identification. Systematic and taxonomic studies of nudibranch molluscs, to include molecular phylogenetics, are also of interest.

Staff

Kuzirian, Alan M., Associate Scientist

Visiting Scientists

Chikarmane, Hemant, Research Scientist, Aphios Corporation,
Woburn MA: Assistant Scientist, MBL
Clay, John R., NINDS/NIH

Laboratory of Rudolf Oldenbourg

The laboratory investigates the molecular architecture of living cells and of biological model systems using optical methods for imaging and manipulating these structures. For imaging non-invasively and non-destructively cell architecture dynamically and at high resolution, we have developed a new polarized light microscope (Pol-Scope). The Pol-Scope combines microscope optics with new electro-optical components, video, and digital image processing for fast analysis of specimen birefringence over the entire viewing field. Examples of biological systems currently investigated with the Pol-Scope are: microtubule-based structures (asters, mitotic spindles, single microtubules); actin-based structures (acrosomal process, stress fibers, nerve growth cones); zona pellucida of vertebrate oocytes; and biopolymer liquid crystals.

Staff

Oldenbourg, Rudolf, Associate Scientist
Katoh, Kaoru, Postdoctoral Research Associate
Geer, Thomas, Research Assistant
Knudson, Robert, Instrument Development Engineer
Maccaro, Jackie, Laboratory Assistant

Laboratory for Reproductive Medicine, Brown University and Woman and Infants Hospital, Providence

Work in this laboratory centers on the investigation of the underlying mechanisms behind female infertility. Particular emphasis is placed on the physiology of the oocyte or early embryo, with the aim of assessing developmental potential and mitochondria dysfunction arising from mtDNA deletions. The studies taking place at the MBL branch of the Brown Laboratory use some of the unique instrumentation available through the resident programs directed by Rudolf Oldenbourg and Peter J. S. Smith. Most particularly, non-invasive methods for oocyte and embryo study are being sought. Of several specific aims, one is to use the new Pol-Scope to analyze the

birefringence of the preimplantation mammalian zona pellucida—a structure most predictive of successful implantation. We also have used this instrument to examine meiotic spindles. An additional aim is to continue the studies on transmembrane ion transport using the non-invasive electro-physiological techniques available at the BioCurrents Research Center. Preliminary studies indicate that the calcium transport may form an accurate predictor of oocyte and embryo health. The newly developed oxygen probe also offers the possibility of looking directly at abnormalities in the mitochondria arising from accumulated mtDNA damage. Ultimately, in addition to investigating the mechanisms behind cellular aging underlying infertility, this laboratory aims to produce clinical methods for assessing preimplantation embryo viability, a development that will make a significant contribution to the health of women and children.

Staff

Keefe, David, Director
Liu, Lin, Research Associate
Pepperell, John, Visiting Investigator
Sokhal, Emily, Research Assistant
Trimarchi, James, Post-doc Fellow

Laboratory of Sensory Physiology

Members of this laboratory have conducted research on various facets of vision since 1973. Current investigations use UV/VIS light microspectrophotometry on vertebrate retinal photoreceptors for the determination of visual pigment absorbance characteristics. One aim is to arrive at a better understanding of the method of spectral tuning that forms the chemical basis of color vision. Polarized light microscopic techniques are used to measure linear dichroism and linear birefringence aimed at revealing structure-function relationships and biophysical mechanisms. An area of interest is polarization discrimination, the mechanisms that could account for the ability of some fish species to detect the direction of polarization of light collected by their eyes. As a recent development, investigations are carried out on sickling in fish red blood cells due to hemoglobin polymerization, once again making extensive use of polarized light microscopic techniques.

Staff

Hárosi, Ferenc I., Senior Scientist, MBL, and Boston University
School of Medicine
Novales Flamarique, I., Postdoctoral Fellow

Visiting Scientists

Van Keuren, Jeffrey R., Postdoctoral Fellow, Woods Hole
Oceanographic Institution
Hunt von Herbing, I., Assistant Professor, University of Maine

Laboratory of Osamu Shimomura

Biochemical mechanisms involved in the bioluminescence of various luminescent organisms are investigated. Based on the results obtained, various improved forms of bioluminescent and chemiluminescent probes are designed and produced for the measurements of intracellular free calcium and superoxide anion.

Staff

Shimomura, Osamu, Senior Scientist, MBL, and Boston University
School of Medicine
Shimomura, Akemi, Research Assistant



Laboratory of Robert B. Silver

The members of this laboratory study how living cells make decisions. The focus of the research, typically using marine models, is on two main areas: the role of calcium in the regulation of mitotic cell division (sea urchins, sand dollars, etc.) and structure and function relationships of hair cell stereociliary movements in vestibular physiology (oyster, toadfish). Other related areas of study, *i.e.* synaptic transmission (squid), are also, at times, pursued. Tools include video light microscopy, multispectral, subwavelength, and very high speed (sub-millisecond frame rate) photon counting video light microscopy, telemanipulation of living cells and tissues, and modeling of decision processes. A cornerstone of the laboratory's analytical efforts is high performance computational processing and analysis of video light microscopy images and modeling. With luminescent, fluorescent, and absorptive probes, both empirical observation and computational modeling of cellular, biochemical, and biophysical processes permit interpretation and mapping of space-time patterns of intracellular chemical reactions and calcium signaling in living cells. A variety of *in vitro* biochemical, biophysical, and immunological methods are used. In addition to fundamental biological studies, the staff designs and fabricates optical hardware, and designs software for large video image data processing, analysis, and modeling.

Staff

Silver, Robert, Associate Scientist
Luders, Bruce, Research Assistant

Interns

Hurwitz, Layne R., REU Intern, Adelphi University
Sheikh, Sarah I., REU Intern, University of Edinburgh & Oxford
University
Strongin, Daniel E., REU Intern, Boston University

Visiting Scientists

Att. Maxim, MikroPhotonische Universität von CZI, Germany
Reeves, Anthony, Cornell University
Searby, Nancy, NASA Ames Research Center
Stromboli, Emilio, Stazione de Napoli, Italy

The Marine Resources Center

The Marine Resources Center (MRC) is one of the world's most advanced facilities for maintaining and culturing aquatic organisms essential to advanced biological, biomedical, and ecological research. Service and education also play an important and complimentary role in the modern, 32,000-square-foot facility.

The MRC and its life support systems have already increased the ability of MBL scientists to conduct research and have inspired new concepts in scientific experiments. Vigorous research programs focusing on basic biological and biomedical aquatic models are currently being developed at the Center. These programs will enhance and build upon the MRC's existing research activities by the University of Pennsylvania's Laboratory of Aquatic Animal Medicine and Pathology (LAAMP) and in the Laboratory of Roger Hanlon.

In addition to research, the MRC provides a variety of services to the MBL community through its Aquatic Resources Division, the Water Quality and System Engineering Division, the Administrative Division, and the Laboratory for Aquatic Animal Medicine and Pathology.

Research and educational opportunities are available at the facility

to established investigators, postdoctoral fellows, graduate, and undergraduate students. Investigators and students will find that the MRC's unique life support and seawater engineering systems make this a favorable environment in which to conduct independent research and masters and doctoral theses using a variety of aquatic organisms and flexible tank space for customized experimentation on live animals. Prospective investigators and students should contact the Director of the MRC for further information.

The MRC also hosts several courses: the annual AQUAVETS® courses sponsored by LAAMP, and an aquaculture course, the theme of which changes according to regional and national interests.

Staff

Hanlon, Roger, Director and Senior Scientist
Kuzirian, Alan, Associate Scientist
Boal, Jean, Postdoctoral Fellow
Shashar, Nadav, Postdoctoral Fellow

Visiting Investigators

Baker, Robert, New York University
Gilland, Edwin, Postdoctoral Fellow
Adamo, Shelly, Dalhousie University, Canada
Spotte, Stephen, University of Connecticut
Wittenberg, Kim, Graduate Student, Boston University Marine Program
Gabr, Howaida, Graduate Student, Suez Canal University, Panama



Honors

Friday Evening Lectures

June 20	Roger Y. Tsien, Howard Hughes Medical Institute, University of California, San Diego "Molecular Spies Reveal Cell Signals in Living Color"
June 27	Charles F. Stevens, The Salk Institute for Biological Studies "Synapses and Memory" (Lang Lecture)
July 4	Marianne Bronner-Fraser, California Institute of Technology "Development of the Neural Crest"
July 11	Clara Franzini-Armstrong, University of Pennsylvania "How Muscle Contraction is Turned On"
July 18	Jerry M. Melillo, Marine Biological Laboratory "Ecological Research and Global Environmental Policy: New Challenges for an Essential Partnership"
July 24, 25	Semir Zeki, University College London "The Functions of the Visual Brain" and "The Autonomy of the Visual Areas" (Forbes Lectures)
August 1	Eric Wieschaus, Princeton University "Zygotic Transcription and the Control of Embryonic Development in <i>Drosophila</i> " (Glassman Lecture)
August 8	Daniel Barry, NASA/Johnson Space Center "Space Flight from a Physician-Scientist's Perspective"
August 15	Rudolf A. Ralf, Indiana University "Development, Genes, and the Evolution of Animal Body Plans"

Fellowships and Scholarships

Robert Day Allen Fellowship

Drs. Joseph W. and Jean M. Sanger

ASCB Summer Research Award

American Society for Cell Biology

Frederik B. Bang Fellowship

Mrs. Betsy G. Bang

Frank A. Brown, Jr. Memorial Readership

Dr. and Mrs. Francis D. Carlson

The Jean and Katsuma Dan Fellowship Fund

Dr. Howard Holtzer
Dr. and Mrs. Shinya Inoué
Drs. Joseph W. and Jean M. Sanger
Mrs. H. Burr Steinbach

Bernard Davis Fund

Mrs. Elizabeth M. Davis

Aline D. Gross Scholarship Fund

Mrs. Mona Gross
Drs. Joan and Gerald Ruderman
Mr. and Mrs. Alfred M. Weisberg

Keffer Hartline Fellowship Fund

Dr. Edward F. MacNichol, Jr.

William Randolph Hearst Educational Endowment

William R. Hearst Foundation

Fred Karush Endowed Library Readership

Dr. and Mrs. Laszlo Lorand
Dr. and Mrs. Arthur M. Silverstein

MBL Summer Fellowships

Dr. and Mrs. Shinya Inoué

**Charles Baker Metz and Charles
William Metz Scholarship Fund**

Mr. Ronald H. Abel
Mrs. Grace S. Metz

Mountain Memorial Fund

Ms. Brenda J. Bodian
Dr. and Mrs. Benjamin Kaminer
Dr. and Mrs. R. Walter Schlesinger

**James A. and Faith Miller
Fellowship Fund**

Mr. and Mrs. David A. Miller
Mr. Robert K. Schlessinger

Frank Morrell Fund

Dr. Jack C. Berger
Ms. Elena N. Cohen
Ms. Kathleen A. Dunn
Dr. Leyla de Toledo Morrell
Dr. Serge J.C. Pierre-Louis
Rush-Presbyterian-St. Luke's
Dr. Susan Stefoski

Nikon Fellowship

Nikon, Inc.

Pfizer Scholarship Fund

Pfizer, Inc.

**William Townsend Porter
Scholarship**

William Townsend Porter Foundation

Ruth Sager Scholarship Fund

Dr. and Mrs. Harlyn O. Halvorson
Dr. and Mrs. Laszlo Lorand

Dr. Arthur B. Pardee
Dr. and Mrs. David Shepro

**The Ann Osterhout Edison/
Theodore Miller Edison and Olga
Osterhout Sears/Harold Bright
Sears Endowed Scholarship Fund**

Ms. Elizabeth F. Brewster
Mr. and Mrs. John W. Child
Ms. Jane T. Claffey
Mr. and Mrs. Putnam P. Flint
Dr. and Mrs. Paul L. Goodrich
Mr. and Mrs. Allan C. Henry
Mr. and Mrs. Robert L. Loud
Ms. Elaine M. Medeiros
Mr. Maren Miles and Ms. Nancy Douglas
Ms. Nancy L. Olsen
Dr. and Mrs. Miles H. Robinson
Mr. and Mrs. Christopher A. Sims
Mr. and Mrs. Peter E. Sloane
Dr. and Mrs. Thomas R. Stetson
Ms. Marsden Williams

**Science Writing
Fellowships Program**

American Society for Biochemistry &
Molecular Biology
American Society for Neurochemistry, Inc.
American Society for Photobiology
Association for Research in Vision and
Ophthalmology
Biophysical Society
Charles A. Dana Foundation
Federation of American Society for
Experimental Biology
Foundation for Microbiology
Friendship Fund
New York Times Foundation
Nicholas B. Ottaway Foundation

Society for Integrative and Comparative
Biology
The Washington Post Company

**The Moshe Shilo Memorial
Scholarship Fund**

Dr. and Mrs. John J. Lee
Dr. and Mrs. Richard I. Mateles

**The Evelyn and Melvin Spiegel
Fellowship Fund**

Drs. Joseph W. and Jean M. Sanger
Dr. Melvin and Evelyn Spiegel and the
Sprague Foundation

H. B. Steinbach Fellowship

Mrs. H. Burr Steinbach

Horace W. Stunkard Fellowship

Mrs. Eunice Latham
Dr. Albert J. Stunkard and Dr. Margaret
Maurin

**The Walter L. Wilson Endowed
Scholarship Fund**

Mrs. Irmgard Alexander (deceased)
Dr. Paul N. Chervin
Mrs. Marian Rigault
Dr. Jean R. Wilson

Young Scholars/Fellows Program

Merck Research Laboratories

Fellowships Awarded

MBL Summer Research Fellows

• Elena Barbieri, M.Sc., the *Bernard Davis Fellow*, is a researcher in the Bay Paul Center for Comparative Molecular Biology and Evolution at the MBL. She is also a fellow at the University of Urbino, Urbino Italy. She worked with Dr. Norman Wainwright on the role of symbiotic bacteria in the accessory nidamental gland (ANG) of the squid, *Loligo pealei*. She measured secondary metabolites derived from these symbiotic bacteria. These metabolites may have antimicrobial activity in the capsule-like membranes of the squid eggs. This study may lead to the

development of new antibiotics or potential treatments in clinical chemotherapy.

• Barbara C. Boyer, Ph.D., was an *Erik B. Fries* and an *MBL Associates Fellow*. She is a professor in the Department of Biology at Union College, Schenectady, New York. Dr. Boyer studied the evolution of development using the turbellarian flatworms *Hoploplana*, *Stylochus* and *Neochildia*.

• Mario H. Burgos, M.D., was supported by the *Frank R. Lillie Fellowship* while working with Dr. Shinya Inoué during the summer of 1997. Dr. Burgos is Founder and Director of the Institute of Histology and Embryology in Mendoza, Argentina. He used video

microscopy and confocal fluorescence microscopy in his research on gossypol, a male anti-fertility agent produced from cottonseed. Dr. Burgos used the male gamete of the sea urchin as a model system in which to test the effects of the agent. Research on gossypol may eventually result in a birth control drug for men.

- Edwin DeMont, Ph.D., is an associate professor in the Biology Department at St. Francis Xavier University, Antigonish, Nova Scotia, Canada. Dr. DeMont was supported by the *Esther A. and Joseph Klingenstein Fund* during the summer of 1997 while he studied the biomechanics of jet-propelled swimming in the squid *Loligo pealei*.

- Leah Devlin, Ph.D., was supported by the *NASA Life Sciences Program Fellowship*, the *M.G.F. Fuortes Fellowship*, and the *Lucy B. Lemann Fellowship*. She is an assistant professor of Biology at Penn State University in Abington, Pennsylvania. Dr. Devlin used a vibrating calcium-selective electrode to explore the movement of calcium in cardiac and smooth muscle. Her primary research organisms were the channeled whelk, *Busycon canaliculatum*, and the sea cucumber, *Sclerodactyla briareus*. Dr. Devlin's research is significant in assessing the effects of anti-arrhythmic and anti-hypertensive drugs, such as calcium blockers, on calcium channel activity in cardiac and smooth muscle.

- Gregg G. Gunderson, Ph.D., is an associate professor in the Department of Cell Biology and Anatomy at Columbia University in New York, New York. As the 1997 *Nikon Fellow*, Dr. Gunderson studied the dynamics and assembly of adhesion complexes during cell migration. Dr. Gunderson's research on the basic mechanism of cell motility may eventually aid clinicians' abilities to combat cancer and infectious diseases.

- Gwendolyn B. Howze, Ph.D., is an associate professor in the Biology Department of Texas Southern University. Dr. Howze's research at the MBL last summer was supported by the *William Townsend Porter Fellowship for Minority Investigators*, as well as an *MBL Associates Fellowship*. Dr. Howze did on-line research of DNA sequence databases. She characterized proteins that play a role in the condensation of chromatin. Chromatin is the mass of material that condenses into individual distinguishable chromosomes just before a cell nucleus divides. Dr. Howze's research may lead to a better understanding of certain pathologies that are due to abnormal gene expression.

- Samantha B. Joye, Ph.D., is an assistant professor in the Department of Oceanography at Texas A&M University. She was supported by an *MBL Associates Fellowship* and worked with Dr. Ivan Valiela during the summer of 1997. Dr. Joye studied the reduction of nitrogen loading to estuaries by denitrification in fringing salt marshes.

- Kamran Khodakhah, Ph.D., is a post-doctoral researcher in the Department of Physiology at the University of Pennsylvania School of Medicine. His research last summer was supported by the *H.B. Steinbach Fellowship*, the *Frederik B. Bang Fellowship Fund*, and an *MBL Associates Fellowship*. Dr. Khodakhah used the American eel and catfish to study the regulation of liver metabolism. His research may have applications in the treatment of diabetes.

- J.H.E.M. (Anka) Klerkx, M.Sc., is a graduate student in the Department of Experimental Zoology at Utrecht University, Utrecht, The Netherlands. Her research last summer was sponsored by the *Evelyn and Melvin Speigel Fellowship Fund*, the *James A. and Faith Miller Memorial Fund*, and the *Charles R. Crane Fellowship*. She studied the mechanisms that evolved to control development in the spiralians, *Chaetopterus* and *Nereis*.

- Donald L. Lovett, Ph.D., is an associate professor in the Department of Biology at The College of New Jersey in Trenton, New Jersey. His research was supported by the *John O. Crane Fellowship Fund*, the *Esther A. and Joseph Klingenstein Fund*, and an *MBL*

Associates Fellowship. Dr. Lovett studied the effects of methyl farnesoate on the cellular mechanisms of the green crab, *Carcinus maenas*. This research has potential economic applications in crustacean aquaculture and biomedical applications in the use of crustacean chitin, which is being examined for biomedical uses.

- Mark Q. Martindale, Ph.D., was supported by the *Erik B. Fries Endowed Fellowship* and an *MBL Associates Fellowship*. He is an assistant professor of Organismal Biology and Anatomy at the University of Chicago, Illinois. Dr. Martindale continued his research on the evolution of embryonic development. He studied the ctenophore, *Mnemiopsis leidyi*, and the flatworms, *Hoploplana*, *Neochilidia*, and *Stylochus*. His research could lead to a better understanding of birth defects.

- Allen Mensinger, Ph.D., is a research instructor in the Department of Otolaryngology at the Washington University School of Medicine, St. Louis, Missouri. His research was supported by a *NASA Life Sciences Program Fellowship* and the *Esther A. and Joseph Klingenstein Fund*. To understand nerve regeneration more fully, Dr. Mensinger studied the physiology of the toadfish, *Opsanus tau*.

- Charles G. Minkoff, B.A., is a graduate student in the Department of Molecular Cancer Biology at Duke University Medical Center in Durham, North Carolina. His work last summer was supported by the *Frank A. Brown, Jr. Memorial Readership*. Mr. Minkoff studied the effects of cholesterol-lowering drugs on the cell cycle in the surf clam, *Spisula solidissima*.

- Takehito Saito, Ph.D., is a professor in the Institute of Biological Sciences at the University of Tsukuba, Tsukuba, Japan. The *Herbert W. Rand Fellowship* supported Dr. Saito's research on the circadian rhythm of the horseshoe crab (*Limulus polyphemus*) eye. Dr. Saito hopes to gain a better understanding of how circadian clocks influence vision.

- Alastair Simpson, B.S., is a graduate student in the Protist Research Laboratory at the University of Sydney, Sydney, Australia. His work last summer on the evolutionary relationships among protozoa was supported by the *Bernard Davis Fund*. By illustrating the relationships among structurally primitive protists, Mr. Simpson hopes to gain insight into the evolution of cells and a better understanding of microbial biodiversity in sediments.

- Peter A. Siver, Ph.D., is a professor in the Department of Botany and Chair of the Environmental Studies Program at Connecticut College. His work was supported by the *Lucy B. Lemann Fellowship*. Dr. Siver studied the remains of golden algae (*Chrysophytes*) archived in lake sediments to understand more fully the effects of environmental stresses on aquatic resources.

- Timothy P. Spann, Ph.D., is a research associate in the Department of Cell and Molecular Biology at Northwestern University Medical School, Chicago, Illinois. He worked with Dr. Robert Goldman as a *NASA Life Sciences Program Fellow* and a *Frederik B. Bang Fellow*. Dr. Spann studied the organization of the surf clam (*Spisula*) nucleus as a model system to understand more fully the relationship between nuclear architecture and nuclear function. His research could lead to new methods of regulating cell growth and gene expression.

- Walter Steffen, Ph.D., is an assistant professor at the Institute of Biochemistry and Molecular Cell Biology in Vienna, Austria. He was a *Herbert W. Rand Fellow* and an *MBL Associates Fellow*. Dr. Steffen's research focused on the transport of membranous organelles by motor proteins in the frog, *Xenopus laevis*.

- Megumi Takahashi, M.D., Ph.D., is a psychiatrist at the Kanagawa Psychiatric Center in Yokohama, Japan. His research was supported by the *Stephen W. Kuffler Fellowship* and the *Ann E. Kammer Memorial Fellowship Fund*. Dr. Takahashi used the squid as a model for understanding the basic mechanisms of neurodegenerative diseases.

• Phong T. Tran, B.A., the *Robert Day Allen Fellow* and a *Lucy B. Lemann Fellow*, is a graduate student in the Department of Biology at the University of North Carolina, Chapel Hill. Last summer Mr. Tran continued his research using the digital polarization microscope to obtain images of microtubules within the spindles during mitosis and kinetochore fibers during chromosome movement. He used lung cells from the newt, *Taricha granulosa*.

• Matt Wachowiak, Ph.D., is a research associate in the Department of Molecular and Cell Biology at the University of California, Berkeley, California. His research on how the brain processes odors was supported by the *Esther A. and Joseph Klingenstein Fund* as well as an *MBL Research Fellowship*. Dr. Wachowiak studied how neurons in the brain of the Florida spiny lobster (*Panulirus argus*) process, code, and identify odors.

• E. Jennifer Weil, M.D., is a research fellow at the Josephine Bay Paul Center for Comparative Molecular Biology and Evolution at the Marine Biological Laboratory. Dr. Weil's research was supported by a *NASA Life Sciences Program Fellowship*. She investigated the evolution of the systems that control blood pressure and contribute to heart disease and other pathological states. She used the killifish, *Fundulus heteroclitus*, as a model. Her research could lead to a better understanding of diseases like congestive heart failure, nephrotic syndrome, and cirrhosis of the liver.

Grass Fellows

• Janet L. Casagrand, Ph.D., University of Colorado. Project: Pressure-sensitive auditory input to the mauthner cells in the goldfish: origin, response properties, and connectivity.

• John Gray, Ph.D., Queen's University, Canada. Project: Neural circuitry underlying a novel motor pattern expressed during metamorphosis of the hawkmoth *Manduca sexta*.

• Matthew Halstead, University of Auckland, New Zealand. Project: Electrophysiology of the electrosensory midbrain of the little skate *Raja erinacea* to biologically realistic stimuli.

• John Layne, Duke University Marine Laboratory. Project: Coordination of optokinesis and locomotion during course control in the fiddler crab, *Uca pugilator*.

• Mark Levandowski, Ph.D., Brown University. Project: Chimeric analysis of α -bungarotoxin binding sequences in nicotinic acetylcholine receptors.

• Quoc Thang Nguyen, Ph.D., University of California, Irvine. Project: Neurotransmitter synthesis in mRNA-injected *Xenopus* oocytes.

• Eleanora Palma, Ph.D., Regina Elena Cancer Research Institute, Italy. Project: Functional expression of neuronal nAChRs subunits in the lower vertebrate using *Xenopus* oocytes.

• Nadav Shashar, Ph.D., University of Maryland, Baltimore County. Project: Polarization sensitivity in cephalopods.

• Hiroshi Tokumaru, Ph.D., Duke University Medical Center. Project: The role of synapin/complexin in transmitter release at the squid giant synapse.

• Martina Wicklein, Ph.D., University of Arizona. Project: Motion sensitive neurons in the visual system of the fiddler crab.

MBL Science Writing Fellowships Program

Fellows

Marc Airhart, Assistant Producer, Earth & Sky Radio Series

Rita Baron-Faust, Producer, "Report on Medicine"

Steven Benowitz, Senior Editor, *The Scientist*

Lynne Cherry, Children's Book Author

Carol Ezzell, Science Editor, *Journal of NIH Research*

(Ms.) Ronny G. Frishman, Managing Editor, *INQUIRY*

John Fleischman, Freelance

Marguerite Holloway, Contributing Editor, *Scientific American*

Meredith Small, Freelance

Terra Ziporyn, Freelance

Program Directors

Robert D. Goldman, Northwestern University

Boyce Rensberger, *The Washington Post*

Hands-On Laboratory Course Directors

Rex Chisholm, Northwestern University

Robert Palazzo, University of Kansas

Hands-On Laboratory Course Instructors

Shuo Ma, Northwestern University

Brad Schnackenberg, University of Kansas

Wendy Wolf, Northwestern University

SPINES—Summer Program in Neuroscience Ethics and Survival

SPINES is a month-long program directed by Joe L. Martinez, Jr., and James Townsel. The program is supported by grants from NIMH administered by the American Psychological Association and the Association of Neuroscience Departments and Programs. SPINES offers an introduction to the opportunities available at the MBL and in the field of neuroscience in general. Fellows are taught responsible conduct in research and other survival skills such as scientific writing, poster construction, presentations, grant mechanisms, and how to seek a postdoctoral or job position.

Predoctoral

Adwoa Aduonum-McKinney

Marcus McFarren

Jonathan Reasor

Dani Smith

Kenira Thompson

Desiree Villarreal

Nicole Wicha

Postdoctoral

Gary O. Gaufo

Scholarships Awarded

Aline D. Gross Scholarship Fund

Brown, Elizabeth A., Medical College of Virginia

American Society for Cell Biology Minorities Affairs Committee

Chitwood, Randy, University of Texas, San Antonio
DePass, Anthony, University of Massachusetts, Amherst
McKnight, Spontaneous, University of Arizona
Norman, Eric, University of Pittsburgh
Quintero, Omar, Duke University Medical Center
Reese, Eric, University of California

Arthur Klorfein Scholarship Fund

Cooper, Brian, National Institute of Medical Research, London, UK
Damen, Wim, University of Munich (LMU), Germany
Melfi, Raffaella, Universita Delgi Studi di Palermo, Italy

Biology Club of the City of New York Scholarships Fund

Yamaguchi, Ayako, Columbia University

Burroughs Wellcome Fund—Biology of Parasitism Course

Brouwer, Kimberly, Johns Hopkins School of Public Health
Camargo, Maristela, Federal University of Minas Gerais, Brazil
Gantt, Soren, New York University Medical Center
Gleeson, Michelle, University of Technology, Sydney, Australia
Hensmann, Meike, Yale School of Public Health
Jiang, David, Johns Hopkins University
Lingnau, Andreas, Washington University Medical School
Mair, Gunnar, Queen's University of Belfast, UK
Marsh, Antoinette, University of California, Davis
Onko, Lillian, University of Pennsylvania
Treutiger, Carl Johan, Karolinska Institute, Sweden
Wille, Ulrike, University of Tübingen, Germany

Burroughs Wellcome Fund—Molecular Mycology Course

Buchanan, Kent, University of Oklahoma Health Sciences Center
Clarke, Enda E., Royal Postgraduate Medical School, London, UK
Doering, Tamara, Cornell Medical School
Hopfer, Roy, University of North Carolina Hospitals
Mathews, Herbert, Loyola University of Chicago
Zhang, Mason, University of Nevada

Caswell Grave Scholarship Fund

Evans, Kelly L., Queen's University, Canada
Osborne, Leslie, University of California, Berkeley
Thongmee, Acharawan, University of North Texas

C. Lalor Burdick Fellowship Fund

Melfi, Raffaella, Universita Delgi Studi di Palermo, Italy

Daniel S. Grosch Endowed Scholarship Fund

Johnson, Hope, Stanford University
Vasconcelos, Crisogono, Universidade Federal Fluminense, Brazil

Edwin Grant Conklin Scholarship Fund

Wenuganen, S., Bogor Agricultural University, Indonesia

Frank R. Lillie Scholarship Fund

Davis, Gregory, University of Chicago
de Sa, Virginia R., University of California, San Francisco
Stone, Alexandra, Ohio State University
Valster, Aline, University of Massachusetts
Wang, Gang, University of Iowa

Gary Nathan Calkins Memorial Scholarship Fund

Giuliano, Paola, Stazione Zoologica, Italy

Herbert W. Rand Scholarship Fund

Giuliano, Paola, Stazione Zoologica, Italy
Kaufmann, Christoph, Massachusetts General Hospital, Boston
Ladurner, Peter P., University of Innsbruck, Austria
Lerchner, Walter, National Institute for Medical Research,
London, UK
Takke, Christina, University of Köln, Germany

Howard A. Schneiderman Endowed Scholarship Fund

Hess, Samuel, Cornell University

Howard Hughes Medical Institute Educational Program Scholarship Funding

Aanstad, Pia, University of Newcastle upon Tyne, UK
Bacci, Alberto, University of Milano, Italy
Bayliss, Richard, University of Cambridge, UK
Faure, Jean-Emmanuel, University of California
Gasser, Paul, Arizona State University
Gries, Gundula, University of Pennsylvania
Hess, Samuel, Cornell University
Holzmann, Maria, University of Geneva, Switzerland
Karthikeyan, G., Tata Institute of Fundamental Research, India
Nelson, Craig, Harvard University
Nilsson, Helen, University of Göteborg, Sweden
Ozoren, Nesrin, University of Pennsylvania
Polnaú, Dorit, Northeastern University
White, Kathryn, Scripps Institute of Oceanography
Zurek, Ludek, University of Alberta

Jacques Loeb Founder's Scholarship Fund

Ketelaar, Tijs J., Wageningen Agricultural University,
The Netherlands

Marjorie Roloff Stetten Scholarship Fund

Krause, Sabine, Max-Planck-Institut für Molekulare Genetik,
Germany

Massachusetts Space Grant Consortium

Blank, Carrine, University of California, Berkeley
Gaidos, Eric, Massachusetts Institute of Technology

Merek and Company, Inc.

Shoda, Lisl, Washington State University
Treutiger, Carl Johan, Karolinska Institute, Sweden
Triplett, Elisabeth, Cornell University
Villegas, Eric, University of Pennsylvania
Wille, Ulrike, University of Tübingen, Germany

Moshe Shilo Memorial Scholarship Fund

Banin, Ehud, Tel Aviv University, Israel

Mountain Memorial Fund

Bayliss, Richard, University of Cambridge, UK
Bell, George, University of Arizona
Broome, Jill, University of North Carolina, Chapel Hill
Diggins, John, Providence College
Ozoren, Nesrin, University of Pennsylvania
Ream, Rachael A., Stanford University, Hopkins Marine Station

**Phillip H. Presley Memorial Scholarships,
Carl Zeiss, Inc.**

Bauer, Eric, University of Texas, Austin
Bonham, Ben, University of California, San Francisco
Broome, Jill, University of North Carolina, Chapel Hill
Hughes, Deborah, Scripps Institution of Oceanography
Jaspers, Elke, Universität Oldenburg, Germany
Kilroy, Christopher, University of North Carolina, Wilmington
Ream, Rachael A., Stanford University, Hopkins Marine Station

Pioneers Fund

Barghuthy, Fikry, The Hebrew University of Jerusalem, Israel
Evans, Kelly L., Queen's University, Canada

Planetary Biology Internships

Johnson, Hope, Stanford University
Vasconcelos, Crisogono, Universidade Federal Fluminense, Brazil

Post-Course Research Awards

Dale L. Beach, University of North Carolina, Chapel Hill, Physiology
Julie Canman, University of North Carolina, Chapel Hill, Physiology
Gregory Davis, University of Chicago, Embryology
Anthony DePass, University of Massachusetts, Amherst, Physiology
Gundula E. Gries, University of Pennsylvania, Physiology
Xiang Dong (Edward) Guo, Columbia University, Physiology
Kaoru Katoh, University of Tsukuba, Japan, Physiology
Matteus Ketelaar, Wageningen Agricultural University,
The Netherlands, Physiology
Peter Ladurner, University of Innsbruck, Austria, Embryology
Susan Laessig, University of Maryland, Baltimore, Neural Systems
& Behavior
Laura Linz, Louisiana State University, Physiology

S. O. Mast Founders' Scholarship Fund

Meyer, Axel, State University of New York

Society of General Physiologists' Scholarships

Gregory K. Davis, University of Chicago
Timothy E. Holy, Princeton University
Justin S. Koble, Children's Hospital of Pennsylvania

Surdna Foundation

Banin, Ehud, Tel Aviv University, Israel
Jaspers, Elke, Universität Oldenburg, Germany
Krause, Sabine, Max-Planck-Institut für Molekulare Genetik,
Germany
Wenuganen, S., Bogor Agricultural University, Indonesia
Zurek, Ludek, University of Alberta, Canada

Walter L. Wilson Endowed Scholarship Fund

Katoh, Kaoru, Marine Biological Laboratory
Nilsson, Helen, University of Göteborg, Sweden

William F. and Irene C. Diller Scholarship Fund

Melli, Raffaella, Università Degli Studi di Palermo, Italy
Stone, Alexandra, Ohio State University

**William Morton Wheeler Family Founder's
Scholarship Fund**

Wenuganen, S., Bogor Agricultural University, Indonesia

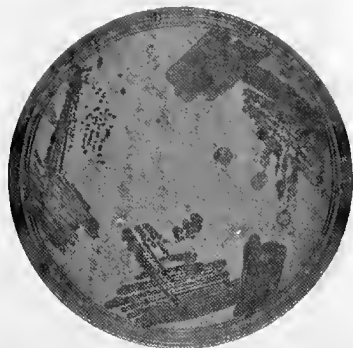
**William Randolph Hearst Educational
Endowment Scholarships**

Kim, Warren, Yale University School of Medicine
Nelson, Craig, Harvard University
Shelton, Marilee, University of North Carolina, Chapel Hill

William Townsend Porter Scholarship Fund

DePass, Anthony, University of Massachusetts, Amherst
McKnight, Spontaneous, University of Arizona
Norman, Eric, University of Pittsburgh
Quintero, Omar, Duke University Medical Center

Paul Maddox, University of North Carolina, Chapel Hill, Physiology
Lynne Merchant, University of California, San Diego, Neural
Systems & Behavior
Helen Nilsson, University of Göteborg, Sweden, Physiology
Yasushi Satoh, University of Tokyo, Japan, Physiology
Elaine Seaver, University of Texas, Austin, Embryology
Sen Song, Brandeis University, Neural Systems & Behavior
Aline Valster, University of Massachusetts, Amherst, Physiology
Cris Vasconcelos, ETH Zentrug, Zurich, Switzerland,
Microbial Diversity
Gang Wang, University of Iowa, Physiology
S. Wenuganen, Bogor Agricultural University, Indonesia,
Microbial Diversity



Board of Trustees and Committees

Corporation Officers and Trustees

Chairman of the Board of Trustees, Sheldon J. Segal, The Population Council

Co-vice Chair of the Board of Trustees, Frederick Bay, Josephine Bay Paul and C. Michael Paul Foundation

Co-vice Chair of the Board of Trustees, Mary J. Greer, New York, NY

President of the Corporation, James D. Ebert, The Johns Hopkins University

Director and Chief Executive Officer, John E. Burris, Marine Biological Laboratory*

Treasurer of the Corporation, Mary B. Conrad, Fiduciary Trust International*

Clerk of the Corporation, Neil Jacobs, Hale and Dorr

Chair of the Science Council, Ronald L. Calabrese, Emory University*

Class of 1998

Norman Bernstein, Diane and Norman Bernstein Foundation, Inc.

John R. Lakian, The Fort Hill Group, Inc.

Joan V. Ruderman, Harvard Medical School

Sheldon J. Segal, The Population Council

William T. Speck, Columbia-Presbyterian Medical Center

Alfred Zeien, The Gillette Company

Class of 1999

Mary-Ellen Cunningham, Grosse Pointe Farms, MI

Neil Jacobs, Hale and Dorr

Darcy Brisbane Kelley, Columbia University

Laurie J. Landeau, Marinetics, Inc.

Burton J. Lee, III, Edgartown, MA

Robert E. Mainer, The Boston Company

Class of 2000

Alexander W. Clowes, University of Washington School of Medicine

Story C. Landis, Case Western Reserve University

Irwin B. Levitan, Brandeis University

G. William Miller, G. William Miller & Co., Inc., Washington, DC

Frank Press, Carnegie Institution of Washington, DC

Christopher M. Weld, Sullivan & Worcester, Boston

Class of 2001

Porter Anderson, North Miami Beach, FL

Frederick Bay, Josephine Bay Paul and C. Michael Paul Foundation, Inc.

Martha W. Cox, Hobe Sound, FL

Mary J. Greer, New York, NY

William C. Steere, Jr., Pfizer Inc.

Gerald Weissmann, New York University School of Medicine

Honorary Trustees

William T. Golden, New York, NY

Ellen R. Grass, The Grass Foundation

Trustees Emeriti

Edward A. Adelberg, Yale University, New Haven, CT

John B. Buck, Sykesville, MD

Seymour S. Cohen, Woods Hole, MA

Arthur L. Colwin, Key Biscayne, FL

Laura Hunter Colwin, Key Biscayne, FL

Donald Eugene Copeland, Woods Hole, MA

Sears Crowell, Indiana University, Bloomington, IN

Alexander T. Daignault, Falmouth, MA

Teru Hayashi, Woods Hole, MA

Ruth Hubbard, Cambridge, MA

Lewis Kleinholz, Reed College, Portland, OR

Maurice E. Krahl, Tucson, AZ

Charles B. Metz, Miami, FL (deceased)

Keith R. Porter, University of Pennsylvania, Philadelphia, PA (deceased)

C. Ladd Prosser, University of Illinois, Urbana, IL

W. D. Russell-Hunter, Syracuse University, Syracuse, NY

Mary Sears, Woods Hole, MA (deceased)

David Shepro, Boston University, Boston, MA

D. Thomas Trigg, Wellesley, MA

Walter S. Vincent, Woods Hole, MA

George Wald, Cambridge, MA (deceased)

**Ex officio*

Science Council

Ronald L. Calabrese, Chair
Donald Abt
Clay Armstrong
Robert Barlow, Jr. (from 8/97)
Kerry S. Bloom
John Burris,*
Vincent E. Dionne (from 8/97)
John Dowling
Barbara Ehrlich
Bruce J. Peterson (1998)
Mitch Sogin (1998)
Ann E. Stuart (ending 8/97)

Executive Committee of the Board of Trustees

Sheldon J. Segal, Chair
Frederick Bay, Co-vice Chair
Mary J. Greer, Co-vice Chair
John E. Burris*
Ronald L. Calabrese
Mary B. Conrad
Mary-Ellen Cunningham
Robert Mainer
Joan V. Ruderman
Gerald Weissmann

Standing Committees of the Board of Trustees

Development

Mary-Ellen Cunningham, Chair
Porter W. Anderson
Robert Barlow
Frederick Bay
Mary B. Conrad
Martha Cox
James Ebert
Neil Jacobs
John Lakian
Burton Lee
Irwin Levitan
G. William Miller
William Speck
William Steere
Christopher Weld

Finance and Investment

Robert Mainer, Chair
Norman Bernstein
Alexander Clowes
Mary B. Conrad
Donald DeHart
Neil Jacobs
Darcy Kelley
John Lakian
Laurie Landeau
Werner Loewenstein
Robert Manz
G. William Miller
Ronald P. O'Hanley
Irving Rabb
Alfred Zeien

Facilities and Capital Equipment

Joan Ruderman, Chair
Porter W. Anderson
Lawrence Cohen
Neal Cornell
Story Landis
Irwin Levitan
Frank Press
Christopher M. Weld

Nominating

Gerald Weissmann, Chair
Ronald Calabrese
Alexander Clowes
Martha Cox
Mary-Ellen Cunningham
Mary Greer
Story Landis
Tom Pollard
Sheldon Segal
William Steere

Standing Committees of the Corporation and Science Council

Buildings and Grounds

Lawrence B. Cohen, Chair
Barbara C. Boyer
Alfred B. Chaet
Richard Cutler*

William R. Eckberg
Barry Fleet*
Ferenc Hárosi
Joe Hayes*
Bruce J. Peterson
Kenyon S. Tweedell

**Ex officio*

Education

John E. Dowling, Chair
 Elaine L. Bearer
 Vincent E. Dionne
 Paul V. Dunlap
 Rachel D. Fink
 Roger T. Hanlon
 Holger W. Jannasch
 George M. Langford
 Dorianne Mebane*
 Michael E. Mendelsohn
 John D. Rummel*
 Steven J. Zottoli

Fellowships

Thoru Pederson, Chair
 Kathleen Dunlap
 Barbara E. Ehrlich
 Anne E. Giblin
 José Lemos
 Carol L. Reinisch
 John D. Rummel*

Housing, Food Service, and Child Care

Kerry S. Bloom
 Carole L. Browne
 LouAnn King*
 Robert P. Malchow
 Darrell R. Stokes
 Ann E. Stuart
 Janis C. Weeks

MBL/WHOI Library Joint Advisory Committee

David Shepro, Chair, MBL
 Judy Ashmore, MBL*
 Cabell Davis, WHOI
 David Dow, NMFS
 John Hobbie, MBL
 Colleen Hurter, WHOI*
 Mark Kurz, WHOI
 Cathy Norton, MBL*
 Monica Riley, MBL
 Jim Robb, USGS
 Peter J. S. Smith, MBL
 Bruce Warren, WHOI

Research Services and Space

Hans Laufer, Chair
 Peter B. Armstrong
 Neal W. Cornell
 Richard Cutler*
 Kenneth H. Foreman
 Louis M. Kerr
 David Landowne
 Andy Mattox*
 Jerry M. Melillo
 Merle Mizell
 Peter J. S. Smith
 Paul A. Steudler
 Ivan Valiela

Discovery: The Campaign for Science at the Marine Biological Laboratory Steering Committee

Frederick Bay, Campaign Chair
 William T. Golden, Honorary Campaign Chair
 Ellen R. Grass, Honorary Campaign Chair
 Alexander Clowes, Campaign Vice-chair
 Martha W. Cox, Campaign Vice-chair
 G. William Miller, Campaign Vice-chair
 Gerald Weissmann, Campaign Vice-chair
 Porter Anderson
 Robert B. Barlow, Jr.
 Norman Bernstein
 Jewel Plummer Cobb
 Mary B. Conrad
 Mary-Ellen Cunningham
 John E. Dowling

James D. Ebert
 Gerald D. Fischbach
 Robert D. Goldman
 Mary J. Greer
 M. Howard Jacobson
 Laurie J. Landeau
 George M. Langford
 Burton J. Lee, III
 Robert A. Prendergast
 David Shepro
 William T. Speck
 William C. Steere, Jr.
 Christopher M. Weld, Esq.
 Alfred M. Zeien

*Ex officio

Administrative Support Staff¹

Biological Bulletin

Greenberg, Michael J., Editor-in-Chief
Clapp, Pamela L., Managing Editor
Burns, Patricia
DeBenedictis, Lisa M.
Gibson, Victoria R.
Pennington, Susan M.
Schachinger, Carol H.

Financial Services Office

Roddy, Timothy, Chief Financial Officer
Bowman, Richard, Controller
Ghetti, Pamela M., Controller
Afonso, Janis
Cornette, Ruth
Dwyer, Patricia E.
Hopkins, Ann E.
Iwaszko, Roxanne M.²
Lancaster, Cindy
Pacheco, Anthony F.²
Palmer, Pamela²
Poravas, Maria
Ranzinger, Laura
Sprague, Patricia A.
Stark, Judy

Stock Room

Schorer, Timothy M., Supervisor
Cameron, Alicia A.²
Nelson, Beth A.
O'Connor-Lough, Susan
Robinson, Mary M.²

Purchasing

Hall Jr., Lionel E., Supervisor
Mancini, Mary
Nelson, Beth A.
Shamon, Lynne R.²
Stone, Janice G.²



Director's Office

Burris, John E., Director and Chief Executive Officer
Burthuis, I. Elaine
Donovan, Marcia H.
MacNeil, Jane L.

External Affairs

Carotenuto, Frank C., Director
Black, Nancy O.
Faxon, Wendy P.
Martin, Theresa H.
Martinez, Mario R.²
Maxwell, Thanh L.²
Patch-Wing, Dolores
Quigley, Barbara A.
Scibek, John C.
Shaw, Kathleen L.
Wessling, Gail M.
Wicklund, Eileen R.

Associates Program

Bohr, Kendall B.
Pratt, Jennifer A.²

Communications Office

Clapp, Pamela, L. Director
Clowes, Sarah W.²
Dykstra, Margaret L.²
Furfey, Susan C.²
Kenna, Laura M.
Liles, Beth R.
Pratt, Sara
Williams, Sara V.

Housing and Conferences

King, LouAnn D., Director
Barry, Manreen J.
Johnson, Frances N.
Hanlon, Arlene K.²

Switchboard

Baker, Ida M.
Dunn-Fall, Martha F.²
Ridley, Alberta W.

¹ Including persons who joined or left the staff during 1997.

² Summer or temporary.

Human Resources

Goux, Susan P., Director
 Donovan, Marcia H.
 Drange, Stacey B.

Marine Resources Center Administrative Staff

Hanlon, Roger T., Director
 Moniz, Priscilla

Aquatic Resources Department

Enos, Jr., Edward G., Superintendent
 Bourque, Ryan M.²
 Chappell, P. Dreux²
 DeGiorgis, Joseph A.²
 Erlingsson, Erik C.²
 Freeman, Darren M.²
 Grossman, William M.
 Klimm III, Henry W.
 Luther, Herbert
 Mansfield, Darren P.²
 Parent, Scott M.²
 Schneider, Peter J.²
 Sexton, Andrew W.
 Sullivan, Daniel A.
 Tassinari, Eugene

MRC Life Support System

Mebane, William N., Systems Operator
 Hanley, Janice S.
 Kuzirian, Alan
 Stukey, Jetley M.
 Till, Geoffrey A.

MBLWHOI Library

Norton, Catherine N., Director
 Ashmore, Judith A.
 Connelly, Michelle F.A.
 Costa, Marguerite E.
 Cullen, Cynthia M.²
 Deveer, Joseph M.
 Duda, Laurel E.
 Farrar, Stephen R. L.
 Jackson, James R.
 Medeiros, Melissa
 Monahan, A. Jean
 Moniz, Kimberly L.
 Nelson, Heidi
 Pratson, Patricia F.
 Riley, Jacqueline
 Ulbrich, Ciona²
 Zuwallack, Barbara
 Zuwallack, Raymond
 Zuwallack, Ronald L.

Copy Center

Mountford, Rebecca J., Supervisor
 Abisla, Richard L.²
 Adams, Cathryn L.²
 Clark, Tamara L.²
 Johnson, Courtney M.²
 Kefeauver, Lee
 LaPlante, Robert F.

Mancini, Mary E.
 Warner, Kathleen²

Information Systems Division

Smith, Adrian P., Assistant Director
 Ennis, Douglas E.²
 Gage, Timothy J.²
 Mahoney, Timothy P.
 Moynihan, James V.
 Mountford, Rebecca J.
 Remsen, David P.
 Renna, Denis J.
 Space, David B.
 Swasey, Anne E.²

Safety Services

Mattox, Andrew H., Environmental, Health, and Safety Manager
 Kelly, Niamh O.²
 O'Neill, Maureen D.²

Service, Projects, and Facilities

Cutler, Richard D., Director
 Enos, Joyce B.

Apparatus

Baptiste, Michael G.
 Barnes, Franklin D.
 Haskins, William A.

Building Services and Grounds

Hayes, Joseph H., Superintendent
 Anderson, Lewis B.
 Atwood, Paul R.
 Baker, Harrison S.
 Barnes, Susan M.
 Berrios, Jessica L.²
 Boucher, Richard L.
 Brereton, Richard S.²
 Callahan, John J.
 Cameron, Lawrence M.²
 Collins, Paul J.
 Cowan, Matthew B.²
 Cutler, Matthew D.²
 Dole, Adam J.²
 Dorris, John J.
 Fernandez, Peter R.²
 Gibbons, Roberto G.
 Gonsalves, Nelson
 Hannigan, Catherine
 Harrington, James D.
 Illgen, Robert F.
 Kennette, Kirsten E.²
 Lawrence, Adam G.²
 Lawson, Christina C.²
 Leary, Jason C.²
 Luther, Herbert
 Lynch, Henry L.
 Maccaro, Jackie
 McNamara, Noreen M.
 Massey Eric²
 Rattacasa, Frank D.
 Sholkovitz, Nathan²

Schrontz, Mathieu D.²
Silva, Cynthia C.
Wessling, Kellen A.²
Varao, John²
Ware, Lynn M

Plant Operations and Maintenance

Fleet, Barry M., Superintendent
Barnes, John S.
Blunt, Hugh F.
Bourgoin, Lee E.
Cadose, James W.
Carini, Robert J.
Carroll, James R.
Fish Jr., David L.
Fuglister, Charles K.
Gonsalves, Jr., Walter W.
Hathaway, Peter J.
Henderson, Jon R.
Justason, C. Scott
Lochhead, William M.
McAdams III, Herbert M.
McHugh, Michael O.
Mills, Stephen A.
Olive, Jr., Charles W.
Schoepf, Claude
Serrano, Robert A.
Shepherd, Denise M.
Toner, Michael

Machine Shop

Sylvia, Frank E.
Wetzel, Ernest D.²

Photolab

Nelson, Linda M., Supervisor
Clark, Tamara L.²
Golder, Robert J.
Hong, Theresa H.²
Richmond, Hazel E.²

Research Administration and Educational Programs

Rummel, John D., Director
Barry, Kevin²
Chandler, Marsha J.
Hamel, Carol C.
Hunt, Sharon L.
Huffer, Linda
Kaufmann, Sandra J.
Mebane, Dorianne C.
Moynihan, Brenda L.²

Central Microscopy Facility and General Use Rooms
Kerr, Louis M., Supervisor
DeProto, Jamin E.²
Lavalli, Kari Lee²
Peterson, Martha B.
Soucy, Lori A.²

*Josephine Bay Paul Center for Comparative Molecular
Biology and Evolution Administrative Staff*

Amit, Udeni

Journal of Membrane Biology

Loewenstein, Werner R., Editor
Cicora, Judith M.²
Fay, Catherine H.
Howard, Linda L.
Lynch, Kathleen F.

*NASA Center for Advanced Studies in the Space Life
Sciences Administrative Staff*

Dawidowicz, Eliezar A., Administrator
Amit, Udeni P.
Nixon, Jennifer L.

Satellite/Periwinkle Children's Programs

Robinson, April²
Robinson, Paulina H.²
Brown, Shannon K.²
Browne, Jennifer L.²
Douglas, Alicia D.²
Gallant, Carolyn A.²
Griffin, Courtney A.²
Lee, Annette M.²
Martinez, Adria E.²
Robinson, Jayma L.²
Robinson, Milton G.²
Simpson, Christopher F.²
Strout, Kerry L.²

Ecosystems Center Administrative Staff

Berthel, Dorothy J.
Donovan, Suzanne J.
Nunez, Guillermo
Seifert, Mary Ann



Members of the Corporation¹

Life Members

- Acheson, George H.**, 25 Quissett Avenue, Woods Hole, MA 02543
- Adelberg, Edward A.**, Lincoln Tower Apt. 802, 2400 Presidential Way, West Palm Beach, FL 33401
- Afelius, Bjorn**, University of Stockholm, Wenner-Gren Institute, Department of Ultrastructure Research, Stockholm, SWEDEN
- Amatnick, Ernest**, 1112 Northwest 5th Avenue, Gainesville, FL 32601
- Arnold, John M.**, 329 Sippewissett Road, Falmouth, MA 02540
- Bang, Betsy G.**, 76 F. R. Lillie Road, Woods Hole, MA 02543
- Bartlett, James H.**, University of Alabama, Department of Physics, Box 870324, Tuscaloosa, AL 35487-0324
- Berne, Robert M.**, University of Virginia School of Medicine, Dept. of Physiology, Box 1116, MR4, Charlottesville, VA 22903
- Bernheimer, Alan W.**, New York University Medical Center, Dept. of Microbiology, 550 First Avenue, New York, NY 10016
- Bertholf, Lloyd M.**, Westminster Village, #2114, 2025 E. Lincoln Street, Bloomington, IL 61701-5995
- Bosch, Herman F.**, Box 617, Woods Hole, MA 02543
- Buck, John B.**, 7200 Third Avenue, #C-020, Sykesville, MD 21784
- Burbanck, Madeline P.**, Box 15134, Atlanta, GA 30333
- Burhanek, William D.**, P.O. Box 15134, Atlanta, GA 30333
- Carlson, Francis D.**, Johns Hopkins University, Biophysics Dept., Jenkins Hall, N. Charles Street, Baltimore, MD 21218
- Clark, Arnold M.**, 53 Wilson Road, Woods Hole, MA 02543
- Clark, James M.**, 210 Emerald Lane, Palm Beach, FL 33480
- Cohen, Seymour S.**, 10 Carrot Hill Road, Woods Hole, MA 02543
- Colwin, Arthur L.**, 320 Woodcrest Road, Key Biscayne, FL 33149-1322
- Colwin, Laura Hunter**, 320 Woodcrest Road, Key Biscayne, FL 33149
- Cooperstein, Sherwin J.**, University of Connecticut, School of Medicine, Department of Anatomy, Farmington, CT 06030-3405
- Copeland, D. Eugene**, 41 Fern Lane, Woods Hole, MA 02543
- Corliss, John O.**, P.O. Box 2729, Bala Cynwyd, PA 19004-2116
- Costello, Helen M.**, Carolina Meadows, Villa 137, Chapel Hill, NC 27514-8512
- Crouse, Helen**, Rte. 3, Box 213, Hayesville, NC 28904
- DeHaan, Robert L.**, Emory University School of Medicine, Department of Anatomy and Cell Biology, 1648 Pierce Drive, Rm. 108, Atlanta, GA 30322
- Dudley, Patricia L.**, 3200 Alki Avenue SW, #401, Seattle, WA 98116
- Edwards, Charles**, 2244 Harbour Court Drive, Longboat Key, FL 34228
- Elliott, Gerald F.**, The Open University Research Unit, Foxcombe Hall, Berkeley Road, Boars Hill, Oxford OX1 5HR, UK
- Failla, Patricia M.**, 2149 Loblolly Lane, Johns Island, SC 29455
- Ferguson, James K. W.**, 56 Clarkehaven Street, Thornhill, Ontario L4J 2B4, Canada
- Glusman, Murray**, New York State Psychiatric Institute, 722 W. 168 Street, Unit #70, New York, NY 10032
- Goldman, David E.**, 140 Ter Heun Drive, Rm 212, Falmouth, MA 02540
- Graham, Herbert**, 36 Wilson Road, Woods Hole, MA 02543
- Hamburger, Viktor**, Washington University, Department of Biology, 740 Trinity Avenue, St. Louis, MO 63130
- Hamilton, Howard L.**, University of Virginia, Department of Biology, 238 Gilmer Hall, Charlottesville, VA 22901
- Harding, Clifford V.**, 54 Two Ponds Road, Falmouth, MA 02540
- Haschemeyer, Audrey E. V.**, 21 Glendon Road, Woods Hole, MA 02543-1406
- Hauschka, Theodore S.**, 333 Fogler Road, Bremen, ME 04551
- Hayashi, Teru**, 15 Gardiner Road, Woods Hole, MA 02543-1113
- Hisaw, Frederick L.**, 1765 SW Tamarack Street, Apt 11, McMinnville, OR 97128-7416
- Hoskin, Francis C. G.**, c/o Dr. John E. Walker, U.S. Army Natick RD&E Center, SAT NC-YSM, Kansas Street, Natick, MA 01760-5020
- Hubbard, Ruth**, Harvard University, Biological Laboratories, Cambridge, MA 02138
- Humes, Arthur G.**, Marine Biological Laboratory, Boston University Marine Program, Woods Hole, MA 02543
- Hnrwitz, Charles**, Stratton VA Medical Center, Research Service, Albany, NY 12208
- Katz, George**, Merck, Sharp and Dohme, Fundamental & Experimental Research Laboratory, P.O. Box 2000, Rahway, NJ 07065
- Kingsbury, John M.**, Cornell University, Dept. of Plant Biology, Plant Science Building, Ithaca, NY 14853

¹ Including action of the 1997 Annual Meeting.

R66 Annual Report

- Kleinholz, Lewis**, Reed College, Department of Biology, 3203 SE Woodstock Blvd., Portland, OR 97202
- Laderman, Ezra**, Yale University, New Haven, CT 06520
- LaMarche, Paul H.**, Eastern Maine Medical Center, 489 State Street, Bangor, ME 04401
- Lauffer, Max A.**, Penn State University Medical Center, Dept. of Biophysics & Physiology, Hershey, PA 17033
- LeFevre, Paul G.**, 15 Agassiz Road, Woods Hole, MA 02543
- Levine, Rachmiel**, City of Hope Medical Center, Shapiro Building, Duarte, CA 91010 (deceased)
- Lochhead, John H.**, 49 Woodlawn Road, London SW6 6PS, UK
- Loewus, Frank A.**, Washington State University, Institute of Biological Chemistry, Pullman, WA 99164
- Lofffield, Robert B.**, University of New Mexico, School of Medicine, Albuquerque, NM
- Malkiel, Saul**, Allergic Diseases Inc., 130 Lincoln Street, Worcester, MA 01609
- Marsh, Julian B.**, Medical College of Pennsylvania, Dept. of Physiology & Biochemistry, Philadelphia, PA 19129
- Martin, Lowell V.**, 10 Buzzards Bay Avenue, Woods Hole, MA 02543
- Mathews, Rita W.**, East Hill Road, P.O. Box 237, Southfield, MA 01259-0237
- Moore, John A.**, University of California, Department of Biology, Riverside, CA 92521
- Moscona, A. Aaron**, University of Chicago, Dept. of Molecular Genetics & Cell Biology, 920 East 58 Street, Chicago, IL 60637
- Musacchia, X. J.**, P.O. Box 5054, Bella Vista, AR 72714-0054
- Nasatir, Maimon**, P.O. Box 379, Ojai, CA 93024
- Passano, Leonard M.**, University of Wisconsin, Department of Zoology, Birge Hall, Madison, WI 53706
- Prosser, C. Ladd**, University of Illinois, Dept. of Physiology, 524 Burrill Hall, Urbana, IL 61801
- Prytz, Margaret McDonald**, address unknown
- Ratner, Sarah**, Public Health Research Institute, Department of Biochemistry, 455 First Avenue, New York, NY 10016
- Renn, Charles E.**, address unknown
- Reynolds, George T.**, Department of Physics, Princeton University, Jadwin Hall, Princeton, NJ 08544
- Rice, Robert V.**, 30 Burnham Drive, Falmouth, MA 02540
- Rockstein, Morris**, 600 Biltmore Way, Apartment 805, Coral Gables, FL 33134
- Ronkin, Raphael R.**, 3212 McKinley Street, NW, Washington, DC 20015-1635
- Sanders, Howard L.**, Woods Hole Oceanographic Institute, Woods Hole, MA 02543
- Sato, Hidemi**, Professor Emeritus, Nagoya University, 3-24-101, Oakinishi Machi, Toba Mie 517-0023, Japan
- Saz, Arthur K.**, Georgetown University Medical School, Department of Immunology, Washington, DC 20007
- Schlesinger, R. Walter**, 7 Langley Road, Falmouth, MA 02540-1809
- Scott, Allan C.**, Colby College, Waterville, ME 04901
- Silverstein, Arthur M.**, John Hopkins University, Institute of the History of Medicine, 1900 E. Monument Street, Baltimore, MD 21205
- Sjodin, Raymond A.**, University of Maryland, Department of Biophysics, Baltimore, MD 21201
- Smith, Paul F.**, P.O. Box 264, Woods Hole, MA 02543-0264
- Sonnenblick, Benjamin P.**, 515A Heritage Hill Village, Southbury, CT 06488 (deceased)
- Speer, John W.**, 293 West Main Road, Portsmouth, RI 02871
- Spereklakis, Nicholas**, University of Cincinnati, Dept. of Physiol./Biophysics, 231 Bethesda Avenue, Cincinnati, OH 45267-0576
- Spiegel, Evelyn**, Dartmouth College, Dept. of Biological Sciences, 204 Gilman, Hanover, NH 03755
- Spiegel, Melvin**, Dartmouth College, Dept. of Biological Sciences, 204 Gilman, Hanover, NH 03755
- Steinhardt, Jacinto**, 1508 Spruce Street, Berkeley, CA 94709
- Stephens, Grover C.**, University of California, School of Biological Sciences, Dept. of Ecology & Evolutionary/Biology, Irvine, CA 92717
- Strehler, Bernard L.**, 2310 N. Laguna Circle Drive, Agoura, CA 91301-2884
- Sussman, Maurice**, 72 Carey Lane, Falmouth, MA 02540
- Sussman, Raquel B.**, Marine Biological Laboratory, Woods Hole, MA 02543
- Szent-Gyorgyi, Gwen P.**, 45 Nobska Road, Woods Hole, MA 02543
- Taylor, Robert E.**, 339 Gifford Street, Apt. 303, Falmouth, MA 02540
- Thorndike, W. Nicholas**, Wellington Management Company, 200 State Street, Boston, MA 02109
- Trager, William**, The Rockefeller University, 1230 York Avenue, New York, NY 10021-6399
- Trinkaus, J. Philip**, Yale University, Dept. of Biology, New Haven, CT 06511
- Villee, Claude A.**, Harvard Medical School, Carrel L. Countway Library, 10 Shattuck Street, Boston, MA 02115
- Vincent, Walter S.**, 16 F. R. Lillie Road, Woods Hole, MA 02543
- Waterman, Talbot H.**, Yale University, Box 208103, 912 KBT Biology Department, New Haven, CT 06520-8103
- Wigley, Roland L.**, 35 Wilson Road, Woods Hole, MA 02543
- Wilber, Charles G.**, Colorado State University, Department of Biology, Forensic Science Laboratory, Fort Collins, CO 80523
- Zweifach, Benjamin W.**, 8811 Nottingham Place, La Jolla, CA 92037 (deceased)

Members

- Abt, Donald A.**, Marine Biological Laboratory, Laboratory of Aquatic Animal Medicine & Pathology, Woods Hole, MA 02543
- Adams, James A.**, 3481 Paces Ferry Road, Tallahassee, FL 32308
- Adelman, William J.**, 160 Locust Street, Falmouth, MA 02540
- Alkon, Daniel L.**, NIH Lab. of Adaptive Systems, 36 Convent Drive, MSC 4124, 36/4A21, Bethesda, MD 20892-4124
- Allen, Garland E.**, Washington University, Dept. of Biology, Box 1137, One Brookings Drive, St. Louis, MO 63130-4899
- Allen, Nina S.**, No. Carolina State University, Department of Botany, Box 7612, Raleigh, NC 27695
- Alliegro, Mark C.**, Louisiana State University Medical Center, Dept. of Cell Biology & Anatomy, 1901 Perdido Street, New Orleans, LA 70112

- Anderson, Everett**, Harvard Medical School, Dept. of Cell Biology, 240 Longwood Avenue, Boston, MA 02115-6092
- Anderson, John M.**, 110 Roat Street, Ithaca, NY 14850
- Anderson, Porter W.**, 100 Bayview Drive, Apt. 2224, North Miami Beach, FL 33160
- Armnett-Kibel, Christine**, University of Massachusetts, Boston, Dean of Science Faculty, Boston, MA 02125
- Armstrong, Clay M.**, University of Pennsylvania School of Medicine, B701 Richards Bldg., Department of Physiology, 3700 Hamilton Walk, Philadelphia, PA 19104-6085
- Armstrong, Ellen Prosser**, 57 Millfield Street, Woods Hole, MA 02543
- Armstrong, Peter B.**, University of California, Davis, Dept. of Molec. & Cell. Biology, Davis, CA 95616-8755
- Arnold, William A.**, Oak Ridge National Laboratory, Biology Division, 102 Balsalm Road, Oak Ridge, TN 37830
- Ashton, Robert W.**, Bay Foundation, 17 West 94th Street, New York, NY 10025
- Atema, Jelle**, Boston University Marine Program, Marine Biological Laboratory, Woods Hole, MA 02543
- Baccetti, Baccio**, University of Sienna, Institute of Zoology, 53100 Siena, Italy
- Baker, Robert G.**, New York University Medical Center, Dept. of Physiol. & Biophysics, 550 First Avenue, New York, NY 10016
- Baldwin, Thomas O.**, Texas A & M University, Department of Biochemistry and Biophysics, College Station, TX 77843
- Baltimore, David**, California Institute of Technology, 256-80, Pasadena, CA 91125
- Barlow, Robert B.**, SUNY Health Science Center, Dept. of Physiology, 750 East Adams St., Weiskotten Hall, Syracuse, NY 13210
- Barry, Daniel T.**, 2415 Fairwind Drive, Houston, TX 77062-4756
- Barry, Susan R.**, Mount Holyoke College, Dept. of Biological Sciences, So. Hadley, MA 01075
- Bass, Andrew H.**, Cornell University, Dept. of Neurobiology & Behavior, Seely Mudd Hall, Ithaca, NY 14853
- Battelle, Barbara-Anne**, University of Florida, Whitney Laboratory, 9505 Ocean Shore Boulevard, St. Augustine, FL 32086
- Bay, Frederick**, Bay Foundation, 17 W. 94th Street, First Floor, New York, NY 10025-7116
- Baylor, Martha B.**, P.O. Box 93, Woods Hole, MA 02543
- Bearer, Elaine L.**, Brown University, Div. of Biology & Medicine, Dept. of Pathology, Box G, Providence, RI 02912
- Beatty, John M.**, University of Minnesota, Dept. of Ecology & Behavioral, Biology, 1445 Gortner, St. Paul, MN 55108
- Beauge, Luis Alherto**, Instituto M. & M. Ferreyra, Dept. of Biophysics, Casilla de Correo 389, Cordoba, 5000, Argentina
- Begenisich, Ted**, University of Rochester, Medical Center, Box 642, 601 Elmwood Avenue, Rochester, NY 14642
- Begg, David A.**, University of Alberta, Faculty of Medicine, Dept. of Cell Biology & Anatomy, Edmonton, Alberta T6G 2H7, Canada
- Bell, Eugene**, 305 Commonwealth Avenue, Boston, MA 02115
- Benjamin, Thomas L.**, Harvard Medical School, Pathology, D2-230, 200 Longwood Avenue, Boston, MA 02115
- Bennett, Michael V. L.**, Albert Einstein College of Medicine, Dept. of Neuroscience, 1300 Morris Park Avenue, Bronx, NY 10461
- Bennett, Miriam F.**, Colby College, Department of Biology, Waterville, ME 04901
- Berg, Carl J.**, P.O. Box 681, Kilauea, Kauai, HI 96754-0681
- Berlin, Suzanne T.**, 5 Highland Street, Gloucester, MA 01930
- Bernstein, Norman**, Diane and Norman Bernstein Foundation, 5301 Wisconsin Ave., NW, #600, Washington, DC 20015-2015
- Bezanilla, Francisco**, Health Science Center, Department of Physiology, 405 Hilgard Avenue, Los Angeles, CA 90024
- Biggers, John D.**, Harvard Medical School, Department of Physiology, Boston, MA 02115
- Bishop, Stephen H.**, Iowa State University, Dept. of Zoology, Ames, IA 50010
- Blaustein, Mordecai P.**, University of Maryland, School of Medicine, Department of Physiology, Baltimore, MD 21201
- Blennemann, Dieter**, 1117 E. Putnam Avenue, Apt. #174, Riverside, CT 06878-1333
- Bloom, George S.**, University of Texas Southwestern, Medical Center, Cell Bio. & Neuroscience Dept., 5323 Harry Hines Blvd., Dallas, TX 75235-9039
- Bloom, Kerry S.**, University of North Carolina at Chapel Hill, Department of Biology, 623 Fordham Hall, CB #3280, Chapel Hill, NC 27599
- Bodznick, David A.**, Wesleyan University, Department of Biology, Lawn Avenue, Middletown, CT 06497-0170
- Boettiger, Edward G.**, 17 Eastwood Road, Storrs, CT 06268-2401
- Boooloofian, Richard A.**, Science Software Systems, Inc., 3576 Woodcliff Road, Sherman Oaks, CA 91403
- Borgese, Thomas A.**, Lehman College, CUNY, Department of Biology, Bedford Park Blvd., West, Bronx, NY 10468
- Borst, David W.**, Illinois State University, Department of Biological Sciences, Normal, IL 61790
- Bowles, Francis P.**, Marine Biological Laboratory, The Ecosystems Center, Woods Hole, MA 02543
- Boyer, Barbara C.**, Union College, Biology Department, Schenectady, NY 12308
- Brandhorst, Bruce P.**, Simon Fraser University, Inst. of Molec. Biol./Biochem, Barnaby, B.C. V5A 1S6, Canada
- Brinley, F. J.**, NINCDS/NIH, Neurological Disorders Program, Rm. 812 Federal Building, Bethesda, MD 20892
- Bronner-Fraser, Marianne**, California Institute of Technology, Division of Biology 139-74, Pasadena, CA 91125
- Brown, Stephen C.**, SUNY, Dept. of Biological Sciences, Albany, NY 12222
- Brown, William L.**, BankBoston, 100 Federal Street, 01-23-11, Boston, MA 02106-2016
- Browne, Carole L.**, Wake Forest University, Dept. of Biology, Box 7325, Winston-Salem, NC 27109
- Browne, Robert A.**, Wake Forest University, Dept. of Biology, Box 7325, Winston-Salem, NC 27109
- Bucklin, Anne C.**, University of New Hampshire, Ocean Process Analysis Lab, 142 Morse Hall, Durham, NH 03824
- Bullis, Robert A.**, Marine Biological Laboratory, Laboratory of Aquatic Animal Medicine, Woods Hole, MA 02543
- Burger, Max M.**, Friedrich Miescher Institute, P.O. Box 2543, CH 4002 Basel, Switzerland
- Burgess, David R.**, University of Pittsburgh, Dept. of Biological Sciences, 234 Langley, Pittsburgh, PA 15260
- Burgos, Mario**, IHEM Medical School, UNC Conicet, Casilla de Correo 56, Mendoza, 5500, Argentina
- Burky, Albert**, University of Dayton, Department of Biology, Dayton, OH 45469
- Burris, John E.**, Marine Biological Laboratory, 7 MBL Street, Woods Hole, MA 02543
- Burstyn, Harold Lewis**, United States Air Force, Air Force Materiel Command, Rome Research Site RL/JA, 26 Electronic Parkway, Rome, NY 13441-4514
- Bursztajn, Sherry**, LSU Medical Center, 1501 Kings Highway, Building BRIF 6-13, Shreveport, LA 71130
- Calabrese, Ronald L.**, Emory University, Department of Biology, 1510 Clifton Road, Atlanta, GA 30322

R68 Annual Report

- Callaway, Joseph C.**, New York Medical College, Dept. of Physiology, Basic Sciences Bldg., Valhalla, NY 10595
- Cameron, R. Andrew**, California Institute of Technology, Division of Biology 156-29, Pasadena, CA 91125
- Campbell, Richard H.**, Bang-Campbell Associates, Eel Pond Place, Box 402, Woods Hole, MA 02543
- Candelas, Graciela C.**, University of Puerto Rico, Department of Biology, P.O. Box 23360, UPR Station, San Juan, PR 00931-3360
- Carew, Thomas J.**, Yale University, Department of Psychology, P.O. Box 11A, Yale Station, New Haven, CT 06520
- Cariello, Lucio**, Stazione Zoologica Villa Comunale, 80121 Naples, Italy
- Case, James F.**, University of California, Santa Barbara, Marine Science Institute, Santa Barbara, CA 93106
- Cassidy, J. D.**, Providence College, Priory of St. Thomas Aquinas, Providence, RI 02918-0001
- Cavanaugh, Colleen M.**, Harvard University, Biological Laboratories, 16 Divinity Avenue, Cambridge, MA 02138
- Chaet, Alfred B.**, University of West Florida, Dept. of Cell & Molec. Biol., 11000 University Parkway, Pensacola, FL 32514
- Chambers, Edward L.**, University of Miami School of Medicine, Dept. of Physiology & Biophys., P.O. Box 016430, Miami, FL 33101
- Chang, Donald C.**, Hong Kong University of Science and Technology, Department of Biology, Clear Water Bay, Kowloon, Hong Kong
- Chappell, Richard L.**, Hunter College, CUNY, Dept. of Biological Sciences, Box 210, 695 Park Avenue, New York, NY 10021
- Chikarmane, Hemant M.**, 12 Middle Street, Reading, MA 01867
- Child, Frank M.**, 28 Lawrence Farm Road, Woods Hole, MA 02543-1416
- Chisholm, Rex Leslie**, Northwestern University, Medical School, Department of Cell Biology, Chicago, IL 60611
- Citkowitz, Elena**, Hospital of St. Raphael, Lipid Disorders Clinic, 1450 Chapel Street, New Haven, CT 06511
- Clark, Eloise E.**, Bowling Green State University, Biological Sciences Department, Bowling Green, OH 43403
- Clark, Hays**, 26 Deer Park Drive, Greenwich, CT 06830
- Clark, Wallis H.**, 12705 NW 112th Avenue, Alachua, FL 32615
- Claude, Philippa**, University of Wisconsin, Dept. Zoology, Zoology Research Building 125, 1117 W Johnson St., Madison, WI 53706
- Clay, John R.**, NIH-NINDS, Building 36, Room 2-CO2, Bethesda, MD 20892
- Clowes, Alexander W.**, University of Washington, School of Medicine, Dept. of Surgery, Box 356410, Seattle, WA 98195-6410
- Clutter, Mary**, 2555 Pennsylvania Avenue, N.W., Apt. 611, Washington, DC 20037-1646
- Cohh, Jewel Plummer**, California State University, Office of the President, 5151 University Drive, Los Angeles, CA 90032-8500
- Cohen, Carolyn**, Brandeis University, Rosenstiel Basic Medical Sciences Research Center, Waltham, MA 02254
- Cohen, Lawrence B.**, Yale University School of Medicine, Dept. of Physiology, 333 Cedar Street, New Haven, CT 06520
- Cohen, Maynard M.**, Rush Medical College, Dept. of Neurological Sciences, 600 South Paulina, Chicago, IL 60612
- Cohen, William D.**, Hunter College, Dept. of Biological Sciences, 695 Park Avenue, Box 79, New York, NY 10021
- Coleman, Annette W.**, Brown University, Div. of Biology and Medicine, Providence, RI 02912
- Colinvaux, Paul**, Smithsonian Tropical Research Institute, Unit 0948, Apo AA 34002-0948, USA
- Collier, Jack R.**, P.O. Box 139, 3431 Highway, #107, Effie, LA 71331
- Collier, Marjorie McCann**, P.O. Box 139, 3431 Highway 107, Effie, LA 71331
- Collin, Carlos**, NIH, Dept. of LAS, NINDS, Bldg. 36, 36 Convent Drive, Room B306, Bethesda, MD 20892-4124
- Cook, Joseph A.**, Edna McConnell Clark Foundation, 250 Park Avenue, New York, NY 10177-0026
- Cornell, Neal W.**, Marine Biological Laboratory, Woods Hole, MA 02543
- Cornwall, Melvin C.**, Boston University, School of Medicine, Dept. of Physiology L714, Boston, MA 02118
- Corson, D. Wesley**, Storm Eye Institute, Room 537, 171 Ashley Avenue, Charleston, SC 29425
- Corwin, Jeffrey T.**, University of Virginia, School of Medicine, Dept. of Otolaryngology, HNS and Neuroscience, Charlottesville, VA 22908
- Couch, Ernest F.**, Texas Christian University, Department of Biology, TCU Box 298930, Fort Worth, TX 76129
- Cox, Rachel Llanelly**, Woods Hole Oceanographic Institution, Biology Department, Woods Hole, MA 02543
- Crane, Sylvia E.**, 438 Wendover Drive, Princeton, NJ 08540
- Cremer-Bartels, Gertrud**, Universitäts Augenklinik, 44 Munster, Germany
- Crow, Terry J.**, University of Texas Medical School, Dept. of Neurobiol. & Anatomy, Houston, TX 77225
- Crowell, Sears**, Indiana University, Department of Biology, Bloomington, IN 47405
- Crowthier, Robert J.**, Shriners Burns Institute Research Center, One Kendall Square, Building 1400, Cambridge, MA 02139
- Cunningham, Mary-Ellen**, 62 Cloverly Road, Grosse Pointe Farms, MI 48236-3313
- Cutler, Richard D.**, Marine Biological Laboratory, Woods Hole, MA 02543
- Daignault, Alexander T.**, Edgewood, 575 Osgood Street, North Andover, MA 01875
- Davidson, Eric H.**, CA Institute of Technology, Division of Biology, 156-29, 1201 E. California Blvd., Pasadena, CA 91125
- Daw, Nigel W.**, 5 Old Pawson Road, Branford, CT 06405
- De Weer, Paul J.**, University of Pennsylvania, B400 Richards Bldg., Department of Physiology, 3700 Hamilton Walk, Philadelphia, PA 19104-6085
- Deegan, Linda A.**, Marine Biological Laboratory, The Ecosystems Center, Woods Hole, MA 02543
- DeGroof, Robert C.**, 145 Water Crest Drive, Doylestown, PA 18901-3267
- Denckla, Martha B.**, Johns Hopkins University, School of Medicine, Kennedy-Krieger Inst., 707 North Broadway, Baltimore, MD 21205
- DePhillips, Henry A.**, Trinity College, Department of Chemistry, 300 Summit Street, Hartford, CT 06106
- DeSimone, Douglas W.**, University of Virginia, Department of Cell Biology, Box 439, Health Sciences Ctr., Charlottesville, VA 22908
- Detbarn, Wolf-Dietrich**, Vanderbilt University, School of Medicine, Department of Pharmacology, Nashville, TN 37232
- Dionne, Vincent E.**, Boston University Marine Program, Marine Biological Laboratory, Woods Hole, MA 02543
- Dixon, Keith E.**, Flinders University, School of Biological Sciences, Bedford Park, 5042, SO, Australia
- Dowling, John E.**, Harvard University, Biological Laboratories, 16 Divinity Street, Cambridge, MA 02138
- Drapeau, Pierre**, Montreal General Hospital, Dept. of Neurology, 1650 Cedar Avenue, Montreal H3G 1A4, Canada
- DuBois, Arthur Brooks**, John B. Pierce Foundation Lab., 290 Congress Avenue, New Haven, CT 06519

- Duncan, Thomas K.**, Nichols College, Environmental Sciences Dept., Dudley, MA 01571
- Dunham, Philip B.**, Syracuse University, Department of Biology, Syracuse, NY 13244
- Dunlap, Paul V.**, University of Maryland Biotechnology Institute, Center of Marine Biotechnology, Columbus Center, Suite 236, 701 East Pratt Street, Baltimore, MD 21202
- Ebert, James D.**, Johns Hopkins University, Dept. of Biology, Homewood, 3400 No. Charles Street, Baltimore, MD 21218-2685
- Eckberg, William R.**, Howard University, Department of Biology, P.O. Box 887, Admin. Bldg., Washington, DC 20059
- Edds, Kenneth T.**, R&D Systems, Inc., Hematology Division, 614 McKinley Place, NE, Minneapolis, MN 55413
- Eder, Howard A.**, Albert Einstein College of Medicine, 1300 Morris Park Avenue, Bronx, NY 10461
- Edstrom, Joan**, 53 Two Ponds Road, Falmouth, MA 02540
- Egyud, Laszlo G.**, Cell Research Corporation, P.O. Box 67209, Chestnut Hill, MA 02167-0209
- Ehrlich, Barbara E.**, Yale University Medical School, B207 SHM, New Haven, CT
- Eisen, Arthur Z.**, Washington University, Division of Dermatology, St. Louis, MO 63110
- Eisen, Herman N.**, Massachusetts Institute of Technology, Center for Cancer Research, E17-128, 77 Massachusetts Ave., Cambridge, MA 02139-4307
- Elder, Hugh Young**, University of Glasgow, Institute of Physiology, Glasgow G12 8QQ, Scotland, UK
- Englund, Paul T.**, Johns Hopkins Medical School, Dept. of Biological Chemistry, 725 N. Wolfe Street, Baltimore, MD 21205
- Epel, David**, Stanford University, Hopkins Marine Station, Ocean View Blvd., Pacific Grove, CA 93950
- Epstein, Herman T.**, 18 Lawrence Farm Road, Woods Hole, MA 02543
- Epstein, Ray L.**, 1602 W. Olympia Street, Hernando, FL 34442
- Farb, David H.**, Boston University School of Med., Dept. of Pharmacology L603, 80 East Concord Street, Boston, MA 02118
- Farmanfarmaian, A.**, Rutgers University, Dept. of Biological Sciences, Nelson Biology Lab, POB 1059, Piscataway, NJ 08855
- Feldman, Susan C.**, University of Medicine & Dentistry, New Jersey Medical School, 100 Bergen Street, Newark, NJ 07103
- Festoff, Barry William**, VA Medical Center, Neurology Service (151), 4801 Linwood Blvd., Kansas City, MO 64128
- Fink, Rachel D.**, Mount Holyoke College, Dept. of Biological Sciences, Clapp Laboratories, South Hadley, MA 01075
- Finkelstein, Alan**, Albert Einstein College of Medicine, 1300 Morris Park Avenue, Bronx, NY 10461
- Fischbach, Gerald D.**, Harvard Medical School, Neurobiology Department, 220 Longwood Avenue, Boston, MA 02115
- Fishman, Harvey M.**, University of Texas Medical Branch, Dept. of Physiology & Biophys., 301 University Blvd., Galveston, TX 77555-0641
- Flanagan, Dennis**, 12 Gay Street, New York, NY 10014
- Fluck, Richard Allen**, Franklin & Marshall College, Department of Biology, Box 3003, Lancaster, PA 17604-3003
- Foreman, Kenneth H.**, Marine Biological Laboratory, The Ecosystems Center, Woods Hole, MA 02543
- Fox, Thomas Oren**, Harvard Medical School, Division of Medical Sciences, 260 Longwood Avenue, Boston, MA 02115
- Franzini-Armstrong, Clara**, University of Pennsylvania, School of Medicine, 330 S. 46th Street, Philadelphia, PA 19143
- Frazier, Donald T.**, University of Kentucky Medical Center, Dept. of Physiology & Biophysics, Lexington, KY 40536
- French, Robert J.**, University of Calgary, Health Sciences Centre, Alberta, T2N 4N1, Canada
- Fulton, Chandler M.**, Brandeis University, Department of Biology, Waltham, MA 02254
- Furie, Barbara C.**, Beth Israel Deaconess Medical Center, BIDMC Cancer Center, Kirstein 1, 330 Brookline Avenue, Boston, MA 02215
- Furie, Bruce**, Beth Israel Deaconess Medical Center, BIDMC Cancer Center, Kirstein 1, 330 Brookline Avenue, Boston, MA 02215
- Furshpan, Edwin J.**, Harvard Medical School, Department of Neurophysiology, 220 Longwood Avenue, Boston, MA 02115
- Futrelle, Robert P.**, Northeastern University, College of Computer Science, 360 Huntington Avenue, Boston, MA 02115
- Gabriel, Mordecai L.**, Brooklyn College, Department of Biology, 2900 Bedford Avenue, Brooklyn, NY 11210
- Gadsby, David C.**, The Rockefeller University, Laboratory of Cardiac Physiol., 1230 York Avenue, New York, NY 10021-6399
- Gainer, Harold**, National Institutes of Health, NINDS, BNP, DIR, Neurochemistry, Building 36, Room 4D20, Bethesda, MD 20892-4130
- Galatzer-Levy, Robert M.**, 180 North Michigan Avenue, Suite 2401, Chicago, IL 60601
- Gall, Joseph G.**, Carnegie Institution, 115 W. University Parkway, Baltimore, MD 21210
- Garber, Sarah S.**, Medical College of Pennsylvania, Dept. of Physiology, 2900 Queen Lane, Philadelphia, PA 19129
- Gascoyne, Peter**, University of Texas, M. D. Anderson Cancer Center, Experimental Pathology, Box 89, Houston, TX 77030
- Gelperin, Alan**, AT & T Bell Labs, Dept. of Biophysics, Rm. 1C464, 600 Mountain Avenue, Murray Hill, NJ 07974
- German, James L.**, The New York Blood Center, Lab. of Human Genetics, 310 East 67th Street, New York, NY 10021
- Gibbs, Martin**, Brandeis University, Institute for Photobiology of Cells and Organelles, Waltham, MA 02254
- Giblin, Anne E.**, Marine Biological Laboratory, The Ecosystems Center, Woods Hole, MA 02543
- Gibson, A. Jane**, Cornell University, Dept. of Biochemistry, Biotech. Building, Ithaca, NY 14850
- Gifford, Prosser**, 540 N Street, SW, Apt. #S-903, Washington, DC 20024-4557
- Gilbert, Daniel L.**, NIH/NINDS, Biophys. Sec., BNP, Bldg. 36, Rm. 5A-27, Bethesda, MD 20892
- Giudice, Giovanni**, Universita di Palermo, Dipartimento di Biologia, Cellulare e Dello Sviluppo, I-90123 Palermo, Italy
- Giuditta, Antonio**, University of Naples, Dept. of Gen. Physiology, Via Mezzocannone 8, Naples, 80134, 80134 Italy
- Glynn, Paul**, P.O. Box 6083, Brunswick, ME 04011-6083
- Golden, William T.**, Golden Family Trust, Room 4201, 42nd Floor, 40 Wall Street, New York, NY 10005
- Goldman, Robert D.**, Northwestern University Medical School, Dept. of Cell & Molecular Biology, 303 E. Chicago Avenue, Chicago, IL 60611-3008
- Goldsmith, Paul K.**, National Institutes of Health, Bldg. 10, Room 9C-101, Bethesda, MD 20892
- Goldsmith, Timothy H.**, Yale University, Department of Biology, New Haven, CT 06510
- Goldstein, Moise H.**, Johns Hopkins University, ECE Department, Barton Hall, Baltimore, MD 21218
- Goodman, Lesley Jean**, Queen Mary College, Dept. of Biological Sciences, Mile End Road, London E1 4NS, England, UK
- Gould, Robert Michael**, Institute for Basic Research in

R70 Annual Report

- Developmental Disabilities, 1050 Forest Hill Road, Staten Island, NY 10314-6399
- Govind, C. K.**, Scarborough College, Life Sciences Division, 1265 Military Trail, West Hill, Ontario, M1C 1A4 Canada
- Grace, Dick**, Doreen Grace Fund, The Brain Center, Promontory Point, New Seabury, MA 02649
- Graf, Werner M.**, College of France, 11 Place Marcelin Berthelot, 75231 Paris Cedex 05, France
- Grant, Philip**, National Institutes of Health, NINDS, BN, DIR, Neurochemistry, Bldg. 36, Rm. 4D20, Bethesda, MD 20892-4130
- Grass, Ellen R.**, The Grass Foundation, 77 Reservoir Road, Quincy, MA 02170-3610
- Grassle, Judith P.**, Rutgers University, Institute of Marine & Coastal Studies, Box 231, New Brunswick, NJ 08903
- Graubard, Katherine G.**, University of Washington, Dept. of Zoology, NJ-15, Box 351800, Seattle, WA 98195-1800
- Greenberg, Everett Peter**, University of Iowa, College of Medicine, Dept. of Microbiology, Iowa City, IA 52242
- Greenberg, Michael J.**, University of Florida, The Whitney Laboratory, 9505 Ocean Shore Boulevard, St. Augustine, FL 32086-8623
- Greer, Mary J.**, 176 West 87 Street, #12A, New York, NY 10024
- Griffin, Donald R.**, Harvard University, Concord Field Station, Old Causeway Road, Bedford, MA 01730
- Grnss, Paul R.**, 53 Two Ponds Road, Falmouth, MA 02540
- Grossman, Albert**, New York University Medical Center, 550 First Avenue, New York, NY 10016
- Grossman, Lawrence**, Johns Hopkins University, Dept. of Biochemistry, 615 North Wolfe Street, Baltimore, MD 21205
- Gruener, John A.**, Cephalon, Inc., 145 Brandywine Parkway, W. Chester, PA 19380-4245
- Gunning, A. Robert**, P.O. Box 165, Falmouth, MA 02541
- Gwilliam, G. F.**, Reed College, Department of Biology, Portland, OR 97202
- Haimo, Leah T.**, University of California, Department of Biology, Riverside, CA 92521
- Hajduk, Stephen L.**, University of Alabama, Dept. of Biochemistry and Molecular Genetics, 1918 University Blvd., Birmingham, AL 35294
- Hall, Linda M.**, SUNY at Buffalo, Dept. of Biochem. Pharmacol., 329 Hochstetter Hall, Buffalo, NY 14260-3850
- Hall, Zach W.**, NINDS/NHS, Office of the Director, Bldg. 31-8A52, Rockville Pike, Bethesda, MD 20892-2540
- Halvorson, Harlyn O.**, Policy Center for Marine Biosciences & Technology, UMass Boston, 100 Morrissey Blvd., Boston, MA 02125-3393
- Haneji, Tatsuji**, Kyushu Dental College, Dept. of Anatomy, 2-6-1, Manazuru, Kokurakita-Ku, Kitakyushu 803, Japan
- Hanton, Roger T.**, Marine Biological Laboratory, Marine Resources Center, 7 MBL Street, Woods Hole, MA 02543-1015
- Hárosi, Ferenc**, Marine Biological Laboratory, Laboratory of Sensory Physiology, Woods Hole, MA 02543
- Harrigan, June F.**, 7415 Makaa Place, Honolulu, HI 96825
- Harrington, Glenn W.**, Weber State University, Dept. of Microbiology, Ogden, UT 84408
- Harrison, Stephen C.**, Harvard University, Dept. of Molecular & Cell Biology, 7 Divinity Avenue, Cambridge, MA 02138
- Haselkorn, Robert**, University of Chicago, Dept. of Molecular Genetics & Cell Biology, Chicago, IL 60637
- Hastings, J. Woodland**, Harvard University, The Biological Laboratories, 16 Divinity Street, Cambridge, MA 02138-2020
- Haydon-Baillie, Wensley G.**, Porton Int., 2 Lowndes Place, London SW1 X8D, England, UK
- Hayes, Raymond L.**, Howard University, College of Medicine, 520 W Street, NW, Washington, DC 20059
- Heck, Diane E.**, EOHSI, Dept. of Pharmacology and Toxicol., 681 Frelinghuysen Road, Piscataway, NJ 08855
- Henry, Jonathan Joseph**, University of Illinois, Dept. of Cell & Struct. Biol., 505 South Goodwin Avenue, Urbana, IL 61801
- Hepler, Peter K.**, University of Massachusetts, Department of Biology, Morrill III, Amherst, MA 01003
- Herndon, Walter R.**, University of Tennessee, Department of Botany, Knoxville, TN 37996-1100
- Herskovits, Theodore T.**, Fordham University, Dept. of Chemistry, John Mulcahy Hall, Rm. 638, Bronx, NY 10458
- Hiatt, Howard H.**, Brigham and Women's Hospital, Department of Medicine, 75 Francis Street, Boston, MA 02115
- Highstein, Stephen M.**, Washington University School of Medicine, Dept. of Otolaryngology, Box 8115, 4566 Scott Avenue, St. Louis, MO 63110
- Hildebrand, John G.**, University of Arizona, ARL Div. of Neurobiology, 603 Gould-Simpson Sci. Bldg., Tucson, AZ 85721
- Hill, Richard W.**, Michigan State University, Department of Zoology, East Lansing, MI 48824
- Hill, Susan**, Michigan State University, Department of Zoology, East Lansing, MI 48824
- Hillis, Llewellya W.**, Smithsonian Tropical Research Institute, Unit 0948 APO, AA 34002-0948 USA
- Hinegardner, Ralph T.**, University of California, Division of Natural Sciences, Santa Cruz, CA 95064
- Hinsch, Gertrude W.**, University of South Florida, Department of Biology, Tampa, FL 33620
- Hinsch, Jan**, Leica, Inc., 110 Commerce Drive, Allendale, NJ 07401
- Hobbie, John E.**, Marine Biological Laboratory, The Ecosystems Center, Woods Hole, MA 02543
- Hodge, Alan J.**, 3843 Mt. Blackburn Avenue, San Diego, CA 92111
- Hoffman, Joseph F.**, Yale University School of Medicine, Dept. of Cellular and Molecular Physiology, New Haven, CT 06520
- Holz, George G.**, Massachusetts General Hospital, Lab. of Molec. Endocrinology, Wellman 320, 50 Blossom St., Boston, MA 02114
- Houk, James C.**, Northwestern University Medical School, 303 E. Chicago Ave., Ward 5-315, Chicago, IL 60611-3008
- Hoy, Ronald R.**, Cornell University, Section of Neurobiology & Behavior, 215 Mudd Hall, Ithaca, NY 14853
- Huang, Alice S.**, California Institute of Technology, Mail Code 1-9, Pasadena, CA 91125
- Hufnagel-Zackroff, Linda A.**, University of Rhode Island, Department of Microbiology, Kingston, RI 02881
- Hummon, William D.**, Ohio University, Dept. of Biological Sciences, Athens, OH 45701
- Humphreys, Susie H.**, Food and Drug Administration, HFS-308, 200 C Street, SW, Washington, DC 20204-0001
- Humphreys, Thomas D.**, University of Hawaii, Kewalo Marine Lab., 41 Ahui Street, Honolulu, HI 96813
- Hunt, Richard T.**, ICRF, Clare Hall Laboratories, South Mimms Potter's Bar, Herb EN6-3LD, England, UK
- Hunter, Robert D.**, Oakland University, Dept. of Biological Sciences, Rochester, MI 48309-4401
- Huxley, Hugh E.**, Brandeis University, Rosenstiel Center, Biology Department, Waltham, MA 02154
- Ilan, Joseph**, Case Western Reserve University, School of Medicine, Department of Anatomy, Cleveland, OH 44106
- Ingolia, Nicholas A.**, New Jersey Medical School, Dept. of Pharmacology/Physiology, 185 South Orange Avenue, Newark, NJ 07103

- Inoue, Saduyki**, McGill University, Dept. of Anatomy, 3640 University Street, Montreal, PQ H3A 2B2, Canada
- Inoué, Shinya**, Marine Biological Laboratory, 7 MBL Street, Woods Hole, MA 02543
- Isselbacher, Kurt J.**, Massachusetts General Hospital, Cancer Center, Charlestown, MA 02129
- Issidorides, Marietta Radovic**, University of Athens, Department of Psychiatry, Monis Petraki 8, Athens, 140, Greece
- Izzard, Colin S.**, SUNY, Albany, Dept. of Biological Sciences, 1400 Washington Avenue, Albany, NY 12222
- Jacobs, Neil**, Hale & Dorr, 60 State Street, Boston, MA 02109
- Jaffe, Laurinda A.**, University of Connecticut Health Center, Dept. of Physiology, Farmington Avenue, Farmington, CT 06032
- Jaffe, Lionel**, Marine Biological Laboratory, Woods Hole, MA 02543
- Jannasch, Holger W.**, Woods Hole Oceanographic Institution, Department of Biology, Woods Hole, MA 02543
- Jeffery, William R.**, Penn State University, Dept. of Biology, 208 Mueller Lab, University Park, PA 16802
- Johnston, Daniel**, Baylor College of Medicine, Division of Neuroscience, 1 Baylor Plaza, Houston, TX 77030
- Josephson, Robert K.**, University of California, Irvine, School of Biological Science, Dept. of Psychobiology, Irvine, CA 92697
- Kaczmarek, Leonard K.**, Yale University School of Medicine, Dept. of Pharmacology, 333 Cedar Street, New Haven, CT 06520
- Kaley, Gabor**, New York Medical College, Department of Physiology, Basic Sciences Building, Valhalla, NY 10595
- Kaltenbach, Jane**, Mount Holyoke College, Department of Biological Sciences, South Hadley, MA 01075
- Kaminer, Benjamin**, Boston University Medical School, Physiology Dept., 80 East Concord Street, Boston, MA 02118
- Kaneshiro, Edna S.**, University of Cincinnati, Biological Sciences Department, JL 006, Cincinnati, OH 45221-0006
- Kaplan, Ehud**, Mt. Sinai School of Medicine, Dept. of Ophthalmology, 1 Gustave Levy Place, Box 1183, New York, NY 10029
- Karakashian, Stephen J.**, Apartment 16-F, 165 West 91st Street, New York, NY 10024
- Karlin, Arthur**, Columbia University, Ctr. for Molecular Recognition, 630 West 168th St., Rm. 11-401, New York, NY 10032
- Keller, Hartmut Ernst**, Carl Zeiss, Inc., One Zeiss Drive, Thornwood, NY 10594
- Kelley, Darcy B.**, Columbia University, Dept. of Biological Sciences, 911 Fairchild, Mailcode 2432, New York, NY 10027
- Kelly, Robert E.**, 5 Little Harbor Road, Woods Hole, MA 02543
- Kemp, Norman E.**, University of Michigan, Department of Biology, Ann Arbor, MI 48109
- Kendall, John P.**, Faneuil Hall Associates, 176 Federal Street, 2nd Flr, Boston, MA 02110
- Kerr, Louis M.**, Marine Biological Laboratory, Woods Hole, MA 02543
- Keynan, Alexander**, Israel Academy of Science and Humanity, P.O. Box 4040, Jerusalem, Israel
- Khan, Shahid M. M.**, Albert Einstein College of Medicine, Dept. of Physiol. & Biophysics, 1300 Morris Park Avenue, Bronx, NY 10461
- Khodakhah, Kamran**, University of Pennsylvania, Dept. of Physiology, Philadelphia, PA 19104
- Kiehart, Daniel P.**, Duke University Medical Center, Dept. of Cell Biol., Box 3709, 307 Nanaline Duke Bldg., Durham, NC 27710
- Kleinfeld, David**, University of California, San Diego, Physics Department, 0319, 9500 Gilman Drive, La Jolla, CA 92093
- Klessen, Rainer**, Carl Zeiss, Inc., 1 Zeiss Drive, Thornwood, NY 10594
- Klotz, Irving M.**, Northwestern University, Department of Chemistry, Evanston, IL 60201
- Knudson, Robert A.**, Marine Biological Laboratory, Instrument Development Laboratory, Woods Hole, MA 02543
- Koide, Samuel S.**, The Rockefeller University, The Population Council, 1230 York Avenue, New York, NY 10021
- Kornberg, Hans**, 134 Sewall Ave., #2, Brookline, MA 02146
- Kosower, Edward M.**, Tel-Aviv University, Dept. of Chemistry, Ramat-Aviv, Tel Aviv, 69978, Israel
- Krahl, Maurice E.**, 2783 W. Casas Circle, Tucson, AZ 85741
- Krane, Stephen M.**, Massachusetts General Hospital, Arthritis Unit, Fruit Street, Boston, MA 02114
- Krauss, Robert**, P.O. Box 291, Denton, MD 21629
- Kravitz, Edward A.**, Harvard Medical School, Dept. of Neurobiology, 220 Longwood Avenue, Boston, MA 02115
- Kriebel, Mahlon E.**, SUNY Health Science Center, Dept. of Physiology, Syracuse, NY 13210
- Kristan, William B.**, University of California, San Diego, Dept. of Biology, B-0357, La Jolla, CA 92093-0357
- Kropinski, Andrew M.**, Queen's University, Dept. of Microbiol./Immunology, Kingston, Ontario K7L 3N6, Canada
- Kuffler, Damien P.**, Insitute of Neurobiology, 201 Blvd. del Valle, San Juan, PR 00901
- Kuhns, William J.**, Hospital for Sick Children, Biochemistry Research, 555 University Ave., Toronto, Ontario, M5G 1X8 Canada
- Kunkel, Joseph G.**, University of Massachusetts, Dept. of Biology, Amherst, MA 01003
- Kusano, Kiyoshi**, National Institutes of Health, Bldg. 36, Room 4D-20, Bethesda, MD 20892
- Kuzirian, Alan M.**, Marine Biological Laboratory, Woods Hole, MA 02543-1015
- Laderman, Aimlee D.**, Yale University, School of Forestry & Environmental Studies, 370 Prospect Street, New Haven, CT 06511
- Landeau, Laurie J.**, Listowel, Inc., 2 Park Avenue, Suite 1525, New York, NY 10016
- Landis, Dennis M.D.**, University Hospital of Cleveland, Dept. of Neurology, 11100 Euclid Ave., Cleveland, OH 44106
- Landis, Story C.**, National Institutes of Health, Bldg. 36, Room 5A05, 36 Convent Drive, Bethesda, MD 20892-4150
- Landowne, David**, University of Miami Medical School, Dept. of Physiology, PO Box 016430, Miami, FL 33101
- Langford, George M.**, Dartmouth College, Dept. of Biological Sciences, 6044 Gilman Laboratory, Hanover, NH 03755
- Laskin, Jeffrey**, University of Medicine & Dentistry of New Jersey, Robert Wood Johnson Medical School, 675 Hoes Lane, Piscataway, NJ 08854
- Lasser-Ross, Nechama**, New York Medical College, Dept. of Physiology, Valhalla, NY 10595
- Laster, Leonard**, University of Massachusetts, Medical School, 55 Lake Avenue, North, Worcester, MA 01655
- Laties, Alan**, Scheie Eye Institute, Myrin Circle, 51 North 39th Street, Philadelphia, PA 19104
- Laufer, Hans**, University of Connecticut, Dept. of Molec. & Cell Biol., U-125, 75 North Eagleville Rd., Storrs, CT 06269-3125
- Lazarow, Paul B.**, Mt. Sinai School of Medicine, Dept. of Cell Biol. & Anatomy, Box 1007, 5th Ave. & 100th St., New York, NY 10029

- Lazarus, Maurice**, Federated Department Stores, Sears Crescent, City Hall Plaza, Boston, MA 02108
- Leadbetter, Edward R.**, University of Connecticut, Dept. of Molec. & Cell Biology, U-131, Storrs, CT 06266-2131
- Lederberg, Joshua**, The Rockefeller University, 1230 York Avenue, New York, NY 10021
- Lee, John J.**, City College of CUNY, Department of Biology, Convent Avenue & 138th Street, New York, NY 10031
- Lehy, Donald B.**, 35 Willow Field Drive, No. Falmouth, MA 02556
- Leibovitz, Louis**, 3 Kettle Hole Road, Falmouth, MA 02540
- Leighton, Joseph**, Aeron Biotechnology, Inc., 1933 Davis Street #310, San Leandro, CA 94577
- Leighton, Stephen B.**, National Institutes of Health, Bldg. 13, 3W13, Bethesda, MD 20892
- Lemos, Jose Ramon**, University of Massachusetts Medical Center, Worcester Foundation Campus, 222 Maple Avenue, Shrewsbury, MA 01545-2737
- Lerner, Aaron B.**, Yale University School of Medicine, Department of Dermatology, P.O. Box 3333, New Haven, CT 06510
- Levin, Jack**, Veterans Administration, Medical Center, 111 H2, 4150 Clement Street, San Francisco, CA 94121
- Levine, Michael**, University of California, Molecular & Cell Biology, 401 Barker Hall #3204, Berkeley, CA 92093-3204
- Levine, Richard B.**, Univ. of Arizona, ARL, Div. of Neurobiology, Room 611, Gould-Simpson Bldg., Tucson, AZ 85721
- Levinthal, Francoise**, Columbia University, Dept. of Biological Sciences, Broadway & 116th Street, New York, NY 10026
- Levitan, Herbert**, National Science Foundation, 4201 Wilson Boulevard, Room 835, Arlington, VA 22230
- Levitan, Irwin B.**, Brandeis University, Volen Center for Complex Sys., 415 South Street, Waltham, MA 02254
- Linck, Richard W.**, University of Minnesota, School of Medicine, Cell Biology & Neuroanatomy Dept., 4-135 Jackson Hall, 321 Church St., Minneapolis, MN 55455
- Lipicky, Raymond J.**, FDA/CDER/ODEI/ HFD-110, 5600 Fishers Lane, Rockville, MD 20857
- Lisman, John E.**, 199 Coolidge Avenue, #902, Watertown, MA 02172-1572
- Liuzzi, Anthony**, 320 Beacon Street, Boston, MA 02116
- Llinas, Rodolfo R.**, NYU Medical Center, Dept. of Physiology & Neurosc., 550 First Ave, Rm 442, New York, NY 10016
- Lobel, Phillip S.**, Boston University Marine Program, Marine Biological Laboratory, Woods Hole, MA 02543
- Loew, Franklin M.**, Medical Foods, Inc., 5 Cambridge Ctr. Ste. 8, Cambridge, MA 02142
- Loewenstein, Birgit Rose**, Marine Biological Laboratory, Woods Hole, MA 02543
- Loewenstein, Werner R.**, Marine Biological Laboratory, Woods Hole, MA 02543
- London, Irving M.**, Johnson & Johnson, Harvard-MIT Division, E-25-551, Cambridge, MA 02139
- Longo, Frank J.**, University of Iowa, Department of Anatomy, Iowa City, IA 52442
- Lorand, Laszlo**, Northwestern University Medical School, CMS Biology, Searle 4-555, 303 East Chicago Avenue, Chicago, IL 60611-3008
- Luckenbill, Louise M.**, Ohio University, Dept. of Biological Sciences, Irvine Hall, Athens, OH 45701
- Macagno, Eduardo R.**, Columbia University, Department of Biosciences, 1003B Fairchild, New York, NY 10027
- MacNichol, Edward F.**, Boston University School of Medicine, Dept. of Physiol., 80 E. Concord Street, Boston, MA 02118
- Maglott-Duffield, Donna R.**, American Type Culture Collection, 12301 Parklawn Drive, Rockville, MD 20852-1776
- Maienschein, Jane Ann**, Arizona State University, Department of Philosophy, P.O. Box 872004, Tempe, AZ 85287-2004
- Mainer, Robert E.**, The Boston Company, Inc., One Boston Place, OBP-15-D, Boston, MA 02108
- Malbon, Craig C.**, SUNY, Stony Brook, Univ. Medical Center, Pharmacology-HSC, Stony Brook, NY 11794-8651
- Manalis, Richard S.**, Indiana-Purdue University, Dept. of Biological Science, 2101 Coliseum Blvd. E., Fort Wayne, IN 46805
- Mangum, Charlotte P.**, College of William and Mary, Department of Biology, Williamsburg, VA 23187-8795
- Manz, Robert D.**, 304 Adams Street, Milton, MA 02186
- Margulis, Lynn**, University of Massachusetts, Amherst, Dept. of Geosciences, Morrill Science Center, Box 35820, Amherst, MA 01003-5820
- Marinucci, Andrew C.**, 102 Nancy Drive, Mercerville, NJ 08619
- Martinez, Joe L.**, University of Texas, San Antonio, Division of Life Sciences, 6900 North Loop 1604 West, San Antonio, TX 78249-0662
- Martinez-Palomo, Adolfo**, CINVESTAV-IPN, Sec. de Patologia Experimental, 07000 Mexico, D.F.A.P. 140740, Mexico
- Mastroianni, Luigi**, Hospital of University of Pennsylvania, 106 Dulles, 3400 Spruce Street, Philadelphia, PA 19104-4283
- Mauzerall, David**, Rockefeller University, 1230 York Avenue, New York, NY 10021
- McCann, Frances V.**, Dartmouth Medical School, Department of Physiology, Lebanon, NH 03756
- McLaughlin, Jane A.**, Marine Biological Laboratory, Woods Hole, MA 02543
- McMahon, Robert F.**, University of Texas, Arlington, Department of Biology, Box 19498, Arlington, TX 76019
- Meedel, Thomas**, Rhode Island College, Biology Dept., 600 Mt. Pleasant Avenue, Providence, RI 02908
- Meinertzhagen, Ian A.**, Dalhousie University, Dept. Psychology, Halifax, NS B3H 4J1, Canada
- Meiss, Dennis E.**, Immunodiagnostic Laboratories, 488 McCormick Street, San Leandro, CA 94577
- Melillo, Jerry M.**, Marine Biological Laboratory, The Ecosystems Center, Woods Hole, MA 02543
- Mellon, DeForest**, University of Virginia, Department of Biology, Gilmer Hall, Charlottesville, VA 22903
- Mellon, Richard P.**, P.O. Box 187, Laughlintown, PA 15655-0187
- Mendelsohn, Michael E.**, Harvard Medical School, Cardiovascular Division, 75 Francis Street, Boston, MA 02115
- Merriman, Melanie Pratt**, 7511 Beachview Dr., N. Bay Village, FL 33141
- Meselson, Matthew**, Harvard University, Fairchild Biochem. Building, 7 Divinity Avenue, Cambridge, MA 02138
- Metuzals, Janis**, University of Ottawa, Dept. of Pathology & Lab. Med., 451 Smyth Rd., Ottawa, Ontario, K1H 8M5 Canada
- Miledi, Ricardo**, University of California, Irvine, Dept. of Psychobiology, 2205 Bio. Sci. II, Irvine, CA 92697-4550
- Milkman, Roger D.**, University of Iowa, Dept. of Biological Sciences, 138 Biology Building, Iowa City, IA 52242-1324
- Miller, Andrew L.**, Hong Kong University, Dept. of Biology, Clearwater Bay, Kowloon, Hong Kong
- Mills, Robert**, 10315 44th Avenue, W. 12 H Street, Brandenton, FL 34210
- Misevic, Gradimir**, University Hospital of Basel, Dept. of Research, Mehelstr. 20, CH-4031 Basel, Switzerland
- Mitchell, Ralph**, Harvard University, Division of Applied Sciences, 29 Oxford Street, Cambridge, MA 02138

- Miyakawa, Hiroyoshi**, Tokyo College of Pharmacy, Lab. of Cellular Neurobiology, 1432-1 Horinouchi, Hachioji, Tokyo 192-03, Japan
- Miyamoto, David M.**, Drew University, Department of Biology, Madison, NJ 07940
- Mizell, Merle**, Tulane University, Dept. of Cell & Molecular Biology, New Orleans, LA 70118
- Moore, John W.**, Duke University Medical Center, Department of Neurobiology, Box 3209, Durham, NC 27710
- Moreira, Jorge E.**, NIH/NICHHD, Dept. of Cell and Molec. Biol., Bethesda, MD 20852
- Morin, James G.**, University of California, Department of Biology, Los Angeles, CA 90024
- Morrell, Leyla de Toledo**, Rush-Presbyterian-St. Lukes Medical Center, 1653 West Congress Parkway, Chicago, IL 60612
- Morse, M. Patricia**, Northeastern University, Marine Science Center, Nahant, MA 01908
- Morse, Stephen S.**, DARPA/DSO, 3701 N. Fairfax Drive, Arlington, VA 22203-1714
- Mote, Michael I.**, Temple University, Department of Biology, Philadelphia, PA 19122
- Muller, Kenneth J.**, University of Miami Medical School, Dept. of Physiol./Biophysics, RMSB-5092 1600 NW 10th Avenue, Miami, FL 33136
- Murray, Andrew W.**, University of California, Dept. of Physiology, Box 0444, 513 Parnassus Avenue, San Francisco, CA 94143-0444
- Nabrit, S. M.**, 686 Beckwith Street, SW, Atlanta, GA 30314
- Nadelhoffer, Knute J.**, Marine Biological Laboratory, The Ecosystems Center, Woods Hole, MA 02543
- Naka, Ken-ichi**, 2-9-2 Tatum Higashi, Okazaki, 444, Japan
- Nakajima, Yasuko**, University of Illinois, College of Medicine, Anat. & Cell Biol. Dept., M/C 512, Chicago, IL 60612
- Narahashi, Toshio**, Northwestern University Medical School, Dept. of Pharmacology, 303 E. Chicago Avenue, Chicago, IL 60611
- Nasi, Enrico**, Boston University School of Medicine, Dept. of Physiology, R-406, 80 E. Concord Street, Boston, MA 02118
- Neill, Christopher**, Marine Biological Laboratory, The Ecosystems Center, Woods Hole, MA 02543
- Nelson, Leonard**, Medical College of Ohio, Department of Physiology, CS 10008, Toledo, OH 43699
- Nelson, Margaret C.**, Cornell University, Section of Neurobiology, and Behavior, Ithaca, NY 14850
- Nicholls, John G.**, Biocenter, Klingelbergstrasse 70, 4056 Basel, Switzerland
- Nickerson, Peter A.**, SUNY, Buffalo, Dept. of Pathology, Buffalo, NY 14214
- Nicosia, Santo V.**, University of South Florida, College of Medicine, Box 11, Department of Pathology, Tampa, FL 33612
- Noe, Bryan D.**, Emory University School of Medicine, Dept. of Anatomy & Cell Biol., Atlanta, GA 30322
- Northcutt, R. Glenn**, University of California, San Diego, Neuroscience 0201, 9500 Gilman Drive, La Jolla, CA 92093-0201
- Norton, Catherine N.**, Marine Biological Laboratory, Woods Hole, MA 02543
- Nusbaum, Michael P.**, University of Pennsylvania School of Medicine, Dept. of Neuroscience, 215 Stemmler Hall, Philadelphia, PA 19104-6074
- O'Herron, Jonathan**, Lazard Freres & Co., 30 Rockefeller Plaza, 59th Flr. New York, NY 10020-1900
- Obaid, Ana Lia**, University of Pennsylvania School of Medicine, Neuroscience Department, 234 Stemmler Hall, Philadelphia, PA 19104-6074
- Ohki, Shinpei**, SUNY, Buffalo, Dept. of Biophysical Sciences, 224 Cary Hall, Buffalo, NY 14214
- Oldenbourg, Rudolf**, Marine Biological Laboratory, 7 MBL Street, Woods Hole, MA 02543
- Olds, James L.**, American Association of Anatomists, 9650 Rockville Pike, Ste. 4514, Bethesda, MD 20814-3998
- Olins, Ada L.**, University of Tennessee, Oak Ridge, Grad. School of Biomed. Sci., Biology Div. ORNL-POB 2009, Oak Ridge, TN 37831-8077
- Olins, Donald E.**, University of Tennessee, Oak Ridge, Grad. School of Biomed. Sci., Biology Division ORNL-POB 2009, Oak Ridge, TN 37831-8077
- Oschman, James L.**, 31 Whittier Street, Dover, NH 03820
- Palazzo, Robert E.**, University of Kansas, Dept. of Physiol. & Cell Biol., Haworth Hall, Lawrence, KS 66045
- Palmer, John D.**, University of Massachusetts, Department of Zoology, 221 Morrill Science Center, Amherst, MA 01003
- Pant, Harish C.**, NINCDS/NIH, Lab. of Neurochemistry, Building 36, Room 4D20, Bethesda, MD 20892
- Pappas, George D.**, University of Illinois, College of Medicine, Department of Anatomy, Chicago, IL 60612
- Pardee, Arthur B.**, Dana-Farber Cancer Institute, D810, 44 Binney Street, Boston, MA 02115
- Pardy, Rosevelt L.**, University of Nebraska, School of Life Sciences, Lincoln, NE 68588
- Parmentier, James L.**, 175 S. Great Road, Lincoln, MA 01773-4112
- Pederson, Thoru**, University of Massachusetts Medical Center, Worcester Foundation Campus, 222 Maple Avenue, Shrewsbury, MA 01545
- Perkins, Courtland D.**, 400 Hilltop Terrace, Alexandria, VA 22301
- Person, Philip**, 137-87 75th Road, Flushing, NY 11367
- Peterson, Bruce J.**, Marine Biological Laboratory, The Ecosystems Center, Woods Hole, MA 02543
- Pethig, Ronald**, University College of No. Wales, School of Electronic Eng. Sci., Bangor, Gwynedd, LL 57 IUT, UK
- Pfohl, Ronald J.**, Miami University, Department of Zoology, Oxford, OH 45056
- Pierce, Sidney K.**, University of Maryland, Department of Zoology, College Park, MD 20742
- Pleasure, David E.**, Children's Hospital, Neurology Research, 5th Floor, Abramson Building, Philadelphia, PA 19104
- Poindexter, Jeanne S.**, Barnard College, Columbia University, 3009 Broadway, New York, NY 10027-6598
- Pollard, Harvey B.**, NIH/NIDDKD, Lab. of Cell Biol. & Genetics, Bldg. 8, Rm. 401, Bethesda, MD 20892
- Pollard, Thomas D.**, Salk Institute for Biological Studies, 10010 N. Torrey Pines Road, La Jolla, CA 92037
- Porter, Beverly H.**, 5542 Windysun Ct., Columbia, MD 21045
- Porter, Mary E.**, University of Minnesota Medical School, Dept. of Cell Biol. & Neuroanatomy, 4-135 Jackson Hall, 321 Church St. SE, Minneapolis, MN 55455
- Potter, David D.**, Harvard Medical School, Department of Neurobiology, 25 Shattuck Street, Boston, MA 02115
- Potts, William T.**, University of Lancaster, Department of Biology, Lancaster, England, UK
- Powers, Maureen K.**, Vanderbilt University, Dept. of Psychology, 301 Arts & Sci. Psych. Bldg, Nashville, TN 37240
- Prendergast, Robert A.**, Wilmer Institute, Johns Hopkins Hospital, 457 Wilmer-Woods Building, 600 N. Wolfe Street, Baltimore, MD 21287-9142
- Price, Carl A.**, Rutgers University, Waksman Inst. of Microbiology, P.O. Box 759, Piscataway, NJ 08855-0759

R74 Annual Report

- Prior, David J.**, Northern Arizona University, Arts and Sci. Dean's Office, Box 5621, Flagstaff, AZ 86011
- Prusch, Robert D.**, Gonzaga University, Department of Life Sciences, Spokane, WA 99258
- Purves, Dale**, Duke University Medical Center, Dept. of Neurobiology, Bx 3209, 1011 Bryan Res. Bldg., Durham, NC 27710
- Quigley, James P.**, SUNY Health Sciences Center, Dept. of Pathology, BHS Tower 9, Rm. 140, Stony Brook, NY 11794-8691
- Rabb, Irving W.**, 1010 Memorial Drive, Cambridge, MA 02138
- Rabin, Harvey**, P.O. Box 4022, Wilmington, DE 19807
- Rabinowitz, Michael B.**, Marine Biological Laboratory, 7 MBL St., Woods Hole, MA 02543
- Rafferty, Nancy S.**, Marine Biological Laboratory, 7 MBL, Woods Hole, MA 02543
- Rakowski, Robert F.**, UHS/The Chicago Medical School, Dept. of Physiol. & Biophysics, 3333 Greenbay Road, N. Chicago, IL 60064
- Ramon, Fidel**, UNAM-CU, Div. Est. Posgrado E Invest., Facultad de Medicina, 04510, D.F., Mexico
- Ranzi, Silvio**, Sez. Zoologia Scienze Naturali, Dip. Di Biologia, Via Celoria, 26, 20133 Milano, Italy
- Rastetter, Edward B.**, Marine Biological Laboratory, The Ecosystems Center, Woods Hole, MA 02543
- Rehman, Lionel I.**, University of Virginia, Department of Biology, Gilmer Hall 45, Charlottesville, VA 22901
- Reddan, John R.**, Oakland University, Dept. of Biological Sciences, Rochester, MI 48309-4401
- Reese, Thomas S.**, NIH, Bldg. 36, Room 2A21, 9000 Rockville Pike, Bethesda, MD 20892
- Reinisch, Carol L.**, Marine Biological Laboratory, Woods Hole, MA 02543
- Rickles, Frederick R.**, 2633 Danforth Lane, Decatur, GA 30033
- Rieder, Conly L.**, Wadsworth Center, Division of Molecular Medicine, P.O. Box 509, Albany, NY 12201-0509
- Riley, Monica**, Marine Biological Laboratory, Woods Hole, MA 02543
- Ripps, Harris**, University of Illinois at Chicago, Dept. of Ophthalmol/Vis. Sci., 1855 West Taylor Street, Chicago, IL 60612
- Ritchie, J. M.**, Yale University School of Medicine, Dept. of Pharmacology, 333 Cedar Street, New Haven, CT 06510
- Rome, Lawrence C.**, University of Pennsylvania, Dept. of Biology, Philadelphia, PA 19104
- Rosenbaum, Joel L.**, University of Pennsylvania School of Medicine, c/o Brian Salzberg, Dept. of Physiology, Philadelphia, PA 19104
- Rosenbluth, Jack**, New York University School of Medicine, Dept. of Physiology, RF 714, 400 East 34th Street, New York, NY 10016
- Rosenbluth, Raja**, Simon Fraser University, Inst. of Molec. Biology & Biochem., Burnaby, BC, Canada, V5A 1S6
- Rosenfield, Allan**, Columbia University School of Public Health, 600 West 168th Street, New York, NY 10032-3702
- Rosenkranz, Herbert S.**, University of Pittsburgh, Dept. of Environ. & Occup. Hlth., 260 Kappa Drive, Pittsburgh, PA 15238
- Roslansky, John D.**, 57 Buzzards Bay Avenue, Woods Hole, MA 02543
- Roslansky, Priscilla F.**, Associates of Cape Cod, Inc., P.O. Box 224, Woods Hole, MA 02543-0224
- Ross, William N.**, New York Medical College, Department of Physiology, Valhalla, NY 10595
- Roth, Jay S.**, P.O. Box 692, Woods Hole, MA 02543-0692
- Rottenfusser, Rudi**, Carl Zeiss, Inc., Marine Biological Laboratory, Woods Hole, MA 02543
- Rowland, Lewis P.**, Neurological Institute, 710 West 168th Street, New York, NY 10032
- Ruderman, Joan V.**, Harvard Medical School, Dept. of Cell Biology, 240 Longwood Avenue, Boston, MA 02115
- Rummel, John D.**, Marine Biological Laboratory, Woods Hole, MA 02543
- Rushforth, Norman B.**, Case Western Reserve University, Department of Biology, Cleveland, OH 44106
- Russell-Hunter, W. D.**, 711 Howard Street, Easton, MD 21601-3934
- Saffo, Mary Beth**, Arizona State University, Life Sci. Dept., MC 2352, P.O. Box 37100, Phoenix, AZ 85069-7100
- Salama, Guy**, University of Pittsburgh, Department of Physiology, Pittsburgh, PA 15261
- Salmon, Edward D.**, University of North Carolina, Dept. of Biology, Wilson Hall, CB 3280, Chapel Hill, NC 27599
- Salyers, Abigail**, University of Illinois, Dept. of Microbiology, 407 S. Goodwin Avenue, Urbana, IL 61801
- Salzberg, Brian M.**, University of Pennsylvania School of Medicine, Dept. of Neuroscience, 215 Stemmler Hall, Philadelphia, PA 19104-6074
- Sanger, Jean M.**, University of Pennsylvania School of Medicine, Dept. of Anatomy, 36th and Hamilton Walk, Philadelphia, PA 19104
- Sanger, Joseph W.**, University of Pennsylvania Medical Center, Dept. of Cell and Devel. Biol., 36th and Hamilton Walk, Philadelphia, PA 19104-6058
- Saunders, John W.**, 118 Metoxit Road, P.O. Box 3381, Waquoit, MA 02536
- Schachman, Howard K.**, University of California, Berkeley, Molecular & Cell Biology Dept., 229 Stanley Hall, #3206, Berkeley, CA 94720-3206
- Schatten, Gerald P.**, University of Wisconsin, 1117 W. Johnson Street, Madison, WI 53706
- Schatten, Heide**, University of Wisconsin, Department of Zoology, Madison, WI 53706
- Schmeer, Arlene C.**, Mercene Cancer Research Institute, 790 Prospect Street, New Haven, CT 06511
- Schuel, Herbert**, SUNY, Buffalo, Dept. of Anatomy/Cell Biology, Buffalo, NY 14214
- Schwartz, James H.**, New York State Psychiatric Institute, Research Annex, 722 West 168th St., 7th floor, New York, NY 10032
- Schwartz, Lawrence**, University of Massachusetts, Amherst, Department of Biology, Morrill Science Center, Amherst, MA 01003
- Schweitzer, A. Nicola**, Brigham & Women's Hospital, Immunology Division, Dept. of Pathology, 221 Longwood Ave., LMRC 521, Boston, MA 02115
- Segal, Sheldon J.**, The Population Council, One Dag Hammarskjold Plaza, New York, NY 10036
- Shanklin, Douglas R.**, University of Tennessee, Dept. of Pathology, Rm. 576, 800 Madison Avenue, Memphis, TN 38117
- Shashoua, Victor E.**, Harvard Medical School, Ralph Lowell Labs, McLean Hospital, 115 Mill St., Belmont, MA 02178
- Shaver, Gaius R.**, Marine Biological Laboratory, The Ecosystems Center, Woods Hole, MA 02543
- Shaver, John R.**, Michigan State University, Dept. of Zoology, East Lansing, MI 48824
- Sheetz, Michael P.**, Duke University Medical Center, Dept. of Cell Biology, Bx 3709, 388 N. Nanaline Duke Bldg., Durham, NC 27710
- Shepro, David**, Boston University, CAS Biology, 5 Cummington Street, Boston, MA 02215

- Shimomura, Osamu**, Marine Biological Laboratory, Woods Hole, MA 02543
- Shibley, Alan M.**, P.O. Box 2036, Sandwich, MA 02563
- Silver, Robert B.**, Marine Biological Laboratory, Woods Hole, MA 02543
- Siwicki, Kathleen K.**, Swarthmore College, Biology Department, 500 College Avenue, Swarthmore, PA 19081-1397
- Skinner, Dorothy M.**, Oak Ridge National Laboratory, Biology Division, P.O. Box 2009, Oak Ridge, TN 37831
- Sloboda, Roger D.**, Dartmouth College, Dept. of Biological Sciences, 6044 Gilman Laboratory, Hanover, NH 03755
- Sluder, Greenfield**, University of Massachusetts Medical Center, Worcester Foundation Campus, 222 Maple Avenue, Shrewsbury, MA 01545
- Smith, Peter J. S.**, Marine Biological Laboratory, Woods Hole, MA 02543
- Smith, Stephen J.**, Stanford University School of Medicine, Dept. of Cell. & Molec. Phys., Beckman Center, Stanford, CA 94305-5426
- Smolowitz, Roxanna S.**, Marine Biological Laboratory, Laboratory of Aquatic Animal Medicine, Woods Hole, MA 02543
- Sogin, Mitchell L.**, Marine Biological Laboratory, Woods Hole, MA 02543
- Sorenson, Martha M.**, Cidade Universitaria-UFRJ, Dept. Bioquimica Medica-ICB, 21941-590 Rio de Janeiro, Brazil
- Speck, William T.**, Columbia-Presbyterian Medical Center, 161 Fort Washington Avenue, 14th Floor, Room 1470, New York, NY 10032-3784
- Spector, Abraham**, Columbia University, Dept. of Ophthalmology, 630 West 168th Street, New York, NY 10032
- Speksnijder, Johanna E.**, University of Groningen, Dept. of Genetics, Kerklaan 30, 9751 NN Haren, The Netherlands
- Spray, David C.**, Albert Einstein College of Medicine, Dept. of Neurosci., 1300 Morris Park Avenue, Bronx, NY 10461
- Spring, Kenneth R.**, National Institutes of Health, Building 10, Room 6N260, 10 Center Drive, MSC 1603, Bethesda, MD 20892-1603
- Steele, John H.**, Woods Hole Oceanographic Institution, Woods Hole, MA 02543
- Steinacker, Antoinette**, University of Puerto Rico, Medical Sciences, Institute of Neurobiology, 201 Boulevard Del Valle, San Juan, PR 00901
- Steinberg, Malcolm**, Princeton University, Dept. of Molecular Biology, M-18 Moffett Laboratory, Princeton, NJ 08544-1014
- Stemmer, Andreas C.**, Institut für Robotik, ETH-Sentrum, 8092 Zurich, Switzerland
- Stenflo, Johan**, University of Lund, Dept. of Clinical Chemistry, Malmö General Hospital, S-205 02 Malmö, Sweden
- Stetten, Jane Lazarow**, 4701 Willard Ave #1413, Chevy Chase, MD 20815-4627
- Stuedler, Paul A.**, Marine Biological Laboratory, The Ecosystems Center, Woods Hole, MA 02543
- Stokes, Darrell R.**, Emory University, Department of Biology, 1510 Clifton Rd., NE, Atlanta, GA 30322-1100
- Stommel, Elijah W.**, Dartmouth-Hitchcock Medical Center, Neurology Dept., Lebanon, NH 03756
- Stracher, Alfred**, SUNY Health Science Center, Dept. of Biochemistry, 450 Clarkson Avenue, Brooklyn, NY 11203
- Strumwasser, Felix**, 39 Fox Run Drive, Hatchville, MA 02536
- Stuart, Ann E.**, University of North Carolina, Department of Physiology, Medical Res. Bldg. 206H, Chapel Hill, NC 27599-7545
- Sugimori, Mutsuyuki**, New York University Medical Center, Dept. of Physiology & Neuroscience, Rm 442, 550 First Avenue, New York, NY 10016
- Summers, William C.**, Western Washington University, Huxley Coll. of Environ. Stud., Bellingham, WA 98225
- Suprenant, Kathy A.**, University of Kansas, Dept. of Physiol. & Cell Biol., 4010 Haworth Hall, Lawrence, KS 66045
- Sweet, Frederick**, Washington University, School of Medicine, Dept. of OB & GYN, Box 8064, St. Louis, MO 63110
- Swenson, Katherine I.**, Duke University Medical Center, Dept. of Molec. Cancer Biology, Box 3686, Durham, NC 27710
- Sydlik, Mary Anne**, Hope College, Peale Science Center, 35 East 12th St., PO Box 9000, Holland, MI 49422
- Szent-Gyorgyi, Andrew**, Brandeis University, Department of Biology, Bassine 244, 415 South Street, Waltham, MA 02254
- Tabares, Lucia**, University of Seville School of Medicine, Dept. of Physiology, Avda. Sanchez Prizjuan, 4, Seville 41009, SPAIN
- Tamm, Sidney L.**, Boston University, 725 Commonwealth Avenue, Boston, MA 02215
- Tanzer, Marvin L.**, University of Connecticut School of Dental Medicine, Dept. of Biostructure & Funct., Farmington, CT 06030-3705
- Tasaki, Ichiji**, NIMH/NIH, Laboratory of Neurobiology, Building 36, Room 2B-16, Bethesda, MD 20892
- Taylor, D. Lansing**, Carnegie Mellon University, Ctr. for Fluorescence Res., 4400 Fifth Avenue, Pittsburgh, PA 15213
- Taylor, Edwin W.**, University of Chicago, Dept. of Mol. Gen. & Cell Bio., 920 E. 58th Street, Chicago, IL 60637
- Teal, John M.**, Woods Hole Oceanographic Institution, Department of Biology, Woods Hole, MA 02543
- Telfer, William H.**, University of Pennsylvania, Department of Biology, Philadelphia, PA 19104
- Telzer, Bruce**, Pomona College, Dept. of Biol., Thille Bldg., 175 W. 6th Street, Claremont, CA 91711
- Townsel, James G.**, Meharry Medical College, Dept. of Physiology, 1005 D. B. Todd Boulevard, Nashville, TN 37208
- Travis, David M.**, 19 High Street, Woods Hole, MA 02543-1221
- Treisman, Steven N.**, University of Massachusetts Medical Center, Department of Pharmacology, 55 Lake Avenue North, Worcester, MA 01655
- Trigg, D. Thomas**, One Federal Street, 9th Floor, Boston, MA 02211
- Troll, Walter**, NYU Medical Center, 550 First Avenue, New York, NY 10016
- Troxler, Robert F.**, Boston University School of Medicine, Dept. of Biochem., 80 East Concord Street, Boston, MA 02118
- Tucker, Edward B.**, Baruch College, CUNY, Dept. of Natural Sciences, 17 Lexington Avenue, New York, NY 10010
- Turner, Ruth D.**, Harvard University, Museum of Comparative Zoology, Mollusk Department, Cambridge, MA 02138
- Tweedell, Kenyon S.**, University of Notre Dame, Dept. of Biological Sciences, Notre Dame, IN 46656
- Tykocinski, Mark L.**, Case Western Reserve University, Institute of Pathology, 2085 Adelbert Road, Cleveland, OH 44106
- Tytell, Michael**, Wake Forest University, Bowman Gray School of Medicine, Dept. of Anatomy & Neurobio., Winston-Salem, NC 27157
- Ueno, Hiroshi**, Kyoto University, AGR Chemistry Faculty, Sakyo, Kyoto, 606-8502, Japan
- Valiela, Ivan**, Boston University Marine Program, Marine Biological Laboratory, Woods Hole, MA 02543
- Vallee, Richard**, University of Massachusetts Medical Center, Worcester Foundation Campus, Cell Biol., 222 Maple Avenue, Shrewsbury, MA 01545

R76 Annual Report

Valois, John J., 420 Woods Hole Road, Woods Hole, MA 02543
Van Dover, Cindy Lee, University of Alaska, P.O. Box 757220,
Fairbanks, AK 99775
Van Holde, Kensal E., Oregon State University, Biochemistry &
Biophysics Dept., Corvallis, OR 97331-7503
Vogl, Thomas P., Environmental Research Institute of Michigan,
1101 Wilson Boulevard, Arlington, VA 22209

Wainwright, Norman R., Marine Biological Laboratory, Woods
Hole, MA 02543
Waksman, Byron, NYU Medical Center, Department of Pathology,
550 First Avenue, New York, NY 10016
Wall, Betty, 9 George Street, Woods Hole, MA 02543
Wang, Hsien-Yu, SUNY, Stony Brook, Univ. Medical Center,
Physiology & Biophysics-HSC, Stony Brook, NY 11794-8633
Wangh, Lawrence J., Brandeis University, Dept. of Biology, 415
South Street, Waltham, MA 02254
Warner, Robert C., University of California, Irvine, Molecular
Bio. & Biochemistry, Irvine, CA 92717
Warren, Leonard, Wistar Institute, 36th and Spruce Streets,
Philadelphia, PA 19104
Waterbury, John B., Woods Hole Oceanographic Institution, Dept.
of Biology, Woods Hole, MA 02543
Waxman, Stephen G., Yale Medical School, Neurology Department,
333 Cedar Street, P.O. Box 208018, New Haven, CT 06510
Webb, H. M., 426 Woods Hole Road, Woods Hole, MA 02543
Weher, Anne Marie, University of Pennsylvania School of
Medicine, Dept. of Biochem. & Biophysics, Philadelphia, PA
19066
Weeks, Janis C., Institute for Neuroscience, University of Oregon,
Box 1254, Eugene, OR 97403-1254
Weidner, Earl, Louisiana State University, Dept. of Zoology &
Physiology, Baton Rouge, LA 70803
Weiss, Alice Sara, 105 University Blvd. West, Silver Spring, MD
20901
Weiss, Dieter, University of Rostock, Biology, Institute of Zoology,
D-18051 Rostock, Germany
Weiss, Leon P., University of Pennsylvania School of Veterinary
Medicine, Department of Animal Biology, Philadelphia, PA 19104
Weiss, Marisa C., Paoli Memorial Hospital, Department of Radiation
Oncology, 255 W. Lancaster Avenue, Paoli, PA 19301
Weissmann, Gerald, New York University Medical Center, Dept. of
Med/Div. Rheumatology, 550 First Avenue, New York, NY 10016
Westerfield, R. Monte, University of Oregon, Institute of
Neuroscience, Eugene, OR 97403

Whittaker, J. Richard, University of New Brunswick, Dept. of
Biology, BS 4511, Fredericton, NB E3B 6E1, Canada
Wilkens, Lon A., University of Missouri, St. Louis, Dept. of
Biology, 8001 Natural Bridge Road, St. Louis, MO 63121-4499
Wilson, Darcy B., San Diego Regional Cancer Center, 3099 Science
Park Road, San Diego, CA 92121
Wilson, T. Hastings, Harvard Medical School, Department of
Physiology, 25 Shattuck Street, Boston, MA 02115
Witkovsky, Paul, NYU Medical Center, Department of
Ophthalmology, 550 First Avenue, New York, NY 10016
Wittenberg, Beatrice, Albert Einstein College of Medicine, Dept. of
Physiol. & Biophysics, Bronx, NY 10461
Wittenberg, Jonathan B., Albert Einstein College of Medicine,
Dept. of Physiol. & Biophysics, Bronx, NY 10461
Wolken, Jerome J., Carnegie Mellon University, Dept. of Biological
Sciences, 440 Fifth Avenue, Pittsburgh, PA 15213
Wonderlin, William F., West Virginia University, Pharmacology &
Toxicology Dept., Morgantown, WV 26506
Worden, Mary Kate, University of Virginia, Dept. of Molecular
Physics and Biological Physics, P.O. Box 10011, Charlottesville,
VA 22906
Worgul, Basil V., Columbia University, Department of
Ophthalmology, 630 West 168 Street, New York, NY 10032
Wu, Chau Hsiung, Northwestern University Medical School, Dept.
of Pharmacology (S215), 303 E. Chicago Avenue, Chicago, IL
60611-3008
Wytenbach, Charles R., University of Kansas, Biological Sciences
Dept., 2045 Haworth Hall, Lawrence, KS 66045-2106
Yeh, Jay Z., Northwestern University, Medical School, Department
of Pharmacology, Chicago, IL 60611
Zacks, Sumner I., 65 Saconeset Road, Falmouth, MA 02540-1851
Zigman, Seymour, University of Rochester Medical School,
Ophthalmol. Research, Box 314, 601 Elmwood Avenue, Rochester,
NY 14640
Zigmond, Michael J., University of Pittsburgh, Dept. of
Neuroscience, 570 Crawford Hall, Pittsburgh, PA 15260
Zimmerberg, Joshua J., LCMB, NICHD, NIH, Building 10, Room
10D14, 10 Center Drive, MSC 1855, Bethesda, MD 20892-1855
Zntoli, Steven J., Williams College, Dept. of Biology,
Williamstown, MA 01267
Zucker, Robert S., University of California, Neurobiology Div.,
Molecular & Cellular Biol. Dept., Berkeley, CA 94720
Zukin, R. Suzanne, Albert Einstein College of Medicine, Dept. of
Neurosci., 1410 Pelham Parkway South, Bronx, NY 10461

MBL Associates

Executive Board

Julie S. Child, President
Ruth Ann Laster, Vice President
Priscilla Roslansky, Secretary
Hanna Hastings, Treasurer
Mary Ulbrich, Membership Chair
Duncan Aspinwall
Barbara Atwood
Kitty Brown

Seymour Cohen
Molly Cornell
Elizabeth Farnham
Michael Fenlon
Megan Jones
Alice Knowles
Rebecca Lash
Barbara Little
Jack Pearce
Joan Pearlman

Deborah Senft
John Valois
Kensal Van Holde

Sustaining Associate

Josephine B. Crane Foundation
George Frederick Jewett Foundation
Mr. Edward F. MacNichol, Jr.
Plymouth Savings Bank
Mr. and Mrs. William A. Putnam, III

Supporting Associate

Mrs. George H. A. Clowes
 Dr. and Mrs. James D. Ebert
 Dr. and Mrs. Prosser Gifford
 Drs. Alfred and Joan Goldberg
 Mr. and Mrs. Lon Hocker
 Drs. Luigi and Elaine Mastroianni
 Dr. and Mrs. William M. McDermott
 Dr. and Mrs. Courtland D. Perkins
 Mr. Michael Fenlon and Ms. Linda Sallop
 Mrs. Anne W. Sawyer
 Ms. Maxine F. Singer
 Dr. John Tochko and Mrs. Christina
 Myles-Tochko
 Drs. Walter S. Vincent and Dore J. Butler
 Mr. and Mrs. Leslie J. Wilson

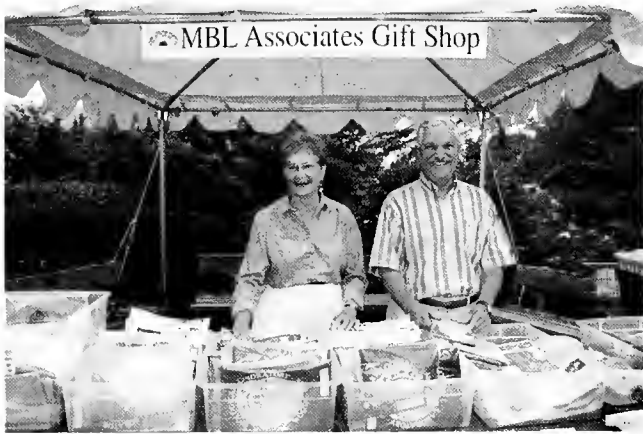
Dual Membership

Mr. David C. Ahearn
 Mr. and Mrs. Douglas F. Allison
 Drs. James and Helene Anderson
 Dr. and Mrs. Samuel C. Armstrong
 Mr. and Mrs. Duncan P. Aspinwall
 Mr. and Mrs. Donald R. Aukamp
 Mr. and Mrs. John M. Baitsell
 Mr. and Mrs. William L. Banks
 Dr. and Mrs. Robert B. Barlow, Jr.
 Mr. and Mrs. John E. Barnes
 Drs. Harriet and Alan Bernheimer
 Mr. and Mrs. Robert O. Bigelow
 Dr. and Mrs. Edward G. Boettiger
 Dr. and Mrs. Alfred F. Borg
 Dr. and Mrs. Thomas A. Borgese
 Dr. and Mrs. Francis P. Bowles
 Dr. and Mrs. John B. Buck
 Dr. and Mrs. John E. Burris
 Mr. and Mrs. D. Bret Carlson
 Dr. and Mrs. Alfred B. Chaet
 Dr. and Mrs. Arnold M. Clark
 Mr. and Mrs. James Cleary
 Mr. and Mrs. Lawrence H. Coburn
 Dr. and Mrs. Neal W. Cornell
 Mr. and Mrs. Norman C. Cross
 Mr. and Mrs. Bruce G. Daniels
 Mr. and Mrs. Richard C. Dierker
 Dr. and Mrs. Arthur Brooks DuBois
 Mr. and Mrs. John Eustis, II
 Dr. and Mrs. James J. Ferguson, Jr.
 Mr. and Mrs. Harold Frank
 Mr. and Mrs. Howard G. Freeman
 Dr. and Mrs. Robert A. Frosch
 Dr. and Mrs. Mordecai L. Gabriel
 Dr. and Mrs. David Garber
 Dr. and Mrs. James L. German, III
 Dr. and Mrs. Philip Grant
 Dr. and Mrs. Thomas C. Gregg
 Prof. and Mrs. Lawrence Grossman
 Dr. and Mrs. Harlyn O. Halvorson
 Capt. and Mrs. Frederick J. Hancox
 Dr. and Mrs. Richard B. Harvey
 Dr. and Mrs. J. Woodland Hastings

Mr. and Mrs. Gary G. Hayward
 Dr. and Mrs. John E. Hobbie
 Drs. Francis C. G. Hoskin and Elizabeth M.
 Farnham
 Dr. and Mrs. Robert J. Huettner
 Dr. and Mrs. Shinya Inoué
 Dr. and Mrs. Benjamin Kaminer
 Mr. and Mrs. Paul W. Knaplund
 Dr. and Mrs. George M. Langford
 Dr. and Mrs. Leonard Laster
 Dr. and Mrs. Hans Laufer
 Mr. William Lawrence and Mrs. Barbara
 Buchanan
 Mr. and Mrs. James E. Lloyd
 Dr. and Mrs. Julian B. Marsh
 Mr. and Mrs. Joseph C. Martyna
 Mr. and Mrs. John E. Matthews
 Dr. and Mrs. Robert T. McCluskey
 Dr. and Mrs. Jerry M. Melillo
 Mr. and Mrs. Richard Meyers
 Dr. and Mrs. Daniel G. Miller
 Dr. and Mrs. Charles H. Montgomery
 Dr. and Mrs. John E. Naugle
 Mr. and Mrs. Frank L. Nickerson
 Dr. and Mrs. Clifford T. O'Connell
 Mr. David Palmer
 Dr. and Mrs. George D. Pappas
 Dr. and Mrs. John B. Pearce
 Mr. and Mrs. William J. Pechilis
 Mr. and Mrs. John B. Peri
 Dr. and Mrs. Philip Person
 Mr. and Mrs. George H. Plough
 Dr. and Mrs. Aubrey Pothier, Jr.
 Mr. and Mrs. Allan Ray Putnam
 Dr. and Mrs. George T. Reynolds
 Mr. and Mrs. John Ripple
 Dr. and Mrs. Harris Ripps
 Mr. and Mrs. Jean Roberts
 Drs. Priscilla and John Roslansky
 Dr. and Mrs. John W. Saunders, Jr.
 Dr. and Mrs. R. Walter Schlesinger
 Mr. and Mrs. Harold H. Sears
 Dr. and Mrs. Sheldon J. Segal
 Dr. and Mrs. David Shepro
 Mr. and Mrs. Bertram R. Silver
 Mr. and Mrs. Jonathan O. Simonds
 Drs. Frederick and Marguerite Smith
 Dr. and Mrs. Heinz Specht
 Drs. William and Phoebe Speck
 Dr. and Mrs. William K. Stephenson
 Mr. and Mrs. Gerard L. Swope, III
 Mr. and Mrs. Emil D. Tietje, Jr.
 Dr. and Mrs. Walter Troll
 Mr. and Mrs. Volker Ulbrich
 Mr. and Mrs. Samuel Vincent
 Mr. and Mrs. Samuel Ward
 Mr. J. Ware and Ms. Sharon McCarthy
 Dr. and Mrs. Henry B. Warren
 Dr. and Mrs. Paul S. Wheeler
 Dr. Martin Keister White
 Mr. and Mrs. Leonard M. Wilson
 Mr. Dick S. Yeo
 Dr. and Mrs. Sumner I. Zacks

Individual Associate

Mrs. Constance M. Allard
 Mrs. Douglas P. Amon
 Mr. Dean N. Arden
 Mrs. Ellen Prosser Armstrong
 Mrs. Kimball C. Atwood, III
 Mr. Everett E. Bagley
 Mr. C. John Berg
 Mrs. Elinor W. Bodian
 Mr. Thomas C. Bolton
 Mrs. Frank A. Brown, Jr.
 Mrs. M. Kathryn S. Brown
 Dr. Alan H. Burghauer
 Mrs. Barbara Burwell
 Mr. William O. Burwell
 Dr. Graciela C. Candelas
 Mrs. Winslow G. Carlton
 Mr. Frank Carotenuto
 Dr. Robert H. Carrier
 Mrs. Patricia A. Case
 Dr. Richard L. Chappell
 Dr. Sallie Chisholm
 Mrs. Octavia C. Clement
 Mr. Allen W. Clowes
 Dr. Jewel Plummer Cobb
 Dr. Seymour S. Cohen
 Ms. Anne S. Concannon
 Mr. Robert J. Cook
 Prof. D. Eugene Copeland
 Dr. Helen M. Costello
 Dr. Vincent Cowling
 Ms. Dorothy Crossley
 Miss Helen Crossley
 Mrs. Villa B. Crowell
 Mrs. Francis J. DeYoung
 Dr. Marie A. DiBerardino
 Mr. Stephen Doyle
 Ms. Suzanne Droban
 Roy A. Duffus
 Mrs. Charles E. Eastman
 Dr. Frank Egloff
 Mr. William M. Ferry
 Ms. Sylvia M. Flanagan
 Mr. Robert P. Flynn, Jr.
 Mr. John H. Ford
 Dr. Krystyna Frenkel
 Mr. Paul J. Freyheit
 Dr. John J. Funkhouser
 Mrs. Paul M. Fye
 Dr. Patricia E. Garrett
 Mrs. Rebeckah Glazebrook
 Murray Glusman, M.D.
 Mrs. Mary L. Goldman
 Ms. Muriel Gould
 Mrs. Deborah Ann Green
 Dr. B. Herold Griffith
 Mrs. Edith T. Grosch
 Mrs. Valerie A. Hall
 Ms. Mary Elizabeth Hamstrom
 Ms. Elizabeth E. Hathaway
 Dr. Robert R. Haubrich
 Mr. Michael W. Herlihy
 Mrs. Nathan Hirschfeld



Mrs. Eleanor D. Hodge
 Miss Elizabeth B. Jackson
 Gary Jacobson
 Dr. Joseph Jacobson
 Mrs. Margaret H. Jones
 Mrs. Barbara Kanellopoulos
 Mrs. Marcella Katz
 Ms. Patricia E. Keoughan
 Dr. Peter N. Kivy
 Ms. Norma Kumin
 Mrs. Rodney C. Larcom
 Ms. Rebecca Lash
 Dr. Marian E. LeFevre
 Dr. Mortimer Levitz
 Mr. Edwin M. Libbin
 Mr. Lennart Lindberg
 Mrs. Sarah J. Loessel
 Mr. Richard C. Lovering
 Mrs. Margaret M. Macleish
 Dr. Phillip B. Maples
 Mr. Daniel R. Martin
 Dr. G. C. Matbiessen
 Mrs. Mary Hartwell Mavor
 Mrs. Jane C. McCormack
 Ms. Suzanne McDermott
 Mr. Paul McGonigle
 Ms. Mary W. McKoan
 Ms. Geraldine G. McLean
 Ms. Cornelia Hanna McMurtrie
 Dr. Martin Mendelson
 Mrs. James A. Miles
 Mrs. Florence E. Mixer
 Ms. Cynthia Moor
 Mr. Stephen A. Moore
 Mr. Alan F. Morrison
 Mrs. Eleanor M. Nace
 Mr. William G. Neall
 Dr. Pamela Nelson
 Mr. Thomas J. Novitsky
 Mr. John J. O'Connor
 Dr. Judith Pederson
 Ms. Joyce S. Pendery
 Dr. Murray E. Pendleton
 Mr. Raymond W. Peterson
 Ms. Victoria A. Powell
 Mrs. Julia S. Rankin
 Mr. Fred J. Ravens, Jr.

Mrs. Adell R. Rawson
 Dr. Lionel I. Rebbun
 Dr. Robert M. Reece
 Dr. Mary Rice
 Mr. John Riina
 Dr. Monica Riley
 Mrs. Alison A. Robb
 Mrs. Lola E. Robertson
 Mrs. Arlene Rogers
 Mrs. Elsie M. Scott
 Dr. Cecily C. Selby
 Mrs. Deborah G. Senft
 Mrs. Charlotte Shemin
 Mrs. Cynthia C. Smith
 Mrs. Perle Sonnenblick
 Dr. Evelyn Spiegel
 Dr. Guy L. Steele, Sr.
 Mrs. Judith G. Stetson
 Mrs. Jane Lazarow Stetten
 Dr. Dorothy A. Stracher
 Mr. Robert Stump
 Dr. Maurice Sussman
 Mr. Albert H. Swain
 Mr. James K. Taylor
 Mrs. Alice Todd
 Mr. Arthur D. Traub
 Ms. Natalie Trousof
 Ms. Ciona Ulbrich
 Mrs. Barbara Van Holde
 Mrs. Eve Warren
 Mr. John T. Weeks
 Ms. Lillian Wendorff
 Mrs. Barbara Whitehead
 Mrs. A.A.T. Wickersham
 Mrs. Clare M. Wilber
 Mr. Albert Wilson
 Dr. T. Hastings Wilson
 Ms. Nancy Woitkoski
 Mrs. Elizabeth S. Yntema
 Mrs. Donald J. Zinn

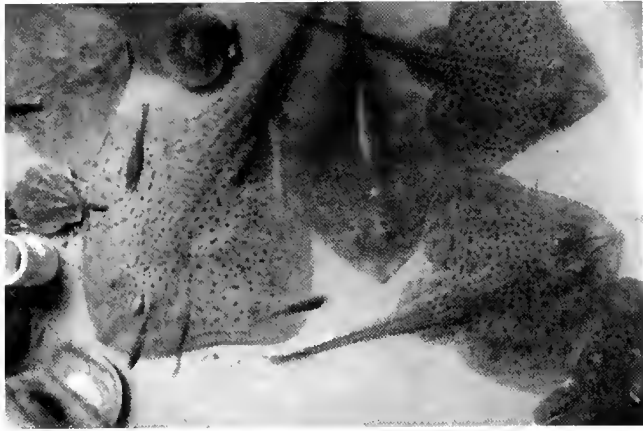
*MBL Associates Gift Shop
 Volunteers*

Marion Adelberg
 Marianne Angell
 Barbara Atwood

Harriet Bernheimer
 Gloria Borgese
 Jennie Brown
 Elizabeth Buck
 Jewel Cobb
 Janet Daniels
 Carol DeYoung
 Fran Eastman
 Alma Ebert
 Pat Ferguson
 Becky Glazebrook
 Muriel Gould
 Rose Grant
 Edie Grosch
 Bobbie Grossman
 Pat Hancox
 Hanna Hastings
 Sally Karush
 Alice Knowles
 Barbara Little
 Sally Loessel
 Winnie Mackey
 Miriam Mauzerall
 Mary Mavor
 Elizabeth Mosley
 Jane McCormack
 Polly Miles
 Florence Mixter
 Lorraine Mizell
 Eleanor Nace
 Bertha Person
 Liz Price
 Julie Rankin
 Jean Ripps
 Arlene Rogers
 Lilyan Saunders
 Marilyn Shepro
 Cynthia Smith
 Peggy Smith
 Louise Specht
 Jane Stetten
 Elaine Troll
 Natalie Trousof
 Mary Ulbrich
 Barbara Van Holde
 Mabel Whelpley
 Barbara Whitehead
 Clare Wilber

MBL Summer Tour Guides

Kevin Barry
 John Buck
 Sears Crowell
 Barbara Little
 Giselle Magnusson
 Kathy Mullin
 Julie Rankin
 Lola Robertson
 Priscilla Roslansky
 Erin Smyth
 Mary Ulbrich
 John Valois



Certificate of Organization Articles of Amendment Bylaws

Certificate of Organization

(On File in the Office of the Secretary of the Commonwealth)

No. 3170

We, Alpheus Hyatt, President, William Stanford Stevens, Treasurer, and William T. Sedgwick, Edward G. Gardiner, Susan Mims and Charles Sedgwick Minot being a majority of the Trustees of the Marine Biological Laboratory in compliance with the requirements of the fourth section of chapter one hundred and fifteen of the Public Statutes do hereby certify that the following is a true copy of the agreement of association to constitute said Corporation, with the names of the subscribers thereto:

We, whose names are hereto subscribed, do, by this agreement, associate ourselves with the intention to constitute a Corporation according to the provisions of the one hundred and fifteenth chapter of the Public Statutes of the Commonwealth of Massachusetts, and the Acts in amendment thereof and in addition thereto.

The name by which the Corporation shall be known is
THE MARINE BIOLOGICAL LABORATORY.

The purpose for which the Corporation is constituted is to establish and maintain a laboratory or station for scientific study and investigations, and a school for instruction in biology and natural history.

The place within which the Corporation is established or located is the city of Boston within said Commonwealth.

The amount of its capital stock is none.

In Witness Whereof, we have hereunto set our hands, this twenty seventh day of February in the year eighteen hundred and eighty-eight, Alpheus Hyatt, Samuel Mills, William T. Sedgwick, Edward G. Gardiner, Charles Sedgwick Minot, William G. Farlow, William Stanford Stevens, Anna D. Phillips, Susan Mims, B. H. Van Vleck.

That the first meeting of the subscribers to said agreement was held on the thirteenth day of March in the year eighteen hundred and eighty-eight.

In Witness Whereof, we have hereunto signed our names, this thirteenth day of March in the year eighteen hundred and eighty-eight, Alpheus Hyatt, President, William Stanford Stevens, Treasurer, Edward G. Gardiner, William T. Sedgwick, Susan Mims, Charles Sedgwick Minot.

(Approved on March 20, 1888 as follows:

I hereby certify that it appears upon an examination of the within written certificate and the records of the corporation duly submitted to my inspection, that the requirements of sections one, two and three of chapter one hundred and fifteen, and sections eighteen, twenty and twenty-one of chapter one hundred and six, of the Public Statutes, have been complied with and I hereby approve said certificate this twentieth day of March A.D. eighteen hundred and eighty-eight.

Charles Endicott
Commissioner of Corporations)

Articles of Amendment

(On File in the Office of the Secretary of the Commonwealth)

We, James D. Ebert, President, and David Shepro, Clerk of the Marine Biological Laboratory, located at Woods Hole, Massachusetts 02543, do hereby certify that the following amendment to the Articles of Organization of the Corporation was duly adopted at a meeting held on August 15, 1975, as adjourned to August 29, 1975, by vote of 444 members, being at least two-thirds of its members legally qualified to vote in the meeting of the corporation:

Voted. That the Certificate of Organization of this corporation be and it hereby is amended by the addition of the following provisions:

"No Officer, Trustee or Corporate Member of the corporation shall be personally liable for the payment or satisfaction of any obligation or liabilities incurred as a result of, or otherwise in connection with, any commitments, agreements, activities or affairs of the corporation.

"Except as otherwise specifically provided by the Bylaws of the corporation, meetings of the Corporate Members of the corporation may be held anywhere in the United States.

"The Trustees of the corporation may make, amend or repeal the Bylaws of the corporation in whole or in part, except with respect to any provisions thereof which shall by law, this Certificate or the bylaws of the corporation, require action by the Corporate Members."

The foregoing amendment will become effective when these articles of amendment are filed in accordance with Chapter 180, Section 7 of the General Laws unless these articles specify, in accordance with the vote adopting the amendment, a later effective date not more than thirty days after such filing, in which event the amendment will become effective on such later date.

In Witness whereof and Under the Penalties of Perjury, we have hereto signed our names this 2nd day of September, in the year 1975, James D. Ebert, President; David Shepro, Clerk.

(Approved on October 24, 1975, as follows:

I hereby approve the within articles of amendment and, the filing fee in the amount of \$10 having been paid, said articles are deemed to have been filed with me this 24th day of October, 1975.

Paul Guzzi
Secretary of the Commonwealth)

Bylaws

(Revised August 7, 1992 and December 10, 1992)

ARTICLE I—THE CORPORATION

A Name and Purpose. The name of the Corporation shall be The Marine Biological Laboratory. The Corporation's purpose shall be to establish and main-

tain a laboratory or station for scientific study and investigation and a school for instruction in biology and natural history.

B. Nondiscrimination. The Corporation shall not discriminate on the basis of age, religion, color, race, national or ethnic origin, sex or sexual preference in its policies on employment and administration or in its educational and other programs.

ARTICLE II—MEMBERSHIP

A. Members. The Members of the Corporation ("Members") shall consist of persons elected by the Board of Trustees (the "Board"), upon such terms and conditions and in accordance with such procedures, not inconsistent with law or these Bylaws, as may be determined by the Board. At any regular or special meeting of the Board, the Board may elect new Members. Members shall have no voting or other rights with respect to the Corporation or its activities except as specified in these Bylaws, and any Member may vote at any meeting of the Members in person only and not by proxy. Members shall serve until their death or resignation unless earlier removed with or without cause by the affirmative vote of two-thirds of the Trustees then in office. Any Member who has retired from his or her home institution may, upon written request to the Corporation, be designated a Life Member. Life Members shall not have the right to vote and shall not be assessed for dues.

B. Meetings. The annual meeting of the Members shall be held on the Friday following the first Tuesday in August of each year, at the Laboratory of the Corporation in Woods Hole, Massachusetts, at 9:30 a.m. The Chairperson of the Board shall preside at meetings of the Corporation. If no annual meeting is held in accordance with the foregoing provision, a special meeting may be held in lieu thereof with the same effect as the annual meeting, and in such case all references in these Bylaws, except in this Article II.B., to the annual meeting of the Members shall be deemed to refer to such special meeting. Members shall transact business as may properly come before the meeting. Special meetings of the Members may be called by the Chairperson or the Trustees, and shall be called by the Clerk, or in the case of the death, absence, incapacity or refusal by the Clerk, by any other officer, upon written application of Members representing at least ten percent of the smallest quorum of Members required for a vote upon any matter at the annual meeting of the Members, to be held at such time and place as may be designated.

C. Quorum. One hundred (100) Members shall constitute a quorum at any meeting. Except as otherwise required by law or these Bylaws, the affirmative vote of a majority of the Members voting in person at a meeting attended by a quorum shall constitute action on behalf of the Members.

D. Notice of Meetings. Notice of any annual meeting or special meeting of Members, if necessary, shall be given by the Clerk by mailing notice of the time and place and purpose of such meeting at least 15 days before such meeting to each Member at his or her address as shown on the records of the Corporation.

E. Waiver of Notice. Whenever notice of a meeting is required to be given a Member, under any provision of the Articles or Organization or Bylaws of the Corporation, a written waiver thereof, executed before or after the Meeting by such Member, or his or her duly authorized attorney, shall be deemed equivalent to such notice.

F. Adjournments. Any meeting of the Members may be adjourned to any other time and place by the vote of a majority of those Members present at the meeting, whether or not such Members constitute a quorum, or by any officer entitled to preside at or to act as Clerk of such meeting, if no Member is present or represented. It shall not be necessary to notify any Members of any adjournment unless no Member is present or represented at the meeting which is adjourned, in which case, notice of the adjournment shall be given in accordance with Article II.D. Any business which could have been transacted at any meeting of the Members as originally called may be transacted at an adjournment thereof.

ARTICLE III—ASSOCIATES OF THE CORPORATION

Associates of the Corporation. The Associates of the Marine Biological Laboratory shall be an unincorporated group of persons (including associations and corporations) interested in the Laboratory and shall be organized and operated under the general supervision and authority of the Trustees. The Associates of the Marine Biological Laboratory shall have no voting rights.

ARTICLE IV—BOARD OF TRUSTEES

A. Powers. The Board of Trustees shall have the control and management of the affairs of the Corporation. The Trustees shall elect a Chairperson of the Board who shall serve until his or her successor is elected and qualified. They shall annually elect a President of the Corporation. They shall annually elect a Vice Chairperson of the Board who shall be Vice Chairperson of the meetings of the

Corporation. They shall annually elect a Treasurer. They shall annually elect a Clerk, who shall be a resident of Massachusetts. They shall elect Trustees-at-Large as specified in this Article IV. They shall appoint a Director of the Laboratory for a term not to exceed five years, provided the term shall not exceed one year if the candidate has attained the age of 65 years prior to the date of the appointment. They shall choose such other officers and agents as they shall think best. They may fix the compensation of all officers and agents of the Corporation and may remove them at any time. They may fill vacancies occurring in any of the offices. The Board shall have the power to choose an Executive Committee from their own number as provided in Article V, and to delegate to such Committee such of their own powers as they may deem expedient in addition to those powers conferred by Article V. They shall, from time to time, elect Members to the Corporation upon such terms and conditions as they shall have determined, not inconsistent with law or these Bylaws.

B. Composition and Election.

(1) The Board shall include 24 Trustees elected by the Board as provided below.

(a) At least six Trustees ("Corporate Trustees") shall be Members who are scientists, and the other Trustees ("Trustees-at-Large") shall be individuals who need not be Members or otherwise affiliated with the Corporation.

(b) The 24 elected Trustees shall be divided into four classes of six Trustees each, with one class to be elected each year to serve for a term of four years, and with each such class to include at least one Corporate Trustee. Such classes of Trustees shall be designated by the year of expiration of their respective terms.

(2) The Board shall also include the Chief Executive Officer, Treasurer and the Chairperson of the Science Council, who shall be *ex officio* voting members of the Board.

(3) Although Members or Trustees may recommend individuals for nomination as Trustees, nominations for Trustee elections shall be made by the Nominating Committee in its sole discretion. The Board may also elect Trustees who have not been nominated by the Nominating Committee.

C. Eligibility. A Corporate Trustee or a Trustee-at-Large who has been elected to an initial four-year term or remaining portion thereof, of which he/she has served at least two years, shall be eligible for re-election to a second four-year term, but shall be ineligible for re-election to any subsequent term until one year has elapsed after he/she has last served as a Trustee.

D. Removal. Any Trustee may be removed from office at any time with or without cause, by vote of a majority of the Members entitled to vote in the election of Trustees; or for cause, by vote of two-thirds of the Trustees then in office. A Trustee may be removed for cause only if notice of such action shall have been given to all of the Trustees or Members entitled to vote, as the case may be, prior to the meeting at which such action is to be taken and if the Trustee to be so removed shall have been given reasonable notice and opportunity to be heard before the body proposing to remove him or her.

E. Vacancies. Any vacancy in the Board may be filled by vote of a majority of the remaining Trustees present at a meeting of Trustees at which a quorum is present. Any vacancy in the Board resulting from the resignation or removal of a Corporate Trustee shall be filled by a Member who is a scientist.

F. Meetings. Meetings of the Board shall be held from time to time, not less frequently than twice annually, as determined by the Board. Special meetings of Trustees may be called by the Chairperson, or by any seven Trustees, to be held at such time and place as may be designated. The Chairperson of the Board, when present, shall preside over all meetings of the Trustees. Written notice shall be sent to a Trustee's usual or last known place of residence at least two weeks before the meeting. Notice of a meeting need not be given to any Trustee if a written waiver of notice executed by such Trustee before or after the meeting is filed with the records of the meeting, or if such Trustee shall attend the meeting without protesting prior thereto or at its commencement the lack of notice given to him or her.

G. Quorum and Action by Trustees. A majority of all Trustees then in office shall constitute a quorum. Any meeting of Trustees may be adjourned by vote of a majority of Trustees present, whether or not a quorum is present, and the meeting may be held as adjourned without further notice. When a quorum is present at any meeting of the Trustees, a majority of the Trustees present and voting (excluding abstentions) shall decide any question, including the election of officers, unless otherwise required by law, the Articles of Organization or these Bylaws.

H. Transfers of Interests in Land. There shall be no transfer of title nor long-term lease of real property held by the Corporation without prior approval of not less than two-thirds of the Trustees. Such real property transactions shall be finally acted upon at a meeting of the Board only if presented and discussed at a prior meeting of the Board. Either meeting may be a special meeting and no less than four weeks shall elapse between the two meetings. Any property acquired by the

Corporation after December 1, 1989 may be sold, any mortgage or pledge of real property (regardless of when acquired) to secure borrowings by the Corporation may be granted, and any transfer of title or interest in real property pursuant to the foreclosure or endorsement of any such mortgage or pledge of real property may be effected by any holder of a mortgage or pledge of real property of the Corporation, with the prior approval of not less than two-thirds of the Trustees (other than any Trustee or Trustees with a direct or indirect financial interest in the transaction being considered for approval) who are present at a regular or special meeting of the Board at which there is a quorum.

ARTICLE V—COMMITTEES

A. *Executive Committee.* There shall be an Executive Committee of the Board of Trustees which shall consist of not more than eleven (11) Trustees, including *ex officio* Trustees, elected by the Board.

The Chairperson of the Board shall act as Chairperson of the Executive Committee and the Vice Chairperson as Vice Chairperson. The Executive Committee shall meet at such times and places and upon such notice and appoint such subcommittees as the Committee shall determine.

The Executive Committee shall have and may exercise all the powers of the Board during the intervals between meetings of the Board except those powers specifically withheld, from time to time, by vote of the Board or by law. The Executive Committee may also appoint such committees, including persons who are not Trustees, as it may, from time to time, approve to make recommendations with respect to matters to be acted upon by the Executive Committee or the Board.

The Executive Committee shall keep appropriate minutes of its meetings, which shall be reported to the Board. Any actions taken by the Executive Committee shall also be reported to the Board.

B. *Nominating Committee.* There shall be a Nominating Committee which shall consist of not fewer than four nor more than six Trustees appointed by the Board in a manner which shall reflect the balance between Corporate Trustees and Trustees-at-Large on the Board. The Nominating Committee shall nominate persons for election as Corporate Trustees and Trustees-at-Large, Chairperson of the Board, Vice Chairperson of the Board, President, Treasurer, Clerk, Director of the Laboratory and such other officers, if any, as needed, in accordance with the requirements of these Bylaws. The Nominating Committee shall also be responsible for overseeing the training of new Trustees. The Chairperson of the Board of Trustees shall appoint the Chairperson of the Nominating Committee. The Chairperson of the Science Council shall be an *ex officio* voting member of the Nominating Committee.

C. *Science Council.* There shall be a Science Council (the "Council") which shall consist of Members of the Corporation elected to the Council by vote of the Members of the Corporation, and which shall advise the Board with respect to matters concerning the Corporation's mission, its scientific and instructional endeavors, and the appointment and promotions of persons or committees with responsibility for matters requiring scientific expertise. Unless otherwise approved by a majority of the members of the Council, the Chairperson of the Council shall be elected annually by the Council. The chief executive officer of the Corporation shall be an *ex officio* voting member of the Council.

D. *Board of Overseers.* There shall be a Board of Overseers which shall consist of not fewer than five nor more than eight scientists who have expertise concerning matters with which the Corporation is involved. Members of the Board of Overseers may or may not be Members of the Corporation and may be appointed by the Board of Trustees on the basis of recommendations submitted from scientists and scientific organizations or societies. The Board of Overseers shall be available to review and offer recommendations to the officers, Trustees and Science Council regarding scientific activities conducted or proposed by the Corporation and shall meet from time to time, not less frequently than annually, as determined by the Board of Trustees.

E. *Board Committees Generally.* The Trustees may elect or appoint one or more other committees (including, but not limited to, an Investment Committee, a Development Committee, an Audit Committee, a Facilities and Capital Equipment Committee and a Long-Range Planning Committee) and may delegate to any such committee or committees any or all of their powers, except those which by law, the Articles of Organization or these Bylaws the Trustees are prohibited from delegating; provided that any committee to which the powers of the Trustees are delegated shall consist solely of Trustees. The members of any such committee shall have such tenure and duties as the Trustees shall determine. The Investment Committee, which shall oversee the management of the Corporation's endowment funds and marketable securities shall include as *ex officio* members, the Chairperson of the Board, the Treasurer and the Chairperson of the Audit Committee,

together with such Trustees as may be required for not less than two-thirds of the Investment Committee to consist of Trustees. Except as otherwise provided by these Bylaws or determined by the Trustees, any such committee may make rules for the conduct of its business, but, unless otherwise provided by the Trustees or in such rules, its business shall be conducted as nearly as possible in the same manner as is provided by these Bylaws for the Trustees.

F. *Actions Without a Meeting.* Any action required or permitted to be taken at any meeting of the Executive Committee or any other committee elected by the Trustees may be taken without a meeting if all members of such committees consent to the action in writing and such written consents are filed with the records of meetings. Members of the Executive Committee or any other committee elected by the Trustees may also participate in any meeting by means of a telephone conference call, or otherwise take action in such a manner as may, from time to time, be permitted by law.

G. *Manual of Procedures.* The Board of Trustees, on the recommendation of the Executive Committee, shall establish guidelines and modifications thereof to be recorded in a Manual of Procedures. Guidelines shall establish procedures for: (1) Nomination and election of members of the Corporation, Board of Trustees and Executive Committee; (2) Election of Officers; (3) Formation and Function of Standing Committees.

ARTICLE VI—OFFICERS

A. *Enumeration.* The officers of the Corporation shall consist of a President, a Treasurer and a Clerk, and such other officers having the powers of President, Treasurer and Clerk as the Board may determine, and a Director of the Laboratory. The Corporation may have such other officers and assistant officers as the Board may determine, including (without limitation) a Chairperson of the Board, Vice Chairperson and one or more Vice Presidents, Assistant Treasurers or Assistant Clerks. Any two or more offices may be held by the same person. The Chairperson and Vice Chairperson of the Board shall be elected by and from the Trustees, but other officers of the Corporation need not be Trustees or Members. If required by the Trustees, any officer shall give the Corporation a bond for the faithful performance of his or her duties in such amount and with such surety or sureties as shall be satisfactory to the Trustees.

B. *Tenure.* Except as otherwise provided by law, by the Articles of Organization or by these Bylaws, the President, Treasurer, and all other officers shall hold office until the first meeting of the Board following the annual meeting of Members and thereafter, until his or her successor is chosen and qualified.

C. *Resignation.* Any officer may resign by delivering his or her written resignation to the Corporation at its principal office or to the President or Clerk and such resignation shall be effective upon receipt unless it is specified to be effective at some other time or upon the happening of some other event.

D. *Removal.* The Board may remove any officer with or without cause by a vote of a majority of the entire number of Trustees then in office, at a meeting of the Board called for that purpose and for which notice of the purpose thereof has been given, provided that an officer may be removed for cause only after having an opportunity to be heard by the Board at a meeting of the Board at which a quorum is personally present and voting.

E. *Vacancy.* A vacancy in any office may be filled for the unexpired balance of the term by vote of a majority of the Trustees present at any meeting of Trustees at which a quorum is present or by written consent of all of the Trustees, if less than a quorum of Trustees shall remain in office.

F. *Chairperson.* The Chairperson shall have such powers and duties as may be determined by the Board and, unless otherwise determined by the Board, shall serve in that capacity for a term coterminous with his or her term as Trustee.

G. *Vice Chairperson.* The Vice Chairperson shall perform the duties and exercise the powers of the Chairperson in the absence or disability of the Chairperson, and shall perform such other duties and possess such other powers as may be determined by the Board. Unless otherwise determined by the Board, the Vice Chairperson shall serve for a one-year term.

H. *Director.* The Director shall be the chief operating officer and, unless otherwise voted by the Trustees, the chief executive officer of the Corporation. The Director shall, subject to the direction of the Trustees, have general supervision of the Laboratory and control of the business of the Corporation. At the annual meeting, the Director shall submit a report of the operations of the Corporation for such year and a statement of its affairs, and shall, from time to time, report to the Board all matters within his or her knowledge which the interests of the Corporation may require to be brought to its notice.

I. *Deputy Director.* The Deputy Director, if any, or if there shall be more than one, the Deputy Directors in the order determined by the Trustees, shall, in the absence or disability of the Director, perform the duties and exercise the powers

of the Director and shall perform such other duties and shall have such other powers as the Trustees may, from time to time, prescribe.

J. President. The President shall have the powers and duties as may be vested in him or her by the Board.

K. Treasurer and Assistant Treasurer. The Treasurer shall, subject to the direction of the Trustees, have general charge of the financial affairs of the Corporation, including its long-range financial planning, and shall cause to be kept accurate books of account. The Treasurer shall prepare a yearly report on the financial status of the Corporation to be delivered at the annual meeting. The Treasurer shall also prepare or oversee all filings required by the Commonwealth of Massachusetts, the Internal Revenue Service, or other Federal and State Agencies. The account of the Treasurer shall be audited annually by a certified public accountant.

The Assistant Treasurer, if any, or if there shall be more than one, the Assistant Treasurers in the order determined by the Trustees, shall, in the absence or disability of the Treasurer, perform the duties and exercise the powers of the Treasurer, shall perform such other duties and shall have such other powers as the Trustees may, from time to time, prescribe.

L. Clerk and Assistant Clerk. The Clerk shall be a resident of the Commonwealth of Massachusetts, unless the Corporation has designated a resident agent in the manner provided by law. The minutes or records of all meetings of the Trustees and Members shall be kept by the Clerk who shall record, upon the record books of the Corporation, minutes of the proceedings at such meetings. He or she shall have custody of the record books of the Corporation and shall have such other powers and shall perform such other duties as the Trustees may, from time to time, prescribe.

The Assistant Clerk, if any, or if there shall be more than one, the Assistant Clerks in the order determined by the Trustees, shall, in the absence or disability of the Clerk, perform the duties and exercise the powers of the Clerk and shall perform such other duties and shall have such other powers as the Trustees may, from time to time, prescribe.

In the absence of the Clerk and an Assistant Clerk from any meeting, a temporary Clerk shall be appointed at the meeting.

M. Other Powers and Duties. Each officer shall have in addition to the duties and powers specifically set forth in these Bylaws, such duties and powers as are customarily incident to his or her office, and such duties and powers as the Trustees may, from time to time, designate.

ARTICLE VII—AMENDMENTS

These Bylaws may be amended by the affirmative vote of the Members at any meeting, provided that notice of the substance of the proposed amendment is stated in the notice of such meeting. As authorized by the Articles of Organization, the Trustees, by a majority of their number then in office, may also make, amend or repeal these Bylaws, in whole or in part, except with respect to (a) the provisions of these Bylaws governing (i) the removal of Trustees and (ii) the amendment of these Bylaws and (b) any provisions of these Bylaws which by law, the Articles of Organization or these Bylaws, requires action by the Members.

No later than the time of giving notice of meeting of Members next following the making, amending or repealing by the Trustees of any Bylaw, notice thereof stating the substance of such change shall be given to all Members entitled to vote on amending the Bylaws.

Any Bylaw adopted by the Trustees may be amended or repealed by the Members entitled to vote on amending the Bylaws.

ARTICLE VIII—INDEMNITY

Except as otherwise provided below, the Corporation shall, to the extent legally permissible, indemnify each person who is, or shall have been, a Trustee, director or officer of the Corporation or who is serving, or shall have served at the request of the Corporation as a Trustee, director or officer of another organization in which the Corporation directly or indirectly has any interest as a shareholder, creditor or otherwise, against all liabilities and expenses (including judgments, fines, penalties, and reasonable attorneys' fees and all amounts paid, other than to the Corporation or such other organization, in compromise or settlement) imposed upon or incurred by any such person in connection with, or arising out of, the defense or disposition of any action, suit or other proceeding, whether civil or criminal, in which he or she may be a defendant or with which he or she may be threatened or otherwise involved, directly or indirectly, by reason of his or her being or having been such a Trustee, director or officer.

The Corporation shall provide no indemnification with respect to any matter as to which any such Trustee, director or officer shall be finally adjudicated in such action, suit or proceeding not to have acted in good faith in the reasonable belief that his or her action was in the best interests of the Corporation. The

Corporation shall provide no indemnification with respect to any matter settled or comprised unless such matter shall have been approved as in the best interests of the Corporation, after notice that indemnification is involved, by (i) a disinterested majority of the Board of the Executive Committee, or (ii) a majority of the Members.

Indemnification may include payment by the Corporation of expenses in defending a civil or criminal action or proceeding in advance of the final disposition of such action or proceeding upon receipt of an undertaking by the person indemnified to repay such payment if it is ultimately determined that such person is not entitled to indemnification under the provisions of this Article VIII, or under any applicable law.

As used in the Article VIII, the terms "Trustee," "director," and "officer" include their respective heirs, executors, administrators and legal representatives, and an "interested" Trustee, director or officer is one against whom in such capacity the proceeding in question or another proceeding on the same or similar grounds is then pending.

To assure indemnification under this Article VIII of all persons who are determined by the Corporation or otherwise to be or to have been "fiduciaries" of any employee benefits plan of the Corporation which may exist, from time to time, this Article VIII shall be interpreted as follows: (i) "another organization" shall be deemed to include such an employee benefit plan, including without limitation, any plan of the Corporation which is governed by the Act of Congress entitled "Employee Retirement Income Security Act of 1974," as amended, from time to time, ("ERISA"); (ii) "Trustee" shall be deemed to include any person requested by the Corporation to serve as such for an employee benefit plan where the performance by such person of his or her duties to the Corporation also imposes duties on, or otherwise involves services by, such person to the plan or participants or beneficiaries of the plan, (iii) "fines" shall be deemed to include any excise tax plan pursuant to ERISA; and (iv) actions taken or omitted by a person with respect to an employee benefit plan in the performance of such person's duties for a purpose reasonably believed by such person to be in the interest of the participants and beneficiaries of the plan shall be deemed to be for a purpose which is in the best interests of the Corporation.

The right of indemnification provided in this Article VIII shall not be exclusive of or affect any other rights to which any Trustee, director or officer may be entitled under any agreement, statute, vote of Members or otherwise. The Corporation's obligation to provide indemnification under this Article VIII shall be offset to the extent of any other source of indemnification of any otherwise applicable insurance coverage under a policy maintained by the Corporation or any other person. Nothing contained in the Article shall affect any rights to which employees and corporate personnel other than Trustees, directors or officers may be entitled by contract, by vote of the Board or of the Executive Committee or otherwise.

ARTICLE IX—DISSOLUTION

The consent of every Trustee shall be necessary to effect a dissolution of the Marine Biological Laboratory. In case of dissolution, the property shall be disposed of in such a manner and upon such terms as shall be determined by the affirmative vote of two-thirds of the Trustees then in office in accordance with the laws of the Commonwealth of Massachusetts.

ARTICLE X—MISCELLANEOUS PROVISIONS

A. Fiscal Year. Except as otherwise determined by the Trustees, the fiscal year of the Corporation shall end on December 31st of each year.

B. Seal. Unless otherwise determined by the Trustees, the Corporation may have a seal in such form as the Trustees may determine, from time to time.

C. Execution of Instruments. All checks, deeds, leases, transfers, contracts, bonds, notes and other obligations authorized to be executed by an officer of the Corporation in its behalf shall be signed by the Director or the Treasurer except as the Trustees may generally or in particular cases otherwise determine. A certificate by the Clerk or an Assistant Clerk, or a temporary Clerk, as to any action taken by the Members, Board of Trustees or any officer or representative of the Corporation shall as to all persons who rely thereon in good faith be conclusive evidence of such action.

D. Corporate Records. The original, or attested copies, of the Articles of Organization, Bylaws and records of all meetings of the Members shall be kept in Massachusetts at the principal office of the Corporation, or at an office of the Corporation's Clerk or resident agent. Said copies and records need not all be kept in the same office. They shall be available at all reasonable times for inspection by any Member for any proper purpose, but not to secure a list of Members for a purpose other than in the interest of the applicant, as a Member, relative to the affairs of the Corporation.

E. *Articles of Organization.* All references in these Bylaws to the Articles of Organization shall be deemed to refer to the Articles of Organization of the Corporation, as amended and in effect, from time to time.

F. *Transactions with Interested Parties.* In the absence of fraud, no contract or other transaction between this Corporation and any other corporation or any firm, association, partnership or person shall be affected or invalidated by the fact that any Trustee or officer of this Corporation is pecuniarily or otherwise interested in or is a director, member or officer of such other corporation or of such firm, association or partnership or in a party to or is pecuniarily or otherwise interested in such contract or other transaction or is in any way connected with any person or person, firm, association, partnership, or corporation pecuniarily or otherwise interested therein; provided that the fact that he or she individually

or as a director, member or officer of such corporation, firm, association or partnership in such a party or is so interested shall be disclosed to or shall have been known by the Board of Trustees or a majority of such Members thereof as shall be present at a meeting of the Board of Trustees at which action upon any such contract or transaction shall be taken, any Trustee may be counted in determining the existence of a quorum and may vote at any meeting of the Board of Trustees for the purpose of authorizing any such contract or transaction with like force and effect as if he/she were not so interested, or were not a director, member or officer of such other corporation, firm, association or partnership, provided that any vote with respect to such contract or transaction must be adopted by a majority of the Trustees then in office who have no interest in such contract or transaction.

THE BIOLOGICAL BULLETIN

PUBLISHED BY
THE MARINE BIOLOGICAL LABORATORY

Associate Editors

JAMES A. BLAKE, ENSR Marine & Coastal Center, Woods Hole
LOUIS E. BURNETT, Grice Marine Biological Laboratory, College of Charleston
WILLIAM D. COHEN, Hunter College, City University of New York
CHARLES D. DERBY, Georgia State University
SHINYA INOUÉ, Marine Biological Laboratory
RUDOLF A. RAFF, Indiana University

NOV 09 1998

Editorial Board

PETER B. ARMSTRONG, University of California, Davis	MARK W. MILLER, Institute of Neurobiology, University of Puerto Rico
ANDREW R. CAMERON, California Institute of Technology	TATSUO MOTOKAWA, Tokyo Institute of Technology
THOMAS H. DIETZ, Louisiana State University	YOSHITAKA NAGAHAMA, National Institute for Basic Biology, Japan
RICHARD B. EMLET, Oregon Institute of Marine Biology, University of Oregon	SHERRY D. PAINTER, Marine Biomedical Institute, University of Texas Medical Branch
DAVID EPEL, Hopkins Marine Station, Stanford University	K. RANGA RAO, University of West Florida
DAPHNE GAIL FAUTIN, University of Kansas	BARUCH RINKEVICH, Israel Oceanographic & Limnological Research Ltd.
WILLIAM F. GILLY, Hopkins Marine Station, Stanford University	RICHARD STRATHMANN, Friday Harbor Laboratories, University of Washington
ROGER T. HANLON, Marine Biological Laboratory	STEVEN VOGEL, Duke University
GREGORY HINKLE, University of Massachusetts, Dartmouth	J. HERBERT WAITE, University of Delaware
MAKOTO KOBAYASHI, Hiroshima University of Economics	SARAH ANN WOODIN, University of South Carolina
MICHAEL LABARBERA, University of Chicago	RICHARD K. ZIMMER-FAUST, University of California, Los Angeles
DONAL T. MANAHAN, University of Southern California	
MARGARET MCFALL-NGAI, Kewalo Marine Laboratory, University of Hawaii	

Editor: MICHAEL J. GREENBERG, The Whitney Laboratory, University of Florida

Managing Editor: PAMELA L. CLAPP, Marine Biological Laboratory

OCTOBER, 1998

Printed and Issued by
LANCASTER PRESS, Inc.

3575 HEMPLAND ROAD
LANCASTER, PA

Cover

The bobtail squid *Euprymna scolopes* is a benthic nocturnal predator endemic to the Hawaiian archipelago. Each individual of this species—like the adult (2–3 cm) resting on the sandy substrate in the upper right photograph—entertains a colony of bioluminescent bacterial symbionts (*Vibrio fischeri*) which it houses in a specialized light organ. The light produced by these bacteria, having been diffused into the environment, is used in anti-predatory behavior.

Each day at dawn, a fraction of the bacterial colony is vented into the ambient seawater—a form of population control. If the light organ of an adult squid is exposed at dawn by ventral dissection of the mantle, freshly released bacteria-rich exudate can be seen emerging from the right lobe of the organ (bottom photograph). In this issue, Spencer V. Nyholm and Margaret J. McFall-Ngai exploit this regulatory behavior; they sample the exudate, study its contents—the cellular components of the light organ, both animal and bacterial—and explore the mechanisms that sustain this stable, dynamic mutualism.

Newly hatched *E. scolopes* are typically 2 to 3 mm long (on sand pebbles, upper left photograph). Such hatchling squid obtain their symbionts from the environment and undergo a series of developmental changes that are induced by *V. fischeri*. Once the symbiosis is established, the association is maintained throughout the life history of the host. Fortunately, the host and its bacterial symbionts can be reared and cultured separately under laboratory conditions; thus, the effects of the mutualistic bacteria on the development of animal tissues can be readily studied. In the December issue of the *Bulletin*, Mary K. Montgomery and McFall-Ngai will describe the final developmental stages of the light organ system.

CONTENTS

SYMBIOSIS

- Nyholm, Spencer V., and Margaret J. McFall-Ngai**
Sampling the light organ microenvironment of *Euprymna scolopes*: description of a population of host cells in association with the bacterial symbiont *Vibrio fischeri* 89

CELL BIOLOGY AND DEVELOPMENT

- Rinkevich, Baruch, Irving L. Weissman, and Anthony W. DeTomaso**
Transplantation of Fu/HC-incompatible zooids in *Botryllus schlosseri* results in chimerism 98
- Yamada, Katsuyuki, and Koshin Mihashi**
Temperature-independent period immediately after fertilization in sea urchin eggs 107
- Abdu, Uri, Peter Takac, Hans Laufer, and Amir Sagi**
Effect of methyl farnesoate on late larval development and metamorphosis in the prawn *Macrobrachium rosenbergii* (Decapoda, Palaemonidae): a juvenoid-like effect? 112

ECOLOGY AND EVOLUTION

- Bavestrello, Giorgio, Umberto Benatti, Barbara Calcinai, Riccardo Cattaneo-Vietti, Carlo Cerrano, Anna Favre, Marco Giovine, Serena Lanza, Roberto Pronzato, and Michele Sarà**
Body polarity and mineral selectivity in the demosponge *Chondrosia reniformis* 120
- Wendt, Dean E.**
Effect of larval swimming duration on growth and reproduction of *Bugula neritina* (Bryozoa) under field conditions 126

PHYSIOLOGY

- Ellers, Olaf, Amy S. Johnson, and Philip E. Moberg**
Structural strengthening of urchin skeletons by collagenous sutural ligaments 136
- Thorington, Glyne U., and David A. Hessinger**
Efferent mechanisms of discharging cnidae: II. A nematocyst release response in the sea anemone tentacle 145

NEUROBIOLOGY AND BEHAVIOR

- Herberholz, Jens, and Barbara Schmitz**
Role of mechanosensory stimuli in intraspecific agonistic encounters of the snapping shrimp (*Alpheus heterochaelis*) 156

RESEARCH NOTE

- Tankersley, Richard A., Maria G. Wieber, Marco A. Sigala, and Kristen A. Kachurak**
Migratory behavior of ovigerous blue crabs *Callinectes sapidus*: evidence for selective tidal-stream transport 168

SHORT REPORTS FROM THE 1998 GENERAL SCIENTIFIC MEETINGS OF THE MARINE BIOLOGICAL LABORATORY

FEATURED ARTICLES

- Atema, Jelle**
Introduction. Tracking turbulence: processing the bimodal signals that define an odor plume 179
- Weaver, Matthew, and Jelle Atema**
Hydrodynamic coupling of lobster antennule motion to oscillatory water flow 180
- Guenther, Carla M., and Jelle Atema**
Distribution of setae on the *Homarus americanus* lateral antennule flagellum 182

SENSORY BIOLOGY

- Mead, Kristina S.**
The biomechanics of odorant access to aesthetascs in the grass shrimp, *Palaemonetes vulgaris* 184
- Quinn, Elizabeth, Kristen Paradise, and Jelle Atema**
Juvenile *Limulus polyphemus* generate two water currents that contact one proven and one putative chemoreceptor organ 185
- Shashar, Nadav, Ferenc I. Hárosi, Anastazia T. Banaszak, and Roger T. Hanlon**
UV radiation blocking compounds in the eye of the cuttlefish *Sepia officinalis* 187
- Ruta, Vanessa J., Frederick A. Dodge, and Robert B. Barlow**
Efferent modulation of physiological properties of the *Limulus* lateral eye 189
- Edds-Walton, P. L., and R. R. Fay**
Directional auditory responses in the descending octaval nucleus of the toadfish (*Opsanus tau*) 191

BEHAVIOR AND NEUROBIOLOGY

- King, Jane Roche, and Hans Straka**
Effects of vestibular nerve lesions on orientation turning in the leopard frog, *Rana pipiens* 193

Mensinger, Allen F., and Max Deffenbaugh Prototype rechargeable tag for acoustical neural telemetry	194
Billack, Blase, Jeffrey D. Laskin, Prudence T. Heck, Walter Troll, Michael A. Gallo, and Diane E. Heck Alterations in cholinergic signaling modulate contraction of isolated sea urchin tube feet: potential role of nitric oxide	196
Hoskin, Francis C. G., and John E. Walker A closer look at the natural substrate for a nerve-gas hydrolyzing enzyme in squid nerve	197
Kuzirian, Alan M., Herman T. Epstein, Thomas J. Nelson, and Nancy S. Rafferty Lead, learning, and calectxin in <i>Hermisenda</i>	198
Tamse, Catherine T., Katherine Hammar, D. Marshall Porterfield, and Peter J. S. Smith Transmembrane calcium flux in Pb^{2+} -exposed <i>Aplysia</i> neurons	201
Malchow, Robert Paul, Michael P. Verzi, and Peter J. S. Smith Extracellular pH gradients measured from isolated retinal cells	203
Andersen, Kristen A., and Robert Paul Malchow Fluorometric analysis of intracellular sodium concentrations in isolated retinal horizontal cells	204
Jessen-Eller, Kathryn, Marjorie Steele, Carol Reinisch, and Nicholas Spitzer Blockade of ryanodine receptors stimulates neurite outgrowth in embryos of <i>Spisula solidissima</i>	206

CELL AND DEVELOPMENTAL BIOLOGY

Porterfield, D. M., J. R. Trimarchi, D. L. Keefe, and P. J. S. Smith Characterization of oxygen and calcium fluxes from early mouse embryos and oocytes	208
Silver, Robert B., Leslie A. King, and Alyssa F. Wise Calcium regulatory endomembranes of the prophase mitotic apparatus of sand dollar cells contain enzyme activities that produce leukotriene B ₄ but not 1,4,5-inositol triphosphate	209
Lee, Kyeng G., Nishal Mohan, Zoya Koroleva, Li-Fang Huang, and William D. Cohen Fluorescence localization of cytoskeletal proteins in fibrin-trapped cells	211
Goda, Makoto, Shinya Inoué, and Robert Knudson Oocyte maturation in <i>Chaetopterus pergamentaceus</i> observed with centrifuge polarizing microscope	212
Miyake, Katsuya, and Paul L. McNeil A little shell to live in: evidence that the fertilization envelope can prevent mechanically induced damage of the developing sea urchin embryo	214
Kuhns, William J., Xavier Fernandez-Busquets, Max M. Burger, Michael Ho, and Eva Turley Hyaluronic acid-receptor binding demonstrated by synthetic adhesive proteoglycan peptide constructs and by cell receptors on the marine sponge <i>Microciona prolifera</i>	216

Kubke, M. F., E. Gilland, and R. Baker Lipophilic dye labeling distinguishes segregated central components of the eighth cranial nerve in embryonic chicken	218
Straka, Hans, Edwin Gilland, and Robert Baker Rhombomeric organization of brainstem motor neurons in larval frogs	220

ANIMAL HUSBANDRY AND DISEASE

Hanley, Janice S., Nadav Shashar, Roxanna Smolowitz, Robert A. Bullis, William N. Mebane, Howaida R. Gabr, and Roger T. Hanlon Modified laboratory culture techniques for the European cuttlefish <i>Sepia officinalis</i>	223
Maxwell, Michael R., William K. Macy, Shobu Odate, and Roger T. Hanlon Evidence for multiple spawning by squids (<i>Loligo pealei</i>) in captivity	225
Weidner, Earl, and Teresa King <i>In vivo</i> and <i>in vitro</i> growth of nerve parasite from <i>Lophius americanus</i>	227
O'Neill, Maureen D., Heather M. Wesp, Allen F. Mensinger, and Roger T. Hanlon Initial baseline blood chemistry of the oyster toadfish, <i>Opsanus tau</i>	228
Smolowitz, Roxanna, Elizabeth Wadman, and H. M. Chikarmane <i>Pseudomonas putida</i> infections of the oyster toadfish (<i>Opsanus tau</i>)	229

ECOLOGY

Schmitt, Catherine, Nathaniel Weston, and Charles Hopkinson Preliminary evaluation of sedimentation rates and species distribution in Plum Island Estuary, Massachusetts	232
Griffin, Martin P. A., Marci L. Cole, Kevin D. Kroeger, and Just Cebrian Dependence of herbivory on autotrophic nitrogen content and on net primary production across ecosystems	233
Rogers, Jennifer, Jennifer Harris, and Ivan Valiela Interaction of nitrogen supply, sea level rise, and elevation on species form and composition of salt marsh plants	235
Sweeney, Jennifer, Linda Deegan, and Robert Garritt Population size and site fidelity of <i>Fundulus heteroclitus</i> in a macrotidal saltmarsh creek	238
Kirkpatrick, John, Ken Foreman, and Ivan Valiela Dissolved inorganic nitrogen flux and mineralization in Waquoit Bay sediments as measured by core incubations	240
Graham, Suzanne, Jessica Davis, Linda Deegan, Just Cebrian, Jeff Hughes, and Jennifer Hauxwell Effect of eelgrass (<i>Zostera marina</i>) density on the feeding efficiency of mummichog (<i>Fundulus heteroclitus</i>)	241

Legra, Jessica C., Roselle E. Safran, and Ivan Valiela Lead concentration as an indicator of contamination history in estuarine sediments	243
Safran, Roselle E., Jessica C. Legra, and Ivan Valiela Effects of nitrogen loading on eelgrass seed coat abun- dance, C to N ratios, and $\delta^{15}\text{N}$ in sediments of Waquoit Bay	245

Costello, John H., and Rebecca Coverdale Planktonic feeding and evolutionary significance of the lobate body plan within the Ctenophora	247
--	-----

ABSTRACTS

Papers listed by title only	249
--	------------

THE BIOLOGICAL BULLETIN

THE BIOLOGICAL BULLETIN is published six times a year by the Marine Biological Laboratory, 7 MBL Street, Woods Hole, Massachusetts 02543.

Subscriptions and similar matter should be addressed to Subscription Manager, THE BIOLOGICAL BULLETIN, Marine Biological Laboratory, 7 MBL Street, Woods Hole, Massachusetts 02543. Subscription per year (six issues, two volumes): \$195 for libraries; \$95 for individuals. Subscription per volume (three issues): \$97.50 for libraries; \$50 for individuals. Back and single issues (subject to availability): \$40 for libraries; \$20 for individuals.

Communications relative to manuscripts should be sent to Michael J. Greenberg, Editor-in-Chief, or Pamela L. Clapp, Managing Editor, at the Marine Biological Laboratory, 7 MBL Street, Woods Hole, Massachusetts 02543. Telephone: (508) 289-7428. FAX: 508-457-1924. E-mail: pclapp@mbl.edu.

<http://www.mbl.edu/BiologicalBulletin/>

The home page for the electronic companion to THE BIOLOGICAL BULLETIN—the *Marine Models Electronic Record*—and other BIOLOGICAL BULLETIN publications is available on the World Wide Web at the address shown above.

THE BIOLOGICAL BULLETIN is indexed in bibliographic services including *Index Medicus* and MEDLINE, *Chemical Abstracts*, *Current Contents*, *Elsevier BIOBASE/Current Awareness in Biological Sciences*, and *Geo Abstracts*.

Printed on acid free paper,
effective with Volume 180, Issue 1, 1991.

POSTMASTER: Send address changes to THE BIOLOGICAL BULLETIN, Marine Biological Laboratory, 7 MBL Street, Woods Hole, MA 02543.

Copyright © 1998, by the Marine Biological Laboratory
Periodicals postage paid at Woods Hole, MA, and additional mailing offices.
ISSN 0006-3185

INSTRUCTIONS TO AUTHORS

The Biological Bulletin accepts outstanding original research reports of general interest to biologists throughout the world. Papers are usually of intermediate length (10–40 manuscript pages). A limited number of solicited review papers may be accepted after formal review. A paper will usually appear within four months after its acceptance.

Very short, especially topical papers (less than 9 manuscript pages including tables, figures, and bibliography) will be published in a separate section entitled "Research Notes." A Research Note in *The Biological Bulletin* follows the format of similar notes in *Nature*. It should open with a summary paragraph of 150 to 200 words comprising the introduction and the conclusions. The rest of the text should continue on without subheadings, and there should be no more than 30 references. References should be referred to in the text by number, and listed in the Literature Cited section in the order that they appear in the text. Unlike references in *Nature*, references in the Research Notes section should conform in punctuation and arrangement to the style of recent issues of *The Biological Bulletin*. Materials and Methods should be incorporated into appropriate figure legends. See the article by Lohmann *et al.* (October 1990, Vol. 179: 214–218) for sample style. A Research Note will usually appear within two months after its acceptance.

The Editorial Board requests that regular manuscripts conform to the requirements set below; those manuscripts that

do not conform will be returned to authors for correction before review.

1. **Manuscripts.** Manuscripts, including figures, should be submitted in quadruplicate, with the originals clearly marked. (Xerox copies of photographs are not acceptable for review purposes.) The submission letter accompanying the manuscript should include a telephone number, a FAX number, and (if possible) an E-mail address for the corresponding author. The original manuscript must be typed in no smaller than 12 pitch or 10 point, using double spacing (including figure legends, footnotes, bibliography, etc.) on one side of 16- or 20-lb. bond paper, 8 by 11 inches. Please, no right justification. Manuscripts should be proofread carefully and errors corrected legibly in black ink. Pages should be numbered consecutively. Margins on all sides should be at least 1 inch (2.5 cm). Manuscripts should conform to the *Council of Biology Editors Style Manual*, 5th Edition (Council of Biology Editors, 1983) and to American spelling. Unusual abbreviations should be kept to a minimum and should be spelled out on first reference as well as defined in a footnote on the title page. Manuscripts should be divided into the following components: Title page, Abstract (of no more than 200 words), Introduction, Materials and Methods, Results, Discussion, Acknowledgments, Literature Cited, Tables, and Figure Legends. In addition, authors should supply a list of words and phrases under which the article should be indexed.

2. **Title page.** The title page consists of a condensed title or running head of no more than 35 letters and spaces, the manuscript title, authors' names and appropriate addresses, and footnotes listing present addresses, acknowledgments or contribution numbers, and explanation of unusual abbreviations.

3. **Figures.** The dimensions of the printed page, 7 by 9 inches, should be kept in mind in preparing figures for publication. We recommend that figures be about 1 times the linear dimensions of the final printing desired, and that the ratio of the largest to the smallest letter or number and of the thickest to the thinnest line not exceed 1:1.5. Explanatory matter generally should be included in legends, although axes should always be identified on the illustration itself. Figures should be prepared for reproduction as either line cuts or halftones. Figures to be reproduced as line cuts should be unmounted glossy photographic reproductions or drawn in black ink on white paper, good-quality tracing cloth or plastic, or blue-lined coordinate paper. Those to be reproduced as halftones should be mounted on board, with both designating numbers or letters and scale bars affixed directly to the figures. All figures should be numbered in consecutive order, with no distinction between text and plate figures and cited, in order, in the text. The author's name and an arrow indicating orientation should appear on the reverse side of all figures.

Color: *The Biological Bulletin* will publish color figures and plates, but must bill authors for the actual additional cost of printing in color. The process is expensive, so authors with more than one color image should—consistent with editorial concerns, especially citation of figures in order—combine them into a single plate to reduce the expense. On request, when supplied with a copy of a color illustration, the editorial staff will provide a pre-publication estimate of the printing cost.

4. **Tables, footnotes, figure legends, etc.** Authors should follow the style in a recent issue of *The Biological Bulletin* in preparing table headings, figure legends, and the like. Because of the high cost of setting tabular material in type, authors are asked to limit such material as much as possible. Tables, with their headings and footnotes, should be typed on separate sheets, numbered with consecutive Roman numerals, and placed after the Literature Cited. Figure legends should contain enough information to make the figure intelligible separate from the text. Legends should be typed double spaced, with consecutive Arabic numbers, on a separate sheet at the end of the paper. Footnotes should be limited to authors' current addresses, acknowledgments or contribution numbers, and explanation of unusual abbreviations. All such footnotes should appear on the title page. Footnotes are not normally permitted in the body of the text.

5. **Literature cited.** In the text, literature should be cited by the Harvard system, with papers by more than two authors cited as Jones *et al.*, 1980. Personal communications and material in preparation or in press should be cited in the text only, with author's initials and institutions, unless the material has been formally accepted and a volume number can be supplied. The list of references following the text should be headed Literature Cited, and must be typed double spaced on separate

pages, conforming in punctuation and arrangement to the style of recent issues of *The Biological Bulletin*. Citations should include complete titles and inclusive pagination. Journal abbreviations should normally follow those of the U. S. A. Standards Institute (USASI), as adopted by BIOLOGICAL ABSTRACTS and CHEMICAL ABSTRACTS, with the minor differences set out below. The most generally useful list of biological journal titles is that published each year by BIOLOGICAL ABSTRACTS (BIOSIS List of Serials; the most recent issue). Foreign authors, and others who are accustomed to using THE WORLD LIST OF SCIENTIFIC PERIODICALS, may find a booklet published by the Biological Council of the U.K. (obtainable from the Institute of Biology, 41 Queen's Gate, London, S.W.7, England, U.K.) useful, since it sets out the WORLD LIST abbreviations for most biological journals with notes of the USASI abbreviations where these differ. CHEMICAL ABSTRACTS publishes quarterly supplements of additional abbreviations. The following points of reference style for THE BIOLOGICAL BULLETIN differ from USASI (or modified WORLD LIST) usage:

A. Journal abbreviations, and book titles, all underlined (for *italics*)

B. All components of abbreviations with initial capitals (not as European usage in WORLD LIST *e.g.*, *J. Cell. Comp. Physiol.* NOT *J. cell. comp. Physiol.*)

C. All abbreviated components must be followed by a period, whole word components *must not* (*e.g.*, *J. Cancer Res.*)

D. Space between all components (*e.g.*, *J. Cell. Comp. Physiol.*, not *J.Cell.Comp.Physiol.*)

E. Unusual words in journal titles should be spelled out in full, rather than employing new abbreviations invented by the author. For example, use *Rit Visindaffjélags Íslendinga* without abbreviation.

F. All single word journal titles in full (*e.g.*, *Veliger, Ecology, Brain*).

G. The order of abbreviated components should be the same as the word order of the complete title (*i.e.*, *Proc.* and *Trans.* placed where they appear, not transposed as in some BIOLOGICAL ABSTRACTS listings).

H. A few well-known international journals in their preferred forms rather than WORLD LIST or USASI usage (*e.g.*, *Nature, Science, Evolution* NOT *Nature, Lond., Science, N.Y.; Evolution, Lancaster, Pa.*)

6. **Reprints, page proofs, and charges.** Authors of articles in black and white (no color figures) receive their first 50 reprints (without covers) free of charge. Color reprints and additional black-and-white reprints may be purchased; authors will receive order forms. Reprints normally will be delivered about 2 to 3 months after the issue date. Authors (or delegates for foreign authors) will receive page proofs of articles shortly before publication. They will be charged the current cost of printers' time for corrections to these (other than corrections of printers' or editors' errors). Other than these charges for authors' alterations, *The Biological Bulletin* does not have page charges.

Sampling the Light-Organ Microenvironment of *Euprymna scolopes*: Description of a Population of Host Cells in Association With the Bacterial Symbiont *Vibrio fischeri*

SPENCER V. NYHOLM AND MARGARET J. MCFALL-NGAI*

Pacific Biomedical Research Center, University of Hawaii, 41 Ahui Street, Honolulu, Hawaii 96813

Abstract. The symbiosis between the squid *Euprymna scolopes* and the luminous bacterium *Vibrio fischeri* has a pronounced diel rhythm, one component of which is the venting of the contents of the light organ into the surrounding seawater each day at dawn. In this study, we explored the use of this behavior to sample the microenvironment of the light-organ crypts. Intact crypt contents, which emerge from the lateral pores of the organ as a thick paste-like exudate, were collected from anesthetized host animals that had been exposed to a light cue. Microscopy revealed that the expelled material is composed of a conspicuous population of host cells in association with the bacterial symbionts, all of which are embedded in a dense acellular matrix that strongly resembles the bacteria-based biofilms described in other systems. Assays of the viability of expelled crypt cells revealed no dead bacterial symbionts and a mixture of live and dead host cells. Analyses of the ultrastructure, biochemistry, and phagocytic activity of a subset of the host cell population suggested that some of these cells are macrophage-like molluscan hemocytes.

Introduction

The microenvironment surrounding extracellular bacterial symbionts that associate with animal hosts is the dynamic zone of interchange between the partners. In a number of associations, most notably the cow rumen (Flint, 1997) and the termite hindgut (Breznak, 1982;

Breznak and Brune, 1994), the characterization of this interface has provided insight into the basic nature of the symbiosis, including aspects of nutrient exchange, host immune response, and the control of symbiont number. In such consortial associations, the contribution of any given symbiont species to the dynamics of the whole has been difficult to assess. Thus, the precise mechanisms by which the environment is created and maintained have not been determined.

The symbiosis between the Hawaiian bobtail squid *Euprymna scolopes* and its bioluminescent bacterial partner *Vibrio fischeri* provides a research system complementary to the more prevalent consortial symbioses (Ruby, 1996; McFall-Ngai and Ruby, 1998). Because both partners are culturable outside of the symbiosis, and the bacterial symbiont can be genetically manipulated, this two-species association can be used to study the underlying biochemical and molecular contributions of each partner to the dynamics of the symbiosis.

The microenvironment surrounding the bacterial symbionts in this symbiosis can now be readily analyzed (Graf and Ruby, 1998). The squid houses its extracellular symbionts in the epithelial crypts of a conspicuous bilobed light organ located in the center of its mantle cavity (McFall-Ngai and Montgomery, 1990). Lee and Ruby (1994) and Boettcher *et al.* (1996) showed that the symbiosis is characterized by a pronounced diel rhythm, one aspect of which is the daily venting of 90% of the bacterial culture into the surrounding seawater. At dawn, each day, the animal expels the bacteria-containing crypt material into the mantle cavity through lateral pores on either side of the light organ (see Fig. 1). This daily venting appears to have a variety of consequences for the symbiosis. Lee

Received 30 April 1998; accepted 22 July 1998.

* To whom correspondence should be addressed. E-mail: mcfallng@hawaii.edu

and Ruby (1994) provided evidence that, in addition to the obvious function of controlling symbiont number, venting increases population densities of *V. fischeri* in the ambient seawater, which is essential for the horizontal transmission of the symbiosis between generations; specifically, they showed that the natural seawater is only infective to newly hatched squids when it is sampled from environments with large populations of adults. Under laboratory conditions, Graf and Ruby (1998) exploited this diel venting behavior of the host to show that the squid host provides the bacteria in the symbiosis with amino acids.

In the present study, we explore the cellular components of the vented crypt contents. Our data show that the host vents a dense assemblage of its own cells in association with the bacterial symbionts. This mixed population of cells is embedded in a conspicuous acellular matrix. Among the host cell population, there is a subset of cells that have a morphology, biochemistry, and phagocytic activity suggestive of macrophage-like molluscan hemocytes. In addition, we demonstrate that the animals can be experimentally induced to vent their crypt contents at times of day other than dawn, a feature that will provide an opportunity for future studies of diel fluctuations in the microenvironment of the light organ crypts.

Materials and Methods

General procedures

Adult *E. scolopes* were collected with the use of dip nets from shallow, subtidal regions surrounding Oahu, Hawaii, and were either transported to the University of Southern California, Los Angeles, and maintained in a 265-liter recirculating aquarium at 23°C, or maintained in flow-through seawater aquaria at Kewalo Marine Laboratory, University of Hawaii, Manoa.

All chemicals were obtained from Sigma Chemical Co. (St. Louis, Missouri) unless otherwise stated. Fixatives, embedding media, and supplies for electron microscopy were purchased from Ted Pella, Inc. (Redding, California).

Characterizing natural venting behavior and obtaining crypt contents

We used the methods of Graf and Ruby (1998) to induce venting behavior and to acquire the contents of the light organ crypts for further analysis. Briefly, adult animals were maintained under natural environmental light conditions of about 12 h of light and 12 h of darkness. Minutes prior to dawn, just before venting normally occurs (Lee and Ruby, 1994), animals were anesthetized in 2% ethanol in seawater. Under red light, we made a midventral transection of the mantle to expose the light organ. The animals were then subjected to a constant

light stimulus, using a 150-W halogen light source placed several centimeters above the eyes. Either immediately or within 60 min of the onset of the stimulus, they vented their light organ contents. This variation in the timing of venting following the stimulus did not affect the factors that were characterized in this study. As they were vented, the crypt contents were collected with a 5- μ l hematocrit tube fitted with a plunger. To determine whether light, and not another aspect of our procedure (*i.e.*, anesthesia or dissection), was the necessary stimulus for the induction of venting, animals were anesthetized during their natural dark period and dissected, but not given a light stimulus.

The possibility that venting behavior occurs in newly hatched squid at the first dawn following hatching was tested as follows. Juvenile squid were anesthetized for 60 s in a solution containing 0.37 M MgCl₂ and seawater (1:1). Acridine orange was added to the solution to a final concentration of 5 ng/ml, which uniformly stained the host cells. The light organs were exposed by removing the mantle tissue, animals were exposed to a light stimulus, and the vented contents were viewed under confocal microscopy.

Preparation for electron microscopy

For scanning electron microscopy (SEM), the exuded crypt contents were placed on a nitrocellulose membrane, which was then immersed and fixed for 15 min in a solution of 5% formalin in filtered seawater (FSW). The samples were rinsed in FSW, dehydrated in a 15%–100% ethanol series, desiccated with hexamethyldisilazane, sputter coated with gold, and examined with a Cambridge 360 scanning electron microscope.

For transmission electron microscopy (TEM), the exudate was fixed in 4% glutaraldehyde in 0.1% sodium cacodylate with 0.45 M NaCl, pH 7.4 (Fixative A), for 30 min. Samples were rinsed for 15 min in 0.1% sodium cacodylate with 0.45 M NaCl, pH 7.4 (Buffer A) and then postfixed in 1% osmium tetroxide in Buffer A for 20 min followed by rinsing with Buffer A for 10 min. Samples were then dehydrated through a graded series from 30% to 100% ethanol in distilled water followed by infiltration with propylene oxide. Samples were placed in a 50:50 mixture of propylene oxide and unaccelerated Spurr (Spurr, 1969) for 15 min, and then transferred first to 100% unaccelerated Spurr for 3 h, and then 100% accelerated Spurr for 2 h. Samples were embedded in freshly prepared accelerated Spurr at 67°C for 48 h. The embedded exudate was sectioned (80 to 90 nm thick), stained with Reynolds lead citrate solution and 3% uranyl acetate, and viewed with a JEOL CX-100 transmission electron microscope.

To determine whether the composition of vented mate-

rial was influenced by the experimental procedure by which it was obtained (*i.e.*, from anesthetized, ventrally dissected animals), we analyzed the crypt contents in intact, unanesthetized animals just prior to venting. Whole adult animals were placed at dawn directly in Fixative A. The light organs were then dissected out and prepared for TEM as described previously (McFall-Ngai and Montgomery, 1990).

Analysis of animal and bacterial cells in the exudate

The total numbers of bacterial and animal cells present in fresh exudate were determined for adult specimens [$n = 3$; average mantle length, 25 mm]. To quantify culturable bacterial cells per microliter in the exudate, serial dilutions of fresh exudate were plated on seawater tryptone (SWT) agar medium and allowed to incubate at 25°C overnight (Ruby and Asato, 1993). The resulting colonies were counted, giving the number of colony forming units (CFUs) in the exudate material. This plating technique detects culturable bacterial cells with greater than 95% efficiency (Ruby and Asato, 1993). *In situ* viability of bacterial cells in the exudate was determined by fluorescence viability staining (*BacLight Live/Dead Viability Assay Kit*, Molecular Probes, Eugene, OR). We used two nucleic acid stains, which are provided separately and mixed immediately prior to application: SYTO-9, which is taken up by all cells and fluoresces green, and propidium iodide, which fluoresces red and is only taken up by dead or dying bacterial cells with damaged membranes (Lloyd and Hayes, 1995). Cells were observed by confocal microscopy immediately after collection, and then 2 h later to ensure that propidium iodide had penetrated dead *V. fischeri*.

The number of animal cells was determined as follows. Fresh exudate of a known volume was placed in a Petroff-Hauser hemacytometer, and the cells were either counted under phase contrast microscopy or stained with acridine orange and counted under fluorescent microscopy. Viability of animal cells in the exudate was determined by exposing the material to trypan blue, which is excluded from healthy animal cells but taken up freely by dead and dying cells with compromised membranes. Samples were exposed to 0.1% trypan blue in FSW for 3.0 min, rinsed in FSW, and examined under light microscopy.

To determine the abundance of acidic compartments (*e.g.*, lysosomes) within the animal cells, fresh exudate was exposed to a 1 μM solution of LysoTracker Green (Molecular Probes, Eugene, OR) for 30 min, rinsed in FSW, and viewed under confocal microscopy. LysoTracker consists of a fluorophore moiety linked to a weak base that permeates cell membranes; it concentrates in cellular compartments with low internal pH, such as lysosomes, where it fluoresces under acidic conditions (Diwu *et al.*, 1994).

Experimental manipulation of venting behavior

To determine whether crypt contents could be obtained at times other than dawn, we attempted to induce venting behavior by exposing *E. scolopes* adults to our experimental conditions (*i.e.*, anesthetic, ventral dissection, and a light stimulus) at different times during the day. Specifically, we assayed in the hours preceding [-12 h, -9 h, -6 h, -4 h, and -1 h] and following [+4 h, +6 h, +8 h, and +10 h] dawn, when the light organ would presumably have either abundant or depleted crypt contents, respectively. In addition, to determine whether the crypt contents would be retained past dawn in the absence of the natural light cue, adult animals were maintained in the dark for up to 8 h after their natural venting time and then exposed to our experimental conditions.

Results

Natural venting behavior

After a continuous light stimulus of 5–60 min, the release of the crypt contents (Fig. 1) was preceded by a large contraction of the light organ. The exudate that resulted from this event emerged from the pores of the light organ as a thick, white, paste-like material (Fig. 1B). An adult animal with a mantle length of 25 mm typically vented between 10 and 20 μl of exudate material, which was then collected intact for further analyses. Animals that were anesthetized and ventrally dissected, but not exposed to a light stimulus, did not expel their crypt contents—neither during the natural dark cycle nor after dark adaptation. Therefore, a light stimulus is required to induce venting, and the experimental conditions themselves did not cause this behavior.

Under the experimental conditions used for adults, juvenile animals also exhibited venting behavior beginning with the first dawn after hatching. Large eukaryotic cells of a diameter similar to those seen in adults (about 10 μm) were observed emerging from the pores leading to the juvenile crypts (Fig. 1C).

Cellular constituents of the exudate

Observations of exudate under light microscopy revealed a mixture of animal and bacterial cells. SEM of the exudate showed that the population of animal and bacterial cells is surrounded by a dense matrix (Fig. 2A–C). Animal cells in the exudate were 10 to 20 μm in diameter. Their membranes often had a ruffled appearance, and cytoplasmic blebbing was regularly observed, but these cells otherwise appeared healthy (Fig. 2D). Both SEM and TEM revealed a close association between the animal cells and bacterial cells within the exudate, with bacterial cells often adhering to the surface of the eukaryotic cells (Fig. 2C–D). TEM of the exudate matrix

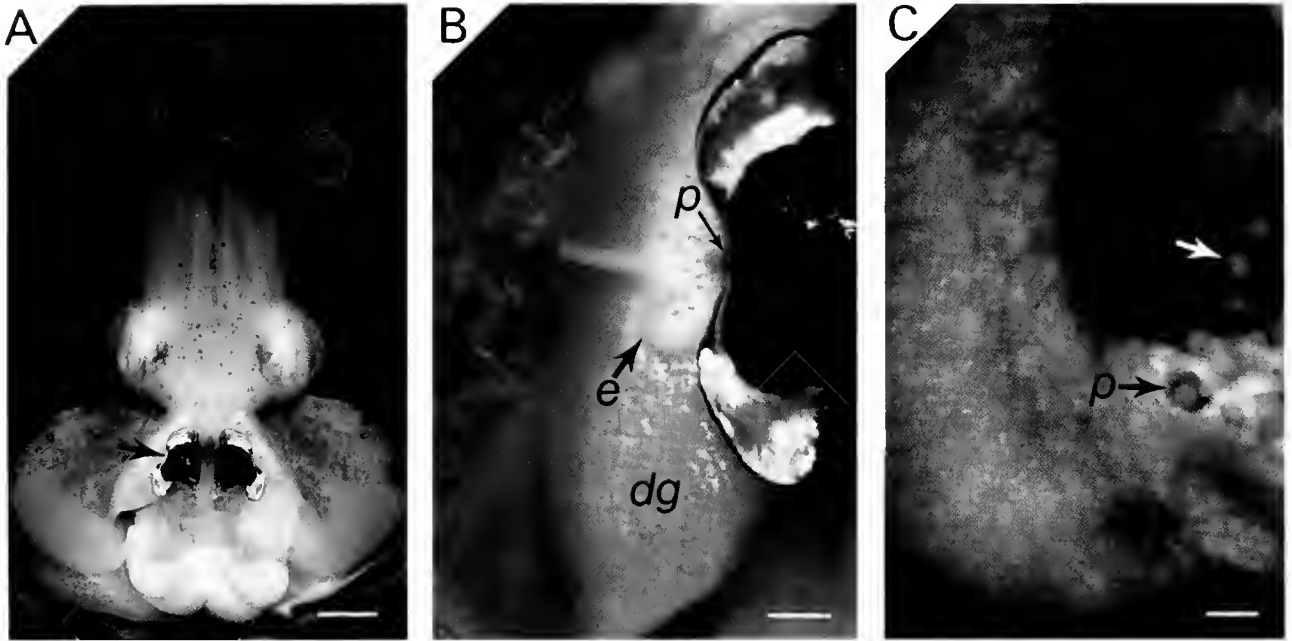


Figure 1. Venting of crypt contents by *Euprymna scolopes*. (A) Ventral dissection of an adult, revealing the bilobed light organ (arrow). Scale, 5 mm. (B) Exudate emerging from one of the lateral pores of the light organ. The exudate can be seen lying across the digestive gland (yellow), which is directly dorsal to the light organ. Scale, 1 mm. (C) Animal cells (white arrow) emerging from the pore of a 48-h juvenile squid. Scale, 25 μm . p, pore; e, exudate; dg, digestive gland.

showed a mixture of particulate material suggestive of cell membranes, possibly of lysed host cells (Fig. 2D).

Based on counts of CFUs, an average of 2.8×10^9 ($\pm 1.3 \times 10^9$, $n = 3$) bacterial cells were contained within the exudate of an *E. scolopes* adult. After venting, homogenates of the bacteria-containing crypt epithelia of the light organ of these same animals contained, on average, 10^8 bacterial cells; thus, 5% to 10% of the symbiont population remained in the hosts. This number of bacteria corresponds to estimates of symbiont retention in animals that were allowed to vent naturally (Lee and Ruby, 1994). In adult squid (average mantle length, 25 mm), the number of animal cells in the exudate, as determined by light and fluorescence microscopy, averaged between 10^3 and 10^4 total cells.

Control studies with fixed, intact, unvented light organs showed animal and bacterial cells in the collection ducts leading up to and in the crypt spaces (Fig. 3). These cells were similar in appearance to cells found in freshly vented exudate samples. TEM revealed that the accompanying matrix material was also similar to that observed in exudate (data not shown).

Viability of animal and bacterial cells

About half the freshly vented animal cells that were stained with trypan blue were observed to exclude the

dye, indicating that they were viable. The remainder took up the blue stain, indicating that they were dead or dying cells with compromised membranes (Fig. 4A). Staining patterns under confocal microscopy, with two nucleic acid stains that distinguish live and dead bacterial cells, indicated that the vast majority of bacteria in the exudate are viable (Fig. 4B). To ensure that these nucleic acid stains could reveal dead cells, the crypt contents were stained 2 h after being expelled. An increase in bacterial cells fluorescing red was observed 2 h after venting, so the propidium iodide revealed dying or dead *V. fischeri* (data not shown).

Acidic compartments of animal cells in the exudate

The animal cells in the exudate were examined for the presence of acidic compartments characteristic of phagocytic or macrophage-like cells. To this end, fresh exudate stained with LysoTracker dye was observed with both light and fluorescence microscopy. Under differential interference contrast (DIC) microscopy, exudate cells appeared to be surrounded by matrix and adherent bacterial cells (Fig. 5A). In the presence of LysoTracker, fluorescent compartments were seen within the animal cells, whereas the nucleus and surrounding extracellular matrix, as well as bacterial cells in the mixture, showed no fluorescence (Fig. 5B).

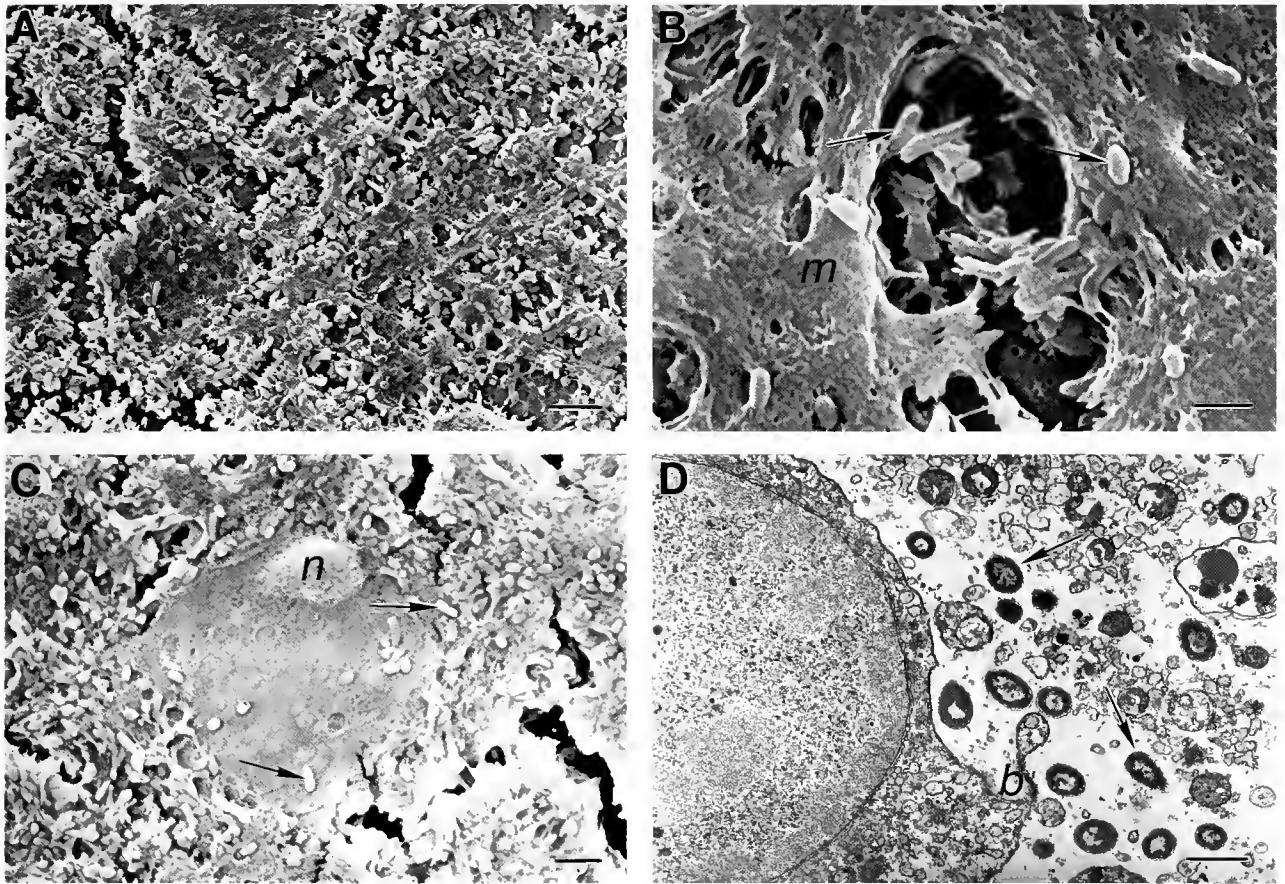


Figure 2. Electron micrographs of freshly collected exudate (A–C were taken with a scanning scope, and D with a transmission scope). (A) Bacterial cells embedded in a thick matrix. Scale, 3 μm . (B) Higher magnification, showing individual bacteria (arrows) surrounded by the matrix. Scale, 1 μm . (C) The outline of animal cells surrounded by bacteria (arrows). Scale, 2 μm . (D) Bacterial cells (arrows) adjacent to a larger animal cell. The membrane exhibits ruffling, and cytoplasmic blebbing is evident. The bacteria are surrounded by a mixture of particulate matter that constitutes the matrix. Scale, 1 μm . m, matrix; n, nucleus; b, cytoplasmic blebbing of the host cell.

Evidence of bacterial phagocytosis in light organ cells

Eukaryotic cells in the crypt spaces of intact light organs occasionally contained intracellular bacteria (Fig. 6). Like the majority of the animal cells within the exudate, these cells averaged 10 μm in diameter and often contained 3–5 bacterial cells each. The bacteria appeared to be contained within membrane-bound vacuoles of the animal cells, and many of these bacterial cells appeared to be undergoing degradation.

Manipulation of venting behavior

Under our experimental conditions, we were able to induce venting behavior between 1 and 12 h prior to dawn, *i.e.*, during the dark portion of the animal's natural cycle—the time period when the bacterial population of the light organ is at its highest. This behavior could not be

induced, however, during the light portion of the animal's natural cycle: this is the period between 4 and 10 h after dawn, when the crypt spaces should have the lowest amount of extracellular constituents, *i.e.*, matrix material, as well as animal and bacterial cells.

Animals kept in the dark past dawn retained their crypt contents until given a light stimulus. Under these conditions, we could induce expulsion up to 8 h past the natural venting time. These data suggest that the behavior is not under an independent circadian rhythm, but requires a light cue each day.

Discussion

The opportunity to sample the microenvironment surrounding bacterial symbionts is rare because, in most associations, the bacteria are embedded deeply within tissues that are difficult to access. In the present study, taking

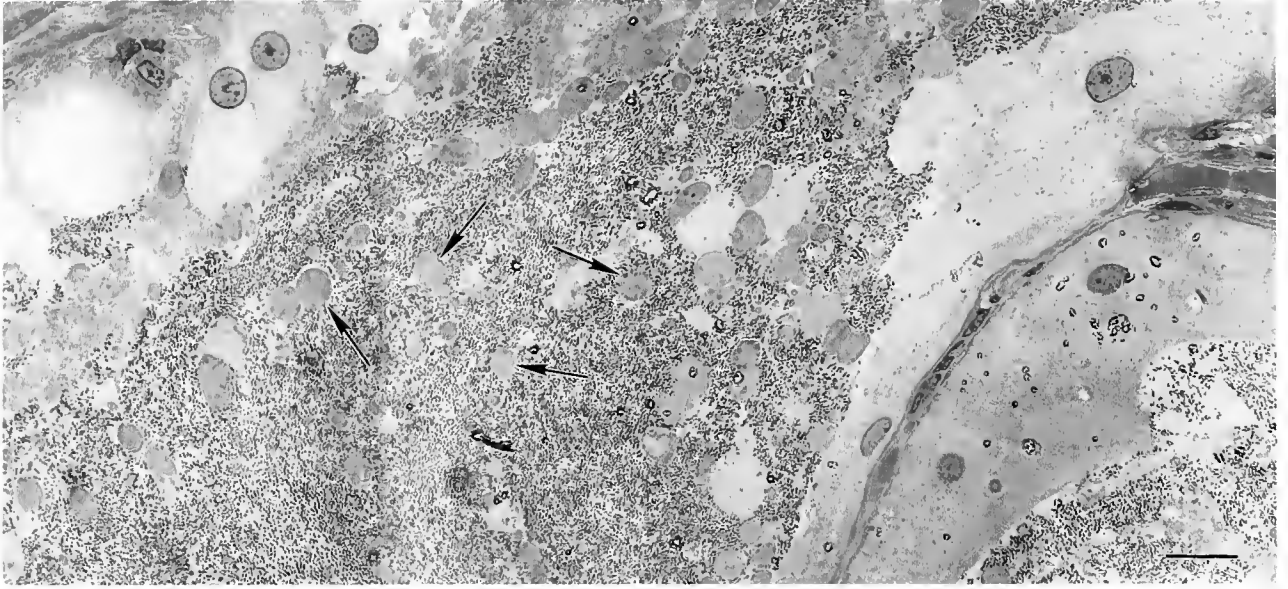


Figure 3. Exudate in the duct and anterior crypt spaces of a sectioned adult light organ. The image is a montage of light micrographs of tissue that was fixed at dawn, just before the natural venting. The typical experimental conditions that produce venting (e.g., anesthetic and light stimulus) were not applied. Eukaryotic cells (arrows) in the crypt and duct spaces are surrounded by bacterial cells. The sample was stained with 2% toluidine blue. Scale, 20 μm .

advantage of a natural behavior of the host squid, we have described the cellular components of the microenvironment of the symbiotic light organ and have determined

the feasibility of sampling this microenvironment under experimental conditions.

These studies have revealed that (1) the diel venting

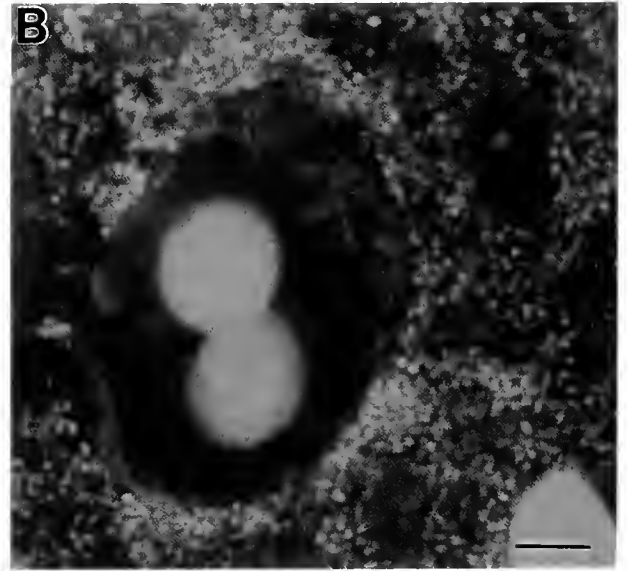
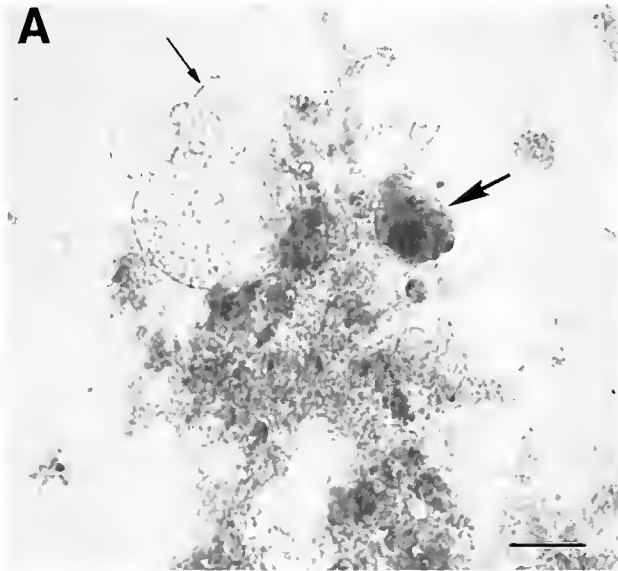


Figure 4. Viability of cells in the exudate. (A) Results of staining the exudate with 0.1% trypan blue to test viability of animal cells. The exudate contains a mixture of living cells, which exclude the stain and remain a golden hue (small arrow), and dead or dying cells, which do not exclude the stain (large arrow). The matrix also interacted with the dye and appears blue. Magnification, 400 \times . Scale, 10 μm . (B) Results of two nucleic acid fluorescent stains that distinguish viable from dead bacterial cells. The vast majority of freshly emerged bacterial cells were viable, as indicated by the green field of bacteria surrounding the animal cell. Scale, 5 μm .

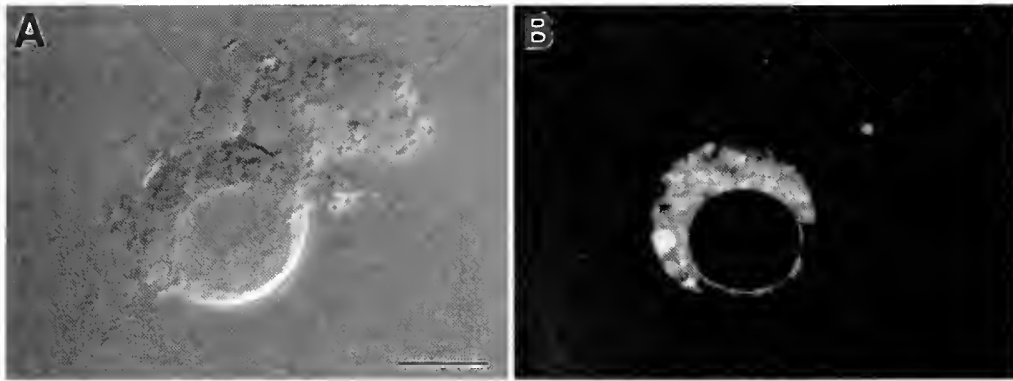


Figure 5. Stained acidic compartments within a freshly vented animal cell. (A) Differential interference microscopy; the cell is surrounded by bacteria and matrix material. Scale, 10 μm . (B) The same cell stained with 1 μM LysoTracker; note the acidic compartments, possibly lysosomes. Scale, 10 μm .

of the symbiotic organ contents by the host squid provides an intact sample of the light organ crypt microenvironment; (2) this diel behavior, which occurs in juveniles as well as adults, is dependent upon a light cue; (3) the cellular constituents of the crypts consist of a population of viable *V. fischeri* cells in association with a mixture of live and dead host cells; (4) the characteristics of some of the animal cells found in the exudate suggest that these cells are molluscan phagocytic hemocytes (Cheng, 1981; Sminia, 1981; Cowden and Curtis, 1981); (5) these host and bacterial cells are embedded in a conspicuous matrix

similar in appearance to other bacteria-based biofilms; and (6) the venting of crypt contents can be experimentally induced at times in the diel cycle other than dawn.

Our finding that about 90% of the symbiont culture is vented suggests strongly that this behavior is controlling the number of symbionts in the light organ (Lee and Ruby, 1994; present study). Research on symbiotic associations between animals and their bacterial partners has demonstrated that symbiont population density is regulated in a variety of ways. These control mechanisms can be grouped into two broad categories that work either alone or in concert: control of bacterial growth rate and elimination of excess bacterial cells. In the former mode, the host environment, while sustaining the viability of the symbionts, presents a biochemical milieu that attenuates bacterial cell division. In the latter, elimination of supernumerary symbionts is typically accomplished by the regular venting of the bacterial cells from the host tissues, the digestion by the host of the bacterial cells, or both. Digestion can be either extracellular or intracellular, the latter typically following the engulfment of the bacterial cell by a phagocytic host cell. Previous research and the results presented here provide evidence for a multifaceted control of the symbiont population in the squid-vibrio symbiosis. Lee and Ruby (1994) demonstrated that the bacterial growth rate in the adult light organ (average doubling time of approximately 4.8 h) is suppressed in comparison with the physiological potential for growth seen under culture conditions (average doubling time of 0.5 h; Ruby and Asato, 1993). However, the former growth rate is still sufficiently high that, although the numbers of bacteria are set back at dawn to a lower population density by the venting behavior, the light organ will be repopulated with symbionts over the course of the day. Slow growth rates, coupled with shedding of symbionts into the environment, have been documented previously in symbioses between animal hosts and their

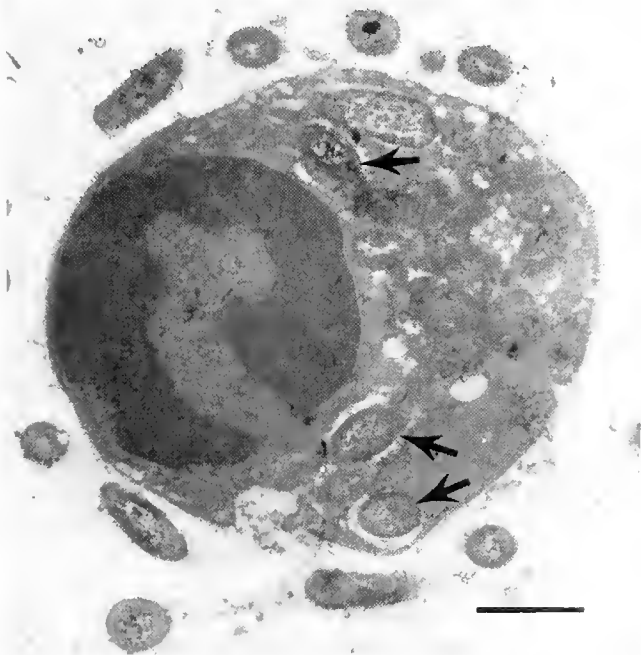


Figure 6. Bacteria within a crypt cell. A TEM of a eukaryotic cell found within the crypt spaces of a juvenile *E. scolopes* light organ. This cell contains several intracellular bacteria (arrows). Scale, 1 μm .

luminous bacterial partners, although no rhythm or dependency on cues was noted (Haygood *et al.*, 1984).

In addition to the suppression of growth rate and the diel venting of symbionts, the phagocytosis of bacterial cells by host macrophage-like cells that we observed in this study (Fig. 6) may represent yet another level of control of the symbionts in these associations. Tebo *et al.* (1979) showed bacteria in host cells in the light organ of the monocentrid fish *Monocentris japonicus*, whose light organ contains the symbiont *V. fischeri*. However, those bacterial cells were in the epithelium rather than in the macrophage-like cells seen in the light organ of *E. scolopes*. At this point, neither they nor we have determined whether the bacteria within host cells are *V. fischeri* or other bacterial species that are being eliminated to maintain *V. fischeri* as the sole symbiont; *i.e.*, we do not know whether the macrophage-like host cells in the squid light organ function principally in control of *V. fischeri* symbiont number or in maintenance of light organ specificity, or both. Thus, the determination of the precise function of these cells in the dynamics of this symbiosis awaits their further characterization. However, to our knowledge, this report represents the first documentation of macrophage-like cells in direct association with the symbionts in a light organ.

Whatever the function of these host macrophage-like cells in the crypt spaces, their association with the population of bacterial symbionts is not unexpected. In molluscs, macrophage-like hemocytes are reported to be involved in phagocytosis and digestion of pathogens in many tissues and their associated lumina (Cheng, 1981; Sminia, 1981; Cowden and Curtis, 1981). Vertebrate macrophages, which are thought to be derived evolutionarily from this invertebrate cell type (Ottaviani and Franceschi, 1997), are also found in similar circumstances. For example, mononuclear phagocytes are released into the blood stream and spread to all tissues including epithelia (Stewart *et al.*, 1994), and lymphocytes are a common constituent of the cellular community that lines the mammalian intestine (James and Zeitz, 1994).

The other animal cells in the crypt environment that do not resemble healthy, functioning macrophage-like molluscan hemocytes may be dead or dying hemocytes, or they may be epithelial cells shed from the lining of the crypt spaces. The shedding of epithelial cells in response to interaction with bacteria or bacterial by-products is known to occur in other instances. For example, bacterial lipopolysaccharide will induce shedding of murine uroepithelial cells, which is believed to be a mechanism by which the host evades pathogenic bacteria (Aronson *et al.*, 1988). The exact definition of the host cell types in the crypt space and the origin of these cells, thus, also awaits future studies.

All of the bacterial and animal cells contained in the

exudate are suspended in a thick, heterogeneous matrix. SEM showed that this matrix resembles other bacteria-associated biofilms, including those associated either with inorganic substrates or animal tissues (Pearl, 1985). TEM revealed a complex mixture of membranes and particulate matter. Matrix ultrastructure of the squid light organ appears similar to that described in the light organs of the macrourid fish *Caelorhincus* (W. Loh, University of Sydney, pers. comm.). The exact nature of the constituents, as well as the relative contributions of the animal host and the bacterial symbionts to the matrix material, remain to be determined. To date, only one constituent has been defined, *i.e.*, the host-derived amino acids that supply the growing symbiont population with these metabolic building blocks (Graf and Ruby, 1998).

The finding that venting behavior can be induced experimentally during the 12 h preceding the natural expulsion event at dawn paves the way for examination of the microenvironment of the crypts during this portion of the diel cycle of the symbiosis. Boettcher *et al.* (1996), in studies of the diel rhythm of the light organ, showed that this 12-h period contains the highest and lowest per cell luminescence of *V. fischeri*. They interpreted this finding to suggest that significant fluctuations in the biochemistry and physiology of the crypt environment occur between the hours around dusk and the hours around dawn. After venting, the remaining 10% of the symbiont population divides and repopulates the light organ, so that by dusk, there is once again a full complement of bacteria in the crypts. Whether the animal delivers nutrients steadily over the period of about 12 h following venting, sustaining a slow bacterial growth rate over this period, or whether it maintains a low bacterial population until the late afternoon, when it delivers a large pulse of nutrients that stimulates rapid bacterial growth, remains to be determined. Defining changes in the biochemistry of the microenvironment during the day may provide insight into the mechanisms by which luminescence is controlled. In addition, such analyses will define other types of metabolic and regulatory changes that accompany the diel rhythm of this symbiosis. At present, we cannot experimentally induce venting of the crypt contents during the light portion of the animal's cycle. Thus, a full understanding of the dynamics of symbiont population growth in the light organ over the entire day awaits refinement of our current method or reliance on alternative methods of sampling this environment.

The accessibility of the bacterial microenvironment in this symbiosis makes a rich frontier available for the study of the dynamics of an animal-bacterial association. Future studies will focus on defining both the biochemical constituents of the matrix material and the nature of the animal cells that occur among the bacterial symbionts.

Acknowledgments

We thank B. DeCaires, J. Doino, J. Foster, J. Kimbell, L. Lamarcq, C. Phillipson, E. Ruby, E. Stabb, and K. Visick for helpful comments on the manuscript. We are also grateful for technical assistance from A. Thompson and W. Ormerod of the Center for Electron Microscopy and Materials Analysis at the University of Southern California. This work was supported by NSF grant IBN 96-01155 to MMN and E. G. Ruby and NIH grant RO1 RR10926-O1A1 to E. G. Ruby and MMN.

Literature Cited

- Aronson, M., O. Medalia, D. Amichay, and O. Nativ. 1988. Endotoxin-induced shedding of viable uroepithelial cells is an antimicrobial defense mechanism. *Infect. Immun.* **56**: 1615–1617.
- Boettcher, K. J., E. G. Ruby, and M. J. McFall-Ngai. 1996. Bioluminescence in the symbiotic squid *Euprymna scolopes* is controlled by a daily biological rhythm. *J. Comp. Physiol. A.* **179**: 65–73.
- Breznak, J. A. 1982. Intestinal microbiota of termites and other xylophagous insects. *Annu. Rev. Microbiol.* **36**: 323–343.
- Breznak, J. A., and A. Brune. 1994. Role of microorganisms in the digestion of lignocellulose by termites. *Annu. Rev. Entomol.* **39**: 453–487.
- Cheng, T. C. 1981. Bivalves. Pp. 233–300 in *Invertebrate Blood Cells*, N. A. Ratcliffe and A. F. Rowley, eds., Academic Press, New York.
- Cowden, R. R., and S. K. Curtis. 1981. Cephalopods. Pp. 301–323 in *Invertebrate Blood Cells*, N. A. Ratcliffe and A. F. Rowley, eds., Academic Press, New York.
- Diwu, Z., Y. Z. Zhang, and R. P. Haugland. 1994. Novel site-selective fluorescent probes for lysosome and acidic organelle staining and long-term tracking. *Cytometry* **77**: 426B.
- Flint, H. J. 1997. The rumen microbial ecosystem—some recent developments. *Trends Microbiol.* **5**: 483–488.
- Graf, J., and E. G. Ruby. 1998. Host-derived amino acids support the proliferation of symbiotic bacteria. *Proc. Natl. Acad. Sci. USA* **95**: 1818–1822.
- Haygood, M. G., B. M. Tebo, and K. H. Nealson. 1984. Luminous bacteria of a monocentrid fish (*Monocentrus japonicus*) and two anomalopoid fishes (*Photoblepharon palpebratus* and *Kryptophanaron olfredi*): population sizes and growth within the light organs, and rates of release into the seawater. *Mar. Biol.* **78**: 249–254.
- James, S. P., and M. Zeitz. 1994. Human gastrointestinal mucosal T cells. Pp. 275–285 in *Handbook of Mucosal Immunology*, P. L. Ogra, M. E. Lamm, J. R. McGhee, J. Mestecky, W. Strober, and J. Bienenstock, eds., Academic Press, San Diego.
- Lee, K., and E. G. Ruby. 1994. Effect of the squid host on the abundance and distribution of symbiotic *Vibrio fischeri* in nature. *Appl. Environ. Microbiol.* **60**: 1565–1571.
- Lloyd, D., and A. J. Hayes. 1995. Vigour, vitality, and viability of microorganisms. *FEMS Microbiol. Lett.* **133**: 1–7.
- McFall-Ngai, M., and M. K. Montgomery. 1990. The anatomy and morphology of the adult bacterial light organ of *Euprymna scolopes* Berry (Cephalopoda: Sepiolidae). *Biol. Bull.* **179**: 332–339.
- McFall-Ngai, M. J., and E. G. Ruby. 1998. Sepioids and vibrios: when first they meet. *BioScience* **48**: 257–265.
- Ottaviani, E., and C. Franceschi. 1997. The invertebrate phagocytic immunocyte: clues to a common evolution of immune and neuroendocrine systems. *Immunol. Today* **18**: 169–174.
- Pearl, H. W. 1985. Influence of attachment on microbial metabolism and growth in aquatic ecosystems. Pp. 363–400 in *Bacterial Adhesion: Mechanisms and Physiological Significance*, D. C. Savage and M. Fletcher, eds., Plenum Press, New York.
- Ruby, E. G. 1996. Lessons from a cooperative bacterial-animal association: the *Vibrio fischeri*-*Euprymna scolopes* light organ symbiosis. *Annu. Rev. Microbiol.* **50**: 591–624.
- Ruby, E. G., and L. M. Asato. 1993. Growth and flagellation of *Vibrio fischeri* during initiation of the sepiolid squid light organ symbiosis. *Arch. Microbiol.* **159**: 160–167.
- Sminia, T. 1981. Gastropods. Pp. 191–232 in *Invertebrate Blood Cells*, N. A. Ratcliffe and A. F. Rowley, eds., Academic Press, New York.
- Spurr, A. 1969. A low-viscosity epoxy resin embedding medium for electron microscopy. *J. Ultrastruct. Res.* **26**: 31–43.
- Stewart, C. C., M. C. Riedy, and S. J. Stewart. 1994. Induction: the proliferation and differentiation of macrophages. Pp. 3–27 in *Macrophage-Pathogen Interactions*, B. S. Zwilling and T. K. Eisenstein, eds., Marcel Dekker, New York.
- Tebo, B. M., D. S. Linthicum, and K. H. Nealson. 1979. Luminous bacteria and light emitting fish: ultrastructure of the symbiosis. *BioSystems* **11**: 269–280.

Transplantation of Fu/HC-Incompatible Zooids in *Botryllus schlosseri* Results in Chimerism

BARUCH RINKEVICH¹, IRVING L. WEISSMAN², AND ANTHONY W. DE TOMASO^{2,*}

¹*National Institute of Oceanography, Tel Shikmona, P.O. Box 8030, Haifa 31080, Israel;*

²*Department of Pathology, Stanford University School of Medicine, Stanford, California 94305; and Hopkins Marine Station, Pacific Grove, California 93950*

Abstract. The colonial urochordate *Botryllus schlosseri* undergoes a genetically defined, natural transplantation reaction that is controlled by a single Mendelian locus (called the Fu/HC). This Fu/HC-based allorecognition system is initiated when peripheral elements of the vasculature interact on the edges of two asexually expanding colonies. To better understand the spatial organization of the cellular elements responsible for Fu/HC-based allorecognition, we bypassed the normal site of interaction (the ampullae) and experimentally transplanted zooids between Fu/HC-noncompatible *Botryllus schlosseri* pairs. The results show that (1) instead of the expected rejections (tissue necroses) that develop after natural contacts between peripheral blood vessels, the transplanted organs are morphologically eliminated within a few days in conjunction with the normal blastogenic cycle; and (2) donor-recipient chimerism is established after complete morphological elimination of transplanted tissues. These results suggest that Fu/HC-based allorecognition responses in *Botryllus schlosseri* occur exclusively at the ampullae and that once cells have crossed this barrier, they are able to survive and proliferate in the new host colony.

Introduction

Colonies of the urochordate *Botryllus schlosseri* undergo a genetically defined, natural transplantation reaction following allogeneic contacts between peripheral blood vessels. Upon contact, the allogeneic vessels either fuse to form a single colony with a common blood supply or reject each other in a blood-based, inflammatory reaction, after which the two colonies no longer interact. His-

tocompatibility discrimination resides in a single, highly polymorphic fusion/histocompatibility locus (called the Fu/HC; Scofield *et al.*, 1984) with a large number of codominantly expressed alleles (Rinkevich *et al.*, 1995). Allogeneic fusion occurs between colonies that share at least one Fu/HC allele; in contrast, partners will reject each other if they share no Fu/HC alleles (Bancroft, 1903; Oka and Watanabe, 1957, 1960; Sabbadin, 1962; Scofield *et al.*, 1982).

Several interesting phenomena may occur after two colonies have undergone a Fu/HC-mediated fusion event. In the laboratory, we have observed that, after fusion, the genetic colonial descendants (zooids) from one partner in the chimera cease normal development, and these dying zooids are resorbed by massive phagocytosis, leaving the zooids of the other colony intact (Rinkevich and Weissman, 1987). This phenomenon, called colony resorption, occurs at the end of the synchronized weekly blastogenic cycle in which the old generation of zooids dies through a programmed apoptotic event (Lauzon *et al.*, 1993). We have used genetically defined laboratory colonies to show that the ability of one colony to resorb another is consistent, and that different genotypes can be grouped into a reliable hierarchy. However, analysis of the segregation of these traits in defined crosses suggests that it is a complex phenomenon involving at least several loci, possibly including the Fu/HC locus (Rinkevich *et al.*, 1993). Thus, resorption in *Botryllus* has been compared to the minor histocompatibility loci seen in the vertebrates (Rinkevich, 1993).

Several laboratories have also shown that, after fusion, each colony can exchange germ and somatic stem cells which are then able to survive and replicate in the allogeneic colony. In fact, as first described by Sabbadin and Zaniolo (1979), the germ cells from one colony can actually completely parasitize the other colony in a fused

Received 5 December 1997; accepted 8 June 1998.

* To whom correspondence should be addressed. E-mail: idet@leland.stanford.edu

chimera, such that only one of the genotypes is represented in the mature germ cells. This can occur up to a month after two fused colonies have been experimentally separated, demonstrating that cells from one colony survive and proliferate in the other (Sabbadin and Zaniolo, 1979; Pancer *et al.*, 1995; Stoner and Weissman, 1996).

These two postfusion events appear to be opposite in nature and are difficult to reconcile. On one hand, the resorption phenomenon suggests that in an allogeneic chimera there is still a form of directed allorecognition occurring, and the ability to demonstrate a hierarchy among laboratory-bred colonies suggests a genetic component to this process. Conversely, the precursors of germ and somatic cells clearly can proliferate inside an Fu/HC-matched, allogeneic colony, suggesting that there is not a secondary form of allorecognition occurring, particularly on a global scale. This is further complicated by recent observations that, in a fused colony in which one of the partners had been resorbed, only the genotype of the resorbed partner was present in the germ line. Thus a somatic loser (by resorption) can be a gametic winner (by successful germ cell competition) (Pancer *et al.*, 1995; Stoner and Weissman, 1996).

The above observations led us to ask whether any allogeneic effector systems are present throughout the entire colony. To investigate this question, we decided to circumvent the natural manifestation of incompatibility, which occurs when peripheral blood vessels interact, by grafting whole zooids between colonies with rejecting Fu/HC genotypes. Results from these experiments provide further evidence that Fu/HC-mediated allorecognition, the rejection effector system, or both, may be restricted to the ampullar tips, suggesting that allorecognition responses are not a colony-wide phenomenon in *Botryllus*.

Materials and Methods

Animals

We used colonies of *B. schlosseri* that were originally collected from the Monterey Marina (California) but have been growing in the laboratory at Haifa, Israel, and at Hopkins Marine Station, Pacific Grove, California. Colonies were born and reared separately on glass slides (5 × 7 cm) in glass staining racks within 17-l tanks as described (Boyd *et al.*, 1986). Subclones of individual colonies were Fu/HC phenotyped using a cut colony assay (Rinkevich *et al.*, 1993), and rejecting pairs of colonies were identified. These subclones were not used in the transplantation assays.

Transplantation

Reciprocal transplantation of whole zooids between rejecting *B. schlosseri* pair genets was performed during developmental stages A–C of the blastogenic cycle (de-

scribed in Milkman, 1967). A longitudinal incision was made (with a thin needle) between the atrial and branchial siphons of a single zooid (highlighted in Fig. 1b). Both edges of the incision were then retracted with fine forceps. The incision went through the tunic and upper body wall of the individual zooid, and retraction of the edges exposed the body cavity, which contained the body of the zooid, the bud, and the gonads (see Berrill, 1941, for an in-depth description of *B. schlosseri* anatomy). The zooid was lifted and removed with a fine needle and forceps, leaving behind a "cup" consisting of the outer and lower tunics lined with epithelium, connective tissues, cut blood vessels, and, in many cases, all or part of the buds and the gonads. Bleeding from the cut blood vessels (either from the removed zooids or from the leftover vessels) was always seen. The removed zooid was then replaced by another zooid taken from a naive subclone of a rejecting genet, or in the case of controls, from another subclone of the same genet. A control zooid and the experimental zooid were transplanted within the same system, separated by 1–3 zooids (Exps. I–III, Table 1A) or in adjacent systems (Exps. IV–VI, Table 1B). The transplanted zooids were carefully inserted within the empty cups, one zooid per cup, pushed slightly inside with the blunt end of a forceps, and covered with the almost enclosing, cut surface of the outer tunic layer. In all cases of transplantation a mixture of blood cells coming from the introduced zooid and from the local bleeding was documented. Bleeding stopped within a few minutes.

Tissue sampling

Amplified fragment length polymorphism (AFLP) analysis was performed on tissue samples from Exps. I–III. Exps. IIc and IIIc died prematurely. Sampling was usually done 3–4 weeks after the final transplantation. Before tissue was sampled, each subclone was carefully checked under a dissecting microscope to determine whether the transplanted zooids had been completely resorbed. In one case (Exp. IIc, Table I) the whole subclone, which started to degenerate, was isolated as is. All other seven subclones were photographed, their general structure was outlined, and three to seven tissue samples per subclone were separated with a razor blade and individually snap-frozen in liquid nitrogen.

Amplified fragment length polymorphism (AFLP) analysis

All enzymes were purchased from New England Biolabs (Beverly, Massachusetts), and the chemical reagents were purchased from Sigma (St. Louis, Missouri). Oligonucleotides were synthesized at the PAN facility at the Stanford University Medical School. Frozen tissue samples were ground to a fine powder with a mortar and pestle. DNA was extracted on silica columns (Nucleo-

Table I

Experimental procedures and major results for allogeneic and isogenic zooid transplantation

Experiment #	Allogeneic* combination	Pair #	Donor genotype	Initial size (# zooids)†		Major outcomes‡
				Recipient	Exp. system	
A = One-month experiments I	1 vs. 2	a	1	23	10	4 repeated zooid transplantations (within 21 days from first event), all resorbed together with isogenic controls and before the takeover phase of blastogenesis. No single case of POR. The ramet died during the 5th transplantation, before completion.
		b	1	20	9	Same as Ia.
		c	2	20	7	6 sets done within 1 month. Resorption of transplanted allogeneic and isogenic zooids in all cases started after transplantation and terminated during takeover. No POR. Sampled for AFLP analysis.
		d	2	11	7	Same as Ic: sampled for AFLP analysis.
II	3 vs. 4	a	3	30	13	Same as Ic: sampled for AFLP analysis.
		b	3	32	10	Same as Ic: sampled for AFLP analysis.
		c	4	16	7	The first 4 sets of transplantations as in Exp. Ia. During the 5th set (day 25), the ramet degenerated and was sacrificed for AFLP analysis as one sample. No POR.
		d	4	15	10	Morphology same as Ic, died on day 25, no further sampling.
III	5 vs. 6	a	5	31	7	Same as Ic: sampled for AFLP analysis.
		b	5	13	6	Same as Ic: sampled for AFLP analysis.
		c	6	21	10	Same as Ic: sampled for AFLP analysis.
		d	6	26	12	Same as Ic: died prior to sampling.
B = Two-month experiments IV	7 vs. 8	a	7	27	11	Same as Ic: but zooids transplanted within two months. No AFLP sampling was done on these experiments.
		b	8	19	9	Same as IVa.
V	9 vs. 10	a	9	22	8	Same as IVa.
		b	10	18	7	Same as IVa.
VI	11 vs. 12	a	11	30	9	Same as IVa.
		b	12	31	8	Same as IVa.

* Each of the 12 genets was used in only one set of experiments.

† The size of the recipient subclone at the day of the first transplantation, and the size of the experimental system within the recipient subclone on which both transplanted zooids (experimental and control) were introduced. Follow-up transplantations were performed on daughter zooids, produced through blastogenesis from intact buds, of these same systems.

‡ POR, point of rejection; AFLP, amplified fragment length polymorphism.

bond C+T Kit, Macherey Nagel, Duren, Germany) using proprietary buffers according to the manufacturer's instructions. AFLPs were performed as described previously (Vos *et al.*, 1995). Briefly, 200 ng of DNA was cut to completion with restriction enzymes *Eco* RI and *Mse* I for 2 h at 37°C in a 30- μ l reaction volume. Oligonucleotide adaptors, 1 mM ATP, and T4 DNA ligase were then added (total volume, 40 μ l), and the incubation was continued for 3 h. The DNA was preamplified with one

selective nucleotide on each primer (*Eco* RI = A; *Mse* I = T). The preamplification mix was diluted 1:20 and 3 μ l was used for AFLP fingerprinting with each primer containing three selective nucleotides (*Eco* RI = ATg; *Mse* I = TCg). The *Eco* RI primer was end-labeled with ³³P-ATP (New England Nuclear) using polynucleotide kinase. PCR reactions were diluted 1:1 in stop solution (98% formamide, 10 mM EDTA pH 8, 0.1% bromophenol blue, 0.1% xylene cyanol), denatured for 5 min at

95°C, and resolved on a standard sequencing gel at 70 W for 2.5 h. Gels were dried, and the autoradiograms were exposed for 36 h. Each experiment was repeated two times to ensure that the AFLP fingerprints were consistent. In some sets, different primer sets were used, and the results were equivalent (not shown).

Results

Twelve *B. schlosseri* colonies were organized into six rejecting pairs, providing six independent experiments (see Table I). Within each pair, two types of transplantations were done in parallel (described in the Methods). Zooids were reciprocally transplanted between the two rejecting colonies to make allografts; and zooids were transplanted from another ramet of each colony to make isografts. Allograft and isograft transplantations were carried out within a single system of the recipient, usually a few zooids apart (see Fig. 1). There were no observed differences in response if allografts or isografts were done independently (not shown).

The initial transplantation procedure was followed by four to six sequential transplantations over the course of 1 (Exps. I–III) or 2 (Exps. IV–VI) months (Table I). Multiple transplantations into the same ramet were done to test for the induction of a rejection response after repeated exposures to the same allogeneic tissue. Transplantations were also done at different points of the blastogenic cycle (Milkman, 1967) to test for any variability in the alloresponse. In Exps. I–III (Table IA) the subsequent transplantation was performed immediately after the takeover phase of blastogenesis (Milkman, 1967), while in Exps. IV–VI (Table IB), one full blastogenic cycle separated the two sequential transplantations.

Apart from the zooids that were completely excised during the transplantation procedure, other zooids in the experimental system and in all the other systems within the same colony were usually not affected. A few hours after transplantation, the implanted tissues were covered by the matrix of the cut tunic, sealing them within the recipient colony.

Under normal conditions in a *Botryllus* colony all zooids and buds are connected by vascular outgrowths to the colonial circulatory system (Milkman, 1967). Vascular anastomoses were not observed in any of the 114 allogeneic and isogeneic zooids transplanted in these experiments. Although there was no long-term vascularization, hemocytes from the donor and recipient were in contact for several hours following the transplantation procedure: there was bleeding from the cut vasculature of the recipient colony, as well as from the open circulatory system of the donor zooid. This allowed mixing of host hemocytes with donor hemocytes and tissue for several hours. After 12–24 h, the disconnected blood vessels of the colony regenerated, sometimes forming a circular pattern

of blood vessels around the transplanted zooid (not shown). Thus the allogeneic interactions in these experiments can be summarized as follows: the donor zooid was in contact with the recipient hemocytes, while the donor hemocytes were allowed to mix with the colonial circulation of the recipient, analogous to injection of hemocytes across a Fu/HC incompatible barrier.

Within 24 h, many of the implants were completely covered by the upper tunic wall (Fig. 1a). In some cases, especially when a large zooid was transplanted, part of the zooid extended out of the "cup," closed around by a "collar" made of the colony epidermal wall (not shown). Within the next few days, all of the implants degenerated, a phenomenon coinciding with the regular colony blastogenesis (Fig. 1b) in which all zooids go through a systemic programmed apoptotic cycle, followed by massive phagocytosis (Lauzon *et al.*, 1992). There was no observable difference between resorption of isografts or allografts (Fig. 1a, c). For instance, in Figure 1c, the isograft appears to be resorbing faster than the allograft. Any variations in the time scale of resorption (2–5 days) were related to the blastogenic cycle. More importantly, no visible points of rejection (POR; Table I) were ever observed in these transplantations (Fig. 1a, b), although natural contact assays done on other ramets of the same six pairs of genets (Table I) always resulted in typical, distinct POR within 24–48 h after first ampullae contacts (not shown). After the takeover phase of blastogenesis, all or most parts of the allogeneic and isogeneic tissues were resorbed and had disappeared, leaving behind a clear tunic matrix or a space occupied by the new generation of developing zooids (Fig. 1b). In some cases, remnants were found trapped in the bare tunic (Fig. 1d) in a manner similar to that recorded in regular colonies (Rinkevich and Weissman, 1987).

Two major morphological variations in the outcomes of transplantation were documented, although neither was related to the type of transplant (autograft or allograft). The first was a partial resorption of an intact zooid bordering the area of transplantation (Fig. 1c), probably resulting from the experimental manipulation of zooid excision and transplantation. Morphological resorption as a result of stress conditions has already been documented in *Botryllus* (Rinkevich *et al.*, 1993). This type of partial resorption (Fig. 1c) occurred within 24 h of zooid transplantation, but was never completed before the takeover phase (Lauzon *et al.*, 1992) of blastogenesis. The second type of variation was the resorption rate of the implant. In some cases, the implants were resorbed completely or mainly within 24 h of transplantation (Fig. 1e, f). Where partial resorption was recorded (Fig. 1f), the leftover parts remained within the tunic for the whole blastogenic cycle and were completely resorbed only during the takeover stage.

To analyze the possibility for donor cell proliferation

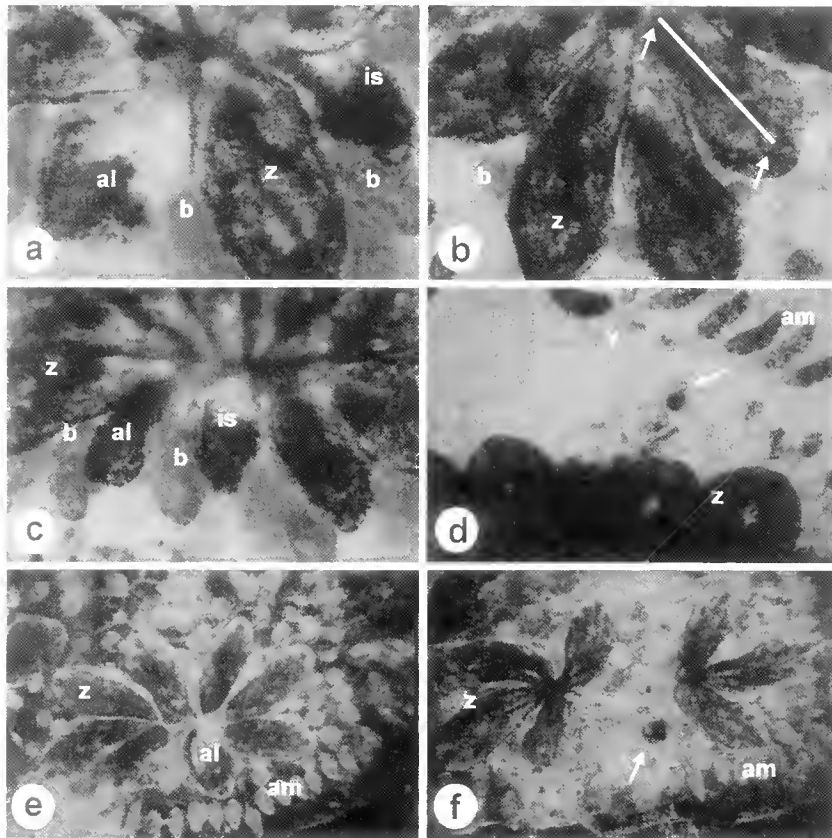


Figure 1. Morphological outcomes for zooid transplantation in Fu/HC-noncompatible colonies of *Botryllus schlosseri*. al = allogeneic transplant, am = ampulla, b = bud, is = isograft, v = blood vessel, z = zooid. Length of each zooid = 2 mm. (a) Results from Exp. 1c (Table I): The second set of allogeneic and isogenic grafts, 24 h after implantation, when the colony is at blastogenic stage C. (b) The same area, photographed 72 h later, following a takeover event. Both implanted zooids are completely resorbed, and there is no difference between control and allograft; the zooid between them as well as adjacent buds are unaffected. After the takeover process, all transplanted materials were morphologically eliminated, no point of rejection (POR) is observed. Note the top right zooid: the incision for transplanting the zooids is highlighted; white arrows point to the atrial and branchial siphons, and the white line highlights the incision made for the transplantation procedure (see Methods). (c) Results from Exp. 1d (Table I) 24 h after first set of implants was established. The control isograft appears to be resorbing faster than the allograft. The zooid to the right of the isograft is also partly resorbed. The colony is at blastogenic stage C, and the developed buds in the area of implantation are not affected. (d) Exp. 1b, after resorption of most of the allogeneic implant. Resorption is not complete, and a remnant of the graft (arrow) is trapped in the tunic matrix. (e, f) Results from Exp. 5a (Table I): The third set of allografts, immediately after implantation (a), and 24 h later (f). By 24 h, most of the graft has been resorbed and only a small part of it (arrow) is left. This remnant remained for an additional 3 days, and was resorbed during the takeover stage of blastogenesis.

in the recipient (Sabbadin and Zaniolo, 1979; Pancer *et al.*, 1995; Stoner and Weissman, 1996), all the available subclones from the 1-month experiment (five or six consecutive transplantation events; Table 1A) were sampled (1–7 fragments/subclone) 3 to 4 weeks after complete resorption of the donor's zooids (except for Exp. 1c, see Table I). The genotype of the recipient was then analyzed using amplified restriction fragment polymorphisms (AFLPs; Vos *et al.*, 1995). AFLPs identify DNA polymorphisms between individuals; these polymorphisms can then be used as molecular genetic markers. AFLP

polymorphisms are often single base-pair substitutions, and since these are the most abundant polymorphisms available, a large number of AFLP genetic markers can be identified, even between closely related colonies (Fig. 2). In these experiments, 6 to 12 unique AFLP markers were first identified in the naïve donor subclones. Following a transplantation, we then looked for the unique donor AFLPs in samples of recipient DNA.

Tissue samples were taken such that the transplanted area (including the relevant system of zooids and the surrounding tissue matrix) was isolated from the rest of

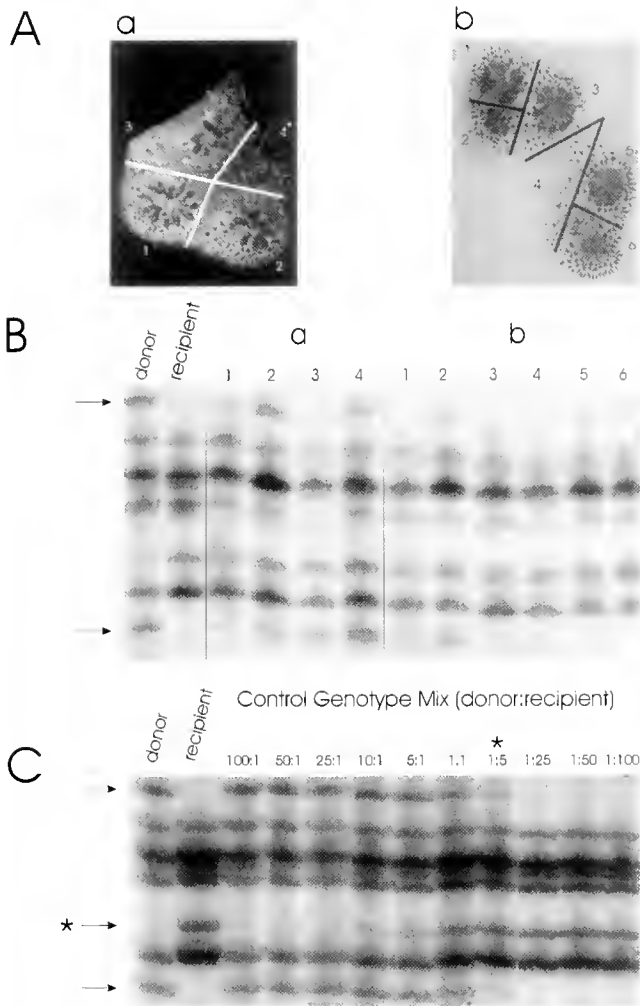


Figure 2. Amplified fragment length polymorphism (AFLP) fingerprints reveal the presence of donor alleles in the recipient after zooid transplantation. Panels a and b correspond to Experiment II, pair number a and b, in Table I. (A) Photographs of the recipient ramets after six sets of zooid transplantation and before subcloning. The areas sampled for DNA extraction and AFLP analysis are delineated and numbered. An asterisk indicates the site to which the donor zooids were originally transplanted; boxed numbers indicate a sample that contained peripheral vascular tissue only. (B) AFLP fingerprints of the donor, the naive recipient, and samples taken from the recipient after transplantation, as shown in A. Arrows indicate polymorphic AFLP alleles present in the donor and absent in the naive recipient. The appearance of these bands in the recipient ramets after transplantation indicates the presence of donor DNA. The recipient bands are invariable, indicating that the recipient genotype is stable and the resulting animal is a chimera. A section of the complete gel is shown for clarity. (C) A control experiment showing the independent sensitivity of each polymorphic AFLP donor locus in known mixtures of genotypes. DNA from the donor and naive recipient were mixed in the indicated ratios and the corresponding AFLP fingerprints were produced. The closed arrows indicate the same polymorphic donor loci as shown in B. The asterisk denotes a DNA mixture in which the top allele is present and the bottom allele is very faint. In this section of the gel a recipient locus can also be seen (arrow plus asterisk) and demonstrates that polymorphic loci can differ as much as 10-fold in their ability to be amplified from low concentrations.

the sublone. Then each sublone was further divided into several parts, including bare-tunic ampullae zones. Figures 2 and 3 depict the sampling details for seven sublones. One sublone (Exp. IIc) was not separated, but was used whole for a single AFLP analysis. In seven of the eight sublones (Fig. 2, Fig. 3 except Exp. IIc) donor AFLPs were clearly documented in all samples, including zooid-free areas and zones away from the transplantation areas. However, the degree of chimerism was not consistent among all parts of the recipients; different regions showed a higher or lower percentage of the donor genotype. In other words, not all of the donor AFLP markers were amplified from each recipient DNA sample (Fig. 2b). This is because the ability to amplify a particular AFLP marker from a mixed sample of DNA is unique for that marker; some AFLP markers can be identified when they represent less than 1% of the total DNA, while others are less sensitive (Fig. 2c). Thus, if the amount of chimerism is very low (e.g., donor DNA < 1% of the total DNA in the sample), only the most sensitive donor AFLP marker will be identified (see Fig. 2c). In contrast, in a sample that contains a higher amount of donor cells, the other, less sensitive AFLP markers will also be identified (Figs. 2 and 3). This provides a nice tool for estimating the amount of chimerism, but because the AFLP technique includes an initial PCR amplification of the total genomic DNA sample (Vos *et al.*, 1995), these comparisons are relative and can only be made in a side-by-side comparison to the controls (Fig. 2b, c).

Chimerism was detected globally in the recipient colonies more than 3 to 4 weeks after the final transplantation, and the degree of chimerism was variable in different samples. This suggests that donor cells proliferated in the host colonies; the small number of hemocytes from several transplanted zooids are unlikely to have been passively circulated and then detected several weeks later, after several rounds of blastogenesis.

Exp. IIIc (Table I; Fig. 3) was the only case in which we did not observe the donor genotype in any sample, although in the reciprocal tests (Exp. IIIa, b; Fig. 3) the other partner's DNA was clearly evident in all tissue samples. This is reminiscent of the directionality observed in resorption, where hierarchies were demonstrated in laboratory-reared colonies (Rinkevich *et al.*, 1993).

In summary, chimerism between the donor and recipient appeared to be the rule rather than the exception in these experiments. In 11 of 12 cases, donor AFLP markers could be identified in the recipient more than 3 to 4 weeks after the donor transplant had been eliminated. Furthermore, high amounts of chimerism were detected throughout the recipient colony. This suggests that once donor cells have crossed the ampullar barriers, they are able to survive and proliferate in the recipient colony, and are not being eliminated by an Fu/HC-based, or any other, allorecognition system.

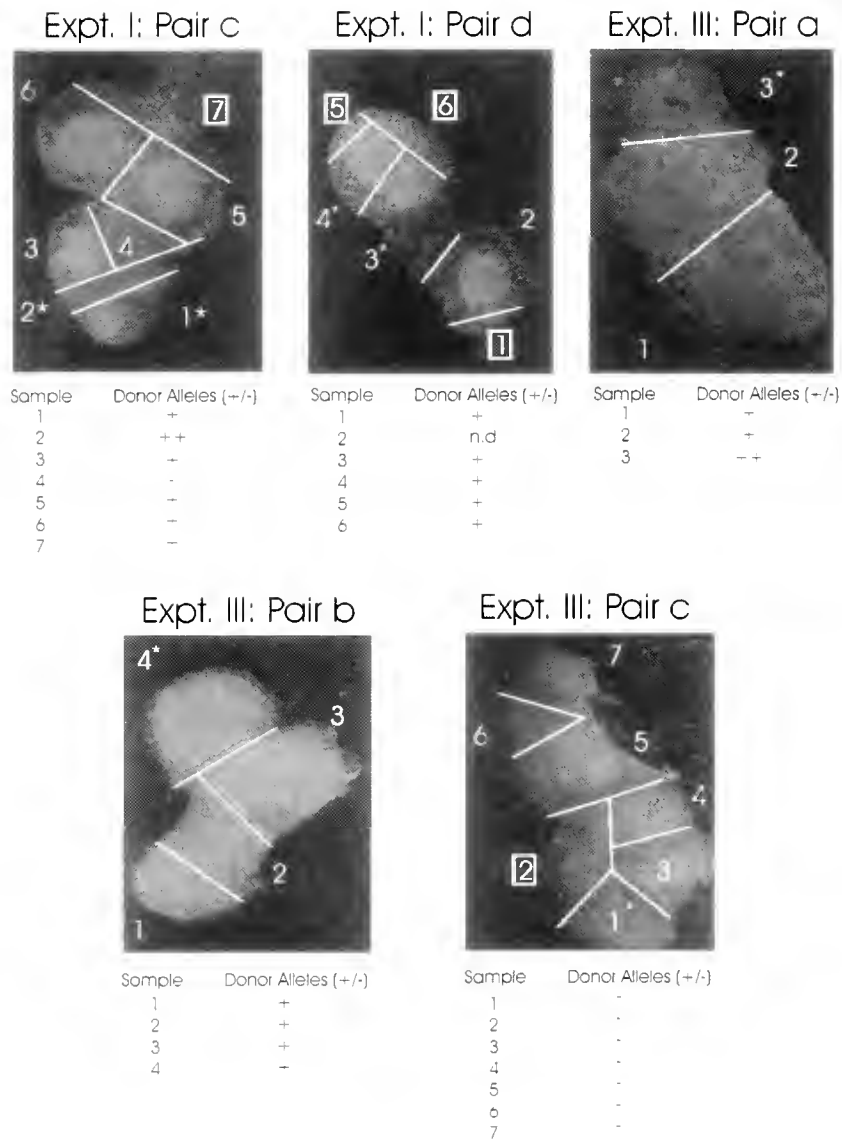


Figure 3. A summary of amplified fragment length polymorphism (AFLP) data from experiments described in Table I. Photographs show five recipient ramets after transplantation. The areas sampled for DNA extraction and AFLP analysis are delineated and numbered. Asterisks indicate the sites to which the donor zooids were originally transplanted; boxed numbers indicate a sample that contained vascular tissue only. Because of the independent sensitivity of each polymorphic donor locus (illustrated in Fig. 2C), not all of the polymorphic donor loci were seen in each of the transplanted recipient samples. Samples were scored as (++) if they contained over 50% of the polymorphic donor loci, (+) if under 50%, and (-) if none were seen. "n.d." indicates that the sample was not determined.

Discussion

This study produces two interesting results. First, zooid transplantation between noncompatible Fu/HC *B. schlosseri* genotypes does not result in the typical formation of visible PORs (reviewed in Weissman *et al.*, 1990). Rather, transplantation is followed by a morphological resorption similar to the allogeneic resorption that takes place after fusion between Fu/HC-compatible colonies (Rinkevich

and Weissman, 1987). Second, the Fu/HC-noncompatible genotypes continue to thrive within the host, even away from the transplantation zone; this phenomenon had previously been recorded only from Fu/HC-compatible encounters (Sabbadin and Zaniolo, 1979; Pancer *et al.*, 1995; Stoner and Weissman, 1996). Circumvention of the natural contact areas in *B. schlosseri* demonstrates that once cells have crossed the allogeneic barriers at the ampullae, they are no longer subject to elimination from an

Fu/HC-based allorecognition system, as demonstrated by the ability of cells to survive and proliferate in a completely allogeneic host.

The idea that Fu/HC-based allorecognition responses in botryllid ascidians could be limited to the ampullae is not new. The differences in rejection mechanisms between *B. scalaris*, *B. primigenus*, *B. schlosseri*, and several species of the genus *Botrylloides* have been postulated to reflect the change in the cells responsible for allorecognition from freely circulating (in *B. scalaris*), to residing outside the tip of the ampullae or in the tunic (*Botrylloides*) (reviewed in Saito *et al.*, 1994). Further evidence for this theory comes from experiments on *Botrylloides fuscus*, where fusion always occurs in a cut surface assay (where nonampullar vasculature elements are brought into contact), even between colonies that reject each other at the growing surface (*i.e.*, ampullar contacts; Hirose *et al.*, 1994). Furthermore, recent fine-scale EM observations on rejection in *Botrylloides simodensis* and *B. fuscus* strongly suggest that allorecognition responses are limited to the tunic in these species (Hirose *et al.*, 1997).

However, the situation in *B. schlosseri* is not as clear. There are no detailed reports of cut surface assays from this species. In our hands, cut surface assays are not definitive; we often see structures that look like POR between rejecting colonies, but this has never been consistent, nor as vigorous as the response at the ampullae (Rinkevich, 1992; unpubl. data). Furthermore, in experiments described by Sabbadin (1982), secondary buds were transplanted to zooid-free colonies that were both Fu/HC isogenic and allogeneic, and the ability of these transplanted buds to vascularize, develop, and mature was analyzed. Although the survival of the transplanted bud in an isogenic colony was clearly different from that in an allogeneic colony, there was no mention of the typical rejection response observed at the ampullae. Since, in Monterey *B. schlosseri*, rejection occurs prior to complete tunic fusion (see Saito *et al.*, 1994), allorecognition elements may be restricted to the vascular epithelia, or to a small subset of cells that did not contact the transplanted zooids in these experiments. It is also possible that Fu/HC-based allorecognition events were occurring but were not detected. Typical, visible POR formation may be a complex event, involving cells and signaling pathways not available at the interface between zooid and vasculature. There is a difference between recognition and response, and since none of the molecules involved in allorecognition in the botryllid ascidians have been identified, only the response is truly assayed. Thus, in these experiments, recognition could be occurring, but without a subsequent response, which would be analogous to effector cell function in the adaptive immune system of the higher vertebrates. In that system, two signals are often required for a response; recognition by the effector cell, and a

costimulatory signal from another cell. If the costimulation signal is absent, there is no effector response (reviewed in Matzinger, 1994).

The ability of donor cells to survive and be detected in the recipient for 3 to 4 weeks after transplantation is the best evidence that Fu/HC-based allorecognition responses are spatially segregated in *B. schlosseri*. But the specific components of the Fu/HC allorecognition response that are spatially segregated are unknown; they could be cells involved in the recognition of allogeneic colonies, in the downstream effector mechanisms responsible for POR formation, or both.

This leads us to ask why the site and severity of fusion/rejection reactions have changed between the different botryllid ascidians (discussed above). One answer might be to lower the costs (*e.g.*, cell death, loss of ampullae) of allogeneic reactions. Another possibility is to limit the amount of cell-cell interaction during an allogeneic reaction, thereby limiting the ability of any cells to cross to an allogeneic colony and begin to parasitize it. Questions like this will be answered only when the Fu/HC and receptors have been characterized at a molecular level, which will allow the cells involved in allorecognition to be identified.

These results also bring up intriguing questions about the resorption phenomenon hypothesized to be a global allorecognition system analogous to minor histocompatibility in the vertebrates (Rinkevich, 1993). In previous studies, we have shown that some cells, notably those that are able to parasitize the germ line of the host colony, are not resorbed (Pancer *et al.*, 1995; Stoner and Weissman, 1996). But in these studies, the cells that survived the resorption event had at least one Fu/HC allele in common with the host colony and were therefore acceptable according to the rules of Fu/HC-based colony specificity. In this study, Fu/HC-mismatched cells continued to survive in a host colony, although we do not know what type of cells they were, or whether they would have been able to parasitize the germline of the host colony. Resorption may not include cells circulating in the vascular system, but the ability of cells to survive and proliferate in an allogeneic colony (Fu/HC-matched, or not) makes us wonder what the effector mechanisms responsible for resorption are responding to. Why would it be that the zooids are resorbed, but cells circulating in the bloodstream—especially those that could parasitize the host colony—are not? Since we did not assay for chimerism after a single transplantation event, it might be postulated that the repetitive transplantations in these experiments are either overwhelming, or inducing tolerance in, the resorption machinery. This seems unlikely since, in previous experiments, one partner of a natural (*i.e.*, Fu/HC-matched) chimera could resorb another, even when the losing (resorbed) partner was three times larger. Further-

more, resorption could occur months after a chimera had become established (Rinkevich and Weissman, 1987).

The ability of transplanted cells to survive and proliferate in an Fu/HC-incompatible colony, while revealing something of alloresponses in *B. schlosseri*, may also seem to be a complete artifact of a laboratory experiment. The existence of the Fu/HC-based allorecognition system and the maintenance of such incredibly high levels of polymorphism at the Fu/HC locus have been hypothesized to limit fusion, and the possibility of subsequent germ and somatic cell parasitism, to kin (Buss, 1982; Pancer *et al.*, 1995; Stoner and Weissman, 1996). Yet, although this system has been investigated for many years, the ability of the Fu/HC-based rejection response to block the transfer of cells capable of germ or somatic cell parasitism during an allogeneic interaction has never been directly tested. Interestingly, cells that appear to be able to transfer from one colony to another during a rejection reaction have recently been observed (Rinkevich *et al.*, 1998), and we have found possible cases of parasitism in unfused, adjacent colonies in the wild (Stoner and Weissman, 1996). While much work remains to be done to confirm these results, the ability of cells to survive and proliferate in an Fu/HC-incompatible colony may not be a completely unnatural phenomenon, particularly if a Fu/HC-based rejection reaction does not provide complete protection against somatic or germ cell parasitism. The ability of cells to survive in Fu/HC-mismatched allogeneic colonies has interesting implications for the study of allorecognition in *B. schlosseri*.

Acknowledgments

Portions of this study were carried out at the Minerva Center for Marine Invertebrate Immunology and Developmental Biology, and were supported by grants from the US-Israel Binational Science Foundation and the Human Frontiers program. Part of the research was supported by a grant from SyStemix/Novartis to ILW. AWD was supported by an NIH Postdoctoral Fellowship.

Literature Cited

- Bancroft, F. W. 1903. Variation and fusion of colonies in compound ascidians. *Proc. Calif. Acad. Sci.* **3**: 138–186.
- Berrill, N. J. 1941. Size and morphogenesis in the bud of *Botryllus*. *Biol. Bull.* **80**: 185–193.
- Boyd, H. C., S. K. Brown, J. A. Harp, and I. L. Weissman. 1986. Growth and sexual maturation of laboratory-cultured Monterey *Botryllus schlosseri*. *Biol. Bull.* **170**: 91–109.
- Buss, L. W. 1982. Somatic cell parasitism and the evolution of somatic tissue compatibility. *Proc. Natl. Acad. Sci. USA* **79**: 5337–5341.
- Hirose, E., Y. Saito, and H. Watanabe. 1994. Surgical fusion between incompatible colonies of the compound ascidian, *Botrylloides fuscus*. *Dev. Comp. Immunol.* **18**: 287–294.
- Hirose, E., Y. Saito, and H. Watanabe. 1997. Subcuticular rejection: an advanced mode of the allogeneic rejection in the compound ascidians *Botrylloides sinodensis* and *B. fuscus*. *Biol. Bull.* **192**: 53–61.
- Lauzon, R. J., K. J. Ishizuka, and I. L. Weissman. 1992. A cyclical, developmentally-regulated death phenomenon in a colonial urochordate. *Dev. Dynam.* **194**: 71–83.
- Lauzon, R. J., C. W. Patton, and I. L. Weissman. 1993. A morphological and immunohistochemical study of programmed cell death in *Botryllus schlosseri* (Tunicata, Ascidiacea). *Cell Tissue Res.* **272**: 115–127.
- Matzinger, P. 1994. Tolerance, danger, and the extended family. *Annu. Rev. Immunol.* **12**: 991–1045.
- Milkman, R. 1967. Genetic and developmental studies on *Botryllus schlosseri*. *Biol. Bull.* **132**: 229–243.
- Oka, H., and H. Watanabe. 1957. Colony specificity in compound ascidians as tested by fusion experiments. *Proc. Jpn. Acad. Sci.* **33**: 657–664.
- Oka, H., and H. Watanabe. 1960. Problems of colony specificity in compound ascidians. *Bull. Biol. Stn. Asamushi.* **10**: 153–155.
- Pancer, Z., H. Gershon, and B. Rinkevich. 1995. Coexistence and possible parasitism of somatic and germ cell lines in chimeras of the colonial urochordate *Botryllus schlosseri*. *Biol. Bull.* **189**: 106–112.
- Rinkevich, B. 1992. Aspects of incompatibility nature in botryllid ascidians. *Anim. Biol.* **1**: 17–28.
- Rinkevich, B. 1993. Immunological resorption in *Botryllus schlosseri* (Tunicata) chimeras is characterized by multilevel hierarchical organization of histocompatibility alleles. A speculative endeavor. *Biol. Bull.* **184**: 342–345.
- Rinkevich, B., and I. L. Weissman. 1987. A long-term study of fused sublones in the ascidian *Botryllus schlosseri*: the resorption phenomenon (Protochordata; Tunicata) *J. Zool. (Lond.)* **213**: 717–733.
- Rinkevich, B., Y. Saito, and I. L. Weissman. 1993. A colonial invertebrate species that displays a hierarchy of allorecognition responses. *Biol. Bull.* **184**: 79–86.
- Rinkevich, B., R. Porat, and M. Goren. 1995. Allorecognition elements on a protochordate histocompatibility locus indicate unprecedented extensive polymorphism. *Proc. R. Soc. Lond. B* **259**: 319–324.
- Rinkevich, B., S. Tartakover, and H. Gershon. 1998. Contribution of morula cells to allogeneic responses in the colonial urochordate, *Botryllus schlosseri*. *Mar. Biol.* **131**: 227–236.
- Sabbadin, A. 1962. Le basi genetiche della capacita di fusione fra colonie in *Botryllus schlosseri* (Ascidiacea). *Atti Accad. Naz. Lincei. Re.* **32**: 1031–1035.
- Sabbadin, A. 1982. Formal genetics of ascidians. *Am. Zool.* **22**: 765–773.
- Sabbadin, A., and G. Zaniolo. 1979. Sexual differentiation and germ cell transfer in the colonial ascidian *Botryllus schlosseri*. *J. Exp. Zool.* **207**: 289–304.
- Saito, Y., E. Hirose, and H. Watanabe. 1994. Allorecognition in compound ascidians. *Int. J. Dev. Biol.* **38**: 237–247.
- Scolfield, V. L., J. M. Schlumberger, L. A. West, and I. L. Weissman. 1982. Protochordate allorecognition is controlled by a MHC-like gene system. *Nature* **295**: 499–502.
- Stoner, D. S., and I. L. Weissman. 1996. Somatic and germ cell parasitism in a colonial ascidian: possible role for a highly polymorphic allorecognition system. *Proc. Natl. Acad. Sci. USA* **93**: 15254–15259.
- Vos, P., R. Hogers, M. Bleeker, M. Reijans, T. Van De Lee, M. Hornes, A. Frijters, J. Pot, J. Peleman, M. Kuiper, and M. Zabeau. 1995. AFLP: a new technique for DNA fingerprinting. *Nuc. Acids Res.* **23**: 4407–4414.
- Weissman, I. L., Y. Saito, and B. Rinkevich. 1990. Allorecognition histocompatibility in a protochordate species: Is the relationship to MHC semantic or structural? *Immunol. Rev.* **113**: 227–245.

Temperature-Independent Period Immediately After Fertilization in Sea Urchin Eggs

KATSUYUKI YAMADA^{1,*} AND KOSHIN MIHASHI²

¹*Department of Physics, Graduate School of Science, Nagoya University, Chikusa-ku, Nagoya 464-8602, Japan; and* ²*Graduate School of Polymathematics, Nagoya University, Chikusa-ku, Nagoya 464-8602, Japan*

Abstract. The experiments described here explore the regulation of the duration of cleavage cycles in sea urchin eggs. We measured the timing of early cleavages in individual fertilized eggs under various temperature conditions and applied methods of statistical analysis to the data obtained. At least for the first three cleavages, the temperature dependence of the cleavage intervals was nearly equal. In addition, we identified a temperature-independent period at the beginning of the first cleavage cycle. This period occurs immediately after fertilization and lasts for several minutes. Our results suggest that this interval of temperature independence is related to the process of egg activation.

Introduction

Various studies have been conducted on the mechanisms that regulate the cell cycle at the molecular level, *e.g.*, the cyclic accumulation and destruction of cyclins and the cyclic activity of M phase-promoting factor (MPF) (Meijer *et al.*, 1991; Edgcombe *et al.*, 1991). Such studies have used conventional methods that determine the timing of an event in the cell cycle by measuring some condition or activity in a whole group of cells at given time intervals—for example, by plotting the percentage of cells that had reached a certain stage or the amount of a particular biochemical activity over time.

However, such methods have limited value because the average behavior of a group of cells reveals little about individual cells. Questions such as how much fluctuation is experienced by individual cells in the duration of inter-

cleavage periods cannot be answered. Thus it is difficult to apply methods of statistical analysis, including the so-called method of moments, confidence interval determination, and regression analysis, especially to the cleavage intervals.

If cell cycle events differ greatly in their degree of temperature dependence, we should be able to use those differences to detect the events. Therefore, we attempted to measure the timing of several early cleavages in sea urchin eggs of various temperatures. These eggs are arrested in post-meiotic interphase and undergo a series of rapid and highly synchronous cleavages after fertilization.

We developed a system by which we can determine the length of several early cleavage cycles in sea urchin eggs by timing these cleavages in tens of individual eggs. Using this system, we found that the effect of temperature on the duration of the cleavage cycle is approximately equal for successive cycles. However, by applying methods of statistical analysis, we also discovered a temperature-independent period of several minutes immediately after fertilization, which has not been found previously (Hoadley and Brill, 1937; Matsumoto *et al.*, 1988).

Materials and Methods

Handling of eggs

Gametes of the sea urchins *Pseudocentrotus depressus* and *Hemicentrotus pulcherrimus* were obtained by injection of 1 mM acetylcholine chloride into the body cavity. Semen was collected "dry" and stored at 4°C until use. The eggs were washed several times with artificial seawater (ASW) and stored as a gently stirred suspension at 5°–10°C. In each experiment, gametes obtained from the same parents were used throughout.

Received 16 April 1997; accepted 25 February 1998.

* Current address: Department of Cellular and Molecular Physiology, National Institute for Physiological Sciences, Okazaki 444-8585, Japan.

Time-lapse video microscopy

The time course of early cleavage was recorded for groups of fertilized eggs (about 30 in each group). The eggs were photographed with a CCD camera (Hamamatsu, C2400) that was mounted on an inverted phase-contrast microscope and attached to a videocassette recorder (Sony, EVT-820).

While the fertilized eggs were being videotaped, it was necessary to regulate the temperature of the ASW that flowed through the observation vessel. For this purpose, a homemade thermo-control chamber was positioned on the stage of the microscope and the observation vessel—a glass laboratory dish, which was filled with 1.5 ml of ASW—was placed into it. The control chamber, which was made of acrylic resin, held water to a depth less than the height of the glass dish. A ring-shaped copper pipe that was immersed in the water of the chamber encircled the glass dish and circulated water from a thermostat bath. The temperature of the ASW in the dish was kept constant by passing it through a tube coiled around the pipe before it entered the dish. (The difference in temperature among locations in the field of the microscope was at most 0.1°C.) To prevent the eggs from being flushed out of the glass dish during observation, they were placed on a nylon mesh that was fixed to the bottom of the dish with wax. A sensor set next to the mesh confirmed that the temperature of the ASW was stable to within 0.1°C throughout each observation.

In all except the temperature-jump experiments described below, gametes were inseminated and after 1 min were added to the glass dish in the thermo-control chamber. After the observation period, the videotape was played back and forth so that the time interval between insemination and the beginning of first cleavage could be determined for each egg. Cleavage of the plural blastomeres of each egg was nearly synchronous in the second and third cycles, so these cleavages were judged from a single blastomere. In this manner the time intervals up to the third cleavage were determined for individual eggs. The length of the first cleavage cycle (u_1) was defined as the time interval between insemination and first cleavage. The length of the second cleavage cycle (u_2) was determined by subtracting the time of the first cleavage from the time of the second, and so on.

The temperature-jump experiments required two observation setups. A sample of fertilized eggs was suspended in a test tube in a 9.6°C constant-temperature water bath. At each predetermined time after insemination, a drop of the egg suspension was added to a glass observation dish that had been set at 17.3°C in one thermo-control system. This constituted the "jump" in temperature. (Measured temperature recovered from a fall in temperature to within 0.1°C at about 1 min after addition of the eggs.) As a

control, another sample of the fertilized eggs was dropped into an observation dish, which had also been set at 17.3°C, in the second thermo-control system, at 1 min after insemination. Cleavage cycles for the eggs in the temperature-jump experiments were determined as previously described.

Results

Temperature dependence of cleavage cycles

Figure 1 shows the reciprocal of the length of the cleavage cycles (*i.e.*, cleavage rates) in *P. depressus* eggs. This plot is analogous to an Arrhenius plot, with log rate ($\ln(1/\langle u_i \rangle)$) as a function of the reciprocal of absolute temperature; where $\langle u_i \rangle$ is the mean for the length of the *i*-th cleavage cycles, as defined in the Materials and Methods. Plotted in this manner, the three curves run parallel to one another (with the curve for u_1 shifted along the ordinate axis from the two other curves). This suggests that the temperature dependence of the three cleavage cycles is similar. The rationale follows.

Because temperature dependence is a change in relative rate (compared with the rate at one standard temperature)

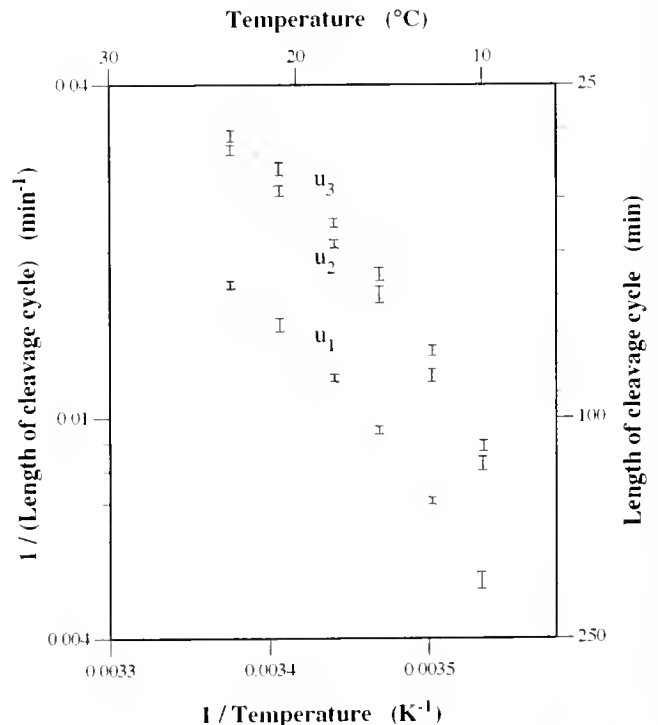


Figure 1. Temperature dependence of the length of cleavage cycles. Each set of the reciprocals of the averages for the first three cleavage cycles (u_1 , u_2 , and u_3) in *Pseudocentrotus depressus* eggs is plotted against the temperature at which each sample was kept. The number of eggs in each sample is about 30. Error bars show 99% confidence intervals of the averages.

with temperature, each cleavage rate is represented by the product of the temperature-dependent term and the cleavage rate at a standard temperature, which is a constant that differs between cleavages. The logarithm of this product is thus the sum of the logarithm of the term representing the temperature dependence and the logarithm of the constant. So, if all terms of the temperature dependence are equal to one another from one cleavage cycle to the next, all curves as a function of temperature will have the same shape with different ordinate intercepts.

To further examine the temperature dependence of cleavage cycles, the same data used in Figure 1 are replotted in Figure 2. As seen in the figure, u_3 has a linear relation to u_2 , with the straight line passing through the

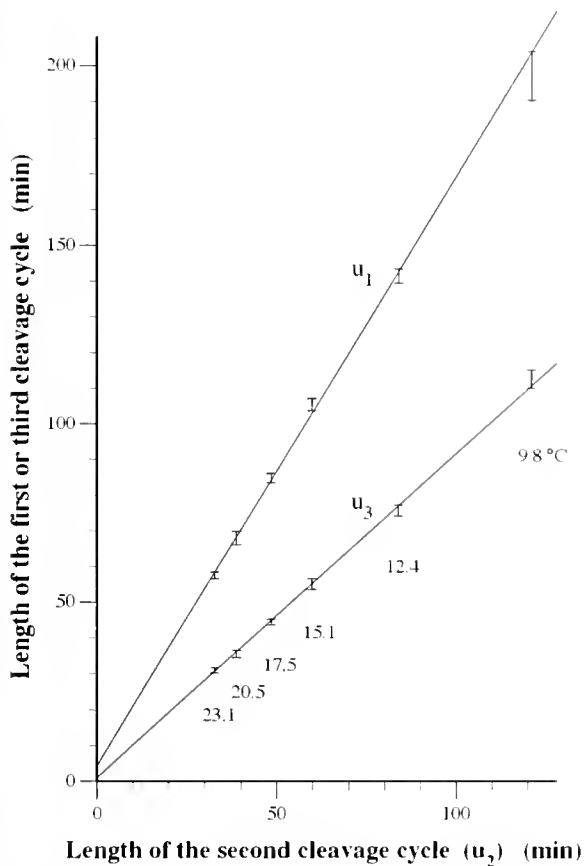


Figure 2. The data in Figure 1 plotted to show the relation between cleavage cycles at various temperatures. The abscissa is the mean length of the second cleavage cycle, and the ordinate is the mean length of the first or third cleavage cycles. Error bars show 99% confidence intervals of the averages. The error bars for u_2 were omitted for clarity in this figure (the magnitude of error bars for u_2 is similar to the magnitude of error bars for u_3). Each straight line was obtained by at least-squares method applied to the data points for u_1 or u_3 , using the squares of SEM for both variables as the variances (Awaya, 1983). The ordinate intercept of the line is 4.1 min for u_1 and 0.8 min for u_3 .

origin; its slope is 0.9. The ordinate intercept is not significantly different from zero ($P = 0.16$). This relation shows that the temperature dependence of u_2 is equal to that of u_3 , since the lengths of two cleavage cycles should be in direct proportion to one another only if the temperature dependence of the cycles is unchanged from one to the other.

Cycle u_1 also has a linear relation with u_2 . However, the ordinate intercept for this straight line is 4.1 min and significantly non-zero ($P < 0.001$). Its slope is not 1 but 1.6, corresponding to the vertical shift of the curve for u_1 from the two other curves. That is, in extrapolating to a hypothetical condition in which u_2 is zero (corresponding to a rate of cleavage that has been raised to infinity by imaginary heating), u_1 does not become zero but has a limited value. Therefore, u_1 appears to include a temperature-independent period of several minutes that does not exist in u_2 or in u_3 .

Temperature-jump experiment

To determine when the temperature-independent period occurs within the first cleavage cycle, we used temperature-jump experiments. Fertilized eggs of *H. pulcherrimus* were kept under constant low temperature (9.6°C) for various incubation times, then placed into ASW at a higher temperature (17.3°C); the total length of the first cleavage cycle was measured for each cell. Because a temperature-independent term should remain constant when temperature changes, whereas a temperature-dependent term will get longer when temperature falls and shorter when it rises, we can distinguish the temperature-independent term from the temperature-dependent term.

Figure 3 shows the results of nine pair of measurements—that is, control and experimental values for 9 incubation times. The average of the duration times measured for the first cleavage cycle for the temperature-jump sample was subtracted from the control value, and these differences were plotted to show cycle delay as a function of incubation time. No delay in u_1 is observed when the incubation time is shorter than several minutes. Thereafter the length of the first cleavage cycle increases linearly with the incubation time. An abscissa intercept given by the linear least-squares method, to which all data pairs were subjected, was significantly different from zero ($P < 0.001$). An abscissa intercept was 5.2 min when the linear least-squares method was applied to all data pairs except the one for the shortest incubation time. This shows that a temperature-independent period of several minutes exists immediately after fertilization. (Note that if a temperature-independent term appeared later in the first cleavage cycle, a corresponding horizontal segment of the plotted data would appear further to the right than at the beginning of the ascending line.)

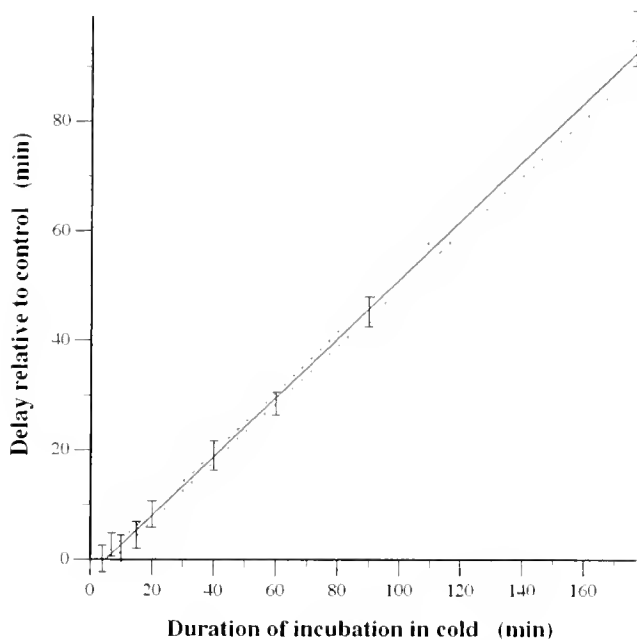


Figure 3. Temperature-jump experiment showing the delay in u_1 relative to control in *Hemicentrotus pulcherrimus* eggs as a function of the duration of incubation at low temperature. Each error bar shows the 99% confidence interval of the difference between the average for u_1 in the temperature-jump sample and the average for u_1 in its control, at each of various incubation times (given in the abscissa). The data point for the longest incubation time is from the measurement in which eggs were incubated at 9.6°C throughout; its abscissa value is the mean length of the first cleavage cycle of the eggs. The straight solid line was obtained by applying least-squares fitting to all the data points except the one for the shortest incubation time, using the sum of the squares of the SE of two coupled averages as the variance. The broken lines give the endpoints of the 99% confidence interval for the true mean of the ordinate value for a given abscissa value (Green and Margerison, 1977). The 99% confidence interval for the abscissa intercept of the regression line, which is predicted from the above endpoints (Draper and Smith, 1981), is between 3.0 and 7.2 min.

Discussion

Temperature dependence of the processes affecting the length of cleavage cycles

Various processes, acting in sequence or in parallel, make up the cell cycle, but only some of these affect the length of the cycle (Nurse, 1990). The observation of the temperature-independent period immediately after fertilization means that there are one or more temperature-independent processes affecting the length of the first cleavage cycle.

The cleavage cycles differ in absolute length, and thus they must also differ in the ratio between the duration of the processes governing the length of the cleavage cycles and the total duration of the cycles. Nevertheless, as shown in the Arrhenius plot (Fig. 1), and the plot of u_1 versus u_2 or u_3 versus u_2 (Fig. 2), the cleavage cycles are

very nearly equal in temperature dependence. Apparently, then, the specific processes that affect the length of cleavage cycles at a given temperature differ little from each other in temperature dependence, with the exception of the temperature-independent process or processes immediately after fertilization. This conclusion is supported by the high linearity of the plot for the temperature-jump experiment (Fig. 3; a value of $\chi^2 = 11$ for 6 degrees of freedom, corresponding to $P = 0.09$ in a χ^2 test for goodness of fit (Bevington and Robinson, 1992)).

Although we have classified the processes that affect the length of cleavage cycles as either independent of or dependent on temperature, the period immediately after fertilization is not absolutely temperature-independent, but only relatively by comparison with the later periods of the cycle. In reality, the first period may have a weak dependence on temperature that might cause the deviation from the linear relation in the plot of u_1 versus u_2 (Fig. 2).

Temperature-independent event associated with egg activation

Both the relationship between cleavage cycles (Fig. 2), whose durations are a function of temperature, and the results of the temperature-jump experiment (Fig. 3) showed that the first cleavage cycle contains a unique temperature-independent term that lasts for several minutes. In addition, the temperature-jump experiment demonstrated that this term takes place immediately after fertilization.

The first cleavage cycle is relatively long in comparison to the ones that follow. This is partly because egg activation, which triggers the resumption of the cell cycle of the egg immediately after fertilization, includes a large number of processes (reviewed by Whitaker and Steinhardt, 1985; Whitaker and Patel, 1990). Considering that the temperature-independent period is specific to the initiation of the cleavage cycles and is transient, this term probably originates in an event related to the activation of the egg rather than to the cell cycle *per se*. Since the temperature-independent term affects the length of the first cleavage cycle, this event is presumably important in egg activation. Furthermore, because it is not preceded by a temperature-dependent period, the temperature-independent event is probably the overriding change during egg activation, and the temperature-dependent events that follow presumably cannot take place until it occurs.

When a sea urchin egg is fertilized, the cytoplasmic concentration of calcium and hydrogen ions changes markedly. These ionic signals are the necessary and sufficient stimuli for the activation of protein synthesis, DNA synthesis, and other metabolic processes that constitute egg activation (Whitaker and Steinhardt, 1985). In particular, cytoplasmic alkalization, which is mediated by the

activation of a $\text{Na}^+\text{-H}^+$ exchange (Johnson *et al.*, 1976) similar to the mechanism that functions in cultured cells (Payan *et al.*, 1983), is the major immediate cause of the increase in the synthesis rate of these macromolecules. The length of the temperature-independent period we have observed coincides with the increase in intracellular pH, which begins 1 minute after fertilization and lasts for several minutes (Whitaker and Steinhardt, 1985). In addition, the rate of $\text{Na}^+\text{-H}^+$ exchange is relatively insensitive to temperature in cells of the opossum kidney (Graber *et al.*, 1992). This period of cytoplasmic alkalization may correspond to the temperature-independent period.

Acknowledgments

We thank the staff of the Sugashima Marine Biological Station, especially Dr. Toyoki Kato, and the Program in Architectural Dynamics in Living Cells at the Marine Biological Laboratory, Woods Hole, for their support. Our thanks are also due to Dr. Fumio Oosawa of the Aichi Institute of Technology and 1996 MBL Lillie Fellow for his encouragement and making KY's visit to the MBL possible; to Dr. Kensal van Holde of Oregon State University and Dr. J. Woodland Hastings of Harvard University for valuable remarks on an early version of the manuscript; and to Dr. Shinya Inoué of the MBL for critically reviewing the manuscript and for encouragement to finish it.

Literature Cited

- Awaya, T. 1983. Two-dimensional curve fitting in counting experiments. *Nucl. Instrum. Methods Phys. Res.* **212**: 311–317.
- Bevington, P. R., and D. K. Robinson. 1992. *Data Reduction and Error Analysis for the Physical Sciences*, 2nd ed. McGraw-Hill, New York.
- Draper, N. R., and H. Smith. 1981. *Applied Regression Analysis*, 2nd ed. John Wiley, New York.
- Edgecombe, M., R. Patel, and M. Whitaker. 1991. A cyclin-abundance cyclin-independent $\text{p34}^{\text{cdc}2}$ tyrosine phosphorylation cycle in early sea urchin embryos. *EMBO J.* **10**: 3769–3775.
- Graber, M., C. Barry, J. Dipaola, and A. Hasagawa. 1992. Intracellular pH in OK cells. II. Effects of temperature on cell pH. *Am. J. Physiol.* **262** (*Renal, Fluid and Electrolyte Physiology* **31**): F723–F730.
- Green, J. R., and D. Margerison. 1977. *Statistical Treatment of Experimental Data*. Elsevier Scientific, Amsterdam, The Netherlands.
- Hoadley, L., and E. R. Brill. 1937. Temperature and the cleavage rate of *Arbacia* and *Chactopterus*. *Growth* **1**: 234–244.
- Johnson, J. D., D. Epel, and M. Paul. 1976. Intracellular pH and activation of sea urchin eggs after fertilization. *Nature* **262**: 661–664.
- Matsumoto, Y., T. Kominami, and M. Ishikawa. 1988. Timers in early development of sea urchin embryos. *Develop. Growth Differ.* **30**: 543–552.
- Meijer, L., L. Azzi, and J. Y. J. Wang. 1991. Cyclin B targets $\text{p34}^{\text{cdc}2}$ for tyrosine phosphorylation. *EMBO J.* **10**: 1545–1554.
- Nurse, P. 1990. Universal control mechanism regulating onset of M-phase. *Nature* **344**: 503–508.
- Payan, P., J.-P. Girard, and B. Ciapa. 1983. Mechanisms regulating intracellular pH in sea urchin eggs. *Dev. Biol.* **100**: 29–38.
- Whitaker, M., and R. Patel. 1990. Calcium and cell cycle control. *Development* **108**: 525–542.
- Whitaker, M. J., and R. A. Steinhardt. 1985. Ionic signaling in the sea urchin egg at fertilization. Pp. 167–221 in *Biology of Fertilization*, vol. 3. C. B. Metz and A. Monroy, eds. Academic Press, San Diego.

Effect of Methyl Farnesoate on Late Larval Development and Metamorphosis in the Prawn *Macrobrachium rosenbergii* (Decapoda, Palaemonidae): A Juvenoid-like Effect?

URI ABDU¹, PETER TAKAC², HANS LAUFER³, AND AMIR SAGI^{1*}

¹Department of Life Sciences, Ben-Gurion University of the Negev, P. O. Box 653, Beer-Sheva 84105, Israel; ²Institute of Zoology, Slovak Academy of Sciences, Bratislava 84206, Slovak Republic; and ³Department of Molecular and Cell Biology, University of Connecticut, Storrs, Connecticut 06269-3125

Abstract. Methyl farnesoate (MF), the unepoxidated form of insect juvenile hormone III, was detected in larvae of the freshwater prawn *Macrobrachium rosenbergii*, which metamorphose to post-larvae following 11 larval stages. The possible role of MF as a morphogen was studied by administering the compound to *M. rosenbergii* larvae via an *Artemia* vector. Higher MF levels caused earlier retardation of late larval growth, and the highest dose retarded larval development. Furthermore, MF significantly affected the patterns of metamorphosis and the appearance of intermediate individuals exhibiting both larval and post-larval morphology and behavior. Three intermediate types were defined, two of which were found only at the MF-treated groups and one that was exclusive to the higher dose treatments. The relative abundance of intermediate specimens increased from 2% in the control to 32% in the high MF concentration, which suggests that MF has a juvenoid-like effect in this decapod crustacean.

Introduction

Juvenile hormones (JHs)—a family of epoxidated sesquiterpenoids—act as growth regulators in insects (Wigglesworth, 1970). Methyl farnesoate (MF), the unepoxidated form of JH III, has been detected in some insect species (Slama, 1971; Lanzrein *et al.*, 1984; Bruning *et*

al., 1985), but its physiological significance is not clear. The first report of the presence of MF in Crustacea was that of Laufer *et al.* (1987), who demonstrated that MF is secreted by the mandibular organ of the spider crab *Libinia emarginata* and is found in its hemolymph. Since then, MF has been found in a variety of crustaceans (Borst *et al.*, 1987; Laufer and Borst, 1988; Landau *et al.*, 1989), including the freshwater prawn *Macrobrachium rosenbergii* (Sagi *et al.*, 1991).

JHs are involved in the regulation of a substantial number of insect functions, including development, reproduction, and behavior. JHs are probably best known for their effect on the growth and differentiation of insect epidermal cells. When JHs are present during larval instars, the cuticle that is secreted has larval characteristics; in the absence of JHs, the cuticle exhibits pupal characteristics (see Laufer and Borst, 1983, for a review). Exogenous application of JHs may cause the appearance of various intermediate forms, and in some cases, of supernumerary larvae, as a result of differences in the growth rates of various parts of the body (allometric growth) (reviewed in Sehna, 1983). It has been suggested that exogenous JH applied during a critical period may function at the cellular level, resulting in mosaic animals with characteristics of two different stages (see Riddiford, 1994, for a review). Thus, it is likely that the effect of a particular juvenoid on insect development is determined by the developmental timing and the effective concentration of the juvenoid (Slama, 1995).

The regulation of larval development and metamorpho-

Received 6 November 1997; accepted 10 July 1998.

* Author to whom correspondence should be addressed. E-mail: sagia@bgumail.bgu.ac.il

Abbreviations: MF, methyl farnesoate; JH, juvenile hormone.

sis in crustaceans is not fully understood. In cyprids of barnacles, JH I and JH analogs caused premature metamorphosis without attachment of the cyprid to the substrate (Gomez *et al.*, 1973; Ramenofsky *et al.*, 1974; Tighe-Ford, 1977). In decapods, JH analogs retarded the development of larvae of the mud crab *Rhithropanopeus harrisi* (Christiansen *et al.*, 1977a, b) and the growth of early larval stages and post-larvae of the estuarine shrimp *Palaemonetes pugio*. In contrast, growth was enhanced in the premetamorphic stages of *P. pugio* (McKenney and Celestial, 1993). Treatment of *Homarus americanus* larvae with JH III increased the duration of larval development and influenced the size of the carapace and appendages (Hertz and Chang, 1986). Injections of JH I into *H. americanus* larvae gave rise to a number of intermediate stages (Charmantier *et al.*, 1988).

MF is the only JH-like compound found thus far in crustaceans. A few studies have targeted its regulatory role in development and metamorphosis in decapods. Application of MF to *H. americanus* larvae prolonged metamorphosis by a small but significant amount of time (Borst *et al.*, 1987). In *M. rosenbergii*, MF retarded growth and development in larval stages 5 to 9 (Abdu *et al.*, 1998).

In some crustaceans the processes of larval development and metamorphosis are similar to those in hemimetabolous insects (Snyder and Chang, 1986). Such is the case for *M. rosenbergii*, which exhibits a "common type" of larval development (Sollaud, 1923), encompassing 11 stages, followed by metamorphosis into post-larvae (Uno and Soo, 1969). Larval development in *M. rosenbergii* is characterized by significant growth of the carapace from stage 1 through stage 11. During metamorphosis (from stage 11 to post-larva), growth is allometric, with increases in size being limited to certain parts of the body (excluding the carapace) (Abdu, 1996).

In this study, *M. rosenbergii* was used as a model species for studying the role of MF in the late larval development and metamorphosis of crustaceans. MF was indeed detected in the larvae, and its effect on the manifestation of morphological features during metamorphosis was studied.

Materials and Methods

Detection of methyl farnesoate in Macrobrachium rosenbergii larvae

M. rosenbergii larvae were hatched and reared according to Daniels *et al.* (1992). Larval stages were determined according to Uno and Soo (1969). To detect the presence of MF, about 1 g of larvae at each of the stages 4, 6, 9, 10, and 11, and post-larvae were collected and homogenized in 2 ml of 4% NaCl and 5 ml of acetonitrile. The homogenates were filtered through α -cellulose,

washed with 4% NaCl and acetonitrile, and extracted with hexane. The hexane fraction was evaporated by means of a rotary evaporator. The dry matter was dissolved in hexane and passed through a Sep-Pak silica cartridge (Waters, Milford, MA), and the cartridge was rinsed with methylene chloride (Abdu *et al.*, 1998). The methylene chloride was evaporated, and the residue was dissolved in 100 μ l of hexane, loaded into a Beckman HPLC and analyzed according to Sagi *et al.* (1991). The nonbiological isomer, *cis-trans* MF, was used as the internal standard, and the retention times were compared to an external standard containing both the biological (*all-trans* MF) and nonbiological isomers. The putative *trans-trans* MF peaks of larvae at stages 4, 6, 9, 10, and 11 were collected from the HPLC and loaded onto a Hewlett Packard gas chromatograph with a 30-m cross-linked and surface-bound dimethylpolysiloxane column (0.5 min to 70°C, 70°–280°C, 20°C/min) connected to a mass spectrometer.

Effect of methyl farnesoate on late larval growth and development

Three experimental groups, each containing 15 *M. rosenbergii* stage-9 larvae, were fed with *Artemia* enriched with 0.21, 0.35, or 0.59 μ g MF/ml according to Abdu *et al.* (1998). A control group was fed with *Artemia* enriched with the vehicle alone (ethyl alcohol and SUPER-SELCO). Each treatment was performed in three replicates. The experimental system consisted of 12 dark plastic containers (300 ml) that were constantly aerated. The water was replaced daily, and the temperature was maintained at $27^\circ \pm 1^\circ$ C. The larvae were fed *ad libitum* with *Artemia* nauplii that were enriched daily with MF. Five larvae per replicate were randomly sampled twice a week; larval stage was determined and the length of the carapace was measured with an ocular micrometer; the larvae were then returned to the growth chamber. In the calculation of the average larval stage for each sampling, all post-11 stages (including both post-larvae and intermediate individuals) were designated as 12. The average larval stage and the average carapace length were compared between treatments, and the statistical significance was tested using one-way ANOVA followed by the least significant difference (LSD) test $P \leq 0.05$. The experiment was repeated three times with similar results; each experiment contained 180 larvae.

Assessment of metamorphosis in Macrobrachium rosenbergii

Among the many changes occurring during metamorphosis (Ling, 1969; Uno and Soo, 1969), the following six predominant changes were selected to distinguish between larvae and post-larvae of *M. rosenbergii* in this study: (1) In larvae, the abdomen is bent such that the

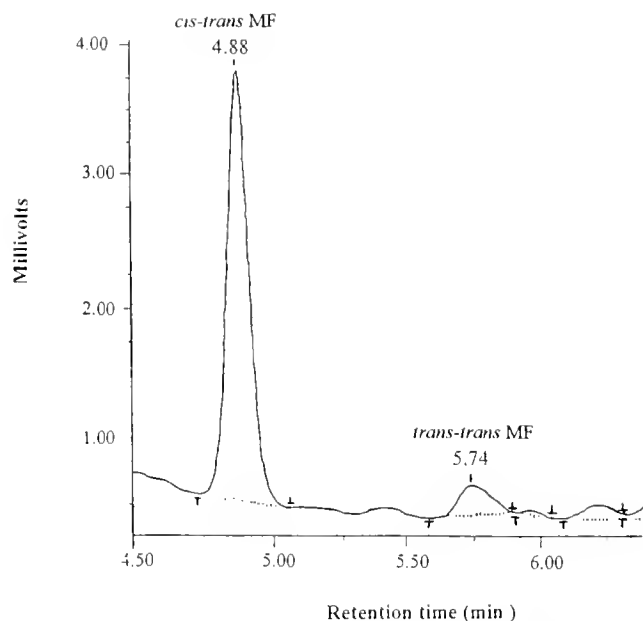


Figure 1. HPLC detection of methyl farnesoate in *Macrobrachium rosenbergii* larvae at stage 4. *Cis-trans* methyl farnesoate was used as the internal standard.

pleopods and the walking legs are not in the same plane, whereas in post-larvae, the abdomen is straight, with the pleopods and the walking legs in the same plane. (2) Larvae swim mainly by beating the long exopodites of

the pereopods. During the metamorphic process these long exopodites degenerate and become reduced to knobs at the postmetamorphic molt (Ling, 1969). (3) In stage 11 larvae, the endopodite of the second pereopod has three segments, the second and third segments being at an angle to the first, which is not fully developed. In contrast, in post-larvae there are four segments, all of which are straight, and the first segment is fully developed, as in the adult. (4) The carapace median tooth is evident from larval stage 4 onward, but disappears during metamorphosis and is absent in the post-larva. (5) In stage 11 larvae, the entire dorsal margin of the rostrum is equipped with numerous small teeth, but no ventral teeth are present, whereas the rostrum of the post-larva has 11 large dorsal teeth and 5 ventral teeth. (6) Larvae are planktonic, swimming tail up, and in most cases tail first, ventral side up; during metamorphosis, they settle to the bottom. Post-larvae are benthic, swimming and behaving as do the juveniles.

The relative abundance of the different intermediate types were compared between treatments, and the statistical significance was tested using the Mann-Whitney *U* test.

Results

Presence of methyl farnesoate in Macrobrachium rosenbergii larvae

MF was found in hexane extracts of *M. rosenbergii* larvae at stages 4, 6, 9, 10, and 11, and in post-larvae. A

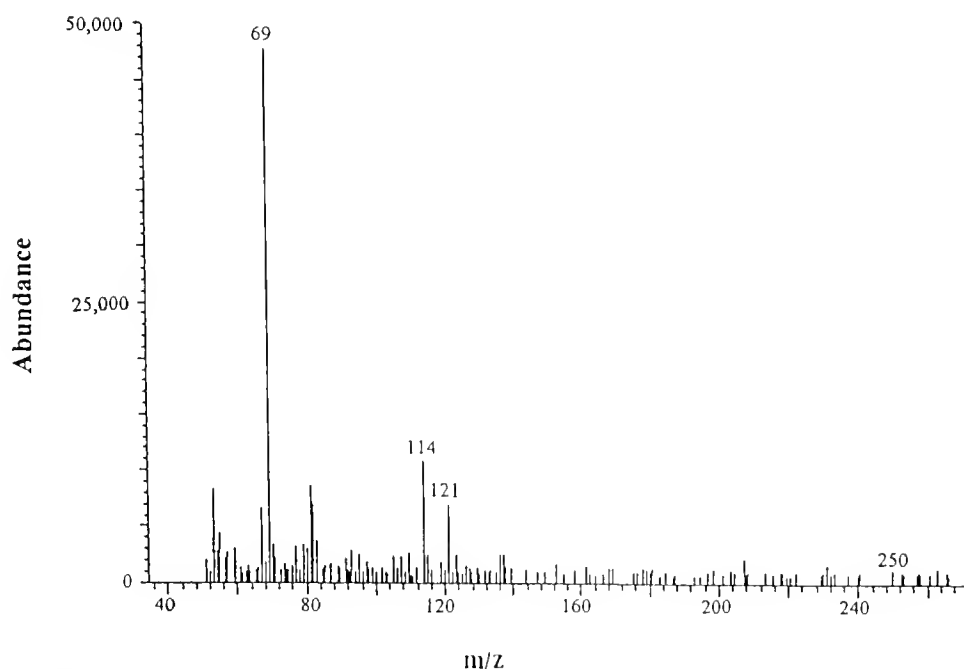


Figure 2. Mass spectrum of methyl farnesoate extracted from *Macrobrachium rosenbergii* larvae. Methyl farnesoate peaks were collected from HPLC separation of larvae extract and analyzed by GC-MS.

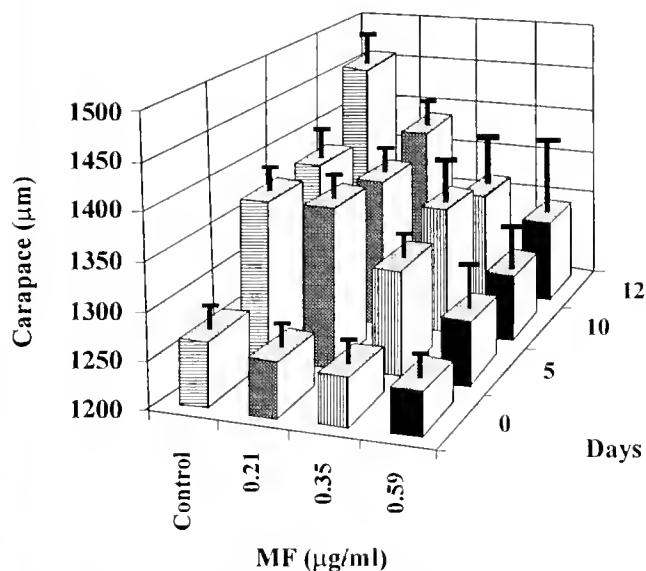


Figure 3. Average carapace length of *Macrobrachium rosenbergii* larvae during 12 days of feeding on *Artemia* enriched with different concentrations of methyl farnesoate. Each bar represents mean \pm SE ($n = 15$). The results presented are taken from one representative experiment out of the three identical experiments performed. Using the *Artemia* vector, approximately 0.0325% of the MF added to the *Artemia* enrichment medium (referred to as MF ($\mu\text{g/ml}$)) was found in *M. rosenbergii* larva feeding for 8 h on the enriched *Artemia* (Abdu *et al.*, 1998). This suggests that the level of MF in the present study did not exceed 0.191 ng MF per larva exposed to the highest dose and 0.068 ng MF per larva exposed to the lowest dose. Since the average weight of a larva is about 0.002 g, these levels could be expressed as 34–95.5 ng MF/g. The calculated level for the low MF exposure is in the range of physiological level found in *M. rosenbergii* larvae (up to 25 ng/g, data not shown) and adults (up to 40 ng/ml, Sagi *et al.*, 1991). Growth retardation in larvae fed on *Artemia* enriched with the median dose of MF was significant ($P < 0.001$) only on day 12. Growth of larvae fed on *Artemia* that were enriched with the highest concentration of MF was markedly slower than that of the control group, the difference being significant ($P < 0.001$) from day 5 onward.

representative HPLC chromatogram of one such hexane extract of larvae shows the presence of the biological *all-trans* MF, identified by comparing its retention time with that of the external standard (data not shown) and that of the internal standard (Fig. 1). Gas chromatography-mass spectrometry of the putative peaks from larval stages 4, 6, 9, 10, and 11 showed a typical methyl farnesoate profile exhibiting selected ion monitoring at m/z 69, 114, and 121 (Fig. 2).

Effect of methyl farnesoate on late larval growth and development

Survival was similar in the control and all the treatment groups (35% in control, and 47%, 41%, and 46% in the treated groups from the low to the high MF concentration, respectively). An earlier retardation of cara-

pace length was observed in the late larval stages of *M. rosenbergii* exposed to higher doses of MF (Fig. 3). The control group and the larvae fed on *Artemia* that were enriched with the lowest concentration of MF exhibited the fastest growth. Growth retardation in larvae fed on *Artemia* enriched with the median dose of MF was significant ($P < 0.001$) only on day 12. Growth of larvae fed on *Artemia* that were enriched with the highest concentration of MF was markedly slower than that of the control group, the difference being significant ($P < 0.001$) from day 5 onward; after that time, the "high-dose" group almost ceased growing. MF also retarded larval development, as manifested by larval stage (Fig. 4). The control group and the larvae fed on *Artemia* enriched with the lowest concentration of MF developed rapidly, reaching an average larval stage above 10 after 5 days and an average larval stage of above 11 at the

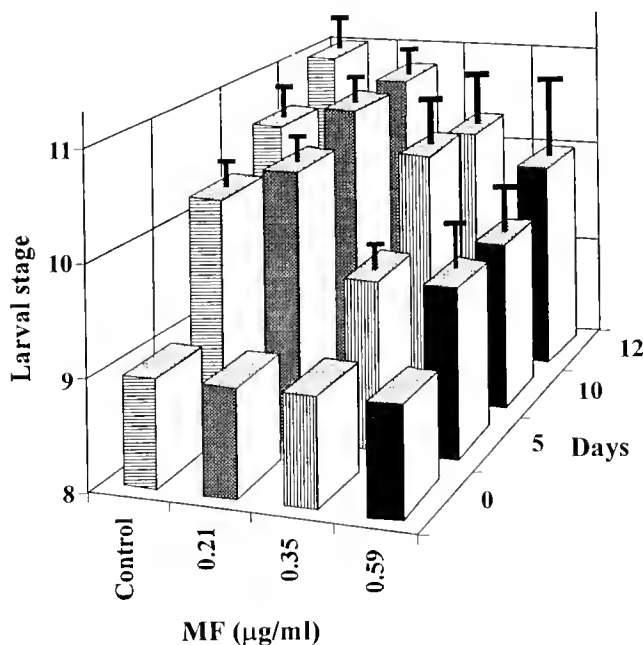


Figure 4. Average larval stage of *Macrobrachium rosenbergii* during 12 days of feeding on *Artemia* enriched with different concentrations of methyl farnesoate. Each bar represents mean \pm SE ($n = 15$). The results presented are taken from one representative experiment out of the three identical experiments performed. MF ($\mu\text{g/ml}$) refers to the amount of MF added to the medium in which the *Artemia* were incubated prior to being provided as food to *M. rosenbergii* larvae. In the larvae fed on *Artemia* enriched with the median dose of MF, further development was significantly retarded up to the 5th day ($P < 0.001$, vs. control group), but not from day 5 to day 10. After day 10, developmental progress was again markedly slower, and on day 12 the average stage of this treatment group was significantly behind that of the control group ($P < 0.001$). Larvae fed on *Artemia* enriched with the highest dose of MF showed significantly slower development to advanced stages than the control group, starting on day 5 ($P < 0.001$); this effect lasted till the end of the experiment.

end of the experiment (after 12 days). In the larvae fed on *Artemia* enriched with the median dose of MF, further development was significantly retarded up to the 5th day ($P < 0.001$, vs. control group), but not from day 5 to day 10. After day 10, developmental progress was again markedly slower, and on day 12 the average stage of this treatment group was significantly behind that of the control group ($P < 0.001$). Larvae fed on *Artemia* enriched with the highest dose of MF showed significantly slower development to advanced stages than the control group, starting on day 5 ($P < 0.001$); this effect lasted till the end of the experiment, and only a small progression of larval stages was recorded from that day onward.

Effect of methyl farnesoate on metamorphosis

Metamorphosis—which takes place after the 11th larval stage—was delayed in a dose-dependent manner in larvae treated with MF, but survival was similar to that in the control. In summary, the three experiments showed that among the surviving control individuals, 28 (58%) reached the postlarval stage at the end of the experiment. In the low MF concentration 20 (31%) normal post-larvae were found, and as higher MF concentrations were used, significantly fewer post-larvae were found—only 8 (14%) and 5 (8%), respectively. In addition to the delay in metamorphosis, different forms possessing both larval

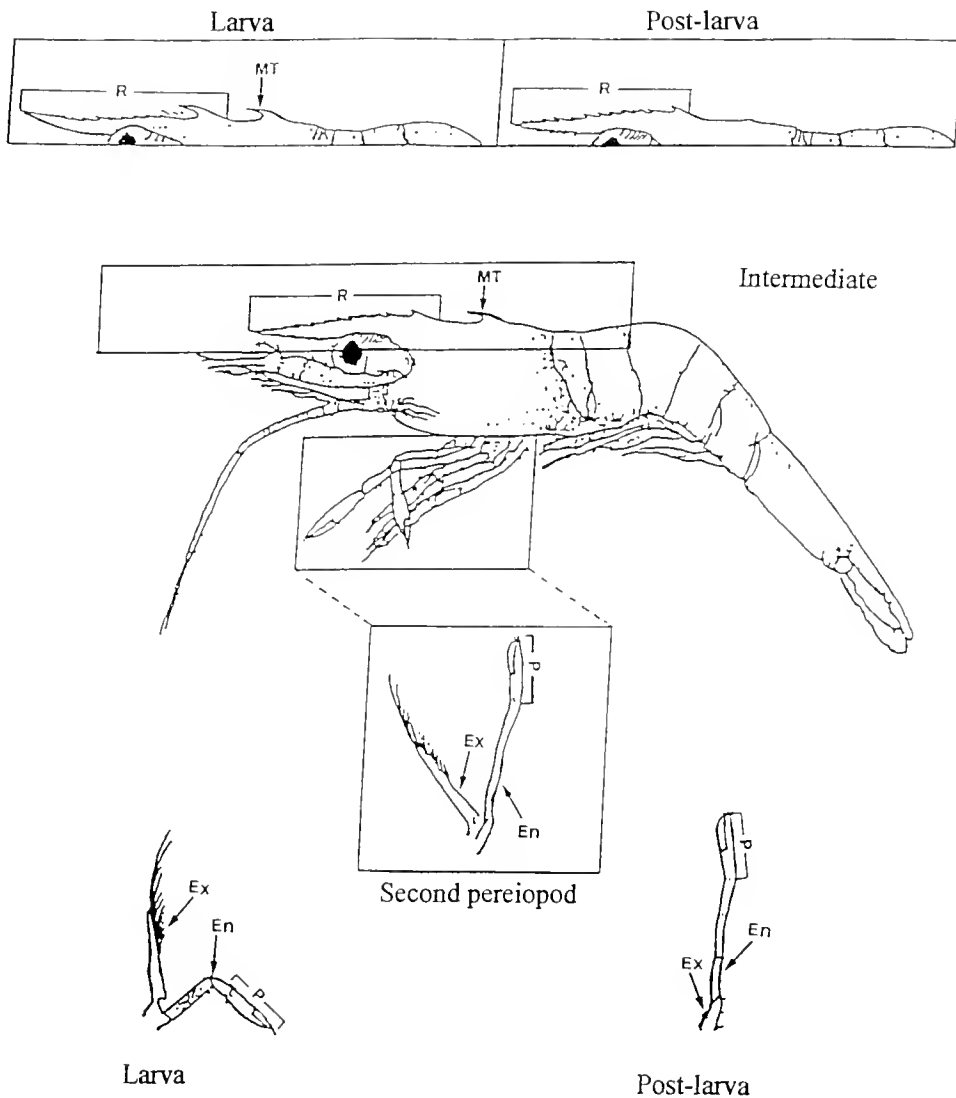


Figure 5. Schematic drawing of larval and postlarval features in a representative intermediate *Macrobrachium rosenbergii*. R - rostrum, MT - median teeth, P - propodus, Ex - exopod of the second pereiopod, En - endopod of the second pereiopod.

	Larvae Stage II	Intermediate			Post-larvae
		Larval-like	Intermediate	Postlarval-like	
Shape of body	Bent			Straight	
Exopods of pereiopods	Long			Short	
Second pereiopod	Larval	Post larval			
Carapace median tooth	Present				Absent
Rostrum	Larval	Postlarval			
Behavior	Planktonic			Benthic	

Figure 6. Typical morphological and behavioral profiles of the three intermediate types of *Macrobrachium rosenbergii* possessing both larval and postlarval features. The clear and shaded backgrounds represent larval and postlarval features, respectively.

and post-larval features of the six defining characteristics (see Materials and Methods) were observed. Figure 5 illustrates these features in a representative intermediate specimen. At the end of the experiment, three such types were defined; their morphological and behavioral features are summarized in Figure 6. The first type, whose features were mainly larval, was termed "larval-like intermediate" (Fig. 6). It retained five larval features but possessed a postlarval-like second pereiopod (Fig. 5). The second type, which exhibited a more equally divided set of features, was termed "intermediate" (Figs. 5 and 6). It retained three larval features, while possessing a postlarval-like rostrum and second pereiopod (Figs. 5 and 6), and exhibited mixed—partly benthic and partly planktonic—behavior. The third type—termed "postlarval-like intermediate"—retained the larval carapace median tooth but had four of the morphological postlarval features as well as postlarval benthic behavior (Fig. 6).

The relative abundances of the above-described types in the treated and control groups, as well as in a sample from a normal hatchery population, are compared in Figure 7. The postlarval-like intermediate was present in all groups (1%–7%), with no significant difference in relative abundance among the groups. The larval-like intermediate was not found in the source population or in the control group, but it was present in all the MF-treated groups in similar relative abundance (11%–17%). The intermediate type was found only in the two highest MF treatments. In general, the different intermediate types were more significantly abundant ($P < 0.001$) in the two higher MF-treated groups than in the lowest MF treatment group, the normal population, and the untreated control group. The abundance of all three intermediate types in-

creased with the increase in MF concentration (from 2% in the control to 32% in the high MF concentration).

Discussion

A great deal of evidence already supports the idea that MF is a crustacean hormone (Homola and Chang, 1997b), *i.e.*, the existence of a specific endocrine gland (Laufer *et al.*, 1987); specific MF-binding proteins in the circulation (Laufer and Albrecht, 1990; King *et al.*, 1993; Prestwich *et al.*, 1996; Tamone *et al.*, 1997); prompt degradation of MF by specific esterases (King *et al.*, 1993; Homola and Chang, 1997a; Takac *et al.*, 1997); and neuroendocrine regulation of MF secretion (Liu and Laufer, 1996; Wainwright *et al.*, 1996). However, the regulatory importance of MF as a juvenile hormone in the larval development of crustaceans has not been clearly demonstrated, except by circumstantial evidence for its juvenilizing effect on morphogenesis in *Libinia emarginata* (Laufer *et al.*, 1997). The only instances in which such a regulatory role for MF has been suggested are the retardation of metamorphosis reported by Borst *et al.* (1987) in *Homarus americanus* larvae exposed to MF; the retardation of early larval development in *Macrobrachium rosen-*

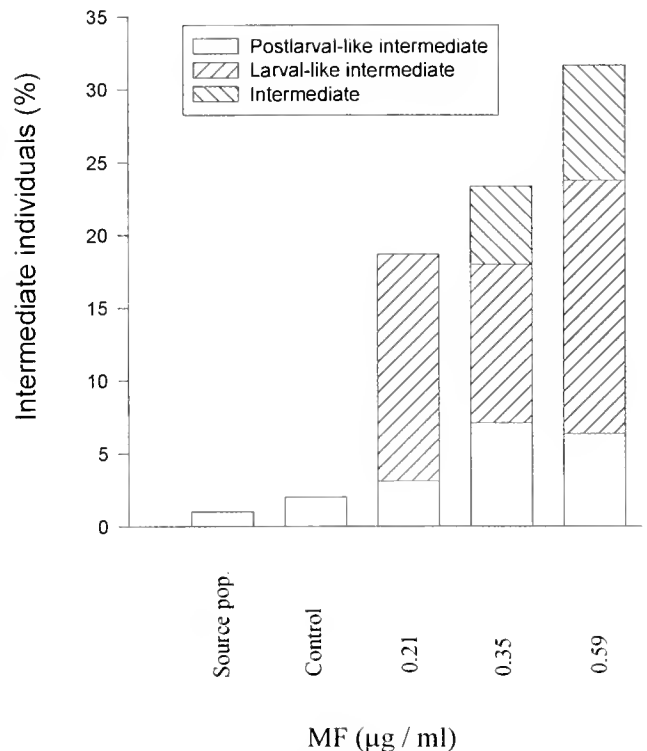


Figure 7. Relative abundance of *Macrobrachium rosenbergii* intermediate types in experimental groups exposed to different doses of methyl farnesoate, in an untreated control group and a sample from a normal hatchery population.

bergii (Abdu, 1996; Abdu *et al.*, 1998); and finally, the findings of the present study in which the retardation of metamorphosis and the appearance of intermediate *M. rosenbergii* types were observed after larvae were exposed to exogenous MF.

In insects, inhibition of metamorphosis is primarily due to the morphogenetic action of a juvenoid. This morphogenetic effect is routinely scored by recording the preservation of juvenile characters after the metamorphic ecdysis. Typically, early treatment of the last-instar larvae induces molting into supernumerary larval instars. Later treatment results in a reduced effect—appearance of intermediates between the juvenile and metamorphosed stages—since the various body tissues gradually become insensitive to juvenoids (for review see Sehnal, 1983). As with insects, the most striking result of this study was the appearance, in the MF-treated groups, of intermediate *M. rosenbergii* individuals. It is not clear how our findings relate to those in insects—whether the different intermediate individuals in the present study correspond to the supernumerary larvae or the intermediate forms known in insects.

The retardation in larval growth found in this study may be due to a molt inhibition, as in some insect species in which continuous exposure to juvenoids can cause a permanent molting block (see Sehnal, 1983, for a review). On the other hand, juvenoids can accelerate the molting process in insects (Sehnal, 1983), and in crustaceans MF may stimulate the production of 20-hydroxyecdysone (Chang *et al.*, 1993); this suggests that in *M. rosenbergii* the retardation may be due to continuous molting to further larval stages, as is the case for the supernumerary larvae in certain insect species (Sehnal, 1983). Further study of the relationship between MF and molting is necessary to determine whether the retardation of growth results from molt inhibition or molt acceleration.

Although the levels of MF administered to the *M. rosenbergii* larvae were within the physiological range (Takac, pers. comm. and Abdu *et al.*, 1998), the possibility of nonspecific toxicity could not be entirely ruled out. In crustaceans, intermediate larval forms may be produced by eyestalk removal during a "critical period," as has been shown for *Rhithropanopeus harrisi* (Costlow, 1966a), *Sesarma reticulatum* (Costlow, 1966b), *H. americanus* (Charmantier and Aiken, 1987), *Palaemonetes varians* (Le Roux, 1984), and *Alpheus heterochaelis* (Knowlton, 1994). Snyder and Chang (1986) suggested that intermediate larval forms in *H. americanus* were probably a manifestation of inadequate nutrition or other stresses. However, Knowlton (1994) showed that the appearance of intermediate forms in *A. heterochaelis* larvae, which have a lecithotropic mode of nutrition, was due to direct or indirect hormonal control from the eyestalk. The reports of the isolation and characterization of mandibular

organ-inhibiting hormone (MOIH) from the sinus gland in the eyestalk (Liu and Laufer, 1996; Wainwright *et al.*, 1996), together with the present work, suggest that MF could be the direct hormonal agent controlling metamorphosis in crustaceans through an indirect effect of eyestalk neuropeptides.

MF has recently been described as a "crustacean juvenile hormone in search of functions" (Homola and Chang, 1997b). The findings of the present study—the delay in larval development and metamorphosis in *M. rosenbergii*, together with the increase in the abundance of intermediate specimens with the increase in exogenous MF—contribute to the debate over the physiological function of MF, supporting its possible role as a juvenile hormone in the development and metamorphosis of crustaceans.

Acknowledgments

We thank Ms. Hanna Ben-Galim and Ms. Galit Yehezkel for their technical assistance, and Ms. Inez Mureinik for editorial review of the manuscript. A. S. is the incumbent of the Judith and Murray Shusterman Chair for Career Development in Physiology.

Literature Cited

- Abdu, U. 1996. The involvement of methyl farnesoate, administered through *Artemia* vector, in the endocrine regulation of larval development and metamorphosis in the freshwater prawn *Macrobrachium rosenbergii*. M.Sc. Thesis, Ben-Gurion University of the Negev, Israel. 55 pp.
- Abdu, U., P. Takac, G. Yehezkel, R. Chayoth, and A. Sagi. 1998. Administration of methyl farnesoate through the *Artemia* vector, and its effect on *Macrobrachium rosenbergii* larvae. *Isr. J. Aquacult.* 50(2): 73–81.
- Borst, D. W., H. Laufer, M. Landau, E. S. Chang, W. A. Hertz, F. C. Baker, and D. A. Schooley. 1987. Methyl farnesoate and its role in crustacean reproduction and development. *Insect Biochem.* 17: 1123–1127.
- Bruning, E., R. R. Shivers, and B. Lanzrein. 1985. Methyl farnesoate and juvenile hormone III in normal and precocene-treated embryos of the ovoviparous cockroach *Nauphaeta cinerea*. *Int. J. Invertebr. Reprod. Dev.* 8: 269–278.
- Chang, E. S., M. J. Bruce, and S. L. Tamone. 1993. Regulation of crustacean molting: a multi-hormonal system. *Am. Zool.* 33: 324–329.
- Charmantier, G., and D. E. Aiken. 1987. Intermediate larval and postlarval stages of *Homarus americanus* H. Milne Edwards, 1837 (Crustacea: Decapoda). *J. Crust. Biol.* 7: 525–535.
- Charmantier, G., M. Charmantier-Daures, and D. E. Aiken. 1988. Larval development and metamorphosis of the American lobster *Homarus americanus* (Crustacea: Decapoda): effect of eyestalk ablation and juvenile hormone injection. *Gen. Comp. Endocrinol.* 70: 319–333.
- Christiansen, M. E., J. D. Costlow, Jr., and R. J. Monroe. 1977a. Effects of the juvenile hormone mimic ZR-515 (Altosid) on larval development of the mud-crab *Rhithropanopeus harrisi* in various salinities and cyclic temperatures. *Mar. Biol.* 39: 269–279.
- Christiansen, M. E., J. D. Costlow, Jr., and R. J. Monroe. 1977b.

- Effects of the juvenile hormone mimic ZR-512 (Altozar) on larval development of the mud-crab *Rhithropanopeus harrisi* in various salinities and cyclic temperatures. *Mar. Biol.* **39**: 281–288.
- Costlow, J. D., Jr. 1966a.** The effect of eyestalk extirpation on larval development of the mud crab, *Rhithropanopeus harrisi* (Gould). *Gen. Comp. Endocrinol.* **3**: 120–130.
- Costlow, J. D., Jr. 1966b.** The effect of eyestalk extirpation on larval development of the crab *Sesarma reticulatum* Say. Pp. 209–224 in *Some Contemporary Studies in Marine Science*. H. Barnes, ed. Appleton-Century-Crofts, New York.
- Daniels, W. H., L. R. D'Abramo, and L. D. Parseval. 1992.** Design and management of a closed, recirculating "clearwater" hatchery system for freshwater prawns, *Macrobrachium rosenbergii* De Man, 1879. *J. Shellfish Res.* **11**: 65–73.
- Gomez, E. D., D. J. Faulkner, W. A. Newman, and C. Ireland. 1973.** Juvenile hormone mimics: effects on cirriped crustacean metamorphosis. *Science* **179**: 813–814.
- Hertz, W. A., and E. S. Chang. 1986.** Juvenile hormone effects on metamorphosis of lobster larva. *Int. J. Invertebr. Reprod. Devel.* **10**: 71–77.
- Homola, E., and E. S. Chang. 1997a.** Distribution and regulation of esterases that hydrolyze methyl farnesoate in *Homarus americanus* and other crustaceans. *Gen. Comp. Endocrinol.* **106**: 62–72.
- Homola, E., and E. S. Chang. 1997b.** Methyl farnesoate: crustacean juvenile hormone in search of functions. *Comp. Biochem. Physiol.* **117B**: 347–356.
- King, L. E., Q. Ding, G. D. Prestwich, and S. S. Tohe. 1993.** The characterization of haemolymph methyl farnesoate binding protein and the assessment of methyl farnesoate metabolism by the haemolymph and other tissues from *Procambarus clarkii*. *Insect Biochem. Mol. Biol.* **25**: 495–501.
- Knowlton, R. E. 1994.** Effects of larval eyestalk extirpation on morphogenesis and molting in the snapping shrimp *Alpheus heterochaelis* Say. *J. Exp. Zool.* **270**: 162–174.
- Landau, M., H. Laufer, and E. Homola. 1989.** Control of methyl farnesoate synthesis in the mandibular organ of the crayfish *Procambarus clarkii*: evidence for peptide neurohormones with dual functions. *Invertebr. Reprod. Devel.* **16**: 165–168.
- Lanzrein, B., H. Imboden, C. Burgin, E. Bruning, and H. Gfeller. 1984.** On titers, origin, and functions of juvenile hormone III, methyl farnesoate, and ecdysteroids in embryonic development of the ovoviparous cockroach *Nauphoeta cinerea*. Pp. 454–465 in *Biosynthesis, Metabolism and Mode of Action of Invertebrate Hormones*. J. Hoffman and M. Porchet, eds. Springer-Verlag, New York.
- Laufer, H., and K. H. Albrecht. 1990.** Metabolism of methyl farnesoate *in vitro* by peripheral tissues of the spider crab *Libinia emarginata* (Decapoda). Pp. 217–222 in *Advances in Invertebrate Reproduction 5*. M. Hoshi and O. Yamashita, eds. Elsevier, Amsterdam.
- Laufer, H., and D. W. Borst. 1983.** Juvenile hormone and its mechanism of action. Pp. 203–216 in *Endocrinology of Insects*. R. G. H. Downer and H. Laufer, eds. Alan R. Liss, New York.
- Laufer, H., and D. W. Borst. 1988.** Juvenile hormone in Crustacea. Pp. 305–313 in *Endocrinology of Selected Invertebrate Types*. R. G. H. Downer and H. Laufer, eds. Alan R. Liss, New York.
- Laufer, H., D. W. Borst, F. C. Baker, C. Carrasco, M. Sinkus, C. C. Reuter, L. Tsai, and D. A. Schooley. 1987.** The identification of a crustacean juvenile hormone. *Science* **235**: 202–205.
- Laufer, H., P. Takac, J. S. B. Ahl, and M. R. Laufer. 1997.** Methyl farnesoate and the effect of eyestalk ablation on the morphogenesis of the juvenile female spider crab *Libinia emarginata*. *Invertebr. Reprod. Devel.* **31**: 63–68.
- Le Roux, A. 1984.** Quelques effets de l'ablation des pedoncles oculaires sur les larves et les premiers stades juveniles de *Palaemonetes varians* (Leach) (Decapoda, Palaemonidae). *Bull. Soc. Zool. Fr.* **109**: 43–60.
- Ling, S. W. 1969.** The general biology and development of *Macrobrachium rosenbergii*, De Man. *FAO Fish. Rep.* **57**: 589–606.
- Liu, L., and H. Laufer. 1996.** Isolation and characterization of sinus gland neuropeptides with both mandibular organ inhibiting and hyperglycemic effects from the spider crab, *Libinia emarginata*. *Arch. Insect Biochem. Physiol.* **32**: 375–385.
- McKenney, C. L., Jr., and D. M. Celestial. 1993.** Variations in larval growth and metabolism of an estuarine shrimp *Palaemonetes pugio* during toxicosis by an insect growth regulator. *Comp. Biochem. Physiol.* **105C**: 239–245.
- Prestwich, G. D., H. Wojtasek, A. J. Lentz, and J. M. Rabinovich. 1996.** Biochemistry of proteins that bind and metabolize juvenile hormone. *Arch. Insect Biochem. Physiol.* **32**: 407–419.
- Ramenofsky, M., D. J. Faulkner, and C. Ireland. 1974.** Effects of juvenile hormone on cirriped metamorphosis. *Biochem. Biophys. Res. Commun.* **60**: 172–178.
- Riddiford, L. M. 1994.** Cellular and molecular actions of juvenile hormone I. General considerations and premetamorphic actions. Pp. 213–274 in *Advances in Insect Physiology vol 24*, P. D. Evans, ed. Academic Press, London.
- Sagi, A., E. Homola, and H. Laufer. 1991.** Methyl farnesoate in the prawn *Macrobrachium rosenbergii*: synthesis by the mandibular organ *in vitro*, and titers in the hemolymph. *Comp. Biochem. Physiol.* **99B**: 879–882.
- Sehnal, F. 1983.** Juvenile hormone analogues. Pp. 657–672 in *Endocrinology of Insects*, R. G. H. Downer and H. Laufer, eds. Alan R. Liss, New York.
- Slama, K. 1971.** Insect juvenile hormone and analogues. *Annu. Rev. Biochem.* **40**: 1079–1102.
- Slama, K. 1995.** The present status of the mode of action of insect juvenile hormone. *Neth. J. Zool.* **45**: 71–78.
- Snyder, M. J., and E. S. Chang. 1986.** Effects of eyestalk ablation on larval molting rates and morphological development of the American lobster, *Homarus americanus*. *Biol. Bull.* **170**: 232–243.
- Sollaud, M. E. 1923.** Le développement larvaire des "Palaemoninae". I. Partie descriptive. La condensation progressive de l'ontogenèse. *Bull. Biol.* **57**: 509–603.
- Takac, P., J. S. B. Ahl, and H. Laufer. 1997.** Seasonal differences in methyl farnesoate esterase activity in tissues of the spider crab *Libinia emarginata*. *Invertebr. Reprod. Devel.* **31**: 211–216.
- Tamone, S. L., G. D. Prestwich, and E. S. Chang. 1997.** Identification and characterization of methyl farnesoate binding proteins from the crab. *Cancer Magister. Gen. Comp. Endocrinol.* **105**: 168–175.
- Tighe-Ford, J. D. 1977.** Effects of juvenile hormone analogues on larval metamorphosis in the barnacle *Eliminus modestus* Darwin. (Crustacea: Cirripedia). *J. Exp. Mar. Biol. Ecol.* **25**: 163–176.
- Uno, Y., and K. C. Soo. 1969.** Larval development of *Macrobrachium rosenbergii* De Man, reared in the laboratory. *J. Tokyo Univ. Fish.* **55**: 179–190.
- Wainwright, G., S. G. Webster, M. C. Wilkinson, J. S. Chung, and H. H. Rees. 1996.** Structure and significance of mandibular organ-inhibiting hormone in the crab, *Cancer pagurus*. *J. Biol. Chem.* **271**: 12749–12754.
- Wigglesworth, V. B. 1970.** *Insect Hormones. University Reviews in Biology*, p. 159. Oliver and Boyd, Edinburgh.

Body Polarity and Mineral Selectivity in the Demosponge *Chondrosia reniformis*

GIORGIO BAVESTRELLO¹, UMBERTO BENATTI², BARBARA CALCINAI¹,
RICCARDO CATTANEO-VIETTI¹, CARLO CERRANO¹, ANNA FAVRE³, MARCO
GIOVINE², SERENA LANZA¹, ROBERTO PRONZATO¹, AND MICHELE SARA¹

¹Istituto di Zoologia dell'Università di Genova, Via Balbi, 5 I-16126 Genova; ²Istituto di Chimica Biologica dell'Università di Genova, Viale Benedetto XV, 8 I-16132 Genova; and ³Istituto di Anatomia Patologica dell'Ospedale G. Gaslini, Lg. G. Gaslini 5, I-16100 Genova

Abstract. The skeleton of the common Mediterranean demosponge *Chondrosia reniformis* lacks endogenous spicules; but exogenous siliceous material is selectively incorporated into its collagenous ectosome, strengthening this layer. Nevertheless, the settling of sponge buds during asexual reproduction necessitates an active incorporation of the calcareous substratum through the sponge lower ectosome. This fact suggests the presence of a polarity in the sponge, with the lower surface selecting primarily carbonates, and the upper surface selecting exclusively silicates and quartz. Our observations under experimental conditions showed that the strong selectivity of the upper ectosome is realized only when the sponge is fixed to the substratum; if detached, the sponge incorporates both quartz and carbonates. In laboratory experiments, the incapacity of both kinds of ectosome to regenerate into a new complete sponge suggests that this polarity arises early in ontogeny.

Introduction

Chondrosia reniformis is a cushion-shaped, Atlanto-Mediterranean demosponge that usually lives on shallow rocky bottoms. A section through the sponge reveals two distinct regions: a cortical zone called ectosome, and an internal zone, the choanosome, which contains the choanocyte chambers. The ectosome is composed of a layer of flattened cells, exopinacocytes, that surround dense interwoven bundles of fibrils of collagen. In many circumstances the pinacocyte layer is loose, and the collagen

fibrils can be in direct contact with water (Garrone *et al.*, 1975).

C. reniformis lacks the opaline spicules that are the main constituents of the skeleton of other demospoenges; rather, the collagenous ectosome is strengthened by sand grains and exogenous spicules, which are actively incorporated by the sponge (Bavestrello *et al.*, 1995). Studies of foreign matter incorporation have been carried out on the sponge *Dysidea etheria*. In this species, the particles are incorporated by contraction of the dermal membrane, which probably separates or disrupts the thin exopinacocyte layer on the dermal membrane surface (Teragawa, 1986a, b). The ectosome of *C. reniformis* behaves similarly (Bavestrello *et al.*, in press).

In *C. reniformis*, the upper ectosome is able to select the minerals that settle on the sponge: thus, siliceous material is engulfed while the calcareous fragments that are the main sediments available in the surrounding environment are eliminated (Bavestrello *et al.*, 1996). In contrast, however, *C. reniformis* settles on calcareous rocks through the partial incorporation of outgrowths of this substratum by the lower ectosome. This process suggests a polarization in the sponge body, with a specificity for the incorporation of minerals that varies from the lower ectosome to the upper one.

Indeed, the polarization of the adult sponge body was already demonstrated 45 years ago with *Sycon raphanus*. When specimens of these sponges were bisected transversely, both halves could develop a complete new animal with the same polarity, from osculum to base, as the original (Tuzet and Paris, 1963).

The polarization of sponges relative to their position on the substratum probably arises in the larval stage. In

the amphiblastula larvae of *Calcarea*, the flagellate cells of the anterior pole make the initial contact with the substratum (Bergquist and Green, 1977). In Demospongiae, several authors have suggested that the coeloblastula or parenchymella larvae express an existing polarity in their attachment to the substrate. But such views are highly speculative, because distinguishing between an anterior and a posterior hemisphere in these animals is difficult (see Simpson, 1984, for a review).

The aims of this work are to verify—through laboratory experiments and scanning electron microscopy (SEM)—the capacity of both kinds of ectosome of *Chondrosia reniformis* to develop specificity towards siliceous and calcareous materials, and to demonstrate the cellular basis of that specificity.

Materials and Methods

Along the rocky cliff of the Portofino Promontory (Ligurian Sea, Italy) *Chondrosia reniformis* lives from the surface to the base of the cliff (about 50 m depth). The specimens used in this study were collected during January 1997, at 10 m depth, on calcareous substrates.

We performed our experiments with specimens having a surface area of 112–156 cm². These specimens were reared at 15°C in 200-l aquaria containing natural seawater with a salinity of 37‰. The medium was aerated by bubbling, and it was replaced twice a week. The collected sponges attached to the aquarium bottom in about 10 days.

The sandy materials used in testing sponge selectivity were white polycrystalline quartz with a particle size of 0.25–0.5 mm (BDH laboratory sand); red calcareous sand of the same particle size obtained from the organ-pipe coral *Tubipora musica*; and fragments of a coralline alga, *Lithothamnium* sp., 3–5 mm in size.

To test the differences in behavior between the upper and lower surfaces of the sponge ectosome, a thin layer of a mixture (1:1) of the BDH siliceous and *Tubipora* calcareous sands was laid down on the upper ectosome of five specimens that had attached to the bottom of an aquarium covered by the same mixture. Two experiments were carried out with these specimens. First, cores through the sponge, from upper to lower surface, were inverted and then transplanted, upside-down, inside the same specimen (five replicas). Second, 40 half-cores (20 mm in diameter) were taken from the upper and lower ectosome and reared for 3 months (see Fig. 1).

Observations made with SEM allowed us to distinguish differences in the organization of the two ectosomal surfaces. The samples used for these observations were collected by scuba divers and fixed *in situ* in 10% formalin.

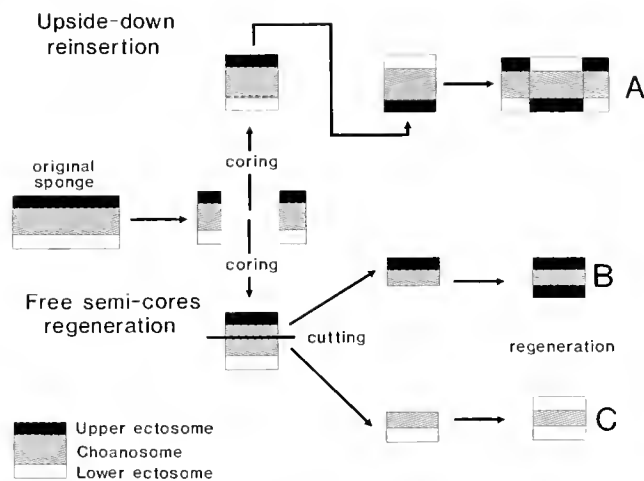


Figure 1. Scheme of coring experiments in *Chondrosia reniformis*. (A) Showing that differences in the mineral selectivity of the upper and lower sides of the ectosome are related to their histology. Cores (about 5–6 cm²) were cut from the upper to the lower surface and reinserted upside-down in the hole. The central portion of the resulting reconstituted sponges thus had an upper-lower orientation that was reversed. (B, C) Determining whether isolated upper and lower ectosomes can reconstitute an entire animal. Cores were produced and cut transversely to make half-cores. After 2 weeks' regeneration, the upper and lower ectosomes proliferated, enveloping the half-cores.

Results

When a mixture of siliceous and calcareous sand was allowed to settle on the upper ectosome of specimens that had attached to the bottom of the aquarium, only the quartz fragments (white) were incorporated. The calcareous grains (red) were never engulfed; rather they were quickly removed from the sponge surface (Fig. 2a). In contrast, the lower ectosome showed a remarkable preference for incorporating the calcareous grains of the mixture lying on the bottom (Fig. 2b).

The upper ectosome of newly collected specimens that had not yet attached to the aquarium bottom actively incorporated both kinds of minerals (Fig. 2c). Ten days later, after attachment, the upper surface of all the tested specimens began to select siliceous material exclusively.

To verify the difference in mineral selectivity between the two sides of the ectosome, cores (about 5–6 cm²) extending from the upper to the lower surface were cut from five large specimens and reinserted upside-down, to produce sponges with a portion of their lower surface having an upward orientation (Figs. 1, 2e). A week later, when the explants were perfectly fused in their anomalous positions and the sponges were attached to the aquarium floor, 5 g of *Lithothamnium* calcareous sand was laid on their surface (Fig. 2f). The subsequent behavior of the two types of surface was very different. The upper ectosome (brown) behaved normally, quickly removing calcareous particles (Fig. 2g–h); but the inverted, originally lower

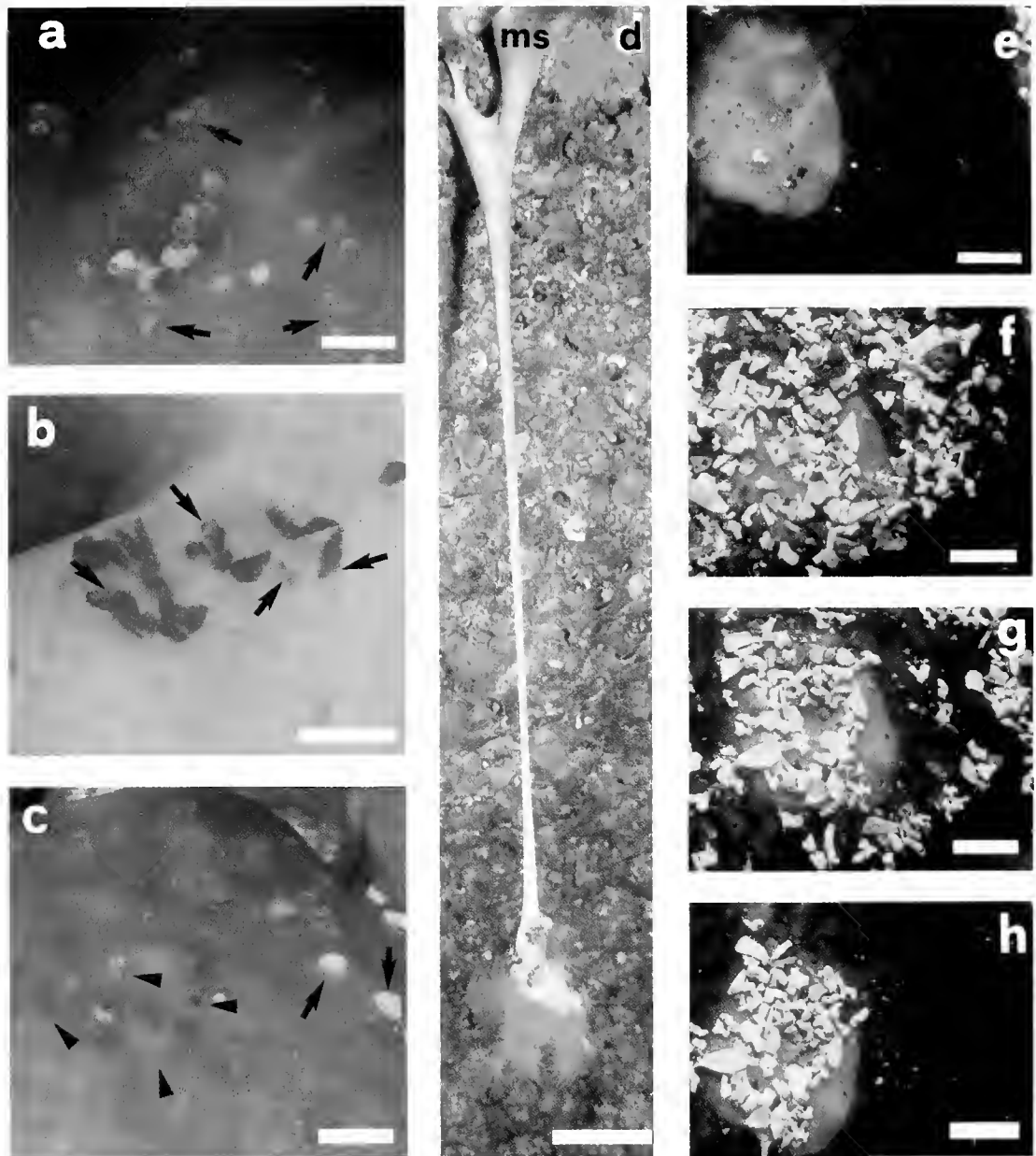


Figure 2. Mineral selectivity experiments. A 1:1 mixture of calcareous (red) and quartz (white) grains were allowed to settle on the upper and lower ectosome of *Chondrosia reniformis* specimens. (a) The upper ectosome (brown) has incorporated several quartz grains (arrows), while almost all the calcareous particles have been eliminated. (b) The opposite happens in the lower ectosome (white), which incorporates the calcareous fraction. Arrows indicate the thin collagenous sheet growing on the calcareous fragments. (c) The upper ectosome of a free, unattached specimen incorporates both quartz (arrows) and carbonatic particles (arrow heads). (d) Asexual reproduction in *C. reniformis*. The underwater photograph shows a long (1 m), stretched filamentous outgrowth hanging from a mother sponge (ms) that lives attached to the vault of a cave. A new sponge has formed at the free tip of the filament. (e) A core (about 6 cm²) cut and newly inserted upside-down in a large specimen of *C. reniformis*. When the explant was perfectly fused in its anomalous position, and the sponge had attached to the aquarium floor, calcareous grains were laid on its surface (f). Afterwards, the behavior of the two portions was very different. The upper surface (brown) behaves normally, quickly removing calcareous particles; shown at 24 h (g) and 48 h (h). The section that was originally the lower surface (whitish) did not move the particles. Scale bars: a–c = 1 mm; d = 10 cm; e–h = 1 cm.

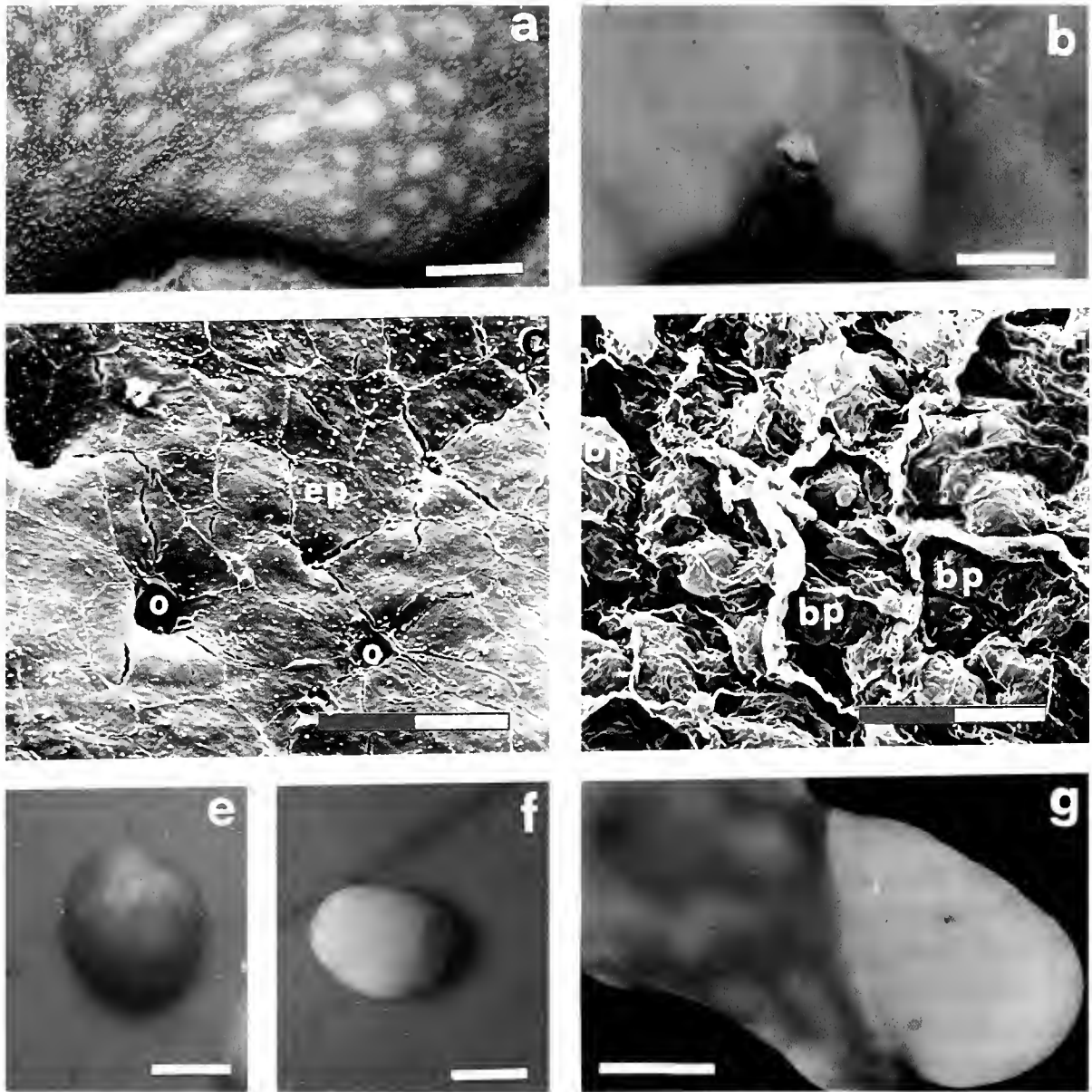


Figure 3. (a) The upper ectosome of *Chondrosia reniformis*, brown in color due to the presence of numerous melanocytes, and (b) the lower whitish one. SEM observations reveal differences between the two zones. (c) The upper surface is covered by polygonal flattened exopinacocytes (ep) and pierced by the incurrent openings, or ostia (o). (d) The lower surface shows no pores, and the basopinacocytes (bp) are covered by a collagenous sheet. Twelve weeks after preparation, the half-cores contain only an upper (e) or lower (f) ectosome. Two half-cores (g) derived from the upper (left) and lower (right) ectosomes, brought together and fused maintaining the characteristics of their original position. Scale bars: a–b, e–g = 1 cm; c–d = 50 μ m.

surfaces (whitish) did not move the particles, and 3 months later, they were all incorporated.

The gross morphological differences between the upper (Fig. 3a) and lower surfaces of the sponge (Fig. 3b) were supported by SEM observations: the upper ectosome is entirely covered by polygonal flattened pinacocytes and perforated by the incurrent openings (*ostia*) (Fig. 3c),

whereas the pinacoderm of the lower surface is covered by a collagenous sheet that lacks ostia (Fig. 3d).

To verify that the polarization between the upper and lower ectosome arises very early in development, experiments were performed with half-cores; these are fractions of sponge tissue that contain a portion of choanosome covered on one side by either upper or lower ectosome

(see Fig. 1). In the first 2 weeks of culture, the ectosome of both kinds of free half-cores actively proliferated, and the pieces assumed a spherical shape (Fig. 3e–f). The half-cores covered with lower ectosome (Fig. 3f) settled on the smooth bottom of the aquarium in 3–4 weeks, whereas those with the upper ectosome (Fig. 3e) settled after about 10–12 weeks. Furthermore, 3 months after the beginning of the experiment, the half-cores with lower ectosome were covered by a collagenous, non-cellularized layer that remained white and formed no osculum; the half-cores with the upper ectosome produced a new oscule in 12–15 weeks and showed a normal pinacoderm perforated by pores. Sometimes, when half-cores deriving from the upper and lower ectosome came in contact, they fused together; but a normal sponge was never reconstituted, although the two kinds of ectosome remained distinct on the opposite sides of the sponge (Fig. 3g).

Discussion

The structural and functional differences between the two sides of the ectosome of the sponge *Chondrosia reniformis* suggest a strong polarization—upper pole versus lower pole—along the axis of the sponge. The activity of the upper ectosome is likely due to the pinacocyte-mineral interaction. More problematic is the basis for the preferences of the lower ectosome for calcareous substrata. In other sponges, a nonspecific attachment to the substratum is probably due to the secretion by the basopinacocytes of a complex basal lamella (Pavans de Ceccatty, 1981) that anchors the sponge but prevents any contact between the cells and the substratum.

The ability of the upper ectosome to discriminate between silica and carbonates is present only in attached specimens and vanishes in free, nonattached ones, which incorporate both materials indiscriminately. This distinction is interpretable if we consider the asexual reproductive strategy of the species: Sponges living on overhanging ledges or on the vaults of submarine grottos give rise to long, thin pendant filaments (Fig. 2d). Cell reorganization within the apical region of these filaments produces a new, functional, but suspended animal. When the filament breaks, the bud is separated from the maternal sponge (Gaino *et al.*, 1995); it falls and must attach quickly irrespective of the side of the ectosome that comes in contact with the substratum. This behavior indicates, not only that mineral receptors are distributed evenly on the sponge surface, but also that these receptors may be activated or deactivated under particular conditions by an environmental switch. We suppose that the mineral discrimination of the upper ectosome is switched on by the adhesion of the sponge to the bottom.

Our studies indicate two modalities of mineral incorporation that are associated with the two sides of the ecto-

some. The upper side collects quartz and silicates, which strengthens the collagenous structure; this is a dynamic process comprising incorporation of the particles and re-sizing of the quartz grains, with their elimination *via* the aquiferous system (Bavestrello *et al.*, 1995). The lower side specifically engulfs the calcareous substrata, thus fixing the sponge to the bottom.

There is a rich literature about the very wide potential for cytodifferentiation in sponges (see Simpson, 1984). Our data indicate that, at least in *C. reniformis*, the morphological differences between the upper and lower regions of the ectosome are sharp, probably arising in a very early stage of sponge ontogeny; that is, a functionally complete specimen cannot be reconstituted from a portion of only upper or lower ectosome with its adjacent choanosome. Connes (1966, 1968) has demonstrated that the ectosome and choanosome of *Tethya aurantium* have different potentials for reconstructing an entire sponge, but our data provide the first indication of differences in this process associated with distinct zones of the same ectosome.

In higher metazoans, the spatiotemporal development of morphological structures is regulated by homeobox genes (Lawrence, 1992). These genes have also been observed in lower metazoans such as sponges (Kruse *et al.*, 1994; Coutinho *et al.*, 1994; Degnan *et al.*, 1995; Seimiya *et al.*, 1997), but their meaning has been obscure until now. We hypothesize that the acquisition of an axial polarity in the sponge may be controlled by these genetic structures.

Acknowledgements

This research was supported by Italian MURST funds.

Literature Cited

- Bavestrello, G., A. Arillo, U. Benatti, C. Cerrano, R. Cattaneo-Vietti, L. Cortesogno, A. Gaggero, M. Giovine, M. Tonetti, and M. Sarà. 1995. Quartz dissolution by the sponge *Chondrosia reniformis* (Porifera, Demospongiae). *Nature* **378**: 374–376.
- Bavestrello, G., C. Cerrano, R. Cattaneo-Vietti, M. Sarà, F. Calabria, and L. Cortesogno. 1996. Selective incorporation of foreign material in *Chondrosia reniformis* (Porifera, Demospongiae). *Ital. J. Zool.* **63**: 215–220.
- Bavestrello, G., A. Arillo, B. Calcinaï, C. Cerrano, R. Cattaneo-Vietti, S. Lanza, and M. Sarà. Interaction between different kinds of silica and the exo-pinacocytes of the demosponge *Chondrosia reniformis*. *Ital. J. Zool.* (in press).
- Bergquist, P. R., and C. R. Green. 1977. An ultrastructural study of settlement and metamorphosis in sponge larvae. *Calif. Biol. Mar.* **18**: 289–302.
- Connes, R. 1966. Aspects morphologiques de la régénération de *Tethya lyncurium* Lamarck. *Bull. Soc. Zool. Fr.* **91**: 43–53.
- Connes, R. 1968. Etude histologique, cytologique et expérimentale de la régénération asexuée chez *Tethya lyncurium* Lamarck (= *Tethya aurantium* Pallas) (Demosponges). Thesis, Univ. Montpellier, France. 193 pp.

- Coutinho, C., S. Vissers, and G. Van de Vyver. 1994.** Evidence of homeobox genes in the freshwater sponge *Ephydatia fluviatilis*. Pp. 385–388 in *Sponges in Time and Space*. R. W. M. van Soest, Th. M. G. van Kempen, and J. C. Braekman, eds. Balkema, Rotterdam.
- Degnan, B. M., S. M. Degnan, A. Giusti, and D. E. Morse. 1995.** A hox/hom homeobox gene in sponges. *Gene* **155**: 175–177.
- Gaino, E., R. Manconi, and R. Pronzato. 1995.** Organizational plasticity as a successful conservative tactics in sponges. *Anim. Biol.* **4**: 31–43.
- Garrone, R., A. Huc, and S. Junqua. 1975.** Fine structure and physicochemical studies on the collagen of the marine sponge *Chondrosia reniformis* Nardo. *J. Ultrastruct. Res.* **52**: 261–275.
- Lawrence, P. A. 1992.** *The Making of a Fly: The Genetics of Animal Design*. Blackwell Scientific, Oxford.
- Kruse, M., A. Mikoc, H. Cetkovic, V. Gamulin, B. Rinkevich, I. M. Muller, and W. E. Muller. 1994.** Molecular evidence for the presence of a developmental gene in the lowest animals: identification of a homeobox-like gene in the marine sponge *Geodia cydonum*. *Mech. Ageing Dev.* **77**: 43–54.
- Pavans de Ceccatty, M. 1981.** Demonstration of actine filaments in sponge cells. *Cell Biol. Int. Rep.* **5**: 945–952.
- Seimiya, M., H. Ishiguro, K. Miura, Y. Watanabe, and Y. Kurosawa. 1997.** Homeobox-containing genes in the most primitive metazoa, the sponges. *Eur. J. Biochem.* **221**: 219–225.
- Simpson, T. L. 1984.** *Cell Biology of Sponges*. Springer, New York.
- Teragawa, C. K. 1986a.** Particle transport and incorporation during skeleton formation in a keratose sponge: *Dysidea etheria*. *Biol. Bull.* **170**: 321–334.
- Teragawa, C. K. 1986b.** Sponge dermal membrane morphology: histology of cell-mediated particle transport during skeletal growth. *J. Morphol.* **190**: 335–347.
- Tuzet, O., and J. Paris. 1963.** Recherches sur la régénération de *Sycon raphanus*. *Vie Milieu* **14**: 285–298.

Effect of Larval Swimming Duration on Growth and Reproduction of *Bugula neritina* (Bryozoa) Under Field Conditions

DEAN E. WENDT

*Department of Organismic and Evolutionary Biology, Harvard University,
Cambridge, Massachusetts 02138*

Abstract. A growing body of evidence indicates that even subtle events occurring during one portion of an animal's life cycle can have detrimental, and in some cases, lasting effects on later stages. Using a laboratory-field transplant design, postmetamorphic costs associated with the duration of larval swimming were investigated in the bryozoan *Bugula neritina*. Larvae were induced to metamorphose in the laboratory after swimming for either less than 1 h or between 23 and 24 h; colonies that developed from these two groups of larvae are referred to hereafter as "1-h colonies" and "24-h colonies," respectively. After completing metamorphosis, individuals were transplanted to the field, where rates of growth and reproduction were monitored. In a study of the interaction between colony orientation (up or down) and larval swimming duration, both factors significantly affected the number of autozooids produced. For example, 14 days after metamorphosis, 1-h colonies facing up were approximately 40% smaller than 1-h colonies facing down. In another study, the effects of larval swimming duration, orientation, and a neighboring conspecific colony on growth and reproduction were examined. In this experiment, proximity to a conspecific colony and orientation did not significantly affect growth or fecundity, whereas increased larval swimming duration significantly reduced both. For example, 14 days after metamorphosis, the 24-h colonies were 35% smaller than 1-h colonies. Furthermore, from the time metamorphosis was initiated, the onset of reproduction was delayed by about 1.5 days in 24-h colonies when compared to 1-h colonies; and a slight delay (*ca.* 1 day) was associated with proximity of a

developing conspecific in 1-h and 24-h colonies. In addition, 17 days after metamorphosis, 24-h colonies had about half as many brood chambers (an index of fecundity) as 1-h colonies. Costs associated with increasing the larval swimming phase by only 24 h are significant in postmetamorphic individuals, and they clearly compromise colony fitness.

Introduction

Possession of a larval stage is common in a wide range of animals, including many fish, amphibians, and both terrestrial and aquatic invertebrates. Occurrence across such an array of taxa suggests that some benefits are associated with a motile larval stage (Strathmann, 1993; Havenhand, 1995; Wray, 1995). For marine invertebrates, a major benefit is dispersal ability, which, for example, reduces parent-offspring competition and facilitates the recolonization of disturbed habitats. In species with sedentary or sessile adults, larvae help to increase gene flow between geographically separated populations and extend species' ranges. However, there are also costs associated with a free-living larval stage (Pechenik, 1990). These costs can be lethal (advection from suitable habitats, predation, and loss of metamorphic competence), or sublethal (slower growth after metamorphosis and delayed onset of reproduction). Thus, by severely limiting dispersal, these costs probably contribute to the speciation of marine invertebrates with aplanktotrophic larvae (see Wendt, 1996, for a discussion of this term).

Models used to examine the life-history strategies and population dynamics of marine invertebrates have focused on the lethal costs of dispersal (*e.g.*, Vance, 1973; Strathmann, 1985; Roughgarden *et al.*, 1988); the suble-

that costs have been largely overlooked. Recent work demonstrates that sublethal effects can dramatically influence juvenile growth and survival under laboratory conditions (Woollacott *et al.*, 1989; Pechenik and Cerulli, 1991; Pechenik *et al.*, 1993; Wendt, 1996). This study assesses the costs of larval swimming duration on growth and reproduction under field conditions in the cheilostome bryozoan *Bugula neritina*.

Larvae of marine invertebrates commonly metamorphose in response to cues indicative of a favorable habitat for the adult (Scheltema, 1974; Hadfield, 1978; Crisp, 1984; Chia, 1989; Pawlik, 1992). Once physiologically competent to metamorphose, a larva can remain in the swimming phase because it has not encountered a suitable cue to trigger metamorphosis or because it does not respond to the normal metamorphic cue as a consequence of additional factors. For example, Young and Chia (1981) demonstrated that competent larvae of *Bugula pacifica* delay metamorphosis in the presence of extracts of the compound ascidian *Diplosoma macdonaldi*, a dominant competitor. An extended larval swimming period occurs when an individual becomes physiologically capable of responding to cues that elicit metamorphosis, but instead continues swimming. The benefit of remaining in the swimming phase is the increased likelihood of synchronizing the onset of metamorphosis with encountering a favorable adult site. On the other hand, the longer a larva swims the greater its exposure to the potentially lethal and sublethal effects of a planktonic existence (Rumrill, 1990; Morgan, 1995).

The adverse effects of an extended larval swimming phase are well documented in laboratory studies of marine invertebrates. Increasing larval swimming time in the polychaete *Capitella* sp. 1 significantly decreased postsettlement survivorship from 100% to 12.5% over 216 h of larval swimming (Pechenik and Cerulli, 1991). In bryozoans identified as *Bugula* spp., the ability to initiate and complete metamorphosis was inversely proportional to larval swimming duration (Woollacott *et al.*, 1989; Hunter and Fusetani, 1996; Wendt, 1996). Furthermore, a loss of metamorphic competence was observed after 24 h of larval swimming in *Celleporella hyalina*, another cheilostome bryozoan (Orellana and Cancino, 1991).

The size of postmetamorphic individuals is affected by the duration of larval swimming. Unusually small ancestrulae developed from larvae of the bryozoan *Hippodiplosia insculpta* that swam for longer than 6 h (Nielson, 1981). Wendt (1996) quantitatively extended Nielson's qualitative observations on *H. insculpta* to *B. neritina*, showing that ancestrulae developed from larvae that swam for 28 h had lophophores (the feeding apparatus) 25% smaller in height, 40% smaller in surface area, and 50% smaller in volume, compared to ancestrulae that developed from larvae induced to metamorphose within 1 h of release.

Only short-term effects of increased larval swimming duration on growth have been assessed. For example, in 12 out of 14 cases, Woollacott *et al.* (1989) found that after 11 h of swimming, larvae of *B. stolonifera* developed into juveniles that grew significantly slower than juveniles from larvae that swam for only 6 h. Likewise, for the barnacle *Balanus amphitrite*, increasing the swimming period of cyprids for 3–5 days depressed juvenile growth rate compared to controls (Pechenik *et al.*, 1993). Long-term effects on growth and reproduction have not been explored.

Effects associated with increased swimming duration are common, but not universal. For example, Highsmith and Emlet (1986) found no significant correlation between "delay time" and juvenile growth rate in the sand dollar *Echinaraclinius parma*, which has planktotrophic larvae. In the gastropod *Crepidula fornicata*, which also has a planktotrophic larva, no significant differences were observed in average rates of survival, feeding, respiration, or growth between juveniles that were induced to metamorphose shortly after attaining competence and those that kept swimming until metamorphosis occurred spontaneously (Pechenik and Eyster, 1989).

In general, the adverse effects associated with larval swimming duration are common in species with aplanktotrophic larvae, whereas species with planktotrophic larvae typically are buffered from these costs. Information on the long-term effects of larval swimming duration on adults are confined to a single laboratory study (Pechenik and Cerulli, 1991) of a polychaete. No study has yet evaluated the performance of individuals in the field. I assess, under field conditions, the long-term costs of increasing larval swimming duration on colony growth and reproduction of *Bugula neritina*. In addition, I investigate the effects of colony orientation and intraspecific competition in relation to larval swimming duration.

Materials and Methods

Collection of specimens

Gravid colonies of *Bugula neritina* were collected from the undersides of floating docks near the Smithsonian Marine Station at Link Port in Fort Pierce, Florida, during February and March 1997. Colonies were maintained in light-tight, flow-through plastic containers. Natural seawater from the Indian River (salinity *ca.* 32 ppt) was continuously pumped through the containers, providing the colonies with ambient levels of food and oxygen.

Larval release

Larvae were obtained from several colonies to foster genetically heterogeneous populations for experiments, and larvae used in experiments were obtained only from

parent colonies kept in the laboratory less than 5 days. There were no qualitative differences between colonies kept in the light-tight boxes for 1 day and those kept for 5 days; in fact, colonies stayed healthy under these conditions for several weeks after the experiments. Colonies were removed from the light-tight containers, placed in glass bowls with 1.0 l of seawater, and exposed to fluorescent light. Larvae appeared within 10 min of illumination, and release was complete by 1 h. As *B. neritina* larvae are positively phototactic on release, they aggregated at the illuminated side of the dishes, a behavior that facilitated their collection.

Larval swimming

Following release, larvae were transferred to an autoclaved, 1.5-l glass finger bowl containing about 1.0 l of 0.2- μm filtered seawater. Larvae were prevented from initiating metamorphosis by continuous exposure to bright, fluorescent illumination accompanied by stirring (Wendt, 1996). The bowl was placed on an acrylic plastic table to reduce UV exposure and illuminated from below with four 20-W, 24-in. full-spectrum DayCycle lamps. An additional two 20-W, 24-in. fluorescent lamps were used to increase the overall lighted area. Pieces of aluminum foil were placed around the finger bowl to create a constant reflection and constant levels of illumination from all directions. Illumination levels ranged from 130 to 170 $\mu\text{E m}^{-2} \text{s}^{-1}$. Fans were installed under the acrylic table to maintain ambient room temperatures (*ca.* 22°C) during larval swimming.

Metamorphosis

Groups of larvae were induced to metamorphose in small polystyrene dishes by adding 10 mM excess KCl to the seawater (Wendt and Woollacott, 1995). Metamorphosis is the time from eversion of the larval metasomal sac to eversion of the lophophore of the ancestrular polypide. To synchronize completion of metamorphosis for 1-h and 24-h individuals, larvae released on two consecutive days were used for each experiment. Those released on the first day were kept swimming for 24 h before metamorphosis was initiated. On the second day, the same adult colonies were used for another release of larvae. This release was 6 h later than on the previous day to allow for the increased time individuals take to metamorphose after swimming for 24 h (Wendt, 1996). This release schedule ensured that 1-h and 24-h individuals finished metamorphosis at about the same time (*ca.* 48 h). Spontaneous metamorphosis was generally rare and occurred at very low levels. If more than 5% of the larvae metamorphosed during larval swimming, the experiment was aborted.

Growth in these experiments was estimated by counting

the number of autozooids and bifurcations in a colony. Bryozoans grow by asexual reproduction of modular units, zooids, from a sexually produced individual, the ancestrula. Zooids are connected to one another by a strand of tissue, the funiculus. Most generally there are two types of zooids: autozooids, which are present in all species, are specialized for feeding and digestion; heterozooids, which are not found in all species, function in defense, attachment, and reproduction. In *B. neritina*, brood chambers are the sole type of heterozooid. Thus, the number of autozooids is a good estimator of colony growth and has an advantage over dry weight or colony length in that it can be determined nondestructively over many days in the same individuals.

Effect of larval swimming duration and colony orientation on adult growth

Larvae were released and metamorphosed as described above. Two polystyrene dishes were attached with low-temperature hot glue to a clear acrylic plastic plate. Three to five larvae were pipetted into dishes to ensure successful metamorphosis of at least one. On completion of metamorphosis, all but a single individual were removed and the sides of the dish were trimmed away so that only the flat bottom portion remained. Each replicate consisted of two plates, each with two dishes and a total of four individuals: colony orientation was up (high siltation) or down (low siltation), and each plate had a 1-h and a 24-h individual (Fig. 1). The relative positions of the individuals were changed between replicates so as to nullify any micro-environmental effects associated with the plates. The replicate plates were then attached to nylon

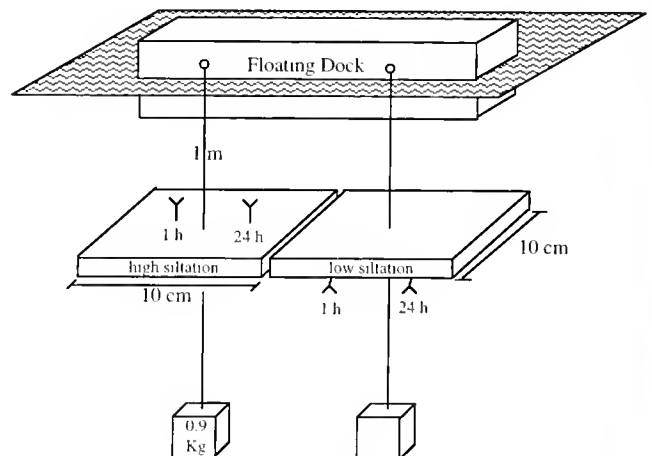


Figure 1. Experimental apparatus for assessing the effect of colony orientation and swimming duration on growth. See text for details on the placement of ancestrulae (Y). The colonies were placed far enough apart so that no competition for food and space occurred. Colonies grew for 14 days and then were returned to the laboratory for scoring.

line at intervals of about 35 cm and suspended from floating docks. Lead ballasts weighing 0.90 kg were hung 0.5 m below the plates to keep them level, and the plates were submerged about 1 m below the surface. A rain gauge modified to serve as a sediment trap was submerged at the same level as the plates to provide a rough estimate of the amount of sediment accumulation over the course of the experiment. After 14 days, the plates were returned to the laboratory and the number of autozooids and bifurcations counted for each colony. Each condition started with 18 replicates, totaling 72 individuals.

Effect of larval swimming duration, orientation, and the presence of a conspecific colony on growth and reproduction

Larvae were released and metamorphosed as described above. About 50 individuals were pipetted into polystyrene dishes and allowed to metamorphose. The dishes were carved into thin strips such that each strip had a newly metamorphosed individual on its end (Fig. 2). The experimental apparatus was a plastic box that contained "lanes" with walls made of dense, chemically inert foam. Tiny slits were made in the foam, which allowed one end of the strip to be inserted in the wall of the lane. Another individual was placed in a slit directly opposite the first, so that the individuals shared space in the center of a lane. For each apparatus there were eight individuals in a total of four lanes. The individuals were either in the presence or absence of competition with a neighboring conspecific (*i.e.*, with a conspecific in a slit directly across the lane facing the same direction) and were either 1-h or 24-h colonies. Another factor in this experiment was orientation (up or down; Fig. 2). However, orientation in this experiment did not expose colonies to different amounts of siltation, as the apparatus was designed to shield colonies from the downward flux of particulate matter. After metamorphosis (*ca.* 48 h), individuals were arranged in blocks and transplanted to the field.

Each apparatus was removed daily and the numbers of autozooids, bifurcations, and brood chambers were counted for each colony. Because the blocks were designed to hold a small volume of seawater, colonies were never exposed to the air during this process. As the colonies grew it became difficult to score all parameters in a single day, so only bifurcations and brood chambers were counted for all colonies after day 12. The number of autozooids was counted for replicate boxes 1–15 on day 13 and for boxes 16–30 on day 14. Due to time constraints, autozooids were not counted after day 14. The experiment was ended on day 17, because the largest colonies began to overgrow the apparatus, potentially introducing additional effects. Analysis of variance (ANOVA) was applied to zooid data from day 12 and

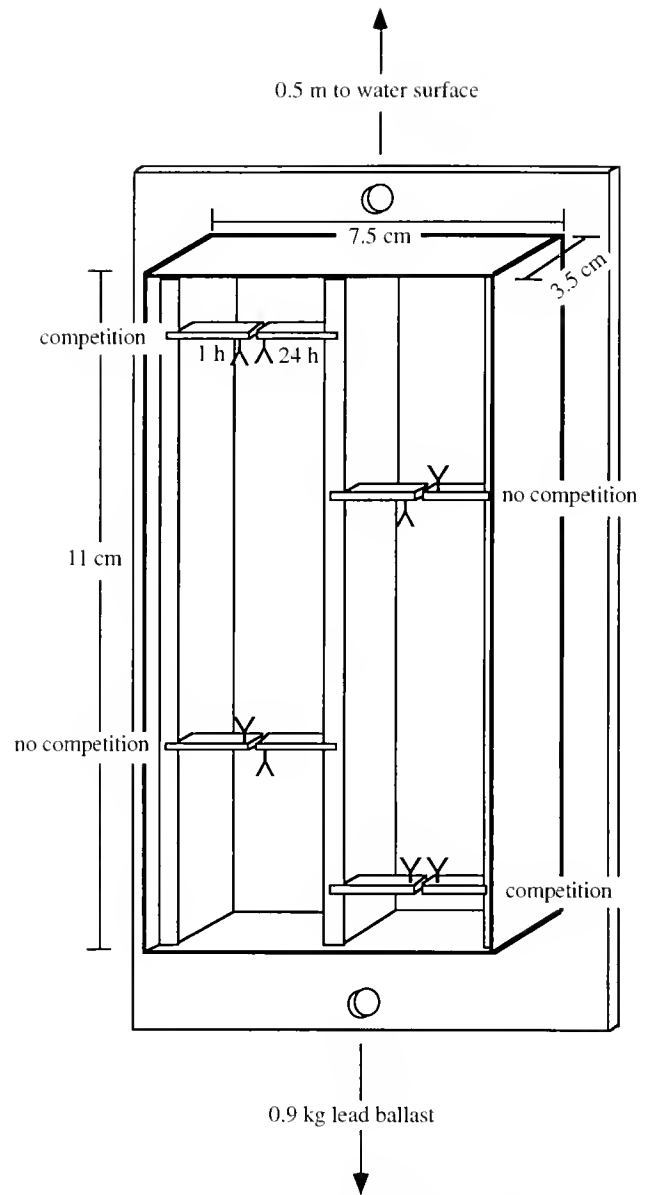


Figure 2. Experimental apparatus for assessing the effect of competition and swimming duration on growth and reproduction. See text for details on placement of ancestrulae (Y).

bifurcation and brood chamber data from day 17; these were the last days the respective data were collected for all colonies.

Data analysis

The data were not significantly different from a normal distribution, and a square root transformation was used to remove heteroscedasticity. The data were back-transformed for presentation in graphs and text. Since all factors were fixed, a Model 1 ANOVA was used. For the

experiment on swimming time and colony orientation a 2-way factorial ANOVA was used to identify heterogeneity of variances within the data sets. The main effects were swimming duration and orientation. For the experiment on competition and swimming duration a 3-way ANOVA was used and the main effects were swimming duration, presence of a conspecific, and orientation. Non-linear regressions were done in SYSTAT using simple and general allometry models (Ebert and Russell, 1994).

Results

Increased duration of larval swimming significantly reduced growth and reproduction in both experiments with *B. neritina*. Colony orientation, when designed to expose colonies to different amounts of siltation pressure, also affected growth: colonies facing down were significantly larger than those facing up. The proximity of a conspecific (*i.e.*, intraspecific competition), did not significantly affect growth, although it slightly delayed the onset of reproduction. Growth between experiments cannot be compared since there was a temperature difference of more than 5°C between the first and second experiments. On average, colonies grew faster under warmer conditions.

Effect of larval swimming duration and colony orientation on growth

During the 14 days of this experiment, approximately 0.2 cm of sediment accumulated in the trap and on the surfaces of the plates. Larval swimming duration and col-

ony orientation significantly affected growth as measured by the number of autozooids and bifurcations in a colony (Fig. 3A, B; Table 1). In no case was the interaction between swimming duration and orientation significant ($P = 0.53$ for zooid number and $P = 0.65$ for bifurcations). On average, 1-h colonies facing down (light siltation load) had twice the number of autozooids and bifurcations as 24-h colonies facing up; whereas 1-h colonies facing up had almost the same number of autozooids and bifurcations as 24-h colonies facing down (Fig. 3). Reproduction of colonies did not occur at levels high enough to warrant statistical analysis.

Effect of larval swimming duration, colony orientation, and the presence of a conspecific on growth and reproduction

Neither orientation nor development next to a conspecific colony significantly affected growth and reproductive output as determined by ANOVA (Table II). Orientation did not expose animals to different amounts of siltation in this experiment, because the apparatus was shielded from the downward flux of particulate matter. Colony proximity appears to have some effect on the onset of reproduction (Fig. 4). Among 1-h colonies, those in the presence of a conspecific reached 50% reproduction 12 h later than those without a conspecific neighbor. Likewise, in the absence of a conspecific neighbor, 24-h colonies reached 50% reproduction more than 31 h later than 1-h colonies (Fig. 4). On average, both the presence of a

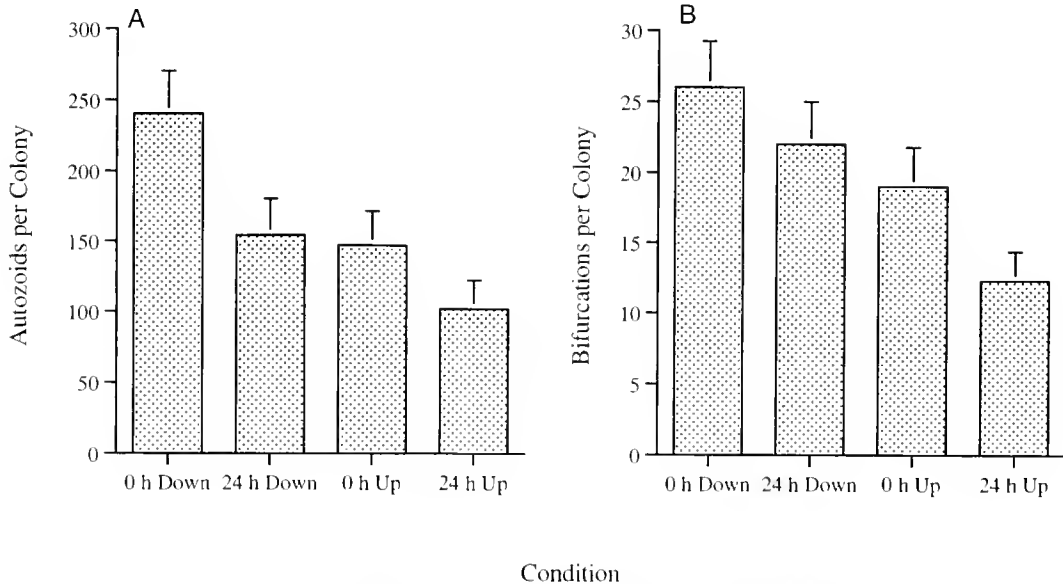


Figure 3. Number of autozooids and bifurcations in 1-h and 24-h colonies, 14 days after metamorphosis. Colonies were oriented up ("high siltation") or down ("low siltation"). Error bars = 95% confidence interval; $n = ca.$ 50 colonies.

Table I

Results of two-way factorial ANOVA for the effect of larval swimming duration and colony orientation (up or down) on the number of zooids and bifurcations in *Bugula neritina* colonies ($n = 53$ colonies)

Measurement	Source of variation	df	SS	MS	F_c	P value
Bifurcations	Swimming duration	1	5.19	5.19	3.74	0.05
	Orientation	1	11.5	11.5	8.28	0.006
	Interaction	1	0.55	0.55	0.40	0.53
	Residual	49	68.1	1.39	—	—
Autozooids	Swimming duration	1	88.7	88.7	5.11	0.02
	Orientation	1	108	108	6.22	0.01
	Interaction	1	3.56	3.56	0.21	0.65
	Residual	52	903	17.4	—	—

conspecific colony and increased duration of larval swimming delayed the onset of reproduction; differences of less than 12 h cannot be resolved.

Longer larval swimming leads to reduced growth and reproductive output (Table II; Figs. 5, 6, and 7). For example, 14 days after metamorphosis the average number of autozooids was 113 ± 7 ($n = 50$; mean \pm 95% confidence) for 1-h colonies, compared to 74 ± 6 ($n = 49$), for 24-h colonies. However, the slopes of the regression lines for autozooid number as a function of days after metamorphosis were statistically indistinguishable; an indication that both groups of colonies were growing at about the same rates, despite differences in the absolute number of autozooids at day 14 (Fig. 5). The number of brood chambers, a measure of reproductive output, was significantly lower in 24-h colonies ($P < 0.001$). The average number of brood chambers was 149 ± 19 ($n = 94$; mean \pm 95% confidence)

for 1-h colonies and 76 ± 11 ($n = 93$) for 24-h colonies. Thus, 17 days after metamorphosis, 1-h colonies had, on average, more than twice the number of brood chambers as did 24-h colonies. Furthermore, unlike the rate of production of new autozooids, which was similar in 1-h and 24-h colonies very soon after metamorphosis, the rate of brood-chamber production was significantly less in 24-h colonies for the duration of the experiment (Fig. 7). Similar trends were observed in bifurcations (Fig. 6).

The only significant interaction between main factors was between colony orientation and proximity of a conspecific ($F = 7.6$, $P = 0.006$ for brood chambers; $F = 6.5$, $P = 0.01$ for autozooids).

Discussion

Most empirical evidence that nonlethal larval experiences have long-term effects comes from observations

Table II

Results of three-way factorial ANOVA for the effect of larval swimming duration, colony orientation (up or down), and competition on the number of zooids, bifurcations, and brood chambers in *Bugula neritina* colonies ($n = 180$ colonies)

Measurement	Source of variation	df	SS	MS	F_c	P value
Bifurcations	Swimming duration	1	24.1	24.1	23.8	0.0001
	Competition	1	1.83	1.83	1.81	0.18
	Orientation	1	0.16	0.16	0.16	0.69
	Interactions	4	3.03	0.76	0.08	>0.5
	Residual	180	181	1.01	—	—
Autozooids	Swimming duration	1	42.8	42.8	30.3	0.0001
	Competition	1	0.46	0.46	0.32	0.57
	Orientation	1	0.62	0.62	0.44	0.51
	Interactions*	4	2.58	0.64	0.46	>0.5
	Residual	179	252	1.41	—	—
Brood chambers	Swimming duration	1	584	584	33.8	0.0001
	Competition	1	1.51	1.51	0.09	0.77
	Orientation	1	2.49	2.49	0.14	0.71
	Interactions*	4	167	41.7	2.43	0.11
	Residual	178	3100	17.3	—	—

For clarity, the interactions of main effects were collapsed into a single interaction term.

* There was a significant interaction between orientation and competition; see Discussion for an examination of this outcome.

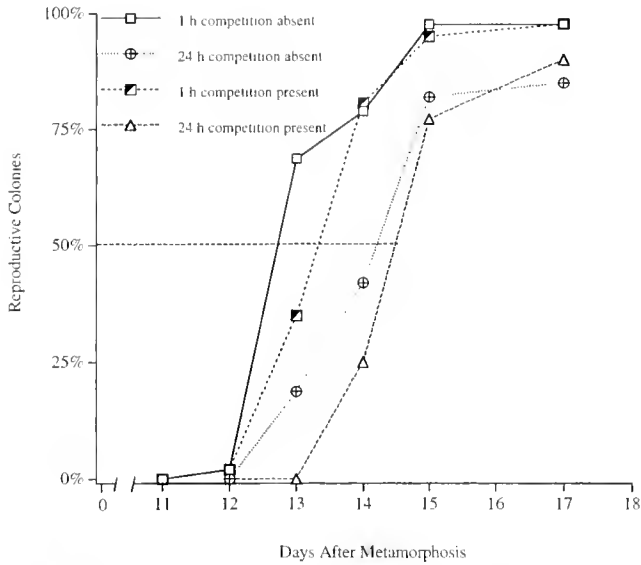


Figure 4. Onset of reproduction in *Bugula neritina* as a function of larval swimming duration, competition, and time after metamorphosis. $n = 40-50$ colonies for each curve.

on marine invertebrates with aplanktotrophic larvae. The influence of such experiences on postmetamorphic performance is not restricted to marine invertebrates, however. For example, the feeding history of larval reef fish affects the average diameter of tail muscle fibers, average size at settlement, and average juvenile feeding rates (McCor-

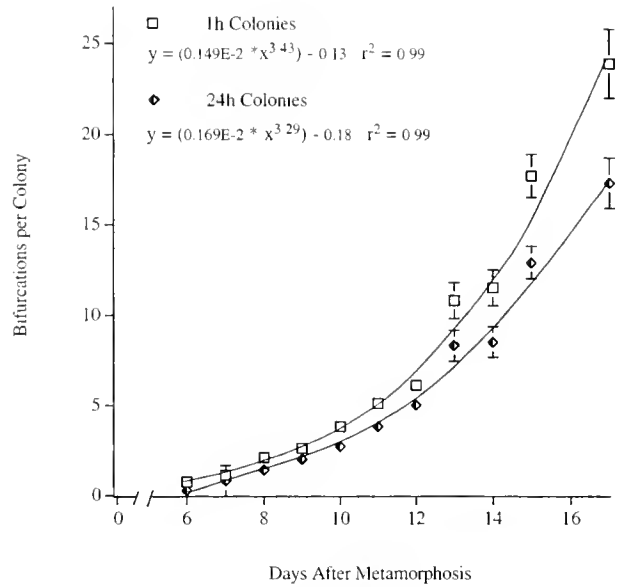


Figure 6. Mean number of bifurcations as a function of larval swimming duration and time after metamorphosis in *Bugula neritina*. Error bars = 95% confidence interval of the means. $n = ca. 90$ colonies for each curve, and all nonsignificant data were pooled. Regressions were calculated using all zero values for y .

mick and Molony, 1992). In amphibians, food deprivation at different periods of tadpole ontogeny can precipitate metamorphosis at smaller sizes (Audo *et al.*, 1995). In insects, the reproductive fitness of the adult female flesh

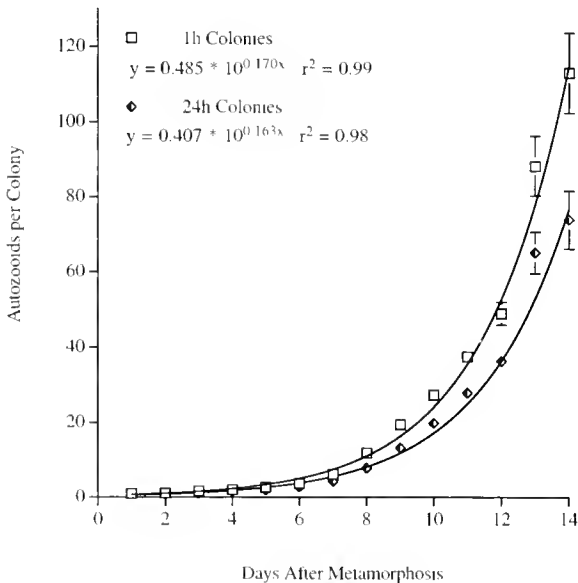


Figure 5. Mean number of autozooids as a function of larval swimming duration and time after metamorphosis in *Bugula neritina*. Error bars = 95% confidence interval of the means. $n = ca. 90$ colonies for each curve, and all nonsignificant data were pooled. Regressions were calculated using all zero values for y .

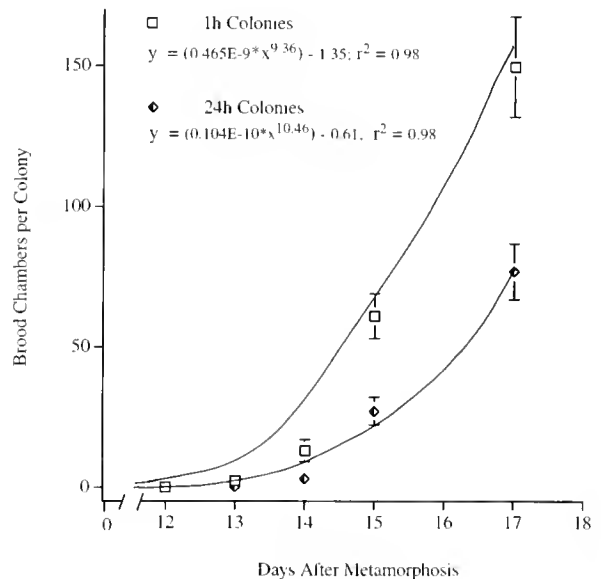


Figure 7. Mean number of brood chambers as a function of larval swimming duration and time after metamorphosis in *Bugula neritina* colonies. Error bars = 95% confidence interval of the means. $n = ca. 90$ colonies for each curve, and all nonsignificant data were pooled. Regressions were calculated using all zero values for y .

fly is inversely correlated with the amount of time the larva spends in diapause (Denlinger, 1981).

Effect of larval swimming duration on growth and reproduction

In both the siltation and the competition experiments, a 24-h increase in the larval swimming period significantly reduced growth and reproduction compared to 1-h colonies (Tables I and II). Since growth in *B. neritina* is an exponential process, small differences during early colony development will translate into large differences in colony size (Figs. 5 and 6). On average, 24-h colonies had half as many autozooids, bifurcations, and brood chambers as did 1-h colonies over the same time of development. The observed difference is not a result of 24-h colonies finishing metamorphosis 23 h later than 1-h colonies, as experiments were designed so that both groups of animals finished metamorphosis and began feeding at nearly the same time. Thus, the lower values observed for 24-h colonies cannot be attributed to a shorter period of postmetamorphic development—in fact, 24-h larvae take an additional 6–8 h to metamorphose (Wendt, 1996). Overall, then, the differences observed between 1-h and 24-h colonies are conservative.

Because 24-h colonies initially grow more slowly, they will always have fewer autozooids, bifurcations, and brood chambers at a given point in time and, assuming similar growth potentials, they will never "catch up" to their 1-h counterparts. But is there a point at which the two groups have equal rates of growth or reproduction? For growth rate, as measured by the number of autozooids, this happens several days after metamorphosis when the slope of the regression lines are virtually identical (Fig. 5). For reproduction, however, the slopes of the regression lines appear to be different throughout the duration of the experiment (Fig. 6), indicating that, 17 days after metamorphosis, 24-h colonies have not produced brood chambers at the same rate as 1-h colonies. Considering that colonies in the Indian River in the vicinity of the Smithsonian Marine Station at Link Port persist in the field for 5 or 6 weeks at most (L. J. Walters, pers. comm.; DEW, pers. observ.), the rate of reproductive output would be severely compromised as the larval swimming phase increases.

Effect of colony orientation on growth

Orientation of developing colonies significantly affected growth in *B. neritina* (Table I; Fig. 3), presumably by influencing the amount of siltation the colonies encountered. Colonies on the upper surfaces of the plates, which experienced a higher concentration of silt particles, grew more slowly. The hypothesis that the additional particles interfered with feeding is supported by evidence

from colonies of the intertidal bryozoan *Flustrellidra hispida*. In that species, the concentration of inorganic suspended particulate matter (*i.e.*, silt) is inversely related to the number of autozooids actively feeding (Best and Thorpe, 1996). A colony with fewer feeding autozooids is likely to capture less food and consequently have less energy available for growth and reproduction. Sedimentation has also been shown to be a significant source of mortality in newly settled solitary ascidians (Young and Chia, 1984).

That colonies on the undersides of surfaces grow significantly larger than those on the upper surfaces suggests that facing downward is beneficial. Many invertebrate larvae are known to settle and metamorphose in environments that favor the chances of adult survival (Olson, 1983; Young and Chia, 1985; Walters and Wethey, 1991; Walters, 1992; Hurlbut, 1993). In the field, *B. neritina* colonies are most often found growing on the undersides of objects and ledges. Whether this distribution is the result of larval behavior, differential postmetamorphic mortality, or some combination of the two has not been explicitly investigated. However, certain larval behaviors may, in part, account for the patterns observed in the field. Larvae of *B. neritina* settle preferentially on the undersides of plates in the field, and they also settle in shaded areas (Ryland, 1977; Table II). At the time of attachment, larvae settle such that the incipient zooid and the resultant colony face away from light (McDougall, 1943). Under natural conditions with light from above, the colony is oriented with its frontal surface and lophophore facing away from the water surface; thus, the colony is shielded from the downward flux of particulate matter. Not all behaviors produce this result, however. Colonies of *B. avicularia* and *B. neritina* show a positive phototropism (Aymes, 1956; Schneider, 1959), which, according to the results of the current study, would retard growth, since the colonies would grow frontal surface up.

Orientation did not significantly affect growth in the competition experiment, which is not surprising in that orientation in this experiment did not expose colonies to different amounts of siltation. All colonies were shielded from sedimentation, and no sediment accumulated on the surfaces where colonies were growing. One factor not controlled for in this experiment was UV radiation. Although UV light has the potential to affect growth, the overall exposure for any colony in the experiment was minimal because none of the replicates were ever exposed to direct sunlight.

Effect of the presence of a conspecific colony on growth and reproduction

The adjacency of a conspecific colony (*i.e.*, a potential competitor) did not significantly affect growth and repro-

duction (Table II). Either postmetamorphic competitive ability is not compromised by increased duration of larval swimming or the individuals did not experience a limiting resource and were not subjected, therefore, to a competitive situation. *A priori*, the former reason appears less satisfactory given that lophophore size decreases significantly as a function of larval swimming duration (Wendt, 1996) and that smaller lophophores generate currents with lower velocities (Best and Thorpe, 1986). Both lophophore size and current velocity can influence interactions as colonies grow and compete for space and food (Buss, 1979). The more likely explanation is that individuals did not experience a limited supply of food. The effects of inter- and intraspecific competition in the context of increased duration of larval swimming remain unresolved.

Interaction between orientation and competition

In the competition experiment, neither competition nor orientation as main factors had a significant effect on growth and reproduction. However, there was a significant interaction between these factors ($F = 7.6$, $P = 0.006$ for brood chambers; $F = 6.5$, $P = .01$ for autozooids), which suggests that some combination of orientation and competition may result in reduced growth and reproduction. *Ad hoc* analysis showed that in 4 out of 5 cases, individuals that faced competition and were oriented upward (*i.e.*, had a light siltation load in this experiment) had, on average, fewer zooids, brood chambers, and bifurcations. This result indicates that competition and upward orientation acting individually were not strong enough factors to reduce growth and reproduction, but that in concert they may compromise colony fitness.

Mechanisms of action

The observed difference in the rates of autozooid budding is probably a result of a delay in the time to first bud, because the increased larval swimming period undoubtedly uses energy that would otherwise go to form the first autozooid. Any energetic deficiency of the ancestrula should not persist, however, so the growth rate should approach normal by the time the first several buds have formed. The difference in the quantity and production rate of brood chambers between 1-h and 24-h colonies is enigmatic. The difference is unlikely to result solely from the energetic deficiency caused by a lengthened period of larval swimming. One other mechanism that might play a part in producing these long-term effects is interspecific competition between bryozoans and stalked protozoans (*e.g.*, *Canthidium* sp., *Zoothanium* sp., *Vorticella* sp.). Unfortunately it was impossible to exclude these pervasive interspecific competitors, which colonized the surfaces of colonies. Consequently, all conditions had a background of interspecific competition and

there could be some difference in interspecific competitive ability of 1-h and 24-h colonies. An alternative explanation suggested by Pechenik *et al.* (in press) is that certain gene products transcribed early in development may be needed for organogenesis and that certain environmental stresses encountered in larval life may interfere with transcriptional or translational processes. Furthermore, it is well known that environmental stress can damage populations of cells and even entire organs during development. In any case, it seems that the effects observed in *B. neritina* may not be attributed entirely to energetic causes.

Effect of larval dispersal ability on species evolution

Taylor (1988) proposed that the major radiation of cheilostome bryozoans 150 million years ago was in part due to the evolution of nonfeeding larvae (like those of *B. neritina*), which severely limited the dispersal of these species. In general, species with this type of larva (short-lived, aplanktotrophic) have lower gene flow between subpopulations—and thus a greater subpopulation genetic structure—than species with long-lived, planktotrophic larvae (Palumbi, 1994). My results support Taylor's hypothesis by demonstrating that individuals of *B. neritina* (and probably of all bryozoans with aplanktotrophic larvae) incur substantial lethal and nonlethal costs after relatively short periods of larval swimming (hours to days). These costs limit the dispersal of bryozoans with aplanktotrophic larvae and may contribute significantly to subpopulation genetic structure. On evolutionary time scales, these costs and their consequences have probably played a central role in speciation within the Bryozoa.

Acknowledgments

I thank Sherry Reed, Hugh Reichardt, and Dr. Mary E. Rice, all of the Smithsonian Marine Station at Fort Pierce, Fort Pierce, Florida, for their assistance in carrying out this research. Colleen Cavanaugh, Peter Goss, Ed Seling, and Robert Woollacott (all of Harvard University) provided thoughtful discussions and comments which greatly improved the study. I thank Wendy Lynn Wendt for editing the manuscript. This research was supported by a Smithsonian Fellowship and by a Grant-in-Aid of Research from Sigma Xi to Dean E. Wendt. This paper is contribution #448 to the Smithsonian Marine Station at Fort Pierce, Fort Pierce, Florida.

Literature Cited

- Audo, M. C., T. M. Mann, T. L. Polk, C. M. Loudenslager, W. J. Diehl, and R. Altig. 1995. Food deprivation during different periods of tadpole (*Hyla chrysoscelis*) ontogeny affects metamorphic performance differently. *Oecologia* 103: 518–522.

- Aymes, Y. 1956. Croissance phototropique chez les Bryozoaires du genre *Bugula*. C. R. Hebd. Seances Acad. Sci. **242**: 1237–1238.
- Best, M. A., and J. A. Thorpe. 1986. Effects of food concentration on feeding current velocity in six species of marine Bryozoa. *Mar. Biol.* **93**: 255–262.
- Best, M. A., and J. A. Thorpe. 1996. The effect of suspended particulate matter (silt) on the feeding activity of the intertidal ctenostomate bryozoan *Flutrellidra hispida* (Fabricius). Pp. 39–45 in *Bryozoa in Space and Time*, D. P. Gordon, A. M. Smith, and J. A. Grant-Mackie, eds. Colorographic International, Wellington, New Zealand.
- Buss, L. W. 1979. Bryozoan overgrowth interaction—the interdependence of competition for space and food. *Nature* **281**: 475–477.
- Chia, F.-S. 1989. Differential larval settlement of benthic marine invertebrates. Pp. 3–12 in *Reproduction, Genetics, and Distribution of Marine Organisms*, J. S. Ryland and P. A. Tyler, eds. Olsen & Olsen, Fredensborg, Denmark.
- Crisp, D. J. 1984. Overview of research on marine invertebrate larvae, 1940–1980. Pp. 103–125 in *Marine Biodeterioration: An Interdisciplinary Study*, J. D. Costlow and R. C. Tipper, eds. Naval Institute Press, Annapolis, Maryland.
- Denlinger, D. L. 1981. Basis for a skewed sex ratio in diapause-destined flesh flies. *Evolution* **34**: 1247–1248.
- Ebert, T. A., and M. P. Russell. 1994. Allometry and model II non-linear regression. *J. Theor. Biol.* **168**: 367–372.
- Hadfield, M. G. 1978. Metamorphosis in marine molluscan larvae: an analysis of stimulus and response. Pp. 165–175 in *Settlement and Metamorphosis of Marine Invertebrate Larvae*, F.-S. Chia and M. E. Rice, eds. Elsevier North-Holland, New York.
- Havenhand, J. N. 1995. Evolutionary ecology of larval types. Pp. 79–122 in *Ecology of Marine Invertebrate Larvae*, L. R. McEdward, ed. CRC Press, Boca Raton, Florida.
- Highsmith, R. C., and R. B. Emlet. 1986. Delayed metamorphosis: effect on growth and survival of juvenile sand dollars (Echinoidea: Clypeasteroidea). *Bull. Mar. Sci.* **39**: 347–361.
- Hunter, E., and N. Fusetani. 1996. Studies of the effects of larval swimming time on settlement, metamorphosis, and post-larval development of *Bugula neritina* (Cheilostomatida). Pp. 139–148 in *Bryozoa in Space and Time*, D. P. Gordon, A. M. Smith, and J. A. Grant-Mackie, eds. Colorographic International, Wellington, New Zealand.
- Hurlbut, C. J. 1993. The adaptive value of larval behavior of a colonial ascidian. *Mar. Biol.* **115**: 253–262.
- McCormick, M. I., and B. W. Molony. 1992. Effects of feeding history on the growth characteristics of a reef fish at settlement. *Mar. Biol.* **114**: 165–173.
- McDougall, K. D. 1943. Sessile marine invertebrates at Beaufort, North Carolina. *Ecol. Monogr.* **13**: 321–374.
- Morgan, S. G. 1995. Life and death in the plankton: larval mortality and adaptation. Pp. 279–321 in *Ecology of Marine Invertebrate Larvae*, L. R. McEdward, ed. CRC Press, Boca Raton, Florida.
- Olson, R. R. 1983. Ascidian-Prochloron symbiosis: the role of larval photoadaptation in midday larval release and settlement. *Biol. Bull.* **165**: 221–240.
- Orellana, M. R., and J. M. Cancino. 1991. The effects of delaying larval settlement on metamorphosis and early colonial growth in *Celleporella hyalina* (Bryozoa: Cheilostomata). Pp. 309–316 in *Bryozoa Living and Fossil*, F. P. Bigley, ed. Bull. Soc. Sci. Nat. Quest. Fr., Mém. HS1, Saint-Herblain, Nantes, France.
- Nielsen, C. 1981. On morphology and reproduction of *Hippodiplosia insculpta* and *Fenestulina malusii* (Bryozoa, Cheilostomata). *Ophelia* **20**: 91–125.
- Palumbi, S. R. 1994. Genetic divergence, reproductive isolation, and marine speciation. *Annu. Rev. Ecol. Syst.* **25**: 547–572.
- Pawlik, J. R. 1992. Chemical ecology of marine invertebrates. *Oceanogr. Mar. Biol. Annu. Rev.* **30**: 273–335.
- Pechenik, J. A. 1990. Delayed metamorphosis of benthic marine invertebrates: Does it occur? Is there a price to pay? *Ophelia* **32**: 63–94.
- Pechenik, J. A., and T. R. Cerulli. 1991. Influence of delayed metamorphosis on survival, growth, and reproduction of the polychaete *Capitella* sp. 1. *J. Exp. Mar. Biol. Ecol.* **151**: 17–27.
- Pechenik, J. A., and L. S. Eyster. 1989. Influence of delayed metamorphosis on the growth and metabolism of young *Crepidula fornicata* (Gastropoda) juveniles. *Biol. Bull.* **176**: 14–24.
- Pechenik, J. A., D. Rittschof, and A. R. Schmidt. 1993. Influence of delayed metamorphosis on survival and growth of juvenile barnacles *Balanus amphitrite*. *Mar. Biol.* **115**: 287–294.
- Pechenik, J. A., J. N. Jarret, and D. E. Wendt. Metamorphosis is not a new beginning. *BioScience* (in press).
- Roughgarden, J., S. Gaines, and H. Possingham. 1988. Recruitment dynamics in complex life cycles. *Science* **241**: 1460–1466.
- Rumrill, S. S. 1990. Natural mortality of marine invertebrate larvae. *Ophelia* **32**: 163–198.
- Ryland, J. S. 1977. Taxes and tropisms of bryozoans. Pp. 411–436 in *Biology of Bryozoans*, R. M. Woollacott and R. L. Zimmer, eds. Academic Press, New York.
- Scheltema, R. S. 1974. Biological interactions determining larval settlement of marine invertebrates. *Thalassia Jugosl.* **10**: 263–296.
- Schneider, D. 1959. Der Aufbau der *Bugula*-tierstocke und seine Beeinflussung durch Aussenfaktoren. *Biol. Zentbl.* **78**: 250–283.
- Strathmann, R. R. 1985. Feeding and nonfeeding larval development and life-history evolution in marine invertebrates. *Annu. Rev. Ecol. Syst.* **16**: 339–361.
- Strathmann, R. R. 1993. Hypotheses on the origins of invertebrate larvae. *Annu. Rev. Ecol. Syst.* **24**: 89–117.
- Taylor, P. D. 1988. Major radiation of cheilostome bryozoans: triggered by the evolution of a new larval type? *Hist. Biol.* **1**: 45–64.
- Vance, R. R. 1973. On reproductive strategies in marine bottom invertebrates. *Am. Nat.* **107**: 353–361.
- Walters, L. J. 1992. Post-settlement success of the arborescent bryozoan *Bugula neritina* (L.): the importance of structural complexity. *J. Exp. Mar. Biol. Ecol.* **164**: 55–71.
- Walters, L. J., and D. S. Wetthey. 1991. Settlement, refuges, and adult body form in colonial marine invertebrates: a field experiment. *Biol. Bull.* **180**: 112–118.
- Wendt, D. E. 1996. Effect of larval swimming duration on success of metamorphosis and size of the ancestrular lophophore in *Bugula neritina* (Bryozoa). *Biol. Bull.* **191**: 224–233.
- Wendt, D. E., and R. M. Woollacott. 1995. Induction of larval settlement by KCl in three species of *Bugula* (Bryozoa). *Invertebr. Biol.* **114**: 345–351.
- Woollacott, R. M., J. A. Pechenik, and K. M. Imbalzano. 1989. Effects of duration of larval swimming period on early colony development in *Bugula stolonifera* (Bryozoa: Cheilostomata). *Mar. Biol.* **102**: 57–63.
- Wray, G. A. 1995. Evolution of larvae and developmental modes. Pp. 413–448 in *Ecology of Marine Invertebrate Larvae*, L. R. McEdward, ed. CRC Press, Boca Raton, Florida.
- Young, C. M., and F.-S. Chia. 1981. Laboratory evidence for delay of larval settlement in response to a dominant competitor. *Int. J. Invertebr. Reprod.* **3**: 221–226.
- Young, C. M., and F.-S. Chia. 1984. Microhabitat-associated variability in survival and growth of subtidal solitary ascidians during the first 21 days after settlement. *Mar. Biol.* **81**: 61–68.
- Young, C. M., and F.-S. Chia. 1985. An experimental test of shadow response function in ascidian tadpoles. *J. Exp. Mar. Biol. Ecol.* **85**: 165–175.

Structural Strengthening of Urchin Skeletons by Collagenous Sutural Ligaments

OLAF ELLERS¹, AMY S. JOHNSON^{2,*}, AND PHILIP E. MOBERG³

¹*Section of Evolution and Ecology, Division of Biological Sciences, University of California, One Shields Ave., Davis, California 95616;* ^{2,*}*Biology Department, Bowdoin College, Brunswick, Maine 04011;* and ³*Marine Biology Research Division, Scripps Institution of Oceanography, University of California, San Diego, La Jolla, California 92093-0202*

Abstract. Sea urchin skeletons are strengthened by flexible collagenous ligaments that bind together rigid calcite plates at sutures. Whole skeletons without ligaments (removed by bleaching) broke at lower apically applied forces than did intact, fresh skeletons. In addition, in three-point bending tests on excised plate combinations, sutural ligaments strengthened sutures but not plates. The degree of sutural strengthening by ligaments depended on sutural position: in tensile tests, ambital and adapical sutures were strengthened more than adoral sutures. Adapical sutures, which grow fastest, were also the loosest, suggesting that strengthening by ligaments is associated with growth. In fed, growing urchins, sutures overall were looser than in unfed urchins. Looseness was demonstrated visually and by vibration analysis: bleached skeletons of unfed urchins rang at characteristic frequencies, indicating that sound traveled across tightly fitting sutures; skeletons of fed urchins damped vibrations, indicating loss of vibrational energy across looser sutures. Furthermore, bleached skeletons of fed urchins broke at lower apically applied forces than bleached skeletons of unfed urchins, indicating that the sutures of fed urchins had been held together relatively loosely by sutural ligaments. Thus, the apparently rigid dome-like skeleton of urchins sometimes transforms into a flexible, jointed membrane as sutures loosen and become flexible during growth.

Introduction

Animal skeletons commonly consist of rigid ossicles connected by flexible ligaments. In this design, rigid ele-

ments resist compression and bending, whereas flexible elements resist tension and allow flexion. Vertebrate limb joints and echinoderm skeletons are examples of this design. Echinoderm skeletons are composed of calcite ossicles and collagenous connective tissues in a ratio that differs among taxa (Moss and Meehan, 1967). In sea cucumbers, for instance, collagenous tissues predominate, whereas in most sea urchins, calcite plates predominate. In the current study, we investigate the structural role of the collagenous ligaments that bind together the calcite plates in urchin skeletons.

The perforated calcite plates are attached to each other at sutures by ligaments (Fig. 1) that wrap around calcite rods (trabeculae), thus sewing together adjacent plates (Moss and Meehan, 1967). In addition, trabeculae project from one plate into holes in the adjacent plates, thus interlocking the plates. Ligaments are present to various degrees depending on the species and on the position of a suture on an urchin (Telford, 1985a). For instance, meridional (= vertical or radial or zig zag) sutures tend to have more ligaments than do circumferential (= horizontal or hoop) sutures. Also, some regions of the skeleton have relatively many sutures and smaller plates. For instance, the ambulacral regions (where the tube foot rows are located), are composed of many small plates (one plate per tube foot). In contrast, the interambulacral regions have larger plates and fewer sutures. The skeletal structure is completed by the peristomial membrane, which is attached at the oral margin. This membrane is a tough but flexible collagenous tissue (sometimes with calcite ossicle inclusions) that bridges the gap between the Aristotle's lantern (or jaw) and the skeleton (Wilkie *et al.*, 1993).

Urchin skeletons grow both by the accretion of calcite

Received 30 January 1998; accepted 12 June 1998.

* To whom correspondence should be addressed. E-mail: ajohnson@polar.bowdoin.edu

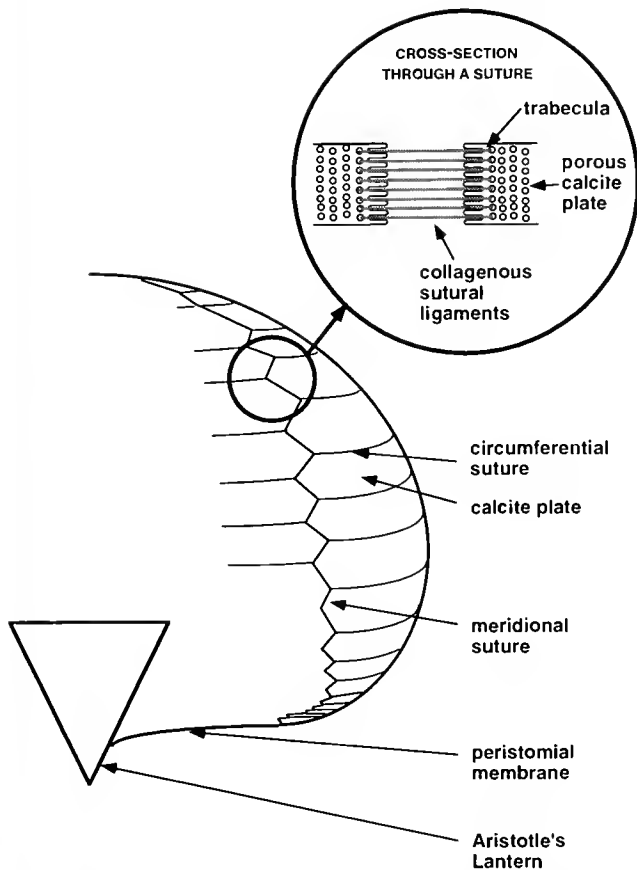


Figure 1. Schematic of interambulacral suture geometry and sutural ligament attachment. Interambulacral, meridional, and circumferential sutures are illustrated. Ligaments bind together adjacent plates (magnified inset of cross-section of a suture).

at the edges and faces of the plates and by the addition of new plates at the apex (Deutler, 1926). Initially apical, new plates gradually migrate adorally during growth. Skeletal plates may show seasonal or yearly growth rings that reflect changes in growth rate (Gage, 1991, 1992a, b) or spurts of growth (Pearse and Pearse, 1975). Urchins may also shrink under conditions of lowered food availability or overcrowding, as observed, for example, in *Diadema antillarum* (Levitan, 1988), and in *Strongylocentrotus purpuratus* (Ebert, 1967). In *Heliocidaris erythrogramma*, shrinkage is associated with diminution of sutural gaps (Constable, 1993).

That sutural ligaments might strengthen the skeleton was suggested in a taphonomic study in which decomposed urchin skeletons disarticulated at sutures and broke at lower forces than did undecomposed urchin skeletons (Kidwell and Baumiller, 1990). On the basis of histological and morphological evidence, sutural ligaments were interpreted as "stress-breakers" that evenly distribute stresses and thus contribute to the structural integrity of echinoid skeletons (Moss and Meehan, 1967). In other

theoretical and experimental studies of the structural mechanics of echinoid skeletons (Telford, 1985b; Dafni, 1986, 1988; Baron, 1991a, b; Ellers, 1993; Philippi and Nachtigall, 1996), the possible structural role of the sutural ligaments has not been a focus. Nor has a possible structural role for the peristomial membrane been tested. Although this membrane is not flexurally stiff relative to the calcite plates, it might provide tensile reinforcement to the skeleton, as do steel tensile reinforcement rods across the span of concrete bridge arches.

To determine the relative contributions of skeletal components (sutural ligaments, peristomial membrane, and calcite plates) to the structural strength of urchin skeletons, we measured breaking forces of entire skeletons and excised portions of skeletons of *S. purpuratus*, with soft tissues either present or removed. To evaluate possible sutural changes during growth, we used breaking and vibration tests as well as visual inspection to compare the looseness of sutures in fed, growing specimens of *S. purpuratus* with that in unfed, nongrowing specimens.

Materials and Methods

Testing device

A motor-driven device and force beam were used to apply a load at a rate of $200 \mu\text{m s}^{-1}$ to various specimens until they broke. The force signal was amplified, digitized (12-bit, 100 Hz), and stored in a computer. Error in the force measurements was $< \pm 0.1 \text{ N}$. Prior to breaking tests, the height and diameter of all urchins were measured to $\pm 0.1 \text{ mm}$ with calipers.

Crushing of whole skeletons

Strongylocentrotus purpuratus was collected subtidally at Bodega Bay, California. Urchins were assigned at random to three groups, each prepared for crushing tests in a different way: (i) live unaltered, *i.e.*, with peristomial membrane and sutural ligaments intact; (ii) peristomial membrane and Aristotle's lantern removed, *i.e.*, with sutural ligaments intact; and (iii) bleached and air-dried, *i.e.*, with no soft tissues intact. The bleaching chemical was 5.25% sodium hypochlorite. Sufficient bleach was added until all soft tissues had been dissolved and washed away. The prepared skeletons were crushed along the oral-aboral axis.

Three-point breakage of plates and meridional sutures

S. purpuratus was collected intertidally at Pillar Point, California. Urchins were kept in a 12°C recirculating seawater system for less than a week prior to mechanical tests.

Pieces of skeleton consisting of various combinations of plates and sutures were prepared for mechanical testing as follows. From each urchin, two homonomous, ambital, interambulacral plates were cut out using a Dremel tool.

As a control, one plate was bleached overnight prior to testing, and the other plate was tested to breakage while fresh (held for less than 1 h in 12°C seawater prior to testing). In addition, two sets of homonomous, three-plate combinations, joined to each other at a meridional, ambital, interambulacral suture were cut out. Again, one set was bleached overnight prior to testing and the other was tested to breakage while fresh.

For mechanical testing, each test piece was placed on the base platform, which was coated lightly with mineral oil to reduce friction. Each test piece formed a shallow arch and, as the piece was driven into the platen to which the load cell was attached, force was applied by a cylindrical rod (diameter 1 mm) to the apex of the arch, till breakage occurred. Thickness and width at the broken section were measured to ± 0.1 mm using calipers. Breaking forces were compared to determine if there was a significant reduction in breaking force after bleaching. Because of the complex geometry of the beams, we compared breaking forces of homonomous specimens paired for size rather than comparing estimated stresses.

Tensile tests of circumferential sutures

S. purpuratus was obtained from a subtidal population near Bodega Bay. One group was bleached and air-dried before testing; the other group was tested fresh. Groups of interambulacral plates were excised from three regions on the skeleton: adapical, ambital, and adoral. The ambital region was defined to be four plates wide, centered at the widest diameter of the urchin. The adapical region was defined as starting three plates above the uppermost ambital plate. The adoral region was defined as starting two plates below the lowest ambital plate.

For each tensile test, the strength of a circumferential suture was measured. Each test piece was excised and consisted of a column of four plates. The test piece was attached to the testing device using strands of copper wire that were looped through holes (1.2 mm in diameter) drilled in the test piece. The holes in the test piece were located in the middle of the plates immediately adjacent to the suture being tested. Thickness and length of the cross-sectional area being broken were measured to ± 0.1 mm using calipers. These measurements were used to calculate a nominal stress; nominal because the porous nature of the plates and sutures makes it impractical to measure an actual cross-sectional area.

Diet and sutural gaps

S. purpuratus was collected subtidally near Bodega Bay and kept for one year in flow-through seawater aquaria at Bodega Marine Laboratory. Urchins were assigned randomly to one of two diet treatments. The fed group received seaweed *ad libitum* (180 kg over 1 year, or an average of

5 g per urchin per day), unfiltered seawater, and normal room light. The starved group was given no seaweed, filtered incoming water, and reduced light, which reduced algal growth on the aquarium walls. At the start of the experiment, all urchins were marked with a tetracycline label as in Ebert (1982). After one year the urchins were sacrificed and bleached and the tetracycline label was inspected. Skeletal diameter (± 0.5 mm) and weight (± 0.1 g) were measured, and the sutures were visually inspected.

To quantify sutural looseness, vibrational properties of the skeletons were measured as follows. A 3.5-g weight was hung on the end of a string attached to a crossbeam hanging above a rubber-lined box of dimensions 28 by 18 by 12 cm. An urchin skeleton's vibrational properties were tested by placing the skeleton in the box and positioning the cross-beam so that the weight hung vertically down to a point just 2 mm from the ambitus. The weight was then lifted to a 30° angle to the vertical and released. The weight swung and hit the skeleton, causing a sound that was recorded with a microphone and analyzed with spectral and cross-correlation procedures. The pattern of frequencies at which a particular urchin vibrated was analyzed statistically with respect to diet, urchin diameter, and skeletal strength under apical loading.

Results

Crushing of whole skeletons

Removal of the peristomial membrane had no effect on diameter-specific breaking forces of skeletons with intact sutural ligaments (Fig. 2). A simultaneous regres-

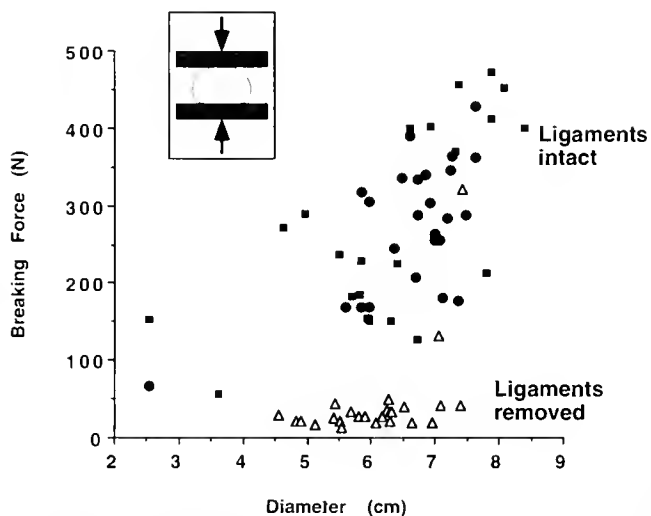


Figure 2. Breaking force of *Strongylocentrotus purpuratus* skeletons as a function of diameter. Bleached skeletons (open triangles) broke at much lower forces than did fresh skeletons with ligaments intact (solid circles). Removing the peristomial membrane from fresh intact skeletons (solid squares) did not decrease the strength of the skeleton relative to intact skeletons.

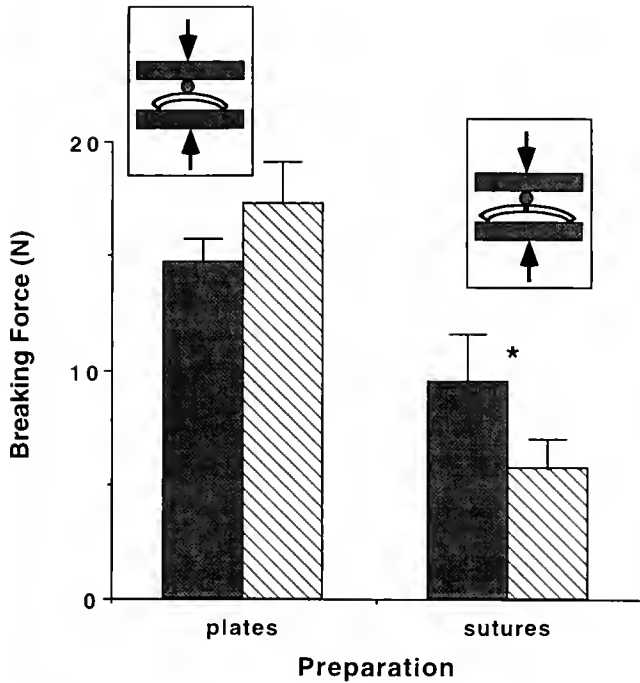


Figure 3. In three-point bending, bleached (hatched) meridional sutures broke at significantly lower forces than did fresh (solid) meridional sutures, whereas bleaching did not affect the breaking force of plates. Asterisk indicates significant difference. Error bars indicate one standard error.

sion with two slopes and two intercepts did not explain significantly more variation than did a single slope with a single intercept ($P = 0.5$, F test, d.f. = 1,44; regression with dummy variables; Weisberg, 1980). For all skeletons with intact ligaments: breaking force = $-79 + 55$ diameter, where diameter is in centimeters and force is in newtons; the intercept was not significantly different from zero, but the slope was significantly different from zero ($P < 0.001$, F test, d.f. = 1,45, $r^2 = 0.42$).

In contrast, with the exception of two high outliers, bleached skeletons had much lower breaking strength than skeletons with intact ligaments (Fig. 2). When data from all urchins with intact ligaments were pooled and the two outliers were excluded, simultaneous regression of force on diameter showed that a model with two slopes and two intercepts for the intact versus removed ligaments explained significantly more variation than did a model with one slope and two intercepts ($P < 0.05$, F test, d.f. = 1,66; regression with dummy variables; Weisberg, 1980). Further, among bleached urchins, there was no significant variation of breaking force with diameter; neither intercept nor slope were significantly different from zero ($P = 0.1$, F test, d.f. = 1,21).

Three-point breakage of plates and meridional sutures

The urchins ranged in diameter from 4.1 to 7.3 cm, with only one being more than 5.3 cm. Over this limited

size range, breaking force of test pieces was independent of urchin diameter, height, or nominal cross-sectional area (plate or suture thickness multiplied by plate or suture width) (linear regressions, probabilities of slope equal to zero ranging between 0.17 and 0.90). Fresh sutures broke at a higher mean force than did bleached sutures ($P < 0.05$, Mann-Whitney U test, 13 pairs of sutures), whereas fresh and bleached plates broke at similar forces ($P = 0.5$, Mann-Whitney U test, 14 pairs of plates) (Fig. 3). (We used the nonparametric U test instead of a paired t test to compare bleached and fresh specimens because the differences between the breakage forces of the paired sutures were not normally distributed; Shapiro-Wilk W test, $P < 0.003$).

Tensile tests of circumferential sutures

The nominal breaking stress of circumferential sutures (Fig. 4) was significantly different (2-way ANOVA) by position of the suture on the skeleton ($P < 0.0001$, d.f. = 2,95) and in bleached versus fresh sutures ($P < 0.0001$, d.f. = 1,95); furthermore, there was an interaction between position and bleaching ($P < 0.0001$, d.f. = 2,95). Grouping all positions, the 54 bleached sutures had a lower nominal breaking stress than the 47 fresh sutures ($P \leq 0.0001$, Mann-Whitney U test). Also, at each position bleached sutures had a lower nominal breaking stress than fresh sutures (all $P < 0.05$, Mann-Whitney U tests).

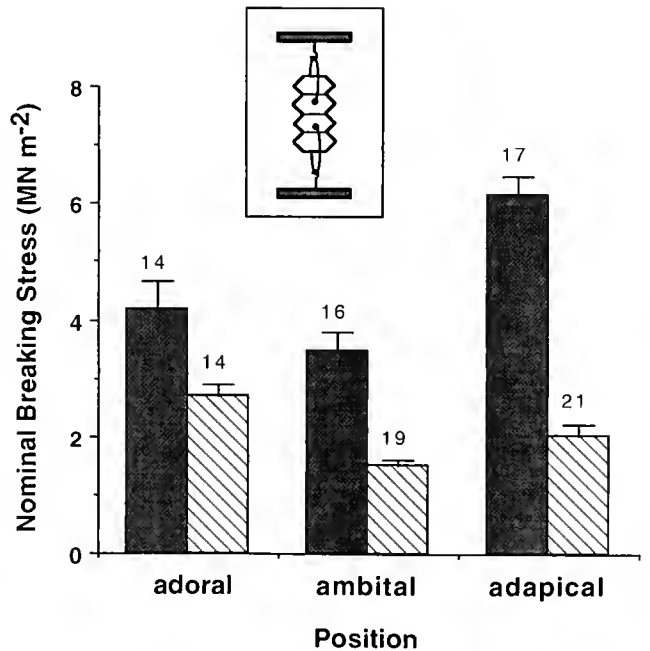


Figure 4. At each position, nominal breaking stress was significantly greater for fresh (solid) than for bleached (hatched) circumferential sutures. Error bars indicate one standard error. Numbers shown are sample sizes.

Among bleached sutures, position had a significant effect ($P \leq 0.0001$, 1-way ANOVA, d.f. = 2,53), with all positions differing significantly from all other positions (all $P < 0.05$, Fisher PLSD). Among fresh sutures, position also had a significant effect ($P \leq 0.0001$, 1-way ANOVA, d.f. = 2,26), with adapical sutures being significantly stronger than ambital or adoral sutures ($P < 0.05$, Fisher PLSD).

Diet and sutural gaps

At the edges of plates, the skeletons of all fed urchins showed tetracycline marks (visualized under ultraviolet light) plus a band of new unmarked calcite added at the edge of plates. In contrast, in the skeletons of unfed urchins

the tetracycline mark could not be found or was only dimly detectable at the very edge of plates. In the unfed urchins in which a trace of tetracycline mark was detectable, no new calcite was visible around the tetracycline marks at the plate edges. Thus, fed urchins had grown, whereas unfed urchins had shrunk or maintained size during the year.

Fed urchins had wider sutural gaps than did unfed urchins (Fig. 5). In 23 of 99 fed urchins, the sutural gaps were large enough to be visible to the naked eye, and 14 of those 23 urchins fell apart (disarticulated) under their own skeletal weight when bleached. Sutural gaps were most prominent in adapical regions. For example, in the 9 urchins with visible gaps, but in which the skeletons did not disarticulate, the visibly gaping sutures always

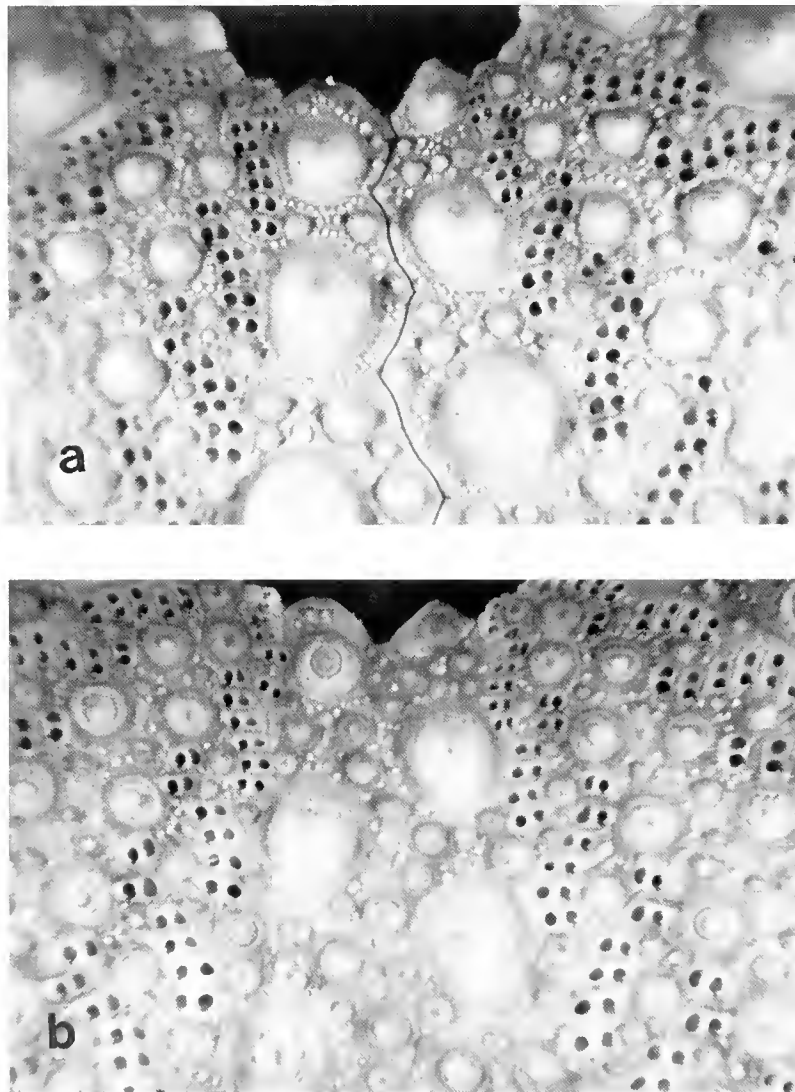


Figure 5. A gap is visible in the apical sutures of skeletons of many well-fed (A) but of no unfed (B) urchins. Typically, well-fed urchins have looser sutures than do unfed urchins.

occurred above the ambitus; the most adapical plate rows tended to fall out of the skeleton, and vertically gaping sutures tended to be more widely gaped adapically. In contrast, the skeletons of the 100 unfed urchins did not fall apart when bleached and no sutural gaps were visible.

The looseness of the sutures of fed urchins was reflected in a smaller weight for a given diameter in comparison to unfed urchins (Fig. 6). A simultaneous regression of $\log[\text{weight}]$ on $\log[\text{diameter}]$ with two slopes and two intercepts does not explain significantly more variation than does a model with a single slope and two intercepts ($P = 0.7$, F test, d.f. = 1,195: regression with dummy variables; Weisberg, 1980). A model with one slope and two intercepts, however, does explain significantly more variation than a model with just a single slope and a single intercept ($P < 0.001$, F test, d.f. = 1,196. $r^2 = 0.9$; regression with dummy variables; Weisberg, 1980). Thus, the bleached skeletons of fed urchins had a significantly lower weight for a given diameter.

Another indication of sutural looseness in urchins is given by the frequency composition of the sound created when a bleached urchin skeleton vibrates after being struck by a weight (Fig. 7). Bleached skeletons of unfed urchins vibrated, or rang, at a series of discrete frequencies, which made a piny sound like a bell. In contrast, bleached skeletons of fed urchins vibrated for a shorter time at a broad range of frequencies without identifiable discrete frequency components, which makes a dull sound.

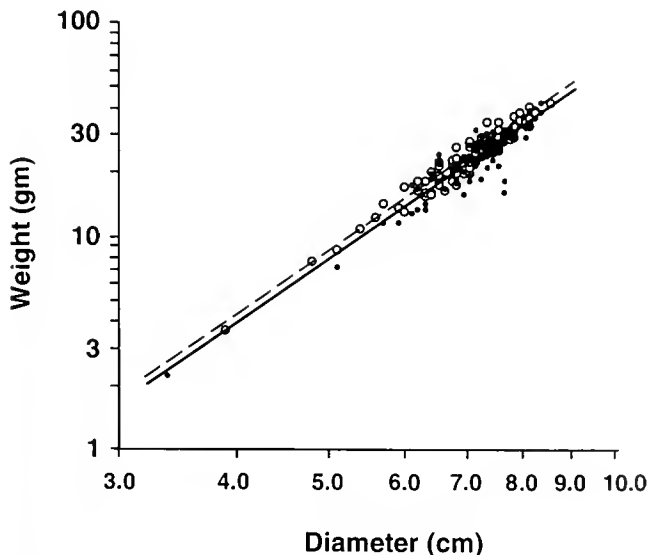


Figure 6. Fed urchins (solid points and line) have significantly lighter skeletons for a given diameter than do unfed urchins (open circles and dashed line). This difference is interpreted as reflecting the larger sutural gaps and general looseness of the plates of fed urchins in comparison to unfed urchins. Regression lines shown have equal slopes but different intercepts.

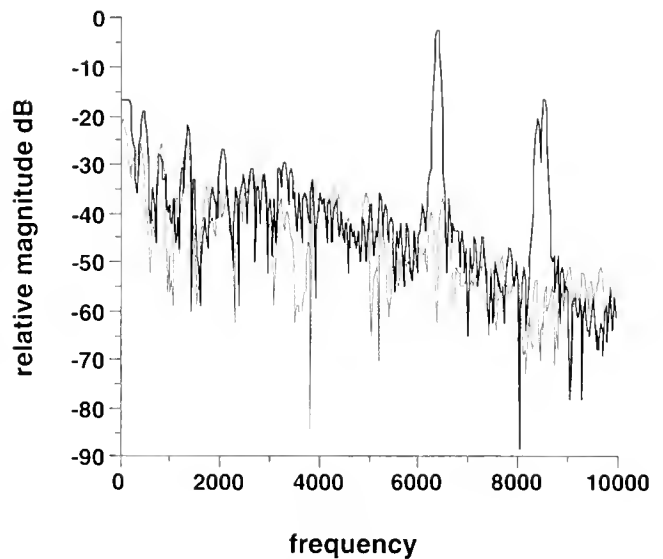


Figure 7. Characteristic frequency spectra of sounds emitted by vibrating, bleached urchin skeletons. Fed urchins ring or ping like a bell when struck; a skeleton-specific set of discrete frequencies of vibration are detectable (solid line). In contrast, unfed urchins emit a dull "thud"; no discrete frequencies are identifiable (dotted line).

For bleached skeletons of unfed urchins, the frequency spectrum is similar to that typical of three-dimensional vibrating objects such as drums or rectangular blocks (Kinsler *et al.*, 1982). The lowest of the identifiable frequency peaks is correlated with urchin diameter ($P \leq 0.0001$, correlation = -0.81 , $r^2 = 0.66$, $n = 100$, frequency = $-940 \text{ diameter} + 1.1 \times 10^4$, with diameter in centimeters and frequency in hertz). The negative correlation between frequency and diameter indicates that the size of the urchin skeleton determines some of the modes of vibration, and thus that vibrations are transmitted across sutures and throughout the skeleton. In contrast, bleached skeletons of fed urchins had no identifiable frequency peaks, thus indicating that vibrational energy was lost at loose sutures and that the structure as a whole did not vibrate.

Skeletal vibrations can be used as a measure of sutural looseness. The cross-correlation between the sound produced by a bleached skeleton and the predicted ringing frequency is a measure of looseness. The predicted ringing frequency is calculated using the empirical linear relationship between frequency and diameter given above. Bleached skeletons of 9 fed urchins that produced the qualitatively dullest sounds had lower cross-correlations ($P < 0.001$, U test) and lower breaking forces ($P < 0.001$, U test) than did 25 randomly chosen skeletons of fed urchins (Fig. 8). The 25 randomly chosen fed urchin skeletons had lower cross-correlations ($P < 0.01$, U tests) and lower breaking forces ($P < 0.01$, U tests) than did 25 randomly chosen unfed skeletons. Within the randomly

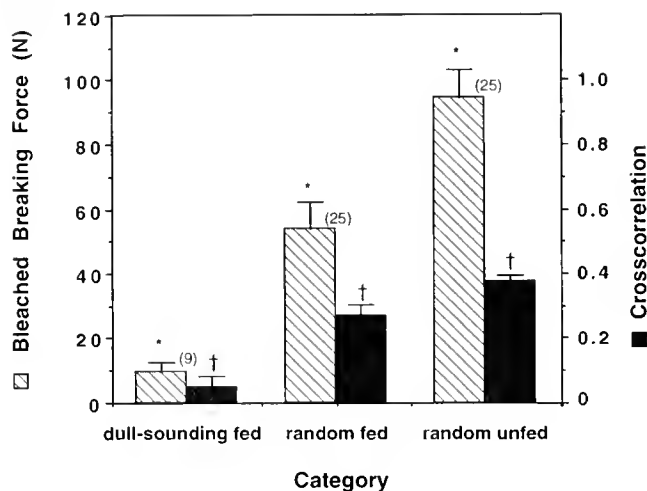


Figure 8. The qualitatively dullest sounding of the fed urchin skeletons had lower mean breaking force and cross-correlation than did randomly chosen fed urchin skeletons. Randomly chosen unfed urchin skeletons have significantly higher mean breaking force and cross-correlation than do randomly chosen fed urchin skeletons. The relationship between breaking force and cross-correlation indicate that loose sutures weaken bleached skeletons. Crosses indicate significant differences in cross-correlation, asterisks indicate significant differences in bleached breaking force.

chosen fed skeletons, breaking force was significantly correlated with the cross-correlation ($P \leq 0.01$, $r = 0.51$, $r^2 = 0.26$, $n = 25$); in contrast, there was no significant correlation between breaking force and cross-correlation for randomly chosen unfed urchin skeletons.

Discussion

Sutural ligaments strengthen urchin skeletons under a variety of loadings. Under apical loading, whole skeletons broke at higher, size-specific forces when ligaments were intact than when they were removed by bleaching (Fig. 2). In three-point bending, meridional interambulacral sutures with ligaments broke at higher forces than did paired sutures without ligaments (Fig. 3). And in circumferential interambulacral sutures with ligaments, sutures broke at higher nominal stresses than did sutures without ligaments (Fig. 4). The consistency of skeletal strengthening by ligaments, despite differences in imposed stresses, suggests that sutural ligaments reinforce urchin skeletons under natural loads as varied as crushing forces from crab claws, apical or lateral forces from waves, and forces generated when an urchin wedges itself in a crack.

The importance of sutural ligaments in strengthening an urchin's skeleton depended on urchin size. Smaller *Strongylocentrotus purpuratus* were strengthened less by ligaments than were larger ones (Fig. 2). Size-specific strengthening may be important across taxa as well; the echinoid *Echinocyamus pusillus*, which is the only species

reported to lack ligaments, is a very small echinoid (Telford, 1985b) growing to a typical maximum size of only about 1 cm in diameter. Sutural ligaments were present in all eight other regular and irregular echinoid genera surveyed (Moss and Meehan, 1967; Telford, 1985a), and are present (pers. obs.) in four Strongylocentrotidae (*S. purpuratus*, *S. droebachiensis*, *S. franciscanus*, and *Allocentrotus fragillis*), all of which grow to larger sizes.

The degree of structural strengthening by sutural ligaments depends on the position of a suture. The faster growing ambital and adapical sutures (Deutler, 1926) were strengthened more than slower growing adoral sutures (Fig. 4). The faster growing adapical sutures also had the largest sutural gaps (Fig. 5), and larger gaps are associated with more and longer ligaments (Telford, 1985a). Such differences in composition and properties of different skeletal regions can influence deformation, stress distribution, and breakage. For instance, interambulacral areas were slightly stiffer than ambulacral areas in *Echinus esculentus*, and that difference influenced deformations and bending stresses calculated using finite element analysis (Philippi and Nachtigall, 1996). The lower stiffness of ambulacra compared to interambulacra of *E. esculentus* might be attributable to the difference in the relative proportion of sutures and plates because ambulacral areas have a higher proportion of sutures. The material properties of different portions of the skeleton may generally depend on the relative area covered by sutures, especially gaping sutures with relatively more and longer ligaments.

Not only do the faster growing sutures (adapical and ambital) gape more than the slower growing (adoral) sutures on an individual urchin, but sutures on faster growing urchins are looser than corresponding sutures on non-growing urchins (Figs. 5–8). Similarly, in *S. franciscanus*, fed urchins develop looser sutures than starved urchins (pers. obs.).

The relationship between sutural looseness and growth has potential implications for interpretation of the taphonomy of fossil urchins and other echinoderms. Disarticulated skeletons have often been used to imply the species composition, biodiversity, and relative abundance of fossil assemblages of echinoderm species (e.g.: Gordon and Donovan, 1992; Nebelsick, 1996). In an attempt to identify taphonomic biases in such studies, the species-specific tendency to disarticulate has been estimated (Greenstein, 1991) and possible biases interpreted (Greenstein, 1992). Disarticulation times dependent on temperature have also been demonstrated and their taphonomic consequences explored (Kidwell and Baumiller, 1990). Our study adds another variable to these temperature- and species-specific effects. Specifically, the tendency to disarticulate depends on the growth status of a given urchin at the time of fossilization. Since looseness

is growth-rate dependent, taphonomic biases likely exist between faster and slower growing age classes as well as between faster and slower growing taxa.

In some urchins, differences in sutural gaping due to diet have been attributed to shrinkage of the starved urchins (Ebert, 1967; Levitan, 1988; Constable, 1993), but in *S. droebachiensis* we have observed that sutural gaping was due mainly to expansion of sutures in the fed group (Johnson, A. S., Bowdoin College, *et al.*, unpubl. data). In that study, we additionally observed that as fed urchins grew, the viscoelastic material properties of the sutures changed. Those changes were probably due to changes both in the degree of interlocking of trabeculae and in the material properties of the sutural ligaments. Similarly, material property changes in ligaments have been observed in the continuously growing teeth of sand dollars (Ellers and Telford, 1996) and sea urchins (Birenheide and Motokawa, 1996; Birenheide, *et al.*, 1996), in which the teeth are held in place on the jaw by dental ligaments. These dental ligaments soften periodically and enable a tiny muscle to advance the teeth (Ellers and Telford, 1997; Telford and Ellers, 1997). Thus, material property changes and rearrangements of ligaments occur during growth of echinoids.

Such viscoelastic properties of ligaments may be important in modeling the mechanical behavior of an urchin skeleton. They are important for three reasons. Firstly, as we demonstrated in the current study, the ligaments have a predominant role in providing structural strength, at least during times of growth. Secondly, as we demonstrated here, the gaping of the sutures varies during growth, and therefore the relative contribution of the calcite trabeculae and the ligaments to structural strength also varies during growth. Thirdly, the material properties of the ligaments may change during growth, or possibly over behavioral time spans. Therefore, time-dependent material behaviors such as creep and stress-relaxation must be considered in modeling the mechanics of urchin skeletons. Previous mechanical finite-element models have only considered more conventional measures such as stiffness (Baron, 1991b; Philippi and Nachtigall, 1996). Time-dependent properties of sutural ligaments could change very rapidly if they were mutable collagenous tissue (MCT) (Wilkie, 1996). MCT is a special tissue, known only in echinoderms, that is innervated and that can change material properties over behavioral time spans. Alternatively, sutural ligaments may change material properties over developmental time spans by reorganizing connective tissue constituents as is common in vertebrate connective tissues, *e.g.*, the cervix in late pregnancy (Winn *et al.*, 1993).

The flexibility of sutural joints resulting from sutural gaping and the predominant role of ligaments in growing urchins also has consequences for determining the shape

of urchin skeletons. The shape of a sea urchin's skeleton is closely approximated by a mathematical mechanical model that is more conventionally used to describe the shape of water droplets (Ellers, 1993). This model assumes that the droplet's surface, or urchin's skeleton, has zero flexural stiffness. That assumption seems initially unreasonable given that calcite plates are flexurally stiff, but the looseness of sutures during growth provides the flexibility assumed by the model. An urchin's skeleton, with its combination of flexurally stiff plates and more flexible sutures, thus behaves as a flexible jointed membrane during times of growth.

The calculation of urchin shapes (Ellers, 1993) also assumes that an urchin's skeleton behaves like a thin membrane in which bending stresses are negligible. A shell is conventionally considered "thin" if the ratio of the radius of curvature to the thickness is greater than 20. In *E. esculentus* that ratio is less than 20, and accordingly a finite-element model was used to calculate bending stresses in the skeleton of that species (Philippi and Nachtigall, 1996). Many urchins, however, have much thinner shells and correspondingly higher ratios, in which a thin membrane model is appropriate. Some urchins, such as *Allocentrotus fragillis*, have extremely thin shells. Others, such as the diadematoïd urchins *Astropyga pulvinata* and *Chaetodiadema pallidum*, are sufficiently thin-walled and loose-sutured that their skeletons deform by bending when touched lightly. Finally, the "soft-tested" echinothurioid urchins have numerous small, thin imbricate plates imbedded in a meshwork of collagenous ligaments and can deform and contort their skeleton flexibly. (They can even adjust their shape to fit in right angles and corners of an aquarium, pers. obs.) They have internal sheets of radial muscles (Tsuchiya and Amemiya, 1977) that control the bending of their flexible, thin-walled, membranous skeleton.

Thus, urchin skeletons can be viewed statically as a continuum of flexibility and thickness, from relatively rigid and thick-walled (*e.g.*, *Echinus*) to quite flexible and thin-walled (*e.g.*, echinothurioids). All urchin skeletons can be better understood dynamically as flexible, jointed membranes with varying degrees of flexibility and sutural looseness depending on growth stage.

Acknowledgments

Thanks to two anonymous reviewers who provided helpful suggestions; S. Keen, H. Leddy, and E. Pearson who critically read the manuscript; and S. Franklin and B. Lindsay who assisted with the experiments. This research was supported by grants from the University of California: Agricultural Research Station Grant #5134-H and a Bodega Marine Lab Travel Grant both to O. Ellers; as well as a President's Undergraduate Fellowship and a Howard Hughes SHARP Fellowship, both to P. Moberg.

Literature Cited

- Baron, C. 1991a.** What functional morphology cannot explain, a model of sea urchin growth and a discussion of the role of morphogenetic explanations in evolutionary biology. Pp. 471–488 in *The Unity of Evolutionary Biology, Vols. 1 & 2; Fourth International Congress of Systematic and Evolutionary Biology, College Park, Maryland, 1990*, E. C. Dudley, ed. Dioscorides Press, Portland, Oregon.
- Baron, C. J. 1991b.** The structural mechanics and morphogenesis of extant regular echinoids having rigid tests. Ph.D. thesis, University of California at Berkeley.
- Birenheide, R., and T. Motokawa. 1996.** To be stiff or to be soft—the dilemma of the echinoid tooth ligament. I. Morphology. *Biol. Bull.* **190**: 218–230.
- Birenheide, R., A. Tsuchi, and T. Motokawa. 1996.** To be stiff or to be soft—the dilemma of the echinoid tooth ligament. II. Mechanical properties. *Biol. Bull.* **190**: 231–236.
- Constable, A. J. 1993.** The role of sutures in shrinking of the test in *Helicoidaris erythrogramma* (Echinoidea: Echinometridae). *Mar. Biol.* **117**: 423–430.
- Dafni, J. 1986.** A biomechanical model for the morphogenesis of regular echinoid tests. *Paleobiology* **12**: 143–160.
- Dafni, J. 1988.** A biomechanical approach to the ontogeny and phylogeny of echinoids. Pp. 175–188 in *Echinoderm Phylogeny and Evolutionary Biology*, C. R. C. Paul and A. B. Smith, eds. Clarendon Press, Oxford.
- Deutler, F. 1926.** Über die Wachstum des Seeigelskeletts. *Zool. Jb. Abt. Anat. Ontog. Tier.* **48**: 119–200.
- Ebert, T. A. 1967.** Negative growth and longevity in the purple sea-urchin *Strongylocentrotus purpuratus* (Stimpson). *Science* **157**: 557–558.
- Ebert, T. A. 1982.** Longevity, life history, and relative body wall size in sea urchins. *Ecol. Monogr.* **52**: 353–394.
- Ellers, O. 1993.** A mechanical model of growth in sea urchins: predictions of shape and a developmental morphospace. *Proc. R. Soc. Lond. B* **254**: 123–129.
- Ellers, O., and M. Telford. 1996.** Advancement mechanics of growing teeth in sand dollars (Echinodermata, Echinoidea): a role for mutable collagenous tissue. *Proc. R. Soc. Lond. B* **263**: 39–44.
- Ellers, O., and M. Telford. 1997.** Muscles advance the teeth in sand dollars and other sea urchins. *Proc. R. Soc. Lond. B* **264**: 1525–1530.
- Gage, J. D. 1991.** Skeletal growth zones as age-markers in the sea urchin *Psammechinus miliaris*. *Mar. Biol.* **110**: 217–228.
- Gage, J. D. 1992a.** Growth bands in the sea urchin *Echinus esculentus*: results from tetracycline-mark recapture. *J. Mar. Biol. Assoc. UK* **72**: 257–260.
- Gage, J. D. 1992b.** Natural growth bands and growth variability in the sea urchin *Echinus esculentus*—results from tetracycline tagging. *Mar. Biol.* **114**: 607–616.
- Gordon, C. M., and S. K. Donovan. 1992.** Disarticulated echinoid ossicles in paleoecology and taphonomy: the last interglacial Fal-mouth formation of Jamaica. *Palaios* **7**: 157–166.
- Greenstein, B. J. 1991.** An integrated study of echinoid taphonomy: predictions for the fossil record of four echinoid families. *Palaios* **6**: 519–540.
- Greenstein, B. J. 1992.** Taphonomic bias and the evolutionary history of family Cidaridae (Echinodermata: Echinoidea). *Paleobiology* **18**: 50–79.
- Kidwell, S. M., and T. Baumiller. 1990.** Experimental disintegration of regular echinoids: roles of temperature, oxygen, and decay thresholds. *Paleobiology* **16**: 247–271.
- Kinsler, L. E., A. R. Frey, A. B. Coppers, and J. V. Sanders. 1982.** *Fundamentals of Acoustics*, 3rd Ed. John Wiley, New York.
- Levitan, D. R. 1988.** Density-dependent size regulation and negative growth in the sea urchin *Diadema antillarum* Philippi. *Oecologia* **76**: 627–629.
- Moss, M. L., and M. M. Meehan. 1967.** Satural connective tissues in the test of an echinoid *Arbacia punctulata*. *Acta Anat.* **66**: 279–304.
- Nebelsick, J. H. 1996.** Biodiversity of shallow-water red sea echinoids: implications for the fossil record. *J. Mar. Biol. Ass. UK* **76**: 185–194.
- Pearse, J. S., and V. B. Pearse. 1975.** Growth zones in echinoid skeleton. *Am. Zool.* **15**: 731–753.
- Philippi, U., and W. Nachtigall. 1996.** Functional morphology of regular echinoid tests (Echinodermata, Echinoidea): a finite element study. *Zoomorphology* **116**: 35–50.
- Telford, M. 1985a.** Domes, arches and urchins: the skeletal architecture of echinoids (Echinodermata). *Zoomorphology* **1105**: 114–124.
- Telford, M. 1985b.** Structural analysis of the test of *Echinocyamus pusillus* (O. F. Muller). Pp. 353–360 in *Fifth International Echinoderm Conference, Galway, Ireland, 1984*, B. F. Keegan and B. D. S. O'Connor, eds. Balkema, Rotterdam.
- Telford, M., and O. Ellers. 1997.** Tooth advancement muscles in the sand dollar, *Echinarachnius parma*. *Invert. Biol.* **116**: 255–261.
- Tsuchiya, T., and S. Amemiya. 1977.** Studies on the radial muscle of an echinothuriid sea-urchin, *Asthenosoma*—I. Mechanical responses to electrical stimulation and drugs. *Comp. Biochem. Physiol.* **57**: 69–73.
- Weisberg, S. 1980.** *Applied Linear Regression*, John Wiley, New York.
- Wilkie, I. C. 1996.** Mutable collagenous tissues: extracellular matrix as mechano-effector. Pp. 61–102 in *Echinoderm Studies 5*, M. Jan-goux and J. M. Lawrence, eds. Balkema, Rotterdam.
- Wilkie, I. C., M. D. C. Carnevali, and F. Andrietti. 1993.** Variable tensility of the peristomial membrane of the sea-urchin *Paracentrotus lividus* (Lamarck). *Comp. Biochem. Physiol.* **105A**: 493–501.
- Winn, R. J., M. B. O'day-Bowman, and O. D. Sherwood. 1993.** Hormonal control of the cervix in pregnant gilts IV. Relaxin promotes changes in the histological characteristics of the cervix that are associated with cervical softening during late pregnancy in gilts. *Endocrinology* **133**: 121–128.

Efferent Mechanisms of Discharging Cnidae: II. A Nematocyst Release Response in the Sea Anemone Tentacle

GLYNE U. THORINGTON AND DAVID A. HESSINGER

*Department of Physiology and Pharmacology, School of Medicine, Loma Linda University,
Loma Linda, California 92350*

Abstract. Feeding behavior in cnidarians is a sequence of coordinated responses beginning with nematocyst discharge. The nematocyst response produces prey capture by envenomating prey and attaching prey to the tentacle. The strength of attachment of discharged nematocysts to the tentacle is termed intrinsic adherence and is calculated from measurements of adhesive force. Following prey capture, the feeding response involves movement of the tentacles toward the mouth and mouth opening. For ingestion to occur, nematocysts attaching the prey to the tentacles must be released from the tentacle. A nematocyst release response has been proposed, but never documented nor measured. Our criterion for a nematocyst release response is that the intrinsic adherence of discharged nematocysts must decrease to zero. The unit of nematocyst discharge in sea anemone tentacles is the cnidocyte/supporting cell complex (CSCC). The nematocyst response includes nematocysts discharged from Type C CSCCs by physical contact alone and nematocysts discharged from the more numerous Type B CSCCs that require both chemosensitization and physical contact. We identify two prey-derived substances, N-acetylneuraminic acid (NANA) and glycine, both of which chemosensitize nematocyst discharge from Type B CSCCs at low concentrations. At higher concentrations NANA stimulates the release response of Type Cs, and glycine stimulates the release response of Type Bs.

Introduction

Cnidarians are obligate predators. Prey captured by cnidarians are attached to tentacles by discharged nematocysts. The discharged nematocysts, with attached prey, must be released in order for ingestion to proceed (Ewer, 1947). It is not known how the discharged nematocysts are released from the tentacles, and it is not known whether such release is under physiological control. In this paper, we hypothesize a "nematocyst release response." Using methods we have developed to measure the strength of attachment of discharged nematocysts to the tentacles of sea anemones (Thorington and Hessinger, 1996), we experimentally test and measure the nematocyst release response.

We have coined the term "afferent mechanisms" of cnida discharge to refer to those processes acting *to* or *toward* the undischarged cnida to regulate or initiate discharge, and to distinguish them from mechanisms acting *out of* or *from* the discharged cnida's effector functions, which we have termed "efferent mechanisms" (Thorington and Hessinger, 1996). Cnidae are the eversible secretory products of specialized cells called cnidocytes. The three known classes of cnidae are nematocysts, spirocysts, and ptychocysts (Mariscal, 1974). We have defined and measured an efferent mechanism termed "tentacle adherence." Tentacle adherence indicates how tightly the tentacle holds the capsules of discharged cnidae and is a measure of how tightly targets, such as captured prey, are retained on the tentacles. The force required to remove an average discharged spirocyst or nematocyst from tentacles is the "intrinsic adherence." The intrinsic adherence is calculated from measurements of adhesive force and of the numbers of nematocyst discharged.

Received 21 April 1998; accepted 15 July 1998.

E-mail: dhessinger@ccmail.llu.edu

Abbreviations: CSCC, cnidocyte/supporting cell complex; D-600, 2-methoxyverapamil; i_m , intrinsic adherence of nematocysts; NANA, N-acetylneuraminic acid; S_t , tentacle stickiness.

We measure adhesive force directly by using a sensitive force-transducer. The adhesive force is the applied force needed to separate a target from the tentacle (Thorington and Hessinger, 1988a). Specifically, adhesive force, as measured from sea anemone tentacles, is the sum of contributions arising from the stickiness of the tentacle mucus to the target (S_t) and the product of the number of cnidae (mastigophore nematocysts, n_m , and spirocysts, n_s) discharging onto the target and their intrinsic adherence (mastigophore nematocysts, i_m , and spirocysts, i_s) (Thorington and Hessinger, 1996):

Adhesive force

$$= S_t + (n_m) (i_m) + (n_s) (i_s) \quad (\text{Equation 1})$$

Adhesive force and intrinsic adherence may be expressed in units of micronewtons (μN) or in hybrid units of milligram-force (mgf), since adhesive force is measured without a significant acceleration component and, thereby, does not involve Newton's Second Law (Miller, 1959).

We measured the intrinsic adherence of discharged spirocysts (i_s) and of nematocysts (i_m) in the sea anemone *Aiptasia pallida* (Thorington and Hessinger, 1996) and found that the values of i_s are consistently very low relative to the values of i_m . We concluded that the values of i_s are too low to significantly contribute to the measurement of adhesive force or to participate in the retention of struggling prey on feeding tentacles. Thus, equation 1 may be simplified:

$$\text{Adhesive force} = S_t + (n_m) (i_m) \quad (\text{Equation 2})$$

In anemone tentacles, each cnidocyte is surrounded by two or more supporting cells. The supporting cells possess chemoreceptors (Watson and Hessinger, 1988) and mechanoreceptors (Watson and Hessinger, 1991) that detect prey and trigger nematocyst discharge. The cnidocyte, surrounded as it is by two or more supporting cells, constitutes a cnidocyte/supporting cell complex (CSCC), which we contend is the functional and morphological unit for triggering nematocyst discharge in the sea anemone tentacle.

Two of the three known types of CSCC in sea anemone tentacles are germane to the present study: Types B and C (Thorington and Hessinger, 1990). Some of the CSCCs in anemone tentacles can be made to discharge by mechanical stimulation alone; others require conjoint mechanical and chemical stimulation. We term the former (CSCCs that respond to mechanical stimulation alone) Type C CSCCs; and the latter (which require both chemical and mechanical stimulation) Type B CSCCs. Sensitizing chemoreceptors for N-acetylated sugars (e.g., N-acetylneuraminic acid, NANA) and for certain amino compounds (e.g., glycine, alanine, and proline) have thus far been identified. Stimulation of the chemoreceptors predis-

poses contact-sensitive mechanoreceptors to respond to contact mechanical stimuli that trigger discharge (Thorington and Hessinger, 1988a; 1990). Type C CSCCs, which are present in lower numbers than Type Bs, do not require chemosensitization but discharge in response to mechanical contact alone.

In addition to proposing the nematocyst release response, we hypothesize that the response is controlled by prey-derived chemicals, as are nematocyst-mediated prey capture (Thorington and Hessinger, 1988b) and the subsequent feeding response (Lindsted, 1971; Lenhoff and Heagy, 1977). Together, our hypotheses predict that certain prey-derived chemicals will lower the intrinsic adherence of discharged nematocysts.

Using methoxyverapamil (D-600) to selectively inhibit discharge from Type Bs, we show that (i) NANA inhibits the intrinsic adherence of nematocysts discharged from Type C CSCCs and, therefore, controls the release response of Type Cs; and (ii) glycine inhibits the intrinsic adherence of nematocysts discharged from Type B CSCCs and, therefore, controls the release response of Type Bs. We conclude that a nematocyst release response exists in sea anemones and that it is controlled by prey-derived chemicals that also control prey capture.

Materials and Methods

Maintenance of sea anemones

Monoclonal sea anemones (*A. pallida*, Carolina strain) were maintained individually in glass finger bowls containing natural seawater at $24^\circ \pm 1^\circ\text{C}$ as previously described (Hessinger and Hessinger, 1981; Thorington and Hessinger, 1988a). Briefly, anemones were fed daily with freshly hatched brine shrimp nauplii (*Artemia salina*) and washed 4–6 h after feeding (Hessinger and Hessinger, 1981). Anemones were maintained on a 12/12-h photoperiod using white fluorescent lights at an intensity of 5.5 klux ($66 \mu\text{Es}^{-1}\text{m}^{-2}$). Animals were starved for 72 h prior to experiments.

Experimental animals and test solutions

Filtered, natural seawater was obtained from Kerckoff Marine Laboratory of California Institute of Technology at Corona del Mar, California. Animals of same size were starved 72 h prior to experimentation and kept under constant fluorescent light at 4.5 klux ($54 \mu\text{Es}^{-1}\text{m}^{-2}$) during the last 48 h of starvation. Exposure to continuous light enhanced the uniformity of anemone behavior and cnidocyte responsiveness. Just prior to use, the animals were gently rinsed to remove soluble waste, and the medium was replaced with test solutions. Unless otherwise stated, animals were permitted to adapt to the change of medium for 10 min before cnidocyte responsiveness was mea-

sured. N-acetylneuraminic acid (NANA), glycine, and methoxyverapamil (D-600) were obtained from Sigma Chemical Co., St. Louis, Missouri. Solutions of D-600 were made up fresh on the day of the experiment and protected from light. All test solutions were prepared in artificial seawater (ASW) adjusted to pH 7.62 with 1 N HCl or NaOH. The ASW consisted of 423 mM NaCl, 10 mM KCl, 24 mM MgCl₂, 25 mM MgSO₄, 10 mM CaCl₂, and 1.2 mM NaHCO₃. Calcium-free artificial seawater (Ca-free ASW) was prepared with the same components as ASW except that calcium chloride was omitted, the NaCl concentration was increased to 438 mM, and EGTA (ethyleneglycoltetraacetic acid) was added to a final concentration of 1 mM; and then the final pH was adjusted to 7.62.

Assays of cnidocyte responsiveness

Physical contact of a tentacle with a gelatin-coated probe triggers discharge of local nematocysts and spirocysts, and adherence of the tentacle to the probe (Thorington and Hessinger, 1988b, 1990). Four parameters were measured to analyze nematocyst-mediated adhesive force: total adhesive force; number of discharged nematocysts; number of discharged spirocysts; and adhesive force in tentacles in which nematocyst and spirocyst discharge had been inhibited by pretreatment with formaldehyde to measure tentacle stickiness. The methods have been described in detail previously (Thorington and Hessinger, 1990). The number of cnidae on the probes is a direct measure of the number of cnidae discharged.

Measurement of adhesive force. Cnida-mediated adhesive force was measured as previously described (Thorington and Hessinger, 1988a). This technique involves using small gelatin-coated nylon beads of defined diameter attached to a strain gauge by means of a fine stainless steel shaft. The gel-coated bead is made to contact the distal third of a primary tentacle on an anemone in a finger bowl containing the test solution. The discharge of cnidae initiated by contact of the probe with the tentacle causes the tubules of everting cnidae to either adhere to or penetrate the gelatin surface. Withdrawing the probe from the tentacle causes the discharged cnidae to exert an opposing force on the probe; this force is measured with a gravimetrically calibrated force-transducer connected to a potentiometric recorder. The force necessary to separate the probe from the tentacle is called the adhesive force and is expressed in hybrid units of milligram-force (mgf). It is an aggregate measure of the "inherent" stickiness of the tentacle plus the nematocyst-mediated adhesive force.

Counting discharged nematocysts. After adhesive force measurements, the same probes are processed for counting nematocysts as detailed previously (Geibel *et al.*,

1988). Briefly, the gelatin coating of the probes is enzymatically digested to release the nematocysts of the discharged mastigophores. The highly refractive mastigophores, which are resistant to proteolysis, are then counted with an inverted microscope from the flat bottoms of microtiter wells.

Counting discharged spirocysts. To determine the number of discharged spirocysts, we used an indirect, solid-state enzyme-linked lectin sorbant assay (ELLSA), the details of which have been published (Thorington and Hessinger, 1990). In principle, the assay is based upon the high affinity of conjugated N-acetylated sugars to the everted tubules of discharged spirocysts on the surface of the test probes. The assay involves use of a microtiter-plate spectrophotometer for colorimetric determination of bound peroxidase activity after the sequential treatment of test probes with solutions of asialomucin and *Vicia villosa* lectin/peroxidase conjugate.

Collection and analysis of data

Individual animals were tested at each concentration of sensitizer. Twelve probes (one per tentacle) were used on each animal to determine adhesive force and to count discharged nematocysts or spirocysts. Daily experimental means were calculated from these experiments. Replicate experiments were carried out on three different days. Each data point represents the mean of the three daily experimental means, and the range bar represents the standard error of the mean.

Results

Selective discharge of cnidae from Type C cnidocyte/supporting cell complex

To test our hypotheses that a nematocyst release response exists and is under the control of prey-derived chemicals, we ask the research question: Do known chemosensitizers of nematocyst discharge lower, in a dose-dependent manner, the values of i_m for nematocysts discharged from either Type B or Type C CSCCs? To answer this question we proposed to determine the intrinsic adherence (i_m values) for nematocysts discharged from Type B and from Type C CSCCs as a function of chemosensitizer concentration. We selectively blocked chemosensitized discharge of nematocysts from Type B CSCCs by using 2-methoxyverapamil (D-600) (Thorington and Hessinger, 1992; Watson and Hessinger, 1994b), a diphenylalkylamine inhibitor of vertebrate L-type calcium channels (Spedding and Paoletti, 1992). With discharge from Type B CSCCs blocked, we directly determined the effect of chemosensitizers on the intrinsic adherence of nematocysts discharged from Type Cs. By subtracting the responses of the Type Cs from the combined responses

of Type B and Type C CSCCs (in the presence of chemosensitizer, but the absence of D-600), we calculated the intrinsic adherence of nematocysts from the Type Bs.

D-600 inhibits discharge from Type B CSCCs. D-600 potently and dose-dependently inhibits nematocyst discharge from NANA-sensitized Type Bs (Fig. 1; open circles). D-600 also inhibits glycine-sensitized nematocyst discharge (Fig. 1; open squares), but less potently and over a wider range of D-600 concentrations. In the absence of chemosensitizers, mechanical contact elicits discharge only from Type C CSCCs (Thorington and Hessinger, 1990). D-600 has no detectable effect on nematocyst discharge from Type Cs at any tested dose (Fig. 1; closed circles). The half-inhibitory doses (IC_{50}) for D-600 on NANA- and glycine-sensitized discharge is below 10^{-16} M for NANA and 10^{-15} M for glycine, and the minimal doses that maximally inhibit (IC_{100}) sensitized discharge are about 10^{-10} M for NANA and 10^{-6} M for glycine. Thus, D-600 blocks nematocyst discharge from Type B CSCCs, but not from Type Cs.

D-600 lowers tentacle stickiness (S_t). We tested the effects of D-600 on tentacle stickiness (Table 1) by incubating anemones at room temperature in ASW and in Ca-free ASW with and without D-600. After 20 min we added formalin to 10% for 5 min to measure S_t with

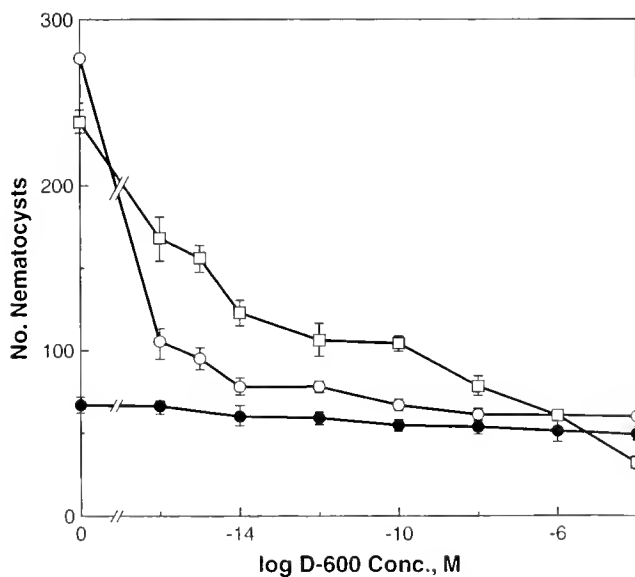


Figure 1. Effects of methoxyverapamil (D-600) on nematocyst discharge in the presence and absence of N-acetylneuraminic acid (NANA) or glycine. The number of nematocysts discharged from sea anemone tentacles onto probes at different molar concentrations of D-600 are indicated on the ordinate and abscissa, respectively, for anemones pre-exposed for 10 min to D-600 in seawater and then for 10 min more to D-600 with 1.8×10^{-5} M NANA in seawater (open circles; $n = 31$), or D-600 with 10^{-7} M glycine in seawater (open squares; $n = 13$), or D-600 in seawater (closed circles; $n = 33$). Data points are the mean \pm standard error of the mean.

adhesive force probes in the absence of any cnida discharge. The value of S_t is not altered by 10% formalin (Thorington and Hessinger, 1996). As expected, neither nematocysts nor spirocysts are discharged in 10% formalin (Table 1). The mean value of S_t in ASW is 36.6 ± 0.9 mgf ($358.7 \pm 8.8 \mu\text{N}$; Table 1), which is in close agreement with the value of 34.6 ± 0.7 mgf ($339.1 \pm 6.9 \mu\text{N}$) that we previously reported for similar experimental conditions (Thorington and Hessinger, 1996). The values of S_t are decreased 44% from ASW controls by 10^{-10} M D-600 in ASW ($P < 0.001$) and 49% from ASW controls by 10^{-8} M D-600 in ASW ($P < 0.005$). In Ca-free ASW, the mean value of S_t is 31.3 ± 0.9 mgf ($306.7 \pm 8.8 \mu\text{N}$, a value 15% lower ($P < 0.02$) than in ASW containing 10 mM Ca^{2+} ; the combination of Ca-free ASW and 10^{-10} M D-600 causes a decrease of 55% from ASW ($P < 0.001$; Table 1). Thus, D-600 significantly and dose-dependently lowers tentacle stickiness (S_t).

Effects of N-acetylneuraminic acid on intrinsic adherence

The combined dose-responses of Type B and Type C CSCCs to NANA for nematocyst discharge, spirocyst discharge, and adhesive force are characteristically biphasic (Fig. 2A–C, open circles; Thorington and Hessinger, 1990). In the presence of 10^{-10} M D-600, the dose-responses of Type Cs to NANA for nematocyst and spirocyst discharge are level and at control levels, showing no significant changes (Fig. 2A and B, closed circles). Thus, discharge from Type B CSCCs to NANA is totally inhibited by 10^{-10} M D-600, whereas discharge from Type Cs is unaffected.

NANA lowers i_m^c . Nematocyst-mediated adhesive force is calculated by subtracting tentacle stickiness (S_t) from adhesive force. To obtain nematocyst-mediated adhesive force in dose-responses to NANA, we subtracted from adhesive force measurements the appropriate value of S_t from Table 1 depending upon whether D-600 was or was not present during the experimental measurements. Nematocyst-mediated adhesive force from Type Cs steadily declines as the NANA concentration increases (Fig. 2C, closed circles). Since the numbers of nematocysts and spirocysts discharging from Type Cs do not significantly decrease (Fig. 2A and B, closed circles), the decline in adhesive force is probably due to a decrease in the value of i_m from the Type C CSCCs (*i.e.*, i_m^c).

We calculated the i_m values of nematocysts discharging from Type Cs (*i.e.*, i_m^c) across a wide range of NANA concentrations (10^{-16} to 10^{-3} M; Fig. 2D, closed circles) by using the values for nematocyst discharge and nematocyst-mediated adhesive force of Type C CSCCs in Equation 2. The values of i_m^c decrease with increasing levels of NANA, from about 0.20 mgf ($1.96 \mu\text{N}$) in ASW to

Table 1

Cnida-independent adhesive force (tentacle stickiness)

Treatment	Nematocysts ^a (n _m)	Spirocysts ^b (n _s)	Stickiness (mgf) ^c (S _t)
Pretreatment time = 90 min.			
ASW (without formalin) ^d	68.6 ± 0.7	136.7 ± 6.0	60.09 ± 1.00 ^e
ASW ^f	0.30 ± 0.10	0.91 ± 0.35	36.55 ± 0.86
Ca-free ASW ^g	0.20 ± 0.12	3.45 ± 2.0	31.25 ± 0.88
Pretreatment time = 70 min.			
ASW + 10 ⁻¹⁰ M D-600 ^h	0.22 ± 0.15	0.54 ± 0.14	20.44 ± 1.0
ASW + 10 ⁻⁸ M D-600 ⁱ	0.31 ± 0.02	0.34 ± 0.25	18.49 ± 0.21
Ca-free ASW + D-600 ^j	0.50 ± 0.28	0.30 ± 0.21	16.55 ± 2.0

Note: All anemones were pretreated with artificial seawater (ASW) at room temperature (23° ± 1°C) for either 70 or 90 min. If the treatment took place in Ca-free ASW, the pretreatment seawater was also Ca-free. After treatment, the anemones were contacted with test probes. Number of individuals (*n*) = 30 for all treatments except ASW without formalin, for which *n* = 34.

^a Mean number of discharged nematocysts ± SEM.

^b Mean number of discharged spirocysts ± SEM.

^c Mean stickiness value measured as adhesive force, mgf ± SEM.

^d Pretreatment only; no further treatment.

^e Values include stickiness plus contributions from discharged nematocysts and spirocysts.

^f Pretreatment + exposure to 10% formalin in ASW for 5 min.

^g Pretreatment + exposure to 10% formalin in Ca-free ASW for 5 min.

^h Pretreatment + exposure to ASW containing 10⁻¹⁰ M D-600 for 15 min, then exposure to 10% formalin in ASW for 5 min.

ⁱ Pretreatment + exposure to ASW containing 10⁻⁸ M D-600 for 15 min, then exposure to 10% formalin in ASW for 5 min.

^j Pretreatment + exposure to Ca-free ASW containing 10⁻¹⁰ M D-600 for 15 min, then exposure to 10% formalin in Ca-free ASW for 5 min.

near zero at 10⁻⁴ M NANA. The concentration of NANA that half-inhibits *i_m^c* is approximately 10⁻¹² M NANA. Thus, NANA dose-dependently lowers the intrinsic adherence of nematocysts discharged from Type Cs.

NANA biphasically modulates i_m^b. The dose-responses for discharge and adhesive force from Type Bs (Fig. 2A–C, closed squares) are calculated by subtracting the discharge (or adhesive force) of Type Cs in D-600 (closed circles) from the discharge (or adhesive force) of both Type Bs and Cs in the absence of D-600 (open circles). The calculated Type B dose-responses of both mastigophore and spirocyst discharge are narrow and biphasic. Maximum discharge (*E_{max}*) of nematocysts and spirocysts from Type Bs is about two times and one time, respectively, that of Type C ASW controls, suggesting that Type Bs and Type Cs coexist in the tentacle in ratios of 2:1 and 1:1 for nematocyst-bearing and spirocyst-bearing CSCCs, respectively. The concentration at which maximal discharge occurs (*EC₁₀₀*) is about 10⁻⁵ M NANA, and the concentration at which half-maximum discharge occurs (*K_{0.5}*) is about 10⁻⁶ M NANA. The NANA dose-response of nematocyst-mediated adhesive force from Type Bs is broadly biphasic, with an *EC₁₀₀* of 10⁻⁵ M NANA and a *K_{0.5}* of about 10⁻¹⁰ M NANA (Fig. 2C, open circles).

Using the values for nematocyst discharge and nematocyst-mediated adhesive force of Type B CSCCs in Equation 2, we calculate the *i_m^b* values of nematocysts discharging from Type Bs (*i.e.*, *i_m^b*) across a wide range of NANA

concentrations (Fig. 2D, closed squares). The *i_m^b* dose-response to NANA is biphasic, with maximum *i_m^b* values of about 0.8 mgf (7.8 μN) occurring at 10⁻¹⁰ M NANA and the *K_{0.5}* occurring at about 10⁻¹² M NANA. The peak of the *i_m^b* dose-response is about five orders of magnitude lower than the peak of the dose-response of Type B nematocyst discharge (Fig. 2A). We conclude that NANA dose-dependently modulates a biphasic change in the intrinsic adherence of nematocysts discharging from Type B CSCCs, but does not reduce the value of *i_m^b* to zero.

Effects of glycine on intrinsic adherence

Glycine suppresses discharge from Type Cs. The minimum dose of D-600 that totally inhibits glycine-sensitized nematocyst discharge from Type Bs is 10⁻⁶ M (Fig. 1). To minimize possible side effects from such a relatively high dose, we elected to use 10⁻⁸ M D-600 rather than 10⁻⁶ M. The dose-responses to glycine for nematocyst discharge, spirocyst discharge, and adhesive force are characteristically biphasic (Fig. 3A–C; Thorington and Hessinger, 1990). In 10⁻⁸ M D-600 the dose-responses to glycine for discharge of both nematocysts and spirocysts and for adhesive force do not exceed those of controls (Fig. 3A–C, closed circles). Thus, 10⁻⁸ M D-600 appears to inhibit cnida discharge from Type B CSCCs in response to glycine.

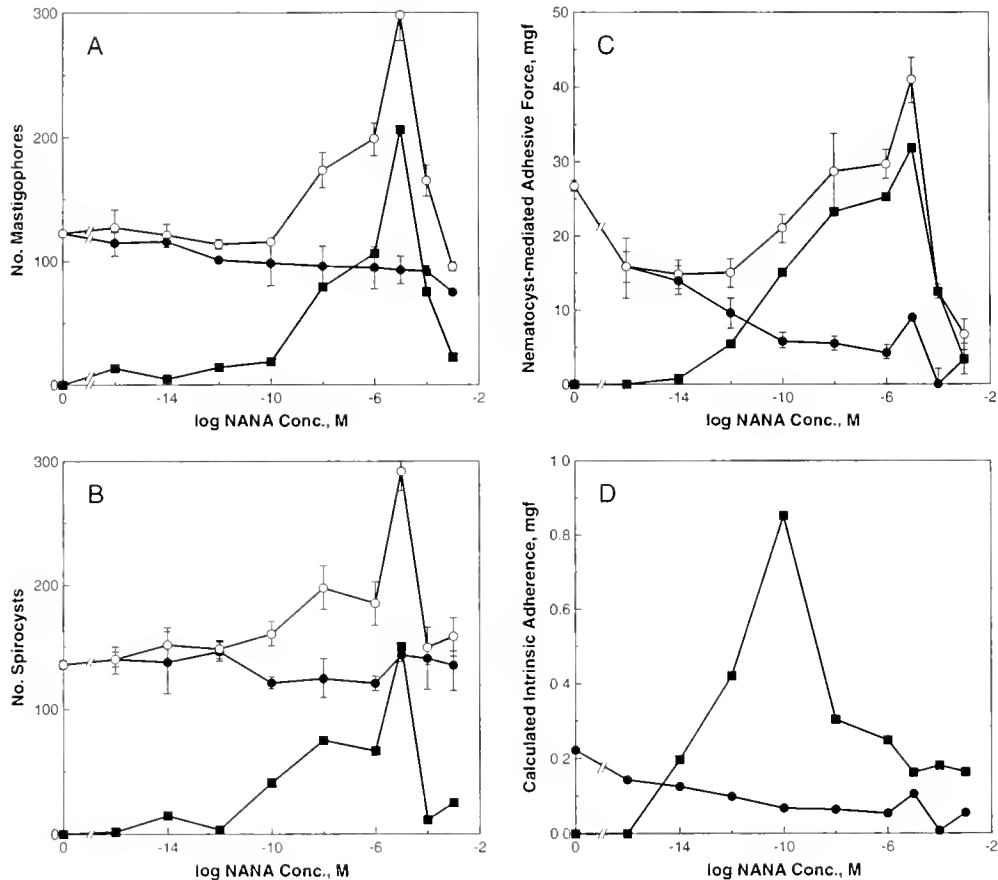


Figure 2. Afferent and efferent cnida dose-responses to N-acetylneuraminic acid (NANA). Combined cnida responses from Type B plus Type C cnidocyte/supporting cell complexes (CSCCs) are measured in seawater (open circles). Cnida responses from Type Cs only are measured in the presence of 10^{-10} M D-600 (closed circles). Calculated responses from Type Bs (closed squares) are obtained by subtracting Type C responses from combined Type B plus Type C responses. Values express the mean of three experiments. Each experiment consists of replicate probes for each NANA concentration; each probe and each tentacle is used only once. Vertical bars represent standard errors of the mean and are applied to all measured means, but not to calculated means. (A) Effect of NANA on nematocyst discharge ($n = 34$). (B) Effect of NANA on spirocyst discharge ($n = 35$). (C) Effect of NANA on nematocyst-mediated adhesive force ($n = 36$). (D) Effect of NANA on calculated intrinsic adherence.

On the other hand, in the presence of 10^{-8} M D-600, we observe about a 50% decrease in both nematocyst and spirocyst discharge from Type Cs at the lowest tested doses of glycine (*i.e.*, 10^{-16} M glycine). Nematocyst discharge gradually recovers to control levels of discharge at about 10^{-7} M glycine and then declines again at higher concentrations. Spirocyst discharge recovers at lower concentrations of glycine and reaches control levels at 10^{-6} M glycine before it, like nematocyst discharge, declines again at higher concentrations. Thus, low concentrations of glycine suppress both nematocyst and spirocyst discharge from Type C CSCCs.

Glycine modulates i_m^s . Nematocyst-mediated adhesive force from Type Cs remains constant (between 12 and

15 mgf or 118 and 147 μ N) at all tested glycine concentrations except 10^{-7} M glycine, at which concentration the adhesive force increases to 20 mgf (196 μ N; Fig. 3C; closed circles). Using Equation 2, we calculated the i_m^c values of nematocysts discharging from Type Cs (*i.e.*, i_m^c) across the range of tested glycine concentrations (10^{-16} to 10^{-4} M; Fig. 3D, closed circles). The values of i_m^c are relatively high (about 0.6 mgf/nematocyst or 5.9 μ N/nematocyst) in seawater controls and in 10^{-16} to 10^{-12} M glycine. But between 10^{-10} and 10^{-7} M glycine, the values of i_m^c decrease by about one-half (to about 0.3 mgf/nematocyst or 2.9 μ N/nematocyst) and then increase (to about 0.4 mgf/nematocyst or 3.9 μ N/nematocyst) at 10^{-6} M and higher concentrations. Overall, there appears to be a

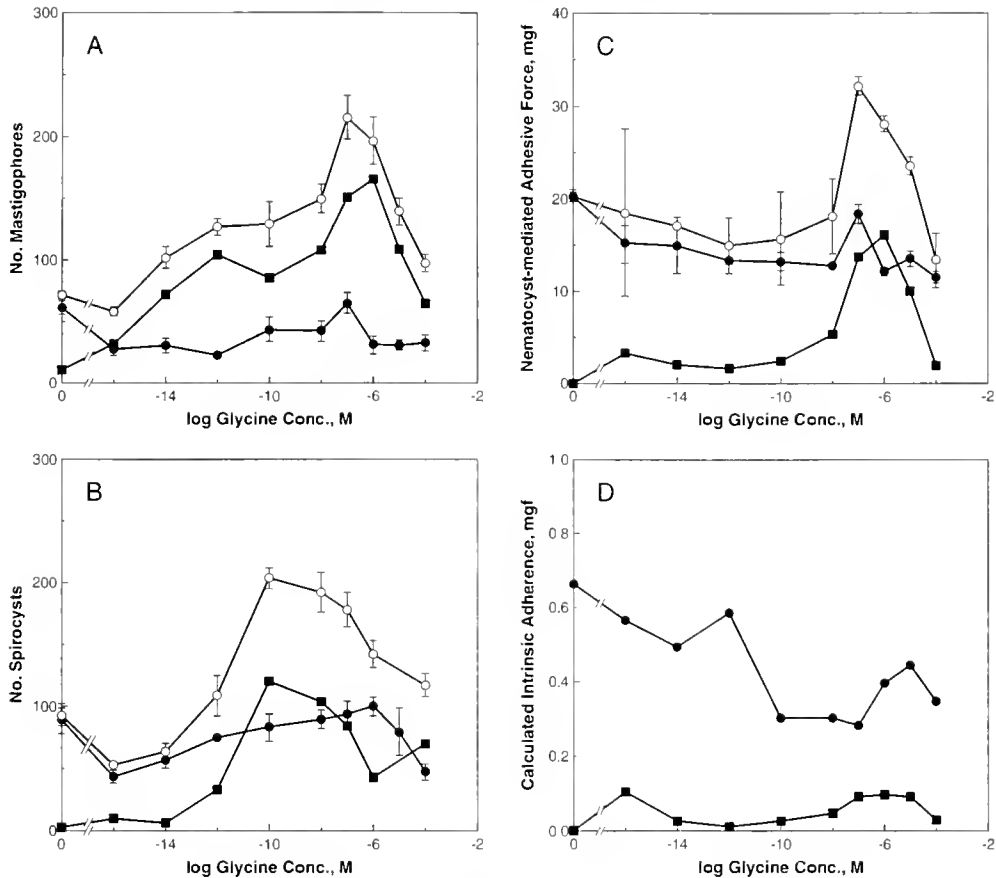


Figure 3. Afferent and efferent cnida dose-responses to glycine. Combined responses from Type B plus Type C cnidocyte/supporting cell complexes (CSCCs) are measured in seawater (open circles). Cnida responses from Type Cs only are measured in the presence of 10^{-8} M D-600 in seawater (closed circles). Calculated responses from Type Bs (closed squares) are obtained by subtracting Type C responses from combined Type B plus Type C responses. Values express the mean of duplicate experiments. Each experiment consists of replicate probes for each glycine concentration; each probe and each tentacle is used only once. Vertical bars represent standard error of the mean and are applied to all measured means, but not to calculated means. (A) Effect of glycine on nematocyst discharge ($n = 15$). (B) Effect of glycine on spirocyst discharge ($n = 15$). (C) Effect of glycine on nematocyst-mediated adhesive force ($n = 14$). (D) Effect of glycine on calculated intrinsic adherence.

downward trend in i_m^c with increasing glycine concentrations.

Glycine suppresses i_m^b . In contrast to NANA, in which NANA-sensitized discharge of nematocysts from Type Bs spans a narrow range of NANA concentrations (Fig. 2A, closed squares), glycine-sensitized discharge of nematocysts spans a wide range of glycine concentrations (Fig. 3A, closed squares). At all tested glycine concentrations (except 10^{-16} M), the numbers of nematocysts discharged from Type Bs exceed those discharged from Type Cs. Yet the values of i_m^b in glycine never exceed 0.1 mgf/nematocyst ($0.98 \mu\text{N/nematocyst}$; Fig. 3D, closed squares), unlike the values in NANA which never drop below 0.2 mgf/nematocyst ($1.96 \mu\text{N/nematocyst}$; Fig. 2D, closed squares).

Discussion

Cnidarians capture swimming prey by discharging nematocysts from their tentacles. These same nematocysts also secure the struggling prey to the tentacle during coordinated tentacle movements that transport the prey to the oral disk and mouth. For ingestion to occur, however, the nematocysts securing captured prey to the tentacle must then be released from the tentacle (Ewer, 1947).

We proposed a so-called nematocyst release response controlled by soluble, prey-derived chemicals also known to both chemosensitize nematocyst discharge and initiate the feeding response. We stipulated that the

strength of attachment of discharged nematocysts to sea anemone tentacles (*i.e.*, intrinsic adherence) must be reduced to or near zero for the mechanism to qualify as a nematocyst release response.

Effects of N-acetylneuraminic acid and glycine on discharge and intrinsic adherence

NANA does not affect discharge from Type Cs. Because low concentrations of D-600 block both NANA-sensitized and glycine-sensitized discharge from Type B CSCCs without affecting discharge from Type Cs (Figs. 1 and 2A, B), we were able to measure the response from Type Cs without interfering contributions from discharging Type Bs. Throughout the range of 10^{-16} to 10^{-3} M NANA, nematocyst and spirocyst discharge from Type Cs was constant (Fig. 2A, B). We concluded that neither nematocyst nor spirocyst discharge from Type Cs is affected by NANA chemoreceptor stimulation.

NANA controls the release response of Type Cs. Despite constant nematocyst discharge from Type Cs at all tested NANA concentrations, nematocyst-mediated adhesive force from Type Cs declined with increasing NANA concentrations (Fig. 2C). The decline in adhesive force was caused by a dose-dependent decrease (from 0.2 to 0 mgf/nematocyst, or 1.96 to 0 μ N/nematocyst; Fig. 2D) in the intrinsic adherence of nematocysts discharged from Type Cs (i_m^c). The dose-dependent decrease in i_m^c fits our criterion of a nematocyst release response. We concluded that a release response of nematocysts discharged from Type Cs is under the control of NANA chemoreceptors.

NANA controls i_m^b . We calculated the NANA dose-responses of Type B CSCCs by subtracting NANA dose-responses in the presence of 10^{-10} M D-600 from NANA dose-responses in the absence of D-600 (Fig. 2). The calculated NANA dose-responses of both nematocyst and spirocyst discharge from Type Bs were narrow and biphasic, with maximal discharge occurring at 10^{-5} M NANA (EC_{100}) and half-maximal discharge ($K_{0.5}$) occurring at 10^{-6} M NANA (Fig. 2A, B). The calculated NANA dose-response of nematocyst-mediated adhesive force from Type Bs was also biphasic, but over a much broader range of NANA concentrations, with the EC_{100} still occurring at 10^{-5} M NANA, but with the $K_{0.5}$ occurring much lower (at 10^{-10} M NANA; Fig. 2C).

In NANA, the intrinsic adherence of nematocysts discharged from Type Bs (i_m^b) varied biphasically with NANA concentration (Fig. 2D). The maximal i_m^b value of 0.8 mgf/nematocyst (7.8 μ N/nematocyst) occurred at 10^{-10} M NANA, but decreased to about 0.2 mgf (1.96 μ N) at 10^{-5} M NANA and at higher concentrations. The values of i_m^c in NANA varied from 0.2 to 0 mgf/nematocyst (1.96 to 0 μ N/nematocyst). Thus, in seawater containing NANA, i_m^b will exceed i_m^c . It therefore appears

that in the presence of NANA, nematocysts discharged from Type Bs will predominate in both prey capture and prey retention over nematocysts discharged from Type Cs. Although the NANA dose-response of i_m^b never goes to zero, we conclude that NANA controls i_m^b over a wide range of values, in a dose-dependent manner, but without affecting the release response of nematocysts discharged from Type Bs.

Glycine inhibits discharge from Type Cs. In addition to N-acetylated sugars, amino sensitizers, such as glycine, also predispose nematocysts and spirocysts to discharge in response to mechanical stimuli (Thorington and Hessinger, 1988a, 1990). In the present study, we showed that glycine sensitizes Type B CSCCs to discharge nematocysts and spirocysts (Fig. 3A, B). However, unlike NANA, which had no effect on discharge from Type Cs, glycine suppressed nematocyst and spirocyst discharge from Type Cs (Fig. 3A, B). The inhibitory effect of glycine was partial and occurred at both low and high concentrations, but reversed at intermediate concentrations. The inhibitory effect of glycine on discharge from Type Cs is probably different from the inhibitory effects of certain homogenate fractions of *Artemia* on prey capture in *Hydra* (Grosvenor and Kass-Simon, 1987) since the inhibitory action of glycine in *Aiptasia* is restricted to Type Cs and the net effect of glycine is to increase nematocyst discharge due to its sensitizing effect on the more numerous Type Bs (Fig. 3A). To the best of our knowledge, this is the first report of an identified chemoreceptor inhibiting nematocyst discharge.

The value of i_m^c varied from 0.6 mgf/nematocyst (5.9 μ N/nematocyst; in seawater and in lower glycine concentrations) to about 0.3 and 0.4 mgf/nematocyst (2.9 and 3.9 μ N/nematocyst; at higher glycine concentrations). Although NANA lowers the i_m^c to zero at higher concentrations, thereby constituting a nematocyst release response, glycine also lowers i_m^c , but without bringing the value to zero. Glycine inhibits discharge from Type Cs, but it does not affect the Type C nematocyst release response.

Glycine controls the release response of Type Bs. Although glycine-sensitized nematocyst discharge from Type Bs is robust at all concentrations greater than 10^{-14} M, the value of i_m^b is consistently low, never exceeding values of 0.1 mgf/nematocyst and reaching 0 mgf/nematocyst (0.98 and 0 μ N/nematocyst) at 10^{-4} M glycine. We conclude that the action of glycine on the intrinsic adherence of nematocysts discharged from Type B CSCCs is consistent with glycine control of the release response of nematocysts discharged from Type Bs.

D-600 affects Type Bs differently than Type Cs. The inhibition of nematocyst discharge from Type B CSCCs by verapamil and other organic and inorganic inhibitors of voltage-gated calcium channels was first reported in the anemone *Haliplanella luciae* (Watson and Hessinger,

1994a). We now show that D-600, a water-soluble derivative of verapamil, inhibits both nematocyst and spirocyst discharge from Type Bs in *Aiptasia pallida* (Fig. 2A, B). The effects on nematocyst discharge of calcium depletion and of standard organic and inorganic calcium channel blockers (Watson and Hessinger, 1994a) are consistent with the involvement of calcium channels, pharmacologically resembling L-type calcium channels, in the chemosensory signaling pathway of Type B CSCCs. Our finding that NANA-sensitized discharge of nematocysts is much more sensitive to D-600 than is glycine-sensitized discharge (Fig. 1) suggests that the NANA and glycine chemosensory pathways utilize calcium in different ways.

Both D-600 and calcium-free seawater reduce tentacle stickiness, and these effects are additive (Table I), suggesting common modes of action. Tentacle stickiness is mediated by the interaction of the mucus layer covering the tentacle surface with the probe. Tentacle mucus originates, in part, by a constitutive secretory process of apical secretory cells. Under conditions of injury or stress, the amount of surface mucus increases. Thus, tentacle mucus may also be contributed by regulated secretion. The nematocyst is a secretory product of the cnidocyte (Slautterback, 1961; Skaer, 1973). Exocytotic processes (*i.e.*, mucus secretion and nematocyst discharge [Holstein and Tardent, 1984]), in general, require extracellular calcium and calcium influx mediated by calcium channels (Bennett *et al.*, 1979). We hypothesize that D-600 and calcium-free seawater reduce tentacle stickiness and inhibit discharge from Type B CSCCs by affecting involved calcium channels.

Roles of N-acetylneuraminic acid and glycine in prey capture and prey ingestion

Prey capture. In our view the "NANA" receptor is the primary chemoreceptor for capturing prey since N-acetylated sugars are ubiquitous constituents of the surfaces of most aquatic prey. On the other hand, the activators of the "amino" chemoreceptors (glycine, alanine, and proline) occur in high concentrations in the hemolymph of crustacean prey (Gilles, 1979) and of *Artemia* nauplii (Clegg and Conte, 1980), the typical prey of laboratory-reared cnidarians. Presumably the amino sensitizers leak into the ambient medium from wounds inflicted by NANA-sensitized nematocysts, as originally suggested by Loomis of the glutathione-effected feeding response of *Hydra* (Loomis, 1955) and later confirmed by Lenhoff (1961). Proline, for instance, potently and negatively modulates NANA-induced tuning of vibration-sensitive mechanoreceptors associated with Type A CSCCs in a related anemone, *Haliplanella luciae* (Watson and Hessinger, 1994b). Alanine inhibits NANA-sensitized discharge from Type Bs in *Aiptasia* (unpubl. findings). And

glycine inhibits discharge of nematocysts and spirocysts from Type C CSCCs (Fig. 3A, B). Thus, we view the "amino" receptors to be secondary chemoreceptors in prey capture, involved in negatively modulating the primary prey capture response to N-acetylated sugars. As secondary chemoreceptors, the amino receptors respond to chemicals leaking from wounded prey and assure that only the minimum adequate number of nematocysts are discharged. By conserving nematocysts and avoiding "overkill," the anemone devotes fewer prey nutrients to replacement of nematocysts and more to growth and reproduction.

Prey ingestion. Following prey capture and transport to the mouth, glycine from wounded prey acts in concert with NANA to stimulate the release responses of discharged nematocysts so that prey can be ingested. Our present work shows that NANA controls the release response of nematocysts discharged from Type Cs (Fig. 2D), whereas glycine controls the release response of nematocysts from the more numerous Type Bs (Fig. 3D).

It has been observed, although not, to our knowledge, published, that many cnidarians do not ingest dead prey, even though the dead prey elicit nematocyst discharge and adhere to tentacles (*e.g.*, pers. obs. by C. Hand, UC, Davis; K. Heidelberg, U. Maryland; H. M. Lenhoff, UC, Irvine). Discrimination between living and dead prey appears to occur after prey capture and may involve the detection of amino substances leaking from wounded prey. On the one hand, the very short timescale for a successful nematocyst response dictates that chemical discrimination in prey capture be cursory and based upon a single chemical cue, the external N-acetylated sugars. These sugars are common to living and dead prey, so discrimination is sacrificed for response speed and the drifting remains of dead prey containing no nutrients are occasionally captured. On the other hand, the subsequent release response and prey ingestion take place on a much longer timescale than prey capture. The release response is based upon dual chemosensory cues, N-acetylated sugars and glycine. Dead and nutrient-depleted prey, if captured, will not provide the amino chemosensory cue needed to stimulate a complete nematocyst release response, and such prey will not be ingested. The dual chemoreceptor requirement for the release response ensures that captured dead prey are not ingested and digestive resources are not committed to nutrient-poor prey.

The i_m -discharge plot explained

We showed previously (Thorington and Hessinger, 1996) that a plot of the weighted average i_m values *versus* the total number of discharged nematocysts (the so-called i_m -discharge plot) was inversely hyperbolic in shape for NANA and several amino chemosensitizers. Except for

the steepness of the i_m -discharge plot, our dilution/recruitment model, in general, simulated the plot. The dilution/recruitment model assumed that (i) the i_m values of mastigophore nematocysts from both Type B and Type C CSCCs are constant, (ii) the value of i_m^c is larger than the value of i_m^b , and (iii) the number of nematocysts discharged from Type C CSCCs is constant. (iv) while the number discharged from Type B CSCCs varies biphasically with increasing concentrations of chemosensitizer. In this model the discharge of a constant number of high- i_m nematocysts from Type C CSCCs is numerically diluted by the discharge of progressively greater numbers of lower- i_m nematocysts recruited by chemosensitization of Type B CSCCs.

Our present findings indicate that the recruitment/dilution model is incomplete in several ways. Firstly, the i_m values from Type Bs and Cs are not constant. We have shown that NANA biphasically varies i_m^b and glycine monophasically varies i_m^c . Secondly, the values of i_m^c are not always larger than the values of i_m^b . We have found that i_m^b is greater than i_m^c in the presence of NANA. Thirdly, the number of nematocysts discharged from Type C CSCCs is not always constant. In the presence of glycine the number of nematocysts discharging from Type Cs decreases. On the positive side, our assumption that the numbers of nematocysts discharged from Type B CSCCs varies biphasically with increasing concentrations of chemosensitizer was confirmed for both NANA and glycine.

Conclusions

1. Nematocysts perform at least three feeding-related functions. (i) Discharging nematocysts subdue swimming prey by penetrating and envenomating prey. (ii) Discharged nematocysts secure struggling prey to the tentacles by a combination of barbed nematocyst tubules fastened into the integument of prey and the initially high intrinsic adherence of nematocyst capsules' attachment to the tentacle. (iii) Discharged nematocysts subsequently facilitate prey ingestion by being released from the tentacle as a result of a large decrease in intrinsic adherence.

2. Each of the feeding-related functions of nematocysts is under the control of at least two chemoreceptor systems. One system is for N-acetylated sugars, such as N-acetylneuraminic acid (NANA), which occur on the surface of prey; the other is for "amino" substances, such as glycine, which occur in the blood of prey and are leaked into the medium from nematocyst-inflicted wounds.

3. The "NANA" receptor is the primary chemoreceptor controlling prey capture, while the "amino" receptors act to negatively modulate nematocyst discharge. Glycine, for instance, inhibits the discharge of nematocysts (and spirocysts) from Type C CSCCs over a wide range of concentrations.

4. To ensure that captured prey are tightly secured to the tentacle, the "NANA" receptor raises the intrinsic adherence of nematocysts discharged from Type B CSCCs at low concentrations of NANA (about 10^{-10} M).

5. To ensure that captured prey are subsequently ingested, the nematocyst release response is activated for nematocysts discharged from Type C CSCCs and from Type B CSCCs by higher concentrations (10^{-4} M) of NANA and glycine, respectively.

6. Cnida-independent tentacle stickiness, presumably due to surface mucus, is dose-dependently decreased by D-600 and by removal of extracellular calcium. The inhibitory actions of D-600 and low calcium on tentacle stickiness are additive.

Acknowledgments

Supported in part by NSF grant MCB-8919269.

Literature Cited

- Bennett, J. P., S. Cockcroft, and B. D. Gomperts. 1979. Ionomycin stimulates mast cell histamine secretion by forming a lipid-soluble calcium complex. *Nature* **282**: 851-853.
- Clegg, J. S., and F. P. Conte. 1980. A review of the cellular and developmental biology of *Artemia*. Pp. 11-54 in *The Brine Shrimp Artemia, vol. 2. Physiology, Biochemistry, Molecular Biology*, G. Personne, P. Sorgeloos, O. Roels, and E. Jaspers, eds. Universa Press, Wetteren, Belgium.
- Ewer, R. F. 1947. On the functions and mode of action of the nematocysts of hydra. *Proc. Zool. Soc. Lond.* **117**: 365-376.
- Geibel, G., G. Thorington, and D. A. Hessinger. 1988. Control of cnida discharge: II. Microbasic p-mastigophore nematocysts are regulated by two classes of chemoreceptors. *Biol. Bull.* **175**: 132-136.
- Gilles, R. 1979. Intracellular organic osmotic effectors. Pp. 111-154 in *Mechanisms of Osmoregulation in Animals: Maintenance of Cell Volume*, R. Gilles, ed. John Wiley, New York.
- Grosvenor, W., and G. Kass-Simon. 1987. Feeding behavior in *Hydra*. I. Effects of *Artemia* homogenate on nematocyst discharge. *Biol. Bull.* **173**: 527-538.
- Hessinger, D. A., and J. A. Hessinger. 1981. Methods for rearing sea anemones in the laboratory. Pp. 153-179 in *Marine Invertebrates*, Committee on Marine Invertebrates, ed. National Academy Press, Washington, DC.
- Holstein, T., and P. Tardent. 1984. An ultra-high speed analysis of exocytosis: nematocyst discharge. *Science* **223**: 830-832.
- Lenhoff, H. M. 1961. Activation of the feeding reflex in *Hydra littoralis*. I. Role played by reduced glutathione and quantitative assay of the feeding reflex. *J. Gen. Physiol.* **45**: 331-344.
- Lenhoff, H. M., and W. Haegy. 1977. Aquatic invertebrate model systems for study of receptor activation and evolution of receptor proteins. *Annu. Rev. Pharmacol. Toxicol.* **17**: 243-258.
- Lindsted, K. J. 1971. Biphasic feeding response in a sea anemone: control by asparagine and glutathione. *Science* **173**: 333-334.
- Loomis, W. F. 1955. Glutathione control of the specific feeding reactions of hydra. *Ann. N. Y. Acad. Sci.* **62**: 209-228.
- Mariscal, R. N. 1974. Nematocysts. Pp. 129-178 in *Coelenterate Biology: Reviews and New Perspectives*, L. Muscatine and H. M. Lenhoff, eds. Academic Press, New York.
- Miller, F., Jr. 1959. Dynamics. Pp. 52-54 in *College Physics*, Harcourt, Brace and World, New York.

- Skaer, R. J., 1973.** The secretion and development of nematocysts in a siphonophore. *J. Cell Sci.* **13**: 371–393.
- Slautterback, D. B., 1961.** Nematocyst development. Pp. 77–130 in *The Biology of Hydra*, D. A. Hessinger and H. M. Lenhoff, eds., Academic Press, San Diego.
- Spedding, M., and R. Paoletti., 1992.** III. Classification of calcium channels and the sites of action of drugs modifying channel function. *Pharmacol. Rev.* **44**: 363–376.
- Thorington, G. U., and D. A. Hessinger., 1988a.** Control of cnida discharge: I. Evidence for two classes of chemoreceptors. *Biol. Bull.* **174**: 163–171.
- Thorington, G. U., and D. A. Hessinger., 1988b.** Control of cnida discharge: factors affecting discharge of cnidae. Pp. 233–253 in *The Biology of Nematocysts*, D. A. Hessinger and H. M. Lenhoff, eds., Academic Press, San Diego.
- Thorington, G. U., and D. A. Hessinger., 1990.** Control of cnida discharge: III. Spirocysts are regulated by three classes of chemoreceptors. *Biol. Bull.* **178**: 74–83.
- Thorington, G. U., and D. A. Hessinger., 1992.** Nifedipine blocks desensitization of chemo-receptors regulating nematocyst discharge in sea anemones (*Aiptasia pallida*). *Molec. Biol. Cell* **3**: 250a
- Thorington, G. U., and D. A. Hessinger., 1996.** Efferent mechanisms of discharging cnidae: I. Measurements of intrinsic adherence of cnidae discharged from tentacles of the sea anemone, *Aiptasia pallida*. *Biol. Bull.* **190**: 125–138.
- Watson, G. M., and D. A. Hessinger., 1988.** Localization of a purported chemoreceptor involved in triggering cnida discharge in sea anemones. Pp. 255–272 in *The Biology of Nematocysts*, D. A. Hessinger and H. M. Lenhoff, eds., Academic Press, San Diego.
- Watson, G. M., and D. A. Hessinger., 1991.** Chemoreceptor-mediated elongation of stereocilium bundles tunes vibration-sensitive mechanoreceptors on cnidocyte-supporting cell complexes to lower frequencies. *J. Cell. Sci.* **99**: 307–316.
- Watson, G. M., and D. A. Hessinger., 1994a.** Antagonistic frequency tuning of hair bundles by different chemoreceptors regulates nematocyst discharge. *J. Exp. Biol.* **187**: 57–73.
- Watson, G. M., and D. A. Hessinger., 1994b.** Evidence for calcium channels involved in regulating nematocyst discharge. *Comp. Biochem Physiol.* **107A**: 473–481.

Role of Mechanosensory Stimuli in Intraspecific Agonistic Encounters of the Snapping Shrimp (*Alpheus heterochaelis*)

JENS HERBERHOLZ AND BARBARA SCHMITZ*

Institut für Zoologie, Technische Universität München, Lichtenbergstr. 4, 85747 Garching, Germany

Abstract. Intraspecific agonistic encounters in snapping shrimp (*Alpheus heterochaelis*) were analyzed using single-frame video analysis. The pair of conspecifics in such an encounter are designated as the snapper, which emits a fast water jet by very rapid closure, or snap, of the large modified snapper claw, and the receiver, which is the target of the water jet. The behavior of both snapper and receiver was evaluated before, during, and after the snap. Interactions between two intact shrimp (experimental series I) were compared with those between an intact shrimp and a "deprived" opponent (one with mechanosensory occlusion produced by coating the setae on the snapper claw with clear lacquer) (experimental series II). The behavior of the receiver is significantly changed by the occlusion, but that of the snapper is not. Intact and deprived opponents usually face each other during snapping, which is often preceded by touching of frontal appendages. The mean duration of claw cocking before snapping is about 500 ms. More than 50% of all snaps (and especially initial snaps) are directed towards the opponent, the water jet usually hitting the snapper claw of the receiver from a mean distance of 0.9 cm. Male shrimp show longer cocking durations, keep a shorter distance, and hit their opponents more often than do females. Intact and deprived snappers usually retreat immediately after snapping, but intact receivers usually approach. In contrast, deprived receivers retreat in most cases and show significantly prolonged latencies compared to intact receivers. Thus, mechanoreceptors on the snapper claw of the receiver play a significant role in intraspecific agonistic encounters.

Introduction

Agonistic encounters in competition for space, shelter, and access to mates or food are very common in crustaceans and have been studied extensively in different orders and families (Dingle, 1983; Hyatt, 1983) such as mantis shrimp (Stomatopoda; Caldwell and Dingle, 1975), freshwater prawns (Palaemonidae; Barki *et al.*, 1991), lobsters (Homaridae; Huber and Kravitz, 1995), crayfish (Astacidae, Cambaridae and Parastacidae; Copp, 1986; Söderbäck, 1991; Pavey and Fielder, 1996), and hermit crabs (Paguridae; Elwood and Neil 1992). Snapping shrimp differ from these crustaceans by having the ability to produce a rapid water jet, which is used in interactions with conspecifics and prey.

Alpheus heterochaelis, the big-clawed snapping shrimp of the family Alpheidae, which comprises about 425 species worldwide in subtropical and tropical oceans, reaches 5.5 cm in body length (Williams, 1984; Gruner, 1993). The animals used in this study originate from the Gulf of Mexico in northern Florida, where they live either individually or as heterosexual pairs in the littoral zone within oyster banks. Both sexes show a large, modified snapper claw on one (left or right) side, claw length reaching nearly half the body length, and a small pincer claw on the other side. Both claws are densely covered with setae of at least six different types (Read and Govind, 1991; Sullivan and Schmitz, 1997). The morphological differences between sexes include a broader pincer claw with fringes of plumoserrate setae on dactyl (movable finger) and propus in the male (Read and Govind, 1991), and a slightly broader abdomen with larger pleurites in the female (Nolan and Salmon, 1970).

In *Alpheus heterochaelis* the dactyl of the snapper claw possesses a huge stopper-like tooth (the plunger), which

Received 1 October 1997; accepted 16 June 1998.

* To whom correspondence should be addressed. E-mail: bschm@cip1.zoo.chemie.tu-muenchen.de

fits into a socket in the propus (Brooks and Herrick, 1891). Prior to snapping, the dactyl is cocked in a 100° position by cocontraction of claw opener and closer muscles, while the closer apodeme is lifted over a pivot point, so that tension is generated until a second closer muscle contracts (Ritzmann, 1974). During the following extremely rapid closure of the snapper claw (within about 1 ms; Schmitz and Herberholz, 1998) a short, very intense sound is produced (Knowlton and Moulton, 1963; Schmitz *et al.*, 1995) when the two claw surfaces hit each other. Furthermore, a rapid jet of water is formed when the dactyl plunger is driven into the propus socket, displacing water that escapes through a narrow anterior groove. Water jets elicited by slight tactile stimulation of the snapper claw in tethered animals show a well-focused main flow of water (width: about 30° at 3 cm distance) along an extension of the long axis of the snapper claw with maximum velocities of 3–10 m/s as revealed by flow visualization, high-speed video recordings, and laser Doppler anemometry (Herberholz and Schmitz, 1998; Schmitz and Herberholz, 1998).

Snapping can be used in offensive actions and to stun or even kill small prey such as grass shrimp and small pearl or goby fish (MacGinitie, 1937; MacGinitie and MacGinitie, 1949; Hazlett, 1962). In addition, by transferring hydrodynamic information toward the opponent via the water jet, snapping may warn the (usually conspecific) opponent not to enter an occupied shelter or territory. Intraspecific agonistic interactions in *A. heterochaelis* were previously studied by Nolan and Salmon (1970), Schein (1977), Conover and Miller (1978), and Hughes (1996a). In a thorough study of aggressive, submissive, and other acts in encounters between two snapping shrimp, Nolan and Salmon (1970) established general sequences of behaviors. Schein (1977) subsequently found that larger animals usually win, and that the eventually dominant shrimp displays more aggressive acts (*e.g.*, snaps). Chemical communication in *A. heterochaelis* was studied by Schein (1975) and Hughes (1996b), and the use of the cocked snapper claw as a visual signal was shown by Conover and Miller (1978) and Hughes (1996a); but the function of mechanosensory stimuli has not been studied previously.

The present paper is a quantitative analysis of the behaviors of the snapper shrimp and the receiver shrimp before, during, and after the snap. To understand the role of hydrodynamic stimuli in these interactions, we compared the responses of intact animals with those of snapping shrimp whose snapper claw had been occluded with clear lacquer.

This occlusion affects four types of setae, which have been morphologically described by Read and Govind (1991) as well as by Sullivan and Schmitz (1997), who also suggested possible functions for these setae. (1) Long

serrulate setae, up to 2.4 mm in length, show various types of serrulations and are found in groups (distally) or individually (proximally), especially near the lateral edges of the claw. These setae are usually loosely jointed at their bases and often show a preferential direction of movement; thus they are possible candidates for water jet reception and analysis. (2) Plumose setae, up to 1 mm in length, are restricted to the dorsal surface and are aligned along the closing edge of the propus. They may play a role in guiding and focusing the water jet. (3) Simple short setae, up to 0.1 mm in length, are evenly scattered over all the claw surfaces except the claw tip and the dactyl plunger. They appear to be fixed in a deep socket, and thus might represent contact mechanoreceptors. (4) Tubercles, which reach a diameter of 45 μm and a cone height of 35 μm , are restricted to three areas on the dorsal surface of the snapper claw. They are also thought to be contact mechanoreceptors.

The presence of these setae on the snapper claw suggests that occlusion of the claw might impede tactile interactions between the snapping shrimp and both production and reception of the water jet. Consequently, we have analyzed the behavior of intact and occluded shrimp during intraspecific agonistic encounters. Parts of the results have been published previously in abstract form (Schmitz and Iturrizaga, 1995; Herberholz and Schmitz, 1997a, b).

Materials and Methods

Forty adult snapping shrimp (*Alpheus heterochaelis*, length from rostrum tip to telson = 2.5–5.1 cm; 18 males and 22 females) were used in our behavioral experiments. Of these, 16 animals participated in encounters between two intact shrimp (experimental series I), and 24 different animals participated in encounters between one mechanosensorily deprived and one intact shrimp (experimental series II). The animals were caught among other snapping shrimp in waters of the gulf coast of Florida at the Florida State University Marine Laboratory in Sopchoppy and near Panacea. Prior to the experiments the animals were labeled with small numbers designed for marking queen bees and were kept individually in perforated plastic containers (11 × 11 × 15 cm) furnished with gravel and oyster shells for shelter. The containers were placed within a large tank (90 × 195 × 33 cm) with 330 l of circulating filtered seawater (salinity, 23–28‰; temperature, 22°–23°C). Proteins were removed from the water and pH, carbonate, oxygen, CO₂, and NO₃ were regularly controlled. The shrimp were exposed to an illumination cycle of 12 h light/12 h dark and fed frozen shrimp, fish, mussel, or *Artemia salina* three times a week.

Experiments were conducted within a 25 × 15 × 16 cm aquarium (water level, 8 cm; temperature, 22°C; floor, covered with black cloth to facilitate walking) on a platform

isolated from vibration (Breithaupt *et al.*, 1995). The short sides of the aquarium were covered with transparent paper, and two Schott KL 50 light guides on each side were used to enhance contrast for video recordings (average intensity = 50 lux). For mechanosensory occlusion the setae on the snapper claw of one shrimp were covered with clear lacquer (Pigrol Farben GmbH, Ansbach) while being viewed under a microscope. The intact opponent was treated in the same way, but did not receive the occlusion. Prior to the experiments two animals (both intact or one intact and one occluded, of the same or different sex) were placed in the aquarium for 10 min for acclimatization; the shrimp were separated by an opaque partition to prevent visual and tactile contact. After removal of the partition, all interactions between the shrimp were videotaped (camera, Panasonic AG 455; videorecorder, Panasonic AG 7355; monitor, Sony Trinitron) for 20 min from above and from the side by means of a mirror set at a 45° angle from the base of the aquarium. After each encounter with deprived animals the occlusion was reexamined, and behavioral data were evaluated only if the snapper claw was still completely covered with lacquer, which was true in the majority of cases. A snapping shrimp met the same conspecific only once and was usually tested no more than once a day. Seventy-two experiments with a total of 326 snaps were subsequently characterized using single-frame analysis (50 frames/s) and statistical procedures. Statgraphics Plus 6.0 and SPSS 6.0.1. were used for conventional statistics and circular statistics (Batschelet, 1981) for evaluating the mean vector direction, the angular deviation, and the length r of the mean vector.

For each animal, sex, body length, and snapper claw side, length, width, and thickness were determined in the living shrimp. Each snapping interaction was characterized by the latency between a preceding tactile interaction and the snap (disregarding durations of 5 s or more); the cocking duration, *i.e.* the time between completely opening the snapper claw (cocking the dactyl in a 100° position) and the beginning of claw closure; the distance between the opponents and the body alignment (head-head, head-tail, tail-head, tail-tail) during the snap; the goal of the snap; and the behavior and latency of both animals after the snap. The following angles were also measured:

1. The body axis angle β between the longitudinal body axes of the interacting animals (ranging from 0° to $\pm 180^\circ$, positive when ipsilateral to the snapper claw of the snapping animal and negative when contralateral to it; see Fig. 1A).

2. The position angle δ between the longitudinal body axis of the snapper and the line connecting the midpoints of both shrimp (range and sign definition as for the angle β ; see Fig. 1A).

3. The snapper claw angle γ between the snapper

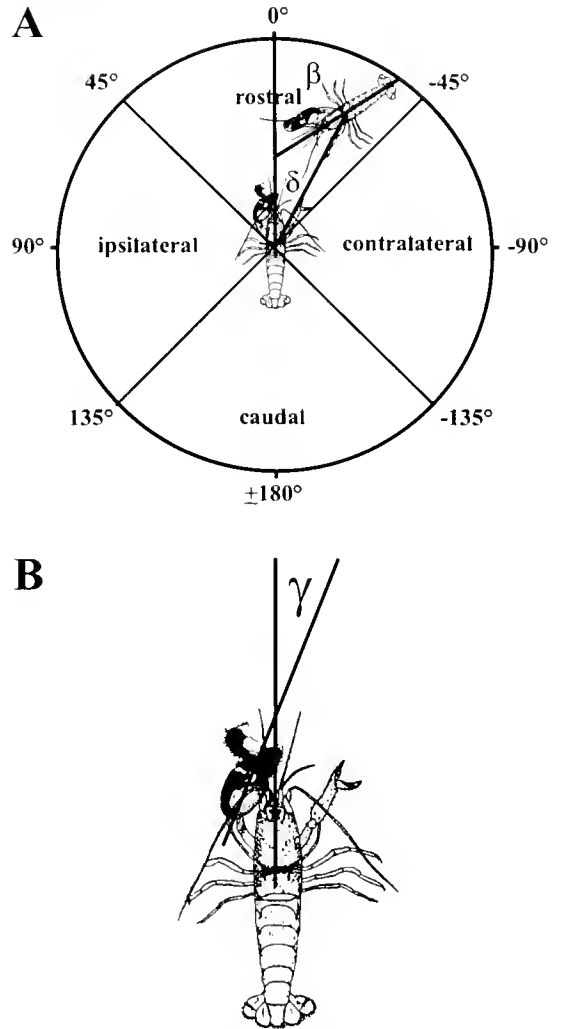


Figure 1. Definitions of the body axis angle β , the position angle δ , and the snapper claw angle γ in snapping shrimp interactions during snapping. (A) The body axis angle β is given by the angle between the longitudinal body axes of both animals, ranging from 0° to $\pm 180^\circ$; it is positive when ipsilateral to the snapper claw of the snapper and negative when contralateral to it. The position angle δ is given by the angle between the longitudinal body axis of the snapper and the line connecting the midpoints of both shrimp (range and sign definition as for β). (B) The snapper claw angle γ is given by the angle between the snapper claw long axis and the longitudinal body axis in the snapping animal; it is negative when crossing the animal's midline.

4. The tailfan angle with respect to the abdomen in the snapper (0°—fully folded, 90°—bent downwards, 180°—stretched out) during the snap.

Results

Our experiments with *Alpheus heterochaelis* were designed to compare the interactions of an intact snapping

shrimp and an intact conspecific (experimental series I) with the interactions of a snapping shrimp having an occlusion of the setae on its snapper claw and an intact conspecific (experimental series II). The deprived animal in experimental series II—like both intact shrimp in experimental series I—acted as the snapper, the receiver, or both during an experiment. Except for general characteristics, the behavior of the intact opponent in experimental series II was not analyzed; thus independent behavioral data are shown in most cases.

General characteristics and behavior before snapping

Intact shrimp produced an average of 3.4 ± 2.8 ($\bar{X} \pm SD$, $n = 218$) snaps per experiment towards each other (series I). Shrimp with an occluded snapper claw showed significantly fewer snaps per experiment ($\bar{X} \pm SD = 1.1 \pm 1.0$, $n = 45$) towards the intact opponent (Mann-Whitney U test: $P < 0.01$), but did not differ significantly from intact shrimp in the same series (II), which produced 1.6 ± 1.6 ($\bar{X} \pm SD$, $n = 63$) snaps per experiment towards them (Mann-Whitney U test: $P > 0.05$). In interaction experiments with two intact snapping shrimp, the mean body size of the snapping animal ($\bar{X} \pm SD = 3.7 \pm 0.8$ cm, $n = 218$) and the receiving animal ($\bar{X} \pm SD = 3.6 \pm 0.6$ cm, $n = 218$) did not differ significantly, which is also true for the body size of the snapper ($\bar{X} \pm SD = 4.0 \pm 0.2$ cm, $n = 108$) and the receiver ($\bar{X} \pm SD = 4.0 \pm 0.3$ cm, $n = 108$) in experiments with one mechanosensorily deprived shrimp.

To obtain information about the stimuli that elicit snapping, we analyzed the tactile interactions between the opponents before snapping occurred and measured the interval between the last contact and the snap, that is, the moment when the cocked snapper claw closed rapidly. Regardless of the condition of the snapper claw, frontal appendages (antennae, snapper claw, and pincer claw) were most frequently used in tactile interactions before snapping, while carapace, tailfan, and legs (summarized as B for "body") were less often contacted (Fig. 2A, B). There is a tendency for deprived animals—in comparison to intact ones—to be touched less often at the antenna and more often at the (occluded) snapper claw before snapping, and to be touched more often at the antenna before receiving a snap. However, χ^2 tests did not reveal any significant differences between intact or occluded snappers or receivers with regard to the touched body parts. The interval between touch and snap (disregarding durations of 5 s or more, which were rare) is 1.4 ± 1.1 s ($\bar{X} \pm SD$, $n = 169$) for intact snappers and 1.6 ± 0.8 s ($\bar{X} \pm SD$, $n = 29$) for mechanosensorily deprived snappers, and does not differ significantly (Mann-Whitney U test: $P > 0.1$) between these animals.

The cocking duration of the snapper claw before snap-

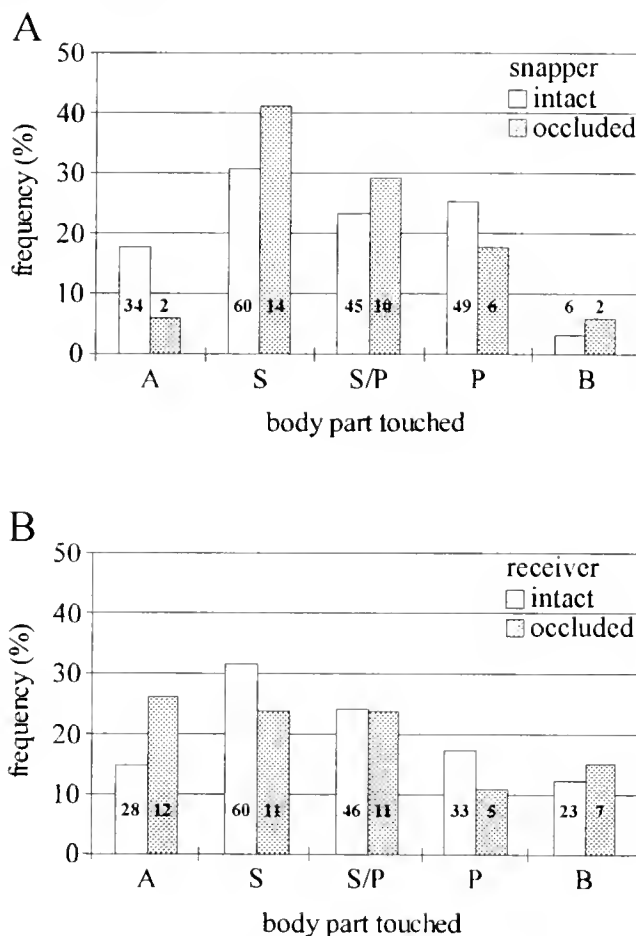


Figure 2. Frequency histogram of body parts of (A) the snapper and (B) the receiver touched by the opponent before snapping occurred in interactions between two intact animals (experimental series I, white columns) and in interactions of a shrimp with an occluded snapper claw and an intact shrimp (experimental series II; only data for the occluded animal are shown, dotted columns). A, antenna; S, snapper claw; S/P, snapper and pincer claw; P, pincer claw; B, body, *i.e.*, carapace, tailfan or legs. Here and in all following figures the numbers illustrate the numbers of observations.

ping (see Materials and Methods) is 513 ± 172 ms ($\bar{X} \pm SD$, $n = 193$) in agonistic encounters of intact shrimp and does not differ significantly (Mann-Whitney U test: $P > 0.1$) from the cocking duration of deprived snappers ($\bar{X} \pm SD = 532 \pm 136$ ms, $n = 37$). Cocking duration is not correlated with snapper claw length or body length.

Behavior during snapping

The snapper keeps its snapper claw parallel to its longitudinal body axis or slightly crossing the midline; the snapper claw angle γ is $-9.6^\circ \pm 15.4^\circ$ ($n = 203$, $r = 0.964$, circular statistics) for intact shrimp and $-0.9^\circ \pm 16.0^\circ$ ($n = 39$, $r = 0.960$, circular statistics) for deprived animals. The tailfan is usually kept at about a right angle

downward from the abdomen (circular mean for intact snappers: $73.6^\circ \pm 35.8^\circ$, $n = 205$, $r = 0.805$; circular mean for deprived snappers: $89.0^\circ \pm 41.0^\circ$, $n = 26$, $r = 0.750$), which simultaneously stabilizes the stance of the snapping animal and prepares it for escape after the snap (see below).

The body axis angle β between the longitudinal body axes of both animals during the snap is $7.8^\circ \pm 58.9^\circ$ ($n = 215$, $r = 0.471$, circular statistics) for intact shrimp and $8.9^\circ \pm 53.7^\circ$ ($n = 45$, $r = 0.558$, circular statistics) for shrimp with an occluded snapper claw (Fig. 3A). Thus, the distribution is rather symmetrical with respect to 0° in both cases. The absolute body axis angle $|\beta|$ is $44.8^\circ \pm 47.4^\circ$ ($r = 0.658$, circular statistics) for intact animals and $37.5^\circ \pm 44.8^\circ$ ($r = 0.690$, circular statistics) for deprived ones; that is, the longitudinal body axes of the interacting animals usually encompass small angles. The position angle δ between the longitudinal body axis of the snapper and the line connecting the midpoints of both animals is $2.4^\circ \pm 42.8^\circ$ ($n = 215$, $r = 0.721$, circular statistics) for intact snappers and $2.0^\circ \pm 29.6^\circ$ ($n = 44$, $r = 0.866$, circular statistics) for deprived snappers (Fig. 3A), and the absolute position angle $|\delta|$ is $29.1^\circ \pm 34.0^\circ$ ($r = 0.824$, circular statistics) for intact animals and $17^\circ \pm 24.9^\circ$ ($r = 0.905$, circular statistics) for deprived ones. Thus, regardless of the occlusion, the receiver is usually positioned in the rostral quadrant with respect to the snapper during the snap (see Fig. 1A). As illustrated in Figure 3A, small body-axis angles in combination with small position angles predominate in both cases. In addition, the shrimp usually face each other during the snap (h-h, head of snapper oriented towards head of receiver: 87% for intact animals, 89% for deprived animals); only rarely does the snapper face the tail of the receiver (h-t) or its tailfan closest to the receiver (t-h, t-t; Fig. 3B).

The distance between opponents during snapping is related to whether the snap is undirected or directed. In an undirected snap, the snapper claw of the snapper is not pointed toward the receiver. In a directed snap, the snapper claw is positioned so that the main flow of water (along an extension of the long axis of the claw; see Introduction) hits the receiver. The latter type, which is more frequent, occurs with shorter distances between the opponents (Fig. 4A). As shown in Figure 4A left, for directed snaps the distance between the tip of the snapper claw and the nearest body part of the receiver in extension of the snapper claw long axis is 0.9 ± 1.0 cm ($\bar{X} \pm \text{SD}$, $n = 117$, 54%) for intact shrimp and 0.9 ± 0.8 cm ($\bar{X} \pm \text{SD}$, $n = 25$, 56%) for mechanosensorily deprived animals. For undirected snaps (Fig. 4A right) the distance between snapper claw tip and the nearest body part of the receiver in any direction is 4.1 ± 3.0 cm ($\bar{X} \pm \text{SD}$, $n = 100$, 46%) for intact shrimp and 4.6 ± 4.2 cm ($\bar{X} \pm \text{SD}$, $n = 18$, 44%) for mechanosensorily deprived animals. Values for

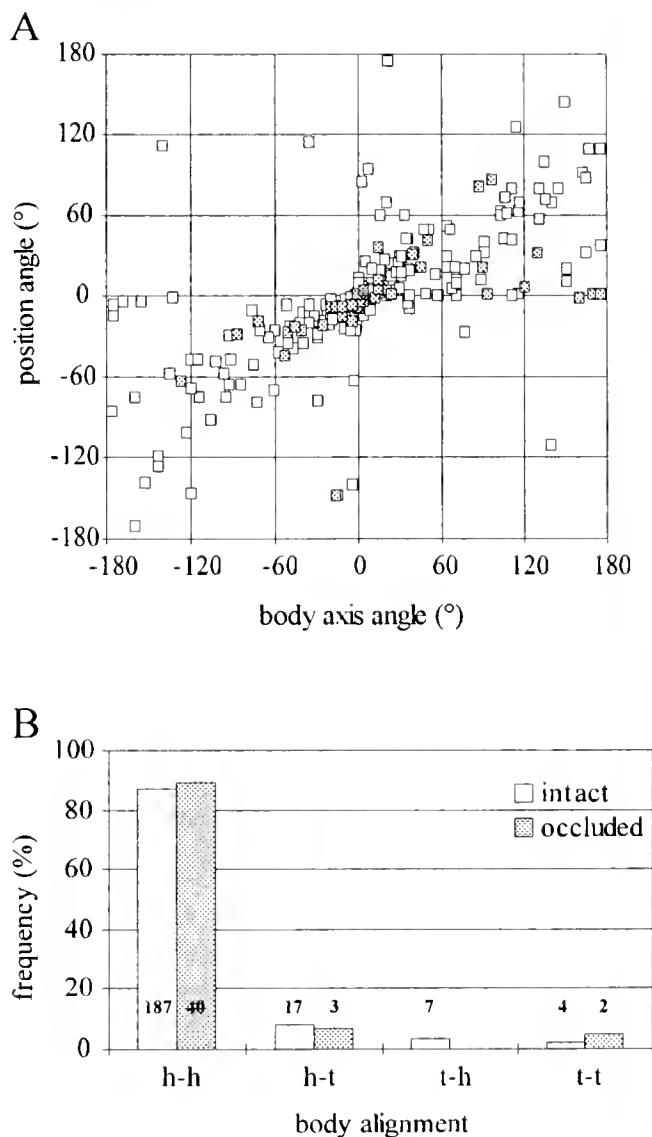


Figure 3. (A) Scatter plot of the position angle δ between the longitudinal body axis of the snapper and the line connecting the midpoints of both shrimp versus the body axis angle β between the longitudinal body axes of the opponents during snapping for intact shrimp (\square , $n = 215$) and animals with an occluded snapper claw (\square , $n = 44$); see Fig. 1 and text for definitions and details. (B) Frequency histogram of body alignments of both shrimp during the snap for intact shrimp (white columns, $n = 215$) and animals with an occluded snapper claw (dotted columns, $n = 45$). h, head, t, tail, first letter for the snapping animal and second one for the receiver; *i.e.*, h-t means that the head of snapper is closest to the tail of receiver.

intact and mechanosensorily deprived animals do not differ significantly (Mann-Whitney U test: $P > 0.5$), whereas in both groups of animals the mean distance for directed snaps is significantly smaller than that for undirected snaps (Wilcoxon test, $P < 0.01$ or < 0.05 , respectively). In interactions between intact snapping shrimp and in

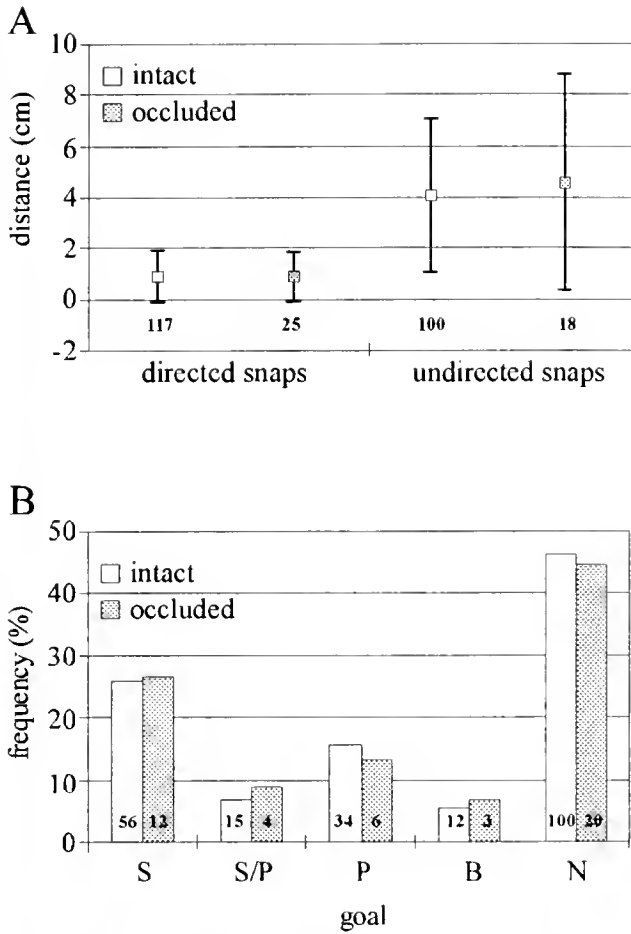


Figure 4. (A) Distance between opponents for intact snapping shrimp (open symbols) and animals with an occluded snapper claw (dotted symbols) during directed (left) and undirected (right) snaps. Values are means \pm SD. (B) Frequency histogram of the goal, i.e., the receiver body part first hit by the water jet of the snapping animal for intact shrimp (white columns) and animals with an occluded snapper claw (dotted columns). S, snapper claw; S/P, between snapper and pincer claw; P, pincer claw; B, body, i.e., carapace, tailfan or legs; N, none.

those between a shrimp with an occluded snapper claw and an intact animal, the goal of the directed snap is usually either the snapper claw or (less often) the pincer claw (Fig. 4B), both of which are densely covered with setae in intact animals. The area between the claws and other body parts is hit less often.

In our experiments, 30 snaps of intact snapping shrimp and 4 snaps of shrimp with an occluded snapper claw (initial snaps) were immediately (within 1 s) followed by a return snap of the opponent. In 3 of the 30 cases in experimental series I, the exchange of snaps was followed by a second snap from the initial snapper. As shown in Figure 5A (white columns), in intact snapping shrimp, initial snaps were more often directed towards the receiver; that is, they hit it more often (24 out of 30, 80.0%)

than return snaps (16 out of 30, 53.3%) and other snaps (77 out of 157, 49.0%). Similarly, as shown by the dotted columns in Figure 5A, all initial snaps of mechanosensorily deprived shrimp hit the receiver (4 out of 4, 100%), while subsequent snaps were less accurate (return snaps: 3 out of 8, 37.5%; other snaps: 18 of 33, 54.5%).

Averaging the distances for directed and undirected snaps reveals that for intact snapping shrimp the mean distance progressively increases from initial snaps ($\bar{X} \pm SD = 0.8 \pm 1.0$ cm, $n = 30$) to return snaps ($\bar{X} \pm SD = 1.7 \pm 1.6$ cm, $n = 30$) and to the other snaps ($\bar{X} \pm SD = 2.8 \pm 3.0$ cm, $n = 157$) with significant differences for initial and return snaps *versus* the remaining snaps (Wilcoxon test, $P < 0.05$, open symbols in Fig. 5B). For mechanosensorily deprived shrimp (dotted symbols in Fig. 5B) the mean distance for initial snaps amounts

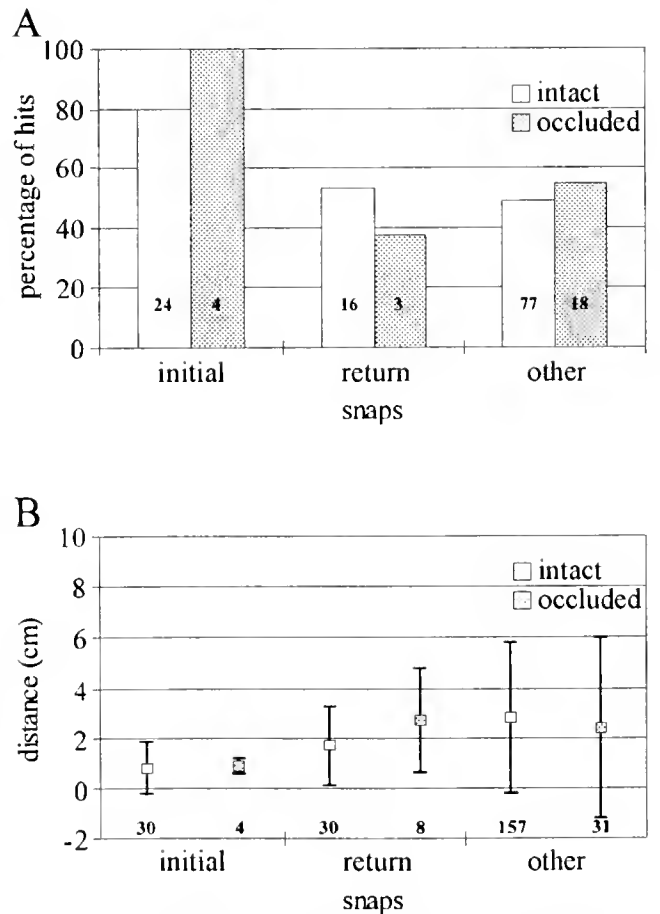


Figure 5. Comparison of different snap types. (A) Percentage of hits, i.e., of snaps directed towards the opponent, for initial snaps, return snaps, and the remaining snaps in intact shrimp (white columns) and animals with an occluded snapper claw (dotted columns). Numbers illustrate the numbers of hits. (B) Mean distance and standard deviation between the tip of the snapper claw of the snapping animal and the receiver for the three snap types in intact animals (open symbols) and mechanosensorily deprived shrimp (dotted symbols).

to 0.9 ± 0.3 cm ($\bar{X} \pm SD$, $n = 4$) and is lower than for return snaps ($\bar{X} \pm SD = 2.7 \pm 2.1$ cm, $n = 8$) and for the other snaps ($\bar{X} \pm SD = 2.4 \pm 3.6$ cm, $n = 31$).

Agonistic encounters between snapping shrimp were also analyzed with respect to the sex of the snapping animal. We analyzed 14 female/female, 5 male/male, and 13 female/male experiments from experimental series I (with two intact snapping shrimp) and 6 female/female, 8 male/male, and 14 female/male experiments from experimental series II (with one mechanosensorily deprived and one intact snapping shrimp).

As shown in Figure 6A, the percentage of hits (*i.e.*, of directed snaps) is significantly higher in males than in females (intact males: 52 of 79, 65.8%; intact females: 65 of 138, 47.1%; occluded males: 17 of 25, 68.0%; occluded females: 8 of 20, 40.0%; χ^2 tests, $P < 0.01$ for intact animals and < 0.05 for mechanosensorily deprived shrimp). In addition, as shown in Figure 6B, snapping distances of intact male snappers ($\bar{X} \pm SD = 1.6 \pm 2.2$ cm, $n = 79$) are significantly shorter than those of intact female snappers ($\bar{X} \pm SD = 2.8 \pm 2.9$ cm, $n = 138$) (Mann-Whitney U test: $P < 0.01$). The snapping distance of occluded males ($\bar{X} \pm SD = 1.9 \pm 3.3$ cm, $n = 24$) shows a trend towards being smaller than that of occluded females ($\bar{X} \pm SD = 2.8 \pm 3.1$ cm, $n = 19$), but does not differ significantly (Mann-Whitney U test: $P > 0.2$). As shown in Figure 6C, the mean cocking duration of intact males ($\bar{X} \pm SD = 583 \pm 173$ ms, $n = 66$) significantly exceeds that of intact females ($\bar{X} \pm SD = 477 \pm 160$ ms, $n = 127$) (Mann-Whitney U test: $P < 0.01$), whereas the difference between the cocking duration of occluded males ($\bar{X} \pm SD = 540 \pm 164$ ms, $n = 21$) and that of occluded females ($\bar{X} \pm SD = 521 \pm 82$ ms, $n = 16$) is not statistically significant (Mann-Whitney U test: $P > 0.6$). Thus, in intraspecific agonistic encounters, snapping shrimp exhibit sex-specific differences: males show a longer cocking duration than females, keep a shorter distance to the receiver during snapping, and hit it more often.

Behavior after snapping

In interactions between two intact animals, the first behavioral response after *directed* snaps differs remarkably between the snapper and the receiver (*cf.* white columns in Fig. 7A and 7B). The intact snapper usually retreats, *i.e.* either tailflips or withdraws more slowly (73.9% of the cases); less often it does not change its behavior (13.0%) or even approaches the receiver (13.0%). In contrast, the intact receiver usually approaches the snapper (51.3% of the cases); more rarely it retreats (28.2%) or does not change its behavior (20.5%). Intact snappers thus retreat significantly more often than intact receivers (Wilcoxon test, $P < 0.05$), and the latter

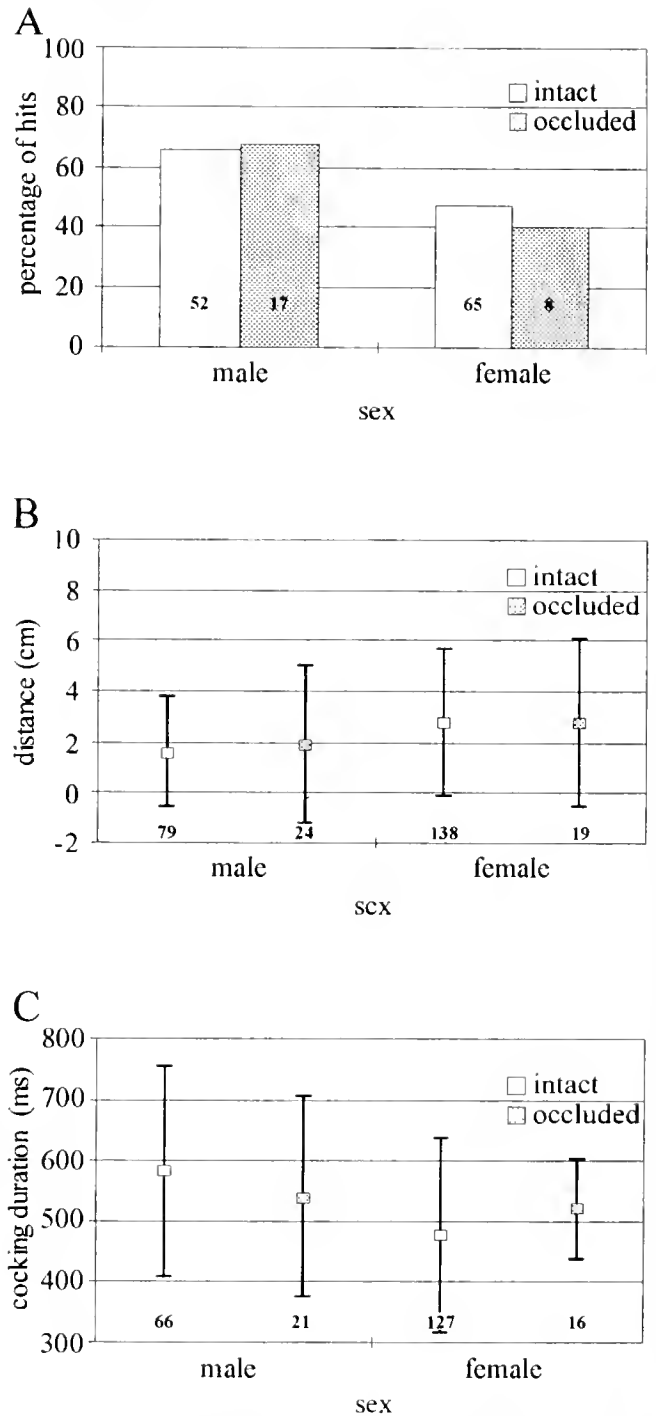


Figure 6. Comparison of male and female behavior before and during snapping. (A) Percentage of hits, *i.e.*, of snaps directed towards the opponent, (B) mean distance and standard deviation between the tip of the snapper claw of the snapping animal and the receiver, and (C) mean cocking duration and standard deviation for intact (white columns and open symbols) and mechanosensorily deprived (dotted columns and symbols) males (left) and females (right). *Cf.* Fig. 5.

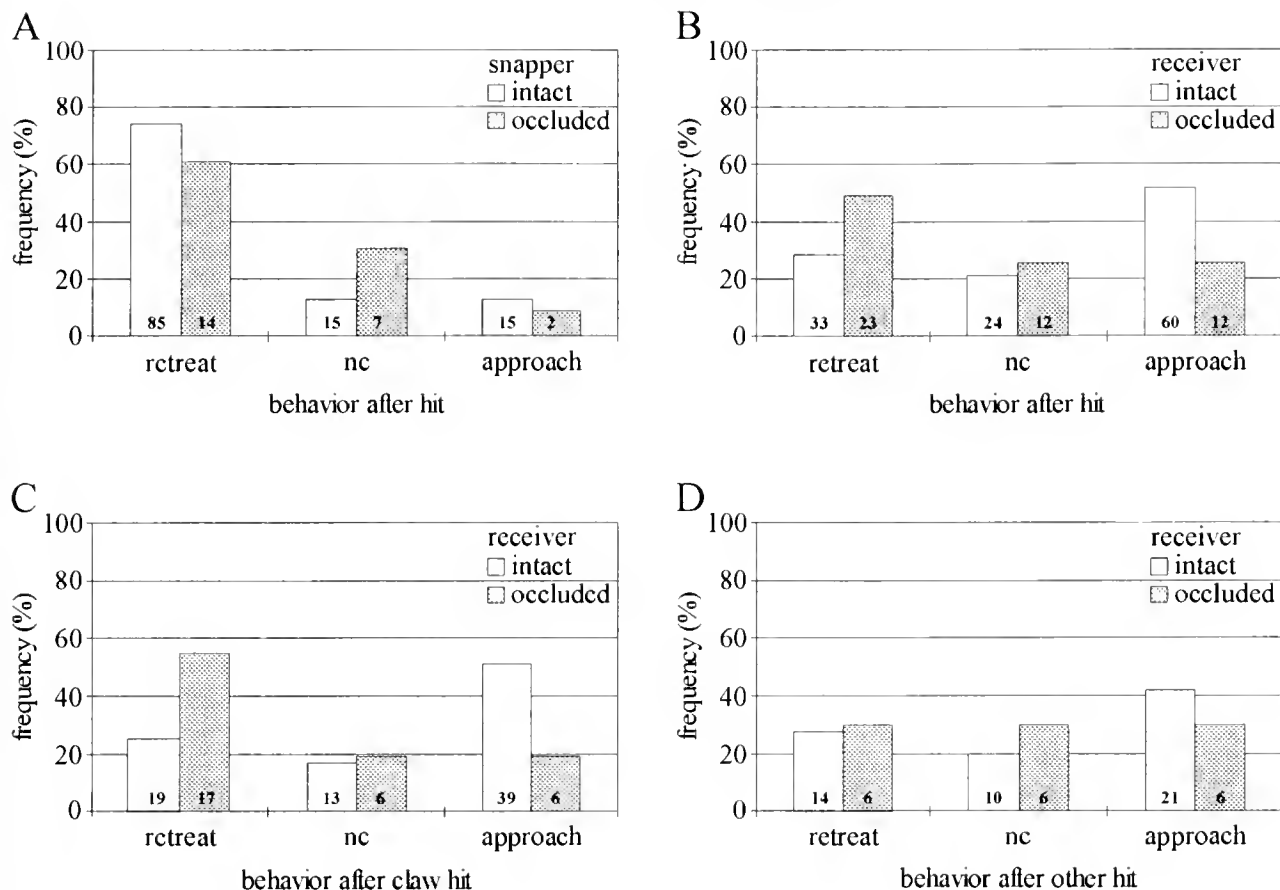


Figure 7. Frequency histograms of behaviors after directed snaps in the snapper (A), in the receiver (B), in the receiver after the snapper claw was hit (C), and in the receiver after other body parts were hit by the water jet (D); nc, no change. Data for intact animals are illustrated by white columns, data for shrimp with an occluded snapper claw by dotted columns.

approach significantly more often than intact snappers (Wilcoxon test, $P < 0.01$).

As illustrated in Figure 7A, the behavior of snappers with an occluded snapper claw (dotted columns) does not differ significantly from that of intact snappers (white columns; χ^2 test: $P > 0.1$). Deprived snappers likewise usually retreat (60.9% of the cases), less often do not change their behavior (30.4%), and only rarely approach the receiver (8.7%). Receivers with an occluded snapper claw, on the other hand, differ significantly (χ^2 test: $P < 0.01$) from intact receivers in their behavior after being hit by the water jet (Fig. 7B). They retreat in most cases (48.9%—more often than intact receivers), approach the snapper less often (25.5%) than intact ones, and show no change in their behavior somewhat more frequently (25.5%). It can be shown that this behavior is a result of snapper claw occlusion, since these animals exhibit a significant behavioral change (χ^2 test: $P < 0.01$, Fig. 7C) only when the water jet hits the snapper claw (goal = S or S/P, cf. Fig. 4B): when they

are hit on other body parts they behave like intact receivers (χ^2 test: $P > 0.5$; Fig. 7D).

Latencies between the directed snap and the first behavioral response are significantly higher for receivers than for snappers (Mann-Whitney U tests: $P < 0.01$ each for intact and mechanosensorily deprived snapping shrimp; Fig. 8A). In addition, latencies of deprived snappers ($\bar{X} \pm \text{SD} = 49 \pm 70$ ms, $n = 13$) are significantly higher than those of intact snappers ($\bar{X} \pm \text{SD} = 29 \pm 73$ ms, $n = 98$, Mann-Whitney U test: $P < 0.01$; Fig. 8A left), though the difference is small when considering the 20-ms resolution of the single-frame video analysis. Furthermore, deprived receivers show significantly higher latencies ($\bar{X} \pm \text{SD} = 156 \pm 190$ ms, $n = 34$) than intact receivers ($\bar{X} \pm \text{SD} = 41 \pm 75$ ms, $n = 90$, Mann-Whitney U test: $P < 0.001$; Fig. 8A right). It can be shown that this extremely prolonged latency is mainly due to occlusion of the snapper claw. In comparison to intact receivers, deprived snap receivers react with significantly higher latencies when being hit on the occluded snapper claw

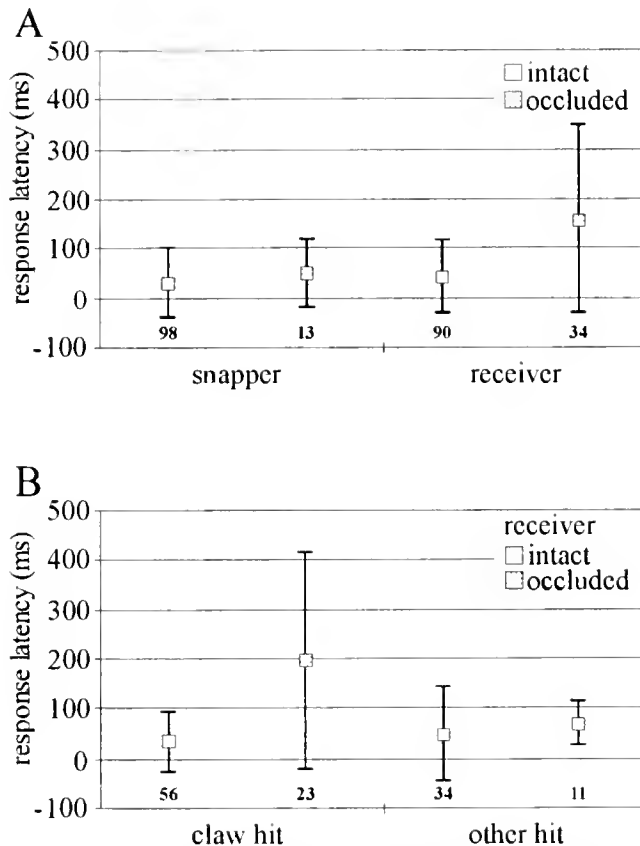


Figure 8. Response latency (means and standard deviations) after directed snaps in snappers (A, left) and receivers (A, right), in receivers after snapper claw hits (B, left), and receivers after hits of other body parts (B, right). Data for intact animals are illustrated by open symbols, data for shrimp with an occluded snapper claw by dotted symbols.

(intact: $\bar{X} \pm SD = 35 \pm 61$ ms, $n = 56$; occluded: $\bar{X} \pm SD = 197 \pm 219$ ms, $n = 23$; Mann-Whitney U test: $P < 0.01$; Fig. 8B right). There are also significant differences when other body parts are hit (intact: $\bar{X} \pm SD = 51 \pm 95$ ms, $n = 34$; occluded: $\bar{X} \pm SD = 71 \pm 44$ ms, $n = 11$; Mann-Whitney U test: $P < 0.05$; Fig. 8B left); however, here again the absolute difference is rather small.

These results show that snapping shrimp strongly depend on the mechanosensory system in intraspecific agonistic encounters. Intact mechanosensory equipment on the snapper claw is of great importance for snap receivers, while snapper claw occlusions have no effect, apart from slightly increased response latencies, on the behavior of the snapper.

Discussion

Snapping shrimp produce a fast, well-focused water jet by rapidly closing their large modified snapper claw, which is used in defensive and offensive interactions with conspecifics and prey. We quantitatively analyzed intra-

specific agonistic interactions between adults of the snapping shrimp species *Alpheus heterochaelis* to gain insights in the mechanisms of detection, identification, and localization of the opponent; the preparations for snapping (such as the approach and alignment of both shrimp, the positioning and cocking of the snapper claw); the snap itself (including the goal of the water jet); and finally the behaviors of both animals after the snap (approach and return snap, retreat, etc.). Our comparison of intact snapping shrimp and shrimp whose snapper claw had been occluded with clear lacquer did not reveal significant differences in the behavior of the two groups before and during snapping, but mechanosensorily deprived snap receivers differed significantly from intact shrimp in their behavior after receiving a snap. These issues are discussed in the following sections.

Behavior before and during snapping

Body alignment. The sequence of events during agonistic interactions of two snapping shrimp (*Alpheus heterochaelis*) starts with the approach of the animals as described by Nolan and Salmon (1970). At this point the shrimp might be aware of each other by visual, hydrodynamic, or chemical information. The opponents align their body axes during the approach. Shortly before snapping, the shrimp are thus facing each other in most cases: the receiver is usually situated in the rostral quadrant with respect to the snapper, and the body axes of both mostly encompassing small angles (Fig. 3). This alignment does not differ in intact shrimp and animals with an occluded snapper claw. Thus, any hydrodynamic receptors on the snapper claw (long serrulate setae; see Introduction) do not play an essential role in the alignment of the shrimp.

Tactile interactions. The reduced distance between the animals allows additional tactile interactions, which (when disregarding durations of 5 s or more) occurred about 1.5 s before the snap. The short latencies indicate that most snaps were actually elicited by the tactile stimulus, especially in view of the 0.5-s duration of snapper claw cocking, which is included in these latencies. The last contact before snapping predominantly involves frontal appendages, with the overall touch frequency for intact and occluded snappers and receivers decreasing from the snapper claw to both claws to the pincer claw to the antennae (Fig. 2). These tactile interactions include active antennal probing—see also the mutual antennulation mentioned by Nolan and Salmon (1970)—and active claw probing. Thus, contact mechano- and chemoreceptors on the antennae and claws are presumably stimulated in these interactions, which can provide information for the localization and recognition of the opponent. Shrimp with an occluded snapper claw do not differ significantly from intact animals in this behavior, indicating that the

presence of mechanoreceptors (long serrulate setae, simple short setae, and tubercles) or chemoreceptors on the snapper claw is not essential in this process.

Claw cocking. In the next step of the encounter, one of the opponents starts to cock the dactyl of its snapper claw in a 100° position. While cocking this claw the snapping animal usually shields its frontal body parts by keeping the claw slightly across the midline. Thus, the snapper claw represents not only a weapon but also a protective device (apart from its function in the analysis of received water jets—see below). During the cocking of the snapper claw, tension is built up by cocontraction of a claw opener and a claw closer muscle (Ritzmann, 1974). Release of this tension produces extremely rapid claw closure with a mean velocity of about 6 m/s (Schmitz and Herberholz, 1998), generating a water jet of similar initial velocity. The duration of cocking in our experiments ranged, on average, from 510 to 530 ms, did not depend on the claw or body size of the shrimp, and was significantly longer in males than in females (Fig. 6C). In addition, cocking duration did not change significantly after occlusion of the setae on the snapper claw; thus the clear lacquer, which covered the entire snapper claw surface except for the dactyl plunger, did not impede the cocking mechanism. Interestingly, the velocity of the water jet did not increase systematically with the cocking duration, but flow visualization, high-speed video recordings (1000 frames/s), and laser Doppler anemometry showed that the jet velocities were highest after cocking durations of about 550 ms (Herberholz and Schmitz, unpubl. data). Therefore, according to our measurements of cocking duration, males should produce faster water jets than females, and intact and mechanosensorily deprived shrimp should, on average, both show optimal cocking durations.

Snapping frequency. The number of snaps per experiment in deprived shrimp was significantly lower than in intact shrimp facing intact opponents (experimental series I), but did not differ significantly from that of the intact animals in the same experiment (experimental series II). This might be caused by a different snapping motivation in the animals of the two experimental series. On the other hand, snapping in mechanosensorily deprived shrimp might be reduced by the lack of information about the water jet of the intact opponent (see below), who in turn reduces its own snapping frequency, thereby saving energy in the interaction with a less aggressive and thus presumably subordinate opponent. The snapping frequency certainly influences the success of a shrimp in intraspecific interactions. Conover and Miller (1978) immobilized the snapper claw dactyl in *Alpheus heterochaelis* and showed that these shrimp—no longer able to snap—could not compete successfully with intact individuals in acquiring or holding a shelter.

Goal of water jets. As was mentioned by Volz (1938)

in an early study of *Alpheus dentipes* and *Synalpheus laevimanus*, the snapping sound may merely represent a side effect of the rapid claw closure. Furthermore, auditory organs have not been detected in snapping shrimp. We thus suppose that the water jet is analyzed by the receiving shrimp and that mechanosensory sensilla are used to analyze these hydrodynamic signals.

More than 50% of all snaps are directed towards the opponent. The percentage of hits is increased for initial snaps, which appear to be better prepared than return or other snaps (Fig. 5A), as well as for snaps produced by males as compared to females (Fig. 6A). Directed snaps of intact and mechanosensorily deprived snappers usually hit the receiver on its snapper claw (Fig. 4B), an accessible target because of the "face-to-face" alignment of the shrimp (Fig. 3), the large size of the snapper claw, and in case of return snaps, the fact that this claw usually shields the frontal body parts during the preceding snap. On the basis of their morphology and distribution, the long serrulate setae on the snapper claw are good candidates for a role in the analysis of water jet velocity and direction (Sullivan and Schmitz, 1997). However, the velocity of the water jet is so high at short distances that other receptors such as the simple short setae and even the tubercles (supposed contact mechanoreceptors) might also respond to this strong stimulation.

Interindividual distance and water jet velocity. The amplitude of the hydrodynamic signal at the receptors of the receiver depends on the intensity of the signal as well as on the angle and distance between the sender and the receiver. The average interindividual distance for directed snaps of both intact and mechanosensorily deprived snappers is 0.9 cm—significantly smaller than for undirected snaps (Fig. 4A). According to flow visualization experiments videotaped at 1000 frames/s, water jets produced by animals with a large snapper claw (more than 2 cm in length) cover the distance of 0.9 cm within 2.0 ms, and the velocity of the jet is 2.1 m/s when it reaches the target (Herberholz and Schmitz, 1998). In spite of these high velocities, obvious damage to the receiving shrimp has not been observed. Furthermore, the reception of a water jet does not impede the behavior of an intact receiver, since in a first response it usually does not retreat, but rather approaches the snapper (Fig. 7B) and may even launch a return snap. On the other hand, small sympatric crabs (*Eurypanopeus depressus*), which represent a prey or a competitor for *Alpheus heterochaelis*, are attacked with a water jet from even shorter distances (on average 0.3 cm) than conspecifics and can be physically injured by this jet (Schultz *et al.*, 1998). Thus, we conclude that snapping in intraspecific encounters in *A. heterochaelis* is not used to damage the opponent, but that water jets can be viewed as threat displays that allow the receiver to assess the strength, fighting ability, and possibly other

characteristics of the snapping animal. These results agree well with those of Knowlton and Keller (1982), who showed that in the snapping shrimp *Alpheus armatus*, physical damage sustained during intraspecific fights does not result from water jets during snapping but from direct contact between the animals.

Sex-specific differences in snapping. If transfer of hydrodynamic information rather than damage is the main function of the snapping behavior, sex-specific characteristics of the water jet should also be important. In *Alpheus heterochaelis*, the male has a larger snapper claw than a female of equal size, and the female in field-caught pairs is usually larger in body size, which increases her egg-carrying capacity (Nolan and Salmon, 1970; Schein, 1975; Hughes, 1996a). In sexually selected species, males usually are more aggressive than females. Although *A. armatus* is an exception to this rule (Knowlton and Keller, 1982), *A. heterochaelis* conforms to it. One example of the female's lower aggressiveness in this species comes from laboratory experiments (Conover and Miller, 1978) in which two females were more likely than two males to co-occupy a shelter. Furthermore, in our experiments, the males showed longer cocking durations, snapped from smaller distances, and hit the opponent more frequently than the females did (Herberholz and Schmitz, 1997b; Fig. 6). Thus, the magnitude of the male's cocking durations and the timidity of the female (which prevents her from getting close to the opponent before snapping) both lead to higher water jet velocities at the receptor site when the signal is produced by a male shrimp. In this way hydrodynamic information allows the shrimp receiving the water jet to identify the sex of its conspecific opponent, provided that the distance of the opponent is also perceived (e.g., visually). In addition, visual, chemical, or tactile cues may be used for sex recognition. Hughes found that the female of *A. heterochaelis*, in contrast to the male, does not assess the size of its opponent on the basis of the open-claw display (Hughes, 1996a) and also does not distinguish between male or female chemical cues (Hughes, 1996b). On the other hand, Jeng (1994) showed that distant chemoreception using the antennular flagella plays an important role in sex recognition and pairing in the snapping shrimp *A. edwardsii*.

Behavior after snapping

Although snaps not aimed at the opponent (i.e., undirected snaps) may also produce perceivable hydrodynamic signals, we restricted our analysis to the behavior of the snapper and the receiver after directed snaps. Intact snappers usually retreat whereas intact receivers usually approach the opponent (Fig. 7A, B), the receiver latency slightly exceeding that of the snapper (Fig. 8A). Thus, the retreat of the snapping animal might not be a response

to the approach of the receiver but rather an action that was initiated before the snap by bending the tailfan downward. On the other hand, the snapper might receive a rebound of its water jet from the snapper claw of the opponent, which in turn stimulates its own mechanosensory system and induces the withdrawal. The retreat of the snapper increases the distance between the opponents, which is compensated for by the approach of the receiver. About 24% of these approaches were followed within 1 s by a return snap of the receiver; for these cases the retreat of the initial snapper represents an evasive strategy, while the receiver by approaching increases its chances to hit the opponent more strongly. Only rarely are return snaps answered immediately by a second snap of the initial snapper. This can be explained by the high energetic costs of snapping—or at least we know that the intensity of the acoustic signal decreases in a series of successive snaps (Schmitz *et al.*, 1995), and we suppose that the same is true for the velocity of the water jet.

The behavior of receivers with an occluded snapper claw differs significantly from that of intact receivers. Deprived receivers predominantly show the withdrawal behavior that is characteristic for snappers (Fig. 7A, B), and this is especially true when the water jet hits the occluded snapper claw (Fig. 7C). These findings show that hydrodynamic receptors on the snapper claw (presumably the long serrulate setae) play an important role in analyzing the water jet. These receptors are suited to transmitting information about the frequency, the amplitude, and the direction of the hydrodynamic signal. Once this information is missing, the opponent cannot be assessed and localized properly, and it is safer for the deprived shrimp to withdraw. Animals with an occluded snapper claw in general show increased latencies in their behavior (Fig. 8A, B). The largest latencies, however, are shown by deprived receivers—especially when the snapper claw is hit. Thus, although different mechanoreceptors may also be used to analyze the water jet, receptors on the snapper claw—the body part that is most exposed and hit first and often—certainly are essential in guiding the behavior. For this reason, future studies will investigate the functional properties of snapper claw mechanoreceptors.

Acknowledgments

We thank the Florida State University Marine Laboratory at Sopchoppy and especially Cheryl Morrison for help in collecting the animals. We also thank Georg Heine for writing a circular statistics program, Raffael Iturrizaga and Eva Tiedge for help with video recordings and data analysis, and Peter Fraser for critically reading an earlier draft of the manuscript. Supported by grants of the Deutsche Forschungsgemeinschaft (Schm 693/5-1 and 5-2).

Literature Cited

- Barki, A., I. Karplus, and M. Goren. 1991.** The agonistic behaviour of the three male morphotypes of the freshwater prawn *Macrobrachium rosenbergii* (Crustacea, Palaemonidae). *Behaviour* **116**: 252–277.
- Batschelet, E. 1981.** *Circular Statistics in Biology*. Academic Press, London. 371 pp.
- Breithaupt, T., B. Schmitz, and J. Tautz. 1995.** Hydrodynamic orientation of crayfish (*Procambarus clarkii*) to swimming fish prey. *J. Comp. Physiol. A* **177**: 481–491.
- Brooks, W. K., and F. H. Herrick. 1891.** The embryology and metamorphosis of the Macrourea. *Mem. Nat. Akad. Sci. Wash.* **5**: 319–576.
- Caldwell, R. L., and H. Dingle. 1975.** Ecology and evolution of agonistic behavior in stomatopods. *Naturwissenschaften* **62**: 214–222.
- Conover, M. R., and D. E. Miller. 1978.** The importance of the large chela in the territorial and pairing behaviour of the snapping shrimp, *Alpheus heterochaelis*. *Mar. Behav. Physiol.* **5**: 185–192.
- Copp, N. H. 1986.** Dominance hierarchies in the crayfish *Procambarus clarkii* (Girard, 1852) and the question of learned individual recognition (Decapoda, Astacidea). *Crustacean* **51**: 9–24.
- Dingle, H. 1983.** Strategies of agonistic behavior in Crustacea. Pp. 85–111 in *Studies in Adaptation: the Behavior of Higher Crustacea*, S. Rebach and D. W. Dunham, eds. Wiley, New York.
- Elwood, R. W., and S. J. Neil. 1992.** *Assessment and Decisions. A Study of Information Gathering by Hermit Crabs*. Chapman & Hall, London. 192 pp.
- Gruener, H.-E. 1993.** *Lehrbuch der speziellen Zoologie*. Band I: Wirbellose. 4. Teil: Arthropoda. Gustav Fischer Verlag, Jena, Germany.
- Hazlett, B. A. 1962.** Aspects of the biology of snapping shrimp (*Alpheus* and *Synalpheus*). *Crustaceana* **4**: 82–83.
- Herberholz, J., and B. Schmitz. 1997a.** The role of visual and mechanosensory input during intraspecific agonistic encounters in the snapping shrimp (*Alpheus heterochaelis*). P. 251 in *Proc. 25th Göttingen Neurobiol. Conf. 1997*. Vol. II, N. Elsner and H. Wässle, eds. Thieme, Stuttgart, Germany.
- Herberholz, J., and B. Schmitz. 1997b.** Sexspecific behaviour in intraspecific agonistic encounters in the snapping shrimp (*Alpheus heterochaelis*). *Verh. Dtsch. Zool. Ges.* **90**: 355.
- Herberholz, J., and B. Schmitz. 1998.** The visible water jet: flow visualisation in snapping shrimp (*Alpheus heterochaelis*). P. 242 in *Proc. 26th Göttingen Neurobiol. Conf. 1998*. Vol. II, N. Elsner and R. Wehner, eds. Thieme, Stuttgart, Germany.
- Huber, R., and E. A. Kravitz. 1995.** A quantitative analysis of agonistic behavior in juvenile American lobsters (*Homarus americanus* L.). *Brain Behav. Evol.* **46**: 72–83.
- Hughes, M. 1996a.** Size assessment via a visual signal in snapping shrimp. *Behav. Ecol. Sociobiol.* **38**: 51–57.
- Hughes, M. 1996b.** The function of concurrent signals: visual and chemical communication in snapping shrimp. *Anim. Behav.* **52**: 247–257.
- Hyatt, G. W. 1983.** Qualitative and quantitative dimensions of crustacean aggression. Pp. 113–139 in *Studies in Adaptation: the Behavior of Higher Crustacea*, S. Rebach and D. W. Dunham, eds. Wiley, New York.
- Jeng, M.-S. 1994.** Effect of antennular and antennal ablation on pairing behavior of snapping shrimp *Alpheus edwardsii* (Audouin). *J. Exp. Mar. Biol. Ecol.* **179**: 171–178.
- Knowlton, N., and B. D. Keller. 1982.** Symmetric fights as a measure of escalation potential in a symbiotic, territorial snapping shrimp. *Behav. Ecol. Sociobiol.* **10**: 289–292.
- Knowlton, R. E., and J. M. Moulton. 1963.** Sound production in the snapping shrimps *Alpheus* (*Crangon*) and *Synalpheus*. *Biol. Bull.* **125**: 311–331.
- MacGinitie, G. E. 1937.** Notes on the natural history of several marine Crustacea. *Am. Midl. Nat.* **18**: 1031–1036.
- MacGinitie, G. E., and N. MacGinitie. 1949.** *Natural History of Marine Animals*. McGraw Hill, New York. 473 pp.
- Nolan, A. N., and M. Salmon. 1970.** The behaviour and ecology of snapping shrimp (Crustacea: *Alpheus heterochaelis* and *Alpheus normanni*). *Forma Functio* **2**: 289–335.
- Pavey, C. R., and D. R. Fielder. 1996.** The influence of size differential on agonistic behaviour in the freshwater crayfish, *Cherax cuspidatus* (Decapoda: Parastacidae). *J. Zool. Lond.* **238**: 445–457.
- Read, A. T., and C. K. Govind. 1991.** Composition of external setae during regeneration and transformation of the bilaterally asymmetric claws of the snapping shrimp, *Alpheus heterochaelis*. *J. Morphol.* **207**: 103–111.
- Ritzmann, R. E. 1974.** Mechanisms for the snapping behavior of two Alpheid shrimp, *Alpheus californiensis* and *Alpheus heterochaelis*. *J. Comp. Physiol.* **95**: 217–236.
- Schein, H. 1975.** Aspects of the aggressive and sexual behaviour of *Alpheus heterochaelis* Say. *Mar. Behav. Physiol.* **3**: 83–96.
- Schein, H. 1977.** The role of snapping in *Alpheus heterochaelis* Say, 1818, the big-clawed snapping shrimp. *Crustaceana* **33**: 182–188.
- Schmitz, B., and J. Herberholz. 1998.** Snapping movements and laser Doppler anemometry analysis of water jets in the snapping shrimp *Alpheus heterochaelis*. P. 241 in *Proc. 26th Göttingen Neurobiol. Conf. 1998*. Vol. II, N. Elsner and R. Wehner, eds. Thieme, Stuttgart, Germany.
- Schmitz, B., and R. Iturrizaga. 1995.** Snapping in intraspecific agonistic encounters in the pistol shrimp (*Alpheus heterochaelis*). P. 465 in *Nervous Systems and Behaviour*, M. Burrows, T. Matheson, P. L. Newland, and H. Schuppe, eds. Thieme, Stuttgart, Germany.
- Schmitz, B., M. van der Wall, and B. Simon. 1995.** Underwater acoustics of snapping in the pistol shrimp (*Alpheus heterochaelis*). *Verh. Dtsch. Zool. Ges.* **88**: 215.
- Schultz, S., K. Wuppermann, and B. Schmitz. 1998.** Behavioural interactions of snapping shrimp (*Alpheus heterochaelis*) with conspecifics and sympatric crabs (*Eurypanopeus depressus*). *Zoology—Analysis of Complex Systems, Suppl. 1*: **101**: 85.
- Söderbäck, B. 1991.** Interspecific dominance relationship and aggressive interactions in the freshwater crayfishes *Astacus astacus* (L.) and *Pacifastacus leniusculus* (Dana). *Can. J. Zool.* **69**: 1321–1325.
- Sullivan, J., and B. Schmitz. 1997.** The mechanosensory system of snapper and pincer claw in snapping shrimp (*Alpheus heterochaelis*). P. 250 in *Proc. 25th Göttingen Neurobiol. Conf. 1997*. Vol. II, N. Elsner and H. Wässle, eds. Thieme, Stuttgart, Germany.
- Volz, P. 1938.** Studien über das "Knallen" der Alpheiden. Nach Untersuchungen an *Alpheus dentipes* Guérin und *Synalpheus laevimanus* (Heller). *Z. Morph. Okol. Tiere* **34**: 272–316.
- Williams, A. B. 1984.** *Shrimps, Lobsters, and Crabs of the Atlantic Coast of the Eastern United States, Maine to Florida*. Smithsonian Inst. Press, Washington, DC.

Migratory Behavior of Ovigerous Blue Crabs *Callinectes sapidus*: Evidence for Selective Tidal-Stream Transport

RICHARD A. TANKERSLEY*, MARIA G. WIEBER, MARCO A. SIGALA,
AND KRISTEN A. KACHURAK

*Department of Biological Sciences, 1000 Hilltop Circle, University of Maryland Baltimore County,
Baltimore, Maryland 21250*

*In the late summer and early fall, newly inseminated female blue crabs (*Callinectes sapidus*) leave low-salinity areas of estuaries and migrate seaward to spawn near the entrance. We tested the hypothesis that migration of female *C. sapidus* to spawning grounds is facilitated by selective tidal-stream transport (STST). We monitored the swimming direction of adult crabs from a stationary platform located about 1 km inside the entrance to the Newport River Estuary (Beaufort, North Carolina). Swimming activity near the surface occurred primarily at night and most crabs avoided swimming against tidal currents. Eighty-one percent of the crabs observed moving down-estuary toward the inlet during ebb tide were ovigerous females. Of the 36 gravid females captured traveling in ebb currents, 97% possessed dark egg masses containing late-stage embryos. Conversely, nearly all (98%) adult crabs observed traveling in flood currents lacked egg masses, and all the females captured while migrating up-estuary exhibited signs of recent spawning. These observations indicate that ovigerous blue crabs use ebb-tide transport to migrate seaward to spawn and flood-tide transport to reenter the estuary shortly after larval release.*

Atlantic blue crabs (*Callinectes sapidus* Rathbun), like many brachyuran crabs, possess a complex life cycle that includes both estuarine and coastal migratory phases, making them ideal models for studying the intricacies of hydrodynamic transport, dispersal, and recruitment [see

(1) and (2) for reviews]. Although populations of *C. sapidus* are found from Cape Cod to Brazil (3), their life history and ecology have been best studied in the estuaries of the western Atlantic and the Gulf of Mexico, where they support a significant commercial fishery. Adult blue crabs are widely distributed throughout the estuary, but their densities are greatest in regions of low salinity. Mating occurs in brackish areas from late spring to early fall. Following insemination, female crabs migrate seaward to high-salinity (euhaline) areas near the mouth of the estuary to spawn (4). Details of the duration of the down-estuary migration for individual crabs are lacking, but results of mark-recapture studies in larger estuaries of the western Atlantic indicate that newly inseminated crabs may take 3–4 months to travel 150–300 km to euhaline regions [see (5) for review]. Spawning occurs after crabs have reached the lower region of the estuary. Females extrude newly fertilized eggs onto the pleopods, forming a large egg mass, or "sponge," under the abdomen (4, 6). Newly oviposited egg masses are yellow-orange, but as embryonic development proceeds, they gradually turn dark brown and eventually black (4, 6). Larvae (zoea) are released at or near the time of nocturnal high tide and remain in surface waters where they are advected seaward to undergo development in the high-salinity waters of the continental shelf [see (2) for review]. Thus, the long-distance migration of female crabs to euhaline areas is thought to ensure the survivorship and development of the larvae, which are unable to tolerate the low-salinity conditions within the estuary (7).

Despite many accounts of newly inseminated crabs migrating to the mouths of bays and rivers to spawn [see (5) for review], details of the migratory behavior of fe-

Received 30 April 1998; accepted 16 June 1998.

* To whom correspondence should be addressed. E-mail: tankersl@umbc.edu

Abbreviations: STST: selective tidal-stream transport.

male crabs and the underlying mechanisms that contribute to down-estuary transport have not been investigated. Horizontal transport of migrating crabs most likely involves the integration of behavioral traits, including oriented swimming and vertical migration, with predictable physical and hydrographic processes such as tidal currents. Gross movements of migrating female *C. sapidus* have been inferred from mark-recapture studies [see (5) for review]. Unfortunately, these studies lack sufficient detail to accurately describe the temporal (lunar, tidal, and diel) and spatial patterns of movement or to elucidate the relevant physical and biological processes that influence transport.

Most recent models of hydrodynamic transport of marine and estuarine organisms with complex life cycles focus on the integration of physical processes with complex behaviors, especially tidally synchronized vertical migrations (*e.g.*, 1, 2, 8, 9). Although the exact behaviors and mechanisms that female blue crabs employ for down-estuary migration have not been identified, it is likely that females use ebb-tide currents to enhance the rate and efficiency of seaward transport. Selective tidal-stream transport (STST) is a common life-history trait of many estuarine-dependent organisms and involves appropriately timed vertical migrations into the water column to exploit tidal currents. Up-estuary migration is accomplished through flood-tide transport, in which animals ascend into the water column during flood tides and remain on or near the bottom during ebb tides. Similarly, seaward migration, or ebb-tide transport, involves vertical migrations toward the surface during ebb tides and maintenance near the bottom during flood tides. Although examples of ebb-tide transport are rare, many estuarine organisms, including crab megalopae and juveniles (*e.g.*, 10), have been shown to possess tidally timed activity patterns and vertical migrations that result in flood-tide (up-estuary) transport. The objective of the present study was to document the STST behavior of ovigerous female blue crabs and to examine the relationship between the direction of migratory movements and tidal currents.

During the summer of 1997, we monitored the frequency of adult blue crabs entrained in surface currents in Beaufort Inlet, North Carolina. The observation point—a stationary platform suspended from a bridge about 1 km inside the entrance to the Newport River Estuary—hung approximately 1 m above the water surface at high tide. It provided a convenient vantage point for monitoring the migratory activity of adult crabs as they traveled down-estuary toward the inlet or up-estuary toward more brackish regions. During two 24-h periods, on 13–14 August and 16–17 August 1997, we continuously surveyed the swimming direction (down-estuary or up-estuary) and reproductive state (ovigerous or non-ovigerous) of adult crabs traveling past the platform. An ovigerous crab was

identified by its large egg mass and exposed semicircular abdomen. Since we were unable to differentiate between non-ovigerous female crabs and male crabs on the basis of observation alone, we used a dip net to capture crabs that came within a few meters of the platform and recorded their size (carapace width), sex, and egg mass color (if present). The study was repeated on 19–20 and 20–21 September 1997. On these dates, we restricted our observations to the hours between dusk and dawn since during the initial observation periods few crabs were spotted swimming near the surface during the day.

The results of the initial two 24-h observation periods are presented in Figure 1. Although fewer crabs were observed migrating during the September sampling periods, their movement patterns relative to tidal currents were similar to those recorded in August. Crabs swam primarily at night, and the frequency and swimming direction of those traveling past the platform was strongly correlated with the magnitude and direction of tidal currents (Fig. 1 and Table 1A). Although blue crabs are excellent swimmers, most of the animals we observed appeared to be transported passively (*i.e.*, “treading water”), and few were seen displaying the stereotypical sideways posture and rapid 5th pereopod movement associated with swimming in *C. sapidus* (11).

Most (81%) crabs observed moving down-estuary toward the inlet during ebb tide were ovigerous “sponge” crabs (Table 1A). Since we were unable (based on observations) to accurately determine the sex of crabs without egg masses, the remaining 19% were either non-ovigerous female or male crabs. Of the 36 gravid females captured traveling in ebb currents, 35 (97%) possessed dark sponges (brown or black) containing late-stage embryos. Microscopic examination of the larvae inside the eggs revealed they were within 2–3 days of hatching. Only one crab carrying early-stage eggs (yellow-orange sponge) was captured swimming near the surface (Table 1A) even though female crabs with newly oviposited egg masses frequently inhabit the area surrounding the platform from June to October (12; R. Tankersley, pers. obs.). Conversely, nearly all (98%) adult crabs observed traveling in flood currents lacked egg masses (Table 1A). Moreover, all crabs captured while migrating up-estuary exhibited signs of recent spawning, including the discoloration of the abdomen near the site of egg attachment and the presence of egg-mass fragments on the pleopods (Table 1B). Thus, the migratory behavior of *C. sapidus* females appears to be influenced by the presence of an egg mass and the developmental state of the embryos.

These observations support the hypothesis that ovigerous blue crabs undergo vertical migrations that are synchronized with tidal cycles and result in unidirectional seaward transport toward the entrance of estuaries (*i.e.*,

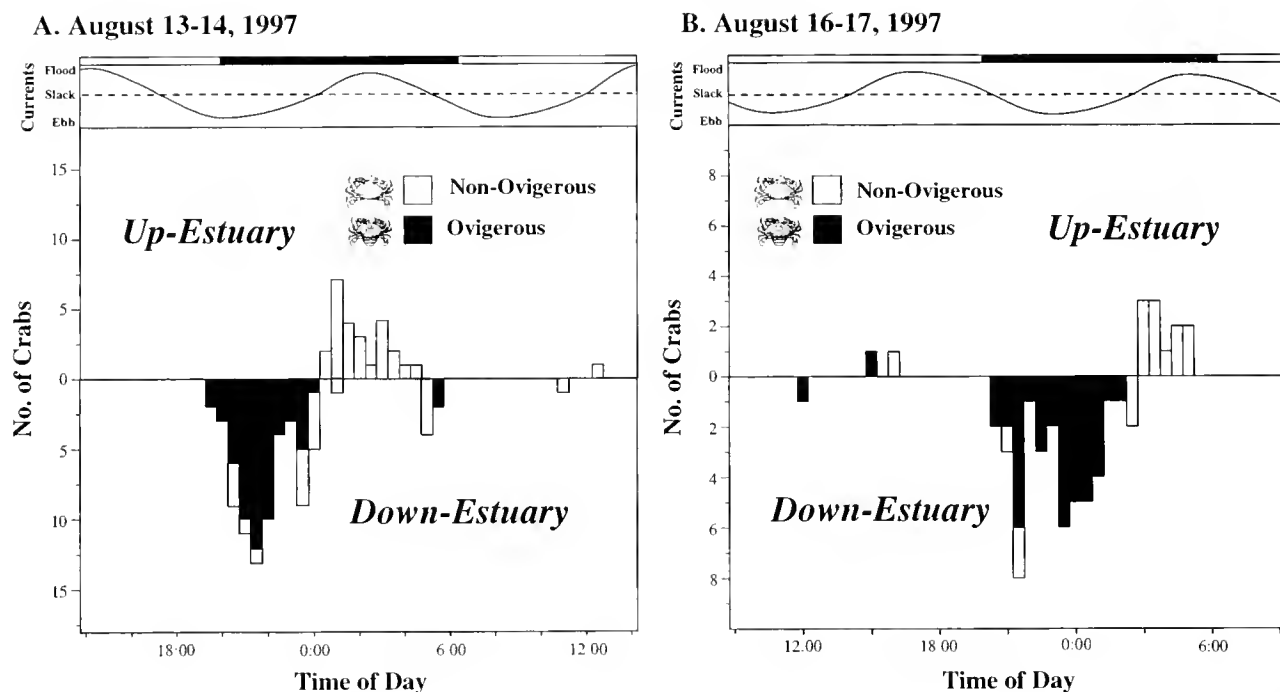


Figure 1. Frequency (plotted at 30-min. intervals) of adult blue crabs observed traveling either up-estuary or down-estuary near the surface during two 24-h observation periods (13–14 and 16–17 August 1997). Only crabs that entered a 6.8-m \times 10.1-m rectangular area surrounding the observation platform were censused and included in the study. At night, the area surrounding the platform was illuminated with a diffuse overhead light that had no apparent effect on the swimming behavior or activity of migrating crabs. Secchi disk depths ranged from 1.0 m to 2.5 m. The light:dark cycle and direction and magnitude of tidal currents are depicted in the top panels. Tidal current velocities were obtained from the computer program Tides and Currents Pro 2.5 (Nautical Software, Inc.).

Table 1

Number (in parentheses) and relative frequency of crabs traveling in flood and ebb currents

A. Observed crabs: From observations alone, only two categories of crabs could be distinguished				
Direction of transport	Crab type			
	Non-ovigerous crabs	Ovigerous females		
Up-estuary (Flood tides)	98% (48)	2% (1)		
Down-estuary (Ebb tides)	19% (24)	81% (103)		
Log-likelihood ratio test: $G = 105.2$, $df = 1$, $P < 0.0001$				
B. Captured crabs: Crabs caught for closer examination could be separated into four categories				
Direction of transport	Crab type			
	Pre-ovigerous females	Ovigerous females	Post-spawning females	Males
Up-estuary (Flood tides)	0% (0)	0% (0)	86% (6)	14% (1)
Down-estuary (Ebb tides)	5% (2)	88% (36)	0% (0)	7% (3)
Log-likelihood ratio test: $G = 35.7$, $df = 3$, $P < 0.0001$				

Note: Associations between crab type (*i.e.*, sex and reproductive condition) and direction of transport (up-estuary and down-estuary) were tested using a log-likelihood ratio test (G -test). Table values represent the pooled observations from four sampling periods in August and September 1997.

ebb-tide transport). The results also suggest that after spawning, female crabs reverse direction and move up the estuary in a saltatorial fashion (*i.e.*, flood-tide transport). A change in the direction of migration requires that the mechanisms responsible for synchronizing the vertical migratory behavior of female crabs with the appropriate tidal currents must shift 180° (*i.e.*, ≈ 6 h) following larval release. Alternatively, ovigerous and post-spawning crabs may rely on different mechanisms or cues to time their forays into the water column.

This migratory pattern is apparently not unique to the Newport River Estuary. In an extensive mark-recapture study conducted in the St. Johns River, Florida, Tagatz (13) found that females with developing eggs migrate from the river to the ocean just prior to larval release. Ovigerous crabs collected within the river had primarily yellow-orange egg masses, whereas most of those collected near the river's mouth and in coastal waters had dark brown or black sponges. Blue crabs that had recently possessed sponges were also observed reentering the lower 40 km of the river and developing a second sponge. Tagatz (13) also reported that several sponge crabs tagged in coastal waters lacked egg masses when they were recaptured in the river within a couple of weeks of their release.

Based upon our observations of the migratory behavior of ovigerous blue crabs in the Newport River Estuary and the results of previous mark-recapture studies [see (5) for

review], we have developed a conceptual model for the seaward migration of female blue crabs for spawning. The model is divided into two phases—a long-distance down-estuary phase in which newly inseminated non-ovigerous crabs travel seaward toward the lower reaches of the estuary (Phase I; Fig. 2), and a shorter distance spawning phase in which ovigerous crabs migrate from euhaline areas to the entrance of the estuary and coastal waters to release larvae (Phase II; Fig. 2). Although the timing of various components of the model may differ among estuaries, we believe that the sequence of events is similar.

Phase I (down-estuary migration) is initiated when, shortly after mating, newly inseminated crabs migrate seaward from brackish water toward the mouth of the estuary. Male crabs remain in low-salinity regions and do not migrate. Down-estuary migration of the females most likely occurs at night and is facilitated by STST on ebb tides. Depending upon the size of the estuary and their distance from the mouth, individual crabs may take weeks to months to complete their down-estuary migration. Upon reaching high-salinity regions, female crabs cease ebb-tide transport as their ovaries and eggs complete development. Crabs that mate in late spring may reach euhaline areas in time to spawn (*i.e.*, undergo Phase II) that same year (6). Crabs reaching the lower estuary in late fall overwinter near the mouth of the estuary and spawn the following spring.

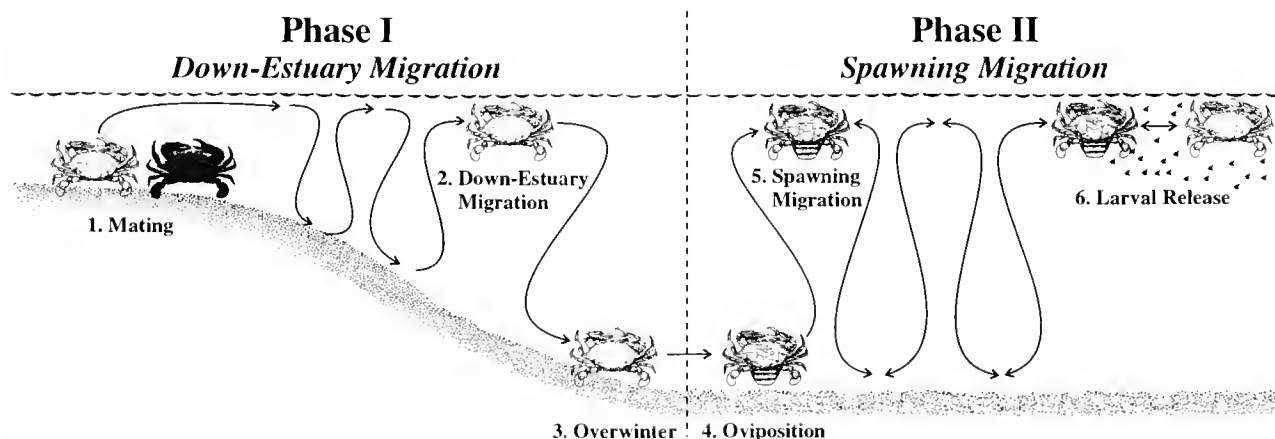


Figure 2. Diagram of the proposed conceptual model of the migratory behavior of female blue crabs. The model is divided into two phases, a down-estuary phase (Phase I) and a spawning phase (Phase II). (1) From late spring to early fall, adult crabs mate in the brackish regions of the estuary (dark crabs represent males; light crabs represent females). (2) Following insemination, female crabs migrate seaward using selective tidal-stream transport (STST) on nocturnal ebb tides. Male crabs remain in low-salinity areas. (3) After reaching euhaline regions, female crabs cease STST and may overwinter near the mouth of the estuary. (4) Spawning is initiated by the attachment of the egg mass (sponge) to the underside of the abdomen. About 10–12 days following extrusion of the sponge, female crabs with late-stage eggs migrate to the mouth of the estuary and possibly into coastal waters using STST on nocturnal ebb tides. (5) At the entrance to the estuary, larvae are released near the time of high tide at night. Shortly after larval release, female crabs reenter the estuary using STST on flood tides. Since some female crabs are capable of producing more than one brood, steps 4–6 may be repeated several times during a single season.

Phase II (spawning migration) of the model is initiated by the oviposition of fertilized eggs under the abdomen. Sponge crabs with early-stage eggs remain in the lower portion of the estuary and do not engage in STST. About 10–12 days after oviposition, female crabs with late-stage eggs migrate vertically toward the surface during nocturnal ebb tides and are transported seaward toward the entrance of the estuary and possibly into coastal waters. Upon reaching the mouth of the estuary, ovigerous females release their larvae near the time of nocturnal high tide. Due to the number of eggs in the egg mass, larvae may be released over several consecutive nights, as has been observed for the lobsters *Homarus gammarus* (14) and *Nephrops norvegicus* (15). Subsequently, post-spawning crabs reenter the estuary by migrating toward the surface during nocturnal flood tides. Since female blue crabs are capable of producing more than one egg mass (4, 5), individual crabs may undergo multiple spawning migrations in a single season.

The success of tidal-stream transport depends upon the time of entry into and exit from the water column, the length of time in the water column, and the animal's vertical position relative to tidal currents (8, 9, 16). Therefore, to be effective, vertical migrations underlying STST must be precisely timed with the correct tidal currents (8, 9). There are two alternative mechanisms that crabs might use to achieve this synchrony. First, these behaviors could be cued by a change in hydrologic variables, which is associated with the tides. Ovigerous crabs on the bottom at the start of a falling tide would experience an increase in water temperature and a decrease in salinity and pressure. Post-spawning crabs near the mouth of the estuary would be exposed to a decrease in water temperature and increases in hydrostatic pressure and salinity during flood tides. The kinetic and directional responses of crustacean early-larval stages to changes in pressure, salinity, and temperature have been well documented (*e.g.*, 17, 18, 19, 20, 21); similar environmental cues appear to mediate up-estuary transport of blue crab megalopae, which ascend into the water column during flood tides in response to an increase in salinity (22). Second, instead of responding to environmental stimuli, behavioral patterns could be synchronized with the tides by an endogenous tidal rhythm in vertical migration or activity. Juvenile eels (23) and fiddler crab postlarvae (24) have circatidal rhythms in swimming activity that appear to underlie STST. Regardless of the underlying mechanism, vertical migratory behaviors contributing to seaward transport toward the mouth of the estuary seem to be restricted to gravid female crabs carrying late-stage embryos (Table IB). Similarly, up-estuary migration on flood tides seems to be restricted to post-spawning females (Table IB). Male blue crabs and females with yellow-orange egg masses containing early-stage embryos do not appear to undergo STST. Thus,

we hypothesize that only egg-bearing females with dark sponges and crabs that have recently released larvae should respond to environmental cues associated with changing tidal conditions or possess an endogenous tidal rhythm that regulates swimming or activity and could be used for saltatory down-estuary or up-estuary transport.

Larvae of most estuarine crabs are hatched at specific times in the diel, tidal, and semilunar or lunar cycles. Although larval release for most brachyurans is under endogenous control, the timing may be controlled by the female, the developing embryos, or both [see (25) for review]. In the subtidal crabs studied (*Rhithropanopeus harrisi* and *Neopanope sayi*), egg hatching is mediated by communication between the larvae and the female (26, 27, 28). Near the time of hatching, substances released by the developing embryos induce ovigerous crabs to exhibit stereotypic larval release behaviors, including rhythmic pumping of the abdomen. Pheromones responsible for triggering this pumping response have been well studied [see (29) for review], and it is possible that similar substances released by the late-stage eggs may initiate the ebb-tide transport behaviors exhibited by ovigerous blue crabs.

Our conceptual model suggests that the transport behaviors responsible for down-estuary migration from brackish water (Phase I) are similar to those that produce the spawning migration (Phase II). Nevertheless, the adaptive value of STST during each phase may be different. For newly inseminated female crabs (Phase I), STST on ebb tides may be an energy-saving strategy since it would increase the speed and efficiency of transport and reduce the energy required for migration. Energy conserved during down-estuary transport may ultimately be used for reproduction. Conversely, migration toward coastal areas just prior to larval release (Phase II) may ensure the successful offshore transport of zoeae, which require high-salinity oceanic water for development (7). Other elaborate spawning behaviors and hatching patterns of estuarine crabs have been linked to the successful transport of larvae to coastal areas [see (23) for review]. Furthermore, recent computer simulations of the dispersal and recruitment of blue crab larvae in Delaware Bay indicate that biological and physical processes that favor offshore advection of newly hatched larvae may be more important than stock size in controlling levels of recruitment of older larvae or juveniles to adult habitats (30). Thus, hydrologic or meteorologic factors that either promote or impede STST by ovigerous females may have a significant impact on the reproductive success of the crabs and may be partially responsible for annual fluctuations in recruitment.

Acknowledgments

We are grateful to R. B. Forward, Jr., and D. Rittschof for their support, input, and critical review of the manu-

script, to the National Marine Fisheries Service for the use of the Pivers Island platform, and to D. I. Rubenstein for helping us design and execute the study. The project was funded in part by a summer research grant from UMBC and a project development grant from Maryland Sea Grant. M. A. Sigala was supported by a Ford Foundation Predoctoral Fellowship.

Literature Cited

1. Forward, R. B., Jr., R. A. Tankersley, M. C. DeVries, and D. Rittschof. 1995. Sensory physiology and behavior of blue crab (*Callinectes sapidus*) postlarvae during horizontal transport. *Mar. Fresh. Behav. Physiol.* **26**: 233–248.
2. Epifanio, C. E. 1995. Transport of blue crab (*Callinectes sapidus*) larvae in the waters off the mid-Atlantic states. *Bull. Mar. Sci.* **57**: 713–725.
3. Williams, A. B. 1974. The swimming crabs of the genus *Callinectes* (Decapoda: Portunidae). *Fish. Bull. U.S.* **72**: 685–789.
4. Van Engel, W. A. 1958. The blue crab and its fishery in Chesapeake Bay. Part I. Reproduction, early development, growth and migration. *Comm. Fish. Rev.* **20**: 6–17.
5. Millikin, M. R., and A. B. Williams. 1984. Synopsis of biological data on the blue crab, *Callinectes sapidus* Rathbun. FAO Fisheries Synopsis 138. NOAA Tech. Rep. NMFS 1, 43 pp.
6. Churchill, E. P. 1921. Life history of the blue crab. *Bull. U.S. Bureau of Fisheries for 1917–1918.* **36**: 95–128.
7. Costlow, J. D., and C. G. Bookhout. 1965. The effect of environmental factors on larval development of crabs. Pp. 77–86 in *Biological Problems in Water Pollution, 3rd Seminar.* C. M. Tarzwell, ed. U.S. Public Health Service, Pub. No. 999-WP-25.
8. Hill, A. E. 1991a. Vertical migration in tidal currents. *Mar. Ecol. Prog. Ser.* **75**: 39–54.
9. Hill, A. E. 1991b. A mechanism for horizontal zooplankton transport by vertical migration in tidal currents. *Mar. Biol.* **111**: 485–492.
10. DeVries, M. C., R. A. Tankersley, R. B. Forward, Jr., W. W. Kirby-Smith, and R. A. Luettich. 1994. Abundances of crab megalopae are associated with estuarine tidal hydrologic variables. *Mar. Biol.* **118**: 403–413.
11. Spirito, C. P. 1972. An analysis of swimming behavior in the portunid crab *Callinectes sapidus*. *Mar. Behav. Physiol.* **1**: 261–276.
12. Dudley, D. L., and M. H. Judy. 1971. Occurrence of larval, juvenile, and mature crabs in the vicinity of Beaufort Inlet, North Carolina. *NMFS Spec. Sci. Rep., Fisheries* **637**: 1–10.
13. Tagatz, M. E. 1968. Biology of the blue crab, *Callinectes sapidus* Rathbun, in the St. Johns River, Florida. *Fish. Bull.* **67**: 17–33.
14. Ennis, G. P. 1973. Endogenous rhythmicity associated with larval hatching in the lobster *Homarus gammarus*. *J. Mar. Biol. Assoc. U.K.* **53**: 531–538.
15. Møller, T. H., and J. R. Branford. 1979. A circadian hatching rhythm in *Nephrops norvegicus* (Crustacea: Decapoda). Pp. 391–397 in *Cyclic Phenomena in Marine Plants and Animals. Proceedings of the 13th European Marine Biological Symposium*, E. Naylor and R. G. Hartnoll, eds. Pergamon Press, Oxford.
16. Wippelhauser, G. S., and J. D. McCleave. 1987. Precision of behavior of migrating juvenile American eels (*Anguilla rostrata*) utilizing selective tidal stream transport. *J. Cons. Int. Explor. Mer* **44**: 80–89.
17. Sulkin, S. D. 1984. Behavioral basis of depth regulation in the larvae of brachyuran crabs. *Mar. Ecol. Prog. Ser.* **15**: 181–205.
18. Forward, R. B., Jr. 1990. Response of larval crustaceans to rates of change in temperature. *Biol. Bull.* **178**: 195–204.
19. Forward, R. B., Jr. 1989. Behavioral responses of crustacean larvae to rates of salinity change. *Biol. Bull.* **176**: 229–238.
20. Forward, R. B., Jr., and C. A. Wellins. 1989. Behavioral responses of a larval crustacean to hydrostatic pressure: *Rhithropanopeus harrisi* (Brachyura: Xanthidae). *Mar. Biol.* **101**: 159–172.
21. Forward, R. B., Jr., C. A. Wellins, and C. U. Buswell. 1989. Behavioral responses of larvae of the crab *Neopanope sayi* to hydrostatic pressure. *Mar. Ecol. Prog. Ser.* **57**: 267–277.
22. Tankersley, R. A., L. M. McKelvey, and R. B. Forward, Jr. 1995. Responses of estuarine crab megalopae to pressure, salinity, and light: implications for flood-tide transport. *Mar. Biol.* **122**: 391–400.
23. Wippelhauser, G. S., and J. D. McCleave. 1988. Rhythmic activity of migrating juvenile American eels *Anguilla rostrata*. *J. Mar. Biol. Assoc. U.K.* **68**: 81–91.
24. Tankersley, R. A., and R. B. Forward, Jr. 1994. Endogenous swimming rhythms in estuarine crab megalopae: implications for flood-tide transport. *Mar. Biol.* **118**: 415–423.
25. Forward, R. B., Jr. 1987. Larval release rhythms of decapod crustaceans: an overview. *Bull. Mar. Sci.* **41**: 165–176.
26. Forward, R. B., Jr., and K. J. Lohmann. 1983. Control of egg hatching in the crab *Rhithropanopeus harrisi*. *Biol. Bull.* **165**: 154–166.
27. Forward, R. B., Jr., D. Rittschof, and M. C. DeVries. 1987. Peptide pheromones synchronize crustacean egg hatching and larval release. *Chem. Senses* **12**: 491–498.
28. DeVries, M. C., D. Rittschof, and R. B. Forward, Jr. 1991. Chemical mediation of larval release behaviors in the crab *Neopanope sayi*. *Biol. Bull.* **180**: 1–11.
29. Rittschof, D. 1993. Body odors and neutral-basic peptide mimics: a review of responses by marine organisms. *Am. Zool.* **33**: 487–493.
30. Garvin, R. W., C. E. Epifanio, C. C. Epifanio, and K. C. Wong. 1997. Transport and recruitment of blue crab larvae: a model with advection and mortality. *Est. Coast. Shelf Sci.* **45**: 99–111.

Reports of Papers Presented at
THE GENERAL SCIENTIFIC MEETINGS
OF THE MARINE BIOLOGICAL LABORATORY,
Woods Hole, Massachusetts
10 to 12 August 1998

Program Chairs:
BARBARA BOYER, Union College
WILLIAM ECKBERG, Howard University
CHARLES HOPKINSON, Ecosystems Center, MBL
ROBERT PAUL MALCHOW, University of Illinois at Chicago

Each of these reports was reviewed by two members of a special editorial board drawn from the research community of Woods Hole, Massachusetts.

Reviewers included scientists from
THE MARINE BIOLOGICAL LABORATORY,
THE WOODS HOLE OCEANOGRAPHIC INSTITUTION,
AND THE NATIONAL MARINE FISHERIES SERVICE.

SHORT REPORTS FROM THE 1998 GENERAL SCIENTIFIC MEETINGS OF THE MARINE BIOLOGICAL LABORATORY

FEATURED ARTICLES

Atema, Jelle

Introduction. Tracking turbulence: processing the bimodal signals that define an odor plume 179

Weaver, Matthew, and Jelle Atema

Hydrodynamic coupling of lobster antennule motion to oscillatory water flow 180

Guenther, Carla M., and Jelle Atema

Distribution of setae on the *Homarus americanus* lateral antennule flagellum 182

SENSORY BIOLOGY

Mead, Kristina S.

The biomechanics of odorant access to aesthetascs in the grass shrimp, *Palaemonetes vulgaris* 184

Quinn, Elizabeth, Kristen Paradise, and Jelle Atema

Juvenile *Limulus polyphemus* generate two water currents that contact one proven and one putative chemoreceptor organ 185

Shashar, Nadav, Ferenc I. Hárosi, Anastazia T. Banaszak, and Roger T. Hanlon

UV radiation blocking compounds in the eye of the cuttlefish *Sepia officinalis* 187

Ruta, Vanessa J., Frederick A. Dodge, and Robert B. Barlow

Efferent modulation of physiological properties of the *Limulus* lateral eye 189

Edds-Walton, P. L., and R. R. Fay

Directional auditory responses in the descending octaval nucleus of the toadfish (*Opsanus tau*) 191

BEHAVIOR AND NEUROBIOLOGY

King, Jane Roche, and Hans Straka

Effects of vestibular nerve lesions on orientation turning in the leopard frog, *Rana pipiens* 193

Mensingher, Allen F., and Max Deffenbaugh

Prototype rechargeable tag for acoustical neural telemetry 194

Billack, Blase, Jeffrey D. Laskin, Prudence T. Heck, Walter Troll, Michael A. Gallo, and Diane E. Heck

Alterations in cholinergic signaling modulate contraction of isolated sea urchin tube feet: potential role of nitric oxide 196

Hoskin, Francis C. G., and John E. Walker

A closer look at the natural substrate for a nerve-gas hydrolyzing enzyme in squid nerve 197

Kuzirian, Alan M., Herman T. Epstein, Thomas J. Nelson, and Nancy S. Rafferty

Lead, learning, and calyculin in *Hermisenda* 198

Tamse, Catherine T., Katherine Hammar, D. Marshall Porterfield, and Peter J. S. Smith

Transmembrane calcium flux in Pb^{2+} -exposed *Aplysia* neurons 201

Malchow, Robert Paul, Michael P. Verzi, and Peter J. S. Smith

Extracellular pH gradients measured from isolated retinal cells 203

Andersen, Kristen A., and Robert Paul Malchow

Fluorometric analysis of intracellular sodium concentrations in isolated retinal horizontal cells 204

Jessen-Eller, Kathryn, Marjorie Steele, Carol Reinisch, and Nicholas Spitzer

Blockade of ryanodine receptors stimulates neurite outgrowth in embryos of *Spisula solidissima* 206

CELL AND DEVELOPMENTAL BIOLOGY

Porterfield, D. M., J. R. Trimarchi, D. L. Keefe, and P. J. S. Smith

Characterization of oxygen and calcium fluxes from early mouse embryos and oocytes 208

Silver, Robert B., Leslie A. King, and Alyssa F. Wise

Calcium regulatory endomembranes of the prophase mitotic apparatus of sand dollar cells contain enzyme activities that produce leukotriene B_4 but not 1,4,5-inositol triphosphate 209

Lee, Kyeng G., Nishal Mohan, Zoya Koroleva, Li-Fang Huang, and William D. Cohen

Fluorescence localization of cytoskeletal proteins in fibrin-trapped cells 211

Goda, Makoto, Shinya Inoué, and Robert Knudson

Oocyte maturation in *Chaetopterus pergamentaceus* observed with centrifuge polarizing microscope . . . 212

Miyake, Katsuya, and Paul L. McNeil

A little shell to live in: evidence that the fertilization envelope can prevent mechanically induced damage of the developing sea urchin embryo 214

Kuhns, William J., Xavier Fernandez-Busquets, Max M. Burger, Michael Ho, and Eva Turley

Hyaluronic acid-receptor binding demonstrated by synthetic adhesive proteoglycan peptide constructs and by cell receptors on the marine sponge *Microciona prolifera* 216

Kubke, M. F., E. Gilland, and R. Baker

Lipophilic dye labeling distinguishes segregated central components of the eighth cranial nerve in embryonic chicken 218

Straka, Hans, Edwin Gilland, and Robert Baker Rhombomeric organization of brainstem motor neurons in larval frogs	220
---	-----

ANIMAL HUSBANDRY AND DISEASE

Hanley, Janice S., Nadav Shashar, Roxanna Smolowitz, Robert A. Bullis, William N. Mebane, Howaida R. Gabr, and Roger T. Hanlon Modified laboratory culture techniques for the European cuttlefish <i>Sepia officinalis</i>	223
Maxwell, Michael R., William K. Macy, Shobu Odate, and Roger T. Hanlon Evidence for multiple spawning by squids (<i>Loligo pealei</i>) in captivity	225
Weidner, Earl, and Teresa King <i>In vivo</i> and <i>in vitro</i> growth of nerve parasite from <i>Lophius americanus</i>	227
O'Neill, Maureen D., Heather M. Wesp, Allen F. Mensinger, and Roger T. Hanlon Initial baseline blood chemistry of the oyster toadfish, <i>Opsanus tau</i>	228
Smolowitz, Roxanna, Elizabeth Wadman, and H. M. Chikarmane <i>Pseudomonas putida</i> infections of the oyster toadfish (<i>Opsanus tau</i>)	229

ECOLOGY

Schmitt, Catherine, Nathaniel Weston, and Charles Hopkinson Preliminary evaluation of sedimentation rates and species distribution in Plum Island Estuary, Massachusetts	232
--	-----

Griffin, Martin P. A., Marci L. Cole, Kevin D. Kroeger, and Just Cebrian Dependence of herbivory on autotrophic nitrogen content and on net primary production across ecosystems	233
Rogers, Jennifer, Jennifer Harris, and Ivan Valiela Interaction of nitrogen supply, sea level rise, and elevation on species form and composition of salt marsh plants	235
Sweeney, Jennifer, Linda Deegan, and Robert Garritt Population size and site fidelity of <i>Fundulus heteroclitus</i> in a macrotidal saltmarsh creek	238
Kirkpatrick, John, Ken Foreman, and Ivan Valiela Dissolved inorganic nitrogen flux and mineralization in Waquoit Bay sediments as measured by core incubations	240
Graham, Suzanne, Jessica Davis, Linda Deegan, Just Cebrian, Jeff Hughes, and Jennifer Hauxwell Effect of eelgrass (<i>Zostera marina</i>) density on the feeding efficiency of mummichog (<i>Fundulus heteroclitus</i>)	241
Legra, Jessica C., Roselle E. Safran, and Ivan Valiela Lead concentration as an indicator of contamination history in estuarine sediments	243
Safran, Roselle E., Jessica C. Legra, and Ivan Valiela Effects of nitrogen loading on eelgrass seed coat abundance, C to N ratios, and $\delta^{15}\text{N}$ in sediments of Waquoit Bay	245
Costello, John H., and Rebecca Coverdale Planktonic feeding and evolutionary significance of the lobate body plan within the Ctenophora	247

ABSTRACTS

Papers listed by title only	249
--	-----

Introduction to the Featured Articles

Tracking Turbulence: Processing the Bimodal Signals That Define an Odor Plume

When an odor is released from a source into the ambient air or water, it is carried with the current to form a scented (or flavored) plume. Many animals can track these odor plumes to their source to locate mates, food, or home areas. Odors elicit different behaviors in different species, such as the rheotaxis triggered in moths, and the odor-biased random walk observed in bacteria. Such well-known behavioral strategies are meant to facilitate plume tracking, but they are quite distinct from those of the American lobster (*Homarus americanus*) and related species.

Odor plumes in nature are complex hydrodynamic or aerodynamic structures, and most of them are turbulent (Fig. 1, left). American lobsters appear to rely, not just on the bulk movement of scent, but also on the internal fine structure of odor plumes—local fluctuations in both chemical concentration and microflow—to provide landmarks that aid in orientation and in tracking a plume to its source. We speculate, therefore, that tracking behavior requires the simultaneous guidance of two different sensory modalities—chemoreception and hydrodynamic mechanoreception; and we have referred to this behavior as eddy chemotaxis.

Support for this hypothesis comes from detailed statistical analyses of the rate of dispersal of odor concentration and the decay of turbulence-related velocity in flavored wakes and jets (complex odor plumes). Because chemical dispersal in the macroscopic world is always closely associated with its carrier flow, we would expect that the best information about odor plume structure would come from coincidence detection—the spatially and temporally coincident measurement of odor and flow. One would further expect that the scale of measurement should be matched to that of the flavored eddies in the plume.

Among the lobster's many and varied chemoreceptor organs, the lateral flagellum of the antennule not only has a pivotal role in social chemical communication (1), but is also the most important organ for tracking odors and locating their sources (2, 3, 4) (Fig. 1, center). The temporal filter properties of its chemoreceptor cells match the chemical dispersal patterns measured at the scale of the aesthetasc sensilla borne on the antennule (5, 6). The idea of coincidence detection, however, leads us to predict that the lateral flagellum is also the site of hydrodynamic receptors tuned to the scale of eddy flows characteristic of the lobster's odor world. The results of preliminary lesioning experiments support this notion. Lesions that are exclusively chemosensory (method of Derby and Atema, 7) are less damaging to tracking efficiency than is



Figure 1. (Left) Dye released near the sea bottom dispersed in a turbulent plume. The dye, as an analog of an odor, reveals the local variations in concentration due to turbulence. But as a marker, the dye also reveals small-scale patterns of flow. Odor patches and flow eddies appear to be coincident, so detection of both odor and flow might provide more information than either alone. (Center) An American lobster among the rocks and algae typical of this animal's benthic marine habitat. The antennules (see arrow) project upward toward an ambient stream, where sensilla on the lateral flagellum can sample passing chemical and hydrodynamic signals. (Right) Diversity of sensilla on the lateral flagellum of the American lobster. Borne on the ventral side of the flagellum (facing down) are long guard hairs and, between them, a thick tuft of chemoreceptive aesthetascs. Other types of sensory hairs can be seen on the dorsal and lateral surfaces; they are described by Guenther and Atema.

removal of the entire lateral flagellum (2, 4). This could mean that the hydrodynamic receptors, still intact, provide partial, but substantial information for tracking.

In the two papers that follow, we begin to focus on the lateral flagellum as a detector of hydrodynamic perturbations. Weaver and Atema analyze the hydrodynamic coupling of this organ to imposed water motion and conclude that both stretch and flow receptors could be detecting the observed frequency-dependent pivoting and whipping motions of the flagellum. Guenther and Atema describe the distribution of setae on the flagellum, including those with the potential for detecting relative water flow (Figure 1, right).

Chemoreception is not infrequently coincident with mechanoreception. Taste in vertebrates—from fish to humans—is mediated by taste buds that are innervated by both chemoreceptor and mechanoreceptor cells. The two receptor systems obtain information from exactly the same locations—*i.e.*, each single taste bud—then carry their information separately to the brain; there the systems project again in close proximity, interact, and form a joint spatial map of the mouth and gut, leading to bimodal output (8). The functional aim is obvious: animals need to sort the tasty items from among the others in the mouth. The flavored eddies of interest to the lobster present similar bimodal signals to its olfactory system, and that coincidence detection then provides superior information for tracking odor plumes.

—Jelle Atema
August 1998

Literature Cited

1. Karavanich, C., and J. Atema. *Anim. Behav.* (in press).
2. Devine, D. V., and J. Atema. 1982. *Biol. Bull.* 163: 144–153.
3. Reeder, P. and B. W. Ache. 1980. *Anim. Behav.* 28: 831–839.
4. Beglane, P. F., F. W. Grasso, J. A. Basil, and J. Atema. 1997. *Biol. Bull.* 193: 214–215.
5. Atema, J. 1996. *Biol. Bull.* 191: 129–138.
6. Gomez, G., and J. Atema, 1996. *J. Exp. Biol.* 199: 1771–1779.
7. Derby, C. and J. Atema. 1982. *J. Exp. Biol.* 98: 317–327.
8. Finger, T. 1982. Pp. 339–363 in *Sensory Biology of Aquatic Chemicals*, J. Atema *et al.*, eds. Springer Verlag, New York.

Reference: *Biol. Bull.* 195: 180–182, (October, 1998)

Hydrodynamic Coupling of Lobster Antennule Motion to Oscillatory Water Flow

Matthew Weaver and Jelle Atema (Boston University Marine Program,
Woods Hole, Massachusetts 02543)

Many animals use chemical, hydrodynamic, or aerodynamic signals to track odor plumes and thus locate odor sources. We have characterized some of the chemical signal dynamics, chemoreceptor filter properties, and behavioral responses involved in the tracking behavior of the lobster *Homarus americanus* (1). Now we have begun to analyze the hydrodynamic signal processing involved in this behavior. From the physics of odor dispersal, we predict that eddy size and velocity should contain important signals for tracking spatial gradients in jets and wakes, both of which are common dispersal patterns in nature. Antennules are important sensory organs, best known for their olfactory capabilities and for the application of this function to tracking behavior. We hypothesize that the antennule is also a detector of hydrodynamic flow, designed particularly to track “flavored” eddies (2). These organs do indeed respond to mechanical stimuli, but the structure and function of the relevant mechanoreceptors is not understood. The present study was designed to determine the coupling of antennule motion to water

motion over a range of frequencies and amplitudes that are found in the eddies of natural odor plumes.

We clamped excised antennules at their natural attachment point—the distal basal segment—to allow for natural motion. We placed them perpendicular to oscillatory flow in the central axis of a cylinder made of clear acrylic plastic (length, 30 cm; diameter, 20 cm) with the sensillar tuft facing in the direction of flow; application of an oscillatory flow is a convenient physical approach to characterizing the antennule’s potential as a detector of water motion. We then measured the displacement of the lateral flagellum over a frequency range of 1–50 Hz in response to sinusoidal water displacements of 10, 30, 60, and 100 μm (peak to peak). Water motion was measured visually from the movement of naturally occurring, suspended particles (the error for 15 repeated independent measurements was <5%). The same method was used to measure flagellar motion at three locations: the tip, the most distal tuft segment, and the center of the tuft. The measurements were taken frame by frame from a

videotape recorded through a dissecting microscope; on-screen magnification was 100×. Water movement was generated with a motor that vibrated the diaphragms fitted to each end of the cylinder. The motor was powered with a sine wave generator and an amplifier.

The resulting flagellar motion had a resonance frequency of 7–12 Hz that was evident at all imposed amplitudes of water motion (Fig. 1A). Furthermore, the flagellar motion consisted of two components: pivoting at the base, and an additional whipping at the tip. The pivoting motion of the flagellum causes differences in relative water flow along its length. In particular, water displacement is greater than flagellar displacement at the basal region, whereas the reverse is true at the tip. Between these two extremes lies a "null" region where the water motion and flagellar displacement are equal (Fig. 1C), but phase differences (not measured) could still cause relative water motion in the null region. This "null" region changes in location along the flagellum in response to changes in frequency. Additional whip action (resulting from the gradual decrease in diameter and stiffness toward the tip of the flagellum) causes complex, frequency-dependent changes in flagellar motion among the three locations (Fig. 1B). Since the flagellum has different characteristic motions for different frequencies of water oscillation, it could provide the lobster with an analysis of frequency.

From these biomechanical results, we conclude that the lateral flagellum could measure water motion with two different types of sensors: external flow detectors that would analyze relative water flow over the flagellar surface, and intersegmental stretch receptors that would measure flagellar bending. Uniform oscillatory flow within the frequency range used in this study may not be a common occurrence in the lobster's natural environment, but the water velocities that were created with this method (0.033 mm/s–4.9 mm/s) are a real part of the lobster's hydrodynamic world. The mechanical properties of the flagellum could be used to discriminate eddies of a particular size range from the general hydrodynamic noise of the lobster's surroundings. The pronounced 7–12 Hz resonance may be linked to velocities and accelerations characteristic of eddies of interest to lobsters.

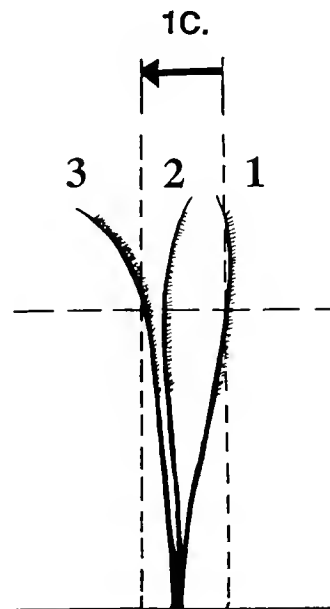
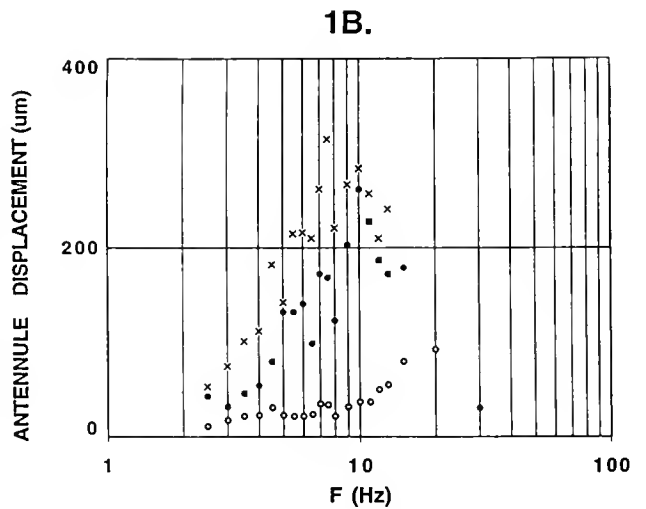
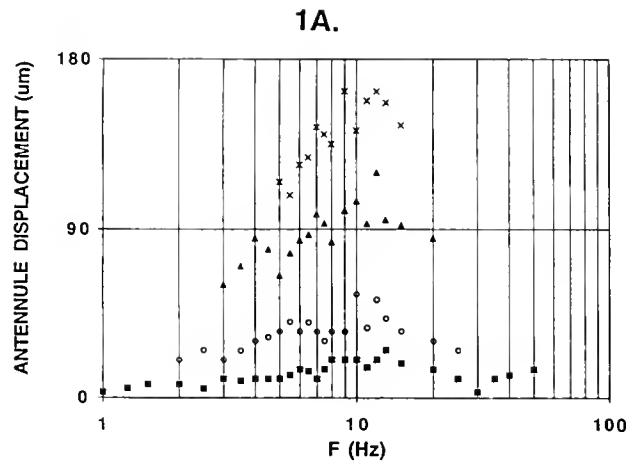


Figure 1. Hydrodynamic coupling of lateral antennular flagellum to water oscillation over a range of 1–50 Hz. (A) In this example the water was oscillated to produce four water displacements: 10 (■), 30 (○), 60 (▲), and 100 µm (×) peak to peak. The resulting flagellar displacement was always measured at the most distal aesthetasc segment, and it peaked at about 10 Hz. (B) In this example the water was oscillated to produce a 60 µm displacement. The resulting flagellar displacement was measured at three locations: tip (×), distal tuft segment (●), and mid-tuft segment (○). Note that the peak displacement of the most flexible area (tip) occurs at a relatively low frequency; at stiffer locations, the peak in displacement occurs at a higher frequency. (C) Sketch of complex flagellar motion in which the flagellum moves from its resting position (1), to an intermediate position (2), then to a final position (3). The motion of the flagellum is driven by water flow; the arrow represents half of an oscillation. This motion has two components: pivoting at the base of the flagellum and whipping at the tip. The broken horizontal line separates the distal and basal regions. At the distal region, the flagellar displacement exceeds water displacement; at the basal region, the reverse holds. Displacement is exaggerated by about 100× for clarity.

We focus here on the potential of the lateral flagellum as a "passive" detector of water flow. The well-known flicking of the antennule, with maximum rates of 5 Hz, is thought to subserve chemosensory sampling. Moreover, the flow velocity of 10 cm/s during flicking far exceeds the maximum velocities used in this study. Flicking is rare during odor plume tracking.

We thank Drs. Richard Fay and Thomas Breithaupt for valu-

able advice and discussions. Special thanks to T. B. for loan of the shaker apparatus. Supported by NSF grant IBN# 9723542 and an REU supplement.

Literature Cited

1. Atema, J. 1995. *Proc. Natl. Acad. Sci.* **92**: 62–66.
2. Atema, J. 1996. *Biol. Bull.* **191**: 129–138.

Reference: *Biol. Bull.* **195**: 182–183. (October, 1998)

Distribution of Setae on the *Homarus americanus* Lateral Antennular Flagellum

Carla M. Guenther and Jelle Atema (Boston University Marine Program, Woods Hole, Massachusetts 02543)

The lateral antennular flagellum of the lobster *Homarus americanus* is a well-studied chemoreceptor organ, but it may have an additional hydrodynamic receptor function. Its chemoreceptive function is linked to both social behavior and feeding behavior; reversible lesions of the chemoreceptor cells, but not mechanoreceptors, abolish individual recognition via urine-borne pheromones (1) and suppress chemotactic orientation and tracking of food odors (2). Most chemical stimuli are received by the 1000 or more aesthetasc sensilla located in a prominent "tuft" on the distal two-thirds of each bilateral flagellum. Each aesthetasc is innervated by some 300 chemoreceptor cells. Several other sensillar types are present that remain rather poorly known in all respects: morphology, physiology, and behavioral function. The most prominent among these sensilla are the "guard" and "companion" hairs, and more recently an "asymmetric" hair has been identified (3). Stimulation of these types of hairs causes clear mechanoreceptor responses in the flagellar nerve (C. Balint, pers. comm.). Other mechanoreceptive structures such as proprioceptors may be present.

We hypothesize that the antennules may function, not only as critical chemoreceptor organs, but also as essential hydrodynamic detectors of eddy features in odor plumes (4). Coincident detection of chemical and hydrodynamic features would allow the animal to track a plume of flavored eddies to the source of an odor. Here we present the first comprehensive study of the setal arrangement of the lateral flagellum. If we combine this work with studies of hydrodynamic coupling (5), we can begin to identify the receptor structures that are most likely involved in the analysis of water motion, especially motion in the range of eddy sizes and velocities common to odor plumes of interest to lobsters.

We examined 24 intact flagella, ranging in length between 32 mm and 53 mm from 21 animals that ranged in carapace length from 78 mm to 91 mm; most animals were ablated unilaterally. We used light and scanning electron microscopy to identify the different setal types and to map them onto the lateral flagellum (Fig. 1). Based on the distribution of the prominent aesthetasc sensilla, the flagellum can be divided into three regions with transition zones between them. The BASE is the

mechanically stiff (5) proximal region of 27 (± 4.5 SEM) segments, each bearing few setae. A 5 (± 3.0 SEM)-segment BASE TRANSITION zone has at least one aesthetasc sensillum, but fewer than two full rows of aesthetasc per segment; it contains a greater variety of setae. The TUFT region is defined by segments each of which bear at least two full rows of aesthetases; the region comprises 57 (± 10.0 SEM) segments, each supplied with a variety of different setae. A short, 2 (± 3.3 SEM)-segment TIP TRANSITION zone with poorly organized aesthetases and other setae leads to the 7 (± 5.2 SEM)-segment TIP region, which lacks aesthetases and most other setae. The number of segments within each region varies from one antennule to the next, even on the same animal. The tip can be missing entirely, and the transition zones can be very short as well.

We recognized 7 setal types grouped into 2 classes according to Watling (6):

Type I annulate, with setules

Supracuticular plumose: ball socket, setules emerge along

shaft in two opposite rows; 170 μm long \times 10 μm diameter

Serrulate: woven setules on one side only; 80–120 μm

long \times 20 μm diameter

Cupped serrulate: cuticular lip, woven setules over $\frac{3}{4}$ of

surface; 90 μm long \times 25 μm diameter

Type II annulate, without setules

Aesthetasc: cylindrical shaft, multiannulate, thin cuticle;

600 μm long \times 20 μm diameter

Guard (slim acuminate): smooth, thick cuticle, tapering

shape after mid-length annulation; 900 μm long \times 40 μm

diameter

Companion (slim acuminate): similar to guard; 580 μm

long \times 30 μm diameter

Asymmetric (simple): smooth, wiry, twisted, tapering;

180 μm long \times 12 μm diameter

A typical tuft segment contains all seven setal types arranged as follows. Two straight rows of 10–12 aesthetasc sensilla perpendicular to the long axis of the antennule occur on the ventral side. The distal row is flanked on either side by a guard hair; these are flanked in turn by one or two companion hairs; an asymmetric hair is irregularly found between aesthetasc and guard hairs on the lateral side; and a plumose hair can be found

Sheet 1

Setae	Location					
	Regions	Base	Transition	Tuft	Transition	Tip
Segment Number	[no./region]	1-27 [27]	28-32 [5]	33-89 [57]	90-91[2]	92-98 [7]
Type I						
1	supracuticular plumose		x	x		
2	serrulate	x	x	x	x	x
3	cupped serrulate	x	x	x	x	
Type II						
4	aesthetasc		x	x	x	
5	guard (slim acuminate)		x	x	x	
6	companion (slim acuminate)		x	x	x	
7	asymmetric (simple)			x		

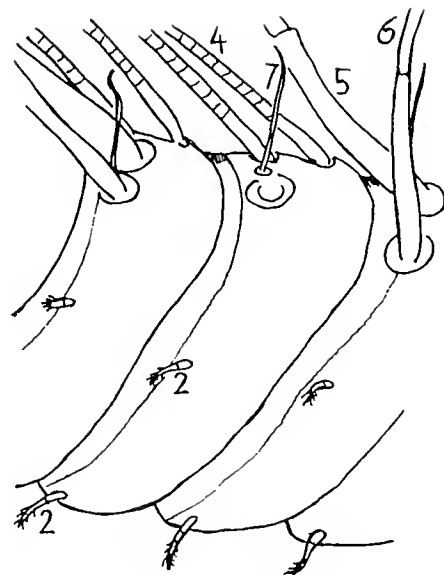


Figure 1. Table: Location of 7 setal types along the 5 regions of the lateral flagellum of the lobster antennule. The regions are defined by the presence and arrangement of aesthetasc sensilla (see text). Segments are numbered sequentially from the base to the tip; the number of segments per region [in brackets] is an average derived from a study of 15 antennules. All scale bars: 100 μ m; the smaller scale bar applies to the Type II setae, excluding the asymmetric form. Two forms of asymmetric hairs are shown.

Diagram: Setal arrangement on tuft segments. Three segments of medial flank of left flagellum shown in ventro-lateral view (ventral: up; distal: left). Setae numbered as in the table. Plumose setae (typical of lateral flank) and cupped serrulate setae (mostly dorsal) are not shown.

in the same position on the medial side. Serrulate setae are located distally on the flanks, with one larger one (120 μ m) on the lateral flank and one smaller one (80 μ m) on the medial flank; other serrulates, including the cupped serrulate setae, are found along the dorsal edge of the segment bordering the distal intersegmental joint.

Inferring function from external morphology has often proved misleading. But we know from preliminary electrophysiological experiments (C. Balint, pers. comm.) that the guard, companion, and asymmetric hairs are mechanoreceptive, responding to tactile and hydrodynamic stimuli. The mechanical filter properties of these hairs remain unknown, and the sensory function of the remaining setae has not been studied. The size and drag-producing morphology of the plumose setae suggests that they could respond to water flow in the antennular boundary layer. The regular spacing of the

serrulate setae along the medial and lateral flanks of the antennule give the appearance of a "lateral line," as seen in fish. The variety of setal types could provide specific filters for hydrodynamic as well as tactile stimuli.

We thank Louie Kerr and Jamin DeProto for their help with microscopy and Dr. Kari Lavalli for discussions on setal morphology. Supported by NSF.IBN 9723542.

Literature Cited

1. Karavanich, C., and J. Atema. 1998. *Anim. Behav.* 56: In Press.
2. Devine, D., and J. Atema. 1982. *Biol. Bull.* 163: 144-153.
3. Gleeson, R., W. Carr, and H. Trapido-Rosenthal. 1993. *Chem. Senses.* 118: 67-75.
4. Atema, J. 1996. *Biol. Bull.* 191: 129-138.
5. Weaver, M., and J. Atema. 1998. *Biol. Bull.* 195: 180-182.
6. Watling, L. 1989. Pp. 15-26 in *Crustacean Issues*, B. Felgenhauer, L. Watling, and A. Thistle, eds. A. A. Balkema, Rotterdam.

The Biomechanics of Odorant Access to Aesthetascs in the Grass Shrimp, *Palaemonetes vulgaris*
Kristina S. Mead (Department of Integrative Biology, University of California at Berkeley, California 94720)

Like many marine crustaceans, the grass shrimp *Palaemonetes vulgaris* can detect odors from distant sources; the receptors are within chemosensory sensillae (aesthetascs) that are borne on its antennules. Odor access to the chemosensory recep-

tors inside the aesthetascs is critical for olfaction. The transport and diffusion of odor molecules to the aesthetasc surface is greatly affected by the pattern of fluid flow around the aesthetascs, which depends on the morphology and distribution of those structures, and their movement relative to ambient flow. One simple way to analyze the fluid flow around the aesthetascs is to calculate the Reynolds number, a dimensionless parameter that indicates the relative importance of inertial and viscous forces in a given flow situation, and thus affects odorant access. Most crustaceans whose flicking has been analyzed to date conserve Reynolds number (and thus flow geometry) over a range of body sizes. This study investigates whether grass shrimp maintain Reynolds numbers, or whether flow around their aesthetascs changes as the shrimp grow.

P. vulgaris is a small marine shrimp that lives in eelgrass beds and has a well-developed chemical sense. Ablation experiments in *P. pugio* suggest that their ability to track odor plumes is largely dependent on their aesthetascs (1). Like many crustaceans, grass shrimp sample their chemical environment by moving their antennules in a rapid reciprocation called flicking. These shrimp flick in a rapid anterior to posterior sweep over 60–120 degrees, with a slower return stroke. The Reynolds number (Re) describing fluid flow around aesthetascs during flicking is $Re = \rho LV/\mu$, where ρ is the density of seawater (1023 kg/m^3), L is the diameter of the aesthetasc, V is the tangential velocity of the aesthetasc-bearing filament during different parts of the flick, and μ is the dynamic viscosity of seawater at 20°C (0.0011 Pa s).

To study aesthetasc morphology, antennules from 19 shrimp (rostrum-telson lengths of 14–40 mm) were excised and examined through a Wild Heerbrugg dissecting scope with a 30×–60× objective. Images were recorded with a Javelin Electronics CCD camera (model JE3462RGB) attached to a video cassette recorder. The number of aesthetasc rows, the number of aesthetascs per row, aesthetasc length, and aesthetasc diameter were measured both through the dissecting scope lens and from a monitor screen. Flicking velocity was measured by filming 14 freely moving *P. vulgaris* (rostrum-telson lengths 15–38 mm) from the side and from above with a Sony Handycam with a 24× zoom lens (CCD-TRV40). When the resultant videos were shown on a monitor, the position of the base and tip of the aesthetasc-bearing filament on successive frames was recorded on transparencies and used to calculate the tangential flicking velocities of the filament tip. Reynolds numbers were calculated for the backward and return parts of the flick for the full range of body sizes.

The *P. vulgaris* antennule consists of a base with three flagellae: two are long and slender and one is short and robust, carrying the aesthetascs along the length of the ventral side. Two rows of 2–4 aesthetascs are inserted perpendicularly and symmetrically into each segment of this short flagellum, with a total

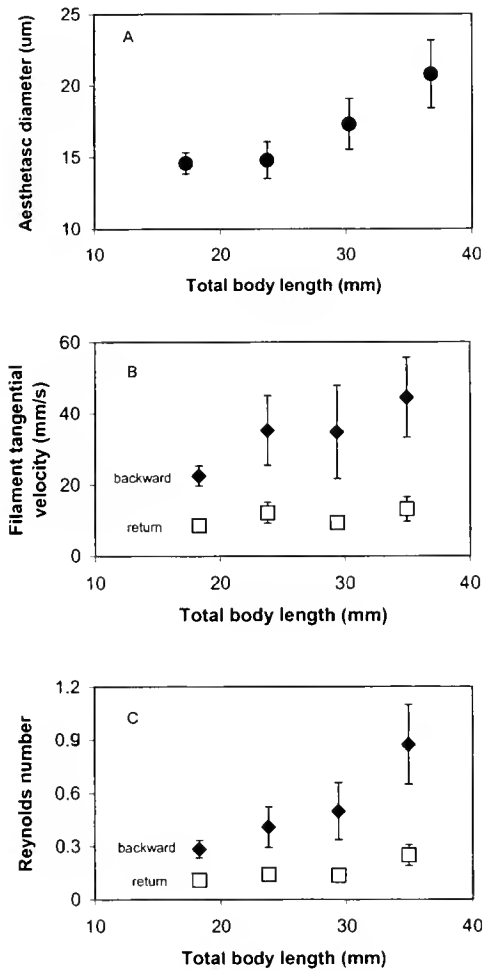


Figure 1. Aesthetasc diameter, tangential velocity of the aesthetasc-bearing flagellum tip, and Reynolds numbers during flicking in *Palaemonetes vulgaris*. In panel A, each symbol represents the mean of measurements from 3–8 animals (one measurement per animal) in a given size class: 14–20.5 mm ($n = 8$), 20.5–27 mm ($n = 3$), 27–33.5 mm ($n = 4$), and 33.5–40 mm ($n = 4$) total body length. Bars indicate standard errors. In panels B and C, each symbol represents the mean of 2–9 measurements each from 3–4 animals in a given size class: 15–21 mm ($n = 8$), 21–27 mm ($n = 3$), 27–33 mm ($n = 4$), and 33–39 mm ($n = 4$). Bars represent standard errors. In both panels, the filled diamonds refer to the backward stroke, and the open circles correspond to the return stroke.

of 8–40 rows of aesthetascs per animal. Aesthetasc diameter is constant along the 400–600 μm length of the aesthetasc, except for a slight swelling at the base and a narrowing at the tip. Mean aesthetasc diameter increases from about 14 μm to 21 μm as body length increases from 18 to 36 mm (Fig. 1, panel A).

Analysis of flicking sequences indicates that the aesthetascs are perpendicular to the water motion during the flick. Mean tangential velocity of the aesthetasc-bearing flagellum tip doubles over the range of tested body sizes (panel B). Mean velocity is 2–3 times greater during the backward part of the flick than during the return stroke. The mean Reynolds number describing flow around the aesthetascs during the backward stroke increases from 0.3 to 0.9, as the animal increases in size from 18 mm to 35 mm (panel C). The corresponding Reynolds number for the return stroke increases from 0.1 to 0.3 over the same size range. These velocities and Reynolds numbers apply primarily to the aesthetascs near the flagellum tip. More proximal aesthetascs will experience correspondingly lower velocities and Reynolds numbers.

In contrast with these observations, the spiny lobster *Paululus argus* maintains an Re of 2 for the downstroke and an Re of 0.5 for the recovery over the range of body sizes tested (2), and the American lobster *Homarus americanus* aesthetascs operate at Re = 3–4 over a 20-fold range of body sizes (3, 4).

Previous physical and mathematical models suggest that the changes in Re observed in *P. vulgaris* lie within a sensitive range (for this particular geometry), where the proportion of fluid moving through, rather than around, the aesthetascs can be significantly affected by both the diameter of the aesthetasc and its velocity through the surrounding fluid (5, 6, 7). At the low end of this range (small animals, the return stroke), a lot

of fluid is dragged along with the antennule as it flicks, so most of the fluid containing new odorant flows around the aesthetascs rather than penetrating the spaces between the sensillae. At the high end of this range (large animals, the backward stroke), the amount of fluid dragged along with the aesthetascs is small, so that most of the fluid containing new odorant flows between the aesthetascs and thus has a shorter diffusion distance to the chemoreceptors inside the aesthetascs. Since diffusion time increases as the square of the distance, these changes in Re (and therefore in odorant access) are likely to affect the shrimp's ability to respond to new odorants. These data suggest that *P. vulgaris* may alter its odor sampling paradigm as it grows. Further investigation into the flow geometry, odor-plume tracking behavior, and the ecological and behavioral olfactory requirements are necessary before further conclusions can be drawn.

This project was funded by a 1998 Grass Fellowship.

Literature Cited

1. Carr, W. E. S., and Charles D. Derby. 1986. *Chem. Senses* 11: 49–64.
2. Gleeson, R. A., W. E. S. Carr, and H. G. Trapido-Rosenthal. 1993. *Chem. Senses* 18: 67–75.
3. Moore, P. A., J. Atema, and G. A. Gerhardt. 1991. *Chem. Senses* 16: 663–674.
4. Best, B. 1995. *Am. Zool.* 35: 53A.
5. Cheer, A., and M. A. R. Koehl. 1987. *J. Theor. Biol.* 129: 17–39.
6. Loudon, C., B. Best, and M. A. R. Koehl. 1994. *J. Exp. Biol.* 193: 233–254.
7. Koehl, M. A. R. 1996. *Mar. Fresh. Behav. Physiol.* 27: 127–141.

Reference: *Biol. Bull.* 195: 185–187. (October, 1998)

Juvenile *Limulus polyphemus* Generate Two Water Currents That Contact One Proven and One Putative Chemoreceptor Organ

Elizabeth Quinn, Kristen Paradise, and Jelle Atema (Boston University Marine Program, Woods Hole, Massachusetts 02543)

In contrast to mandibulate arthropods, horseshoe crabs have no antennae. The absence of such chemo- and mechanoreceptive appendages invites questions about the mechanisms involved in bringing odor to the chemoreceptor organs, the gnathobases (1) and the dactyls (2). Selective chemoreceptor lesion experiments of these organs in our laboratory have shown that locating distant food-odor sources is dependent on the gnathobases, whereas the dactyls are involved in local grasping for food (Abromaitis and Talarski, unpubl. data). A third, putative, chemoreceptor organ is the flabellum, located laterally to the last pair of legs (3). Flabella are not involved in regulating respiration despite their location in the major respiratory water current (3) (Fig. 1). We investigate here the currents that may carry odor to both the known and the suspected chemoreceptor organs.

We tested six juvenile *Limulus polyphemus*, ranging in size

from 5 to 8 cm (prosomal width), collected from a salt marsh on the east shore of Buzzards Bay and maintained at the Marine Biological Laboratory in running seawater. The animals were fed about once every two weeks. More than 40 trials were recorded on videotape. Other trials relied on the observations of the experimenters. To measure and visualize currents created by *Limulus*, we needed to see underneath the carapace while the animal rested on the substrate, so that natural pressure differences would be generated. For this purpose, we placed a 56 cm \times 56 cm, glass-bottomed tank over a mirror held at a 45-degree angle. We used a camcorder to record the reflection of the bottom of the tank and the ventral surface of the animal onto videotape. We glued a nut to the carapace of the animal so it could be bolted in place from above during trials. The animals were fixed in natural position on the glass substrate. All trials

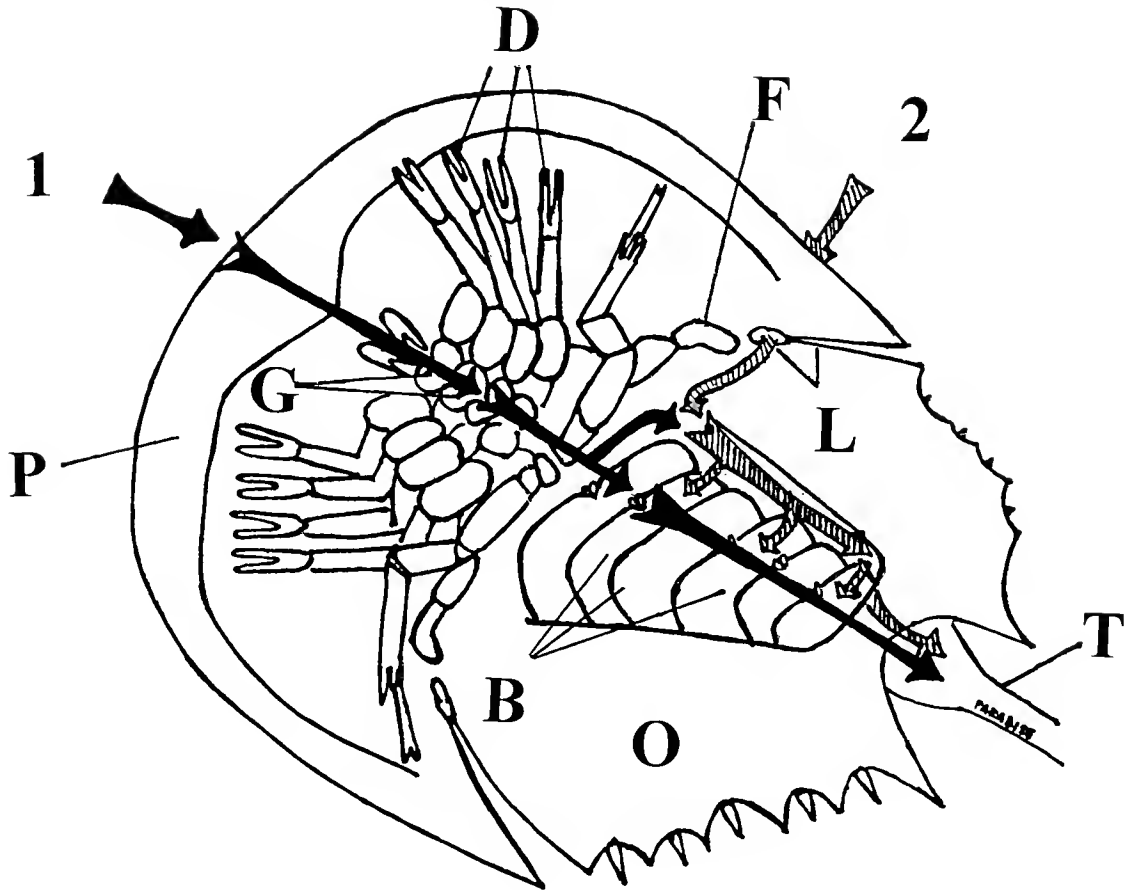


Figure 1. The two currents generated by juvenile *Limulus polyphemus* are a result of the activity of the book gills. The anterior current (#1, solid arrows) enters under the prosoma (P), passes directly over the gnathobases (G), and may be directed laterally by the first two pairs of legs. The anterior current continues over the book gills (B) and is expelled ventromedially at the telson (T). The respiratory current (#2, hatched arrows) is drawn in through the lateral slits (L) between the prosoma and opisthosoma (O), passes by the flabella (F), is drawn through the book gills, and is expelled by the telson. Neither of the currents targets the dactyls (D).

took place in still seawater about 6–10 cm deep. For flow visualization, we dispensed dye, one part red food coloring and two parts chilled seawater, using a 1-cm³ syringe.

Dye was placed in different locations around the animals. First, we placed dye on the substrate, 1–2 cm in front of the prosoma, and observed until the dye was either drawn entirely under the carapace or became too diffuse to see clearly. Then, we placed multiple dots of dye on the substrate around the prosoma and the opisthosoma, starting as close as 1 cm away from the flare and extending to 38 cm in front of the animal and 15 cm to either side, to measure the “reach” of the incoming, anterior current (Fig. 1). Third, we placed dye under the carapace at distinct locations, including the gnathobases, the lateral slits, the left and right sides of the prosoma above the pusher legs, and the book gills, to observe the movement and expulsion of the dye. Fourth, we placed dye in the water column directly above the lateral slits, a few millimeters from the carapace, to observe the strength of the respiratory current.

Book gill activity creates currents in *Limulus*. When the book gills beat, negative pressure is created under the opisthosoma

and water flows toward that area. Although the legs are capable of stirring up the water and even creating small currents, their effect on net flow is minor relative to book gill activity. A distinct incoming current enters underneath the prosoma, at the flare, and passes directly over the centrally located gnathobases (Fig. 1); the first two pairs of legs may direct this current off-center, to the right or left. When dye was placed within 1 cm of the flare, water-current velocity could reach up to 9.8 mm/s; depending on book gill activity, this anterior current drew in dye spots placed up to 18 cm away. When dye spots were placed adjacent to the prosoma, current velocities decreased. However, the animal could still entrain dye placed up to 8 cm to the left or right side of the prosoma. There was no conclusive evidence to suggest that larger animals could pull in dye placed further away. Because the observed currents were flowing in immediate synchrony with book gill movement, we believe that it is unlikely that the incoming currents were significantly affected by the expulsion current. In summary, the anterior current may function as an information current targeting the gnathobases.

Close examination of the second current, previously de-

scribed as the respiratory current (1), shows that when the book gills are active, the lateral slits entrain dye ventrally and dorsally. In both cases, dye passes the flabella. The flabella are therefore situated in the respiratory current where they can monitor chemical stimuli drawn in from a distance. However, when the last pair of legs, known as the "pusher" legs, are active and the book gills are inactive, these slits can serve as expulsion sites. The book gills were also able to entrain dye placed within 2 cm lateral to the opisthosoma. *Limulus* spends time with its prosoma burrowed in the sand (4); as a result, we hypothesize that the flabella allow the animal to sense chemical signals in its environment while partially buried. Both currents described above are expelled posteriorly under the telson when the book gills are active. Currents can be reversed and dye forced out

the flare, however, when an animal flaps its opisthosoma and telson forward.

Although the specific sensory functions of the flabella remain unclear, the two currents we describe target two different (chemo)receptor organs, the gnathobases and the flabella. Our findings indicate that *Limulus* may be more capable of long-range chemoreception than previously thought.

Supported by NSF IBN 9723542.

Literature Cited

1. Barber, S. B. 1956. *J. Exp. Zool.* **131**: 51-74.
2. Wyse, G. A. 1971. *Z. Vgl. Physiol.* **73**: 249-273.
3. Waterman, T. H., and D. F. Travis. 1953. *J. Cell Comp. Physiol.* **41**: 261-287.
4. Vosatka, E. D. 1970. *Ohio J. Sci.* **70**: 267-283.

Reference: *Biol. Bull.* **195**: 187-188. (October, 1998)

UV Radiation Blocking Compounds in the Eye of the Cuttlefish *Sepia officinalis*

Nadav Shashar, Ferenc I. Hárosi, Anastazia T. Banaszak¹, and Roger T. Hanlon
(Marine Biological Laboratory, Woods Hole, Massachusetts 02543)

UV-absorbing compounds are well documented in the light-passing components (cornea and lens) of vertebrate eyes, including numerous fish species (reviewed in [1, 2]). In fishes, three main classes of such compounds have been found: aromatic amino acids of proteins, such as tryptophan, tyrosine, and phenylalanine; mycosporine-like amino acids (MAAs); and derivatives of tryptophan such as kynurenine and 3-hydroxykynurenine (2, 3). Whereas aromatic amino acids may be contained in structural proteins of cornea and lens, the role of the MAAs and the kynurenine type molecules is believed to be primarily the filtering of UV radiation. Of the latter two classes, MAAs, which are of algal or bacterial origin, are obtained from the animals' diet, whereas kynurenine and 3-hydroxykynurenine are synthesized within the lens.

Cuttlefish, *S. officinalis*, live in shallow waters along the east coast of the Atlantic ocean and in the Mediterranean sea. These waters are classified (4) as types I, IA, IB, II (open waters) and I and 3 (coastal waters). In these waters, UV radiation penetrates to considerable depths (4) including a large portion of the shallow waters that *S. officinalis* inhabits. In this study, we examined the light transmission properties of the lens and cornea of *S. officinalis*, identified compounds that modify these properties, and compared lens and corneal transmission with the sensitivity of the animal's photoreceptors.

High performance liquid chromatography (HPLC)

Cornea and lenses were frozen (-70°C) until further analysis. Samples were extracted overnight in 100% HPLC-grade metha-

nol at 4°C. Individual pigments were separated by reverse-phase, isocratic HPLC on a Brownlee RP-8 column (Spheri-5, 4.6 mm ID × 250 mm) that was protected with an RP-8 guard column (Spheri-5, 4.6 mm ID × 30 mm). The mobile phase consisted of 25% methanol (v:v) and 0.1% glacial acetic acid (v:v) in water with a flow rate of 0.7 ml·min⁻¹. Detection of the peaks was carried out using a diode array, UV absorbance detector (Beckman Gold System). Standards (originally isolated by W. Dunlap) were available for seven MAAs (mycosporine-glycine, shinorine, porphyra-334, palythine, asterina-330, palythanol, and palythene); and 3-hydroxykynurenine was identified following Truscott *et al.* (3). Identities of the peaks were confirmed by co-chromatography with standards and by on-line diode array spectroscopy.

Three MAAs, 3-hydroxykynurenine, and two unknown compounds were found in the lens and cornea of cuttlefish (Fig. 1B). The two unknown compounds and one of the MAAs (palythanol) were found in both lens and cornea, whereas 3-hydroxykynurenine and palythene were limited to the lens, and shinorine was identified only in the cornea.

Bon *et al.* (5) noted a non-protein compound in the lens of *Octopus vulgaris* with maximal absorption at 334 nm. It is likely that octopus, like cuttlefish, also possess UV-absorbing compounds such as MAAs in their lenses.

Microspectrophotometry (MSP)

Samples of cornea and lens, used whole or in 40 μm slices (lenses), were mounted between quartz cover slips and examined through a microspectrophotometer capable of measuring light fluxes passing through microscopic samples (6). By this technique we were able to measure light absorbance through a biologically significant optical path in the sample and visually

¹ Smithsonian Environmental Research Center, P.O. Box 28, Edgewater, Maryland 21037.

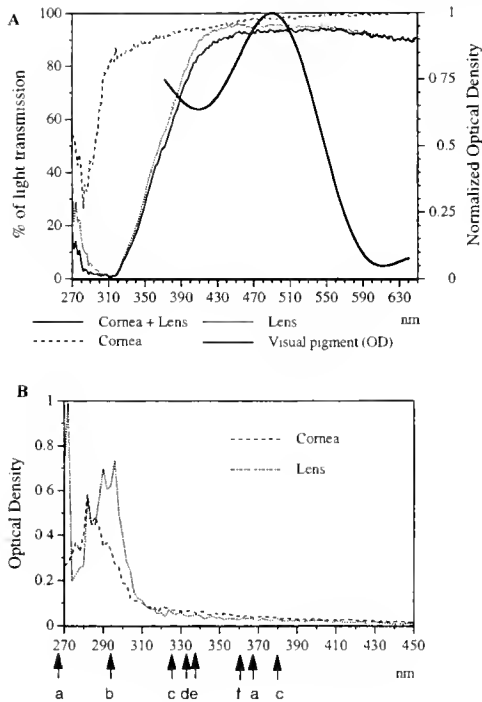


Figure 1. (A) Transmission spectra (left scale) through a lens (5 mm in diameter, animal age is 5 months) and a cornea of a cuttlefish, each measured intact, and the combined transmission through cornea and lens; and normalized optical density (right scale) of the cuttlefish visual pigment having a λ_{max} at 490 nm (light-scatter by screening pigments and possibly by visual products interfered with the signal at short wavelengths and hence the spectra is plotted only at the 370–640 nm range). Transmission spectra show that the lens acts as a UV-A blocking filter with 50% transmission at about 365 nm, while the cornea's 50% cut-off is at about 295 nm. (B) Optical density of a cornea and a 40 μ m thick section of a lens. Low levels of scattering and higher absorption are revealed at wavelengths shorter than 390 nm. Arrows indicate λ_{max} of compounds identified in the lens and cornea (a, 3-hydroxykynurenine 267 and 368 nm; b, unknown #1–295 nm; c, unknown #2–324 and 380 nm; d, palythanol–332 nm; e, shinorine–334 nm; f, palythene–360 nm). Values demonstrate that the combined effect of these compounds is responsible for attenuating UV radiation.

ensure the quality of the part of the sample examined. Fresh corneas and lenses were rapidly frozen, cut frozen, and thawed only on the measuring slide. Sivak (7) and Thorpe *et al.* (2) found that this method does not distort the transmittance of light through the tissue. Additionally, a fresh lens, 5 mm in diameter, was examined within a specially prepared water well, using 10 \times Ultrafluor lenses as objective and condenser. Each sample

was measured at 5 different locations. Each recording consisted of 16 scans in which the light transmittance of the tissue was measured over the range of 270–650 nm, in 2 nm intervals. These measurements were compared to a 16-scan reference measurement of a clear portion of the sample, and the optical density of the tissue was computed. Repetitive measurements of each sample type showed very little variation and were averaged together. No differences were found between the anterior and posterior parts of the lens and the measurements were averaged as well.

MSP recordings were further performed on photoreceptors of a dark-adapted, 4-month-old cuttlefish. The technique followed Hárosi (6), but recordings were taken from groups of photoreceptors. In 22 measurements, a single photopigment was found having maximal absorption at 490 nm (Fig. 1A).

Both lens and cornea showed high transmittance in the 470–550 nm range, to which cuttlefish are most sensitive (Fig. 1A). The lens was found to be somewhat less transparent in the long wavelengths (>590 nm), and both lens and cornea absorbed short-wavelength radiation, acting together as a long pass filter with 50% transmission at about 370 nm. Close examination of the optical density of cornea and lens revealed that most absorption can be correlated with that of proteins and 3-hydroxykynurenine, with a smaller impact by MAAs. However, since MAAs are derived from the diet, the concentrations of MAAs in the eye may be food-dependent.

UV-absorbing compounds in lenses were suggested to function both in preventing damage to the retina and in absorbing short-wavelengths that have a greater tendency to cause blurring (2). As cuttlefish are likely to have a single visual pigment (8) with maximal absorption near 490 nm (Fig. 1A), such short-wavelength blocking compounds would be expected to have a small impact on the cuttlefish visual sensitivity.

We thank D. Karentz and M. Lesser for providing chemical standards. This study was partly supported by NSF grant IBN-9729598 and NIH grant RR01024 to RTH. ATB was supported by a Smithsonian Postdoctoral Fellowship.

Literature Cited

1. Dunlap, W. C., D. McB. Williams, B. E. Chalker, and A. T. Banaszak. 1989. *Comp. Biochem. Physiol.* **93B**: 601–607.
2. Thorpe, A., R. H. Douglas, and R. J. W. Truscott. 1993. *Vision Res.* **33**: 289–300.
3. Truscott, R. J. W., J. A. Carver, A. Thorpe, and R. H. Douglas. 1992. *Exp. Eye Res.* **54**: 1015–1017.
4. Jerlov, N. G. 1976. *Marine Optics*. Elsevier, Amsterdam.
5. Bon, W. F., A. Dohrn, and H. Batink. 1967. *Biochim. Biophys. Acta.* **140**: 312–318.
6. Hárosi, F. I. 1987. *J. Gen. Physiol.* **89**: 717–743.
7. Sivak, J. G. 1991. *Can. J. Zool.* **69**: 2501–2506.
8. Marshal, N. J., and J. B. Messenger. 1996. *Nature* **382**: 409.

Reference: *Biol. Bull.* 195: 189–190. (October, 1998)

Efferent Modulation of Physiological Properties of the *Limulus* Lateral Eye

Vanessa J. Ruta, Frederick A. Dodge, and Robert B. Barlow (Marine Biological Laboratory, Woods Hole, Massachusetts 02543)

The visual system of the horseshoe crab *Limulus polyphemus* undergoes marked circadian changes in sensitivity that are controlled by a clock in the animal's brain (1). At night, efferent optic nerve activity to the lateral eyes induces multiple physiological, anatomical and metabolic changes in all retinal cell types (2). These changes function together to facilitate detection of a mate as the animals come to the water's edge during the nighttime high tide (3). The three circadian changes that have the most pronounced effect on retinal responses are an increase in "photon catch" (the number of photons absorbed by each ommatidium), an increase in "gain" (the steady-state optic nerve response to each absorbed photon), and a decrease in "noise" (spontaneous optic nerve activity in the absence of light). We report here that the latter two changes are rapid physiological events induced by the clock's efferent input and occur well in advance of the slower structural transformations that increase photon catch. We also report on the efficacy of the efferent activity of the optic nerve in modulating the gain and noise level of the retina in the absence of structural changes.

To record optic nerve activity *in situ*, we secured a male horseshoe crab to a rigid platform in an aquarium filled to the level of the specimen's lateral eye with continuously aerated seawater and placed the aquarium in a lightproof shielded cage. A hole, 1.9 cm in diameter, was cut in the carapace 3 cm anterior to one of the lateral eyes to expose the optic nerve trunk, which was cleaned of surrounding tissue, cut, and pulled into a small recording chamber mounted on the carapace. To measure response gain, a single active optic nerve fiber was teased free of the nerve trunk and pulled into the glass tip (100- μ m opening) of a suction electrode. A cluster of optic nerve fibers was pulled into a second suction electrode to monitor retinal noise (spontaneous activity). The remainder of the optic nerve was then pulled into a third suction electrode that was connected to the stimulus isolation unit of a pulse stimulator (Models PSU6 and S44, Grass Instruments). Current pulses (1 ms duration) delivered to the optic nerve by the third suction electrode simulated the clock's efferent input (3). The electrodes and the recording chamber were filled with a modified *Limulus* Ringer solution containing 100 units/ml of penicillin and 100 μ g/ml of streptomycin. The final step was to optically isolate the ommatidium of the single active nerve fiber by aligning a fiber optic light pipe (70 μ m diameter) along the axis of the ommatidium and in contact with the cornea (4). We measured the gain of the optic nerve response by averaging the firing rate over the last 4 s of a 5-s light flash. We measured the level of spontaneous optic nerve activity by averaging the activity of the cluster of optic nerve fibers over a 20-s period in the dark. Electroretinograms (ERGs) elicited by brief (10-ms) flashes of light from an LED were recorded from the dark-adapted lateral eye with corneal electrodes. We used the peak-to-peak amplitude of the ERG as a measure of the photon catching ability of the retina (5).

Figure 1A shows the rapid effects of the efferent activity on

retinal gain and noise. In less than 1 min after a brief period of efferent input, the light-driven response of the single optic nerve fiber increased by about 40%, and the level of spontaneous activity of the cluster of nerve fibers decreased by about 95%. Previous experiments (R. Barlow, unpubl. observations) have shown that the stimulation paradigm used in the experiment in Figure 1A is insufficient to induce significant structural changes and thus does not change the eye's photon-catching ability. Such changes require longer periods of repetitive efferent stimulation and are readily detected by changes in ERG amplitudes. Although the effects of efferent input on retinal gain and noise are rapid and coincident, the dynamics of their decay are not. Twenty minutes after the cessation of efferent input, the increased gain decayed about 50%, and the decreased noise returned to 67% of its original level. In other experiments, we found that delivering a single current pulse to the optic nerve evoked a discernible change in gain without affecting the level of spontaneous activity or the ERG amplitude. Changes in gain appear to have a lower threshold for efferent input than do the other two circadian components.

Figures 1B and 1C show that increasing the level of efferent input to the retina increases the magnitude of the changes in gain and noise. We found that doubling the efferent input doubled the evoked effects at low levels of efferent input. The linearity in response was lost at higher levels of efferent stimulation. While the onset of the changes in gain and noise appear coincident at moderate efferent inputs, their sensitivities differ: changes in gain can be induced without changes in noise. The onset of efferent activity begins slowly in the late afternoon, increasing in intensity until it reaches its peak at about midnight (4). From the findings reported here, the first step in the transformation of the eye to its more sensitive nighttime state would be an increase in retinal gain. The decrease in the level of retinal noise would follow as the level of efferent activity increases as dusk approaches. These two physiological changes would occur in advance of the slower changes in the structure of the ommatidia.

Limulus has evolved elegant circadian mechanisms that enhance visual sensitivity at night. How these fast physiological changes in retinal gain and noise are linked is not yet known. Because these mechanisms have different thresholds, they may be activated independently of one another in a sequential manner. Although the mechanism underlying the circadian increase in gain is not completely understood, our working hypothesis is that at night, an efferent neurotransmitter (octopamine; 6) decreases the efficacy of a light-adapting mechanism that would otherwise reduce the eye's response to light. With little need for a strong light-adapting mechanism at night, the animal appears to have developed a mechanism to suppress it, yielding the increase in response gain we report here. The mechanism underlying the nighttime decrease in retinal noise appears to result from a stabilization of rhodopsin via an efferent-evoked reduction in pH in the vicinity of the photoreceptor cells (7). Such stabilization reduces the rate of thermal isomeriza-

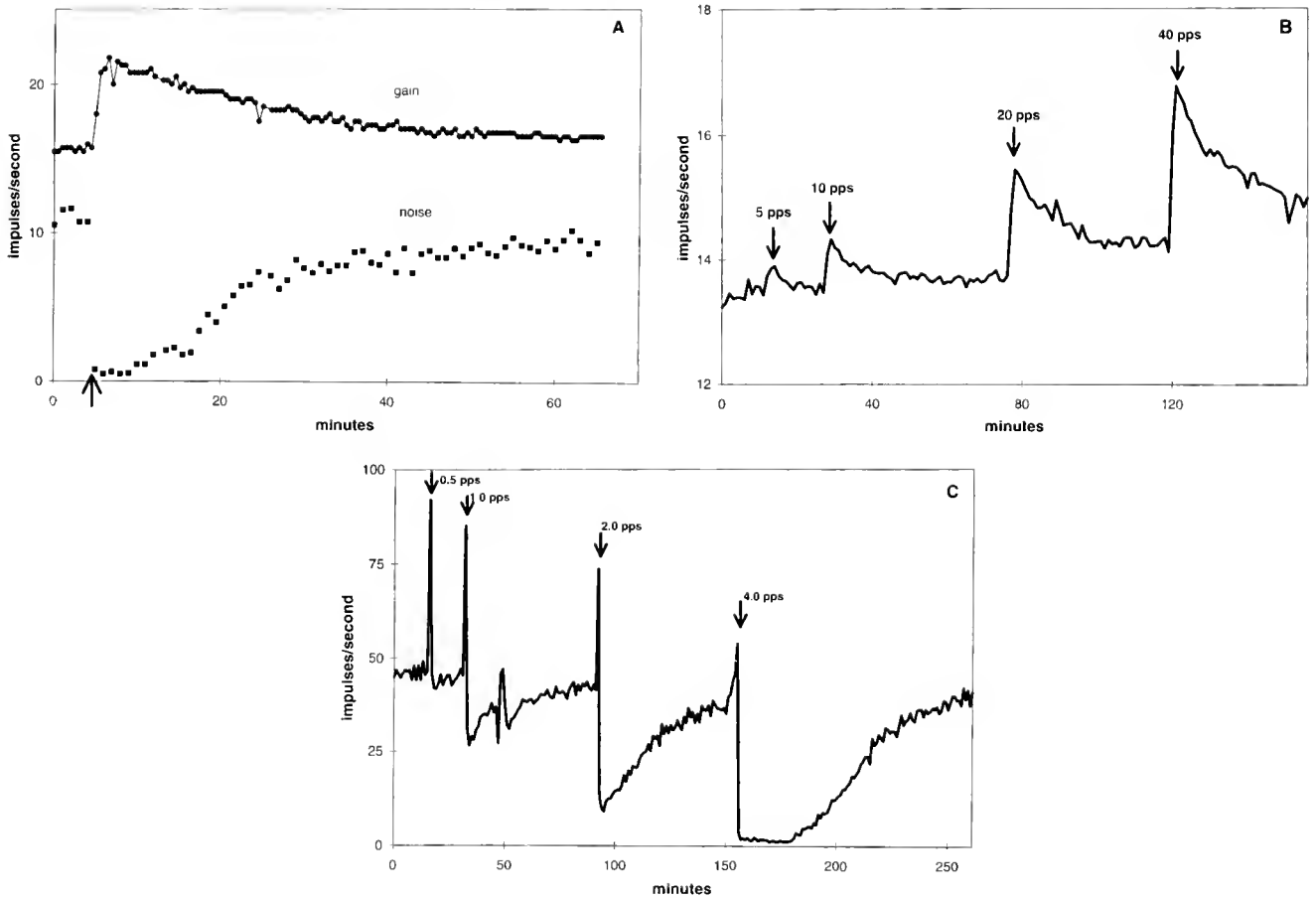


Figure 1. Efferent optic nerve activity increases gain and decreases noise in the Limulus retina. (A) Simultaneous recording in situ of changes in gain and noise in the lateral eye following the delivery of a single episode of efferent stimulation consisting of 8 pulses per second (pps) for 10 s as indicated by the arrow. The efferent input induced an increase of ~40% in retinal gain and a decrease of ~95% in retinal noise within 1 min of nerve stimulation. Although the changes in gain and noise are equally rapid, their decay after cessation of the efferent input is not. Light intensity incident on the recorded ommatidium was 10^9 photon/s during the 5-s stimulus. (B) Effect of varying levels of efferent input on the gain of a single optic nerve fiber in response to light. One-second episodes of shock were delivered at various times (arrows) and the number of pulses administered in the 1-s period was successively increased. The resulting increase in retinal gain was directly proportional to the level of efferent input for 5 pps, 10 pps, and 20 pps but not for 40 pps where the linearity was lost. (C) Increasing the level of efferent input also increases the effect on retinal noise. The changes in retinal noise were monitored after the delivery of a 10-s period of shock (arrows) consisting of 0.5 pps, 1 pps, 2 pps, and 4 pps. Large peaks at the times of stimulation are artifacts of the stimulus. A fluctuation of unknown origin in the level of spontaneous activity occurs at 50 min. As was the case with efferent-induced changes in gain, there is a nearly linear relationship between efferent input and the induced change in the level of noise at the lower three stimulation levels, but the effect saturated at the highest efferent inputs. Different levels of efferent input are required to induce discernible changes in gain and noise. Gain is more sensitive to efferent input than noise.

tion of rhodopsin, which is thought to be the primary source of spontaneous optic nerve activity.

Supported in part by REU Fellowships from the National Science Foundation and NSF grant IBN9696208 and NIH grants MH49741 and EY00667.

Literature Cited

1. Barlow, R. B., Jr., S. J. Bolanowski, and M. L. Brachman. 1977. *Science* 197: 86–89.
2. Barlow, R. B., Jr., S. C. Chamberlain, and H. K. Lehman. 1989. *Facets of Vision: Circadian Rhythms in the Invertebrate Retina*. Springer-Verlag, Berlin.
3. Barlow, R. B., Jr., L. C. Ireland, and L. Kass. 1982. *Nature*, 296:65–66.
4. Barlow, R. B., Jr. 1983. *J. Neurosci.* 3: 856–870.
5. Kaplan, E., and R. B. Barlow, Jr. 1975. *J. Gen. Physiol.* 66: 303–326.
6. Kass, L., and R. B. Barlow, Jr. 1984. *J. Neurosci.* 4: 908–917.
7. Barlow, R. B., Jr., R. R. Birge, E. Kaplan, and J. R. Tallent. 1993. *Nature* 366: 64–66.

Reference: *Biol. Bull.* 195: 191-192. (October, 1998)

Directional Auditory Responses in the Descending Octaval Nucleus of the Toadfish (*Opsanus tau*)
P. L. Edds-Walton and R. R. Fay (Marine Biological Laboratory, Woods Hole, Massachusetts 02543)

Afferents from the toadfish saccule have directional auditory sensitivity that we have documented previously with extracellular and intracellular recordings (1,2). In this study, we have begun to characterize the response properties of one of the target nuclei of saccular afferents: the descending octaval nucleus (DON) (3,4). The DON has an extensive rostral-caudal distribution in the lateral medulla between the entrances of the anterior ramus of cranial nerve VIII and cranial nerve X (Fig. 1A). In horizontal section, the nucleus is wedge-shaped with greatest width rostrally in the "dorsal zone" above the descending tract of cranial nerve V. Saccular afferents project most heavily to the dorsal zone of the descending octaval nucleus (dDON) (3,4).

Incoming saccular afferent fibers travel the length of dDON laterally, and terminal fields from those fibers are seen medial and lateral to the main axon (unpubl. obs.). Individual neurobiotin-filled cells revealed that all primary auditory axons branch

repeatedly in the rostral-caudal axis of the dDON; however, variation was seen in the lateral to medial extent of terminal fields among afferents with different best elevations and best azimuths. Therefore, the goal of this preliminary study was to evaluate directional responsiveness across the lateral to medial axis of the dDON.

In preparation for the experiments, the toadfish was anesthetized and the tail muscles paralyzed. An incision was made in the dorsal surface of the skull, and the medulla was exposed carefully. The fish's head was then secured in a cylindrical dish filled with fresh seawater on a three dimensional shaker table. A system of moving-coil shakers created a sinusoidal motion of the dish along linear pathways (5). A calibration program produced the appropriate starting phases and amplitudes to create movements in the horizontal and mid-sagittal planes (0°, 30°, 60°, 90°, 120°, 150°). Movement of the dish simulated the particle motion component of underwater sound at 100 Hz, a frequency to which the toadfish is extremely sensitive (5).

Extracellular recordings were made with indium electrodes designed for use in the central nervous system (6). The electrode tips were approximately 12 μm in diameter, which enhanced the likelihood that the electrodes were recording activity from secondary cell bodies in the dDON; recordings from axon collaterals or their terminal fields are not likely to be made with a large electrode tip. Multiple recordings were made in the same fish whenever possible; e.g., beginning laterally and moving medially on successive electrode penetrations. A three-axis micromanipulator was used to systematically change electrode position. Drawings were made to show electrode locations relative to VIII rami and IX in the rostro-caudal axis, and relative to the lateral edge of the brain and a large blood sinus that runs medially along the length of the medulla. Although "0" readings on the vertical scale of the micromanipulator were made at the surface of the medulla, the relative depth of the electrode was difficult to control at consecutive recording sites due to the curvature of the medulla. In some cases, a lesion was produced at the site of the last cell recorded to confirm our location in the dDON.

We have recorded more than 50 single units from the dDON in seven toadfish. We believe that the units are secondary cells of the dDON based on their response characteristics and the consistency of the data that we have recorded independent of location in the dDON. Although the dDON cells show phase-locking to the 100 Hz sinusoid, spikes are not produced for each cycle, which is unlike the regular phase-locked spiking patterns we have recorded from over 400 primary afferents. In addition, the activity of cells recorded at lateral sites does not differ from the activity of cells in the most medial locations of dDON. Recording from the small primary axon collaterals and terminal fields found medially would be extremely difficult with this large electrode. Secondary cell bodies in both lateral and medial locations are the most likely sources of the activity we have recorded.

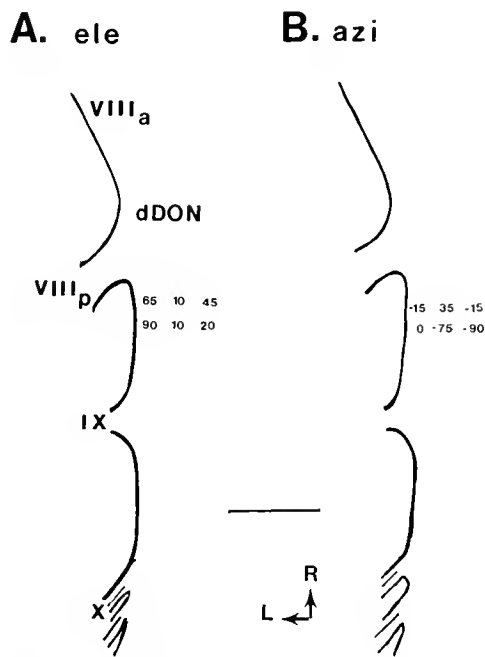


Figure 1. Directional response data obtained from extracellular recordings in the dorsal zone of the descending octaval nucleus (dDON) of the toadfish. A portion of the left medulla is shown as a horizontal section; the distance between sites of recording are exaggerated to allow the plotting of best axis values. The distance between the most lateral and the most medial sites was about 400 μm. (A) Best elevations (ele), in degrees, at relative recording sites for six cells. L, lateral; R, rostral; VIII, IX, X, cranial nerves; a, anterior ramus; p, posterior ramus. The scale bar is 500 μm. (B) Best azimuths (azi), in degrees, for the same cells whose elevations appear in "A." Negative numbers indicate that the cell's best direction is to the left; 0° is directly in front of the fish.

Thirty-seven of the dDON units were phase-locked to the 100 Hz sinusoidal stimuli with root mean square displacement amplitudes between 10 and 30 dB (re 1 nm) and were clearly directional. The "best" axis for each cell was determined by plotting the cell's response to the six different angles of stimulation in each plane at three displacement amplitudes. All but one unit showed a directional response pattern with a consistent best axis of greatest phase-locked response, and an orthogonal "null" axis of minimal response in both the horizontal and mid-sagittal planes. These data indicate that the directional encoding among individual primary afferents is maintained at the level of the dDON, and the dDON may be a site of directional sound analyses.

The data collected from six cells in the dDON of a single fish are plotted by their relative locations in Figure 1. A portion of the dDON is represented in a horizontal section. Best elevation (Fig. 1A) and best azimuth (Fig. 1B) are shown separately for each cell at the appropriate relative location. Following our first successful recording, the micromanipulator was used to change the position of the electrode in the lateral-medial axis with no change in the electrode's location in the rostral-caudal axis. In some fish, such as the one illustrated in Figure 1, a second lateral to medial series of recordings was successful at a second more caudal (or more rostral) site.

We were able to obtain best elevations and best azimuths in consecutive lateral to medial sites in seven fish (37 cells). A

comparison of the most lateral sites with the most medial sites indicated that elevation and azimuth vary widely along that axis of the dDON. For example, the range of best elevations most laterally was 0–90° ($n = 14$ cells); the range of best elevations most medially was 0–95° ($n = 13$ cells). The remaining ten cells were located between a most lateral and a most medial site; the range of best elevations at those sites was 0–45°.

To our knowledge, this is the first study to show directional auditory responses in the dDON. Our future research will explore directional response properties along all three axes of the dDON (lateral-medial, rostral-caudal, dorsal-ventral) to determine whether direction is mapped systematically in this nucleus.

Research funded by a National Institutes of Health, RO1 grant.

Literature Cited

1. Edds-Walton, P. L., and R. R. Fay. 1995. *Biol. Bull.* **189**: 211–212.
2. Fay, R. R., and P. L. Edds-Walton. 1997. *Hear. Res.* **111**: 1–21.
3. Highstein, S. M., R. Kitch, J. Carey, and R. Baker. 1992. *J. Comp. Neurol.* **319**: 501–518.
4. Edds-Walton, P. L. 1998. *Hear. Res.* **115**: 45–60.
5. Fay, R. R., and P. L. Edds-Walton. 1997. *Hear. Res.* **113**: 235–246.
6. Dowben, R. M., and J. E. Rose. 1953. *Science* **118**: 22–24.

Effects of Vestibular Nerve Lesions on Orientation Turning in the Leopard Frog, *Rana pipiens*

Jane Roche King (University of Arizona, Tucson, Arizona 85721) and Hans Straka¹

Many behaviors are driven by centrally patterned programs or commands. These central programs may then be modified on-line by various forms of sensory information to produce an adaptive behavior. Here we examine the contribution of the vestibular system to two different types of spatially organized orientation movements, prey capture and escape turning, in *Rana pipiens*.

Prey capture turning was at one time considered ballistic because, once in motion, visual information is not required to complete the movement (1, 2). However, prey capture turns are in fact dependent upon sensory afferent input from the vestibular system. Frogs with lesions of the anterior branch of the vestibular (VIIIth) nerve overshoot, or turn past, prey targets (3).

Escape turns may be ballistic or may be influenced by vestibular information. We investigate the effects of lesions to vestibular nerve fibers on the turning component of prey capture and escape to understand how one sensory modality influences and contributes to two different behaviors.

Rana pipiens was used for all experiments. The animals were housed in 10-gallon aquaria and fed crickets and meal worms. Pre- and post-lesion escape and prey capture trials were recorded using methods previously described in detail (4). Briefly, animals were placed inside a round, uniform arena with a video camera mounted overhead. Escape turns were elicited by moving a hand-held stimulus, an 8 × 10 cm black card mounted on a handle, toward the frog on a collision course. Prey capture turns were elicited with a mealworm placed in a small glass vial. Escape and prey capture stimuli were presented at 15 locations randomly chosen within the visual field during one recording session. All trials were recorded on videotape at a rate of 30 frames per second (60 fields per second). The behavioral sequences were analyzed with a frame-by-frame play-back video deck. From videotapes, the angle of stimulus and the angle of initial turn were measured for each trial and plotted on a Cartesian graph using previously described methods (4) (see Fig. 1). Unilateral lesions of the peripheral vestibular system were performed under tricaine (MS-222) anesthesia. The labyrinthine organs were accessed through the roof of the mouth. Post-ganglionic lesions of the entire VIIIth nerve ($n = 2$) and two VIIIth nerve branchlets, the horizontal canal (HC) nerve ($n = 2$) and posterior canal (PC) nerve ($n = 1$), were made by cutting the nerve with sharp iridectomy scissors under visual control. After surgery, the frogs were awake and behaving within 2 hours.

Following unilateral lesion of the complete VIIIth nerve, frogs exhibited postural deficits due to asymmetrical utricular information (5). These deficits were not present after lesion of the HC or PC nerve. Unilateral HC nerve lesions were verified by the presence of asymmetrical dynamic deficits in the hori-

zontal vestibular-colic reflex. Since turning for both escape and prey capture consists mainly of movement in the horizontal plane, lesion of the PC nerve, which senses movement in the vertical plane, served as a surgical control. Behavioral data were collected before the lesion and 1 to 30 days post-lesion. Pre- and post-lesion turn amplitudes from each animal were compared using the Mann-Whitney rank sum test (SigmaStat, Jandel Scientific).

Following complete VIIIth nerve lesions, frogs displayed an overshooting in prey capture turns toward stimuli placed on the side of the lesion; that is, turn amplitude increased post-lesion ($P < 0.001$ for both animals, Fig. 1A). The degree to which frogs overshoot increased with increasing azimuthal position of the stimulus. A smaller post-lesion increase in turn amplitude was also present on the side opposite the lesion ($P < 0.05$ for both animals). For escape, pre- and post-lesion turn amplitudes were not significantly different (Fig. 1B).

Following HC nerve lesions, frogs exhibited prey capture

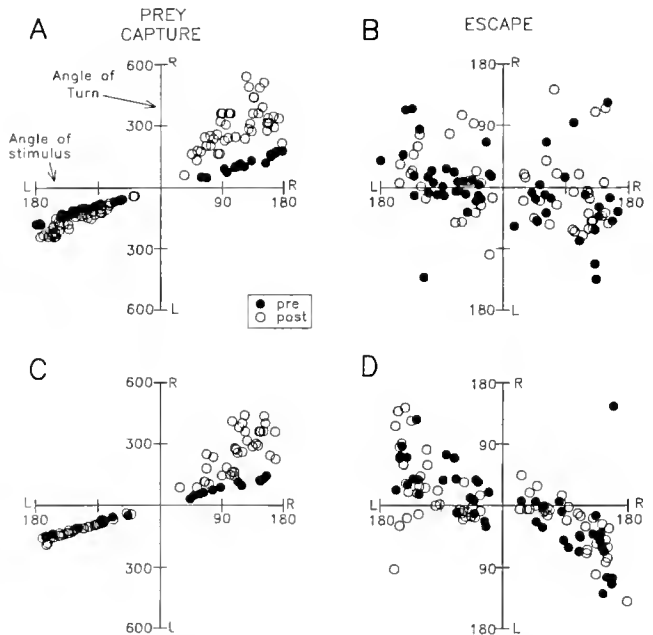


Figure 1. Scatterplots illustrating the spatial organization of escape and prey capture turns pre- and post-damage to the vestibular system. (A and B) Data collected from one individual animal with a postganglionic VIIIth nerve lesion. Prey capture turning is plotted in A and escape turning is plotted in B. (C and D) Data collected from one animal with a lesion to the horizontal canal nerve. Turning for prey capture and escape is shown in panels C and D, respectively. R = right visual hemifield, L = left visual hemifield. Note that the frame of reference is opposite for the two behaviors. For escape, 0° = stimulus at vent, 180° = stimulus at snout. For prey capture, 0° = stimulus at snout, 180° = stimulus at vent.

¹ New York University Medical Center, New York, New York.

overshooting in response to stimuli placed on the side of the lesion ($P < 0.001$ for both animals, Fig. 1C). In contrast to VIIIth nerve lesions, turn amplitude did not increase on the side opposite the lesion. Complete VIIIth nerve lesions disrupt input from all end organs which may result in more widespread turning deficits. For escape, pre- and post-lesion turn amplitudes were not significantly different (Fig. 1D). While lesions to the peripheral vestibular system did not affect the turning component of escape, they may affect the airborne phase and landing.

Following PC nerve lesion, the amplitudes of prey capture and escape turns did not change (data not shown). This result implies that the turning deficits described here for prey capture are specific to horizontal canal nerve lesion and not a result of non-specific damage to the nervous system or to general surgical trauma.

These data support the idea that on-line vestibular input is required for prey capture turning and not required for escape turning. This is consistent with the fact that turn accuracy is of greater importance for prey capture than for escape. Since the HC measures angular acceleration in the horizontal plane, it is well suited to supply the animal with on-line information about

the actual position and velocity of the body in space. This information could be used to guide the centrally generated movement of the body and head toward the prey target. For escape turns, the spatial organization is more variable and the peak velocity is greater than for prey capture turns (4). This suggests that the speed of the escape turn is more important than accuracy; thus vestibular input may not be required. The initial phase of the escape response, the turn, may be truly ballistic in nature allowing the frog to maximize the speed of the response.

This work was supported by the Grass Foundation.

Literature Cited

1. Ingle, D. 1973. *Science* **181**: 1053–1055.
2. Comer, C. M., and P. Grobstein. 1981. *J. Comp. Physiol.* **142**: 141–150.
3. Comer, C. M., J. Schotland, and P. Grobstein. 1985. *Soc. Neurosci. Abstr.* **11**: 289.
4. King, J. R., and C. M. Comer. 1996. *J. Comp. Physiol.* **178**: 293–305.
5. Dieringer, N. 1995. *Prog. Neurobiol.* **46**: 97–129.

Reference: *Biol. Bull.* **195**: 194–195. (October, 1998)

Prototype Rechargeable Tag for Acoustical Neural Telemetry

Allen F. Mensinger (Washington University School of Medicine, St. Louis, Missouri)
and Max Deffenbaugh¹

It has long been a goal of neuroethologists to record continuous neural activity from electrodes integrated into the nervous system of an unrestrained, naturally behaving animal. Recent studies have produced stable neural recordings in tethered toadfish (*Opsanus tau*) from sieve microelectrodes chronically implanted into the regenerated VIIIth nerve (1). The telemetry tag will advance the sieve electrode technology one step further by allowing acoustic telemetry of neural signals from a freely swimming animal in a quasi-natural environment; it will also advance our understanding of the vestibular and auditory system. The toadfish, *Opsanus tau*, presents an excellent model for this study. Its large, flat skull provides ample room for subcutaneous implantation of the tag. Moreover, the central projections (2, 3) and morphophysiology (4, 5) of its vestibular and auditory fibers have been well characterized.

Recording from freely swimming marine animals, in contrast to terrestrial animals, presents a different array of problems. The conductivity of seawater precludes the use of radio telemetry for practical bio-monitoring frequencies, except at ranges much less than one meter (6). In contrast, acoustic telemetry offers adequate ranges but can be limited by echoes (multipath) in enclosed environments like tanks. However, acoustic telemetry systems have been used in recent studies to transmit full electro-

myogram waveforms from free-swimming dogfish and tuna (7, 8) demonstrating the feasibility of the system.

Additionally, the increased drag of the aqueous medium dictates that telemetry devices must be small and streamlined, or implanted subcutaneously. Implantation greatly reduces the risk of infection or damage to the device but this advantage is offset, either by limited battery life, or by the need for invasive battery changes. The inductive recharging system used in this study solves these problems by providing a mechanism for noninvasive charging.

Fish were anesthetized with 0.001% MS-222 (Sigma) and injected with 0.1 ml of 1% pancuronium bromide. A small craniotomy was made directly over the anterior ramus of the VIIIth nerve. Twin microwire electrodes of insulated 20 μm diameter platinum/iridium wire were connected with conductive epoxy to 50 gauge multistranded gold wires, 6 cm in length, that terminated into a multipin connector. The post microwire assembly was encased in silastic to insure water tightness. The electrodes were inserted proximal to the anterior ramus of the VIIIth nerve, which contains the fibers for the anterior and horizontal semicircular canals and utricle. Neural activity was confirmed by recording differentially from the two microwires with an AM systems 1800 differential amplifier. The electrode was affixed with cyanoacrylate to the edge of the craniotomy, and the remaining opening was sealed with cyanoacrylate gel, the wound sutured, and the fish allowed to recover overnight. The micro-

¹ Marine Biological Laboratory, Woods Hole, Massachusetts.

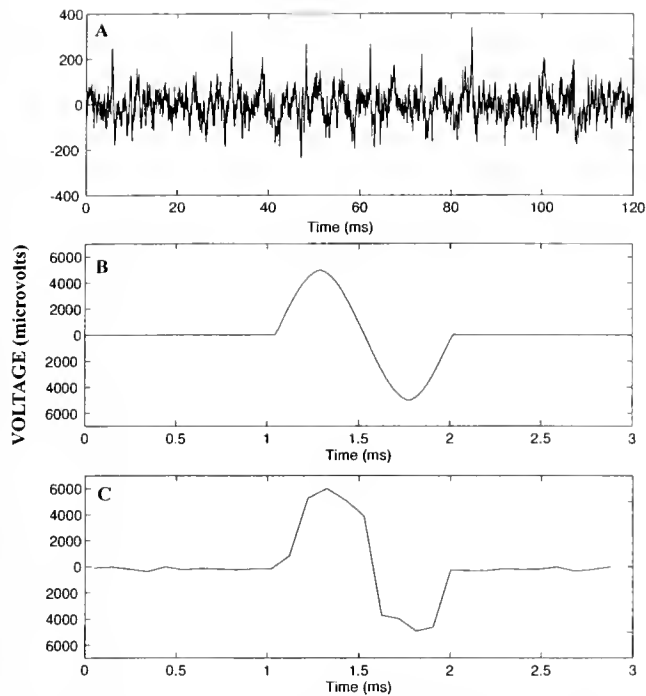


Figure 1. (A) An example of spontaneous neural data from micro-wire electrodes implanted into the VIIIth nerve of the toadfish. The signals in this example were transmitted via a direct hardwire connection between the telemetry tag and receiver. (B) The output of the amplifier when synthetic neural data from a function generator was transmitted into the telemetry tag. (C) The capture and reconstruction of the same neural signal by the receiver software after the signal in Figure 1B was acoustically transmitted to the receiver.

wire connector was then inserted into the telemetry tag mounted on the fish's head.

The transmitter tag consists of a flat cylinder, 2 cm diameter \times 1 cm high, weighing 8 g. Contained within the tag are two miniature 0.2 Farad ultra-high-capacity, energy-storage capacitors, which provide power to the tag, a circular inductive coil used to recharge the tag, and a piezoelectric transducer for transmitting data acoustically and high and low pass filters. The tag is recharged with a "recharging wand" that produces a 150 kHz oscillating magnetic field. When placed near the tag, this field induces an oscillating current in the inductive coil on the tag. This current is rectified and used to recharge the energy storage capacitors. At present, recharging takes 20 seconds, and a fully charged tag will operate for 15 minutes. The tag electronics include a differential electrode amplifier with 20 M Ω input impedance, a gain of 1000, a low pass frequency of 100 Hz, and a high pass frequency of 4000 Hz. A voltage-controlled oscillator converts the varying electrode voltage into a varying

frequency, which is amplified and transmitted acoustically by the piezoelectric transducer. This acoustic frequency modulated signal has a center frequency of 90 kHz and a 20 kHz bandwidth. The acoustic signal from the tag is detected by a receiver hydrophone and mixed down to a 0–20 kHz bandwidth. This demodulated signal is digitized and decoded by the receiver computer to reconstruct the full neural waveform.

Neural activity was recorded from the microwire electrodes over a period of several days using the tag, which was recharged several times during the one-hour recording sessions. Figure 1A shows an example of neural data from the electrode amplifier when the tag was wired to the receiver. Figure 1B displays the output of the amplifier when synthetic neural data from a function generator were transmitted to the amplifier; and Figure 1C shows the same signal after acoustical transmission by the tag and capture by the receiver. The synthetic data were displayed because the signal processing software is currently unable to discriminate individual action potentials from background noise within the multi-path environment of the small aquarium used for testing.

The results show that this inductively charged telemetry tag can transmit neural data through the water acoustically. The tag is presently in the preliminary stages of development. Future improvements will include extending the operational life by increasing energy storage capacitance on the tag and by replacing continuous full-waveform transmission with a level discriminator that will emit a short ping when the neural signal exceeds a preset threshold. Work is underway to increase signal resolution by mitigating the multi-path environment of the aquarium. This involves shielding the receiver hydrophone, coating the aquarium walls with materials that absorb or disperse reflections, and processing signals at the receiver.

Funding provided by a NASA Life Sciences Fellowship, MBL Associates Fellowship and NIH grant 1 R21 RR12623.

Literature Cited

1. Mensinger, A. F., S. M. Highstein, C. Buchko, D. Martin, R. Silver, and D. Anderson. 1998. *Soc. Neurosci. Abstracts* (In press).
2. Highstein, S. M., R. Kitch, J. Carey, and R. Baker. 1992. *J. Comp. Neurol.* 319: 501–518.
3. Edds-Walton, P. L. 1998. *Hearing Res.* 115: 45–60.
4. Boyle, R., J. P. Carey, and S. M. Highstein. 1991. *J. Neurophysiol.* 66: 1504–1521.
5. Mensinger, A. F., J. Carey, R. Boyle, and S. M. Highstein. 1997. *J. Comp. Neurol.* 384: 71–85.
6. Simon, H., E. O. Lewis, R. K. Raney, and J. R. Rossiter. 1994. *Remote Sensing of Sea Ice and Ice Bergs*. J Wiley and Sons, New York, p. 70.
7. Dewar, H., M. Deffenbaugh, B. Block, K. Lashkari, S. Lowder, G. Thurman, and P. McGill. 1996a. *5th European Conference on Wildlife Telemetry*. Strasbourg, France.
8. Dewar, H., M. Deffenbaugh, D. Marcinek, and B. Block. 1996b. *Proceedings of the 47th Tuna Conference*, Lake Arrowhead, CA.

Reference: *Biol. Bull.* 195: 196–197. (October, 1998)

Alterations in Cholinergic Signaling Modulate Contraction of Isolated Sea Urchin Tube Feet: Potential Role of Nitric Oxide

Blase Billack, Jeffrey D. Laskin¹, Prudence T. Heck, Walter Troll², Michael A. Gallo¹, and Diane E. Heck
(Environmental & Occupational Health Sciences Institute, Rutgers University,
Piscataway, New Jersey 08855)

The tube feet of the sea urchin are contractile appendages that are important in anchoring, locomotion, and sensory perception. Tube feet are composed of three distinct cylindrical layers. The outermost layer is a squamous epithelium that is closely associated with a nerve plexus. The epithelium is underlain by a dense layer of connective tissue. The innermost layer consists largely of smooth muscle separated from the lumen by a thin layer of epithelial cells. Sea urchin tube feet can extend from about 0.1 to 5 cm in length, and they contract spontaneously or when mechanically stimulated (1). Contraction can also be induced by electrical stimulation or exposure to acetylcholine (2). Previous studies indicate that electrical stimulation of tube feet is potentiated by anticholinesterase agents and antagonized by cholinergic blocking agents (2, 3). Low concentrations of acetylcholine have been found in the muscle layer or in the internal epithelium and the connective tissue sheath, and high concentrations have been reported in the layers that include the nerve plexus and the external epithelium (4). However, neither neuromuscular synapses, nor axons that cross the connective tissue layer separating muscle fibers from the subepithelial nerve plexus, have been detected (4), and thus, the signaling mechanisms that regulate smooth muscle movement are unclear. It has been proposed that acetylcholine slowly diffuses through the connective matrix in the absence of cholinesterase (2); however, the mechanism by which signals initiated by acetylcholine are transduced has not been determined. In the present studies we provide evidence that nitric oxide plays a role in this process.

Nitric oxide, an important signaling molecule derived from L-arginine, is important in the regulation of neurotransmission and smooth muscle contraction (5). We have found that the tube feet of the sea urchin *Arbacia punctulata* are relaxed by S-nitroso-N-acetylpenicillamine (SNAP, 4.5 nM), a nitric oxide donor (Fig. 1); moreover, this response is independent of the presence of sodium in the seawater. In contrast, N-nitroarginine methyl ester (NAME, 1 mM), an inhibitor of nitric oxide synthase, induced tube foot contraction (Fig. 1). The addition of nitric oxide was found to partially oppose the contraction of tube feet induced by acetylcholine (10–100 μ M). Nitroblue tetrazolium, a nitric oxide/superoxide free-radical trapping agent, induced contraction of tube feet. This reagent, which forms blue formazan in the presence of oxidants, such as nitric oxide, that are capable of single electron transfer, produced distinct staining patterns in the tube

feet. These were composed of concentric rings regularly spaced along the longitudinal axis of the tube feet.

In the mammalian enteric epithelium, nitric oxide production is stimulated by alpha bungarotoxin (BG)-sensitive acetylcholine receptors (type 1 nicotinic acetylcholine receptor, 6). In these cells, BG inactivates sensitive acetylcholine receptors and inhibits nitric oxide production (6). We found that BG caused contraction of isolated tube feet, an effect that was reversed by the addition of the nitric oxide donor SNAP (0.1–10 nM), suggesting that nitric oxide produced by activation of type 1 nicotinic acetylcholine receptors regulates tube foot relaxation. BG-induced contraction was not observed in the absence of calcium, or both calcium and magnesium. In calcium- or calcium and magnesium-free seawater, SNAP continued to induce relaxation, suggesting that extracellular calcium is required for BG-induced contraction, but that events downstream of nitric oxide production are independent of extracellular calcium. A question remains as to the nature of the receptors that mediate the contractile response to acetylcholine. Studies are in progress using cholinergic blocking agents to characterize this response.

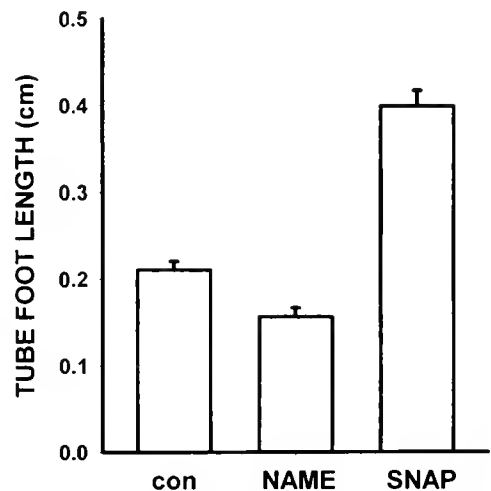


Figure 1. SNAP-induced relaxation of sea urchin tube feet. Tube feet were collected from *Arbacia punctulata* by ligation of the distal 2 cm of fully extended feet and placed in artificial seawater. Upon ligation, the hydraulically extended tube feet spontaneously contract. con, Untreated control tube foot; NAME, tube feet treated with 1 mM of the nitric oxide synthase inhibitor; SNAP, tube feet treated with 4.5 nM of the nitric oxide donating drug. Changes in the length of the tube feet were visualized microscopically and recorded with a graded measuring device 10 min after the addition of the drugs. Each bar represents the mean \pm SE, n = 6.

¹ University of Medicine and Dentistry of New Jersey—Robert Wood Johnson Medical School, 675 Hoes Lane, Piscataway, New Jersey 08854.

² New York University, 550 First Avenue, New York, New York 10016.

Taken together, these data indicate that acetylcholine mediates both the contraction and relaxation of sea urchin tube feet. We speculate that nitric oxide induces relaxation in response to the activation of BG-sensitive acetylcholine receptors. We hypothesize, further, that outer layer epithelial cells produce nitric oxide in response to acetylcholine released from the nerve plexus, and that nitric oxide, a lipid soluble gas, diffuses through the connective matrix to mediate relaxation of tube foot muscle.

Supported in part by NIH grants ES 03647, ES 05022 and ES 06897.

Literature Cited

1. Kabat-Zinn, J., and R. H. Singer. 1981. *J. Cell Biol.* **89**: 109–114.
2. Florey, E., and M. A. Cahill. 1980. *J. Exp. Biol.* **88**: 281–292.
3. Florey, E., M. A. Cahill, and M. Rathmayer. 1975. *Comp. Biochem. Physiol.* **51C**: 5–12.
4. Florey, E., and M. A. Cahill. 1977. *Cell Tissue Res.* **177**: 195–214.
5. Moncada, S. 1997. *Funct. Neurol.* **12**: 134–140.
6. Worl, J., B. Mayer, and W. L. Neuhuber. 1997. *Cell Tissue Res.* **287**: 113–118.

Reference: *Biol. Bull.* **195**: 197–198. (October, 1998)

A Closer Look at the Natural Substrate for a Nerve-Gas Hydrolyzing Enzyme in Squid Nerve

Francis C. G. Hoskin (Marine Biological Laboratory, Woods Hole, Massachusetts 02543)
and John E. Walker¹

In 1946, Abraham Mazur first described an enzyme that hydrolyzes and thus detoxifies the powerful organophosphorus acetylcholinesterase inhibitors termed "nerve gases." In 1966, a similar enzyme, but with markedly different properties, was found in nervous tissue from the squid *Loligo pealei*. The criteria differentiating "squid type" OPAA (organophosphorus acid anhydrolase) from "Mazur type" OPAA were summarized in a 1990 review (1), that also contains references to the earlier work. In brief, squid type OPAA hydrolyzes DFP, (iC₃H₇O)₂P(=O)F about five times faster than another nerve gas, Soman, CH₃(C₆H₁₃O)P(=O)F; it has a molecular weight of about 30,000; and it is narrowly limited to cephalopod nerve, hepatopancreas, and saliva despite a wide search covering representative samples in various kingdoms and phyla. Although the "Mazur type" characterization is less rigorous, these properties emerge: hydrolyzes Soman 5 to 50 times faster than DFP; has molecular weights ranging from 45,000 to 90,000; is widely distributed; and is stimulated 2- to 20-fold and more by Mn²⁺, a property not displayed by the squid-type enzyme.

There are exceptions to our simplistic classification. We ourselves reported a squid-like enzyme from *Pseudomonas diminuta* that hydrolyzes the P-S bond of the VX-type nerve agents (R₁R₂P(=O)SR₃) and, more to the point, hydrolyzes DFP about eight times faster than Soman (2). And on the other hand, a "Mazur"-like enzyme from *Alteromonas* has recently been described (3) that hydrolyzes Soman faster than DFP and also hydrolyzes the dipeptide Leu-Pro (leucine-proline). The subtitle of that report (3), "Nerve agent-detoxifying enzyme is a proli-dase" leads us to ask whether this applies to the squid type OPAA as well.

We have reasoned that, if a DFP-hydrolyzing enzyme also hydrolyzes Leu-Pro, then Leu-Pro should inhibit the hydrolysis of DFP. In a typical experiment to test this idea, 0.05 ml purified OPAA (diluted sufficiently to give a measurable reaction rate)

is added to 4.95 ml 0.02 M Pipes buffer, pH 7, made 0.003 M in both DFP and Leu-Pro. The hydrolysis of DFP is followed with a fluoride-sensitive electrode. In the control experiment, the enzyme is added to the same buffer made to 0.003 M in DFP only. The results, presented in Table 1, show that squid-type OPAA and the comparable enzyme from *Pseudomonas diminuta*, termed OPH (2), are not inhibited by Leu-Pro. This finding seems to be correlated with the Soman/DFP hydrolysis ratio of approximately 0.2, and with a lack of Mn²⁺ stimulation, which has previously been reported for squid-type OPAA. The other three Mazur-like sources tested show inhibition by Leu-Pro, and suggest a correlation with greater hydrolysis of Soman than of DFP and with Mn²⁺ stimulation. Thus, only Mazur-like OPAA's appear to be inhibited by Leu-Pro.

Three conclusions emerge from the data. First, squid-type OPAA is not a proli-dase. Second, some of the other OPAA's have active sites that, indeed, seem to be occupied by Leu-Pro.

Table 1

Effect of Leu-Pro on DFP hydrolysis by purified nerve gas hydrolyzing enzymes in relation to other properties

Enzyme source	% Inhibition by Leu-Pro	Soman/DFP hydrolysis ratio ¹	Mn ²⁺ stimulation ¹
Squid	-3, -5 ²	0.2-0.25	0
<i>Ps. diminuta</i>	0, 2, 3	0.125	0 ¹
Hog kidney	93, 93	~5	~5 X
<i>E. coli</i>	72, 76	~50	~5 X
<i>Alteromonas</i>	55, 68	~2 ⁴	Yes ⁴

¹ Previously published by senior author and colleagues over many years; see, e.g., ref. (1).

² Negative values = stimulation.

³ New data.

⁴ Ref. (3).

¹ U.S. Army Natick RD&E Center, Natick, Massachusetts 01760.

Third, for the first time, a bacterial OPAA, namely that from *Pseudomonas diminuta*, shows a close resemblance to the squid enzyme. The first two conclusions, while appearing valid, should be verified when DFP and Leu-Pro concentrations are widely different; *i.e.*, a K_i should be determined for Leu-Pro. The third conclusion suggests that a new criterion for the so-called squid type OPAA has emerged, namely, the lack of inhibition by Leu-Pro.

Two questions are now to be examined: Do either Leu or Pro, as hydrolysis products, inhibit the Mazur type OPAA's? And if so, do any other amino acids inhibit the squid type OPAA? Because the latter category now includes the enzyme

from *Pseudomonas diminuta* as well as from squid nerve, a new approach to the question of a natural substrate for this enzyme may be emerging.

Literature Cited

1. Hoskin, F. C. G. 1990. Pp. 469–480 in *Squid as Experimental Animals*, D. L. Gilbert, W. J. Adelman, Jr., and J. M. Arnold, eds. Plenum Press, New York.
2. Hoskin, F. C. G., J. E. Walker, W.-D. Dettbarn, and J. M. Wild. 1995. *Biochem. Pharmacol.* 49: 711–715.
3. Cheng, T.-C., L. Liu, J. Wu, J. J. DeFrank, D. M. Anderson, V. K. Rastogi, and A. B. Hamilton. 1997. *J. Ind. Microbiol. Biotechnol.* 18: 49–55.

Reference: *Biol. Bull.* 195: 198–201. (October, 1998)

Lead, Learning, and Calcectin in *Hermisenda*

Alan M. Kuzirian, Herman T. Epstein, Thomas J. Nelson¹, Nancy S. Rafferty
(Marine Biological Laboratory, Woods Hole, Massachusetts 02543), and Daniel L. Alkon¹

Calcectin (cp20)(CE) is a unique Ca^{+2} /GTP binding protein with two EF-hands that, when phosphorylated by Ca^{2+} -dependent isozymes (α , σ , δ) of protein kinase-C (PKC), reduces two voltage-dependent K^+ currents (I_A ; $I_{\text{Ca-K}^+}$)(1, 2). These currents are thought to be responsible for the enhanced long-lasting depolarization (LLD) exhibited in *Hermisenda* photoreceptors when these animals are exposed to Pavlovian conditioning, and for the increased EPSP summation seen in the vertebrate hippocampus after nictitating membrane conditioning. Although immunoreactivity to CE has been found in the central nervous systems of squid, rabbits, and rats, and in human fibroblasts, its presence in *Hermisenda* had not been demonstrated. The purpose of this report is to document, by immunocytochemical methods, the occurrence of CE in the central nervous system (CNS) and photoreceptors of *Hermisenda*, as well as its modulation by Pavlovian conditioning and its possible involvement in lead-induced neurotoxicity.

As part of a continuing investigation focused on lead toxicity in the CNS of *Hermisenda*, the training paradigms and lead exposure levels used here follow previously proven methods that have demonstrated training acquisition and neurotoxic effects of lead (2, 3). Nudibranchs were chronically exposed to lead (Pb acetate added to natural seawater (NSW); 0, 2, 4 mg/l) for 3 days prior to and throughout their first training paradigm, which consisted of random presentations of light (conditioned stimulus; CS) and agitation (unconditioned stimulus; UCS), 50 trials/day for 3 days. The animals were then tested for learning acquisition on the 4th day by measuring their response (change in body length: contraction indicates positive training; no response or body extension indicates no training) to the CS alone. After 4 days with no training and no lead exposure, each group

was acutely re-exposed to lead (0, 2, 4 mg/l PbAc), re-trained (3 days) with explicitly paired CS/UCS stimuli, and tested again for learning acquisition (4th day). Nudibranchs used for the immunocytochemical demonstration of calcectin underwent either paired or random training regimes, with or without the presence of lead (2 mg/l). Naive animals receiving no training were used as controls. Throughout the experimental period, the treatment seawater was changed daily and the nudibranchs were fed a daily diet of the colonial ascidian *Diplosoma mcdonaldi*.

For immunocytochemistry, the CNS of each animal was dissected after testing, then fixed (4% paraformaldehyde in artificial seawater), dehydrated, and embedded in polyethylene glycol-400-distearate; 4- μm sections were cut and mounted on subbed slides. Sections were de-waxed, incubated in anti-CE (cloned peptide sequence from squid optic lobes, designated 25U2, raised in rabbit; 1:1000 dil.), and then in biotinylated horse anti-rabbit secondary antibody, followed by avidin-bound microperoxidase (ABC method, Vector), and finally reacted with the chromogen, 3-amino-9-ethylcarbazole (AEC). Bovine serum albumin (BSA) and normal horse serum (at 1%) served as negative controls.

Hermisenda experiencing random presentations of light and agitation demonstrated no significant learning, and statistical analyses (ANOVA: $F = 0.33$, $P = 0.726$, $n = 13$) confirmed that their behavior was unaltered by lead exposure (only 16%–23% of the animals contracted; Table I, Fig. 1). However, when the same animals were re-trained with paired CS/UCS stimuli, in the absence of lead, significant learning occurred; assessed in terms of the percentage of animals contracting (random [16%] vs. paired [69%]). Moreover, lead exposure (4 mg/l PbAc) statistically suppressed learning (paired, 0 vs. 4 mg/l PbAc [69% vs. 31% respectively]) to within comparable (statistically non-significant) performance levels demonstrated by randomly trained animals (23%). The results were similar whether the

¹ Laboratory of Adaptive Systems, NINDS-NIH, Bethesda, Maryland 20892.

Table 1

Training responses of *Hermisenda* to paired and random stimuli presentations, with and without lead exposure

Pb conc. (mg/l)	Random stimuli	Paired stimuli
I. Animals Contracting (%)		
0	16.25	68.75
2	24.5	45.0
4	22.8	31.25
Student's <i>t</i> tests		
Random vs. Paired stimuli, 0 mg/l Pb: $t = -2.645$, $P = 0.038$, $n = 8$		
Paired stimuli, 0 vs. 4 mg/l Pb: $t = -2.778$, $P = 0.032$, $n = 8$		
II. Change in Foot Length (in millimeters)*		
0	0.333	-2.50
2	1.667	-2.25
4	0.167	-0.75
Student's <i>t</i> tests		
Random vs. Paired stimuli, 0 mg/l Pb: $t = -3.279$, $P = 0.011$, $n = 12$		
Paired stimuli, 0 vs. 4 mg/l Pb: $t = 4.583$, $P = 0.0038$, $n = 8$		

* Negative number = foot contraction, positive training response; positive number = foot extension, negative training response.

percentage of animals contracting or the actual change in body length (in millimeters) was used as a measure of learning.

Immunocytochemical labeling with anti-CE was demonstrated in specific neurons in the CNS and, in particular, in the medial-B photoreceptors in the eye (Fig. 2). Preliminary evidence suggests that the intensity of immunolabeling may reflect the animal's training experience as well as its lead exposure. Thus, animals that had undergone paired CS/UCS training had intensely labeled B photoreceptors (Fig. 2A). In contrast, naive, non-trained control animals (Fig. 2B) and randomly trained animals (not illustrated) showed only minimal photoreceptor immunostaining. Finally, lead-exposed (2 mg/l), paired CS/UCS-trained nudibranchs showed an intermediate staining intensity (Fig. 2C). The negative immuno-controls (1% BSA, horse serum) were unstained in all aspects (Fig. 2D). CE immunocytochemistry also revealed the existence of several specifically located and intensively labeled interneurons of unknown function in both the cerebropleural and pedal ganglia. One of these cells, which may be part of the photic network and was unaffected both by training and lead exposure, interacts synaptically with a similarly labeled neuron from the contralateral side. Squid optic lobe (8- μ m-thick cryosections) was used as a positive control tissue and gave positive results similar to those of Nelson *et al.* (1).

A significant finding of this study is that animals trained with presentations of random stimuli demonstrated no significant training acquisition and that no behavioral differences were recorded in the conditioned response (CR) that could be correlated with lead exposure (0-4 mg/l). Also of importance, when

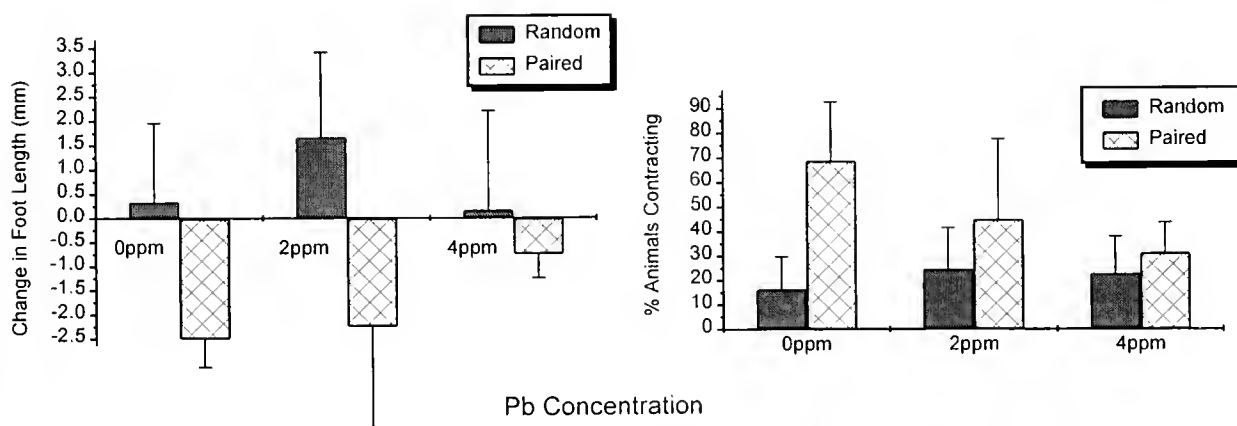


Figure 1. Lead effects at 2 ppm and 4 ppm lead acetate (PbAc) on behavioral responses of *Hermisenda*. First, the nudibranchs were exposed to lead, trained with random presentations of light (conditioned stimulus: CS) and agitation (unconditioned stimulus: UCS) for 50 trials/day for 3 days and tested on day 4. After 4 days of re-acclimation to non-experimental conditions, the same groups were re-exposed to lead, re-trained with paired light and agitation (3 days) and again re-tested (4th day). (Left panel) Amount of foot contraction (conditioned response [CR] in mm) of test animals exposed as above, in response to CS. No significant amount of positive learning (foot contraction) occurred with randomized stimuli presentations, and locomotory behavior was unaffected by lead exposure. When re-trained with paired stimuli, control animals (0 mg/l PbAc) demonstrated positive conditioning by exhibiting marked foot shortening (negative length changes) compared to randomly trained animals (positive length changes; normal locomotion). Foot-length differences between paired stimuli groups at 0 and 4 mg/l PbAc indicated significant learning depression within the lead-exposed animals, while foot-length changes between 0 and 2, and 2 and 4 mg/l PbAc were not significant. (Right panel) Percentage of animals responding with positive foot contraction (CR) when tested with light alone. Statistical analyses confirmed there were no significant lead effects within or between groups trained with randomized presentations of the two stimuli. Significant learning did occur with paired stimuli in control animals that were not exposed to lead, but learning responses were statistically depressed in animals exposed to 4 mg/l PbAc. Again, statistical comparisons of the percentage of animals contracting between 0 and 2, and 2 and 4 mg/l PbAc were not significant.

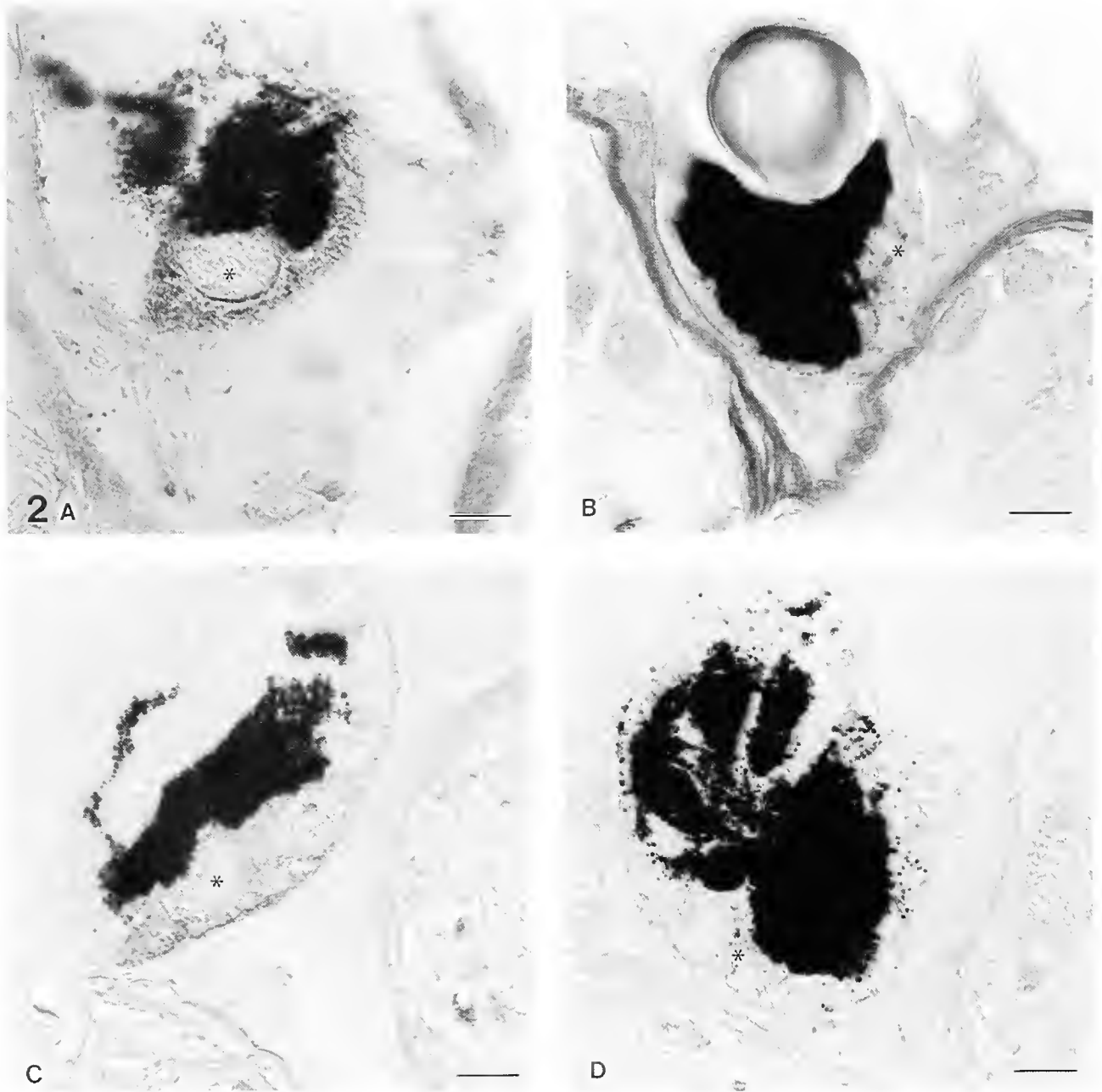


Figure 2. Photomicrographs of 4- μ m-thick sections of polyester-embedded *Hermisenda* nervous systems immunolabeled with a rabbit antibody to calnexin (25U2, 1:1000 dilution) and reacted with the chromogen, 3-amino-9-ethylcarbazole. Photoreceptors of interest are indicated by asterisks. (A) Section of the eye of an animal conditioned with paired stimuli (CS-Light/UCS-agitation), illustrating the 4⁺ positive staining for calnexin in the medial-B photoreceptor. (B) Similarly labeled medial-B photoreceptor from a naive (non-trained) animal showing minimal staining (1⁺) for calnexin. (C) Immunolabeled medial-B photoreceptor of a paired (CS/UCS) trained, lead-exposed (2 ppm PbAc) animal showing much less intense antibody labeling (2⁺) for calnexin. (D) Negative control in which 1% BSA, 1% normal horse serum was substituted for the primary antibody (25U2), and applied to a serial section of same eye as in (A). Photomicrograph illustrates no non-specific staining (scale bars = 20 μ m).

the same groups of nudibranchs were retrained with the paired CS/UCS stimuli, significant statistical differences in learning acquisition were evident in comparisons between lead exposed (4 mg/l) and non-exposed groups. Non-exposed animals underwent the expected, normal training acquisition, but lead-exposed

animals again failed to demonstrate learning. These results are unlikely to be caused by some general physiological impairment or loss of motor ability. Rather, they continue to support the hypothesis that the reduced behavioral performances of lead-exposed animals are due to sensory processing deficits in the

CNS. They also confirm and reinforce the previously published lead toxicity data on lead-induced declines in the training (or learning) performance in *Hermisenda* (3, 4).

This preliminary antibody study suggests that CE levels, as detected by the intensity of immunolabeling in the medial-B photoreceptors, reflect (at least qualitatively) positive learning effects in *Hermisenda*, as well as lead-induced learning neurotoxicity. The immunolabeling results are consistent with the cellular electrophysiology of the photoreceptors and with the biochemistry of this unique $\text{Ca}^{+2}/\text{GTP}$ binding protein. It has been shown in *Hermisenda* that paired Pavlovian conditioning induces an increased input resistance and reduced voltage-dependent K^{+} currents in the photoreceptors as a result of increased intracellular calcium levels (5). Concurrent second messenger changes involve autophosphorylation and translocation of PKC and phosphorylation of CE (6, 1). CE inactivates the K^{+} channels and activates ryanodine receptors (RyR), which in turn maintain long-term increases in intracellular calcium. This rise in intracellular calcium underlies the long-term changes in neuronal excitability (LLD) associated with memory (7). The increased levels of intracellular calcium could be sustained by increased levels of CE occurring concurrently with the up-regulated mRNA levels for RyR (8). The more intense immunolabeling of photoreceptors from animals experiencing paired training supports this hypothesis, while also suggesting a possible interference by lead with intracellular calcium homeostasis (9).

Future efforts using quantitative labeling of preparations with

immuno-colloidal gold will be undertaken to confirm our hypothesis that CE levels increase with learning. The immuno-EM labeling will also allow us to document the cytologic location of CE and to determine whether learning causes any translocation of the protein within or between the cytosol and plasma membrane or between membrane organelles, as is known for PKC.

Literature Cited

1. Nelson, T. J., S. Cavallaro, C-L. Yi, D. McPhie, B. G. Schreurs, P. A. Gusev, A. Favitt, O. Zohar, J. Kim, S. Beushausen, G. Ascoli, J. Olds, R. Neve, and D. L. Alkon. 1996. *Proc. Natl. Acad. Sci.* **93**: 13808–13813.
2. Ascoli, G. A., K. X. Luu, J. L. Olds, T. J. Nelson, P. A. Gusev, C. Bertucci, E. Bramanti, A. Raffaelli, P. Salvadori, and D. L. Alkon. 1997. *J. Biol. Chem.* **272**(40): 24771–24779.
3. Kuzirian, A. M., F. M. Child, H. T. Epstein, P. J. S. Smith, and C. T. Tamse. 1996. *Biol. Bull.* **191**: 260–261.
4. Kuzirian, A. M., H. T. Epstein, and N. R. Rafferty. 1997. *Biol. Bull.* **193**: 263–264.
5. Nelson, T. J., C. Collin, and D. L. Alkon. 1990. *Science* **254**: 1479–1483.
6. McPhie, D. L., L. D. Matzet, J. L. Olds, D. S. Lester, A. M. Kuzirian, and D. L. Alkon. 1993. *J. Neurochem.* **60**: 646–651.
7. Alkon, D. L., T. N. Nelson, W. Zhao, and S. Cavallaro. 1998. *Trends Neurosci.* **21** (in press).
8. Cavallaro, S., N. Meiri, C-L. Yi, S. Musco, J. Goldberg, and D. L. Alkon. 1997. *Proc. Natl. Acad. Sci.* **94**: 9669–9673.
9. Gilbert, M. E. 1997. *Am. Zool.* **37**: 389–398.

Reference: *Biol. Bull.* **195**: 201–202. (October, 1998)

Transmembrane Calcium Flux in Pb^{+2} -Exposed *Aplysia* Neurons

Catherine T. Tamse¹, Katherine Hammar, D. Marshall Porterfield, and Peter J. S. Smith
(BioCurrents Research Center, Marine Biological Laboratory, Woods Hole, Massachusetts 02543)

Lead (Pb^{+2}) continues to be a major health and environmental hazard, especially for young children. This neurotoxin affects the development of the central nervous system and causes cognitive and behavioral perturbations (1). Decades of extensive clinical and laboratory research on Pb^{+2} , with both vertebrate and invertebrate model systems, attest to its biomedical importance. Studies have shown that Pb^{+2} can interfere with important calcium (Ca^{+2})-mediated cellular processes and enter cells through Ca^{+2} channels and other molecule-mediated pathways (2, 3, 4, 5). However, the dynamic interaction between Pb^{+2} and Ca^{+2} remains poorly understood. Scientists have only recently reported that Pb^{+2} uptake across the plasma membrane is enhanced by the depletion of intracellular Ca^{+2} stores (6).

By observing its effects on calcium flux, we have asked how Pb^{+2} can be transported into and sequestered within the cell. In particular, we have tested the hypothesis that Pb^{+2} , upon enter-

ing the cell, disrupts Ca^{+2} homeostasis by displacing intracellular Ca^{+2} . A non-invasive, Ca^{+2} -selective self-referencing probe was used to directly measure any changes in the net transmembrane Ca^{+2} flux after Pb^{+2} exposure. To examine how Pb^{+2} might use Ca^{+2} transport mechanisms to enter the cell, non-specific and specific pharmacological blockers of Ca^{+2} channels such as cobalt (Ca^{+2}) and verapamil were applied during Pb^{+2} exposure. Thapsigargin, an intracellular Ca^{+2} -ATPase inhibitor (7) acting principally at the endoplasmic reticulum, was used to examine the relationship between Pb^{+2} , Ca^{+2} , and the reticular store.

The bag cell neurons from specimens of the gastropod mollusc, *Aplysia californica*, were used in this study; the animals were maintained at the Marine Resources Center, Marine Biological Laboratory, Woods Hole, Massachusetts. *Aplysia* is a well-established model for diverse neurobiological and toxicological investigations (3, 5, 8, 9), and Ca^{+2} currents in the bag cell neurons have been well-characterized (10). Primary cultures of bag cells were prepared according to standard protocols (8, 9) and were studied between 24 and 48 hours after isolation.

¹ Department of Biological Sciences, University of Rhode Island, Kingston, Rhode Island 02881.

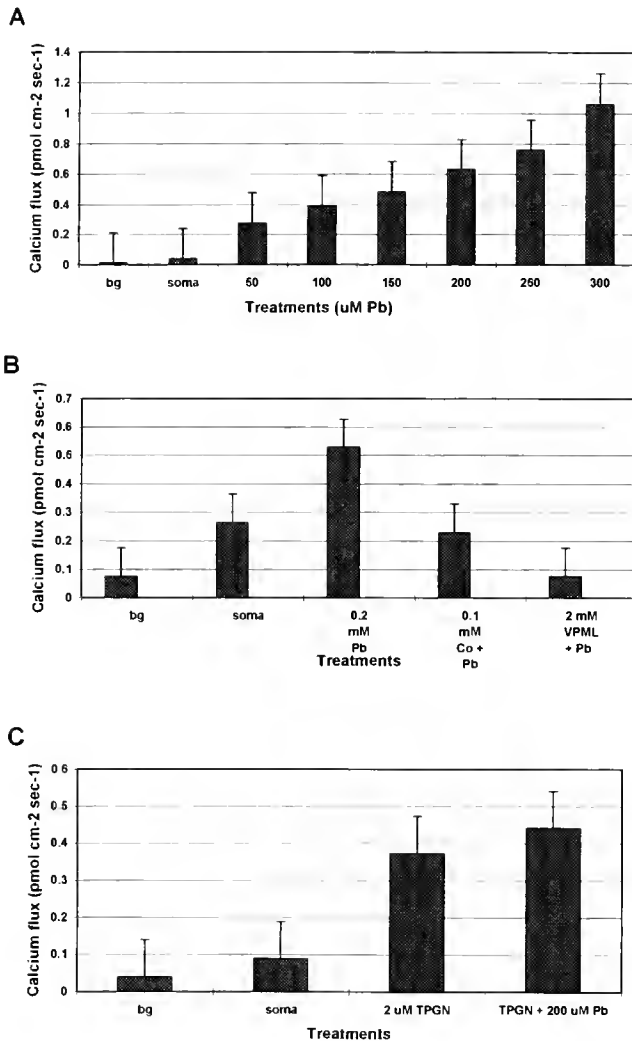


Figure 1. Effects of lead and pharmacological agents on the calcium flux observed in *Aplysia* bag cell neurons. **A.** Increasing Pb^{+2} concentrations stimulated a corresponding increase in Ca^{+2} efflux signals. **B.** Ca^{+2} channel blocker verapamil (VPML) markedly reduced the Pb^{+2} -induced Ca^{+2} efflux while Co^{+2} (Co) slightly diminished the signals. **C.** Thapsigargin (TPGN), a Ca^{+2} -ATPase inhibitor, generates a sustained increase in efflux, a level not significantly altered by the subsequent addition of Pb^{+2} . Background (bg) measurements or negative controls were done at 60–200 μ m away from the plasmamembrane, while positive controls (soma) were measured at the neuronal membrane before any of the treatments were added.

To record the transmembrane Ca^{+2} signals, a Ca^{+2} -selective self-referencing probe was used. This instrument and method of operation have been described in detail (8, 11, 12); the probe takes advantage of the inherent, albeit low voltage signals caused by the movement of ions across cell membranes. Silanized microelectrodes tipped with a 30- μ m column of Ca^{+2} -selective liquid membrane (Fluka Calcium Ionophore 1, Cocktail A) were moved alternately at 0.3 Hz, orthogonal to the plasma membrane, between a near pole within 1 μ m of the surface and a distant point 10 μ m away. The circuit was completed with a 3 M KCl bridge electrode.

Calcium flux was calculated with the Fick equation using the differential voltage recorded between the two extremes of oscillation (12). Background measurements were made at points further than 60 μ m from the cell membrane. This whole set-up was mounted on a Zeiss IM 35 inverted microscope, in a Faraday cage, on an air table.

Addition of lead acetate in 50- μ M increments (50–300 μ M concentrations) to the bathing medium caused a dose-dependent increase in Ca^{+2} efflux signals (Fig. 1A) and demonstrates a concentration-dependent flux. Furthermore, verapamil (2 mM) greatly reduced Pb^{+2} -induced Ca^{+2} efflux, while 100 μ M Co^{+2} (as cobalt chloride) diminished the signals (Fig. 1B). Therefore, we propose that Pb^{+2} is entering the cells through Ca^{+2} channels. Other studies have already suggested that Ca^{+2} channels are involved in the entry of Pb^{+2} into both vertebrate and invertebrate cells (3, 4, 6). The enhanced efflux seen with Pb^{+2} could be due either to (1) a direct action on the transmembrane Ca^{+2} transporters, ATPases and exchangers, or (2) the displacement of Ca^{+2} by Pb^{+2} from internal stores. In the latter case, we suggest that Pb^{+2} is causing the release of Ca^{+2} from the endoplasmic reticulum into the cytosol, from which it is subsequently removed by the plasmamembrane transporters.

To test the possibility that Pb^{+2} interacts with the endoplasmic reticular Ca^{+2} stores, we applied thapsigargin (2 μ M) 10–15 min before treatment with Pb^{+2} . After such a pre-treatment with thapsigargin, Pb^{+2} caused no additional significant increase in the transmembrane flux (Fig. 1C). The simplest interpretation of this result is that Pb^{+2} , like Ca^{+2} , is transported into the reticular lumen via a Ca^{+2} -ATPase pump. But with thapsigargin blocking the pump, Pb^{+2} is therefore unable to enter the endoplasmic reticulum and displace the Ca^{+2} store. Thus, the subsequent addition of Pb^{+2} did not significantly increase the plasma membrane Ca^{+2} flux beyond what was measured from thapsigargin treatment alone.

We hypothesize, therefore, that Pb^{+2} enters the cells through Ca^{+2} channels and can displace reticular Ca^{+2} stores via transport mechanisms of the endoplasmic reticulum.

This project was funded by grants from SICB and IWFA to CTT and by NIH-P41 RR01395 to PJSS.

Literature Cited

1. Silbergeld, E. K. 1992. *FASEB J.* 6: 3201–3206.
2. Markovac, J., and G. W. Goldstein. 1988. *Nature.* 334: 71–73.
3. Busselberg, D., M. L. Evans, H. Rahmann, and D. O. Carpenter. 1991. *J. Neurophysiol.* 65: 786–795.
4. Ujihara, H., and E. X. Albuquerque. 1992. *J. Pharmacol. Exp. Ther.* 263: 868–875.
5. Audesirk, G. 1993. *Neurotoxicol.* 14: 137–148.
6. Kerper, L. E., and P. M. Hinkle. 1997. *J. Biol. Chem.* 272: 8346–8352.
7. Knox, R. J., L. S. Kao, E. Jonas, P. J. S. Smith, and L. Kaczmarek. 1996. *J. Physiol.* 494: 627–639.
8. Kaczmarek, L. K., M. Finbow, J. P. Revel, and F. Strumwasser. 1979. *J. Neurobiol.* 10: 535–550.
9. Dagan, D., and I. B. Levitan. 1981. *J. Neurosci.* 7: 736–740.
10. Fieber, L. A. 1995. *J. Exp. Biol.* 198: 2337–2347.
11. Smith, P. J. S., R. H. Sanger, and L. F. Jaffe. 1994. Pp. 115–134 in *Methods in Cell Biology*. R. Nuccitelli, ed. Academic Press, CA.
12. Smith, P. J. S. 1995. *Nature.* 378: 645–646.

Reference: *Biol. Bull.* **195**: 203–204. (October, 1998)

Extracellular pH Gradients Measured From Isolated Retinal Cells

Robert Paul Malchow (University of Illinois at Chicago, 1855 West Taylor Street, Chicago, Illinois 60612), Michael P. Verzi¹, and Peter J. S. Smith²

Neuronal signaling within the vertebrate retina is highly dependent upon the pH of the extracellular fluid. For example, the alteration of external pH from 7.8 to 7.0 has been shown to suppress almost completely the light-induced responses of second order neurons in the retina of the tiger salamander (1–3). Further, stimulation of the retina by light can induce significant changes in extracellular pH (4, 5), raising the possibility that normal light-induced alterations in the extracellular H⁺ concentration might play an important role in modulating the flow of visual information within the retina. Ratiometric imaging techniques using fluorescent pH indicator dyes such as BCECF have begun to expand our knowledge of the control of pH within retinal neurons (cf. 6, 7). However, this method does not readily permit direct examination of fluxes of hydrogen ions across the membranes of neurons and glia. This limitation, coupled with the cellular heterogeneity of the vertebrate retina, has made it difficult to study the cellular and molecular mechanisms responsible for the maintenance of extracellular pH and its alteration during light stimulation. The purpose of the present study was to determine whether a different method could be used to examine H⁺ flux directly from isolated retinal neurons, setting the stage for future experiments designed to understand the mechanisms that might be responsible for changes in external pH.

pH-selective microelectrodes can be used to address this question, but drift in the signal of such electrodes can often obscure the small signals expected to be generated adjacent to the membrane of individual cells. A method that greatly improves both the stability and sensitivity of such recordings involves the use of the electrode in a self-referencing format. In this method, an electrode is moved alternately from a position close to the membrane of the cell to a position further away in the surrounding medium. The difference between the voltage readings at the two positions is indicative of differences in free ion concentrations at the two locations. This procedure permits the examination of the small ionic gradients expected to be generated at the plasma membrane-saline interface (see Smith, Sanger and Jaffe [8] for review).

We prepared pH-selective electrodes by pulling thin-wall glass capillary tubes (o.d. 1.5 mm) to a tip diameter of ~2 μm. The pulled pipettes were silanized and back-filled to about 1 cm with 100 mM potassium chloride. The electrolyte was forced into the end tip of the pipette by air pressure supplied to the back of the pipette from a syringe. The pipette tip was then placed into contact with a pH-selective resin (hydrogen ionophore 1-Cocktail B, Fluka Chemica) and approximately 50 μm of the resin was drawn into the silanized tube. This resin has

an especially high degree of selectivity for hydrogen ions, as compared to other ions; for example it is more than 10⁹ times more sensitive to H⁺ than to potassium or sodium ions (9). A voltage is generated across the small column of resin, and this voltage is directly proportional to the ion activity at the tip of the electrode. In referring to our measurements as net fluxes we are assuming that the major force driving the movement of hydrogen ions between the two points of measurement is diffusion, and that the effect of the net voltage gradient associated with steady state currents (10) will be minimal. Finally, isolated retinal neurons from skate (*Raja erinacea* or *R. ocellata*) were prepared according to the enzymatic dissociation protocol described in Malchow *et al.* (11).

Figure 1 shows that a robust and easily detectable signal could indeed be detected from isolated external horizontal cells using these techniques. The leftmost portion of the trace indicates the size of the differential signal recorded from one cell bathed in a skate-modified Ringer containing 2 mM of the pH buffer HEPES and adjusted to pH 7.60 with NaOH. With the electrode within 1 μm of the cell membrane at the closest extent of its travel, and 50 μm from the cell at the distant position, a differential signal of approximately 85 μV was recorded. The electrode was then moved in the vertical plane 160 μm away ("background"); at this distance, no differential signal could be detected. When the electrode was returned to its initial position the signal was restored. The solution surrounding the cell was then changed for one containing 25 mM HEPES, again adjusted to pH 7.60. The higher concentration of this pH buffer was expected to reduce the extracellular concentration of free hydrogen ions near the cell and thus significantly reduce the signal detected by the electrode. Indeed, the signal recorded

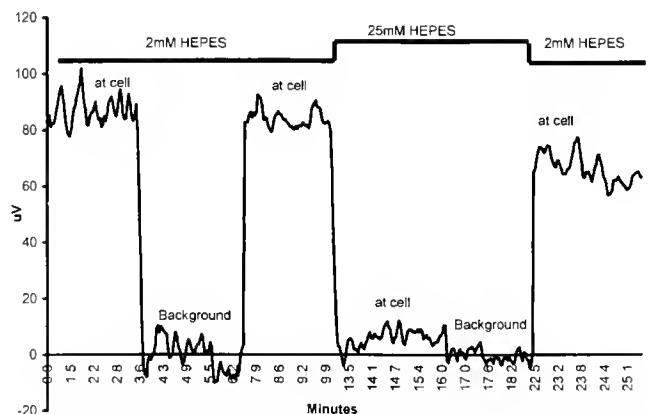


Figure 1. Example of a recording made with a self-referencing pH-selective microelectrode placed in close apposition to an external horizontal cell isolated from the retina of the skate.

¹ Department of Biology, College of New Jersey, Ewing, New Jersey 08628

² Biocurrents Research Center, Marine Biological Laboratory, Woods Hole, Massachusetts 02543

under these conditions was lowered to approximately 10 μ V, supporting the contention that the differential voltage being measured by the electrode results from hydrogen ions. A background recording was then again made 160 μ m away from the cell. Finally, the electrode was returned to the cell and the dish refreshed with 2 mM HEPES Ringer, resulting in restoration of the signal.

Our results demonstrate that self-referencing pH-selective microelectrodes can indeed be used to examine H⁺ net flux across the membranes of isolated retinal neurons. We are now employing specific pharmacological probes that selectively inhibit various pH transport mechanisms in an effort to clarify the mechanisms responsible for the net fluxes we have detected.

We are grateful to Richard H. Sanger for electronic and computer assistance and Rudi Rottenfusser of the Zeiss Corporation for the generous loan of microscope equipment. This work was supported by grants EYO 9411 from the National Eye Institute, P41 RR01395 from the National Center for Research Resources, and grant DBI-9605155 from the National Science Foundation.

Literature Cited

1. Kleinschmidt, J. 1990. *Soc. Neurosci. Abstr.* **16**: 465.
2. Kleinschmidt, J. 1991. *Ann. N. Y. Acad. Sci.* **635**: 468–470.
3. Barnes, S., V. Merchant, and F. Mahmud. 1993. *Proc. Natl. Acad. Sci.* **90**: 10081–10085.
4. Oakley, B. II, and R. Wen. 1989. *J. Physiol. (Lond.)* **419**: 353–378.
5. Borgula, G. A., C. J. Karwowski, and R. H. Steinberg. 1989. *Vision Res.* **29**: 1069–1077.
6. Haugh-Scheidt, L., and H. Ripps. 1998. *Exp. Eye Res.* **66**: 449–464.
7. Saarikoski, J., E. Ruusuvaori, A. Koskelainen, and K. Donner. 1997. *J. Physiol. (Lond.)* **498**: 61–72.
8. Smith, P. J. S., R. H. Sanger, and L. F. Jaffe. 1994. *Methods Cell Biol.* **40**: 115–134.
9. Fluka. 1991. *Sectophore, Ionophores for Ion-Selective Electrodes and Optodes*. Fluxa Chemie A. G. Ronkonkoma, New York.
10. Robinson, K. R. 1989. Endogenous and applied electrical currents: their measurement and application. Pp. 1–26 in: R. B. Borgens, K. R. Robinson, J. W. Vanable, and M. E. McGinnis. *Electric Fields in Vertebrate Repair*. Alan R. Liss, New York.
11. Malchow, R. P., II, Qian, H. Ripps, and J. E. Dowling. 1990. *J. Gen. Physiol.* **95**: 177–198.

Reference: *Biol. Bull.* **195**: 204–205. (October, 1998)

Fluorometric Analysis of Intracellular Sodium Concentrations in Isolated Retinal Horizontal Cells

Kristen A. Andersen and Robert Paul Malchow (University of Illinois at Chicago, 1855 West Taylor Street, Chicago, Illinois 60612)

Horizontal cells of the vertebrate retina are interneurons; they form a lateral inhibitory pathway in the visual system mediating interactions between photoreceptors and bipolar cells at the first stage of signal transduction. In the all-rod retina of the skate (*Raja erinacea* and *R. ocellata*), evidence suggests that horizontal cells control information processing through the actions of the inhibitory neurotransmitter gamma-aminobutyric acid (GABA), and through extensive electrical-coupling by membrane proteins called gap junctions. Electrical-coupling allows signals at the outer plexiform layer to be summed over a large spatial domain.

Immunoreactive antibodies directed against GABA and its rate-limiting enzyme glutamic acid decarboxylase (GAD) indicate that horizontal cells of the skate are most likely GABAergic (1). Uptake of GABA into the skate horizontal cells occurs through GABA transporters which co-transport sodium and chloride (2). Furthermore, horizontal cells may release internal GABA into the extracellular space due to sodium-dependent reversal of the transporters. Therefore, measurement of the internal concentration of sodium in the horizontal cells may predict the direction in which the GABA transporter will allow co-transport of sodium, chloride and GABA to occur in the resting cell. Measurements made with intracellular ion-selective microelectrodes in the horizontal cells of another elasmobranch, the stingray, have suggested that these cells contain surprisingly

high levels of internal sodium (123 mM) (3), values that may favor release as opposed to uptake.

The cinchona alkaloid quinidine is a powerful antiarrhythmic agent that has been used to examine the properties of conductances in a variety of neuronal cell types, including retinal horizontal cells. This compound blocks sodium, potassium and calcium channel conductances in isolated skate horizontal cells (4). However, quinidine also promotes the opening of a large, non-specific conductance, termed the Q-current, which reflects the opening of "hemi-gap" junctional channels (4). These non-selective channels allow the movement of small ions as well as large molecules. Since quinidine both closes and opens different sets of channels, the effect of this compound on intracellular sodium levels and consequent GABA transport remains unclear. In the present study, we have used the dual excitation, sodium-sensitive fluorescent indicator, sodium-binding benzofuran isophthalate, SBFI, to examine the effect of quinidine on intracellular sodium.

Skate horizontal cells are isolated as follows: the eyes are removed, and the retina separated from eyecup pieces. The tissue was placed in a modified Leibovitz L-15 culture medium containing L-cysteine and the enzyme papain, and kept under constant agitation for one hour. The tissue was then rinsed with enzyme-free medium, mechanically triturated, plated onto small culture dishes, and stored at 14°C. Cells were loaded with the

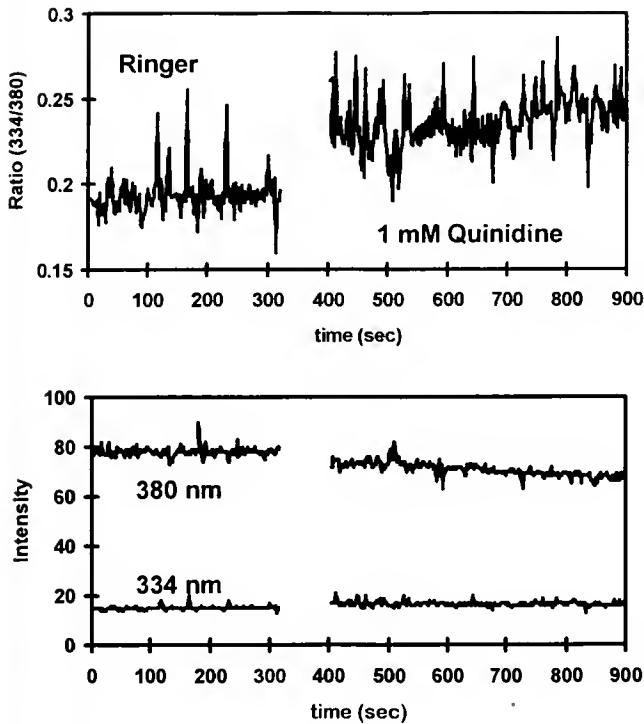


Figure 1. Fluorescence ratio of 1 mM quinidine. (A) The internal sodium concentration in one cell increased by 63 mM over baseline (from 42 mM to 105 mM). The average increase for six cells was 102 mM \pm 6 mM (SE) over the resting concentration. The trial was momentarily stopped for a whole-bath exchange of solutions between \sim 300 and 400 sec. (B) The intensity of the signals at 380 nm (upper trace) and 334 nm (lower trace) were recorded and used to measure the value of the ratiometric fluorescence per unit time.

cell-permeant AM-ester form of SBFI for one hour, then rinsed with skate Ringer's (2). Light at two wavelengths, 334 nm and 380 nm, was alternately applied to induce fluorescence of the dye, allowing the fluorescence data—measured with the Zeiss digital fluorescence imaging system equipped with an Attofluor Intensified CCD Camera—to be expressed as a ratio rather than an absolute intensity. The advantage of the ratio method is that variable dye concentrations, cell thickness, dye leakage, and bleaching are eliminated, since these factors similarly affect the recorded intensities at both wavelengths and are canceled in the measurement.

The intracellular sodium concentration at rest was determined through an *in vivo* calibration. Typically, there were eight regions of interest (ROIs) from which measurements were made; ratiometric measurements for each cell are the averaged signals from the ROIs. The fluorescence ratio of a single cell was recorded in normal Ringer's, followed by application of 10 μ M gramicidin, an ionophore that inserts into the plasma membrane forming a pore permeable to small ions. After gramicidin treatment, calibration solutions (0–250 mM NaCl, equimolar potas-

sium substitution) were bath-applied. The equation $[Na]_i = K_d(R - R_{min}) / (R_{max} - R) F$ was used to estimate the internal sodium concentration, where K_d is the dissociation constant of the dye, R is the fluorescence ratio at rest, R_{min} and R_{max} are the ratiometric responses at 0 mM and 250 mM, respectively, and F is the ratio of fluorescence recorded at 380 nm in zero sodium over the response at 380 nm in saturating sodium. The average values of R_{min} and R_{max} were 0.136 ± 0.005 (SE) and 0.181 ± 0.008 (SE), respectively, for three cells. Using this method, we estimate the resting internal sodium concentration of the skate horizontal cells to be 49 mM \pm 0.82 (SE). The internal sodium concentration of skate horizontal cells measured by the fluorescence imaging technique is markedly different from the reported sodium concentration in the horizontal cells of the stingray, measured with a double-barreled electrode (3). The apparent disparity between these estimates may be due to the fact that the sodium concentration in stingray horizontal cells was measured in the intact retina where glutamate is likely to be released from photoreceptors, possibly causing intracellular sodium to be considerably increased. Our measurements were made in isolated cells in the absence of glutamate, and therefore a lower resting concentration of internal sodium may not be surprising.

The response of a resting cell to bath application of 1 mM quinidine is shown in Figure 1. Application caused a marked increase in the fluorescence ratio, indicating a rapid flux of sodium into the cell ($n = 6$). Although an *in vivo* calibration following application of quinidine could not be performed, an estimate of the change in intracellular sodium as a result of quinidine application, based on the calibration of the instrumentation with the cell impermeant form of SBFI, reveals an increase of approximately 102 \pm 6 mM (SE) intracellular sodium over baseline levels. This suggests that, despite the block of voltage-gated sodium channels, significant increases in sodium can occur through the opening of hemi-gap junctional channels.

Our data demonstrate that the internal resting concentration of sodium in the isolated horizontal cells of the skate retina can be measured *in vivo* with the fluorescent indicator for sodium, SBFI. Further, quinidine can promote a notable increase in intracellular sodium concentrations that may have a significant effect on the sodium-dependent transport of GABA by these cells.

We thank Laura Haugh-Scheidt and Kasia Hammar for their guidance with the ratiometric measurements, and Rudi Rotenfusser of the Zeiss corporation for assistance with the Attofluor imaging system.

Supported by grant EY 09411 from the National Eye Institute.

Literature Cited

1. Agardh, E., A. Bruun, B. Ehinger, P. Ekstrom, T. van Veen, and J. Y. Wu. 1987. *J. Comp. Neurol.* 258(4): 622–630.
2. Malchow, R. P., and H. Ripps. 1990. *Proc. Natl. Acad. Sci.* 87(22): 9845–9849.
3. Fujimoto, M., and J. Katayama. 1993. *Exp. Eye Res.* 57: 487–491.
4. Malchow, R. P., H. Qian, and H. Ripps. 1994. *J. Gen. Physiol.* 104(6): 1039–1053.

Blockade of Ryanodine Receptors Stimulates Neurite Outgrowth in Embryos of *Spisula solidissima*

Kathryn Jessen-Eller, Marjorie Steele, Carol Reinisch (Marine Biological Laboratory, Woods Hole, Massachusetts), and Nicholas Spitzer¹

Transient elevations of intracellular calcium regulate specific aspects of differentiation in embryonic cells (1–4). Neuronal calcium transients are necessary for the developmental increase in the rate of activation of delayed rectifier potassium current, expression of the neurotransmitter, GABA, and regulation of the rate of neurite extension at growth cones; moreover, calcium transients in striated muscle are necessary for normal sarcomere assembly (1–4). Release of calcium from ryanodine receptor-activated intracellular stores contributes to all of these regulatory pathways. To test the generality of these findings, we investigated embryos of the surf clam *Spisula solidissima*, in which serotonergic neurons differentiate during the first day after fertilization. Embryos were chronically exposed to ryanodine, and the appearance of serotonin (5HT) and neurite outgrowth were assessed with antibodies to 5HT and actin.

Embryos were generated by *in vitro* fertilization (5). To evaluate calcium entry and calcium release mechanisms, 7 and 17 h embryos were incubated *in vivo* with 10 μ M Fluo3-AM (in 0.4% pluronic acid and 0.4% DMSO) for 1 h at 18°C., washed in artificial filtered seawater (AFSW), adhered to glass coverslips with Cell-Tak (Sigma) and immobilized with a 20 μ m Nitex net. Fluo-3 fluorescence was assessed with a Zeiss LSM 510 confocal laser scanning microscope in the same embryos (to control for variability in calcium loading) before and after application of pharmacological agents (ionomycin, caffeine; Sigma). Concentrated solutions of compounds were added to small drops of AFSW containing embryos, to achieve the final concentrations reported below. Other embryos were rotated continuously (3-D rotator, Lab-Line) in 20 ml AFSW containing 100 μ M ryanodine (Calbiochem) starting at 6 h after fertilization. Ryanodine is a highly specific toxin (6) that blocks ryanodine receptors without altering other physiological parameters when applied at these concentrations (3).

Samples were collected at 72 h, fixed in formalin, rinsed, and processed to develop immunofluorescence due to 5HT (rabbit anti-5HT Incstar; Alexa 594 Molecular Probes) and actin (mouse anti-actin Oncogene Research; Alexa 488 Molecular Probes). Standard whole mount procedure was followed, and observations were made with the Zeiss LSM 510 confocal scanning microscope. Neurite lengths and cell perimeters, reconstructed from a series of up to 20 confocal z-sections, were analyzed with Image Tool (University of Texas Health Science Center in San Antonio) and calibrated against a 10 μ m bar for each image. Processes connecting the clusters of 5HT cells were not counted since they were often obscured by the cell body immunoreactivity.

Application of 5 μ M ionomycin at either 7 or 17 h post-fertilization stimulated an increase in intracellular calcium which was detectable by the elevated fluorescence of Fluo 3 ($n = 4$). This test indicated that embryos incubated with Fluo 3-AM at these times must have taken up the dye. Moreover, although these embryos were about 50 μ m in diameter, increases in fluorescence were observed at their centers, suggesting that the dye was loaded into deep as well as superficial tissues. Stimulation with 300 mM KCl elevated intracellular calcium at both ages ($n > 3$), suggesting the presence of voltage-gated calcium channels. Stimulation with 50 mM caffeine gave a signal in 17 h embryos ($n = 4$), but not in 7 h embryos ($n = 3$). This response to caffeine was blocked by pre-incubation with 100 μ M ryanodine ($n = 4$), indicating not only that caffeine acts via ryanodine receptors, but that these receptors can be blocked (Fig. 1A–D). These results further suggest that any

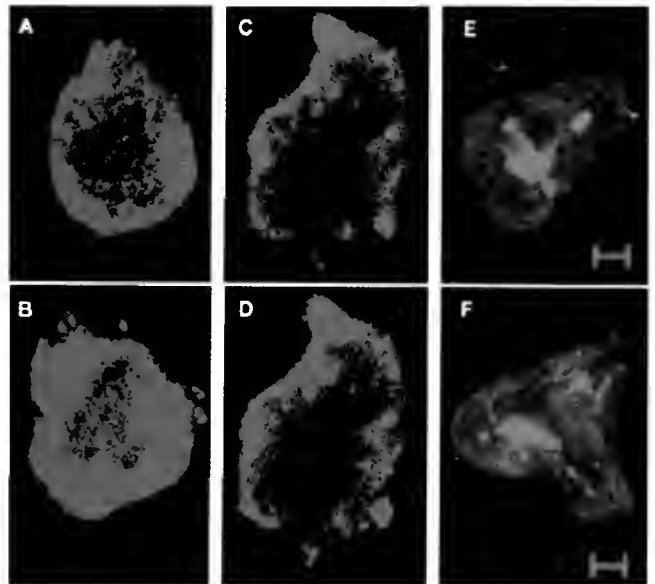


Figure 1. Confocal images (1.2 μ m sections) of *Spisula* embryos demonstrate the presence of ryanodine receptor-activated stores and the effects of suppressing them during development. Caffeine (50 mM) stimulated an increase in intracellular calcium (green), as illustrated by these images of the same 17 h embryo before (A) and after (B) application of caffeine. This response was not evident in ryanodine-treated animals (100 μ M), as shown here in another 17 h embryo both before (C) and after (D) caffeine exposure. The size of the clusters of 5HT-immunoreactive cell bodies (red) located in the center of 72 h *Spisula* embryos counterstained for actin (green) did not differ between embryos cultured in the absence (E) and presence (F) of ryanodine. However, embryos exposed to ryanodine (F) had almost double the total length of 5HT-immunoreactive neurites extending from cell clusters (red) as the controls (E). Bars represent 10 μ m.

¹ Biology Department, UCSD, La Jolla, California.

spontaneous calcium transients that are generated in part by ryanodine receptors will be suppressed by sustained application of ryanodine.

We observed no change in 5HT immunoreactivity in the somata of cells in response to chronic blockade of ryanodine receptors with 100 μ M ryanodine. This concentration also had no influence on survival or swimming behavior. Embryos were incubated in AFSW containing ryanodine starting at 6 h after fertilization, and samples were fixed at 72 h for immunocytochemical analysis. 5HT immunoreactivity was clustered in 2–5 groups of cell bodies of 10–15 μ m diameter (Fig. 1E, F). Cortical actin appeared to line the cell perimeters, giving the embryos a tiled appearance. The size (total perimeter across a stack of confocal images) of the 5HT-containing cell bodies was not affected by chronic exposure to 100 μ M ryanodine (Mann-Whitney test statistic = 0.33; P = 0.56; n = 8). In contrast, the total length of 5HT-immunoreactive neurites from confocal stacks (80.18 μ m \pm 18.11, mean \pm S.D.) was nearly double that of controls (44.16 μ m \pm 29.57) at 72 h (Fig. 1E, F). We were able to recognize neurite tips within growth cones by the colocalization of actin and 5HT. This difference was only significant at P = 0.08 (Mann Whitney test statistic = 3.0; n = 8) because 1 of the control embryos (87 μ m in total length) did not fall within the range of the 3 other animals (20–36 μ m in total neurite length).

We conclude that (1) caffeine-stimulated elevations of intracellular calcium are blocked by pre-incubation with ryanodine in *Spisula* embryos; and (2) continuous exposure to ryanodine does not influence the size of 5HT-immunoreactive neurons but appears to stimulate production of longer neurites. These conclusions are consistent with the view that spontaneous calcium transients involving ryanodine receptor-activated stores are generated during early stages of develop-

ment, and that neurite lengths are increased when calcium transients in neuronal growth cones are blocked (3). However, we cannot exclude the possibility that axons are of equal length, and that ryanodine affects the export of 5HT. There was no obvious effect on levels of 5HT immunoreactivity in neuronal cell bodies; small changes may have gone undetected. We will test these conclusions by analyzing larger sample sizes, studying the dose-dependence of the effects of ryanodine, and applying agents that block calcium pumps. Early differentiation of serotonergic neurons is observed in other molluscs (7, 8) and may be regulated in a manner similar to that in *Spisula* embryos. The initial results reported here inspire us to image spontaneous calcium transients in *Spisula* serotonergic neurons.

We thank the Grass Foundation for support of K. Jessen-eller (Fellow) and N. Spitzer (Forbes Lecturer). We are grateful to the Grass Fellows for many stimulating discussions. This work was also supported by NIH grant CA44307 to C.R.

Literature Cited

1. Gu, X., E. C. Olson, and N. C. Spitzer. 1994. *J. Neurosci.* **14**: 6325–6335.
2. Watt, S. D., X. Gu, and N. C. Spitzer. 1997. *Soc. Neurosci. Abstr.* **23**: 117.
3. Gu, X. and N. C. Spitzer. 1995. *Nature* **375**: 784–787.
4. Ferrari, M. B., K. Ribbeck, D. J. Hagler, Jr., and N. C. Spitzer. 1998. *J. Cell Biol.* **141**: 1349–1356.
5. Allen, R. H. 1953. *Biol. Bull.* **105**: 213–239.
6. Coronado, R., J. Morrissette, M. Sukhareva, and D. M. Vaughan. 1994. *Am. J. Physiol.* **266**: C1485–C1504.
7. Goldberg, J. I. and S. B. Kater. 1989. *Dev. Biol.* **131**: 483–495.
8. Diefenbach, T. J., R. Koss, and J. I. Goldberg. 1998. *J. Neurobiol.* **34**: 361–376.

Reference: *Biol. Bull.* **195**: 208–209, (October, 1998)

Characterization of Oxygen and Calcium Fluxes From Early Mouse Embryos and Oocytes

D. M. Porterfield¹, J. R. Trimarchi², D. L. Keefe^{2,3}, and P. J. S. Smith¹

Despite the importance of the mammalian embryo to clinical and biomedical sciences, the physiology of pre-implantation embryos and oocytes is largely unexplored. For example, although calcium is known to participate in the early events of fertilization (1) and also plays a brief but critical role at each cleavage (2, 3), the regulation of transmembrane calcium flux during the interim between cleavages or during blastocoel formation is unknown. One reason for this gap in our knowledge lies in the difficulty in studying a single oocyte or embryo. The goal of the project reported here is to take advantage of new techniques for monitoring physiological parameters from individual cells and to begin to characterize changes in embryo physiology during development. This work is part of larger study on the viability of the pre-implantation embryo.

The self-referencing electrode technique (4) pioneered by the BioCurrents Research Center at the MBL is ideal for exploring the physiology of the early embryo. The technique allows the derivation of flux values by measuring the concentrations of free ions or dissolved oxygen at two probe positions micrometers apart, where the electrode is moved in a square wave oscillation. One pole of this oscillation is brought close to the zona pellucida (within about 1 μm). With this approach, physiological measurements can be obtained from individual oocytes or embryos. Being noninvasive, the self-referencing electrode can be used to record from oocytes or developing embryos without perturbation, an assumption recently confirmed by the successful birth of implanted, post-experimental blastocysts (Trimarchi and Liu, unpub. obs.).

We employed self-referencing electrode techniques to characterize calcium and oxygen flux from a series of developmental stages of mouse embryos. The embryos were collected at stages ranging from unfertilized oocytes to expanded blastocysts and cultured in M2 medium according to standard techniques (5). Physiological experiments were conducted in M2 medium with reduced calcium (50 μM) at 37°C in a Faraday box mounted on an airtable.

For the measurement of oxygen fluxes, oxygen microelectrodes, with a tip diameter of 2–3 μm , were purchased from Diamond General Development Corp. (Model 723, Ann Arbor, MI). These were calibrated in N_2 and air-bubbled dH_2O . The measured current was converted to a flux value as previously described (6). The ion-selective electrodes were constructed as described by Smith *et al.* (4), incorporating a short (30 μm) column of ion-selective resin (ETH 1001; Fluka). Unlike the oxygen electrode response, which is linear with concentration,

these electrodes are Nernstian, with voltages being converted to flux values by the following equation:

$$J = -D \frac{C_{av} 10^{S\Delta V} - C_{av}}{\Delta r}$$

where, J is flux, D is the diffusion coefficient ($0.79 \cdot 10^{-5} \cdot \text{cm}^2 \cdot \text{s}^{-1}$), ΔV is the differential voltage measurement (mV) between the measurement positions separated by Δr (cm), S is the inverse of the Nernst slope of the electrode, and C_{av} is the average free Ca^{2+} concentration measured in the medium between the poles of the electrode movement. This equation is modified from Kühtreiber and Jaffe (7). For both oxygen and calcium detection, all electrodes were oscillated at 0.3 Hz over 10 μm . A return electrode (Ag/AgCl) completed the circuit via a bridge of 3M KCl in 5% agar.

Measurements taken with calcium and oxygen selective, self-referencing electrodes demonstrate that developing embryos exhibit measurable net oxygen influx and calcium efflux at all stages examined (oocyte to blastocyst; Fig. 1). In particular, oxygen influx measured from blastocysts is three times that measured from earlier stages. These data are consistent with oxygen consumption measurements obtained from groups of embryos by ultra-microfluorescence techniques (8). The increase in oxygen consumption coincident with blastocyst formation is thought to reflect an increased metabolic demand generated by the pumping of sodium and potassium ions that drives the enlargement of the blastocoel (9).

In contrast to oxygen influx, calcium efflux was relatively

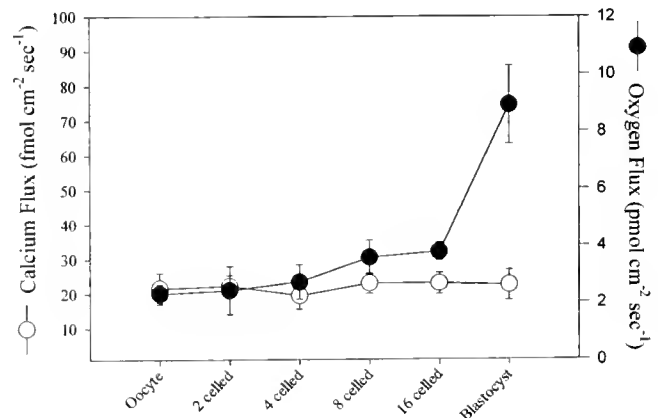


Figure 1. Net calcium efflux (open symbols) and oxygen influx (solid symbols) measured from pre-fertilization mouse oocytes and developing embryos. Calcium efflux is constant throughout the developmental series. In contrast, oxygen influx dramatically increases in blastocysts relative to the lower levels at earlier stages of development. Each data point (mean \pm stdev) represents measurements from nine embryos. Calcium efflux and oxygen influx were measured in different sets of embryos.

¹ BioCurrents Research Center, Marine Biological Laboratory, Woods Hole, Massachusetts 02543.

² Laboratory for Reproductive Medicine, Marine Biological Laboratory

³ Women and Infants Hospital, Brown University, Providence, Rhode Island 02905.

constant ($\sim 22 \text{ fmol} \cdot \text{cm}^{-2} \cdot \text{s}^{-1}$) throughout the developmental series (Fig. 1). Mouse embryos are known to be able to develop from embryos through the blastocyst stage in the absence of external calcium (10). We have not yet determined the physiological mechanisms underlying this net efflux. We could be measuring a steady-state loss of calcium from the internal stores or, as is more likely, an efflux linked to calcium uptake from the medium via channels. As the probe technique is based on considerable signal averaging, with both high and low pass filters (4), rapid channel events occurring over periods of a second or less may not be recorded. The increase in oxygen influx in the absence of a change in the calcium efflux that we observed in blastocyst-stage embryos demonstrates that the physiological state of the embryo changes markedly between the 16-cell stage and blastocyst formation. Characterization of the transmembrane movement of other ion species will continue to improve our understanding of the physiological mechanisms underlying early embryo development. This study demonstrates the utility of the noninvasive probes for the characterization of the early embryo.

Literature Cited

1. Jaffe, L. A. 1996. Pp. 367–378 in *Molecular Biology of Membrane Transport Disorders*, S. G. Shultz et al., eds. Plenum Press, New York.
2. Stachecki, J. J., and D. R. Armant. 1996. *Development* **122**: 2485–2496.
3. Stricker, S. A. 1995. *Dev. Biol.* **170**: 496–518.
4. Smith, P. J. S., R. H. Sanger, and L. F. Jaffe. 1994. *Methods Cell Biol.* **40**: 115–134.
5. Hogan, B., R. Beddington, F. Costantini, and E. Lacy. 1994. *Manipulating the Mouse Embryo*. CSHL Press, Cold Spring Harbor, New York.
6. Malchow, R. P., S. C. Land, L. S. Patel, and P. J. S. Smith. 1997. *Biol. Bull.* **193**: 231–232.
7. Kühtreiber, W. M., and L. F. Jaffe. 1990. *J. Cell Biol.* **110**: 1565–1573.
8. Houghton, F. D., J. G. Thompson, C. J. Kennedy, and H. J. Leese. 1996. *Mol. Reprod. Dev.* **44**: 476–485.
9. Biggers, J. D., J. E. Bell, and D. J. Benos. 1988. *Am. J. Physiol.* **255**: C419–C432.
10. Santaló, J., M. Grossmann, and J. Egozcue. 1996. *Hum. Reprod. Update* **2**: 257–261.

Reference: *Biol. Bull.* **195**: 209–210. (October, 1998)

Calcium Regulatory Endomembranes of the Prophase Mitotic Apparatus of Sand Dollar Cells Contain Enzyme Activities That Produce Leukotriene B₄ but Not 1,4,5-Inositol Trisphosphate

Robert B. Silver, Leslie A. King, and Alyssa F. Wise (Marine Biological Laboratory, Woods Hole, Massachusetts 02543)

The calcium signal that precedes nuclear envelope breakdown (NEB) (1, 2) is generated, acts, and is degraded very near to the site of action, and the signal does not diffuse over distances greater than 1 micrometer (2). Reduced leukotriene B₄ (LtB₄), but not other products of the arachidonic acid (AA) pathway, can evoke Ca²⁺ release from endomembrane stores in a pattern quite similar to that of the pre-NEB calcium signal (3) in eggs and mitotic cells of the sand dollar (*Echinarracnius parma*). Under physiological conditions, LtB₄ undergoes spontaneous oxidation to a form that does not evoke calcium release from cell stores *in vivo* or *in vitro* (4–6). Of course, 1-4-5 inositol trisphosphate (IP₃) also evokes calcium quantum emission domains (Ca²⁺-QEDs) (3, 7–10), but IP₃ rapidly diffuses through the cell, releasing calcium in a pattern markedly different from that of LtB₄. LtB₄ is much more effective at eliciting endomembrane calcium *in vivo* release than is IP₃ (2, 10). Reduced LtB₄ elicits calcium release from endomembranes both *in vivo* and *in vitro* (3).

PLA₂ acts on phospholipids to yield AA and monoacylglycerols (4). In turn, AA is converted to LtB₄ through the 5'-lipoxygenase (5-LO) branch of the AA pathway. The precursor of LtB₄, leukotriene A₄ (LtA₄), can be converted by glutathione S-transferase (GST) to leukotriene C₄ (LtC₄) by the addition of reduced glutathione to LtA₄. Thus, GST can provide a shunt to help regulate the production of LtB₄. By comparison, IP₃ is

produced by the direct action of PLC on phosphatidyl 4,5-bisphosphate inositide (8).

In our initial study of phospholipase activity in sea urchin endomembrane we found that phospholipase A₂ (PLA₂) and phospholipase C (PLC) were differentially distributed among endomembrane fractions in whole cells (10). That distribution was consistent with the products of PLA₂ and PLC activity acting on distinct endomembrane calcium stores. If LtB₄ is used as the agonist for the pre-NEB calcium signal, then enzymes needed for production and regulation of LtB₄ would have to be present—if not concentrated—among the calcium regulatory endomembranes of prophase mitotic apparatus (MA).

We have now identified PLA₂ and PLC enzyme activities on endomembranes from prophase cells and isolated native prophase MA of the sand dollar. Eggs were obtained from mature female sand dollars as previously described (1), and endomembranes were subfractionated as previously described (7, 11). Native prophase MA were isolated according to our standard methods (7, 11). Spectrophotometric assays for PLA₂, PLC, and glutathione S-transferase (GST) activities were developed for these studies; they are adaptations of previously published methods for PLA₂ (12), PLC (13), and GST (14). Endomembrane subfractions were also assayed for glucose-6-phosphate dehydrogenase, a marker enzyme found in the endoplasmic reticulum, and for creatine kinase (14, 15). Standard curves for

enzyme product were generated for each experiment at $\log/2$ and $\text{linear}/2$ concentration steps (R^2 typically > 0.995). Triplicate assays were performed for each membrane subfraction. Specific and total activities for the enzyme activities of each subfraction were determined and the values compared.

PLA₂ and PLC enzyme activities are differentially distributed among endomembrane subfractions isolated from whole cells and prophase MA. In whole cells and prophase MA, PLA₂ is present primarily in the less dense subfractions. In whole cells and prophase MA, the majority of total PLA₂ activity was found in the less dense endomembrane subfractions, which are the same endomembranes that exhibit ATP-dependent calcium uptake activity and which release calcium on exposure to LtB₄ and IP₃. Results from these assays are summarized in Table I. Thus, within the prophase MA, PLA₂ appears to be selectively concentrated, and the relative distribution of its activity is shifted to the same endomembrane subfraction (subfraction B) that exhibits the majority of ATP-dependent calcium uptake activity and agonist-induced calcium release.

The distribution of PLC enzyme activity is markedly different in whole cells and isolated native prophase MA, and is also different from that seen with PLA₂ (Table I). In whole cells, PLC is present primarily in the more dense subfractions. In stark contrast, no PLC activity was detected in any of the prophase MA endomembrane subfractions, even when the membrane content was increased 5-fold and the duration of the assay was increased 6-fold to 90 minutes. Thus, while PLC is distributed among the whole-cell endomembranes of greater specific gravity, it is absent and presumably excluded from the prophase MA.

Activity of the enzyme GST is differentially distributed among the endomembrane subfractions isolated from whole cells and prophase MA in patterns that mimic those described above for PLA₂ (Table I). In whole cells and prophase MA, GST is present primarily in the less dense subfractions. Thus,

the low density, calcium regulatory, endomembrane subfraction (smooth endoplasmic reticulum) converts LtA₄ to LtC₄, and thus provides a shunt to draw away LtA₄ from LtA₄-hydrolase production of LtB₄, preventing potential premature expression of calcium QEDs in prophase MA.

It is now clear that enzymes necessary for production of LtB₄ and IP₃ are selectively localized within prophase cells. PLA₂ and GST, enzymes essential for production and regulation of LtB₄, are present within the prophase MA. PLC, which is essential for production of IP₃, is apparently omitted from the prophase MA. These findings are entirely consistent with our prediction that LtB₄, and not IP₃, is used as the calcium agonist which is generated, acts, and is degraded locally and without diffusion over distances greater than 1 micrometer, to produce the space-time patterned calcium QEDs essential for NEB (3). The common endomembrane distribution of GST in whole cells and prophase MA is consistent with a general need for production of leukotriene C₄, perhaps to prevent untimely production of LtB₄, and thus Ca²⁺-QEDs. Apparently, therefore, the 5-LO branch of the AA pathway is a component of the calcium regulatory endomembranes that exhibit ATP-dependent Ca²⁺ uptake activity and LtB₄-sensitive Ca²⁺ release, and are the source of calcium for the pre-NEB calcium signal imaged in aequorin-labeled mitotic cells (3, 7, 11, 15). Note that the amount of LtB₄ that could be produced in prophase MA, based on the measured enzyme activities for PLA₂ and anticipated stoichiometric conversion of AA to LtB₄, closely coincides with the number of QEDs observed in pre-NEB calcium signals (2). These results support the hypothesis that LtB₄ is the agonist of choice for generating the non-random, space-time patterns of pre-NEB Ca²⁺-QEDs.

Grant support by NSF (MCB-9602056) is gratefully acknowledged.

Literature Cited

1. Silver, R. B. 1989. *Dev. Biol.* **131**: 11–26.
2. Silver, R. B. 1996. *Cell Calcium* **20**: 161–179.
3. Silver, R. B. 1995. *Biol. Bull.* **189**: 203–204.
4. Samuelsson, B. 1983. *Science* **220**: 568–575.
5. Rich, A. M., G. Weissmann, C. Anderson, L. Vossball, K. A. Haines, T. Humphreys, and P. Dunham. 1984. *Biochem. Biophys. Res. Commun.* **121**: 863–870.
6. Abdel-latif, A. A. 1986. *Pharmacol. Rev.* **38**: 227–272.
7. Silver, R. B., R. D. Cole, and W. Z. Cande. 1980. *Cell* **19**: 505–516.
8. Bansal, V. S., and P. W. Majernus. 1990. *Annu. Rev. Cell Biol.* **6**: 41–67.
9. Chow, S. C., and M. Jondel. 1990. *J. Biol. Chem.* **265**: 902–907.
10. Silver, R. B., D. E. Strongin, L. R. Hurwitz, and A. P. Reeves. 1997. *Biol. Bull.* **193**: 236–237.
11. Silver, R. B. 1986. *Methods Enzymol.* **134**: 200–217.
12. Reynolds, L. J., L. L. Hughes, L. Yu, and E. A. Dennis. 1994. *Anal. Biochem.* **217**: 25–32.
13. Kurioka, S., and M. Matsuda. 1976. *Anal. Biochem.* **75**: 281–289.
14. Keen, J. H., W. H. Habig, and W. B. Jakoby. 1976. *J. Biol. Chem.* **251**: 6183–6188.
15. Silver, R. B. 1986. *Proc. Nat. Acad. Sci. U.S.A.* **83**: 4302–4306.

Table I

*Distribution of the percent of total activity of phospholipase A₂, phospholipase C, and glutathione S-transferase among endomembrane density subfractions isolated from sand dollar (Echinarracnius parma) whole cells and prophase mitotic apparatus**

Enzyme	Source	Subfractions†			
		A	B	C	D
Phospholipase A ₂	Whole cells‡	73.5	14	4	7
	Prophase MA	35	35	16	14
Phospholipase C	Whole cells‡	4	28.7	29.4	38.3
	Prophase MA	0	0	0	0
Glutathione S-transferase	Whole cells	83.9	6.9	4.4	4.7
	Prophase MA	84	9	4	1

* $n = 3$ or more replicate assays performed at 13°C. Additional details are provided in the text.

† Details of preparation of endomembrane subfractions are provided in reference 11.

‡ Data for PLA₂ activity in whole cells is from reference 10, with permission.

Reference: *Biol. Bull.* **195**: 211–212. (October, 1998)

Fluorescence Localization of Cytoskeletal Proteins in Fibrin-Trapped Cells

Kyeng G. Lee^{1,2}, Nishal Mohan^{1,2}, Zoya Koroleva^{1,2}, Li-Fang Huang¹, and William D. Cohen
(Hunter College, New York, New York 10021)²

Several difficulties arise when fluorescence localization of cytoskeletal proteins is attempted in cells that normally exist in suspension, such as the nucleated erythrocytes used as a model system in our laboratory (e.g., 1). Artificially induced attachment of living cells or their cytoskeletons to coverslips or slides with polylysine (2) or other adhesives can distort three-dimensional structure. Material is often lost due to poor or selective adhesion, so that the sample is not representative, and cytoskeletons of pre-selected living cells cannot be readily relocated after labeling. In addition, processing small numbers of cells is difficult.

Here we describe a new method that avoids many of these problems. The major steps are: (a) trapping living cells in physiological media within fibrin "clots"; (b) treating the trapped cells with detergents or other agents to produce cytoskeletons; and (c) after fixation, exposing the trapped cytoskeletons to antibodies or other fluorescent probes. In developing the procedure, "blood clam" and amphibian erythrocytes, sea urchin sperm, and sea urchin zygotes were used as test material.

Living cells were trapped by mixing one volume of a cell suspension in artificial seawater or Ringer's solution with four volumes of the same medium containing 10 mg/ml fibrinogen (Sigma Chemical Co., St. Louis, MO; F8630 from bovine plasma; final conc. = 8 mg/ml). Thrombin (Sigma T4648; from bovine plasma; 50 U/ml frozen stock in Ringer's or artificial seawater) was added to 1 U/ml or, for some amphibian Ringer's solutions, lower concentrations, so that a firm clot formed in about 10 min. Samples (5–25 μ l) were delivered to coverslips within this time window, and were usually spread inside self-adhesive plastic rings that remained attached to the coverslips throughout the procedure (Avery #05729 white ring-binder reinforcements, 7 mm interior diameter). In some cases, the suspension was thinly spread without using the rings. To prevent the clots from drying during formation or incubation with probes, the coverslips were kept in moist chambers; for detergent treatment (lysis), fixation, and washes, they were transferred to coverslip staining jars. When seawater was used, the clots were optically clear, whereas in amphibian Ringer's, they were translucent. This reduction in clarity interfered with phase contrast to some extent, but did not affect fluorescence microscopy.

Coverslips bearing fibrin-trapped cells were immersed in a cytoskeleton-stabilizing lysing medium containing Triton X-100, with or without protease inhibitors (1, 3), to produce cytoskeletons within the clot. After 4–8% formaldehyde fixation (either post-lysis, or simultaneously with lysis), the coverslips were washed in PBS and incubated with probes for

detection of microtubules and F-actin. These probes included monoclonal anti- α -tubulin and anti- β -tubulin (Sigma T9026, T-4046) as a primary mixture, with FITC-goat anti-mouse IgG (Fab; F-8521) as secondary, FITC-monoclonal anti- β -tubulin (F-2043) for direct labeling, and Texas Red-X phalloidin (Molecular Probes, Eugene OR) for F-actin. We found that the antibodies penetrated the clots within 1–2 hours, and that both direct and indirect anti-tubulin immunofluorescence was successful. Controls lacking primary antibody were blank, and most clots exhibited little background fluorescence, even though blocking was not performed.

We examined fibrin-trapped specimens by both epifluorescence and confocal fluorescence microscopy; the latter was particularly useful for thicker clots. Tubulin was localized in the marginal bands of both molluscan (*Noetia ponderosa*; Fig. 1a,a') and amphibian erythrocytes (*Notophthalmus viridescens*, *Ambystoma mexicanum*; not shown), in sea urchin sperm flagella (*Lytechinus pictus*; Fig. 1b,b'), and in mitotic spindles and asters of dividing sea urchin zygotes (*L. pictus*, Fig. 1c,c'). Sperm distributed throughout the clots showed specific flagellar labeling. In addition, the distribution of F-actin was examined with Texas Red phalloidin in cytoskeletons of molluscan (*N. ponderosa*, Fig. 1d,d') and amphibian erythrocytes (*N. viridescens*, Fig. 1e).

To determine whether the clotting process or the resulting confinement might be detrimental to cells, we followed the development of fertilized sea urchin eggs (*L. pictus*, *Arbacia punctulata*) in clots incubated in filtered natural seawater contained in coverslip staining jars. The same trapped cells could be repeatedly located and examined during the time preceding lysis (Fig. 1, f vs. g). Development appeared to progress normally in the clots, with the percentage of dividing cells similar to that in seawater alone. Many ciliated blastulae (Fig. 1h) rotated within their confined space, and larvae (Fig. 1i) ultimately escaped from the clot and were found free-swimming in the coverslip jars (2 days at 21.5°C). Thus, long-term exposure to the clot did not block development.

Although the optimal conditions for various steps remain to be determined for specific cell types, results to date suggest that fibrin trapping will be a useful alternative to methods involving polylysine or other adhesives (2). The images of blood clam erythrocyte cytoskeletons obtained with the new method (e.g., Fig. 1a,a') are superior, in terms of three-dimensional structure and retention of representative samples to those obtained previously with polylysine. The method has also begun to yield improved data on cytoskeletal organization in blood clam erythrocytes that have undergone a naturally-induced shape transformation (4). Potential additional advantages include the processing of small cell populations with minimal losses, and the opportunity to observe the same

¹ Hunter College, New York, New York 10021.

² Marine Biological Laboratory, Woods Hole, Massachusetts 02543.

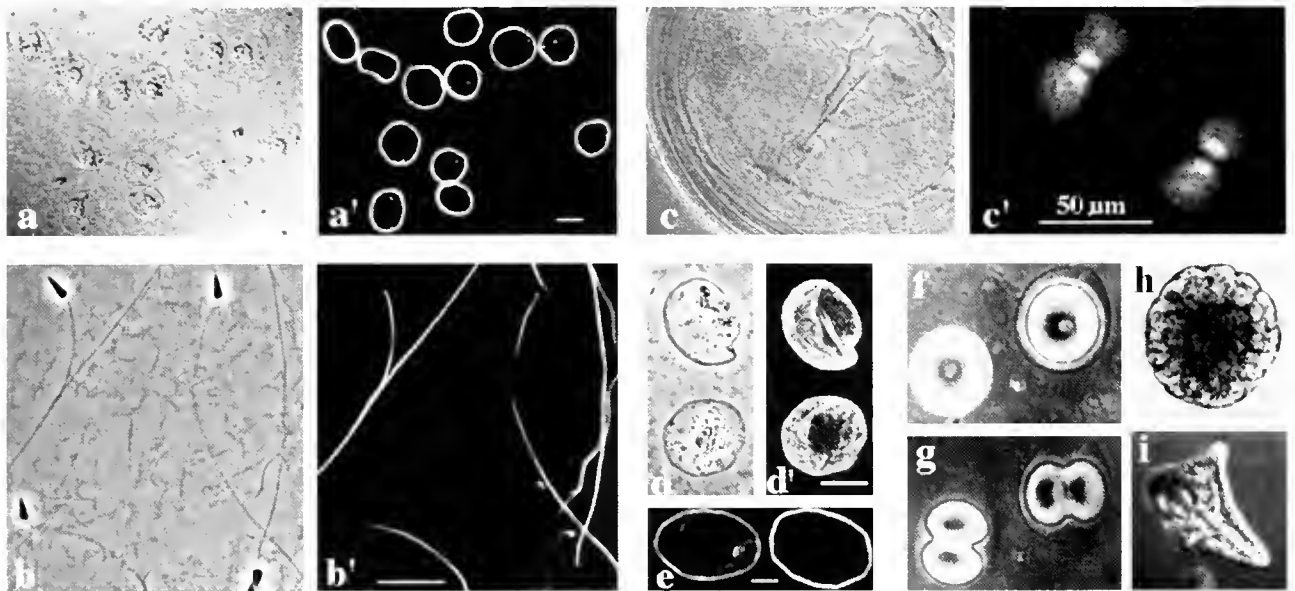


Figure 1. Fluorescence localization of cytoskeletal proteins in cells trapped in fibrin clots. Abbreviations: PC = phase contrast, DIC = differential interference contrast, FL = fluorescence. (a,a') Clam erythrocytes (*N. ponderosa*); indirect anti-tubulin labeling of marginal bands, DIC-FL pair. (b,b') Sea urchin sperm (*L. pictus*); indirect anti-tubulin labeling of flagellae, PC-FL pair. (c,c') *L. pictus* zygote, 2-cell stage; indirect anti-tubulin labeling of spindles and asters, DIC-FL pair. (d,d') *N. ponderosa* erythrocytes; Texas Red phalloidin labeling of F-actin, PC-FL pair. (e) Salamander erythrocytes (*N. viridescens*); Texas Red phalloidin labeling of marginal band-associated F-actin, PC-FL pair. (f,g) Same sea urchin zygotes (*A. punctulata*) viewed before and after first cleavage in clot, PC. (h,i) *A. punctulata* at blastula stage, and larva after escape from clot, PC. Bars = 10 μ m, except as noted.

cells before and after lysis and labeling. In addition, though not yet tested, the firmness with which living cells, such as sea urchin zygotes, are initially trapped suggests that microinjection of antibodies or other probes may be possible prior to processing.

Support from PSC-CUNY 666180, NIGMS-MBRS GM08176-18, the MBL Erik Fries Fellowship Fund (to WDC), and National Science Foundation grant MCB9808368, is gratefully acknowledged. We thank Drs. Mel Spiegel and Roger Sloboda for *L. pictus* gametes.

Literature Cited

1. Cohen, W. D., Y. Sorokina, and I. Sanchez. 1998. *Cell Motil. Cytoskeleton*. **40**: 238-248.
2. Mazia, D., G. Schatten, and W. Sale. 1975. *J. Cell Biol.* **96**: 527-540.
3. Cohen, W. D., I. Sanchez, N. Rayos, and A-V Dadacay. 1996. *Marine Models Electronic Record*. [Online]. Available: <http://www.mbl.edu/html/BB/MMER/COH/CohTit.html> [1998, July 31].
4. Dadacay, A-V. M., J. C. Huerta, C. J. Theiner, S. Swarnakar, and W. D. Cohen. 1996. *Biol. Bull.* **191**: 276-277.

Reference: *Biol. Bull.* **195**: 212-214. (October, 1998)

Oocyte Maturation in *Chaetopterus pergamentaceus* Observed With Centrifuge Polarizing Microscope

Makoto Goda, Shinya Inoué, and Robert A. Kuudson (*Marine Biological Laboratory, Woods Hole, Massachusetts 02543*)

We explored the polarized organization in maturing oocytes of *Chaetopterus pergamentaceus* using a centrifuge polarizing microscope (CPM). The CPM, developed jointly by MBL, Olympus Optical, and Hamamatsu Photonics, displays birefringence and differential interference contrast images resolved to better than 1 μ m at up to 10,000 times gravity ($\times g$) (1, 2).

When a *Chaetopterus* oocyte is shed into normal seawater, its germinal vesicle breaks down, and meiotic spindle formation

proceeds to metaphase-I, where it is arrested for several hours unless the egg is fertilized or otherwise activated. When an oocyte is shed into calcium-free seawater, the germinal vesicle does not break down and no spindle is formed; the oocyte remains "immature" (3).

In the CPM, the metaphase-arrested oocytes and the immature oocytes show strikingly different patterns of stratification. The immature cells stratify into three apparent zones, with a broad

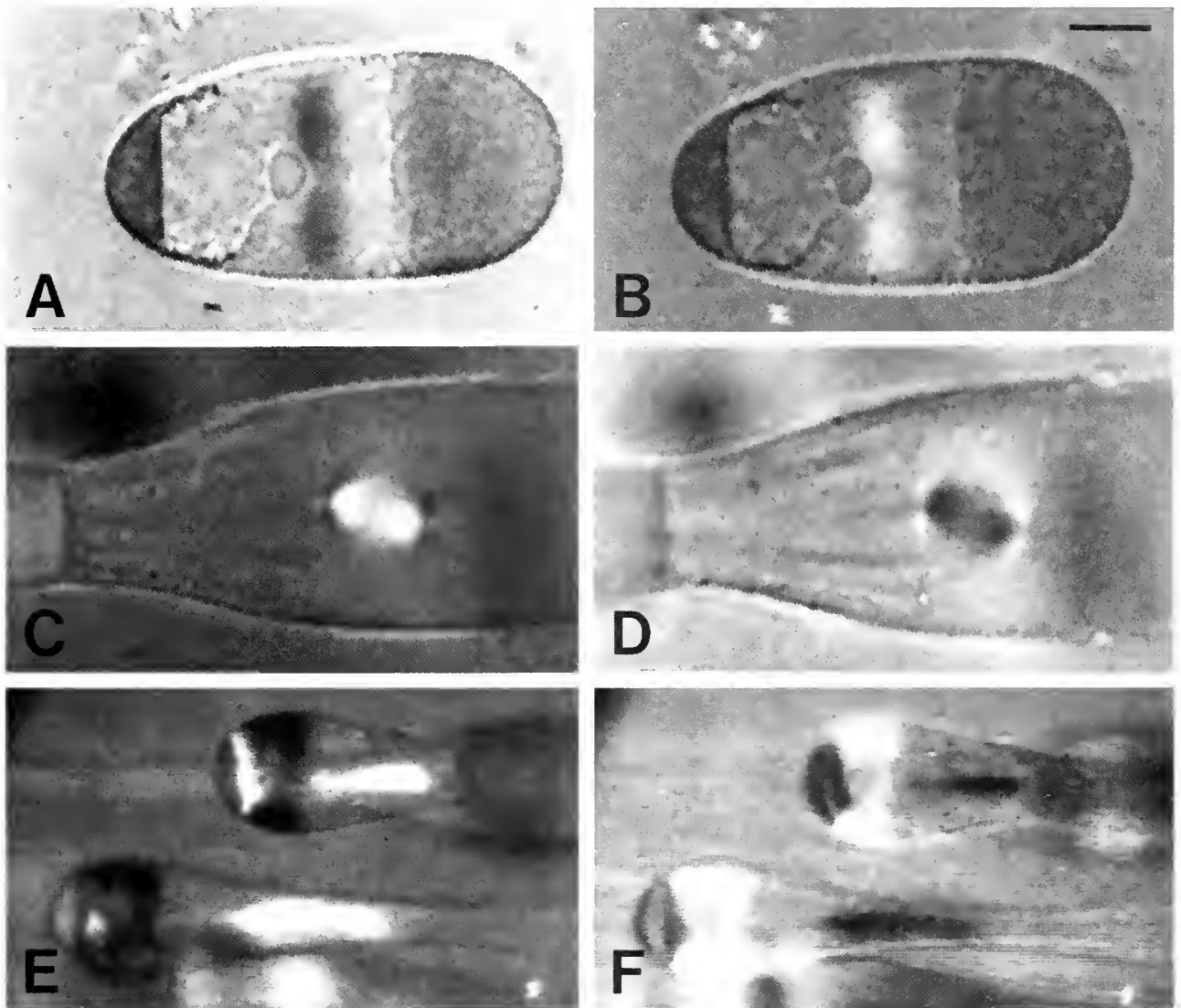


Figure 1. Live *Chaetopterus* oocytes observed with the spinning centrifuge polarizing microscope (CPM). The images were taken from video sequences that were shown at the General Scientific Meetings. The g-force in all panels points to the right; i.e., the left side is the centripetal end ("top of the cell" where the lighter components of the cell accumulate). (A, B) Oocyte shed in calcium-free seawater and centrifuged at about 5600 RPM for over half an hour. (C, D) Oocyte exposed to calcium-containing seawater after stratification, as shown in A and B. (E, F) Oocytes shed into normal seawater, then stratified after spindle formation in the CPM at about the same RPM as in A and B. In Panels A, C, and E, the compensator slow axis runs horizontally; in B, D, and F, vertically. Scale bar in Panel B is 20 μm for all panels.

clear zone separating the lighter and heavier polar caps. In the clear zone, the large germinal vesicle abuts the lighter cap, with the nucleolus eventually appearing prominently at its bottom, or centrifugal, end (Fig. 1, Panels A, B). By that time, a broad band (or curtain) of as-yet-unidentified negatively birefringent material, with its substructures oriented along the centrifuge axis, appears in the clear zone just below the nucleolus. Although its sign of birefringence is opposite to that of the spindle and astral fibrils, there is some indication that this negatively birefringent material, reminiscent of "streaks" in developing sea urchin zygotes (4,5), may give rise to microtubules in the spindle.

When calcium-containing seawater is applied to such cells,

the nucleoli, germinal vesicle, and negatively birefringent material quickly disappear in sequence within a few seconds. Concurrently, the cortical gel appears to weaken suddenly, since trapped particles become dislodged and start to "rain down" within the cell. The cell, floating on an isopycnic density gradient in the CPM, also becomes less resistant to stretch. After a few minutes, small, positively birefringent astral rays emerge. The poles of the asters are then separated over the next 15 to 20 minutes by a growing meiotic spindle, which exhibits prominent positive birefringence in the middle of the clear zone (Fig. 1, C, D). The spindle thus formed has rounded poles similar to those formed in undeformed cells.

Oocytes that were exposed to normal seawater and had already formed the meiotic metaphase spindles responded totally differently than the oocytes centrifuged while still immature. The stratified lighter and heavier contents stretch the oocyte into a highly elongated dumbbell, with a much smaller space occupied by the clear zone than in oocytes that were centrifuged while still immature. Within the narrow clear zone, the meiotic spindle, as though stretched by its poles along the centrifuge radius, takes on a very strong positive birefringence, and the shape of its poles becomes acute (Fig. 1, E, F). Above the spindle and below the oil cap, three to four layers of as-yet-unidentified material, mostly with prominent, negative birefringence, are stacked. Yolk and other heavy contents stretch the centrifugal end of the oocyte into an extended teardrop.

Thus, live oocytes of *Chaetopterus pergamentaceus* showed strikingly different patterns of stratification and fine structural organization before and after nuclear envelope breakdown. The differences may well be induced by changes in cytosolic cal-

cium-pumping activity that could be associated with maturation of the oocytes, since we find that oocytes that were aged before shedding mature spontaneously, even when shed into calcium-free seawater.

Support by Olympus Optical Co. and Hamamatsu Photonics Co. is gratefully acknowledged.

Literature Cited

1. Inoué, S., R. A. Knudson, K. Suzuki, N. Okada, H. Takahashi, M. Iida, and K. Yamanaka. 1997. *Am. Soc. Cell Biol. Abstract* #H-117.
2. Inoué, S., R. A. Knudson, K. Suzuki, N. Okada, H. Takahashi, M. Iida, and K. Yamanaka. 1998. *Microsc. Microanal.* 4(Suppl. 2): 36–37.
3. Ikegami, S., T. S. Okada, and S. Koide. 1975. *Dev. Growth Differ.* 18: 33–43.
4. Monné, L. 1944. *Ark. Zool.* 35A(13): 1–27.
5. Inoué, S., and K. Dan. 1951. *J. Morphol.* 89: 423–456.

Reference: *Biol. Bull.* 195: 214–215. (October, 1998)

A Little Shell to Live In: Evidence That the Fertilization Envelope Can Prevent Mechanically Induced Damage of the Developing Sea Urchin Embryo

Katsuya Miyake¹ and Paul L. McNeil (Institute for Molecular Medicine and Immunology and Department of Cellular Biology and Anatomy, Medical College of Georgia, Augusta, Georgia 30912-2000)

The fertilization envelope begins to form within seconds after the fertilizing sperm fuses with the egg surface. It is the product of cortical granule exocytosis and subsequent chemical modifications that result in a hardening of the egg's surface (1). The function most often ascribed to the fertilization envelope of sea urchins and other animals is prevention of polyspermy. Indeed, in the laboratory, where sperm often greatly outnumber eggs, the sperm are obviously unable to penetrate this physical barrier. But there is an earlier, electrically-based block to polyspermy, suggesting that the fertilization envelope may have a function other than preventing polyspermy (2).

Another possible function of the fertilization envelope is protection, particularly from damage imposed by mechanical forces present in the natural environment of the egg and early embryo (3). We have tested this possibility by comparing the degree of damage caused by exposure of fertilized and unfertilized eggs to equal amounts of shear stress.

Shear stress was imposed on *Lytechinus variegatus* eggs by repeatedly drawing these cells up into a 1 ml syringe through an 18-gauge syringe needle, and then ejecting them. The fluid uptake part of the cycle is dependent on the vacuum produced by retraction of the syringe piston, i.e., the volume displaced. Ejection force is the major variable in this maneuver; it was maintained at an equivalent level throughout by positioning a

rubber band such that its elastic recoil produced the requisite force. The degree of egg damage resulting from imposition of shear stress in this manner was assessed in three ways. First, by observation of the eggs before and after various rounds of syringing. The unfertilized eggs were mostly broken into many smaller fragments after 10 rounds of syringing (Fig. 1a), whereas many of the fertilized eggs remained intact (Fig. 1b). This observation suggested a second, quantitative way of assessing damage: measurement of the degree of light scattered by the supernatant remaining after all of the whole eggs were allowed to sediment under gravity. The amount of light scattered by such supernatants was higher for unfertilized than for fertilized eggs over a wide range of shear-injury (Fig. 1c). This difference was largely eliminated when trypsin (0.2%, 10 min) was used to remove the fertilization envelope before syringing. We have obtained this result on five separate occasions, when fertilized (30–90 post-fertilization) and unfertilized eggs from the same batch of de-jellied eggs (two for the trypsin experiment) were compared.

This light scattering assay did not, however, rule out the possibility that fragmentation was also occurring in the fertilized egg, but was unnoticed, perhaps because the envelope trapped the fragments. Therefore an alternative assay for damage was developed—one that could measure the release from the damaged egg of a small molecule, ATP, that is normally membrane-impermeant. Syringing, controlled by a rubber band, as described, was carried out within the sample chamber of a luminometer in seawater containing luciferin and luciferase. Thus,

¹ Second Department of Anatomy, Fukushima Medical School, Fukushima, Japan.

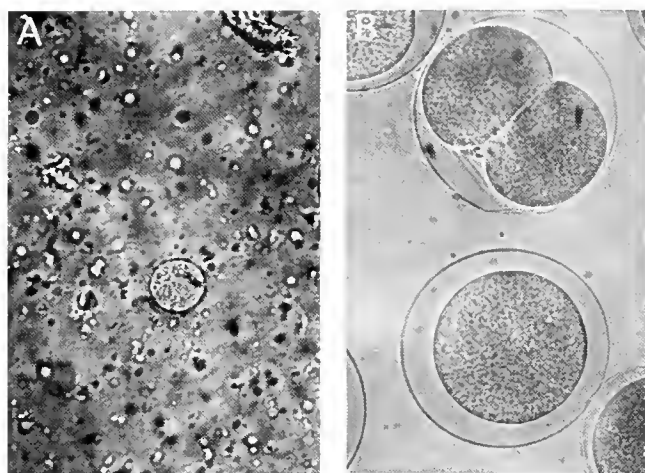
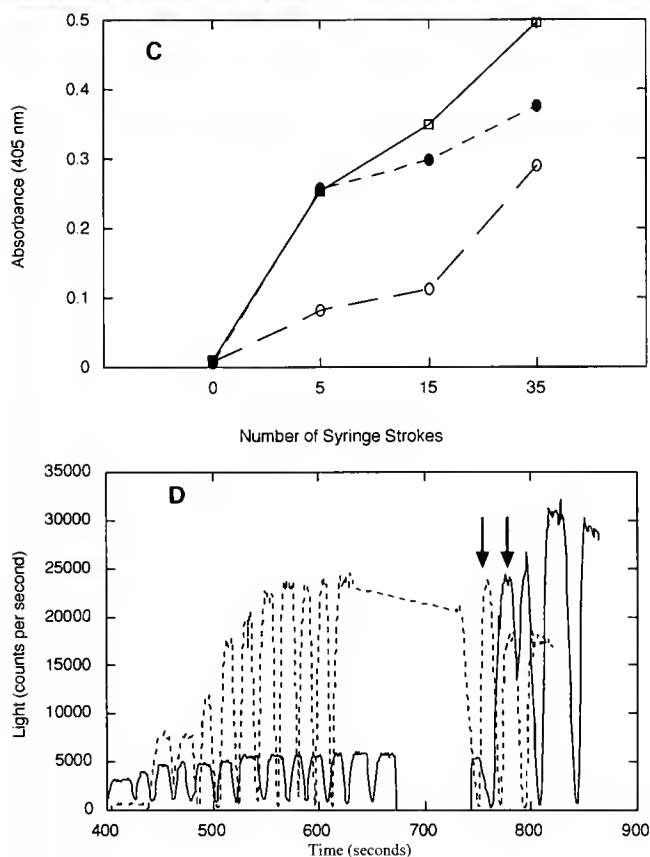


Figure 1. (A) Light micrograph of unfertilized eggs of *Lytechinus variegatus* subjected to 10 syringe strokes. Instead of whole eggs, egg fragments predominate. (B) Light micrograph of fertilized eggs also subjected to 10 syringe strokes. Note that intact eggs and early embryos predominate. (C) The absorbance, measured in a standard microtiter plate reader from the supernatant that formed in a 1.5 ml microcentrifuge tube after 2 min at 1 g, as a function of the number of syringe strokes administered. The readings were higher for unfertilized (open squares) and fertilized eggs treated with trypsin (solid circles) than for normal fertilized eggs (open circles). (D) The light produced by fertilized (solid line) and unfertilized (dotted line) eggs in the presence of seawater containing luciferin (1 mM) and luciferase (2 mM). Note the steep increase in light produced with each syringe stroke (each downward deflection followed by upward deflection) by the fertilized eggs in comparison to that produced by the unfertilized eggs. After syringing with the 18-gauge needle was completed (first arrow), the eggs were completely lysed by syringing with a much smaller (22-gauge) needle (second arrow) so that the total ATP-generated signal could be measured.



the light produced by the luciferin/luciferase mixture in response to ATP released from damaged cells could be recorded as a function of syringe injury. At the end of the experiment, the sample was lysed, allowing us to determine the total, measurable ATP. There was a striking difference between the fertilized and unfertilized eggs in the pattern and extent of ATP

release (Fig. 1d). Upon each syringe stroke, the unfertilized eggs released a greater proportion of the total ATP than did fertilized eggs. Indeed, the typical result of 10 rounds of syringe injury was that the unfertilized egg released maximally measurable amounts of ATP into the external medium, whereas the fertilized egg released only a small fraction of this amount.

Only a very few of the eggs released by a sea urchin survive to produce a reproductively competent adult. This high rate of mortality most likely has a number of causes. We propose that the fertilized egg and developing embryo are protected by the fertilization envelope from hydrodynamic-, predator-, and collision-generated mechanical forces present within the planktonic zone of the sea. We and others have shown elsewhere that an additional, and perhaps equally important adaptation of the urchin egg to life in a mechanically stressful environment, is its highly developed capacity to reseal and thereby to survive disruption of the plasma membrane (4). Although not often investigated, adaptations such as these may have great importance biologically for the sea urchin egg and embryo and for many other cell types that normally reside in mechanically stressful environments.

Dr. McNeil was an R. D. Allen/NASA fellow during the summer of 1998. The authors are grateful to Lionel Jaffe, for use of his luminometer, and R. Créton, for graciously helping us use this instrument; to Laurinda Jaffe for suggesting the first half of our title; and to M. Terasaki for conveying this suggestion to us by e-mail.

Literature Cited

1. Runnström, J. 1966. *Adv. Morphog.* 5: 221-325.
2. Jaffe, L. A. 1976. *Nature* 261: 68-71.
3. Harvey, E. B. 1956. *The American Arabacia and other Sea Urchins*. Princeton University Press, Princeton, NJ.
4. Terasaki, M., K. Miyake, and P. L. McNeil. 1997. *J. Cell Biol.* 139: 63-74.

Hyaluronic Acid-Receptor Binding Demonstrated by Synthetic Adhesive Proteoglycan Peptide Constructs and by Cell Receptors on the Marine Sponge *Microciona prolifera*

William J. Kulms¹, Xavier Fernandez-Busquets², Max M. Burger², Michael Ho¹, and Eva Turley¹
(Marine Biological Laboratory, Woods Hole, Massachusetts 02543)

The aggregation factor (MAF) of *Microciona* sponge is depicted as a species specific, adhesive proteoglycan molecule configured as a sunburst-type structure with a central ring, or core, from which numerous elongated arms project (1). Although the carbohydrate content of MAF is very high, the core is considered to be a protein (2). Fernandez-Busquets *et al.* have demonstrated, in a cloned peptide MAF fragment, a putative hyaluronic acid (HA) binding sequence bearing a chemical similarity to some other HA binding proteins on vertebrate cell membranes (3, 4) that are known to be involved in growth, and cell cycle and motility events (5, 6). The sequence of predominantly basic amino acids is generally designated by the formula B (X₇) B, where B is arginine or lysine, and X is any non-acidic amino acid; there is also at least one additional basic amino acid within, or adjacent to, the basic unit (7, 8). By these criteria, the deduced MAF peptide sequence is shown to be B (X₆) B, and is thus analogous to its vertebrate counterparts. In an earlier study, we used a biotin-labeled HA (BHA) probe to demonstrate HA receptors on *Microciona* cells; we also used antibodies against RHAMM (receptor for HA mediated motility, having the chemical formula shown above) to demonstrate that RHAMM is present on some of these cells (9). These results led us to hypothesize that HA, known to be present on MAF, might serve as a ligand for these chemically similar binding peptides, one on the MAF core peptide, the other on cell membranes, and that it might, thereby, be capable of signal transduction, as is known to occur in higher organisms. The aim of this study was to provide evidence in support of these notions.

Synthetic peptide constructs of RHAMM isoforms were prepared as described by Zhang *et al.* (10). The putative HA binding sequence of MAF core protein was synthesized in the Biotechnology Laboratories at the University of Toronto. This thirteen amino acid construct possessed short sequences that flanked the eight primarily basic amino acids believed to possess HA binding affinities. The structure was as follows: GLY-VAL-SER-VAL-ARG-ARG-TYR-ARG-ASN-ARG-VAL-ARG-ILE-OH. Dot blots were carried out by spotting 10 micrograms of a peptide at a site on nitrocellulose. After blocking non-specific reactive sites with 1%

buffered bovine serum albumin, BHA was applied and, after incubation and washings, was followed in sequence by streptavidin peroxidase and color development with diaminobenzidine. The negative controls consisted of peptide-free MAF glycans and a peptide-free color development site (Fig. 1E).

The reactivities of cellular RHAMM sites toward specific anti-RHAMM antibodies and HA were studied comparatively by immunohistochemical experiments in which sponge cells were double-labeled with mouse anti-RHAMM antibodies and with BHA. Sections of formalin-fixed and paraffin-embedded sponge cell pellets, cut at 5 μ m, were deparaffinated and were double-labeled with: (a) BHA stain as the first reagent, followed by mouse anti-RHAMM and FITC anti-mouse antibodies; and (b) anti-RHAMM FITC anti-mouse as the first reagent, followed by BHA and color development. Stained sections were viewed under tungsten and UV light.

The presence of color development at all sites that were blotted with RHAMM peptide and MAF peptide constructs indicated that they were reactive with hyaluronic acid (BHA). On the other hand, there was no demonstrable staining at a control site treated with peptide-free MAF, or at a site lacking MAF and peptide. The staining patterns shown on microscopic sections indicated that the reactivity of BHA toward RHAMM sites could be blocked by the prior application of anti-RHAMM antibodies (Fig. 1C, D), in which case some immunofluorescence by the anti-RHAMM FITC preparation could be shown. Conversely, the activity of anti-RHAMM toward RHAMM foci was greatly reduced when the BHA stain had been applied beforehand (Fig. 1A, B). This indicated that either one or the other reagent could compete effectively for cellular RHAMM based upon its ability to block the reaction of the alternate probe.

Taken together, the evidence indicates that (a) the postulated HA binding sequence of MAF core peptide actually functions in this role as determined by the behavior of an HA binding mimetic, and (b) this MAF HA binding sequence, in addition to the RHAMM on *Microciona* cell membranes, may serve as anchorage points for HA molecules. In this role, the entire construct may provide a conduit for the transduction of signals that specify motility and perhaps other phenomena. As a final point, sponges like *Microciona* are the most primitive species with multiple cell lineages, in which cell-cell recognition occurs by clumping, (11). The presence of HA receptors on MAF and on sponge cells suggests a highly conserved function that may

¹ Hospital for Sick Children, Toronto, Ontario, Canada M5G 1X8

² Friedrich Miescher Institute, CH4002, Basel, Switzerland.

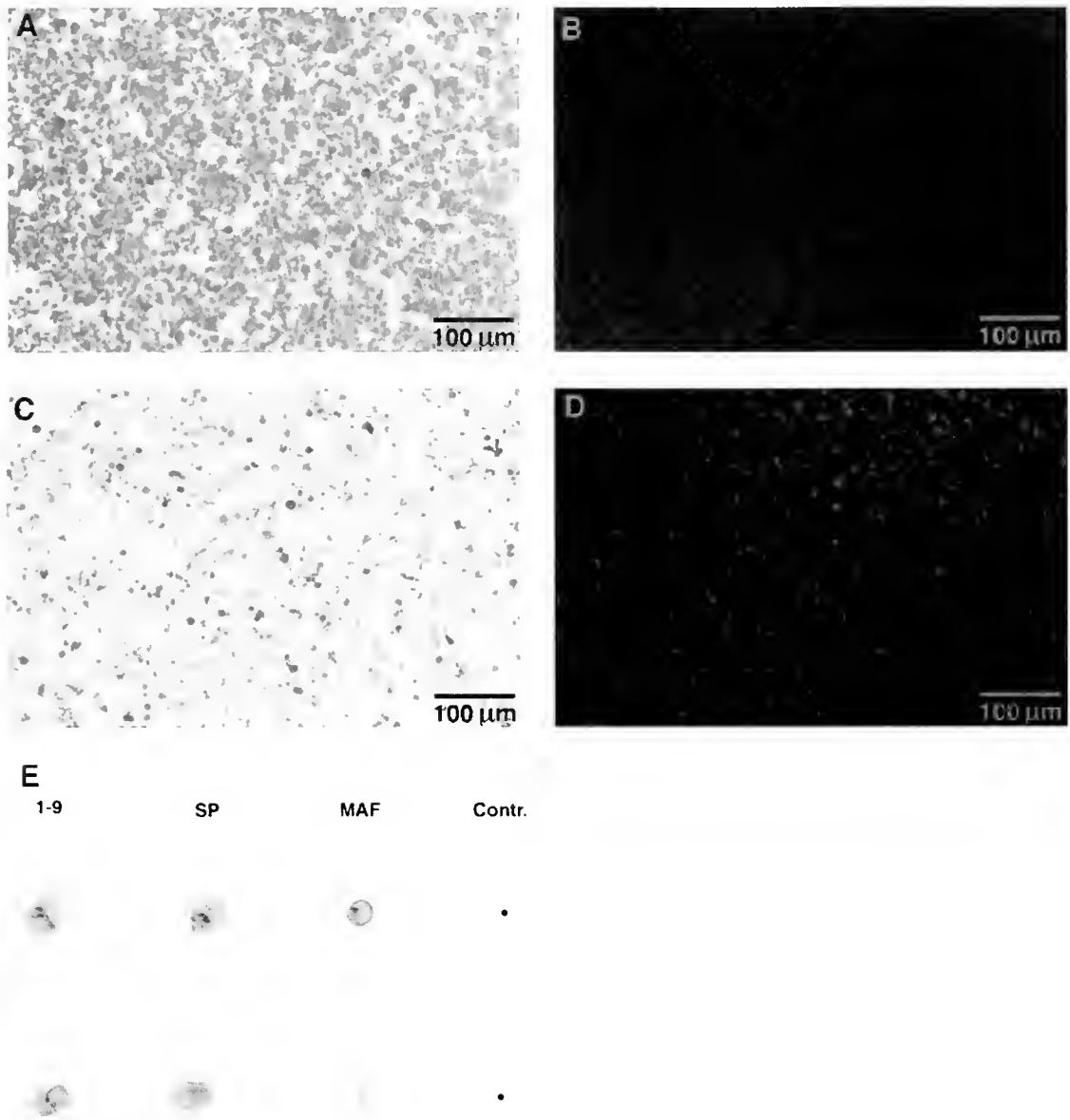


Figure 1. Sections of pelleted *Microciona* cells double-labeled with biotinylated hyaluronic acid (BHA) at a dilution of 1/100, and with mouse anti-RHAMM-FITC anti-mouse globulin. Frames A and B depict the same microscopic field of a section that had first been stained with BHA, and then by anti-RHAMM-FITC. Photographs of this field were taken with tungsten (A) and with UV illumination (B). Prominent BHA staining of most cells was observed, whereas only muted fluorescence could be seen. Frames C and D demonstrate the staining patterns of the two reagents when they are applied in reverse order; i.e., anti-RHAMM-FITC followed by BHA. In this instance, there is fluorescence (D), but BHA staining (C) is strongly reduced relative to the picture seen in (A). Frame E shows the results of dot blot studies. Positive blots were demonstrated by RHAMM isoform constructs (columns 1–9 and SP). A strong reaction was shown by the MAF peptide construct (upper) and a small signal was given by MAF proteoglycan (lower). The black dots in the control column (right) were pencil marks indicating the positions at which reagents were applied; peptide-free MAF glycans (upper) and peptide-free color development control (lower) gave no reactions.

possess a specific role in motility. This function may thus help to bring about cell sorting and aggregation, in synergy with other MAF-binding epitopes that have been referred to in earlier publications (12–15).

Literature Cited

1. Henkart, P., S. Humphreys, and T. Humphreys. 1973. *Biochemistry* 12: 3045–3050.

2. Fernandez-Busquets, X., R. Kammerer, and M. Burger. 1996. *J. Biol. Chem.* **271**: 23558–23565.
3. Underhill, C., S. Green, P. Comoglio, and G. Tarone. 1987. *J. Biol. Chem.* **262**: 13142–13146.
4. Lesley, J., R. Hyman, and P. Kincade. 1993. *Adv. Immunol.* **54**: 271–335.
5. Hall, C., C. Wang, L. Lange, and E. Turley. 1994. *J. Cell Biol.* **126**: 575–588.
6. Entwistle, J., C. Hall, and E. Turley. 1996. *J. Cell Biochem.* **61**: 569–577.
7. Yang, B., L. Zhang, and E. Turley. 1993. *J. Biol. Chem.* **268**: 8617–8623.
8. Yang, B., B. L. Yang, R. Savani, and E. Turley. 1994. *EMBO J.* **13**: 286–296.
9. Kuhus, W., M. Ho, M. Burger, and E. Turley. 1997. *Biol. Bull.* **193**: 243–244.
10. Zhang, S., M. Chang, D. Zylka, S. Turley, R. Harrison, and E. Turley. 1998. *J. Biol. Chem.* **273**: 11342–11347.
11. Weissmann, G., W. Riesen, S. Davidson, and M. Waite. 1988. *Biochim. Biophys. Acta* **960**: 351–364.
12. Spillmann, D., K. Hard, J. Thomas-Oates, J. Vliegthart, G. Misevic, M. Burger, and J. Finne. 1993. *J. Biol. Chem.* **268**: 13378–13387.
13. Spillmann, D., J. Thomas-Oates, A. van Kuik, J. Vliegthart, G. Misevic, M. Burger, and J. Finne. 1995. *J. Biol. Chem.* **270**: 5089–5097.
14. Misevic, G., J. Jumblatt, and M. Burger. 1982. *J. Biol. Chem.* **257**: 6931–6936.
15. Misevic, G., and M. Burger. 1990. *J. Cell. Biochem.* **43**: 307–314.

Reference: *Biol. Bull.* **195**: 218–220. (October, 1998)

Lipophilic Dye Labeling Distinguishes Segregated Central Components of the Eighth Cranial Nerve in Embryonic Chicken

M. F. Kubke (University of Maryland, Department of Biology, College Park, Maryland 20742),
E. Gilland¹, and R. Baker²

Central nuclei of the auditory and vestibular systems are organized in spatially and functionally discrete subdivisions (1). For example, cochlear nucleus magnocellularis and nucleus angularis receive inputs from the cochlear nerve but process information on time and intensity, respectively, through parallel pathways (2). In addition, each of these nuclei is tonotopically organized and receives an equally orderly projection from the auditory nerve (1). The embryological origin (3), as well as the later development of the central auditory and vestibular nuclei (4, 5), has been established in the chicken. The vestibular nuclei arise from hindbrain rhombomeres r1–r8, and the auditory nuclei arise exclusively from rhombomeres r3–r8 (4). In the chicken, the cells that will give rise to the auditory nuclei begin their migration at about Stage 25, but discrete auditory nuclei

cannot be readily identified until after Stage 30 (4). Less is known about the early development of the VIIIth nerve. Cranial nerve VIII contains the axons of afferent and efferent neurons in the auditory and vestibular systems. The aim of this study was to identify the topographical organization of the components of the VIIIth nerve in embryonic chicken at stages before any obvious spatial segregation can be seen in the developing central targets.

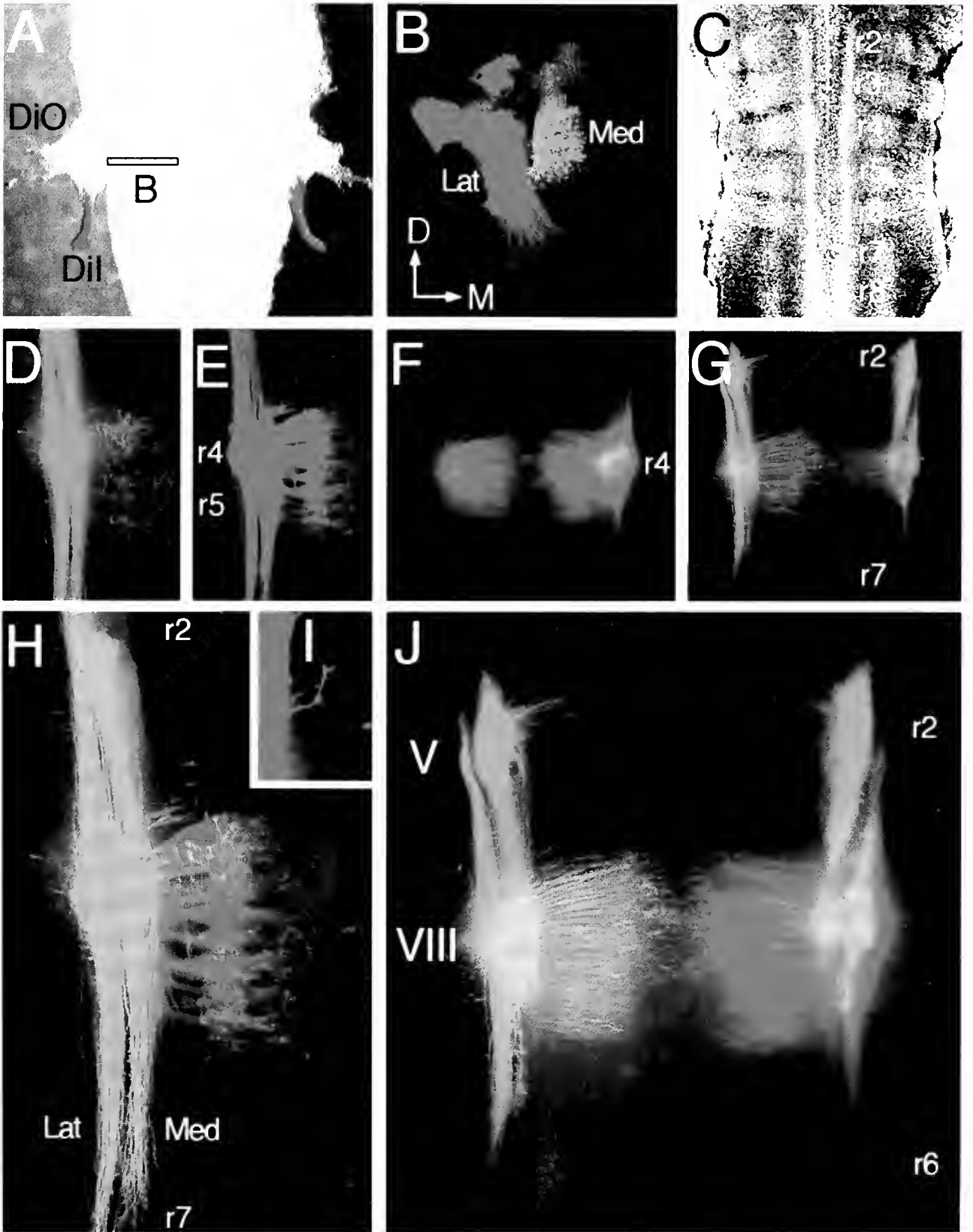
Eighteen chicken embryos, stages 20–32 (6), were fixed in 4% paraformaldehyde in 0.1 M phosphate buffer (PB). The brains were dissected in PB, leaving the cranial roots intact. Crystals of lipophilic dyes (DiI and DiO, Molecular Probes) were selectively applied to different regions of the VIIIth nerve roots (Fig. 1A). The brains were then incubated in PB at 38°C for 24 h, after which the nerve roots were removed. The brains were cleared in a glycerol series and whole-mounted for examination under epifluorescence in transmission and confocal microscopy.

Application of crystals to the entire nerve root labeled both

¹ Marine Biological Laboratory, Woods Hole, Massachusetts 02543.

² New York University, Department of Physiology and Neuroscience, New York, New York 10016.

Figure 1. Lipophilic dye analysis of VIIIth nerve compartmentalization. (A) Application of DiI and DiO onto anterior and posterior divisions, respectively, of the VIIIth nerve. The medially located root of the VIIth nerve was removed on both sides. (B) Cross section through the brainstem at the level of the VIIIth nerve (see box in A) showing differential labeling of the sensory tracts as shown in A. Medial (Med) and lateral (Lat) columns can be distinguished, with no overlap between the labeled components in A. (C) Pial view of a Stage 24 hindbrain distinguishing rhombomeres r2–r8. The root of the VIIIth nerve arises entirely within rhombomere 4. (D, E, H) Pial view of the left side of a Stage 24 embryo after dye application throughout the VIIIth nerve. Two distinct sensory tracts (Lat and Med) were identified after double labeling of the nerve. (D) Labeling pattern after DiI application; (E) labeling pattern after DiO application; (H) Composite view of both fluorescent channels. (F, G, J) Separate dye labeling in a Stage 24 embryo (see text). (F) Labeling pattern after DiI application; (G) labeling pattern after DiO application; (J) Composite view of both fluorescent channels. Although the nerve subdivisions are not visible at the gross level, spatially restricted labeling of the VIIIth nerve root showed distinct central projections. I: Axon exiting the lateral tract at Stage 24 and exhibiting a robust growth cone



fferent and afferent components of the cranial nerves. At Stage 28 and beyond, the rostral and caudal branches of the VIIIth nerve roots presumably contain, respectively, vestibular components and a mixed population of auditory and vestibular fibers (1). The root of the VIIth nerve could be isolated and dissected, either for removal or for dye application (Fig. 1A). Separate application of dyes to each region (anterior and posterior) of the VIIIth nerve at Stage 28 (such as shown in Fig. 1A) resulted in differential labeling of two lateral afferent sensory tracts (Fig. 1B), with the projections of the vestibular sensory portion being found in a more medial position (seen in green in Fig. 1B). At Stage 24, when rhombomeric borders are still evident (Fig. 1C), neither central nor peripheral targets can be identified (4). In addition, dye applications at these stages could not entirely exclude spread to the VIIth nerve. In spite of the absence of obvious landmarks in the nerve, the different components of the VIIIth nerve were found experimentally to be segregated both centrally and peripherally. This is shown in Figure 1D–H. J. Application of DiI and DiO to the entire VIIIth nerve root resulted in the labeling of two distinct fiber tracts that ran along the lateral margins of the hindbrain (shown at higher magnification on the left side of the brain, Fig. 1D, E; lat and med in H). The appearance of some axons exiting the main fiber tracts and exhibiting expanded growth cones suggests that afferent fiber extension was still underway (Fig. 1I). Figure 1 F, G, and J show the results obtained after local application of dye to different areas of the VIIIth nerve in a Stage 24 embryo. On the right side of the embryo, DiI (red, Fig. 1F) was applied to the more rostral component of the nerve root, and DiO (green, Fig. 1G) was selectively applied to the more caudal region of the root. At this stage, afferent and efferent fibers were seen to project through both the rostral and caudal regions of the nerve. In the

left side of the embryo, DiI was applied to the most medial portion of the nerve root (Fig. 1F), and DiO was applied selectively on the lateral half of the root (Fig. 1G). The resulting labeling pattern suggests that afferent fibers enter the brain primarily within the medial component of the nerve, whereas the lateral component carries both afferent and efferent fibers (see composite in Fig. 1J).

These results show that at the time when the anterior and posterior components of the VIIIth nerve are identifiable, their respective central projections are spatially segregated. The appearance of two similar afferent tracts in younger embryos suggests the hypothesis that segregation in the primary vestibular and cochlear afferents precedes the differentiation of the central nuclei. Hence, combined labeling of peripheral and central structures may be used to resolve the spatial relationship between auditory and vestibular afferents with respect to their central targets early during development.

This work was supported by NIH EY02007, DCD00436 and a Grass Fellowship to MFK.

Literature Cited

1. Rubel, E. W., A. N. Popper, and R. R. Fay. 1998. Development of the Auditory System. Springer Verlag, New York.
2. Takahashi, T., A. Moiseff, and M. Konishi. 1984. *J. Neurosci.* **4**: 1781–1786.
3. Marin, F. and L. Puelles. 1995. *Eur. J. Neurosci.* **7**: 1714–1738.
4. Book, K. J., and D. K. Morest. 1990. *J. Comp. Neurol.* **297**: 55–76.
5. Rubel, E. W., D. J. Smith, and J. C. Miller. 1976. *J. Comp. Neurol.* **166**: 469–489.
6. Hamburger, V., and H. L. Hamilton. 1951. *J. Morphol.* **88**: 49–92.

Reference: *Biol. Bull.* **195**: 220–222. (October, 1998)

Rhombomeric Organization of Brainstem Motor Neurons in Larval Frogs

Hans Straka (New York University Medical Center, New York 10016), Edwin Gilland¹, and Robert Baker

The vertebrate hindbrain develops from a series of eight neuroepithelial segments called rhombomeres, each of which expresses specific subsets of developmentally regulated genes including 3' members of the Hox gene clusters (1). Rhombomeres give rise to particular neuronal populations and are generally visible only during embryonic stages. However, lampreys, which have a prolonged larval period, retain visible rhombomeric patterning through much of their postembryonic development (2). In addition, reticulospinal neurons in teleosts retain a clear segmental organization even at adult stages, forming neu-

ronal units termed rhombomeric segments (rhs) (3). Neurons underlying specific vestibulo-oculomotor behaviors have also been shown to reside in characteristic segmental positions within this persisting hindbrain scaffold in goldfish and zebrafish (4). Since anurans have a prolonged larval period and are also extensively studied in terms of adult brainstem circuitry, they are suitable subjects for research into the relationship between embryonic segmental origins and functional neuronal phenotypes. We therefore examined larval ranid frogs for evidence of visible rhombomeric compartments and labeled cranial nerves with dye to permit the functionally distinct neuronal populations to be mapped with reference to their segmental locations.

Populations of efferent neurons in the hindbrain of stage

¹Marine Biological Laboratory, Woods Hole, Massachusetts 02543.

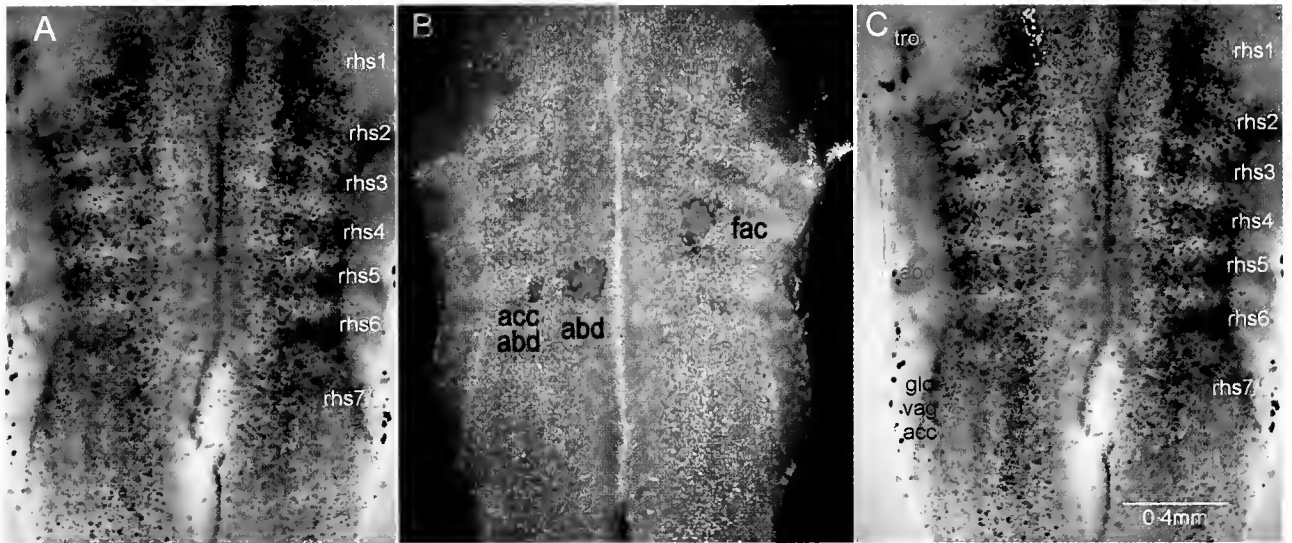


Figure 1. Whole-mount preparations of the hindbrains of 2-cm frog tadpoles viewed from the ventral surface. (A) Brightfield photomicrograph showing the rhombomeric segments (rhs 1–8) as a series of dark and light stripes. (B) Combined brightfield-epifluorescence overlay of a hindbrain after labeling of the VIth nerve on the right side and the VIIth nerve on the left side with rhodamine-dextran. Facial motoneurons (fac) reside in rhs 4 only, while abducens (abd) and accessory abducens (acc abd) reside in rhs 5 only. (C) Location of the trochlear (tro), trigeminal (tri), facial (fac), abducens (abd) and glossopharyngeal (glo), vagal (vag), accessory (acc) motor neurons as imaged in confocal preparations superimposed on the brightfield micrograph shown in A. Calibration bar in C applies to A and B as well.

24–26 larval frogs (*Rana clamitans*) were reconstructed with confocal microscopy after the cranial nerves were labeled with fluorescent tracers. The locations of the labeled neurons were correlated with rhombomeric compartments imaged in the same preparations by using oblique transmitted illumination. Crystals of 3000 mw dextran-conjugated rhodamine, fluorescein, or Texas red (Molecular Probes) were placed on the cut ends of the IVth, Vth, VIth, VIIth, and IX–XIth cranial nerves. After transport times ranging from 24 to 48 h, the samples were fixed in 4% paraformaldehyde. Whole brains were cleared in glycerol and were either scanned on a Zeiss LSM-510 confocal microscope at 4–7 μm z-axis intervals or photographed with transmitted and epi-illumination with a Spot digital camera on a Zeiss Axiophot microscope.

The larval frog hindbrain appears as a rostro-caudal series of eight darkly pigmented regions of similar size, separated by narrower, more lightly pigmented stripes (Fig. 1A). In the youngest tadpoles studied, an undulating pattern of sulci and gyri was superimposed on and correlated with the stripes. These units demonstrate retention of the embryonic rhombomeric pattern at larval stages, with the first six segments (rhs 1–6) clearly separated from each other, but the border between rhs 7 and 8 not evident in all animals. In addition, rhs 1 appeared to be slightly larger than the others, with a more triangular shape (Fig. 1A).

After the IVth cranial nerve was labeled, trochlear motoneurons were found exclusively on the contralateral side in rhs 1. Tracer applied to the Vth cranial nerve labeled trigeminal motoneurons in two clusters on the ipsilateral side in rhs 2 and 3. Application of tracer onto the VIth cranial nerve labeled medially located abducens motoneurons and more

laterally located accessory abducens motoneurons exclusively in rhs 5 (Fig. 1B, abd and acc abd). Facial motoneurons, labeled after tracer application to the VIIth cranial nerve, were found only in rhs 4 on the ipsilateral side (Fig. 1B, fac). In some preparations, additional efferent neurons with axons running parallel to the VIIth nerve were found in rhs 5 and are likely anterior lateral-line efferent neurons. Tracer applied to the IX–XI complex of the cranial nerves labeled motoneurons in rhs 7 and 8, with only occasional cells visible rostral to the rhs 6–7 border.

These results show that visible rhombomeric segments, similar in number and appearance to those found in all embryonic vertebrates, are still present in post-embryonic frog larvae. The rhombomeric organization of cranial motor neurons is likewise similar to the pattern described in other vertebrate groups, with the notable exception of facial and abducens motoneurons (Fig. 1C). Restriction of facial motoneurons to rhs 4, as opposed to rhs 4 and 5 in most vertebrates, might be a premetamorphic condition, or it might be due to the fact that the superior salivary regions, which are innervated by motoneurons located in rhs 5 in mammals, are not well developed in anurans. In the latter case, the presence of facial motoneurons in only one rhombomere might represent a modification specific to amphibians. In contrast to lampreys, teleosts, birds, and reptiles, in which abducens motoneurons are located in rhs 5 and 6, in frogs these motoneurons were found only in rhs 5, a condition previously thought to be unique to mammals (1, 5).

The origin of abducens motoneurons in two segments appears to be the basic vertebrate pattern, with restriction to only one segment (rhs 5 in anurans and mammals and rhs 6 in elasmobranchs) being unique to particular taxa. Comparative

studies have shown that the Hox b3 gene is expressed at high levels in rh5 in mammals and in rh5 and 6 in teleosts, thus correlating with the location of abducens motoneurons (5). Analysis of the rhombomeric pattern of Hox b3 gene expression in anurans and sharks will therefore provide further tests of causal relations hypothesized to exist between particular developmentally regulated genes and functionally distinct neuronal phenotypes.

This work was supported by the Max-Kade Foundation, New York.

Literature Cited

1. Gilland, E., and R. Baker. 1993. *Acta Anat.* **148**: 110–123.
2. Gilland, E., and R. Baker. 1995. *Soc. Neurosci. Abstr.* **21**: 779.
3. Lee, R. K., R. C. Eaton, and S. J. Zottoli. 1993. *J. Comp. Neurol.* **329**: 539–556.
4. Suwa, H., E. Gilland, and R. Baker. 1996. *Biol. Bull.* **191**: 257–259.
5. Prince, V. E., C. B. Moens, C. B. Kimmel, and R. K. Ho. 1998. *Development* **125**: 393–406.

Modified Laboratory Culture Techniques for the European Cuttlefish *Sepia officinalis*

Janice S. Hanley, Nadav Shashar, Roxanna Smolowitz¹, Robert A. Bullis¹, William N. Mebane, Howaida R. Gabr, and Roger T. Hanlon (Marine Resources Center, Marine Biological Laboratory, Woods Hole, Massachusetts 02543)

The cuttlefish *Sepia officinalis* Linnaeus, 1758, is an important model for a variety of biological and biomedical investigations (1). To introduce this organism to the North American research communities, and make it readily available, various methods have been used to maintain or culture the species. The most intensive efforts and successes have been achieved by Forsythe and colleagues at the University of Texas Medical Branch in Galveston (2,3). Their most noteworthy achievement was to culture seven consecutive generations in large-scale recirculating seawater systems.

Recently, cuttlefish were brought to the Marine Resources Center (MRC) of the Marine Biological Laboratory, where they have also been cultured successfully through their life cycle. Presently the third laboratory generation is under culture. Unlike previous work on *Sepia* culture in the United States, our focus has been to use a mostly open (flow-through) seawater system modified to function well through a northern winter, and to develop feeding methods that are suitable for our locale.

Seawater filtration

Unlike the recirculating systems used recently, in the MRC the cuttlefish were cultured in systems that were largely open, or flow-through. The basic system was a semi-closed loop containing about 34,500 liters of water, of which a high percentage—9.7%—was exchanged in the loop every hour. Thus, we used local seawater that had a long residence time (approximately 10 hours) in the loop. This water was heated or chilled at different times of the year to maintain a temperature in the range of 18°–20°C. However, adult cuttlefish could tolerate a wider range of 15°–22°C. Biological filters were still used in the loop, but with the rapid water turnover and low biomass of cuttlefish in the system (generally varying from 80–140 kg), the water quality was always excellent. The major water quality parameters were pH, 7.80–8.10; salinity, 29–33 ppt; dissolved oxygen, 7.0–9.0 mg/l (cephalopods have high respiration rates and require highly aerated water); NH₃, less than 0.5 mg/l; NO₂, less than 0.2 mg/l; and NO₃, less than 1 mg/l. This last parameter is important, because cuttlefish often jet and ink more in closed systems in which nitrate exceeds 80 mg/l (2). In addition to helping to maintain good water quality, the rapid exchange of seawater prevented depletion of trace elements which are needed for cephalopod development. To lower bacterial counts in the tanks, we used UV sterilization rather than ozone treatment (for which the loops were designed), because mechanical failures of the UV system do not affect the water system ad-

versely, and UV radiation has relatively little effect on the water chemistry. Space requirements are described in Table I and they are roughly comparable to those determined in other studies (3).

Fecundity

Spawning females usually laid about 2000 eggs each over several weeks (the number varied greatly). The range of egg fertility rates was 32–80% (avg. = 48%, out of 2850 eggs subsampled from 6 females) and, because our present needs are limited, several thousands of eggs or hatchlings were shipped to Galveston for rearing. Although we are culturing only about 50–100 cuttlefish to full adult size (many are used for experiments at smaller sizes), the adult males usually grow to about 2 kg (max 4.3 kg), and the females to 1 kg. Presently (August 1998), there are 170 cuttlefish in culture at three months of age.

Feeding

Various methods for feeding in captivity have been developed previously (2–4). We wished to improve on the performance of brine shrimp (*Artemia* sp.) as a food source for hatchlings. Due to the high cost of live food needed by young cuttlefish, we wanted to develop a method that would train the young cuttlefish to accept frozen food at as early an age as possible. The current feeding schedule is described in Table 1. Hatchlings (0–8 weeks old) were fed either with (i) a mixture of brine shrimp, mysid shrimp and amphipods (mainly *Gammarus* sp.), or (ii) with brine shrimp that were enriched with fatty acids and amino acids by a soaking in Super Selco (INVE Inc.). At the age of approximately 6 weeks, food was occasionally augmented with live grass shrimp (*Palaemonetes* sp.) for both groups. Survival rates of the cuttlefish fed with a mixture of foods were significantly higher than the group fed only with enriched brine shrimp ($P < 0.001$, χ^2 with equal expected frequency, 91% vs. 41% respectively, $n = 1304$).

When the cuttlefish reached an age of 2 months (body length = 19.8 ± 2.4 mm, mantle length = 14.8 ± 1.3 mm, wet weight = 0.9 ± 0.2 g), they were hand-trained to accept frozen food. Training involved presenting the animals with small pieces of food on plastic rods, and even touching and stroking their arms with the food. At training sessions, performed 3 times a day, each animal was presented with food for up to 1 min. After 3 days of training, the animals would accept the food, and after a week they actively sought it. Thereafter, small pieces of frozen food were dropped directly into the tank. Of the different types of food pieces presented (fish, squid, shrimp, and clam), shrimp was accepted best. However, after the week of training, most animals would accept any type of food presented in thin, prefer-

¹ Laboratory for Aquatic Animal Medicine and Pathology, University of Pennsylvania, MBL.

Table I

Maintenance schedule for cuttlefish, Sepia officinalis

Age (month)	Total length (cm)	Animal density (cm ² /animal)	Substrate in tank	Food
0-1.25	0.50-1.25	3	no substrate—animals held in sieves with 150 μ m mesh	brine shrimp
1.25-2	1.25-2	200	fine sand	brine shrimp + grass shrimp
1.75-2	ca. 2			training for frozen food
2-4	2-8	500	gravel 5-15 mm mesh size	frozen shrimp, squid, fish or clam
4-6	8-12	2000 separation by sex to reduce interactions	no substrate	frozen shrimp, squid, fish or clam
6+	12+	8900	no substrate	frozen shrimp, squid, fish or clam

ably long, slices. It was not essential to train all animals in a tank during the first week because, if more than 75% of the animals accepted the food within a 24-h period, the other animals in the tank would follow and seek the frozen food. Although the cuttlefish would occasionally eat food left in the tank after it was presented, food left for more than 2 h was rejected and had to be removed.

Substrate

Cuttlefish hatchlings were held in shallow sieves with 150- μ m mesh bottom liners and water flowing in from the top. At the age of 6 weeks, they were transferred to wide shallow tray tanks with a shallow sand substrate. To avoid damage to the skin, the substrate had to present a smooth surface to the cuttlefish, hence crushed oyster shells were rejected. On the other hand, to reduce bacterial settlement and fouling of the surface, large-grain particles, having a small surface-to-volume ratio, were used in the tanks. When the cuttlefish reached a size of about 2 cm in total length (2 months old), they were transferred to tanks having a thin layer of gravel (grain size of 5-15 mm) as the substrate (Table I).

Animal Health

Various diseases of cuttlefish in captivity have been described (5). Small numbers of cuttlefish developed severe, focally extensive, ulcerative dermatitis and cellulitis of the dorsal apex of the mantle (Fig. 1A), which caused mortality if not treated. Such lesions were caused by an animal jetting against the tank walls during flight responses. Secondary problems accompanying this initial lesion were septicemias and, more rarely, fluid accumulation (sometimes up to 100 ml of clear to slightly milky fluid) between the cuttlebone and the overlying dermis of the mantle (see also 6).

Another problem in very old adults was the occurrence of multifocal, erosive-to-deep, ulcerative lesions (Fig. 1B) over the mantle, head, and arms. These lesions seem to result from sucker-induced trauma during confrontations between males and during reproductive behavior. In less severe cases of traumatically induced dermatitis, treatment with 5-min dips (1 \times /day for 3 consecutive days) in an Argentine solution (25 ppm) was successful in healing the ulcers. Healed ulcers appeared white to slightly translucent (no chromatophores were present

in the newly formed dermis). A less common, but distinctive, lesion was the separation of the median angle of the collar ("Pen Point") from the underlying supportive connective tissues. Such a separation could produce a cavity underlying the cuttlebone up to 4 cm in diameter. The cause of such separations was not identified, but was probably traumatic in origin. Juveniles occasionally developed idiopathic bulbus protrusions of one or both eyes. This condition was associated with opaque corneas and swelling of periorbital tissues.

Measures of containment from the local environment

Sepia officinalis is not native to the western Atlantic Ocean. Hence, special care is required to prevent their introduction to the local marine environment. Small-mesh screens on all water outlets prevented hatchlings or eggs from escaping the tank. Water was heavily sterilized with ozone before being discharged to the ocean. Discarded eggs were frozen and then incinerated.

In summary, these techniques have enabled further development of this species as a marine model in the United States.

We gratefully thank Geoff Till for helping maintain the water system, Alan Kuzirian and Jean Boal for assistance with water quality and animal care, and Kim Boyle, Anne Petz, Nicolas

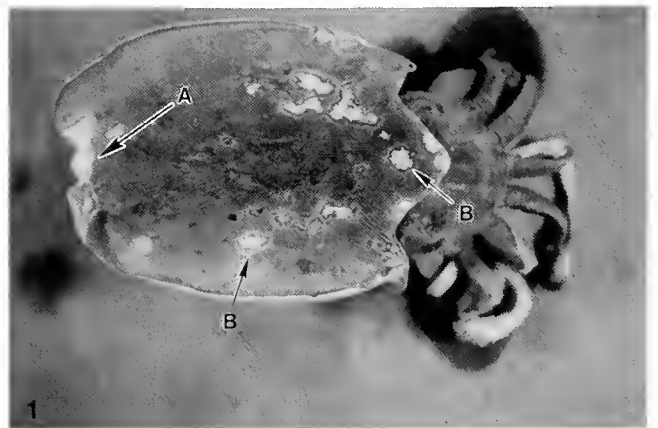


Figure 1. A case of severe ulcerative dermatitis of the mantle apex (A), and multifocal ulcerative dermatitis of the mantle (B) in an adult cuttlefish.

Offner and Aimee Vasse for help in feeding and training the cuttlefish. This study was partly supported by NIH grant RR01024 and a Grass fellowship to NS.

Literature Cited

1. Boucaud-Camou, E. 1991. *The Cuttlefish. First Int. Symp. on the Cuttlefish Sepia*. Centre de publication de l'Université de Caen, France.
2. Forsythe, J. W., R. T. Hanlon, and R. DeRusha. 1991. Pp. 313–323 in *The Cuttlefish. First Int. Symp. on the Cuttlefish Sepia*, E. Boucaud-Camou, ed. Centre de publication de l'Université de Caen, France.
3. Forsythe, J. W., R. H. DeRusha, and R. T. Hanlon. 1994. *J. Zool. (Lond.)* 233: 175–192.
4. DeRusha, R. H., J. W. Forsythe, F. D. DiMarco, and R. T. Hanlon. 1989. *Lab. Anim. Sci.* 39: 306–312.
5. Hanlon, R. T., and J. F. Forsythe. 1990. Pp. 23–46 in *Diseases of Marine Animals, Vol 3*, O. Kinne, ed. Biologische Anstalt Helgoland, Hamburg, Germany.
6. Oestmann, D. J., J. M. Scimeca, J. Forsythe, R. T. Hanlon, and P. Lee. 1997. *Lab. Anim. Sci. Contemporary Topics* 36: 89–92.

Reference: *Biol. Bull.* 195: 225–226. (October, 1998)

Evidence for Multiple Spawning by Squids (*Loligo pealei*) in Captivity

Michael R. Maxwell (Marine Biological Laboratory, Woods Hole, Massachusetts 02543),
William K. Macy¹, Shobu Odate, and Roger T. Hanlon

The long-finned squid (*Loligo pealei*) is an important commercial resource that is experiencing increasing fishing pressure in the northwestern Atlantic (1), and is also used in biomedicine and studies of sexual selection (2, 3). The actual fecundity of females of this species remains unknown, despite the importance of fecundity to fishery management and to behavioral and ecological research. Because many cephalopods are thought to be semelparous (4)—that is, individuals undergo only one bout of reproduction before death—an outstanding question for *L. pealei* and other squids is whether females spawn multiple times. When a female loliginid squid lays eggs, she typically lays several egg capsules (gelatinous strands that usually contain 100–200 embryos) over the course of a few hours. For *L. pealei*, we follow Harman *et al.* (5) in defining multiple spawning by a female as the occurrence of two processes: at least two bouts of egg-laying (during each of which she lays several egg capsules), and the maturation of new oocytes between these bouts. Previous studies of fecundity in squids have relied on morphological examinations of the size-frequency distribution of ovarian oocytes (reviewed in 6), in which small oocytes are taken as evidence of the development of oögonia. No study has yet linked the condition of the ovaries to the actual reproductive histories of female squids. Here, we investigate multiple spawning in *L. pealei* by combining anatomical information with actual reproductive output, an approach that contributes to a more accurate representation of female fecundity.

Squids were jig-caught in Nantucket and Vineyard Sounds in the periods May–September 1997 and May–July 1998. We placed single females into large tanks maintained at ambient temperature, and checked each tank daily for egg capsules. In 1997, each female ($n = 36$) was paired with a male throughout her captive life; each tank received 2–10 fish (*Fundulus hetero-*

clitus) per day. In 1998, 32 females were kept without males. All of these females had sperm in their seminal receptacles, so males were not essential for the laying of fertilized eggs. Each female received 2–6 *F. heteroclitus* per day.

Our analysis focused on females that lived for at least 3 days in captivity and laid clutches of five or more egg capsules on at least 2 separate days. In 1997, 12 of the 36 females met these conditions; in 1998, 14 of the 32 females did so. We dissected these females *post mortem*, measured mantle length (ML, dorsal surface), and extracted the ovary; in 1997, we also removed the two statoliths to determine age. Each ovary was fixed in 10% formalin, weighed, and then two 0.10-g pieces were removed, one from the anterior and the other from the posterior part of the ovary. We counted the oocytes in these two subsamples to derive a measure of oocytes per gram of ovarian tissue. The two values from each female were averaged, and the mean was multiplied by the mass of the ovary, providing an estimate of the total number of oocytes in the ovary. Statoliths were preserved in 70% ethanol, and the rings of the left statolith were counted by the method described in Brodziak and Macy (7); one statolith ring is laid down daily.

The reproductive histories of the captive females are depicted in Figure 1. Many females laid eggs frequently over 1–2 weeks; other females spaced their egg clutches over 2–3 weeks.

Our results reveal considerable variation in mantle length (ML) and age among the multiply-spawning females. In 1997, ML ranged from 9.6 to 22.5 cm (mean \pm SD = 14.8 \pm 3.6 cm, $n = 12$); in 1998, the range was 11.4–20.7 cm (mean \pm SD = 15.3 \pm 3.0 cm, $n = 14$). The number of statolith rings varied from 118 to 181 among the 1997 females (mean \pm SD = 163 \pm 21 rings). A comparison of two females from 1997 illustrates how egg output can vary between females. One female measured 9.6 cm ML and had 138 statolith rings. She laid 138 egg capsules over 15 days, with the mean \pm SD number of fertilized ova per egg capsule being 111 \pm 19 (random subsample of five egg capsules). Upon dissection, we were not able to differentiate

¹ Graduate School of Oceanography, University of Rhode Island, Narragansett, Rhode Island 02882.

oocytes from the surrounding ovarian tissue, suggesting that she had laid all of her ovarian oocytes before death (this animal, however, had deteriorated before preservation). The second female was roughly twice as long, 18.6 cm ML, and about a month older (176 statolith rings). She laid 62 egg capsules over 7 days, with a mean \pm SD of 151 ± 9 fertilized ova per egg capsule (random subsample of five egg capsules). Upon dissection, her ovary held an estimated 3521 oocytes.

In both years, most females had oocytes remaining in the ovary, suggesting that these females did not exhaust their supply of gametes before dying. In 1997, the mean \pm SD ovarian mass was 2.83 ± 3.13 g. Eight of the 12 females had oocytes in the ovary (mean \pm SD number of oocytes per gram of ovary = 611.4 ± 574.5). The estimated number of oocytes in the ovary of each of these eight females ranged from 345 to 17,323 (mean \pm SD = 3838 ± 5631 oocytes). For 1998, the mean \pm SD ovarian mass was 3.19 ± 2.14 g. Thirteen of the fourteen females had oocytes in the ovary (mean \pm SD = 736.8 ± 261.1 oocytes per gram of ovary). For these 13 females, the estimated total number of oocytes in the ovary ranged from 604 to 5455 (mean \pm SD = 2386 ± 1502 oocytes).

In both years, the ovarian oocytes showed a range of size and structure: our counts included two classes of oocytes. We found small oocytes (less than 1 mm in diameter) that were characterized by a veined texture due to follicle cells that surrounded the developing oocyte (8). The presence of these oocytes suggests that the females had indeed developed oogonia that had yet to undergo vitellogenesis (8). We also found larger, translucent, amber-colored oocytes (1–2 mm diameter) that resembled the fully mature amber-colored oocytes in the oviduct.

This study demonstrates that individual *L. pealei* females are capable of multiple egg-laying events over several weeks at least. During this period of multiple oviposition, the females appear to produce new oocytes, as suggested by the presence of the small and large oocytes in the ovaries; the congeners *L. forbesi* and *L. vulgaris* show similar ranges in oocyte size (9, 10), but their reproductive output has not been examined. Taken together, these results strongly indicate that *L. pealei* females are multiple spawners. Furthermore, this study contributes to a shift in thought about the life cycles of this and other loliginid squids. Previously, *L. pealei* females were thought to live for 2 years in the northwestern Atlantic and to die after spawning (11), implying that reproduction would encompass a very small fraction of an individual's life. Recent data suggest that a shorter life span of less than 1 year (7) and an egg-laying period of at least 2–3 weeks appear to be more typical for females of this population. Egg laying, then, may cover a substantial proportion of a female's life. Additionally, some females, perhaps the majority, might lay all or most of their mature ova and then develop more oocytes for another bout of egg laying. Overall, this study indicates the possibility of higher reproductive output by *L. pealei* females than previously thought.

We thank Ed Enos, Bill Mebane, Bill Klimm, Dan Sullivan, and Geoff Till of the Marine Resources Center at the Marine Biological Laboratory for support in the collection and maintenance of the squid. Kim Boyle, Joseph Cavanaugh, Florent Guyennet, Coren Milbury, Nicolas Offner, Anne Petz, Andrew

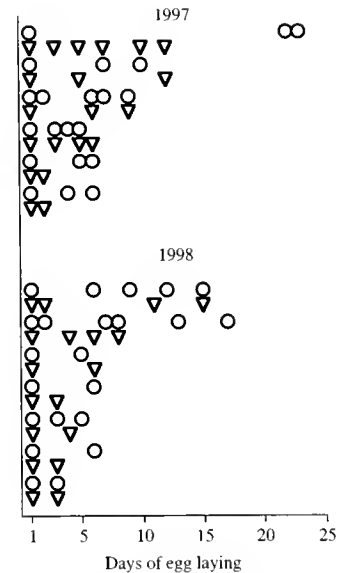


Figure 1. Production of egg capsules by captive females in 1997 and 1998. Each symbol represents the laying of five or more egg capsules, and each row of symbols reflects the activity of a single female; symbols alternate to aid viewing. The horizontal axis refers to the days after the laying of the first clutch of egg capsules (i.e., the first clutch of egg capsules is laid on day 1).

McTurner, and Anne-Sophie Voisin assisted in dissecting the squid, in sorting the egg capsules, and in caring for the animals. We are especially grateful for funding from Saltonstall-Kennedy Grant NA76FD0111 to RTH.

Literature Cited

1. NEFSC (Northeast Fisheries Science Center). 1995. *Status of Fishery Resources off the Northeastern United States for 1993*. NOAA Tech. Mem. NMFS-F/NEC. Woods Hole, Massachusetts.
2. Gilbert, D. L., W. J. Adelman, and J. M. Arnold, eds. 1990. *Squid as Experimental Animals*. Plenum Press, New York.
3. Hanlon, R. T., M. R. Maxwell, and N. Shashar. 1997. *Biol. Bull.* **193**: 212–214.
4. Boyle, P. R., ed. 1987. *Cephalopod Life Cycles, Vol. 2 Comparative Reviews*. Academic Press, London.
5. Harman, R. F., R. E. Young, S. B. Reid, K. Mangold, T. Suzuki, and R. F. Hixon. 1989. *Mar. Biol.* **101**: 513–519.
6. Mangold, K. M., R. E. Young, and M. Nixon. 1993. Pp. 697–703 in *Recent Advances in Cephalopod Fisheries Biology*. T. Okutani, R. K. O'Dor and T. Kubodera, eds. Tokai University Press, Tokyo.
7. Brodziak, J. K. T., and W. K. Macy. 1996. *Fish. Bull.* **94**: 212–236.
8. Beag, G. H., Y. Sakurai, and K. Shimazaki. 1993. *Veliger* **36**: 228–235.
9. Boyle, P. R., G. J. Pierce, and L. C. Hastie. 1995. *Mar. Biol.* **121**: 501–508.
10. Rocha, F., and A. Guerra. 1996. *J. Exp. Mar. Biol. Ecol.* **207**: 177–189.
11. Summers, W. C. 1971. *Biol. Bull.* **141**: 189–201.

Reference: *Biol. Bull.* 195: 227–228. (October 1998)

In vivo and *in vitro* Growth of Nerve Parasite from *Lophius americanus*

Earl Weidner and Teresa King (Biology, Louisiana State University, Baton Rouge, Louisiana)

Microsporidian parasites of the genus *Spraguea* develop in neuronal cells in the central nervous system of different species of the genus *Lophius* (1). Large colonies (0.5–1 mm in diameter) of parasites locate in the trigeminal ganglia, dorsal spinal root ganglia, and supramedullary cells (SMCs). All of these neurons appear to send fibers to the skin. Recent tracer studies by Fanakoshi *et al.* (2) indicate that SMCs extend single or branched fibers directly to the skin. The infective spore stages of *Spraguea* are activated to discharge in *Lophius* surface mucus, and it is therefore believed that peripheral fibers of the fish may be parasitized directly upon the injection of sporoplasm from the activated spore into the nerve fiber.

The parasitism of *Lophius* by *Spraguea* begins during the first year of the fish's growth, presumably after the shift from a pelagic to benthic existence. The development of the parasites into colonies is primarily confined to neuronal processes proximal to the cell body (Fig. 1). The parasites locate freely within the cytoplasm of the host cell, although each colony appears to be confined to specific domains by the accumulation of intermediate filaments that surround the parasites. In older fish, the colonies consist primarily of spores, although vegetative (meronts) elements persist even in the old colonies. The size of the parasite colony within the nerve process effectively blocks axonal flow; nevertheless, the cell body of host retains viability.

For *in vitro* studies, colonies were removed from the surrounding host cells; the dense network of intermediate filaments

surrounding the parasites permits their easy removal and separation from the cytoplasm of the host cell. Colonies were transferred to a modified Trager medium supplemented with nucleotides and the gel Matrigel (3). During 24-h incubations *in vitro*, meront stages remained within the colony matrix of intermediate filaments and showed evidence of motor activity, including some endocytosis.

Nerve cell infections by *Spraguea* are thought to become established by the discharge of spores that introduce infective sporoplasm into neuronal fibers near the skin surface. Subsequently, the sporoplasm migrates up the fiber and begins to replicate in areas adjoining the cell body. To examine newly discharged sporoplasms *in vitro*, spores were placed on coverslips with activation medium (4). The discharging sporoplasms remained attached to the coverslips while the spore ghosts were being removed with 0.5% concanavalin A rinses. Isolated sporoplasms were transferred to culture dishes in Medium 199 containing nucleotides, pentose sugars, Matrigel, and antibiotics (penicillin/streptomycin). In these *in vitro* studies, sporoplasms showed limited endocytic activity, a slight size increase with no clear evidence of cytokinesis after 32 h in incubation.

In all microsporidian invasions of target cells, the sporoplasm stage is introduced directly into the host cell cytoplasm. The meronts of *Spraguea* usually reside and replicate in the fiber next to the neuronal cell body; infrequently, the meronts locate in more distal positions in the fiber. Current investigations are in search of the motor that transfers the sporoplasms or developing meronts from the skin, up the fiber, toward the cell body.

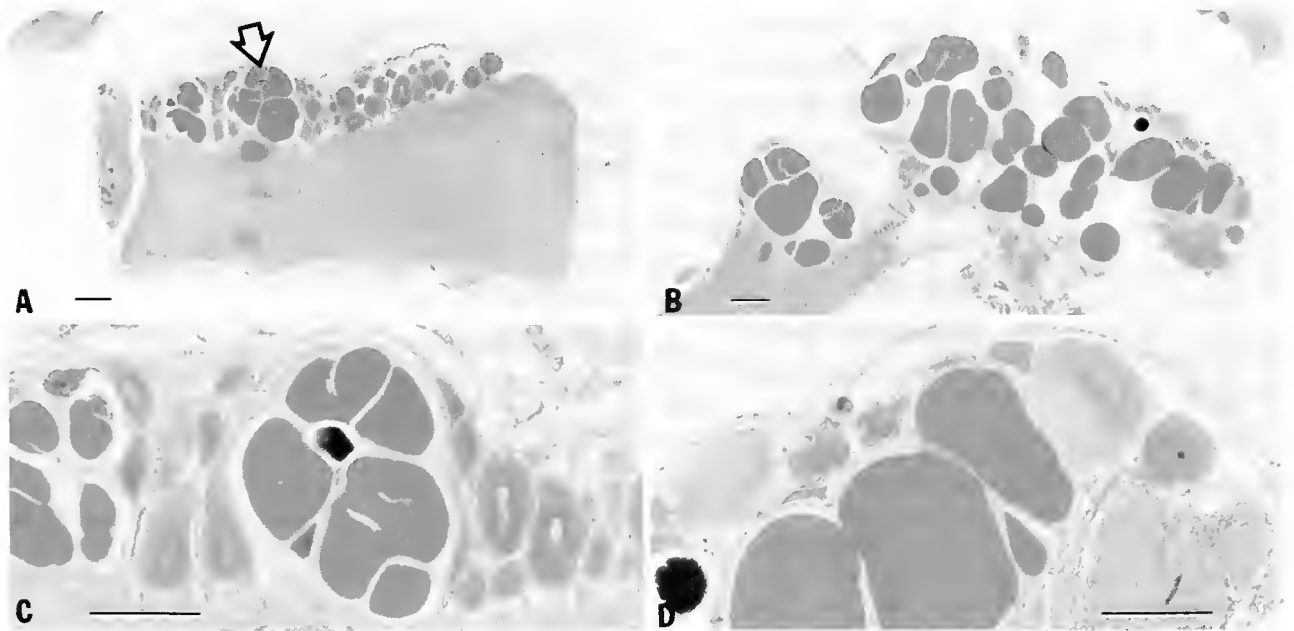


Figure 1. Supramedullary Cells (SMCs) with parasite colonies. (A) Arrow indicates parasite colonies in a light infection of SMCs. (B) SMCs from fish with a heavy infection. (C & D) Lightly magnified view of parasite colonies in SMCs. Note that colony in D adjoins neuron cell body. Bar scale represents 400 μ m.

Literature Cited

1. Fanakoshi, K., T. Abe, and R. Kishida. 1995. *J. Comp. Neurol.* **358**: 552–562.
2. Canning, E. U., and J. Lom. 1986. *The Microsporidia of Vertebrates*. Academic Press, London.
3. Williams, J. H., G. S. Gill, and W. Trager. 1995. *Proc. Natl. Acad. Sci. USA* **92**: 566–568.
4. Weidner, E. 1976. *J. Cell Biol.* **71**: 23–34.

Reference: *Biol. Bull.* **195**: 228–229. (October, 1998)

Initial Baseline Blood Chemistry of the Oyster Toadfish, *Opsanus tau*

Maureen D. O'Neill¹, Heather M. Wesp², Allen F. Mensinger (Washington University School of Medicine, St. Louis, Missouri), and Roger T. Hanlon¹

Blood chemistry is commonly used to explore the dynamics of health in captive animals in biomedical facilities. Yet, studies of blood serum chemistry in teleost fish are almost nonexistent (1). Such information would be beneficial in determining the baseline health and physiology of captive animals. Physiological assays would allow pre-screening of experimental subjects and decrease the loss of time, effort, and animals by indicating which fish are most suited to survive the rigors of surgery, experimentation, and long-term maintenance. In mariculture, early indication of disease or infection would allow therapeutic measures to be taken to alleviate adverse conditions and resultant death or disease. The oyster toadfish, *Opsanus tau*, is a valuable vertebrate model for biomedical research (2, 3), but little is known about its blood chemistry. This study's objective is to establish some initial baseline values for blood parameters that may be important in understanding the health of the captive toadfish.

Male and female toadfish of various sizes (200–1200 g; 18–33 cm—standard length) were selected from the holding tanks in the Marine Resources Center (MRC) of the Marine Biological Laboratory. Selection was based on the alertness (erect fin position), integument appearance, and regular respiration of the fish—the same characteristics investigators currently use to choose toadfish for experiments. Blood was collected in July 1997 ($n = 20$), and June 1998 ($n = 40$), between 0800 and 1000 h. from recently captured fish that had been acclimated for 1–2 weeks in MRC holding tanks. These fish were taken from the general population in the holding tanks, and therefore their health status was unknown. Consequently, any fish that died within 45 days of the initial blood sampling (less than 10%) were excluded from the study. Within 15 min after the fish were anesthetized in a 0.001% solution of MS-222 (tricaine methanesulfonate), blood was drawn by caudal puncture. A 3-ml heparinized syringe and a 25-gauge needle were used to extract 1–3 ml of mixed arterio-venous blood. Each fish was then weighed, measured, sexed, and tagged with an Avid radio tag. Only one blood sample was taken from each fish.

The percentage of the blood volume composed of red blood cells (hematocrit) was determined by transferring a portion of each blood sample directly from the syringe into capillary tubes, which were centrifuged and then read using a Monoject Scientific Crito-caps micro-hematocrit capillary tube reader. The remaining blood

was placed in microcentrifuge tubes and centrifuged in an Eppendorf Centrifuge 5402 for 10 min at 4°C at 10,000 rpm. In 1997, a DadeAnalyst benchtop chemistry system was used to analyze the blood serum for blood urea nitrogen (BUN), cholesterol, calcium, aspartate aminotransferase (GOT), and alanine aminotransferase (GPT). In 1998, a DU-640 Beckman spectrophotometer was used to analyze samples for BUN, cholesterol, and glucose using diagnostic kits (Sigma). Blood serum was then frozen at -80°C to be tested later in 1998 for corticosteroid levels.

The results of these analyses (Table I) illustrate a range of baseline blood chemistry values for the captive oyster toadfish during the summer months of June and July. Excretory function was monitored by BUN, digestive function by cholesterol and glucose, reproduction activity by calcium, liver function by GOT and GPT, and respiratory function by red blood cell volume percentage (hematocrit). Tests for gamma-glutamyl transpeptidase (GGT), amylase, uric acid, creatine, and bilirubin fell below the minimum range of the DadeAnalyst system. Values for parameters affected by feeding may be variable due to the lack of information of the feeding schedules of toadfish kept in the MRC holding tanks.

Previous published studies show a wide range of blood chemistry values for toadfish. The BUN value, 8.4 ± 0.8 mg/dl ($n = 48$), of the present study was only slightly elevated from the 8.1 ± 1.3 mg/dl that was reported for the gulf toadfish (*Opsanus beta*) (4). The cholesterol value of 116.3 ± 5.1 mg/dl ($n = 47$) differs from the 302 ± 23 mg/dl ($n = 70$) found in the Spanish toadfish, *Halobatrachus didactylus* (5). Chavin and Young (6) reported a mean glucose value for *Opsanus tau* of 30 mg/dl ($n = 57$) with a range of 58.0 mg/dl, which was consistent with our present values. Rosety *et al.* (7) reported a calcium value of 9.9 ± 0.4 mg/dl for *H. didactylus* males during the reproductive period, which deviated little from the 9.6 ± 0.3 mg/dl ($n = 17$) found in the present study for *Opsanus tau*.

The discrepancies between our results and those published previously may be explained by differences in variables such as species, age, reproductive factors, season, location, experimental conditions, and analytical procedures. Therefore, our goal is to establish year-round values for this species of toadfish. A long-term study of the effects of stocking densities on blood chemistry would provide greater insight into seasonal changes. Seasonal differences in blood chemistry due to winter hibernation and reproduction have been recorded by Munoz-Cueto *et al.* (5). Influences from laboratory conditions such as overcrowding are known to affect blood chemistry values (8), and these effects should be explored in the future.

We would like to thank Stephen M. Highstein, Roxanne M.

¹ Marine Biological Laboratory, Woods Hole, Massachusetts 02543.

² Hope College, Holland, Michigan 49423.

Table 1

Blood chemistry values measured for the oyster toadfish, *Opsanus tau*, in July 1997 and June 1998

Parameter	1997	1998	Combined
BUN (mg/dl)	6.8 ± 0.8 (n = 17) (2.1–13.7)	9.3 ± 1.2 (n = 31) (1.2–26.3)	8.4 ± 0.8 (n = 48) (1.2–26.3)
Cholesterol (mg/dl)	123.6 ± 8.2 (n = 16) (69–202)	112.6 ± 6.5 (n = 31) (53.3–195.4)	116.3 ± 5.1 (n = 47) (53.2–202)
Hematocrit (%)	30.9 ± 3.6 (n = 16) (13–57.5)	24.7 ± 1.0 (n = 34) (13–33.5)	—
Calcium (mg/dl)	9.6 ± 0.3 (n = 17) (8.5–12.8)	9.3 ± 0.3 (n = 17) (7.6–11.8)	9.5 ± 0.2 (n = 34) (7.6–12.8)
GOT (U/l)	33.5 ± 4.8 (n = 16) (13.0–84.0)	2.68 ± 1.8 (n = 17) (10–40)	30.1 ± 2.6 (n = 33) (10–84)
Glucose (mg/dl)	Not Determined	27.3 ± 1.4 (n = 31) (11.6–44.9)	—
GPT (U/l)	Not Applicable* (<5–14.00)	8.9 ± 0.3 (n = 18) (7–11)	—

The data represent the mean ± standard error, with sample size (n) in parentheses and the range listed below. On the basis of the Student's *t* test, data for BUN, cholesterol, calcium, and GOT were not significantly different between 1997 and 1998 ($P > 0.10$) and thus could be combined for the two years; for hematocrit, 1997 and 1998 values were significantly different ($P < 0.05$) and could not be combined.

* Mean and standard error are not available for GPT in 1997 because about 50% of the samples fell below the minimum range of the DadeAnalyst. Initial summer 1997 tests for GGT and amylase (<5 U/l), uric acid (<1.0 mg/dl), creatine (<0.2 mg/dl), and bilirubin (<0.1 mg/dl) also fell below the minimum range.

Smolowitz, Patrick J. Walsh, Michael K. Stoskopf, J. Hanley, W. Mebane, G. Till, and Seth Ament for their contributions to this project. This experiment was funded by the Five-College Coastal and Marine Science Summer 1997 Scholarship, NSF grant NSFDBI-9605155, the NASA Life Science Fellowship, NIH grant PO1-DC01837-05, NSF grant AD93-0LMSA, and NASA grants 088 and NAG2-945-97-233.

Literature Cited

1. Stoskopf, M. K. 1993. Page 127 in *Fish Medicine*. W. B. Saunders, Philadelphia.
2. Mensinger, A. F., J. Carey, R. Boyle, and S. M. Highstein. 1997. *J. Comp. Neurol.* 384: 71–85.
3. Highstein, S. M., R. Kitch, J. Carey, and R. Baker. 1992. *J. Comp. Neurol.* 319: 501–518.
4. Walsh, P. J., E. Danulat, and T. P. Mommsen. 1990. *Mar. Biol.* 106: 323–328.
5. Munoz-Cueto, J. A., M. Alvarez, M. Blanco, M. L. Gonzalez de Canales, A. Garcia-Garcia, and C. Sarasquete. 1996. *Sci. Mar.* 60: 289–296.
6. Chavin, W., and J. E. Young. 1970. *Comp. Biochem. Physiol.* 33: 629–653.
7. Rosety, M., M. Blanco, M. L. Gonzalez de Canales, A. Grau, and M. C. Sarasquete. 1992. *Sci. Mar.* 56: 87–94.
8. Walsh, P. J., and C. L. Milligan. 1995. *J. Exp. Biol.* 198: 1559–1566.

Reference: *Biol. Bull.* 195: 229–231. (October, 1998)

Pseudomonas putida Infections of the Oyster Toadfish (*Opsanus tau*)

Roxanna Smolowitz (Laboratory for Aquatic Animal Medicine and Pathology [LAAMP], U. of Penn., Marine Biological Laboratory, Woods Hole, Massachusetts), Elizabeth Wadman¹, and H. M. Chikarmane²

The oyster toadfish, *Opsanus tau*, is an important laboratory animal used in the study of diabetes, muscle physiology, sound reception, and equilibrium. Toadfish are collected from estuaries surrounding Woods Hole, Massachusetts, and maintained in the seawater tanks at the Marine Resources Center (MRC) at the

Marine Biological Laboratory. Unfortunately, because these fish are collected from the wild and are held in a flow-through salt-water system, they may harbor or be exposed to infectious agents before or during utilization in research.

During the period from August 1997 to March 1998, 17 of about 50 toadfish from two experimental tanks at the MRC developed *Pseudomonas putida* infections. *Pseudomonas* sp. are normal inhabitants of fresh and salt water and tend to cause disease in fish under "stress" (1). They have only rarely been

¹ LAAMP.

² MBL.

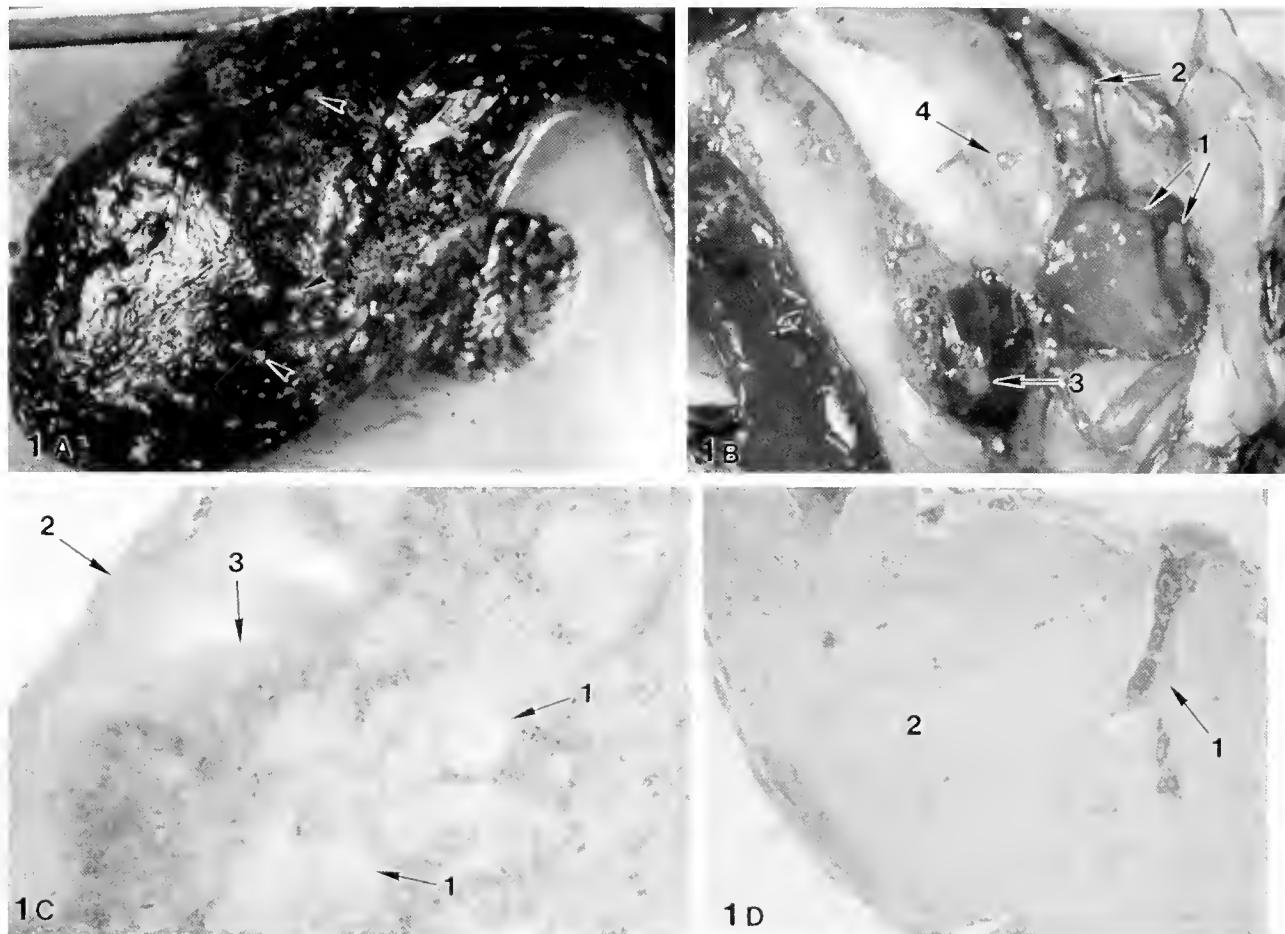


Figure 1. Clinical and microscopic appearance of *Pseudomonas putida* infection in laboratory-held *Opsanus tau*. (A) Multifocal beads of mucus are present over the dorsal and lateral body surfaces of this specimen (arrowheads). (B) The open peritoneal cavity of the toadfish shows foci of inflammation in the accessory sex gland (1), testis (2), spleen (3), and on the surface of the edematous swim bladder (4). (C) In the spleen were foci of tissue necrosis with macrophagic and heterophilic inflammation containing abundant bacteria (1). Inflammation covered the serosal surface of the spleen (2), and the capsule was irregular in shape (3). (Paraffin section stained with hematoxylin and eosin.) (D) Inflammation (1) associated with the liver capsule tracked with the trabeculae of the capsule into the parenchyma of the liver (2). (Paraffin section stained with hematoxylin and eosin.)

identified as a cause of disease in fish in the wild (2). *Pseudomonas* sp. infections have been identified in other fish species, both from fresh water and from salt water, but not in *Opsanus tau*. The study in which these fish had been used attempted to create a stressed and a non-stressed environment. It is not known if the tank simulating the non-stressed conditions truly eliminated stress or if the fish it held were being subjected to other important medical or potentially stressful conditions such as proximity of healthy to infected fish, colonization of the tank with *Pseudomonas* sp., or either water temperatures or reproductive activity that depressed the immune system of the fish.

Animals affected by this disease were adults averaging 33 cm in length and 800 g in weight. An abnormality observed upon necropsy (5 of 17 animals) was the occurrence of multifocal beads of mucus over the dorsal and lateral body surfaces (Fig. 1A). The external surface of 6 of 17 animals was covered with abundant thick mucus. Gill filaments were meaty and also pro-

fusely covered with mucus. Internally, the peritoneal surfaces were thickened and dull (normally these surfaces are thin and shiny), indicating peritonitis, which was confirmed histologically. White/tan, flocculent to fluid exudate was visible grossly in the peritoneal cavities of 8 of 17 fish. The splenic outline was botryoid, with foci of small white nodules visible in the dark red parenchyma (diameter <1 to occasionally 3 mm). Only rarely were small white/tan nodules noted in the liver or kidney parenchyma. In 7 of the 11 male fish examined, the accessory sex glands contained white/tan nodules and stripes (Fig. 1B). A similar finding was often present in the male gonads. White/tan nodules were seen in the gonads of 2 of 3 females. The swim gland rete was congested, edematous, and reddish brown in 7 of 17 animals.

Histopathologic examination of tissue sections stained with hematoxylin and eosin (3) showed a severe, diffuse, macrophagic bacterial peritonitis. Multifocally in the kidney, spleen

(Fig. 1C), swim bladder gland, muscle, ovary, intestinal serosa, mesenteries and subcutis, and dermis were areas of tissue necrosis containing abundant, predominately macrophagic inflammatory cells. Bacteria were easily identified in the macrophages. These inflammatory foci formed the white/tan nodules noted grossly in the organs. In some foci, the inflammation was organized into granulomas. Rarely were nodules of inflammatory necrosis seen in the parenchyma of the liver. More frequently, inflammation associated with the liver capsule tracked with the trabeculae of the capsule into the parenchyma of the liver (Fig. 1D). Multifocally, the accessory sex gland and the male gonad showed inflamed septal walls and lumens filled by inflammatory exudate full of bacteria. In many foci of the secondary gill lamellae, severe inflammation consisting of macrophages, lymphocytes, heterophils, and proliferative chloride, mucus and gill epithelial cells expanded the lamellae, sometimes resulting in adhesion of adjacent secondary lamellae. Evaluation of blood smears demonstrated an increase in the circulating monocytes of the blood (monocytosis) (44%–50%; normal, 1%–4%) (4). Bacteria were commonly present in monocytes identified in Giemsa-stained blood smears from these animals.

Pseudomonas sp. was identified from 10 toadfish: traditional biochemical methods of identification were used in 6 cases and visual examination of cultures in the other 4 cases. Bacterial cultures were not taken from severely autolyzed animals. Using the MIDI System to analyze phospholipid-linked fatty acids from the isolates of 4 of the fish resulted in identification of

three isolates as *Pseudomonas putida* and one isolate as *P. fluorescens*. Random amplified polymorphic DNA (RAPD) fingerprinting of all 4 isolates (5), using four different primers, showed identical polymerase chain reaction (PCR) amplification profiles, demonstrating that the isolates were clonal and most likely *P. putida*.

The toadfish used in this study were affected with a subacute to chronic bacterial disease that resulted in mortality in fish from both stressed and non-stressed environments. The origin of the *Pseudomonas putida*, the cause of this disease, is not known. It is important that disease be recognized in laboratory animals, including toadfish, because its effects not only are detrimental to the infected animal but can significantly affect the results of the study in which the animal (or its parts) is used.

Literature Cited

1. Noga, E. 1996. Pp. 160–161 in *Fish Disease Diagnosis and Treatment*. Mosby-Year Book, St. Louis, MO.
2. Post, G. 1983. Pp. 41–44 in *Textbook of Fish Health*. TFH Publications, Neptune City, NJ.
3. Humanson, G. L. 1962. Pp. 3–126 in *Animal Tissue Techniques*. W. H. Freeman, San Francisco.
4. Shapiro, L., R. A. Bullis, and R. M. Smolowitz. 1997. *Biol. Bull.* 193: 272.
5. Williams, J. G., A. R. Kubelik, K. J. Livak, J. A. Rafalski, and S. V. Tingey. 1990. *Nucl. Acids Res.* 18: 6531–6535.

Preliminary Evaluation of Sedimentation Rates and Species Distribution in Plum Island Estuary, Massachusetts

Catherine Schmitt¹, Nathaniel Weston, and Charles Hopkinson (The Ecosystems Center, Marine Biological Laboratory, Woods Hole, Massachusetts 02543)

Tidal salt marshes exist in estuaries throughout the temperate zone of the world. Their presence in the future is threatened by accelerating rates of sea level rise associated with the temperature increases predicted by models of global climate change. In northern Massachusetts, sea level has been increasing at a rate of about 2.4 mm yr⁻¹ since 1921 (calculated from data obtained from National Ocean Survey/NOAA Boston tide gauges). If marshes are to remain common features of the coastline, salt marsh accretion must occur at rates greater than the rising sea. Marshes can increase in elevation by the accumulation of plant material within the sediment profile and by the deposition of organic and mineral matter on the surface. Deposition requires the availability of suspended material and a transport mechanism, such as tides and floods, to distribute the material onto the marsh surface (1). The importance of these processes is likely to vary along a range of elevations that determines both the frequency and duration of tidal inundation and the distribution of plant species. Here we report measures of deposition, elevation, and species distribution in salt marshes of the tidal Rowley River in the estuary of Plum Island Sound, Massachusetts.

Five 150–250-m transects were established across Rowley River salt marshes that varied in elevation, species composition, flooding frequency, and distance from the ocean and from freshwater inputs. We measured variables at three sites representative of the range of elevation and species along each transect. Relative elevation for each site was determined by measuring water depth at high tide. Short-term sedimentation rates were estimated by deploying three sets of ashed, pre-weighed 9-cm glass-fiber filters placed on inverted petri dishes secured to the marsh surface at each site from 17 June to 14 July 1998. Filters were collected every two weeks; dry weight was determined after drying at 60°C (1, 2, 3) and organic matter content by dry weight loss on ignition (4). The weight of salt has not been accounted for, so results represent maximum deposition (3). We used duplicate quadrats at each site on 1 July to measure the species composition, density, and biomass of marsh vegetation (5). We also determined bulk density and organic matter content of sediment by loss on ignition from 50-cm cores collected at each site.

The relative elevation range of the sites was 85 cm. Deposition rates decreased with increasing elevation (Fig. 1a). Sites with *Spartina alterniflora* had higher sedimentation rates (Fig. 1b), were significantly lower in elevation (Fig. 1c), had lower percentages of organic matter in the sediment deposited (Fig. 1d), and lower stem densities than sites dominated by *Spartina patens* ($P < 0.01$). The average biomasses were 490 g and 539 g

dry weight m⁻² for *S. alterniflora* and *S. patens*, respectively, but were not significantly different. The bulk density of the sediments averaged 0.247 g cm⁻³ in the *S. alterniflora* sites and 0.294 g cm⁻³ in the *S. patens* sites ($P = 0.06$). The organic content to a depth of 50 cm averaged 23% in the *S. alterniflora* sites and 31% in the *S. patens* sites. We did not find a significant effect of distance from the ocean or from freshwater inputs on sedimentation rates.

Marsh elevation determines the frequency and duration of flooding. Flooding transports suspended material onto the marsh surface, and also influences the distribution of plant species (1, 6, 7). The species distribution observed along the elevation gradient is similar to that reported for other salt marsh systems (8). We found that areas of low relative elevation (and therefore frequent flooding) had lower stem densities and higher sedimentation rates (Fig. 1a). Although high stem densities slow the flow of water over the marsh surface, which should increase sediment deposition (6), our observations show that the denser

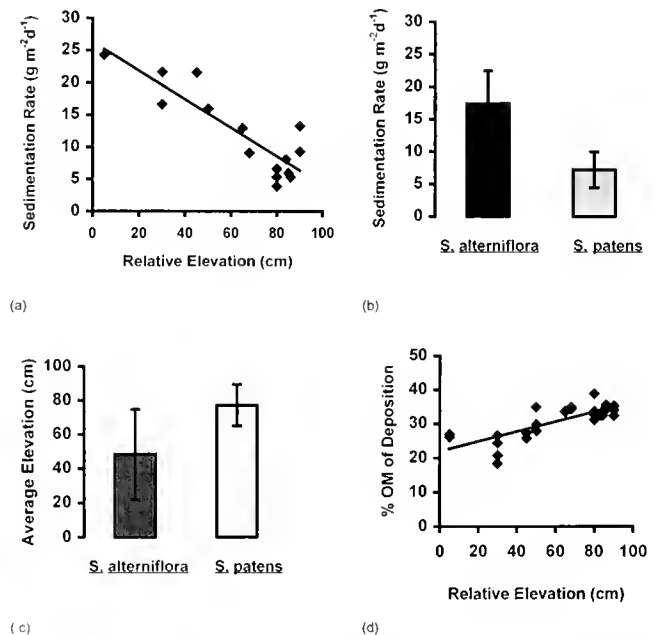


Figure 1. Elevations are relative to the elevation of the site flooded to the greatest depth. (a) Relationship between short-term measures of sedimentation (g dry weight m⁻² d⁻¹) and marsh elevation along Rowley marsh transects. $R^2 = 0.7678$, $P < 0.01$. (b) Average sedimentation rates in marshes with different species composition. $P < 0.01$. (c) Average elevation of marshes with different species composition. $P < 0.01$. (d) Percentage of organic matter in the sediment deposited on filters on the marsh surface at different elevations. $R^2 = 0.6297$, $P < 0.01$.

¹ University of Massachusetts, Amherst, Massachusetts 01003.

S. patens sites had lower sedimentation rates. Because of their higher elevations, the sites dominated by *S. patens* were subject to less frequent and shorter periods of flooding, and therefore had less opportunity to receive suspended material. Both the percentage of organic matter deposited and the sediment content of organic matter to a depth of 50 cm increased with elevation. Not only is sediment less available to these higher sites, but inorganic constituents are heavier and fall out of suspension before flooding reaches the elevation of the high marsh (8). The high marsh sites have a higher percentage of organic matter below the surface because they are accumulating peat (8), and the sediment deposited on the surface is mostly organic.

The sedimentation patterns we have observed give a brief picture of a two-month period. Factors not within the scope of our study, such as marsh microtopography, seasonal storm events, and mussel densities may also influence marsh sedimentation. Our estimates of sedimentation rates for this period indicate that elevation (or flooding frequency) is the most significant factor in determining the rate of sedimentation in salt marshes of the Rowley River. At first, these results seem to suggest that marshes will always be able to keep up with a rising sea level

because they will become lower in elevation and will thus be flooded more frequently. However, determining whether there will be a sufficient supply of sediment for salt marshes to rise at the same pace as the sea requires further investigation.

This work was funded by the Woods Hole Marine Sciences Consortium, the Plum Island Sound LTER NSF #OCE-9726921, and the Sweetwater Trust. Special thanks to Sarah Turner and Simon Punal for their assistance.

Literature Cited

1. Reed, D. 1989. *Estuaries* 12: 222–227.
2. Reed, D. 1992. *Environ. Manage.* 16: 55–65.
3. Hensel, P. F., J. W. Day, Jr., D. Pont, and J. N. Day. 1998. *Estuaries* 21: 52–65.
4. Wetzel, R. G., and G. E. Likens. 1991. P. 338 in *Limnological Analyses*, Second Edition. Springer-Verlag, New York.
5. Morris, J. T., and B. Haskin. 1990. *Ecology* 71: 2209–2217.
6. Leonard, L., and M. Luther. 1995. *Limnol. Oceanogr.* 40: 1474–1484.
7. Rozas, L. P. 1995. *Estuaries* 18: 579–590.
8. Redfield, A. C. 1971. *Ecol. Monogr.* 42: 201–237.

Reference: *Biol. Bull.* 195: 233–234. (October, 1998)

Dependence of Herbivory on Autotrophic Nitrogen Content and on Net Primary Production Across Ecosystems

Martin P. A. Griffin, Marci L. Cole, Kevin D. Kroeger, and Just Cebrian (Boston University Marine Program, Marine Biological Laboratory, Woods Hole, Massachusetts 02543)

To determine what factors control the abundance of herbivores in an ecosystem (1), and thus the effects these consumers have on autotrophic biomass (2), we must first understand why and how much herbivory differs among ecosystems. Previous reports suggest that ecosystems dominated by richer autotrophs (*i.e.*, those with a higher nutrient content) support higher rates of herbivory (2) and that the same is true for more productive ecosystems (1,3). If ecosystems composed of richer autotrophs are indeed subject to higher herbivory rates, the association between net primary production (NPP) and herbivory across ecosystems may point to a contradiction, because more productive ecosystems are not necessarily dominated by autotrophs with higher nutrient contents (4). For instance, although forests and phytoplanktonic communities may reach similar values of NPP, they are dominated by autotrophs with contrasting nutrient contents (5). Therefore, the interaction between NPP and autotrophic nutrient content in controlling herbivory in ecosystems needs to be further explored and clarified.

Here, we investigate, through a compilation of published data, the relationship between NPP, autotrophic nitrogen content, and herbivory across different types of ecosystems. We chose nitrogen because it is the nutrient most frequently reported in the literature. All the reports compiled met these requirements: first, they were representative of the ecosys-

tem considered—that is, they included the dominant autotrophs and herbivores (>75% of total abundance) in the ecosystem; second, they were annual or exceeded the growing period for seasonal producers; and finally, they referred only to natural conditions. Some reports of macrophyte-dominated ecosystems included only the above-ground compartment, but the patterns obtained overrode this variability. NPP and herbivory rates were expressed as grams of carbon per square meter per day, and autotrophic nitrogen concentration was expressed as percent dry weight. In some reports these units were derived by using standard conversion factors. The data set used is available from the first author. Relationships between variables were examined with least-square regression techniques. Variables were log-transformed to remove heteroscedasticity.

NPP is unrelated to autotrophic nitrogen content across ecosystems (Fig. 1a). This finding shows that, as suggested by previous reports (4), across ecosystems the magnitude of NPP is independent of its quality to herbivores (*i.e.*, nitrogen content). We further show that ecosystems composed of richer autotrophs lose a higher percentage of NPP to herbivores (Fig. 1b). This tendency indicates that herbivore feeding rates in ecosystems are limited by the nitrogen content of the dominant autotrophs. Hence, ecosystems composed of richer autotrophs have enhanced rates of herbivore feeding

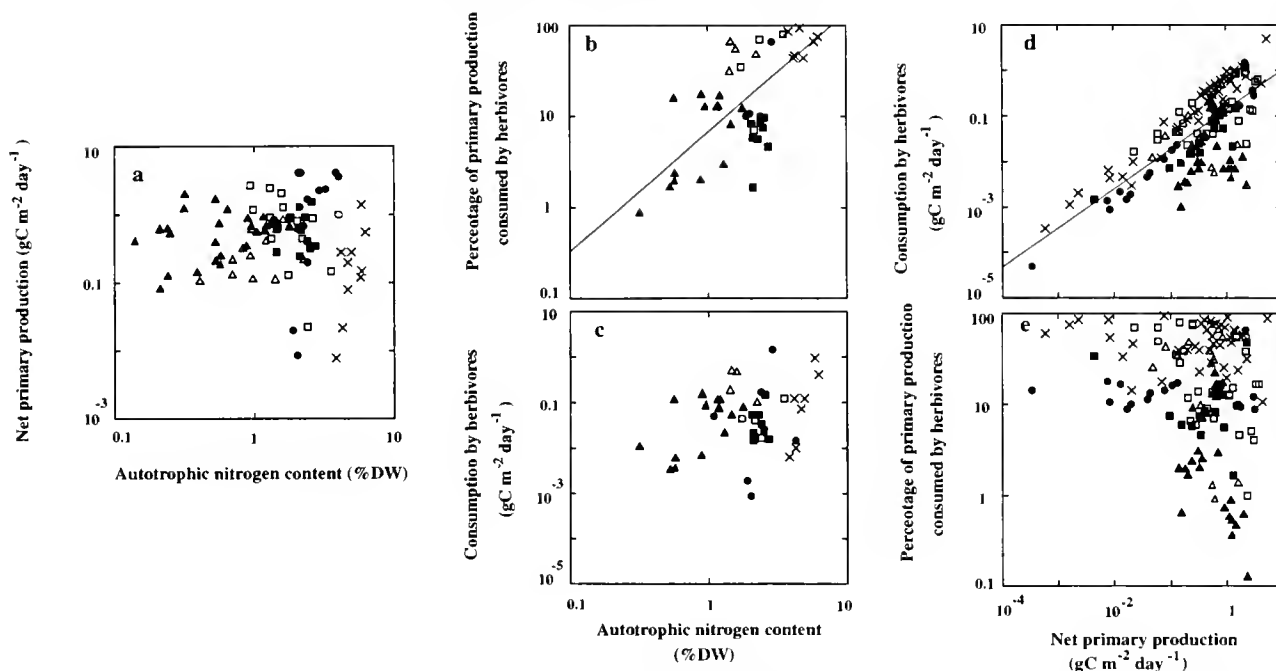


Figure 1. Relationships between pairs of variables across the range of ecosystems for which data were compiled. Symbols denote phytoplanktonic and microphytobenthic communities (\times), benthic macroalgal beds (\bullet), seagrass meadows (\blacksquare), salt and freshwater marshes (\square), grasslands (Δ), and shrublands and forests (\blacktriangle). Lines correspond to the regressions adjusted. (a) Net primary production versus autotrophic nitrogen content ($r^2 = 0.02$, $n = 87$, F ratio = 0.03, $P = 0.86$) (b) Percentage of production consumed by herbivores versus autotrophic nitrogen content (log percentage consumed = $0.82 (\pm 0.09) + 1.3 (\pm 0.2) \log$ nitrogen content, $r^2 = 0.43$, $n = 41$, F ratio = 31.6, $P < 0.01$) (c) Absolute consumption by herbivores versus autotrophic nitrogen content ($r^2 = 0.07$, $n = 43$, F ratio = 4.3, $P = 0.046$) (d) Absolute consumption versus NPP (log absolute consumption = $-0.90 (\pm 0.06) + 0.84 (\pm 0.06) \log$ NPP, $r^2 = 0.54$, $n = 147$, F ratio = 169.9, $P < 0.01$) (e) Percentage of production consumed versus NPP ($r^2 = 0.04$, $n = 147$, F ratio = 6.4, $P = 0.01$).

and, as a consequence, lose larger percentages of NPP. This reveals that autotrophic nitrogen content is a major control of herbivory in ecosystems and overrides differences in herbivore characteristics (such as migratory vs. resident behavior or dissimilar metabolic constraints) among ecosystems (6).

Because ecosystems composed of richer autotrophs lose a higher percentage of NPP to herbivores (Fig. 1b) but reach relatively similar values of NPP (Fig. 1a), it would seem that they would also support a higher absolute consumption (in $\text{g C m}^{-2} \text{ day}^{-1}$) by herbivores. However, we found that absolute consumption is poorly ($r^2 = 0.07$), albeit significantly ($P = 0.046$), related to autotrophic nitrogen content across ecosystems (Fig. 1c). Instead, absolute consumption is associated with NPP, as indicated by previous results (1) and generalized here for a broader range of ecosystems (Fig. 1d). Absolute consumption is the product of NPP and the percentage of NPP consumed by herbivores. Among ecosystems, NPP varies by four orders of magnitude, whereas the fraction of NPP consumed varies by less than three (Fig. 1e). Consequently, the variability in absolute consumption among ecosystems is mostly dictated by the variability in NPP (Fig. 1d). This tendency combined with the finding that ecosystems with similar values of NPP differ remarkably in their autotrophic nitrogen contents (Fig. 1a) explain why absolute consumption and autotrophic nitrogen content are poorly related across ecosystems (Fig. 1c).

Our results clarify the role and interaction of NPP and autotrophic nitrogen content as controls of herbivory in ecosystems. If herbivory is regarded as percentage of NPP consumed, differences among ecosystems are related to differences in autotrophic nitrogen content, probably because higher nitrogen contents enhance herbivore feeding rates. On the other hand, when herbivory is regarded as absolute consumption, differences among ecosystems are associated with differences in NPP, because NPP variability among ecosystems overrides any enhancement of herbivore feeding rate that is caused by a higher autotrophic nitrogen content.

Literature Cited

1. Cyr, H., and M. Pace. 1993. *Nature* 361: 148–150.
2. Cebrian, J., and C. M. Duarte. 1994. *Funct. Ecol.* 8: 518–525.
3. McNaughton, S. J., M. Oesterheld, D. A. Frank, and K. J. Williams. 1989. *Nature* 341: 142–144.
4. Borum, J., and K. Sand-Jensen. 1996. *Oikos* 76: 406–410.
5. Whittaker, R. H., and G. E. Likens. 1973. Pp. 281–302 in *Carbon in the Biosphere*, G. M. Woodwell and E. V. Pecan, eds. National Technical Information Service, New York.
6. Crawley, M. J. 1983. *Herbivory: The Dynamics of Animal-Plant Interactions*. University of California Press, Los Angeles, 437 pp.

Reference: *Biol. Bull.* **195**: 235–237. (October, 1998)

Interaction of Nitrogen Supply, Sea Level Rise, and Elevation on Species Form and Composition of Salt Marsh Plants

Jennifer Rogers¹, Jennifer Harris², and Ivan Valiela (Boston University Marine Program, Marine Biological Laboratory, Woods Hole, Massachusetts 02543)

Supply of nitrogen (1), elevation within the intertidal range (2), and changes in sea level (3) are among the many factors that structure the vegetation of salt marshes. Here, we examine interactions between these three factors in long-term experimental plots maintained in Great Sippewissett Marsh since 1970 (1).

The vegetation of Great Sippewissett Marsh is dominated by *Spartina alterniflora* and a few other species. The distribution of forms of *S. alterniflora* varies along the intertidal gradient in salt marshes, with the shorter forms found above creek banks on the high parts of the marsh and the taller form lower in the intertidal and along creek banks. The intermediate form lies between the short and tall forms in the marsh. The higher parts of the marsh support a few other species including *Spartina patens*, *Distichlis spicata*, *Salicornia europaea*, and *Iva frutescens*.

There were changes in the relative abundance of the forms of *S. alterniflora*, as well as shifts in species cover, from 1976 to 1992, in experimental salt marsh plots subject to nutrient additions (3,4). In this paper we examine changes in the cover of the three forms and in the overall species composition in these plots to determine what long-term changes have occurred since the earlier reports.

The effects of nitrogen supply were studied in replicate plots, 10 m in radius, that had been subjected to experimental enrichment since 1970 (3,4). Each year, fertilizer (a commercially available sewage-sludge-based material) was broadcast by hand every 2 weeks throughout the growing season, at dosages of 0.85 g m⁻² wk⁻¹ (LF), 2.5 g m⁻² wk⁻¹ (HF; urea), and 7.6 g m⁻² wk⁻¹ (XF). Untreated plots are referred to as C. These plots had been subjected to a chronic treatment that ran long enough to permit the expression of possible effects of changing sea level. Plots were situated at slightly different elevations, and we measured these elevations to ascertain their possible influence on the changes in vegetation.

Beginning in 1976, plots were mapped visually (4,5) to examine changes in vegetation. Visual estimates were well correlated with biomass measurements taken in separate 20-cm² plots to verify our visual assessments (Fig. 1, top left, $r^2 = 0.96$). The 10 experimental plots were mapped in mid-June 1998 by recording the position and extent of cover of either single species or mixtures within each square meter of each plot.

We mapped the patches of *S. alterniflora* (tall, intermediate, and short), *D. spicata*, *S. patens*, *S. europaea*, *I. frutescens*, and bare sediment. In patches with a mixture of species, we visually estimated the relative percent cover for each species. Maps

were scanned into a computer file, the area of each patch was measured, and the area for each taxon was summed for the whole plot. To determine differences in elevation between the plots, six to eight wooden stakes painted with colored glue that was soluble in water were driven into high marsh and low marsh areas of the plot, and three to four were placed outside of the plot. Tide heights were recorded as the height of glue removed by tidal water, to the nearest centimeter.

The data collected in 1998 shows that after 28 years of fertilization, the increased supply of nitrogen had changed the composition of the vegetation (Fig. 1, top right). At the lowest rates of nitrogen supply, *S. alterniflora* remained the dominant species, covering about 70% of the surface of the plots (Fig. 1, top right). In plots subjected to higher fertilization rates, the dominance of *S. alterniflora* was less marked, and other species, particularly *D. spicata*, covered larger proportions of the plots.

The relative cover by the forms of *S. alterniflora* also was changed by the different fertilization dosage. As fertilizer increased, the stands of *S. alterniflora* became transformed to the tall form (Fig. 1, bottom left), with very little of the short form remaining at the highest dosages.

Plots that were fertilized had elevations significantly higher than the surrounding marsh surface and the untreated plots (Fig. 1, bottom right). The pace of accretion, or turf-building, prompted by the XF treatment, more than compensated for the submergence caused by the rise in sea level. Examination of a vertical profile of sediments in the XF plots suggests that this accumulation is composed largely of thatch and detritus left by the high marsh plants rather than of undecomposed fertilizer (Valiela, pers. observ.).

Hersh (1996; ref 4) mapped the same plots, using methods similar to ours, and we combined our 1998 data with his results to obtain a long-term view of vegetation change under chronic nitrogen enrichment. The changes in species form and cover in the experimental plots since the treatments began result from interactions between sea level rise, plot elevation, and nitrogen supply.

In C plots, *S. alterniflora* showed a modest increase in percent cover, from 45% to 65% (Fig. 2, top right), which seems to have taken place mainly at the expense of cover by the high-marsh species, *D. spicata*. This shift may also have been caused by rising sea level during the 28 years of the fertilization experiments. More evidence of the effects of sea level rise can be seen in the relative proportion of cover among the forms of *S. alterniflora* in C plots (Fig. 2, top left): the tall form, characteristic of an ecophenotype that grows in creek banks (6), proliferated from minimal cover to about 20% cover by 1998. Sea level in the area rose 2.9 mm/yr (7). Keeping up with this rise would require an 8.1-cm increase in elevation of the marsh surface, a

¹ Lafayette College, Easton, Pennsylvania.

² Yale University, New Haven, Connecticut.

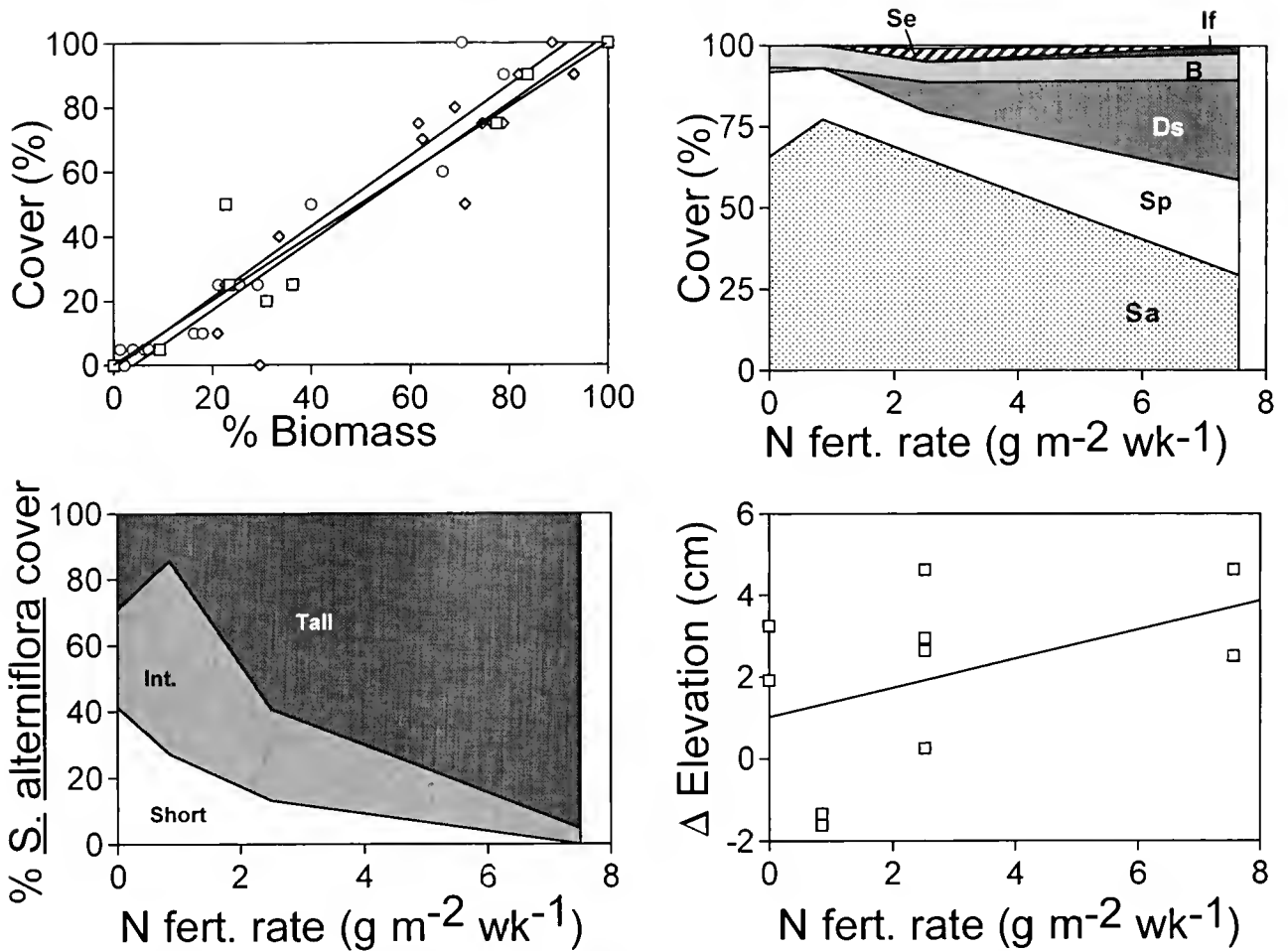


Figure 1. Left top: Percent biomass (determined as wet weight of the species divided by total wet weight) versus species cover as determined by visual estimation. The regressions for each species were statistically indistinguishable from each other ($\text{cover} = 1.001 \times \text{biomass} + 0.311$, $r^2 = 0.96^{**}$; $\text{cover} = 1.07 \times \text{biomass} - 4.105$, $r^2 = 0.91^{**}$; $\text{cover} = 1.100 \times \text{biomass} - 0.734$, $r^2 = 0.95^{**}$). Left bottom: Response of cover by the different species to increased nitrogen dosage. Sa = *S. alterniflora*; Sp = *S. patens*; Ds = *D. spicata*; B = bare sediment; If = *Iva frutescens*; Se = *S. europaea*. Right top: Percent cover of tall, intermediate, and short forms of *Spartina alterniflora* plotted versus rate of nitrogen enrichment ($\text{g m}^{-2} \text{wk}^{-1}$) in the 10 experimental plots of Great Sippewissett Marsh. Right bottom: Changes in elevation (inside plot - outside plot, for high-marsh and low-marsh areas within the plot) of the marsh surface in plots subjected to different nitrogen dosages.

change that seems large enough to prompt large changes in vegetation bands (3.8).

The fertilized plots (Fig. 2, left center and bottom) show larger changes from one year to the next, as though an increased supply of nitrogen, the element that is limiting to growth of marsh plants, augmented year-to-year changes among forms. Increased nitrogen supply, as in the HF and XF plots (Fig. 2, right middle and bottom), altered the long-term pattern of vegetation. The major effect was to reduce dominance of *S. alterniflora* and increase cover by *D. spicata*. The response by *D. spicata* apparently took place before 1976; this species seems to be an opportunist that responds rather quickly to increased nitrogen supply (3). In addition, the higher the rate of fertilization, the more the existing *S. alterniflora* was converted to the tall form (Fig. 2, left center and bottom). At the larger nitrogen dosages, the tall form became the dominant one, constituting

up to 90% of the cover of *S. alterniflora* that remained (Fig. 2, bottom left).

As sea level rise outpaced vertical accretion of marsh peat, the boundary between low-marsh and high-marsh vegetation may have shifted upslope (4), but only in the C plots. This shift did not occur in the HF plot, where some complex interaction between *S. alterniflora*, *S. europaea*, and bare space took place. By 1998, *D. spicata* began to take over bare space, replacing *S. europaea* (Fig. 2, center right). The XF treatment stimulated *D. spicata* to develop a thick thatch of dead material, which accumulated to raise the level of the plot (4).

The overall effects of higher nitrogen supply are that low-marsh plants are replaced by high-marsh plants; most of the *S. alterniflora* that remains becomes the tall form; and the shift in vegetation increases the level of the marsh surface. Nitrogen enrichment thus counters the effects of an increase in sea level

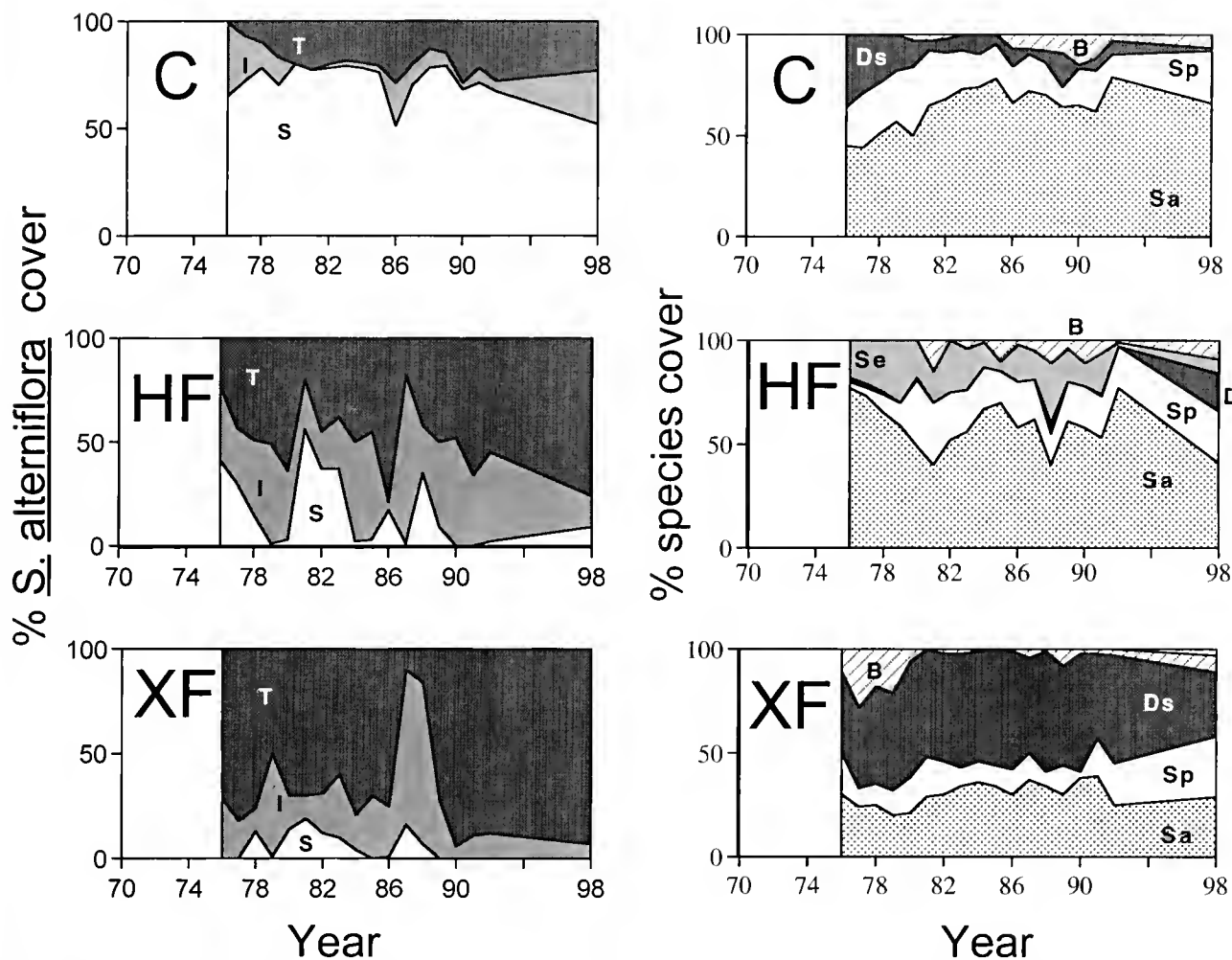


Figure 2. Long-term changes in the cover of different salt marsh plants in C (unfertilized), HF (intermediate fertilization), and XF (high fertilization) plots in Great Sippewissett Marsh. Fertilization was started in 1970; mapping began in 1976. No maps were done between 1993 and 1997. Pre-1998 data from Hersh (4). Left panels: Percent tall (T), intermediate (I), and short (S) *S. alterniflora* cover. Right panels: Changes in overall cover for the different species with increasing nitrogen supply. Sa = *S. alterniflora*; Sp = *S. patens*; Ds = *D. spicata*; B = bare sediment; I = *Iva frutescens*; Se = *S. europaea*.

by changing the species composition of marsh vegetation, and may allow salt marshes to persist even in situations of rising sea level.

This research was supported by an NSF Research Experience for Undergraduates grant. The order of first and second author of this paper was determined by lot.

Literature Cited

1. Valiela, I., B. Howes, R. Howarth, A. Giblin, K. Foreman, J. Teal, and J. Hobbie. 1982. Pp. 151–168 in *Wetlands: Ecology and Management*, B. Gopal, R. E. Turner, R. G. Wetzel, and D. E. Whigham, eds. National Institute of Ecology, Jaipur, India.

2. Day, J. W., Jr., and P. H. Temple. 1989. *Coastal Manage.* 17: 2412–257.
 3. Valiela, I., and C. Rietsma. 1995. *Oecologia* 102: 106–112.
 4. Hersh, D. A. 1996. *Abundance and Distribution of Intertidal and Subtidal Macrophytes in Cape Cod: The Role of Nutrient Supply and Other Controls*. Ph. D. Thesis, Boston University. 143 pp.
 5. Dethier, M. N., E. S. Graham, S. Cohen, and L. M. Tear. 1993. *Mar. Eco. Prog. Ser.* 96: 93–100.
 6. Valiela, I., J. M. Teal, and W. Deuser. 1978. *Am. Nat.* 112: 461–470.
 7. Nixon, S. W. 1982. *The Ecology of New England High Salt Marshes: A Community Profile*. U.S. Fish and Wildlife Service, Office of Biological Services, Washington, D.C.
 8. Niering, W. A., and R. S. Warren. 1980. *Bioscience* 30: 301–307.

Population Size and Site Fidelity of *Fundulus heteroclitus* in a Macrotidal Saltmarsh Creek

Jennifer Sweeney (Marine Biological Laboratory, Woods Hole, Massachusetts 02543),
Linda Deegan¹, and Robert Garritt¹

Fundulus heteroclitus (mummichog) is the numerically dominant fish species found in salt marshes from Florida to Nova Scotia. These areas exhibit a wide range of fluctuation in environmental conditions such as temperature, salinity, and tidal range. Mummichogs are known to be eurythermal and euryhaline, but there is little information about the influence of tidal range on population dynamics. Our purpose was to determine whether extreme tides (>3 m) in a tidal creek system would affect the population density and site fidelity of *F. heteroclitus*.

Both population density and site fidelity were measured by mark-recapture experiments in a primary saltmarsh creek (named here Sweeney Creek) off the Rowley River in Plum Island Estuary, a macrotidal (>3 m) estuary (Fig. 1). Both branches were approximately 300 m long from the confluence to the upland end. From 18 June to 31 July 1998, temperature (data logger), salinity (refractometer), and fish abundance were monitored. Six, 6.35-mm-mesh minnow traps were set in the center and randomly apart on both branches at around 180 m (East) and 120 m (West) from the confluence (Fig. 1). Specimens of *F. heteroclitus* ≥ 40 mm caught in the traps were counted and marked yellow (West) and blue (East) by injection of acrylic dye under the skin on the left dorsal side, then released. Population size was estimated using the Bailey model (1). Site fidelity was measured as the number of marked fish recaptured in different locations. Opposite-colored fish found in a marking zone were recorded and re-marked on the opposite dorsal side with the color of the branch in which captured. To determine how far and by what path fish moved, we set traps in three locations. In the secondary creek, two traps were set at five stations 22 to 106 m from the confluence. Nine traps were set in the mosquito ditches, and traps were set upstream of the marking locations. The pannes and secondary creek were also seined. Time intervals between mark and recapture were variable, averaging a 14.75 hour catch per unit effort.

Temperature and salinity were within the normal range for *F. heteroclitus*. Water temperature averaged 20°C at night and 26°C during the day for both branches. Salinity ranged from 8 to 25 ppt for the East branch, and 10 to 26 ppt for the West.

The population of the East branch is estimated to be 28,548 individuals (14.8 individuals in a square meter area), and the West branch 23,527 individuals (13.75 individuals per square meter). These estimates assume a closed population. Recapture rate was 16% for both creeks (East: 865 recaptured out of 4558 marked; West: 731 out of 3800 marked). The smaller number of individuals in the West branch may be due to the shorter length of this branch, a low tidal volume, and emigration.

Mummichogs in this macrotidal creek ranged farther than previous studies have suggested (2,3,4). Of the 2086 fish caught in the confluence/secondary, 21 were marked blue and 71 were marked yellow. This suggests that the fish traveled between 110 m and 320 m downstream to reach the confluence. Marked fish were found 335 m downstream from the confluence (Fig. 1), indicating that they traveled between 450 m and 650 m from the marking locations. In addition, opposite-colored fish were found in the marking areas of the branches. These fish traveled either by using the ditches (~132 m of travel) or by traveling to the confluence and back up (~300 m). Marked fish were also found in the traps set in the mosquito ditches. Of the 1112 fish captured, 37 were marked yellow, and 11 were marked blue. This suggests that they move between branches via the ditches.

Marked fish were found as far upstream as water was available and up on the marsh surface in pannes. Yellow-marked fish were found in pannes near the West branch. None were found in the pannes by the confluence.

F. heteroclitus has the ability to move farther up and down the creek system and onto the high marsh in macrotidal systems than in mesotidal systems, but it appears to be site specific. Lotrich (2,3) found a home range of ~36 m in mesotidal creeks of Delaware Bay. An earlier study by Butner and Brattstrom (4) in Long Island, New York, contradicts this information by concluding that there is not a definitive home range for *F. heteroclitus*. Chidester (5) discovered that members of the species are highly mobile in a New Jersey saltmarsh. Though these studies were done in lower tidal environments, the home range identified in our study (~650 m) is 17 times larger than the 36 m found in Delaware Bay (2,3) and supports the findings by Butner and Brattstrom (4) and Chidester (5).

The home-range expansion we observed may be due to the larger flux of water in the system and the strong current. It might not be energy efficient to oppose such a current.

¹The Ecosystems Center, Marine Biological Laboratory, Woods Hole, Massachusetts 02543.

Sweeney Creek

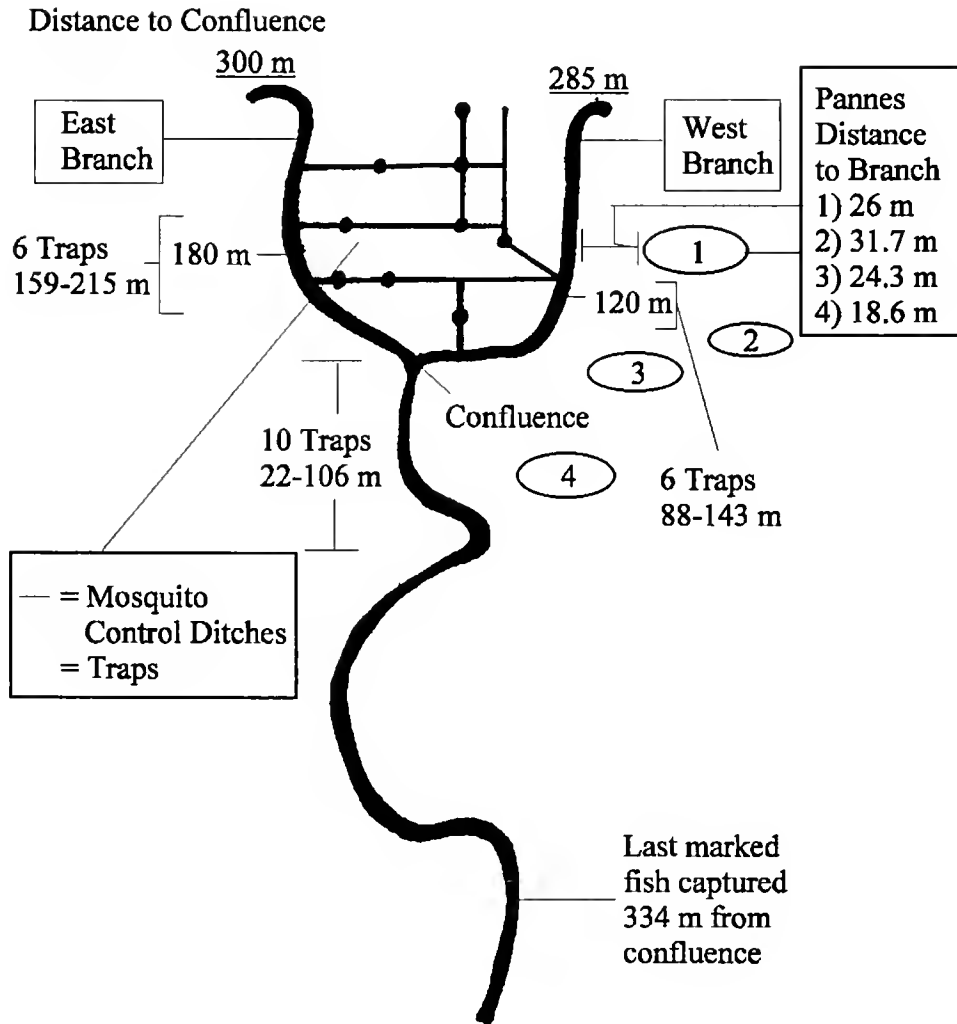


Figure 1. Map of Sweeney Creek showing the dimensions of the East and West branches and the locations at which fish were marked and recaptured.

Also, the population may be forced to leave the creeks because of factors such as lack of water, increased predation, season, and temperature. *F. heteroclitus* could be altering its behavior to fit the tidal environment and habitat.

This study was funded through the NSF Research Experience for Undergraduates and the Plum Island Sound LTER Program. We thank Sarah Turner, Alejandro Filgueira, and Simon Punal for their help on the project.

Literature Cited

1. Bailey, N. T. J. 1951. *Biometrika* 38: 293-306.
2. Lotrich, V. A. 1975. *Ecology* 56: 191-198.
3. Meredith, W. H., and V. A. Lotrich. 1979. *Estuarine Coastal Mar. Sci.* 8: 99-118.
4. Butner, A., and B. H. Brattstrom. 1960. *Copeia* 2: 139-141.
5. Chidester, F. E. 1920. *Am. Nat.* 54: 551-557.

Dissolved Inorganic Nitrogen Flux and Mineralization in Waquoit Bay Sediments as Measured by Core Incubations

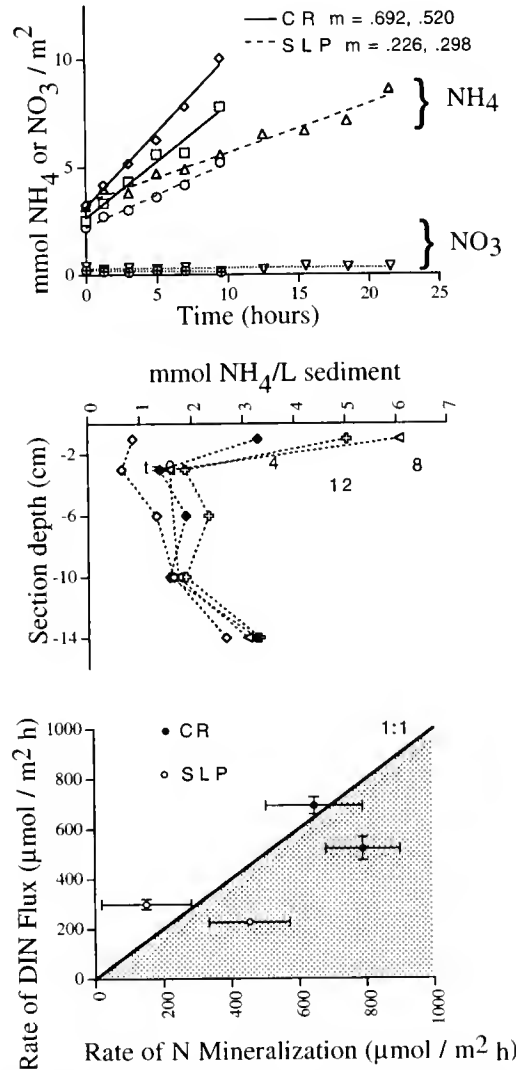
John Kirkpatrick and Ken Foreman (Ecosystems Center, Marine Biological Laboratory, Woods Hole, Massachusetts, 02543), and Ivan Valiela²

Globally, human activities have doubled the rate at which atmospheric dinitrogen is fixed into bioavailable forms such as ammonium and nitrate (1). Locally, this increase in N fixation is manifested as greater nitrogen loading to coastal ecosystems, systems in which nitrogen is often the principal limiting nutrient for primary producers (2). In these systems, mineralization is the primary process by which organic nitrogen deposited to sediments is regenerated. This mineralized N can flux out of the sediments or be denitrified (3). N that fluxes out of the sediments and enters the water column can be taken up by producers. As a result, N may be recycled several times before being transported out of the ecosystem. One important control on the proportion of N input that is recycled within an ecosystem is the rate of denitrification.

Here we report on N cycling in sediments at two sites in Waquoit Bay, the Childs River estuary, which receives high inputs of N ($410.1 \text{ kg N ha}^{-1} \text{ y}^{-1}$), and Sage Lot Pond, which receives much lower N inputs ($5.2 \text{ kg N ha}^{-1} \text{ y}^{-1}$) due to its relatively pristine watershed (unpubl. data). To assess the effects of nitrogen loading on these processes, we measured rates of mineralization and dissolved inorganic nitrogen (DIN) flux from the sediment in two cores collected from each site. We were also able to estimate the maximum rate of denitrification, which can be calculated as the difference between mineralization and flux (4).

We measured N flux as the change in concentration of NH_4 and NO_3 over 24 hours in the water-filled headspace over the sealed sediment cores. Nutrient analyses were done using standard colorimetric techniques, either by hand (5) or on a Lachat Auto-Analyzer. We also measured oxygen consumption in the cores with an Orbisphere Laboratories stirring oxygen probe.

After these measurements were complete, we horizontally sectioned each core at depths of 0–2, 2–4, 4–8, 8–12, and 12–16 cm. Sediment from each section was homogenized under N_2 in a glove bag, and subsamples were placed into sealed test tubes. These tubes were incubated anaerobically at the same temperature as measured during the flux determinations ($21^\circ \pm 0.5^\circ\text{C}$) for 0, 4, 8, and 12 days. Nitrogen mineralization was



¹ Harvard University, Cambridge, Massachusetts 02138.

² Boston University Marine Program, Marine Biological Laboratory, Woods Hole, Massachusetts 02543.

Figure 1. (Top) Flux of ammonium and nitrate per square meter of sediment. Childs River (CR) cores (squares and diamonds, solid line) had a higher rate of ammonium production, as is seen in the higher slopes over Sage Lot Pond (SLP) cores (triangles and circles, dashed

line). More data are available for SLP 1 because of a larger headspace volume. (Middle) Production of ammonium (i.e., mineralization) with depth, using core CR 1 as an example. Each progressive line indicates an increment in time (squares were from $t = 0$ days; circles, $t = 4$; diamonds, $t = 8$; and triangles, $t = 12$). The vertical axis, depth, represents the distance from the surface of the sediment to the midpoint of the section sampled. Note that in the top section, at -1 cm, NH_4 increases with time, while the lower depths do not show as much change. (Bottom) Rate of N flux compared to mineralization: Childs River rates are indicated by black dots, Sage Lot Pond by empty circles. Points falling in the shaded area, below the 1:1 line, are values for which the rate of mineralization is greater than that of DIN flux. The difference between the two is the rate of denitrification. Note that the Childs River rates are high, while the Sage Lot Pond rates are low.

measured as the accumulation of NH_4^+ in KCl extracts of the sediments through the incubation period (6,7). Rates for both DIN flux and mineralization were calculated from regression fit to the time courses, with standard error included.

The rates of NH_4^+ increase were higher in the sediments from Childs River than in those from Sage Lot Pond (Fig. 1, top). In contrast, no NO_3^- was released (Fig. 1, top). The lack of nitrate flux indicates either low rates of nitrification or close coupling of nitrification and denitrification. The rate of DIN flux was about twice as high in the two Childs River cores (520 ± 47 and $692 \pm 33 \mu\text{mol N m}^{-2} \text{h}^{-1}$) as in the two Sage Lot Pond cores (298 ± 20 and $226 \pm 16 \mu\text{mol N m}^{-2} \text{h}^{-1}$) (Fig. 1, top, bottom). These values fall within previously measured ranges (8).

Production of ammonium occurred largely in the top layers of sediment (Fig. 1, middle), as found in other studies (7). The rates of mineralization, calculated from the regression line fit to the time course, were not different from the rates of flux in one core from each estuary (Fig. 1, bottom). However, rates of mineralization were higher than flux rates in the other core taken from each estuary. This difference represents a maximum rate of denitrification. We found denitrification rates of 269 ± 120 and $-48 \pm 146 \mu\text{mol N m}^{-2} \text{h}^{-1}$ (an average of $111 \pm 94 \mu\text{mol N m}^{-2} \text{h}^{-1}$) in the Childs River cores, with rates of -148 ± 149 and $227 \pm 119 \mu\text{mol N m}^{-2} \text{h}^{-1}$ (an average of $79 \pm 95 \mu\text{mol N m}^{-2} \text{h}^{-1}$) for Sage Lot Pond.

These results suggest that N loading causes higher rates of N flux and mineralization. This would seem to imply that N

loading causes faster N cycling in estuary sediments. On average, however, denitrification does not appear to be occurring at a high enough rate in these sediments, during the season we sampled, to create differences measurable by this method. The rates of land-derived N loading seem relatively uncorrelated to rates of denitrification in estuary sediments.

This work was supported by an NSF Research Experience for Undergraduates grant. Special thanks to Anne Giblin, Jane Tucker, Gabby Tomasky, Roselle Safran, and Jessica Legra.

Literature Cited

1. Vitousek, P. M. 1975. *Ecology* 75: 1861–1876.
2. Vitousek, P. M., and R. W. Howarth. 1991. *Biogeochemistry* 13: 87–115.
3. Fenchel, T., and T. H. Blackburn. 1979. Pp. 101–126 in *Bacteria and Mineral Cycling*. Academic Press, London.
4. Banta, G. T. 1992. *Decomposition and Nitrogen Cycling in Coastal Marine Sediments—Controls by Temperature, Organic Matter Inputs, and Benthic Macrofauna*. Ph.D. Thesis, Boston University. 278 pp.
5. Parsons, T. R., Y. Maita, and C. M. Lalli. 1984. Pp. 14–17 in *A Manual of Chemical and Biological Methods for Seawater Analysis*. Pergamon Press, Oxford.
6. Rosenfeld, J. K. 1979. *Limnol. Oceanogr.* 24: 356–364.
7. Rosenfeld, J. K. 1981. *Am. J. Sci.* 281: 436–462.
8. LaMontagne, M. G. 1996. *Denitrification and the Stoichiometry of Organic Matter Degradation in Temperate Estuarine Sediments—Seasonal Pattern and Significance as a Nitrogen Sink*. Ph.D. Thesis, Boston University. 172 pp.

Reference: *Biol. Bull.* 195: 241–243. (October, 1998)

Effect of Eelgrass (*Zostera marina*) Density on the Feeding Efficiency of Mummichog (*Fundulus heteroclitus*)

Suzanne Graham¹, Jessica Davis², Linda Deegan (Marine Biological Laboratory, Woods Hole, Massachusetts 02543),
Just Cebrian³, Jeff Hughes (Marine Biological Laboratory), and Jennifer Hauxwell³

Eelgrass (*Zostera marina*) beds are important coastal nursery habitats for a variety of fishes. Eelgrass beds also provide food for many fish species by supporting an abundant and diverse benthic community (1). Nitrogen loading from anthropogenic sources alters eelgrass shoot density and may, in turn, affect the feeding efficiency of benthivorous fishes (2). For instance, decreases in eelgrass shoot densities significantly enhance the feeding efficiency of predators as well as the vulnerability of prey to predation (3). However, the dynamic response of fish feeding efficiency to varying eelgrass densities is not well known. This study examined the functional relationship between eelgrass shoot density and the feeding efficiency of the mummichog (*Fundulus heteroclitus*), a benthivorous fish. Natural eelgrass densities were studied in the field and, in the laboratory, eelgrass densities were manipulated.

Specimens of second-year (55–70 mm total length) *F. heteroclitus* were obtained by seining in subestuaries of Waquoit Bay, Massachusetts. All fish were starved for 24 h to ensure that the gut was completely empty and were given 30 min to acclimate to environmental conditions prior to use in experiments.

During the field experiment, the fish were allowed to feed on naturally occurring prey in habitats with different eelgrass shoot densities. Four experimental sites with contrasting shoot densities ($0, 40 \pm 11.31, 80 \pm 14.79, \text{ and } 375 \pm 9.24$ shoots/ m^2 , mean \pm SE) were established in subestuaries of Waquoit Bay. Ten exclusion cages, each containing three *F. heteroclitus*, were placed on the substrate at random locations within each site. A cage consisted of a 500- μm -mesh bag sealed to a 30-cm-diameter ring (0.07 m^2). After 2 h, the fish were retrieved from the cages and preserved with 95% ethanol in preparation for gut analysis. Preliminary experiments had indicated that prey were completely digested approximately 3 h after ingestion. Stomach contents were identified and enumerated under a dissecting microscope ($50\times$). The average density of invertebrate prey was determined by collecting three random samples

¹ San Diego State University, San Diego, CA (First and second authorship was determined by the flip of a coin).

² Roger Williams University, Bristol, RI.

³ Boston University Marine Program, MBL.

from each site with an Ekman grab (0.02 m²), and enumerating the organisms retained on a 250- μ m-mesh screen.

The parallel laboratory experiment was conducted using 33-l tanks with 19 densities (0-800 shoots per m²) of artificial eelgrass clusters ($n = 3$). Artificial eelgrass was designed from green polypropylene and consisted of four blades per shoot. Eelgrass shoots were randomly attached to a 1-cm-mesh grid within each tank. The grids were covered with washed beach sand, and the tanks were filled with running seawater at ambient temperature ($\sim 20^{\circ}\text{C}$). Prey were a mixture of amphipods (*Amphipoe* sp., *Cyanea* sp., *Microdeutopus* sp., and *Gammarus* sp.) that are commonly associated with eelgrass beds in Waquoit Bay. Two *F. heteroclitus* and 20 amphipods were placed in each tank. After 2 h, the fish were removed and preserved in 95% ethanol for gut analysis.

The field experiment revealed that amphipods were the preferred prey of mummichogs (74%–94% of total contents, mean = 85%) (Fig. 1 top). Other prey items were polychaetes (7%), snails (5%), and other crustaceans (3%). However, amphipods represented a lower percentage of total prey abundance (10%–65%, mean = 39.3%) in field collections than in the gut contents at all field sites. These data indicate that mummichogs selected amphipods regardless of total prey abundance. Feeding efficiency (*i.e.*, average number of amphipods consumed per fish

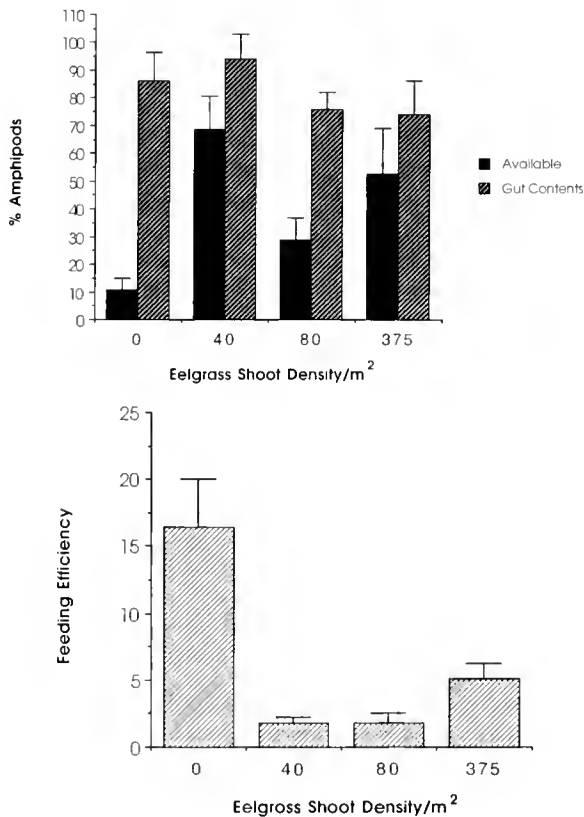


Figure 1. (Top) Percent occurrence of amphipods in total invertebrate sample and percent of amphipods found in *Fundulus heteroclitus* guts at sites with different eelgrass shoot densities. (bottom) Mean feeding efficiency of *F. heteroclitus* (\pm SE) (% amphipods consumed per fish per hour).

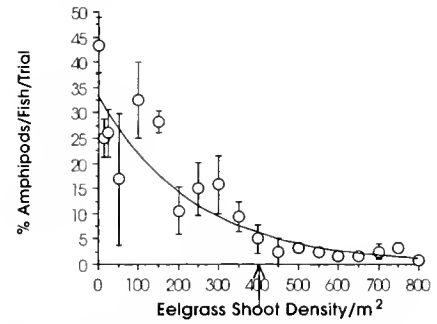


Figure 2. Mean feeding efficiency (\pm SE) as a function of eelgrass shoot density in laboratory experiments. Regression line shown is an exponential curve fit relating consumption rate (y) to eelgrass density (D): ($y = 79.2 (\pm 1.6)e^{-0.0043(\pm 0.0004)D}$, $r^2 = 0.880$, $D =$ density constant). The arrow indicates an intermediate density beyond which consumption rate is largely unchanged. Trial duration = 2 h.

per h) was normalized to the number of amphipods available and was reported as a percentage of those available.

Mummichogs consumed virtually all (96%) the amphipods in the zero eelgrass treatment and might have consumed even larger quantities had more been available, since fish in other treatments were observed to have eaten up to 16 amphipods/h. An expected maximal consumption rate can be derived for the other treatments by multiplying the rate observed in the zero eelgrass treatment by the relative difference in prey availability between the zero eelgrass and other treatments. These expected values (expressed as number of amphipods consumed in 2 hours by three fish) are as follows: 96 consumed at 40 shoots, 40 consumed at 80 shoots, 67 consumed at 375 shoots. In each instance, fish consumed far fewer amphipods than expected: actual values were 12 amphipods consumed at 40 shoots, 4 consumed at 80 shoots, 18 consumed at 375 shoots. The discrepancy between expected and actual values implies that prey accessibility was diminished in treatments with eelgrass.

Feeding efficiency of *F. heteroclitus* was significantly higher (16.4% fish⁻¹ h⁻¹) in the site with no eelgrass (Fig. 1 bottom) than in the sites with eelgrass ($\sim 3\%$ fish⁻¹ h⁻¹) (Tukey HSD, $P < 0.01$). Feeding efficiency did not differ significantly among the three sites with eelgrass.

Laboratory experiments revealed that eelgrass shoot density had a significant effect on fish feeding efficiency ($P < 0.0001$, one-factor ANOVA) (Fig. 2). Feeding efficiency decreased sharply at lower densities (0 to ~ 400 shoots/m²) and approached a constant value for densities higher than 400 shoots/m² (Fig. 2). The relationship between feeding efficiency and shoot density can be described as a decreasing exponential function ($P < 0.0001$, Fig. 2). This finding contrasts with that of Nelson (2), who found that the feeding efficiency of perch (*Perca fluviatilis*) was linearly related to habitat complexity.

Field and laboratory results both suggest that a simple linear relationship between feeding efficiency and habitat complexity does not exist for mummichog and its amphipod prey. Laboratory data show that there is a critical level of habitat complexity (~ 400 shoots/m²) beyond which feeding efficiency is low but unaffected by further increases in structural density. The feeding

response observed in the field experiment suggests that this critical density is lower. These differences could be due to other structural elements of the habitat that are not mimicked in the experimental tanks. At the field sites, the presence of macroalgae and a canopy of dead eelgrass leaves may have provided additional refuge for amphipods.

In laboratory trials at zero eelgrass density, mean amphipod consumption approached the maximum amount of prey available, possibly explaining the low amphipod abundance found in field sites with no eelgrass. Laboratory trials at 12 shoots/m² revealed a 42% decrease in the amphipod consumption rate from that at 0 shoots/m². Field experiments indicated a 89% decrease in the amphipod consumption rate from the zero eelgrass habitat to that with 37 shoots/m². These results suggest that relatively low habitat complexity provides refuge for amphipod prey.

Both field and laboratory experiments suggest that there is a critical habitat complexity at which the feeding efficiency of the fish is strongly affected. Many healthy eelgrass beds have higher shoot densities than the laboratory-determined critical value of 400 shoots/m². Hence, fishes may have a limited feeding efficiency in dense eelgrass beds. However, fish abundance

in healthy eelgrass beds has been observed to be substantially greater than that in adjacent unvegetated habitats (Deegan *et al.*, unpubl. data). The high abundance of invertebrates in eelgrass beds offers greater food availability for fishes despite, and maybe because of, enhanced protection for individual prey (3, 4). Further field investigations should be conducted to clearly define the minimum shoot density necessary to sustain a stable and diverse eelgrass community.

We are grateful to G. Breed, A. Filgueira, and J. Wyda for valuable suggestions and assistance in our experiments. This work was supported by funds from a grant from the NSF Research Experience for Undergraduates Program.

Literature Cited

1. Valiela, I., K. Foreman, M. LaMontagne *et al.* 1992. *Estuaries* 15: 443-457.
2. Nelson, W. G., and E. Bonsdorff. 1990. *J. Exp. Mar. Biol. Ecol.* 141: 183-194.
3. Heck, K. L., and T. A. Thoman. 1981. *J. Exp. Mar. Biol. Ecol.* 53: 125-134.
4. R. J. Orth, K. J. Heck, J. van Montfrans *et al.* 1984. *Estuaries* 7: 339-350.

Reference: *Biol. Bull.* 195: 243-244. (October, 1998)

Lead Concentration as an Indicator of Contamination History in Estuarine Sediments

Jessica C. Legra¹, Roselle E. Safran², and Ivan Valiela (Boston University Marine Program, Marine Biological Laboratory, Woods Hole, Massachusetts 02543)

Exposure to lead has increased over the century, but has not been of concern until recently. Atmospheric lead concentration worldwide has increased 200-fold during the past 3000 years (1). The lead found in estuarine sediment cores comes from regional, large-scale atmospheric sources such as automobile exhaust and industry or from local sources such as gasoline outboard motors or street runoff (2). Thus, local sources, produced by human activities as coastal watersheds urbanize, will add to the more global atmospheric sources. Local urbanization of watersheds could further alter the accumulation of Pb in the sediments of receiving estuaries.

In this study we measured Pb concentrations in vertical sediment profiles of three estuaries of Waquoit Bay, Massachusetts, to (a) document the historical record of concentrations of Pb and (b) compare the effects of different degrees of watershed urbanization on the lead content of sediments in each estuary. Waquoit Bay comprises a series of estuaries with different histories of urbanization (3): Childs River has the most urbanized watershed, Quashnet River is moderately urbanized, and Sage Lot Pond is still in a near-pristine forested state.

We sampled two sediment cores (6.5 cm in diameter and 50 cm deep) from the three estuaries of Waquoit Bay. The cores were sectioned into 1-cm intervals for the first 10 cm and into 5-cm intervals for the remainder of the core. The sections were

oven dried at 60°C for 2-3 days and then ground with a mortar and pestle. For Pb analysis, weighed samples of sediment (0.18-0.22 g) were digested with 8 ml of HNO₃ and shaken overnight. The following day, 2.5 ml of HNO₃ was added to the shaken mixture and centrifuged for 1 min. The supernatant was decanted, and the Pb in the supernatant was measured by flame atomic absorption spectrometry. To learn more about possible biogeochemical controls of Pb in the sediment, we also measured other chemical properties, including % C, on a Perkin-Elmer 2400 CHN elemental analyzer (4). The sediments were also ashed at 490°C overnight.

The Pb profiles of the sediments (Fig. 1, top) show the changing history of Pb in the sediments of the three estuaries of Waquoit Bay. In general, Pb concentrations are low near the bottom of the profile and increase in the upper layers. The Pb depth profiles are similar to others from California (2) and New England (4). ²¹⁰Pb-dated cores taken in New England show increases in Pb concentrations around 1900 (4). In our samples, the Pb concentration in sediments of all three estuaries rose between 30 and 37 cm. This initial rise could signal a date of about 1930, determined on the basis of Pb and ²¹⁰Pb data from Connecticut lakes (P. Siver, University of Connecticut, pers. comm.). This agrees with the date of 1931-1932 estimated for the 30-37 cm layer in our cores by using the abundance of eelgrass seed coats (5).

We assumed that the rise in Pb concentration from 35-15 cm in the Childs River core (Fig. 1, top left), was of a similar origin, and that the rise continued into the 1970s when Pb concentrations

¹ Lafayette College, Easton, Pennsylvania.

² Princeton University, Princeton, New Jersey.

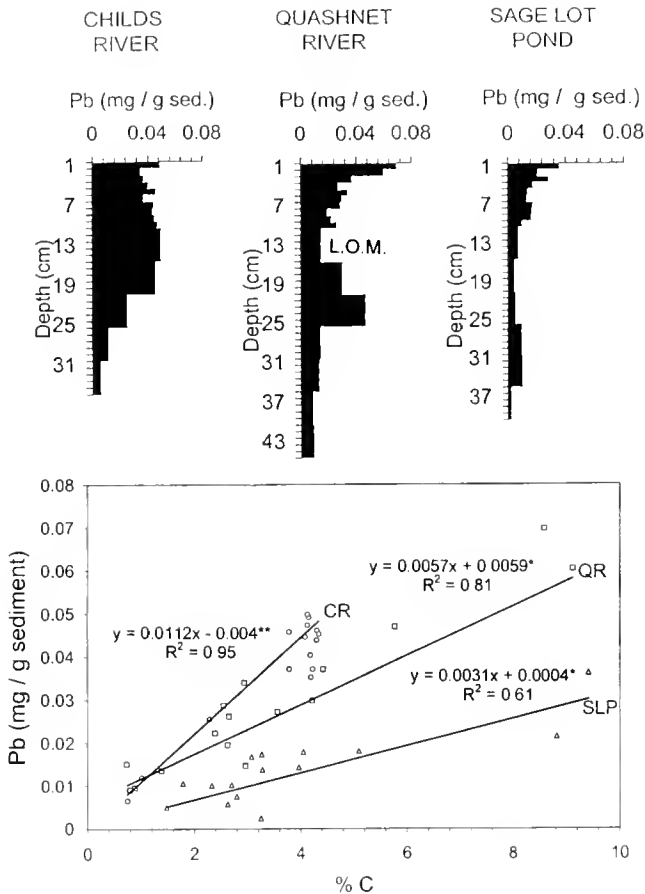


Figure 1. Top: Depth profiles of lead concentration (mg/g sediment) in cores from Childs River, Quashnet River, and Sage Lot Pond, average of two cores. L.O.M indicates a layer with much lower organic content. Bottom: Lead concentration vs. the % carbon in cores of sediment for all three estuaries. CR = Childs River, QR = Quashnet River, SLP = Sage Lot Pond.

peaked as a result of the use of leaded gasoline. Pb concentrations decreased after 1973, when the United States banned the addition of lead to gasoline for automotive fuel. There is a near-surface peak of Pb concentrations in the uppermost layers of sediments in the Childs River profile (as well as in those of the other two estuaries). This feature is unexplained; we speculate that lead sources from recent increases in boat traffic might be responsible because the use of leaded gasoline in boats was not officially banned until 1995. Further, there could be increased leaching of Pb deposited in roads and roadsides.

The depth profiles for Pb vary among the estuaries; for example, the Quashnet River profile shows a marked trough at 11–15 cm (Fig. 1, top middle). This trough in Pb concentrations was associated with a significant decrease in organic content.

It is difficult to compare Pb loads to the different estuaries by just comparing Pb concentrations; we must also account for possible differences in sediment accretion. To get a better comparison of lead inputs into the three estuaries, we calculated the total inventory of Pb received by each estuary, across the time period represented by the top 31 cm in the sediment cores

(Fig. 1, top). The total lead per volume of sediment per core section was calculated by using data on porosity of the sediment (6). The Pb inventory in the Childs River sediment was 0.446 g cm^{-3} , 3 times higher than that of Sage Lot Pond (0.134 g cm^{-3}). This suggests that the atmospheric, regional sources represent about a third of the inputs and that local sources derived from human activities associated with urban land use are responsible for at least $\frac{2}{3}$ of the Pb load to urbanized estuaries.

The vertical profiles of % C suggested that within the sediment of each estuary, lead content might be closely related to carbon content (data not shown). To define this relationship between lead and % C we plotted Figure 1 (bottom). In all sediments, lead concentrations increased as carbon increased, but the specific response differed among estuaries. The estuary with the highest urbanization accumulated lead in sediments more effectively than the less urbanized estuary. Moreover, the carbon content of sediments in the urbanized estuary did not reach the value found in sediments of the less urbanized estuary. This might be related to the different C/N ratios and higher biogeochemical activity of sediments exposed to larger loads of nitrogen. Increased N loads increase ecosystem metabolism (7), which may result in greater consumption of organic matter and explain the decreased amount of C in Childs River. Hence, for each square meter of estuarine sediment, the amount of Pb deposited is associated with a lower amount of carbon in Childs River than in the two less urbanized estuaries.

These data show that estuarine sediments have variable concentrations of Pb and that historical changes are evident, but the effects of different lead sources are hard to discern. In urbanized watersheds, regional atmospheric sources contribute perhaps a third of the Pb in estuarine sediment and local sources contribute two thirds. Pb concentrations are closely related to the organic content of sediments. Nitrogen associated with land use therefore indirectly affects lead content through its effects on nitrogen supply and ecosystem metabolism.

This research was supported by an NSF Research Experience for Undergraduates grant. Very special thanks to Anne Giblin and Ken Foreman for all of their help with the Pb analysis. Also, thanks to Gabrielle Tomasky for obtaining some of our cores. Finally, we are grateful to Suzanne Thomas, Martha Peterson, and Sarah Thompson for assistance with the Perkin-Elmer 2400 CHN elemental analyzer.

Literature Cited

1. Ng, A., and C. C. Patterson. 1982. *Geochim. Cosmochim. Acta* 46: 2307–2317.
2. Chow, T. J., K. W. Bruland, K. Bertine, A. Soutar, M. Koide, and E. D. Goldberg. 1973. *Science* 181: 551–552.
3. Valiela, I., and others. 1992. *Estuaries* 15: 443–457.
4. Giblin, A., G. E. Likens, D. White, and R. W. Howarth. 1990. *Limnol. Oceanogr.* 35: 852–869.
5. Safran, R. E., J. C. Legra, and I. Valiela. 1998. *Biol. Bull.* 195: 245–246.
6. LaMontagne, M. G. 1986. *Denitrification and the Stoichiometry of Organic Matter Degradation in Temperate Estuarine Sediments: Seasonal Pattern and Significance as a Nitrogen Sink*. Ph.D. Thesis, Boston University.
7. D'Avanzo, C., J. N. Kremer, and S. C. Wainright. 1996. *Mar. Ecol. Prog. Ser.* 141: 263–274.

Reference: *Biol. Bull.* **195**: 245–246. (October, 1998)

Effects of Nitrogen Loading on Eelgrass Seed Coat Abundance, C to N Ratios, and $\delta^{15}\text{N}$ in Sediments of Waquoit Bay

Roselle E. Safran¹, Jessica C. Legra², and Ivan Valiela (Boston University Marine Program, Marine Biological Laboratory, Woods Hole, Massachusetts 02543)

Increased watershed urbanization has increased land-derived nitrogen loads entering some estuaries of Waquoit Bay. The N loads originate from wastewater, fertilizer, and atmospheric deposition, and consist of NO_3 , NH_4 , and dissolved organic nitrogen (1, 2). As a result of the increase in nitrogen load, areas of eelgrass (*Zostera marina*) meadows have been reduced (3, 4, 5), but not to the same extent in all estuaries. Different Waquoit Bay estuaries have been subject to different rates of nitrogen loading, and areas of eelgrass habitat seem to mirror N loading (6). We compared three estuaries in the Waquoit system (Childs River, Quashnet River, and Sage Lot Pond) that receive different land-derived N loads, to define how N load affects survival of eelgrass meadows. To assess relative abundance of eelgrass meadows and to document historical changes in the abundance of eelgrass, we counted eelgrass seed coats buried at each layer within sediment profiles (7).

To measure eelgrass seed coat abundance in vertical profiles of sediment, we collected six cores from unvegetated sediment at each estuary and divided them into 1-cm horizontal sections. Each section was wet sieved through a 1-mm sieve (7). To examine other biochemical properties that may be involved in controlling seed coat abundance, two additional cores were obtained from each location and were used to measure % C and N, and $\delta^{15}\text{N}$ values. The sections from these cores were dried, ground, and % carbon and % nitrogen were evaluated with a Perkin-Elmer 2400 elemental analyzer. $\delta^{15}\text{N}$ values were determined with a Finnigan Delta-S isotope ratio mass spectrometer (8).

The abundance of eelgrass seed coats varied with depth in the sediment (Fig. 1, top three panels). Interpretation of the vertical sequence is difficult because variations in sediment accretion as well as eelgrass abundance could have contributed to the differences (7). The eelgrass wasting disease of 1931–1932 eliminated eelgrass in our region, and the lack of seed coats seen at 30–37 cm in QR and SLP (Fig. 1, top center and top right panel) and lower than 36 cm in CR (Fig. 1, top left panel) could mark that date. A similar conclusion was reached by Costa (7), who first examined seed coat distributions. Further evidence supporting this premise was obtained by P. Siver of the University of Connecticut, who analyzed Pb and ^{210}Pb profiles in sediments of Connecticut lakes and found that the depths of 30–37 cm corresponded to a date of about 1930 (pers. comm.).

Since the early 1930s, eelgrass had recovered in all three estuaries, reaching the greatest abundance in SLP. CR sediments apparently lost eelgrass earlier than QR. In contrast, eelgrass seed coats were still found in the most recent upper layers in SLP. These results agree with what is known about urbanization of the three estuaries. CR was the earliest to become urbanized, while the watershed of SLP remains undeveloped. There was an unexplained decrease in seed coat abundance at the top few centimeters of SLP; this decrease may simply reflect our taking of core samples from bare patches where eelgrass was not growing.

The data from the cores show a historical relationship between nitrogen supply and seed coat abundance (Fig. 1, bottom left). As a way to examine the time course of nitrogen loads, we used C/N as a proxy. We calculated C/N using the average values for percent carbon and percent nitrogen of the two cores from each estuary for each section and found that, as the C/N increased (*i.e.*, there was a smaller amount of N in relation to C), the relative abundance of eelgrass seed coats increased. This suggests that indeed eelgrass seemed sensitive to historical changes in nitrogen supply.

We have calculated current nitrogen loads (1) and can thus determine whether we can use our space-for-time inter-estuary comparison to relate the decrease in eelgrass abundance in recent sections (upper 10 cm) of the cores to N load rates (Fig. 1, bottom center). Indeed, C/N did become lower as N load increased. More evidence of the clear link between land-derived N loads and the N in estuarine sediment is provided by the $\delta^{15}\text{N}$ results (Fig. 1, bottom right). The $\delta^{15}\text{N}$ values in sediments were heavier in estuaries receiving larger N loads. The change in $\delta^{15}\text{N}$ is probably derived from the relatively heavy contributions of isotope N made by wastewater nitrogen in the more urbanized watersheds (2). These two lines of evidence show that there is a link between what happens on land and the quality of sediment in the receiving estuaries. Moreover, the linkages betray differences in nitrogen loads that can be the cause of changing eelgrass abundance. The results thus show that eelgrass seed coat surveys reflect historical changes in the different estuaries, and that nitrogen delivery rates from adjoining watersheds were significantly related to the occurrence of eelgrass beds.

This project was funded by the NSF's REU program. Special thanks to Gabby Tomasky, Anne Giblin, Suzanne Thomas, and Sarah Thompson for their help at various stages of the research.

¹ Princeton University, Princeton, New Jersey 08544.

² Lafayette College, Easton, Pennsylvania 18043.

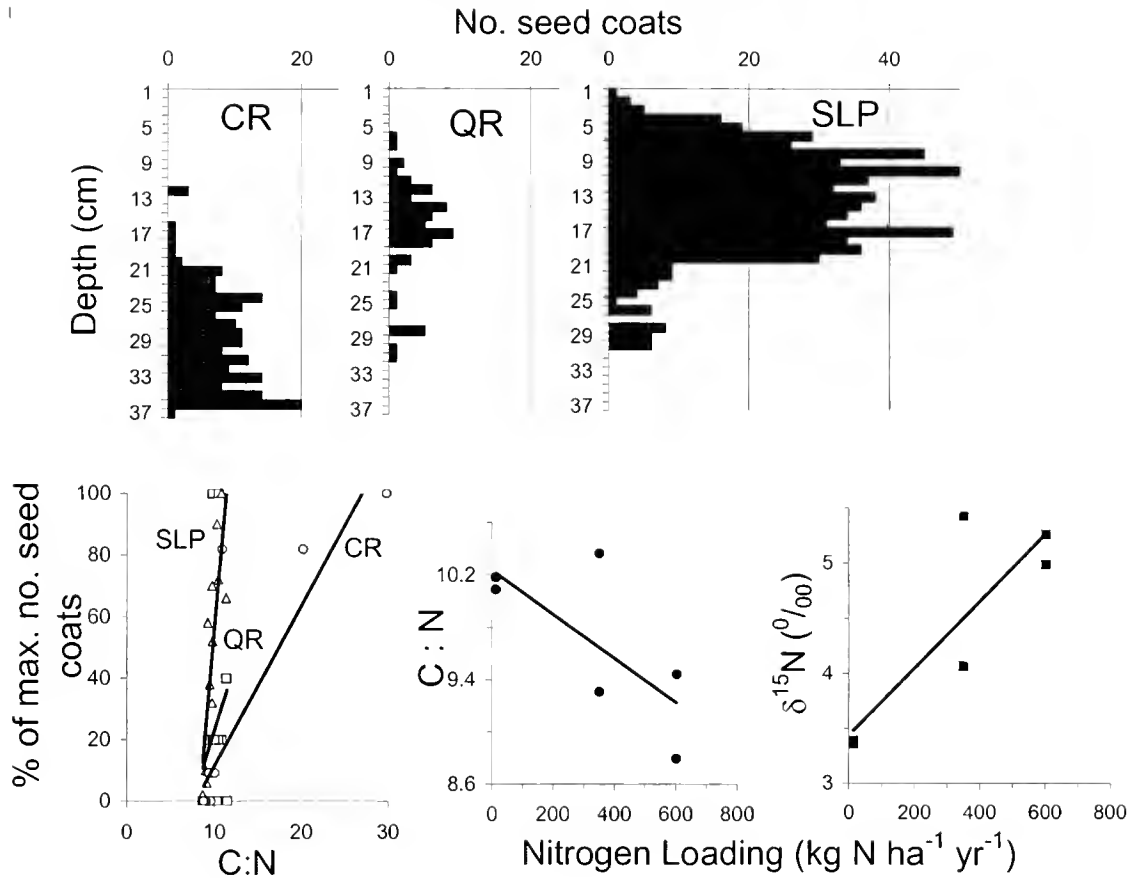


Figure 1. Top: Abundance of seed coats in cores taken from Childs River (CR), Quashnet River (QR), and Sage Lot Pond (SLP). Sum of 6 cores per estuary. Bottom Left: Relationship of seed coat abundance to C:N of sediments. % of max. is the number of seed coats in a section divided by the maximum number in the estuary. For CR, $y = 5.2176x - 40.81^*$ and $R^2 = 0.71$. For SLP, $y = 32.556x - 269.57^*$ and $R^2 = 0.63$. The regression was not significant for QR. Bottom Center: C:N in recent sediment (upper 10 cm of sediment) vs. nitrogen loading rates ($y = -0.0017x + 10.238^*$ and $R^2 = 0.53$). Bottom Right: $\delta^{15}\text{N}$ vs. nitrogen loading rates where $\delta^{15}\text{N}$ is averaged for top 10 cm ($y = 0.003x + 3.4376^*$ and $R^2 = 0.74$).

Literature Cited

1. Valiela, I., G. Collins, J. Kremer, K. Lajtha, M. Geist, B. Seely, J. Brawley, and C. H. Sham. 1997. *Ecol. Appl.* **7**: 358–380.
2. Valiela, I., K. Foreman, M. LaMontagne, D. Hersh, J. Costa, P. Peckol, B. DeMeo-Anderson, C. D'Avanzo, M. Babione, C. H. Sham, J. Brawley, and K. Lajtha. 1992. *Estuaries* **15**: 443–457.
3. Duarte, C. M. 1995. *Ophelia* **41**: 87–112.
4. Burkholder, J. M., K. M. Mason, and H. B. Glasgow, Jr. 1992. *Mar. Ecol. Prog. Ser.* **61**: 163–178.
5. Burkholder, J. M., H. B. Glasgow, Jr., and J. E. Cooke. 1994. *Mar. Ecol. Prog. Ser.* **105**: 121–138.
6. Valiela, I., J. McClelland, J. Hauxwell, P. J. Behr, D. Hersh, and K. Foreman. 1997. *Limnol. Oceanogr.* **42**: 1105–1118.
7. Costa, J. 1988. *Distribution, Production, and Historical Changes in Abundance of Eelgrass (Zostera marina L.) in Southeastern Massachusetts*. Ph.D. Thesis. Boston University, Massachusetts, Pp. 63–84.
8. McClelland, J. W., I. Valiela, and R. H. Michener. 1997. *Limnol. Oceanogr.* **42**: 930–936.

Reference: *Biol. Bull.* **195**: 247–248. (October, 1998)

Planktonic Feeding and Evolutionary Significance of the Lobate Body Plan Within the Ctenophora
John H. Costello (Biology Department, Providence College, Providence, Rhode Island 02918)
and Rebecca Coverdale¹

Ctenophores are gelatinous marine invertebrates that prey upon zooplankton. The two main ctenophoran orders that affect planktonic communities are the Cydippida and the Lobata. The Cydippida possess two elongate tentacles. In the Lobata, two large lobes surround comparatively reduced tentacles, and water is drawn through the inter-lobe space by four flap-like ciliated auricles. Both groups are successful predators and are widespread in the world's oceans (1). In coastal regions, members of the genera *Bolinopsis* (Lobata) and *Pleurobrachia* (Cydippida) may co-occur and often reach high densities simultaneously.

The co-occurrence of *Bolinopsis* and *Pleurobrachia* suggests the possibility of dietary overlap and feeding competition between these genera, because both are commonly believed to consume copepods as their primary prey (2, 3). To examine this hypothesis, we recorded the gut contents of individuals from two species, *Bolinopsis infundibulum* (Lobata) and *Pleurobrachia pileus* (Cydippida); the animals were collected simultaneously on six dates between March and May 1998 from the Woods Hole Oceanographic Institution pier in Woods Hole, Massachusetts. *Bolinopsis infundibulum* preserved poorly (total disintegration within 24 h in 0.5% formalin solution), did not tolerate vessel containment well, and often regurgitated prey when held in a container for more than 30 min. As a result, ctenophore gut contents were observed microscopically and recorded at the sample site within 30 min of hand collection. Gut contents were easily observed in intact animals due to transparency of the body wall. On each sample date, 20–30 individual ctenophores of each species were sampled.

Although the day-to-day selection by the ctenophore predators was subject to the availability of specific prey types, a pattern of prey partitioning between the ctenophore orders was evident (Fig. 1). The cydippid *Pleurobrachia pileus* consistently consumed larger, more strongly swimming prey such as gammarid amphipods, crab zoea, calanoid copepods, and barnacle cyprid larvae. In contrast, the lobate *Bolinopsis infundibulum* selected smaller, more weakly swimming prey such as copepod nauplii, gastropod veligers, rotifers, and tintinnids.

Differences in patterns of prey selection reflected the mechanical bases of prey capture by each species. *P. pileus* sits motionless while its tentacles are extended and set in a wide net that ensnares highly mobile prey. *B. infundibulum* uses the ciliary lining of its auricles to create a feeding current that entrains low-speed and weakly swimming prey that are entrapped on a network of fine tentillae located near the oral region (4). The two mechanisms favor capture of a different fraction of the

available plankton and allow co-occurring ctenophores with different body plans to partition available prey.

Although the prey capture mechanism of cydippid ctenophores such as *P. pileus* have long been appreciated (3, 5, 6), the mechanics of lobates such as *B. infundibulum* have been less studied and are poorly understood. However, evidence on the mechanics of prey capture by lobates has been growing (Costello, unpubl. data) and now indicates that both of the lobate genera examined to date share the ability to utilize the smaller, less mobile fraction of plankton classified as microzooplankton. This ability is a consequence of the lobate body plan: funnel-like oral lobes; ciliated auricles; and in the genera *Bolinopsis*

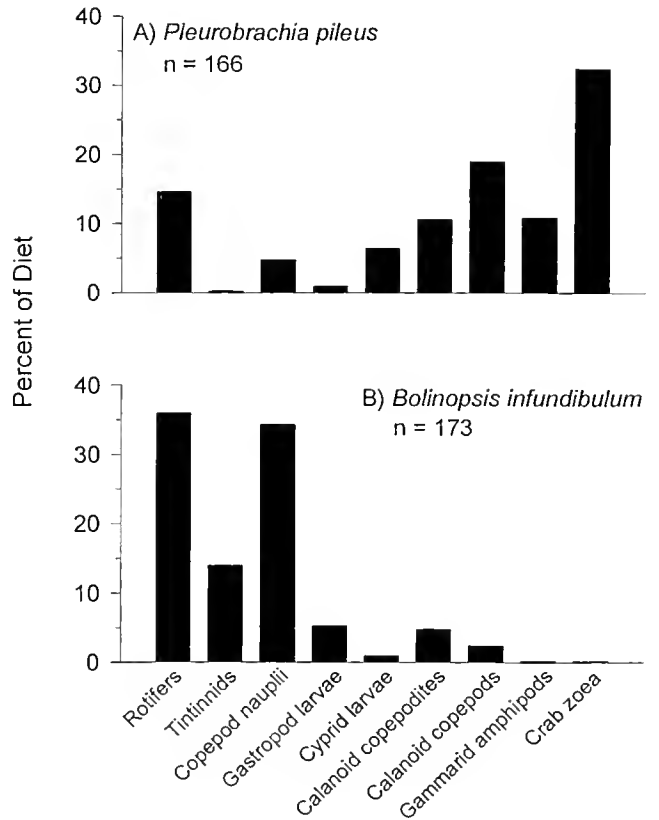


Figure 1. The percentages of various prey types in the gut contents of two ctenophores: (A) *Pleurobrachia pileus* (Cydippida) and (B) *Bolinopsis infundibulum* (Lobata). These values are based on the total prey numbers consumed over the 6-day sampling period. The ctenophores were collected adjacent to Great Harbor in Woods Hole, Massachusetts. The proportional contribution of each prey item was significantly different between the two ctenophores (χ^2 , $P < 0.01$ for all comparisons). Prey types are arranged sequentially by approximate length and varied from rotifers (0.15–0.35 mm) to crab zoea (1.5–3.0 mm).

¹ Biology Department, Woods Hole Oceanographic Institution, Woods Hole, Massachusetts 02543.

and *Mnemiopsis*, modification of elongate tentacles into a finely spaced sieve of tentillae.

We propose that the capacity to exploit the microzooplankton was a major selective force favoring evolution of lobate ctenophores from cydippid ancestors. Cydippid groups such as the Pleurobrachiidae are physically constrained by tentacle thread spacing from successfully preying on microzooplankton taxa. By making this prey group available, the lobate characteristics enabled a substantial radiation of forms within the Ctenophora, particularly in open-ocean communities, where the planktonic size spectrum is shifted downward relative to coastal and upwelling areas. Note that lobates, such as *Mnemiopsis*, never completely abandoned the capacity to prey on calanoid copepods and other macrozooplankton. Rather, they developed mechanosensory abilities and behavioral responses (Costello, unpubl. data) that allow predation both on macrozooplankton, using primarily the oral lobes, as well as on microzooplankton, using the tentacles (Costello and Waggett, unpubl. data). Thus, we suggest that the evolution of the lobate body plan allowed an expansion of prey niche dimensions rather than a complete reallocation of predatory effort. However, design options in-

volve tradeoffs in performance, and the *in-situ* gut contents data (Fig. 1) demonstrate that, while enabling feeding on microzooplankton, the lobate design may perform less favorably than that of the cydippid at capturing the larger, more mobile end of the zooplankton prey spectrum.

JHC expresses gratitude to the Marine Biological Laboratory for a summer fellowship, and to the National Science Foundation (ROA supplement, OCE-9632654 to L. Madin). RAC gratefully acknowledges dissertation support from The Seaver Institute and NOAA, Office of Sea Grant NA46RG0470 (R/B-143).

Literature Cited

1. Harbison, G. R., L. P. Madin, and N. R. Swanberg. 1978. *Deep-Sea Res.* **25**: 233-256.
2. Bishop, J. W. 1968. *Ecology* **49**: 996-997.
3. Reeve, M. R., and M. A. Walter. 1978. *Adv. Mar. Biol.* **15**: 249-287.
4. Nagabhushanam, A. K. 1959. *Nature* **184**: 829.
5. Hyman, L. H. 1940. Pp. 662-695 in *The Invertebrata: Protozoa through Ctenophora*. McGraw-Hill, New York.
6. Greene, C. H., M. R. Landry, and B. C. Monger. 1986. *Ecology* **67**: 1493-1501.

ABSTRACTS

In addition to the work described here in Short Reports, the following papers were also presented. The abstracts of these papers are available from the Marine Biological Laboratory Archives, 7 MBL Street, Woods Hole, MA 02543.

Appleman, Gregory M., Frank W. Grasso, and Jennifer A. Basil

A learning algorithm of crayfish spatial representation embodied in a biomimetic robot

Dale, Jonathan

Odor dispersal and its ramifications for chemotaxis in *Asterias forbesi*

Freidenfelds, Jason L., Takashi Yamamoto, Frederick A. Dodge, and Robert B. Barlow

Limulus vision in the laboratory

Kam, Adrienne W., Frank W. Grasso, and Jelle Atema

Use of antennule flicking in odor source tracking of the lobster, *Homarus americanus*

Lazenby, Gweneth B., Louisa O. Nakanuku, Jennifer A. Basil, Jelle Atema, and Roger T. Hanlon

Nautilus are attracted to conspecific odor

Tran, P. T., P. Bermei, S. Inoué, and E. D. Salmon

High guanosine-5'-triphosphate (GTP) concentrations promote microbutule catastrophe

THE BIOLOGICAL BULLETIN

PUBLISHED BY
THE MARINE BIOLOGICAL LABORATORY

Associate Editors

JAMES A. BLAKE, ENSR Marine & Coastal Center, Woods Hole

LOUIS E. BURNETT, Grice Marine Biological Laboratory, College of Charleston

WILLIAM D. COHEN, Hunter College, City University of New York

CHARLES D. DERBY, Georgia State University

SHINYA INOUÉ, Marine Biological Laboratory

RUDOLF A. RAFF, Indiana University

Editorial Board

PETER B. ARMSTRONG, University of California, Davis

ANDREW R. CAMERON, California Institute of Technology

THOMAS H. DIETZ, Louisiana State University

RICHARD B. EMLET, Oregon Institute of Marine Biology,
University of Oregon

DAVID EPEL, Hopkins Marine Station, Stanford University

GREGORY HINKLE, Cereon Genomics, Cambridge, Massachusetts

MAKOTO KOBAYASHI, Hiroshima University of Economics

MICHAEL LABARBERA, University of Chicago

DONAL T. MANAHAN, University of Southern California

MARGARET McFALL-NGAI, Kewalo Marine Laboratory,
University of Hawaii

MARK W. MILLER, Institute of Neurobiology, University
of Puerto Rico

TATSUO MOTOKAWA, Tokyo Institute of Technology

YOSHITAKA NAGAHAMA, National Institute for Basic
Biology, Japan

SHERRY D. PAINTER, Marine Biomedical Institute, University
of Texas Medical Branch

BARUCH RINKEVICH, Israel Oceanographic & Limnological
Research Ltd.

RICHARD STRATHMANN, Friday Harbor Laboratories,
University of Washington

J. HERBERT WAITE, University of Delaware

SARAH ANN WOODIN, University of South Carolina

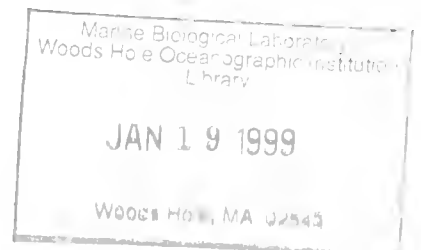
RICHARD K. ZIMMER-FAUST, University of California,
Los Angeles

Editor: MICHAEL J. GREENBERG, The Whitney Laboratory, University of Florida

Managing Editor: PAMELA L. CLAPP, Marine Biological Laboratory

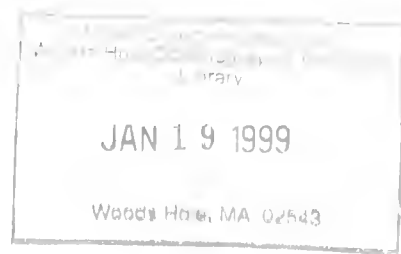
DECEMBER, 1998

Printed and Issued by
LANCASTER PRESS, Inc.
3575 HEMPLAND ROAD
LANCASTER, PA



Cover

Photograph of an adult specimen of the mesopelagic lobate ctenophore *Bathocyroe fosteri*. This species was discovered in 1976 during a dive in the submersible *Alvin*; it appears to be cosmopolitan in distribution and fairly common at lower mesopelagic depths. This particular specimen (~ 12 cm long) was captured from the *Johnson-Sea-Link* submersible at a depth of about 700 meters in Oceanographer Canyon on the southern rim of Georges Bank. *B. fosteri* is highly transparent. Indeed, some degree of transparency is found in almost all oceanic zooplankters that are neither camouflaged by small size or mirrored surfaces nor protected by rapid swimming speeds or chemical defenses. Little is known about the physical basis of transparency or its ecological significance. Now, Johnsen and Widder (this issue) have measured the transparency of *B. fosteri* and specimens of 28 other common species of gelatinous zooplankton from the Northwestern Atlantic Ocean and Gulf of Mexico. The results were fit to models of contrast and light scattering, enabling predictions to be made about the ultrastructure of transparent animals and their visibility to predators and prey. Photograph by Dr. E. Widder, Harbor Branch Oceanographic Institution © 1998.



CONTENTS

Volume 195, No. 3: December 1998

RESEARCH NOTES

- Mankad, Raj V., Alexander A. Gimelbrant, and Timothy S. McClintock**
Consensus translational initiation sites of marine invertebrate phyla 251
- Bishop, Jamie J., Thomas L. Vandergon, David B. Green, Jeannette E. Doeller, and David W. Kraus**
A high-affinity hemoglobin is expressed in the notochord of amphioxus, *Branchiostoma californiense* . . . 255
- Stach, Thomas**
Coelomic cavities may function as a vascular system in amphioxus larvae 260

PHYSIOLOGY

- Ellington, W. Ross, and Stephen T. Kinsey**
Functional and evolutionary implications of the distribution of phosphagens in primitive-type spermatozoa . . . 264

NEUROBIOLOGY AND BEHAVIOR

- Linser, Paul J., William E. S. Carr, Holly S. Cate, Charles D. Derby, and James C. Netherton III**
Functional significance of the co-localization of taste buds and teeth in the pharyngeal jaws of the largemouth bass, *Micropterus salmoides* 273
- Webster, S. G.**
Peptidergic neurons in barnacles: an immunohistochemical study using antisera raised against crustacean neuropeptides 282

CELL BIOLOGY

- Nowel, Mark S., P. M. J. Shelton, and P. J. Herring**
Cuticular photophores of two decapod crustaceans, *Oplophorus spinosus* and *Systellapsis debilis* 290

DEVELOPMENT AND REPRODUCTION

- Ram, Jeffrey L., Carlos S. Gallardo, Michal L. Ram, and Roger P. Croll**
Reproduction-associated immunoreactive peptides in the nervous systems of prosobranch gastropods 308
- Sakai, Kazuhiko**
Effect of colony size, polyp size, and budding mode on egg production in a colonial coral 319

- Montgomery, Mary K., and Margaret J. McFall-Ngai**
Late postembryonic development of the symbiotic light organ of *Euprymna scolopes* (Cephalopoda: Sepioliidae) 326

ECOLOGY AND EVOLUTION

- Johnsen, Sönke, and Edith A. Widder**
Transparency and visibility of gelatinous zooplankton from the northwestern Atlantic and Gulf of Mexico . . . 337
- Pernet, Bruno, and Alan J. Kohn**
Size-related obligate and facultative parasitism in the marine gastropod *Trichotropis cancellata* 349

GENETIC REGULATORY NETWORKS IN EMBRYOGENESIS AND EVOLUTION

- Cameron, R. Andrew**
Introduction 361
- Henry, Jonathan Q., and Mark Q. Martindale**
Evolution of cleavage programs in relationship to axial specification and body plan evolution 363
- van Loon, A. E., and J. A. M. van den Biggelaar**
Changes in cell lineage specification elucidate evolutionary relations in Spiralia 367
- Shankland, Marty, and Ashley E. E. Bruce**
Axial patterning in the leech: developmental mechanisms and evolutionary implications 370
- Akam, Michael**
Hox genes in arthropod development and evolution . . . 373
- Slack, Frank, and Gary Ruvkun**
Heterochronic genes in development and evolution . . . 375
- Hobert, Oliver, and Gary Ruvkun**
A common theme for LIM homeobox gene function across phylogeny? 377
- Satoh, Noriyuki**
Mechanisms of specification in ascidian embryos 381
- Published by title only** 384
- Chairs and speakers** 384

1997-98 PHOTOGRAPHY AND PHOTOMICROGRAPHY CONTEST

- Prize-winning photographs** 387

* * *

- Index for Volume 195** 391

THE BIOLOGICAL BULLETIN

THE BIOLOGICAL BULLETIN is published six times a year by the Marine Biological Laboratory, 7 MBL Street, Woods Hole, Massachusetts 02543.

Subscriptions and similar matter should be addressed to Subscription Manager, THE BIOLOGICAL BULLETIN, Marine Biological Laboratory, 7 MBL Street, Woods Hole, Massachusetts 02543. Subscription per year (six issues, two volumes): \$195 for libraries; \$95 for individuals. Subscription per volume (three issues): \$97.50 for libraries; \$50 for individuals. Back and single issues (subject to availability): \$40 for libraries; \$20 for individuals.

Communications relative to manuscripts should be sent to Michael J. Greenberg, Editor-in-Chief, or Pamela L. Clapp, Managing Editor, at the Marine Biological Laboratory, 7 MBL Street, Woods Hole, Massachusetts 02543. Telephone: (508) 289-7428. FAX: 508-457-1924. E-mail: pclapp@mbl.edu.

<http://www.mbl.edu/BiologicalBulletin/>

The home page for the electronic companion to THE BIOLOGICAL BULLETIN—the *Marine Models Electronic Record*—and other BIOLOGICAL BULLETIN publications is available on the World Wide Web at the address shown above.

THE BIOLOGICAL BULLETIN is indexed in bibliographic services including *Index Medicus* and MEDLINE, *Chemical Abstracts*, *Current Contents*, *Elsevier BIOBASE/Current Awareness in Biological Sciences*, and *Geo Abstracts*.

Printed on acid free paper,
effective with Volume 180, Issue 1, 1991.

POSTMASTER: Send address changes to THE BIOLOGICAL BULLETIN, Marine Biological Laboratory, 7 MBL Street, Woods Hole, MA 02543.

Copyright © 1998, by the Marine Biological Laboratory

Periodicals postage paid at Woods Hole, MA, and additional mailing offices.

ISSN 0006-3185

INSTRUCTIONS TO AUTHORS

The Biological Bulletin accepts outstanding original research reports of general interest to biologists throughout the world. Papers are usually of intermediate length (10–40 manuscript pages). A limited number of solicited review papers may be accepted after formal review. A paper will usually appear within four months after its acceptance.

Very short, especially topical papers (less than 9 manuscript pages including tables, figures, and bibliography) will be published in a separate section entitled "Research Notes." A Research Note in *The Biological Bulletin* follows the format of similar notes in *Nature*. It should open with a summary paragraph of 150 to 200 words comprising the introduction and the conclusions. The rest of the text should continue on without subheadings, and there should be no more than 30 references. References should be referred to in the text by number, and listed in the Literature Cited section in the order that they appear in the text. Unlike references in *Nature*, references in the Research Notes section should conform in punctuation and arrangement to the style of recent issues of *The Biological Bulletin*. Materials and Methods should be incorporated into appropriate figure legends. See the article by Lohmann *et al.* (October 1990, Vol. 179: 214–218) for sample style. A Research Note will usually appear within two months after its acceptance.

The Editorial Board requests that regular manuscripts conform to the requirements set below; those manuscripts that

do not conform will be returned to authors for correction before review.

1. **Manuscripts.** Manuscripts, including figures, should be submitted in quadruplicate, with the originals clearly marked. (Xerox copies of photographs are not acceptable for review purposes.) The submission letter accompanying the manuscript should include a telephone number, a FAX number, and (if possible) an E-mail address for the corresponding author. The original manuscript must be typed in no smaller than 12 pitch or 10 point, using double spacing (including figure legends, footnotes, bibliography, etc.) on one side of 16- or 20-lb. bond paper, 8 by 11 inches. Please, no right justification. Manuscripts should be proofread carefully and errors corrected legibly in black ink. Pages should be numbered consecutively. Margins on all sides should be at least 1 inch (2.5 cm). Manuscripts should conform to the *Council of Biology Editors Style Manual*, 5th Edition (Council of Biology Editors, 1983) and to American spelling. Unusual abbreviations should be kept to a minimum and should be spelled out on first reference as well as defined in a footnote on the title page. Manuscripts should be divided into the following components: Title page, Abstract (of no more than 200 words), Introduction, Materials and Methods, Results, Discussion, Acknowledgments, Literature Cited, Tables, and Figure Legends. In addition, authors should supply a list of words and phrases under which the article should be indexed.

2. **Title page.** The title page consists of a condensed title or running head of no more than 35 letters and spaces, the manuscript title, authors' names and appropriate addresses, and footnotes listing present addresses, acknowledgments or contribution numbers, and explanation of unusual abbreviations.

3. **Figures.** The dimensions of the printed page, 7 by 9 inches, should be kept in mind in preparing figures for publication. We recommend that figures be about 1 times the linear dimensions of the final printing desired, and that the ratio of the largest to the smallest letter or number and of the thickest to the thinnest line not exceed 1:1.5. Explanatory matter generally should be included in legends, although axes should always be identified on the illustration itself. Figures should be prepared for reproduction as either line cuts or halftones. Figures to be reproduced as line cuts should be unmounted glossy photographic reproductions or drawn in black ink on white paper, good-quality tracing cloth or plastic, or blue-lined coordinate paper. Those to be reproduced as halftones should be mounted on board, with both designating numbers or letters and scale bars affixed directly to the figures. All figures should be numbered in consecutive order, with no distinction between text and plate figures and cited, in order, in the text. The author's name and an arrow indicating orientation should appear on the reverse side of all figures.

Color: *The Biological Bulletin* will publish color figures and plates, but must bill authors for the actual additional cost of printing in color. The process is expensive, so authors with more than one color image should—consistent with editorial concerns, especially citation of figures in order—combine them into a single plate to reduce the expense. On request, when supplied with a copy of a color illustration, the editorial staff will provide a pre-publication estimate of the printing cost.

4. **Tables, footnotes, figure legends, etc.** Authors should follow the style in a recent issue of *The Biological Bulletin* in preparing table headings, figure legends, and the like. Because of the high cost of setting tabular material in type, authors are asked to limit such material as much as possible. Tables, with their headings and footnotes, should be typed on separate sheets, numbered with consecutive Roman numerals, and placed after the Literature Cited. Figure legends should contain enough information to make the figure intelligible separate from the text. Legends should be typed double spaced, with consecutive Arabic numbers, on a separate sheet at the end of the paper. Footnotes should be limited to authors' current addresses, acknowledgments or contribution numbers, and explanation of unusual abbreviations. All such footnotes should appear on the title page. Footnotes are not normally permitted in the body of the text.

5. **Literature cited.** In the text, literature should be cited by the Harvard system, with papers by more than two authors cited as Jones *et al.*, 1980. Personal communications and material in preparation or in press should be cited in the text only, with author's initials and institutions, unless the material has been formally accepted and a volume number can be supplied. The list of references following the text should be headed Literature Cited, and must be typed double spaced on separate

pages, conforming in punctuation and arrangement to the style of recent issues of *The Biological Bulletin*. Citations should include complete titles and inclusive pagination. Journal abbreviations should normally follow those of the U. S. A. Standards Institute (USASI), as adopted by BIOLOGICAL ABSTRACTS and CHEMICAL ABSTRACTS, with the minor differences set out below. The most generally useful list of biological journal titles is that published each year by BIOLOGICAL ABSTRACTS (BIOSIS List of Serials; the most recent issue). Foreign authors, and others who are accustomed to using THE WORLD LIST OF SCIENTIFIC PERIODICALS, may find a booklet published by the Biological Council of the U.K. (obtainable from the Institute of Biology, 41 Queen's Gate, London, S.W.7, England, U.K.) useful, since it sets out the WORLD LIST abbreviations for most biological journals with notes of the USASI abbreviations where these differ. CHEMICAL ABSTRACTS publishes quarterly supplements of additional abbreviations. The following points of reference style for THE BIOLOGICAL BULLETIN differ from USASI (or modified WORLD LIST) usage:

A. Journal abbreviations, and book titles, all underlined (for *italics*)

B. All components of abbreviations with initial capitals (not as European usage in WORLD LIST e.g., *J. Cell. Comp. Physiol.* NOT *J. cell. comp. Physiol.*)

C. All abbreviated components must be followed by a period, whole word components *must not* (i.e., *J. Cancer Res.*)

D. Space between all components (e.g., *J. Cell. Comp. Physiol.*, not *J.Cell.Comp.Physiol.*)

E. Unusual words in journal titles should be spelled out in full, rather than employing new abbreviations invented by the author. For example, use *Rit Vísindaffélag Islandinga* without abbreviation.

F. All single word journal titles in full (e.g., *Veliger, Ecology, Brain*).

G. The order of abbreviated components should be the same as the word order of the complete title (i.e., *Proc. and Trans.* placed where they appear, not transposed as in some BIOLOGICAL ABSTRACTS listings).

H. A few well-known international journals in their preferred forms rather than WORLD LIST or USASI usage (e.g., *Nature, Science, Evolution* NOT *Nature, Lond., Science, N.Y.; Evolution, Lancaster, Pa.*)

6. **Reprints, page proofs, and charges.** Authors of articles in black and white (no color figures) receive their first 50 reprints (without covers) free of charge. Color reprints and additional black-and-white reprints may be purchased; authors will receive order forms. Reprints normally will be delivered about 2 to 3 months after the issue date. Authors (or delegates for foreign authors) will receive page proofs of articles shortly before publication. They will be charged the current cost of printers' time for corrections to these (other than corrections of printers' or editors' errors). Other than these charges for authors' alterations, *The Biological Bulletin* does not have page charges.

CONTENTS

for Volume 195

NO. 1, AUGUST 1998

IMAGING AND MICROSCOPY

- Piston, David W.**
Concepts in Imaging and Microscopy. Choosing objective lenses: the importance of numerical aperture and magnification in digital optical microscopy 1

RESEARCH NOTES

- Hárosi, Ferenc I., Ione Hunt von Herbing, and Jeffrey R. Van Keuren**
 Sickling of anoxic red blood cells in fish 5
- Stuart, J. A., E. L. Ooi, J. McLeod, A. E. Bourns, and J. S. Ballantyne**
 D- and L- β -hydroxybutyrate dehydrogenases and the evolution of ketone body metabolism in gastropod molluscs 12
- Rodhouse, Paul G.**
 Physiological progenesis in cephalopod molluscs 17

DEVELOPMENT AND REPRODUCTION

- Holm, Eric R., Brian T. Nedved, Eugenio Carpizo-Ituarte, and Michael G. Hadfield**
 Metamorphic-signal transduction in *Hydroides elegans* (Polychaeta: Serpulidae) is not mediated by a G protein 21

SYMBIOSIS

- Nyholm, Spencer V., and Margaret J. McFall-Ngai**
 Sampling the light organ microenvironment of *Euprymna scolopes*: description of a population of host cells in association with the bacterial symbiont *Vibrio fischeri* 89

PHYSIOLOGY

- Leys, Sally P., and Henry M. Reiswig**
 Transport pathways in the neotropical sponge *Aplysina* 30
- Nair, P. Satish, and William E. Robinson**
 Calcium speciation and exchange between blood and extrapallial fluid of the quahog *Mercenaria mercenaria* (L.) 43
- Nakatani, Isamu, Yoshinori Okada, and Takuji Kitahara**
 Induction of extra claws on the chelipeds of a crayfish, *Procambarus clarkii* 52

ECOLOGY AND EVOLUTION

- Ogasawara, Michio, and Noriyuki Satoh**
 Isolation and characterization of endostyle-specific genes in the ascidian *Ciona intestinalis* 60
- Maruyama, Tadashi, Masaharu Ishikura, Satoru Yamazaki, and Satoru Kanai**
 Molecular phylogeny of zooxanthellate bivalves 70

NEUROBIOLOGY AND BEHAVIOR

- Cobb, Christopher S., and Roddy Williamson**
 Electrophysiology and innervation of the photosensitive epistellar body in the lesser octopus *Eledone cirrhosa* 78
- * * *
- Annual Report of the Marine Biological Laboratory R1**

NO. 2, OCTOBER 1998

CELL BIOLOGY AND DEVELOPMENT

- Rinkevich, Baruch, Irving L. Weissman, and Anthony W. DeTomaso**
 Transplantation of Fu/HC-incompatible zooids in *Botryllus schlosseri* results in chimerism 98

Yamada, Katsuyuki, and Koshin Mihashi Temperature-independent period immediately after fertilization in sea urchin eggs	107
Abdu, Uri, Peter Takac, Hans Laufer, and Amir Sagi Effect of methyl farnesoate on late larval development and metamorphosis in the prawn <i>Macrobrachium rosenbergii</i> (Decapoda, Palaemonidae): a juvenoid-like effect?	112

ECOLOGY AND EVOLUTION

Bavestrello, Giorgio, Umberto Benatti, Barbara Calcinai, Riccardo Cattaneo-Vietti, Carlo Cerrano, Anna Favre, Marco Giovine, Serena Lanza, Roberto Pronzato, and Michele Sarà Body polarity and mineral selectivity in the demosponge <i>Chondrosia reniformis</i>	120
Wendt, Dean E. Effect of larval swimming duration on growth and reproduction of <i>Bugula neritina</i> (Bryozoa) under field conditions	126

PHYSIOLOGY

Ellers, Olaf, Amy S. Johnson, and Philip E. Moberg Structural strengthening of urchin skeletons by collagenous sutural ligaments	136
Thorington, Glyne U., and David A. Hessinger Efferent mechanisms of discharging cnidae: II. A nematocyst release response in the sea anemone tentacle	145

NEUROBIOLOGY AND BEHAVIOR

Herberholz, Jens, and Barbara Schmitz Role of mechanosensory stimuli in intraspecific agonistic encounters of the snapping shrimp (<i>Alpheus heterochaelis</i>)	156
--	-----

RESEARCH NOTE

Tankersley, Richard A., Maria G. Wieber, Marco A. Sigala, and Kristen A. Kachurak Migratory behavior of ovigerous blue crabs <i>Callinectes sapidus</i> : evidence for selective tidal-stream transport	168
---	-----

SHORT REPORTS FROM THE 1998 GENERAL SCIENTIFIC MEETINGS OF THE MARINE BIOLOGICAL LABORATORY

FEATURED ARTICLES

Atema, Jelle Introduction. Tracking turbulence: processing the bimodal signals that define an odor plume	179
Weaver, Matthew, and Jelle Atema Hydrodynamic coupling of lobster antennule motion to oscillatory water flow	180

Guenther, Carla M., and Jelle Atema Distribution of setae on the <i>Homarus americanus</i> lateral antennule flagellum	182
--	-----

SENSORY BIOLOGY

Mead, Kristina S. The biomechanics of odorant access to aesthetascs in the grass shrimp, <i>Palaemonetes vulgaris</i>	184
Quinn, Elizabeth, Kristen Paradise, and Jelle Atema Juvenile <i>Limulus polyphemus</i> generate two water currents that contact one proven and one putative chemoreceptor organ	185
Shashar, Nadav, Ferenc I. Hárosi, Anastazia T. Banaszak, and Roger T. Hanlon UV radiation blocking compounds in the eye of the cuttlefish <i>Sepia officinalis</i>	187
Ruta, Vanessa J., Frederick A. Dodge, and Robert B. Barlow Efferent modulation of physiological properties of the <i>Limulus</i> lateral eye	189
Edds-Walton, P. L., and R. R. Fay Directional auditory responses in the descending octaval nucleus of the toadfish (<i>Opsanus tau</i>)	191

BEHAVIOR AND NEUROBIOLOGY

King, Jane Roche, and Hans Straka Effects of vestibular nerve lesions on orientation turning in the leopard frog, <i>Rana pipiens</i>	193
Mensingher, Allen F., and Max Deffenbaugh Prototype rechargeable tag for acoustical neural telemetry	194
Billack, Blase, Jeffrey D. Laskin, Prudence T. Heck, Walter Troll, Michael A. Gallo, and Diane E. Heck Alterations in cholinergic signaling modulate contraction of isolated sea urchin tube feet: potential role of nitric oxide	196
Hoskin, Francis C. G., and John E. Walker A closer look at the natural substrate for a nerve-gas hydrolyzing enzyme in squid nerve	197
Kuzirian, Alan M., Herman T. Epstein, Thomas J. Nelson, and Nancy S. Rafferty Lead, learning, and calyxitin in <i>Hermisenda</i>	198
Tamse, Catherine T., Katherine Hammar, D. Marshall Porterfield, and Peter J. S. Smith Transmembrane calcium flux in Pb^{2+} -exposed <i>Aplysia</i> neurons	201
Malchow, Robert Paul, Michael P. Verzi, and Peter J. S. Smith Extracellular pH gradients measured from isolated retinal cells	203
Andersen, Kristen A., and Robert Paul Malchow Fluorometric analysis of intracellular sodium concentrations in isolated retinal horizontal cells	204
Jessen-Eller, Kathryn, Marjorie Steele, Carol Reinisch, and Nicholas Spitzer Blockade of ryanodine receptors stimulates neurite outgrowth in embryos of <i>Spisula solidissima</i>	206

Porterfield, D. M., J. R. Trimarchi, D. L. Keefe, and P. J. S. Smith
 Characterization of oxygen and calcium fluxes from early mouse embryos and oocytes 208

Silver, Robert B., Leslie A. King, and Alyssa F. Wise
 Calcium regulatory endomembranes of the prophase mitotic apparatus of sand dollar cells contain enzyme activities that produce leukotriene B₄ but not 1,4,5-inositol triphosphate 209

Lee, Kyeng G., Nishal Mohan, Zoya Koroleva, Li-Fang Huang, and William D. Cohen
 Fluorescence localization of cytoskeletal proteins in fibrin-trapped cells 211

Goda, Makoto, Shinya Inoué, and Robert Knudson
 Oocyte maturation in *Chaetopterus pergamentaceus* observed with centrifuge polarizing microscope . . . 212

Miyake, Katsuya, and Paul L. McNeil
 A little shell to live in: evidence that the fertilization envelope can prevent mechanically induced damage of the developing sea urchin embryo 214

Kuhns, William J., Xavier Fernandez-Busquets, Max M. Burger, Michael Ho, and Eva Turley
 Hyaluronic acid-receptor binding demonstrated by synthetic adhesive proteoglycan peptide constructs and by cell receptors on the marine sponge *Microciona prolifera* 216

Kubke, M. F., E. Gilland, and R. Baker
 Lipophilic dye labeling distinguishes segregated central components of the eighth cranial nerve in embryonic chicken 218

Straka, Hans, Edwin Gilland, and Robert Baker
 Rhombomeric organization of brainstem motor neurons in larval frogs 220

ANIMAL HUSBANDRY AND DISEASE

Hanley, Janice S., Nadav Shashar, Roxanna Smolowitz, Robert A. Bullis, William N. Mebane, Howaida R. Gabr, and Roger T. Hanlon
 Modified laboratory culture techniques for the European cuttlefish *Sepia officinalis* 223

Maxwell, Michael R., William K. Macy, Shobu Odate, and Roger T. Hanlon
 Evidence for multiple spawning by squids (*Loligo pealei*) in captivity 225

Weidner, Earl, and Teresa King
In vivo and *in vitro* growth of nerve parasite from *Lophius americanus* 227

O'Neill, Maureen D., Heather M. Wesp, Allen F. Mensinger, and Roger T. Hanlon
 Initial baseline blood chemistry of the oyster toadfish, *Opsanus tau* 228

Smolowitz, Roxanna, Elizabeth Wadman, and H. M. Chikarmane
Pseudomonas putida infections of the oyster toadfish (*Opsanus tau*) 229

ECOLOGY

Schmitt, Catherine, Nathaniel Weston, and Charles Hopkinson
 Preliminary evaluation of sedimentation rates and species distribution in Plum Island Estuary, Massachusetts 232

Griffin, Martin P. A., Marci L. Cole, Kevin D. Kroeger, and Just Cebrian
 Dependence of herbivory on autotrophic nitrogen content and on net primary production across ecosystems 233

Rogers, Jennifer, Jennifer Harris, and Ivan Valiela
 Interaction of nitrogen supply, sea level rise, and elevation on species form and composition of salt marsh plants 235

Sweeney, Jennifer, Linda Deegan, and Robert Garritt
 Population size and site fidelity of *Fundulus heteroclitus* in a macrotidal saltmarsh creek 238

Kirkpatrick, John, Ken Foreman, and Ivan Valiela
 Dissolved inorganic nitrogen flux and mineralization in Waquoit Bay sediments as measured by core incubations 240

Graham, Suzanne, Jessica Davis, Linda Deegan, Just Cebrian, Jeff Hughes, and Jennifer Hauxwell
 Effect of eelgrass (*Zostera marina*) density on the feeding efficiency of mummichog (*Fundulus heteroclitus*) 241

Legra, Jessica C., Roselle E. Safran, and Ivan Valiela
 Lead concentration as an indicator of contamination history in estuarine sediments 243

Safran, Roselle E., Jessica C. Legra, and Ivan Valiela
 Effects of nitrogen loading on eelgrass seed coat abundance, C to N ratios, and $\delta^{15}\text{N}$ in sediments of Waquoit Bay 245

Costello, John H., and Rebecca Coverdale
 Planktonic feeding and evolutionary significance of the lobate body plan within the Ctenophora 247

ABSTRACTS

Papers listed by title only 249

NO. 3, DECEMBER 1998

RESEARCH NOTES

Mankad, Raj V., Alexander A. Gimelbrant, and Timothy S. McClintock
 Consensus translational initiation sites of marine invertebrate phyla 251

Bishop, Jamie J., Thomas L. Vandergon, David B. Green, Jeannette E. Doeller, and David W. Kraus
 A high-affinity hemoglobin is expressed in the notochord of amphioxus, *Branchiostoma californiense* . . . 255

Stach, Thomas
 Coelomic cavities may function as a vascular system in amphioxus larvae 260

PHYSIOLOGY

Ellington, W. Ross, and Stephen T. Kinsey
 Functional and evolutionary implications of the distribution of phosphagens in primitive-type spermatozoa 264

NEUROBIOLOGY AND BEHAVIOR

Linser, Paul J., William E. S. Carr, Holly S. Cate, Charles D. Derby, and James C. Netherton III
 Functional significance of the co-localization of taste buds and teeth in the pharyngeal jaws of the largemouth bass, *Micropterus salmoides* 273

Webster, S. G.
 Peptidergic neurons in barnacles: an immunohistochemical study using antisera raised against crustacean neuropeptides 282

CELL BIOLOGY

Nowel, Mark S., P. M. J. Shelton, and P. J. Herring
 Cuticular photophores of two decapod crustaceans, *Oplophorus spinosus* and *Systellapsis debilis* 290

DEVELOPMENT AND REPRODUCTION

Ram, Jeffrey L., Carlos S. Gallardo, Michal L. Ram, and Roger P. Croll
 Reproduction-associated immunoreactive peptides in the nervous systems of prosobranch gastropods 308

Sakai, Kazuhiko
 Effect of colony size, polyp size, and budding mode on egg production in a colonial coral 319

Montgomery, Mary K., and Margaret J. McFall-Ngai
 Late postembryonic development of the symbiotic light organ of *Euprymna scolopes* (Cephalopoda: Sepioliidae) 326

ECOLOGY AND EVOLUTION

Johnsen, Sönke, and Edith A. Widder
 Transparency and visibility of gelatinous zooplankton from the northwestern Atlantic and Gulf of Mexico 337

Pernet, Bruno, and Alan J. Kohn
 Size-related obligate and facultative parasitism in the marine gastropod *Trichotropis cancellata* 349

**GENETIC REGULATORY NETWORKS
 IN EMBRYOGENESIS AND EVOLUTION**

Cameron, R. Andrew
 Introduction 361

Henry, Jonathan Q., and Mark Q. Martindale
 Evolution of cleavage programs in relationship to axial specification and body plan evolution 363

van Loon, A. E., and J. A. M. van den Biggelaar
 Changes in cell lineage specification elucidate evolutionary relations in Spiralia 367

Shankland, Marty, and Ashley E. E. Bruce
 Axial patterning in the leech: developmental mechanisms and evolutionary implications 370

Akam, Michael
 Hox genes in arthropod development and evolution 373

Slack, Frank, and Gary Ruvkun
 Heterochronic genes in development and evolution 375

Hobert, Oliver, and Gary Ruvkun
 A common theme for LIM homeobox gene function across phylogeny? 377

Satoh, Noriyuki
 Mechanisms of specification in ascidian embryos 381

Published by title only 384

Chairs and speakers 384

**1997-98 PHOTOGRAPHY AND
 PHOTOMICROGRAPHY CONTEST**

Prize-winning photographs 387

* * *

Index for Volume 195 391

Notice to Subscribers

1999 SUBSCRIPTION RATES FOR *THE BIOLOGICAL BULLETIN*

	Libraries	Individuals
Per year (six issues, two volumes):	\$205.00	\$95.00
Per volume (three issues):	\$102.50	\$47.50
Back and single issues: (subject to availability)	\$ 40.00	\$20.00

For additional information, please contact our subscription manager at the Marine Biological Laboratory, 7 MBL Street, Woods Hole, MA 02543; tel: (508) 289-7402.

Consensus Translational Initiation Sites of Marine Invertebrate Phyla

RAJ V. MANKAD, ALEXANDER A. GIMELBRANT, AND TIMOTHY S. MCCLINTOCK*

Department of Physiology, University of Kentucky, 800 Rose St., Lexington, Kentucky 40536-0298

The efficiency of translational initiation depends upon the sequence context surrounding the AUG codon (1, 2, 3). A purine at position -3 contributes critically to context, but other neighboring nucleotides are also important. Nucleotide frequencies at these neighboring positions vary among distant taxa (4, 5). We have analyzed the translational initiation sites of cnidarian, echinoderm, molluscan, annelid, and crustacean sequences in nucleotide sequence databases. These taxa conform to the pattern of a strong preference for a purine at -3, but the frequencies of nucleotides at neighboring positions are characteristic for each taxon. The consensus translational initiation sequences of the marine invertebrate taxa are also different from those of vertebrates and single-celled eukaryotes. These consensus sequences are useful guides for predicting translational initiation sites in cDNA clones.

The initiation of translation in eukaryotes requires the function of several complexes of proteins (6, 7, 8, 9, 10). In cap-dependent translation, a ternary complex of eukaryotic initiation factor 2B (eIF2B), GTP, and Met-tRNA interacts with a 40 S ribosomal subunit complex containing eIF1A and eIF3 to form the 43 S preinitiation complex. The 43 S complex is recruited to the cap at the 5' end of the mRNA by eIF4F (composed of eIF4E, eIF4G, and eIF4A). The 43 S complex then scans the mRNA in the 3' direction. The melting of RNA secondary structure, which can interfere with binding of the 43 S complex to the RNA and with scanning, is accomplished by the helicase activity of eIF4A and eIF4B. When an AUG is encountered, the 43 S complex pauses or slows. During the pause, the hydrolysis of GTP by eIF2 is associ-

ated with the release of the initiation factors and the binding of the 60 S ribosomal subunit to the 40 S subunit to form the 80 S ribosome, and translation is initiated. Because the 43 S complex scans the mRNA from the 5' end to the 3', the most 5' AUG is often the site of initiation of translation. However, mRNAs in which downstream AUGs are translational initiation sites are common. In cases where an upstream AUG codon is followed by a short open reading frame, the 40 S subunit can reinitiate scanning and initiate translation from a downstream AUG (11). For some mRNAs, a cap-independent mechanism of translation is used, and upstream AUGs can be bypassed completely by the initiation complex (10). In addition, some of the initiation factors are subject to physiological regulation by signaling pathways, supporting the idea that the initiation of translation is a significant component of the regulation of gene expression in cells (6, 12). For further details see reviews by Pain, 1996 (6), Proud and Denton, 1997 (8), Green and Noller, 1996 (9), and Sachs *et al.*, 1997 (10).

One of the contributing factors for arresting the 43 S preinitiation complex at an AUG is the sequence flanking the AUG. For vertebrates, the sequence GCCA/GCCAUGG is a strong context for translational initiation, and deviations from this sequence decrease the efficiency of translation (2, 3, 13, 14, 15). The most conserved nucleotide is a purine, usually an A, at position -3. Translational initiation sites from eukaryotes and prokaryotes alike display a strong preference for a purine at this position (4, 5, 16). Very weak contexts that lack a purine at -3 cause reduced levels of protein or significant initiation of translation from downstream AUG codons with stronger contexts (13, 15). The mechanisms by which the 43 S complex interacts with translational initiation sites are poorly understood, except for the requirement for the Met-tRNA anticodon and evidence for involvement of eIF2 (6). The effects of context on the efficiency of trans-

Received 17 September 1997; accepted 31 August 1998.

* Author to whom correspondence should be addressed. E-mail: mcclint@pop.uky.edu

Crustaceans, n = 98

	-18	-17	-16	-15	-14	-13	-12	-11	-10	-9	-8	-7	-6	-5	-4	-3	-2	-1	+4	+5	+6	+7	+8	+9	+10	+11	+12	+13	
A	31	26	27	24	31	24	41	42	33	36	21	30	35	24	28	65	39	20	33	26	8	28	33	18	23	21	25	36	
C	24	30	26	34	24	39	23	17	29	21	40	30	17	33	46	5	27	42	23	28	17	19	21	37	18	22	31	12	
G	18	16	17	13	18	20	15	18	23	12	21	13	24	15	11	27	16	28	35	26	42	40	27	21	37	32	21	43	
T	28	28	30	29	27	18	21	23	16	31	19	26	24	28	15	3	18	10	9	21	33	13	20	25	23	26	24	8	
	a	c	c	c	a	c	a	a	a	a	c	a/c	a	c	c	A	a	c	ATG	g	c	G/T	g	a	c	g	g	c	A/G

Annelids, n = 51

	-18	-17	-16	-15	-14	-13	-12	-11	-10	-9	-8	-7	-6	-5	-4	-3	-2	-1	+4	+5	+6	+7	+8	+9	+10	+11	+12	+13					
A	30	28	37	54	28	37	25	51	45	38	26	44	46	20	38	75	45	24	20	18	22	32	26	36	24	30	34	26					
C	15	17	26	13	26	17	19	14	20	26	32	26	12	28	36	2	16	29	16	40	22	22	28	20	30	34	10	16					
G	17	26	13	17	22	17	27	16	8	10	14	18	16	12	16	22	12	45	32	18	24	22	28	24	28	16	14	40					
T	37	28	24	15	24	28	29	18	27	26	28	12	26	40	10	2	28	2	32	24	32	24	18	20	18	20	42	18					
	t	a	t	a	A	a	a	t	A	a	a	c	a	a	t	a	A	a	g	ATG	g	t	c	t	a	c	g	a	c	c	A	T	g

Molluscs, n = 249

	-18	-17	-16	-15	-14	-13	-12	-11	-10	-9	-8	-7	-6	-5	-4	-3	-2	-1	+4	+5	+6	+7	+8	+9	+10	+11	+12	+13				
A	35	37	31	31	31	38	35	39	50	34	33	39	31	19	32	73	39	35	28	34	18	25	28	23	28	29	26	35				
C	20	23	27	23	24	30	29	24	19	19	34	22	14	33	45	3	30	35	18	37	14	20	26	37	18	23	25	20				
G	16	15	19	20	17	7	13	17	10	27	16	12	24	16	10	18	10	20	38	18	29	37	18	18	28	13	21	28				
T	29	25	23	26	20	25	22	20	21	20	17	27	31	32	12	5	21	10	17	12	39	18	28	22	26	36	29	17				
	a	a	a	a	a	a	a	A	a	c	a	a	t	c	A	C	A	a	a	c	ATG	g	c	t	g	a	t	c	a	t	t	a

Aplysia californica, n = 66

	-18	-17	-16	-15	-14	-13	-12	-11	-10	-9	-8	-7	-6	-5	-4	-3	-2	-1	+4	+5	+6	+7	+8	+9	+10	+11	+12	+13	
A	11	27	24	31	20	25	28	35	42	30	33	48	33	19	21	75	30	33	20	35	14	27	30	14	21	32	29	33	
C	40	25	24	22	20	35	35	28	30	18	37	21	14	30	48	0	33	38	20	41	18	15	27	35	17	21	27	24	
G	37	27	29	31	27	8	13	15	13	43	18	19	27	18	10	18	8	13	46	17	38	35	14	29	38	23	18	27	
T	12	20	24	17	32	32	23	22	15	10	13	13	25	33	22	8	29	16	15	8	30	23	29	23	24	24	26	15	
	C/G	a/g	g	a/g	t	c	c	a	a	g	c	a	a	t	c	A	c	c	ATG	g	A/C	g	g	a	c	g	a	a	a

Echinoderms, n = 230

	-18	-17	-16	-15	-14	-13	-12	-11	-10	-9	-8	-7	-6	-5	-4	-3	-2	-1	+4	+5	+6	+7	+8	+9	+10	+11	+12	+13	
A	33	41	37	36	33	39	31	41	46	31	33	43	38	19	32	94	33	22	15	20	20	20	29	24	34	27	32	28	
C	27	18	27	25	24	31	27	23	17	22	28	24	13	24	54	2	28	50	15	51	12	19	24	31	21	28	27	18	
G	18	19	16	16	11	14	12	14	16	17	12	14	21	13	6	9	8	18	40	19	25	46	30	16	30	23	15	39	
T	22	22	21	23	31	15	30	22	21	30	27	20	28	44	8	5	31	9	29	10	44	16	17	30	15	22	26	15	
	a	a	a	a	a	a	a	a	a	a	a	a	a	t	A/C	A	a	C	ATG	g	C	t	g	g	c	a	c	a	g

Strongylocentrotus purpuratus, n = 91

	-18	-17	-16	-15	-14	-13	-12	-11	-10	-9	-8	-7	-6	-5	-4	-3	-2	-1	+4	+5	+6	+7	+8	+9	+10	+11	+12	+13			
A	33	39	34	35	31	36	30	39	54	25	29	33	31	18	38	78	37	20	20	26	23	22	26	12	30	28	32	30			
C	21	16	28	22	26	35	30	21	17	24	19	29	17	28	48	4	26	48	14	44	10	14	24	31	24	24	26	18			
G	24	23	21	16	14	11	13	16	12	23	14	12	25	9	7	14	8	20	39	19	27	45	26	25	27	20	18	35			
T	23	23	18	28	29	19	27	24	18	29	38	26	28	45	7	5	29	13	27	11	40	19	23	32	19	28	25	17			
	a	a	a	a	a	a	a/c	a	A	t	t	a	a	t	A/C	A	a	c	ATG	g	c	t	g	a	g	t	a	a	t	a	g

Cnidarians, n = 85

	-18	-17	-16	-15	-14	-13	-12	-11	-10	-9	-8	-7	-6	-5	-4	-3	-2	-1	+4	+5	+6	+7	+8	+9	+10	+11	+12	+13			
A	26	37	42	34	45	47	36	37	37	41	41	47	42	23	48	69	47	43	29	32	24	32	37	34	34	31	37	29			
C	21	19	11	14	18	9	27	16	21	14	12	15	8	31	21	10	15	28	7	39	11	16	18	18	18	18	13	19			
G	16	12	16	10	14	12	8	20	17	14	13	12	21	18	13	13	12	10	35	11	21	31	17	20	33	17	15	33			
T	37	32	31	43	24	32	29	27	24	31	35	26	30	29	19	9	26	19	28	18	44	22	28	28	15	34	35	18			
	t	a	a	A	T	a	A	T	a	a	a	A	T	a	a	c	a	A	a	a	ATG	g	c	t	a	a	a	a	a	a	g

Figure 1. Nucleotide frequencies at positions flanking translational initiation sites of marine invertebrate taxonomic groups. Uppercase letters depict nucleotides that meet the 50/75 consensus rule (18). At all other positions the nucleotide (or nucleotides in cases of equal frequencies) with the highest frequency is shown in lowercase. All nucleotides meeting the 50/75 consensus rule were found by chi-square analysis to differ significantly from expected frequencies.

lational initiation are, however, incremental rather than absolute, because even weak contexts support the initiation of translation. In fact, the vast majority of vertebrate cDNAs possess translational initiation sites that are not identical to the strong context of GCCA/GCCATGG (4, 17).

Nucleotide preferences in sequences that flank translational initiation sites vary among major taxonomic groups (4, 5). Therefore, we have analyzed the frequencies of nucleotides at positions flanking translational initiation sites of cDNAs from several major marine invertebrate taxa (phylum or subphylum) that have been diverging for many millions of years. We have found that nucleotide frequencies at these positions are phylogenetically distinct.

Sequence databases now contain sufficient information from several marine invertebrate phyla that tables of nucleotide frequencies at translational initiation sites can be constructed. Using the sequence databases of the National Center for Biotechnology Information, we analyzed translational initiation sites in sequences from the phyla Cnidaria (376 sequences), Echinodermata (1053), Mollusca (1365), Annelida (270), and the subphylum Crustacea (690). Because many of the sequences analyzed were fragments or were ribosomal or mitochondrial DNAs, the number of sequences with suitable translational initiation sites was much smaller: 85 for cnidarians, 230 for echinoderms, 249 for molluscs, 51 for annelids, and 95 for crustaceans. In addition, sufficient sequences from *Strongylocentrotus purpuratus* and *Aplysia californica* were available that their translational initiation sites could be compared with those of all echinoderms and molluscs, respectively. For each major taxon, the most abundant protein families in the database (and their percent occurrence) were as follows: cytoskeletal elements (11.8%) in annelids, kinases (8.2%) in cnidarians, peptide hormones (14.3%) in crustaceans, histones (22.6%) in echinoderms, and bioactive peptides (11.2%) in molluscs. We believe that the types of cDNA clones in the database were sufficiently diverse as to prevent significant bias in our analyses. For each taxon, the identified sequences were individually inspected, and the sequences surrounding each translational initiation site (positions -20 to +20) were incorporated into a spreadsheet on a personal computer. Using a computer program written in Pascal, the frequencies of occurrence of nucleotides at each position were calculated.

Figure 1 shows the nucleotide frequencies at each position from -18 to +13 surrounding the translational initiation sites from each taxon. In comparisons of a single species with its own phylum, we observed that the nucleotide frequencies at corresponding positions were similar. This comparison revealed only one position in which the frequency of a nucleotide differed more than 16 percentage points. This occurred in the comparison of *A. californica*

and all molluscs at a position -18, relatively distant from the ATG codon. Clear differences in nucleotide frequencies at positions near translational initiation sites are probably apparent only between distant taxa (see refs. 4, 5).

The nucleotide frequencies at each position were used to determine consensus sequences for each taxon. These sequences are shown in a format (5) that uses uppercase letters for nucleotides that have met the criteria of the 50/75 consensus rule, and lowercase letters for the nucleotide with the highest frequency (the preferred nucleotide) in positions at which no nucleotide reached consensus (Fig. 1 and Table 1). The 50/75 rule (18) specifies that a nucleotide reaches consensus if its frequency is greater than 50% and more than twice the frequency of any other nucleotide at that position. If the sum of the frequencies of any two nucleotides at one position is greater than 75%, the nucleotides are assigned co-consensus. The marine invertebrates conformed to the strong preference for a purine at position -3, with A reaching consensus at this position in all taxa (Fig. 1). Few other positions reached consensus in the marine invertebrate taxa, consistent with previous analyses of other taxonomic groups (4, 5).

These similarities are, however, overshadowed by differences among the consensus translational initiation site contexts of the five marine invertebrate taxa (Fig. 1 and Table 1). These differences include the positions and identities of consensus nucleotides, and trends in preferences for specific nucleotides. The number of positions at which A is the preferred nucleotide correlates positively with early divergence in the inferred phylogenetic relationships of the marine invertebrates, yeast, and vertebrates (19). In yeast, A is the preferred nucleotide at every position from -10 to -1 (4). The cnidarians had A as the preferred

Table 1

Consensus translational initiation sites

Taxon	Position						
	-6	-5	-4	-3	-2	-1	+4
Vertebrata (1)	g	c	c	A/G	c	C	A T G g
<i>Drosophila</i> (4)	a	c	C	A	a	a	A T G g
Crustacea	a	c	c	A	a	c	A T G g/a
Annelida	a	t	a/c	A	a	g	A T G g/t
Mollusca	a/t	c/t	A/C	A	a	a/c	A T G g
Echinodermata	a	t	A/C	A	a/t	C	A T G g
Cnidaria	a	a/c	a	A	a	a	A T G g
Yeast (4)	a	a	a	A	a	a	A T G t

The preferred nucleotide at each position is shown. In cases where the two nucleotides with the highest frequencies at a position were separated by less than two percentage points, or where the 75% rule was met, both nucleotides are shown. Nucleotides that met the 50/75 consensus rule (18) are shown in uppercase.

nucleotide at nine positions over this region: the molluscs, echinoderms, and annelids had seven; and the crustaceans (and *Drosophila*, ref. 4) had six. Vertebrates have A as the preferred nucleotide at only one of these positions (4). Interestingly, the consensus translational initiation sites of plant phyla also show a similar divergence, with a preference for A content in the dicot plants and for G/C content in the monocot plants (4, 5).

We have found that invertebrate phyla representing radial metazoans and the deuterostome and protostome groups of bilateral metazoans have different consensus sequence contexts at translational initiation sites. Consensus for A at position -3 is a common element in sequences that otherwise tend to be distinct. The consensus sequences that we have generated (Table I) are one of several factors that can aid in the identification of translational initiation sites in marine invertebrate phyla.

Acknowledgments

Supported by NIH award DC 02366 and a Lucy B. Lemann Fellowship at the Marine Biological Laboratory to T. S. Mc.

Literature Cited

1. Kozak, M. 1983. Translation of insulin-related polypeptides from messenger RNAs with tandemly reiterated copies of the ribosome binding site. *Cell* **34**: 971-978.
2. Kozak, M. 1986. Point mutations define a sequence flanking the AUG initiator codon that modulates translation by eukaryotic ribosomes. *Cell* **44**: 283-292.
3. Kozak, M. 1987. At least six nucleotides preceding the AUG initiator codon enhance translation by eukaryotic ribosomes. *J. Mol. Biol.* **196**: 947-950.
4. Cavener, D. R., and S. C. Ray. 1991. Eukaryotic start and stop translation sites. *Nucleic Acids Res.* **19**: 3185-3192.
5. Joshi, C. P., H. Zhuo, X. Huang, and V. L. Chang. 1997. Context sequences of translation initiation codon in plants. *Plant Mol. Biol.* **35**: 993-1001.
6. Pain, V. M. 1996. Initiation of protein synthesis in eukaryotic cells. *Eur. J. Biochem.* **236**: 747-771.
7. Sprengart, M. L., and A. G. Porter. 1997. Functional importance of RNA interactions in selection of translation initiation codons. *Mol. Microbiol.* **24**: 19-28.
8. Proud, C. G., and R. M. Denton. 1997. Molecular mechanisms for the control of translation by insulin. *Biochem. J.* **328**: 329-341.
9. Green, R., and H. F. Noller. 1997. Ribosomes and translation. *Annu. Rev. Biochem.* **66**: 679-716.
10. Sachs, A. B., P. Sarnow, and M. W. Hentze. 1997. Starting at the beginning, middle, and end: translation initiation in eukaryotes. *Cell* **89**: 831-838.
11. Dever, T. E., L. Feng, R. C. Wek, A. M. Cigan, T. F. Donahue, and A. G. Hinnebusch. 1992. Phosphorylation of initiation factor 2 α by protein kinase GCN2 mediates gene-specific translational control of *GCN4* in yeast. *Cell* **68**: 585-596.
12. Sachs, A. B., and S. Buratowski. 1997. Common themes in translational and transcriptional regulation. *Trends Biochem. Sci.* **22**: 189-192.
13. Kozak, M. 1989. Context effects and inefficient initiation at non-AUG codons in eucaryotic cell-free translation systems. *Mol. Cell. Biol.* **9**: 5073-5080.
14. Kozak, M. 1994. Determinants of translational fidelity and efficiency in vertebrate mRNAs. *Biochimie* **76**: 815-821.
15. Feng, Y., L. E. Gunter, E. L. Organ, and D. R. Cavener. 1991. Translational initiation in *Drosophila melanogaster* is reduced by mutations upstream of the AUG initiator codon. *Mol. Cell. Biol.* **11**: 2149-2153.
16. Kozak, M. 1987. An analysis of 5' noncoding sequences from 699 vertebrate messenger RNAs. *Nucleic Acids Res.* **15**: 8125-8148.
17. Kozak, M. 1996. Interpreting cDNA sequences: some insights from studies on translation. *Mamm. Genome* **7**: 563-574.
18. Cavener, D. R. 1987. Comparison of the consensus sequences flanking translational start sites in *Drosophila* and vertebrates. *Nucleic Acids Res.* **15**: 1353-1361.
19. Wainwright, P. O., G. Hinkle, M. L. Sogin, and S. K. Stickel. 1993. Monophyletic origins of the metazoa: an evolutionary link with fungi. *Science* **260**: 340-342.

A High-Affinity Hemoglobin Is Expressed in the Notochord of Amphioxus, *Branchiostoma californiense*

JAMIE J. BISHOP^{1,*}, THOMAS L. VANDERGON^{1,†}, DAVID B. GREEN¹,
JEANNETTE E. DOELLER², AND DAVID W. KRAUS²

¹Natural Science Division, Pepperdine University, 24255 Pacific Coast Highway, Malibu, California 90263-4321; and ²Department of Biology, University of Alabama at Birmingham, 1300 University Boulevard, Birmingham, Alabama 35294-1170

In the phylum Chordata, only members of the subphylum Vertebrata were thought to express hemoglobin (Hb). Here we document the existence of intracellular Hb expressed in members of the subphylum Cephalochordata. Hemoglobin is expressed in myotome tissue and in notochord cells within the body of amphioxus. Both notochord and myotome tissue Hbs have a molecular size consistent with a dimeric molecule made up of two non-covalently linked monomers each of approximately 19 kD. The notochord Hb has a relatively high oxygen-binding affinity, with an apparent P_{50} of 0.036 kPa (0.27 mm Hg), and it does not bind oxygen cooperatively. The notochord Hb may be involved in facilitating oxygen delivery and providing a short-term oxygen store within the notochord cells in order to maintain a high level of aerobic metabolism in support of the sustained contraction necessary for notochord function.

Among the metazoa, Hbs are known to exist in members of 12 of the 33 phyla of animals (1,2). In the phylum Chordata, although Hb is nearly universally expressed in members of the subphylum Vertebrata, it has not been identified in any members of the subphyla Urochordata or Cephalochordata. However, these groups of animals share a common ancestor with the vertebrates (3), who

inherited the Hb gene from the common ancestor (4,5). Recently, two of us (Doeller and Kraus) observed absorption spectra characteristic of Hb from the notochord of amphioxus from the Gulf of Mexico, *Branchiostoma floridae* (Subphylum Cephalochordata). We verified this observation and also recorded characteristic Hb spectra from both notochord and myotome tissue of another species, *B. californiense*.

The myotome tissue of cephalochordates consists of chevron-shaped bundles of cells, and the notochord tissue consists of a lamellar structure of stacked cells surrounded by a fibrous sheath. The notochord cells are known to have all the features of muscle cells, including the presence of contractile paramyosin fibers, contractility upon stimulation, and neuro-notochordal junctions possessing acetylcholinesterase activity (6,7,8). The stiffening of the notochord was shown to be under neural control, and the paramyosin filaments found in notochord cells contract when myotome filaments contract (6,7). These features clearly demonstrated the contractile nature of the amphioxus notochord, which allows for changes in stiffening that are important for swimming and burrowing in these animals (9).

Cytoplasmic Hb is commonly expressed in contractile cells of vertebrates and invertebrates, where it is often associated with the facilitation of oxygen into the actively respiring cells (10). The expression of Hb in a skeletal support such as the muscular notochord is therefore not unusual. The occurrence of Hb in two species of amphioxus suggests an important function related to the maintenance of the semi-rigid skeleton by supporting muscular activity. This communication presents data identifying

Received 21 October 1997; accepted 13 August 1998.

* Present address: Division of Molecular, Cellular and Developmental Biology, Department of Biological Sciences, University of California, Santa Barbara, CA 93106-9610.

† To whom correspondence should be addressed. E-mail: tvandergon@pepperdine.edu

Abbreviations: Hb, hemoglobin; SEC, size-exclusion chromatography; TFA, trifluoroacetic acid.

the Hb in *B. floridae* and *B. californiense* and describes structural and functional characteristics of the notochord Hb from *B. californiense*.

The *in situ* optical absorption spectra for notochord Hb from *B. californiense* are shown in Figure 1A; Figure 1B shows equivalent spectra for *B. floridae*. Figure 1C shows the *in vitro* optical absorption spectra for myotome tissue crude extracts prepared in 50 mM Tris, 100 mM NaCl, and 1 mM EDTA, pH 7.6. Notochord Hb spectra are shown for each sample equilibrated with air or with

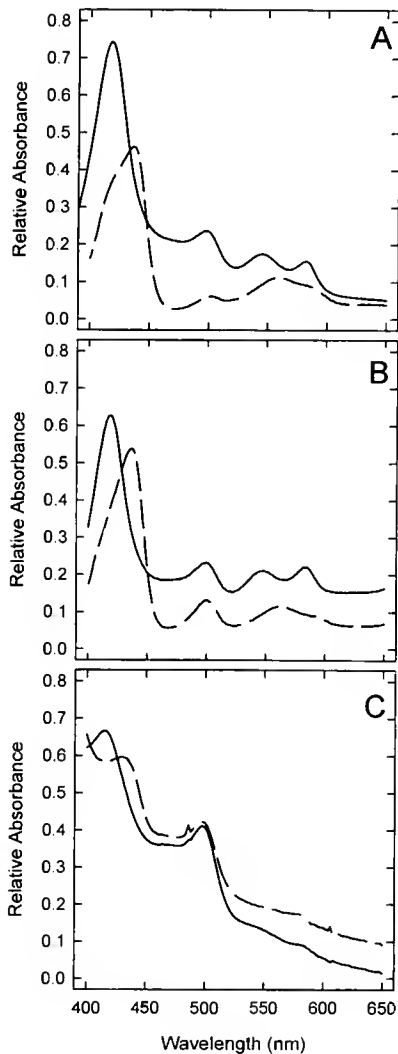


Figure 1. Optical absorption spectra acquired through the anterior region of the isolated notochord of *Branchiostoma californiense* (A) and *B. floridae* (B) equilibrated with air (—) and with 99.999% nitrogen (---). *In vitro* spectra of *B. floridae* myotome extracts (C) are shown equilibrated with air (—) and with added sodium dithionite (---). Specimens of *B. californiense* were purchased from Pacific Biomarine Supply Co. (Torrence, CA), and those of *B. floridae* were collected from shallow waters on the Gulf of Mexico or purchased from Gulf Specimen Co. (Panacea, FL).

99.999% nitrogen. Myotome Hb spectra are shown for the sample equilibrated with air or under anoxic conditions produced by addition of sodium dithionite. The air-equilibrated notochord samples show absorbance maxima at 418 nm, 546 nm, and 582 nm (± 1 nm); the nitrogen-equilibrated samples show absorbance maxima at 435 nm and 556 nm (± 1 nm). The dilute *in vitro* myotome Hb spectra show a distinct Soret band at 416 nm (± 1 nm) in air and 430 nm (± 1 nm) with sodium dithionite; however, the visible peaks were below detectable levels. The observed absorbance maxima and maxima shifts are reversible and are characteristic of the oxygenated and deoxygenated states of a typical Hb (11). Another peak occurs at 500 nm in the *in situ* notochord and *in vitro* myotome spectra, but this peak does not shift upon changes in oxygenation state and disappears following anion-exchange chromatographic purification, indicating that it is not a globin-related absorbance (data not shown). These data clearly demonstrate that Hb capable of reversible oxygen binding is expressed in two species of cephalochordates, thus expanding the known range of expression among chordates to include nonvertebrate chordates.

The size-exclusion chromatography (SEC) elution profile at 415 nm for crude protein extract from notochords is shown in Figure 2A and from myotomes in Figure 2B. The crude-extract proteins elute from the SEC column after bovine serum albumin (66 kD) but before cytochrome *c* (12.4 kD). Only the fraction eluting between 8 and 9 min (30–40 kD) in both extracts showed a characteristic Hb absorption spectrum. The anion-exchange elution profile for the Hb-containing SEC fraction from notochords is shown in Figure 2C and from myotomes in Figure 2D. One major peak with a trailing shoulder elutes near the beginning of the gradient, and no other protein peaks are evident. For both notochord and myotome extracts, the first fraction has the characteristic optical absorption spectrum of Hb.

The reversed-phase elution profiles for the Hb-containing anion-exchange fractions are shown for notochord in Figure 2E and myotome in Figure 2F. The chromatograms from the reversed-phase column showed one broad globin band between 10 and 15 min. Even though the chromatograms are off scale in Figure 2E and 2F, the computing integrator indicated two closely eluting bands in the predominant peak in both cases.

Native Hbs from *B. californiense* notochord and myotome tissues elute at about the same time from the size-exclusion column at an equivalent molecular weight of about 38 kD. Additionally, the native Hbs have similar charge densities based on their elution from the anion-exchange column. All of the globin fractions were analyzed by sodium dodecylsulfate-polyacrylamide gel electrophoresis and showed only one band at about 19 kD. This band is of equivalent size for subunits of both noto-

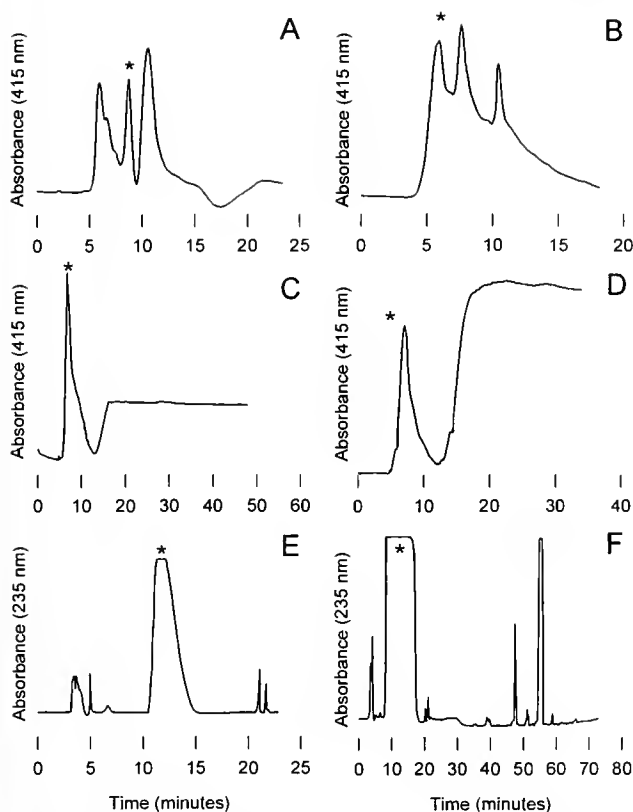


Figure 2. Elution profiles, obtained by high performance liquid chromatography, for extracts of *Branchiostoma californiense* notochord and myotome. Peaks marked with an asterisk represent the Hb-containing fractions. The chromatographic system consisted of a ternary gradient HPLC pump attached to a UV-visible absorption detector via an appropriate column. Size-exclusion chromatography (SEC) was performed on notochord extract (A) or myotome extract (B) using a Polysep-3000 (300 × 7.8 mm) SEC column with a Polysep GFPC (35 × 7.8 mm) guard column equilibrated with 10 mM Tris, pH 7.4, at a flow rate of 1.0 ml · min⁻¹. Sample volumes of 0.2 ml were injected and the eluent was monitored at 415 nm. Hb-containing fractions from the size-exclusion column were lyophilized, then resuspended in 10 mM Tris, pH 7.4. Anion-exchange chromatography was performed on the Hb fraction from A (C) or the Hb fraction from B (D) on a Biosep DEAE-P (75 × 7.8 mm) column with a Polysep GFPC (35 × 7.8 mm) guard column using a solvent program consisting of a 1-min load with 10 mM Tris, pH 7.4, followed by a solvent gradient from 0–80% 10 mM Tris/0.5 M sodium acetate in 40 min at a flow rate of 0.5 ml · min⁻¹. Sample volumes of 0.5 ml were injected and monitored at 415 nm. Hb-containing fractions from the anion-exchange column were lyophilized and resuspended in 0.1% trifluoroacetic acid (TFA) for purification by reversed-phase chromatography. Reversed-phase chromatography was performed on Hb fractions from C (E) or Hb fractions from D (F) on a Spherisorb ODS 5 μm *d_p* (250 × 4.6 mm) column using a solvent program consisting of a 1-min load with 0.1% TFA followed by a solvent gradient from 0–85% 0.1% TFA/acetonitrile in 85 min at a flow rate of 0.8 ml · min⁻¹. Sample volumes of 0.2 ml were injected and the eluent was monitored at 235 nm.

chord and myotome Hb samples. These results, and the reversed-phase chromatographic results, suggest that the notochord and myotome Hbs consist of dimers assembled

from two non-covalently linked monomers. It is unknown whether these globins are expressed from the same genes or different genes in the two distinct tissues. The existence of intracellular Hb dimers in cephalochordates is not unexpected because their nearest vertebrate relatives (the lamprey) also produce Hb dimers (12,13,14). Dimers of Hb are common also among the Echinodermata (15,16), a sister taxon to the chordates and a group that probably shares a common ancestor with the chordates (3).

The diameter of the notochord follows the general body taper and, for a *B. californiense* specimen 50 mm in length, is thinner (0.3 mm) toward the ends and thicker (0.6 mm) in the middle. Hemoglobin is detectable in all regions of the notochord, but concentration varies along its length. The heme concentration is approximately 1 mM in the thinner anterior and posterior regions of the notochord and 0.5 mM in the middle thicker region of the notochord. Concentrations were estimated from absorbance data, determination of the tissue thickness in the region of measurement, and extinction coefficient values for human Hb (11). The oxygen-binding properties of notochord Hb *in situ* were characterized using a computer-controlled Cary Model 14 recording spectrophotometer equipped with a scattered transmission accessory (Aviv Associates, Lakewood, NJ) and a humidified, temperature and gas controlled chamber. Fine forceps were used to completely clean notochord segments of adhering myotome tissue down to the fibrous sheath. The segments were then incubated at 15°C in 0.2 μm filtered 32‰ seawater buffered with 50 mM Tris and 10 mM KCN at pH 7.4 for 30 min prior to measurements. The technique for determination of O₂-binding equilibria using the scatter transmission system is described elsewhere (17). The Hb from *B. californiense* notochord has a relatively high affinity for oxygen (0.036 kPa, SD 0.013 kPa, *n* = 5) and no significant cooperativity (Hill coefficient = 1.15, SD 0.14). Oxygen release from the notochord Hb does not occur until the partial pressure of oxygen drops to near 0.25 kPa, and most of the oxygen is released near the P₅₀ of the Hb.

The oxygen consumption rates of individual animals were determined with a temperature-controlled, dual closed-chamber polarographic respirometer (Oxygraph 60697, Cyclobios Paar, Graz, Austria) (18). Under normoxic conditions (18.6–20.0 kPa) the oxygen consumption rates for six *B. californiense* individuals ranged from 3.6 to 7.9 μmol O₂ · g⁻¹ · h⁻¹; under hypoxic conditions (8.6–10.0 kPa), the oxygen consumption rate dropped to between 1.5 and 3.2 μmol O₂ · g⁻¹ · h⁻¹. Animals were able to initiate swimming motions under hypoxic conditions if disturbed, but otherwise remained quiescent at very low oxygen tensions. All animals survived exposure to the very low oxygen tensions that occurred at the end of the experiments (<0.5 kPa for up to 1 h). In all animals

there appeared to be a general trend of oxyconformity. We tested this phenomenon using the second-degree polynomial (quadratic) model proposed by Mangum and Van Winkle (19). The oxygen tension data (one measurement every 10 s for 6 to 8 h) were standardized as described (19) to millimeters of mercury for X values and fractional oxygen uptake for Y values (ranging from near 0 to 1.0). The data were fit to the quadratic model $Y = B_0 + B_1X + B_2X^2$ by the method of least-squares. The coefficients B_0 , B_1 , and B_2 were optimized by minimizing the sum of the squared residuals between the polynomial model and the data. The standard deviation about the regression (= SD of the Y estimate) was calculated from the sum of the squared residuals. Two data plots representing the curvilinear extremes and their corresponding quadratic model fits are shown in Figure 3. The standard deviation about the regression for the six *B. californiense* oxygen uptake data sets ranged from 0.018 to 0.085, indicating reasonable fit to the quadratic model. Mangum and Van Winkle (19) found that the B_2 coefficient values for the quadratic model were the most informative concerning responses that deviate from strict oxy-conformity in the direction of oxy-regulation (negative B_2 values) or in the direction opposite to regulation (positive B_2 values). The mean B_2 value for the six animals was near zero (2.40×10^{-5} , range -2.99×10^{-6} to 1.24×10^{-4}); however, it often diverged at the ends of the curves (see Fig. 3A), giving slightly negative values (-0.0004) at low PO_2 and slightly positive values ($+0.004$) at high PO_2 . No value for B_2 is very far from zero, suggesting that oxygen uptake in *B. californiense* conforms closely, although not perfectly, to declining oxygen tension.

In animals whose level of aerobic metabolism is highly dependent on PO_2 , a cytoplasmic Hb could support tissue-specific aerobic metabolism in the face of declining tissue PO_2 . Myofibril contraction within contractile cells

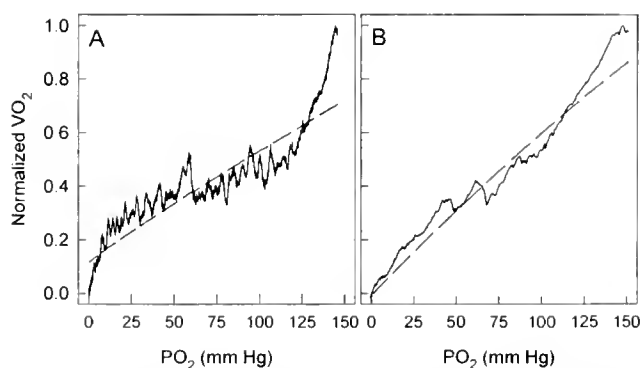


Figure 3. Fractional oxygen uptake of two *B. californiense* single animals (A and B) plotted as a function of the partial pressure of oxygen. The dashed lines represent the best fit of the data to the second-degree polynomial model proposed by Mangum and Van Winkle (19).

causes the intracellular partial pressure of oxygen to drop rapidly as the result of the high energetic demands of contraction (10). Myoglobin in heart muscle cells has been shown to effectively increase O_2 transport to 30 times the amount that can be delivered by diffusion alone (10). Amphioxus notochord Hb. with its high oxygen-binding affinity *in situ* and hyperbolic oxygen saturation curve, may facilitate diffusion of oxygen into the notochord cells (10). Although a lower Hb concentration in the thicker region of the notochord might reduce the amount of facilitated O_2 diffusion, this decrease might also be ascribed to a greater passive stiffness of the larger diameter thick region compared to the thinner regions. When acting as the skeletal support during fast swimming, amphioxus notochord cells maintain high levels of activity in tonic contracture at peak tension (7.9). This high level of activity requires an adequate supply of ATP energy that could be supplied by aerobic metabolism. By providing a constant supply of oxygen to mitochondria in the notochord cells even under active conditions, the notochord Hb may be crucial for the production of ATP by aerobic pathways, thereby supporting the maintenance of a semi-rigid skeleton.

Acknowledgments

This work is dedicated to the memory of Charlotte Preston Mangum. This investigation was supported by The Ralph M. Parsons Foundation, a grant from the University Research Council of Pepperdine University, National Science Foundation Grants IBN9343430 and IBN9219658 to JED and DWK, and NSF Research Experience for Undergraduates Grant BIR9225034 (Pepperdine University).

Literature Cited

1. Vinogradov, S., D. A. Walz, B. Pohajdak, L. Moens, O. H. Kapp, T. Suzuki, and C. N. A. Trotman. 1993. Adventitious variability? The amino acid sequences of nonvertebrate globins. *Comp. Biochem. Physiol.* **106B**: 1–26.
2. Riggs, A. F. 1991. Aspects of the origin and evolution of nonvertebrate hemoglobins. *Am. Zool.* **31**: 535–545.
3. Turbeville, J. M., J. R. Schulz, and R. A. Raff. 1994. Deuterostome phylogeny and the sister group of the chordates: evidence from molecules and morphology. *Mol. Biol. Evol.* **11**: 648–655.
4. Zharkikh, A. A., V. V. Solovyov, and N. A. Kolchanov. 1984. Conformational changes in the globin family during evolution. I. Analysis of the evolutionary role of insertions and deletions. *J. Mol. Evol.* **21**: 42–53.
5. Goodman, M., J. Pedqaydon, J. Czelusniak, T. Suzuki, T. Gotob, L. Moens, F. Shishikura, D. Walz, and S. Vinogradov. 1988. An evolutionary tree for invertebrate globin sequences. *J. Mol. Evol.* **27**: 236–249.
6. Flood, P. R., D. M. Guthrie, and J. R. Banks. 1969. Paramyosin muscle in the notochord of amphioxus. *Nature* **222**: 87–89.
7. Guthrie, D. M., and J. R. Banks. 1970. Observations on the

- function and physiological properties of a fast paramyosin muscle — the notochord of amphioxus (*Branchiostoma lanceolatum*). *J. Exp. Biol.* **52**: 125–138.
8. **Flood, P. R. 1970.** The connection between spinal cord and notochord in amphioxus (*Branchiostoma lanceolatum*). *Z. Zellforsch.* **103**: 115–128.
 9. **Webb, J. E. 1973.** The role of the notochord in forward and reverse swimming and burrowing in the amphioxus *Branchiostoma lanceolatum*. *J. Zool., Lond.* **170**: 325–338.
 10. **Wittenberg J. B., and B. A. Wittenberg. 1990.** Mechanisms of cytoplasmic hemoglobin and myoglobin function. *Annu. Rev. Biophys. Biophys. Chem.* **19**: 217–241.
 11. **Van Assendelft, O. W. 1970.** *Spectrophotometry of Haemoglobin Derivatives*. Charles C. Thomas, Springfield. 152 pp.
 12. **Briehl, R. W. 1963.** The relation between the oxygen equilibrium and aggregation of subunits in lamprey hemoglobin. *J. Biol. Chem.* **238**: 2361–2366.
 13. **Dobi Y., Y. Sugita, and Y. Yoneyama. 1973.** The self-association and oxygen equilibrium of hemoglobin from the lamprey, *Entosphenus japonicus*. *J. Biol. Chem.* **248**: 2354–2363.
 14. **Britain, T., A. J. O'Brian, R. M. G. Wells, and J. Baldwin. 1989.** A study of the role of subunit aggregation in the expression of cooperative ligand binding in the hemoglobin of the lamprey *Mordacia mordax*. *Comp. Biochem. Physiol.* **79**: 363–369.
 15. **Terwilliger, R. C., and N. B. Terwilliger. 1988.** Structure and function of holothurian hemoglobins. Pp. 589–595 in: *Echinoderm Biology*, R. D. Burke, P. V. Mladenov, P. Lambert, and R. L. Parsley, eds. A. A. Balkema, Rotterdam.
 16. **Baker, S. M., and N. B. Terwilliger. 1993.** Hemoglobin structure and function in the rat-tailed sea cucumber, *Paracaudina chilensis*. *Biol. Bull.* **185**: 115–122.
 17. **Kraus, D. W., J. E. Doeller, and C. S. Powell. 1996.** Sulfide may directly modify cytoplasmic hemoglobin deoxygenation in *Solemya reidi* gills. *J. Exp. Biol.* **199**: 1343–1352.
 18. **Haller, T., M. Ortner, and E. Gnaiger. 1994.** A respirometer for investigating oxidative cell metabolism: Toward optimization of respiratory studies. *Anal. Biochem.* **218**: 338–342.
 19. **Mangum, C. P., and W. Van Winkle. 1973.** Responses of aquatic invertebrates to declining oxygen conditions. *Am. Zool.* **13**: 529–541.

Coelomic Cavities May Function as a Vascular System in Amphioxus Larvae

THOMAS STACH

Lehrstuhl für Spezielle Zoologie der Universität Tübingen, Auf der Morgenstelle 28/E, D-72076 Tübingen, Germany

At the level of light microscopy, *Branchiostoma lanceolatum* may be the best studied species of the *Cephalochordata*—the probable sister taxon of the *Craniates* (1, 2, 3, 4). The blood vascular system of adult lancelets was studied by Rähr (5), and the detailed anatomical similarities of the major vessels prompted him to propose their homology with the vascular anatomy of *Craniates*. He also showed that, in contrast to those of the *Craniates*, most of the vessels in *B. lanceolatum* are not lined by an endothelium (6). In addition, there are rarely any hemocytes in the blood of cephalochordates. Nevertheless, certain parts of the circulatory system—endostylar artery, bulbilli, glomus, hepatic portal vein, hepatic vein, sinus venosus, subintestinal vein, and others—are reported to be contractile. Ruppert (7) proposed that the myoepithelial lining of adjacent coelomic cavities may provide the driving force for such contractions. On the basis of an extensive study by transmission electron microscopy as well as light microscopical observations of living larvae, I propose that Ruppert's hypothesis also holds true for larval stages. Moreover, the observations reported here suggest that the coelomic canal system is the functional circulatory system at a stage when the blood vessels are rudimentary.

When amphioxus larvae begin to feed in the plankton (8), the extracellular matrices (ecm) of certain areas of the body are widely expanded (Fig. 1A; methods: (20)). This is particularly evident in those areas where, in adult specimens, major blood vessels will be situated. Fully developed blood vessels in adults are typically enlarged, fluid-filled spaces within the extracellular matrix (6). In

one observation, a rudimentary blood vessel could be demonstrated by electron microscopy in the expanded ecm space below the notochord of a larva with one primary gill slit (Fig. 1B). This vessel, which corresponds to the left anterior aorta (9) in the juvenile, is associated with Hatschek's nephridium, the first excretory organ to appear in the ontogeny of amphioxus. Indeed, the functioning of the nephridium may depend upon the presence of this blood vessel (10).

In living larval stages, the first observable, contractile, longitudinal vessel-like structure is situated in the ventral midline behind the first primary gill slit (labeled *vc* in Figs. 1C and 2A). This ventral structure was termed "Blutgefäß" (11), "blood vessel" (12), "artère" (13), or "longitudinal vessel which will become the endostylar and sub-intestinal vessels of the adult" (14). Peristaltic waves of contraction pass, within about 3 seconds, from the posterior end of the vessel, rostrally over its entire length of about 400 μm (Fig. 2A). Single waves are separated from each other by a period of about 5–6 seconds. Light microscopy reveals small particles (about 0.5–1 μm) floating rostrally in the lumen of this vessel-like structure (Fig. 2B).

Transmission electron micrographs of larvae demonstrate (Fig. 1A) that the ventral coelom, a longitudinally extensive cavity, is situated immediately below the anlage of the sub-intestinal vessel (lower *ecm*; structure labeled *vc* in Fig. 1A; see also Fig. 1C). The location of the sub-intestinal vessel in adult lancelets is in an enlarged area of extracellular matrix of the dense connective tissue type in Rähr's nomenclature (6). This ecm-area is composed of a coarse granulated material; whereas the anlage of the left anterior aorta contains a fine granular substance (Fig. 1B) that, in electron micrographs, resembles the blood of

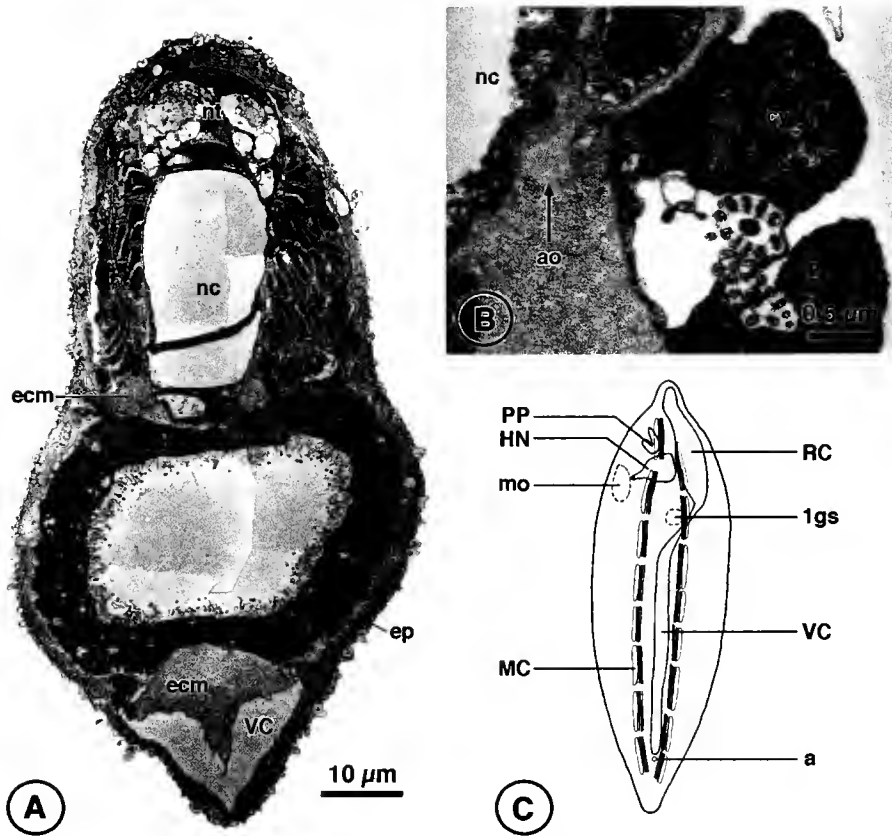


Figure 1. (A & B) Transmission electron micrographs of a larva of *Branchiostoma lanceolatum* [110 h post fertilization, 18°C; methods: (20)]. (A) Cross section of the trunk region. Structures labeled *ecm* are situated in areas where major blood vessels are situated in adults. (B) Hatschek's nephridium. Cyrtopodocytes on the enlarged *ecm* where the rudiment of the left anterior aorta is formed. (C) Diagrammatic dorsal view of coelomic cavities. a, anus; ao, anlage of the left anterior aorta; cy, cyrtopodocytic cell; *ecm*, extracellular matrix; ep, epidermis; HN, Hatschek's nephridium; mo, mouth opening; MC, myocoel; nc, notochord; nt, neural tube; PP, preoral pit; RC, rostral coelom; VC, ventral coelom; 1gs, first primary gill slit.

adults (6). Thus, the anlage of the sub-intestinal blood vessel may not contain blood fluid in this early stage. The lumen of the coelomic cavity below the anlage of the sub-intestinal blood vessel appears empty in TEM (Fig. 1A). The ventral coelom is lined by a sheet of very narrow epithelial cells interspersed with myothelial cells and cells extremely rich in rough endoplasmic reticulum (Fig. 2C, D).

The transmission electron micrographs suggest that the contractile vessel-like structure in the ventral midline of larval cephalochordates is not the sub-intestinal blood vessel, but rather the ventral coelom. The occurrence of peristaltic contractions in living specimens indicates that this system is functional in early larval stages. This precocious coelomic circulatory system could fulfill several (until now speculative) functions (see also Table 1). The observation of microscopic particles in the lumen of the

ventral coelom (Fig. 2B) suggests a role in the distribution of nutrients. This possibility is strengthened by the observation that the coelomic vessel becomes functional when the yolk reserves of nearly all cells are depleted (pers. obs.), and the animals begin to feed actively. Alternatively, since certain free coelomic cells take part in the immunological response of adult cephalochordates (15), such a function could also be hypothesized for the microscopic particles observed. Regarding the developmental stage, we might further speculate that the cells of the coelothelium, equipped with extensive rough endoplasmic reticulum (Fig. 2C), could be producing growth factors. In any event, the interpretation of the contractile vessel-like structure of larval amphioxus as a blood vessel (11, 12, 13, 14) has certainly to be revised. The contractile longitudinal vessel in these stages is a ventral coelomic canal.

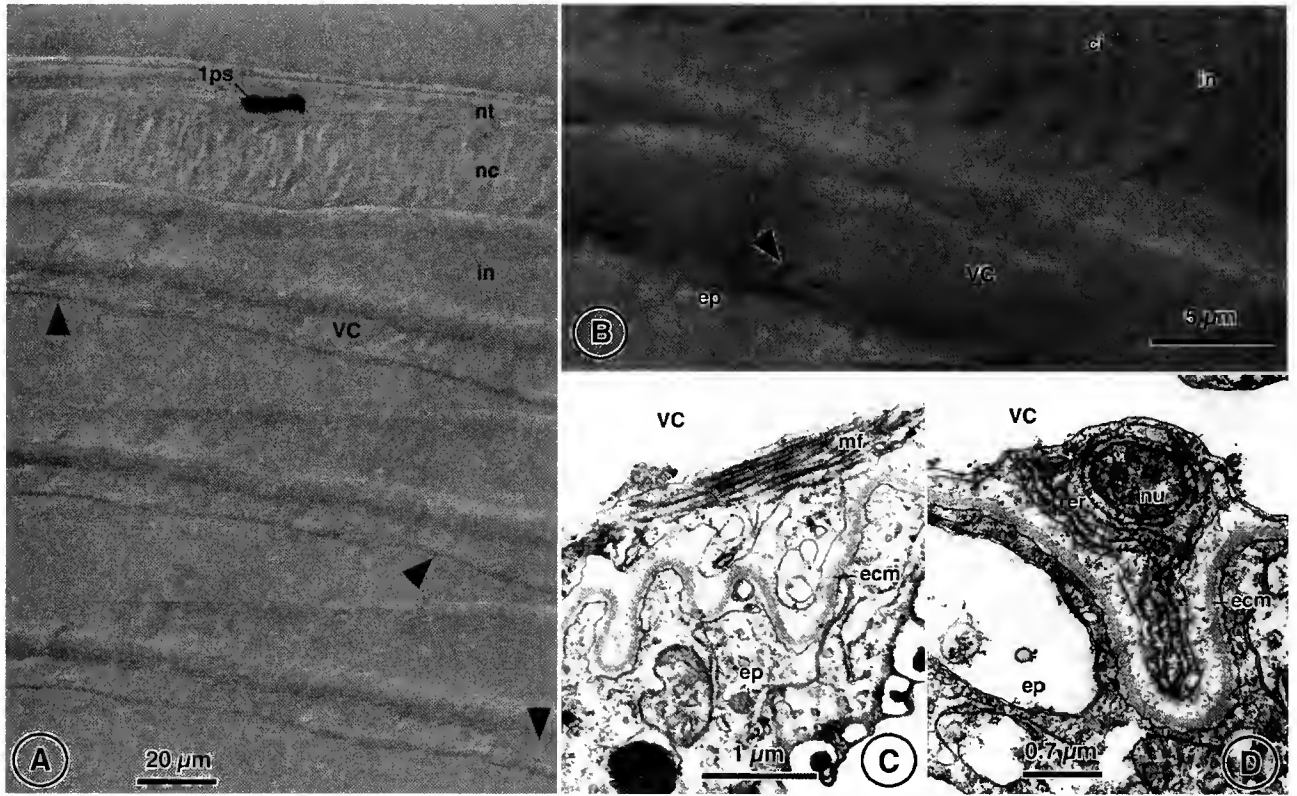


Table 1

Relevant anatomical features and suggested functions of the coelomic system and the blood vascular system of cephalochordates; note: no correlation between anatomical features and functions in the same line intended

Coelom*		Blood vascular system	
Anatomical features	Functions	Anatomical features	Functions†
Adult Epithelial lining (with intercellular junctions) present (16) Smooth myoepithelial cells present (16) Free coelomocytes in perivisceral coelom regular (15, 16) Excretory cells (cyrtopodocytes) in nephridia (e.g., 7, 9, 10)	Excretion (e.g., 7, 9, 10) Propulsion of blood (6, 7) Expulsion of gametes (16) Phagocytosis (15) Storage of nutrients (16, 17) Lubrication (16) Hydrostatic skeleton (18)	Part of the blastocoelic space, vessels usually delimited by connective tissue (mostly basement membranes) only: no endothelial lining present (6, 7) Ameboid hemocytes rarely present (e.g., 6, 7, 15) No blood or respiratory pigments present (7)	Endocytosis (19) Ultrafiltration (e.g., 7) ? Nutrient transport ? No respiratory function‡
Larva Epithelial lining (with intercellular junctions) present (9, 10) Excretory cells (cyrtopodocytes) in Hatschek's nephridium (9, 10) Smooth myoepithelial cells present#	Excretion (9, 10) Distribution of nutrients# ? Secretory function# ? Distribution of secretory products#	Only left anterior aorta distinguishable (10, #) Part of the blastocoelic space, delimited by dense connective tissue <u>not</u> by basement membrane (10, #)	Ultrafiltration (9, 10)

* Not considering the segmental myocoels, the medial walls of which are specialized as the locomotory trunk muscles.

† Physiology and function of the circulatory system of cephalochordates have hardly been investigated, but the lack of respiratory pigment is generally assumed to indicate that this system does not play a crucial role in oxygen supply.

Present study.

? Hypothetical function, not fully substantiated.

Figure 2. (A) Light microscopic aspect of a peristaltic wave passing along the ventral coelom. Anterior is to the right. About 1.2 s elapsed between first and third frame. Arrowheads, area of contraction (compare to other frames). (B) Higher light microscopical magnification of the ventral coelomic canal. Anterior to the right. Note the particulate matter within the ventral coelom (arrowhead). Direction of movement of the particle was antieriad. (C & D) Transmission electron micrographs of mesodermal cells of a larva (110 h post fertilization, 18°C). (C) Mesothelial cell bearing myofilaments. (D) Cell with extensive profiles of rough endoplasmic reticulum around the nucleus. Such cells may be of secretory function. ci, cilia; ecm, extracellular matrix; ep, ventral epidermis; in, intestine; mf, myofilaments; nc, notochord; nt, neural tube; nu, nucleus; rer, rough endoplasmic reticulum; VC, ventral coelom; Ips, first pigment spot.

Acknowledgments

I would like to thank Prof. W. Maier for generously providing support and all the facilities of the Lehrstuhl für Spezielle Zoologie, Tübingen. M. Hohloch assisted with the work in the photo lab. Two anonymous reviewers were exceptionally helpful with their constructive critical remarks.

Literature Cited

- Maisey, J. G. 1986. Heads and tails: a chordate phylogeny. *Cladistics* 2: 201–256.
- Gans, C. 1989. Stages in the origin of vertebrates: analysis by means of scenarios. *Biol. Rev.* 64: 221–268.
- Holland, P. W., L. Z. Holland, N. A. Williams, and N. D. Holland. 1992. An amphioxus homeobox gene: sequence conservation, spatial expression during development and insights into vertebrate evolution. *Development* 116: 653–661.
- Nielsen, C. 1995. *Animal Evolution*. Oxford University Press, New York.
- Rähr, H. 1979. The circulatory system of amphioxus (*Branchiostoma lanceolatum* (Pallas)). A light-microscopic investigation based on intravascular injection technique. *Acta Zool.* 60: 1–18.
- Rähr, H. 1981. The ultrastructure of the blood vessels of *Branchiostoma lanceolatum* (Pallas) (Cephalochordata). *Zoomorphology* 97: 53–74.
- Ruppert, E. E. 1997. Cephalochordata (Acrania). Pp. 349–504 in *Microscopic Anatomy of Invertebrates. Hemichordata, Chaetognatha, and the Invertebrate Chordates* 15. F. W. Harrison and E. E. Ruppert, eds. Wiley-Liss, New York.
- Stokes, M. D., and N. D. Holland. 1995. Ciliary hovering in larval lancelets (= amphioxus). *Biol. Bull.* 188: 231–233.
- Ruppert, E. E. 1996. Morphology of Hatschek's nephridium in larval and juvenile stages of *Branchiostoma virginiae* (Cephalochordata). *Isr. J. Zool.* 42: 161–182.
- Stach, T., and K. Eisler. 1998. The ontogeny of the nephridial system of the larval amphioxus (*Branchiostoma lanceolatum*). *Acta Zool.* 79: 113–118.
- Hatschek, B. 1881. Studien über Entwicklung des *Amphioxus*. *Arbeiten am Zoologischen Institut der Universität Wien und der Zoologischen Station Triest* 4: 1–88.
- Goodrich, E. S. 1934. The early development of the nephridia in amphioxus: introduction and part I, Hatschek's nephridium. *Q. J. Microsc. Sci.* 76: 499–674.
- Drach, P. 1948. Développement de l'amphioxus. Pp. 1001–1027 in *Traité de Zoologie*. P.-P. Grassé, ed. Masson, Saint-Germain, Paris.
- Jefferies, R. P. S. 1986. *Living Acraniates—Amphioxus and Its Relatives*. British Museum (Natural History), London.
- Rhodes, C. P., N. A. Ratcliff, and A. F. Rowley. 1982. Presence of coelomocytes in the primitive chordate amphioxus (*Branchiostoma lanceolatum*). *Science* 217: 263–265.
- Holland, N. D., and L. Z. Holland. 1990. Fine structure of the mesothelia and extracellular materials in the coelomic fluid of the fin boxes, myocoels and sclero-coels of a lancelet *Branchiostoma floridae* (Cephalochordata = Acrania). *Acta Zool.* 71: 225–234.
- Azariah, J. 1965. On the seasonal appearance of fin rays and their bearing on the reproductive cycle of *Branchiostoma lanceolatum*. *J. Mar. Biol. Assoc. India* 7: 459–461.
- Gutmann, W. F. 1971. Was ist urtümlich an *Branchiostoma*? *Nat. Mus.* 101: 340–356.
- Moller, P. C., and C. W. Philpott. 1973. The circulatory system of *Amphioxus* (*Branchiostoma floridae*). II. Uptake of exogenous proteins by endothelial cells. *Z. Zellforsch. Mikrosk. Anat.* 143: 135–141.
- Methods. Developmental stages of *Branchiostoma lanceolatum* were observed alive by means of light microscopy (Leitz, Axioplan) and recorded on videotape (Sony, KSP-60, U-matic). Larvae were fixed for 30 min at 0°C in a glutardialdehyde (8%)–seawater mixture (1:2). Rinsing in seawater was followed by postfixation for 3 h in an OsO₄ (4%)–seawater mixture (1:1). The animals were stained with uranyl acetate en bloc prior to embedding in Epon 812. Serial sections for light and transmission electron microscopy (TEM) were prepared on an LKB ultratome 1 as follows: a survey series of about 20 semi-thin sections 0.5 μm thick was made, followed by a series of ultra-thin sections 0.05 μm in thickness. This pattern was repeated separately for the length and height of the entire animals. Sections were stained with lead citrate (1 min) for TEM and with toluidine blue for light microscopy. TEM micrographs were prepared with a Siemens Elmiskop 102.

Functional and Evolutionary Implications of the Distribution of Phosphagens in Primitive-Type Spermatozoa

W. ROSS ELLINGTON^{1,*} AND STEPHEN T. KINSEY²

¹*Department of Biological Science and Institute of Molecular Biophysics, Florida State University, Tallahassee, Florida; 32306-4370, and* ²*Department of Biological Science, University of North Carolina, 601 South College Road, Wilmington, North Carolina 28403-3297*

Abstract. External fertilization is considered to be the primitive condition in metazoans. The spermatozoa of such organisms typically display a common primitive-type morphology that is present in a range of phyla. These spermatozoa are extremely polarized cells in that the site of ATP synthesis (mitochondria in midpiece) is located at large diffusion distances from the ATP sink (dynein ATPases in the flagellum). Spermatozoa of polychaetes, sipunculids, echiuroids, echinoderms, and tunicates contain the phosphagen creatine phosphate or express the corresponding phosphagen kinase creatine kinase (or both), even when other phosphagens/phosphagen kinases are present in somatic tissues and eggs. The selective expression of the creatine kinase system in these spermatozoa may be related to potential advantages in the cellular transport of energy. To evaluate this possibility, we compared the efficacy of the major phosphagen systems for cellular transport of energy. We used a facilitated diffusion model for spatial ATP buffering, taking into account relative differences in diffusivity and thermodynamic poise. At low ratios of [total phosphagen pool]/[total adenine nucleotide pool] (C_{G+P}/C_{Ad} ratio), creatine phosphate carried a higher fraction of total high-energy phosphate (J) than the other phosphagens. However, J values for all phosphagens were greater than 0.9, and these differences disappeared as the C_{G+P}/C_{Ad} ratio was increased. Thus, the functional benefit of using CP, rather than other phosphagens, in energy transport is quite limited. The creatine kinase system became associated with primitive-type spermatozoa early in metazoan evolution.

This association is not necessarily related to inherent advantages of this phosphagen system for buffering of ATP, but may be linked to historical events in the evolution of the cell phenotype.

Introduction

The energy “content” of ATP is not fixed but rather is related to the extent of displacement of the hydrolysis reaction ($ATP \rightarrow ADP + \text{inorganic phosphate}$) from thermodynamic equilibrium (Nicholls and Ferguson, 1992), as the effective free energy of ATP hydrolysis (ATP chemical potential, ΔG_{ATP}) is a function of the physiological [ATP]/[ADP] ratio. Under normal conditions, cellular energy metabolism maintains the hydrolysis reaction far displaced from equilibrium, which is reflected by high prevailing [ATP]/[ADP] ratios and correspondingly high values for ΔG_{ATP} (Nicholls and Ferguson, 1992; Kammermeier, 1993). Physiological conditions that lead to increases in cellular ADP concentrations lead to disproportionately larger decreases in the [ATP]/[ADP] ratio. The net effect is substantial reductions in ΔG_{ATP} that dramatically impact the functioning of critical ATP-requiring processes in cells (Kammermeier *et al.*, 1982; Kammermeier, 1987, 1993).

Phosphagens are phosphorylated guanidine compounds that are involved in buffering cellular ATP levels. These compounds are typically found in cells with high and variable rates of energy turnover. A diverse array of phosphagens is found in the animal kingdom, including arginine phosphate (AP), creatine phosphate (CP), glycoyaminate phosphate (GP), taurocyamine phosphate (TP), hypotaurocyamine phosphate (HTP), and lombricine phosphate (LP). Corresponding phosphagen (guanidino)

Received 23 March 1998; accepted 9 September 1998.

* Author to whom correspondence should be addressed. E-mail: elling@bio.fsu.edu

kinases—arginine kinase [AK], creatine kinase [CK], glycoamine kinase [GK], taurocyamine kinase [TK], hypotaurocyamine kinase [HTK] and lombricine kinase [LK]—catalyze the reversible transfer of phosphate from phosphagen to ADP, yielding ATP (phosphagen + ADP \leftrightarrow ATP + guanidine acceptor).

The traditional view of phosphagen systems is that they function as temporal ATP buffers (Meyer *et al.*, 1984). Typically, phosphagen concentrations are higher than adenine nucleotide concentrations (Beis and Newsholme, 1975; Meyer *et al.*, 1984). During periods of intense energy turnover, ΔG_{ATP} is kept high by the transphosphorylation of ADP to ATP at the expense of the phosphagen. This role of the phosphagen system has been likened to that of the discharge of a capacitor (Meyer, 1988; Kammermeier, 1993). Ellington (1989) showed that the apparent equilibrium constants ($K' = ([ATP] * [guanidine]) * ([phosphagen] * [ADP])^{-1}$) for the phosphagen kinase reactions span a range of values from 13.2 (AK) to 100 (CK); others are intermediate. This means that the CK reaction can buffer ATP over higher ranges of ΔG_{ATP} than other phosphagen systems (Ellington, 1989). However, CP might be viewed as being disadvantageous in certain invertebrate systems in which lower pH values and reduced set-point ΔG_{ATP} values may prevail, thereby inducing rapid dissipation of the CP pool (Wyss *et al.*, 1992).

A second hypothesized function of phosphagens is a potential role (particularly CP) in the transport of high-energy phosphate from "source" (typically mitochondria) to "sink" (ATPases). One perspective on the transport role, formulated as the CP "shuttle" (Bessman and Geiger, 1981) and later CP "circuit" (Wallimann *et al.*, 1992), hypothesizes that there are separate pools of adenine nucleotides at source and sink and that the CP/CK system provides the energetic link between the two sites. The net effect is to allow rapid transport of high-energy phosphate while maintaining appropriate ΔG_{ATP} values at source and sink (Mainwood and Rakuson, 1982; Jacobus, 1985; Kammermeier, 1987). The above arguments are based on diffusive constraints (concentration gradients; membrane permeability) of the adenine nucleotides vs. CP/creatine in relation to energy turnover rates. The basic premise for this view is that intracellular diffusion of ATP and particularly ADP is limiting. That is, the conditions that optimize diffusive movement of the adenine nucleotides (high concentration gradients) would produce ΔG_{ATP} values at the site of ATP utilization (sink) that would be incompatible with functioning of the ATPase (Jacobus, 1985; Kammermeier, 1987). Furthermore, additional diffusive constraints for ADP, such as binding to intracellular surfaces and reduced permeability for entry into the mitochondrion, have been identified (Saks *et al.*, 1993, 1996).

Phosphagens are distributed along distinct phylogenetic

lines (for reviews see Watts, 1968, 1971, and 1975). The CP/CK system is found in the vertebrates, lower chordates, and lower and higher invertebrate groups. The AP/AK system is widely distributed throughout the invertebrates and is present in lower chordates but absent in the vertebrates. The remaining phosphagen systems are primarily found in vermiform groups best typified by polychaetes, which as a group have all phosphagen systems (Watts, 1968, 1971, 1975). Of great interest is the observation that in such groups as polychaetes, echinoderms, and tunicates, regardless of which phosphagen system is present in somatic cells and eggs, the CP/CK system is always present in the primitive-type spermatozoa of these animals (Watts, 1968, 1971, 1975; Tombes and Shapiro, 1989). It has long been recognized that the diffusion of ATP (and ADP) might limit motility in cells that use flagella and cilia (Raff and Blum, 1968; Nevo and Rickenspoel, 1970; Lin, 1972). Thus, energy transport by phosphagens should be especially important in more highly polarized cells such as primitive-type spermatozoa, which have mitochondria in the midpiece and dynein ATPases distributed along the flagellum (Tombes and Shapiro, 1989). Here we evaluate differences in the energy transport properties of the various phosphagen systems in an effort to explain the selective expression of the CP/CK system in these primitive-type spermatozoa.

Materials and Methods

Rationale for approach

The functioning of the phosphagen systems in energy transport should be dependent on a number of parameters—thermodynamic properties of the phosphagen kinase reaction (Meyer *et al.*, 1984; Ellington, 1989) and diffusive constraints such as relative diffusivities and concentration differences. Thermodynamic differences have been documented (Ellington, 1989). The various phosphagens span a range of relative molecular masses (M_r). According to the Stokes-Einstein equation, diffusivity (diffusion coefficient, D) is given by the following expression:

$$D = k*T/(6*\pi*n*r)$$

where

k = Boltzman's constant,

T = absolute temperature,

n = viscosity,

r = molecular radius

Molecular volume should be roughly proportional to M_r . If one assumes a spherical molecule, then D values for each phosphagen should be proportional to the cubed root of the M_r . In the present study we empirically determined

the relative diffusivities of five major phosphagens and ATP. We then used these data to model the functional impact of differences in D , K' , and phosphagen concentrations on energy transport, using the steady-state, facilitated diffusion model of Meyer *et al.* (1984), in which energy transport by phosphagens is viewed as spatial ATP buffering.

Phosphagens

Five major phosphagens were used in this study (see Fig. 1 for chemical structures and Mr values). CP and AP are available commercially from Sigma Chemical Co. (St. Louis, MO). The remaining phosphagens were enzymatically synthesized using the appropriate guanidine acceptor and phosphagen kinase. We followed the protocol of Poat *et al.* (1980) with an ATP-regenerating system consisting of phosphoenolpyruvate and pyruvate kinase. CK catalyzes the phosphorylation of glycoxyamine, albeit at a much lower rate than creatine. Thus, GP was synthesized using glycoxyamine (Sigma) and muscle CK (Boehringer Mannheim, Indianapolis, IN). LK catalyzes the phosphorylation of both lombricine and taurocyamine (Suzuki *et al.*, 1997). LK was purified from the body wall of the earthworm *Eisenia foetida* according to the protocol of Suzuki *et al.* (1997). Lombricine was isolated as a natural product from the body wall of the earthworm *Lumbricus terrestris* according to the protocol of Ellington (1989). Purity was verified using thin-layer chromatography, NMR spectroscopy, and enzymatic assay. Taurocyamine was synthesized as previously described (Ellington, 1989). Both LP and TP were enzymatically

synthesized using LK as described above. All other biochemical reagents were from Sigma or Boehringer Mannheim.

Measurement of diffusion coefficients using pulsed gradient NMR spectroscopy

Diffusion coefficients for phosphagens and ATP were determined using a Bruker DMX-WB600 NMR spectrometer equipped with XYZ gradients. Phosphagens and ATP were dissolved in a model solution consisting of 50 mM HEPES buffer, 200 mM KCl, 100 mM glycine, and 25 mM $MgCl_2$ (pH of solution adjusted to 7.4). Samples were placed in 10-mm NMR tubes and mounted in a microimaging probe. Phosphorus NMR spectra were acquired at 242 MHz. Temperature was maintained at 20°C. Diffusion coefficients were determined with pulsed gradient spin echo NMR (PGSE) using a bipolar gradient sequence with a longitudinal eddy current delay period (BPP-LED) (Wu *et al.*, 1995). In this protocol, spin echo experiments were conducted with increasing applied gradients that resulted in attenuation of the ^{31}P -NMR signal. The slope of this attenuation curve is directly proportional to the mobility of the molecule being observed. Due to this dependence on mobility, it was possible to calculate the D values under these circumstances. Since AP, GP, TP, and LP have nearly identical chemical shifts, these phosphagens were investigated in independent experiments.

Mathematical treatments

Numerical simulations were conducted using Mathcad Plus version 6 (Mathsoft, Cambridge, MA) on a Pow-

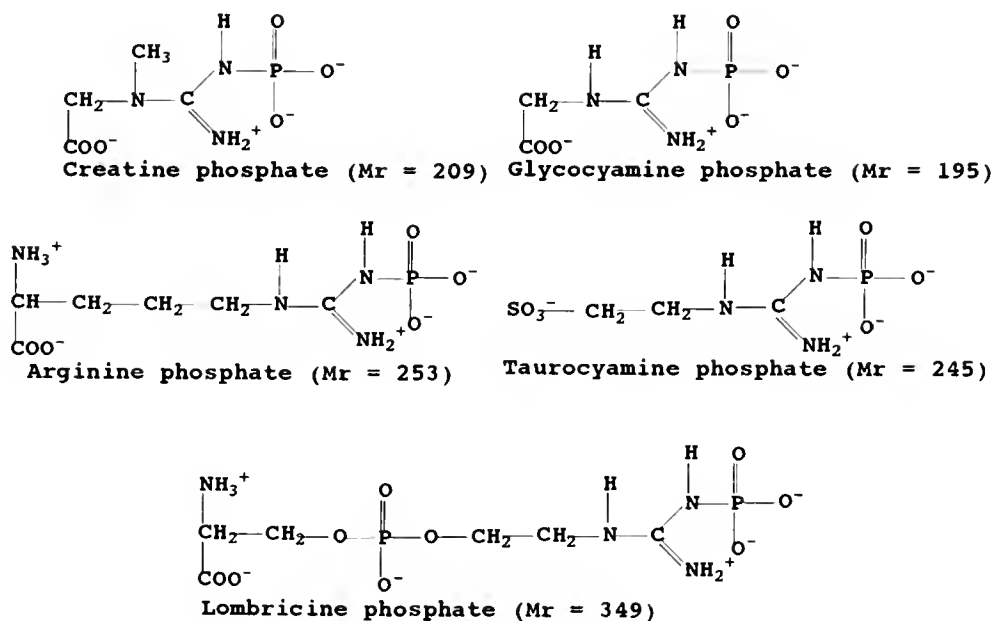


Figure 1. Structures of five of the major phosphagens.

erMac 7600 microcomputer and SlideWrite Plus version 4 (Advanced Graphics Software, Carlsbad, CA) on a Pentium 133 MHz microcomputer. Equations and boundary conditions are described in the text.

Results and Discussion

Diffusion coefficient

PGSE NMR determinations of diffusion coefficients for phosphagens and ATP yielded very consistent results within replicates for each treatment (Table I; Fig. 2). As expected according to the Stokes-Einstein equation, the D values were indirectly proportional to Mr. That is, there was a linear relationship between the diffusion coefficient and the reciprocal of the cube root of the Mr (Fig. 2). In the context of cellular energy transport, the more physiologically relevant parameter is the ratio $D_{\text{phosphagen}}/D_{\text{ATP}}$, which reflects relative mobilities of the "high energy" phosphates. The ratios range from 1.222 for the largest phosphagen, LP, to 1.597 for the smallest, GP (Table I). The $D_{\text{PC}}/D_{\text{ATP}}$ ratio observed in the present study is highly comparable to values obtained in model solutions by other groups (Yoshizaki *et al.*, 1987; Moonen *et al.*, 1990; Hubley *et al.*, 1995).

Simulation of spatial ATP buffering

Meyer *et al.* (1984) pointed out that under conditions of submaximal rates of aerobic energy turnover, the role of phosphagens can be viewed as a form of facilitated diffusion in which the phosphagen and its corresponding guanidine base, in effect, substitute for ATP and ADP, respectively. If one assumes that the phosphagen kinase reaction is globally near equilibrium throughout the cell,

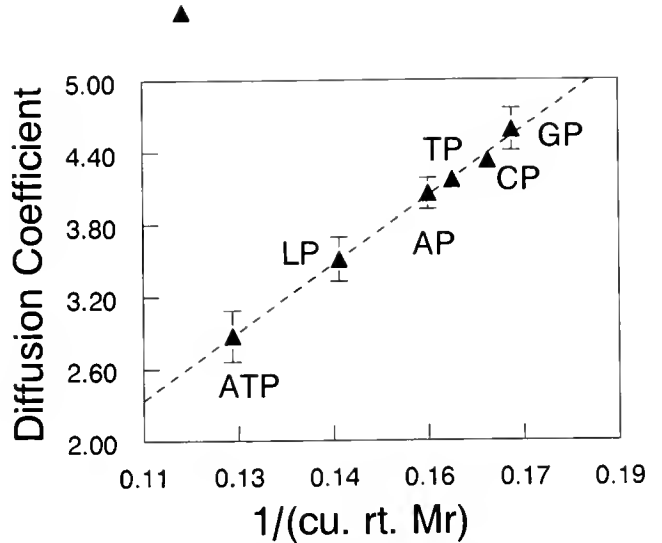


Figure 2. Relationship between diffusion coefficient ($\times 10^{-6}$ cm²/s) and the cubed root of the relative molecular mass. Each value represents a mean ± 1 SD (*n* size is reported in Table I).

then the importance of phosphagens in energy transport can be described by the following relation (Meyer *et al.*, 1984):

$$J_{\text{phos.}}/J_{\text{ATP}} = (D_{\text{phosphagen}}/D_{\text{ATP}}) * (C_{\text{G+P}}/C_{\text{Ad}}) * K' * [(R + 1)/(R + K')]^2$$

where

- $J_{\text{phos.}}/J_{\text{ATP}}$ = ratio of phosphate carried by the phosphagen over phosphate carried by ATP
- $C_{\text{G+P}}/C_{\text{Ad}}$ = ratio of concentration of total phosphagen pool over total adenine nucleotide pool
- K' = apparent equilibrium constant of phosphagen kinase
- $R = [\text{ATP}]/[\text{ADP}]$ ratio

In this context, it is assumed that the diffusion coefficients for phosphagen vs. guanidine base and ATP vs. ADP are not substantially different (Meyer *et al.*, 1984). Implicit in our use of *in vitro* D values and $D_{\text{phosphagen}}/D_{\text{ATP}}$ ratios is the assumption that these ratios do not change appreciably *in vivo*. This assumption appears to be valid for $D_{\text{PC}}/D_{\text{ATP}}$ in vertebrate skeletal muscle (Hubley *et al.*, 1995). The Meyer *et al.* (1984) model was originally developed to look at high-energy phosphate diffusion in skeletal muscle fibers. Although the geometry of spermatozoa is somewhat different, we consider the application of the model appropriate in the context of comparing relative capacities for energy transport amongst the phosphagens.

For the purposes of establishing boundary conditions, we chose a physiologically reasonable value of 300 for the $[\text{ATP}]/[\text{ADP}]$ ratio. Boundary limits for $D_{\text{phosphagen}}/D_{\text{ATP}}$ ratios and K' were 1.1 to 1.6 and 10 to 100, respectively, which bracket the range of values in Table I. For

Table I

Properties of phosphagens and corresponding phosphagen kinase reactions; data for diffusion coefficients (D) correspond to means ± 1 SD

	D (cm ² /s) $\times 10^{-6}$	$D_{\text{phosphagen}}/D_{\text{ATP}}$	Apparent equilibrium constant ¹
ATP	2.872 \pm 0.212 (<i>n</i> = 23)	—	—
Lombrocinine phosphate	3.509 \pm 0.184 (<i>n</i> = 12)	1.222	32.3
Arginine phosphate	4.054 \pm 0.129 (<i>n</i> = 5)	1.412	13.2
Taurocyamine phosphate	4.169 \pm 0.063 (<i>n</i> = 6)	1.452	27.3
Creatine phosphate	4.329 \pm 0.089 (<i>n</i> = 5)	1.508	100
Glycoeyamine phosphate	4.586 \pm 0.177 (<i>n</i> = 6)	1.597	29.0

¹ From Ellington (1989).

values of the C_{G+P}/C_{Ad} ratio we chose a range of values of 1 to 8, which brackets the observed pool ratios for a range of contractile/motile cells (Beis and Newsholme, 1975; Tombes *et al.*, 1985; Hamm and Yue, 1987; Schneider *et al.*, 1989). Numerical solutions to the above equation were calculated and expressed as the fraction of total high-energy phosphate flux carried by the phosphagen (J).

Figure 3 depicts the relationship between J, $D_{\text{phosphagen}}/D_{\text{ATP}}$ ratio, and K' at a $C_{G+P}/C_{Ad} = 1$ and a $[ATP]/[ADP]$ ratio = 300. It is apparent that there is a steep dependence of J on K' , especially in the lower K' range. The dependence of J on relative diffusivity is much less pronounced (Fig. 3). When one plots the individual 3-dimensional coordinates for each phosphagen type on the response surface, the positions of each are well dispersed (Fig. 3). However, CP's position on the surface shows that it carries the highest fraction of phosphate while AP carries the lowest. The other three phosphagens show intermediate J values (Fig. 3). Note that under the conditions used in the Figure 3 simulation, all of the phosphagens are responsible for transporting over 90% of high-energy phosphate. The impact of incrementally increasing C_{G+P}/C_{Ad} ratios on J is shown in Figure 4. The dependence of J on the $D_{\text{phosphagen}}/D_{\text{ATP}}$ ratio and K' becomes increasingly compressed so that these latter two parameters have minimal impact at higher C_{G+P}/C_{Ad} ratios.

The above analyses were conducted using the limiting condition of the ATP/ADP ratio being equal to 300. Although within physiological limits, this ratio reflects an upper extreme of energy state condition that may exist in

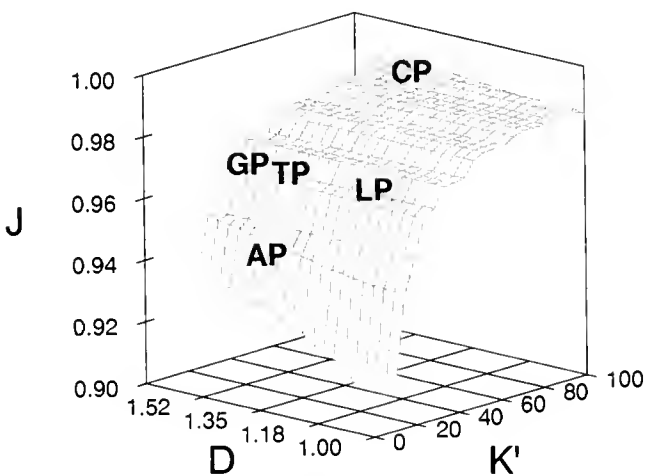


Figure 3. Impact of $D_{\text{phosphagen}}/D_{\text{ATP}}$ ratio (denoted D in figure) and apparent equilibrium constant (K') on the fraction of total high-energy phosphate (J) carried by phosphagens according to the facilitated diffusion model of Meyer *et al.* (1984). ATP/ADP and C_{G+P}/C_{Ad} ratios were set at 300 and 1, respectively. Specific J values for the various phosphagens (CP, GP, TP, LP, and AP) were calculated based on their respective D and K' values. The positions of these phosphagens are indicated on the response surface.

cells. Thus, we modeled J at a range of ATP/ADP ratios (10–300). The results (Table II) show that differences in the transport capabilities of the phosphagens are minimal except at the lowest ATP/ADP ratio (10). In this extreme case, the CK system is the least effective in transport, as was first noted by Meyer *et al.* (1984).

Before assessing the physiological implications of these results, it is useful to comment on the validity of the above simulation. In addition to the facilitated diffusion approach, high-energy phosphate transport *in vivo* has also been investigated extensively using reaction-diffusion models (Raff and Blum, 1968; Nevo and Rikenspoel, 1970; Lin, 1972; Tombes *et al.*, 1985; Hubley *et al.*, 1997); these models require the use of *in vivo* D values that are typically somewhat lower than corresponding *in vitro* D values (Moonen *et al.*, 1990; Hubley *et al.*, 1995). Furthermore, intracellular barriers dramatically decrease *in vivo* D values in a time-dependent manner (Kinsey *et al.*, 1998), which must be taken into account in reaction-diffusion analyses of energy transport. However, in our analyses we used $D_{\text{phosphagen}}/D_{\text{ATP}}$ ratios that should be minimally affected by such restrictions to diffusion and, consequently, would not compromise our overall conclusions.

Furthermore, the facilitated diffusion model is applicable only to situations in which aerobic energy turnover is near or below maximal and the global cellular high-energy phosphate concentrations do not change appreciably (or at least reach a new steady state). These circumstances should prevail in primitive-type spermatozoa of externally fertilizing marine animals that must swim for a considerable time in the water column. Recently, van Dorsten *et al.* (1997) showed that activation of motility in spermatozoa from the sea urchin *Psammechinus miliaris* is accompanied by dramatic increases in both respiration and the forward flux of CK (CP → ATP). In the same study, CP and ATP remained essentially constant for at least 2 h of motility, an observation consistent with steady-state energy transport by the CP/CK system according to the facilitated diffusion model.

Phosphagen kinase equilibrium state and compartmentation are other issues to be considered. The Meyer *et al.* (1984) approach assumes global equilibrium of the phosphagen kinase reaction throughout the cell. A number of workers have questioned the validity of this assumption (Saks and Aliev, 1996; Aliev and Saks, 1997). Recent evidence suggests that a significant fraction of the pool of creatine/creatine phosphate is not in equilibrium with CK in skeletal muscle fibers (Hochachka and Mossey, 1998). Furthermore, the whole issue of diffusion as a paradigm for intracellular transport has recently been questioned (Agutter *et al.*, 1995). In some sense, these issues are experimentally intractable in the sperm system and cannot be addressed in this study. However, on the basis of cell morphology and rates of energy turnover, it

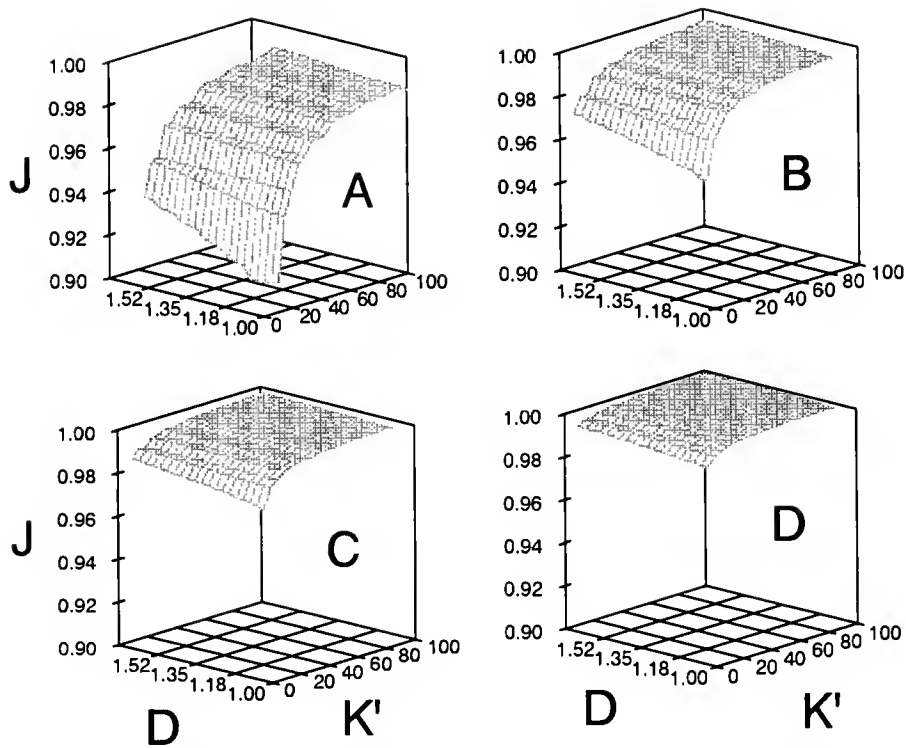


Figure 4. Impact of changes in the C_{G+P}/C_{Ad} ratio on fraction high-energy phosphate transport by phosphagens: (A) $C_{G+P}/C_{Ad} = 1$; (B) $C_{G+P}/C_{Ad} = 2$; (C) $C_{G+P}/C_{Ad} = 4$; and (D) $C_{G+P}/C_{Ad} = 8$. ATP/ADP ratio and Y and X axes are the same as in Fig. 3.

seems clear that there are certain diffusion restrictions on energy transport in primitive-type spermatozoa. Thus, in the present study we use the facilitated diffusion model to look only for broadscale and relative differences between the phosphagen systems—differences that would change the overall diffusive component of energy transport.

Diffusion of phosphagens in physiological context

The above results show that differences in thermodynamic potential and intrinsic diffusivity impact the rela-

tive capacity of phosphagens in facilitated energy transport under typical conditions of ΔG_{ATP} . At lower C_{G+P}/C_{Ad} ratios, CP, because of its higher diffusivity and high K' , carries a greater fraction of high-energy phosphate (J) than other phosphagens. However, even at low C_{G+P}/C_{Ad} ratios J values for all phosphagens fall well above 0.9. Furthermore, these differences become negligible as the C_{G+P}/C_{Ad} ratio is increased (Fig. 4). Meyer *et al.* (1984) pointed out that the spatial ATP buffering role of phosphagens should be “most important in large cells with nonuniform mitochondrial distribution in which diffusion distances are greatest.” Our analyses above show that spatial ATP buffering is moderately dependent on phosphagen type but strongly influenced by the C_{G+P}/C_{Ad} ratio. As indicated previously, primitive-type spermatozoa are highly polarized, with mitochondria separated by large diffusion distances from the dynein ATPases in the flagellum; yet these cells are capable of sustained aerobic energy turnover during swimming. Elegant work by Tombes and Shapiro (1985) and Tombes *et al.* (1985) showed that sea urchin spermatozoa contain creatine kinase (CK) and that sustained swimming is highly dependent on CK activity, presumably due to its role in energy transport.

The CP/CK system is known to be associated with primitive-type spermatozoa. Even though other phosphagen systems may be present in somatic tissues and eggs,

Table II

Impact of changes in the setpoint ATP/ADP ratio on the transport capacities of phosphagen kinase reactions

ATP/ADP ratio	LK	AK	TK	CK	GK
10	0.870	0.913	0.896	0.791	0.902
25	0.953	0.956	0.961	0.942	0.964
50	0.974	0.968	0.977	0.977	0.979
100	0.982	0.974	0.984	0.990	0.986
200	0.987	0.976	0.987	0.994	0.989
300	0.988	0.977	0.989	0.995	0.990

For the purpose of these calculations, the [total phosphagen pool]/[total adenine nucleotide pool] (C_{G+P}/C_{Ad} ratio) was set at 2.5. Data are listed as fraction of the total high-energy phosphate carried by the phosphagen (J, as in Figures 3 and 4).

the spermatozoa of all echinoderms, tunicates, and polychaetes consistently have the CP/CK system only (Watts, 1971; Tombs and Shapiro, 1989; Kamp *et al.*, 1995), with CK activities ranging from 7.1 to 30 $\mu\text{moles} \cdot \text{min}^{-1} \cdot \text{mg protein}^{-1}$ in echinoderms (Ratto *et al.*, 1989). The sipunculid *Sipunculus nudus* has high activities of AK in its somatic tissues (van Thoai *et al.*, 1966) yet the spermatozoa contain CK only (G. Kamp, pers. comm.). Recently, we have shown that sperm of another sipunculid, *Phascolopsis gouldii*, contain significant CK activity ($16.6 \mu\text{moles} \cdot \text{min}^{-1} \cdot \text{mg protein}^{-1}$) while muscle contains HTK activity (W. R. Ellington, unpub. obs.). This phenomenon is also characteristic of sperm of the echiuroid *Urechis caupo*, in which CK activity approaches $10 \mu\text{moles} \cdot \text{min}^{-1} \cdot \text{mg protein}^{-1}$ (W. R. Ellington, unpub. obs.) even though the phosphagen system present in muscle is LP/LK (Robin, 1964; van Thoai *et al.*, 1972).

The above pattern, as seen in major protostome (polychaetes, echiuroids, and sipunculids) and deuterostome (echinoderms, tunicates) groups, indicates that when an organism has the potential to express more than one phosphagen type, if CP/CK is one of the possibilities, it is the type that will, without exception, be expressed in spermatozoa. Thus, the selective expression of the CP/CK system in cells where spatial ATP buffering is critical (using logic of Meyer *et al.*, 1984) could be related to adaptive differences in functional properties amongst the phosphagen systems.

The above adaptationist interpretation of CP/CK system distribution in primitive-type spermatozoa is completely undermined by our analyses, above, which show that the differences in transport properties of the various phosphagen systems are small and that these differences collapse as the C_{G+P}/C_{Ad} ratio is increased. Marine bivalve molluscs have highly motile primitive-type spermatozoa that contain high AK activities (Tombs and Shapiro, 1989). The motility of these spermatozoa does not appear to be compromised by the lack of the CK/CP system. In 1971, Watts pointed out a distinct advantage for sperm to contain CP instead of AP: creatine is a dead-end compound, whereas arginine is in the mainstream of amino acid metabolism and is clearly important in sperm due to histone biosynthesis. This argument is credible for the preference of CP over AP in many spermatozoa but fails to explain the exclusion of phosphagens derived from glycocyamine, taurocyamine, hypotaurocyamine, and lombricine, all of which are dead-end compounds.

Why is CK selectively expressed in many spermatozoa?

Spermatozoa demonstrate a diverse array of morphologies and metabolic capacities that correlate well with mode of fertilization and—for species with external fertilization—the nature of the microhabitat (Kamp *et al.*, 1996; Kaldis *et al.*, 1997). For instance, mammalian sper-

matozoa have very low or no CK activity but generally have a high capacity for fermentative pathways (Kamp *et al.*, 1996; Kaldis *et al.*, 1997), which decreases the effective polarity ATP source and sink. Carp sperm have low CK activity but show motility for only a few minutes after release (Kamp *et al.*, 1996). In contrast, phosphagen kinase activities (especially CK) are much higher in the sperm of externally fertilizing marine invertebrates (Tombs and Shapiro, 1989; Kamp *et al.*, 1996). This dependency on phosphagen kinase is best exemplified by echinoderm sperm, which rely exclusively on mitochondrial fat oxidation (Kaldis *et al.*, 1997) and must sustain long periods of motility in the water column.

Regardless of which model is utilized, the constraints on the diffusion of adenine nucleotides make phosphagen systems critical in the motility of many primitive-type spermatozoa. However, the present simulations suggest that the various phosphagen systems differ only slightly in their capacities for energy transport, as modeled in the context of facilitated diffusion, and that these differences collapse when the C_{G+P}/C_{Ad} ratio is increased (see Fig. 4). Thus, we are hard-pressed to ascribe a functional advantage in terms of energy transport to the possession of the CP/CK system rather than another phosphagen system.

Echinoderm spermatozoa contain an octameric mitochondrial CK isoform (Tombs and Shapiro, 1985; Wyss *et al.*, 1995) that is very similar to the vertebrate mitochondrial CK present in somatic tissues (Wyss *et al.*, 1992, 1995). A unique "contiguous" trimeric CK is found restricted to the flagellum (Tombs and Shapiro, 1985; Wothe *et al.*, 1990). We recently discovered that the spermatozoa of the polychaete *Chaetopterus variopedatus* have octameric mitochondrial and "contiguous" trimeric flagellar CKs which have strikingly similar physical properties to echinoderm sperm CKs (Ellington *et al.*, 1998). Although definitive conclusions about the evolutionary relationships amongst these mitochondrial and flagellar CK's must await completion of our determinations of cDNA sequences for the polychaete forms, it seems likely that both the mitochondrial and flagellar CK isoforms evolved prior to the divergence of protostomes and deuterostomes, at least 670 million years ago (Doolittle *et al.*, 1996).

A number of workers have recently pointed out the uncertainties of attempting to view physiological characters in extant animals as adaptations to current environmental situations (Huey, 1987; Harvey and Pagel, 1991). Historical issues have to be considered. External fertilization is thought to be the primitive metazoan condition (Baccetti and Afzelius, 1976) and primitive-type spermatozoa are very similar in structure regardless of group. It is tempting to speculate that the expression of the CK system may reflect some ancient linkage between the cell

phenotype and the expression of the suite of cell-specific genes, including the two CK isoforms.

Acknowledgments

This research was supported by a grant from the National Science Foundation (IBN 96-31907) to WRE.

Literature Cited

- Agutter, P. S., P. C. Malone, and D. N. Wheatley. 1995. Intracellular transport mechanisms: a critique of diffusion theory. *J. Theor. Biol.* **176**: 261–272.
- Aliiev, M. K., and V. A. Saks. 1997. Compartmentalized energy transfer in cardiomyocytes: use of mathematical modeling for analysis of in vivo regulation of respiration. *Biophys. J.* **73**: 428–445.
- Bacetti, B., and B. A. Afzelius. 1976. *The Biology of the Sperm Cell*. Karger, Basel.
- Beis, I., and E. A. Newsholme. 1975. The contents of adenine nucleotides, phosphagens and some glycolytic intermediates in resting muscles from vertebrates and invertebrates. *Biochem. J.* **102**: 23–32.
- Bessman, S. P., and P. J. Geiger. 1981. Transport of energy in muscle: the phosphorylcreatine shuttle. *Science* **211**: 448–452.
- Doolittle, R. F., D-F Feng, S. Tsang, G. Cho, and E. Little. 1996. Determining the divergence times of the major animal kingdoms of living organisms with a protein clock. *Science* **271**: 470–477.
- Ellington, W. R. 1989. Phosphocreatine represents a thermodynamic and functional improvement over other muscle phosphagens. *J. Exp. Biol.* **143**: 177–194.
- Ellington, W. R., K. Roux, and A. Pineda. 1998. Origin of octameric creatine kinases. *FEBS Lett.* **425**: 75–78.
- Hamm, J. R., and G. M. Yue. 1987. ³¹P nuclear magnetic measurements of intracellular pH in giant barnacle muscle. *Am. J. Physiol.* **252**: C30–C37.
- Harvey, P. H., and M. D. Pagel. 1991. *The Comparative Method in Evolutionary Biology*. Oxford University Press, Oxford.
- Hochachka, P. W., and M. K. Mossey. 1998. Does muscle creatine phosphokinase have access to the total pool of phosphocreatine plus creatine? *Am. J. Physiol.* **274**: R868–R872.
- Huhley, M. J., R. C. Rosanske, and T. S. Moerland. 1995. Diffusion coefficients of ATP and creatine phosphate in isolated muscle: pulsed gradient ³¹P NMR of small biological samples. *NMR Biomed.* **8**: 72–78.
- Huhley, M. J., B. R. Locke, and T. S. Moerland. 1997. Reaction-diffusion analysis of the effects of temperature on high-energy phosphate dynamics in goldfish skeletal muscle. *J. Exp. Biol.* **200**: 975–988.
- Huey, R. B. 1987. Phylogeny, history and the comparative method. Pp. 76–97 in *New Directions in Ecological Physiology*, M. E. Feder, A. F. Bennett, W. E. Burggren, W. W. and R. B. Huey, eds. Cambridge University Press, Cambridge.
- Jacobus, W. E. 1985. Theoretical support for the heart phosphocreatine energy transport shuttle based on the intracellular diffusion limited mobility of ADP. *Biochem. Biophys. Res. Commun.* **133**: 1035–1041.
- Kaldis, P., G. Kamp, T. Piendl, and T. Wallimann. 1997. Functions of creatine kinase isoenzymes in spermatozoa. *Adv. Devel. Biol.* **5**: 275–312.
- Kammermeier, H. 1987. Why do cells need phosphocreatine and a phosphocreatine shuttle? *J. Mol. Cell. Cardiol.* **19**: 115–118.
- Kammermeier, H. 1993. Meaning of energetic parameters. *Basic Res. Cardiol.* **88**: 380–384.
- Kammermeier, H., P. Schmidt, and E. Jungling. 1982. Free energy change of ATP-hydrolysis: a causal factor of early hypoxic failure of the myocardium? *J. Mol. Cell. Cardiol.* **14**: 267–277.
- Kamp, G., H. Englisch, R. Muller, and D. Westhoff. 1995. Comparison of the two different phosphagen systems in the lugworm *Arenicola marina*. *J. Comp. Physiol. B* **165**: 496–505.
- Kamp, G., G. Busselmann, and J. Lauterwein. 1996. Spermatozoa: models for studying aspects of energy metabolism. *Experientia* **52**: 487–494.
- Kinsey, S. T., B. R. Locke, B. Penke, and T. S. Moerland. 1998. Diffusional anisotropy is induced by subcellular barriers in skeletal muscle. *NMR Biomed.* (in press).
- Lin, S. H. 1972. Transient analysis of dual enzyme reaction in cilia. *Biophysik* **8**: 264–270.
- Mainwood, G. W., and K. Rakusan. 1982. A model for intracellular energy transport. *Can. J. Physiol. Pharmacol.* **66**: 98–102.
- Meyer, R. A. 1988. A linear model of muscle respiration explains monoexponential phosphocreatine changes. *Am. J. Physiol.* **254**: C548–C553.
- Meyer, R. A., H. L. Sweeney, and M. J. Kushmerick. 1984. A simple analysis of the 'phosphocreatine shuttle.' *Am. J. Physiol.* **246**: C365–C377.
- Moonen, C. T., P. C. M. van Zihl, D. Le Bihan, and D. DesPres. 1990. In vivo NMR diffusion spectroscopy: ³¹P application to phosphorus metabolites in muscles. *Magn. Reson. Med.* **13**: 467–477.
- Nevo, A. C., and R. Rickenspoel. 1970. Diffusion of ATP in sperm flagella. *J. Theoret. Biol.* **26**: 11–18.
- Nicholls, D. G., and S. J. Ferguson. 1992. *Bioenergetics 2*. Academic Press, San Diego, California.
- Poat, P. C., I. G. Giles, and K. A. Munday. 1980. An investigation into the apparent inhibition by arginine phosphate of the activity of *Carcinus maenas* type-M pyruvate kinase. *Biochim. Biophys. Acta* **613**: 410–419.
- Raff, E. C., and J. J. Blum. 1968. A possible role for adenylate kinase in cilia: concentration profiles in a geometrically constrained dual enzyme system. *J. Theor. Biol.* **18**: 53–71.
- Ratto, A., B. M. Shapiro, and R. Christen. 1989. Phosphagen kinase evolution: expression in echinoderms. *Eur. J. Biochem.* **186**: 195–203.
- Robin, Y. 1964. Biological distribution of guanidines and phosphagens in marine annelida and related phyla from California. *Comp. Biochem. Physiol.* **12**: 347–367.
- Saks, V. A., and M. K. Aliiev. 1996. Is there the creatine kinase equilibrium in working heart cells? *Biochem. Biophys. Res. Commun.* **227**: 360–367.
- Saks, V. A., E. Vasil'eva, Y. O. Belikova, A. V. Kuznetsov, S. Lyapina, L. Petrova, and N. A. Perov. 1993. Retarded diffusion of ADP in cardiomyocytes: possible role of outer mitochondrial membrane and creatine kinase in cellular regulation of oxidative phosphorylation. *Biochim. Biophys. Acta* **1144**: 134–148.
- Saks, V. A., T. Tiivel, L. Kay, V. Novel-Chate, Z. Daneshrad, A. Rossi, E. Fontaine, C. Keriell, X. Lerverve, R. Ventura-Clapier, K. Anfous, J.-L. Samuel, and L. Rappaport. 1996. On the regulation of cellular energetics in health and disease. *Mol. Cell. Biochem.* **160/161**: 195–208.
- Schneider, A., R. J. Niener, and M. K. Grieshaber. 1989. On the role of arginine kinase in insect flight muscle. *Insect Biochem.* **19**: 471–480.
- Suzuki, T., Y. Kawasaki, T. Furukohri, and W. R. Ellington. 1997. Evolution of phosphagen kinase VI. Isolation, characterization and cDNA-derived amino acid sequence of lombricine kinase from the earthworm *Eisenia foetida*, and identification of a possible candidate for the guanidine recognition site. *Biochim. Biophys. Acta* **1343**: 152–159.
- Thoai, N. V., N. V. Thien, G. Lacombe, and J. Roche. 1966. Heteroenzymes d'acide adenosine 5'-triphosphoric: L-arginine phosphotransferase. *Biochim. Biophys. Acta* **122**: 547–550.
- Thoai, N. V., Y. Robin, and Y. Guillou. 1972. A new phosphagen.

- N'-Phosphorylguanidinoethylphospho-O-(α -N,N-dimethyl)serine (phosphothalassemine). *Biochem. J.* **11**: 3890-3895.
- Tombes, R. M., and B. M. Shapiro. 1985.** Metabolite channelling: a phosphocreatine shuttle to mediate high energy phosphate transport between sperm mitochondrion and tail. *Cell* **41**: 325-334.
- Tombes, R. M., and B. M. Shapiro. 1989.** Energy transport and cell polarity: relationship of phosphagen kinase activity to sperm function. *J. Exp. Zool.* **251**: 82-90.
- Tombes, R. M., C. J. Brokow, and B. M. Shapiro. 1985.** Creatine kinase dependent energy transport in sea urchin spermatozoa. *Biophys. J.* **52**: 75-86.
- van Dorsten, F. A., M. Wyss, T. Wallimann, and K. Nicolay. 1997.** Activation of sea urchin sperm motility is accompanied by an increase in the creatine kinase flux. *Biochem. J.* **325**: 411-416.
- Wallimann, T., M. Wyss, D. Brdiczka, K. Nicolay, and H. M. Eppenberger. 1992.** Intracellular compartmentation, structure and function of creatine kinase isoenzymes in tissues with high and fluctuating energy demands: the 'phosphocreatine' circuit. *Biochem. J.* **281**: 21-40.
- Watts, D. C. 1968.** The origin and evolution of the phosphagen phosphotransferases. Pp. 279-296 in *Homologous Enzymes and Biochemical Evolution*, N. V. Thoai and J. Roche, eds. Gordon and Breach, New York.
- Watts, D. C. 1971.** Evolution of phosphagen kinases. Pp. 150-173 in *Biochemical Evolution and the Origin of Life*, E. Schoffenials, ed. North-Holland, Amsterdam.
- Watts, D. C. 1975.** Evolution of phosphagen kinases in the chordate line. *Symp. Zool. Soc. Lond.* **36**: 105-127.
- Wothe, D. D., H. Charbonneau, and B. M. Shapiro. 1990.** The phosphocreatine shuttle of sea urchin sperm: flagellar creatine kinase resulted from a gene triplication. *Proc. Natl. Acad. Sci. USA* **87**: 5203-5207.
- Wu, D., A. Chen, and C. S. Johnson, Jr. 1995.** An improved diffusion-ordered spectroscopy experiment incorporating bipolar gradient pulses. *J. Magn. Reson.* **115A**: 260-264.
- Wyss, M., J. Smeitnik, R. A. Wevers, and T. Wallimann. 1992.** Mitochondrial creatine kinase: a key enzyme of aerobic energy metabolism. *Biochim. Biophys. Acta* **1102**: 119-166.
- Wyss, M., D. Maughan, and T. Wallimann. 1995.** Re-evaluation of the structure and physiological function of guanidino kinases in the fruit fly (*Drosophila*), sea urchin (*Psammechinus miliaris*) and man. *Biochem. J.* **309**: 255-261.
- Yoshizaki, K., H. Nishikawa, and H. Watari. 1987.** Diffusivities of creatine phosphate and ATP in an aqueous solution studied by pulsed field gradient ^{31}P NMR. *Jpn. J. Physiol.* **37**: 923-928.

Functional Significance of the Co-Localization of Taste Buds and Teeth in the Pharyngeal Jaws of the Largemouth Bass, *Micropterus salmoides*

PAUL J. LINSER, WILLIAM E. S. CARR, HOLLY S. CATE¹, CHARLES D. DERBY¹, AND JAMES C. NETHERTON III

The Whitney Laboratory, University of Florida, 9505 Ocean Shore Boulevard, St. Augustine, Florida 32086-8623; and ¹Department of Biology, Georgia State University, P.O. Box 4010, Atlanta, Georgia 30302-4010

Abstract. Studies of feeding behavior in the largemouth bass, *Micropterus salmoides*, revealed that live goldfish or artificial food balls are ingested in three discrete steps: inhalation of the food into the oral cavity, passage through the pharyngeal cavity, and swallowing. Food balls with or without a feeding stimulant were inhaled with equal frequency; thus, vision was clearly the major sense affecting inhalation. However, food balls with defined concentrations of a feeding stimulant were swallowed in a dose-dependent manner, whereas food balls without a feeding stimulant were promptly expelled. Thus, gustation played a major role in stimulating swallowing. Videotaped observations of feeding behavior suggested that both food processing and gustation occur in the pharynx and take place before the swallowing of either goldfish or food balls. The well-developed pharyngeal jaws of largemouth bass consist of six major pads of caniniform teeth in the upper pharynx and two pads in the lower pharynx. Scanning electron microscopy showed that taste buds were abundant around most of these pharyngeal teeth. Histological sections prepared from all pharyngeal pads revealed that both elevated and flattened taste buds occur with the teeth. The morphology of these taste buds was typical of that described in other teleosts. Neuronal profiles, visualized with an HNK-1 monoclonal antibody, were observed entering each taste bud. The antibody also selectively stained a group of one to four putative sensory cells in each taste bud and the distal processes of these cells in the receptor area. The co-

localization of teeth and taste buds on the pharyngeal jaws indicates that food processing and gustation both occur there, and that together these processes determine whether a potential food item is swallowed.

Introduction

Live fish are a major food item in the diet of the largemouth bass, *Micropterus salmoides* (Howick and O'Brien, 1983). Although this species is primarily a visual feeder (McMahon and Holanov, 1995), gustation apparently plays a role in the ultimate acceptance (Kubitza and Lovshin, 1997) or rejection (Kruse and Stone, 1984) of potential food items.

Taste cells present in multicellular taste buds are the major functional units in the gustatory sense of all vertebrates including teleosts (*e.g.*, Roper, 1989; Reutter and Witt, 1993). In fishes, taste buds occur not only within the oral and pharyngeal cavities, but also on external structures such as the barbels and skin (reviewed by Caprio, 1988; Jakubowski and Whitear, 1990; and others). Excitation of taste buds in the oropharyngeal cavity of two species of catfish, *Ictalurus natalis* and *I. punctatus*, is known to induce swallowing of food, whereas taste buds on the barbels and skin are involved in the location and pickup of food (Atema, 1971; Caprio *et al.*, 1993).

In addition to taste buds, teeth are also present in the oropharyngeal cavities of many fishes. Teeth in the pharynx are frequently associated with pharyngeal jaws, which are situated immediately anterior to the esophagus (Casciotta and Arratia, 1993; Vandewalle *et al.*, 1994, 1995). Pharyngeal jaws and teeth in some species are

involved in the processing of food, whereby it is masticated and crushed before being transported to the esophagus for swallowing (Sibbing, 1982; Claes and De Vree, 1991; Vandewalle *et al.*, 1994, 1995).

Preliminary visual and videotaped studies of feeding in largemouth bass revealed that just before swallowing a goldfish, the bass would always dislodge and expel many scales from the prey (Carr and Netherton, unpub. data). These observations indicated that food processing is occurring in the pharynx, which is also the site of well-developed pharyngeal jaws (Lauder, 1983). An indication that gustation also occurs in the pharynx came from observations of the swallowing or rejection of "food balls" after inhalation. Food balls devoid of a feeding stimulant were spit out after being held in the mouth a few seconds. In contrast, food balls containing a feeding stimulant were swallowed within 30 seconds. Food balls were, incidentally, treated like goldfish: small pieces of food balls were often dislodged and ejected from beneath the operculum—not from the mouth—before the balls were swallowed. This finding not only supports our notion that food processing occurs in the pharynx, it also suggests that prompt interactions occur between gustation and food processing.

Hence in a visual feeder such as the largemouth bass, gustatory signals affecting the final swallowing of suitable prey may be provided by taste buds co-located with the pharyngeal teeth that crush and otherwise damage prey organisms prior to swallowing. Although a 1982 study by Ezeasor in rainbow trout, *Salmo gairdneri*, suggested that the co-location of taste buds and pharyngeal teeth may contribute to both food processing and gustation, this important adaptation is not generally acknowledged. For example, the functional significance of taste buds juxtaposed with pharyngeal teeth near the esophagus is not noted in recent reviews or in other current literature on taste buds, pharyngeal teeth, and gustation in fish (*e.g.*, see Jakubowski and Whitear, 1990; Casciotta and Arratia, 1993; Hara, 1994; Sorensen and Caprio, 1997).

Our initial observations prompted us to study feeding behavior in the largemouth bass in more detail, and to employ light and electron microscopy and cytochemical techniques to determine whether pharyngeal teeth and taste buds occur together in the well-developed pharyngeal jaws. We report here the co-location of large numbers of teeth and taste buds in the pharyngeal jaws situated immediately anterior to the esophagus. Moreover, the results of our behavioral and anatomical studies indicate that this organization of teeth and taste buds functions in food selection in this species.

Materials and Methods

Behavior

Sixteen largemouth bass (*M. salmoides*), 230–305 mm long, were caught by hook and line from a lake in central

Florida, and transported to the Whitney Laboratory in an aerated box of lake water. The bass were placed into a 575-liter aquarium of filtered, recirculated well water and fed several times daily with live goldfish, *Carassius auratus* (and occasionally killifish, *Fundulus heteroclitus*). Bricks in the aquarium provided shelters behind which the bass could retreat when alarmed. After 3 weeks of acclimation to captivity, the fish would feed consistently in the presence of an observer, so single fish were next transferred into 76-liter metal-framed glass aquaria. Each aquarium received a constant supply of filtered, aerated well water, and was provided with a brick for shelter. After about 1 month, once the fish had become accustomed to the presence, movements, and siphoning of water and waste material by an observer, the bricks were removed. The sides of the aquaria were covered with an opaque black film to prevent fish from viewing the activities of adjacent animals.

The following regime was then used for about 1 month to condition the test animals to accept "food balls":

1. Bass were fed live goldfish and occasionally killifish at about 5% of body weight per day until at least 12 test animals were eating immediately in the presence of the observer.
2. Feeding with live fish was continued, but the bass were also presented with fresh fish fillets or shrimp pieces threaded onto the end of a monofilament line and moved in front of each test animal. This was continued until all fish were readily accepting the nonliving food.
3. Feeding with live fish was continued. But in addition, diced fish or shrimp was incorporated into "food balls" gelled with carboxymethylcellulose, compressed onto the end of a monofilament line, and presented as described above.
4. Feeding with live fish and food balls was continued, but a shrimp extract or an artificial shrimp mixture replaced the diced flesh in the food balls. Preparation and presentation of the food balls was as above.

Since all largemouth bass were not equally responsive to food on a given day, tests of food balls were preceded by the introduction of a goldfish into the tank of each test animal. On each test day, only bass that inhaled and swallowed the goldfish were subsequently presented with food balls.

Shrimp extract was made by homogenizing defrosted shrimp (*Penaeus sp.*) for 2 min in a blender in cold deionized water (1 g:3 ml; weight:volume). The homogenate was centrifuged at 5°C at 5800 × *g*. The supernatant was removed and referred to as shrimp extract (SE). An artificial shrimp mixture (ASM) was also prepared. The ASM contained the 26 amino acids, quaternary amines, nucleosides, nucleotides, and lactic acid in the same relative concentrations as given in Carr and Derby (1986).

Defined concentrations of SE or ASM were prepared by dilution with deionized water.

Food balls were prepared from a thick malleable gel that was made as follows. One part of sodium carboxymethylcellulose (high viscosity) was mixed with a KitchenAid into 9 parts of liquid composed of defined concentrations of SE, ASM, or deionized water. Portions of the resulting gel, about 2 g each, were shaped by hand into food balls. As a test of their efficacy, food balls were compressed onto the end of a monofilament line and moved in front of individual fish; each fish was given 60 s to respond. The number of food balls inhaled and then either rejected (expelled) or swallowed was recorded. The log likelihood ratio test (Zar, 1984) was used to analyze the data for significant differences.

Some of the tests and other facets of behavior, such as food processing and distinguishing between the roles of vision and gustation, were videotaped with a Sony CCD-V5000 Hi 8 video recorder for further analysis. Chemicals (>98% purity) were obtained from Sigma.

Light microscopy and immunocytochemistry

The pharyngeal jaws together with the gill arches, tongue, and opening to the esophagus were dissected away from sacrificed specimens. The dissected structure was immersed in 4% paraformaldehyde in 0.1 M sodium cacodylate buffer, pH 7.2, at 4°C. The tissue was incubated overnight in the primary fixative and then transferred to ice-cold Carnoy's solution (60% ethanol, 30% chloroform, 10% glacial acetic acid) for 90 min. The tissue was next rinsed 3 × 30 min in 100% ethanol followed by clearing in xylene for 3 × 30 min. The gross anatomy of the pharyngeal jaw apparatus was studied and drawn using a Wild M3 dissecting microscope with a camera lucida attachment.

For histological analysis of material prepared as above, specific pharyngeal pads were dissected free of the remaining pharyngeal jaw structure and infiltrated with and embedded in paraffin. Each pharyngeal pad was next sectioned, at 6–15 μm, perpendicular to the longitudinal axis of the pad. Sections were mounted on gel-subbed slides and rehydrated for either immunohistochemical or standard histological staining, as described below.

Some neuronal components of the pharyngeal pads were visualized using indirect immunofluorescence techniques, with the HNK-1 monoclonal antibody (from the American Type Culture Collection) serving as the probe. Secondary antibodies labeled with Texas red and fluorescein (Jackson Research Laboratories, Inc.) were also employed. Further details of tissue structure were also visualized by fluorescent labeling of cell nuclei with 4',6-diamidino-2-phenylindol (DAPI) as described by Linser *et al.* (1996), and by standard staining with hematoxylin and eosin.

Scanning electron microscopy

The pharyngeal jaws and associated structures described above were dissected away from other parts of the head. The surface of the tissue was rinsed extensively with jets of deionized water to remove some of the mucus and debris. The tissue was fixed in 2.5% glutaraldehyde in 0.1 M sodium phosphate buffer (PB), pH 7.4, for 1 to 4 days at 4°C. The tissue was post-fixed in 1% osmium tetroxide in 0.1 M PB. The material was then thoroughly rinsed with many volumes of 0.1 M PB, and dehydrated in a graded series of ethanol followed by immersion in dimethoxypropane. The tissue was secured onto a stub, vacuum dried, and sputter-coated with gold/palladium (Desk II sputter coater, Denton). The tissue was examined at a voltage of 5–7.5 kV using a Leica S420 scanning electron microscope.

Results

Behavior

Wild largemouth bass, *M. salmoides*, began eating live goldfish after only a few days of acclimation in captivity. Ingestion of live fish consisted of the following steps: inhalation of the prey into the oral cavity, passage through the pharyngeal cavity, and swallowing. Visual observations and video recordings revealed that the swallowing step is always preceded or accompanied by the forceful ejection of many goldfish scales from beneath the operculum. These scales did not appear to be removed during the inhalation process, either by the oral jaws or from within the oral cavity. Indeed, bass were occasionally observed to inhale goldfish, hold them in the oral cavity for several seconds, and then release them unharmed, and with the scales intact. Hence, the scales are apparently removed in the pharyngeal cavity before swallowing.

Captive largemouth bass were readily conditioned to inhale moving food balls. But food balls without a feeding stimulant (= controls) were inhaled as frequently as those containing a natural shrimp extract (SE) or an artificial shrimp mixture (ASM) (Fig. 1 inset). Inhalation of these potential food items was thus induced by the sight of a moving object and not by olfaction or gustation.

Swallowing differs from inhalation in that the decision to swallow a food item occurred only after the object was in the mouth. Food balls flavored with either SE or ASM were swallowed with a frequency that increased in a dose-dependent manner ($P < 0.001$; Fig. 1). Indeed, about 85% of the food balls containing the highest concentration of SE were swallowed, whereas no control food balls were swallowed. Food balls with a concentration of SE greater than 1%, or ASM greater than 0.05%, were swallowed at a significantly greater frequency than the controls ($P < 0.005$). Hence the gustatory sense appears to

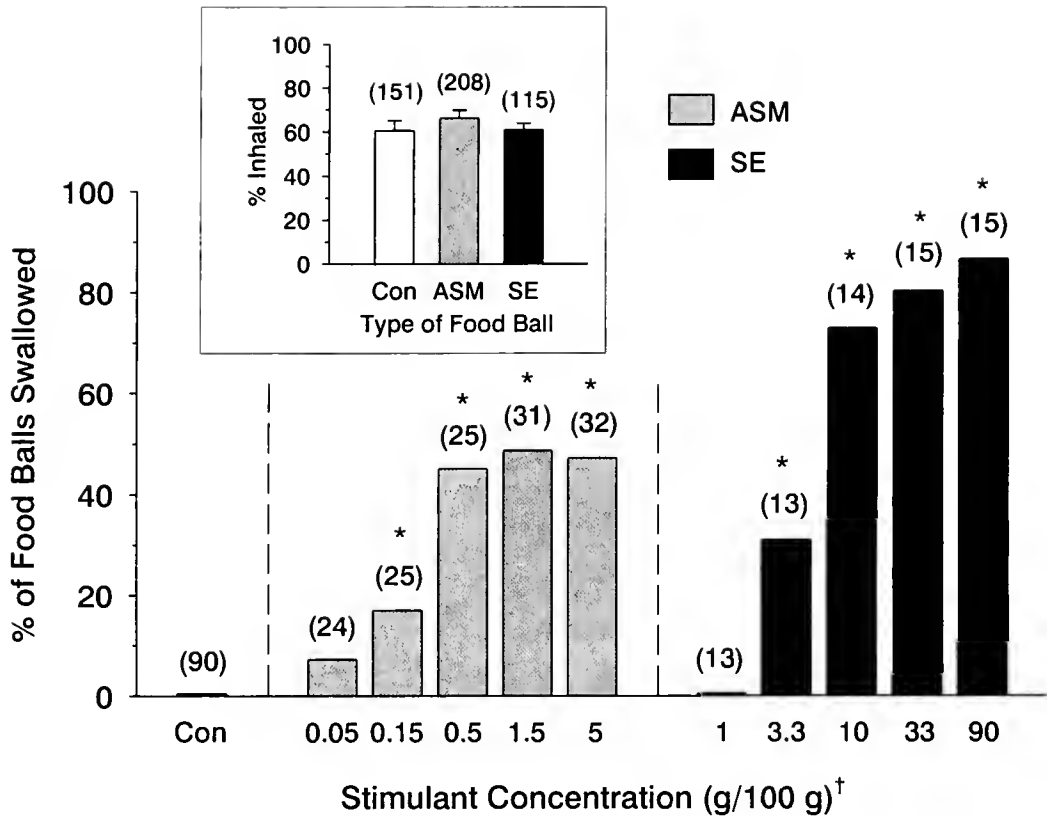


Figure 1. Percentage of food balls with or without feeding stimulant that were inhaled (inset) or swallowed by largemouth bass. Con, control; ASM, artificial shrimp mixture; SE, shrimp extract; parentheses, number of trials. Inhalation of the three types of food balls is not significantly different ($G = 2.38$, $df = 2$; $P > 0.25$). A significant dose dependency existed for the swallowing of food balls with SE ($G = 36.5$; $df = 4$; $P < 0.001$) or ASM ($G = 102.6$; $df = 4$; $P < 0.001$). All food balls with SE $> 1.0\%$ and ASM $> 0.05\%$ were swallowed with a frequency significantly greater than that of the controls (*; $P < 0.005$). Since inhalation of food balls is a prerequisite to swallowing, the percentage of food balls swallowed was calculated as the number swallowed divided by the number inhaled. †Stimulant concentration: ASM = grams of solute per 100 grams of food ball; SE = grams of SE per 100 grams of food ball.

play a major role in the decision to swallow or reject a food ball, whereas vision is the primary sense affecting its initial inhalation. Once a control ball was in the oral cavity, its average rejection time was about 3 seconds after inhalation (data not given).

Before swallowing a food ball, bass would often dislodge and eject small pieces of the ball from beneath the operculum. This process, like the removal of scales from goldfish, occurred in the posterior part of the oropharyngeal cavity. Control food balls that were rejected after inhalation were usually still intact and were always ejected from the mouth, not the operculum.

Gross morphology of pharyngeal jaws

Figure 2 shows the gross morphology of the pharyngeal jaws, teeth, gill arches, and other associated structures. The upper (dorsal) jaw has three major toothed pads

(= pharyngeal pads) on each side of the midline; the most anterior pad is designated as UPI (Fig. 2A). Each pad has a long and a short axis, with the long axis oriented in the general direction of the esophagus. The most posterior upper pad (UP3) possesses a protuberance that juts into the pharyngeal cavity just anterior to the esophageal entrance. The lower (ventral) pharyngeal pads (LP) consist of single elongate pads on each side of the midline (Fig. 2A). Each LP has a truncated triangular shape, with its posterior margin situated just in front of the entrance to the esophagus. Additional smaller pads of teeth occur on the gill arches and elsewhere in the pharynx (Fig. 2A), but our major focus was upon the major upper and lower pads described above.

All teeth on the pharyngeal pads and elsewhere in the pharynx are caniniform. On the upper pads, all teeth are curved, with their tips pointed generally toward the esophagus (Figs. 2B; 3A). The lower pads have straight cani-

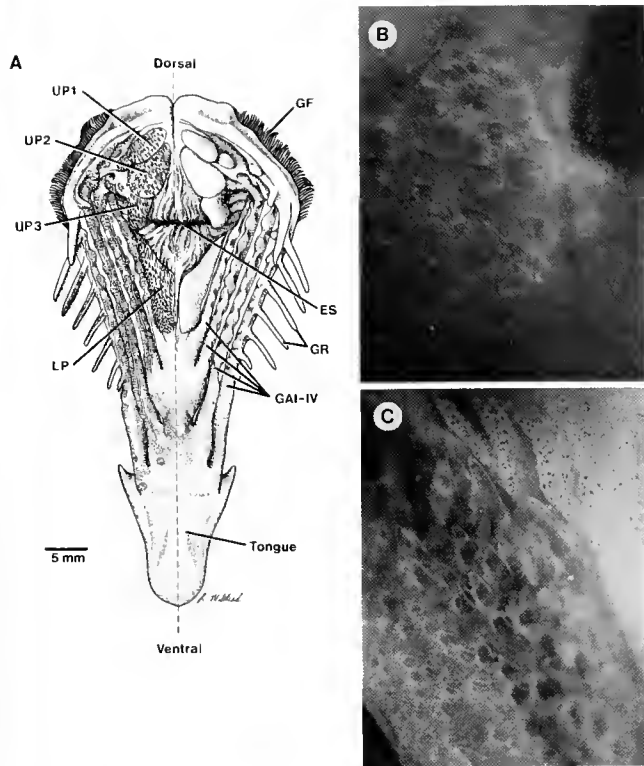


Figure 2. Gross morphology of the pharyngeal jaws, teeth, and associated structures of the largemouth bass. (A) Drawing of the fully distended pharynx and tongue; other parts of the oral cavity are not shown. The structure was opened dorsoventrally to provide a flattened configuration. Details of the dentition on the pharyngeal pads and gill arches are shown on the left half of the figure. Upper (dorsal) pharyngeal pads (UP1–3) and the gill arches (GA 1–IV) are numbered in an anterior to posterior direction. ES, esophagus; GF, gill filaments; GR, gill rakers; LP, lower pharyngeal pad. (B) Curved caniniform teeth on upper pharyngeal pad, UP2. (C) Straight caniniform teeth on medial portion of a lower pharyngeal pad. In panel A, the lines to UP2 and LP terminate in the approximate regions of teeth shown in B and C.

form teeth on the medial half (Fig. 2C) and curved teeth situated toward the periphery, and generally pointed toward the esophagus.

Co-location of pharyngeal teeth and taste buds

Scanning electron microscopy (SEM) showed that taste buds are abundant around and between most teeth of both the upper and lower pharyngeal jaws. Taste buds completely encircle many teeth (Fig. 3B, C). Many taste buds are situated atop distinct mounds or papillae (Fig. 3B–D), whereas others have a flattened surface profile. The relative proportion of the two types of taste buds was not determined because some of the flat buds were difficult to distinguish from other surface structures or debris. Higher magnification SEM showed that each taste bud also had a distinct receptor area, and microplacae (elevated ridges)

on the surrounding epithelium (Fig. 3D); these features have been observed in other fish species (e.g., Reutter *et al.*, 1974).

Histological sections verified the existence of taste buds with an elevated surface profile and a flattened profile (Fig. 4); but no further features that might distinguish the function or distribution of the two types were noted. Taste buds were also seen close to teeth on the gill arches (not shown).

Internal structure and immunoreactivity of taste buds on the pharyngeal jaws

Histological sections prepared from all pharyngeal pads showed distinct ovoid taste buds of about 40 μm in diameter and 70 μm in height (Fig. 4A–E). The taste buds

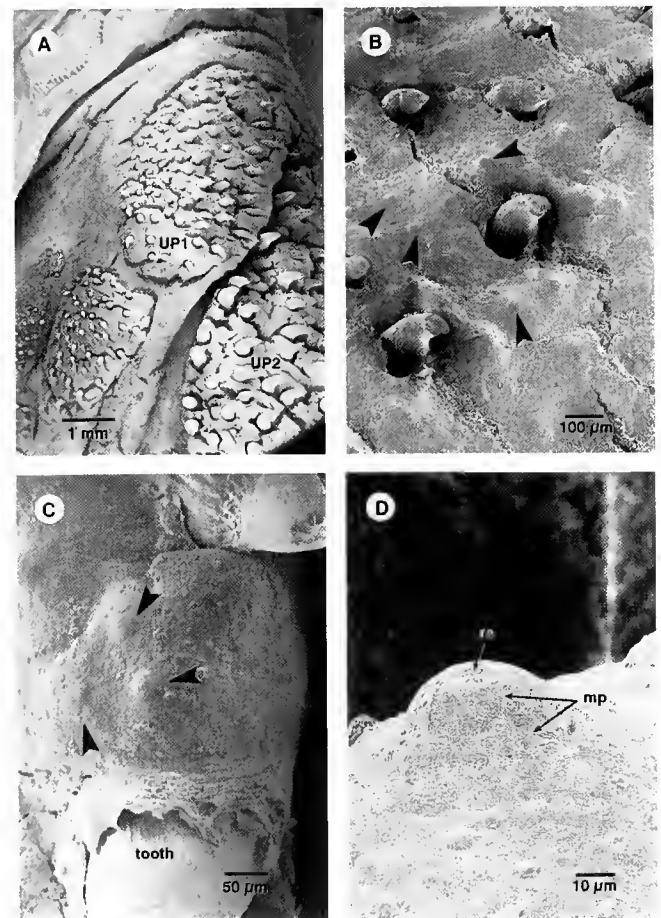


Figure 3. Scanning electron micrographs showing the co-localization of taste buds and pharyngeal teeth on the pharyngeal pads of largemouth bass. (A) Low-magnification view of upper pharyngeal pads, UP1 and UP2, with curved caniniform teeth. (B and C) Higher magnification views of papillae of elevated taste buds (arrowheads) co-located with teeth on UP2 (B) and LP (C). (D) Higher magnification of an elevated taste papilla on UP1. mp, microplacae; ra, receptor area. Other abbreviations as in Fig. 2.

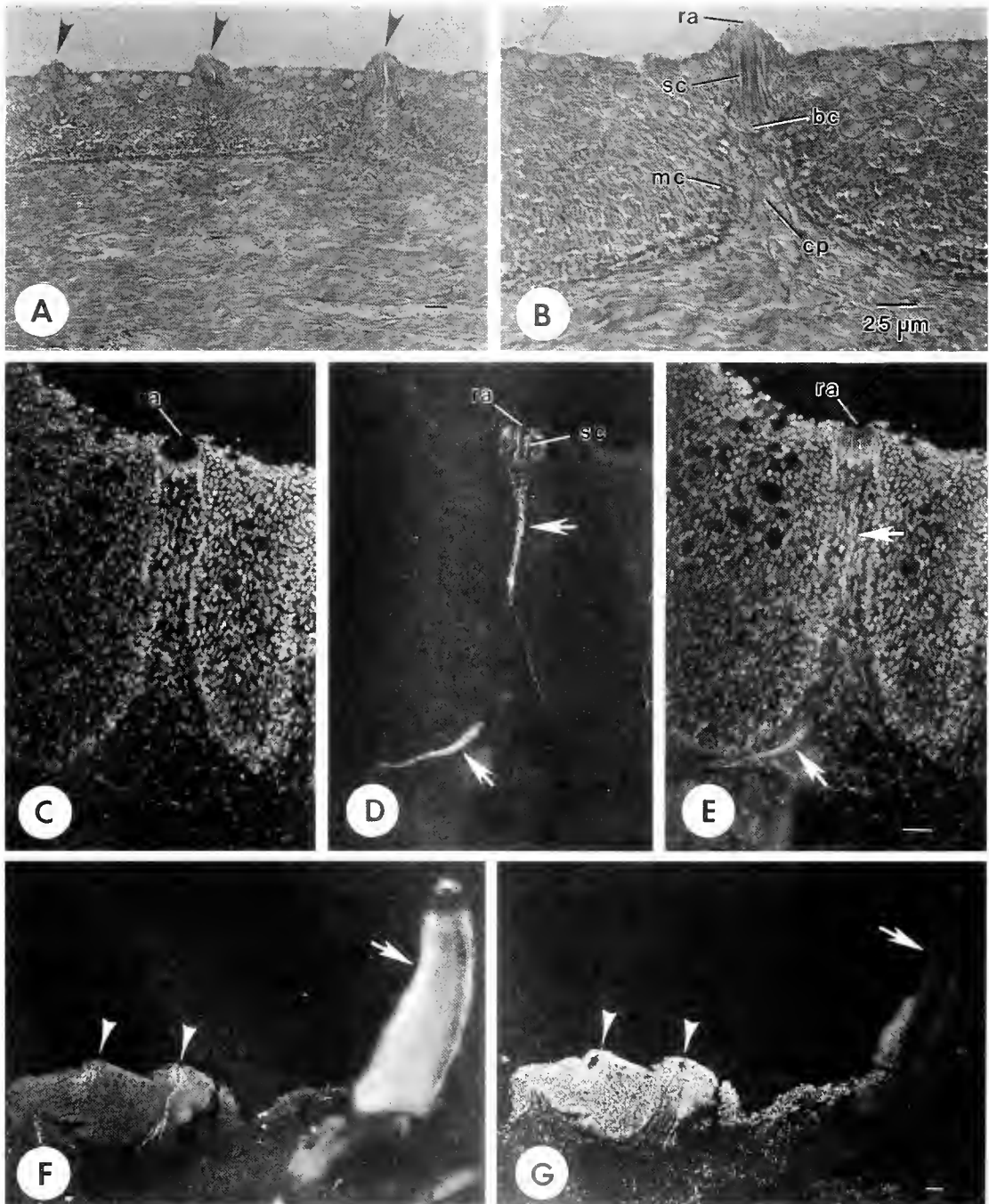


Figure 4. Elevated and flattened taste buds in histological sections of pharyngeal pads of largemouth bass. (A and B) Differential interference contrast images of hematoxylin and eosin stained sections of UP2. (A) Elevated taste buds (arrowheads) in single plane of a section. (B) Higher magnification of an elevated taste bud revealing the details of classical taste bud morphology including sheath of marginal cells (mc), corium papilla (cp), basal cells (bc), receptor area (ra), and elongated putative sensory cells (sc). (C, D, E) Single section from an LP showing a flattened taste bud as revealed by DAPI staining (C), HNK-1 immunofluorescence (D), and a combination of DAPI staining and HNK-1 immunofluorescence (E). HNK-1 fluorescence reveals the relationship between the nerve (arrows) innervating the taste bud and several putative sensory cells (sc) with processes extending into the receptor area (ra) (D and E). Scale bar: 25 μ m. (F and G) Single section from UPI illuminated with HNK-1 immunofluorescence (F) or by DAPI staining (G) at low magnification to show the co-location of a tooth (arrows) and two elevated taste buds (arrowheads). Other abbreviations as in Fig. 2. Scale bar: 25 μ m.

appear typical for teleosts (Reutter, 1992; Sorensen and Caprio, 1997). Each exhibits elongated putative sensory cells, basal cells, a corium papilla, associated neuronal elements, and an apical receptor area; and each is enclosed by a sheath of marginal cells (Fig. 4B–D). Other than the differences in surface profile, the general morphology of the elevated and flattened taste buds was very similar.

Aspects of the neural character of taste buds were examined with immunocytochemical techniques. The HNK-1 antibody recognizes a specific carbohydrate moiety frequently found on membrane glycoproteins of neural cells (Linsler, 1991; Bakker *et al.*, 1997). In the chick, HNK-1 is a powerful marker of neural crest cells and their derivatives (Bronner-Fraser, 1985). Since the sensory cells of taste buds, as well as other components of the peripheral nervous system, may be of neural crest origin (Gans and Northcutt, 1983; Ganchrow and Ganchrow, 1989), we hypothesized that this antibody might be useful for investigating pharyngeal pads.

Sections of a pharyngeal pad immunostained with the HNK-1 antibody are shown in Figure 4D–F. The staining delimited many nerves coursing through the pads and their supportive tissue. These nerves frequently exhibited branches that turn toward the surface of the pad epithelium, where they enter the basal portion of taste buds. Within a taste bud itself, immunostaining for HNK-1 was also evident over the entire length of one or more of the elongated putative sensory cells, with staining continuing distally directly into the receptor area (Fig. 4D–F). Note that only a few of the sensory cells within each taste bud were labeled with HNK-1 antibody (Fig. 4D, E). Serial analyses of several hundred taste buds revealed that in most cases only one to four cells were immunostained. Additional details of taste bud morphology were obtained by the DAPI staining of cell nuclei (Fig. 4C, E, G). This technique showed that marginal cells clearly delineate the periphery of the taste bud.

Discussion

Food processing is a facet of feeding whereby the condition of a food item is modified by mastication, crushing, or tearing prior to swallowing (Vandewalle *et al.*, 1995). In the current study of largemouth bass, videotaped observations of feeding revealed that after inhaling a live goldfish, bass would remove its scales in the oropharyngeal cavity and eject them from beneath the operculum. These observations strongly suggest that the well-developed pharyngeal jaws of the bass are processing food.

We found that, after largemouth bass inhale gelled food balls, a selection process strongly modulated by gustation occurs within their oropharyngeal cavity. Food balls containing a feeding stimulant were swallowed in a dose-dependent manner, whereas food balls without feeding

stimulant were rejected and expelled from the mouth (Fig. 1). Our subsequent finding that large numbers of teeth and taste buds are co-located in the pharyngeal apparatus (Figs. 2–4) indicates that food processing and gustatory sensing occur together in this organ before a potential food item is swallowed.

The co-occurrence of teeth and taste buds in the pharynx of fish has been observed before (Reutter *et al.*, 1974; Ezeasor, 1982; Sibbing, 1982; Hossler and Merchant, 1983; Northcott and Beveridge, 1988). However, these earlier workers failed to include, or to integrate, both behavioral and anatomical evidence demonstrating the interaction of food processing, gustation, and ingestion. For example, in extensive studies of food mastication and transport by the carp, *Cyprinus carpio*, Sibbing (1982) noted the co-occurrence of teeth and taste buds in the pharyngeal apparatus; however, the interaction of food processing and gustation was not mentioned. Likewise, Ezeasor (1982) used scanning and transmission electron microscopy to show that the pharyngeal cavity of the rainbow trout, *Salmo gairdneri*, has both teeth and taste buds, which he concluded could "conceivably" interact to affect the ingestion or rejection of a potential food item. However, Ezeasor did not conduct behavioral studies to show that food processing and gustation do indeed contribute to the decision to swallow.

In the current study with largemouth bass, vision is clearly the major sense inducing inhalation of live fish and food balls, whereas the gustatory sense contributes in a major way to swallowing. Thus these two phases of ingestion are regulated quite differently. In earlier feeding studies with largemouth bass fry, Brandt *et al.* (1987) also showed that food was located by vision, because odorants introduced into the water did not serve as attractants or stimulate feeding behavior. Gustation was, however, important at some point in food ingestion by bass fry because a gustatory stimulant such as freeze-dried krill incorporated into feed pellets increased pellet consumption (Kubitza and Lovshin, 1997). Pellet consumption by largemouth bass was also increased by incorporating artificial mixtures of substances present in a krill extract (Kubitza *et al.*, 1997). The most effective mixtures were those containing the nucleotide and nucleoside, inosine-5'-monophosphate and inosine, plus either eight amino acids or the quaternary amine, betaine. Moreover, in studies with the goldfish, *Carassius auratus*, Lamb and Finger (1995) used gelatin pellets containing feeding stimulants or aversive substances (quinine and caffeine) to show that both gustatory and textural qualities affected the sorting, rejection, or swallowing of pellets after inhalation into the mouth.

The well-developed pharyngeal jaws in largemouth bass and other members of the family Centrarchidae were described by Lauder (1983), who observed that food pro-

cessing in the pharyngeal cavity of centrarchids is especially pronounced in species such as *Lepomis microlophus* and *L. gibbosus*, whose pharyngeal jaws include molariform teeth adapted to crush snails. The adaptation, found in *L. microcephalus*, to discharge shell fragments from crushed snails through the operculum is seemingly similar to the current observations of the discharge of fish scales through the operculum by largemouth bass. However, in contrast to the molariform pharyngeal teeth of *L. microcephalus* and *L. gibbosus*, the largemouth bass has straight and curved caniniform teeth (see Figs. 2 and 3) that are more suitable for piercing flesh and removing scales than for crushing very hard objects such as snails. Phylogenetic aspects of the morphology and function of the pharyngeal apparatus in diverse species are described by Liem and Greenwood (1981) and Liem (1986).

The morphology of pharyngeal taste buds in largemouth bass revealed that many are located beneath the apices of elevated epithelial papillae (see Figs. 3 and 4). Hence their gross structure corresponds closely to Type II taste buds described by Reutter *et al.* (1974). Other taste buds were seen with a flattened surface profile that projected only slightly above the surface of the surrounding epithelium, thereby corresponding somewhat to the Type III taste buds described by Reutter *et al.* (1974). Taste buds are not confined to the pharyngeal jaws of the largemouth bass, but also occur throughout the oropharyngeal cavity on the gill arches, palate, tongue, and elsewhere, as described for other species (see reviews by Kapoor *et al.*, 1975; Reutter and Witt, 1993).

In the current study, the mouse antibody HNK-1 stained neurons entering the taste buds, as well as a limited number of putative sensory cells within the taste buds themselves. The HNK-1 antibody recognizes a specific carbohydrate moiety, sulfated glucuronic acid, associated with cell adhesion and cell-cell recognition molecules (Bakker *et al.*, 1997). The HNK-1 antibody has been widely used to examine aspects of neural development because it stains developing and mature neurons, particularly those of neural crest origin (Bronner-Fraser, 1985; Linser, 1991; Linser *et al.*, 1996). Since taste buds may be derived from both neural crest cells and placodal cells of ectodermal origin (Mistretta, 1991), the staining by HNK-1 of only a limited number of sensory cells in taste buds may indicate that these cells are of neural crest origin. Moreover, the distribution of taste bud cells stained with the HNK-1 antibody in the largemouth bass resembles the distribution of taste cells stained with the carbocyanine dye, dil, in the barbels of the catfish, *Ictalurus punctatus* (Finger and Böttger, 1990). In both cases, the limited number of stained cells within taste buds may, to quote the authors of the catfish study, "indicate a special relationship between these cells and the nerve fibers innervating them."

Our behavioral observations of a functional interaction between food processing and gustation provide a logical explanation for the co-localization of taste buds and teeth in the pharyngeal jaws of the largemouth bass. We now propose that in many fish species, food processing and gustation occur together in the pharynx and may serve as final determinants of the suitability of potential food items prior to swallowing. This hypothesis is supported by several findings. Pharyngeal jaws and teeth exist ubiquitously and have a role in food processing and transport in most families of euteleosteans, including members of both the Protacanthopterygii (soft-finned fishes) and Acanthopterygii (ray-finned fishes) (Vandewalle *et al.*, 1994). Furthermore, the presence of both teeth and taste buds within the pharyngeal cavity has been reported for a variety of fish species (Reutter *et al.*, 1974; Ezeasor, 1982; Sibbing, 1982; Hossler and Merchant, 1983; Hossler *et al.*, 1986). Finally, the hypothesis is consistent with our current behavioral and morphological findings with the largemouth bass.

Acknowledgments

This work was supported by the Whitney Laboratory, a grant from Classic Fishing Products, Inc., Clermont, Florida, to WESC, and NIH grant NICD IDC00312 to CDD. We thank Ms. Leslie Van Ekeris for assistance with the preparation and analysis of histological and immunocytochemical materials, and Dr. Robert Simmons for assistance with scanning electron microscopy. We are grateful to Ms. Marsha Lynn Milstead for preparing the illustrations. We also thank two anonymous reviewers for several very helpful suggestions regarding the manuscript.

Literature Cited

- Atema, J. 1971. Structures and functions of the sense of taste in the catfish (*Ictalurus natalis*). *Brain Behav. Evol.* **4**: 273–294.
- Bakker, H., I. Friedmann, S. Oka, T. Kawasaki, N. Nifant'ev, M. Schachner, and N. Mantei. 1997. Expression cloning of a cDNA encoding a sulfotransferase involved in the biosynthesis of the HNK-1 carbohydrate epitope. *J. Biol. Chem.* **272**: 29942–29946.
- Brandt, T. M., R. M. Jones, Jr., and R. J. Anderson. 1987. Evaluation of prepared feeds and attractants for largemouth bass fry. *Prog. Fish-Cult.* **49**: 198–203.
- Bronner-Fraser, M. 1985. Alterations in neural crest migration by a monoclonal antibody that affects cell adhesion. *J. Cell Biol.* **101**: 610–617.
- Caprio, J. 1988. Peripheral filters and chemoreceptor cells in fishes. Pp. 313–338 in *Sensory Biology of Aquatic Animals*, J. Atema, R. R. Fay, A. N. Popper, and W. N. Tavolga, eds. Springer-Verlag, New York.
- Caprio, J., J. G. Brand, J. H. Teeter, T. Valencic, L. Kalinoski, J. Kohbara, T. Kumazawa, and S. Wegert. 1993. The taste system of the channel catfish: from biophysics to behavior. *Trends Neurosci.* **16**: 192–197.
- Carr, W. E. S., and C. D. Derby. 1986. Behavioral chemoattractants for the shrimp, *Palaemonetes pugio*: identification of active compo-

- nents in food extracts and evidence of synergistic mixture interactions. *Chem. Senses* **11**: 49–64.
- Casciotta, J. R., and G. Arratia. 1993.** Jaws and teeth of American cichlids (Pisces: Labroidae). *J. Morphol.* **217**: 1–36.
- Claes, G., and F. De Vree. 1991.** Kinematics of the pharyngeal jaws during feeding in *Oreochromis niloticus* (Pisces: Perciformes). *J. Morphol.* **208**: 227–245.
- Ezeasor, D. N. 1982.** Distribution and ultrastructure of taste buds in the oropharyngeal cavity of the rainbow trout, *Salmo gairdneri* Richardson. *J. Fish Biol.* **20**: 53–68.
- Finger, T. E. 1997.** Feeding patterns and brain evolution in ostariophyssean fishes. *Acta Physiol. Scand. Suppl.* **638**: 59–66.
- Finger, T. E., and B. Böttger. 1990.** Transcellular labeling of taste bud cells by carbocyanine dye (dil) applied to peripheral nerves in the barbels of the catfish, *Ictalurus punctatus*. *J. Comp. Neurol.* **302**: 884–892.
- Ganchrow, D., and R. Ganchrow. 1989.** Gustatory ontogenesis in the chicken: an avian-mammalian comparison. *Med. Sci. Res.* **17**: 223–228.
- Gans, C., and R. G. Northcutt. 1983.** Neural crest and the origin of vertebrates: a new head. *Science* **220**: 268–274.
- Hara, T. J. 1994.** Olfaction and gustation in fish: an overview. *Acta Physiol. Scand.* **152**: 207–217.
- Hussler, F. E., and L. H. Merchant. 1983.** Morphology of taste buds on the gill arches of the mullet *Mugil cephalus*, and the killifish *Fundulus heteroclitus*. *Am. J. Anat.* **166**: 299–312.
- Hossler, F. E., J. H. Harpole, Jr., and J. A. King. 1986.** The gill arch of the striped bass, *Morone saxatilis*. I. Surface ultrastructure. *J. Submicrosc. Cytol.* **18**: 519–528.
- Howick, G. L., and W. J. O'Brien. 1983.** Piscivorous feeding behavior in largemouth bass: an experimental analysis. *Trans. Am. Fish Soc.* **112**: 508–516.
- Jakubowski, M., and M. Whitear. 1990.** Comparative morphology and cytology of taste buds in teleosts. *Z. Mikrosk.-Anat. Forsch.* **104**: 529–560.
- Kapoor, B. G., H. E. Evans, and R. A. Pevsner. 1975.** The gustatory system of fish. *Adv. Mar. Biol.* **13**: 53–108.
- Kruse, K. C., and B. M. Stone. 1984.** Largemouth bass (*Micropterus salmoides*) learn to avoid feeding on toad (*Bufo*) tadpoles. *Anim. Behav.* **32**: 1035–1039.
- Kubitz, F., and L. L. Lovshin. 1997.** The use of freeze-dried krill to feed train largemouth bass (*Micropterus salmoides*): feeds and training strategies. *Aquaculture* **148**: 299–312.
- Kubitz, F., L. L. Lovshin, and R. T. Lovell. 1997.** Identification of feed enhancers for juvenile largemouth bass *Micropterus salmoides*. *Aquaculture* **148**: 191–200.
- Lamb, C. F., and T. E. Finger. 1995.** Gustatory control of feeding behavior in goldfish. *Physiol. Behav.* **57**: 483–488.
- Lauder, G. V. 1983.** Functional and morphological bases of trophic specialization in sunfishes (Teleostei, Centrarchidae). *J. Morphol.* **178**: 1–21.
- Liem, K. F. 1986.** The pharyngeal jaw apparatus of the Embiidae (Teleostei): a functional and evolutionary perspective. *Copeia* **1986**: 311–323.
- Liem, K. F., and P. H. Greenwood. 1981.** A functional approach to the phylogeny of the pharyngognath teleosts. *Am. Zool.* **21**: 83–101.
- Linsler, P. J. 1991.** Comparative immunohistochemistry of elasmobranch retina Muller cells and horizontal cells. *J. Exp. Zool.* **5**: 88–96.
- Linsler, P. J., R. E. Peterson, J. McClintock, J. Possley, and R. Buono. 1996.** Comparative analysis of Muller cell differentiation in primitive vertebrate retinas. *J. Brain Res.* **37**: 215.
- McMahon, T. E., and S. H. Holanov. 1995.** Foraging success of largemouth bass at different light intensities: implications for time and depth of feeding. *J. Fish Biol.* **46**: 759–767.
- Mistretta, C. M. 1991.** Developmental neurobiology of the taste system. Pp. 35–64 in *Smell and Taste in Health and Disease*, T. V. Getchell, R. L. Doty, L. M. Bartoshuk, and J. B. Snow, Jr., eds. Raven Press, New York.
- Northcott, M. E., and M. C. M. Beveridge. 1988.** The development and structure of the pharyngeal apparatus associated with filter feeding in tilapia (*Oreochromis niloticus*). *J. Zool. (Lond.)* **215**: 133–149.
- Reutter, K. 1992.** Structure of the peripheral gustatory organ, represented by the silurid fish, *Plotosus lineatus* (Thunberg). Pp. 60–78 in *Fish Chemoreception*, T. J. Hara, ed. Chapman and Hall, London.
- Reutter, K., and M. Witt. 1993.** Morphology of vertebrate taste organs and their nerve supply. Pp. 29–82 in *Mechanisms of Transduction*, S. A. Simon and S. D. Roper, eds. CRC Press, Boca Raton, FL.
- Reutter, K., W. Breipohl, and G. J. Bijvank. 1974.** Taste bud types in fishes. II. Scanning electron microscopical investigations on *Xiphophorus helleri* Heckel (Poeciliidae, Cyprinodontiformes, Teleostei). *Cell Tissue Res.* **153**: 151–165.
- Roper, S. D. 1989.** The cell biology of vertebrate taste receptors. *Annu. Rev. Neurosci.* **12**: 329–353.
- Sibbing, F. A. 1982.** Pharyngeal mastication and food transport in the carp (*Cyprinus carpio*): a cineradiographic and electromyographic study. *J. Morphol.* **172**: 223–258.
- Sorensen, P. W., and J. Caprio. 1997.** Chemoreception. Pp. 375–405 in *The Physiology of Fishes*, D. H. Evans, ed. CRC Press, Boca Raton, FL.
- Vandewalle, P., A. Huysseune, P. Aerts, and W. Verraes. 1994.** The pharyngeal apparatus in teleost feeding. Pp. 59–62 in *Biomechanics of Feeding in Vertebrates*. V. L. Bels, M. Chardon, and P. Vandewalle, eds. Springer-Verlag, Berlin.
- Vandewalle, P., P. Saintin, and M. Chardon. 1995.** Structure and movements of the buccal and pharyngeal jaws in relation to feeding in *Diplodus sargus*. *J. Fish Biol.* **46**: 623–656.
- Zar, J. H. 1984.** *Biostatistical Analysis* (2nd ed.). Prentice-Hall, Englewood Cliffs, NJ.

Peptidergic Neurons in Barnacles: An Immunohistochemical Study Using Antisera Raised Against Crustacean Neuropeptides

S. G. WEBSTER

School of Biological Sciences, University of Wales, Bangor, Gwynedd LL57 2UW, UK

Abstract. Antisera raised against neuropeptides from decapod crustaceans were used to investigate whether balanomorph barnacles produce peptides analogous to those identified in some decapods. The distribution and structure of immunoreactive neurons was examined in *Balanus balanus*, *Balanus perforatus*, and *Chirona (Balanus) hameri* by whole-mount immunohistochemistry. In these species, no immunoreactivity was observed to antisera against CHH (crustacean hyperglycemic hormone), MIH (molt-inhibiting hormone), or RPCH (red-pigment-concentrating hormone), but neurons immunoreactive for pigment-dispersing hormone (PDH) and crustacean cardioactive peptide (CCAP) were observed. In all three species, PDH immunoreactivity was primarily associated with a pair of large (30–50 μm diam.) antero-ventral perikarya in the ventral ganglion, projecting prominent axons along the great splanchnic nerves, which branched extensively in the segmental splanchnic nerves, directing several arborizing dendrites to the somatic extensor muscles. Occasionally, three pairs of antero-dorsal perikarya were observed, which projected fine ipsilateral and contralateral axons along the great splanchnic nerves. A further 12 pairs of perikarya, apparently segmentally arranged, were observed in the thoracic ganglion. Several PDH-immunoreactive perikarya and associated branching plexus were observed in the supra-esophageal ganglion. CCAP immunoreactivity was mainly restricted to the ventral ganglion, where three pairs of perikarya (*ca.* 30–50 μm diam.) projected contralateral descending axons to the cirri. Occasionally a single pair of immunoreactive neurons were observed in the supra-esophageal ganglia. Although the anatomy of the CCAP-immunoreactive neurons in the

ventral ganglion of barnacles might be homologous to conserved neural architectures in higher crustaceans, the anatomy of the PDH-immunoreactive neurons seems unique, and the morphology of the two large neurons in the ventral ganglion suggests a neuromodulatory role for this peptide, possibly associated with somatic extension.

Introduction

The morphology of the cirripede central nervous system is unique amongst arthropods in that it has undergone extensive modification associated with the sessile mode of life in the adult barnacle. Indeed, the *Bauplan* of the arthropod nervous system is scarcely discernible. The supra-esophageal ganglion is a simple bilobed structure with no external topographical features distinguishing a proto-, deutero-, or trito-cerebrum, and it appears to be principally involved in neural integration of information from the lateral and median photoreceptors. There is no trace of a sub-esophageal ganglion; the circumesophageal connectives join a ventral ganglionic mass that is sometimes referred to as the thoracic ganglion. There is no trace of an abdominal ganglion (Gwilliam and Cole, 1979).

Although much is known about the neurobiology of the barnacle CNS, particularly with regard to the photoreceptors and the neural networks involved in cirral movement (review by Gwilliam, 1987), very little is known about the nature or anatomy of peptidergic cells in the barnacle CNS. At the light microscopic level, Gomori-positive neurons have been observed in the supra-esophageal and ventral ganglion (Barnes and Gonor, 1958a,b; Van den Bosch de Aguilar, 1976, 1979). At the electron microscopic level, membrane-bound electron-dense vesicles reminiscent of neurosecretory granules have been

observed within axons in the median ocellar nerve of *Semibalanus cariosus* (Fahrenbach, 1965) and *Chirona (Balanus) hameri* (Clare and Walker, 1989); these vesicles apparently constitute a neurohemal area. Recently, Gallus *et al.* (1997) demonstrated the presence of FMRFamide immunopositive neurons in the ventral ganglion of *Balanus amphitrite*.

Because the morphology of the barnacle nervous system is so unusual, and because peptidergic neurons in those systems are so little known, the methods of immunohistochemistry were used to define and map neurons that might be producing peptides homologous to those now identified in some decapod crustaceans. From an evolutionary viewpoint, it was also of interest to determine whether peptidergic neuronal networks structurally homologous to those known in higher crustaceans could be identified in the greatly modified CNS of barnacles.

Materials and Methods

Animals and tissue preparation

Specimens of *Balanus balanus* were collected from rocks at extreme low-tide level at Church Island, Menai Strait, UK, and *Balanus perforatus* from rocks at mid-tide level at Concarneau, Brittany, France. *Chirona (Balanus) hameri* specimens were obtained by dredge from *Modiolus* beds off Langness, Isle of Man. Nervous systems were microscopically dissected under ice-cold saline, and since non-nervous tissue produces unacceptably high background staining, all of it was removed. Complete nervous systems were pinned with cactus spines to small pieces of Sylgard. Tissues were fixed for 8 h at 4°C in Stephanini's fixative (Stephanini *et al.*, 1967), or in 4% paraformaldehyde, 1% EDC (1-ethyl-3,3'-dimethylaminopropyl-carbodiimide) in 0.1 M phosphate buffered saline (PBS), pH 7.4, for 8 h at 0°C, washed in 0.1 M sodium phosphate buffer (pH 7.4) containing 0.5 M sucrose, and permeabilized by extensive (24 h) incubation in PBS containing 0.5% Triton X-100 containing 0.02% sodium azide (PTX).

Immunohistochemical techniques

Nervous systems were incubated in primary antibody, diluted in PTX, for 72 h. Antisera (and dilutions) used were (a) anti-molt-inhibiting hormone (MIH), *Carcinus* 1:500 (Dirksen *et al.*, 1988); (b) anti-crustacean hyperglycemic hormone (CHH), *Carcinus* 1:500 (Dirksen *et al.*, 1988); (c) anti-red-pigment-dispersing hormone (RPCH) 1:250 (Schooneveld and Veenstra, 1985); (d) anti-pigment-dispersing hormone (β -PDH) 1:1000 (Dirksen *et al.*, 1987); and (e) anti-crustacean cardioactive peptide (CCAP), 1:250 (Dirksen and Keller, 1988). After extensive washing in PTX (24 h), nervous systems

were incubated in goat-anti-rabbit fluorescein isothiocyanate (GAR-FITC) (Sigma) 1:50 in PTX for 24–48 h, washed extensively in PTX, mounted in glycerol:PTX 1:1, and viewed under a fluorescence microscope. Permanent preparations were subsequently made by reincubation of tissues in goat-anti-rabbit IgG (Sigma) 1:100 (in PTX without sodium azide) (24 h), washing for 24 h in the same buffer, incubation in peroxidase-anti-peroxidase (PAP) (Sigma) 1:200 (24 h), and visualization with 3-3'-diaminobenzidine hydrochloride as detailed by Dirksen *et al.* (1991); this was followed by graded ethanol dehydration, clearing in methyl benzoate, and mounting in DPX.

Specificity tests (preabsorption controls) were performed for antisera that yielded positive results by incubating (24 h 4°C) 1 μ l of antiserum with 10 nmol of the appropriate (synthetic) peptide dissolved in 10 μ l PBS. After dilution, the antibody was then used for immunohistochemistry as detailed above.

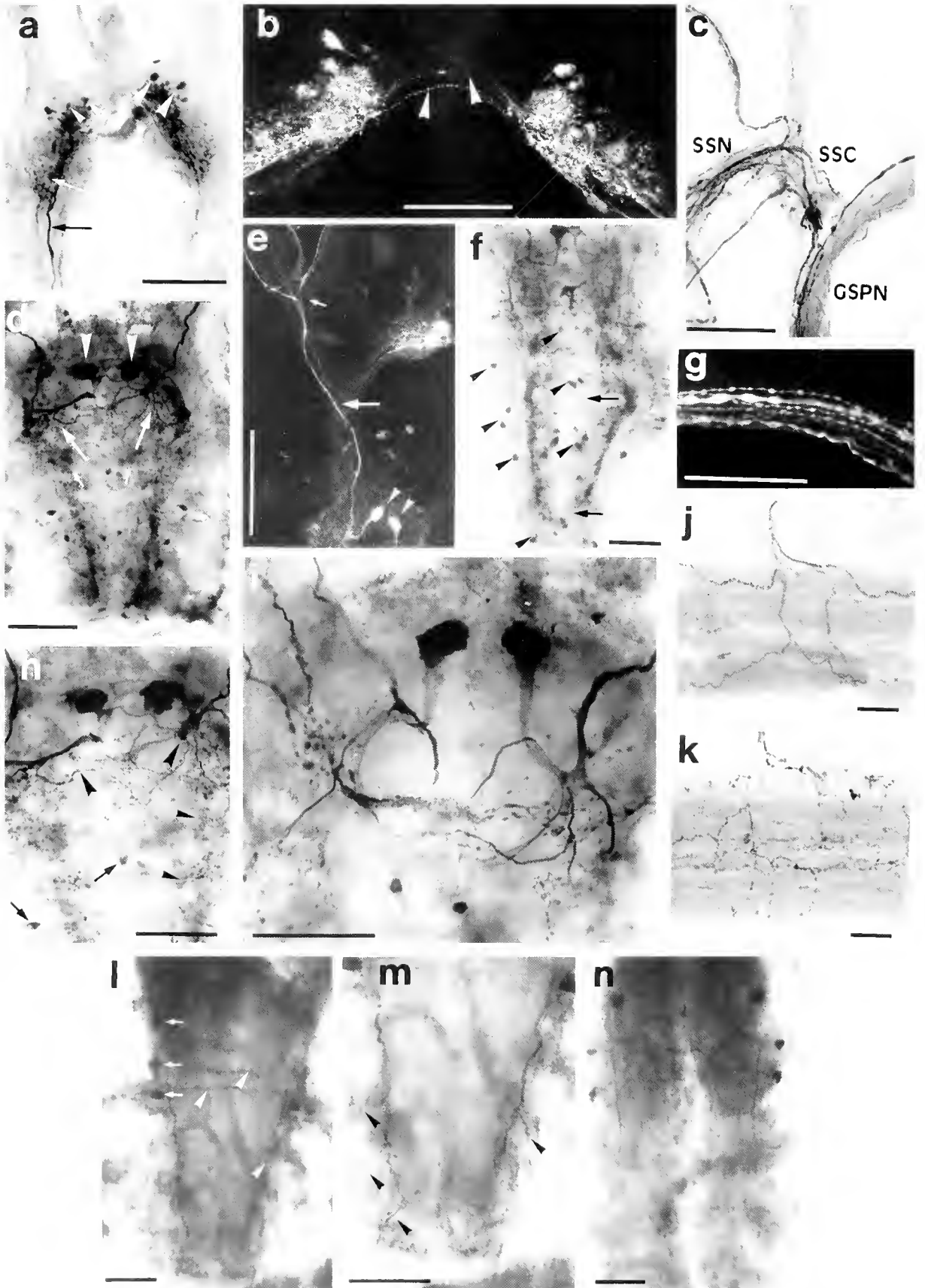
Results

Despite extensive investigation, immunopositive structures were never observed using MIH, CHH, or RPCH antisera. Nevertheless, PDH- and CCAP-immunoreactive (IR) neurons were consistently seen in preparations of *B. balanus*, *B. perforatus*, and *C. hameri*. Essentially, all species exhibited broadly similar PDH- and CCAP-IR structures; species differences were insignificant. Preabsorption controls completely abolished immunoreactivity.

PDH-immunoreactive neurons

The most striking and consistently observed immunoreactive structures seen in all species were a pair of large (30–50 μ m diameter) antero-ventral perikarya on the surface of the neuropil of the ventral ganglion (VG) (Fig. 1d–f, h, i; Fig. 2). These cells projected a large, conspicuous (often beaded) axon along the great splanchnic nerve (GSPN), branching extensively at the junction of this nerve with the segmental splanchnic nerve (SSN) (Fig. 1c). Additional branches from the axons ran to the posterior of the VG, and also to the midline, terminating in an extensive plexus (Fig. 1d, f, h; Fig. 2). Fine nerves from the SSN, each containing immunopositive dendrites, branched extensively over adjacent musculature; the attrahens and anterior prosomal muscles were particularly well innervated. When attrahens muscles were examined, a consistent pattern of immunopositive dendrites were seen (Fig. 1j, k).

In a few (*ca.* 5–10) preparations (particularly *C. hameri*), a group of three pairs of perikarya were seen on the antero-dorsal surface of the VG. The anterior two pairs of perikarya projected fine axons ipsilaterally and contralaterally along the GSPN, whilst the posterior pair pro-



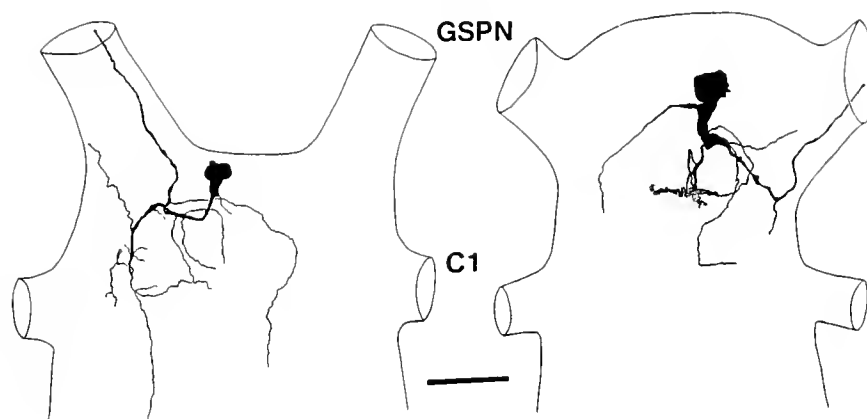


Figure 2. *Camera lucida* tracings of the large ventral PDH-immunopositive perikarya of the ventral ganglion. Left: *Balanus perforatus*, Right: *B. balanus*. GSPN = great splanchnic nerve, C1 = first cirral nerve. Scale bar = 100 μm .

jected axons ipsilaterally towards the GSPN, with a fine, posteriorly directed branch (Fig. 3). It should be emphasized that these neurons were not often visible in *B. perforatus* or *B. balanus*, but occasionally four immunopositive axons were observed in the GSPN. The large axon could invariably be traced to the antero-dorsal perikarya

mentioned earlier, but the fine axons (which exhibited prominent varicosities), could not be traced to the presumed group of three paired perikarya. Within the neuropil of the VG of *B. perforatus* and *B. balanus*, six pairs of small (15–20 μm diameter), weakly immunopositive, lateral perikarya projecting fine axons to the midline

Figure 1. Immunoreactive neurons in the barnacle central nervous system: (a–k) Pigment-dispersing-hormone immunoreactivity (PDH-IR); (l–n) crustacean-cardioactive-peptide immunoreactivity (CCAP-IR). All preparations are peroxidase-anti-peroxidase (PAP) except where noted. (a) The supra-esophageal ganglion of *Balanus perforatus*, showing two pairs of prominent perikarya (large arrowheads) and several less intensely stained, smaller perikarya (small arrowheads) in each hemisphere, arborizing dendrites and axons projecting along the circumesophageal connectives (arrows). (b) Fluorescein isothiocyanate (FITC) preparation of the supra-esophageal ganglion of *B. balanus*, showing the features seen in a, and also fine contralateral projections to each hemisphere (arrowheads). (c) PAP preparation of the origin of the segmental splanchnic nerve (SSN) of *B. balanus*, showing the extensive ramification of the single axon of the great splanchnic nerve (GSPN) in the segmental splanchnic connective (SSC). (d) Ventral ganglion of *B. balanus*. Note the two prominent perikarya (arrowheads), with prominent axons entering the great splanchnic nerve, and extensive dendrites (arrows). Small arrowheads indicate the small, weakly immunopositive neurons. Note the three pairs of perikarya (small arrows) out of the plane of focus. These are the dorsal perikarya, which are described in Fig. 3. (e) FITC preparation of the CNS of *B. balanus*, showing the two large perikarya in the ventral ganglion (arrowheads), directing axons along the great splanchnic nerve (small arrow), branching at the origin of the segmental splanchnic connective (small arrowhead). Note the intense immunoreactivity in the supra-esophageal ganglion (top right) in this preparation. (f) Ventral ganglion of *B. perforatus*; the large ventral perikarya are at the top of the figure. Note the small, weakly immunopositive lateral perikarya and median perikarya (arrowheads). The lateral perikarya project fine axons to the midline (arrows). (g) FITC preparation of the circumesophageal connective of *B. balanus*. The beaded axons are associated with the immunopositive neurons in the supra-esophageal ganglion, but could not be traced to the ventral ganglion. (h) Higher magnification of d, showing the large pair of ventral perikarya and branching dendrites (arrowheads). Note the small, weakly immunopositive median and lateral perikarya (arrows), and the extensive dendritic fields (small arrowheads) associated with branching fibers from the large ventral perikarya. (i) Fine structure of the pair of large ventral perikarya. (j–k) The atrahens muscles of *B. balanus* (upper) and *B. perforatus* (lower), showing branching immunopositive dendrites. (l) Ventral ganglion of *B. balanus*, showing three pairs of CCAP-immunoreactive perikarya (small arrows). The first pair are dorsal (out of the plane of focus); the posterior two pairs are ventral. Note the contralaterally projecting descending axons (arrowheads). (m) Higher magnification of l, showing last pair of perikarya at the top of the figure, detailing the descending axons, which branch into each cirral nerve (arrowheads). (n) Ventral ganglion of *C. hameri*, showing CCAP-immunoreactive cells and axons, with a morphology very similar to those seen in *B. balanus*. (The contralateral projections are broken along the midline in all preparations of this species, due to shrinkage.) Scale bars: a, b, c, f, h, l, m, n = 200 μm ; d, g, j, k, i = 100 μm ; e = 500 μm .

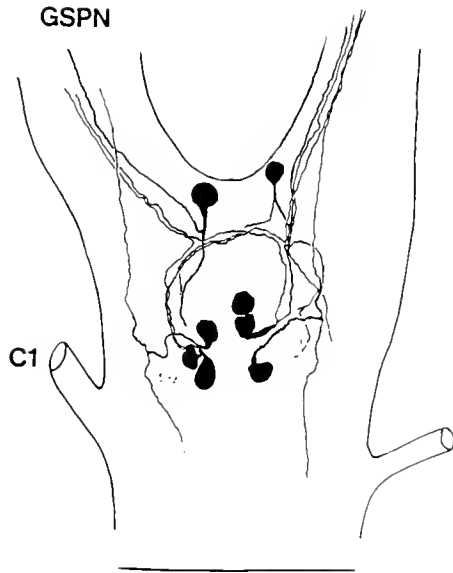


Figure 3. *Camera lucida* tracing of the ventral ganglion of *Chirona hameri*, detailing the gross structure of the large ventral PDH-immunopositive perikarya, and more detailed structures of the two groups (weakly immunoreactive) of three dorsal perikarya. The posterior cells direct axons ipsilaterally, whilst the anterior cells project axons ipsi- and contralaterally. Scale bar = 500 μ . Abbreviations as in Fig. 2.

were observed (Fig. 1f), and a further six pairs of very weakly immunoreactive perikarya were located centrally (Fig. 1d, f).

Apart from the above-mentioned structures, the only PDH-immunoreactive structures consistently seen were in the supra-esophageal ganglia of *B. balanus*, where at least two pairs of strongly immunoreactive and three pairs of weakly immunoreactive neurons were seen, associated with extensive dendritic fields with prominent varicosities on the surface and within the neuropil (Fig. 1a, b). Several contralaterally projecting fine axons were also observed (Fig. 1b). Occasionally, prominent beaded axons originating from the supra-esophageal ganglion were seen in the circumesophageal connectives (Fig. 1g), but these could never be traced to the ventral ganglion (Fig. 1e).

CCAP-immunoreactive neurons

CCAP-immunoreactivity was observed in all species of barnacles examined, although immunoreactivity was weak, and background staining was high, even when nervous systems were fixed in carbodiimide fixative (the fixative of choice for this peptide in whole mounts of arthropod nervous tissue (Dircksen *et al.*, 1991). For both *B. balanus* and *C. hameri*, similar morphologies of CCAP-immunoreactive neurons were observed (Fig. 1, 1–n). The anterior pair of perikarya (*ca.* 50 μ diam.) are dorsal, the posterior two pairs (*ca.* 30 μ diam.) are ventral.

All perikarya project a single axon contralaterally which descends to the posterior margin of the ventral ganglion with fine branches projecting along each cirral nerve. A detailed *camera lucida* reconstruction of these neurons (Fig. 4) shows the branching pattern of fine dendrites. In some preparations a pair of small (10–15 μ m) neurons were seen in the supra-esophageal ganglia (the fine structure of these neurons was not investigated further).

For references, Figure 5 shows a schematic of the PDH- and CCAP-immunoreactive neurons observed.

Discussion

In the present study, several antisera raised to native peptides of decapod crustaceans were used to determine the neuroanatomy of peptidergic neurons in barnacles. Although a limited array of antisera were used, a notable finding was that CHH- and MIH-immunoreactive neurons were never observed in barnacle nervous systems. This might be explained by the considerable group- or even species-specificity of MIH and CHH (Keller, 1992). However, CHH-immunoreactive neurons have been identified in isopods (Nussbaum and Dircksen, 1995) and mapped in the cladoceran *Daphnia magna* and in an anostracan, *Artemia salina* (Zhang *et al.*, 1997). Thus, since CHH-like molecules seem to be a phylogenetically ancient group, the failure to observe CHH-like immunoreactivity in this study may well have been due to unsuitability of

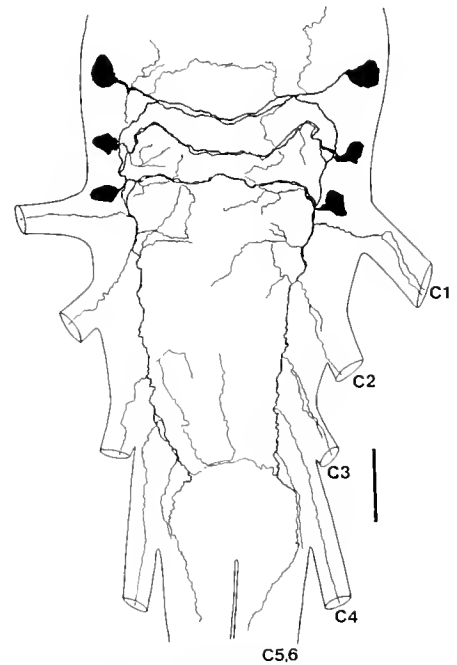


Figure 4. *Camera lucida* tracing of the CCAP-immunoreactive structures in the ventral ganglion of *Balanus balanus*. C1–6 = cirral nerves 1–6. Scale bar = 100 μ .

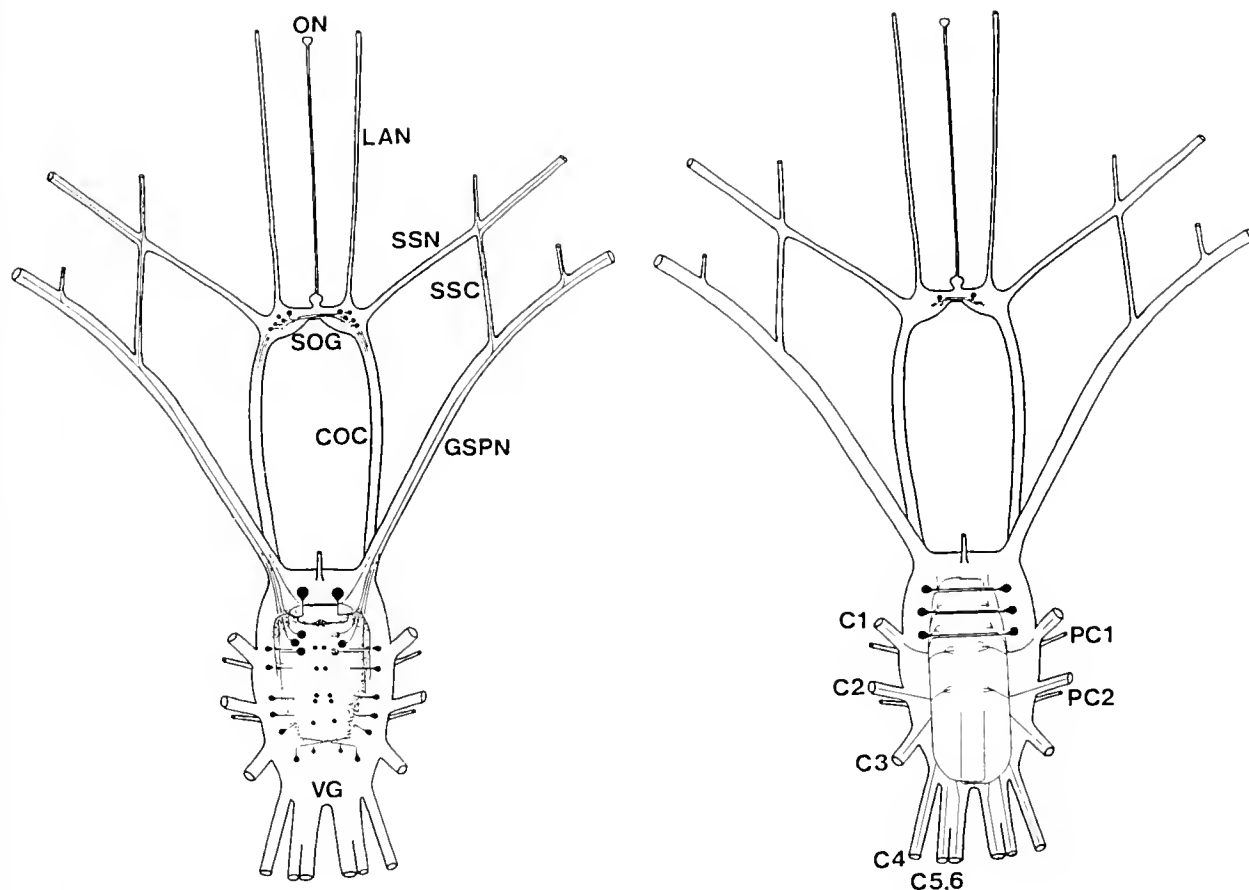


Figure 5. Schematic diagrams of PDH (left) and CCAP (right) immunoreactive neurons in the CNS of balanomorph barnacles. Abbreviations: C1–6: cirral nerves 1–6; COC: circumesophageal connectives; GSPN: great splanchnic nerve; LAN: lateral antennal nerve; OC: ocellar nerve; PC1–2: paracirral nerves 1–2; SOG: supra-esophageal ganglion; SSC: segmental splanchnic connective; SSN: segmental splanchnic nerve; VG: ventral ganglion.

the fixatives used, although the same fixative (Stephanini) was used in all studies mentioned here.

The absence of RPCH immunoreactivity is surprising. This peptide is a member of the ever-expanding adipokinetic hormone (AKH) group. Although many different AKHs have been identified in insects (See Gäde, 1997, for list), it appears likely that only one member, red-pigment-concentrating hormone (RPCH) occurs in crustaceans (Gaus *et al.*, 1990). It might be argued that the absence of RPCH (as a circulating neurohormone) would be expected since chromatophores are present only in malacostracans; however, immunocytochemical studies (Mangerich *et al.*, 1986; Nussbaum and Dirksen, 1995) using the same antiserum that recognizes the N-terminal tetrapeptide sequence common to many AKHs (Schooneveld and Veenstra, 1985) have shown that RPCH-immunoreactive interneurons are very widely distributed in the brain, thoracic and stomatogastric ganglia, and ventral nerve cord in malacostracans. Although RPCH from the

central nervous system of decapods shows red-pigment-concentrating activity in bioassays (Fingerman and Couch, 1967), extracts of CNS from several species of barnacle result in pigment dispersion when injected into *Uca pugilator* (Sandeen and Costlow, 1961). This could indicate an absence of RPCH-like peptides in the CNS of barnacles, but it is more likely that the relative abundance of PDH-like material demonstrated in this study would override any pigment-concentrating effect of RPCH.

Although a pigment-dispersing hormone was first identified in crustaceans (Fernlund, 1976), immunocytochemical studies have not only verified a neurohormonal role for PDH, but have also documented a widespread occurrence in the CNS of crustaceans (Dirksen *et al.*, 1987; Mortin and Marder, 1991) and insects (Homberg *et al.*, 1991; Nässel *et al.*, 1991; Stengl and Homberg, 1994); it seems likely that PDH-like peptides, or more precisely, pigment-dispersing factors (PDFs) have a widespread.

perhaps universal, occurrence in arthropods (review by Rao and Riehm, 1993). Apart from the established role of PDH in controlling pigment migration in malacostracan crustaceans, the physiological significance of PDH-like peptides in arthropods has remained obscure. However, a role for PDH in control of circadian rhythmicity, proposed on the basis of the morphology of the immunoreactive neurons in the brain of orthopterans (Homberg *et al.*, 1991), has been confirmed (Stengl and Homberg, 1994); furthermore, some neurons that express the period (*per*) gene in the *Drosophila* brain also display PDH-immunoreactivity (Helfrich-Förster, 1995). In the present study, PDH immunoreactivity was seen in several types of neuron in the ventral and supra-esophageal ganglia of barnacles. The neuronal system, consisting of a single pair of large cells projecting axons along the GSPN, was extremely prominent. Apart from these PDH-immunopositive structures, the only invariably immunoreactive PDH cells appeared to be interneurons: the perikarya in the supra-esophageal ganglia projected axons along the circumesophageal connectives towards the ventral ganglion. Small perikarya in the VG appeared to be segmentally arranged—although the VG is fused, six pairs of perikarya correspond with the number of thoracic limbs; thus these cells may delineate neuromeres. Additionally, the dendritic areas associated with the posteriorly directed branches of the two large PDH-IR perikarya appeared to show some arrangement reminiscent of a segmentally iterated pattern (Fig. 4d, h).

With respect to the possible functions of PDH-IR material in barnacles, the presence of PDH-IR in neurons terminating on the attrahens and anterior prosomal muscles is of interest. Cotransmission of peptides and neurotransmitters is a widespread, if not universal, phenomenon (review by Kupfermann, 1991). In crustaceans, a thoroughly investigated cotransmitter system is that of the crayfish tonic flexor muscle, which is innervated by five motoneurons, three containing proctolin, that potentiate tonic contraction of these muscles (Bishop *et al.*, 1987). It therefore seems possible that the two PDH-IR neurons innervating the somatic protractor may also have neuromodulatory roles in somatic extension in barnacles.

Crustacean cardioactive peptide (CCAP), originally isolated from pericardial organs of *Carcinus maenas* (Stangier *et al.*, 1987), is another example of a neuropeptide with a wide, if not universal, occurrence in arthropods. The conserved neuronal networks of this peptide in arthropods have recently been reviewed by Dirksen (1998). Although the best known action of this peptide is its cardioacceleratory action, related (myotropic) actions in crustaceans include acceleration of seaphognathite rate and increased hindgut motility (Stangier, 1991). An important recent finding is that CCAP is a potent modulator of the pyloric rhythm of the stomatogastric

ganglion of the crab *Cancer borealis* (Weimann *et al.*, 1997). Immunocytochemical studies on the isopod *Oniscus asellus* (Nussbaum *et al.*, 1995) suggest that CCAP might be involved in the biphasic exuviation pattern seen in isopods. For insects, broadly comparable myotropic roles have been observed, and it is expected (from morphology of CCAP-IR neurons that a multiplicity of functions have yet to be determined (Direksen, 1998). In the present study, three pairs of CCAP-IR neurons observed in the ventral ganglion were notable. The perikarya essentially projected descending contralateral axons towards the cirri, but were too fine to allow the complete neural pathway to be traced. Although backfills have not demonstrated that barnacles have a neuronal architecture equivalent to that of higher crustaceans (Gwilliam and Cole, 1979; Gwilliam, 1987), the arrangement of the CCAP-IR neurons in the barnacle ventral ganglion is broadly reminiscent of the arrangement of the *cdn*-type-2 neurons in the thoracic ganglion of decapod crustaceans (Direksen, 1998) in the sense that they project contralateral descending axons. Further speculation with regard to homology or function would, however, be premature.

Acknowledgements

This work was supported by a Royal Society research grant. I am indebted to Dr. Heinrich Dirksen, University of Bonn, for providing antisera, and especially for his helpful advice and discussion. This paper is dedicated to the memory of the late Professor Dennis Crisp, F.R.S., who initiated and stimulated my interest in barnacle biology with his enthusiasm.

Literature Cited

- Barnes, H., and J. J. Gonor. 1958a. Neurosecretory cells in some cirripedes. *Nature* **181**: 194.
- Barnes, H., and J. J. Gonor. 1958b. Neurosecretory cells in the cirripede, *Pollicipes polymerus* J. B. Sowerby. *J. Mar. Res.* **17**: 81–102.
- Bishop, C. A., J. J. Wine, F. Nagy, and M. R. O'Shea. 1987. Physiological consequences of peptide cotransmission in a crayfish nerve muscle preparation. *J. Neurosci.* **7**: 1767–1779.
- Clare, A. S., and G. Walker. 1989. Morphology of the nervous system of barnacles: the median ocellus of *Balanus hameri* (= *Chirona hameri*). *J. Mar. Biol. Assoc. UK* **69**: 769–784.
- Dirksen, H. 1998. Conserved crustacean cardioactive peptide (CCAP) neuronal networks and functions in arthropod evolution. Pp. 302–333 in *Recent Advances in Arthropod Endocrinology*, G. M. Coast and S. G. Webster, eds. Cambridge University Press.
- Dirksen, H., and R. Keller. 1998. Immunocytochemical localization of CCAP, a novel crustacean cardioactive peptide, in the nervous system of the shore crab, *Carcinus maenas* L. *Cell Tiss. Res.* **254**: 347–360.
- Dirksen, H., C. A. Zahnow, G. Gaus, R. Keller, K. R. Rao, and J. P. Riehm. 1987. The ultrastructure of nerve endings containing pigment-dispersing hormone (PDH) in crustacean sinus glands: identification by an antiserum against synthetic PDH. *Cell Tiss. Res.* **250**: 377–387.
- Dirksen, H., S. G. Webster, and R. Keller. 1988. Immunocytochemi-

- cal demonstration of the neurosecretory systems containing putative moulting-inhibiting hormone and hyperglycemic hormone in the eyestalk of brachyuran crustaceans. *Cell Tiss. Res.* **251**: 3–12.
- Dirksen, H., A. Müller, and R. Keller. 1991.** Crustacean cardioactive peptide in the nervous system of the locust, *Locusta migratoria*: an immunocytochemical study on the ventral nerve cord and peripheral innervation. *Cell Tiss. Res.* **263**: 439–457.
- Fahrenbach, W. H. 1965.** The micromorphology of some simple photoreceptors. *Z. Zellforsch.* **66**: 233–254.
- Fernlund, P. 1976.** Structure of a light-adapting hormone from the shrimp *Pandalus borealis*. *Biochim. Biophys. Acta* **439**: 17–25.
- Fingerman, M., and E. F. Couch. 1967.** The red pigment dispersing hormone of the abdominal nerve cord and its contribution to the physiology of the prawn *Palaemonetes vulgaris*. *Rev. Can. Biol.* **26**: 109–117.
- Gäde, G. 1997.** The explosion of structural information on insect neuropeptides. *Prog. Chem. Org. Nat. Prod.* **71**: 1–128.
- Gallus, L., A. Diaspro, R. Rolandi, M. Fato, and G. Tagliafierra. 1997.** Three-dimensional reconstruction of FMRF-amide immunopositive neurons in the ventral ganglion of the barnacle *Balanus amphitrite* (Cirripedia, Crustacea). *Eur. J. Histochem.* **2**: 99–100.
- Gaus, G., L. H. Kleinholz, G. Kegel, and R. Keller. 1990.** Isolation and characterization of red-pigment-concentrating hormone (RPCH) from six crustacean species. *J. Comp. Physiol. B* **160**: 373–379.
- Gwilliam, G. F. 1987.** Neurobiology of barnacles. Pp. 191–211 in *Barnacle Biology*, A. J. Southward, ed. Balkema, Rotterdam.
- Gwilliam, G. F., and E. S. Cole. 1979.** The morphology of the central nervous system of the barnacle, *Semibalanus cariosus* (Pallas). *J. Morphol.* **159**: 297–310.
- Hellrich-Förster, C. 1995.** The period clock gene is expressed in central nervous system neurons which also produce a neuropeptide that reveals the projections of circadian pacemaker cells within the brain of *Drosophila melanogaster*. *Proc. Natl. Acad. Sci. USA* **92**: 612–616.
- Hamburger, U., S. Würden, H. Dirksen, and K. R. Rao. 1991.** Comparative anatomy of pigment-dispersing hormone-immunoreactive neurons in the brain of orthopteroid insects. *Cell Tiss. Res.* **266**: 343–357.
- Keller, R. 1992.** Crustacean neuropeptides: structures, functions and comparative aspects. *Experientia* **48**: 439–448.
- Kupfermann, I. 1991.** Functional studies of cotransmission. *Physiol. Rev.* **71**: 683–732.
- Mangerich, S., R. Keller, and H. Dirksen. 1986.** Immunocytochemical identification of structures containing putative red pigment-concentrating hormone in two species of decapod crustaceans. *Cell Tiss. Res.* **245**: 377–386.
- Martin, L. L., and E. Marder. 1991.** Differential distribution of (β -PDH)-like immunoreactivity in the stomatogastric nervous system of five species of decapod crustaceans. *Cell Tiss. Res.* **265**: 19–33.
- Nässel, D. R., S. Shiga, E. M. Wikstrand, and K. R. Rao. 1991.** Pigment-dispersing hormone-immunoreactive neurons and their relation to serotonergic neurons in the blowfly and cockroach visual system. *Cell Tiss. Res.* **266**: 511–523.
- Nussbaum, T., and H. Dirksen. 1995.** Neuronal pathways of classical crustacean neurohormones in the central nervous system of the woodlouse, *Oniscus asellus* (L.). *Phil. Trans. R. Soc. Lond. B* **347**: 139–154.
- Rao, K. R., and J. P. Riehm. 1993.** Pigment-dispersing hormones. *Ann. NY Acad. Sci.* **680**: 78–88.
- Sandeen, M. L., and J. D. Castlow. 1961.** The presence of decapod pigment-activating substances in the central nervous system of representative Cirripedia. *Biol. Bull.* **120**: 192–205.
- Schooneveld, H., and J. A. Veenstra. 1985.** Insect neuroendocrine cells and neurons containing various adipokinetic hormone (AKH)-immunoreactive substances. Pp. 425–434 in *Neurosecretion and the Biology of Neuropeptides*, M. Kobayashi, H. A. Bern, and A. Urano, eds. Japan. Sci. Soc. Press, Tokyo; Springer, New York.
- Stangier, J. 1991.** Biological effects of crustacean cardioactive peptide, a putative neurohormone/neurotransmitter from crustacean pericardial organs. Pp. 201–210 in *Comparative Aspects of Neuropeptide Function*, G. B. Stephano and E. Florey, eds. Manchester University Press, UK.
- Stangier, J., C. Hilbich, K. Beyreuther, and R. Keller. 1987.** Unusual cardioactive peptide (CCAP) from pericardial organs of the shore crab *Carcinus maenas*. *Proc. Natl. Acad. Sci. USA* **84**: 575–579.
- Stengl, M., and U. Homberg. 1994.** Pigment-dispersing hormone-immunoreactive neurons in the cockroach *Leucophaea maderae* share properties with circadian pacemaker neurons. *J. Comp. Physiol. A* **175**: 201–213.
- Stephanini, M., C. De Martino, and L. Zamboni. 1967.** Fixation of ejaculated spermatozoa for electron microscopy. *Nature* **216**: 173–174.
- Van den Bosch de Aguilar, Ph. 1976.** Etude histochemique du système neurosécréteur de *Balanus perforatus* et *B. balanoides* (Crustacea; Cirripedia). *Gen. Comp. Endocrinol.* **30**: 228–230.
- Van den Bosch de Aguilar, Ph. 1979.** Neurosecretion in the Entomostraca crustaceans. *Cellule* **73**: 29–48.
- Weimann, J. M., P. Skiehe, H. G. Heinzel, C. Soto, N. Kopell, J. C. Jorge-Riviera, and E. Marder. 1997.** Modulation of oscillator interactions in the crab stomatogastric ganglion by crustacean cardioactive peptide. *J. Neurosci.* **17**: 1748–1760.
- Zhang, Q., R. Keller, and H. Dirksen. 1997.** Crustacean hyperglycaemic hormone in the nervous system of the primitive crustacean species *Daphnia magna* and *Artemia salina* (Crustacea; Branchiopoda). *Cell Tiss. Res.* **287**: 565–576.

Cuticular Photophores of Two Decapod Crustaceans, *Oplophorus spinosus* and *Systellaspis debilis*

M. S. NOWEL^{1,*}, P. M. J. SHELTON², AND P. J. HERRING³

¹*Department of Biology, Providence College, Providence, Rhode Island 02918-0001;* ²*Department of Biology, School of Biological Sciences, University of Leicester, Leicester LE1 7RH, UK; and* ³*Southampton Oceanography Centre, Empress Dock, Southampton SO14 3ZH, UK*

Abstract. The organization, ultrastructure, growth, and development of two types of cuticular photophore in oplophorid shrimps (*Oplophorus spinosus* and *Systellaspis debilis*) are described. Photophores located in the third maxilliped consist of a unit structure comprising a single photocyte and associated pigment cells. Reflecting pigment cells contain white pigment and form an apical cap above the photocyte; sheath cells contain red carotenoid pigment and form a light-absorbing layer around the photophore. Photophores located on the pleopods are compound structures comprising many photocytes. They also contain the same types of pigment cell that are found in the unit photophores of the maxilliped. Paracrystalline bodies at the apical ends of the photocytes in both types of photophore are thought to be associated with light generation. Both types of photophore have mechanisms for tilting in the pitch plane. In the maxilliped, the apices of the photophores are connected to a ligament that has its origin in the propodus. Flexion or extension of the dactylus displaces the ligament, which tilts the photophores synchronously. The cuticular window beneath each photophore remains stationary. The tilt mechanism of the pleopod photophores is quite different, and depends upon muscular contraction. A main and an accessory longitudinal muscle cause backwards rotation of the photophore by deforming the cuticle surface. A loop muscle that passes around the anterior face of the photophore causes forward rotation. The two mech-

anisms optimize the use of the photophores in ventral camouflage. They allow photophore rotation to compensate for changes in the shrimp's orientation in the plane of pitch and thus maintain the ventral direction of the luminescence.

Introduction

Many groups of oceanic animals are bioluminescent (Harvey, 1952; Herring, 1978). In a number of these, the luminescence is produced in single cells or groups of cells without any other associated structures. However, in some animals the bioluminescent cells (photocytes, the "photogenic cells" of Dennell, 1940) are part of a complex organ (photophore) whose additional features may modify the direction, intensity, spectral distribution, or angular distribution of the emitted light (Denton *et al.*, 1972, 1985; Herring, 1985a). In the sea, such photophores are restricted to fish, cephalopods, euphausiids, and decapod crustaceans, and are particularly common in members of the mesopelagic fauna, whose normal daytime depth distribution is between 200 m and 1000 m. These animals tend to direct their luminescence downwards, and the photophores are most numerous along the ventral surface, where their function is primarily that of counterillumination. They camouflage the animal by emitting bioluminescence whose characteristics closely match those of the downwelling light. This eliminates the silhouette that would otherwise be visible from below. In euphausiid shrimps, the ventral directionality is further maintained during swimming by rotating the photophores in response to changes in body tilt (Hardy, 1962, 1964; Land, 1980; Grinnell *et al.*, 1988).

Received 17 June 1998; accepted 31 August 1998.

* To whom correspondence should be addressed. E-mail: mnowel@providence.edu

Among the decapod shrimps, several families of both the Penaeidea and Caridea have such photophores, and they may be formed either as cuticular structures or as modified hepatopancreas tubules (Herring, 1976, 1985b). In the caridean family Oplophoridae, whose species range in depth distribution from the upper mesopelagic to the deep-sea floor, the two shallowest genera—*Systellaspis* and *Oplophorus* (the latter here including the genus *Janicella*)—have many cuticular photophores. These are present on the eyes, limbs, cephalothorax, and abdomen. They take various forms, but in live animals all except those on the pleopods appear to be made up of variable-sized groups of very similar small units. Those on the third maxilliped represent the simplest level of organization, consisting of single photophore units each containing a single photocyte. At the other extreme, the abdominal photophores on the protopodite of each pleopod contain many photocytes that are less obviously composed of multiple units. The morphology of the photophores from various sites on a number of species has been described by Coutière (1905, 1906), Kemp (1910a, b), and later by Dennell (1940, 1942, 1955). Dennell (1940) interpreted his results as evidence for a range of photophore types both within and between species of *Systellaspis* and *Oplophorus*.

In this paper we reexamine some of this apparent variation and conclude that the different appearances of the photophores reflect different degrees of aggregation and merging of fundamentally similar units. We describe the ultrastructure of a typical unit in the maxilliped and the compound nature of the pleopod photophores. We also report the rotation of some of the photophores in the plane of pitch and the anatomical means whereby this is achieved. Similar rotation of some counterilluminating photophores has been described in the thoracic and abdominal photophores of euphausiids, as noted above, and in the hepatic photophores of species of the penaeidean shrimp *Sergestes* (Latz and Case, 1982).

Materials and Methods

Specimens were collected during cruises 195 (1990) and 204 (1993) of RRS *Discovery* in the eastern North Atlantic, between the Canary and Cape Verde Islands. They were taken from depths of up to 600 m, using the RMT 1 + 8 net system (Roe and Shale, 1979). The use of a closing cod end (Wild *et al.*, 1985) maintained the shrimps in good condition. They were processed on board ship. Juvenile and adult specimens were fixed in Karnovsky's (1965) fixative, and most were postfixed in 1% phosphate-buffered osmium tetroxide at pH 7.4. Specimens were dehydrated in a graded acetone series and embedded in either Spurr's resin or in Araldite. On shore, semithin (1 μ m) sections were cut on a Huxley Cambridge

ultramicrotome, mounted on subbed slides (0.1% gelatine; 0.01% chrome alum), and stained with toluidine blue (1% in 1% borax). Ultrathin sections were collected on uncoated grids or on 0.5% pioloform films that were mounted on slot grids; they were stained with aqueous uranyl acetate and lead citrate and examined using a JEOL 100 CX electron microscope (JEOL Ltd, Colindale, London, UK). Light micrographs were taken on Pan F film with a Zeiss Photomicroscope II.

Results

The 3rd maxilliped photophores

The photophores in the dactylus of the 3rd maxilliped are located along its posterior (ventral) surface towards the lateral edge, and they are organized in a single row (Fig. 1). There is a group of relatively large photophores located at the very tip. These are always separate from the main row, are present in the earliest postlarvae, and are among the first to develop. From this distal group the photophore row extends proximally to the joint. In older individuals, both the proximal and distal ends of this row are several photophores wide. We selected this group of photophores in *Oplophorus spinosus* as representative of the basic subunits. We chose these photophores because they are easily visible in the transparent dactylus of juvenile specimens, are not obscured by pigment as in *Systellaspis debilis*, and are organized in a largely linear array that allows their developmental sequence to be readily determined in live animals. At most other sites, the individual subunits are obscured by pigment or by the two-dimensional nature of the arrays.

The photophores of the 3rd maxilliped represent the simplest grade of photophore organization, and their overall structure is summarized in Figure 2. They are ovoid to conical and consist of a single photocyte and two types of pigment cell. In fresh specimens, the clear nucleus of the photocyte can be seen at its basal, most ventral (closest to the cuticle) end (Fig. 3). Its refractile properties suggest that it may have an optical function. This basal end of the photophore is attached to a specialized region of the epidermis. At the dorsal end, the apex of the photophore is connected to a ligament extending the length of the dactylus (Figs. 2 and 3).

The photocyte

The photocyte is more or less ovoid, and electron micrographs reveal its close association with the epidermis (Fig. 4). When treated with uranyl acetate and lead citrate, its nucleus stains lightly compared with those of nearby epidermal cells. In addition, the chromatin is concentrated around the periphery of the nucleus. The shape of the nucleus is plano-convex, with the curved face directed

ventrally towards the limb surface. In *O. spinosus*, there is a dimple in the convex surface, but in *S. debilis* there is not. The shape and distinctive staining properties of the nucleus may relate to its presumed refractive function.

Most of the volume of the photocyte is occupied by a single clear vacuole lacking organelles or inclusions but filled with a material that sometimes shows a very fine granulation (Fig. 6). Dennell (1940) calls this the "clear area" of the "photogenic cell." The rest of the cytoplasm is located at the periphery of the cell and contains cytoskeletal elements, mitochondria, vesicles, and paracrystalline bodies.

The basal cytoplasm of the mature photocyte, ventral to the nucleus (and in *O. spinosus*, extending into its dimpled face) is packed with mitochondria (Fig. 5); in all other regions, the cytoplasm surrounding the clear central region of the cell is devoid of these organelles. The cytoplasm at the apex of the cell, lying above the clear area, contains numerous osmiophilic paracrystalline bodies (Figs. 4 and 6). These bodies are membrane-bound structures stacked into a flat cone in the most apical region of the cell. They usually have flat sides and occur in a range of shapes. Many appear rhomboidal or square while others are triangular in section. In all cases, they have a regular, square lattice substructure, with a periodicity of about 14.8 nm (SD = 0.36 in 15 measurements) (Fig. 7). Cytoplasmic processes arising from the apical region of the photocyte extend into the surrounding reflecting pigment cell processes (Fig. 6). The cytoplasm in the apical

region of the photocyte and the processes arising from it contain microfilamentous cytoskeletal elements.

The pigment cells

Two distinct types of pigment cell contribute to each photophore. In fresh tissue, one type has a broadband white reflectance. The other is scarlet, and the pigment has the typical characteristics of the carotenoid astaxanthin and its esters, which are responsible for most of the animal's color (Herring, 1973). The somata are associated with the ligament dorsal to the row of photophores (Figs. 2 and 4). These somata contain abundant rough endoplasmic reticulum. Cytoplasmic processes that contain most of the pigment granules extend ventrally from the somata.

In material sectioned for light and electron microscopy, the processes containing the white pigment granules form a cap around the apex of each photocyte (Fig. 6). These processes contain relatively uniform, densely packed membrane-bound pigment granules measuring up to about 0.40 μm in diameter in *O. spinosus* and up to about 0.25 μm in diameter in *S. debilis*. The granules contain electron-lucent material around a central core of moderately dense material. There are similarities between the contents of these pigment granules and those of the tapeta of various crustacean eyes (shrimps: Doughtie and Rao, 1984, and Ball *et al.*, 1986; crayfish: Piekos, 1986; lobsters, Shelton *et al.*, 1986), which is evidence for their role as a reflecting layer. The cytoplasm of the reflecting

Figures 1–6. Views of maxilliped photophores in *Oplophorus spinosus*.

Figure 1. Light micrograph of a lateral view of a maxilliped, showing the photophores arranged in a row along the ventral face of the dactylus with a pair of large photophores at the distal tip (arrow). Note the immature photophores within the row (arrowheads). di, distal; do, dorsal; l, ligament. Scale bar: 300 μm .

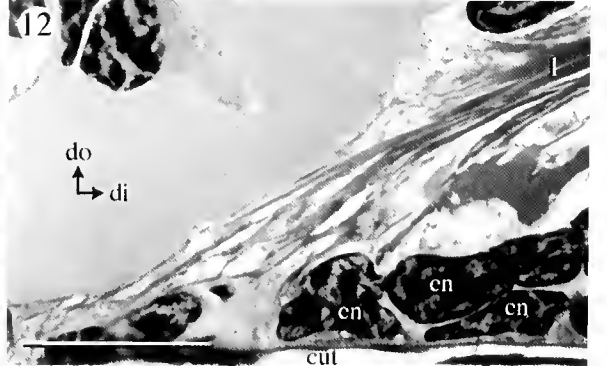
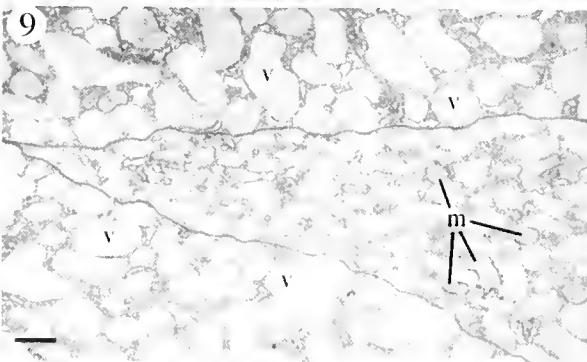
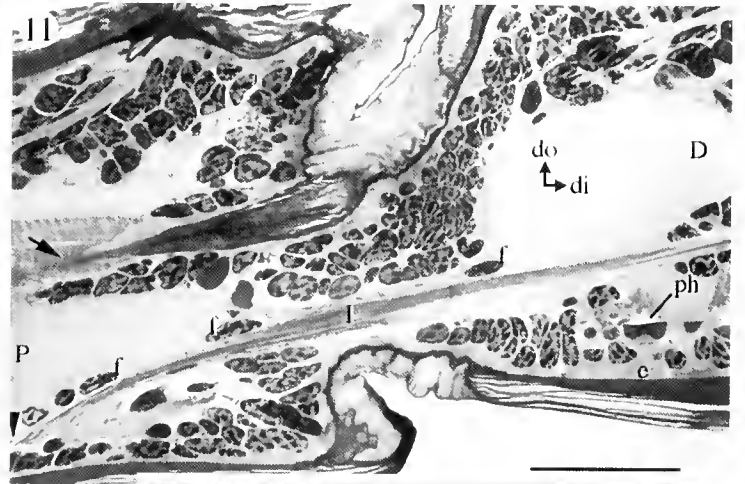
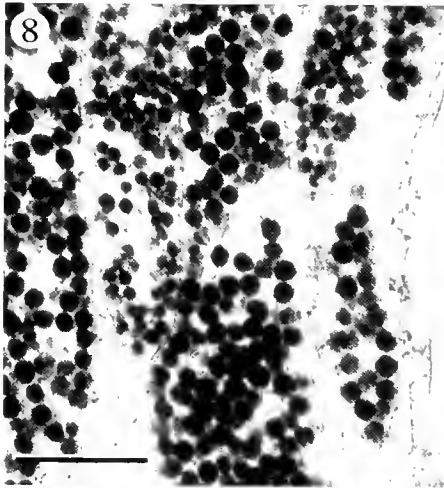
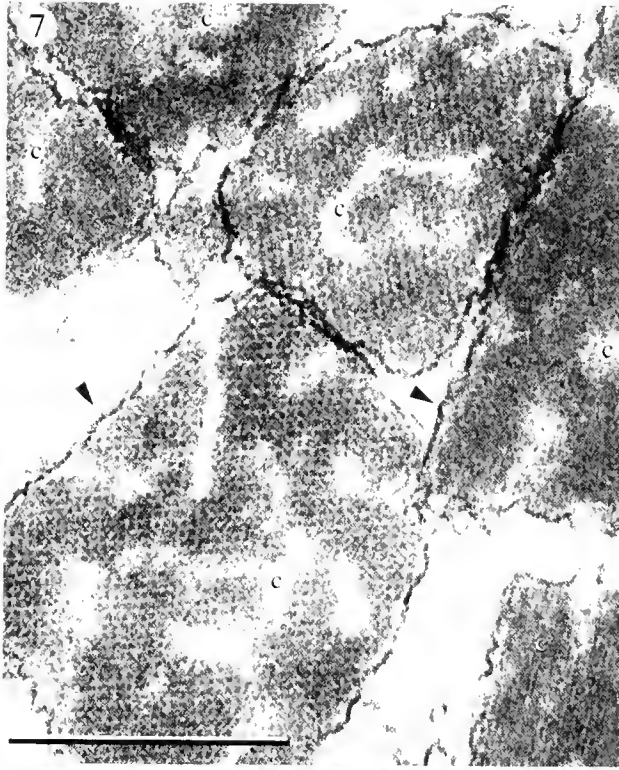
Figure 2. Semi-schematic drawings of portions of the maxilliped to show the arrangement of the photophores lined along the ventro-lateral portion of the dactylus (upper), and the cellular organization of two photophores (lower). Each photophore consists of a photogenic cell with a nucleus (pn) at the base and paracrystalline bodies (c) at the apex; a cap of processes of a reflecting pigment cell (r); and a sheath of processes of carotenoid pigment cells (p). A ligament (l) composed of extracellular fibrils formed by fibroblasts (f) joins the photophores to each other and anchors them to the "window" epidermis (e) below. A blood vessel (b) runs parallel to and above the ligament. di, distal; do, dorsal. Dimensions are approximate. Scale bar: 40 μm .

Figure 3. Light micrograph of a lateral view of the ventral portion of the maxilliped. The ligament (l) is attached to the apex of each photophore. Note the clear, lens-shaped photocyte nuclei (pn). di, distal; do, dorsal. Scale bar: 75 μm .

Figure 4. Light micrograph of a longitudinal section through the maxilliped showing two photophores oriented perpendicular to the cuticular surface. One photocyte is outlined to indicate its boundaries with the "window" epidermal cells. Each photocyte has a lens-shaped nucleus (pn) at its base and an array of paracrystalline bodies (c) above a clear area (ca). The apex of the photocyte is connected to the ligament (l) by a cap of reflecting pigment cell processes (r) and a sheath of carotenoid pigment cells (p). Fibrous strands (arrowhead) extend from the ligament alongside the photophores. cut, surface cuticle; di, distal; do, dorsal; en, "window" epidermal cell nuclei; f, fibroblast; pen, pigment cell nucleus. Scale bar: 40 μm .

Figure 5. Electron micrograph of the basal cytoplasm of the photocyte of the maxilliped photophore showing abundant mitochondria (m) which lie below the nucleus (pn). Scale bar: 1 μm .

Figure 6. Electron micrograph of a section through the apex of a photocyte and the cap of reflecting pigment cell processes (r). c, paracrystalline bodies; ca, clear area. Scale bar: 2 μm .



cell also contains some mitochondria but few other organelles.

Numerous abutting processes of the carotenoid pigment cells surround the photocyte and its associated reflecting cap down to its junction with the epidermis. They contain many electron-dense pigment granules that do not appear to be membrane-bound and resemble those in crustacean chromatophores (Elofsson, 1971). The size of the granules is relatively uniform up to a diameter of about $0.15\ \mu\text{m}$ in *O. spinosus* (Fig. 8) and $0.25\ \mu\text{m}$ in *S. debilis*. As with the reflecting pigment cells, the granules are contained in numerous abutting cytoplasmic processes. The presumed function of the carotenoid pigment is to prevent lateral leakage of light from the photophore.

The underlying epidermis and cuticle

The photophores lie on a strip of a specialized "window" epidermis through which light generated by the photophore is transmitted (Fig. 4). This epidermis is composed of a single layer of epithelial cells in which the cytoplasm is filled with electron-lucent droplets and a few mitochondria (Fig. 9). There is an abrupt transition between the window epidermis and the general cuticular epidermis. The latter contains abundant rough endoplasmic reticulum that gives its cytoplasm a somewhat more electron-dense appearance. The clearly differentiated nature of the window epidermis may relate to the optical requirements of the photophore structure.

The cuticle secreted by the window epidermis differs in two ways from that secreted by the non-photophore epidermis. In both *S. debilis* and *O. spinosus*, the "window" cuticle is thicker than that which surrounds it. In *S. debilis*, the window cuticle ventral to the row of photo-

phores is formed into a lens-like ridge (Fig. 10) that is probably of optical significance; *O. spinosus* has no such obvious ridge. In fresh preparations of both species, the window cuticle has a distinct blue color with an absorption maximum around 560 nm in *O. spinosus* and 530 nm in *S. debilis* (P.J.H., unpub. data), whereas the surrounding cuticle does not. This color is visible over the pleopod photophores in the first zoeas of *S. debilis*, but develops only in later stage larvae of *O. spinosus*.

The ligament

With the exception of the separate group of larger photophores at the distal end of the dactylus, each photophore along the length of the maxilliped is attached to a ligament lying dorsal to the row (Figs. 2, 3, and 4). The ligament arises at the distal end of the propodus (Fig. 11), where it is attached directly to the cuticular epidermis (Fig. 12). It extends to the most distal of the photophores in the main row, but not as far as the large photophores of the terminal group. The ligament consists of thick bundles of fibrils that are parallel to the long axis of the limb. These fibrils have a diameter of 20 nm, and a periodicity of about 9.7 nm (SD = 0.52 in ten measurements) along their length (Figs. 13 and 14). They are associated with fibroblasts distributed along the ligament and are assumed to be formed by them (Figs. 4 and 11).

Smaller bundles of fibrils extend ventrally from the ligament to the apex of each photophore (Figs. 4 and 15). These bundles are found amidst the processes of the pigment cells and in between adjacent photophores at all levels down to the window epidermis. Like the thicker bundles, these are associated with fibroblasts (Fig. 15) and serve to connect each photophore to the ligament or

Figures 7–10. Micrographs of maxilliped photophores; all except Fig. 10 are of *Oplophorus spinosus*.

Figure 7. Electron micrograph of the membrane-bound (arrowheads) paracrystalline bodies (c) of the photocyte showing the square lattice substructure. Scale bar: $0.5\ \mu\text{m}$.

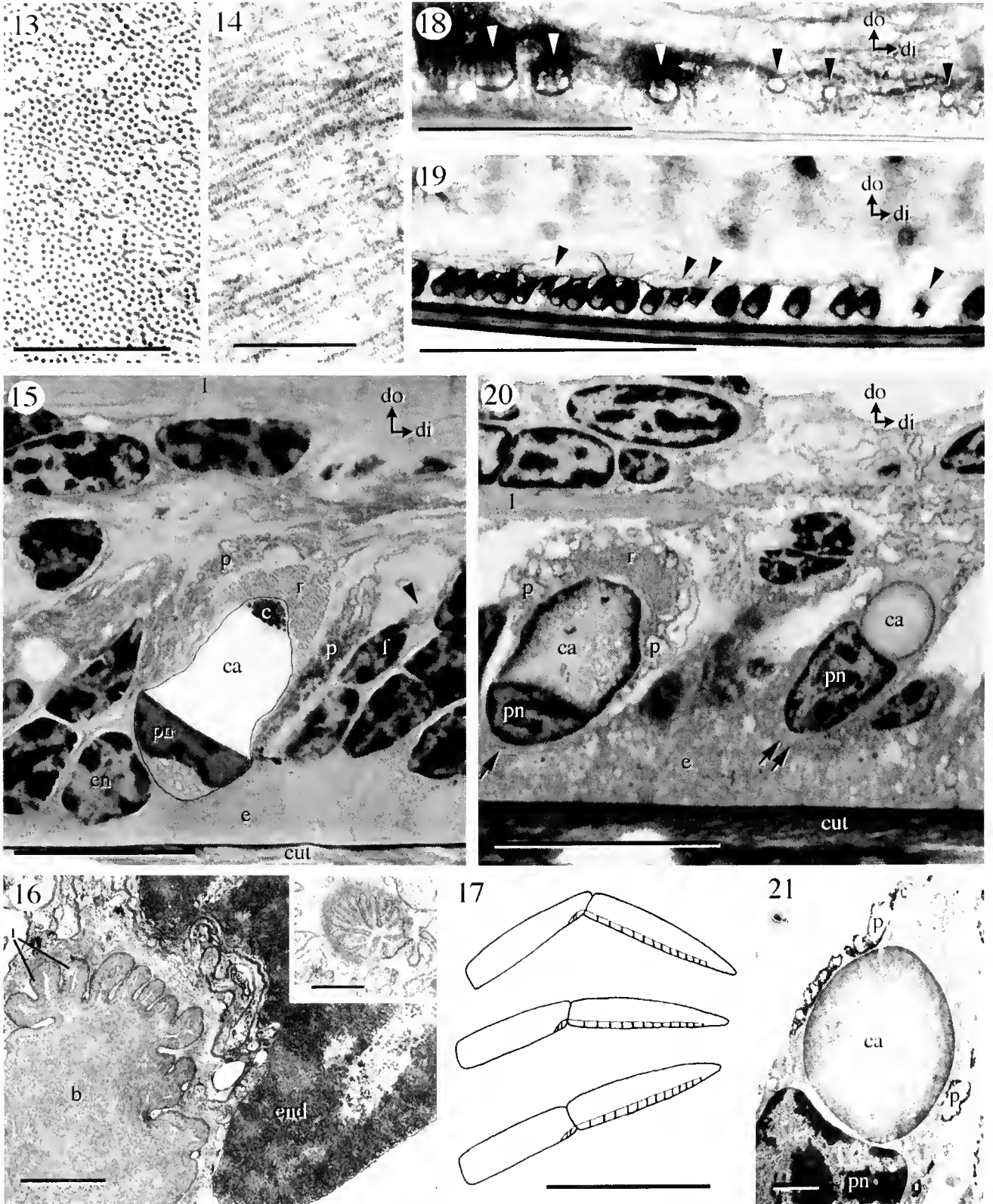
Figure 8. Electron micrograph showing the processes of a carotenoid pigment cell that form a sheath around the photophore. Scale bar: $1\ \mu\text{m}$.

Figure 9. Electron micrograph of a horizontal section through the "window" epidermis of the maxilliped. Note the abundance of membrane-bound vesicles (v), with minimal cytoplasm between them, and the relatively few mitochondria (m). Scale bar: $1\ \mu\text{m}$.

Figure 10. Light micrograph of a section through a photophore in the maxilliped of *Systellaspis debilis*, showing the similarities with those of *O. spinosus*. The photocyte lies above the "window" epidermis (e). The ligament (l), blood vessel (b), and processes of the pigment cells (p) can be seen above the photocyte. In *S. debilis*, the photocyte "clear area" (ca) is invariably filled with an electron-dense material. Note that the cuticle below the simple photophore has a convex lens-like contour (arrowhead). pn, photocyte nucleus. Scale bar: $40\ \mu\text{m}$.

Figure 11. Light micrograph of a longitudinal section through the propodus (P) and dactylus (D), of the maxilliped. The most proximal of the row of photophores (ph) in the dactylus is shown. The insertion of the ligament (l) into the epidermis of the propodus is indicated (arrowhead), as well as the insertion of the flexor muscle to the cuticle of the joint (arrow). di, distal; do, dorsal; e, window epidermis; f, fibroblast. Scale bar: $100\ \mu\text{m}$.

Figure 12. High-power light micrograph showing the attachment of the ligament fibers (l) to the epidermis of the propodus. cut, cuticle; di, distal; do, dorsal; en, epidermal cell nuclei. Scale bar: $40\ \mu\text{m}$.



the ligament to the epidermis between adjacent photophores.

A prominent blood vessel runs the whole length of the ligament, along its dorsal surface. This vessel exhibits a folding of its internal intima and endothelial lining (Figs. 2 and 16), which would facilitate any changes in its diameter. Similar blood vessels have been found in other crustacean systems (Peterson and Loizzi, 1974; Schönenberger, 1977; Martin and Hose, 1992). Capillaries extend from the main blood vessel toward the photophore; these, too, have folded walls (Fig. 16 inset).

Tilt control of the maxilliped photophores

The ligament that is attached to all but the terminal group of photophores in the dactylus appears to have a role in determining their orientations. Examination of fresh and fixed whole-mount preparations and of the longitudinally sectioned dactylus shows that in any one specimen, all the photophores in the main row are oriented

in the same way. However, the orientation varies from specimen to specimen: in some cases they are perpendicular to the surface of the maxilliped (Fig. 4); in others they are tilted (Figs. 15, 20, and 22). The ligament provides the means whereby such changes of orientation occur.

Owing to its origin in the ventral region of the distal propodus, the ligament and the apices of all the photophores connected to it are pulled proximally, with respect to the dactylus, by flexion of the propodus/dactylus joint. Extension of the joint results in distal movement of the ligament and the apices of the photophores connected to it. The photophores are fixed to the integument at their basal surfaces, so these ligament displacements cause them to tilt (Fig. 17).

Because most of our observations were made on preserved material, we have not been able to describe the precise relationship between joint angle and photophore tilt. Nevertheless, one of us (P.J.H.) was able to confirm that in fresh material the photophores do indeed tilt as the dactylus is rotated with respect to the propodus. A

Figures 13–21. Views of maxilliped photophores of *Oplophorus spinosus* (Figs. 13–19) and *Systellapsis debilis* (Figs. 20, 21).

Figure 13. Electron micrograph of a transverse section through the ligament dorsal to the maxilliped photophores showing the dense packing of the fibrils. Scale bar: 0.25 μm .

Figure 14. Electron micrograph of a longitudinal section through the ligament of the maxilliped showing the highly oriented fibrils. Scale bar: 0.25 μm .

Figure 15. Light micrograph of a longitudinal section through the maxilliped showing the photophore tilted proximally. The photocyte has been outlined to show its boundaries. c, paracrystalline bodies of photocyte; ca, clear area of photocyte; cut, cuticle; di, distal; do, dorsal; e, "window" epidermis cytoplasm; en, "window" epidermis nucleus; f, fibroblast (with arrowhead indicating fibers extending toward ligament); l, ligament; p, carotenoid pigment cell processes; pn, nucleus of photocyte; r, reflector pigment cell processes. Scale bar: 40 μm .

Figure 16. Electron micrograph of a transverse section of the blood vessel (b) associated with the ligament of the maxilliped. The wall of the blood vessel is a folded structure comprising an endothelial cell and an internal intima (i). The inset shows a capillary that has branched from the blood vessel toward the photophore and exhibits the same type of folding. end, endothelial cell nucleus. Scale bars: 1 μm .

Figure 17. Schematic drawings of the maxilliped. Top: the limb flexed, with the photophores tilting anteriorly as the ligament pulls their apices posteriorly. Middle: the maxilliped in its resting position with the photophores directed downward. Bottom: the limb extended, with the photophores tilted posteriorly as the ligament pushes their apices anteriorly. In each case, light would be directed ventrally with respect to the animal. Scale bar: 2 mm.

Figure 18. High-power light micrograph of the distal tip of the maxilliped showing early stages in the development of several photophores in the main row. In some, refractile droplets are forming in the photocytes (black arrowheads). In slightly older photophores (white arrowheads), larger droplets are surrounded by the carotenoid pigment cell sheath. di, distal; do, dorsal. Scale bar: 150 μm .

Figure 19. Light micrograph of a lateral view of a maxilliped showing the row of photophores at the ventral surface, all oriented in the same direction (tilted slightly posteriorly). Note the small (*i.e.*, developing) photophores (arrowheads) between more mature neighbors. di, distal; do, dorsal. Scale bar: 400 μm .

Figure 20. Light micrograph of a longitudinal section through the maxilliped of *S. debilis* showing two photophores. The larger (and more mature) photophore (arrow) has a photocyte with a large, moderately electron-dense "clear area" (ca) and a relatively small nucleus (pn). The photocyte of the smaller (and younger) photophore (double arrow) has a larger nucleus and a small clear area growing as an electron-lucent droplet within the supranuclear cytoplasm of the cell. cut, cuticle; di, distal; do, dorsal; e, "window" epidermis; l, ligament; p, carotenoid pigment cell processes; r, reflecting pigment cell cap. Scale bar: 40 μm .

Figure 21. Electron micrograph of a very young photocyte in a simple photophore of *S. debilis*. The small clear area droplet (ca) within the cytoplasm lies above the nucleus (pn). A few carotenoid pigment cell processes (p) surround the photocyte, but neither the cap of reflecting pigment cell processes nor the paracrystalline bodies are present at this stage. Scale bar: 3 μm .

maxilliped was amputated at the mid-propodus level and placed on its side on a layer of Sylgard in a petri dish. It was fixed in position by one pin on either side of the propodus and another on the dorsal side of the dactylus so that the two segments were in line. The dactylus was then displaced ventrally (*i.e.*, flexed) with a pin and the preparation was observed through a binocular microscope. As the dactylus was alternately extended and flexed, the photophores tilted in synchrony, first backwards and then forwards. In addition, live juveniles were pinned so that they lay horizontally but were otherwise free to move all their limbs and abdomen. The maxillipeds were placed under a dissecting microscope and their movements were videotaped. Dactyli of the maxillipeds were occasionally flexed, and the orientations of the photophores in them were compared with those in the extended limb. Similar changes in orientation of the photophores were noted.

To obtain an indication of the possible range of photophore tilt angles, we measured the angle between the normal to the cuticular surface and the long axis of the photophore in 14 fixed specimens. Photophores that had a forward tilt (towards the distal end of the limb) due to joint flexion had a maximum angle of about $+31^\circ$ from the normal. Photophores tilted backwards (due to joint extension) measured a maximum of about -42° from the normal. These results provide the first evidence for a form of photophore tilt control that does not depend on a special muscle attached to each organ. In this case the photophores are displaced passively by movements of the joint using an automatic mechanism that ensures that all photophores in the row move in synchrony. A similar system produces rotation of the abdominal photophores of euphausiids (Hardy, 1964); however, in that case, muscles are involved in displacing the ligament.

The development of the photophores in the maxilliped

The sequence of photophore development in *S. debilis* was fully described by Kemp (1910a), who reported that the maxilliped photophores appear at the first postlarval stage. He did not distinguish the development of separate photophore units within the maxilliped dactylus; we have examined similar early postlarvae and found that in all cases there are two small photophores at the distal tip and three at the proximal end. The photophores in the proximal group form the first of those that are associated with the ligament, and contribute to the main row. The distal group remains independent of the ligament. During later development, photophores appear between the two original groups as a linear array (Fig. 18), while both the distal and (more obviously) the proximal groups add more photophores so that they become several photophores wide.

The spacing of photophores within the main row is fairly irregular, and new photophores develop in the gaps between existing ones (Fig. 19). The photophore precursor cells have not been identified, but they are likely to arise from the epidermis where mitotic figures are often found. The first visible sign that a new photophore is developing is the appearance of a differentiating photocyte (Fig. 18). A single refractile droplet appears within this cell and expands within the cytoplasm dorsal to the nucleus, increasing the total cell volume and resulting in the elongation of the cell dorsally (Fig. 20) to form the "clear area" (Dennell, 1940) of the photocyte. The rest of the cytoplasm—containing ribosomes, vesicles, and cytoskeletal elements—becomes restricted to the periphery of the cell (Fig. 21), with abundant mitochondria in the basal cytoplasm ventral to the nucleus. The electron-dense apical paracrystalline bodies are absent from the youngest photocytes (Fig. 21) and appear only as the cell matures.

While these cytoplasmic changes are taking place, nuclear changes are also occurring. At first the nucleus of the developing photocyte is indistinguishable from those of the epidermal cells around it (ovoid and hyperchromatic). Gradually the nucleus acquires the pale and more homogeneous appearance characteristic of the mature photocyte and assumes its lens-like plano-convex shape (Fig. 4).

The growth of the photocytes occurs within a sheath of the processes of the carotenoid pigment cells (Fig. 21). Inspection of serial sections through a number of differentiating photophores showed that photophores that had a reflecting cap always had a carotenoid pigment cell coat, but those that had a coat of carotenoid pigment sometimes lacked a reflecting cap. Thus the reflecting pigment cell presumably differentiates after the carotenoid pigment cell.

Examination of many fully differentiated photophores revealed significant variations in the appearance of the photocyte. In newly formed photophores the clear area is of uniform appearance and lacks any inclusions; more mature photophores contain non-membrane-bound droplets that may completely fill the "clear area," with an accumulation of electron-dense material between them (Fig. 22). These anatomical changes are accompanied by a change in the consistency of the clear area. Sectioning for transmission electron microscopy reveals that the fixed material becomes harder, and this portion of the cell often falls out of sectioned material. The extent of the modification to the clear area varies from photophore to photophore. The simplest interpretation of these observations is that the changes are part of maturation, and that those photophores with the greatest accumulation of material are the oldest. This maturation process seems to occur earlier in *S. debilis* than in *O. spinosus*, because even

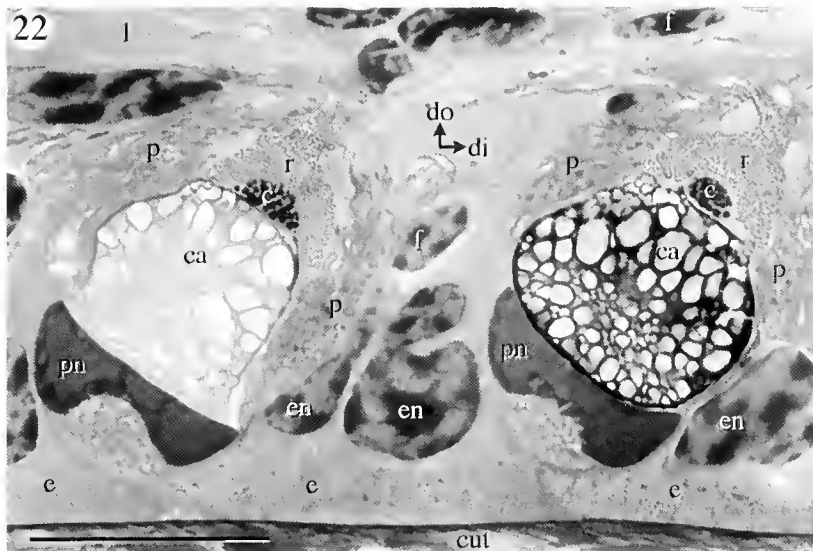


Figure 22. Light micrograph of a longitudinal section through the maxilliped of *Oplophorus spinosus* showing photophores in which the "clear areas" (ca) of the photocytes exhibit stages of increasing osmiophilicity. c, paracrystalline bodies; cut, surface cuticle; di, distal; do, dorsal; e, "window" epidermis cytoplasm; en, "window" epidermis nucleus; f, fibroblast; l, ligament; p, carotenoid pigment cell processes; pn, photocyte nuclei; r, reflector pigment cell cap. Scale bar: 40 μ m.

young photophores of *S. debilis* invariably have darkened "clear areas" (Figs. 20 and 21). This is consistent with the earlier development of the blue cuticular pigment in *S. debilis*.

Pleopod photophores

Each pleopod has a cuticular photophore located in the distal coxa (Fig. 23). It is situated anterior and slightly lateral to the origin of the more distal segments of the pleopod. Externally, its lens is visible as an ovoid region of modified cuticle in which the long axis is more or less transverse with respect to the animal. The convex surface of the lens is surrounded on three sides (anterior, lateral, and medial) by a furrow, the cuticle of which is attenuated; this folded surface acts as a hinge that enables the photophore to be rotated.

Kemp (1910b) described the photophores on the pleopods as the most highly developed. Our studies have shown that, despite their relative complexity, these photophores are composed of the same cell types found in the single-unit (*i.e.*, maxilliped) photophores. They include photocytes, reflecting pigment cells, and carotenoid pigment cells. Most of our observations of pleopod photophores were made on *O. spinosus*, and the general structure of these photophores is summarized in Figure 24.

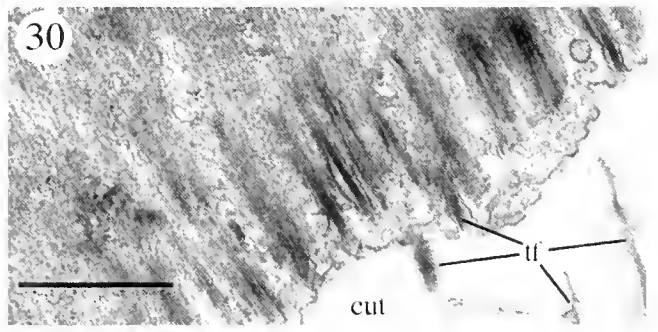
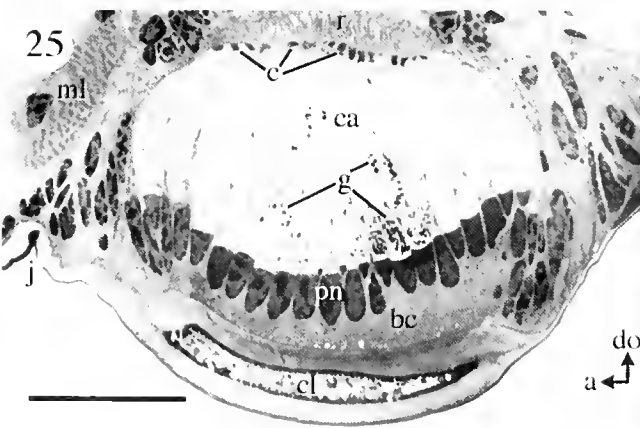
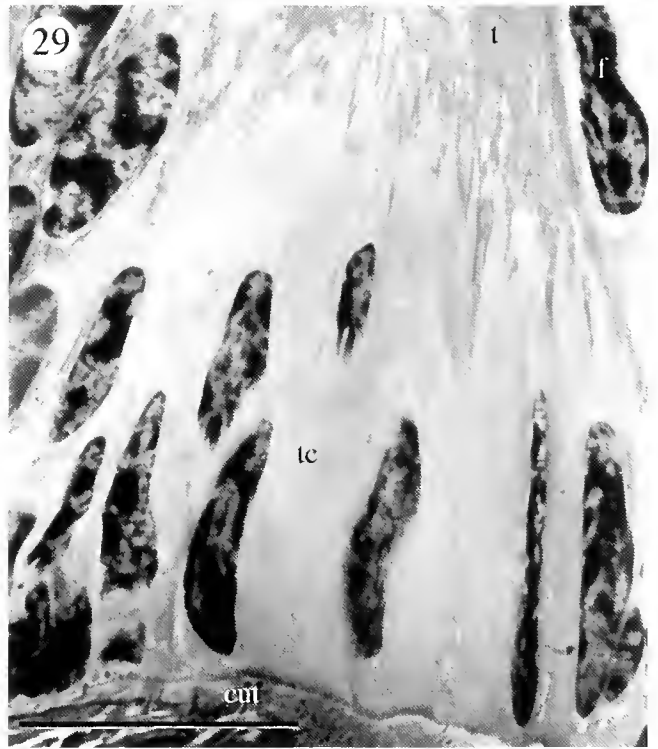
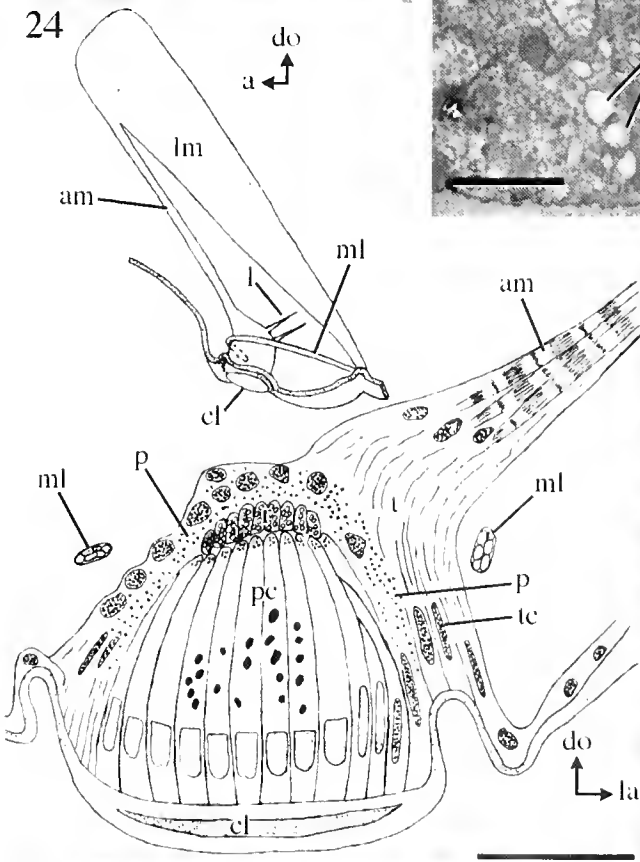
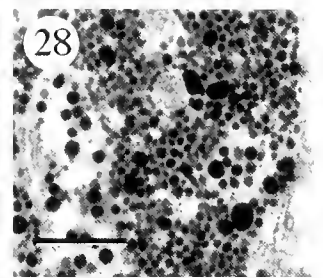
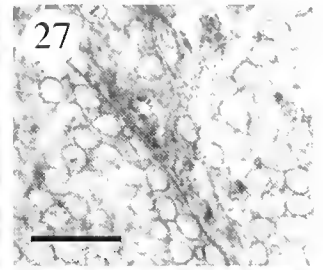
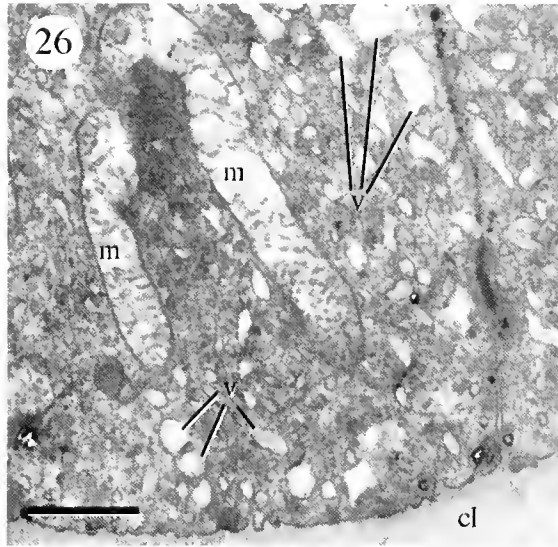
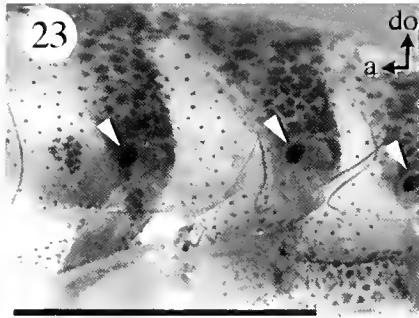
The cuticle covering the photophore forms a concavo-convex lens that in mature specimens is trilaminar (Fig. 25) (Kemp, 1910b; Dennell, 1940). Whereas the photocytes in the simple photophores of the maxilliped are

separated from the cuticle by a layer of epidermis, in the pleopod photophore the photocytes are attached directly to the cuticle and it must be concluded that they secrete the lens structure. The cuticle peripheral to the lens is thinner and often folded (Fig. 25), allowing the cuticular lens to be displaced during photophore tilting movements (see below). This is in contrast to the situation in the maxilliped photophores where the cuticle remains stationary during photophore rotation.

The photocyte

The photocytes of the pleopod photophores are very elongate and somewhat conical (Figs. 24 and 25). The basal cytoplasm lying between the nucleus and the cuticular lens is filled with small, electron-lucent vesicles and a few mitochondria (Fig. 26). These vesicles may contribute to the optical properties of the photophore, or they may simply be related to the secretion or resorption of the cuticle. There are similarities between this portion of the photocyte cytoplasm and the cytoplasm of the specialized window epidermis under the maxilliped photophores—both have abundant vesicles and a few mitochondria, although the vesicles in the pleopod photocytes are smaller and separated by a granular cytoplasm. The similarities of appearance may indicate similarities of function.

The nuclei of the photocytes resemble those of the single-unit maxilliped photophores in that they are pale-staining with diffuse chromatin, have a plano-convex



shape, and often possess a dimple in the distal surface. One difference is in the ratio of length to width: in the pleopod photophores, the photocyte nuclei are about twice as long as they are wide ($\approx 25\text{--}35\ \mu\text{m} \times 12\text{--}15\ \mu\text{m}$), whereas the relationship is reversed in the maxilliped ($\approx 15\ \mu\text{m} \times 30\text{--}35\ \mu\text{m}$). Consequently, the photocyte nuclear layer is thicker in the pleopod photophores than in those of the maxilliped.

The cytoplasm above the nuclei is almost completely occupied by a clear area devoid of organelles, as it is in the maxilliped photocytes. The rest of the cytoplasm is restricted to the periphery of the cell. Membrane-bound paracrystalline bodies in the pleopod photophore are similar in location (at the apex of each of the photocytes) and substructure (a regular square lattice) to those in the maxilliped photophores.

Pigment cells

In the pleopod photophore, the processes of the reflecting pigment cells form a common cap around the apex of the complete set of photocytes (Figs. 24 and 25); in contrast, in the photophores of the maxilliped, each individual photocyte has its own cap of reflecting pigment cell processes. The processes of the carotenoid pigment cells form a sheath peripheral to this reflecting cap. The

sheath covers the photophore down to its base at the level of the integument. Kemp (1910b) suspected the presence of such a pigment coat but was unable to demonstrate it definitively. In *O. spinosus*, the pigment granules in these two types of pigment cell closely resemble those in the maxilliped photophores in appearance and staining properties: the reflecting pigment granules are membrane-bound and electron-lucent, while the carotenoid pigment granules are not membrane-bound and are very electron-dense. Although the reflecting pigment granules are similar in size (up to $0.35\ \mu\text{m}$ in diameter) to those in the maxilliped photophores, the carotenoid pigment granules are larger in the pleopod photophores (up to $0.25\ \mu\text{m}$ in diameter) (Figs. 27 and 28). No observations were made of pigment granule sizes in *S. debilis*.

The musculature and tendon apparatus

Observations of living preparations showed that the photophore can articulate about its anterior margin (see Figs. 31 and 32). Each pleopod photophore has its own anatomically separate mechanism for tilting (unlike the linked arrangement in the maxilliped), and the anatomical findings show that the photophores are controlled by muscles rather than by passive movements of a joint structure as they are in the maxilliped. There are two major muscle

Figures 23–30. Views of pleopod photophores of *Oplophorus spinosus*.

Figure 23. Micrograph of a lateral view of the abdomen showing three of the pleopods with the photophores (arrowheads) visible through the transparent abdominal pleura. a, anterior; do, dorsal. Scale bar: 5 mm.

Figure 24. Semi-schematic drawings showing the arrangement of muscles (upper) and the cellular organization (lower) of the pleopod photophores. The lower is viewed from the medial side; the section is in the transverse of the shrimp. The pleopod is directly influenced by the main longitudinal photophore muscle (lm), the accessory longitudinal muscle (am), and the photophore muscle loop (ml). Short ligaments (l) connect the posterior side of the photophore to the cuticle. The accessory longitudinal muscle is connected to the antero-lateral margin of the photophore by a tendon (t) inserted into tendinous cells (tc). Photogenic cells (pc) are attached basally to the cuticular lens (cl), and the apices of these cells are capped by processes of reflecting pigment cells (r). Processes of carotenoid pigment cells (p) ensheath the photophore. a, anterior; do, dorsal; la, lateral. Dimensions are approximate. Scale bar for section: $100\ \mu\text{m}$.

Figure 25. Light micrograph through a photophore. The photocytes are arrayed in rows above the trilaminar cuticular lens (cl) with their nuclei (pn) above a basal cytoplasm (bc) and below a clear area (ca). Each photocyte contains paracrystalline bodies (c) at the apex of its clear area; in the center of the photophore, many photocytes have accumulated dark granules (g) in the clear areas. The processes of reflecting pigment cells (r) form a cap above the photophore. The pleopod photophore articulates around a thin, cuticular hinge joint (j). a, anterior; do, dorsal. Scale bar: $100\ \mu\text{m}$.

Figure 26. Electron micrograph of the basal cytoplasm of the photocytes. The cytoplasm is filled with numerous membrane-bound vesicles (v) and contains a few mitochondria (m). cl, cuticular lens. Scale bar: $1\ \mu\text{m}$.

Figure 27. Electron micrograph of reflecting pigment cell processes filled with membrane-bound pigment granules. Scale bar: $1\ \mu\text{m}$.

Figure 28. Electron micrograph of a carotenoid pigment cell filled with dark granules. Scale bar: $1\ \mu\text{m}$.

Figure 29. Light micrograph of the lateral margin of a photophore. Tendinous cells (tc) form a sheet that is attached at its base to the cuticle (cut); the articulating tendon (t) of the photophore inserts into the apex of these cells. f, fibroblast. Scale bar: $40\ \mu\text{m}$.

Figure 30. Electron micrograph through tendinous cells of the photophore at their junction with the cuticle (cut). The cytoplasm of these cells is loaded with microtubules oriented perpendicular to the cuticular surface. Tonofibrillae (t) anchor the tendinous cells to the cuticle. Scale bar: $1\ \mu\text{m}$.

sets: a pair of longitudinal muscles concerned with backward rotation of the photophore, and a muscle loop that tilts the photophore forward. The former have their origin on the antero-lateral wall of the coxa dorsal to the photophore. The larger of the two muscles (the main longitudinal muscle) inserts onto the cuticle of the coxa about 0.5 mm posterior to the photophore (Fig. 24). The smaller longitudinal muscle (the accessory longitudinal muscle) arises as a branch of the larger one and runs directly to the photophore itself, inserting into the antero-lateral margin of the photophore by means of a tendon.

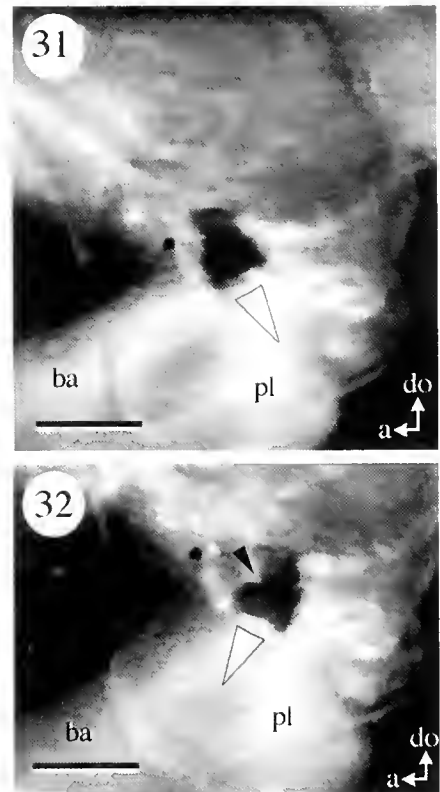
This description differs significantly from that of Dennell (1940), who described only the accessory longitudinal muscle (his "longitudinal photophore muscle") and not the main longitudinal muscle. We do confirm the presence of Dennell's (1940) "photophore muscle loop," which passes around the anterior side of the photophore. One end of the loop inserts outside the cuticular groove that surrounds the photophore, and the other end inserts medially into an invagination of the cuticle at the site where the main longitudinal muscle described above terminates. In addition to these muscles, there is a set of several short ligaments that attach the posterior region of the photophore to the adjacent wall of the coxa (Fig. 24).

Of the various muscles, only the accessory longitudinal muscle is connected directly to the photophore. The tendon that joins the muscle to the photophore is composed of fibrils that have the same dimensions and periodicity as do those making up the ligament that controls tilt in the row of maxilliped photophores. They are produced by fibroblasts found within the tendon (Fig. 29). Bundles of fibrils insert into the apices of a strip of modified epidermal, or "tendinous," cells (Mellon, 1992) at the antero-medial perimeter of the photophore (Figs. 29 and 30).

The cytoplasm of the tendinous cells is densely filled with microtubules oriented perpendicular to the cuticle. The base of each tendinous cell is firmly fixed onto the inner face of the cuticle by means of tonofibrillae that penetrate the layers of cuticle externally and extend into invaginations of the tendinous cells internally (Fig. 30). The attachment of cells to cuticle in this way has been described in various crustaceans such as shrimps (Talbot *et al.*, 1972) and crayfish (Jahromi and Atwood, 1976, 1977), as well as in insects (Lai-fook, 1967). The lateral margins of adjacent attachment cells are often strongly interdigitated.

Tilting behavior

The arrangements described above provide an anatomical basis for the observable tilting behavior of this type of photophore. Contraction of the main longitudinal muscle would result in backward rotation of the cuticular lens about the hinge anterior to it. There is no obvious antago-



Figures 31 and 32. Images from a videotaped sequence of an *Ophiophorus spinosus* juvenile, showing a photophore on the coxa of a pleopod tilted in different orientations: posteriorly in Fig. 31 and anteriorly in Fig. 32. The basis of the pleopod (ba), as well as the photophore itself, is visible beneath the abdominal pleura (pl). The open arrowheads indicate the tilt direction. Note the kink in the anterior face of the pleopod in Fig. 32, which is caused by contraction of the photophore muscle loop (black arrowhead). a, anterior; do, dorsal. Scale bars: 1 mm.

nistic muscle set and it is assumed that when the main longitudinal muscle relaxes, elasticity of the cuticle returns it to its former position. The function of the accessory longitudinal muscle may be to maintain tension on the photophore when the main longitudinal muscle contracts. This would be necessary to keep the photophore pointing in the appropriate direction during movements of the lens. The short ligaments would provide support for the photophore during this process. The anatomical arrangement of the loop muscle means that its contraction would rotate the photophore forwards by pulling on its anterior margin.

To obtain information on tilting behavior, juvenile specimens of both *O. spinosus* and *S. debilis* were restrained and videotaped from the side, as described earlier. Three types of movement were noted: (1) frequent small twitches (approximately 4°), (2) relatively large rotations in which the posterior margin of the photophore was raised to rotate the photophore backwards by as much as -40° from the resting position (Fig. 31), and (3) rela-

tively large rotations in which the anterior wall of the photophore was pulled posteriorly (by the photophore muscle loop) to rotate the photophore to point forward by as much as $+46^\circ$ (Fig. 32). None of these types of movement appears to be related to any aspect of pleopod beating, which involves movements of only those parts of the limb that are distal to the photophore. Observations of videotape sequences showed that the photophores in adjacent segments often but not always rotated similarly and simultaneously, even though the pleopod photophores are anatomically independent from each other. The larger rotations were sometimes but not always associated with flexion of the abdomen. However, forcible flexion of the abdomen did not always induce rotation.

Growth and development

Kemp (1910a) reported that the pleopod photophores of *S. debilis* are present in the first zoea. The photophores in the pleopods of young postlarvae are extremely small, and mid-longitudinal sections of the organ are just a few photocytes wide (Fig. 33). In older shrimps they are much larger, and they can be up to 20 cells wide. The total number of photocytes has been estimated to be over 300 in fully developed photophores (Kemp, 1910b). Growth of the photophore appears to involve the differentiation

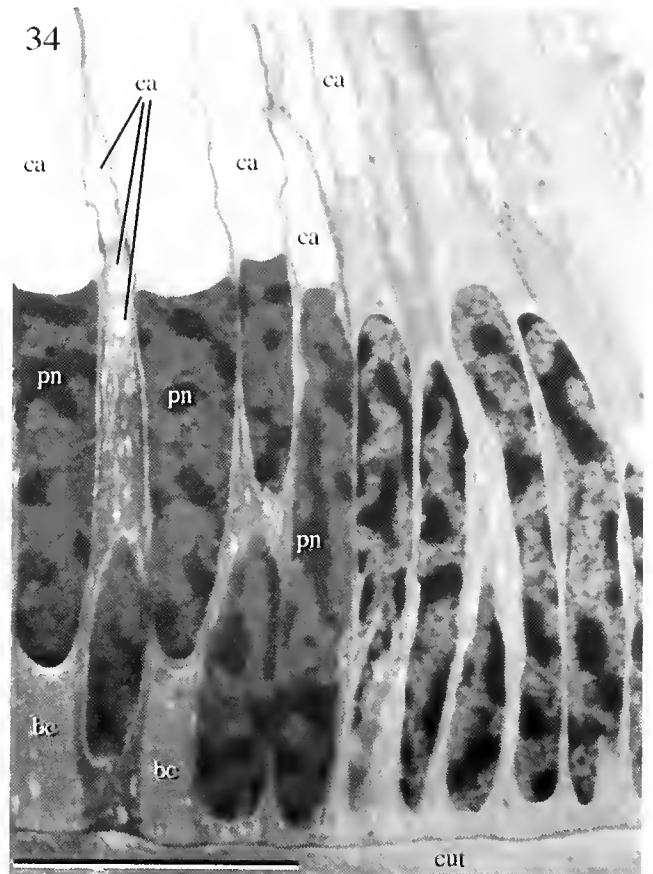


Figure 34. Light micrograph at the growing edge of the pleopod photophore of *Oplophorus spinosus*, where undifferentiated epidermal cells are developing the features of mature photocytes, including the formation of a clear area (ca), lens-shaped, homogeneous nuclei (pn), and vesiculated basal cytoplasm (bc). cut, cuticle. Scale bar: $40\ \mu\text{m}$.

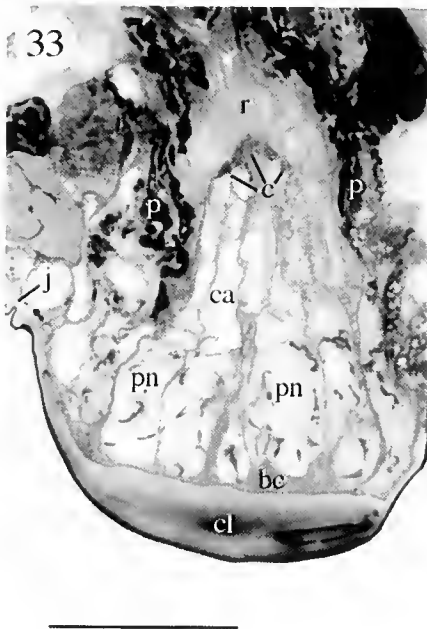


Figure 33. Light micrograph through the pleopod photophore of a postlarval specimen of *Oplophorus spinosus*. The photophore exhibits all the features of the adult organ. bc, basal cytoplasm of photocytes; c, paracrystalline bodies; ca, clear area; cl, cuticular lens; j, articulating joint; p, carotenoid pigment cell processes; pn, photocyte nuclei; r, reflecting pigment cell cap. Scale bar: $40\ \mu\text{m}$.

of immature cells at the periphery of the organ (Fig. 34). This conclusion is based on the observation that photocytes at the edge of the photophore are less mature than those in the center: cells at the edge of the photophore lack a clear area, while the extent of the clear area is greatest in photocytes situated away from the margins of the photophore. Furthermore, the clear area in the most centrally located photocytes shows an accumulation of an electron-dense material that seems to increase with maturation.

Events involved in this differentiation process appear to be similar to stages in the development of photocytes in the maxilliped. The first indication that an epidermal cell at the periphery of the photophore is differentiating into a photocyte is the appearance of a clear area above the nucleus of the cell. Next, the clear area enlarges in the differentiating photocyte, which elongates in an apical direction. This is seen in cells located slightly more centrally. Finally, toward the middle of the organ, the shape of the nucleus changes from ovoid to plano-convex, the

nucleoplasm becomes more homogeneous, and the subnuclear cytoplasm assumes the vesiculated appearance of a mature photocyte (Fig. 34). All of these events occur within the sheath of the carotenoid pigment cell layer.

Additional changes take place in older photocytes, found in the center of the photophore. In these cells, the clear area gradually fills almost completely with osmiophilic granules (see Fig. 25), which eventually coalesce. This differs from what occurs in the maxilliped photocytes. In those cells, the clear area fills with electron-lucent droplets and the material between them becomes increasingly osmiophilic (see Fig. 22). As in the maxilliped, however, the maturation process in photocytes of the pleopod is accompanied by a hardening of the cytoplasm, as evidenced by the material becoming difficult to section for electron microscopy.

Discussion

The term "photophore" is normally used to describe a composite structure in which the light-emitting cells (photocytes) are associated with accessory optical structures. Photophores almost invariably contain numerous photocytes. In *S. debilis* and *O. spinosus*, however, this usage of photophore is clearly applicable to the individual units within the 3rd maxilliped dactylus, each of which contains only a single photocyte but which nevertheless also has refractive, reflective, and light-shielding structures. Examination of a variety of photophores (*sensu* Kemp, 1910b) on these animals (M.S.N., unpub. data) shows that, with the sole exception of the pleopod photophores, they are modular structures made up of a variable number of subunits, each of which is equivalent to one of the photophores containing a single photocyte and present in the maxilliped series. A modular arrangement of photophores at such a small scale has not been described in any other animal. In the few other cases known of photophores with only a single photocyte (e.g., the shark *Euprotomicrus* [Hubbs *et al.*, 1967]), the photophores are widely scattered over the ventral surface and not aggregated into specific groups. Modular assemblages (or groups) of larger photophores are, however, typical of many deep-sea fishes and are particularly prominent in the Sternoptychidae (e.g., *Valenciennellus* and the hatchetfishes). They are also present in a number of cephalopods, notably the Ommastrephidae in which the millimeter-sized subunits may form a very large dorsal photophore. The organs of Pesta, the hepatic photophores of species of *Sergestes*, are modular assemblages of specialized liver tubules, each tubule containing many photocytes and reflective cells (Herring, 1981).

The fine structure of the photophores of *S. debilis* and *O. spinosus* is very similar, as was recognized by Kemp (1910b). There are no other examples of cuticular photo-

phores in the genera within the Caridea, but among the Penaeidea they also occur in some species of the sergestid *Sergia*; the solenocerids *Hymenopenaeus*, *Mesopenaeus*, *Hadropenaeus*, and *Solenocera*; and the penaeid *Gennadas* (see Herring, 1985b, for references). Nothing is known of their ultrastructure in any of these genera, but the early histological descriptions of those in *Sergia* (Kemp, 1910b; Terao, 1917) closely resemble those in similar studies of *O. spinosus* and *S. debilis* (Kemp, 1910b; Dennell, 1940). At the ultrastructural level, the most striking parallel with other decapods is in the paracrystalline bodies that provide the photogenic core of the organs in both *O. spinosus* and *S. debilis*. The photocytes of *Sergestes* have similar paracrystalline bodies or platelets, but with a lattice periodicity of 5–8 nm, considerably lower than the 14.8 nm in *O. spinosus*. The presence of paracrystalline material at the photogenic core is not restricted to these decapods but also occurs in euphausiid shrimp, cranchiid and enoploteuthid squids, and the anglerfish *Liuphryne*. Its functional significance is not known; other complex lattice structures ("photosomes") characterize the photocytes of polynoid worms.

The pleopod photophores are more complex than mere aggregations of subunits because the photocytes are now arranged radially rather than linearly (as Dennell recognized), and the pigment cells are organized to form a common sheath. This complexity is associated with a rotatory capability. The possibility of rotation of these photophores was first suggested by Kemp (1910b), and a general anatomical arrangement that might allow it was described by Dennell (1940). However, our description differs considerably from that of Dennell. His explanation was presumably limited by the state of preservation of the animals and the difficulties of interpreting structures in wax-embedded specimens. He failed to notice the main longitudinal muscle, and described other muscles that were not present in our material. In addition, he described a photophore nerve. We found no evidence for such a structure and believe that what Dennell identified as a nerve was in fact extracellular fibrils of the tendon and carotenoid pigment cell processes.

The configuration of the muscle loop is highly unusual and actually deforms the photophore during forward rotation. Further observations of live shrimps are necessary before the exact roles of the main and accessory longitudinal muscles can be confirmed.

The organs of Pesta in *Sergestes similis* are also capable of rotation as part of a counterillumination mechanism (Latz and Case, 1982), but the structural basis has not yet been described. It is probable that similar antagonistic muscle and ligament systems are involved. In *S. similis*, angular rotation of up to 140° can be achieved in the plane of pitch and is statocyst-mediated, as was demonstrated by an elegant series of ablation experiments. In

euphausiids, the rotation of the photophores is linked to angular movements of the eyestalks in response to directional changes of incident light (Land, 1980; Grinnell *et al.*, 1988). Simultaneous angular rotations of up to 165° were recorded for both the thoracic and abdominal photophores, and spontaneous small movements of the photophores (15°–30°) took place in eyeless animals. The authors concluded that feedback concerning eye movement is not necessary and that parallel signals from the central nervous system control the photophore positions. Our video observations of restrained specimens were made on animals exposed to room lighting and cannot be interpreted as normal behavior. What they do show are changes in orientation of up to 87°. Whether there is normally an element of visual control over the rotation (as in euphausiids) or whether it is statocyst-mediated (as in *S. similis*) has not been determined.

The rotation of the 3rd maxilliped photophores is quite different in that they are linked to a ligament and rotate in mechanical response to local changes in the relative positions of the propodus and dactylus. This permits rotation only in the plane of pitch. The linking mechanism is very similar to that of the two parallel ligaments responsible for the simultaneous rotation of the abdominal photophores of euphausiids. However, in the latter animals there is some very limited capability for lateral (roll) rotation (Land, 1980; Grinnell *et al.*, 1988), which is clearly not possible in the system controlling the maxilliped photophores. In addition, the ligaments in the euphausiid case are under direct muscular control. We do not know of any rotatory capability in the modular photophores elsewhere on the body of *O. spinosus* or *S. debilis*; it is almost certainly impossible for the carapace photophores but cannot be ruled out for others (*e.g.*, the 5th thoracic limb or posterior streak photophores).

The different means of photophore rotation may have different optical consequences. In the pleopod photophore, the lens is an integral part of the structure and rotates with it during contraction of the longitudinal muscles, so the optical output is unaffected. When the photophore muscle loop contracts, the photophore may be displaced relative to the underlying lens. In the maxilliped, the cuticular lens-like thickening remains fixed in position as the photophores rotate above it. Any optical changes (*e.g.*, lens misalignment) consequent on the different orientation are likely to be small because the thickening runs the length of the dactylus and probably acts as a cylindrical lens so that the photophore output will still pass through it, albeit with an altered angle of incidence.

All evidence indicates that the main role of the photophores in these animals is counterillumination (Herring, 1976). The presence and positions of the photophores on the limbs need to be considered in terms of their normal disposition during swimming. The 3rd maxilliped is held

forwards, almost horizontal, which means that the photophores point more or less downwards within the limits of their movement. Those on the pleopod also point ventrally. However, on other limbs, photophores face in different directions in different organs. Consideration of the ways in which the limbs are folded during swimming shows that even in these cases the photophores point in a predominantly downward direction. The thoracic limbs (pereopods) are folded at the meral/carpal joint so that where the anterior margin of the proximal limb segments faces dorsally, that of the distal segments faces ventrally. This explains why the photophores face opposite sides of the limb in distal (carpus and propodus) and more proximal segments. This apparently paradoxical inversion of the photophores on the propodus of the 5th limb, relative to those of the streak behind the limb, greatly perplexed Dennell (1940), who described it in *Oplophorus* (noting that "the inversion . . . is very surprising and cannot be readily explained") and in *Systellaspis* ("a most astonishing and inexplicable feature"). The consistently ventral direction of photophores at different sites strongly suggests that they have a counterillumination function.

Our description of the cellular architecture of oplophorid photophores is simpler than that of Dennell (1940). He described more cell types than we have identified, but this interpretation was almost certainly due to his use of relatively crude fixatives and wax histology. In addition, he interpreted profiles from different levels of the same type of cell as belonging to different cell classes, a misjudgment that often arose from non-ideal planes of section. For example, Dennell described the photophores of the 5th thoracic limb and in the large luminous streak behind its base as showing succeeding stages of differentiation. However, this appearance is the result of oblique sections (see Fig. 35), as becomes clear if sections of carefully oriented material are compared with oblique sections. Dennell's *S. pellucida* (as *S. affinis*) "photogenic unit 1" (his Fig. 26) is a section through the clear area, surrounded by the processes of the reflecting pigment cap; his "photogenic unit 2" is a section through the middle of the reflecting pigment cap; and "photogenic unit 3" is a section through the top of the cap. His interpretation of the luminous streak in *O. spinosus* (as *H. grimaldii*, his Fig. 15) is even more complicated but equally explicable as an obliquely sectioned organ. "Photogenic cell 1" is a section through the photocyte nucleus, "2" is an oblique section through the base of the clear area and grazing the nucleus, "3" is through the middle portion of the clear area, "4" is through the upper third of the clear area and reflecting cell processes, and "5" is through the apex of the photophore. The "central body" (his Fig. 16) consists of the paracrystalline bodies (elsewhere labeled "basal cap of photogenic cell" and, in the pleopod photophore, "granular zone").

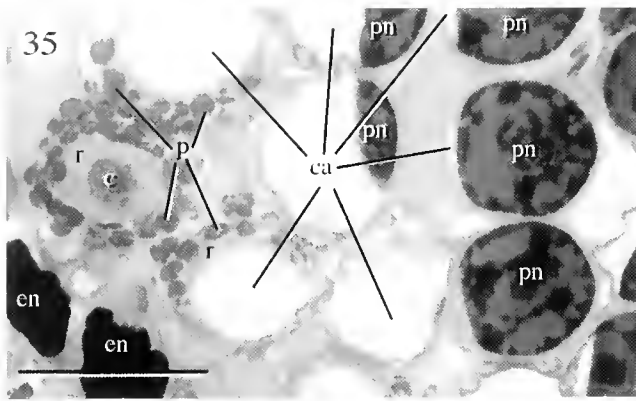


Figure 35. Light micrograph of an oblique section through a group of maxilliped photophores in *Oplophorus spinosus*, which shows the appearance of the photophores at different levels of section. c, paracrystalline bodies; ca, clear area; en, "window" epidermal nuclei; p, carotenoid pigment cell processes; pn, photocyte nuclei; r, reflecting pigment cell processes. Scale bar: 40 μ m.

Dennell (1940) described a fibrous reflector in the pleopod photophores of *O. spinosus*; using electron microscopy, we have found this to be a ligament with associated cell processes of carotenoid pigment cells. He identified the actual reflector as the "striated zone." Nevertheless, Dennell's detailed histological and morphological account is immensely thorough and, if correctly relabeled, provides an invaluable comparative survey.

One unexpected feature of our study of the pleopod photophore is the apparent absence of any identifiable epidermal cells between the photocytes and the lens cuticle, though these are clearly visible as "window" epidermis in the maxilliped photophores. We can only assume that in the pleopod photophores the cuticle is secreted by the photocytes at each molt. The window epidermis structures (small vesicles and few mitochondria) seen also in the basal cytoplasm of the pleopod photocytes suggest that they have a similar function, either in the optics of the photophore or in the secretion of the cuticle. Another surprising feature is the absence of any identifiable direct neural connections to the photophores. Any nerves we have seen have been associated with the muscles. This suggests that light emission is controlled by some indirect mechanism. One possibility is that the circulatory system is involved, as is the case in euphausiids where sphincters control the blood supply to each photophore (Herring and Locket, 1978). Euphausiids, as well as *Oplophorus* and *Styellaspis*, can be induced to luminesce by treatment with low levels of serotonin (5-OH tryptamine). Serotonin also induces luminescence in *Sergestes similis* photophores, and neurohumoral control is implied by the slow induction of bioluminescence by photic stimuli (Latz and Case, 1992; Latz, 1995). Many of the nerves reported by Dennell (1940) were undoubtedly misidentifications of

striated material that were in reality either ligament or pigment cell processes. Nevertheless, we cannot entirely rule out the possibility of some direct neural control, and ventral nerve cord section has produced variable and inconclusive results (Herring, 1976).

The photophores of these shrimps represent an elaborate degree of optical structure on a small scale. The combined output of the many (probably more than a thousand) units over the ventral surface of the body in conjunction with the animal's swimming movements would provide extremely effective counterillumination, probably well beyond the resolution of the eye of a predator. The ability of the photophores to rotate in (presumed) response to changes of the animal's orientation in the water affords an additional refinement to the camouflage capability. Comparisons of fine structure between these photophores and the cuticular photophores of other decapods, particularly species of *Sergia*, are highly desirable. Even more valuable would be direct observations of the behavior of the photophores with respect to the activity of the shrimps.

Acknowledgments

This study was supported by NERC grants GR9/0119A to PMJS and GR3/11212 to PMJS and PJH. MSN gratefully acknowledges a CAFR grant from Providence College, and is grateful for the assistance of Dr. Edward A. Gaten and the staff of the Electron Microscopy Suite of the University of Leicester.

Literature Cited

- Ball, E. E., L. C. Kao, R. C. Stone, and M. F. Land. 1986. Eye structure and optics in the pelagic shrimp *Acetes sibogae* (Decapoda, Natantia, Sergestidae) in relation to light-dark adaptation and natural history. *Phil. Trans. R. Soc. B* 313: 251-270.
- Coutière, H. 1905. Note préliminaire sur les *Eucyphotes* recueillis par S.A.S. le Prince de Monaco. *Bull. Mus. Oceanogr. Monaco* 48: 1-35.
- Coutière, H. 1906. Notes sur la synonymie et le développement de quelques Hoplophoridae. *Bull. Mus. Oceanogr. Monaco* 70: 1-20.
- Dennell, R. 1940. On the structure of the photophores of some decapod Crustacea. *Discovery Rep.* 20: 307-381.
- Dennell, R. 1942. Luminescence in decapod Crustacea. *Sci. J. Roy. Coll. Sci.* 12: 60-68.
- Dennell, R. 1955. Observations on the luminescence of bathypelagic Crustacea Decapoda of the Bermuda area. *J. Linn. Soc. Zool.* 42: 393-406.
- Denton, E. J., J. B. Gilpin-Brown, and P. G. Wright. 1972. The angular distribution on light produced by some mesopelagic fish in relation to their camouflage. *Proc. R. Soc. Lond. B* 182: 145-158.
- Denton, E. J., P. J. Herring, E. A. Widder, M. I. Latz, and J. F. Case. 1985. The roles of filters in the photophores of oceanic animals and their relation to vision in the oceanic environment. *Proc. R. Soc. Lond. B* 225: 63-97.
- Doughtie, D. G., and K. R. Rao. 1984. Ultrastructure of the eyes of the grass shrimp, *Palaemonetes pugio*. General morphology, and light and dark adaptation at noon. *Cell Tiss. Res.* 238: 271-288.

- Elofsson, R. 1971.** The ultrastructure of the chromatophores of *Craggon* and *Pandalus* (Crustacea). *J. Ultrastruct. Res.* **36**: 263–270.
- Grinnell, A. D., P. M. Narins, F. T. Awbrey, W. M. Hamner, and P. P. Hamner. 1988.** Eye/photophore co-ordination and light-following in krill, *Euphausia superba*. *J. Exp. Biol.* **134**: 61–77.
- Hardy, M. G. 1962.** Photophore and eye movement in the euphausiid *Meganyctiphanes norvegica* (G. O. Sars) *Nature* **196**: 790–791.
- Hardy, M. G. 1964.** The rotary mechanism and innervation of the abdominal photophores of the euphausiid crustacean *Meganyctiphanes norvegica*. *J. Physiol. Lond.* **173**: 16P–18P.
- Harvey, E. N. 1952.** *Bioluminescence*. Academic Press, New York.
- Hastings, J. W., and J. G. Morin. 1991.** Bioluminescence. Pp. 131–170 in *Neural and Integrative Animal Physiology*, C. L. Prosser, ed. Wiley-Liss, New York.
- Herring, P. J. 1973.** Depth distribution of the carotenoid pigments and lipids of some oceanic animals. 2. Decapod crustaceans. *J. Mar. Biol. Assoc. U.K.* **53**: 539–562.
- Herring, P. J. 1976.** Bioluminescence in decapod Crustacea. *J. Mar. Biol. Assoc. U.K.* **56**: 1029–1047.
- Herring, P. J. (ed.) 1978.** *Bioluminescence in Action*. Academic Press, London.
- Herring, P. J. 1981.** The comparative morphology of hepatic photophores in decapod Crustacea. *J. Mar. Biol. Assoc. U.K.* **61**: 723–737.
- Herring, P. J. 1985a.** How to survive in the dark: bioluminescence in the deep sea. Pp. 323–350 in *Physiological Adaptations of Marine Animals*, M. S. Laverack, ed. *Symp. Soc. Exp. Biol.* **39**.
- Herring, P. J. 1985b.** Bioluminescence in the Crustacea. *J. Crust. Biol.* **5**: 557–573.
- Herring, P. J., and J. A. Locket. 1978.** The luminescence and photophores of euphausiid crustaceans. *J. Zool., London.* **186**: 431–462.
- Hubbs, C. L., T. Iwai, and K. Matsubara. 1967.** External and internal characters, horizontal and vertical distribution, luminescence and food of the dwarf pelagic shark *Euprotomicrus bispinatus*. *Bull. Scripps Inst. Oceanogr.* **10**: 1–64.
- Jahromi, S. S., and H. L. Atwood. 1976.** Attachments of phasic and tonic abdominal extensor muscles in crayfish. *Can. J. Zool.* **54**: 1256–1269.
- Jahromi, S. S., and H. L. Atwood. 1977.** Normal organization and induced degeneration of the muscle attachment in the crayfish opener muscle. *Can. J. Zool.* **55**: 825–835.
- Karnovsky, M. J. 1965.** A formaldehyde-glutaraldehyde fixative of high osmolality for use in electron microscopy. *J. Cell Sci.* **27**: 137A–138A.
- Kemp, S. 1910a.** The Decapoda Natantia of the coast of Ireland. *Fisheries, Ireland, Sci. Invest. (1908)* **1**: 3–190.
- Kemp, S. 1910b.** Notes on the photophores of decapod Crustacea. *Proc. Zool. Soc. Lond.* **11**: 639–651.
- Lai-fook, J. 1967.** The structure of developing muscle insertions in insects. *J. Morphol.* **123**: 503–527.
- Land, M. F. 1980.** Eye movements and the mechanism of vertical steering in euphausiid crustacea. *J. Comp. Physiol.* **137**: 256–265.
- Latz, M. I. 1995.** Physiological mechanisms in the control of bioluminescent countershading in a midwater shrimp. *Mar. Fresh. Behav. Physiol.* **26**: 207–218.
- Latz, M. I., and J. F. Case. 1982.** Light organ and eyestalk compensation to body tilt in the luminescent midwater shrimp, *Sergestes similis*. *J. Exp. Biol.* **98**: 83–104.
- Latz, M. I., and J. F. Case. 1992.** Slow photic and chemical induction of bioluminescence in the midwater shrimp *Sergestes similis* Hansen. *Biol. Bull.* **182**: 391–400.
- Martin, G. G., and J. E. Hose. 1992.** Vascular elements and blood (hemolymph). Pp. 117–146 in *Microscopic Anatomy of Invertebrates*, Vol. 10: *Decapod Crustacea*, F. W. Harrison and A. G. Humes, eds. John Wiley, New York.
- Mellon, D. 1992.** Connective tissue and supporting structures. Pp. 77–116 in *Microscopic Anatomy of Invertebrates*, Vol. 10: *Decapod Crustacea*, F. W. Harrison and A. G. Humes, eds. John Wiley, New York.
- Peterson, D. R., and R. F. Loizzi. 1974.** Ultrastructure of the crayfish kidney—coelomosae, labyrinth, and nephridial canal. *J. Morphol.* **142**: 241–263.
- Piekos, W. B. 1986.** The role of reflecting pigment cells in the turnover of crayfish photoreceptors. *Cell Tiss. Res.* **244**: 645–654.
- Roe, H. S. J., and D. M. Shale. 1979.** A new multiple rectangular midwater trawl (RMT1 + 8M) and some modifications to the Institute of Oceanographic Sciences' RMT1 + 8. *Mar. Biol.* **50**: 217–236.
- Schönenberger, N. 1977.** The fine structure of the compound eye of *Squilla mantis* (Crustacea, Stomatopoda). *Cell Tiss. Res.* **176**: 205–233.
- Shelton, P. M. J., E. Gaten, and C. J. Chapman. 1986.** Accessory pigment distribution and migration in the compound eye of *Nephrops norvegicus* (L.) (Crustacea: Decapoda). *J. Exp. Mar. Biol. Ecol.* **98**: 185–198.
- Talbot, P., W. H. Clark, and A. L. Lawrence. 1972.** Ultrastructural observations of the muscle insertion and modified branchiostegite epidermis in the larval brown shrimp, *Penaeus aztecus*. *Tissue Cell* **4**: 613–628.
- Terao, A. 1917.** Notes on the photophores of *Sergestes prehensilis* Bate. *Annot. Zool. Jpn.* **9**: 299–316.
- Wild, R. A., E. Darlington, and P. J. Herring. 1985.** An acoustically controlled cod-end system for the recovery of deep-sea animals at *in situ* temperatures. *Deep-Sea Res.* **32**: 1583–1589.

Reproduction-Associated Immunoreactive Peptides in the Nervous Systems of Prosobranch Gastropods

JEFFREY L. RAM¹, CARLOS S. GALLARDO², MICHAL L. RAM¹,
AND ROGER P. CROLL³

¹Department of Physiology, Wayne State University, Detroit, Michigan 48201; ²Department of Zoology, Universidad Austral de Chile, Valdivia, Chile; and ³Department of Physiology and Biophysics, Dalhousie University, Halifax, Nova Scotia, Canada

Abstract. Antibodies against reproductive peptides of *Aplysia* and *Lymnaea* were used to localize homologous immunoreactive peptides in the nervous systems of three prosobranch species: *Busycon canaliculatum*, *Concholepas concholepas*, and *Tegula atra*. Positive control experiments in *L. stagnalis* demonstrated the broad species range of the anti-egg-laying hormone (anti-ELH) antibody used in this study, and showed binding of anti- α -caudodorsal-cell peptide (anti- α -CDCP) to the same cells in cerebral and buccal ganglia. Dot immunoassays with synthetic ELH confirmed the reactivity and sensitivity (<0.1 μ g) of the anti-ELH antibody. Experiments with preadsorbed antibody or no primary antibody confirmed its specificity.

In *B. canaliculatum*, clusters of more than 300 neuronal cell bodies immunoreactive to both anti-ELH and anti- α -CDCP were observed along the medial margins of left and right cerebral ganglia. Anti- α -CDCP reacted with additional small populations of cerebral ganglion neurons not stained by anti-ELH. Anti-ELH and anti- α -CDCP also reacted with overlapping but different small populations of neurons in buccal ganglia. In *C. concholepas* and *T. atra*, ELH-like immunoreactivity was found in cerebral ganglia, and in *T. atra* in fibers in the cerebral ganglia and cerebral-pedal connectives. Thus, cerebral ganglia are the major locus of the ELH-like immunoreactivity in prosobranchs.

Introduction

Prosobranch gastropods are the most ancient and numerous subclass of gastropod molluscs (Solem, 1991). Of

the three extant subclasses, Prosobranchia evolved first—more than 400 million years ago—and radiated strongly; so the species in this subclass now occupy diverse habitats and thus exhibit an extraordinary variety of adaptations, including reproductive mechanisms. The two other gastropod subclasses, Opisthobranchia and Pulmonata, are derived from a common ancestor that diverged—first from the Prosobranchia, and from each other shortly thereafter—about 350 million years ago. Indeed, some classifications join the opisthobranchs and pulmonates under a single taxon known as Euthyneura (Haszprunar, 1988). The euthyneuran species are all hermaphrodites, in striking contrast to the diverse prosobranchs.

Prosobranchs generally have separate sexes, male and female, but sex reversal is known to occur in several species (*e.g.*, *Crepidula fornicata*, Collin, 1995; *Busycon carica*, Castagna and Kraeuter, 1994). Fertilization is usually internal, and the females lay their fertilized eggs in protective egg capsules, but some species discharge gametes into the water column, where external fertilization takes place.

The great abundance, long evolutionary history, and diversity of the prosobranchs should make this taxon ideal for studies of the evolution and mechanisms of reproductive adaptations, from the molecular level to behavior. Unfortunately, relatively little is known about molecular mechanisms in prosobranchs, particularly as applied to the humoral regulation of reproductive behavior. The objective of the present study, therefore, was to investigate

Abbreviations: CDC, caudodorsal cells; CDCH, CDC hormone; α -CDCP, alpha-CDC peptide; ELH, egg-laying hormone; PB, phosphate buffer; PFAPB, 4% paraformaldehyde in PB; TTBS, nonspecific blocker solution for dot immunoassay.

the localization of putative reproductive peptides in the nervous systems of a set of diverse prosobranchs, with the long-term goals of investigating roles of these peptides in the reproductive strategies of prosobranchs and, possibly, exploiting their function in mariculture.

A reproductive role for neuropeptides in prosobranch egg laying is supported by experiments in which nervous system extracts have been injected into mature females. Nervous system extracts elicit laying of eggs or egg capsules in the whelks *Busycon canaliculatum* and *Busycon carica* (Ram, 1977) and in the top snails *Gibbula cineraria*, *G. umbilicalis*, and *Monodonta lineata* (Clare, 1986, 1987). The active factors are protease sensitive (*B. canaliculatum*, Ram, 1977; *G. umbilicalis*, Clare, 1986), and in *B. canaliculatum* its molecular mass is about 5 kDa, as estimated by gel filtration (Ram *et al.*, 1982). These data are consistent with a molecule similar to a pair of homologous neuropeptides that cause egg laying in two euthyneuran species. These neuropeptides are egg-laying hormone (ELH) from the opisthobranch *Aplysia californica* (Kupfermann, 1967; Toevs and Braekenbury, 1969; Chiu *et al.*, 1979) and caudodorsal cell hormone (CDCH) from the pulmonate *Lymnaea stagnalis* (De Vlieger *et al.*, 1980; Ebberink *et al.*, 1985; Geraerts *et al.*, 1988). Some of us have speculated that the substances that activate egg laying in prosobranchs are also homologous with ELH and CDCH (Ram and Ram, 1990). To determine whether prosobranch nervous systems contain peptides homologous to the ELH/CDCH peptide family and to localize them if they are present, we have investigated the immunoreactivity of nervous tissues from several prosobranch species to antibodies to ELH and to alpha-CDCP (the latter is a small peptide derived from the CDCH precursor; Gerearts *et al.*, 1988).

The prosobranch species investigated here were *Busycon canaliculatum* (Neogastropoda, Melongenidae; whelk), *Concholepas concholepas* (Neogastropoda, Muriidae; loco), and *Tegula atra* (Archaeogastropoda, Trochidae; top snail). *B. canaliculatum* has been the subject of several previous studies of humoral control of egg laying in a prosobranch (Ram, 1977; Ram *et al.*, 1982); it is also the basis of a small, but important, fishery in Atlantic waters off the northeastern coast of the United States (Kaplan and Boyer, 1992). *C. concholepas* and *T. atra* are commercially important Chilean prosobranch species (Coloma, 1974; Osorio, 1979). *C. concholepas* is the most intensively studied Chilean prosobranch (for review, see Castilla, 1988), for which there is great concern about over-exploitation (Gallardo and Carrasco, 1996) and interest in its reproduction (Castilla and Cancino, 1976), development (DiSalvo and Carriker, 1994; Rodriguez *et al.*, 1995), and behavior (Serra *et al.*, 1997). As an archaeogastropod, *T. atra* adds phylogenetic diversity to the study; in contrast with the other two species, it exhibits external fertilization and a more primitive neuroanatomy.

We have determined that all three prosobranch species have anti-ELH immunoreactivity in clusters of cell bodies in the cerebral ganglia. In the cerebral ganglia of *B. canaliculatum*, immunoreactivity to anti-alpha-CDCP occurred in the same cells as immunoreactivity to anti-ELH, and it also appeared in several additional cells. Also in this species, anti-ELH and anti-alpha-CDCP immunoreactivity appeared in small overlapping, but distinct, populations of cell bodies in the buccal ganglia. The findings reported here provide a molecular and anatomical basis for investigations into the roles of molluscan reproductive peptides in prosobranch reproductive adaptations.

Materials and Methods

Animals

Experiments on *B. canaliculatum* were performed at Dalhousie University, Halifax, Nova Scotia, Canada. For Chilean species, two of the authors (JLR and MLR) traveled to Chile to collect specimens, and to dissect and fix nervous system preparations (as described below). Fixed material was brought back to Halifax for further processing and analysis. Positive controls on *L. stagnalis* utilized animals that were cultured at Dalhousie University in freshwater aquaria with continuously recirculated, filtered tap water, as previously described (Croll and Chiasson, 1989).

B. canaliculatum was obtained from the Marine Biological Laboratory, Woods Hole, Massachusetts, USA. Specimens were large (>12 cm, length from apex to siphon), and both males and females were used. Animals were maintained for up to 3 months in sea tables at approximately 10°C, and marine mussels were provided for food. *T. atra* was collected from tide pools near the field station of the Universidad Austral de Chile (Valdivia) located at Mehuin Bay, Chile (39°25' S; 73°13' W). *C. concholepas* was collected from tide pools at Playa Rosada, Chile (39°43' S; 73°23' W); other specimens of *C. concholepas* were obtained from A. Pinto of the Instituto de Fomento Pesquero, Castro, Chile (42°29' S; 73°46' W), where they were being grown by aquaculture. Both *C. concholepas* and *T. atra* were dissected shortly after collection.

Dissection, fixation, sectioning, and staining

Nervous systems of each of the above species were removed and further dissected, as needed, in either artificial saline (for *L. stagnalis*; Jansen and ter Maat, 1985) or filtered seawater (all other species). Ganglia were pinned out on Sylgard-coated dishes and cleaned of overlying connective tissue. The relative positions of ganglia were carefully noted so they could be identified accurately in sectioned material.

For *L. stagnalis*, the dissected preparations usually included cerebral, pedal, parietal, and buccal ganglia; cuts were made in the pedal commissure to produce an opened, flat ring of ganglia prior to fixation. For *B. canaliculatum* (Pierce, 1950; Bullock, 1965), cuts were made either between left pleural and left parietal (subesophageal) ganglia, or between cerebral ganglia prior to pinning out for dissection. The latter orientation is shown schematically in the Results to indicate the location of immunoreactive neurons. The nervous system of *C. concholepas*, like that of *B. canaliculatum*, consists of several rings of ganglia closely surrounding the esophagus (Fig. 1); thus, the dissection of the nervous system of *C. concholepas* was similar to that of *B. canaliculatum*. As a more primitive prosobranch, *T. atra* has a less compact set of ganglia than the other species. The nervous system of *T. atra* is almost identical to that of *Trochus* illustrated in Hyman (1967), which was used as a dissection guide. The anteriorly located pair of cerebral ganglia are connected by cerebral-pedal connectives to the pedal ganglia, which were easily identified by their location, shape, and the presence of statocysts. Most preparations included cerebral and pedal ganglia, the cerebral commissure, and the cerebral-pedal connectives, but in some preparations, other ganglia attached to these were also retained.

After dissecting and pinning out preparations in saline

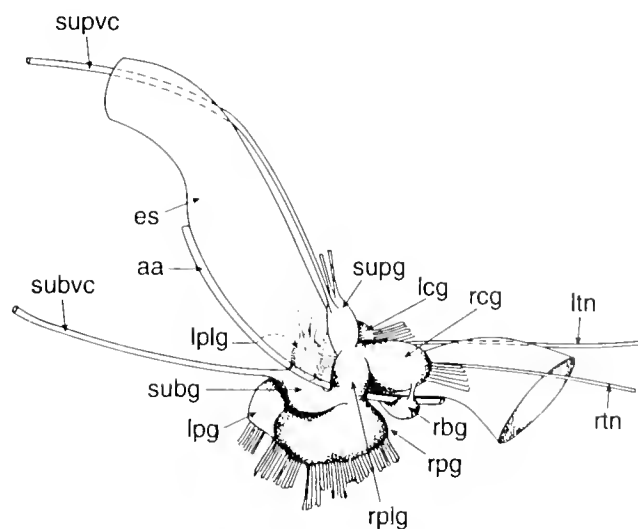


Figure 1. Diagram of the central nervous system of *Concholepas concholepas*, redrawn from original artwork by Huaquin (1966). Abbreviations: aa, anterior aorta; es, esophagus; leg, left cerebral ganglion; lpg, left pedal ganglion; lplg, left pleural ganglion; ltn, left tentacle nerve; rbg, right buccal ganglion; rcg, right cerebral ganglion; rpg, right pedal ganglion; rplg, right pleural ganglion; rtn, right tentacle nerve; subg, subesophageal ganglion; subvc, subesophageal visceral connective; supg, supraesophageal ganglion; and supvc, supraesophageal visceral connective. Lplg and several nerves that are behind the esophagus are shaded as if seen through it. Subvc and supvc connect to the visceral ganglion (not shown).

solution in the desired orientation, the solution was replaced with 4% paraformaldehyde in phosphate buffer (0.1 M, pH 7.4) (PFAPB) at 4°C. For experiments with *L. stagnalis* and *B. canaliculatum*, PFAPB was made fresh weekly and stored at 4°C. For the Chilean species, PFAPB was several weeks older and was maintained at room temperature for significant amounts of time during transport to and within Chile. Ganglia were fixed in PFAPB at 4°C for 24 h, then unpinned from the Sylgard and transferred to 70% ethanol for short- or long-term storage. Ganglia retained their shape and relative orientation after fixation. All preparations of *L. stagnalis* and *B. canaliculatum* were refrigerated while in 70% ethanol, and storage time ranged from 24 h to several days before further processing. Chilean specimens were maintained in 70% ethanol and refrigerated, when possible, for 3 to 4 weeks before further processing.

Prior to cryosectioning, preparations were transferred to 30% sucrose in phosphate buffer (PB, 0.1 M, pH 7.4) and stored overnight at 4°C. Preparations were frozen in TissueTek in the cryostat at -15°C and sectioned at 30 µm. In some experiments, alternate sections were put on separate slides so that different antibodies or control procedures could be compared. Sections were dried, rinsed three times in PB, and incubated overnight at room temperature in primary antibodies (rabbit anti-ELH serum, 1:500 in 2% normal goat serum and 0.2% Triton X-100 in PB; or rabbit anti-α-CDCP, 1:500 in the same medium). They were then rinsed three times in PB, incubated in fluorescein isothiocyanate (FITC)-labeled goat anti-rabbit secondary antibody (1:20, Bio/Can Scientific, Mississauga, Ont.) in the dark at 4°C overnight, rinsed three more times in PB, and then mounted in 75% glycerol in PB. Sections were viewed and photographed through a Leitz Aristoplan microscope for epifluorescence with I3 or L3 filter block.

The primary anti-ELH is an affinity-purified antibody made in rabbits by J. E. Blankenship and G. T. Nagle (Marine Biomedical Institute, University of Texas Medical Branch, Galveston, TX), who used as antigen a synthetic N-terminal fragment of *Aplysia* ELH (ISINQD-LKAITDMLC; the C-terminal Cys was for coupling purposes and is not part of the N-terminal ELH sequence). The antibody was characterized as specifically staining *Aplysia* bag cell neurons and their axons (Blankenship and Nagle, unpub. data). This antibody is further characterized in this paper with regard to its binding to synthetic *Aplysia* ELH in dot immunoassays and its capability of binding to the caudodorsal cell (CDC) neurons and cerebral commissure of *L. stagnalis*. The CDC neurons and cerebral commissure contain the *L. stagnalis* peptide egg-laying neurohormone CDCH (Geraerts and Bohlken, 1976; Geraerts *et al.*, 1988). The N-terminal sequence of CDCH (LSITNDLRAIADSY-; Ebberink *et al.*, 1985) is

50% identical to the ELH sequence (Chiu *et al.*, 1979). Tests of positive staining of CDC neurons and cerebral commissure were used to determine whether the anti-ELH antibody had a sufficiently broad specificity that it would bind to CDCH, a homolog of *A. californica* ELH in a species from a different subclass of gastropods.

The primary anti- α -CDCP is a polyclonal rabbit serum obtained from J. Van Minnen (Vrije Universiteit, Amsterdam) and characterized in previous publications on *L. stagnalis* (Van Minnen *et al.*, 1992; Croll *et al.*, 1993). α -CDCP is biologically synthesized in *L. stagnalis* from the same precursor peptide as CDCH and is a member of a family of "alpha peptides" that are nine amino acids long and have an identical core sequence (amino acids 2 to 6, -PRLRF-) in *L. stagnalis* and *A. californica* (reviewed by Nagle *et al.*, 1989). Staining for α -CDCP-immunoreactivity was used to provide positive identification of CDC neurons and cerebral commissure in *L. stagnalis* and to determine whether immunoreactive alpha peptides were also present in ELH-immunoreactive cells in prosobranchs.

All of the immunohistological experiments reported here included, as positive controls, one or more *L. stagnalis* nervous systems carried through the same sectioning, staining, and micrographic procedures simultaneously with ganglia from other species. Negative control procedures included omitting the primary antibodies and preadsorbing the anti-ELH antibody with 5×10^{-6} mol/l synthetic *Aplysia* ELH (Peninsula Laboratories, Lot 012020).

Dot immunoassay

Synthetic *Aplysia* ELH was dissolved in deionized water at various concentrations, ranging from 0.01 μ g to 2 μ g/ μ l and applied in 1- μ l dots on nitrocellulose membranes. After drying for at least 15 min, the nitrocellulose was immersed in PFAPB for 8–10 min, rinsed, and then incubated for 60 min at room temperature in nonspecific "blocker" solution (5% Carnation nonfat dry milk in TTBS [0.05% Tween 20, 500 mM NaCl, 20 mM Tris, pH 7.5]), with rocking. After the blocker solution was drained off, the membranes were incubated with rocking in anti-ELH (diluted 1:500 in blocker solution) at room temperature for 45–60 min. The membranes were then rinsed 2 times for 7 min in TTBS, incubated 45–60 min in secondary antibody (donkey anti-rabbit Ig horseradish peroxidase-linked F(ab')₂ fragment from Amersham, diluted 1:2000 in blocker solution), rinsed three times in TTBS, and then stored up to several hours in TBS (TTBS without Tween-20). The dot immunoassays were developed using a luminol-based enhanced chemiluminescence procedure (Pierce, SuperSignal Substrate). Immediately after completing the procedure, the location and intensity

of the luminescing luminol produced by the reaction was determined by exposures to X-ray film for 5–10 min. Subsequent longer exposures (several hours) were used to confirm the presence of faint spots, while saturating the responses elsewhere.

Results

Anti-ELH immunoreactivity in Lymnaea stagnalis, a positive control

The antibody to *A. californica* ELH was tested first on nervous systems of *L. stagnalis*, a species from a different subclass of gastropods known to contain an ELH homolog, CDCH, in CDC neurons and the cerebral commissure. CDC neurons were identified by their characteristic clustering and positions, and were further positively identified using antibodies to α -CDCP (Fig. 2A). Few other cell bodies in the central nervous system bind to anti- α -CDCP, but some additional α -CDCP-immunoreactive

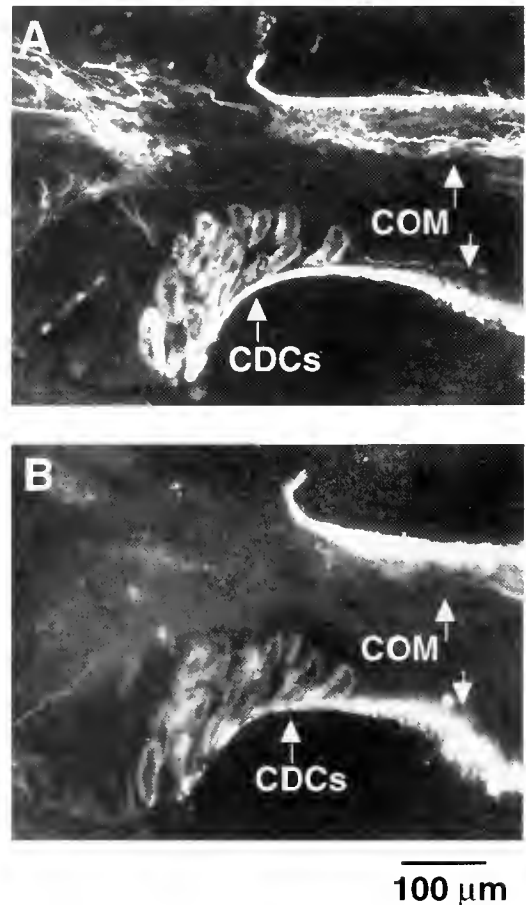


Figure 2. Immunoreactivity to anti- α -CDCP (A) and anti-ELH (B) in adjacent sections of a cerebral ganglion and cerebral commissure of *Lymnaea stagnalis*. Abbreviations: CDCs, caudodorsal cells; COM, cerebral commissure.

fibers were present as previously observed (Van Minnen *et al.*, 1992). Similarly, hormone-containing regions of the cerebral commissure were positively identified by their position and immunoreactivity to anti- α -CDCP. CDC neurons and cerebral commissure were then shown to be immunoreactive to anti-ELH. Figure 2B shows anti-ELH immunoreactivity in a section adjacent to the anti- α -CDCP-stained section in Figure 2A. Few other fibers or neurons were immunoreactive with the anti-ELH antibody, although a faint staining (much lighter than in the CDCs) of metacerebral giant cells was occasionally observed (not shown). This pattern of anti-ELH immunoreactivity was consistently obtained in *L. stagnalis* preparations that were processed in parallel with sections of ganglia from other species. Sections carried through the procedures in the absence of primary antibodies to ELH and α -CDCP, or with anti-ELH that had been preadsorbed with synthetic ELH, showed no staining with the secondary (FITC-labeled) antibody (not shown).

We also examined other ganglia of *L. stagnalis* for immunoreactive cells. As illustrated in Figure 3, the buccal ganglia each had a single neuron containing immunoreactive ELH and α -CDCP, consistent with a previous schematic representation of CDCH distribution (Geraerts *et al.*, 1988), but this is the first illustration of the location

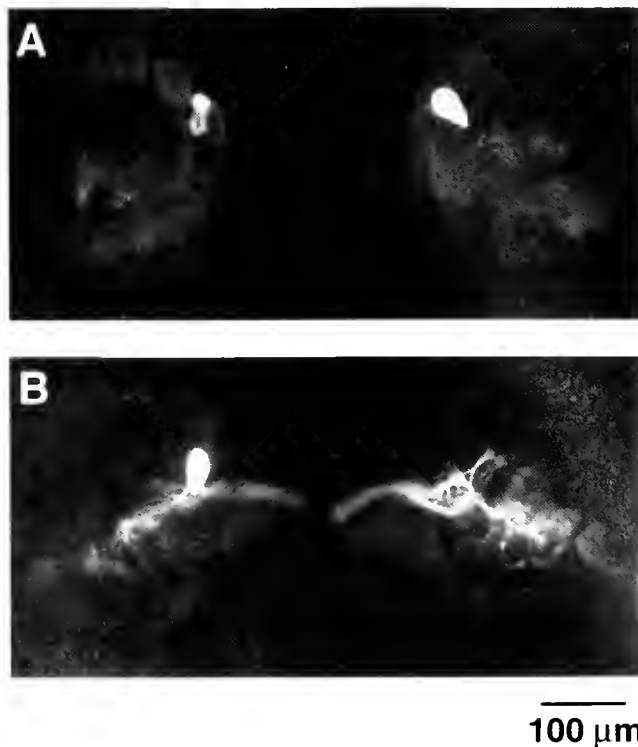


Figure 3. Pair of neurons and associated processes immunoreactive to anti- α -CDCP (A) and anti-ELH (B) in adjacent sections of buccal ganglia of *Lymnaea stagnalis*.

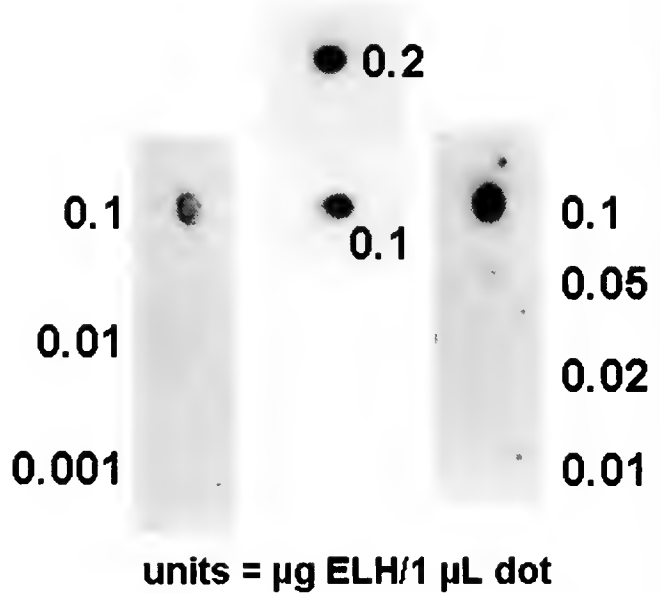


Figure 4. Dot immunoassays of synthetic *Aplysia* ELH, using anti-ELH. The number next to each dot indicates micrograms of ELH, applied to the paper in 1 μ l.

and morphology of fibers of these buccal ganglion cells. Together, these findings demonstrate that the anti-ELH antibody employed here has a broad enough specificity to react with intracellular egg-laying neuropeptides in a species as distantly related as being in another gastropod subclass.

To determine whether the anti-ELH antibody could, in fact, bind to ELH and also to determine, to some degree, the sensitivity of its interaction, we conducted dot immunoassays with synthetic ELH. As illustrated in Figure 4, we could consistently ($n = 3$) detect as little as 0.1 μ g ELH, with possible sensitivity down to 0.05 μ g (slight response observed in one experiment). The antibody to α -CDCP did not bind to synthetic ELH.

Immunoreactive ELH and α -CDCP in Busycon canaliculatum

Cerebral ganglia of *B. canaliculatum* contain neurons immunoreactive to anti-ELH (Fig. 5A, C) and anti- α -CDCP (Fig. 5B, D, E). In serial sections through entire cerebral ganglia, both antibodies consistently labeled clusters of immunoreactive neurons that are located in bilaterally symmetric positions along the medial margins of the cerebral ganglia (Fig. 6). To ascertain that the antibodies were indeed staining the same cells, alternate sections from two preparations were stained with the two antibodies. In the example illustrated in Figure 5A, a large cluster of neurons stained well with the anti-ELH antibody. The same cluster also stained moderately,

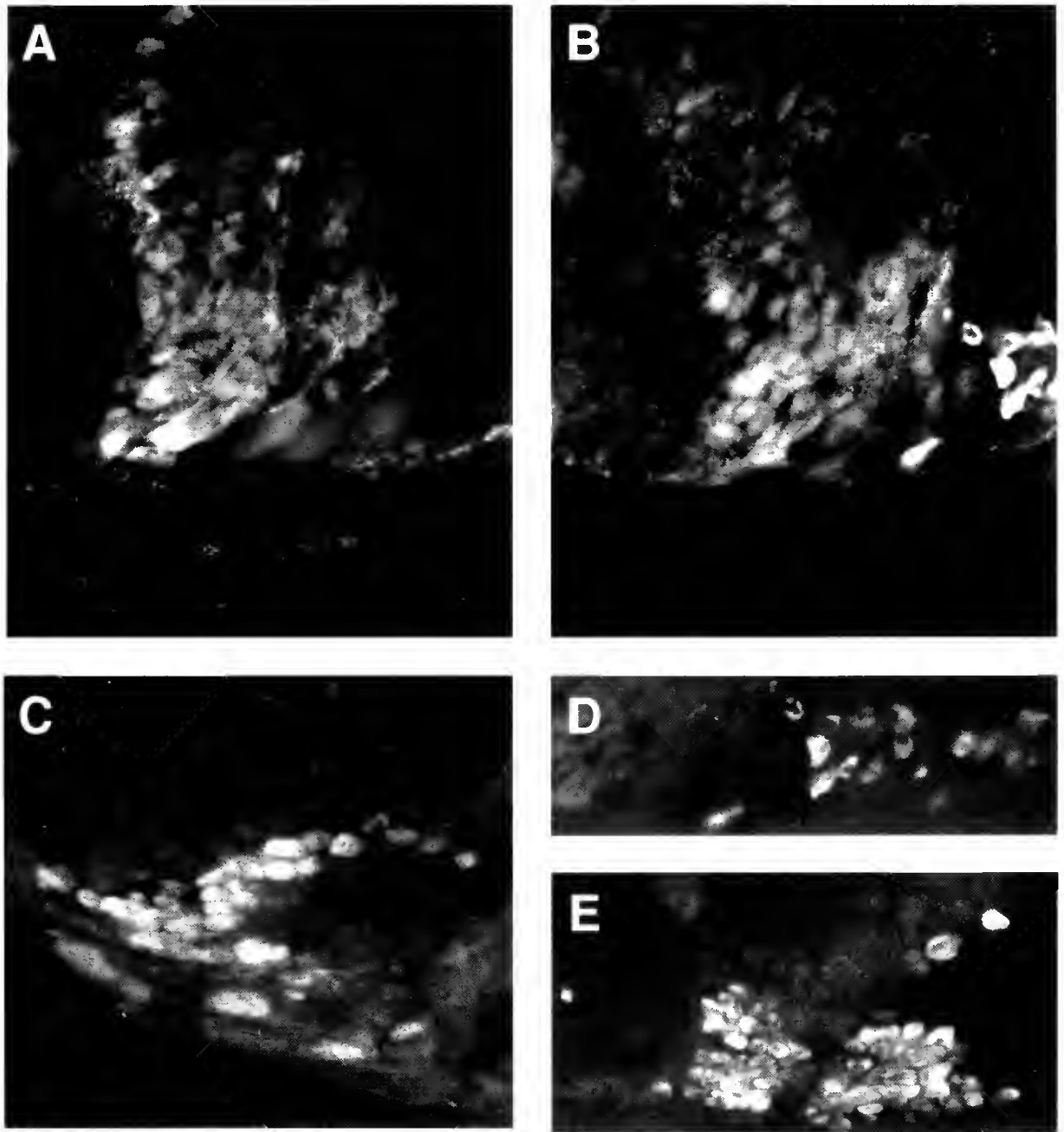


Figure 5. Immunoreactivity to anti-ELH (A, C) and anti- α -CDCP (B, D, E) in cerebral ganglia of *Busycon canaliculatum*. (A, B) Adjacent sections from one cerebral ganglion, showing staining of the same large cluster of cells with both (A) anti-ELH and (B) anti- α -CDCP antibodies. In addition, (B) shows part of a brighter cluster of anti- α -CDCP-immunoreactive cells at the lower right which has no counterpart in the anti-ELH micrograph. The entire cluster of these brighter cells from the same section as in (B) is shown in (D). (C) Anti-ELH-immunoreactive cell bodies from another cerebral ganglion. (E) Anti- α -CDCP-immunoreactive cell bodies from another cerebral ganglion.

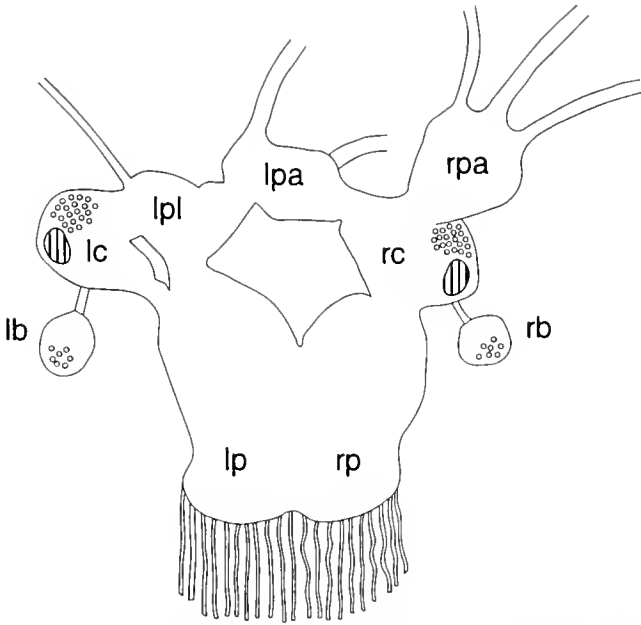


Figure 6. Schematic of locations of cells immunoreactive to anti-ELH and anti- α -CDCP in the nervous system of *Busycon canaliculatum*. The relative sizes and shapes of ganglia are shown for a preparation in which the circumesophageal ring of ganglia was opened by cutting through the cerebral commissure (cross-hatched areas of each cerebral ganglion). Small circles in the cerebral ganglia represent cells immunoreactive to both antibodies; circles in the buccal ganglia represent cell bodies of overlapping clusters of cells reactive to one or the other of the antibodies. Abbreviations: lb, left buccal; lc, left cerebral; lp, left pedal; lpa, left parietal; lpl, left pleural; rb, right buccal; rc, right cerebral; rp, right pedal; rpa, right parietal. Labeling of ganglia is according to Pierce (1950); however, the ganglia labeled as the left and right parietal ganglia probably correspond to ganglia usually described, respectively, as the subesophageal (or subintestinal) and supraesophageal (or supraintestinal) in most prosobranchs (Bullock, 1965).

though clearly above the background level of staining for many adjacent cells, with the anti- α -CDCP antibody (Fig. 5B). The anti- α -CDCP also stained more intensely a small, additional cell population in the region that did not bind the anti-ELH antibody (Fig. 5B, D). The other preparation stained with the antibodies on alternate sections showed a similar picture. In control experiments, alternate sections stained in the absence of primary antibody or with preadsorbed anti-ELH antibody showed no staining of cell bodies in cerebral ganglia.

Figures 5A and 5B were chosen to illustrate staining with anti-ELH and anti- α -CDCP of alternate sections of the same clusters, but they are not the most intense or clearly delineated examples we have of the appearance of the immunoreactive neurons. Accordingly, we illustrate clusters from a similar location in other cerebral ganglia in Figure 5C and Figure 5E. The diameters of the neuronal somata were in the range of 10–25 μ m. Clusters of ELH-immunoreactive neurons comparable to those illustrated

were generally found in 8 to 12 serial sections of each cerebral ganglion, with 30 to 60 stained cells per cluster on most of these sections. The average diameter of these cells is less than the thickness of each section (30 μ m). Therefore, the total number of ELH-immunoreactive neurons per cerebral ganglion is estimated to be greater than 300.

Immunoreactive cell bodies were also seen in buccal ganglia of *B. canaliculatum* (Fig. 7). Immunoreactive ELH- and α -CDCP-containing neurons appeared in about the same location in these ganglia, but based on the number and sizes of the neurons, the two antibodies appear to be staining different subsets of neurons. In Figure 7, showing adjacent sections stained with the two antibodies, the α -CDCP-immunoreactive neurons appear to be smaller and more numerous than the anti-ELH-immunoreactive neurons. This pattern continued through several additional alternating sections (not shown).

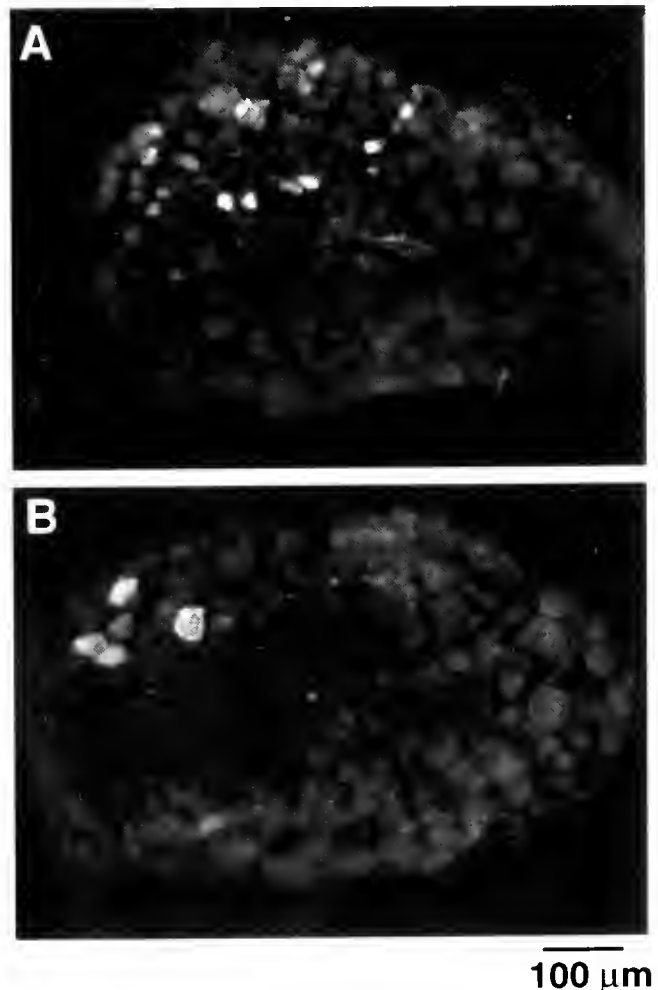


Figure 7. Immunoreactivity to anti- α -CDCP (A) and anti-ELH (B) in adjacent sections of a buccal ganglion of *Busycon canaliculatum*.

No immunoreactive cell bodies were seen in parietal and pleural ganglia. Although staining was observed in the surrounding connective tissue sheath (not shown), control sections stained without primary antibody also showed a significant amount of staining in the connective tissue sheath. Hence, the connective tissue staining in these ganglia might not reflect the presence of specific ELH immunoreactivity in this location. By comparison, there was no staining of cell bodies and relatively little staining of connective tissue in pedal ganglia.

Other prosobranch species

Anti-ELH immunoreactivity was also observed in *C. concholepas* (Fig. 8) and *T. atra* (Fig. 9). In both species, the cerebral ganglia were the only ganglia to show strongly immunoreactive cell bodies. In *C. concholepas*, compact clusters of more than 20 neurons each were present in the cerebral ganglia, whereas, in *T. atra*, numerous immunoreactive neurons appeared in several less compact clusters (e.g., Fig. 9A shows neurons in two clusters). In *T. atra*, these clusters were on the surface of the ganglia and extended through a large number of sections.

T. atra is the only prosobranch in which we have seen unambiguous anti-ELH immunoreactivity in fibers. Figure 9A clearly illustrates several neuronal cell bodies from

which well-stained processes originate. In addition, staining of single fibers (Fig. 9B) and tracts of fibers (Fig. 9C) were consistently (three different preparations) seen in the cerebral-pedal connectives of *T. atra*. These fibers could not be traced back to their cell bodies of origin. They were present almost all of the way from the cerebral ganglia to the pedal ganglia, but no positively stained cell bodies or fibers were seen in the pedal ganglia. When single fibers could be seen in the nerves, the fibers always had a varicose appearance with a diameter less than 0.5 μm .

Staining of sections of the above preparations from *C. concholepas* and *T. atra* for anti- α -CDCP immunoreactivity gave negative results.

Discussion

We report here the first use of immunocytochemistry to localize ELH- and α -CDCP-like peptides in prosobranchs. The anti-ELH antibody used in this study is shown to bind to low concentrations of synthetic ELH and to have a broad species range. The localization of anti-ELH immunoreactivity in cerebral ganglia of three different prosobranch species supports these ganglia as a major locus of peptides that regulate reproduction in this subclass of gastropods. The antibodies used in this study may therefore be useful in future studies to purify prosobranch ELH-like peptides, to study the physiological properties of their secretory neurons, and to identify the location and function of these neurons in other molluscan classes and species.

Observations of immunoreactivity to anti-ELH and anti- α -CDCP support the cerebral ganglia as candidates for the location of secretory neurons regulating egg laying in prosobranchs. The positive control data obtained here in *L. stagnalis* (Figs. 2 and 3) clearly confirm that both antibodies stain the CDC neurons, the cerebral commissure, and a pair of neurons in the buccal ganglia, previously reported to contain CDCH, the egg-laying hormone of *L. stagnalis* (Geraerts *et al.*, 1988). In *B. canaliculatum*, a population of neurons immunoreactive to both anti-ELH and anti- α -CDCP antibodies was found in the cerebral ganglia (Figs. 5A, B and 6). Since cerebral ganglia also produced positive laying bioassays, these neurons are the most likely candidates for the source of the peptide causing this response. A cerebral ganglion localization of ELH-like immunoreactivity was also observed in the top snail *T. atra*. Although no bioassay experiments with *T. atra* have been reported, experiments in the related top snail species *Gibbula* spp. and *M. lineata* demonstrated that spawning could be elicited by cerebral ganglion extracts (Clare, 1986, 1987). ELH-like immunoreactive neurons found in *T. atra* are therefore good candidates for the source of this peptide as well. Likewise,

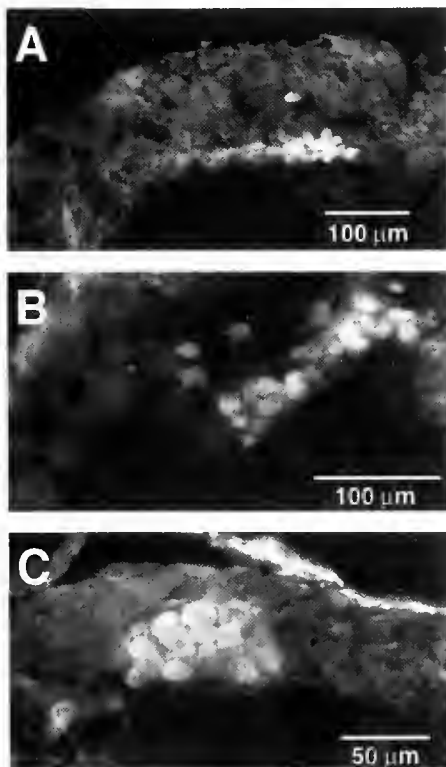


Figure 8. Anti-ELH-immunoreactive cell bodies in cerebral ganglia from three specimens of *Concholepas concholepas*.

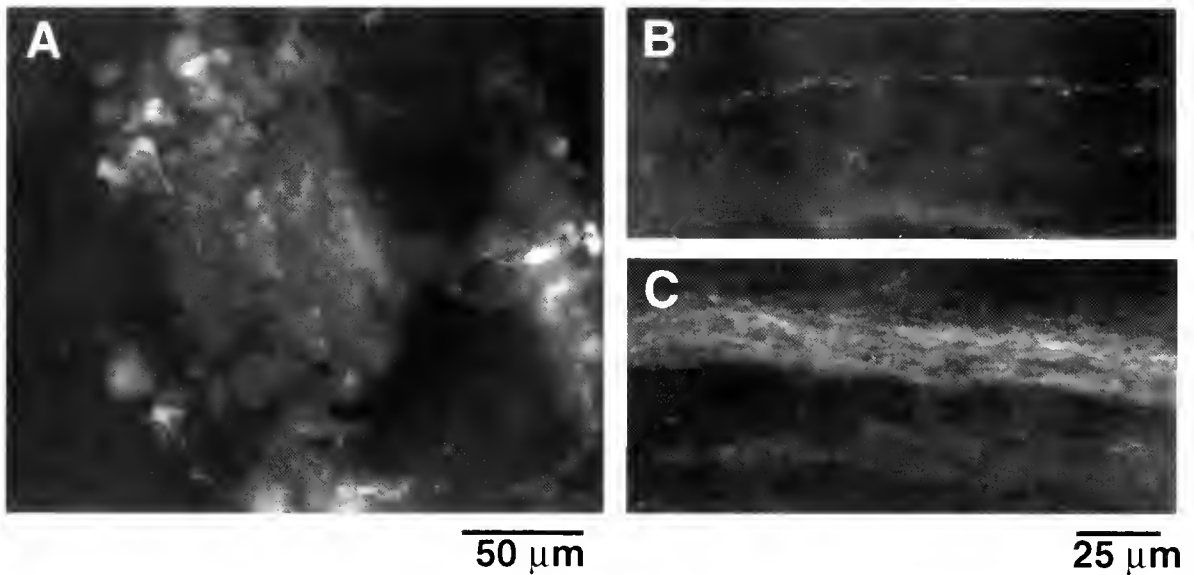


Figure 9. Anti-ELH-immunoreactive cell bodies and fibers in the nervous system of *Tegula atra*. (A) Section of a cerebral ganglion showing immunoreactive cell bodies from two clusters. Several of the neurons also have clearly evident immunoreactive axons. (B, C) Axons in the cerebral-pedal connective: (B) a single fiber; (C) a tract of immunoreactive fibers. The calibration mark at the right is for both (B) and (C).

C. concholepas ELH-like immunoreactivity was found in cerebral ganglia, which are therefore good candidates for secretory neurons controlling egg laying in that species. Among opisthobranchs, extracts of cerebral ganglia of *Archidoris montereyensis* can produce egg laying (Wiens and Brownell, 1994), and small clusters of ELH-immunoreactive neurons are present in cerebral ganglia of *A. californica* (Chiu and Strumwasser, 1984). Thus, according to the present data, a major locus of the secretory neurons regulating egg laying in prosobranchs, as in pulmonates, appears to be cerebral ganglia, and the present data provide a more precise anatomical localization for the cell bodies of these neurons than previous bioassay experiments.

In addition to cerebral ganglia, ELH-like immunoreactivity was also found elsewhere. The buccal ganglia of both *B. canaliculatum* and *L. stagnalis* contained immunoreactive neurons. ELH expression has been reported in buccal ganglia of *A. californica* in immature animals (McAllister *et al.*, 1983; Pulst *et al.*, 1988) but is apparently absent from buccal ganglia of mature *A. californica* (Chiu and Strumwasser, 1984; Pulst *et al.*, 1988). In *B. canaliculatum*, buccal ganglia do not elicit spawning upon bioassay with the amounts of extracts usually tested (*e.g.*, Ram, 1977), possibly indicating that the small number of putative ELH-containing neurons do not contain a large enough amount of the peptide to elicit egg laying. In *A. californica*, ELH is known to have direct effects on neurons, including neurons in buccal ganglia (Ram and Ram, 1989). By analogy, ELH in buccal ganglia of *B. canaliculatum* and *L.*

stagnalis could be acting on local circuits, rather than being released for hormonal activation of egg laying.

This study did not clearly localize ELH-like immunoreactivity in parietal and pleural ganglia of *B. canaliculatum*. Bioassays of extracts of individual parietal and pleural ganglia elicited laying as reliably as did cerebral ganglia (Ram, 1977). Yet, no immunoreactive cell bodies were found in parietal and pleural ganglia. Only the connective tissue sheath was stained, and it could not be distinguished from nonspecific staining of the same tissue in control sections. Possibly the connective tissue sheath of these ganglia is the site of neurohaemal secretion of ELH. Further studies to reduce the nonspecific staining in this region and to identify immunoreactive structures, if any, may help resolve this problem.

With regard to the targets of the anti-ELH antibody, dot immunoassays show, as expected, that the anti-ELH antibody binds to low concentrations of synthetic ELH. It has been estimated that the bag cells of a mature *A. californica* contain approximately 20 μg ELH (Chiu *et al.*, 1979). The dot immunoassays reliably detected 0.1 μg ELH, approximately 1/200th the amount in a mature animal and much less than the amount detectable by bioassay (approximately $\frac{1}{2}$ of the hormone in a bag cell cluster; Toevs, 1970). In other species, where the antigenic peptides may not provide a perfect fit for the antibody, the sensitivity may be much less, but even a 10-fold decrease in the detectable concentration would make it a much more sensitive technique for detecting ELH than bioassays in congeneric species.

Although ELH-like immunoreactivity was observed in all three species of prosobranchs that were examined, anti- α -CDCP staining was obtained only in *B. canaliculatum* and in the positive control pulmonate, *L. stagnalis*. The negative results for α -CDCP-like immunoreactivity in *C. concholepas* and *T. atra* could have a number of explanations. These include lack of these peptides in these species, presence of α -CDCP homologs that are sufficiently dissimilar to α -CDCP to lack immunoreactivity to the serum used, and loss of immunoreactivity due to the differences in fixation of these Chilean specimens. Physiological experiments have indicated that alpha peptides may have an autoregulatory function in neurons that secrete ELH or CDCH (Rothman *et al.*, 1983; Brussaard *et al.*, 1990; Redman and Berry, 1991). Therefore, determination of the presence, location, and structural or functional differences of alpha peptides in prosobranchs may be important in understanding adaptations for regulating secretion of the ELH-like peptides in prosobranchs.

Further studies identifying the peptides to which these antibodies bind in the prosobranchs are needed, to determine whether they are indeed related structurally to ELH/CDCH and the alpha peptides, to measure the sensitivity with which they can be detected with these techniques, and to ascertain their relationship to the substances in nervous system extracts previously shown to cause egg-laying in prosobranch species. Nevertheless, the results shown in this paper demonstrate that antibodies to pulmonate and opisthobranch reproductive peptides bind to specific groups of neurons in cerebral and other ganglia of prosobranchs, identifying these neurons for future functional studies.

Acknowledgments

This research was supported, in part, by a Dalhousie Medical Research Foundation Picchione Visiting Scholarship and NSF grant INT-9724918 to J. L. Ram, by grants from Fondecyt (1960488) and the Volkswagen Foundation (I 96-01) to C. S. Gallardo, and an NSERC (Canada) Strategic Grant to R. P. Croll. The authors gratefully acknowledge Dr. Ariel Pinto, of the Instituto de Fomento Pesquero, Castro, Chile, for specimens and information regarding egg-laying behavior of *Concholepas concholepas*, and Janette Nason for help with histology. Antibodies were obtained from J. E. Blankenship and G. T. Nagle (anti-ELH) and J. Van Minnen (anti- α -CDCP). Dedicated to the memory of Sharon L. Ram.

Literature Cited

- Brussaard, A. B., N. C. M. Schluter, R. H. M. Ebberink, K. S. Kits, and A. ter Maat. 1990. Discharge induction in molluscan peptidergic cells requires a specific set of autoexcitatory neuropeptides. *Neuroscience* **39**: 479–491.
- Bullock, T. H. 1965. Mollusca: Gastropoda. Pp. 1283–1386 in *Structure and Function in the Nervous Systems of Invertebrates, Volume II*. T. H. Bullock and G. A. Horridge, eds. W. H. Freeman, San Francisco.
- Castagna, M., and J. N. Kraenter. 1994. Age, growth-rate, sexual dimorphism and fecundity of knobbed whelk *Busycon carica* (Gmelin, 1791) in a western mid-Atlantic lagoon system, Virginia. *J. Shellfish Res.* **13**: 581–585.
- Castilla, J. C. 1988. Una revisión bibliográfica (1980–1988) sobre *Concholepas concholepas* (Gastropoda, Muricidae): Problemas pesqueros y experiencia de repoblación. *Biol. Pesq. (Chile)* **17**: 9–19.
- Castilla, J. C., and J. Cancino. 1976. Spawning behavior and egg capsules of *Concholepas concholepas* (Mollusca: Gastropoda: Muricidae). *Mar. Biol.* **37**: 255–263.
- Chiu, A. Y., and F. Strumwasser. 1984. Two neuronal populations in the head ganglia of *Aplysia californica* with egg-laying hormone-like immunoreactivity. *Brain Res.* **294**: 83–93.
- Chiu, A. Y., M. W. Hunkapiller, E. Heller, D. K. Stuart, L. E. Hood, and F. Strumwasser. 1979. Purification and primary structure of the neuropeptide egg-laying hormone of *Aplysia californica*. *Proc. Natl. Acad. Sci. USA* **76**: 6656–6660.
- Clare, A. S. 1986. Induction of egg spawning in *Gibbula umbilicalis* (da Costa) by an homogenate of the cerebral ganglia. *Gen. Comp. Endocrinol.* **64**: 85–90.
- Clare, A. S. 1987. Studies on the putative egg-spawning neurohormones of *Gibbula umbilicalis* (da Costa) and *G. cineraria* (L.). *Gen. Comp. Endocrinol.* **66**: 48–49.
- Collin, R. 1995. Sex, size, and position: a test of models predicting size at sex change in the protandrous gastropod *Crepidula fornicata*. *Am. Nat.* **146**: 815–831.
- Coloma, S. L. 1974. Estudio histológico de la gónada de *Tegula atra*. *Bol. Soc. Biol. Concepción* **48**: 359–363.
- Croll, R. P., and B. J. Chiasson. 1989. Post-embryonic development of serotonin-like immunoreactivity in the central nervous system of the snail, *Lymnaea stagnalis*. *J. Comp. Neurol.* **280**: 122–142.
- Croll, R. P., J. Nason, and J. van Minnen. 1993. Characterization of neurons in bivalves using antibodies raised against neuropeptides involved in the control of egg-laying in gastropods. *Invertebr. Reprod. Dev.* **24**: 161–168.
- De Vlieger, T. A., K. S. Kits, A. ter Maat, and J. C. Lodder. 1980. Morphology and electrophysiology of the ovulation hormone producing neuro-endocrine cells of the freshwater snail *Lymnaea stagnalis* (L.). *J. Exp. Biol.* **84**: 259–271.
- DiSalvo, L., and M. R. Carriker. 1994. Planktonic metamorphic and early benthic behavior of the Chilean loco *Concholepas concholepas* (Muricidae, Gastropoda, Mollusca). *J. Shellfish Res.* **13**: 57–66.
- Ebberink, R. H. M., H. van Loenhout, W. P. M. Geraerts, and J. Joosse. 1985. Purification and amino acid sequence of the ovulation neurohormone of *Lymnaea stagnalis*. *Proc. Natl. Acad. Sci. USA* **82**: 7767–7771.
- Gallardo, M. H., and J. I. Carraseo. 1996. Genetic cohesiveness among populations of *Concholepas concholepas* (Gastropoda, Muricidae) in southern Chile. *J. Exp. Mar. Biol. Ecol.* **197**: 237–249.
- Geraerts, W. P. M., and S. Bohlken. 1976. The control of ovulation in the hermaphrodite freshwater snail *Lymnaea stagnalis*. *Gen. Comp. Endocrinol.* **28**: 350–357.
- Geraerts, W. P. M., A. ter Maat, and E. Vreugdenhil. 1988. The peptidergic neuroendocrine control of egg-laying behavior in *Aplysia* and *Lymnaea*. Pp. 141–231 in *Invertebrate Endocrinology, Endocrinology of Selected Invertebrate Types*, H. Laufer and G. H. Downer, eds. Alan R. Liss, New York.
- Haszprunar, G. 1988. On the origin of major gastropod groups, with special reference to the Streptoneura (Mollusca). *J. Molluscan Stud.* **54**: 367–441.

- Huaquin, L. 1966. Anatomía de *Concholepas concholepas* (Bruguière, 1789). Thesis. Facultad de Medicina, Universidad Católica de Chile, Santiago, Chile. 53 pp.
- Hyman, L. H. 1967. Pp. 247–262 in *The Invertebrates. Vol. VI, Mollusca*. McGraw-Hill, New York.
- Jansen, R. F., and A. ter Maat. 1985. Ring neuron control of columnar motor neurons during egg-laying behavior in the pond snail. *J. Neurobiol.* **16**: 1–14.
- Kaplan, I. M., and B. C. Boyer. 1992. Monitoring marine resources: ecological and policy implications affecting the scientific collecting and commercial value of New England conch (*Busycon*). *Biol. Bull.* **183**: 379–380.
- Kupfermann, I. 1967. Stimulation of egg-laying: possible neuroendocrine functions of bag cells of abdominal ganglion of *Aplysia californica*. *Nature* **216**: 814–815.
- McAllister, L. B., R. H. Scheller, E. R. Kandel, and R. Axel. 1983. *In situ* hybridization to study the origin and fate of identified neurons. *Science* **222**: 800–808.
- Nagle, G. T., S. D. Painter, and J. E. Blankenship. 1989. Post-translational processing in model neuroendocrine systems: precursors and products that coordinate reproductive activity in *Aplysia* and *Lymnaea*. *J. Neurosci. Res.* **23**: 359–370.
- Osorio, C. 1979. Moluscos marinos de importancia económica en Chile. *Biol. Pesq. (Chile)* **11**: 3–47.
- Pierce, M. E. 1950. *Busycon canaliculatum*. Pp. 336–344 in *Selected Invertebrate Types*, F. A. J. Brown, ed. John Wiley, New York.
- Pulst, S.-M., D. Gusman, and E. Mayeri. 1988. Immunostaining for peptides of the egg-laying hormone/bag cell peptide precursor protein in the head ganglia of *Aplysia*. *Neuroscience* **27**: 363–371.
- Ram, J. L. 1977. Hormonal control of reproduction in *Busycon*: laying of egg capsules caused by nervous system extracts. *Biol. Bull.* **152**: 221–232.
- Ram, J. L., and M. L. Ram. 1989. Synthetic egg-laying hormone of *Aplysia*: quantitative studies of induction of egg laying in *Stylocheilus* and of the activation of *Aplysia* buccal neuron B16. *Comp. Biochem. Physiol.* **92C**: 131–134.
- Ram, J. L., and M. L. Ram. 1990. Gastropod egg-laying hormones. Pp. 257–264 in *Advances in Invertebrate Reproduction*, M. Hoshi and O. Yamashita, eds. Elsevier, Amsterdam.
- Ram, J. L., M. L. Ram, and J. P. Davis. 1982. Hormonal control of reproduction in *Busycon*: II. Laying of egg-containing capsules caused by nervous system extracts and further characterization of the substance causing capsule-laying. *Biol. Bull.* **162**: 360–370.
- Redman, R. S., and R. W. Berry. 1991. Temperature-dependent peptidergic feedback: potential role in seasonal egg laying in *Aplysia*. *J. Neurosci.* **11**: 1780–1785.
- Rodríguez, S. R., C. Riquelme, E. O. Campos, P. Chavez, E. Brandan, and N. C. Inestrosa. 1995. Behavioral responses of *Concholepas concholepas* (Bruguière, 1789) larvae to natural and artificial settlement cues and microbial films. *Biol. Bull.* **189**: 272–279.
- Rothman, B. S., E. Mayeri, R. O. Brown, P.-M. Ynan, and J. E. Shively. 1983. Primary structure and neuronal effects of alpha-bag cell peptide, a second candidate neurotransmitter encoded by a single gene in bag cell neurons of *Aplysia*. *Proc. Natl. Acad. Sci. USA* **80**: 5753–5757.
- Serra, G., G. Chelazzi, and J. C. Castilla. 1997. Effects of experience and risk of predation on the foraging behavior of the South-eastern Pacific muricid *Concholepas concholepas* (Mollusca: Gastropoda). *J. Anim. Ecol.* **66**: 876–883.
- Solem, G. A. 1991. Gastropods (snails and slugs). Pp. 311–321 in *The New Encyclopedia Britannica, 15th ed.* Encyclopedia Britannica, Chicago.
- Toevs, L. 1970. Identification and characterization of the egg-laying hormone from the neurosecretory bag cells of *Aplysia*. Ph.D. Dissertation. Division of Biology, California Institute of Technology, Pasadena, California.
- Toevs, L., and R. W. Brackenburg. 1969. Bag cell specific proteins and the humoral control of egg laying in *Aplysia californica*. *Comp. Biochem. Physiol.* **29**: 207–216.
- Van Minnen, J., H. D. F. H. Schallig, and M. D. Ramkema. 1992. Identification of putative egg-laying hormone containing neuronal systems in gastropod molluscs. *Gen. Comp. Endocrinol.* **86**: 96–102.
- Wiens, B. L., and P. H. Brownell. 1994. Neuroendocrine control of egg-laying behavior in the nudibranch, *Archidoris montereyensis*. *J. Comp. Neurol.* **344**: 619–625.

Effect of Colony Size, Polyp Size, and Budding Mode on Egg Production in a Colonial Coral

KAZUHIKO SAKAI

Sesoko Station, Tropical Biosphere-Research Center, University of the Ryukyus, Sesoko, Motobu-cho, Okinawa 905-0227, Japan

Abstract. The factors that influence egg production in the massive coral *Goniastrea aspera* were examined in colonies of various sizes collected before the first spawning of the year. Particular attention was given to polyp size, measured in three dimensions as volume.

Although a polyp in a colony containing as few as 13 polyps produced eggs, colonies with fewer than 60 polyps had fewer eggs per unit volume of polyp. The relationship between colony size and colony fecundity suggested that 60 polyps is the minimum size at which a colony can achieve active maturity. Polyp volume of small colonies before maturation was also smaller than that of the larger colonies, suggesting that colony size, as well as polyp size, is crucial for sexual maturity.

The position of a polyp in the colony (and thus its mode of budding) also affects its maturity (and thus its egg production). Marginal polyps (those on the edge of the colony) usually exhibited extratentacular budding, and the resulting polyps were initially immature. Consequently, egg production by such polyps is a function of their age, calculated from the time of their formation by extratentacular budding. In contrast, non-marginal polyps always exhibited intratentacular budding. Moreover, in the non-marginal areas of large colonies (>84 polyps), the polyps produced by intratentacular budding were always mature. In all colonies, marginal polyps were smaller in volume and had a lower number of eggs for each unit of volume than did non-marginal ones. This suggests that polyps play different roles according to their position in a colony: marginal polyps contribute to defense and expansion of the area of attachment, whereas

the role of non-marginal polyps is reproductive. The fecundity of mature colonies increased linearly with colony size, and large colony size cannot be attained without expansion of the attachment area.

Introduction

Recent studies on reproduction of colonial, scleractinian corals have revealed that polyps in small colonies produce no eggs or few eggs, and that in large, fecund colonies polyps at or near the margin of the colony produce fewer eggs than those in central positions (Harriott, 1983; Chornesky and Peters, 1987; Harrison and Wallace, 1990; Szmant, 1991; Soong and Lang, 1992; Van Veghel and Kahmann, 1994; Hall and Hughes, 1996). A coral colony is usually derived from a single polyp by budding, so that the polyps in the colony are usually genetically identical (Jackson and Coates, 1986) and likely to have the same structure and the same potential for any physiological function (Meester and Bak, 1995). Thus, the recent work has demonstrated that coral polyps may differ in reproductive activity even though they share the same structure and genetic identity.

In colonial corals, colony size is considered to be important for the maturation of polyps (reviewed in Harrison and Wallace, 1990), but the size of a coral has another aspect, *i.e.*, polyp size. Although the polyp is the basic unit for physiological activities, its size has not often been studied. Two exceptions are the studies by Harriott (1983) and Van Veghel and Kahmann (1994). Harriott (1983) investigated sexual reproduction in four scleractinian coral species, and suggested that polyp size rather than colony size limits gonad production in the mussid coral *Lobophyllia corymbosa*; she presented no data on polyp size. Van Veghel and Kahmann (1994) studied reproduc-

tion in three morphotypes of the faviid coral *Montastrea annularis*, measuring polyp size two-dimensionally at the base. They found that the fertility (measured as the percentage of polyps with eggs) of polyps from 27 colonies was less than 40% in small polyps (<1.5 mm) and increased with polyp diameter.

To date, however, no study of coral reproduction has quantitatively examined the relationship between the size of a polyp and its egg production. Furthermore, polyp size has previously been measured in two dimensions, even though it is the space within a polyp that limits gamete volume. Thus, I measured the three-dimensional size of polyps in the faviid coral *Goniastrea aspera*.

I examined the effect of colony size, polyp size, and location of polyps on egg production. I show that not only colony size but also polyp size is related to egg production, and further suggest that fertility in *G. aspera* is also affected by polyp age, determined as the time since formation by extratentacular budding.

Materials and Methods

Collection, colony size, and egg count

I collected specimens of *G. aspera* at the lowest low tide level on the fringing reef of Sesoko Island, Okinawa, southern Japan (26° 38'N, 127° 52'E). This coral is a simultaneous hermaphrodite; in Okinawa it has one or two spawning peaks per year, in June and July (Heyward *et al.*, 1987; Hayashibara *et al.*, 1993; Sakai, 1997). To assess egg production by polyps, 23 *G. aspera* colonies of various sizes were collected on 21 May 1991, 10 days before the predicted date of the first spawning of the year. Before collection, the length, width, and height of the colony were measured to the nearest 1 mm. Since egg production may be affected by disease or injury and by contact with large benthic organisms such as neighboring corals, I chose colonies without such features.

The collected colonies were fixed in 10% formalin in seawater for at least 24 h, and decalcified in a solution of 5% formalin + 5% acetic acid. I counted the number of polyps in the colony after decalcification and used this value as a measure of colony size, because the polyp number is highly correlated with colony somatic biomass (Sakai, 1998). Then, randomly selected polyps (n ranged from 1 to 20 according to colony size) were cut from the decalcified colony after the maximum and minimum diameters of the oral side were measured to the nearest 0.1 mm. Polyp height was measured after the polyps were excised from the colony. I estimated the volume of each polyp from its diameter and height. While non-marginal polyps (in polyp row 2 or higher, away from the colony margin; Fig. 1) were always cylindrical, marginal polyps (in the row at the colony edge) were frequently more

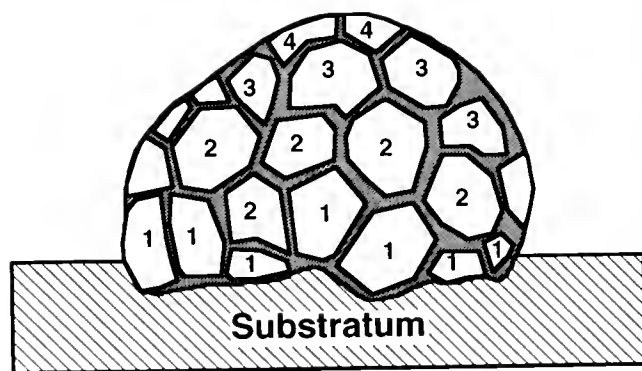


Figure 1. Diagram showing position classification of polyps in a colony. Each white polygon represents a polyp, and the number inside the polygon indicates the row number of that polyp. Row number was determined as the next highest number to the lowest number in adjacent polyps. 1 = marginal polyps; ≥ 2 = non-marginal polyps.

conical. Hence, I estimated the polyp volume as $k \times \pi \times [(\text{maximum diameter} + \text{minimum diameter}) / 4]^2 \times \text{height}$, where k ranged from $1/3$ (conical) to 1 (cylindrical). The value of k was subjectively determined for each polyp according to its shape. Each polyp was dissected under a stereoscopic microscope, and all the eggs within a polyp were counted. I measured the diameter of five eggs, randomly selected from each of four polyps in each of ten fecund colonies. The overall mean of the egg diameter in the polyps was $310 \pm 30 \mu\text{m}$ (Mean \pm SD, $n = 200$). There was no significant colony effect on the egg diameter (Model III nested ANOVA, $df = 9$, $SS = 9663.98$, $F = 0.99$, $P = 0.5$; when polyps were nested in the colonies). Thus, egg production can be compared in terms of number of eggs per polyp volume (NE/PV, see below).

Preliminary examination of the effect of polyp position on egg production in four fecund colonies showed that marginal polyps had significantly lower NE/PV than non-marginal polyps (Table 1). NE/PV of polyps in row 2 or higher did not differ significantly ($P > 0.05$). In subsequent analyses I therefore grouped polyps in a colony into marginal and non-marginal sets. Polyp-group fertility, as percentage of polyps with eggs to total number of sampled polyps, was calculated separately for marginal and non-marginal polyps in each colony.

Budding mode and polyp biomass

To examine the relationship between estimated polyp volume and polyp biomass, I collected 11 colonies of *G. aspera* of various sizes (from 40 to 420 polyps) in October 1993, when reproductive tissue was negligible (Sakai, 1997). These colonies were fixed and decalcified as described for the egg-count specimens. When I counted the number of polyps in the decalcified colonies, I also re-

Table 1

Intracolony variation in NE/PV (number of eggs per polyp volume, mm⁻³) in four fecund colonies

Colony size (number of polyps)	Kruskal-Wallis test among polyp rows (<i>P</i> value)	Tukey-type multiple comparison
84	<0.01	1st <<< 2nd ≈ 3rd+
85	<0.01	1st < 2nd, 1st <<< 3rd+, 2nd ≈ 3rd+
167	<0.01	1st << 2nd, 1st < 3rd, 1st << 4th+, 2nd ≈ 3rd ≈ 4th+
349	<0.001	1st << 2nd, 1st < 3rd, 1st << 4th, 2nd ≈ 3rd ≈ 4th+

Note: Ordinals in the multiple comparison (Zar, 1996) represent polyps of the *i*th row from the colony edge; 3rd+ and 4th+ indicated polyps more central than 2nd and 3rd rows, respectively (Fig. 1). Probability in multiple comparison: ≈, *P* > 0.05; <, *P* < 0.05; <<, *P* < 0.01; <<<, *P* < 0.001. Number of polyps examined in each row ranged from 5 to 10.

corded the mode of budding (*i.e.*, intratentacular or extratentacular) for marginal and non-marginal polyps separately. Formation of a new bud outside the polyp wall was recorded as extratentacular budding, and formation of a new polyp wall dividing the original polyp was recorded as intratentacular budding.

Four polyps, two marginal and two non-marginal, were randomly selected from each colony after decalcification. These 44 polyps were measured and excised from the colonies as described for egg-count polyps, and then rinsed in distilled water and dried at 60°C to constant weight. Each polyp was weighed to the nearest 0.1 mg. The estimated polyp volume showed a strong linear correlation with the somatic biomass, both in marginal ($r^2 = 0.87$, $P < 0.0001$, $n = 22$) and non-marginal ($r^2 = 0.84$, $P < 0.0001$, $n = 22$) polyps, with no significant difference between the two regression lines (ANCOVA, $df = 1$, $SS = 0.29$, $F = 0.17$, $P = 0.7$). Therefore, assuming that the polyp volume represents the somatic biomass, I calculated the average number of eggs per polyp volume (NE/PV, mm⁻³) for marginal and non-marginal polyps in each colony.

Colony fecundity

Egg production by a whole colony (colony fecundity) was estimated as the sum of egg production by marginal and non-marginal polyps. The total egg production for each polyp type was calculated as the mean number of eggs per polyp multiplied by the number of polyps of that type in the colony.

Statistical analyses

I examined the relationship between colony size (polyp number) and fertility and mean NE/PV, fitting a curve using the logistic equation, since egg production by coral polyps over colony size is expected to be sigmoidal (Babcock, 1991). For the remaining regression analyses, I examined linear, exponential, power, and logarithmic functions, and used the one with the highest correlation coefficients after examining the residuals (Zar, 1996). I used Model III ANOVA, nesting random-effects such as individual colonies within fixed-effects such as colony size classes (Zar, 1996). The assumptions for ANOVA (*i.e.*, normality and homogeneity of variance) were examined with the Shapiro-Wilk *W* test and O'Brien's tests. Logarithmic transformation was made if necessary; when the assumptions were severely violated even after the transformation, a nonparametric analysis such as the Wilcoxon paired-sample test was performed using means from colonies. Statistical analyses were performed with computer software packages (Data Desk, Data Description Inc., Ithaca, NY; JMP, SAS Institute, Cary, NC; Kaleida Graph, Synergy Software, Reading, PA).

Results

Marginal and non-marginal polyps

Six of twenty-three colonies smaller than 2 cm in diameter (9 polyps) had only marginal polyps. Hence, the comparisons between marginal and non-marginal polyps were conducted for the 17 colonies that had both polyp types. Values for mean polyp volume, fertility, and mean NE/PV of non-marginal polyps were significantly greater than those of marginal polyps from the same colony (Wilcoxon paired-sample test, all $P < 0.01$; Fig. 2A–C). The mode of budding was also significantly different between the two groups (Fisher exact test, $P < 0.0001$). All the budding (total = 58) in non-marginal polyps was intratentacular, and 96% of the budding (total = 53) in marginal polyps was extratentacular.

Colony size, polyp size, and egg production by polyps

To examine the relationships among colony size, polyp size, and egg production, I grouped the colonies into three size classes: small (S; ≤60 polyps, or ≤4.5 cm in mean colony diameter), medium (M; 60–150 polyps, or 4.5–9 cm), and large (L; >150 polyps, or >9 cm). The classification was made because (1) below 60 polyps, NE/PV was extremely small; and (2) after 150 polyps, the fitted curve using the logistic equation between the colony size and NE/PV leveled off (Table II; Fig. 2C).

No eggs were found in colonies with marginal polyps only or with marginal polyps and one non-marginal polyp

Table IV

Mean polyp volume, polyp fertility, and mean NE/PV (number of eggs per polyp volume) among the colony size classes

Colony size class	Mean polyp volume (mm ³)	Fertility (%)	Mean NE/PV (mm ⁻³)	<i>n</i>
Marginal polyps				
S	33.2 ± 4.8	3.1 ± 3.1	0.004 ± 0.004	13
M	77.4 ± 10.9	63.3 ± 15.8	0.19 ± 0.07	6
L	65.6 ± 17.0	62.5 ± 10.3	0.30 ± 0.14	4
Non-marginal polyps				
S	59.7 ± 9.3	32.1 ± 11.8	0.02 ± 0.01	7
M	131.5 ± 18.7	93.9 ± 3.9	1.02 ± 0.10	6
L	140.7 ± 13.9	100	1.82 ± 0.36	4

Note: The size classes: S, ≤ 60; M, 62–150; L, >150 polyps. Mean ± SE calculated from means of individual colonies are shown. Number of colonies = *n*. Bars connect means that were judged not significantly different ($P > 0.05$) by Scheffé test (for mean polyp volume of marginal and non-marginal polyps after nested ANOVA), Tukey-type test (for fertility of marginal and non-marginal polyps after Kruskal-Wallis test), and nested ANOVA (for mean NE/PV of marginal and non-marginal polyps between the M and the L size classes).

for marginal polyps. The M and the L class colonies did not differ in mean polyp volume for either marginal or non-marginal polyps.

Fertility (Fig. 2B) was significantly lower in the S size class than in the M and L size classes for both marginal and non-marginal polyps (Table IV; $P < 0.001$; Kruskal-Wallis test). As with mean polyp volume, fertility did not differ significantly between the M and the L size classes (Table IV). Fertility of non-marginal polyps was 100% in all the colonies that were larger than 84 polyps. The complete fertility of the non-marginal polyps was not due to large polyp volume. Although the volume was significantly larger in non-marginal polyps than in marginal polyps within a colony, small non-marginal polyps were fertile, whereas some of marginal polyps within the same volume range were not (Fig. 3). The overall fertility of these marginal polyps was 66.7% ($n = 57$), and polyp volume was positively associated with fertility.

ANOVA could not be performed for mean NE/PV among colonies in all the size classes, because the many 0 scores in mean NE/PV in the S size class (Fig. 2C) was a severe violation of ANOVA assumptions. However, mean NE/PV of both marginal and non-marginal polyps in the S size class was an order of magnitude smaller than those in the M and the L size classes (Table IV). I performed Model III nested ANOVAs excluding colonies in the S size class. Mean NE/PV of marginal polyps was not significantly different between the L and the M size classes (Table IIIC); in contrast, the difference was significant for non-marginal polyps (Table IIID).

Colony fecundity

Some colonies in the S size class produced eggs, but their colony fecundity was less than 60 eggs. In contrast, the fecundity of colonies in the M and the L size classes

was more than 4500 eggs, and it increased linearly with colony size (Fig. 4). The *X* intercept of colony size vs. colony fecundity in the regression line for the M and L size class colonies was 58.3 polyps. Hence I considered the colony size for active maturation to be 60 polyps. Marginal polyps contributed less than 1% to the fecundity of colonies in the M size class. The contribution by marginal polyps decreased with colony size, and it was less than 0.1% in the L size class (>150 polyps).

Discussion

The results suggest that the sexual maturation of a polyp is less a function of its size than of the mode of

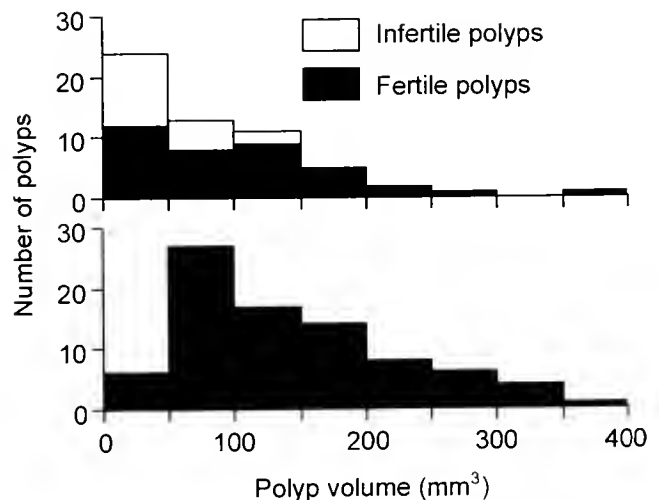


Figure 3. Polyp size distribution for marginal (top) and non-marginal (bottom) polyps from colonies larger than 84 polyps. All the polyps from eight colonies were pooled. Infertile and fertile polyps are shown separately.

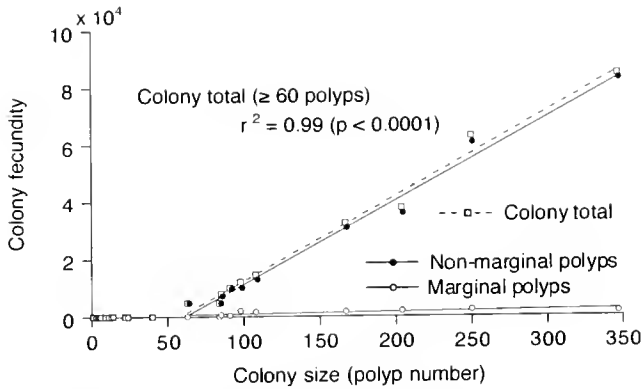


Figure 4. Relationship between colony size (number of polyps) and colony fecundity. The total colony fecundity and the contribution of marginal and non-marginal polyps to colony fecundity are presented separately. Linear regressions were conducted for colonies larger than 60 polyps.

budding that produced it. In large colonies of mature *G. aspera* (>84 polyps), the non-marginal polyps, which showed intratentacular budding, always contained eggs regardless of polyp size, but less than 70% of the marginal polyps were fertile (Fig. 3). New polyps produced by intratentacular budding of mature non-marginal polyps appear to share the developmental stage of their parent polyps, whereas new small polyps produced by extratentacular budding are rarely fertile and may be regarded as developmentally "young" polyps. In the Caribbean massive faviid coral *Montastrea annularis*, not all the polyps in the central area are fertile, and polyp fertility is positively correlated with polyp size (Van Veghel and Kahmann, 1994), as in marginal polyps from the large colonies of *G. aspera* (Fig. 3). One of the generic characters of *Montastrea* is that it exhibits only extratentacular budding (Veron, 1986). So for this species, polyp size likely reflects the polyp age after extratentacular budding; *i.e.*, each polyp has its own developmental clock. In contrast, new polyps produced by intratentacular budding in *G. aspera* are mature from inception. Thus the age of these polyps should also be measured from the time of original formation by extratentacular budding, not from the time of intratentacular budding.

Egg production of *G. aspera* was affected by colony size, polyp size, and budding mode. The colonies became actively reproductive at a size of 60 polyps, and the polyp volume of the reproductive colonies was significantly larger than that of the pre-reproductive colonies (Tables IIIA, IIIB, and IV). An effect of polyp age on egg production has been suggested by Kojis and Quinn (1985). They divided mature colonies of *Goniastrea favulus* into fragments smaller than the minimum size at maturity observed in naturally growing colonies, and found that some of the

fragments produced gametes. In *G. aspera*, non-marginal polyps were formed in colonies with more than eight polyps, which then began intratentacular budding. All non-marginal polyps in colonies larger than 84 polyps were fertile, presumably because all the polyps have attained maturity upon extratentacular budding.

This study demonstrates that polyps within a mature colony of *G. aspera* play different roles according to their position, even though all the polyps in a colony share the same structure and are likely to be genetically identical and physiologically connected to each other. Significant differences in polyp volume, NE/PV, and mode of budding were detected between marginal and non-marginal polyps within a colony. Moreover, NE/PV of marginal polyps was relatively constant in mature colonies, whereas NE/PV of non-marginal polyps was significantly higher in the larger mature colonies (>150 polyps) than in smaller mature colonies (60–150 polyps; Tables IIIC, IIID and IV). This implies that marginal polyps function as a buffer for the non-marginal polyps, which produce the bulk of the gametes (Fig. 4), against external perturbations such as competition and grazing, which are likely to be heavier at the colony edge (Jackson, 1979; Hughes and Jackson, 1985; Chornesky and Peters, 1987; Soong and Lang, 1992). In addition, marginal polyps may also contribute to the expansion of the attachment area of the colony (Chornesky and Peters, 1987). In a massive coral colony, polyps in the central area contribute to colony growth, increasing the surface area of the colony. However, large colony size cannot be attained without expansion of the attachment area as well. As a colony becomes larger, its total fecundity becomes greater with an increase in the number of fecund, non-marginal polyps. Thus, the differences between the marginal and the non-marginal polyps play a role in promoting high colony fecundity.

Acknowledgments

I thank R. A. Kinzie III, E. F. Cox, and J. S. Stimson for comments on the manuscript. I also thank K. Karino, T. Kuwamura, Y. Nakashima, Y. Loya, and H. Yamashiro for comments on the earlier manuscripts, and E. Hirose for discussion on polyp age. This study was partly supported by grants from the Japanese Ministry of Education, Science, Sports and Culture. This is a contribution from Sesoko Station, University of the Ryukyus.

Literature Cited

- Babcock, R. C. 1991. Comparative demography of three species of scleractinian corals using age- and size-dependent classifications. *Ecol. Monogr.* 61: 225–244.
- Chornesky, E. A., and E. C. Peters. 1987. Sexual reproduction and colony growth in the scleractinian coral *Porites astreoides*. *Biol. Bull.* 172: 161–177.

- Hall, V. R., and T. P. Hughes. 1996. Reproductive strategies of modular organisms: comparative studies of reef-building corals. *Ecology* 77: 950-963.
- Harriott, V. J. 1983. Reproductive ecology of four scleractinian species at Lizard Island, Great Barrier Reef. *Coral Reefs* 2: 9-18.
- Harrison, P. L., and C. C. Wallace. 1990. Reproduction, dispersal and recruitment of scleractinian corals. Pp. 133-207 in *Ecosystems of the World, Vol. 25, Coral Reefs*, Z. Dubinsky, ed. Elsevier, Amsterdam.
- Hayashihara, T., K. Shimoike, T. Kimura, S. Hosaka, A. Heyward, P. Harrison, K. Kudo, and M. Omori. 1993. Patterns of coral spawning at Akajima Island, Okinawa Japan. *Mar. Ecol. Prog. Ser.* 101: 253-262.
- Heyward, A., K. Yamazato, T. Yeemin, and M. Minei. 1987. Sexual reproduction of corals in Okinawa. *Galaxea* 6: 331-343.
- Hughes, T. P., and J. B. C. Jackson. 1985. Population dynamics and life histories of foliaceous corals. *Ecol. Monogr.* 55: 141-166.
- Jackson, J. B. C. 1979. Morphological strategies of sessile animals. Pp. 499-555 in *Biology and Systematics of Colonial Organisms*, G. Larwood and B. R. Rosen, ed. Academic Press, New York.
- Jackson, J. B. C., and A. G. Coates. 1986. Life cycles and evolution of clonal (modular) animals. *Phil. Trans. R. Soc. Lond. B* 313: 7-22.
- Jackson, J. B. C., and T. P. Hughes. 1985. Adaptive strategies of coral-reef invertebrates. *Am. Sci.* 73: 265-274.
- Kojis, B. L., and N. J. Quinn. 1985. Puberty in *Goniastrea favulus*: age or size limited? *Proc. 5th Int. Coral Reef Congr., Tahiti* 4: 289-293.
- Meester, E. H., and R. P. M. Bak. 1995. Age-related deterioration of a physiological function in the branching coral *Acropora palmata*. *Mar. Ecol. Prog. Ser.* 121: 203-209.
- Sakai, K. 1997. Gametogenesis, spawning, and planula brooding by the reef coral *Goniastrea aspera* (Scleractinia) in Okinawa, Japan. *Mar. Ecol. Prog. Ser.* 151: 67-72.
- Sakai, K. 1998. Delayed maturation in the colonial coral *Goniastrea aspera* (Scleractinia): whole-colony mortality, colony growth and polyp egg production. *Res. Popul. Ecol. (Kyoto)* 40: (in press).
- Soong, K., and J. L. Lang. 1992. Reproductive integration in reef corals. *Biol. Bull.* 183: 418-431.
- Szmant, A. M. 1986. Reproductive ecology of Caribbean reef corals. *Coral Reefs* 4: 43-54.
- Szmant, A. M. 1991. Sexual reproduction by the Caribbean reef corals *Montastrea annularis* and *Montastrea cavernosa*. *Mar. Ecol. Prog. Ser.* 74: 13-25.
- Van Veghel, M. L. J., and M. E. H. Kahmann. 1994. Reproductive characteristics of the polymorphic Caribbean reef building coral *Montastrea annularis*. II. Fecundity and colony structure. *Mar. Ecol. Prog. Ser.* 109: 221-227.
- Veron, J. E. N. 1986. *Corals of Australia and the Indo-Pacific*. Angus & Robertson, North Ryde, Australia.
- Zar, J. H. 1996. *Biostatistical Analysis*, 3rd ed. Prentice-Hall, Upper Saddle River, NJ.

Late Postembryonic Development of the Symbiotic Light Organ of *Euprymna scolopes* (Cephalopoda: Sepiolidae)

MARY K. MONTGOMERY* AND MARGARET J. McFALL-NGAI†

Pacific Biomedical Research Center, University of Hawaii, 41 Ahui Street, Honolulu, Hawaii 96813

Abstract. The symbiotic light organ of the sepiolid squid *Euprymna scolopes* undergoes significant anatomical, morphological, and biochemical changes during development. Previously we described the embryonic organogenesis and early postembryonic development of the light organ. During embryogenesis, tissues are developed that will promote the onset of an association with *Vibrio fischeri*, the light organ symbiont. Upon inoculation, and in response to the first interactions with the bacterial symbionts, the light organ undergoes a dramatic morphogenesis during the first 4–5 days of postembryonic development. Here we describe the final developmental stage of the light organ system, a period of late postembryonic development in which particular tissues of the light organ mature that eventually mediate the functional symbiosis. The maturation of the light organ occurs within 1 to 2 weeks posthatch and entails two principal processes: (1) changes in the shape of the organ and elaboration of the accessory tissues that modify the bacterially produced light; and (2) branching of the epithelial crypts, where the bacterial symbionts reside, and restriction of epithelial cell proliferation to the deepest branches of the crypts. The gross morphological changes of the organ occur in the absence of *V. fischeri*, although rudiments of the ciliated field of the hatchling remain in animals not exposed to the microbial symbiont.

Introduction

A variety of mutualistic symbioses exist between bacteria and many species of plants and animals. The associations can be highly evolved and complex, involving the development of specific host tissues or organs that directly interact with the bacterial symbionts; examples include the root nodule of leguminous plants (Hirsch, 1992), the rumen of ungulate mammals (Flint, 1997), the light organs of some species of squid and fish (Herring, 1978; Haygood, 1993), the trophosome of vestimentiferans (Jones and Gardiner, 1988), and the bacteriocytes of certain insects (Douglas, 1989). Several of these associations have "indirect" transmission of symbionts between generations; that is, onset of the symbiosis results from interactions with environmental microbes, not microbes that are in or on the eggs.

The early morphology of these organs, prior to the infection with symbionts, is often quite different from that of the fully differentiated symbiotic state (Buchner, 1965; Jones and Gardiner, 1988; Fisher and Long, 1992; Hirsch, 1992; Montgomery and McFall-Ngai, 1993, 1994). In the well-characterized *Rhizobium*-leguminous plant symbioses, stages of the symbiosis have been defined as preinfection, infection, colonization, and maturation (van Rhijn and Vanderleyden, 1995). These stages correspond to specific molecular, biochemical, and anatomical changes in both the host plant and the bacterial symbiont that reflect the progression of the association from initiation to the mature nitrogen-fixing symbiosis. More than 100 years of research on the host plants and bacterial symbionts have revealed that dozens of host and symbiont genes are induced in the progression of these developmental changes.

Received 25 June 1998; accepted 29 September 1998.

* Present address: Macalester College, Department of Biology, 1600 Grand Avenue, St. Paul, Minnesota.

† To whom correspondence should be addressed. E-mail: mcfallng@hawaii.edu

The symbiosis between the sepiolid squid *Euprymna scolopes* and the luminous bacterium *Vibrio fischeri* provides an opportunity to define the events associated with the development of an *animal* symbiosis (McFall-Ngai and Ruby, 1991, 1998; Ruby, 1996). The development of the light organ can be divided into 3 distinct stages—embryonic, early postembryonic, and late postembryonic—reflecting the preinfection, inoculation, and maturation stages of the symbiosis. During embryonic development, an incipient organ that is primarily structured to ensure inoculation with the bacterial symbionts forms in the mantle cavity. This organ includes a complex, superficial, ciliated epithelium that will potentiate inoculation as well as a set of epithelium-lined crypts, or in-pocketings of the surface of the light organ, that will house the symbiotic bacteria (Montgomery and McFall-Ngai, 1993). Early postembryonic development is induced by initiation of the symbiosis and is characterized by the cell-death-mediated loss of the ciliated epithelium and the further differentiation of the crypt cells that directly interact with the symbionts (Montgomery and McFall-Ngai, 1994; Lamarca and McFall-Ngai, 1998). In the mature organ, the luminescent bacterial symbionts are maintained in a complex bilobed light organ. The functional symbiotic organ is composed of several host tissues, including a core of branching epithelial crypts that houses the symbionts; a thick reflector that directs the bacterial luminescence ventrally; diverticula of the ink sac that dynamically control the intensity of luminescence; and a ventral muscle-derived lens that diffuses the point-source light into the environment (McFall-Ngai and Montgomery, 1990). In addition, two bright yellow filters, which are situated ventral to the bacteria-containing tissue and dorsal to the lens, are associated with the ducts of the adult organ (pers. obs.; Fig. 1). The configuration of adult tissues appears to maintain a stable symbiotic association and to control luminescence, which is apparently used in antipredatory behaviors (Moynihan, 1983).

We have previously described the embryonic and early postembryonic stages of light organ development (Montgomery and McFall-Ngai, 1993, 1994). Here, we provide a biochemical, cytological, and morphological analysis of the changes that accompany the transition from the early postembryonic stages to the mature, functional light organ symbiosis.

Materials and Methods

Light microscopic observations of the light organs of live and fixed specimens

Specimens of *Euprymna scolopes* were collected from Hawaii, as previously described (Weis *et al.*, 1993). Field-caught animals at various developmental stages (ranging

in mantle length from 2 to 20 mm) were anesthetized by having their body temperature lowered to 10°C. The ventral side of the mantle and then the funnel were dissected open to expose the light organ within the mantle cavity. Light organs were photographed with a Nikon camera attached to a Wild M-5 stereomicroscope.

Light organs were fixed for light microscopy as previously described (Montgomery and McFall-Ngai, 1993). Serial 1- μ m sections of the organs were reconstructed to reveal morphological features.

BrdU incorporation and visualization

To locate active areas of host cell proliferation, field-caught juveniles ranging in mantle length from 6 to 12 mm were exposed for various times, from 12 h to 5 d, to 10 μ M 5-bromo-2'-deoxyuridine (BrdU), a thymidine analog that was added to filtered seawater. Animals were transferred to filtered seawater for 30 min and then fixed and embedded as described by Montgomery and McFall-Ngai (1994). One-micron sections were dried on gelatin-coated slides. To denature the DNA, sections were treated with 4 N HCl for 10 min, followed by a neutralizing step in 0.1 M sodium borate (Migheli *et al.*, 1991). Sections were incubated for 30 min in blocking solution consisting of a 1:50 dilution of non-immune goat serum in 10 mM sodium phosphate buffer, containing 150 mM NaCl, 0.05% sodium azide, and 0.5% bovine serum albumin (PBS/BSA). The sections were then rinsed in PBS/BSA and incubated overnight in a 1:50 dilution of primary antiserum, *i.e.*, monoclonal anti-BrdU antibody (Becton-Dickinson, CA); the bound antibody was visualized by light microscopy using goat anti-mouse secondary antibody conjugated to 5-nm gold spheres amplified by silver enhancement (Sigma Chemical Co.). The sections were counterstained with 1% acid fuchsin for 20 min, rinsed in water, dried, and mounted in heavy immersion oil.

Immunocytochemistry

Light organs of field-caught *E. scolopes* were fixed and processed for immunocytochemistry as described in Weis *et al.* (1993). Serial sections, 1 to 1.5 μ m thick, were cut with glass knives and dried onto gelatin-coated glass slides. L-crystallin, a light organ lens marker protein, was localized in the tissue sections with anti-L-crystallin rabbit antiserum (Montgomery and McFall-Ngai, 1992; Weis *et al.*, 1993); the antiserum has been shown in previous experiments to be highly specific to this antigen. Bound antibody was visualized in light microscopy with a goat anti-rabbit secondary antibody conjugated to 5-nm gold spheres amplified by silver enhancement (Sigma Chemical Co.). The sections were counterstained with 1% acid fuchsin as described above.

Experiments with aposymbiotic animals

Juvenile animals were maintained aposymbiotically; *i.e.*, they were raised in artificial seawater for 2–3 weeks posthatch at the University of Texas Medical Branch (Galveston, TX). Whole animals were fixed in Texas in 4% formalin in seawater and transported to the University of Hawaii, where they were processed for scanning electron microscopy as previously described (Montgomery and McFall-Ngai, 1994).

Results

Changes in gross morphology of the light organ

Changes in overall gross morphology accompany post-embryonic development of the light organ (Fig. 1). A newly hatched juvenile with an average mantle length of 1.6 mm possesses an incipient light organ located in the center of the ventral surface of the ink sac (Fig. 1A; Montgomery and McFall-Ngai, 1993). This juvenile organ is ovoid and lacks a lens, although the silver reflector that covers the ventral surface of the ink sac is apparent. During the first several days of posthatch development, the anterior and posterior diverticula of the ink sac expand and contract to cover the bacteria-containing crypts of the organ (Fig. 2, top).

By the time a juvenile reaches 2.8 mm in mantle length, the light organ has begun to acquire a more bilobed appearance (Fig. 1B). A medial portion of the ink sac, extending from the posterior end, covers much of the center ventral surface of the organ, and diverticula of the ink sac have moved in from the lateral margins, covering the lateral central portion of each lobe. Most of the growth in each lobe has been directed anteriorly, although some posterior growth has also occurred. In each lobe, the lens, although not very apparent, has begun to differentiate. In addition, a pair of yellow filters has begun to form lateroventral to the bacteria-containing crypt tissue.

In juveniles 4.0 mm in mantle length (Fig. 1C), all the components of the light organ of an adult squid are fully differentiated. The characteristic bilobed shape of the adult light organ is evident, and the medial portion of the ink sac that covers the center of the ventral surface of the organ has begun to expand laterally. The bacteria-containing crypts are now covered by a series of dynamic diverticula that wrap around the organ; these diverticula expand and contract, over a period of seconds to minutes, in the anterior-posterior direction and the medial-lateral direction (Fig. 2, middle). In addition, the yellow filters, which are very conspicuous by this stage, are observed in various positions along the anterior-posterior axis, spreading over the bacteria-containing crypt tissue (Fig. 1B–D).

Continued growth of the light organ beyond this stage results in a structure only slightly more well defined and complexly shaped (Fig. 1D). The lateral "flaps" of the ventral medial portion of the ink sac have expanded so that the central half of each lobe is covered. Laterally, each lobe has grown anteriorly and posteriorly, with the lens forming a thick pad over each end and thinning in the middle near the pore; the medial portion of the organ, however, has been almost completely overlain by the posterior ventral fold of the ink sac. The medial and lateral diverticula of the ink sac have become the primary mechanism by which the bacteria-containing tissue of the organ is shielded (Fig. 2, bottom).

Late postembryonic development of the crypts and ciliated duct

Serial histological sections of the light organs of two squids, one 2 mm and the other 8 mm in mantle length, revealed that, although they are highly branched, there are always only three bacteria-containing crypts in a mature light organ (Fig. 3). Each branching epithelial crypt joins the ciliated duct separately; the crypts were identified on the basis of their relative positions to each other and the sites at which each joins the duct. At hatching, the three crypts empty into three separate ducts that lead to three separate pores on the surface of the light organ (Montgomery and McFall-Ngai, 1993). By 2 mm in mantle length, the three crypts on each side of the light organ are joined to a single tripartite duct leading to a single pore (data not shown). In the fully differentiated light organ of the squid 8 mm in mantle length, the ciliated duct, rather than being tripartite, branches into five parts (Fig. 3); *i.e.*, in addition to branches leading to the three crypts, an anterior portion of the duct leads into the inner core of the anterior yellow filter, and a posterior portion leads into the inner core of the posterior filter.

Proliferating cells could be localized by analyzing the incorporation of the thymidine analog BrdU into replicating DNA. Regional differences were observed in the distribution of dividing cells in the light organ of a squid 8 mm in mantle length (Fig. 4A). Only a few cells were labeled in such accessory tissues as the lens (Fig. 4A, B). Cells in the distal portions of the crypts incorporated BrdU intensely (Fig. 4A, C), whereas none of the cells in either the ciliated duct or portions of the crypts close to the ciliated duct was labeled. The morphology of the cells in the proliferating zones of the crypts appeared different from those nonproliferating cells located closer to the duct. The epithelial cells of the distal portions of the crypts are roughly cuboidal and relatively small (Fig. 4C); as cells are located closer to the ciliated duct, they

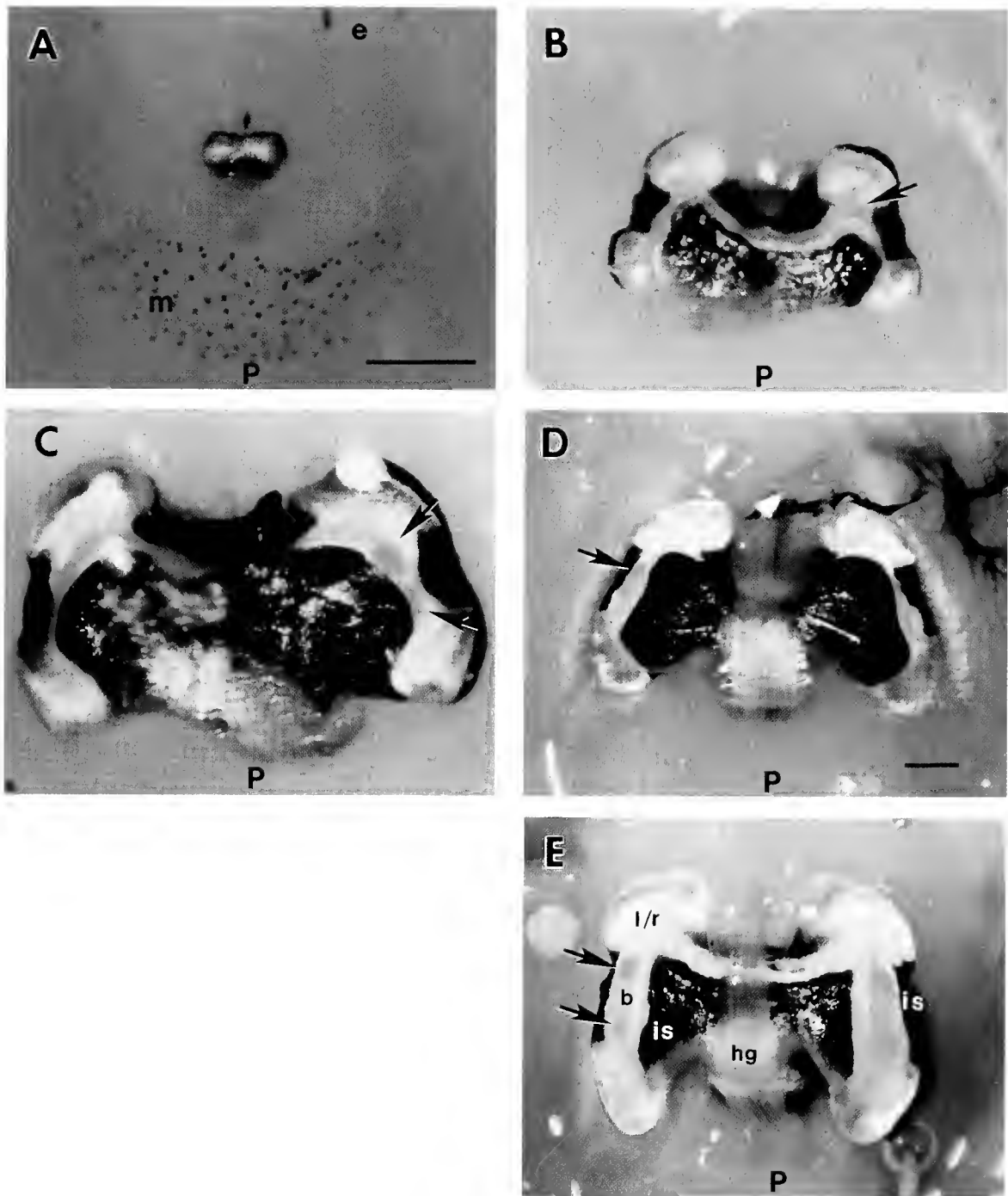


Figure 1. Postembryonic development of the light organ of *Euprymna scolopes*. [Animals were placed against a pink background to provide contrast to the squid light organ tissues.] Ventral views of the light organ of a (A) newly hatched juvenile 1.6 mm in mantle length; m, mantle; e, eye; (B) juvenile 2.8 mm in mantle length; (C) juvenile 4.0 mm in mantle length; (D) sexually mature male 18 mm, and (E) 20 mm in mantle length. The bacteria-containing tissue (b) is dorsal to the yellow filters (arrows in B–D) and appears opaque against the brilliantly silver reflector. The reflector and the lens (l/r), which occurs ventral to the reflector, run much of the length of each lobe. Diverticula of the ink sac (is) expand and contract over the bacteria-containing tissue to control the intensity of light emission. Bar (A–C), 500 μ m, (D–E), 1 mm; hg, hindgut; P, posterior.

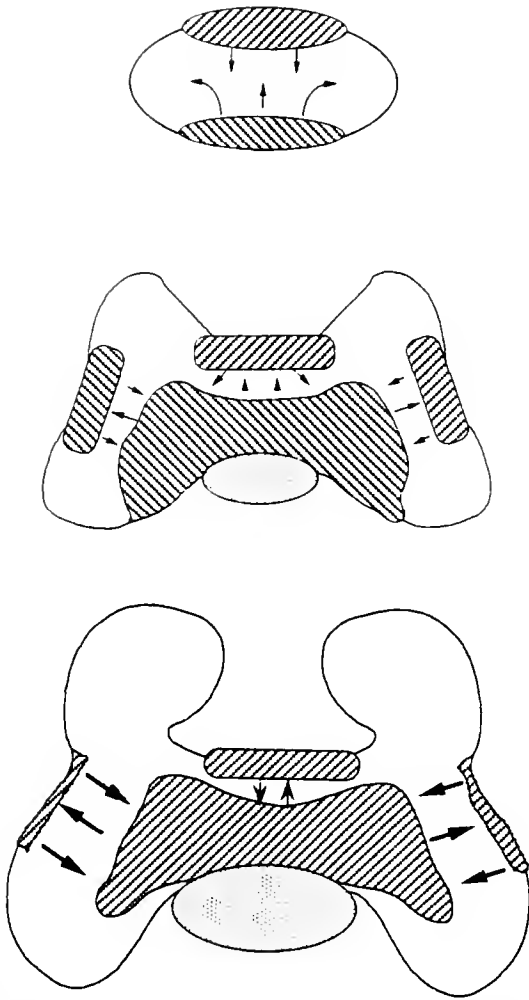


Figure 2. Change in the dynamics of the ink sac diverticula with development of the *Euprymna scolopes* light organ. Top panel, organ of a hatchling (1.6 mm in mantle length); middle panel, juvenile organ (4.0 mm in mantle length); bottom panel, organ of mature adult (20 mm in mantle length). The organs are in the fully "open" position; the arrows indicate the direction of movement of the ink sac diverticula when they expand for full occlusion of the bacteria-containing tissues of the organ. Hatched areas represent diverticula of the ink sac, and stippled areas are the central portions of the ink sac complex that are covered with silvery tissue.

appear progressively larger, and cells in the transition between ciliated duct and nonciliated crypt epithelium appear massively enlarged (data not shown).

Microscopy of the lens and yellow filters

L-crystallin is the major protein component of the light organ's lens (Montgomery and McFall-Ngai, 1992), a structure that covers the entire ventrum of each lobe but thins near the center where the pore is situated (Figs. 5

and 6). The yellow filters, which are hemispherical, are situated between the lens and the bacteria-containing crypts and to either side of the pore— anterior and posterior (see Fig. 1). The filters, both in histological sections (Fig. 5) and in transmission electron micrographs (data not shown), appear to be composed largely of masses of fibrous cells. The inner core of each filter is formed from a branch of the ciliated duct. The epithelial cells of this inner core stained positively with an antibody raised to L-crystallin, although markedly less strongly than lens tissue, in which the majority of the soluble protein is L-crystallin. These data on the yellow filters indicate that the protein pools of these cells are enriched in either L-crystallin or a closely related (ALDH-like) protein that cross reacts with the L-crystallin polyclonal antibody (Fig. 6).

Late development of aposymbiotic animals

Five aposymbiotic animals, between 14 and 18 d post-hatch and averaging 2.0 mm in mantle length, were examined (Fig. 7). The light organs of all specimens were distinctly bilobed (Fig. 7C), and the ink sac diverticula resembled that of the wild-caught juvenile of 2.8 mm in mantle length (see Fig. 1B); *i.e.*, the lateral and medial diverticula had already begun to form. At this stage in development, the lens was not yet evident. Conspicuous on these aposymbiotic animals (Fig. 7D) were the vestiges of the superficial ciliated epithelial field of cells, which

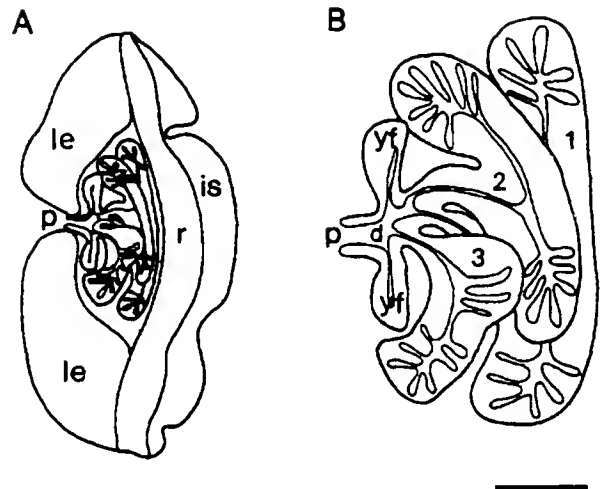


Figure 3. Relationship of the three bacteria-containing crypts (1, 2, and 3) to the ciliated duct (d) and the yellow filters (yf) in the left half of a fully differentiated light organ. (A) Frontal section through the left lobe of the light organ. (B) Enlargement of the crypts, yellow filters, and duct illustrated in (A). Diagrams based on examination of serial frontal sections of the light organ of a squid 8.0 mm in mantle length. is, ink sac; le, lens; p, pore; r, reflector. Bar, 250 μ m.

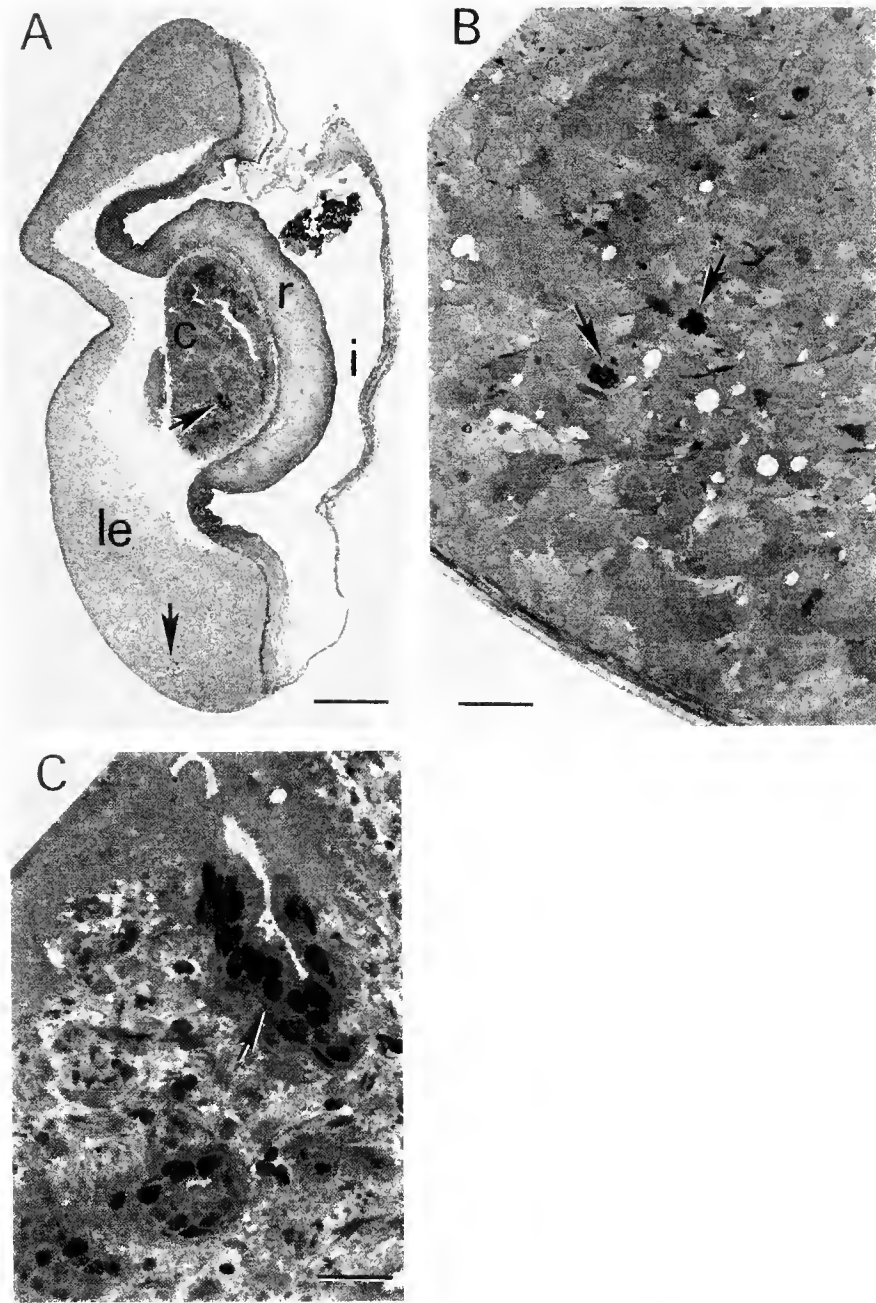


Figure 4. Incorporation of bromodeoxyuridine (BrdU) in a fully differentiated light organ. (A) Low-magnification micrograph of a frontal section through one lobe of a specimen 8.0 mm in mantle length exposed to $10 \mu\text{M}$ BrdU for 5 days. The section was labeled with anti-BrdU; note that the label is localized to cells in the most distal portions of the bacteria-containing crypts [arrow in crypts (c)] and in a few cells scattered throughout the lens [arrow in lens (le)]. The darkly pigmented area at upper right is a portion of the ink sac. Bar, $250 \mu\text{m}$; r, reflector; i, ink sac. (B) The light organ lens at higher magnification; only a few nuclei are labeled in this tissue (arrows). Bar, $25 \mu\text{m}$. (C) Labeled nuclei (arrow) in the distal portion of one of the branches of crypt 3. Bar, $25 \mu\text{m}$.

in normal development and due to a program of bacteria-induced cell death, regresses within 4 d of hatching. Thus, although the change in shape and the elaboration of some

accessory tissues occur in the absence of interaction with the symbionts, normal regression of the superficial ciliated field requires interaction with *V. fischeri*.

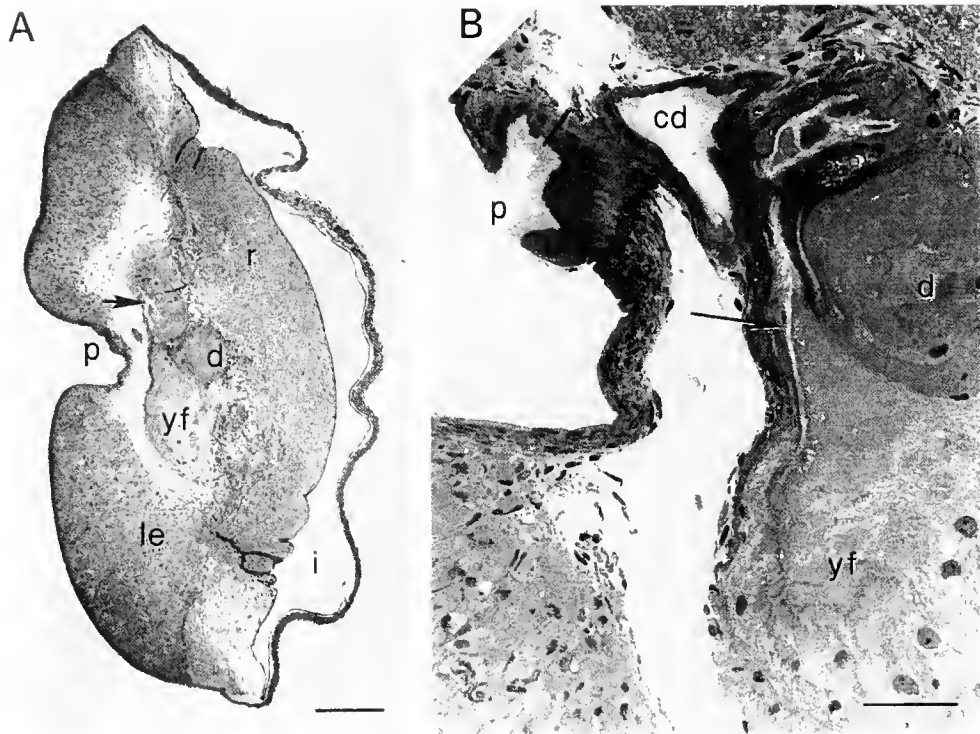


Figure 5. The yellow filters (yf) appear as a fibrous tissue outpocketing from the ciliated duct in these Richardson-stained frontal sections through one lobe of a mature light organ. (A) The posterior filter is shown fully in this section. The arrow indicates the lumen of the ciliated duct leading into the posterior filter. Bar, 250 μm . (B) This section reveals a portion of the ciliated duct (arrow) that leads from the pore region into the posterior filter (for orientation, see Fig. 3B). Bar, 50 μm . cd, ciliated duct; d, duct; le, lens; p, pore; r, reflector.

Discussion

The bacterial light organ of *E. scolopes* progresses through a series of developmental stages that reflect the changing function of the system. Specifically, a morphology associated with inoculation is replaced by a morphology that mediates the mature function of the symbiotic state, *i.e.*, the controlled emission of bacterial luminescence into the host's environment. The results of the present study, and reports from other investigators (Claes and Dunlap, 1998), show that the transition between these stages occurs within the first 2 weeks that follow the initial colonization with symbionts. The maturation program during this period involves significant remodeling of the organ, including (i) changes in shape, (ii) the loss, as well as the addition, of tissue types, and (iii) elaboration of already existing accessory structures (Table 1).

This work, combined with our previous studies of the earlier developmental stages of this symbiosis (McFall-Ngai and Montgomery, 1990; Montgomery and McFall-Ngai, 1993, 1994), enable us now to compare the overall developmental sequence of the squid light organ

with that of the well-described root-nodule symbiosis between leguminous plants and nitrogen-fixing bacteria, or rhizobia (for reviews see Hirsch, 1992; van Rhijn and Vanderleyden, 1995). The legume-rhizobia symbiosis has been studied for over 100 years, and until recently has been the only well-developed experimental system for the analysis of procaryotic-eucaryotic interactions; it has therefore been the system to which many others are compared and contrasted. In both the squid-vibrio and legume-rhizobia symbioses, within hours of the initial interactions of symbiosis-competent bacteria with host tissues (*i.e.*, either the crypt epithelium of hatchling squid light organs or the zone of susceptible root hairs on the legume), morphological changes are triggered both in the cells with which the bacteria directly associate and in remote tissues. Direct cell-cell interactions with *V. fischeri* trigger cell swelling (Montgomery and McFall-Ngai, 1994) and an increase in microvillar density in the crypt epithelium of the host squid (Lamarcq and McFall-Ngai, 1998), whereas rhizobia cause conspicuous root-hair curling. Remotely, an extensive program of apoptosis in the superficial field of host epithelia occurs in response to

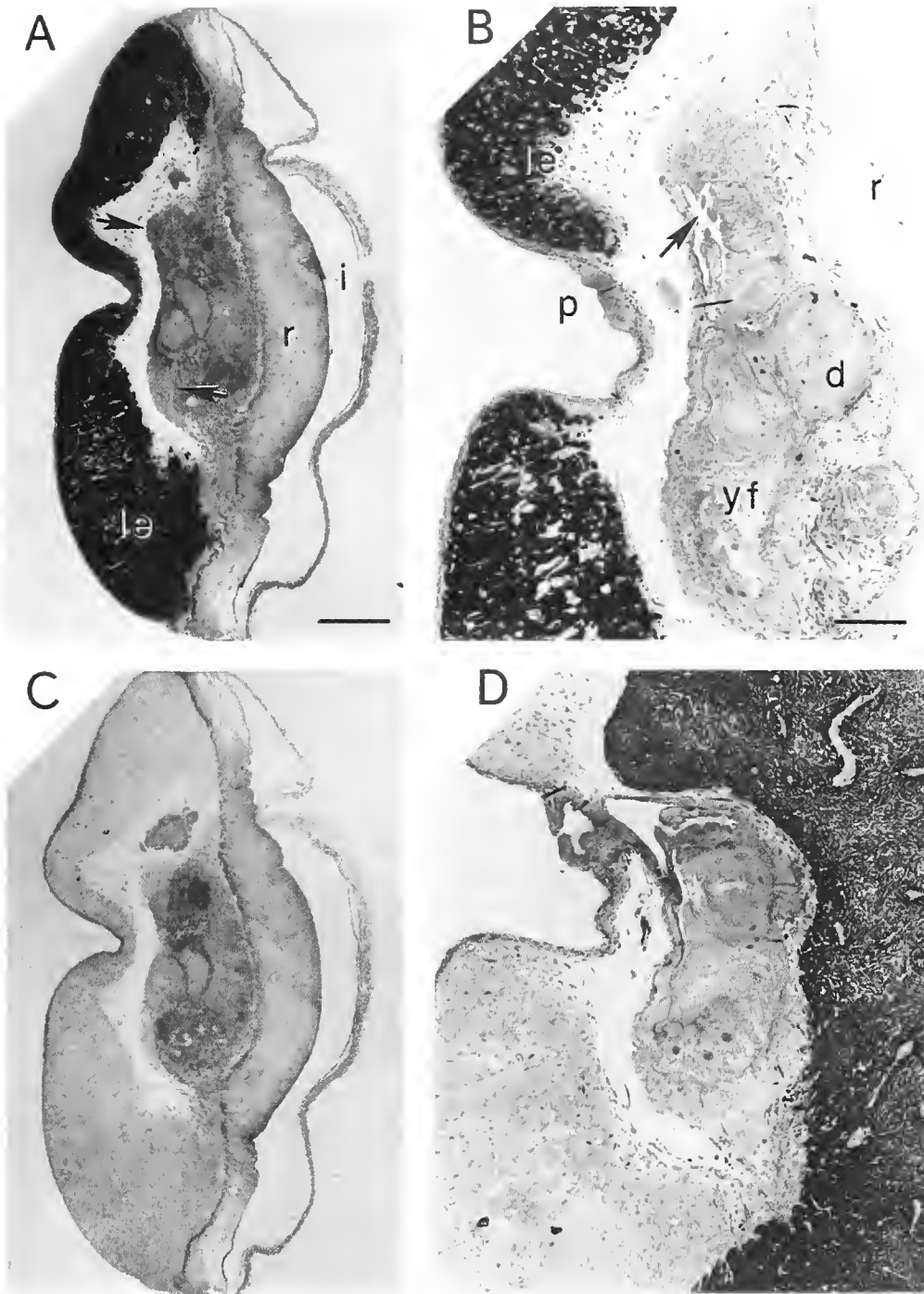


Figure 6. Immunocytochemistry of frontal sections through one lobe of the light organ of *Euprymna scolopes* (8.0 mm in mantle length) revealing production of a light organ lens protein, L-crystallin. (A) Low magnification of a section incubated with antiserum containing L-crystallin antibodies, counterstained with acid fuchsin. The silver granules indicate the high abundance of L-crystallin in the lens (le) (dense black), and the presence of the same or a closely related protein in the yellow filters (arrows), which are stained light gray. The ink in the ink sac has been washed out during fixation. i, ink sac; r, reflector; bar, 250 μ m; anterior at top, ventral at left. (B) Higher magnification of the section in central region of the organ revealing the presence of ALDH-like protein in the posterior yellow filter (yf) and in the portions of the ciliated duct that lead into the yellow filter (arrow); low levels of the protein are also present in the pore (p) and in the portions of the duct (d) that leads to the bacteria-containing crypts. Bar, 100 μ m. (C, D) No silver precipitate is seen in adjacent sections of the same light organ, at the same magnification, incubated with preimmune serum.

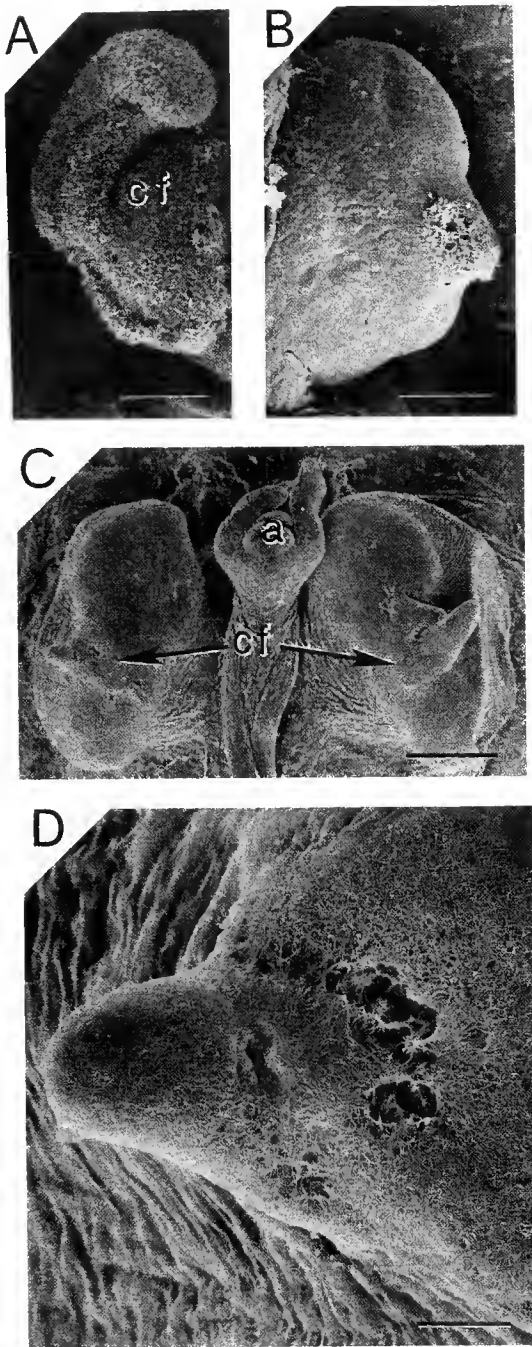


Figure 7. Scanning electron micrographs (ventral views) illustrating the developmental changes in the light organ that are independent of, or dependent upon, interactions with *Vibrio fischeri* (A) One half of the hatchling light organ showing the complex ciliated field (cf) on the lateral face of the ovoid organ. Bar, 50 μ m. (B) One half of a 4-d-old symbiotic animal showing the nearly complete regression of the ciliated field. Bar, 50 μ m. (C) Whole light organ of a 15-d-old aposymbiotic animal showing the bilobed shape of the organ and the retention of vestiges of the ciliated field (cf). a, anus; bar, 200 μ m. (D) Higher magnification of the left side of (C) showing dense cilia on the lateral surface of the organ. Bar, 25 μ m.

interactions with *V. fischeri* (Montgomery and McFall-Ngai, 1994; Foster and McFall-Ngai, 1998), whereas the signals from rhizobia induce cell division deep in the root cortex (Fisher and Long, 1992; Niner and Hirsch, 1998). However, clear differences in the later developmental patterns in these two types of symbiosis are also evident. Whereas bacterial bioluminescence—the principal contribution of the microbial symbiont—is induced in the squid light organ within 8 to 10 hours after inoculation (McFall-Ngai and Ruby, 1991), nitrogen fixation by rhizobia does not occur at maximal levels in the root nodule for days to weeks. In addition, the squid light organ continues to grow throughout the life history of the host, and the bacterial symbionts continue to divide. In the legume-rhizobia symbioses, the active host cells of the root nodule have a finite lifetime, and the intracellular bacteria within the nodule form bacteroids, which represents a terminal differentiation of these cells (Hirsch, 1992).

A further critical difference between these symbioses is that the developmental program of the squid light organ is less reliant on bacterial signals. In the root nodule associations, reciprocal induction of gene expression by the partners is essential for all phases of nodule morphogenesis and maturation (Niner and Hirsch, 1998); *i.e.*, an already existing, functional root hair and root cortex are recruited and transformed into the nitrogen-fixing nodule as a direct result of interaction with rhizobia or their secreted gene products. In contrast, previous studies of the patterns of early development in the squid-vibrio relationship, and the results presented here on late development in this system, indicate that only some stages of development require interaction with *V. fischeri*. During embryogenesis, in the absence of bacteria, tissues are developed that are destined to have no other function than to serve as the future symbiotic light organ. Subsequently, the early posthatch morphogenetic changes, such as apoptotic loss of the ciliated field (Montgomery and McFall-Ngai, 1994) and change in microvillar density of symbiont-associated cells (Lamareq and McFall-Ngai, 1998), have an absolute requirement for interactions with symbiotically competent *V. fischeri*. However, even in the absence of symbionts, the light organ of aposymbiotic animals converts from a rounded to a bilobed shape and elaborates the accessory structures of the organ. This result shows that these aspects of later development are genetically “hard wired”; that is, they do not depend on an inductive interaction with the symbionts.

The differences between the squid-vibrio and the legume-rhizobia symbioses in their requirements for bacterial induction during development may reflect a very basic difference in the nature of these associations. The squid-vibrio symbiosis appears to be obligate throughout the life history of the host; examination of several hundred

Table 1

Postembryonic development of the *Euprymna scolopes* light organ

Light organ feature	Newly hatched (≈ 1.6 mm ML)	Symbiotic (≈ 2.8 mm ML)	Development under <i>V. fischeri</i> induction*	Reference
<i>Early development (hatching through day 4)</i>				
ciliated surface epithelium	present	absent	yes	Montgomery and McFall-Ngai (1994)
microvilli of crypt epithelium	sparse	dense	yes	Lamarcq and McFall-Ngai (1998)
crypt epithelial cell shape	columnar	cuboidal	yes	Montgomery and McFall-Ngai (1994)
<i>Late development (end of week 2 onward)</i>				
light organ shape	ovoid	bilobed	no	This study
ink sac diverticula	anterior/posterior	anterior/posterior + paired medial/lateral	no	This study
lens	absent	present	no	Claes and Dunlap (1998)
crypts	sacculate	branching	no	Claes and Dunlap (1998)
yellow filters	absent	present	n.d.	This study

*n.d. = not determined.

field-caught animals of all ages has revealed that *E. scolopes* always has a functioning bacterial light organ (McFall-Ngai, pers. obs.). Because a symbiosis is always present in this species, we would expect portions of the developmental program to be independent of symbiont induction. In contrast, nodules form in legumes only when soil nitrogen is limiting (van Rhijn and Vanderleyden, 1995). Thus, the developmental program of the legume root has not incorporated nodule formation into its basic pattern, but only the genetic ability to respond and develop nodules under particular environmental conditions.

The coordinated late development of the accessory structures of the squid light organ, including the lens, reflector, and ink sac diverticula, reflects both the accommodation of these tissues to the changing size and shape of the organ and their function in the modulation of bacterial luminescence. However, the role of the yellow filters, which also arise later in development, is not as clear. Such filters are common in bioluminescence systems, and it has been suggested that they serve to shift the wavelength maximum of the emitted luminescence so that it more closely matches the spectral quality of environmental light (Denton *et al.*, 1985; McFall-Ngai, 1990). The notion that the yellow filters of the squid system function in this way is supported by some evidence. The wavelength maximum of *V. fischeri* luminescence is typically 489 nm (Eley *et al.*, 1970), and if the yellow filters of the *E. scolopes* light organ do shift the wavelength of bacterial light emission toward the red, then the luminescence emitted would more closely match the spectrum of downwelling moonlight, as well as the maximum absorp-

tion wavelength of the visual pigment of *E. scolopes*, which is 500–507 nm (F. Crescitelli, unpubl. data).

Although all recognized, late developmental events in the squid-vibrio association appear to be independent of symbiont induction, some of the bacteria-induced signaling of biochemical changes in the light organ that occur in early development are likely to require sustained interaction with the bacterial symbionts. For example, the requirement for continued interaction with bacterial symbionts to maintain the increase in microvillar density of the crypt epithelia has already been described (Lamarcq and McFall-Ngai, 1998). Taking advantage of the ability to eliminate the symbiont population from the light organ by treatment with antibiotics (Doino and McFall-Ngai, 1995), a comparison of the biochemistry of the light organ in cured and uncured adults should reveal the extent to which the composition of the internal environment of the host cells relies on the presence of the bacteria with which they directly interact.

The results obtained on late developmental patterns in the squid-vibrio association have demonstrated that the period during which bacteria induce developmental events is restricted to the first hours to days following inoculation. Studies of the bacterial symbiont have revealed that this is also the period during which *V. fischeri* displays dramatic genetic and morphological changes as it transforms from a free-living member of the bacterioplankton to a resident of the light organ (Ruby, 1996). Taken together, these findings indicate that the first hours to days of this symbiosis will continue to be the most fruitful period for discovering the biochemical and molec-

ular bases of the reciprocal dialogue that occurs between the partners of this symbiosis.

Acknowledgments

We thank S. Nyholm and E. G. Ruby for helpful comments on the manuscript. This work was supported by grant #IBN 9601155 from the National Science Foundation (to M. M.-N. and E. G. Ruby) and by grant #NIH ROI-RR12294-02 to E. G. Ruby and M. M.-N., and the ARCS Foundation (to M. K. M.). We thank P. Lee and L. Walsh of the National Resource Center for Cephalopods (NRCC) for providing specimens for this study. The cultured *Euprymna scolopes* specimens were provided by the NRCC, Galveston, TX, by the NIH's National Center For Research Resources through grant #RR01024 and a matching grant from the Texas Institute of Oceanography.

Literature Cited

- Buchner, P. 1965.** Symbiosis in luminous animals. Pp. 543–571 in *Endosymbiosis of Animals with Plant Microorganisms*. P. Buchner, ed. Interscience Publishers, New York.
- Claes, M. F., and P. V. Dunlap. 1998.** Involvement of *Vibrio fischeri* in light organ tissue development in the sepiolid squid *Euprymna scolopes*. *Abstr. Annu. Mtg. Am. Soc. Microbiol.* **98**: 373.
- Denton, E. J., P. J. Herring, E. A. Widder, M. A. Latz, and J. F. Case. 1985.** The roles of filters in the photophores of oceanic animals and their relation to vision in the oceanic environment. *Proc. R. Soc. Lond. B* **225**: 63–97.
- Doino, J. A., and M. J. McFall-Ngai. 1995.** A transient exposure to symbiosis-competent bacteria induces light organ morphogenesis in the host squid. *Biol. Bull.* **189**: 347–355.
- Douglas, A. E. 1989.** Mycetocyte symbiosis in insects. *Biol. Rev. Camb. Philos. Soc.* **64**: 409–434.
- Eley, M., J. Lee, J.-M. Lhoste, C. Y. Lee, M. J. Cormier, and P. Hemmerich. 1970.** Bacterial bioluminescence: comparison of bioluminescence emission spectra, the fluorescence of luciferase reaction mixtures and the fluorescence of flavin cations. *Biochem.* **9**: 2902–2908.
- Fisher, R. F., and S. R. Long. 1992.** *Rhizobium*-plant signal exchange. *Nature* **357**: 655–660.
- Flint, H. J. 1997.** The rumen microbial ecosystem—some recent developments. *Trends Microbiol.* **5**: 483–488.
- Foster, J. S., and M. J. McFall-Ngai. 1998.** Induction of apoptosis by cooperative bacteria in the morphogenesis of host epithelial tissues. *Develop. Genes Evol.* **208**: 295–303.
- Haygood, M. 1993.** Light organ symbioses in fishes. *Crit. Rev. Microbiol.* **19**: 191–216.
- Herring, P. J. 1978.** *Bioluminescence in Action*. Academic Press, London.
- Hirsch, A. M. 1992.** Developmental biology of legume nodulations. *New Phytol.* **122**: 211–237.
- Jones, M. L., and S. L. Gardiner. 1988.** Evidence for a transient digestive tract in Vestimentifera. *Proc. Biol. Soc. Wash.* **11**: 423–433.
- Lamarcq, L. H., and M. J. McFall-Ngai. 1998.** Induction of a gradual, reversible morphogenesis of its host's epithelial brush border by *Vibrio fischeri*. *Infect. Immun.* **66**: 777–785.
- McFall-Ngai, M. J. 1990.** Crystallization in the pelagic environment. *Am. Zool.* **30**: 175–188.
- McFall-Ngai, M., and M. K. Montgomery. 1990.** The anatomy and morphology of the adult bacterial light organ of *Euprymna scolopes* Berry (Cephalopoda: Sepiolidae). *Biol. Bull.* **179**: 332–339.
- McFall-Ngai, M., and E. G. Ruby. 1991.** Symbiont recognition and subsequent morphogenesis as early events in an animal-bacterial mutualism. *Science* **254**: 1491–1494.
- McFall-Ngai, M., and E. G. Ruby. 1998.** Sepioids and vibrios: When first they meet. *Bioscience* **48**: 257–265.
- Migheli, A., C. Mocellini, and M. T. Giordana. 1991.** Ultrastructural detection of DNA-incorporated bromodeoxyuridine in resin embedded brain tissue. *Histochemistry* **95**: 491–494.
- Montgomery, M. K., and M. McFall-Ngai. 1992.** The muscle-derived lens of a squid bioluminescent organ is biochemically convergent with the ocular lens. Evidence for recruitment of aldehyde dehydrogenase as a predominant structural protein. *J. Biol. Chem.* **267**: 20999–21003.
- Montgomery, M. K., and M. McFall-Ngai. 1993.** Embryonic development of the light organ of the sepiolid squid *Euprymna scolopes* Berry. *Biol. Bull.* **184**: 296–308.
- Montgomery, M. K., and M. McFall-Ngai. 1994.** Bacterial symbionts induce host organ morphogenesis during early postembryonic development of the squid *Euprymna scolopes*. *Development* **120**: 1719–1729.
- Moynihan, M. 1983.** Notes on the behavior of *Euprymna scolopes* (Cephalopoda: Sepiolidae). *Behaviour* **85**: 25–41.
- Niner, B. M., and A. M. Hirsch. 1998.** How many rhizobium genes, in addition to the *nod*, *nif* and *exo*, are needed for nodule development and function? *Symbiosis* **24**: 51–102.
- Ruby, E. G. 1996.** Lessons from a cooperative, bacterial-animal association: The *Vibrio fischeri*-*Euprymna scolopes* light organ symbiosis. *Annu. Rev. Microbiol.* **50**: 591–624.
- van Rhijn, P., and J. Vanderleyden. 1995.** The *Rhizobium*-plant symbiosis. *Microbiol. Rev.* **59**: 124–142.
- Weis, V. M., M. K. Montgomery, and M. J. McFall-Ngai. 1993.** Enhanced production of ALDH-like protein in the bacterial light organ of the sepiolid squid *Euprymna scolopes*. *Biol. Bull.* **184**: 309–321.

Transparency and Visibility of Gelatinous Zooplankton from the Northwestern Atlantic and Gulf of Mexico

SÖNKE JOHNSEN AND EDITH A. WIDDER

*Marine Science Division, Harbor Branch Oceanographic Institution,
5600 US 1 North, Ft. Pierce, Florida 34946*

Abstract. Transparency measurements (at 400 to 700 nm) were made on living specimens of 29 common species of gelatinous zooplankton from the Northwestern Atlantic Ocean and Gulf of Mexico. Percent transparency ranged from 91% for the hydromedusa *Sibogota tya* to 0.51% for the pteropod *Clione limacina*. Percent transparency was linearly and positively correlated with wavelength, with slopes of the regression lines (normalized to the percent transparency at 480 nm) ranging from 0.027%/nm for *Sibogota tya* to 0.51%/nm for the ctenophore *Mnemiopsis macrydi* (average $0.17 \pm 0.019\%/nm$). There was no significant correlation between the percent transparency of an animal and its daytime depth distribution. The relationship between percent transparency and sighting distance when viewed from below was modeled and showed that, due to the increase of the minimum contrast threshold for object detection at lower light levels, the usefulness of transparency as camouflage increases dramatically with depth. A preliminary account of these results was presented by the authors at the fourteenth meeting of the Ocean Optics Society in November 1998.

Introduction

Transparency is an important, but understudied, characteristic of many oceanic zooplankton. A large percentage of oceanic zooplankton are transparent, some achieving almost complete invisibility (Davis, 1955; Hardy, 1956; McFall-Ngai, 1990), and it is generally assumed that transparency is an important method of camouflage from visual predators

and prey in the optically featureless open-ocean environment, particularly in the euphotic region (reviewed in McFall-Ngai, 1990; Hamner, 1996). Indeed, it is difficult to explain the prevalence of transparency in epipelagic and mesopelagic environments and its relative rarity in bathypelagic and coastal environments (McFall-Ngai, 1990) without assuming that it functions as a form of camouflage. Some degree of transparency is found in almost all oceanic zooplankton that are not camouflaged by small size or mirrored surfaces, or protected by fast swimming speeds or chemical defenses. Although these transparent, mostly gelatinous animals are poorly represented in trawls, research using blue-water diving and submersibles has shown they are extremely diverse and abundant (Hamner *et al.*, 1975). However, despite the prevalence and presumed ecological importance of transparency, little work has been done in this area (McFall-Ngai, 1990). In particular, few measurements of the degree of transparency of these animals have been made (Greze, 1963, 1964; Chapman, 1976a, b). This information could help answer several important questions related to the ecological function and importance of transparency. What is the relationship between percent transparency and wavelength? Are animals in shallow water more or less transparent than animals at depth? For a given visual system, what is the maximum distance at which various transparent animals are still detectable?

In this study, 29 species of oceanic zooplankton from seven phyla (Cnidaria, Ctenophora, Annelida, Mollusca, Crustacea, Chaetognatha, and Chordata) were collected from six sites in the Northwestern Atlantic Ocean and Gulf of Mexico. The degree of transparency of various tissues of the animals from different depths was measured at wavelengths ranging from 400 to 700 nm. In addition, the relationship between an animal's degree of transparency and its sighting distance when viewed from below was modeled.

A preliminary account of these experiments was presented at the fourteenth meeting of the ocean optic society in November 1998 (Johnsen and Widder, in press).

Materials and Methods

Source of animals and description of tissues examined

Animals were obtained from the following six locations: Georges Bank; Oceanographer Canyon (on the southern edge of Georges Bank); Tongue of the Ocean (Bahamas); eastern Gulf of Mexico; Panacea, Florida; and Woods Hole, Massachusetts. Animals from the first four locations were obtained during cruises of the RVs *Oceanus* (April 1998), *Edwin Link* (September 1997), *Seward Johnson* (February 1998), and *Pelican* (June 1998) respectively. The animals obtained from Georges Bank were collected using a MOCNESS net system (five nets, 10-m² opening, 3-mm mesh). About half the animals obtained from Oceanographer Canyon were collected at depth using the *Johnson Sea-Link* (JSL) research submersible. These animals were captured in 1-liter clear acrylic cylinders with hydraulically activated, sliding lids. The remaining animals from Oceanographer Canyon were collected using an opening/closing Tucker trawl (4.3-m² opening, 1/4-inch knotless nylon mesh) fitted with a thermally insulated collecting container that could be closed at depth. The animals collected from Tongue of the Ocean were caught in a surface plankton net (0.2-m² opening, 335- μ m mesh). Animals from the eastern Gulf of Mexico were collected either with the above-mentioned Tucker trawl or in jars by divers using blue-water diving techniques (Hamner, 1975). Animals from Panacea and Woods Hole were obtained from Gulf Specimen Marine Supply Inc. and the Aquatic Resources Division at The Marine Biological Laboratory respectively. Table 1 lists the animals collected, their dimensions, and their source and method of collection. The table also lists the conditions of the animals at the times of measurement. Animals listed as "good" were intact and mobile and appeared healthy. Animals listed as "unknown" appeared to be healthy and intact but showed no movement (one of these, *Pyrosoma atlanticum*, generally makes no easily observable movements). Animals collected on cruises were measured within an hour of collection. Animals obtained from the two marine specimen supply companies were measured upon arrival.

Several animals had large regions of obviously different transparency. Therefore, several tissues were measured from these animals. Mesoglea measurements were taken through portions of mesoglea that had no other visible structure. Comb-row measurements in ctenophores were taken through portions of the mesoglea containing one comb row. Lobe measurements in *Bolinopsis infundibulum* were taken through the mesoglea and one of the large oral lobes. Siphosome measurements in *Agalma*

okeni were taken through the siphosome of the animal. Center measurements in *Bathocyroe fosteri* were taken through the translucent region surrounding the gut. Canal measurements in *Sibogita tupa* were taken through the mesoglea and a number of the radial canals. Body measurements were taken through the thickest unpigmented portion of the body. All measurements were taken along an axis perpendicular to the longest axis of the animal. Therefore, ctenophores were measured perpendicular to the oral-aboral axis; hydromeduse were measured perpendicular to the plane of the bell; molluscs, tunicates, crustaceans, and annelids were measured perpendicular to the anterior-posterior axis; etc.

Apparatus and procedure for measurement of transparency

Transparency was measured with an apparatus (Fig. 1) similar to those used for measuring the wavelength dependence of light transmission in human lenses and corneas (Farrell *et al.*, 1973). The light source was a stabilized tungsten halogen source (LSI, Ocean Optics Inc.) coupled to a 1-mm fiber optic and a 200- μ m precision pinhole. The beam was collimated with an achromatic triplet lens and reduced to a diameter of 3 mm with an iris diaphragm. The beam passed through the specimen (held in a glass cuvette) and was focused by an achromatic lens onto a fiber-optic cable (diameter 2 mm) coupled to the detector of an optical multichannel analyzer (OMA-detector model 1420, detector interface model 1461, EG&G Princeton Applied Research). The detector was wavelength calibrated using a low-pressure mercury spectrum lamp (Model 6047, Oriel Inc.). For further details on the theory of operation and calibration of the OMA detector, see Widder *et al.* (1983). Due to space restrictions on the RVs *Oceanus* and *Pelican*, the OMA was replaced with a more compact multichannel spectrometer (PS1000, Ocean Optics Inc.). An iris diaphragm was placed in front of the collection optics to limit the angle of acceptance of scattered light from the sample. The diaphragm was set at a diameter of 3.5 mm, the minimum aperture required to pass the complete uninterrupted beam. Since the base of the sample was 0.07 m from the collection aperture, the detector received forward-scattered light within a cone of half-angle of 1.05° (angle equals arctan (r/d), where r is the radius of the aperture and d is the distance from the sample to the aperture. Angle is corrected for refraction at the air-water surface in the cuvette). Because the collection optics must always have a finite aperture, the detector always collects forward-scattered light in addition to directly transmitted light. There is no standard aperture angle for measuring transmitted light, though a half-angle of approximately 1° is common (Mertens, 1970; Farrell *et al.*, 1973). The angle used was the minimum possible given the problems caused by ship motion. The entire apparatus was placed in a dark room on the ship to eliminate stray light.

Table I

Dimensions, source, and condition of the animals used for transparency measurements

Animal	Specimens (no.)	Optical thickness (mm)	Length* (mm)	Collection		Condition
				Site†	Method‡	
Cnidaria						
<i>Agalma okeni</i> §	8	16 ± 1.2	42 ± 2.5	OC/EGM	T	good/unknown
<i>Athorybia rosacea</i>	1	10	11	EGM	D	good
<i>Cyclocamma welshii</i>	1	15	50	OC	S	good
<i>Halistemma cupulifera</i> §	3	8 ± 0.58	42 ± 1.7	EGM	T	good/unknown
<i>Nemopsis bachei</i>	4	7.3 ± 0.25	7.3 ± 0.25	PFL		good
<i>Orchistoma pileus</i>	4	18 ± 1.7	29 ± 3.3	EGM	D	good
<i>Physophora hydrostatica</i>	1	29	45	GB	T	good
<i>Sibogita typa</i>	1	24	24	OC	T	unknown
Ctenophora						
<i>Bathocyroe fosteri</i>	2	24 ± 4.0	38 ± 2.5	OC	S	good
<i>Beroe cucumis</i>	4	10 ± 0.0	14 ± 0.0	GB	T	good
<i>Bolinopsis infundibulum</i>	2	22 ± 2.0	83 ± 2.5	OC	S	good
<i>Horniphora</i> sp.	3	17 ± 1.3	35 ± 6.7	EGM	T	good
<i>Mnemiopsis macrydi</i>	11	13 ± 1.0	25 ± 1.3	PFL		good
<i>Ocyropsis maculata</i>	1	10	30	TO	T	good
<i>Pleurobrachia bachei</i>	10	16 ± 0.63	18 ± 0.55	WH		good
Annelida						
<i>Tamopteris</i> sp.	2	3.0 ± 1.0	30 ± 9.5	GB	T	good
Mollusca						
<i>Carinaria lamarcki</i>	4	11 ± 0.88	43 ± 1.7	EGM	T/D	good
<i>Clinoe limacina</i>	1	4	23	OC	T	good
<i>Corolla spectabilis</i>	5	39 ± 6.4	13 ± 2.9	OC/EGM	S/D	good
<i>Phylliroe atlantica</i>	4	1.9 ± 0.13	25 ± 2.0	EGM	D	good
<i>Pterotrachea coronata</i>	4	8.0 ± 1.2	85 ± 4.6	OC/EGM	S/D/T	good
Crustacea						
<i>Cystosoma cystosoma</i>	2	7.5 ± 0.50	53 ± 6.5	EGM	T	good
Chaetognatha						
<i>Sagitta hexaptera</i>	8	3 ± 0.19	45 ± 2.5	GB	T	good/unknown
<i>Sagitta maxima</i>	1	4	55	OC	T	good
Chordata						
<i>Cyclosalpa affinis</i> #	1	35	33	EGM	D	good
<i>Pegea confederata</i>	4	20 ± 0.48	39 ± 1.9	TO	T	good
<i>Pyrosoma atlanticum</i>	5	10 ± 1.2	32 ± 4.9	OC/EGM	T/D	unknown
<i>Salpa cylindrica</i>	8	16 ± 0.90	38 ± 1.5	EGM	D	good
<i>Salpa maxima</i>	1	13	30	TO	T	good

* Measured along the axis of greatest length.

† OC, Oceanographer Canyon; GB, Georges Bank; EGM, Eastern Gulf of Mexico; PFL, Panacea, FL; WH, Woods Hole; TO, Tongue of the Ocean.

‡ T, trawl; S, submersible; D, scuba diving.

§ *Agalma* and *Halistemma* (physonect siphonophores) lacked several nectophores and bracts, but still exhibited movement and high transparency.# The salp *Cyclosalpa affinis* is an aggregate of seven individuals.

Each animal to be measured was placed in an appropriately sized cuvette. The water level in the cuvette was slightly greater (<2 mm) than the thickness of the animal. A reference measurement of the water was taken, followed by 4–10 (usually 5) measurements of a given tissue of the animal. Each measurement consisted of 3000 consecutive 0.1-s exposures. The exposures were averaged to reduce noise due to ship motion and other sources. The animal was moved slightly between measurements to get an average value for the tissue measured. Transmission values were calculated by dividing the intensity of the beam after it passed through the

tissue by the intensity of the reference beam (that had passed through an equivalent distance of water). Although both the OMA and PS1000 detectors were calibrated from 350 to 700 nm, the values from 350 to 400 nm were unreliable due to the small output of the tungsten light source in this region. Therefore, only values from 400 to 700 nm are discussed.

The repeatability of the measurements was confirmed by measuring the transmission of a sample of water 15 times and then calculating the standard error. The standard error ranged from 1.00% of the mean value at 700 nm to 1.25% of the mean value at 400 nm.

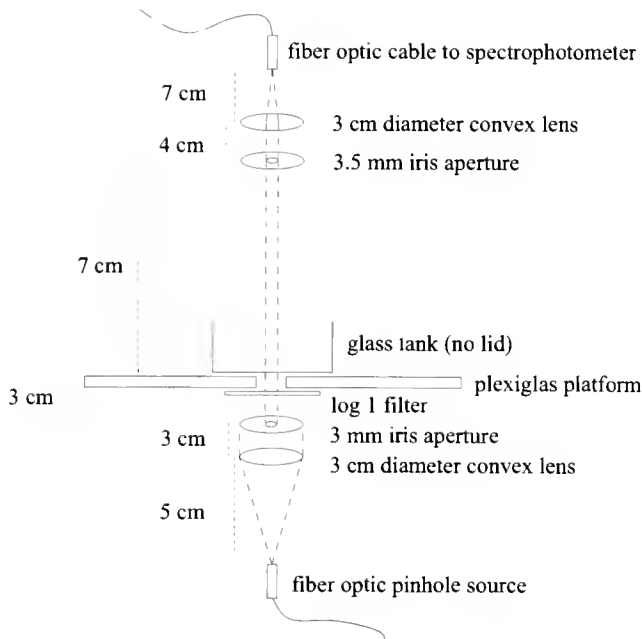


Figure 1. Diagram of the apparatus used to measure transparency.

Calculating the effect of tissue transmission spectra on the spectrum of downwelling light

Unless the percent transmission of a tissue is constant with respect to wavelength, the tissue will have an effect on the spectrum of the downwelling light that passes through it. In general, percent transparency was positively and linearly proportional to wavelength (see *Results*). Hereafter, the slope of the regression of percent transparency on wavelength is referred to as the T-W slope. The alteration of the spectrum of downwelling light after passing through materials with different T-W slopes was calculated. The downwelling spectrum was taken in Oceanographer Canyon at 260 m and 60 m, using the PS1000 multichannel spectrometer. These two depths were chosen because they represent a near-surface and an asymptotic light field. An underwater light field is referred to as asymptotic when the position of the sun has no effect on the light field's spatial characteristics (Jerlov, 1976). Light was transmitted to the PS1000, operated from the back dive chamber of the JSL submersible, via a 1-mm fiberoptic through-hull penetrator. To calculate the effects of tissues with different T-W slopes on the downwelling light spectrum, a spectrum with a given slope was multiplied by the measured downwelling light spectrum and the resultant spectrum was divided by its peak value. To factor out the absolute value of the T-W slope, the slopes used were normalized by percent transmission at 480 nm. Therefore, a normalized T-W slope of 1%/nm describes a linear transmission spectrum that has a value 1% greater than the percent transmission at 480 nm for every nanometer greater than 480 (e.g., if $T_{480} = 30\%$, $T_{490} = 30\% + [10 \times (1\% \times 30\%)] = 33\%$).

Modeling of relationship between percent transparency and sighting distance

The visibility of an object depends upon its contrast with the background. Contrast is defined as $(L_o - L_b)/L_b$, where L_o is the radiance of the background (Mertens, 1970; Jerlov, 1976). Contrast values range from -1 to ∞ . An object of zero radiance on a luminous background has a contrast value of -1 . A luminous object on a background of zero radiance (e.g., a bioluminescent source in the deep ocean) has a contrast value of ∞ . An object whose radiance matches the radiance of the background has a contrast value of zero. In the asymptotic light field that most of the collected animals commonly inhabit, the upward and horizontal radiances are only a small fraction of the downward radiance (ca. 0.5% and 3% respectively), and downward irradiance approximates vertical downward radiance (Denton, 1990). Therefore, animals are most visible when viewed from below. Since $(L_o - L_b)/L_b = L_o/L_b - 1$, and $L_o/L_b = T/100$ (where T is the percent transparency of a given object), the contrast of an animal viewed from below ranges from 0 to -1 and is equal to $T/100 - 1$.

The absolute value of contrast decreases exponentially with distance. When viewed from below, the attenuation coefficient (of contrast) is equal to the beam attenuation coefficient minus the diffuse attenuation coefficient of the water (Mertens, 1970; Jerlov, 1976); i.e.,

$$C = C_o \times e^{-(c-K)d}, \quad (\text{Equation 1})$$

where C is the apparent contrast at distance d , C_o is the inherent contrast of the viewed object (contrast at zero distance, $C_o = T/100 - 1$) of the object, and c and K are the beam and diffuse attenuation coefficients of the water. One can determine the maximum distance at which an object is still detectable by setting C equal to C_{\min} (the minimum contrast threshold for object detection for a given visual system) and solving equation (1) for d . This gives

$$\begin{aligned} d &= \ln(C_{\min}/C_o)/(c - K) \\ &= \ln(C_{\min}/(T/100 - 1))/(c - K). \end{aligned} \quad (\text{Equation 2})$$

The sighting range, d_{opaque} , of an opaque object ($T = 0$) is

$$\begin{aligned} d_{\text{opaque}} &= \ln(C_{\min}/(0/100 - 1))/(c - K) \\ &= \ln(-C_{\min})/(c - K). \end{aligned} \quad (\text{Equation 3})$$

By dividing equation (2) by equation (3), one can factor out the two attenuation coefficients and express the sighting distance as a fraction of the sighting distance of an opaque object of the same size and shape in the same water and light field. This gives

$$d/d_{\text{opaque}} = \ln(C_{\min}/(T/100 - 1))/\ln(-C_{\min}).$$

This ratio gives an estimate of the advantage of a given percent transparency over opacity for a prey item attempting to hide from a visual predator with a given

minimum contrast threshold (the argument, of course, is identical for a predator attempting to hide from a visual prey item). A ratio of zero implies that the object cannot be seen at any distance and can only be detected by nonvisual means. A ratio near one implies that the object is detected at a distance only slightly less than that at which an opaque object of the same size is detected and therefore gains only a slight advantage by being transparent. The ratio d/d_{opaque} as a function of T was calculated for C_{min} values of -0.005 (best value reported for fish), -0.02 (human underwater vision), -0.1 , -0.2 , -0.5 (cod vision at 650 m), and -0.75 (Douglas and Hawryshyn, 1990).

Results

Percent transparency values

Figure 2 shows three typical traces of percent transparency vs. wavelength. Table II is a summary of measured percent transparency values. In general, percent transparency was linearly and positively proportional to wavelength. The slopes of the linear regressions of transparency on wavelength (normalized by dividing by the percent transparency at 480 nm) ranged from $0.027\%/nm$ to $0.51\%/nm$ (average $0.17 \pm 0.019\%/nm$), with most r^2 values approaching unity. The slopes in all animals were significantly different from zero ($P < 0.0005$). The most transparent tissues (at 480 nm) were hydromedusa mesoglea (66%), followed by *Cystosoma* (42%), ctenophore mesoglea (41%), siphonophore mesoglea (39%), pelagic tunicates (excluding *Pyrosoma*) (33%), *Sagitta* (24%), and the translucent portions of the hydromedusae and ctenophores (24%). The least transparent tissues were from the pelagic gastropods (excluding *Clione*) (17%)

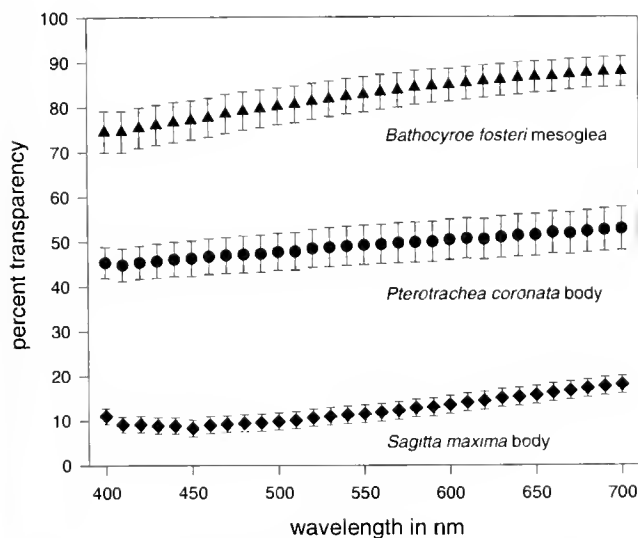


Figure 2. Percent transparency vs. wavelength for individual specimens of *Bathocyroe fosteri*, *Pterotrachea coronata*, and *Sagitta maxima*. The error bars denote standard deviation of the mean.

and *Tomopteris* (9.1%). *P. atlanticum* and *C. limacina* were essentially opaque, with percent transparencies of 1.6% and 0.51% respectively.

Transmission values vs. depth

Because the optical properties of the collecting sites differed greatly and the largest variety of animals was collected from Oceanographer Canyon, data from animals collected at that site were used to evaluate the relationship between the percent transparency (of the major tissue in the animal) and its average daytime depth (Fig. 3). No significant relationship was found ($r = 0.39$, $n = 11$, $P > 0.2$). Highly transparent animals were found at all depths, and nearly opaque animals were found at all depths.

Effect of tissue transmission spectra on the spectrum of downwelling light

The spectrum of downwelling light and the altered spectra after passing through tissues with linear relationships between percent transparency and wavelength with normalized slopes of 0.5%, 2%, 5%, and 10%/nm was analyzed for two depths in Oceanographer Canyon. At 260 m the peak wavelength shifts from 489.5 nm to 489.5, 492.0, 492.5, and 495.0 (Fig. 4a). At 60 m the peak wavelength shifts from 489.5 nm to 492.5, 494.0, 498.0, and 505.0 (Fig. 4b).

Relationship between percent transparency and sighting distance

Figure 5 shows the ratio of sighting distance of a transparent object to sighting distance of an opaque object vs. percent transparency of the transparent object for visual systems with different minimum contrast thresholds. For predators with a low minimum contrast threshold, the sighting distance decreases slowly until high transparency values are reached, after which it decreases rapidly. For high absolute minimum contrast thresholds, the sighting distance decreases rapidly and linearly with increasing transparency. At percent transparencies higher than $100 \times (1 - C_{\text{min}})$, the sighting distance is zero and the tissue is essentially invisible.

Discussion

Transparency and predator/prey relationships among gelatinous zooplankton

Although the effects of prey transparency on visually mediated predation have often been examined in freshwater systems (Zaret and Kerfoot, 1975; Greene, 1983; reviewed in McFall-Ngai, 1990), less work has been done in marine systems (McFall-Ngai, 1990). In addition, the effects of predator transparency on successful capture of visually oriented prey are largely unexplored (Purcell,

Table II

Transparency values (percent transparency: T_λ , at wavelength λ) measured at three wavelengths (λ) for animals and tissues; values are given as mean \pm standard deviation of the mean

Animal	Tissue	n	T_λ			Regression parameters*	
			$\lambda = 400$	$\lambda = 480$	$\lambda = 700$	$\frac{dT/d\lambda}{T_{480}}$	r^2
Cnidaria							
<i>A. okeni</i>	mesoglea	8	40 \pm 4.0	48 \pm 4.1	56 \pm 4.8	0.11	0.95
	siphosome	1 (4)	3.7 \pm 1.4	3.9 \pm 1.4	4.5 \pm 1.4	0.15	0.99
<i>A. rosacea</i>	mesoglea	1 (5)	47 \pm 7.1	53 \pm 8.1	59 \pm 9.7	0.068	0.94
<i>C. welshi</i>	mesoglea	1 (5)	55 \pm 7.2	64 \pm 7.0	80 \pm 8.7	0.13	0.98
<i>H. cupulifera</i>	mesoglea	3	36 \pm 7.7	44 \pm 8.8	53 \pm 8.3	0.10	0.95
<i>N. bachei</i>	mesoglea	4	50 \pm 8.6	56 \pm 8.7	68 \pm 8.8	0.10	0.99
<i>O. pileus</i>	mesoglea	4	49 \pm 8.2	52 \pm 7.9	59 \pm 7.9	0.071	0.97
<i>P. hydrostatica</i>	mesoglea	1 (10)	6.1 \pm 2.4	11 \pm 2.5	14 \pm 2.6	0.21	0.88
<i>S. tya</i>	mesoglea	1 (5)	89 \pm 0.91	91 \pm 1.0	96 \pm 1.8	0.027	0.99
	canal	1 (5)	20 \pm 1.4	22 \pm 1.5	39 \pm 1.6	0.31	0.98
Ctenophora							
<i>B. fosteri</i>	mesoglea	2	70 \pm 4.9	75 \pm 4.0	85 \pm 2.8	0.069	0.98
	center	1 (5)	32 \pm 5.6	36 \pm 6.3	47 \pm 6.9	0.14	0.99
<i>B. cucumis</i>	mesoglea	4	11 \pm 1.7	13 \pm 1.3	17 \pm 1.5	0.13	0.96
<i>B. infundibulum</i>	mesoglea	2	40 \pm 13	45 \pm 12	58 \pm 9.1	0.13	0.99
	lobe	2	14 \pm 2.1	18 \pm 1.9	29 \pm 1.5	0.27	0.99
	comb row	2	22 \pm 7.9	24 \pm 7.4	30 \pm 8.0	0.12	0.99
<i>Horniphora</i> sp.	mesoglea	3	27 \pm 4.7	33 \pm 11	39 \pm 7.6	0.11	0.97
<i>M. macrydi</i>	comb row	11	4.8 \pm 1.3	7.0 \pm 1.5	15 \pm 2.2	0.51	0.99
<i>O. maculata</i>	mesoglea	1 (5)	28 \pm 12	39 \pm 13	48 \pm 8.9	0.14	0.97
<i>P. bachei</i>	comb row	10	12 \pm 1.2	17 \pm 1.6	22 \pm 1.8	0.19	0.95
Annelida							
<i>Tomopteris</i> sp.	body	2	7.7 \pm 4.5	9.1 \pm 3.2	12 \pm 0.22	0.12	0.96
Mollusca							
<i>C. lamarcki</i>	body	4	4.3 \pm 1.0	8.0 \pm 1.4	11 \pm 1.7	0.24	0.92
<i>C. limacina</i>	body	1 (5)	0.76 \pm 0.031	0.51 \pm 0.04	0.93 \pm 0.10	0.33	0.72
<i>C. spectabilis</i>	body	5	12 \pm 5.0	18 \pm 6.2	25 \pm 7.3	0.22	0.96
<i>P. atlantica</i>	body	4	4.9 \pm 1.7	14 \pm 2.8	18 \pm 3.5	0.19	0.74
<i>P. coronata</i>	body	4	25 \pm 9.0	29 \pm 9.0	37 \pm 9.2	0.13	0.99
Crustacea							
<i>C. cystosoma</i>	body	2	36 \pm 7.1	42 \pm 6.5	49 \pm 7.4	0.098	0.96
Chaetognatha							
<i>S. hexaptera</i>	body	8	32 \pm 4.7	38 \pm 5.1	49 \pm 5.9	0.15	0.98
<i>S. maxima</i>	body	1 (5)	11 \pm 1.7	9.4 \pm 1.9	18 \pm 2.0	0.44	0.91
Chordata							
<i>C. affinis</i>	body	1 (5)	9.0 \pm 2.9	8.4 \pm 2.6	8.0 \pm 2.6	-0.036	0.79
<i>P. confederata</i>	body	4	39 \pm 4.0	42 \pm 4.5	47 \pm 4.7	0.060	0.97
<i>P. atlanticum</i>	body	5	0.78 \pm 0.41	1.6 \pm 0.57	2.8 \pm 0.8	0.42	0.96
<i>S. cylindrica</i>	body	8	49 \pm 3.7	55 \pm 3.3	64 \pm 3.0	0.078	0.99
<i>S. maxima</i>	body	1 (5)	22 \pm 2.0	25 \pm 2.3	33 \pm 2.9	0.18	0.99

The number of animals measured is represented by n . If $n = 1$, the number following in parentheses is the number of measurements taken from that animal. When $n > 1$, the reported value for T_λ is the average of the average values for each animal. When $n = 1$, the reported value is the average of the measurements for that animal.

* $dT/d\lambda/T_{480}$ is the slope of the linear regression of percent transparency on wavelength divided by percent transparency at 480 nm, and r^2 is the coefficient of determination for the regression. In general, percent transparency was linearly proportional to wavelength (see Fig. 2).

1980; Mackie *et al.*, 1987), probably because of the difficulty in determining the predators and prey of gelatinous marine animals. However, due to the increasing use of submersible and scuba-based collecting and observing techniques, the role of gelatinous animals in the trophic

ecology of the ocean is becoming clearer (Alldredge, 1984; Madin, 1988; Lalli and Gilmer, 1989). Table III lists documented examples of predator/prey relationships involving transparent animals and animals with well-developed visual systems. Of the phyla containing transpar-

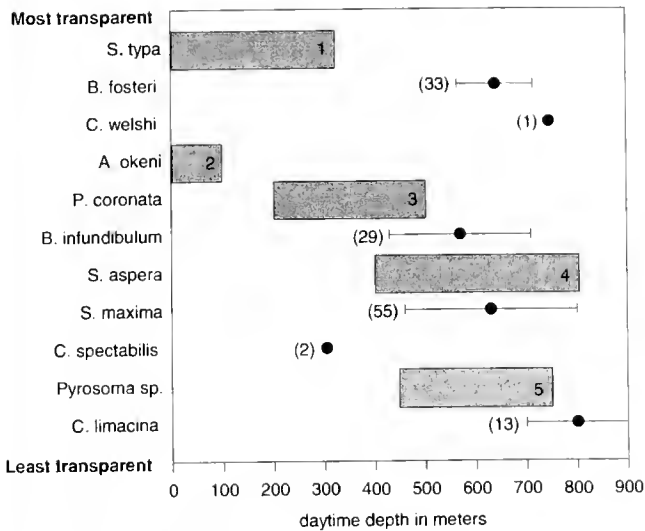


Figure 3. Transparency of species collected from Oceanographer Canyon in relation to depth of daytime distribution. Species are arranged from most transparent (*Sibogita typa*) to least transparent (*Clione limacina*). Transparency values (filled circles) for each species are means of measurements taken from animals collected on the same cruise; bars are standard deviation of the mean, with number of specimens given in parentheses. Daytime depth ranges (bars) are taken from the literature. The number within each bar gives the reference from which it was taken: 1 = Mayer (1910); 2 = Youngbluth (pers. comm.); 3 = Lalli and Gilmer (1989); 4 = Wiebe *et al.* (1979); 5 = Anderson *et al.* (1992).

ent members, all include transparent animals that either prey on, or are preyed upon by animals with well-developed visual systems. In addition, many of these animals (in particular certain cnidarians, ctenophores, and chaetognaths) prey upon copepods (Harbison *et al.*, 1978; Madin, 1988; Baier and Purcell, 1997). Copepods do not have well-developed vision, but have been shown to react defensively to shadows (Buskey *et al.*, 1986), and therefore may react to opaque or translucent predators passing overhead. A large number of transparent animals are thus interacting with animals that respond to visual cues.

Since, in general, transparent animals are more delicate and less agile than their visually oriented predators or prey, their success as predators or prey of such animals depends critically upon their sighting distance (the maximum distance at which they are still detectable by a visually oriented animal). Prey with short sighting distances reduce their number of encounters with visually oriented predators (Greene, 1983). "Ambush" predators (*e.g.*, medusa, siphonophores, cydippid ctenophores) with short sighting distances increase their chances of entangling visually oriented prey before being detected and avoided. Raptors (*e.g.*, chaetognaths, heteropods) with short sighting distances increase their chances of getting within striking distance without being detected.

In certain cases, the relationship between transparent animals and visually oriented animals is quite complex.

The physonect siphonophores *Athorybia rosacea* and *Agalma okeni* are mostly transparent, but they have pigmented regions that mimic copepods and larval fish and are apparently used as lures (Purcell, 1980). Other animals appear to have exploited temporal changes in transparency for defense. The calycophoran siphonophore *Hippododius hippopus* is normally transparent, but rapidly becomes opaque when disturbed, presumably as a defense response (Mackie, 1996). Finally, there is evidence that cephalopods use their well-developed polarization vision to break the camouflage afforded by transparency (Shashar *et al.*, 1998). Certain zooplankton, though trans-

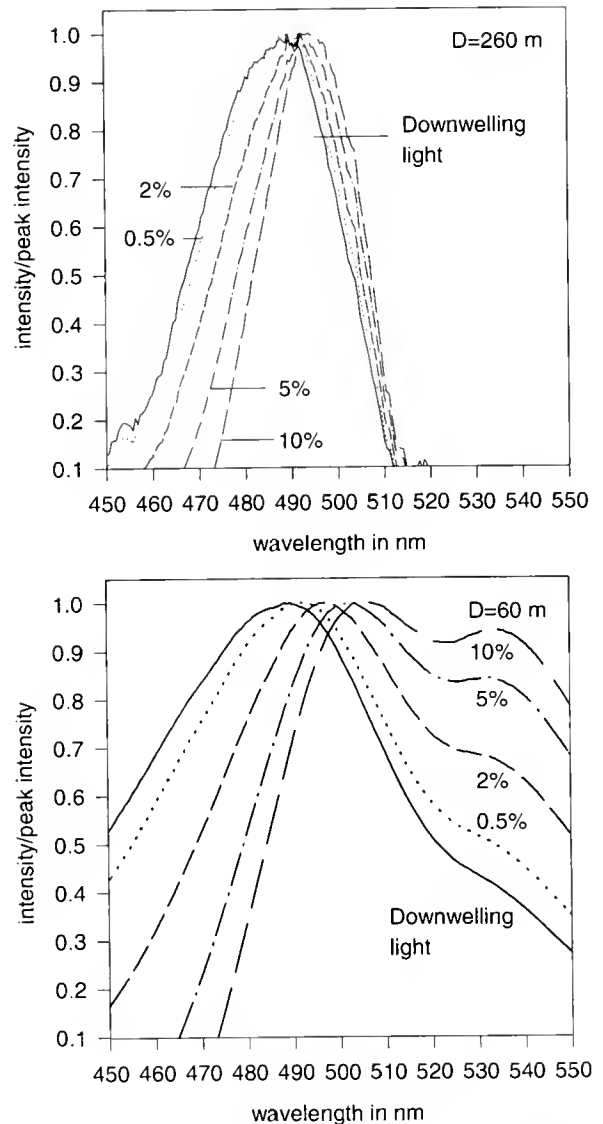


Figure 4. (Top) Spectrum of downwelling light in Oceanographer Canyon at 260 m (solid line) and the spectra after having passed through the tissue with linear transmission spectra with normalized slopes of 0.5%, 2%, 5%, and 10%/nm. All spectra are normalized to have a value of unity at their wavelength of peak intensity. (Bottom) Same as above, but at 60 m.

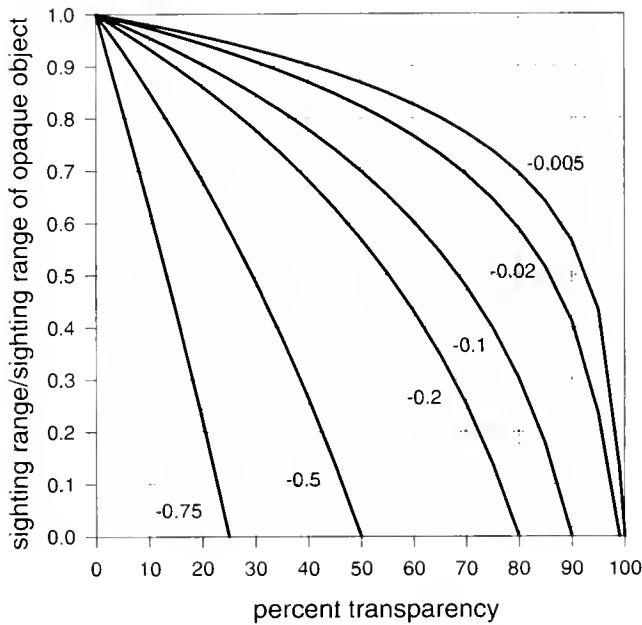


Figure 5. Sighting distance of a prey item vs. its percent transparency when viewed from below by predators with visual systems that have different minimum contrast thresholds for object detection. The sighting distance is divided by the sighting distance of an opaque object to control for water clarity, prey shape, size, etc. The ratio gives an estimate of the advantage of transparency for crypsis in a given situation.

parent, alter the polarization characteristics of transmitted light and are therefore detectable by animals that can detect these characteristics (Shashar *et al.*, 1998). Since many crustaceans have polarization vision (Waterman, 1981), this method of detection may be quite common.

Relationship of measured transparency to in situ light transmission

The great majority of the collected animals either have a mesopelagic daytime distribution in oceanic water or are found at moderate depths in coastal water (see *Results*). In both cases, the light field has reached an asymptotic state. The asymptotic light field is considerably simpler than its epipelagic counterpart. The intensity and spatial and temporal aspects of the epipelagic light field are strongly influenced by solar elevation and azimuth, waves, and clouds (Jerlov, 1976; Lythgoe, 1979; Loew and McFarland, 1990). In addition, downwelling light has a broad angular distribution. Therefore, it can be difficult to relate percent transmission of a narrow beam of light to percent transmission of the *in situ* light field (Chapman, 1976a). In contrast, while the intensity of the asymptotic light field is affected by surface light levels, its spatial characteristics are essentially constant (Jerlov, 1976; Denton, 1990). Additionally, the angular distribution of most of the light is narrow and centered around the vertical. As mentioned in the *Materials and Methods* section, the ver-

tical upward and horizontal radiances are only 0.5% and 3% of the vertical downward radiance. At asymptotic depths, the vertical downward radiance approximates the downward irradiance (reviewed in Denton, 1990). Therefore, measurements of percent transparency in a light beam are comparable to the *in situ* transparency of an animal viewed from below. Since visual acuity and contrast sensitivity are in general proportional to the amount of available light (Douglas and Hawryshyn, 1990), transparent animals are most visible when viewed from below. Therefore an analysis of visibility from this viewing position provides a conservative estimate of the cryptic abilities of these animals.

Wavelength dependence of light transmission

In all but one of the animals (*C. affinis*), the percent transparency increased linearly with wavelength. This linear wavelength dependence can be a disadvantage to an animal using transparency as camouflage. Unless percent transparency of the animal is independent of wavelength, the spectrum of light passing through the animal will be altered. Whereas the peak wavelength is displaced only slightly, there is a considerable reduction in intensity in shorter wavelengths and an increase in longer wavelengths, even for normalized slopes as small as 2%/nm (see *Results*). Therefore, in addition to creating an intensity contrast against the background, the animal will also appear to be a slightly different color from the surrounding water. Because the spectral distribution of the downwelling light broadens near the surface, this effect is stronger at shallow depths, though the peak displacement remains small (Fig. 4). Since there is evidence that the eyes of some mesopelagic predators have certain characteristics (*e.g.*, pigmented lenses, multibanked retinæ) that may give them excellent hue discrimination in the blue-green (Munz, 1976; Denton and Lockett, 1989; Douglas and Thorpe, 1992), it is advantageous that the normalized T-W slope of an animal using transparency for camouflage be as small as possible. In the tissues measured, the normalized slopes are all less than 0.5% and average only 0.17%/nm. Therefore, they have a small and probably undetectable effect on the spectrum of the downwelling light.

Constant percent transparency at all wavelengths is not a general characteristic of materials. Light attenuation ($100-T$) is caused by true absorption and scattering, but scattering dominates in unpigmented organic materials (Chapman, 1976a). The wavelength dependence of attenuation due to scattering depends on the size of the scattering particles, with the general form $S \approx \lambda^k$, where S is the amount of scattering and λ is the wavelength of incident light. For particles with radii that are small relative to λ (Rayleigh scattering), k equals -4 . For particles with radii within an order of magnitude of λ (Mie scattering),

Table III

Examples of transparent zooplankton that have prey or predators with well-developed visual systems

Animal	Preys on	Preyed upon by
Cnidaria		
<i>Aegina</i>		hyperiid amphipods ¹
<i>Aglantha</i>	euphausiids ¹	euphausiids, ¹ fish ¹
<i>Athorybia</i>	mysids, ² heteropods ²	
<i>Aurelia</i>	fish ⁴	sea turtles ³
<i>Carybdea</i>	fish, ⁵ mysids ⁵	
<i>Forskalia</i>	fish ⁶	
<i>Laodicea</i>	fish ⁶	
<i>Liriope</i>	fish, ⁶ alciopid worms ⁶	
<i>Nanomia</i>		heteropods ⁷
cystonect siphonophores	fish ⁸	sea turtles ³
assorted siphonophores		heteropods, ⁷ sea turtles ³
assorted hydromedusae		sea turtles ³
Ctenophora		
<i>Bathocyroe</i>	euphausiids ⁵	
<i>Bolinopsis</i>	euphausiids ⁵	
<i>Cestum</i>		alciopid worms ⁹
<i>Eurhamphaeca</i>		alciopid worms ⁹
<i>Hormiphora</i>	fish, ⁶ heteropods ⁶	
<i>Nmemiopsis</i>		alciopid worms, ⁹ fish ⁴
<i>Ocyropsis</i>	fish, ⁹ euphausiids ⁹	alciopid worms ⁹
<i>Pleurobrachia</i>	fish ⁵	
assorted. ctenophores		hyperiid amphipods, ⁹ sea turtles ³
Annelida		
<i>Tomopteris</i>		heteropods, ⁷ squid ¹¹
Mollusca		
<i>Carianria</i>	euphausiids, ⁷ fish ⁷	sea turtles, ³ fish ¹⁵
<i>Corolla</i>		hyperiid amphipods ⁷
<i>Cymbulia</i>	heteropods ¹⁵	
<i>Phylliroe</i>		heteropods ¹⁰
<i>Pterotrachea</i>		hyperiid amphipods ⁹
assorted heteropods	heteropods ⁷	heteropods, ⁷ fish, ⁷ squid, ¹¹ sea turtles ³
assorted cranchiid squid		birds ¹⁴
Crustacea		
<i>Lucifer</i>		fish ¹²
<i>Phronima</i>		squid ¹¹
Chaetognatha		
assorted chaetognaths	fish, ¹² euphausiids ¹²	heteropods, ⁷ squid, ¹¹ euphausiids, ¹² fish, ¹² decapods ¹²
Chordata		
assorted salps		hyperiid amphipods, ⁹ heteropods, ⁷ euphausiids, ¹³ sea turtles ³
assorted larvaceans		fish ¹⁰

Sources of the data: ¹ Mackie, 1996; ² Purcell, 1981; ³ Bjorndal, 1997; ⁴ Alldredge, 1984; ⁵ Wrobel and Mills, 1998; ⁶ Madin, 1988; ⁷ Lalli and Gilmer, 1989; ⁸ Purcell, 1980; ⁹ Harbison *et al.*, 1978; ¹⁰ Hamner *et al.*, 1975; ¹¹ Hanlon and Messenger, 1996; ¹² Pierrot-Bults and Chidgey, 1988; ¹³ Du and Zhang, 1980; ¹⁴ Imber, 1978; ¹⁵ Van der Spoel, 1976. Most of the sources are reviews to minimize the number of references.

k ranges from -4 to 0.2 . For particles much larger than λ (geometric optics), k equals 0 (see Mertens (1970) for further details). Table IV shows the k values calculated for the transparent tissues by fitting the above power function to $(100 - T)$ vs. wavelength. For the most transparent tissues, k ranges from -2 to -1 . For moderately transparent tissues, k ranges from -0.78 to -0.11 . For the nearly opaque tissues, k approximates zero. Therefore, it is likely that the attenuation of light in the highly and moderately transparent tissues (*e.g.*, *S. typha*, *P. coronata*) is mostly due to light scattering by medium-size particles and that

the attenuation in the nearly opaque tissues (*e.g.*, *C. limacina*) is mostly due to scattering by large particles. In contrast, the k values reported for vertebrate corneas ($T = 90 - 100\%$) range from -5 to -3 , suggesting that attenuation in this tissue is dominated by scattering from small particles (reviewed in Farrell *et al.*, 1973).

Relationship of percent transparency to sighting distance

All other factors being equal, a visual predator will spot an opaque animal at a greater distance than it will

Table 1V

Exponent values (k), calculated when light attenuation ($100 - T$) vs. wavelength (λ) is fit to the power function $100 - T \approx \lambda^k$, that provide information about the size of the ultrastructural components responsible for most of the light scattering; r^2 is the coefficient of determination for the curve fit to the power function

Animal	Tissue	k	r^2
Cnidaria			
<i>A. okeni</i>	mesoglea	-0.57	0.98
	siphosome	-0.041	0.99
<i>A. rosacea</i>	mesoglea	-0.052	0.99
<i>C. welshi</i>	mesoglea	-1.5	0.99
<i>H. cupulifera</i>	mesoglea	-0.47	0.99
<i>N. bachei</i>	mesoglea	-0.78	0.99
<i>O. pileus</i>	mesoglea	-0.44	0.99
<i>P. hydrostatica</i>	mesoglea	-0.14	0.92
<i>S. typha</i>	mesoglea	-2.0	0.93
	canal	-0.58	0.97
Ctenophora			
<i>B. fosteri</i>	mesoglea	-1.3	0.99
	center	-0.50	0.99
<i>B. cucumis</i>	mesoglea	-0.11	0.97
<i>B. infundibulum</i>	mesoglea	-0.64	0.99
	lobe	-0.35	0.99
	comb row	-0.21	0.99
<i>Hormiphora sp.</i>	mesoglea	-0.29	0.99
<i>M. macrydi</i>	comb row	-0.21	0.98
<i>O. maculata</i>	mesoglea	-0.43	0.99
<i>P. bachei</i>	comb row	-0.22	0.98
Annelida			
<i>Tomopteris sp.</i>	body	-0.069	0.97
Mollusca			
<i>Carinaria sp.</i>	body	-0.11	0.96
<i>C. limacina</i>	body	-0.007	0.67
<i>C. spectabilis</i>	body	-0.27	0.99
<i>P. atlantica</i>	body	-0.18	0.81
<i>P. coronata</i>	body	-0.30	0.99
Crustacea			
<i>C. cystosoma.</i>	body	-0.40	0.99
Chaetognatha			
<i>S. hexaptera</i>	body	-0.52	0.99
<i>S. maxima</i>	body	-0.19	0.86
Chordata			
<i>C. affinis</i>	body	0.018	0.85
<i>P. confederata</i>	body	-0.24	0.99
<i>P. atlanticum</i>	body	-0.037	0.98
<i>S. cylindrica</i>	body	-0.54	0.99
<i>S. maxima</i>	body	-0.28	0.99

spot a transparent one. Since a shorter sighting distance for a prey item decreases its encounters with visual predators, transparency can be advantageous. The ratio of the sighting distance of a transparent prey item to the sighting distance for a similar opaque prey item gives an estimate of the advantage of transparency as a form of crypsis in a given situation (Fig. 5). The scale is inverted in that a ratio of zero implies a high advantage (the prey item is essentially invisible) and a ratio of one implies no advantage over an opaque object. The model showed that the

qualitative and quantitative relationship between the percent transparency of an object and its sighting distance depends critically upon the minimum contrast threshold for object detection in the given visual system. Note that in the preceding and following discussion, the terms predator and prey can be exchanged without loss of meaning.

The minimum contrast threshold is known for only a handful of animals and depends on many variables (Douglas and Hawryshyn, 1990). Optimal minimum contrast thresholds have been determined for several species (reviewed in Lythgoe, 1979, and Douglas and Hawryshyn, 1990); for simplicity, quoted values are unsigned: man (0.01), cat (0.01), goldfish (0.009–0.05), eod (0.02), rudd (0.03–0.07), roach (0.02), and bluegill (0.003–0.007). Because these values depend on many aspects of the experimental situation (temperature, position of stimulus on retina, use of one eye or two, assessment method, etc.), they are not directly comparable (Hester, 1968, cited in Douglas and Hawryshyn, 1990). In addition, studies on cod (*Gadus morhua*) have shown that the minimum contrast threshold increases from the optimum (0.02) at a light level of $10^{-1} \text{ W sr}^{-1} \text{ m}^{-2}$ to nearly 0.5 at a light level of $10^{-7} \text{ W sr}^{-1} \text{ m}^{-2}$ (Anthony, 1981). In general, the minimum contrast threshold of visual systems increases with decreasing light levels (Douglas and Hawryshyn, 1990). The minimum contrast threshold also depends on the relative size of the object. Studies on goldfish (*Carassius auratus*) viewing sine wave patterns have shown that the minimum contrast threshold increases from 0.025 at 0.3 cycles/degree to 0.25 at higher and lower spatial frequencies (Northmore and Dvorak, 1979). The same pattern is found in humans, though the optimal minimum contrast threshold is 4 cycles/degree (Uhlrich *et al.*, 1981). For the above reasons, absolute determination of the sighting distance of these animals by their relevant predators and prey is at present impossible.

Despite this limitation, it can be predicted that the usefulness of transparency as camouflage increases dramatically with depth (up to the depth limit for vision for a given predator). This is because, in general, the minimum contrast threshold of a given visual system increases with decreasing light levels. For example, as mentioned above, the minimum contrast threshold of the eod, *Gadus morhua*, increases to 0.5 at light levels of $10^{-7} \text{ W sr}^{-1} \text{ m}^{-2}$. In clear water, daytime vertical downward radiance has this intensity at about 650 m (Denton, 1990). At this depth, the sighting range decreases rapidly with increasing percent transparency, and tissues with percent transparency greater than 50% are invisible at all distances when viewed from below by *G. morhua* (see Fig. 5). Near the surface, the minimum contrast threshold decreases to 0.02, and the sighting distance of a tissue with 50% transparency is only 27% less than that for an opaque object. An interesting corollary is that, unless they are preyed upon by visual predators whose low-light contrast

sensitivity is extraordinarily better than that of humans, many of the animals measured are far more transparent than is necessary to achieve complete invisibility at their daytime depths (e.g., *Bathocyroe fosteri*).

This analysis, however, is limited to one dimension. An extension would be to consider a critical volume within which a prey item could be detected. If the light field were spherically symmetrical, the volume would equal $4\pi d^3/3$, where d is the sighting distance and the above-mentioned 27% decrease in d would correspond to a 61% reduction in the critical volume. However, due to the asymmetry of the asymptotic light field (Denton, 1990) and the complex relationship between percent transparency and visibility in horizontal and downward lines of sight, a determination of the critical volume is beyond the scope of this paper.

The foregoing analysis does not necessarily predict a simple relationship between percent transparency and depth. Indeed, in this study no relationship was found between the percent transparency of an animal and its daytime depth distribution. High transparency at depth may be a consequence of selection for low backscatter to camouflage animals from predators or prey that use directed bioluminescence to illuminate the environment. Shallow-water animals with a low percent transparency when backlit by a narrow beam may be considerably more transparent in the diffuse epipelagic light environment (see Chapman, 1976a). Finally, of course, some animals may be transparent for reasons unrelated to vision and camouflage—e.g., as a result of having gelatinous flotation devices (Marshall, 1979).

Acknowledgments

We thank the captains and crews of the RVs *Edwin Link*, *Oceanus*, *Pelican*, and *Seward Johnson*, and the pilots and crew of the *Johnson Sea-Link* for assistance with all aspects of animal collection. We also thank Dr. Tamara Frank for a critical reading of the manuscript, and Drs. Laurence Madin, Charles Miller, and Dale Calder for help with animal identifications. Sea time aboard the *Seward Johnson*, *Pelican*, and *Oceanus* was generously donated by Dr. Craig Young, Dr. Joseph J. Torres, and GLOBEC, respectively. This work was funded by a grant from the National Oceanic and Atmospheric Administration (subgrant UCAP-95-02b, University of Connecticut, Award No. NA76RU0060) to Drs. Tamara M. Frank and EAW, a grant from the National Science Foundation (OCE-9633784) to Drs. Craig M. Young and Mary E. Rice, a grant from the National Science Foundation (OCE-9712572) to Dr. Joseph J. Torres, the GLOBEC Northwest Atlantic/Georges Bank Program, and by a Harbor Branch Institution Postdoctoral Fellowship to SJ. This is Harbor Branch Contribution No. 1253.

Literature Cited

- Allredge, A. L. 1984.** The quantitative significance of gelatinous zooplankton as pelagic consumers. Pp. 407–434 in *Flows of Energy and Materials in Marine Ecosystems*. M. J. R. Fasham, ed. Plenum Press, New York.
- Anderson, V., J. Sardou, and P. Nival. 1992.** The diel migrations and vertical distributions of zooplankton and micronekton in the northwestern Mediterranean Sea. 2. Siphonophores, hydromedusae, and pyrosomids. *J. Plankton Res.* **14**: 1155–1169.
- Anthony, P. D. 1981.** Visual contrast thresholds in the cod *Gadus morhua*. *J. Fish Biol.* **19**: 87–103.
- Baier, C. T., and J. E. Purcell. 1997.** Trophic interactions of chaetognaths, larval fish, and zooplankton in the South Atlantic Bight. *Mar. Ecol. Prog. Ser.* **146**: 43–53.
- Bjorndal, K. A. 1997.** Feeding ecology and nutrition of sea turtles. Pp. 199–232 in *The Biology of Sea Turtles*. P. L. Lutz and J. A. Musick, eds. CRC Press, New York.
- Buskey, E. J., C. G. Mann, and E. Swift. 1986.** The shadow response of the estuarine copepod *Acartia tonsa*. *J. Exp. Mar. Biol. Ecol.* **103**: 65–75.
- Chapman, G. 1976a.** Reflections on transparency. Pp. 491–498 in *Coelenterate Ecology and Behavior*, G. O. Mackie, ed. Plenum Press, New York.
- Chapman, G. 1976b.** Transparency in organisms. *Experientia* **15**: 123–125.
- Davis, C. C. 1955.** *The Marine and Fresh-water Plankton*. Michigan State Univ. Press, Chicago.
- Denton, E. J. 1990.** Light and vision at depths greater than 200 meters. Pp. 127–148 in *Light and Life in the Sea*. P. J. Herring, A. K. Campbell, M. Whitfield, and L. Maddock, eds. Cambridge University Press, New York.
- Denton, E. J., and N. A. Locket. 1989.** Possible wavelength discrimination by multibank retinæ in deep-sea fishes. *J. Mar. Biol. Assoc. U. K.* **69**: 409–435.
- Douglas, R. H., and C. W. Hawryshyn. 1990.** Behavioral studies of fish vision: an analysis of visual capabilities. Pp. 373–418 in *The Visual System of Fish*. R. H. Douglas and M. B. A. Djamgoz, eds. Chapman and Hall, New York.
- Douglas, R. H., and A. Thorpe. 1992.** Short-wave absorbing pigments in the ocular lenses of deep-sea teleosts. *J. Mar. Biol. Assoc. U. K.* **72**: 93–112.
- Du, J., and Q. Zhang. 1980.** The feeding habits of the striped mullet, *Mugil cephalus*. *J. Fish. China* **4**: 207–216.
- Farrell, R. A., R. L. McCally, and P. E. R. Tatham. 1973.** Wave-length dependencies of light scattering in normal and cold swollen rabbit corneas and their structural implications. *J. Physiol.* **233**: 589–612.
- Greene, C. H. 1983.** Selective predation in freshwater zooplankton communities. *Int. Rev. Gesamten. Hydrobiol.* **68**: 297–315.
- Greze, V. N. 1963.** The determination of transparency among planktonic organisms and its protective significance. *Dokl. Akad. Nauk. S.S.S.R.* **151**: 435–438.
- Greze, V. N. 1964.** The transparency of planktonic organisms in the equatorial part of the Atlantic Ocean. *Okeanologiya* **4**: 125–127.
- Hamner, W. M. 1975.** Underwater observations of blue-water plankton: logistics, techniques and safety procedures for divers at sea. *Limnol. Oceanogr.* **20**: 1045–1051.
- Hamner, W. M. 1996.** Predation, cover, and convergent evolution in epipelagic oceans. Pp. 17–37 in *Zooplankton: Sensory Ecology and Physiology*, P. H. Lenz, D. K. Hartline, J. E. Purcell, and D. L. Macmillan, eds. Overseas Publishers Assoc., Amsterdam.
- Hamner, W. M., L. P. Madin, A. L. Alldredge, R. W. Gilmer, and P. P. Hamner. 1975.** Underwater observations of gelatinous zooplankton: sampling problems, feeding biology, and behavior. *Limnol. Oceanogr.* **20**: 907–917.

- Hanlon, R. T., and J. B. Messenger. 1996.** *Cephalopod Behavior*. Cambridge University Press, Cambridge.
- Harbison, G. R., L. P. Madin, and N. R. Swanberg. 1978.** On the natural history and distribution of oceanic ctenophores. *Deep-Sea Res.* **25**: 233–256.
- Hardy, A. C. 1956.** *The Open Sea, its Natural History: The World of Plankton*. Houghton Mifflin, Cambridge.
- Hester, F. J. 1968.** Visual contrast thresholds of the goldfish (*Carassius auratus*). *Vision Res.* **8**: 1315–1335.
- Imber, M. J. 1978.** The squid families Cranchiidae and Gonatidae (Cephalopoda: Teuthoidea) in the New Zealand region. *N. Z. J. Zool.* **5**: 445–484.
- Jerlov, N. G. 1976.** *Marine Optics*. Elsevier Scientific, New York.
- Johnson, S., and E. A. Widder.** The transparency and visibility of gelatinous zooplankton. *SPIE Ocean Optics XIV* (in press).
- Lalli, C. M., and R. W. Gilmer. 1989.** *Pelagic Snails*. Stanford Univ. Press, Palo Alto, CA.
- Loew, E. R., and W. N. McFarland. 1990.** The underwater visual environment. Pp. 1–44 in *The Visual System of Fish*, R. H. Douglas and M. B. A. Djamgoz, eds. Chapman and Hall, New York.
- Lythgoe, J. N. 1979.** *The Ecology of Vision*. Clarendon Press, Oxford.
- Mackie, G. O. 1996.** Defensive strategies in planktonic coelenterates. Pp. 435–446 in *Zooplankton: Sensory Ecology and Physiology*, P. H. Lenz, D. K. Hartline, J. E. Purcell, and D. L. Macmillan, eds. Overseas Publishers Assoc., Amsterdam.
- Mackie, G. O., P. R. Pugh, and J. E. Purcell. 1987.** Siphonophore biology. Pp. 98–263 in *Advances in Marine Biology*, J. H. S. Blaxter and A. J. Southward, eds. Academic Press, London.
- Madin, L. P. 1988.** Feeding behavior of tentaculate predators: in situ observations and a conceptual model. *Bull. Mar. Sci.* **43**: 413–429.
- Marshall, N. B. 1979.** *Deep-Sea Biology: Developments and Perspectives*. Garland STPM Press, New York.
- Mayer, A. G. 1910.** *Medusae of the World*. Carnegie Institute Press, Washington, DC.
- McFall-Ngai, M. J. 1990.** Crystallin in the pelagic environment. *Am. Zool.* **30**: 175–188.
- Mertens, L. E. 1970.** *In-Water Photography: Theory and Practice*. John Wiley, New York.
- Munz, W. R. A. 1976.** On yellow lenses in mesopelagic animals. *J. Mar. Biol. Assoc. U. K.* **56**: 963–976.
- Northmore, D. P. M., and C. A. Dvorak. 1979.** Contrast sensitivity and acuity of the goldfish. *Vision Res.* **19**: 255–261.
- Pierrot-Bults, A. C., and K. C. Chidgey. 1988.** *Chaetognatha*. Bath Press, Avon, UK.
- Purcell, J. E. 1980.** Influence of siphonophore behavior on their natural diets; evidence for aggressive mimicry. *Science* **209**: 1045–1047.
- Purcell, J. E. 1981.** Selective predation and caloric consumption by the siphonophore *Rosacea cymbiformis* in nature. *Mar. Biol.* **63**: 283–294.
- Shashar, N., R. T. Hanlon, and A. Petz. 1998.** Polarization vision helps detect transparent prey. *Nature* **393**: 222–223.
- Uhlrich, D. J., E. A. Essock, and S. Lehmkuhle. 1981.** Cross-species correspondence of spatial contrast sensitivity functions. *Behav. Brain Res.* **2**: 291–299.
- Van der Spoel, S. 1976.** *Pseudothecosomata, Gymnosomata and Heteropoda*. Bohn, Scheltema & Holkema, Utrecht, The Netherlands.
- Waterman, T. H. 1981.** Polarization sensitivity. Pp. 281–469 in *Handbook of Sensory Physiology*, vol. 7/6B, H. Autrum, ed. Springer, New York.
- Widder, E. A., M. I. Latz, and J. F. Case. 1983.** Marine bioluminescence spectra measured with an optical multichannel detection system. *Biol. Bull.* **165**: 791–810.
- Wiebe, P. H., L. P. Madin, L. R. Haury, G. R. Harbison, and L. M. Philbin. 1979.** Diel vertical migration by *Salpa aspera* and its potential for large-scale particulate organic matter transport to the deep-sea. *Mar. Biol.* **53**: 249–255.
- Wrobel, D., and C. Mills. 1998.** *Pacific Coast Pelagic Invertebrates: A Guide to Common Gelatinous Animals*. Monterey Bay Aquarium, Monterey, CA.
- Zaret, T. M., and W. C. Kerfoot. 1975.** Fish predation on *Bosmina longirostris*: body size selection versus visibility selection. *Ecology* **56**: 2332–237.

Size-Related Obligate and Facultative Parasitism in the Marine Gastropod *Trichotropis cancellata*

BRUNO PERNET* AND ALAN J. KOHN

Department of Zoology, University of Washington, Box 351800, Seattle, Washington 98195-1800

Abstract. The marine gastropod *Trichotropis cancellata*, previously considered to be exclusively a suspension feeder, is also a kleptoparasite, stealing food from several species of suspension-feeding polychaetes. When feeding independently, *T. cancellata* uses its pseudoproboscis, an elongate, ciliated extension of the lower lip, to transport particles captured on its ctenidium to its mouth. When parasitizing, the snail positions its pseudoproboscis in the mouth of a host polychaete and diverts a large proportion of the particles captured by the polychaete to its own mouth. In subtidal habitats around San Juan Island, Washington, most individuals of *T. cancellata* are found in association with the tube openings of suspension-feeding polychaetes. In laboratory experiments, parasitism significantly enhanced fitness in *T. cancellata*. Juvenile snails that parasitized polychaetes grew faster and survived in greater numbers than those deprived of access to hosts, and parasitic adult snails reproduced more than those without hosts. Parasitism in *T. cancellata* and related capulid gastropods may have originated in early post-metamorphic stages as a response to constraints on the efficiency of suspension feeding at small sizes; however, because parasitism is more effective than suspension feeding for snails of all sizes, it now persists throughout life.

Introduction

Animals often vary in trophic mode over the course of their lives. Changes in feeding mechanism at metamorphosis in marine invertebrates are among the most obvious examples of such variation, and are accompanied by

major changes in morphology and often habitat. However, equally major shifts in trophic mode can occur without qualitative morphological change. Some of these are related to increases in body size during ontogeny (Werner and Gilliam, 1984). For example, many fishes switch from feeding on individual particles to suspension feeding after reaching a certain size (Gerking, 1994). On shorter time scales, environmental variation may drive changes in trophic mode. For example, some benthic marine invertebrates deposit feed when the flux of particles in suspension is low, but as it increases they switch to suspension feeding (e.g., Taghon *et al.*, 1980; Turner and Miller, 1991). Variation in the concentration or size of food particles may also drive some behavioral switches in trophic mode in fishes (Crowder, 1985; Gibson and Ezzi, 1985; Ehlinger, 1989). Such ontogenetic and behavioral variation is useful for understanding the functional morphology and evolution of feeding mechanisms in at least two ways. First, shifts in feeding mode focus attention on the costs and benefits associated with particular strategies (Werner and Gilliam, 1984; Taghon and Greene, 1992). Second, trophic polymorphisms provide us with excellent models for exploring evolutionary change in feeding mechanisms (Lauder *et al.*, 1989).

Here we describe a case of within-individual variation in feeding mode of interest from both of these perspectives. The marine gastropod *Trichotropis cancellata* (order Neotaenioglossa, family Capulidae) has previously been considered a suspension feeder, generating a feeding current and collecting suspended particles using its ciliated ctenidium (Yonge, 1962). Our results confirm that it is capable of feeding on suspended particles. However, in subtidal habitats *T. cancellata* is frequently found near the tube openings of several species of suspension-feeding polychaetes (Pernet and Kohn, pers. obs.). Here we show that in addition to independent suspension feeding, *T. cancellata* can also efficiently divert and eat particles cap-

Received 18 February 1998; accepted 3 August 1998.

*Author to whom correspondence should be addressed. Current address: Friday Harbor Laboratories, 620 University Road, Friday Harbor, Washington 98250. E-mail: pernet@fhl.washington.edu

tured by these polychaetes. Kleptoparasitism, the diversion of host food to a parasite that does not otherwise damage the host, is well known in some birds, mammals, and terrestrial arthropods (e.g., Elgar, 1993; Vickery and Brooks, 1994; Carbone *et al.*, 1997), and even in one terrestrial gastropod (Zamora and Gomez, 1996), but it is poorly documented among marine invertebrates, with the exception of annelids in the order Myzostomida (Eeckhaut *et al.*, 1995).

We present the results of observations and experiments intended to assess the relative importance of these two trophic modes to *T. cancellata*. These data show that in the laboratory, (i) parasitism of polychaetes leads to substantial fitness gains for small and large individuals, and (ii) small snails cannot meet their basic metabolic needs solely by independent suspension feeding and thus can be considered obligate parasites. Hence, the use and effectiveness of alternate trophic modes in *T. cancellata* depends both on environmental factors (presence of suitable hosts) and ontogenetic factors (body size). The data suggest that Yonge's (1962) hypotheses on the evolution of suspension-feeding neotaenioglossan limpets—in which *T. cancellata* played a role as a model intermediate form—should be reevaluated. Further, our results suggest a novel hypothesis concerning diversification in feeding modes, an important aspect of animal diversity.

Materials and Methods

Collection of animals

Trichotropis cancellata and host polychaetes (Sabellariidae: *Sabellaria cementarium*; Sabellidae: *Potamilla ocellata* and *Schizobranchia insignis*; Serpulidae: *Serpula columbiana* [cf. *S. vermicularis*; Kupriyanova and Rzhavsky, 1993; Kupriyanova, 1995]) were collected by dredging in the vicinity of San Juan Island, Washington, from depths of 30–60 m. Snails and host polychaetes were also observed and collected by divers in the shallow subtidal zone at Shady Cove and Eagle Cove, San Juan Island. Additional sabellids were collected from the breakwater at the Friday Harbor Laboratories, and additional serpulids from the intertidal zone at Argyle Creek, San Juan Island. All animals were maintained in tanks of flowing seawater until used in observations or experiments.

Feeding behavior

For feeding observations, snails and polychaetes were placed in dishes of seawater and viewed with a dissecting microscope equipped with a video camera and recorder. Particle captures were visualized by introducing suspended *Artemia* cysts (~250 μm diameter) or polystyrene beads (40 μm diameter) into the dishes. To estimate the efficiency of *T. cancellata* in parasitizing host poly-

chaetes, we counted the number of particles (*Artemia* cysts) captured by polychaetes and subsequently removed by snails. A parasitized polychaete (*Potamilla ocellata* or *Serpula columbiana*) was positioned so that its mouth was clearly visible through the microscope. When the associated snail began diverting captured particles, we began videotaping. From the videotapes, we were able to count the total number of particles that were (A) captured by the polychaete and entered its mouth and (B) removed from the polychaete's mouth by the snail. We used the proportion (B/A) as a measure of the snail's efficiency in capturing particles from the host.

Suspension-feeding ability in *Trichotropis cancellata*

To examine the potential for suspension feeding to supply the metabolic needs of *T. cancellata*, we compared the relationships between ctenidium area and body mass in *T. cancellata* and two other suspension-feeding neotaenioglossans, *Calyptraea fastigiata* and *Crepidula dorsata* (family Calyptraeidae). Like *T. cancellata*, *C. fastigiata* and *C. dorsata* use the ctenidium to capture particles from suspension; these last two snails also capture particles with a mucus "pre-filter" that stretches across the upstream opening of the mantle cavity (Werner, 1951, 1953). We used ctenidium area as an indicator of suspension-feeding ability because it is positively correlated with pumping rate, one component of feeding ability, in other suspension-feeding molluscs (Möhlenburg and Riisgård, 1979; Meyhöfer, 1985). *C. fastigiata* and *C. dorsata* were collected by divers from Shady Cove. Ctenidium area was measured by dissecting out the ctenidium and tracing its outline using a camera lucida. The tracing was scanned into a computer and the program NIH Image 1.61 (available at <http://rsb.info.nih.gov/nih-image>) used to calculate its area. The ctenidium and other body tissues (excluding the shell) were then dried at 60°C for 24 h on preweighed foil squares and weighed on a Mettler ARE-100 balance to the nearest milligram.

We used reduced major axis (Model II) regression to describe the relationships between ctenidium area and body mass for the three species (LaBarbera, 1989). All data were ln-transformed. We compared slopes and elevations of these regressions by the Model I method described by Zar (1996, pp. 353–357).

Importance of parasitism to growth, survival, and reproduction

In a direct assessment of the importance of parasitism to several components of fitness in *T. cancellata*, we raised snails in the laboratory with or without hosts and compared growth, survival, and reproduction between treatments. Snails raised with hosts were able to feed by both suspension feeding and parasitism; those raised

without hosts could only suspension feed. We conducted three such experiments, two with small snails (initial shell height 3.0–10.0 mm, measured to the nearest 0.5 mm with vernier calipers) and one with large snails (initial shell height 17.0–23.0 mm). According to Yonge's (1962) data on size and reproductive condition, the small snails were likely immature.

Serpula columbiana served as the host in these experiments; specimens were collected from Argyle Creek on small stones to which they had attached their tubes. Half of the polychaetes were placed into a 7.5% solution of MgCl₂ for 48 h, after which their bodies were completely removed from tubes. All stones were thoroughly scrubbed to remove epifauna other than *S. columbiana*. Each stone, now bearing either a single living host or a single host tube without a living occupant, was placed into its own plastic box (9 × 9 × 9 cm) with walls of plastic screen (mesh size 1 mm). Boxes were submerged in a single tank of flowing seawater, which ranged in temperature from 9° to 13° C over the course of the experiments.

In the first experiment with small individuals of *T. cancellata* (Oct 1995–Jun 1996), 20 snails (initial shell height 4.0–7.0 mm) were distributed among 10 boxes, 5 of which contained hosts and 5 of which contained tubes only. Hence, each box contained two snails and only one host. In the second experiment (Jul 1996–Mar 1997), 40 snails (initial shell height 5.0–10.0 mm) were distributed among 20 boxes, 10 containing hosts and 10 containing tubes only. Again, each box contained two snails and only one host. This distribution of snails (two per host) is seen frequently in field populations (Pernet and Kohn, pers. obs.).

In the single experiment using large individuals of *T. cancellata* (Aug 1996–Mar 1997), 30 snails (initial shell height 17.0–23.0 mm) were distributed among 30 boxes, 15 containing hosts and 15 containing tubes only. In this experiment each box contained only one snail.

Every 4–8 weeks the snails in each box were measured and checked for mortality, as well as for deposition of benthic egg capsules. Growth was calculated as percent increase in shell height. Boxes were cleaned and their positions in the tank were varied haphazardly at each sampling time.

We compared mean growth in the two treatments in each experiment with Student's *t* tests, and survivorship and reproduction with Fisher's exact tests. In the experiments with small snails we could not consider the two snails in a box to be independent replicates, because they shared an experimental environment; for statistical comparisons each box was treated as an independent replicate. Growth rate in each box was calculated as the mean of the growth rates of the snails in the box, and each box was scored as showing mortality if one or both of its resident snails had died.

Results

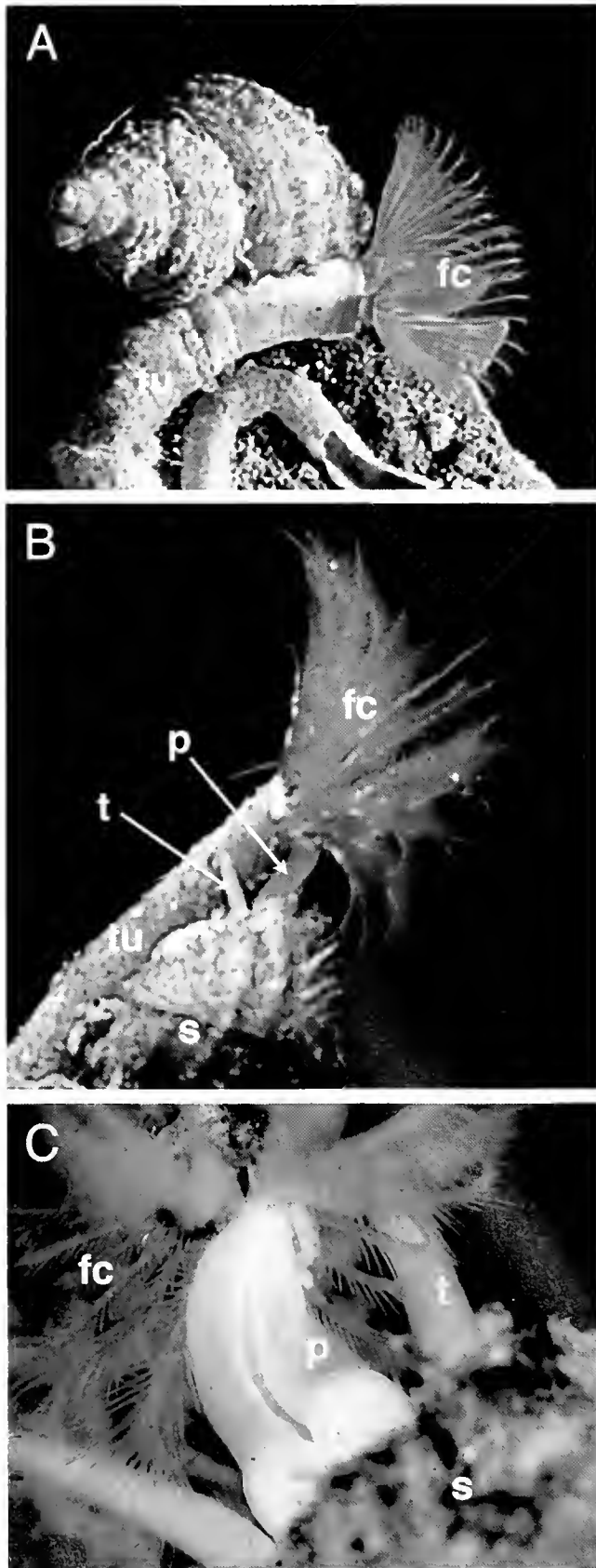
Feeding behavior

Isolated individuals of *Trichotropis cancellata* feed on suspended particles as described by Yonge (1962). Cilia on the ctenidium generate a current through the mantle cavity. Particles drawn into the mantle cavity with the feeding current are captured on the ctenidium, moved down its filaments, and carried around to the right side of the head in a ciliated food groove on the floor of the mantle cavity. Captured particles, often entangled in a bolus of mucus, are then transferred to the pseudoproboscis, a long, tongue-like extension of the lower lip that is bent under the head to the right, where its tip meets the food groove. The particles are carried up the ciliated pseudoproboscis to the mouth, where the radula is used to pull them into the mouth. The snails consumed 40- μ m beads as well as *Artemia* cysts in this fashion.

Snails kept in tanks with a variety of tube-dwelling polychaetes moved onto the worm tubes and positioned themselves near the tube openings (Fig. 1A). Once near a tube opening, snails did not move again unless disturbed. This sessility contrasted with the behavior of snails without hosts; these moved around the tanks frequently. We noticed snails immobile near the tube openings of four species of polychaetes: *Sabellaria cementarium* (Sabellariidae), *Potamilla ocellata* and *Schizobranchia insignis* (Sabellidae), and *Serpula columbiana* (Serpulidae). We did not offer snails other potential host species.

This distribution of *T. cancellata* was also seen repeatedly in the field. Dredged snails were often found attached near the tube openings of sabellariids and sabellids. At Shady Cove, on the east side of San Juan Island, almost all of the many *T. cancellata* seen by divers over a depth range of 5–25 m were found on the tube openings of *Serpula columbiana* (and occasionally of sabellariids and sabellids). Further, host tube openings were frequently attended by as many as five snails. At Eagle Cove, on the west side of the island, almost all of the snails seen by divers were associated with *Sabellaria cementarium*. Again, several snails were often associated with a single host.

We observed interactions between *T. cancellata* and sabellid and serpulid hosts more closely. While host worms were retracted into their tubes, snails used their ctenidia to suspension feed. When the worm's feeding crown eventually emerged from its tube, the snail usually began to probe it gently with its tentacles. This inevitably failed to elicit a reaction from the host, which began feeding, as evidenced by the steady movement of particles down the radioles of the feeding crown and into the worm's mouth. The snail's pseudoproboscis then uncoiled and lengthened (Fig. 1B) and was inserted into



the feeding crown, usually via the dorsal or ventral gap between the radioles of the left and right sides (Fig. 1C). The tip of the pseudoproboscis probed around the base of the radioles until it located and slipped into the polychaete's mouth. At this point particles entering the worm's mouth disappeared briefly into its pharynx, but then reappeared traveling in the opposite direction on the snail's pseudoproboscis towards its mouth. This sudden reversal in particle path was seen most clearly (and could be quantified most easily) with large particles (e.g., *Artemia* cysts), but smaller particles and strings of mucus were also pulled from the worm's mouths and ingested by snails.

Snails fed directly from host mouths in this fashion for periods of minutes to hours. Throughout the snails' feeding activities the worms appeared oblivious to their deprivation. Snail feeding was usually terminated by the worm suddenly retracting into its tube, but this withdrawal usually seemed to be related to external events (e.g., disturbance by the investigator) rather than to the behavior of the snail. On several occasions we observed parasitized sabellids briefly rotating their feeding crowns up to 90°; these actions sometimes dislodged snail pseudoproboscides.

Trichotropis cancellata was extremely efficient in removing *Artemia* cysts from the feeding structures of host polychaetes. In the seven short feeding bouts we observed in unique pairs of snails and worms, *T. cancellata* intercepted 100% of the *Artemia* cysts ($n = 10-40$) captured by hosts *Potamilla ocellata* and *Serpula columbiana*.

Suspension-feeding ability in *Trichotropis cancellata*

Regressions of ctenidium area on body mass for the known suspension feeders *Calyptraea fastigiata* and *Crepidula dorsata* were not significantly different in slope or elevation, so we pooled data from these species for statistical comparison with *T. cancellata*. Over a broad range of body sizes, ctenidium area was significantly smaller relative to body mass in *T. cancellata* than in the

Figure 1. The marine gastropod *Trichotropis cancellata* stealing food from the polychaetes *Serpula columbiana* and *Potamilla ocellata*. (A) *T. cancellata* on the tube of *S. columbiana*, near the crown of feeding tentacles which the worm uses to create a current and capture food particles. *T. cancellata* is also able to suspension feed, using its ciliated ctenidium hidden by the shell in the mantle cavity. (B) *T. cancellata* on the tube of *P. ocellata*. The snail's pseudoproboscis is visible reaching into the worm's feeding crown. (C) A view into the feeding crown of *P. ocellata*, showing the pseudoproboscis of *T. cancellata* entering the mouth of the polychaete, and the snail's tentacles on either side of the pseudoproboscis. Cilia on the pseudoproboscis carry particles from the polychaete's mouth to the snail's mouth. fc = polychaete feeding tentacles, p = pseudoproboscis, s = shell, t = snail tentacles, tu = tube.

two calyptraeids ($P < 0.001$; Fig. 2). Relative growth rates of ctenidia, as indicated by the slopes of regressions of ctenidium area on body mass for *T. cancellata* and the two calyptraeids, were not significantly different ($0.1 < P < 0.2$).

Importance of parasitism to growth, survival, and reproduction

Experimental snails behaved similarly to other *T. cancellata* observed in the laboratory. In particular, those raised with live hosts moved to the openings of host tubes within a few days of being placed in their boxes, and once on the host tubes, they did not move from them for the duration of the experiment. In experiments with small snails, both individuals in a box settled near the tube opening of their shared host. In contrast, individuals of *T. cancellata* raised without hosts moved around on the walls of their boxes.

In both experiments with small snails, those caged with live hosts grew faster and survived better than those caged with empty host tubes. In the first experiment, snails caged with live hosts showed no mortality over 9 months and increased in mean shell height by 25% (Fig. 3A). In contrast, 5 of 10 snails caged without hosts died, and survivors increased in shell length only 9%. Differences between treatments in both growth (t test, $P < 0.05$) and

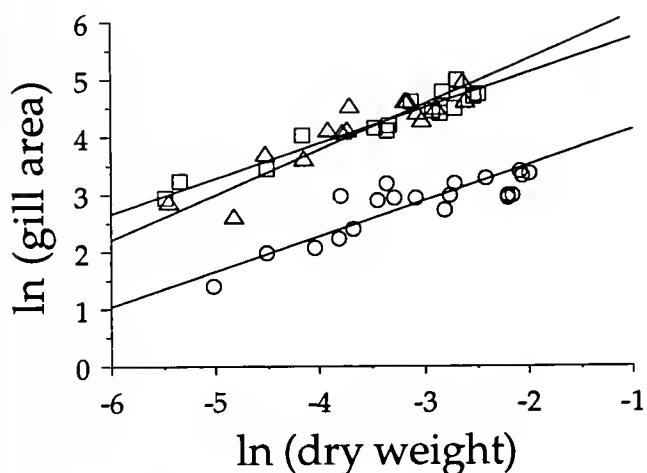


Figure 2. Gill area as a function of dry weight (excluding shell) in *Trichotropis cancellata* (circles, $n = 20$), *Calyptraea fastigiata* (squares, $n = 15$), and *Crepidula dorsata* (triangles, $n = 15$). Lines are reduced major axis regressions of ln-transformed data. Variables (standard error) and coefficients of determination for each of the regressions are *T. cancellata*—intercept 4.649 (0.225), slope 0.593 (0.071), R^2 0.746; *C. fastigiata*—intercept 6.392 (0.333), slope 0.610 (0.089), R^2 0.921; *C. dorsata*—intercept 6.954 (0.171), slope 0.791 (0.048), R^2 0.834. For the regression of pooled *C. fastigiata* and *C. dorsata* data (not shown), the variables and coefficient of determination are intercept 6.607 (0.176), slope 0.692 (0.048), and R^2 0.865.

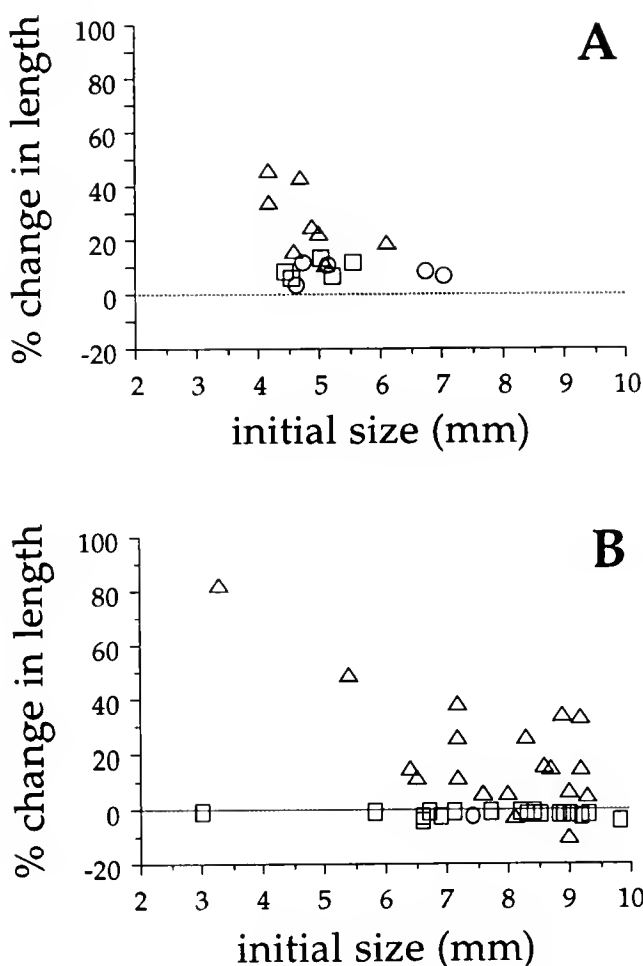


Figure 3. Growth of small *Trichotropis cancellata* maintained in the laboratory with and without living *Serpula columbiana*, measured as percent change in shell height. (A) First experiment, Oct 1995–Jun 1996. *T. cancellata* caged with living hosts (triangles) and with empty host tubes (circles, *T. cancellata* that survived the experiment; squares, *T. cancellata* that died during the experiment). (B) Second experiment, Jul 1996–Mar 1997. *T. cancellata* caged with living hosts (triangles) and with empty host tubes (circle, *T. cancellata* that survived the experiment; squares, *T. cancellata* that died during the experiment).

survivorship (Fisher's exact test, $P < 0.05$) are significant even after sample sizes are adjusted to avoid pseudoreplication. Results of the second experiment were even more dramatic. Here, all snails caged with live hosts survived, and they increased in mean shell length by 19% (Fig. 3B). In contrast, 19 of 20 small snails caged without hosts died, and the single survivor did not grow. The difference in survivorship is highly significant (sample sizes adjusted to avoid pseudoreplication, Fisher's exact test, $P < 0.0001$).

The shell lengths of large snails did not change over the 8-month experiment, whether they were caged with or without hosts. Neither was there a difference in survi-

vorship: 14 of 15 survived the experiment in each treatment. However, the availability of hosts enhanced reproduction of large individuals of *T. cancellata*. Significantly more snails caged with live hosts (7 of 14) deposited egg capsules than those caged with empty host tubes (1 of 14) (Fisher's exact test, $P = 0.03$). All egg capsules contained fertilized, developing embryos, even though none of these snails had had access to mates for at least 6 months prior to capsule deposition.

Discussion

The marine gastropod *Trichotropis cancellata* is able to use two distinct feeding mechanisms, independent suspension feeding and kleptoparasitism of suspension-feeding polychaetes. It employs the former as described by Yonge (1962)—particles are captured on the ctenidium and moved to the mouth *via* the ciliated pseudoproboscis. Parasitism involves inserting the tongue-like pseudoproboscis into the mouth of a suspension-feeding polychaete, where it intercepts particles captured by the worm. Thus *T. cancellata* takes advantage of the large feeding filters of hosts without paying the metabolic costs of generating flow or capturing particles. The frequent association of snails with the tubes of suspension-feeding polychaetes in the field (Pernet and Kohn, pers. obs.) suggests regular use of this feeding strategy.

Several lines of evidence suggest that parasitism is a more important feeding mode than is suspension feeding in *T. cancellata*. First, ctenidial area in *T. cancellata* is significantly smaller relative to body mass than it is in the known suspension feeders *Calyptrea fastigiata* and *Crepidula dorsata*, over a broad range of body sizes (Fig. 2). This result is comparable to that of Meyhöfer (1985), who found that the ctenidial area relative to body mass of a deposit-feeding bivalve was less than those of three suspension-feeding bivalves. The morphology of the ctenidia also differs between the known suspension feeders and *T. cancellata*. The ctenidia of *Calyptrea fastigiata* and *Crepidula dorsata* have the long, filamentous lamellae typical of suspension feeders (Yonge, 1938; Declerck, 1995), whereas the ctenidia of *T. cancellata* have broader, triangular lamellae more similar to those of gastropods that feed by other means (Kohn and Pernet, pers. obs.). These data imply that *T. cancellata* individuals of all sizes are less effective suspension feeders than are members of the Calyptraeidae.

Second, our laboratory experiments show that individuals of *T. cancellata* raised with hosts (and thus able to feed by both parasitism and suspension feeding) are more fit than those raised without hosts (and thus only able to suspension feed). Suspension feeding alone provided insufficient energy to support growth and survival of small snails or reproduction by large snails. These results

should be applied to natural situations with caution, however, because we did not compare the concentration of suspended food particles in the laboratory with natural food levels. If food concentration in our experimental tank was lower than that typically seen in nature (because, for example, suspension-feeding organisms inhabiting the seawater system had depleted incoming water of plankton), growth, survival, and reproduction of snails raised without hosts may have been limited by available food supplies and not by their suspension-feeding abilities. Also, low food levels may have influenced the feeding behavior of serpulids in ways that made parasitism more profitable for snails. For example, low particle concentrations may have stimulated serpulids to feed more frequently, making them available to be parasitized more frequently. Although we suspect that these complications will not alter the main result—that the presence of hosts greatly enhances growth, survival, and reproduction of *T. cancellata*—repeating these experiments in the field is clearly necessary. Preliminary short-term field experiments (E. Iyengar, unpub. data) corroborate our laboratory results that the presence of serpulid hosts greatly enhances growth of small individuals of *T. cancellata*.

Third, the behavior of snails in the laboratory is consistent with the hypothesis that parasitism is more valuable than suspension feeding for *Trichotropis cancellata*. Once a snail finds a host tube, it usually remains there unless it is removed; for example, one *T. cancellata* associated with a *Serpula columbiana* in a laboratory tank did not move from the tube opening for about 11 months (C. E. Mills, pers. comm.). In contrast, snails that are not associated with a host move frequently. Yonge (1962) noted that snails held without hosts invariably move upwards. He interpreted this climbing behavior as an adaptation for enhancing suspension-feeding efficiency by moving to regions of high flow, but it can also be interpreted as a means of locating the tube openings of potential hosts. Although the behavior of *T. cancellata* in the field has not yet been studied, the fact that snails are frequently found on polychaete tubes there is striking (Pernet and Kohn, pers. obs.).

In our laboratory experiments, small snails raised without hosts suffered high mortality, suggesting that they are obligate parasites. In contrast, large snails raised without hosts did not suffer any mortality. What might cause this difference? Declerck (1995) argued that suspension feeding is less efficient in small gastropods than in large ones, for several morphological and mechanical reasons. For example, the ctenidia (and thus the ability to generate flow and capture particles) of small snails may not yet be fully developed. A more fundamental problem with small size may be the increased energy required to generate flow through a mantle cavity of small dimensions. The power required to generate a given volume flux through a

tubular conduit varies inversely with its radius to the fourth power; similarly, the power required to generate a given flow velocity through such a conduit varies inversely with conduit radius squared (Vogel, 1981). For conduits that are not circular in cross-section, these relationships are also inverse (e.g., rectangular conduits: Denny, 1993). Hence, if mantle cavity dimensions increase with body size (e.g., Declerck, 1991), small snails may have to invest relatively more energy than large ones to generate adequate flow through the mantle cavity for suspension feeding.

We observed *T. cancellata* parasitizing four species of polychaetes of three families. This is a minimal estimate of host range, as we did not test other potential hosts. Although our experiments show that parasitism of *Serpula columbiana* is more profitable than independent suspension feeding for *T. cancellata*, the outcome of interactions with other hosts may be different. For example, other host species might have behavioral or morphological traits that might reduce the effectiveness of parasitism. Likewise, though field experiments show that parasitism by *T. cancellata* greatly reduces the growth rates of *S. columbiana* (Pernet and E. Iyengar, unpub. data), the magnitude of such negative effects may vary among host species, for several reasons. Hosts may vary in behavioral parameters like time allocated to feeding, sensitivity to probing pseudoproboscides, and presence or absence of defenses against parasites. Detailed understanding of the effects of *T. cancellata* on its various hosts thus requires more information on the behavioral ecology of suspension-feeding polychaetes (e.g., Wildish and Lobsjger, 1987; Dill and Fraser, 1997), as well as that of *T. cancellata*.

On the basis of his studies of suspension feeding in *T. cancellata* and other gastropods, Yonge (1962) argued that *T. cancellata* might be important in understanding the evolution of suspension-feeding neotaenioglossan limpets. He suggested that limpets such as modern *Calyptraea* and *Crepidula* evolved from an ancestral grazing snail with a typical conispiral shell via a suspension-feeding intermediate like *T. cancellata*. Thus suspension feeding preceded the limpet-shaped shell, the latter evolving as an adaptation for resistance to dislodgement in the sedentary suspension feeder (Yonge, 1962). Our data show that *T. cancellata* is not particularly well-suited as a model intermediate in this scenario. *T. cancellata* is not a very effective suspension feeder; parasitism of suspension-feeding polychaetes is likely a more important contributor to its fitness than is suspension feeding. A convincing test of Yonge's hypothesis awaits phylogenetic analysis of the order Neotaenioglossa.

Morphological characters of its larvae and adults suggest that *T. cancellata* is closely related to the members of the genus *Capulus* (Bouchet and Warén, 1993; Pernet, unpub. data). These are thought to employ both indepen-

dent suspension feeding (Yonge, 1938) and parasitism of other suspension feeders (including bivalves, gastropods, brachiopods, and polychaetes: reviewed by Thorson, 1965). Further studies of the feeding biology of these snails and of their relationships with other neotaenioglossan groups are needed before we can understand the history of these dual feeding modes, but our observations suggest a hypothesis for the evolution of parasitism in capulid gastropods. Ctenidial suspension-feeding molluscs may face constraints on suspension-feeding efficiency when small, for several morphological and mechanical reasons (Declerck, 1995). Some gastropods appear to overcome these constraints by using the alternate feeding mode of benthic grazing at small sizes. As the mantle cavity and ctenidium increase in size with growth, suspension feeding may become energetically more attractive and eventually becomes the primary feeding mode (Declerck, 1995). We suggest that capulid gastropods, including *T. cancellata*, have coped with the high cost of suspension feeding at small sizes by adopting a novel feeding strategy—parasitism of other suspension feeders. The superiority of this parasitic feeding mode for snails of all sizes may explain why it persists throughout life.

Similar size-dependent constraints on feeding efficiency are widespread in animals and may underlie many ontogenetic shifts in trophic mode (Werner and Gilliam, 1984). We suggest that when particular ontogenetic stages adopt novel feeding modes as an evolutionary response to such constraints, the new mode may occasionally supersede the ancestral one throughout the life history, as may have occurred in *Trichotropis cancellata*.

Acknowledgments

B. Pernet was supported by an NSF predoctoral fellowship and awards from the Lerner-Gray Fund for Marine Research and the PADI Foundation. We thank K. Britton-Simmons, R. Collin, and E. Iyengar for assistance with diving and for helpful discussion; R. R. Strathmann for comments on an earlier version of the manuscript; and the director and staff of Friday Harbor Laboratories for facilities and support.

Literature Cited

- Bouchet, P., and A. Warén. 1993. Revision of the northeast Atlantic bathyal and abyssal Mesogastropoda. *Boll. Malacol.*, suppl. 3: 577–840.
- Carbone, C., J. T. Du-Toit, and I. G. Gordon. 1997. Feeding success in African wild dogs: does kleptoparasitism by spotted hyenas influence group hunting size? *J. Anim. Ecol.* 66: 318–321.
- Crowder, L. B. 1985. Optimal foraging and feeding mode shifts in fishes. *Environ. Biol. Fishes* 12: 57–62.

- Declerck, C. H. 1991.** Evolution and comparative functional morphology in suspension feeding prosobranch gastropods. Ph.D. dissertation, University of California, Davis. 141 pp.
- Declerck, C. H. 1995.** The evolution of suspension feeding in gastropods. *Biol. Rev. Camb. Philos. Soc.* **70**: 549–569.
- Denny, M. W. 1993.** *Air and Water*. Princeton University Press, New Jersey.
- Dill, L. M., and A. H. G. Fraser, 1997.** The worm re-turns: hiding behavior of a tube-dwelling marine polychaete, *Serpula vermicularis*. *Behav. Ecol.* **8**: 186–193.
- Eeckhaut, I., B. Dochy, and M. Jangoux. 1995.** Functional morphology of the introvert and digestive system of *Myzostoma cirriferum* (Myzostomida). *Acta Zool.* **76**: 307–315.
- Ehlinger, T. J. 1989.** Foraging mode switches in the golden shiner (*Notemigonus chrysoleucas*). *Can. J. Fish. Aquat. Sci.* **46**: 1250–1254.
- Elgar, M. A. 1993.** Interspecific associations involving spiders: kleptoparasitism, mimicry, and mutualism. *Mem. Queensl. Mus.* **33**: 411–430.
- Gerking, S. D. 1994.** *Feeding Ecology of Fish*. Academic Press, New York.
- Gihson, R. N., and I. A. Ezzi. 1985.** Effect of particle concentration on filter and particulate feeding in the herring, *Clupea harengus*. *Mar. Biol.* **88**: 109–116.
- Kupriyanova, E. K. 1995.** Re-establishment of *Serpula columbiana* Johnson 1901 with a discussion of ontogenetic variability of taxonomic characters. *Am. Zool.* **35**: 114A.
- Kupriyanova, E. K., and A. V. Rzhavsky. 1993.** *Serpula* and *Crucigera* from the Russian far-eastern seas. *Ophelia* **38**: 47–54.
- LaBarbera, M. 1989.** Analyzing body size as a factor in ecology and evolution. *Annu. Rev. Ecol. Syst.* **20**: 97–117.
- Lauder, G. V., A. W. Crompton, C. Gans, J. Hanken, K. F. Liem, W. O. Maier, A. Meyer, R. Prestley, O. C. Rieppel, G. Roth, D. Schluter, and G. A. Zweers. 1989.** How are feeding systems integrated and how have evolutionary innovations been introduced? Pp. 97–115 in *Complex Organismal Functions: Integration and Evolution in Vertebrates*. D. B. Wake and G. Roth, eds. John Wiley, New York.
- Meyhöfer, E. 1985.** Comparative pumping rates in suspension-feeding bivalves. *Mar. Biol.* **85**: 137–142.
- Möhlenburg, F., and H. U. Riisgård. 1979.** Filtration rate, using a new indirect technique, in 13 species of suspension-feeding bivalves. *Mar. Biol.* **54**: 143–147.
- Taghon, G. L., and R. R. Greene. 1992.** Utilization of deposited and suspended particulate matter by benthic “interface” feeders. *Limnol. Oceanogr.* **37**: 1370–1391.
- Taghon, G. L., A. R. M. Nowell, and P. A. Jumars. 1980.** Induction of suspension feeding in spionid polychaetes by high particulate fluxes. *Science* **210**: 562–564.
- Thorson, G. 1965.** A neotenus dwarf-form of *Capulus ungaricus* (Gastropoda: Prosobranchia) commensalistic on *Turritella communis* Risso. *Ophelia* **2**: 175–210.
- Turner, E. J., and D. C. Miller. 1991.** Behavior of a passive suspension-feeder (*Spiochaetopterus oculus* (Webster)) under oscillatory flow. *J. Exp. Mar. Biol. Ecol.* **149**: 123–137.
- Vickery, J. A., and M. D. L. Brooks. 1994.** The kleptoparasitic interactions between great frigatebirds and masked boobies on Henderson Island, South Pacific. *Condor* **96**: 331–340.
- Vogel, S. 1981.** *Life in Moving Fluids*. Princeton University Press, New Jersey.
- Werner, B. 1951.** Über die Bedeutung der Wasserstromerzeugung und Wasserstromfiltration für die Nahrungsaufnahme der ortsgewundenen Meereschnecke *Crepidula fornicata*. *Zool. Anz.* **146**: 97–113.
- Werner, B. 1953.** Über den Nahrungserwerb der Calyptraeidae. Morphologie, Histologie, und Funktion der am Nahrungserwerb beteiligten Organe. *Helgol. Wiss. Meeresunters.* **4**: 260–315.
- Werner, E. E., and J. F. Gilliam. 1984.** The ontogenetic niche and species interactions in size-structured populations. *Annu. Rev. Ecol. Syst.* **15**: 393–425.
- Wildish, D. J., and U. Lohsiger. 1987.** Three-dimensional photography of soft-sediment benthos, S. W. Bay of Fundy. *Biol. Oceanogr.* **4**: 227–241.
- Yonge, C. M. 1938.** Evolution of ciliary feeding in the Prosobranchia, with an account of feeding in *Capulus ungaricus*. *J. Mar. Biol. Assoc. U. K.* **22**: 453–468.
- Yonge, C. M. 1962.** On the biology of the mesogastropod *Trichotropis cancellata* Hinds, a benthic indicator species. *Biol. Bull.* **122**: 160–181.
- Zamora, R., and J. M. Gomez. 1996.** Carnivorous plant-slug interaction: a trip from herbivory to kleptoparasitism. *J. Anim. Ecol.* **65**: 154–160.
- Zar, J. H. 1996.** *Biostatistical Analysis*. 3rd ed. Prentice-Hall, Upper Saddle River, NJ.

GENETIC REGULATORY NETWORKS in Embryogenesis and Evolution

Proceedings
of a workshop
sponsored by
THE CENTER FOR ADVANCED STUDIES
IN THE SPACE LIFE SCIENCES
AT THE MBL

11–14 June 1997

Marine Biological Laboratory,
Woods Hole, Massachusetts

Funded by
THE NATIONAL AERONAUTICS
AND SPACE ADMINISTRATION
under Cooperative Agreement
NCC 2-896



CONTENTS

Genetic Regulatory Networks in Embryogenesis and Evolution

Cameron, R. Andrew			
Introduction	361		
Henry, Jonathan Q., and Mark Q. Martindale			
Evolution of cleavage programs in relationship to axial specification and body plan evolution	363		
van Loon, A. E., and J. A. M. van den Biggelaar			
Changes in cell lineage specification elucidate evolutionary relations in Spiralia	367		
Shankland, Marty, and Ashley E. E. Bruce			
Axial patterning in the leech: developmental mechanisms and evolutionary implications	370		
Akam, Michael			
Hox genes in arthropod development and evolution		373	
Slack, Frank, and Gary Ruvkun			
Heterochronic genes in development and evolution		375	
Hobert, Oliver, and Gary Ruvkun			
A common theme for LIM homeobox gene function across phylogeny?		377	
Satoh, Noriyuki			
Mechanisms of specification in ascidian embryos		381	
Published by title only			384
Chairs and speakers			384



Introduction

The participants in the workshop “Genetic Regulatory Networks in Embryogenesis and Evolution” gathered to consider the challenging and provocative problem of the evolutionary mechanisms that led to the appearance and diversification of animal body plans. They share the conviction that the developmental regulatory circuitry encoded in the genomes of modern invertebrate animals holds the keys to understanding metazoan evolution.

Detailed analyses of gene regulation in a wide variety of invertebrates, considered from a comparative perspective, occupied the attention of the participants. Michael Akam’s group (Cambridge University) has established that, in *Drosophila*, it is the *cis*-regulatory system of the *Ubx* gene that determines exactly where the gene will be expressed. Michael Levine and his group (UC Berkeley) described recent extensions of their elegant analyses of the *cis*-regulatory mechanisms that are required to set the boundaries of expression domains in early *Drosophila* embryos. The first developmental *cis*-regulatory analysis ever carried out in a molluscan embryo, reported by Andre van Loon (Utrecht), revealed that negative controls are required to confine expression of a tubulin gene to the trochoblast lineage. Gary Ruvkun and his group (Harvard Medical School) reported progress in one of the most essential, but generally still unsolved problems in unraveling gene regulatory networks: *viz.*, how to find the downstream target genes of given transcription factors. Work from the Davidson group on sea urchins and the Levine group on *Drosophila* and ascidians has, along with other studies in vertebrates, led to the emerging general view that metazoan *cis*-regulatory regions are organized into modules wherein local interactions between negative and positive elements occur. In many cases, negative interactions are required to set boundaries. This view, in turn, provides a major insight into the evolutionary generation

of novel developmental processes, by exchange, translocation, addition, or subtraction of *cis*-regulatory modules.

Among the most exciting themes of the workshop was phyletic homology in patterns of gene expression. An extensive search for genes that are expressed in the ascidian embryo and that also have homologs in other chordates and related invertebrates was described by Nori Satoh (Kyoto). Prominent among these are the transcription factors, *forkhead* and *Brachyury*. The Levine group reported that the transcriptional activation of *Brachyury* in ascidian embryos is a direct zygotic event in the specification of notochord cells. Satoh showed that *Brachyury* is activated late in embryogenesis at the anterior end of the gut in embryos of *Ptychodera*, an indirectly developing hemichordate; it is also expressed in the secondary mesenchyme that delaminates from the anterior end of the gut in sea urchin embryos.

Homologous cellular processes underlying embryogenesis in various taxa was another major theme of the workshop. Recent work on annelids from Martyr Shankland’s group (UT, Austin) and studies of nemerteans and flatworms by Jonathan Henry (University of Illinois) and Mark Martindale (University of Chicago) have illuminated the homologies—found throughout the Spiralia—that relate the contributions of the micromere quartet to axial symmetry. Martindale extended this comparative view of early embryonic development to the radially organized animals, cnidarians and ctenophores. The morphogenetic processes of later embryogenesis, invagination and ingression, are rapidly being characterized in molecular terms to the sea urchin embryo by Dave McClay’s group (Duke University). The observation, from Chuck Ettensohn (Carnegie-Mellon), that secondary mesenchyme cells can replace the normal skeletogenic lineage of the sea urchin embryo suggests that embryonic skeletogenesis may really be a character of an adult body plan that has been, to different extents, heterochronically inserted into embryogenesis.

Participants in this workshop also focused on the general mechanism used by most invertebrate bilaterian groups to specify the fate of blastomeres during cleavage, largely in response to short-range signals from adjacent blastomeres. Dave McClay’s group showed that beta-

This article introduces a series of papers that were originally presented at a workshop titled *Genetic Regulatory Networks in Embryogenesis and Evolution*. The workshop, which was held at the Marine Biological Laboratory, Woods Hole, Massachusetts, from 11 to 14 June 1997, was sponsored by the Center for Advanced Studies in the Space Life Sciences at MBL and funded by the National Aeronautics and Space Administration under Cooperative Agreement NCC 2-896.

catenin is localized, in sea urchin embryos, to the nuclei of exactly those vegetal plate cells that express the vegetal plate marker *Endo16*. Joel Rothman (UC Santa Barbara) described the successive utilization of the *Notch* signaling pathway that specifies all eight sublineages descendant from the AB blastomere in *Caenorhabditis elegans*.

The experimental proceedings of the workshop were interlaced with theories, arguments, and speculations, which provided an unusual intellectual quality to the proceedings. Davidson, Cameron, and Peterson had previously proposed that the relatively rapid elaboration of the body plans of the large animals that have populated the Earth since before the Cambrian boundary was due to the appearance of populations of undifferentiated cells, set aside from the job of forming the embryo, and equipped with the prerequisite, regional specification capacity to pattern the adult. Davidson and colleagues now inferred further that the *Hox* gene cluster is not utilized in the development of the embryo or larva of a modern

indirectly developing species, but is used at the stage when the adult body plan is generated from the larval imaginal rudiment; *i.e.*, from set-aside cells. Pedro Martinez and Cesar Arenas in Davidson's laboratory recently characterized the *Hox* gene cluster of *Strongylocentrotus purpuratus*, and measured the expression of these genes. None of the "anterior" *Hox* genes, nor some others, are expressed at all until the adult rudiment forms. Are these larvae indeed representative of the earliest metazoans in their regulatory characteristics? The flexible schedule, which left time for extensive discussion, provided the participants in this workshop with the luxury of being able to think in an evolutionary sense about discoveries in both gene regulation and the control of development.

R. ANDREW CAMERON
Division of Biology
California Institute of Technology
Pasadena, California

Evolution of Cleavage Programs in Relationship to Axial Specification and Body Plan Evolution

JONATHAN Q. HENRY¹ AND MARK Q. MARTINDALE²

¹*Department of Cell and Structural Biology, The University of Illinois, Urbana, Illinois 61801; and*

²*Department of Organismal Biology and Anatomy, The University of Chicago, 1027 E. 57th St., Chicago, Illinois 60637*

We examine egg organization and the role of the early cleavage program in establishing the axial properties of larval and adult body plans. Here we review our own work and that of others on various invertebrate metazoans, including cnidarians, ctenophores, polyclad flatworms, and some protostome spiralian—nemerteans, molluscs, and polychaete annelids.

The Ctenophores

Most metazoan body plans can be characterized as having either elements of radial symmetry (such as the Cnidaria and Ctenophora) or bilateral symmetry (e.g., protostomes and deuterostomes). Cnidarians are considered to be radially symmetrical around their longitudinal body axis, called the oral-aboral axis, whereas ctenophores display “biradial symmetry” around their oral-aboral axis. Although their phylogenetic relationship to other metazoans remains controversial, ctenophores may represent the sister-group to the Bilateria. The transition from radial to bilateral symmetry can be viewed as one of the most important events in body plan evolution, and the study of the extant cnidarians and ctenophores may therefore help us to understand the evolution of the anterior-posterior and dorso-ventral axes of bilaterians.

This paper was originally presented at a workshop titled *Genetic Regulatory Networks in Embryogenesis and Evolution*. The workshop, which was held at the Marine Biological Laboratory, Woods Hole, Massachusetts, from 11 to 14 June 1997, was sponsored by the Center for Advanced Studies in the Space Life Sciences at MBL and funded by the National Aeronautics and Space Administration under Cooperative Agreement NCC 2-896.

Virtually all bilaterian metazoan phyla undergo a stereotyped, species-specific cleavage program, but some basal metazoans (i.e., sponges and most cnidarians) do not. This raises the question of how and why stereotypical cleavage programs evolved. One distinct feature of ctenophores, which sets them apart from other radially symmetrical forms, is their phylum-specific, highly stereotyped mode of development (see 1–3 for reviews). Previous work has demonstrated that the cleavage program is causally involved with the establishment of cell fates in the ctenophore (4–6), and that the capacity to replace structures derived from missing blastomeres (“mosaic development”) is lacking. For example, previous chalk-particle marking experiments indicated that the eight rows of comb plates in ctenophores are derived from the four e_1 micromeres of the 16-cell embryo (7), and deletion of these four micromeres results in the absence of comb rows and their associated endodermal canal system (8–10).

Using intracellular cell lineage techniques on embryos of the lobate ctenophore *Mnemiopsis leidyi*, however, we showed that the m_1 micromeres (Fig. 1A) also contribute to comb plate formation during normal development. Thus, if comb plates do not form after e_1 micromere removal, then some blastomere fates in the early embryo must not be precociously specified at the time of their birth, as previously argued. Rather, inductive interactions by the descendants of the e_1 micromeres organize (Fig. 1B) development in adjacent ectodermal and endodermal lineages (11, 12). We suggest that stereotypical cleavage programs arose during metazoan evolution as a reliable means of segregating factors to distinct embryonic lineages, some of which serve as inductively active “signaling centers.” These signaling centers or-

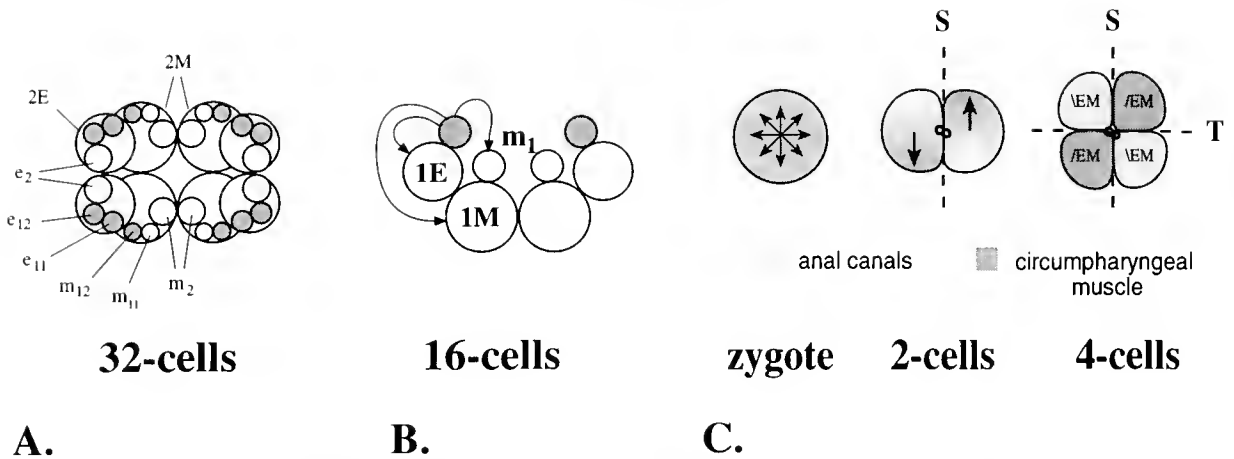


Figure 1. Views of the ctenophore embryo at various stages of development. (A) Aboral view of a 32-cell stage embryo. The shaded cells indicate the blastomeres which normally give rise to comb plates. Note that only one of the two daughter cells of the m_1 micromere makes comb plates (m_{12}). Previous work failed to detect any contribution from the 'M' lineage. (B) Lateral view of a 16-cell stage embryo. The arrows indicate that the e_1 micromeres (shaded) are required to induce comb plates from m_1 micromere lineages (unshaded) and for endodermal derivatives from the 1E and 1M macromeres. (C) Oral views of the changing axial properties. Following fertilization the embryo is radially symmetrical around the pre-emptive oral-aboral axis. By the 4-cell stage two distinctly different types of blastomeres are present. Only one pair, the \EM blastomeres, will give rise to the endodermally derived anal canals, while the other pair, /EM, will give rise to muscle cells around the pharynx. This means that these blastomeres become polarized in opposite orientations sometime before the end of second cleavage.

organize subsequent development in adjacent lineages. Stereotypic cleavage patterns are a means of reliably positioning these organizing centers and the cells that respond to their signals. Other cells may be determined by autonomous mechanisms. These strategies for early patterning are prevalent in many metazoan embryos (13, 14). Although the molecular nature of inductive signals in ctenophores is unknown, several known pathways, such as those involving *wg*/ β -catenin, are reasonable places to start looking.

Most authorities believe that bilaterally symmetrical organisms evolved from a radially symmetrical ancestor. Little is known about how this transition occurred. For example, no agreement about the relationship between the oral-aboral axes of cnidarians and ctenophores and the anterior-posterior axis of bilaterians has been reached. The apparent conservation in the molecular mechanisms leading to the establishment of the dorsoventral axis in the common ancestor of protostomes and deuterostomes (the *dpp/sog* orthologs) adds to speculation that an existing axis was co-opted for the dorso-ventral axis. On the other hand, this axis may have arisen *de novo* (15). We have shown in ctenophores that some mesodermal and endodermal lineages are organized in a pattern that is diagonally opposed to the first and second cleavage planes (Fig. 1C). Because these lineages give rise to the

oral-anal plane, this organization could reflect a transition from a radial to a bilaterally symmetrical body plan (16). We propose different scenarios for generating these changes in body plan organization based on the expression of highly conserved developmental regulatory genes.

The Spiralian

The highly stereotypic cleavage pattern referred to as "spiral cleavage" occurs in most of the extant invertebrate phyla, including the molluscs, annelids, vestimentiferans, pogonophorans, echiurans, sipunculids, nemertean, gnathostomulids, mesozoans, and polyclad turbellarians. Cell lineage analyses, mainly conducted on annelidan and molluscan embryos, suggested that the ultimate fates of blastomeres are tremendously conserved.

More recently, we have been examining the development of representatives from a number of different spiralian phyla to determine the extent of homologies in the spiralian developmental program. For instance, our work in collaboration with Barbara Boyer has confirmed earlier reports that the polyclad flatworms display a cell lineage fate map similar to that of the annelids and molluscs (17, 18, 19). Early investigators suggested that the acoelomate platyhelminthes (flatworms) are basal to the bilaterian metazoans, but more recent phylogenetic analyses place

them as basal members of the protostome spiralian (20, 21). In either case, the developmental pattern exhibited by the polyclads should be more closely representative of the basal condition within the Spiralia.

We have also demonstrated that the Nemertea, a coelomate invertebrate phylum, also exhibits strong homologies to the basic spiralian cleavage program. In addition to possessing cell quadrant identities similar to those found in other spiralian (*i.e.*, A, B, C, and D quadrants), the embryos also give rise to both ecto- and endomesoderm (22, 23). Although the general spiralian developmental program is highly conserved in this group, it does exhibit some modifications in the form of what Lillie referred to as "adaptations in cleavage" (23). These include the formation of a first quartet of micromeres of greatly increased size that generates the majority of the larval ectoderm. Other changes have occurred in the sub-lineages that give rise to certain structures, such as the ciliated band (derived from first, second, and third quartet derivatives) and the ectomesoderm (derived entirely from 3a and 3b).

The most significant modifications in Nemertea of the spiralian developmental program seem to have affected the mechanisms involved in cell fate and axis determination. Those employed by the nemerteans appear to be distinct from those utilized by equal-cleaving molluscs (24, 25), and differences are encountered between different nemertean species. Our research indicates that larval nemertean axial properties are actually specified before cleavage begins, a condition that does not appear to take place in the embryos of equal-cleaving molluscs (24). Furthermore, the embryos of the indirect-developing nemertean *Cerebratulus lacteus* appear to exhibit a great deal of regulation, while those of a direct-developing species, *Nemertopsis bivittata*, do not (25). We believe that nemerteans exhibit a derived developmental condition, and agree with previous reports that the ancestral spiralian developmental condition was one in which equal, quartet spiral cleavage occurred, and quadrant fates and axial properties were established epigenetically *via* inductive interactions (26).

Acknowledgments

The authors thank the organizers of this meeting and NASA for inviting us to this workshop. M.Q.M. was supported by an American Cancer Society Illinois Division Grant #92-43, NSF grant #9315653, and MBL Spiegel, Davis and NASA Fellowships. J.Q.H. (J.J.H.) was supported by an MBL Associates' Fellowship, a Lemann Fellowship, a Spiegel Fellowship, and a NASA Fellowship.

Literature Cited

1. Reverberi, G. 1971. Ctenophores. Pp. 85–103 in *Experimental Embryology of Marine and Fresh-water Invertebrates*, G. Reverberi, ed. North-Holland, Amsterdam.
2. Ortolani, G. 1989. The ctenophores: a review. *Acta Embryol. Morphol. Exp.* **10**: 13–31.
3. Martindale, M. Q., and J. Q. Henry. 1997. The Ctenophora. Pp. 87–111 in *Embryology, The Construction of Life*, S. Gilbert and A. Raunio, eds. Sinauer, Sunderland, MA.
4. Freeman, G. 1976. The role of cleavage in the localization of developmental potential in the ctenophore *Mnemiopsis leidyi*. *Dev. Biol.* **49**: 143–177.
5. Freeman, G. 1976. The effects of altering the position of cleavage planes on the process of localization of developmental potential in ctenophores. *Dev. Biol.* **51**: 332–337.
6. Freeman, G. 1977. The establishment of the oral-aboral axis in the ctenophore embryo. *J. Embryol. exp. Morphol.* **42**: 237–260.
7. Reverberi, G., and G. Ortolani. 1963. On the origin of the ciliated plates and mesoderm in the Ctenophore. *Acta Embryol. Morphol. Exp.* **6**: 175–199.
8. Driesch, H., and T. H. Morgan. 1895. Zur Analysis der ersten Entwicklungsstadien des ctenophoreeies. *Arch. Entwicklungsmech. Organ.* **2**: 204–224.
9. Farfaglio, G. 1963. Experiments on the formation of the ciliated plates in Ctenophores. *Acta Embryol. Morphol. Exp.* **6**: 191–203.
10. Martindale, M. Q. 1986. The expression and maintenance of adult symmetry properties in the ctenophore, *Mnemiopsis mceradyi*. *Dev. Biol.* **118**: 556–576.
11. Martindale, M. Q., and J. Q. Henry. 1996. Development and regeneration of comb plates in the ctenophore *Mnemiopsis leidyi*. *Biol. Bull.* **191**: 290–292.
12. Martindale, M. Q., and J. Q. Henry. 1997. Reassessing embryogenesis in the Ctenophora: The inductive role of e₁ micromeres in organizing ctene row formation in the "mosaic" embryo, *Mnemiopsis leidyi*. *Development* **124**: 1999–2006.
13. Davidson, E. H. 1991. Spatial mechanisms of gene regulation in metazoan embryos. *Development* **113**: 1–26.
14. Schnabel, R. 1997. Why does a nematode have an invariant cell lineage? *Semin. Cell Dev. Biol.* **8**: 341–349.
15. Lacalli, T. 1996. Dorsoventral axis inversion: a phylogenetic perspective. *BioEssays* **18**: 251–254.
16. Martindale, M. Q., and J. Q. Henry. 1995. Diagonal development: establishment of the anal axis in the ctenophore *Mnemiopsis leidyi*. *Biol. Bull.* **189**: 190–192.
17. Henry, J. Q., M. Q. Martindale, and B. C. Boyer. 1995. Axial specification in a basal member of the spiralian clade: lineage relationships of the first four cells to the larval body plan in the polyclad turbellarian *Hoploplana inquilina*. *Biol. Bull.* **189**: 194–195.
18. Boyer, B. C., J. Q. Henry, and M. Q. Martindale. 1996. Dual origins of mesoderm in a basal member of the spiralian clade: cell lineage studies in the polyclad turbellarian *Hoploplana inquilina*. *Dev. Biol.* **179**: 329–338.
19. Boyer, B. C., J. Q. Henry, and M. Q. Martindale. 1998. The cell lineage of a polyclad turbellarian embryo reveals close similarity to coelomate spiralian. *Dev. Biol.* (in press).
20. Aguinaldo, A. M. A., J. M. Turbeville, L. S. Linford, M. C. Rivera, J. R. Garey, R. A. Raff, and J. A. Lake. 1997. Evidence for a clade of nematodes, arthropods and other moulting animals. *Nature* **387**: 489–493.
21. Balavoine, G. 1997. The early emergence of platyhelminths is

- contradicted by the agreement between 18S rRNA and *Hox* genes data. *C. R. Acad. Sci. Paris* **320**: 83–94.
22. **Henry, J. Q., and M. Q. Martindale. 1996.** The origins of mesoderm in the equal-cleaving nemertean worm *Cerebratulus lacteus*. *Biol. Bull.* **191**: 286–288.
 23. **Henry, J. Q., and M. Q. Martindale. 1997.** Conservation of the spiralian developmental program: cell lineage of the nemertean *Cerebratulus lacteus*. *Dev. Biol.* **200** (in press).
 24. **Henry, J. Q., and M. Q. Martindale. 1996.** The establishment of embryonic axial properties in the nemertean, *Cerebratulus lacteus*. *Dev. Biol.* **180**: 713–721.
 25. **Martindale, M. Q., and J. Q. Henry. 1995.** Modifications of cell fate specification in equal-cleaving nemertean embryos: alternate patterns of spiralian development. *Development* **121**: 3175–3185.
 26. **Freeman, G., and J. W. Lundelius. 1992.** Evolutionary implications of the mode of D quadrant specification in coelomates with spiral cleavage. *J. Evol. Biol.* **5**: 205–247.

Changes in Cell Lineage Specification Elucidate Evolutionary Relations in Spiralia

A. E. VAN LOON AND J. A. M. VAN DEN BIGGELAAR

*Department of Experimental Zoology, Utrecht University, Padualaan 8,
3584 CH Utrecht, The Netherlands*

Introduction

Comparative embryology of the various body plans, and an understanding of the molecular regulation of the establishment of these body plans, are powerful tools that can help us reconstruct the evolutionary relations between the animal phyla. The first Metazoa were undoubtedly radially symmetrical animals with two germ layers: ectoderm and endoderm. Examples of these diploblastic creatures can still be found today, in marine and fresh waters throughout the world. The evolution of a third germ layer, the mesoderm, led, in part, to the great Precambrian radiation of the animal kingdom. Elucidation of the developmental mechanisms underlying the formation of mesoderm could shed light on the evolutionary relations among different phyla. Whether this third germ layer evolved once or developed convergently in a number of ancestral diploblastic forms remains to be demonstrated.

Our recent research has focused on the development of two cell lines typical of the Spiralia (*i.e.*, phyla with spiral cleavage): (1) the stem cell of the mesodermal bands (the mesentoblast) and (2) the trochoblasts. The mesentoblast was chosen because the origin of mesoderm is consistently similar in different Spiralia. The mesentoblast is formed from a single primary endodermal cell that is induced to follow a developmental program different from the other endodermal cells. After induction, the mesentoblast divides and gives rise to the stem cell of the left and right mesodermal bands. A comparative study

of mesentoblast formation may be used to elucidate the evolutionary relations within the Spiralia.

Trochoblasts were analyzed because this cell line can be found in a number of Spiralia. These cells are ectodermally derived and form the prototroch—the larval locomotory organ typical of such spiralian animals as molluscs and annelids but absent in other spiralian animals like the nemertean and flatworms.

In this paper, we discuss the molecular and developmental aspects of trochoblast and mesentoblast formation and their significance to the analysis of the phyletic relations between spiralian phyla.

Trochoblasts

The trochoblasts constitute the first fully specified cell line in a number of spiralian embryos (1). Detailed knowledge of trochoblast specification, however, is limited to *Patella vulgata*, the common limpet. Specification in *Patella* requires that the third cleavage is executed correctly (2); if this cleavage is inhibited, no trochoblast-specific gene expression will occur. Trochoblast specification is completed after the fourth cleavage; thereafter the trochoblasts divide only twice more and then differentiate into ciliated cells. From the fourth cleavage onward, specification is autonomous: *i.e.*, cells isolated from the 16-cell embryo go through two cleavages, enter a division arrest, and become ciliated, just as in the intact embryo.

To investigate the molecular mechanism of trochoblast specification, we first focused on genes encoding tubulin as part of this process. Trochoblasts bear a large number of cilia which, in turn, are mainly composed of tubulin. *In situ* hybridization revealed that tubulin genes are expressed one cell cycle before the last division of the trochoblasts (3). One of the tubulin genes that we cloned from the *Patella* genome appeared to be trochoblast spe-

This paper was originally presented at a workshop titled *Genetic Regulatory Networks in Embryogenesis and Evolution*. The workshop, which was held at the Marine Biological Laboratory, Woods Hole, Massachusetts, from 11 to 14 June 1997, was sponsored by the Center for Advanced Studies in the Space Life Sciences at MBL and funded by the National Aeronautics and Space Administration under Cooperative Agreement NCC 2-896.

cific. The promoter of this gene was coupled to the *Lac-Z*-reporter gene, and the construct was injected into 2-cell embryos. Expression of the reporter gene appeared to be limited to the trochal cells, and began about 30 minutes after the appearance of tubulin mRNA (3). Extensive mapping in the promoter showed that only a small region, between -108 and -1 with respect to the transcription start, is absolutely required for correct expression (4). In this region, two elements—located between -108 and -68 and between -52 and -42 —serve different functions in establishing correct spatiotemporal gene expression. Mutation of the $-108/-68$ element results in expression of the reporter gene in non-trochoblasts. Mutation in the $-52/-42$ region completely abolishes expression of the reporter gene. In addition to these two elements, two others located in the regions $-418/-108$ and $+1/+487$, are required for correct expression; these latter elements can be located either before or after the $-108/-1$ region. We therefore consider the region $-108/-1$ to be the core of the promoter.

Nuclear proteins from different stages of development were isolated and a southwestern blot performed; the core region was used as a probe. Each stage shows a specific array of proteins binding to this core region (A. H. E. M. Klerkx and A. E. van Loon, unpub. data). We therefore assume that at different times in development, different proteins bind to the core region.

As trochoblasts are not exclusively formed in gastropods, but also in other molluscan classes, the *Patella* tubulin promoter was coupled to the *Lac-Z* gene and injected into embryos of representatives of other classes of molluscs. Embryos of a polyplacophoran (*Acanthochiton*) and a scaphopod (*Dentalium*) showed an expression pattern completely comparable with that in *Patella* (A. H. E. M. Klerkx, W. G. M. Damen, A. E. van Loon, and J. A. M. van den Biggelaar, unpub. data). Thus, the molecular mechanism for the regulation of a trochoblast-specific gene is conserved in representatives of different molluscan classes.

The spiralian taxon Annelida is presumed to include the closest relatives of the molluscs, and these worms form trochoblasts that originate from the same cell line as in the molluscs. The tubulin promoter gene construct therefore was injected into embryos of the polychaete annelid *Platynereis*. Seven of the resulting embryos survived to the trochophore stage. One of these showed expression, and that expression was limited to trochoblasts. Injections of the construct into a large number of embryos of another polychaete annelid, *Nereis*, have not resulted in *Lac-Z*-expression.

Nemerteans do not develop into larvae with a proto-troch, but are supposed to be ancestral to the molluscs and annelids. We therefore examined the expression of the *Patella* tubulin promoter construct in nemertean em-

bryos (*Cerebratulus lacteus*). Expression was found, but was not restricted to a specific domain of the 24-h larvae. Similarly, embryos of another spiralian taxon, the flatworms, do not develop trochophore larvae. A small number of embryos of the polyclad flatworm *Hoploplana* were injected with the construct, and no expression was found.

The molecular aspects of trochoblast-specific gene expression in molluscs have been conserved in the Polyplacophora, Scaphopoda, and Gastropoda. As the trochoblasts arise from the same cells in molluscs and annelids, we conclude that they are spiralian phyla with a close evolutionary relationship. The conservation, in molluscs and annelids, of the molecular mechanism regulating the expression of a trochoblast-specific gene needs further support. On the other hand, nemerteans and flatworms do not share the formation of trochoblasts, but nemerteans seem to have the molecular mechanism that is required for a cell-specific expression of the *Patella* trochoblast-specific gene. We therefore consider nemerteans, as well as flatworms, to be more distantly related to molluscs and annelids.

Mesentoblast

In many Spiralia, the most important contribution to the mesoderm derives from the mesentoblast, which produces the two mesodermal bands. In ancestral molluscs, the mesentoblast arises from a primary endodermal cell after an inductive interaction with micromeres in the animal hemisphere (5). This induction also establishes the plane of bilateral symmetry and dorsoventral polarity.

In embryos of *Patella*, the endodermal macromeres 3A–3D extend in the animal direction and make contact with the ectodermal micromeres of the opposite animal pole. Of these macromeres, only one maintains these contacts. This macromere becomes the mesentoblast precursor cell (5). Previous work on the development of the dorsoventral axis and mesentoblast formation in a number of gastropod families has shown that gastropod evolution has been accompanied by a heterochronic shift in mesentoblast formation (6, 7, Figure 1). In a series of gastropods, from Archeogastropoda to Pulmonata, mesentoblast formation is shifted from late cleavage stages to much earlier developmental stages.

In annelid embryos a similar extension of the macromeres 3A–3D occurs during the interval between the fifth and the sixth cleavage. But no single macromere is centralized. Despite the uniform contact that these cells have with the micromeres, one is induced to produce the mesentoblast. This inductive event also establishes the dorsoventral axis. A heterochronic shift in the specification of the dorsal quadrant, comparable to that found in gastropods, is also found in annelids (8).

Specification of the dorsoventral axis and mesentoblast

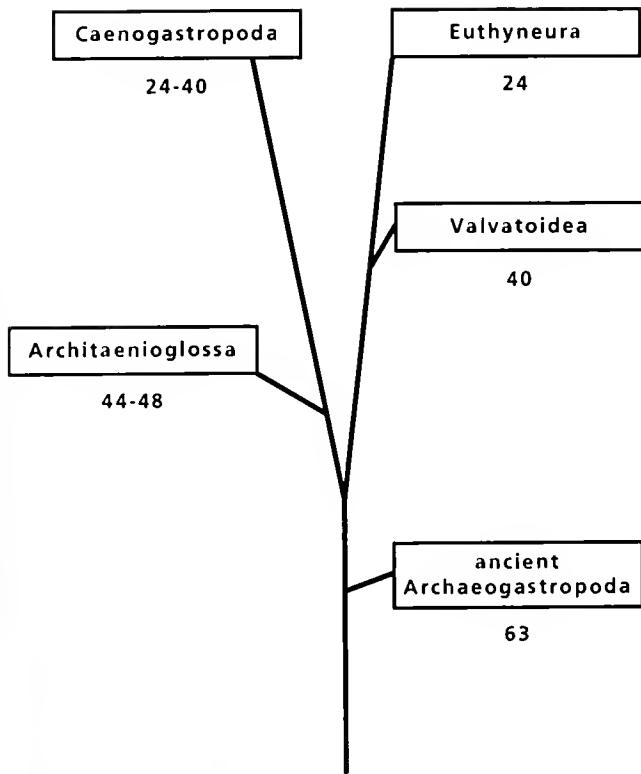


Figure 1. Phylogenetic relations among different gastropod taxa based upon the number of cells in the embryo at the time of the mesentoblast (3D) division (the number of cells is written under the boxed taxon name). The mesentoblast divides into the mesodermal stem cell (4d) and an endoderm precursor (4D). Caenogastropods, together with the Architaenioglossa, probably constitute a separate group, as they form polar lobes during at least the first two cleavages. (After van den Biggelaar and Haszprunar, 1996, ©Allen Press, used with permission)

formation in nemertean and flatworm embryos show similarities and differences compared to molluscs and annelids and to each other. The nemertean embryo is not divided into dorsal, ventral, right, and left quadrants, but into two dorsolateral and two ventrolateral quadrants (9). Despite this alternative quadrant arrangement with respect to the first cleavage planes, bandlets of mesenchymal cells seem to be derived from the same endomesodermal cell (4d) as in annelids and molluscs (10). Like molluscs and annelids, flatworm embryos are also divided into dorsal, ventral, and two lateral quadrants; the specification of the dorsal quadrant, however, must be different. After the formation of the fourth quartet of micromeres, the micromeres 4a–4d extend in the animal direction, in contrast to the macromeres 3A–3D in molluscan and annelid embryos. Finally, it is the micromere of the ventral quadrant (4b) that maintains the contacts with the animal micromeres (van den Biggelaar, unpub. obs.). Micromere 4d of the opposite dorsal quadrant then develops the mesentoblast. These

differences in mesentoblast formation between annelids, molluscs, and nemerteans on the one hand, and flatworms on the other hand, again demonstrate that molluscs, annelids and nemerteans are more close related than with flatworms. The differences between nemerteans and the other two phyla (annelids and molluscs) with respect to the dorsoventral axis specification would argue that annelids and molluscs are more closely related to each other than either is to the nemerteans.

Conclusion

Resemblances in mesentoblast specification and the conservation of the regulatory mechanisms of a trochoblast-specific gene in three different classes of molluscs are consistent with the idea of a monophyletic origin of the molluscs. Trochoblast and mesentoblast specification (coupled to dorsoventral axis formation) in molluscs and annelids strengthens the idea of a close phylogenetic relationship between these phyla. Nemerteans and flatworms have distinct modes of dorsoventral axis formation and do not have a trochoblast cell line, excluding a close evolutionary relation with annelids and molluscs as well as with each other.

Literature Cited

1. Wilson, E. B. 1904. Experimental studies in germinal localization. II Experiments on the cleavage-mosaic in *Patella* and *Dentalium*. *J. Exp. Zool.* **1**: 197–268.
2. Damen, W. G. M., A. H. E. M. Klerkx, and A. E. van Loon. 1996. Micromere formation at third cleavage is decisive for trochoblast specification in the embryogenesis of *Patella vulgata*. *Dev. Biol.* **178**: 238–250.
3. Damen, W. G. M., L. A. van Grunsven, and A. E. van Loon. 1994. Transcriptional regulation of tubulin gene expression in differentiating trochoblasts during early development of *Patella vulgata*. *Development* **120**: 2835–2845.
4. Damen, W. G. M., and A. E. van Loon. 1996. Multiple *cis*-acting elements act cooperatively in directing trochoblast-specific expression of the alpha-tubulin-4 gene in *Patella* embryos. *Dev. Biol.* **176**: 313–324.
5. van den Biggelaar, J. A. M. 1977. Development of dorsoventral polarity and mesentoblast determination in *Patella vulgata*. *J. Morphol.* **154**: 157–186.
6. van den Biggelaar, J. A. M. 1996. The significance of the early cleavage pattern for the reconstruction of Gastropod phylogeny. Pp 155–160 in *Origin and Evolutionary Radiation of the Mollusca*, JD Taylor, ed. Oxford University Press, Oxford.
7. van den Biggelaar, J. A. M., and G. Haszprunar. 1996. Cleavage patterns and mesentoblast formation in the gastropoda: an evolutionary perspective. *Evolution* **50**: 1520–1540.
8. Anderson, D. T. 1973. *Embryology and Phylogeny in Annelids and Arthropods*. Pergamon Press, Oxford.
9. Martindale, M. Q., and J. Q. Henry. 1995. Modifications of cell fate specification in equal-cleaving nemertean embryos: alternate patterns of spiralian development. *Development* **121**: 3175–3185.
10. Henry, J. Q., and M. Q. Martindale. 1996. The origins of mesoderm in the equal-cleaving nemertean worm, *Cerebratulus lacteus*. *Biol. Bull.* **191**: 290–292.

Axial Patterning in the Leech: Developmental Mechanisms and Evolutionary Implications

MARTY SHANKLAND¹ AND ASHLEY E. E. BRUCE²

¹*Department of Zoology, University of Texas at Austin, Austin, Texas 78712; and*

²*Program in Neuroscience, Harvard Medical School, Boston, Massachusetts 02115*

The phylogenetic history of animal body plans, particularly those of the segmented protostomes (arthropods + annelids), is one of the most important topics in the current study of the evolution of developmental mechanisms. Genetic studies of the fruitfly *Drosophila* have uncovered a wealth of information about the molecular biology of development, but the degree to which other animals utilize similar or different mechanisms is not entirely clear, nor is it obvious how and when the mechanisms observed in *Drosophila* first arose during evolution.

Glossiphoniid leeches, such as *Helobdella*, offer numerous advantageous features for embryological research. *Helobdella* embryos are highly amenable to 'classical' embryology: the eggs are large, undergo stereotyped cell lineages, and single cells can be identified and manipulated during the developmental stages when segmentation is being established (1). The segmental body plan of the leech is generated through the iterative cell divisions of teloblastic stem cells situated in a posterior growth zone (2)—a process so outwardly different from what is known of segmentation in insects or vertebrates that a detailed comparison is likely to be informative. Comparing the cellular and molecular mechanisms that underlie pattern formation in different taxa can reveal those aspects of a process that are likely to be homologous or convergent, and can thereby yield significant insight into the evolutionary origin of patterning mechanisms such as segmentation.

This paper was originally presented at a workshop titled *Genetic Regulatory Networks in Embryogenesis and Evolution*. The workshop, which was held at the Marine Biological Laboratory, Woods Hole, Massachusetts, from 11 to 14 June 1997, was sponsored by the Center for Advanced Studies in the Space Life Sciences at MBL and funded by the National Aeronautics and Space Administration under Cooperative Agreement NCC 2-896.

The research in our laboratory has addressed various aspects of pattern formation in *Helobdella*. First, we have examined the establishment of symmetry properties in the unsegmented head and the segmented trunk of the leech. Consistent with the traditional view of spiralian development, the teloblastic stem cells of the posterior growth zone—which generate all of the segmented ectoderm and mesoderm—derive exclusively from the D quadrant of the early 4-cell embryo, with the eventual plane of bilateral symmetry bisecting the derivatives of that quadrant (2). In contrast, lineage tracer analysis of the first quartet of micromeres—progenitors of the unsegmented head ectoderm—reveals that the plane of right-left symmetry falls between bilaterally homologous A and D quadrant derivatives on the left of the embryo, and homologous B and C quadrant derivatives on the right (3). This disparity between the symmetry properties of the first quartet micromeres in the head and the D quadrant derivatives in the trunk is schematized in Figure 1. These results are, in fact, quite consistent with classical studies of polychaete annelids—overlooked by generations of subsequent reviewers—in which the symmetry of the embryonic quadrants was shown to alternate back and forth by 45° between the derivatives from each successive round of micromeres (4, 5).

A second area of interest is the genetic basis of the distinction between the head and the trunk. Studies of fruitflies and mice have shown that a certain group of genes (*otd* and *ems* in flies, and their vertebrate orthologues *Otx* and *Emx*) encode transcription factors that are expressed predominately in head structures—anterior to the boundary of Hox gene expression—in both of these disparate taxa (6). We have cloned and sequenced a *Helobdella* orthologue of *otd* (called *Lox22-Otx*) and, using *in situ* hybridization, have found that it is expressed in every major part of the unsegmented head, including

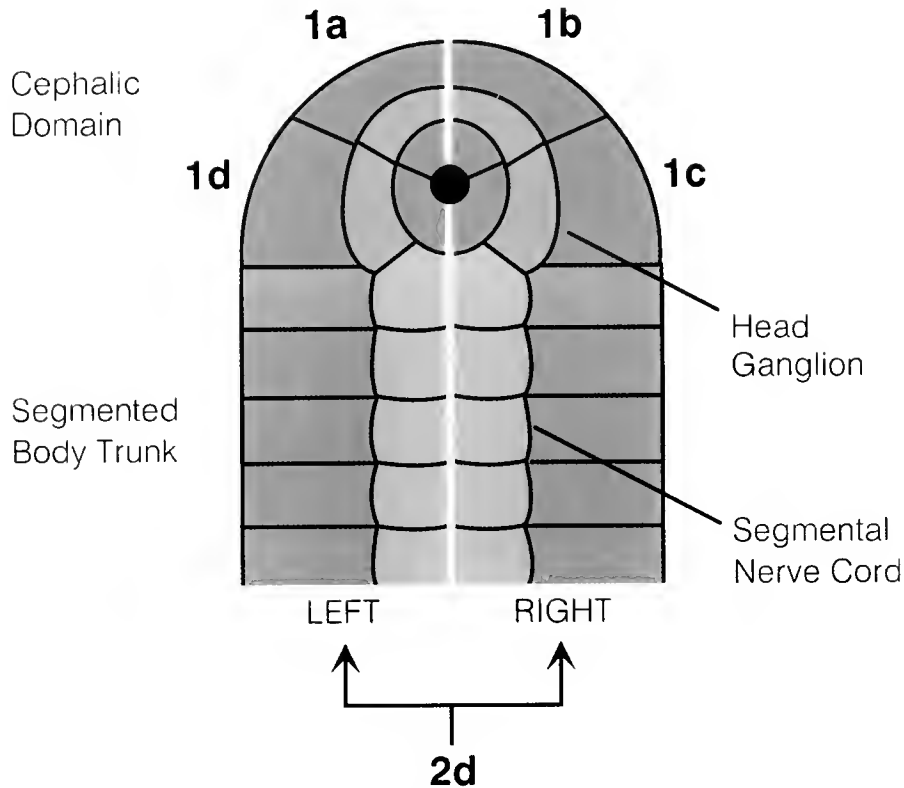


Figure 1. Differing symmetry properties in the progeny of different micromere quartets. Schematic diagram of clonal contributions to ectodermal tissues—body wall and central nervous system—at the head end of the *Helobdella* germinal plate, shown in dorsal view. Four primary micromere clones are shown in shades of orange, with the embryonic mouth or stomadeum situated at the point where the four clones meet. Note that the plane of bilateral symmetry falls between the 1a and 1d clones on the left and the 1b and 1c clones on the right. The definitive ectoderm of the segmented body trunk (turquoise) derives exclusively from the 'micromere' 2d, otherwise known in leeches as cell DNOPQ. In the trunk, the plane of bilateral symmetry thus bisects the derivatives of the D quadrant.

many derivatives of the first quartet of micromeres (7). In contrast, *Lox22-Otx* is not detectably expressed in the body wall of the segmented trunk, and is expressed in only two pairs of segmentally iterated CNS neurons, similar to what is seen in *Drosophila* embryos. This finding further supports the idea that head and trunk were genetically distinct body domains by an early stage in the bilaterian radiation (6).

One possible evolutionary scenario is that the *otd/otx* genes were originally involved in the pattern formation of a radially symmetric pre-bilaterian ancestor, in which they were very likely expressed in patterns concentric about the oral-aboral axis. In the Bilateria, the expression of these genes could then have been relegated to the head by the addition of a trunk domain whose developmental patterning relied on the cooptation or expansion of other genetic pathways. If this model is correct, then the radial organization of micromere cell lineages (3) and *Lox22-Otx* expression (7) that we find around the mouth of the *Helobdella* embryo could be interpreted as the remnants

of a radially organized pre-bilaterian body plan, remnants that have not yet been obscured by the later addition and expansion of trunk-patterning mechanisms.

A third line of research focuses on the analysis—through cloning and expression—of *Helobdella* genes orthologous to known *Drosophila* genes involved in segmentation and segment identity. Most of our work to date has focused on the leech Hox genes (8–10). The leech, like many higher animals, has a number of Hox genes that show segmentally restricted patterns of expression; and the ordering of those expression domains along the anteroposterior body axis corresponds closely with the ordering of their orthologues in other species. The most anteriorly expressed leech Hox gene—the *labial* orthologue *Lox7*—is expressed in all segmental ganglia, but not in the unsegmented head region (10). The majority of leech Hox genes that have been characterized to date are expressed only during the later stages of development, primarily in neurons and mesodermal derivatives that are undergoing terminal differentiation. In addition, cell

transplantation studies have indicated that the segmental founder cells of the leech ('primary blast cells') already possess an intrinsic segment identity several days prior to the onset of Hox gene expression, and will express that original identity—including segment-specific Hox expression—even if their descendant clones are forced to develop in inappropriate segments (9, 11). These findings suggest that, in leeches, the expression of most Hox genes is involved only in the later stages of segmental diversification, and not in the initial establishment of segment identity. However, there are at least two leech Hox genes that do show earlier expression patterns, and their potential significance for segment identity specification is still under investigation.

This work was supported by NSF grant IBN-9506352/IBN-9796063. A.E.E.B. was an Alfred J. Ryan Foundation Fellow, and was also supported by N.I.H. training grants MH18012-09 and NS07009-21 and by the Mahoney Neuroscience Foundation.

Literature Cited

1. Stent, G. S., W. B. Kristan, Jr., S. A. Torrence, K. A. French, and D. A. Weisblat. 1992. Development of the leech nervous system. *Int. Rev. Neurobiol.* **33**: 109–193.
2. Shankland, M., and R. M. Savage. 1997. Annelids, the segmented worms. Pp. 219–235 in *Embryology: Constructing the Organism*, S. F. Gilbert and A. M. Raunio, eds. Sinauer Associates, Sunderland, MA.
3. Nardelli-Haeffliger, D., and M. Shankland. 1993. *Lox10*, a member of the *NK-2* homeobox gene class, is expressed in a segmental pattern in the endoderm and in the cephalic nervous system of the leech *Helobdella*. *Development* **118**: 877–892.
4. Wilson, E. B. 1892. The cell lineage of *Nereis*. *J. Morphol.* **6**: 361–480.
5. Woltereck, R. 1904. Beiträge zur praktischen Analyse der *Polygordius* Entwicklung nach dem "Nordsee"-und "Mittelmeer"-Typus. I. Die für beide Typen gleichverlaufende entwicklungsabschnitt: Vom Ei bis zum jüngsten Trochophora-Stadium. *Arch. Entwickl. Mech. Org.* **18**: 377–403.
6. Holland, P. 1992. Homeobox genes in vertebrate evolution. *BioEssays* **14**: 267–273.
7. Bruce, A. E. E., and M. Shankland. 1998. Expression of the head gene *Lox22-Otx* in the leech *Helobdella* and the origin of the bilaterian body plan. *Dev. Biol.* **201**: 101–112.
8. Nardelli-Haeffliger, D., and M. Shankland. 1992. *Lox2*, a putative leech segment identity gene, is expressed in the same segmental domain in different stem cell lineages. *Development* **116**: 697–710.
9. Nardelli-Haeffliger, D., A. E. E. Bruce, and M. Shankland. 1994. An axial domain of HOM/Hox gene expression is formed by the morphogenetic alignment of independently specified cell lineages in the leech *Helobdella*. *Development* **120**: 1839–1849.
10. Kourakis, M. J., V. A. Master, D. K. Lokhorst, D. Nardelli-Haeffliger, C. J. Wedeen, M. Q. Martindale, and M. Shankland. 1997. Conserved anterior boundaries of Hox gene expression in the central nervous system of the leech *Helobdella*. *Dev. Biol.* **190**: 284–300.
11. Martindale, M. Q., and M. Shankland. 1990. Segmental founder cells of the leech embryo have intrinsic segmental identity. *Nature* **347**: 672–674.

Hox Genes in Arthropod Development and Evolution

MICHAEL AKAM*

Wellcome/CRC Institute, Tennis Court Road, Cambridge, CB2 1QR, UK

The Hox genes have become a paradigm for the conservation of developmental mechanisms throughout the animal kingdom. They encode transcription factors that act as molecular markers for the position of cells along the major body axis (1). Individual Hox genes are activated at different positions in the early embryo, establishing a pattern that is maintained throughout much of development. This differential expression has been shown to control the development of region-specific structures in nematodes, arthropods, and chordates, and may be a shared characteristic of triploblastic metazoan animals.

Hox genes and the diversity of development within insects

The *Drosophila* Hox cluster also contains homeobox genes that have no close homologues in other species. These genes, *bicoid*, *zen*, and *fushi-tarazu* (*ftz*), serve roles in development different from those of the canonical Hox genes. All are involved in establishing the body plan during the early syncytial stage of *Drosophila* development.

Syncytial development is not universal within the insects. Many lower insects make much or all of their segment pattern after cellularization—a point made particularly clear by recent studies of the grasshopper, *Schistocera*, which show that the blastoderm becomes cellular even before the aggregation of cells to form the embryonic primordium (2). Yet more remarkable is the diversity of development among the parasitic Hymenoptera (3).

This paper was originally presented at a workshop titled *Genetic Regulatory Networks in Embryogenesis and Evolution*. The workshop, which was held at the Marine Biological Laboratory, Woods Hole, Massachusetts, from 11 to 14 June 1997, was sponsored by the Center for Advanced Studies in the Space Life Sciences at MBL and funded by the National Aeronautics and Space Administration under Cooperative Agreement NCC 2-896.

*Present address: The University Museum of Zoology, Downing Street, Cambridge CB2 3EJ, UK.

Species within the same family may exhibit extreme differences in early embryogenesis: The Braconidae contain ectoparasitic species, laying yolky eggs that show syncytial development similar to that of *Drosophila*, and endoparasitic species that lay small, yolk-free eggs that undergo total cleavage and “short germ” patterning (M. Grbic and M. Strand, unpub. data).†

It is now clear that at least two of the atypical *Drosophila* Hox genes—*zen* and *ftz*—derive from ancient members of the Hox cluster that have evolved particularly rapidly within the insect lineage (4, 5). We suggest that the developmental role of these genes changed in the ancestors of the insects, with a loss of many of the functional constraints that act on the ‘canonical’ Hox genes.

Hox genes, homeosis, and the evolution of segment identity

It has long been suggested that mutation in the Hox genes may contribute to morphological diversity of the arthropods (6), but this idea has been criticized on the grounds that dramatic homeotic transformations could not possibly contribute to natural evolution because such changes in form would never be selectively advantageous. Recent changes in our understanding of the role and regulation of Hox genes provide a way out of this dilemma.

In the 1970s and 80s, genetic analysis suggested that the Hox genes served to give an identity to all cells in a segment. This was interpreted to mean that Hox genes were ubiquitously and uniformly expressed in whole segments, under ‘monolithic regulation’. It is now clear that the regulation of the Hox genes is more complex (7). Whether or not a given gene will be active in a particular segment is defined in the early embryo, by signals that make certain of the Hox regulatory domains “open for business.” However, each of these regulatory domains

† See addition to Literature Cited.

has a complex modular structure, like that of other patterning genes. In later development, these modules are regulated independently in different cell types and stages of development, even within a single segment. Moreover, this detailed regulation is important for the specification of segment identities. A single Hox gene can specify the development of several different segment types, and our studies on the *Ultrabithorax* gene show that this is in large part dependent on the precise spatial and temporal regulation of the gene (8). Changing this pattern of *Ubx* regulation within segments can alter fine details of segment development (9). Recent work in my laboratory (D. Stern, unpub. data)‡ and elsewhere (10) suggests that allelic variants that affect *Ubx* function can also be observed in natural populations.

From this perspective, it is easy to understand how gradual changes in the regulatory elements of Hox genes may contribute to the evolution of segment morphology. Summed over time, such changes may lead to differences in Hox gene function between species that would be comparable to the effects of overt homeotic mutations—even though no such mutations need ever have been fixed.

To test whether such changes have occurred, we initiated a survey of Hox gene structure and expression in diverse arthropods. Orthologs of all the *Drosophila* Hox genes can be identified in Crustacea and Myriapods (11 and M. L. Smith, unpub.) Surprisingly, three genes that define the identity of diverse trunk segments in insects (*Antp*, *Ubx*, and *abd-A*) are all expressed throughout the thorax of the branchiopod crustacean *Artemia*, but are not expressed in the postgenital abdomen (12). If the Hox genes can be used as markers for homologous segments, these differences suggest a novel relationship between body regions in insects and Crustacea (13).

Within the Crustacea, a wider taxonomic survey of a single class of Hox gene products reveals a striking correlation between the boundaries of Hox gene expression and the diversity of segment types (14). Many basal crustacean lineages have an array of similar thoracic segments, and *Ubx/Abd-A* class Hox genes are typically expressed in all of these segments. In other, more derived crustacean lineages, the most anterior thoracic segments

are transformed into maxillipeds—supplementary feeding appendages that resemble in part the gnathal segments. In these segments, *Ubx/abd-A* proteins are not expressed. It seems that the alteration in segment organization has been achieved by shifting the domains of Hox gene expression relative to a conserved array of segments.

Literature Cited

1. McGinnis, W., and R. Krumlauf. 1992. Homeobox genes and axial patterning. *Cell* 68: 283–302.
 2. Ho, K., O. Dunin-Borkowski, and M. Akam. 1997. Cellularisation in Locust embryos occurs before blastoderm formation. *Development* 124: 2761–2768.
 3. Grbic, M., L. M. Nagy, S. B. Carroll, and M. R. Strand. 1996. Polyembryonic development: insect pattern formation in a cellularized environment. *Development* 122: 795–804.
 4. Dawes, R., I. Dawson, F. Falciani, G. Tear, and M. Akam. 1994. Dax, a Locust Hox gene related to *fushi tarazu* but showing no pair-rule expression. *Development* 120: 1561–1572.
 5. Falciani, F., B. Hausdorf, R. Schröder, M. Akam, D. Tantz, R. Denell, and S. Brown. 1996. Class 3 Hox genes in insects and the origin of *zen*. *Proc. Nat. Acad. Sci. USA* 93: 8479–8484.
 6. Lankester, E. R. 1904. The structure and classification of the arthropoda. *Q. J. Micros. Sci.* 47: 523–582.
 7. Peifer, M., F. Karch, and W. Bender. 1987. The bithorax complex: control of segment identity. *Genes Dev.* 1: 891–898.
 8. Castelli-Gair, J., and M. Akam. 1995. How the Hox gene *Ultrabithorax* specifies two different segments: the significance of spatial and temporal regulation within metameres. *Development* 121: 2973–2982.
 9. Castelli-Gair, J., S. Greig, G. Micklem, and M. Akam. 1994. Dissecting the temporal requirements for homeotic gene function. *Development* 120: 1983–1995.
 10. Gibson, G., and D. S. Hogness. 1996. Effect of polymorphism in the *Drosophila* regulatory gene *Ultrabithorax* on homeotic stability. *Science* 271: 200–203.
 11. Averof, M., and M. Akam. 1993. HOM/Hox genes of *Artemia*: implications for the origin of insect and crustacean body plans. *Curr. Biol.* 3(2): 73–78.
 12. Averof, M., and M. Akam. 1995. Hox genes and the diversification of insect and crustacean body plans. *Nature* 376: 420–423.
 13. Akam, M. 1995. Hox genes and the evolution of diverse body plans. *Phil. Trans. Roy. Soc.* 349: 313–319.
 14. Averof, M., and N. Patel. 1997. Changes in Hox gene regulation associated with the evolution of specialized crustacean appendages. *Nature* 388: 682–686.
- † Grbic, M., and M. R. Strand. 1998. Shifts in the life history of parasitic wasps correlate with pronounced alterations in early development. *Proc. Natl. Acad. Sci. USA* 95: 1097–1101.
- ‡ Stern D. 1998. A role for *Ultrabithorax* in morphological differences between *Drosophila* species. *Nature* 396 (in press).

‡ See addition to Literature Cited.

Heterochronic Genes in Development and Evolution

FRANK SLACK AND GARY RUVKUN

*Department of Genetics, Harvard Medical School, and Department of Molecular Biology,
Massachusetts General Hospital, Wellman 8, Boston, Massachusetts 02114*

Heterochrony is an evolutionary term that describes the comparatively common phylogenetic variation between species in the relative timing of developmental events. Heterochronic variation has also been induced by mutation to identify genes that regulate the timing of developmental events (1, 2). Genes that control the temporal dimension of development, heterochronic genes, can be thought of as the temporal analogs of the homeotic genes, which regulate spatial dimensions (*e.g.*, anterior-posterior, dorsal-ventral axes) during development of metazoans. These pathways generate graded or binary levels of regulatory factors that pattern one axis of the developing animal. Heterochronic genes may be the target of mutations that cause heterochronic change in phylogeny. In the nematode *Caenorhabditis elegans*, heterochronic genes mediate the temporal pattern of stage-specific expression of cell fates. Correct timing of many stage-specific developmental events depends on the time-dependent decrease of the LIN-14 and LIN-28 proteins, two key regulatory factors that promote early larval fates (3, 4, 5). Their decrease is thought to be the result of the time-dependent increase in the LIN-4 RNA, which binds to the mRNAs of both *lin-14* and *lin-28* and somehow inhibits their translation (6, 7). LIN-14 [a novel protein (3)] and LIN-28 [an RNA binding protein (5)] function at the first (L1) and second (L2) larval stages respectively, to prevent the premature activation of LIN-29 (8). LIN-29 is a transcription factor induced at the L4 stage that is required for adulthood. Null mutations in *lin-14*, for example, result in the activation of LIN-29 one stage too early, with the

result that certain adult features are precociously expressed in larval stages. Additional, as yet unknown, heterochronic genes are postulated to function in the genetic pathway between LIN-14/28 and LIN-29. Hormonal control of developmental timing is a common theme throughout phylogeny. For example, heterochronic mutations that involve hormonal signaling have been identified in vertebrates as well as *C. elegans* (9).

The level of LIN-14 protein forms a temporal gradient that specifies stage-specific cell lineages during development of *C. elegans*. Mutations that perturb this level perturb the temporal sequence of cell lineages. LIN-14 is a nuclear protein, but is not homologous to any known protein. To experimentally establish how graded LIN-14 levels act to specify stage-specific cell fates (including the mechanism used by *lin-14* to control downstream genes, *i.e.*, transcription, splicing, etc.) we are identifying factors that mediate *lin-14* action. We expect these to include targets of *lin-14*, as well as factors that act in combination with LIN-14. We have used a genetic analysis to identify genes that function downstream of *lin-14* in the heterochronic pathway. We have isolated suppressors of two heterochronic mutants that respectively result in opposite heterochronic phenotypes, precocious *lin-14(lf)* mutants and retarded *lin-4(lf)*, mutants. Some of these suppressor mutations define new heterochronic genes. We have also succeeded in using epistasis analysis to order various other known heterochronic genes into the heterochronic pathway.

In addition, we have identified mutations in the *let-7* gene that result in a retarded heterochronic phenotype and partially suppress the precocious phenotypes of *lin-14(lf)* mutations. We have also identified mutations in the gene *lin-41* which display a precocious phenotype and partially suppress the retarded phenotypes of *let-7* mutations. We have mapped these genes and are currently attempting to clone them via transformation rescue, as well as to order

This paper was originally presented at a workshop titled *Genetic Regulatory Networks in Embryogenesis and Evolution*. The workshop, which was held at the Marine Biological Laboratory, Woods Hole, Massachusetts, from 11 to 14 June 1997, was sponsored by the Center for Advanced Studies in the Space Life Sciences at MBL and funded by the National Aeronautics and Space Administration under Cooperative Agreement NCC 2-896.

them into the heterochronic pathway using epistasis analysis. This molecular analysis should reveal additional aspects of this pathway, and may hint at the molecular function of LIN-14.

Some of this work was supported by NIH R01 grant (GM44619) to GR and an NRSA postdoctoral fellowship (GM18663) to FS.

Literature Cited

1. Slack, F., and G. Ruvkun. 1997. Temporal pattern formation by heterochronic genes. *Annu. Rev. Genet.* **31**: 611–634.
2. Ambros, V., and E. Moss. 1994. Heterochronic genes and the temporal control of *C. elegans* development. *Trends Genet.* **10**: 123–127.
3. Ruvkun, G., and J. Guisto. 1991. The *Caenorhabditis elegans* heterochronic gene *lin-14* encodes a nuclear protein that forms a temporal developmental switch. *Nature* **338**: 313–319.
4. Arasu P., B. Wightman, and G. Ruvkun. 1991. Temporal regulation of *lin-14* by the antagonistic action of two other heterochronic genes, *lin-4* and *lin-28*. *Genes Dev.* **5**: 1825–1833.
5. Moss, E., R. Lee, and V. Ambros. 1997. The cold shock domain protein LIN-28 controls developmental timing in *C. elegans* and is regulated by the *lin-4* RNA. *Cell* **88**: 637–646.
6. Wightman, B., I. Ha, and G. Ruvkun. 1993. Posttranscriptional regulation of the heterochronic gene *lin-14* by *lin-4* mediates temporal pattern formation. *Cell* **75**: 855–862.
7. Lee, R., R. Feinbaum, and V. Ambros. 1993. The *C. elegans* heterochronic gene *lin-4* encodes small RNAs with antisense complementarity to *lin-14*. *Cell* **75**: 843–854.
8. Bettinger, J., K. Lee, and A. Rougvie. 1996. Stage-specific accumulation of the terminal differentiation factor LIN-29 during *Caenorhabditis elegans* development. *Development* **122**: 2517–2527.
9. Antebi, A., J. Culotti, and E. Hedgecock. 1998. *daf-12* regulates developmental age and the dauer alternative in *Caenorhabditis elegans*. *Development* **125**: 1191–1205.

A Common Theme for LIM Homeobox Gene Function Across Phylogeny?

OLIVER HOBERT AND GARY RUVKUN

*Massachusetts General Hospital, Department of Molecular Biology, and Harvard Medical School,
Department of Genetics, Boston, Massachusetts 02114*

The identification of the molecular components of the developmental neurogenic programs in different organisms has revealed an astounding degree of conservation across phylogeny, suggesting that the basic mechanisms of neural development have also been conserved in evolution. One class of conserved neural regulatory genes, the LIM homeobox genes, encode transcription factors with two Zn-finger-like LIM domains and a DNA-binding homeodomain (1). Vertebrate members of this class have been implicated in neurogenesis by correlative expression evidence; *e.g.*, the combinatorial expression of LIM homeobox genes in the vertebrate spinal cord suggested a "LIM-code" for specific motoneuronal targeting choices (2). Genetic analysis in *Drosophila* also demonstrated their essential role in axon pathfinding and the determination of neurotransmitter identity (3, 4).

The genome of the nematode *Caenorhabditis elegans* is almost completely sequenced, thus allowing the analysis of complete gene families in a metazoan organism. *C. elegans* contains seven LIM homeobox genes. Almost all *C. elegans* LIM homeobox genes fall into subclasses that are defined by the presence of similar genes from arthropods and vertebrates, suggesting a common origin for different subclasses of LIM homeobox genes (Fig. 1; *C. elegans* proteins are underlined).

This paper was originally presented at a workshop titled *Genetic Regulatory Networks in Embryogenesis and Evolution*. The workshop, which was held at the Marine Biological Laboratory, Woods Hole, Massachusetts, from 11 to 14 June 1997, was sponsored by the Center for Advanced Studies in the Space Life Sciences at MBL and funded by the National Aeronautics and Space Administration under Cooperative Agreement NCC 2-896.

Function of the *C. elegans ttx-3* and *lin-11* homeobox genes

We recently described the function of two *C. elegans* LIM homeobox genes, *ttx-3* and *lin-11*, in a neural circuit subserving thermoregulatory behavior (5, 6, 7). The neural pathway for thermotaxis includes the sensory neuron AFD and the connected interneurons AIY and AIZ (Ref. 5; see Fig. 2). The *ttx-3* null mutation causes the same behavioral defect as laser ablation of AIY, implying that AIY does not signal in this mutant (5). A *ttx-3*-GFP reporter construct shows that *ttx-3* is expressed exclusively in the AIY interneuron pair (6). AIY is generated in *ttx-3* mutants, arguing that no fundamental changes in cell fate have taken place. However, AIY exhibits abnormal axonal projections, manifested mainly by the outgrowth of additional small neurites. These defects could be due to misregulation of *ttx-3* downstream target genes involved directly in axonal pathfinding, or they could be due to misregulation of *ttx-3* downstream target genes involved in synaptic signaling, which could, as a secondary consequence, cause axonal sprouting defects.

ttx-3 is continuously expressed in AIY from mid-embryogenesis throughout adulthood and is required to maintain its own expression, suggesting that *ttx-3* may also act in a neural maintenance pathway for AIY. Considering that thermotactic behavior manifests a simple learning and memory task, AIY represents a prime candidate for an interneuron that integrates and memorizes sensory inputs, for example by variable patterns of synaptic connections. We consider the possibility that *ttx-3* is part of an autoregulatory loop that regulates the initial expression of downstream target genes involved in neural

signaling and that may also modulate downstream gene expression in behavioral plasticity (6).

We have identified a second LIM homeobox gene, *lin-11*, that is expressed and functions in the opposing interneuron of the thermoregulatory circuit, AIZ (7). *lin-11* null mutant animals display cryophilic defects that phenocopy laser ablation of the AIZ interneuron. Although the *lin-11* expressing neurons, including AIZ, are formed in *lin-11* null mutant animals, they display neuro-anatomical defects, comparable to those neural defects observed in *ttx-3* mutant animals. Like *ttx-3*, *lin-11* expression is also maintained in postmitotic neurons throughout adulthood. Thus, distinct LIM homeobox genes specify two functionally related antagonistic interneurons within a neural network dedicated for thermoregulatory processes (see Fig. 2).

How are thermoregulatory neural centers organized in more complex organisms? And is there any evidence for a conserved role for *ttx-3* and *lin-11* in the control of these neural centers? In fact, the organization of the *C. elegans* thermoregulatory network into two parallel, warm- and cold-processing pathways is remarkably simi-

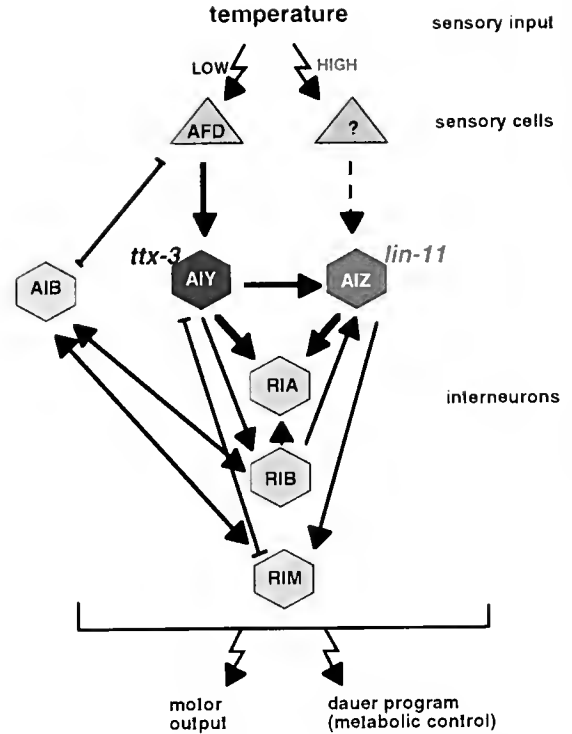


Figure 2. The neural thermoregulatory pathway in *Caenorhabditis elegans*.

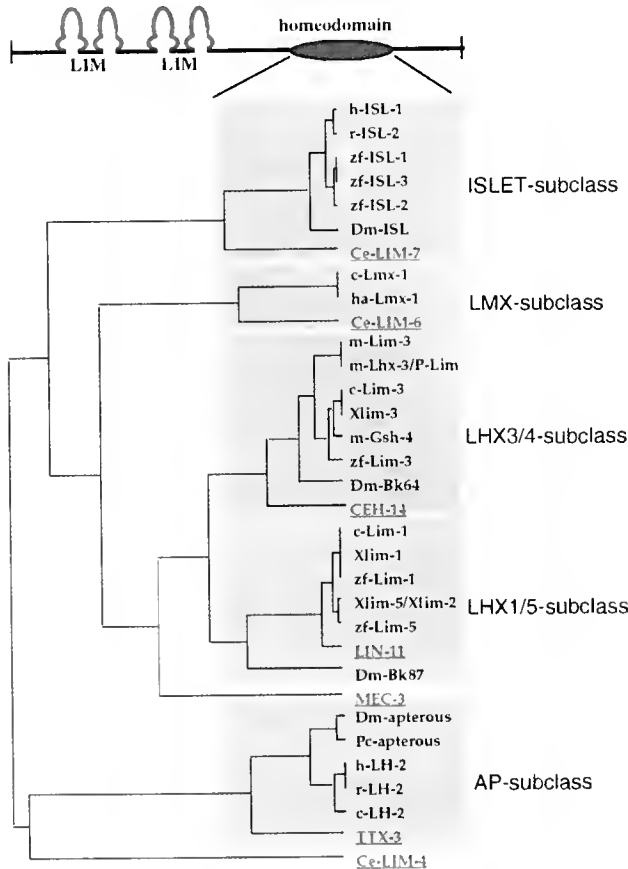


Figure 1. Dendrogram of LIM homeodomain proteins.

lar to thermocontrol in vertebrates. The major thermoregulatory organ of vertebrates, the hypothalamus, contains distinguishable warm- and cold-sensing temperature processing units (8) that may be homologous to the antagonistic high and low temperature sensing pathways of the *C. elegans* thermotactic response pathway (Fig. 2). The vertebrate *ttx-3* homolog *Lhx2* and the *lin-11* homolog *Lhx1* are indeed expressed in the diencephalon, which gives rise to the thermoregulatory hypothalamus (9, 10). *lin-11* and *ttx-3* in *C. elegans*, and their homologs in mammals, may thus play a similar role in the development of two components of these related thermal processing networks.

Apart from their suggested role in the hypothalamus, the vertebrate *lin-11* and *ttx-3* homologs *Lhx1* and *Lhx2* are expressed in several additional places in the nervous system (9, 10). The additional roles of the vertebrate genes might parallel the function of the nematode homologs, making additional cases for a conservation of function throughout evolution. For example, *lin-11* is expressed and functions in the ventral nerve cord of *C. elegans*, where it is required for correct axon bundle fasciculation (7); vertebrate *Lhx1* is similarly expressed in motor neurons of the spinal cord. Additionally, *Lhx1* expression can be observed in sensory structures in the

brain (9), which correlates with *lin-11* expression in *C. elegans* head sensory neurons (7). In contrast, the comparison of expression and functions of nematode *lin-11* and vertebrate *Lhx1* also makes a very strong point for the acquisition of *additional* functions for a regulatory gene (or, alternatively, the loss of a function): While *Lhx1* is involved early in embryogenesis in neural induction (11), no such embryonic role exists for *lin-11* (7). Similarly, as *C. elegans* has no appendages, the function of *apterous*, the *Drosophila* homolog of *C. elegans* *ttx-3* in wing patterning, represents a clear case of co-option of a regulatory gene to a new developmental process.

Is there a common theme for LIM homeobox gene function in *C. elegans*? The functional analysis of the LIM homeodomain-encoding *ttx-3*, *lin-11*, and *mec-3* genes, all of which act late in neural development, demonstrated their role in determining the differentiated neural phenotype (6, 7, 12). To learn whether the other *C. elegans* LIM homeobox genes might share a similar role, we examined their expression pattern using GFP reporter gene fusion. We found *lim-4*, *lim-6*, and *lim-7* to be expressed in a non-overlapping subset of neuronal cells. While the expression of the *isl*-homolog *lim-7* is very dynamic and not confined to the nervous system, we found *lim-4* and *lim-6* to be exclusively expressed in a non-overlapping set of head sensory-, inter- and motorneurons. Note that, like *mec-3*, *ttx-3* and *lin-11*, *lim-4* and *lim-6* are also expressed in neurons after their final division and continue to be expressed throughout adulthood, suggesting that they might be involved in neuronal maintenance. We speculate that a common theme of *C. elegans* LIM homeobox genes is to determine a specific neural phenotype, as manifested perhaps by a specific neural connectivity or neurotransmitter choice. Our findings suggest that this is the phylogenically conserved function of LIM homeobox genes, and that some of the functions of the genes in *C. elegans*—such as the role of *lin-11* in vulval development—represent a later recruitment of these genes into additional cellular processes.

A comparison of expression characteristics of the *C. elegans* LIM homeobox genes leads to another interesting point: the expression of most, if not all of these genes is maintained in neural tissues throughout adulthood. This suggests a nontransient, but constitutive requirement for these genes throughout the life of the neuron, e.g., in the maintenance of specific neural features.

We further propose that LIM homeobox gene function in neural development represents a function of these genes that has been conserved across phylogeny. This hypothesis is based on the functioning of *Drosophila* LIM homeobox genes in axon pathfinding and determination of neurotransmitter identity (3, 4), as well as the maintained

neural expression of vertebrate LIM homeobox genes in postmitotic neurons (1). To our knowledge, LIM homeobox genes have so far been found exclusively in organisms that contain a nervous system, which provides some circumstantial evidence that LIM homeobox genes might have co-evolved with neural structures, whose complexity obviously requires the use of new classes of regulatory genes.

LIM homeobox genes presumably arose in evolution by a recombination event of homeodomain and LIM domain coding exons. This event probably happened only once, since (1) all LIM homeobox genes contain a very similar architecture, with two LIM domains at the N-terminus and one homeodomain at the C-terminus, and since (2) the first LIM domain of LIM homeodomain proteins is usually more similar to the first LIM domain of other LIM homeodomain protein than to their own second LIM domain (1). Gene duplications of a single common ancestor conceivably created the different subclasses of LIM homeodomain proteins; these duplication must have happened before the divergence of nematodes, arthropods, and chordates. This common ancestor, which contained multiple LIM homeobox genes, might have already contained a simple nervous system in which LIM homeodomain protein were employed to define specific neural features.

As mentioned above, LIM homeobox genes have obviously been recruited to function in additional non-neural processes, such as vulval patterning, limb development, and neural induction during gastrulation. These additional and relatively specialized functions of LIM homeobox genes in organs and processes specific for distinct phylogenetic branches presumably have been co-opted by specific phyla at later stages of evolution.

Acknowledgments

This work was supported in part by Hoechst AG to G. R. and by a postdoctoral fellowship from the Human Frontiers Science Program to O. H.

Literature Cited

1. Dawid, I. B., R. Toyama, and M. Taira. 1995. LIM domain proteins. *C. R. Acad. Sci. Paris/Life Sci.* **318**: 295–306.
2. Tsuchida, T., M. Ensigni, S. B. Morton, M. Baldassare, T. Edlund, T. M. Jessell, and S. L. Pfaff. 1994. Topographic organization of embryonic motor neurons defined by expression of LIM homeobox genes. *Cell* **79**: 957–970.
3. Lundgren, S. E., C. A. Callahan, S. Thor, and J. B. Thomas. 1995. Control of neuronal pathway selection by the *Drosophila* LIM homeodomain gene *apterous*. *Development* **121**: 1769–1773.
4. Thor, S., and J. B. Thomas. 1997. The *Drosophila* islet gene governs axon pathfinding and neurotransmitter identity. *Neuron* **18**: 397–409.

5. **Mori, I., and Y. Ohshima. 1995.** Neural regulation of thermotaxis in *Caenorhabditis elegans*. *Nature* **376**: 344–348.
6. **Hobert, O., I. Mori, Y. Yamashita, H. Honda, Y. Ohshima, Y. Liu, and G. Ruvkun. 1997.** Regulation of interneuron function in the *C. elegans* thermoregulatory pathway by the *trx-3* LIM homeobox gene. *Neuron* **19**: 345–357.
7. **Hobert, O., T. d'Albert, Y. Liu, and G. Ruvkun. 1998.** Control of neural development and function in a thermoregulatory network by the LIM homeobox gene *lin-11*. *J. Neurosci.* **18**: 2084–2096.
8. **Boulant, J. A., and J. B. Dean. 1986.** Temperature receptors in the central nervous system. *Annu. Rev. Physiol.* **48**: 639–654.
9. **Fuji, T., J. G. Pichel, M. Taira, R. Toyama, I. B. Dawid, and H. Westphal. 1994.** Expressions patterns of the murine LIM class homeobox gene *lim1* in the developing brain and excretory system. *Dev. Dynam.* **199**: 73–83.
10. **Porter, F. D., J. Drago, Y. Xu, S. Cheema, S. P. Huang, E. Lee, A. Grinberg, J. S. Massalas, D. Bodine, F. W. Alt, and H. Westphal. 1997.** *Lhx2*, a LIM homeobox gene, is required for eye, forebrain and definitive erythrocyte development. *Development* **124**: 2935–2944.
11. **Shawlot, W., and R. R. Behringer. 1995.** Requirement for *Lim1* in head-organizer function. *Nature* **374**: 425–430.
12. **Way, J. C., and M. Chalfie. 1988.** *mec-3*, a homeobox-containing gene that specifies differentiation of the touch receptor neurons in *C. elegans*. *Cell* **54**: 5–16.

Mechanisms of Specification in Ascidian Embryos

NORIYUKI SATOH

Department of Zoology, Graduate School of Science, Kyoto University, Kyoto 606-8502, Japan

Ascidians (subphylum Urochordata, class Ascidiacea) are ubiquitous marine animals. Since the work of Chabry (1) in 1887, which described the first blastomere destruction experiments in the history of embryology, ascidian eggs and embryos have served as an experimental system in developmental biology. The fertilized egg develops quickly into a tadpole larva (about 2600 component cells) consisting of a small number of tissues including epidermis, central nervous system with two sensory organs, nerve cord, endoderm, mesenchyme, notochord, and muscle (2). The lineage of these embryonic cells is described almost completely. In addition, the recent isolation of cDNA clones of various tissue-specific genes by our laboratory provides molecular probes with which to monitor the differentiation of each type of tissue (3). The advantageous features of the embryo, together with tissue-specific molecular probes, allow us to study the mechanisms underlying the specification and subsequent differentiation of embryonic cells (2, 3).

Maternal genes with localized mRNA

Fate restriction in ascidian embryos takes place relatively early; *i.e.*, most of the blastomeres in the 64-cell stage are already restricted to generating one type of tissue. Reflecting such an early fate restriction, the ascidian embryo shows a highly determinate mode of development, which may be dependent on prelocalized egg cytoplasmic determinants. Recently we isolated cDNA clones for several maternal genes with localized mRNA (4, 5). Because all of these mRNAs are localized in the posterior-

vegetal cytoplasm of the egg and they later mark the posterior end of developing embryos, we named the genes *posterior end mark (pem)* (4). Thus far we have obtained cDNA clones for six *pems*: *pem*, *pem-2*, *pem-3*, *pem-4*, *pem-5*, and *pem-6*. *pem-3* encodes a polypeptide with the KH domain and RING finger (a possible homolog of *C. elegans* MEX-3 that may function as an RNA-binding protein), whereas *pem-4* encodes a polypeptide with the C2H2-type zinc finger motif.

Muscle differentiation

The B-line presumptive muscle cells of ascidian embryos have extensive potential for self-differentiation dependent on determinants prelocalized in the myoplasm of fertilized eggs (2). Ascidian larval muscle cells therefore provide an experimental system with which to explore an intrinsic genetic program for autonomous specification of embryonic cells. Experiments with egg fragments suggested that maternal mRNAs are one of the components of muscle determinants (6). Expression of larval muscle actin genes (*HrMA4*) begins as early as the 32-cell stage, prior to the developmental fate restriction of the cells (7). The initiation of actin gene expression begins a few hours before the expression of an ascidian homolog of vertebrate MyoD (8). In addition, mutations in the proximal E-box of the 5' flanking region of *HrMA4* did not alter the promoter activity for muscle-specific expression of a reporter gene (9). These results, together with the effects of deleting constructs of fusion genes, suggest that muscle determinants regulate directly—or indirectly *via* regulatory factors other than MyoD—the transcription of muscle-specific structural genes leading to the terminal differentiation. We have characterized *cis*-elements responsible for muscle-specific expression of *HrMA4*, and have identified two elements within about 100 bp upstream of the transcription initiation site (9).

This paper was originally presented at a workshop titled *Genetic Regulatory Networks in Embryogenesis and Evolution*. The workshop, which was held at the Marine Biological Laboratory, Woods Hole, Massachusetts, from 11 to 14 June 1997, was sponsored by the Center for Advanced Studies in the Space Life Sciences at MBL and funded by the National Aeronautics and Space Administration under Cooperative Agreement NCC 2-896.

Specification of notochord

Recent studies have revealed an important role for cell-cell interactions in the specification of certain types of ascidian embryonic tissue. Differentiation of ascidian notochord cells is induced during the early phase of the 32-cell stage by interaction of the presumptive notochord blastomeres with adjacent endoderm cells, as well as with neighboring presumptive notochord blastomeres (10). Immediately after the induction, an ascidian homolog (*As-T*) of mouse *Brachyury* gene is expressed only in the primordial notochord cells (11). Microinjection of synthetic *As-T* mRNA into fertilized eggs resulted in notochord differentiation in the presumptive notochord blastomeres with no induction process (12). The notochord differentiation was assessed by the appearance of a specific antigen (Not-1) and morphological features (an elongated cell with a large vacuole). In addition, *As-T* mRNA injection promotes notochord differentiation in lineages of nerve cord and endoderm, suggesting that this gene exerts a master control upon notochord differentiation (12).

Evolutionary aspects

Halocynthia roretzi has at least four T-domain genes. Although *As-T* is expressed exclusively in differentiating notochord cells, *As-T2* is expressed in differentiating muscle and the tip of the tail of the embryo (13). In addition, an ascidian homolog of *omb* is expressed in the nervous system, and a maternal *As-mT* mRNA is present in unfertilized eggs.

Because the notochord is one of the characteristic features shared by chordates, and because the *Brachyury* gene is responsible for notochord formation, comparative studies of *Brachyury* gene expression and function between primitive chordates and other deuterostomes (echinoderms and hemichordates) may give us some insight into the developmental mechanisms underlying the appearance of the chordates about 550 million years ago (14). We therefore compared the patterns of *Brachyury* gene expression among the deuterostome groups.

The amphioxus *Branchiostoma belcheri* contains two *Brachyury* genes. These genes are initially expressed in the involuting mesoderm of the gastrula, then in the differentiating somites of the neurula, followed by the differentiating notochord and finally in the tail bud of the 10-somite stage embryo (15). This pattern of expression of the amphioxus *Brachyury* resembles that of the vertebrate *Brachyury*.

The sea urchin *Brachyury* gene (*HpTa*) is transiently expressed in the lineage of secondary mesenchyme cells: first in the vegetal plate of the mesenchyme blastula, extending to the tip of the invaginating archenteron, and finally in the secondary mesenchyme cells at the late-gastrula stage (16). This result suggests that the present

function of the *Brachyury* gene in the notochord of chordates originated prior to the branching of the lineage leading to chordates from that leading to echinoderms; it also suggests that, during sea urchin development, *Brachyury* is likely to specify embryonic cells to the secondary mesenchyme.

We also isolated a cDNA clone encoding a hemichordate (*Ptychodera flava*) homolog (*PfBra*) of the *Brachyury* gene and examined its expression pattern during embryogenesis (17). The *PfBra* is first expressed in the vegetal plate of the early gastrula. However, the expression is not detected in the extending tip of the invaginating archenteron, but remains at the blastopore region. In addition, the gene expression is evident in the ectodermal cells of the stomodium, and this pattern is retained in the 3-day-old tornaria larva. The stomochord, which was once thought to be homologous to chordate notochord (18), is formed in the basal region of the proboscis during metamorphosis. The *PfBra* expression should be determined during this later stage of embryogenesis.

Conclusion

The ascidian tadpole larva is regarded as a prototype of the ancestral chordate. Therefore, studies of developmental mechanisms involved in the formation of ascidian tadpoles provide new insights, not only into the ontogeny, but also into the phylogeny of chordates. Further analyses, particularly of *Brachyury* target genes in ascidians and sea urchins, may facilitate our understanding of the genetic circuitry underlying the origin and evolution of chordates.

Acknowledgments

Our studies is supported by a Grant-in-Aid for Specially Promoted Research (No. 07102012) from the Ministry of Education, Science, Sports and Culture, Japan.

Literature Cited

1. Chabry, L. 1887. Contribution a l'embryologie normale et teratologique des Ascidies simples. *J. Anat. Physiol. (Paris)* **23**: 167–319.
2. Satoh, N. 1994. *Developmental Biology of Ascidians*. Cambridge Univ. Press, New York.
3. Satoh, N., K. W. Makabe, Y. Katsuyama, S. Wada, and H. Saiga. 1996. The ascidian embryo: an experimental system for studying genetic circuitry for embryonic cell specification and morphogenesis. *Dev. Growth Diff.* **38**: 325–340.
4. Yoshida, S., Y. Marikawa, and N. Satoh. 1996. *posterior end mark*: a novel maternal gene encoding a localized factor in the ascidian embryo. *Development* **122**: 2005–2012.
5. Satou, Y., and N. Satoh. 1997. *posterior end mark-2 (pem-2)*, *pem-4*, *pem-5* and *pem-6*: maternal genes with localized mRNA in the ascidian embryo. *Dev. Biol.* **192**: 467–481.
6. Marikawa, Y., S. Yoshida, and N. Satoh. 1995. Muscle determinants in the ascidian egg are inactivated by UV irradiation and the

- inactivation is partially rescued by injection of maternal mRNAs. *Roux's Arch. Dev. Biol.* **204**: 180–186.
7. **Satou, Y., T. Kusakabe, I. Araki, and N. Satoh. 1995.** Timing of initiation of muscle-specific gene expression in the ascidian embryo precedes that of developmental fate restriction in lineage cells. *Dev. Growth Differ.* **37**: 319–327.
 8. **Satoh, N., I. Araki, and Y. Satou. 1996.** An intrinsic genetic program for autonomous differentiation of muscle cells in the ascidian embryo. *Proc. Natl. Acad. Sci. USA* **93**: 9315–9321.
 9. **Satou, Y., and N. Satoh. 1996.** Two *cis*-regulatory elements are essential for the muscle-specific expression of an actin gene in the ascidian embryo. *Dev. Growth Differ.* **38**: 565–573.
 10. **Nakatani, Y., and H. Nishida. 1994.** Induction of notochord during ascidian embryogenesis. *Dev. Biol.* **166**: 289–299.
 11. **Yasuo, H., and N. Satoh. 1993.** Function of vertebrate *T* gene. *Nature* **364**: 582–583.
 12. **Yasuo, H., and N. Satoh. 1998.** Conservation of the developmental role of *Brachyury* in notochord formation in a urochordate, the ascidian *Halocynthia roretzi*. *Dev. Biol.* **200**: 158–170.
 13. **Yasuo, H., M. Kobayashi, Y. Shimauchi, and N. Satoh. 1996.** The ascidian genome contains another T-domain gene that is expressed in differentiating muscle and the tip of the tail of the embryo. *Dev. Biol.* **180**: 773–779.
 14. **Satoh, N., and W. R. Jeffery. 1995.** Chasing tails in ascidians: developmental insights into the origin and evolution of chordates. *Trends Genet.* **11**: 354–359.
 15. **Terazawa, K., and N. Satoh. 1997.** Formation of the chorda-mesoderm in the amphioxus embryo: Analysis with *Brachyury* and *fork head/HNF-3* genes. *Dev. Genes Evol.* **121**: 1–11.
 16. **Harada, Y., H. Yasuo, and N. Satoh. 1995.** A sea urchin homologue of the chordate *Brachyury (T)* gene is expressed in the secondary mesenchyme founder cells. *Development* **121**: 2747–2754.
 17. **Tagawa, K., T. Humphreys, and N. Satoh. 1998.** Novel pattern of *Brachyury* gene expression in hemichordate embryos. *Mech. Dev.* **75**: 139–143.
 18. **Bateson, W. 1885.** The later stages in the development of *B. kowalevski* with a suggestion as to the affinities of the Enteropneusta. *Quart. J. Microsc. Sci.* **25**: 81–122.

Published by Title Only

ROTHMAN, JOEL H., ERIN NEWMAN-SMITH, AND STEVE GENDREAU

Genetic control of germ layer specification, blastomere identity, and differentiation during embryogenesis in *C. elegans*

ETTENSohn, CHARLES A., PAUL G. HODOR, AND HYL A SWEET

Morphogenesis and conditional cell fate specification in the sea urchin embryo

SZE, JI-YING, AND GARY RUVKUN

VP16-activation of the *C. elegans* neural specific transcription factor UNC-86 promotes extra axon outgrowth in adults and sensitizes the olfactory sensation

CORBO, JOE, ALBERT ERIVES, ANNA DIGREGORIO, SHI-GEKI FUJIWARA, AND MICHAEL LEVINE

Tracing the origins of the vertebrate tissues in the ascidian, *Ciona intestinalis*

LOGAN, CATRIONA, DAVID SHERWOOD, AND DAVID McCLAY

Adhesion changes and signaling changes that characterize critical steps in the gastrulation of the sea urchin embryo

DAVIDSON, ERIC H.

Gene regulatory networks in the sea urchin

CAMERON, R. ANDREW, AND ERIC H. DAVIDSON

Larval development in the sea urchin, *Strongylocentrotus purpuratus*

Chairs and Speakers

Workshop Co-Chairs

ERIC DAVIDSON

California Institute of Technology

and

DAVID McCLAY

Duke University

MICHAEL AKAM

Wellcome CRC Institute
Tennis Court Road
Cambridge CB2 1QR UK
Phone: +44 1223 334088
Fax: +44 1223 334089
m.akam@zoo.cam.ac.uk

MARIA ARNONE

California Institute of Technology
1201 E. California Blvd.
Pasadena, CA 91125
miarone@mirsky.caltech.edu

ASHLEY BRUCE

Department of Zoology
University of Texas at Austin
Austin, TX 78712-1064
aeb Bruce@mail.utexas.edu

ANDREW CAMERON

Division of Biology 156-29
California Institute of Technology
Pasadena, CA 91125
Phone: 626/395-8421
Fax: 626/793-3047
acameron@mirsky.caltech.edu

ERIC DAVIDSON

California Institute of Technology
1201 E. California Blvd.
Pasadena, CA 91125
Phone: 626/395-4937
Fax: 626/793-3047
davidson@mirsky.caltech.edu

CHARLES ETTENSOHN
 Department of Biological Sciences
 Carnegie Mellon University
 4400 Fifth Avenue
 Pittsburgh, PA 15213-2683
 Phone: 412/268-5849
 Fax: 412/268-7129
 ettensohn@andrew.cmu.edu

JOHN FINNERTY
 Department of Organismal Biology
 University of Chicago
 1027 E. 57th Street
 Chicago, IL 60637
 jrf3@midway.uchicago.edu

STEVE GENDREAU
 Neuroscience Research Institute
 Department of MCD Biology
 University of California, Santa Barbara
 Biological Sciences Building II, Rm 2125
 Santa Barbara, CA 93106

CATHERINE GOLDEN
 Information Dynamics Inc.
 300 D. Street, SW
 Suite 801
 Washington, DC 20024
 catherine.golden@hq.nasa.gov

JON HENRY
 Department of Cell and Structural Biology
 University of Illinois
 601 S. Goodwin
 Urbana, IL 61801
 Phone: 217/333-4449
 Fax: 217/244-1648
 j_henry4@uiuc.edu

OLIVER HOBERT
 Department of Molecular Biology
 Wellman 8
 Massachusetts General Hospital
 Boston, MA 02114

PAUL HODOR
 Department of Biological Sciences
 Carnegie Mellon University
 4400 Fifth Avenue
 Pittsburgh, PA 15213-2683
 hodor@andrew.cmu.edu

EMILY HOLTON
 NASA Ames Research Center
 MS 236-7
 Moffett Field, CA 94035-1000
 eholton@mail.arc.nasa.gov

MICHAEL LEVINE
 Department of Molecular and Cell Biology
 University of California, Berkeley
 401 Barker Hall
 Berkeley, CA 94720-3201
 Phone: 510/642-5014
 Fax: 510/642-7000
 mlevine@mendel.berkeley.edu

CATRIONA LOGAN
 Duke University
 Department of Cell and Molecular Biology
 Box 91000
 Durham, NC 27708-1000
 cylogan@acpub.duke.edu

MARK MARTINDALE
 Department of Organismal Biology
 University of Chicago
 1027 E. 57th Street
 Chicago, IL 60637
 Phone: 773/702-9228
 Fax: 773/702-0037
 m__martindale@uchicago.edu

DAVID McCLAY
 Duke University
 Department of Cell and Molecular Biology
 Box 91000
 Durham, NC 27708-1000
 Phone: 919/613-8188
 Fax: 919/613-8177
 dmccclay@acpub.duke.edu

ERIN NEWMAN-SMITH
 Neuroscience Research Institute
 Department of MCD Biology
 University of California, Santa Barbara
 Biological Sciences Building II, Room 2125
 Santa Barbara, CA 93106
 newman@lifesci.ucsb.edu

ANDREW RANSICK
 California Institute of Technology
 1201 E. California Blvd.
 Pasadena, CA 91125
 andyr@mirsky.caltech.edu

JOEL ROTHMAN
 Neuroscience Research Institute
 Department of MCD Biology
 University of California, Santa Barbara
 Biological Sciences Building II, Rm 2125
 Santa Barbara, CA 93106
 Phone: 805/893-7885
 Fax: 805/893-4724
 rothman@lifesci.ucsb.edu

GARY RUVKUN
 Department of Molecular Biology
 Wellman 8
 Massachusetts General Hospital
 Boston, MA 02114
 Phone: 617/726-5959
 Fax: 617/726-6893
 ruvkun@frodo.mgh.harvard.edu

NORI SATOH
 Department of Zoology
 Graduate School of Sciences
 Kyoto University
 Sakyo-ku
 Kyoto, 606-01, JAPAN
 satoh@ascidian.zool.kyoto-u.ac.jp

JONATHAN SCHAEFER
 Department of Cell and Structural Biology
 University of Illinois
 601 S. Goodwin
 Urbana, IL 61801
 jjschae@students.uiuc.edu

STEPHAN SCHNEIDER
 Department of Organismal Biology
 University of Chicago
 1027 E. 57th Street
 Chicago, IL 60637
 Phone: 773/702-9228
 Fax: 773/702-0037
 ssch@mail.mpi.tuebingen.mpg.de

ELAINE SEAVER
 Department of Zoology
 University of Texas at Austin
 Austin, TX 78712-1064
 seaver@mail.utexas.edu

MARTIN SHANKLAND
 Department of Zoology
 University of Texas at Austin
 Austin, TX 78712-1064
 Phone: 512/232-1892
 Fax: 512/471-9651
 hastypig@mail.utexas.edu

DAVID SHERWOOD
 Duke University
 Department of Cell and Molecular Biology
 Box 91000
 Durham, NC 27708-1000
 sherwood@acpub.duke.edu

FRANK SLACK
 Department of Molecular Biology
 Wellman 8
 Massachusetts General Hospital
 Boston, MA 02114

HYLA SWEET
 Department of Biological Sciences
 Carnegie Mellon University
 4400 Fifth Avenue
 Pittsburgh, PA 15213-2683
 hsweet+@andrew.cmu.edu

Ji YING SZE
 Department of Molecular Biology
 Wellman 8
 Massachusetts General Hospital
 Boston, MA 02114
 sze@frodo.mgh.harvard.edu

ANDRE E. VAN LOON
 Department of Experimental Zoology
 Utrecht University
 Padualaan 8
 3584 CH Utrecht
 The Netherlands
 Fax: (31)-30-2532837
 a.e.vanloon@biol.ruu.nl

BRYAN WALTER
 Department of Cell and Structural Biology
 University of Illinois
 601 S. Goodwin
 Urbana, IL 61801
 b-walter@students.uiuc.edu

CHIOU-HWA (CATHY) YUH
 California Institute of Technology
 Division of Biology, 156-29
 Pasadena, CA 91125
 Phone: 626/395-4988
 Fax: 626/793-3047
 cathy@mirsky.caltech.edu

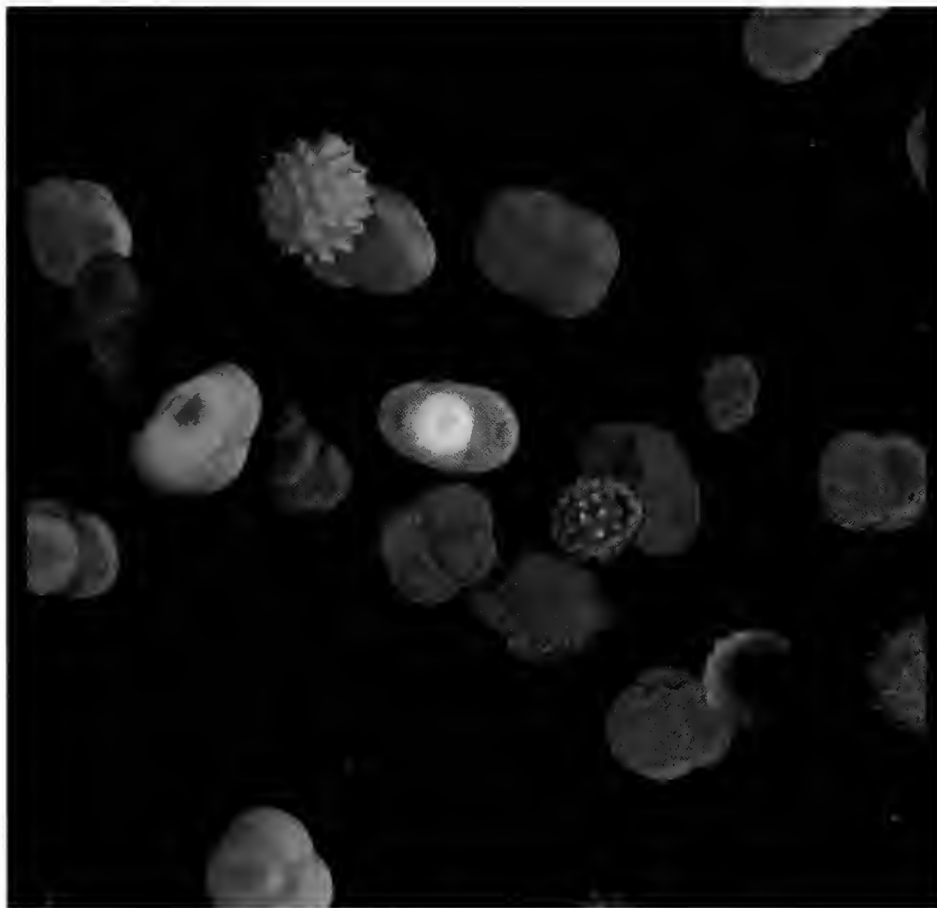
1997–98 MBL Photography/Photomicrography Contest Winners

The following photos won awards in the 1997–1998 MBL Photography and Photomicrography Contest, which is held annually at the Marine Biological Laboratory and sponsored by Carl Zeiss, Inc.

The Contest is meant to encourage contributions to the photographic record of MBL activities. Images submitted to the “MBL-at-Large” category depict science and education at the MBL, including people and their activities, the organisms studied, and the places where all this occurs. The “Scientific Imaging” category includes all forms of macro and micro images that illustrate the research performed at the Laboratory. Submissions in both categories create a composite picture of the MBL through the lens of a camera.

The Biological Bulletin is publishing these photos with the hope that they will inspire authors to contribute papers to the journal’s new section on Imaging and Microscopy. This section is overseen by Associate Editor Shinya Inoué of the Marine Biological Laboratory.

We congratulate all of this year’s winning photographers.



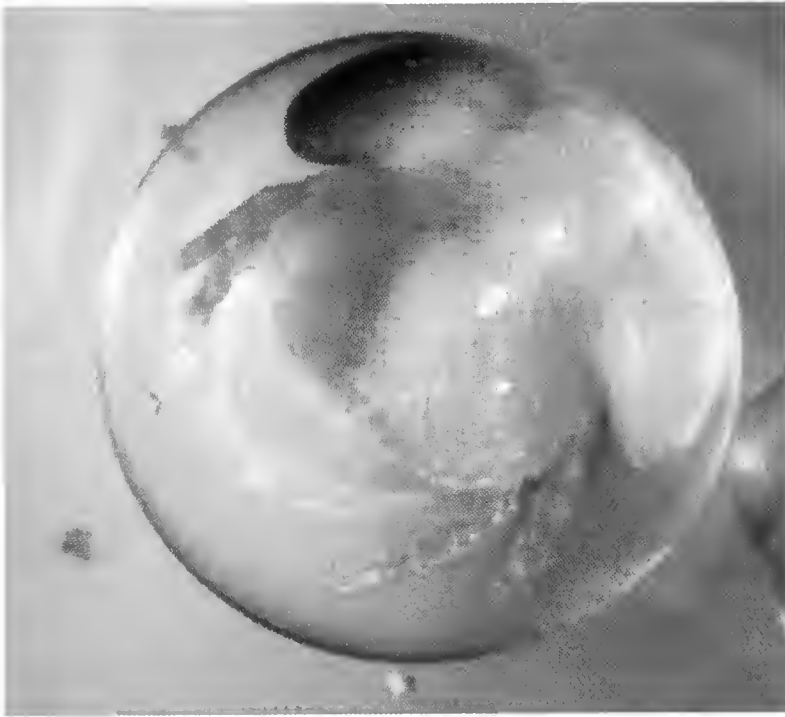
Grand Prize

“Pollen Projection”

JAMIN DEPROTO

Central Microscopy Facility, Marine Biological Laboratory

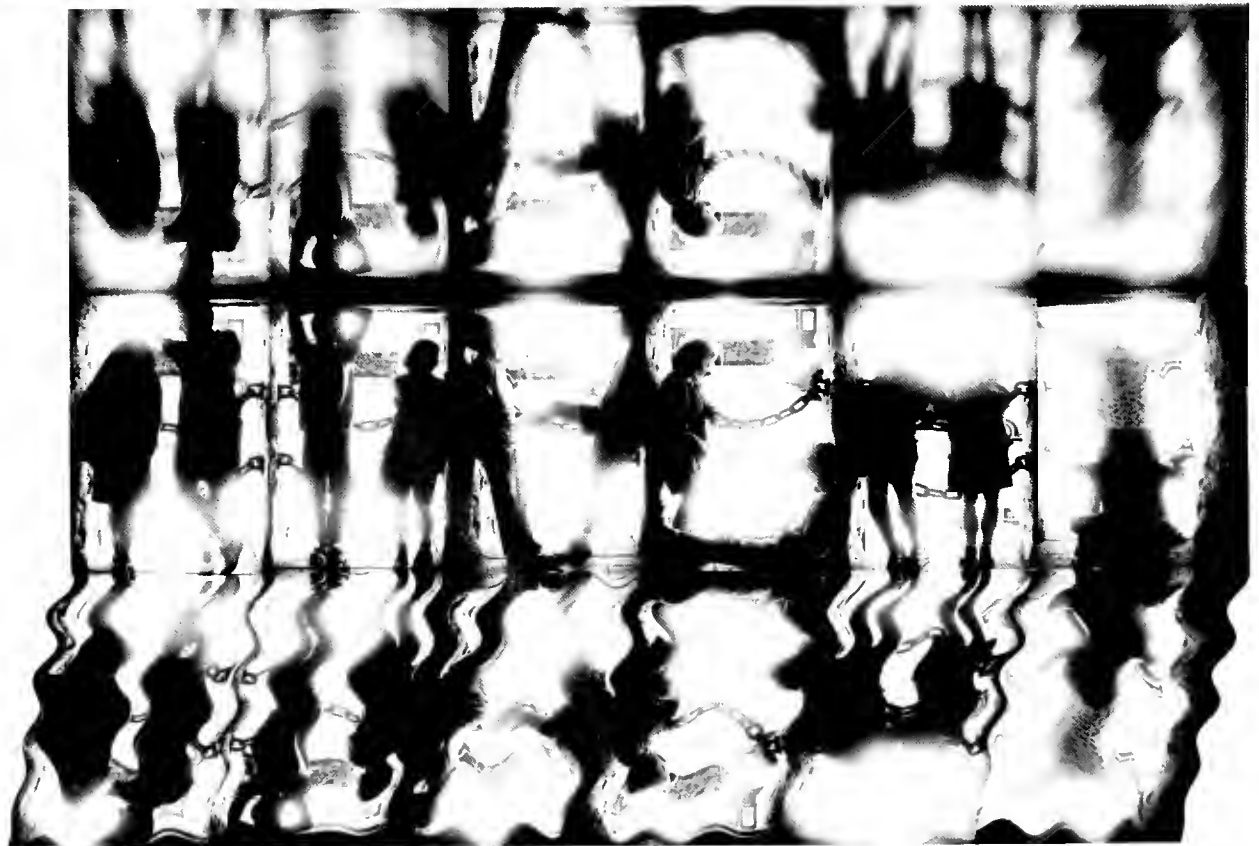
A frame of 360° projections of optical sections from a confocal microscope (3 channel).



First Prize, Scientific Imaging

“*Limulus* Embryo”
JASON FREIDENFELDS
Harvard University

A *Limulus* embryo in its egg sac
one week prior to hatching.



First Prize, MBL-at-Large

“Links”
MARK CHAMPAGNE
Duke University

Mosaic of three people and statues on the MBL campus.

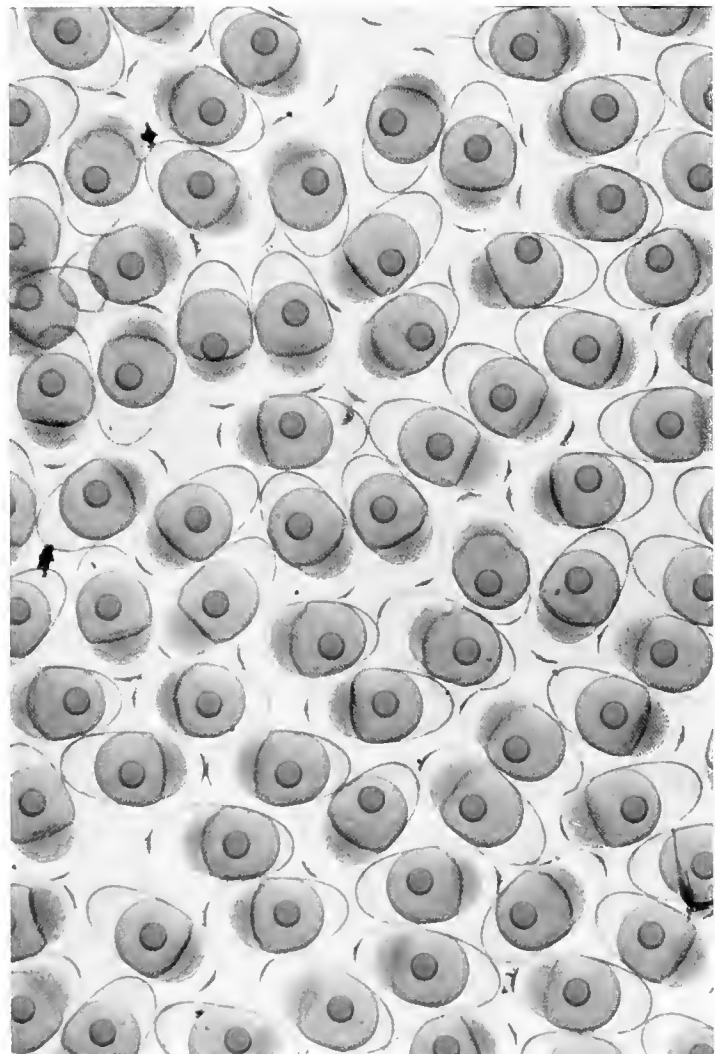


Second Prize, MBL-at-Large

“Chambered Nautilus”

DAVID REMSEN
Marine Biological Laboratory

Chambered Nautilus in an
aquarium in the MBL’s
Marine Resources Center.



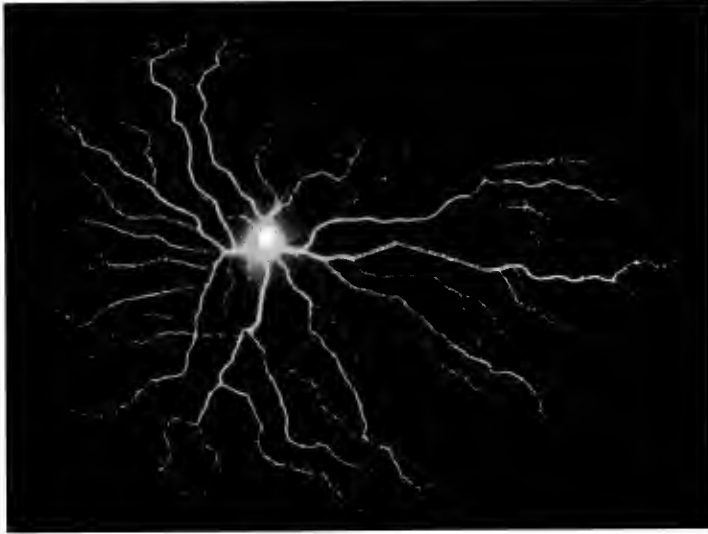
Second Prize, Scientific Imaging

“Damsel Fish Embryos”

LISA KERR-LOBEL
Boston University Marine Program

Abudefduf solidus embryos in early
stage (10 hours).

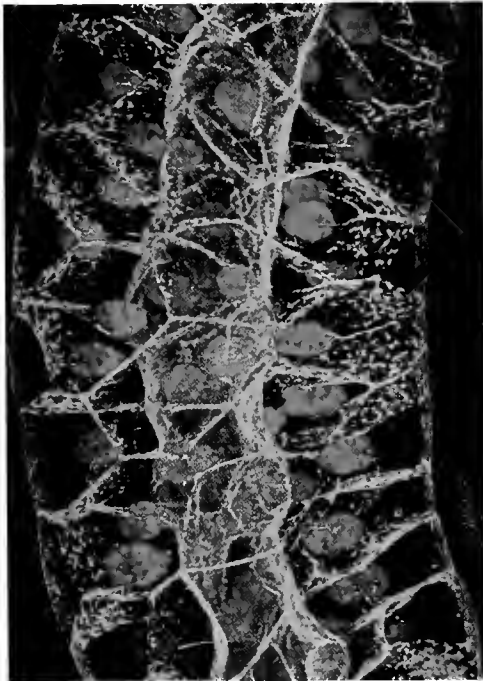
Honorable Mention



“Alpha-Ganglion Cell Retina,” PETER KOULEN, Yale University



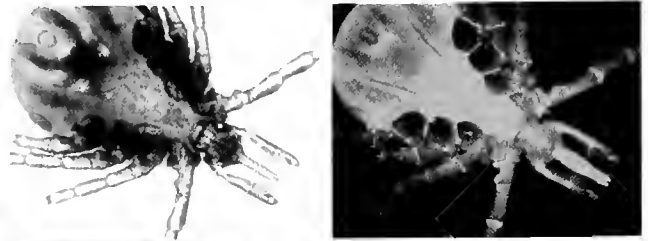
“MYXO Fruiting Body with Fungi”
TOMAS PITTA
Rowland Institute for Science



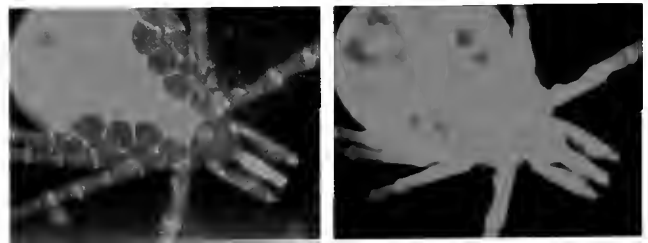
“Confocal View of *Drosophila*
Salivary Gland Cell II”
RICHARD FEHON, Duke University



“Cedar Bog Research,” TOBY AHRENS, Connecticut College



“Common Deer Tick”
MONIKA OLI, University of Alabama



INDEX

A

- A closer look at the natural substrate for a nerve-gas hydrolyzing enzyme in squid nerve, 197
- A common theme for LIM homeobox gene function across phylogeny? 377
- A high-affinity hemoglobin is expressed in the notochord of amphioxus, *Branchiostoma californiense*, 255
- A little shell to live in: evidence that the fertilization envelope can prevent mechanically induced damage of the developing sea urchin embryo, 214
- ABDU, URI, PETER TAKAC, HANS LAUFER, and AMIR SAGI, Effect of methyl farnesoate on late larval development and metamorphosis in the prawn *Macrobrachium rosenbergii* (Decapoda, Palaemonidae): a juvenoid-like effect? 112
- Abducens, 220
- Acetylcholine, 196
- Adhesive force, 145
- Aesthetasc, 184
- Agonistic encounter, 156
- AKAM, MICHAEL, Hox genes in arthropod development and evolution, 373
- Allorecognition, 98
- Alpha peptides, 308
- Alterations in cholinergic signaling modulate contraction of isolated sea urchin tube feet: potential role of nitric oxide, 196
- Amphioxus, 255, 260
- Anatomy, 260
- ANDERSEN, KRISTEN A., and ROBERT PAUL MALCHOW, Fluorometric analysis of intracellular sodium concentrations in isolated retinal horizontal cells, 204
- Annelida, 251
- Annual Report of the Marine Biological Laboratory, R1
- Antennule, 182
- Aplysia* bag cell neurons, 201
- Artemia*, 112
- Ascidian, 60, 98, 381
- ATEMA, JELLE, see Matthew Weaver, 180; Carla M. Guenther, 182; Elizabeth Quinn, 185
- ATEMA, JELLE, Tracking turbulence: processing the bimodal signals that define an odor plume, 179
- Atlantic Ocean, 337
- Auditory system, development, 218
- Axial patterning in the leech: developmental mechanisms and evolutionary implications, 370

B

- BAKER, R., see M. F. Kubke, 218
- BAKER, ROBERT, see Hans Straka, 220
- BALLANTYNE, J. S., see J. A. Stuart, 12
- BANASZAK, ANASTAZIA T., see Nadav Shashar, 187
- BARLOW, ROBERT B., see Vanessa J. Ruta, 189
- Barnacle nervous system, 282
- BAVESTRELLO, GIORGIO, UMBERTO BENATTI, BARBARA CALCINAL, RICCARDO CATTANEO-VIETTI, CARLO CERRANO, ANNA FAVRE, MARCO GIOVINE, SERENA LANZA, ROBERTO PRONZATO, and MICHELE SARA, Body polarity and mineral selectivity in the demosponge *Chondrosia reniformis*, 120
- Behavior
- agonistic, 156
 - feeding, 273
 - migratory, 168
 - orientation, 193
- BENATTI, UMBERTO, see Giorgio Bavestrello, 120
- BILLACK, BLASE, JEFFREY D. LASKIN, PRUDENCE T. HECK, WALTER TROLL, MICHAEL A. GALLO, and DIANE E. HECK, Alterations in cholinergic signaling modulate contraction of isolated sea urchin tube feet: potential role of nitric oxide, 196

- Bioluminescence, 290
- Biomechanics, 136
- Biophysics, 5
- BISHOP, JAMIE J., THOMAS L. VANDERSON, DAVID B. GREEN, JEANNETTE E. DOELLER, and DAVID W. KRAUS, A high-affinity hemoglobin is expressed in the notochord of amphioxus, *Branchiostoma californiense*, 255
- Blockade of ryanodine receptors stimulates neurite outgrowth in embryos of *Spisula solidissima*, 206
- Blood
- plasma, 43
 - serum chemistry, 228
- Blue crab, 168
- Body polarity, 120
- Body polarity and mineral selectivity in the demosponge *Chondrosia reniformis*, 120
- BOURNS, A. E., see J. A. Stuart, 12
- Brachyury, 381
- BRUCE, ASHLEY E. E., see Marty Shankland, 370
- Bryozoans, 126
- Budding mode, 319
- BULLIS, ROBERT A., see Janice S. Hanley, 223
- BURGER, MAX M., see William J. Kuhns, 216
- Busycyon*, 308

C

- C. elegans*, 377
- C to N ratio, 245
- CALCINAL, BARBARA, see Giorgio Bavestrello, 120
- Calcium, 208
- agonist, 209
 - endomembrane stores, 209
 - flux, 201
 - release, 209
 - signal, 209
 - speciation, 43
- Calcium regulatory endomembranes of the prophase mitotic apparatus of sand dollar cells contain enzyme activities that produce leukotriene B₄ but not 1,4,5-inositol triphosphate, 209
- Calcium speciation and exchange between blood and extrapallial fluid of the quahog *Mercenaria mercenaria* (L.), 43
- Calxectin, 198
- Callinectes sapidus*, 168
- CAMERON, R. ANDREW, 361
- Camouflage, 337
- CARPIZO-ITUARTE, EUGENIO, see Eric R. Holm, 21
- CARR, WILLIAM E. S., see Paul J. Linser, 273
- CATE, HOLLY S., see Paul J. Linser, 273
- CATTANEO-VIETTI, RICCARDO, see Giorgio Bavestrello, 120
- CCD camera, 290
- α-CDCP, 308
- CEBRIAN, JUST, see Martin P.A. Griffin, 233; Suzanne Graham, 241
- Cell
- cycle, 107
 - lineage, 363, 367
- Central nuclei, 218
- Centrifuge polarized microscope, 212
- Cephalochordata, 255
- Cephalopod, 17, 78
- CERRANO, CARLO, see Giorgio Bavestrello, 120
- Changes in cell lineage specification elucidate evolutionary relations in Spiralia, 367
- Characterization of oxygen and calcium fluxes from early mouse embryos and oocytes, 208
- Cheliped, 52
- Chemoreception, 185
- CHIKARMANE, H.M., see Roxanna Smolowitz, 229
- Chondrosia reniformis*, 120

- Choosing objective lenses: the importance of numerical aperture and magnification in digital optical microscopy, 1
- Chordate, 60, 381
origin of, 60
- Circadian rhythm, 189
- Circulation, 43
- Circulatory system, 260
- Clam
giant, 70
symbiotic, 70
- Claw, extra, 52
- Cnidae, 145
- Cnidaria, 145, 251
- Cnidocyte, supporting cell complex (CSCC), 145
- Co-localization
pharyngeal teeth, 273
taste buds, 273
- COBB, CHRISTOPHER S., and RODDY WILLIAMSON, Electrophysiology and innervation of the photosensitive epistellar body in the lesser octopus *Eledone cirrhosa*, 78
- Coelom, 260
- Coelomic cavities may function as a vascular system in amphioxus larvae, 260
- COHEN, WILLIAM D., see Kyeng G. Lee, 211
- COLE, MARCI L., see Martin P.A. Griffin, 233
- Collagen, 136
- Colonial coral, 319
- Concepts in Imaging and Microscopy, 1
- Concholepas*, 308
- Confocal, 1
- Consensus translational initiation sites of marine invertebrate phyla, 251
- COSTELLO, JOHN H., and REBECCA COVERDALE, Planktonic feeding and evolutionary significance of the lobate body plan within the Ctenophora, 247
- Counter-illumination, 290
- COVERDALE, REBECCA, see John H. Costello, 247
- Crayfish, 52
- CROLL, ROGER P., see Jeffrey L. Ram, 308
- Crustacea, 112, 251, 290, 373
- Ctenophore, 247, 363
- Cuticular photophores of two decapod crustaceans, *Optalophorus spinosus* and *Systellaspis debilis*, 290
- Cuttlefish, 223
- D**
- D- and L-β-hydroxybutyrate dehydrogenases and the evolution of ketone body metabolism in gastropod molluscs, 12
- DAVIS, JESSICA, see Suzanne Graham, 241
- Decapoda, 112
- DEEGAN, LINDA, see Jennifer Sweeney, 238; Suzanne Graham, 241
- DEFFENBAUGH, MAX, see Allen F. Mensinger, 194
- Denitrification, 240
- Dependence of herbivory on autotrophic nitrogen content and on net primary production across ecosystems, 233
- DERBY, CHARLES D., see Paul J. Linsler, 273
- DE TOMASO, ANTHONY W., see Baruch Rinkevich, 98
- Development, 260, 377
- Di-I dye, 78
- Directional auditory responses in the descending octaval nucleus of the toadfish (*Opsanus tau*), 191
- Dispersal, 126
- Dissolved inorganic nitrogen flux and mineralization in Waquoit Bay sediments as measured by core incubations, 240
- Distribution of setae on the *Homarus americanus* lateral antennule flagellum, 182
- DODGE, FREDERICK A., see Vanessa J. Ruta, 189
- DOELLER, JEANNETTE E., see Jamie J. Bishop, 255
- Dorsoventral axis, 363
- E**
- Echinarachnius*, 209
- Echinodermata, 251
- EDDS-WALTON, P. L., and R. R. FAY, Directional auditory responses in the descending octaval nucleus of the toadfish (*Opsanus tau*), 191
- Eelgrass, 241, 245
- Effect of colony size, polyp size, and budding mode on egg production in a colonial coral, 319
- Effect of eelgrass (*Zostera marina*) density on the feeding efficiency of mummichog (*Fundulus heteroclitus*), 241
- Effect of larval swimming duration on growth and reproduction of *Bugula neritina* (Bryozoa) under field conditions, 126
- Effect of methyl farnesoate on late larval development and metamorphosis in the prawn *Macrobrachium rosenbergii* (Decapoda, Palaemonidae): a juvenoid-like effect? 112
- Effects of nitrogen loading on eelgrass seed coat abundance, C to N ratios, and $\Delta^{15}N$ in sediments of Waquoit Bay, 245
- Effects of vestibular nerve lesions on orientation turning in the leopard frog, *Rana pipiens*, 193
- Efferent modulation, 189
- Efferent modulation of physiological properties of the *Limulus* lateral eye, 189
- Egg, 214
activation, 107
- Egg-laying hormone, 308
- Eighth cranial nerve, 218
- Electrophysiology, 78
- Electrophysiology and innervation of the photosensitive epistellar body in the lesser octopus *Eledone cirrhosa*, 78
- Eledone cirrhosa*, 78
- ELH, see Egg-laying hormone, 308
- ELLERS, OLAF, AMY S. JOHNSON, and PHILIP E. MOBERG, Structural strengthening of urchin skeletons by collagenous sutural ligaments, 136
- ELLINGTON, W. ROSS, and STEPHEN T. KINSEY, Functional and evolutionary implications of the distribution of phosphaagens in primitive-type spermatozoa, 264
- Embryo
chicken, 218
physiology, 208
- Embryology, 370
- Endostyle, 60
- Energetics, 17
- Energy transport, 264
- Enzyme, 12
- Epistellar body, 78
- EPSTEIN, HERMAN T., see Alan M. Kuzirian, 198
- Erythrocytes, 5
- Escape, 193
- Estuarine sediment cores, 243
- Euprymna*, 89, 326
- Evidence for multiple spawning by squids (*Loligo pealei*) in captivity, 225
- Evolution, 12, 264, 363, 370, 373, 377
- Evolution of cleavage programs in relationship to axial specification and body plan evolution, 363
- Expression, 60
- Extracellular pH gradients measured from isolated retinal cells, 203
- Extracellular recording, 191
- Extrapallial fluid, 43
- Eye, invertebrate, 187
- F**
- FAVRE, ANNA, see Giorgio Bavestrello, 120
- FAY, R. R., see P. L. Edds-Walton, 191
- Feeding
ctenophore, 247
fish
efficiency in mummichog, 241
behavior in largemouth bass, 273

- FERNANDEZ-BUSQUETS, XAVIER, see William J. Kuhns, 216
 Fertilization envelope, 214
 Fibrin-trapping method, 211
 Fine structure, oocyte, 212
 Fish, feeding efficiency, 241
 Flow patterns, 185
 Fluorescence
 microscopy, 1
 localization, 211
 Fluorescence localization of cytoskeletal proteins in fibrin-trapped cells, 211
 Fluorometric analysis of intracellular sodium concentrations in isolated retinal horizontal cells, 204
 FOREMAN, KEN, see John Kirkpatrick, 240
 Functional and evolutionary implications of the distribution of phosphagens in primitive-type spermatozoa, 264
 Functional significance of the co-localization of taste buds and teeth in the pharyngeal jaws of the bass, *Micropterus salmoides*, 273

G

- G protein, 21
 GABR, HOWAIDA R., see Janice S. Hanley, 223
 GALLARDO, CARLOS S., see Jeffrey L. Ram, 308
 GALLO, MICHAEL A., see Blase Billack, 196
 GARRITT, ROBERT, see Jennifer Sweeney, 238
 Gastropoda, 349
 Gelatinous zooplankton, 337
 Genetic regulatory networks in embryogenesis and evolution, 357
 GILLAND, E., see M. F. Kubke, 218; Hans Straka, 220
 GIMELBRANT, ALEXANDER A., see Raj V. Mankad, 251
 GIOVINE, MARCO, see Giorgio Bavestrello, 120
 GODA, MAKOTO, SHINYA INOUÉ and ROBERT KNUDSON, Oocyte maturation in *Chaetopterus pergamentaceus* observed with centrifuge polarizing microscope, 212
 GRAHAM, SUZANNE, JESSICA DAVIS, LINDA DEEGAN, JUST CEBRIAN, JEFF HUGHES, and JENNIFER HAUXWELL, Effect of eelgrass (*Zostera marina*) density on the feeding efficiency of mummichog (*Fundulus heteroclitus*), 241
 GREEN, DAVID B., see Jamie J. Bishop, 255
 GRIFFIN, MARTIN P. A., MARCI L. COLE, KEVIN D. KROEGER, and JUST CEBRIAN, Dependence of herbivory on autotrophic nitrogen content and on net primary production across ecosystems, 233
 Growth, 17
 GUENTHER, CARLA M., and JELLE ATEMA, Distribution of setae on the *Homarus americanus* lateral antennule flagellum, 182
 Gulf of Mexico, 337
 Gustation, 273

H

- Habitat complexity, 241
 HADFIELD, MICHAEL G., see Eric R. Holm, 21
 HAMMAR, KATHERINE, see Catherine T. Tamse, 201
 HANLEY, JANICE S., NADAV SHASHAR, ROXANNA SMOLOWITZ, ROBERT A. BULLIS, WILLIAM N. MEBANE, HOWAIDA R. GABR, and ROGER T. HANLON, Modified laboratory culture techniques for the European cuttlefish *Sepia officinalis*, 223
 HANLON, ROGER T., see Nadav Shashar, 187; Janice S. Hanley, 223; Michael R. Maxwell, 225; Maureen D. O'Neill, 228
 HAROSI, FERENC I., IONE HUNT VON HERBING, and JEFFREY R. VAN KEUREN, Sickling of anoxic red blood cells in fish, 5
 HAROSI, FERENC I., see Nadav Shashar, 187
 HARRIS, JENNIFER, see Jennifer Rogers, 235
 HAUXWELL, JENNIFER, see Suzanne Graham, 241
 Head genes, 370
 Hearing, directional, 191
 HECK, DIANE E., see Blase Billack, 196
 HECK, PRUDENCE T., see Blase Billack, 196
 Hemoglobin
 in amphioxus, 255
 sickling, 5

- Hemolymph, 43
 HENRY, JONATHAN Q., and MARK Q. MARTINDALE, Evolution of cleavage programs in relationship to axial specification and body plan evolution, 363
 HERBERHOLZ, JENS, and BARBARA SCHMITZ, Role of mechanosensory stimuli in intraspecific agonistic encounters of the snapping shrimp (*Alpheus heterochaelis*), 156
 Herbivory, 233
Hermisenda, learning, 198
 HERRING, P. J., see Mark S. Nowel, 290
 HESSINGER, DAVID A., see Glyne U. Thorington, 145
 Heterochronic, 377
 Heterochronic genes in development and evolution, 375
 Hindbrain, 220
 HO, MICHAEL, see William J. Kuhns, 216
 HOBERT, OLIVER, and GARY RUVKUN, A common theme for LIM homeobox gene function across phylogeny? 377
 HOLM, ERIC R., BRIAN T. NEDVED, EUGENIO CARPIZO-ITUARTE, and MICHAEL G. HADFIELD, Metamorphic-signal transduction in *Hydroides elegans* (Polychaeta: Serpulidae) is not mediated by a G protein, 21
 Home range, 238
 Homeobox, 377
 HOPKINSON, CHARLES, see Catherine Schmitt, 232
 Horizontal cells, 203, 204
 HOSKIN, FRANCIS C. G., and JOHN E. WALKER, A closer look at the natural substrate for a nerve-gas hydrolyzing enzyme in squid nerve, 197
 Hox gene, 220, 373
 Hox genes in arthropod development and evolution, 373
 HUANG, LI-FANG, see Kyeng G. Lee, 211
 HUGHES, JEFF, see Suzanne Graham, 241
 Hyaluronic acid, receptor binding, 216
 Hyaluronic acid-receptor binding demonstrated by synthetic adhesive proteoglycan peptide constructs and by cell receptors on the marine sponge *Microciona prolifera*, 216
 Hyaluronic receptors of *Microciona* sponges, 216
 Hydrodynamic coupling of lobster antennule motion to oscillatory water flow, 180
Hydroides elegans, 213-hydroxykynurenine, 187
 α -Hydroxykynurenine, 187

I

- Immunohistology, 308
In vivo and *in vitro* growth of nerve parasite from *Lophius americanus*, 227
 Induction of extra claws on the chelipeds of a crayfish, *Procambarus clarkii*, 52
 Initial baseline blood chemistry of the oyster toadfish, *Opsanus tau*, 228
 Innervation, 78
 INOUÉ, SHINYA, see Makoto Goda, 212
 Interaction of nitrogen supply, sea level rise, and elevation on species form and composition of salt marsh plants, 235
 Intrinsic adherence, 145
 ISHIKURA, MASAHARU, see Tadashi Maruyama, 70
 Isolation and characterization of endostyle-specific genes in the ascidian *Ciona intestinalis*, 60

J

- JESSEN-ELLER, KATHRYN, MARJORIE STEELE, CAROL REINISCH, and NICHOLAS SPITZER, Blockade of ryanodine receptors stimulates neurite outgrowth in embryos of *Spisula solidissima*, 206
 JOHNSEN, SÖNKE, and EDITH A. WIDDER, Transparency and visibility of gelatinous zooplankton from the northwestern Atlantic and Gulf of Mexico, 337
 JOHNSON, AMY S., see Olaf Ellers, 136
 Juvenile hormone, 112
 Juvenile *Limulus polyphemus* generate two water currents that contact one proven and one putative chemoreceptor organ, 185

K

- KACHURAK, KRISTEN A., see Richard A. Tankersley, 168
 KANAI, SATORU, see Tadashi Maruyama, 70
 KEEFE, D. L., see D. M. Porterfield, 208
 Ketone body, 12
 KING, JANE ROCHE, and HANS STRAKA, Effects of vestibular nerve lesions on orientation turning in the leopard frog, *Rana pipiens*, 193
 KING, LESLIE A., see Robert B. Silver, 209
 KING, TERESA, see Earl Weidner, 227
 KINSEY, STEPHEN T., see W. Ross Ellington, 264
 KIRKPATRICK, JOHN, KEN FOREMAN, and IVAN VALIELA, Dissolved inorganic nitrogen flux and mineralization in Waquoit Bay sediments as measured by core incubations, 240
 KITAHARA, TAKUJI, see Isamu Nakatani, 52
 KNUDSON, ROBERT, see Makoto Goda, 212
 KOHN, ALAN J., see Bruno Pernet, 349
 KOROLEVA, ZOYA, see Kyeng G. Lee, 211
 KRAUS, DAVID W., see Jamie J. Bishop, 255
 KROEGER, KEVIN D., see Martin P.A. Griffin, 233
 KUBKE, M. F., E. GILLAND, and R. BAKER, Lipophilic dye labeling distinguishes segregated central components of the eighth cranial nerve in embryonic chicken, 218
 KUHNS, WILLIAM J., XAVIER FERNANDEZ-BUSQUETS, MAX M. BURGER, MICHAEL HO, and EVA TURLEY, Hyaluronic acid-receptor binding demonstrated by synthetic adhesive proteoglycan peptide constructs and by cell receptors on the marine sponge *Microciona prolifera*, 216
 KUZIRIAN, ALAN M., HERMAN T. EPSTEIN, THOMAS J. NELSON, and NANCY S. RAFFERTY, Lead, learning, and calcectin in *Hermis-senda*, 198

L

- Lancelet, 255, 260
 LANZA, SERENA, see Giorgio Bavestrello, 120
 Largemouth bass, 273
 Larvae, 112, 126
 LASKIN, JEFFREY D., see Blase Billack, 196
 Late postembryonic development of the symbiotic light organ of *Euprymna scolopes* (Cephalopoda: Sepiolidae), 326
 LAUFER, HANS, see Uri Abdu, 112
 Lead
 concentration in sediments, 243
 effect on *Aplysia*, 201
 neurotoxicity, 198
 Lead concentration as an indicator of contamination history in estuarine sediments, 243
 Lead, learning, and calcectin in *Hermis-senda*, 198
 LEE, KYENG G., NISHAI MOHAN, ZOYA KOROLEVA, LI-FANG HUANG, and WILLIAM D. COHEN, Fluorescence localization of cytoskeletal proteins in fibrin-trapped cells, 211
 Leech, 370
 LEGRA, JESSICA C., ROSELLE E. SAFRAN, and IVAN VALIELA, Lead concentration as an indicator of contamination history in estuarine sediments, 243
 LEGRA, JESSICA C., see Rosell E. Safran, 245
 Leukotriene, 209
 LEYS, SALLY P., and HENRY M. REISWIG, Transport pathways in the neotropical sponge *Aplysina*, 30
 Ligaments, 136
 Light organ, 89
Limulus
 chemoreception, 185
 lateral eye, 189
 LINSER, PAUL J., WILLIAM E.S. CARR, HOLLY S. CATE, CHARLES D. DERBY, and JAMES C. NETHERTON III, Functional significance of the co-localization of taste buds and teeth in the pharyngeal jaws of the bass, *Micropterus salmoides*, 273
 Lipophilic dye labeling distinguishes segregated central components of the eighth cranial nerve in embryonic chicken, 218
 Lobster, 180, 182

- Lophius americanus*, 227
 Lucifer yellow, 78

M

- MAA, see Mycosporin-like amino acid
Macrobrachium rosenbergii, 112
 Macrophage, invertebrate, 89
 MACY, WILLIAM K., see Michael R. Maxwell, 225
 MALCHOW, ROBERT PAUL, MICHAEL P. VERZI, and PETER J.S. SMITH, Extracellular pH gradients measured from isolated retinal cells, 203
 MALCHOW, ROBERT PAUL, see Kristen A. Andersen, 204
 MANKAD, RAJ V., ALEXANDER A. GIMELBRANT, and TIMOTHY S. MCCLINTOCK, Consensus translational initiation sites of marine invertebrate phyla, 251
 Mariculture, 223
 MARTINDALE, MARK Q., see Jonathan Q. Henry, 363
 MARUYAMA, TADASHI, MASAHARU ISHIKURA, SATORU YAMAZAKI, and SATORU KANAI, Molecular phylogeny of zooxanthellate bivalves, 70
 Maternal genes, 381
 Maturation, oocyte, 212
 MAXWELL, MICHAEL R., WILLIAM K. MACY, SHOBU ODATE, and ROGER T. HANLON, Evidence for multiple spawning by squids (*Loligo pealei*) in captivity, 225
 MBL Photography/Photomicrography Contest 1997–1998, 387
 MCCLINTOCK TIMOTHY S., see Raj V. Mankad, 251
 MCFALL-NGAI, MARGARET J., see Spencer V. Nyholm, 89; Mary K. Montgomery, 326
 McLEOD, J., see J. A. Stuart, 12
 McNEIL, PAUL L., see Katsuya Miyake, 214
 MEAD, KRISTINA S., The biomechanics of odorant access to aesthetascs in the grass shrimp, *Palaeomonetes vulgaris*, 184
 MEBANE, WILLIAM N., see Janice S. Hanley, 223
 Mechanisms of specification in ascidian embryos, 381
 Mechanosensory stimulus, 156
 MENSINGER, ALLEN F., and MAX DEFFENBAUGH, Prototype rechargeable tag for acoustical neural telemetry, 194
 MENSINGER, ALLEN F., see Maureen D. O'Neill, 228
 Mesoderm
 amphioxus, 260
 evolution, 367
 Metabolism, 12
 Metal speciation, 43
 Metamorphic-signal transduction in *Hydroides elegans* (Polychaeta: Serpulidae) is not mediated by a G protein, 21
 Metamorphosis, 21, 112, 126
 Methyl farnesoate, 112
Microciona
 adhesive proteoglycan peptide constructs, 216
 hyaluronic receptors in, 216
Micropterus salmoides, 273
 Microscopy
 centrifuge polarizing, 212
 confocal, 1
 Migration, 168
 Migratory behavior of ovigerous blue crabs *Callinectes sapidus*: evidence for selective tidal-stream transport, 168
 MIHASHI, KOSHIN, see Katsuyuki Yamada, 107
 Mineral selectivity, 120
 Mineralization, 240
 MINTEQA2 speciation model, 43
 MIYAKE, KATSUYA, and PAUL L. McNEIL, A little shell to live in: evidence that the fertilization envelope can prevent mechanically induced damage of the developing sea urchin embryo, 214
 MOBERG, PHILIP E., see Olaf Eilers, 136
 Modified laboratory culture techniques for the European cuttlefish *Sepia officinalis*, 223
 MOHAN, NISHAI, see Kyeng G. Lee, 211
 Molecular phylogeny of zooxanthellate bivalves, 70
 Mollusc, ketone body metabolism, 12

Mollusca, 251
 MONTGOMERY, MARY K., and MARGARET J. MCFALL-NGAI, Late post-embryonic development of the symbiotic light organ of *Euprymna scolopes* (Cephalopoda: Sepiolidae), 326
 Morphogenesis, 112
 Mummichog
 feeding, 241
 population size, 238
 site fidelity, 238
 Muscle, 52
 Mycosporine-like amino acid, 187
 Myotome, 255

N

NAIR, P. SATISH, and WILLIAM E. ROBINSON, Calcium speciation and exchange between blood and extrapallial fluid of the quahog *Mercentaria mercenaria* (L.), 43
 NAKATANI, ISAMU, YOSHINORI OKADA, and TAKUJI KITAHARA, Induction of extra claws on the chelipeds of a crayfish, *Procambarus clarkii*, 52
 NASA, Genetic Regulatory Networks in Embryogenesis and Evolution, 357
 National Aeronautics and Space Administration, see NASA, 357
 NEDVED, BRIAN T., see Eric R. Holm, 21
 NELSON, THOMAS J., see Alan M. Kuzirian, 198
 Nematocyst, 145
 Nerve bundle, 52
 Nerve parasites in *Lophius americanus*, 227
 Nerve-gas, 197
 Net primary production, 233
 NETHERTON, JAMES C., III, see Paul J. Linser, 273
 Neurodevelopment, 206
 Neuroethology, 193, 194
 Neuropeptide, 308
 Nitric oxide, 196
 Nitrogen
 fertilization, 180, 235
 loading, 240
 stable isotope, 245
 Notochord, 255, 381
 NOWEL, MARK S., P. M. J. SHELTON, and P. J. HERRING, Cuticular photophores of two decapod crustaceans, *Oplophorus spinosus* and *Systellaspis debilis*, 290
 Nuclear envelope breakdown
 in polychaete, 212
 in sand dollar, 209
 Nucleus, descending octaval, 191
 Nutrient concentration, 233
 NYHOLM, SPENCER V., and MARGARET J. MCFALL-NGAI, Sampling the light organ microenvironment of *Euprymna scolopes*: description of a population of host cells in association with the bacterial symbiont *Vibrio fischeri*, 89

O

O'NEILL, MAUREEN D., HEATHER M. WESP, ALLEN F. MENSINGER, and ROGER T. HANLON, Initial baseline blood chemistry of the oyster toadfish, *Opsanus tau*, 228
 Objective lenses, 1
 ODATE, SHOBU, see Michael R. Maxwell, 225
 OGASAWARA, MICHIO, and NORIYUKI SATOH, Isolation and characterization of endostyle-specific genes in the ascidian *Ciona intestinalis*, 60
 OKADA, YOSHINORI, see Isamu Nakatani, 52
 Oocyte maturation in *Chaetopterus pergamentaceus* observed with centrifuge polarizing microscope, 212
 OOI, E. L., see J. A. Stuart, 12
 Oplophorid shrimps, 290
Opsanus tau
 acoustic tagging, 194
 auditory response, 191

 blood chemistry, 238
 infections in, 229
 Optical anisotropies, 5
 Oxygen, 208

P

PARADISE, KRISTEN, see Elizabeth Quinn, 185
 Parasitism, 227, 349
 Pb²⁺, 201
 Peptidergic neurons, 282
 Peptidergic neurons in barnacles: an immuno-histochemical study using antisera raised against crustacean neuropeptides, 282
 PERNET, BRUNO, and ALAN J. KOHN, Size-related obligate and facultative parasitism in the marine gastropod *Trichotropis cancellata*, 349
 pH, 203
 Pharmacology, 196
 Pharyngeal
 jaws, 273
 teeth, 273
 Phosphagen kinase, 264
 Photophores, 290
 Photoreceptor
 extraocular, 78
 sensitivity of, 187
 Physiological progenesis in cephalopod molluscs, 17
 PISTON, DAVID W., Concepts in Imaging and Microscopy. Choosing objective lenses: the importance of numerical aperture and magnification in digital optical microscopy, 1
 Planktonic feeding and evolutionary significance of the lobate body plan within the Ctenophora, 247
 Polychaete
 metamorphic signal in, 21
 oocyte maturation, 212
 parasitic, 349
 Polymerization, 5
 Population size and site fidelity of *Fundulus heteroclitus* in a macrotidal saltmarsh creek, 238
 Porifera
 development, 120
 hyaluronic receptors, 216
 transport in, 30
 PORTERFIELD, D. M., J. R. TRIMARCHI, D. L. KEEFE, and P. J. S. SMITH, Characterization of oxygen and calcium fluxes from early mouse embryos and oocytes, 208
 PORTERFIELD, D. MARSHALL, see Catherine T. Tamse, 201
 Post-larva, 112
 Preliminary evaluation of sedimentation rates and species distribution in Plum Island Estuary, Massachusetts, 232
 Prey
 capture, 193
 selection, 247
 Progenesis, 17
 PRONZATO, ROBERTO, see Giorgio Bavestrello, 120
 Prophase mitotic apparatus, 209
 Proprioceptor, 52
 Prosobranchia, 308
 Prototype rechargeable tag for acoustical neural telemetry, 194
Pseudomonas, 197, 229
Pseudomonas putida infections of the oyster toadfish (*Opsanus tau*), 229

Q

Quinidine, 204
 QUINN, ELIZABETH, KRISTEN PARADISE, and JELLE ATEMA, Juvenile *Limulus polyphemus* generate two water currents that contact one proven and one putative chemoreceptor organ, 185

R

- RAFFERTY, NANCY S., see Alan M. Kuzirian, 198
- RAM, JEFFREY L., CARLOS S. GALLARDO, MICHAL L. RAM, and ROGER P. CROLL. Reproduction-associated immunoreactive peptides in the nervous systems of prosobranch gastropods, 308
- RAM, MICHAL L., see Jeffrey L. Ram, 308
- REINISCH, CAROL, see Kathryn Jessen-Eller, 206
- REISWIG, HENRY M., see Sally P. Leys, 30
- Release response, 145
- Reproduction
bryozoan, 126
coral, 319
gastropod, 308
- Reproduction-associated immunoreactive peptides in the nervous systems of prosobranch gastropods, 308
- Resolution, 1
- Retina
pH gradients, 203
damage to, 187
- Reynolds number, 184
- Rhombomeric organization of brainstem motor neurons in larval frogs, 220
- RINKEVICH, BARUCH, IRVING L. WEISSMAN, and ANTHONY W. DETOMASO. Transplantation of Fu/HC-incompatible zooids in *Botryllus schlosseri* results in chimerism, 98
- ROBINSON, WILLIAM E., see P. Satish Nair, 43
- RODHOUSE, PAUL G., Physiological progenesis in cephalopod molluscs, 17
- ROGERS, JENNIFER, JENNIFER HARRIS, and IVAN VALIELA. Interaction of nitrogen supply, sea level rise, and elevation on species form and composition of salt marsh plants, 235
- Role of mechanosensory stimuli in intraspecific agonistic encounters of the snapping shrimp (*Alpheus heterochaelis*), 156
- RUTA, VANESSA J., FREDERICK A. DODGE, and ROBERT B. BARLOW. Efferent modulation of physiological properties of the *Limulus* lateral eye, 189
- RUVKUN, GARY, see Frank Slack, 375; Oliver Hobert, 377
- Ryanodine, 206

S

- SAFRAN, ROSELLE E., JESSICA C. LEGRA, and IVAN VALIELA. Effects of nitrogen loading on eelgrass seed coat abundance, C to N ratios, and $\Delta^{15}N$ in sediments of Waquoit Bay, 245
- SAFRAN, ROSELLE E., see Jessica C. Legra, 243
- SAGI, AMIR, see Uri Abdu, 112
- SAKAI, KAZUHIKO. Effect of colony size, polyp size, and budding mode on egg production in a colonial coral, 319
- Salt marsh, 180, 232, 235, 238
- Sampling the light organ microenvironment of *Euprymna scolopes*: description of a population of host cells in association with the bacterial symbiont *Vibrio fischeri*, 89
- SARÀ, MICHELE, see Giorgio Bavestrello, 120
- SATOH, NORIYUKI. Mechanisms of specification in ascidian embryos, 381
- SATOH, NORIYUKI, see Michio Ogasawara, 60
- SBF1, sodium indicator, 204
- SCHMITT, CATHERINE, NATHANIEL WESTON, and CHARLES HOPKINSON. Preliminary evaluation of sedimentation rates and species distribution in Plum Island Estuary, Massachusetts, 232
- SCHMITZ, BARBARA, see Jens Herberholz, 156
- Scleractinian, 319
- Sea anemone, 145
- Sea level rise, 180, 235
- Sea urchin
fertilization, 107, 214
skeleton, 136
tube foot contraction, 196
- Sediments
deposition, 232
lead in, 243
- N flux and mineralization in, 240
organic matter content, 232
- Segment development, 373
- Sepia officinalis*, 223
- Serotonin, 206
- Setae, 182
- SHANKLAND, MARTY, and ASHLEY E. E. BRUCE. Axial patterning in the leech: developmental mechanisms and evolutionary implications, 370
- SHASHAR, NADAV, FERENC J. HAROSI, ANASTAZIA T. BANASZAK, and ROGER T. HANLON. UV radiation blocking compounds in the eye of the cuttlefish *Sepia officinalis*, 187
- SHASHAR, NADAV, see Janice S. Hanley, 223
- SHELTON, P. M. J., see Mark S. Nowel, 290
- Sickling of anoxic red blood cells in fish, 5
- SIGALA, MARCO A., see Richard A. Tankersley, 168
- Signal transduction, 21
- SILVER, ROBERT B., LESLIE A. KING, and ALYSSA F. WISE. Calcium regulatory endomembranes of the prophase mitotic apparatus of sand dollar cells contain enzyme activities that produce leukotriene B₄ but not 1,4,5-inositol triphosphate, 209
- Size-related obligate and facultative parasitism in the marine gastropod *Trichotropis cancellata*, 349
- Skeleton, sea urchin, 136
- SLACK, FRANK, and GARY RUVKUN. Heterochronic genes in development and evolution, 375
- SMITH, PETER J. S., see Catherine T. Tamse, 201; Robert Paul Malchow, 203; D. M. Porterfield, 208
- SMOLOWITZ, ROXANNA, ELIZABETH WADMAN, and H. M. CHIKARMANE. *Pseudomonas putida* infections of the oyster toadfish (*Opsanus tau*), 229
- SMOLOWITZ, ROXANNA, see Janice S. Hanley, 223
- Snapping shrimp, 156
- Spawning, 168
- Specific gene, 60
- Spermatozoa, 264
- Spiralia, 363, 367
- Spirocyst, 145
- SPITZER, NICHOLAS, see Kathryn Jessen-Eller, 206
- Sponge, see Porifera
- Squid
fecundity, 225
fishery, 225
light organ, 326
nerve, 197
- STACH, THOMAS. Coelomic cavities may function as a vascular system in amphioxus larvae, 260
- Start site, 251
- STEELE, MARJORIE, see Kathryn Jessen-Eller, 206
- Stomatopod, 184
- STRAKA, HANS, EDWIN GILLAND, and ROBERT BAKER. Rhombomeric organization of brainstem motor neurons in larval frogs, 220
- STRAKA, HANS, see Jane Roche King, 193
- Strength, 136
- Strongylocentrotus*, 136
- Structural strengthening of urchin skeletons by collagenous sutural ligaments, 136
- STUART, J. A., E. L. OOI, J. MCLEOD, A. E. BOURNS, and J. S. BALLANTYNE. D- and L-β-hydroxybutyrate dehydrogenases and the evolution of ketone body metabolism in gastropod molluscs, 12
- Suspension feeding, 349
- SWEENEY, JENNIFER, LINDA DEEGAN, and ROBERT GARRITT. Population size and site fidelity of *Fundulus heteroclitus* in a macrotidal salt-marsh creek, 238
- Symbiosis
in bivalves, 70
in squid, 89, 326
- Symmetry, 370

T

- TAKAC, PETER, see Uri Abdu, 112
- TAMSE, CATHERINE T., KATHERINE HAMMAR, D. MARSHALL PORTERFIELD, and PETER J. S. SMITH, Transmembrane calcium flux in Pb^{2+} -exposed *Aplysia* neurons, 201
- TANKERSLEY, RICHARD A., MARIA G. WIEBER, MARCO A. SIGALA, and KRISTEN A. KACHURAK, Migratory behavior of ovigerous blue crabs *Callinectes sapidus*: evidence for selective tidal-stream transport, 168
- Taste buds, 273
- Tegula, 308
- Telemetry, 194
- Temperature dependence, 107
- Temperature-independent period immediately after fertilization in sea urchin eggs, 107
- The biomechanics of odorant access to aesthetascs in the grass shrimp, *Palaemonetes vulgaris*, 184
- THORINGTON, GLYNE U., and DAVID A. HESSINGER, Efferent mechanisms of discharging cnidae: II. A nematocyst release response in the sea anemone tentacle, 145
- Toadfish, see *Opsanus tau*
- Tracking turbulence: processing the bimodal signals that define an odor plume, 179
- Translation, 251
- Transmembrane calcium flux in Pb^{2+} -exposed *Aplysia* neurons, 201
- Transparency, 337
- Transparency and visibility of gelatinous zooplankton from the north-western Atlantic and Gulf of Mexico, 337
- Transplantation of Fu/Hc-incompatible zooids in *Botryllus schlosseri* results in chimerism, 98
- Transport pathways in the neotropical sponge *Aplysina*, 30
- Transport, selective tidal-stream, 168
- TRIMARCHI, J. R., see D. M. Porterfield, 208
- Trochoblast, 367
- TROLL, WALTER, see Blase Billack, 196
- TURLEY, EVA, see William J. Kuhns, 216

U

- Ubx* regulation, 373
- Ultrastructure
 amphioxus, 260
 photophore, 290
- Ultraviolet radiation, 187
- Urbanization, 243
- UV radiation blocking compounds in the eye of the cuttlefish *Sepia officinalis*, 187

V

- VALIELA, IVAN, see Jennifer Rogers, 235; John Kirkpatrick, 240; Jessica C. Legra, 243; Rosell E. Safran, 245
- VAN DEN BIGGELAAR, J. A. M., see A. E. van Loon, 367
- VAN KEUREN, JEFFREY R., see Ferenc I. Hárosi, 5
- VAN LOON, A. E., and J. A. M. VAN DEN BIGGELAAR, Changes in cell lineage specification elucidate evolutionary relations in Spiralia, 367
- VANDERSON, THOMAS L., see Jamie J. Bishop, 255
- VERZI, MICHAEL P., see Robert Paul Malchow, 203
- Vestibular system, development, 218
- Vibrio*, 89, 326
- Visibility, 337
- VON HERBING, IONE HUNT, see Ferenc I. Hárosi, 5

W


- WADMAN, ELIZABETH, see Roxanna Smolowitz, 229
- WALKER, JOHN E., see Francis C. G. Hoskin, 197
- Water jet, 156
- WEAVER, MATTHEW, and JELLE ATEMA, Hydrodynamic coupling of lobster antennule motion to oscillatory water flow, 180
- WEBSTER, S. G., Peptidergic neurons in barnacles: an immuno-histochemical study using antisera raised against crustacean neuropeptides, 282
- WEIDNER, EARL, and TERESA KING, *In vivo* and *in vitro* growth of nerve parasite from *Lophius americanus*, 227
- WEISSMAN, IRVING L., see Baruch Rinkevich, 98
- WENDT, DEAN E., Effect of larval swimming duration on growth and reproduction of *Bugula neritina* (Bryozoa) under field conditions, 126
- WESP, HEATHER M., see Maureen D. O'Neill, 228
- WESTON, NATHANIEL, see Catherine Schmitt, 232
- WIDDER, EDITH A., see Sönke Johnsen, 337
- WIEBER, MARIA G., see Richard A. Tankersley, 168
- WILLIAMSON, RODDY, see Christopher S. Cobb, 78
- WISE, ALYSSA F., see Robert B. Silver, 209
- Wounding, on propodus, 52

Y

- YAMADA, KATSUYUKI, and KOSHIN MIHASHI, Temperature-independent period immediately after fertilization in sea urchin eggs, 107
- YAMAZAKI, SATORU, see Tadashi Maruyama, 70

Z

- Zooplankton, 337
- Zooxanthellae, 70
- Zostera marina*, see Eelgrass

MBL WHOI LIBRARY

0 EEBL HM

